TN
1
A5
Vol. 201
NIC

TRANSACTIONS

of the

American Institute of Mining and Metallurgical Engineers

(Incorporated)

VOLUME 201

American Institute of Mining, Metallurgical, and Petroleum Engineers

PETROLEUM DEVELOPMENT AND TECHNOLOGY

1954

PETROLEUM BRANCH

PAPERS AND DISCUSSIONS INCLUDED HAVE BEEN APPROVED FOR PUBLICATION BY THE PETROLEUM BRANCH TRANSACTIONS EDITORIAL COMMITTEE. THEY WERE SELECTED FROM PAPERS PRESENTED BEFORE THE BRANCH AT MEETINGS HELD IN LOS ANGELES, OCT. 1-2, 1953; DALLAS, OCT. 19-21, 1953; NEW YORK, FEB. 13-17, 1954; LOS ANGELES, OCT. 7-8, 1954; SAN ANTONIO, OCT. 17-20, 1954; AND PAPERS NOT PRESENTED AT THESE MEETINGS BUT OFFERED TO THE PETROLEUM BRANCH, AIME, FOR PUBLICATION.

PUBLISHED BY THE INSTITUTE
AT THE OFFICE OF THE PETROLEUM BRANCH
800 FIDELITY UNION BUILDING
DALLAS, TEXAS

Headquarters of the Institute are at 29 West 39th Street, New York, N. Y.

Copyright, 1955, by the
American Institute of Mining and Metallurgical Engineers
(Incorporated)

Printed in the United States of America

STORM PRINTING COMPANY, DALLAS, TEXAS

FOREWORD

DURING 1954 the Petroleum Branch continued its phenomenal growth by accepting 930 new applications for affiliation in one of the three membership grades. Seven new local sections were formed and approved by the AIME Board of Directors, as follows: San Joaquin Valley, Hobbs, Hugoton, Panhandle, New York Petroleum, Illinois Basin Petroleum and Venezuela Petroleum.

Continued growth in advertising income from the JOURNAL OF PETROLEUM TECHNOLOGY resulted in our receiving a new high net income from this source. Our JOURNAL is fast becoming recognized in the advertising field as the best method of reaching the Petroleum Engineer, who recommends a substantial portion of oilfield purchases.

R. W. Taylor was appointed editor of the JOURNAL on March 1st. A complete restyling of the typography and layout of the magazine was initiated with the April issue and subsequent response has indicated that this was a very timely and appropriate move for the long range development of the publication. The Branch published a directory of its membership in the June issue. It is hoped that this practice can be continued.

The Southwest Texas Section acted as host for the annual Petroleum Branch Fall Meeting in San Antonio, Tex., and their efforts were rewarded by a record attendance of 1,777 men and 525 ladies. A new innovation was the Membership Luncheon which attracted a capacity crowd to hear a report covering the business affairs of our Branch. Institute President Leo F. Reinartz honored us with his presence at this luncheon.

Cedric K. Ferguson was a prominent Junior Member who died of polio in Aug., 1953. At the time of his death he was secretary of the Pacific Petroleum Chapter and chairman of the Pacific Petroleum Chapter Junior Group. In his memory, the Cedric K. Ferguson Medal was established by grants from fellow members and the employer of Mr. Ferguson. It will be awarded annually to a member under 33 years of age who contributes an outstanding paper in the field of petroleum technology. The first award was made at the San Antonio Meeting to Cedric K. Ferguson, posthumously, and was accepted by his parents in a touching ceremony. The Branch needs to establish more awards of this type to enable us to recognize technical achievements in our field.

This *Transactions* volume and the ones before it represent the history of the technology of our Petroleum Branch and the men on the Technology and Publications Committees, along with the authors, are to be complimented on another fine contribution to our literature comprising 44 technical papers and two technical notes.

JOHN R. McMILLAN, Chairman
Petroleum Branch, 1954

Los Angeles, California
January 1, 1955

OFFICERS AND STAFF OF THE AIME

For the Year Ending February, 1955

PRESIDENT

L. F. REINARTZ

VICE PRESIDENTS

O. B. J. FRASER
L. E. ELKINS
T. B. COUNSELMAN
J. B. MORROW
A. B. KINZEL
HAROLD DECKER

DIRECTORS

C. H. BENEDICT
E. ISERN
R. E. KIRK
R. B. CAPLES
H. W. JOHNSON
C. C. LONG
M. L. HAIDER
PHILIP KRAFT
P. J. SHENON
T. L. JOSEPH, SR.
E. L. OLIVER
GEORGE DUB
C. E. REISTLE, JR.
P. D. WILSON
E. R. MARBLE
D. C. HELMS
E. C. BABSON

DIRECTORS EX OFFICIIS

J. R. VAN PELT (Mineral Industry Education)
J. H. SCAFF (Institute of Metals)
P. T. STROUP (Extractive Metallurgy)
JOHN R. McMILLAN (Petroleum)
R. C. STEPHENSON (Industrial Minerals)
M. D. COOPER (Coal)
J. S. MARSH (Iron and Steel)
J. D. FORRESTER (Mining, Geology, Geophysics)
S. D. MICHAELSON (Mineral Beneficiation)
J. K. RICHARDSON (Mineral Economics)
R. E. KIRK (Mining Branch Council)
R. R. McNAUGHTON (Metals Branch Council)

TREASURER AND DIRECTOR

G. F. MOULTON

STAFF OF INSTITUTE IN NEW YORK

SECRETARY

EDWARD H. ROBIE

ASSISTANT SECRETARIES

JOE B. ALFORD
ROY E. O'BRIEN
E. J. KENNEDY, JR.
H. NEWELL APPLETON
E. O. KIRKENDALL

ASSISTANT TREASURER

PETER J. APOL

STAFF OF INSTITUTE IN DALLAS

JOE B. ALFORD
EXECUTIVE SECRETARY

R. W. TAYLOR
EDITOR, JOURNAL OF PETROLEUM TECHNOLOGY

VIRGINIA B. DAGGETT
ASSISTANT SECRETARY

CONTENTS

FOREWORD, *by* JOHN R. MCMILLAN iii

AIME OFFICERS AND STAFF iv

PETROLEUM BRANCH OFFICERS AND COMMITTEE CHAIRMEN viii

PETROLEUM BRANCH PAST CHAIRMEN ix

THE ANTHONY F. LUCAS MEDAL AND FUND x

PETROLEUM BRANCH CERTIFICATE OF SERVICE xii

PAPERS

CAPILLARITY-PERMEABILITY

Displacement Experiments in a Consolidated Porous System, by J. S. Levine 57

A Study of Displacements in Microscopic Capillaries, by Charles C. Templeton 162

DRILLING AND PRODUCING — EQUIPMENT, METHODS AND MATERIALS

Effectiveness of Gun Perforating, by T. O. Allen and J. H. Atterbury, Jr. 8

Some Practical Aspects of Gravel Packing, by C. J. Rodgers 15

The Corrosion-Metallurgical Aspects of Sucker Rods and their Oil Well Service Performance, by F. J. Radd and R. L. McGlasson 73

Mechanical Treatment of Weighted Drilling Muds, by Roy A. Bobo and R. S. Hoch 93

Reservoir Fracturing — A Method of Oil Recovery from Extremely Low Permeability Formations, by L. E. Wilsey and W. G. Bearden 169

Optimum Sand Concentrations in Well Treatments, by Peter Dehlinger, W. H. Browne, and C. O. Bundrant 273

A New Tool for Perforating Casing below Tubing, by Blake M. Caldwell and Harrold D. Owen . . . 302

DRILLING FLUIDS AND CEMENTS

A Simplified Cementing Technique for Recompletion Operations, by T. A. Huber, G. H. Tausch, and J. R. Dublin III 1

Filtration from Mud During Drilling, by C. K. Ferguson and J. A. Klotz 29

Drilling Mud Control in the Southwest Louisiana Coastal Area, by C. R. Claus and G. A. Standish . . 87

Mechanical Treatment of Weighted Drilling Muds, by Roy A. Bobo and R. S. Hoch 93

Plugging off Water in Fractured Formations, by George C. Howard and P. P. Scott, Jr. 132

A Ten-Pound Cement Slurry for Oil Wells, by Henry F. Coffer, J. J. Reynolds, and Roscoe C. Clark, Jr. . 146

The Pumpability of Clay-Water Drilling Fluids, by I. Havenaar 287

ELECTRIC LOGGING

An Experimental Investigation of the S.P. and Resistivity Phenomena in Dirty Sands, by M. R. J. Wyllie and P. F. Southwick 43

A Contribution to Electric Log Interpretation in Shaly Sands, by A. Poupon, M. E. Loy, and M. P. Tixier 138

Resistivity Logging in Thin Beds, by Leendert de Witte 155

Interrelation of Resistivity and Potential of Shaly Reservoir Rock, by F. M. Perkins, Jr., H. R. Brannon, Jr., and Weldon O. Winsauer 176

NATURAL GAS TECHNOLOGY

A Simplified Analysis of Unsteady Radial Gas Flow, by J. S. Aronofsky and R. Jenkins 149

Gas Hydrates of Hydrogen Sulfide-Methane Mixtures, by Leslie J. Noaker and Donald L. Katz . . . 237

The Phase and Volumetric Behavior of Natural Gases at Low Temperatures and High Pressures, by P. C. Davis, A. F. Bertuzzi, T. L. Gore, and F. Kurata 245

Viscosity of Hydrocarbon Gases under Pressure, by Norman L. Carr, Riki Kobayashi, and David B. Burrows 264

Measurement of Resistance to Flow of Fluids in Natural Gas Wells, by R. V. Smith, R. H. Williams, and E. J. DeWees. 279

PVT STUDIES

Equilibrium Vaporization Ratios for a Reservoir Fluid Containing a High Concentration of Hydrogen Sulfide, by Harold Vagtborg, Jr. 67

Solution of the Equations of Unsteady State Two-Phase Flow in Oil Reservoirs, by W. J. West, W. W. Garvin, and J. W. Sheldon 217

Study of Undersaturation during Repressuring and Supersaturation during Flow of Oil to Wells, by Ralph V. Higgins 230

The Phase and Volumetric Behavior of Natural Gases at Low Temperatures and High Pressures, by P. C. Davis, A. F. Bertuzzi, T. L. Gore, and F. Kurata 245

Viscosity of Hydrocarbon Gases under Pressure, by Norman L Carr, Riki Kobayashi, and David B. Burrows 264

RESEARCH ON PHASE RELATIONSHIPS

Displacement Experiments in a Consolidated Porous System, by J. S. Levine 57

The Effect of Surface and Interfacial Tensions on the Recovery of Oil by Water Flooding, by Harvey T. Kennedy, and Erasmo T. Guerrero 124

RESERVOIR ENGINEERING EQUIPMENT

A Blotter-Type Electrolytic Model Determination of Areal Sweeps in Oil Recovery by In-Situ Combustion, by H. J. Ramey, Jr., and G. W. Nabor 119

A Simplified Analysis of Unsteady Radial Gas Flow, by J. S. Aronofsky and R. Jenkins 149

A Magnetic Susceptibility Method for the Determination of Liquid Saturation in Porous Materials, by J. W. Whalen 203

Solution of the Equations of Unsteady State Two-Phase Flow in Oil Reservoirs, by W. J. West, W. W. Garvin, and J. W. Sheldon 217

RESERVOIR ENGINEERING — GENERAL

Equilibrium Vaporization Ratios for a Reservoir Fluid Containing a High Concentration of Hydrogen Sulfide, by Harold Vagtborg, Jr. 67

A Method for Determination of Average Pressure in a Bounded Reservoir, by C. S. Matthews, F. Brons, and P. Hazebroek 182

Estimated Effect of Vertical Fractures on Secondary Recovery, by Paul B. Crawford and R. E. Collins. . 192

Production of Water-Driven Reservoirs below their Bubble Point, by A. B. Dyes 240

The Mechanics of Fracture Induction and Extension, by Eugene Harrison, W. F. Kieschnick, Jr., and W. J. McGuire 252

The Role of Bubble Formation in Oil Recovery by Solution Gas Drives in Limestones, by C. R. Stewart, E. B. Hunt, Jr., F. N. Schneider, T. M. Geffen, and V. J. Berry, Jr. 294

Displacement of Oil from Porous Media by Miscible Liquids, by J. Offeringa and C. van der Poel . . 310

RESERVOIR PERFORMANCE FIELD STUDIES

History and Performance of the Coldwater Oil Field, Michigan, by C. R. Criss and R. L. McCormick . . 22

Pressure Maintenance by Gas Injection in the Brookhaven Field, Mississippi, by J. B. Justus, R. W. Cassingham, C. R. Blomberg, and W. H. Ashby 97

Comparison of Methods for Analyzing a Water Drive Field, Torchlight Tensleep Reservoir, Wyoming, by F. M. Stewart, F. H. Callaway, and R. E. Gladfelter 197

SECONDARY RECOVERY

Oil Production after Breakthrough — As Influenced by Mobility Ratio, by A. B. Dyes, B. H. Caudle, and R. A. Erickson 81

Pressure Maintenance by Gas Injection in the Brookhaven Field, Mississippi, by J. B. Justus, R. W. Cassingham, C. R. Blomberg, and W. H. Ashby 97

Development of an Underground Heat Wave for Oil Recovery, by Bruce F. Grant, and Stefan F. Szasz . 108

A Blotter-Type Electrolytic Model Determination of Areal Sweeps in Oil Recovery by In-Situ Combustion, by H. J. Ramey, Jr., and G. W. Nabor 119

The Effect of Surface and Interfacial Tensions on the Recovery of Oil by Water Flooding, by Harvey T. Kennedy and Erasmo T. Guerrero 124

Estimated Effect of Vertical Fractures on Secondary Recovery, by Paul B. Crawford and R. E. Collins . 192

Use of Radioactive Iodine as a Tracer in Water-Flooding Operations, by J. Wade Watkins and E. S. Mardock 209

Study of Undersaturation during Repressuring and Supersaturation during Flow of Oil to Wells, by Ralph V. Higgins 230

Displacement of Oil from Porous Media by Miscible Liquids, by J. Offeringa and C. van der Poel . . 310

TECHNICAL NOTES

Effect of Gas Slip on Unsteady Flow of Gas through Porous Media — Experimental Verification, by G. C. Wallick and J. S. Aronofsky 324

A Rotational High Pressure Viscosimeter, by Murray F. Hawkins, Jr., and Marion L. Kimmel . . . 322

ERRATA

In Technical Paper 3784, "Oil Production after Breakthrough — As Influenced by Mobility Ratio" by A. B. Dyes, B. H. Caudle, and R. A. Erickson, three of the figures are incorrectly positioned. These are Figs. 4, 6, and 8 which appear in this volume on pages 83, 84, and 85, respectively. The figures with the captions correctly placed are shown below.

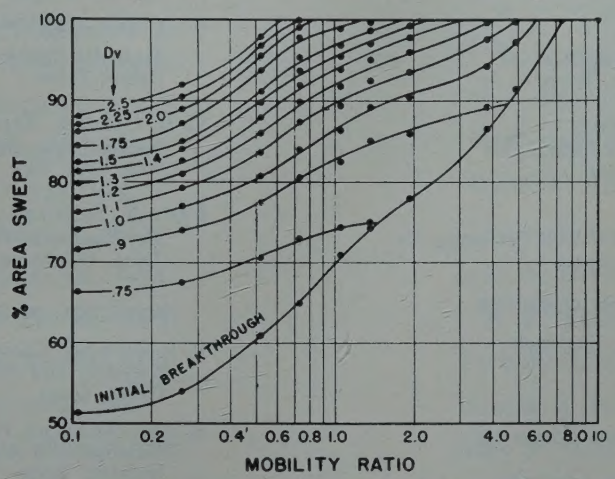

FIG. 4 — EFFECT OF MOBILITY RATIO ON THE DISPLACEABLE VOLUMES INJECTED FOR THE FIVE SPOT PATTERN.

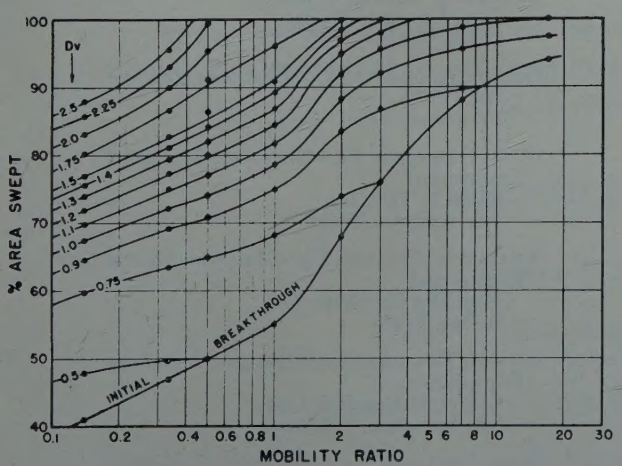

FIG. 6 — EFFECT OF MOBILITY RATIO ON THE DISPLACEABLE VOLUMES INJECTED FOR THE DIRECT LINE DRIVE (SQUARE PATTERN).

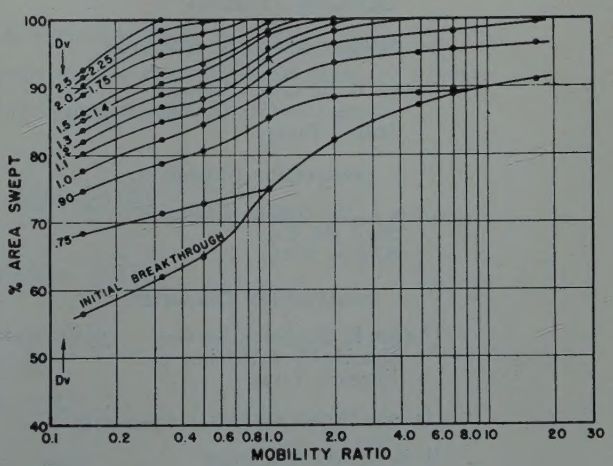

FIG. 8 — EFFECT OF MOBILITY RATIO ON THE DISPLACEMENT VOLUMES INJECTED FOR THE STAGGERED LINE DRIVE.

PETROLEUM BRANCH OFFICERS AND COMMITTEE CHAIRMEN

For the Year Ending February, 1955

CHAIRMAN

JOHN R. McMILLAN
Monterey Oil Co.
Los Angeles, California

VICE-CHAIRMEN

D. W. AKINS
Ohio Oil Co.
Shreveport, Louisiana

THOMAS C. FRICK
The Atlantic Refining Co.
Dallas, Texas

EXECUTIVE COMMITTEE

D. W. AKINS

JOHN R. McMILLAN

THOMAS C. FRICK

BURTON ATKINSON
Pishny & Atkinson
Fort Worth, Texas

THOMAS A. ATKINSON
Douglas Oil Co.
Los Angeles, California

ROLAND GOULDY
Consulting Engineer
Wichita Falls, Texas

CLAUDE R. HOCOTT
Humble Oil & Refining Co.
Houston, Texas

W. D. OWSLEY
Halliburton Oil Well Cementing Co.
Duncan, Oklahoma

E. N. VAN DUZEE
Shell Oil Co.
New Orleans, Lousiana

G. L. YATES
Amstutz and Yates
Wichita, Kansas

T. A. POLLARD, *Treasurer*
Magnolia Petroleum Co.
Dallas, Texas

C. R. DODSON, *Representing MIED*
National City Bank
New York, New York

PAUL R. SCHULTZ, *Representing MED*
The Blackwell Oil & Gas Co.
Tulsa, Oklahoma

ADMISSIONS COMMITTEE

F. G. PRUTZMAN, *Chairman*
Sun Oil Co.
Dallas, Texas

ADVERTISING COMMITTEE

THOMAS C. FRICK, *Chairman*
The Atlantic Refining Co.
Dallas, Texas

EDUCATION COMMITTEE

JACK TARNER, *Chairman*
Phillips Petroleum Co.
Bartlesville, Oklahoma

GENERAL EDITORIAL COMMITTEE

GLENN M. STEARNS, *Chairman*
British-American Oil Producing Co.
Dallas, Texas

MEMBERSHIP COMMITTEE

GENE L. SCHEIRMAN, *Chairman*
Shell Oil Co.
Kilgore, Texas

NOMINATING COMMITTEE

CLAUDE R. HOCOTT, *Chairman*
Humble Oil & Refining Co.
Houston, Texas

TRANSACTIONS EDITORIAL COMMITTEE

H. B. RENFRO, *Chairman*
Petroleum Consultant
Dallas, Texas

STUDENT ACTIVITIES COMMITTEE

PAUL ANDREWS, *Chairman*
Signal Oil & Gas Co.
Los Angeles, California

PRODUCTION REVIEW COMMITTEE

R. B. GILMORE, *Chairman*
DeGolyer and MacNaughton
Dallas, Texas

MILTON WILLIAMS, *Vice-Chairman, Domestic*
Humble Oil & Refining Co.
Houston, Texas

A. H. CHAPMAN, *Vice-Chairman, Foreign*
Arabian-American Oil Co.
Washington, D. C.

TECHNOLOGY COMMITTEE

WILLIAM L. HORNER, *Chairman*
Core Laboratories, Inc.
Dallas, Texas

PRESTON E. CHANEY, *Vice-Chairman, Drilling*
Sun Oil Co.
Beaumont, Texas

W. W. HAMMOND, *Vice-Chairman, Geological Engineering*
Ralph E. Fair, Inc.
San Antonio, Texas

WILLIAM H. SPEAKER, *Vice-Chairman, Natural Gas Engineering*
Magnolia Petroleum Co.
Dallas, Texas

JOHN H. THACHER, *Vice-Chairman, Petroleum Economics*
California Research Corp.
San Francisco, California

LEWIS FINCH, JR., *Vice-Chairman, Production Engineering*
Stanolind Oil & Gas Co.
Tulsa, Oklahoma

L. P. WHORTON, *Vice-Chairman, Reservoir Engineering*
The Atlantic Refining Co.
Dallas, Texas

PETROLEUM BRANCH, AIME

Established as a Division March 24, 1922
Established as a Branch in 1948

PAST CHAIRMEN

Ralph Arnold, 1922
E. DeGolyer, 1923, 1924
F. Julius Fohs, 1925, 1926
John M. Lovejoy, 1927
A. W. Ambrose, 1928
Joseph B. Umpleby, 1929
C. V. Millikan, 1930
C. E. Beecher, 1931
Earl Oliver, 1932
W. E. Wrather, 1933
H. D. Wilde, Jr., 1934
Harry H. Power, 1935
Hallan N. Marsh, 1936
M. Albertson, 1937
George B. Corless, 1938
W. H. Geis, 1939
T. V. Moore, 1940
Eugene A. Stephenson, 1941
Harry P. Stoltz, 1942
C. A. Warner, 1943
W. S. Morris, 1944
M. L. Haider, 1945
H. F. Beardmore, 1946
Howard C. Pyle, 1947
Irwin W. Alcorn, 1948
Lloyd E. Elkins, 1949
John E. Sherborne, 1950
R. W. French, 1951
Paul R. Turnbull, 1952
Claude R. Hocott, 1953
John R. McMillan, 1954

PETROLEUM BRANCH CERTIFICATE OF SERVICE

Established in 1948, the Petroleum Branch Certificate of Service is awarded to recognize and show appreciation for exceptional services of Members of the Branch.

CERTIFICATES AWARDED

Eugene A. Stephenson, 1948

Fred B. Plummer, 1948
(posthumously)

Earl Oliver, 1948

F. Julius Fohs, 1949

Joseph B. Umpleby, 1949

Stuart E. Buckley, 1952

MORRIS MUSKAT
Lucas Medalist, 1953

"For his distinguished achievements in the application of mathematical concepts to the science of petroleum engineering, for his contributions to the knowledge of flow of oil and gas in sands and to the producing patterns of well groupings, and for his efforts in advancing the science of geophysics."

The Anthony F. Lucas Fund and Medal

In 1936 the Institute established the Anthony F. Lucas Gold Medal, to be awarded from time to time "for distinguished achievement in improving the technique and practice of finding and producing petroleum." These awards are sponsored by the Petroleum Branch.

Captain Lucas was a pioneer in the oil industry, one of the early wildcatters, and a leading mining and petroleum engineer. He was famous as the discoverer of Spindletop. He became a member of the Institute in 1895 and in 1913 was the first chairman of the Petroleum and Gas Committee of the Institute, the forerunner of the present Petroleum Branch. He also headed the Committee in 1914, 1917, and 1918.

MEDALS AWARDED

J. Edgar Pew, 1937

Henry L. Doherty, 1938

E. DeGolyer, 1940

Conrad (posthumously) and Marcel Schlumberger, 1941

John Robert Suman, 1943

Charles Van Ormer Millikan, 1944

James Ogier Lewis, 1946

William Noble Lacey, 1947

Wallace Everette Pratt, 1948

William Embry Wrather, 1950

Morris Muskat, 1953

Bruce H. Sage, 1954

BRUCE H. SAGE

Lucas Medalist, 1954

"For his distinguished achievements in research on the phase behavior and thermodynamics of petroleum hydrocarbons; for the development of ingenious techniques and equipment; for the study of these materials under petroleum reservoir conditions; for the resourceful application of mathematics in extending the range of prediction of the behavior of hydrocarbons over a wide range of pressure and temperature; and for his marked contribution to the present-day concepts of good petroleum engineering practice."

COMMITTEE ON AWARD OF LUCAS MEDAL

J. E. Sherborne, *Chairman*

Until Feb. 1955	*Until Feb. 1956*	*Until Feb. 1957*	*Until Feb. 1958*
R. F. Baker	I. W. Alcorn	Paul Andrews	J. N. McGirl
M. L. Haider	E. G. Gaylord	D. V. Carter	W. S. Morris
	W. E. Wrather	R. W. French	Paul R. Turnbull

MEMBERS EX OFFICIIS

John J. Forbes	Frank M. Porter	Morgan J. Davis	Leo F. Reinartz
Director, USBM	President, API	President, AAPG	President, AIME

LOCAL SECTION CHAIRMEN FOR 1954

BILLINGS PETROLEUM SECTION — Howard R. Lowe, *Lowe & Heath, Petroleum Associates*, Billings, Mont.

DALLAS LOCAL SECTION — Guy R. Brainard, Jr., *Lucerne Corp.*, Dallas.

DELTA LOCAL SECTION — A. L. Vitter, Jr., *The California Co.*, New Orleans.

DENVER PETROLEUM SECTION — T. O. H. Mattson, *The Texas Co.*, Denver.

EAST TEXAS LOCAL SECTION — Gene L. Scheirman, *Shell Oil Co.*, Kilgore, Tex.

FORT WORTH LOCAL SECTION — Madison I. Taylor, *Gulf Oil Corp.*, Fort Worth.

GULF COAST LOCAL SECTION — W. B. Hopkins, *Gulf Oil Corp.*, Houston.

HOBBS PETROLEUM SECTION — W. G. Abbott, *Amerada Petroleum Corp.*, Monument, N. Mex.

HUGOTON LOCAL SECTION — Jack Phillippe, *Panhandle Eastern Pipe Line Co.*, Liberal, Kan.

ILLINOIS BASIN PETROLEUM SECTION — Daniel M. Moon, *Schlumberger Well Surveying Corp.*, Mt. Vernon, Ill.

KANSAS LOCAL SECTION — John T. Gary, *Continental Oil Co.*, Wichita, Kan.

LOU-ARK LOCAL SECTION — C. R. Olson, *Ohio Oil Co.*, Shreveport, La.

MID-CONTINENT LOCAL SECTION — M. B. Penn, *Mid-Continent Petroleum Corp.*, Tulsa.

MISSISSIPPI LOCAL SECTION — W. I. Sanderson, *Halliburton Oil Well Cementing Co.*, Natchez, Miss.

NEW YORK PETROLEUM SECTION —H. E. McAuliffe, Jr., *Socony-Vacuum Oil Co.*, New York.

NORTH TEXAS LOCAL SECTION — D. B. Meisenheimer, *The Texas Co.*, Wichita Falls, Tex.

OKLAHOMA CITY SECTION — R. K. MacIvor, *MacIvor Engineering Co.*, Oklahoma City.

PANHANDLE LOCAL SECTION — Donald E. Radtke, *Magnolia Petroleum Co.*, Pampa, Tex.

PERMIAN BASIN SECTION — John R. Brack, *Forest Oil Corp.*, Midland, Tex.

SAN JOAQUIN VALLEY SECTION — H. D. Campbell, *Franco Western Oil Co.*, Bakersfield, Calif.

SOUTH PLAINS LOCAL SECTION — M. C. Gulledge, *Magnolia Petroleum Co.*, Brownfield, Tex.

SOUTHWEST TEXAS LOCAL SECTION — Chester L. Wheless, *La Gloria Oil and Gas Co.*, Corpus Christi, Tex.

VENEZUELA LOCAL SECTION — Section established on Dec. 15, 1954; chairman not elected.

WEST CENTRAL TEXAS SECTION — Dalton Moore, Jr., *Wimberley Field Unit*, Abilene, Tex.

WYOMING LOCAL SECTION — M. O. Hegglund, *Stanolind Oil and Gas Co.*, Casper, Wyo.

PACIFIC PETROLEUM CHAPTER — M. E. Loy, *Schlumberger Well Surveying Corp.*, Los Angeles.

A SIMPLIFIED CEMENTING TECHNIQUE for RECOMPLETION OPERATIONS

T. A. HUBER
G. H. TAUSCH
J. R. DUBLIN III
MEMBERS AIME

HUMBLE OIL & REFINING CO.
HOUSTON, TEXAS

T. P. 3739

ABSTRACT

Simplified equipment and techniques have been developed to permit cementing a completion interval in a well and recompleting higher, lower, or at the same depth in such a manner as to:

1 Eliminate the need for a conventional drilling or workover rig.
2. Eliminate mud and other cement contaminants which have long interferred with ideal cementing.
3. Eliminate need for drilling out cement.
4. Provide a more satisfactory recompletion.
5. Provide a more economical recompletion.

This technique involves the use of a small-diameter, lightweight, tubing extension which is run on a wireline and set in a landing nipple previously installed in the tubing string. Low squeeze pressure and small cement volumes, with their attendant cost reduction, are successfully used when wells are completed and reworked with salt water or other penetrating fluids.

Relatively low-water-loss cement is an integral component of the technique which provides that excess cement be reverse-circulated from the well to leave the casing void of cement when recompleting lower or in the same interval. Substantial cost reductions are realized by using the simplified or low-pressure cementing technique, and the ratio of successful squeeze-cement operations has been increased.

INTRODUCTION

Squeeze-cementing or recementing is the act of filling a channel behind casing or filling holes purposely placed in the casing. To obtain a satisfactory squeeze-cement job, it is necessary only to fill the channel or the perforation holes with a cement filter cake and to allow it to harden in that position. In the past, the presence of mud in a well has been considered the chief deterrent to obtaining a good cement bond and satisfactory cement job; however, late developments in squeeze-cementing have made it possible to eliminate cement contamination or interference. Since it is possible to form a cement filter cake with a small pressure differential, squeeze-cementing with high pressures may not be necessary in most cases.

The amount of cement needed to fill the annulus about the casing and even to fill part of the casing, if necessary, is generally small in quantity. Use of low squeeze-cementing pressures and small quantities of cement provides the following advantages:

1. Longer effective life of well tubing, casing, and other equipment; and less chance of costly equipment failure due to excessive pressure.
2. Monetary savings effected by elimination of retainers and specal squeeze-cementing tools.
3. Monetary savings effected by use of small quantities of cement and fewer squeeze-cementing operations.
4. Future surface squeeze-cementing equipment may be smaller and more economical to operate and maintain.

[1]References given at end of paper.
Manuscript received in the Petroleum Branch office August 3, 1953. Paper presented at the Petroleum Branch Fall Meeting in Dallas, Texas, Oct. 18-21, 1953.

To deposit cement about the casing while squeeze-cementing with low pressure, it is imperative that no mud filter cake be present in the cavities or channels to be filled with cement. To accomplish this, the well must be perforated with clean fluid in the casing and must be killed or reworked with a penetrating fluid, or fluid not depositing a filter cake.

When salt water or other clean fluid is used as a workover fluid, it is often dangerous to pull tubing from a well; therefore, a technique has been developed which does not require removal of the tubing. Tubing is originally set above the anticipated producing intervals, with a landing nipple near its lower extremity. A tubing extension of one-inch aluminum pipe is used to extend the effective length of the tubing for the purpose of conducting cement slurry to the proper location while squeeze-cementing. This extension is suspended from a wireline mandrel which is lowered into or retrieved from the landing nipple with a small steel wireline.

This new technique of squeeze-cementing by using the retrievable tubing extension precludes the use of a bit to remove set or hardened cement. It is often necessary to use a special cement which will form a filter cake of dehydrated cement between casing and formation face and will still remain sufficiently fluid within the casing to be reverse-circulated from the well.

THEORY

The conventional method of perforating with drilling mud in the casing, and of unavoidably having mud ahead of cement when squeezing cement into perforations, necessitates the use of high squeeze pressures to force mud or mud filter cake into the formation or formation fractures so that the cement slurry may enter the perforations. It has never been shown that this action of squeezing large quantities of drilling mud and cement into the formation has enhanced the producing characteristics of an oil or gas well. However, it has definitely been demonstrated that cement does not adhere tightly to a formation which has previously been flushed with drilling mud.[1]

Fig. 1 illustrates the possible condition existing when a well perforated in an oil-producing sand produces water from a lower sand through a channel behind the casing. If conventional techniques were used to cement such a channel, water in the channel would be replaced with mud before cementing or during the act of cementing. This mud in the channel could be replaced by cement only by rupturing the formation below the upper oil sand and forcing mud into the resulting fracture. Were the upper oil-producing sand to rupture and allow cement to enter, the channel would be by-passed and not repaired. If this second operation took place, the well might again produce water when reperforated in the oil sand. Water production would be temporarily halted, however, if a small cement cap entered the channel.

If the new technique of low-pressure squeeze-cementing were used, salt water would be used as a recompletion fluid and water in the channel would be replaced with cement. Only pressure sufficient to force water into the water sand need be applied while cementing. The water or oil sand need never be ruptured. Cement is given every chance to bond with the formation and casing and dehydrate in a channel cleaned by water production. The technique of low-pressure squeeze-

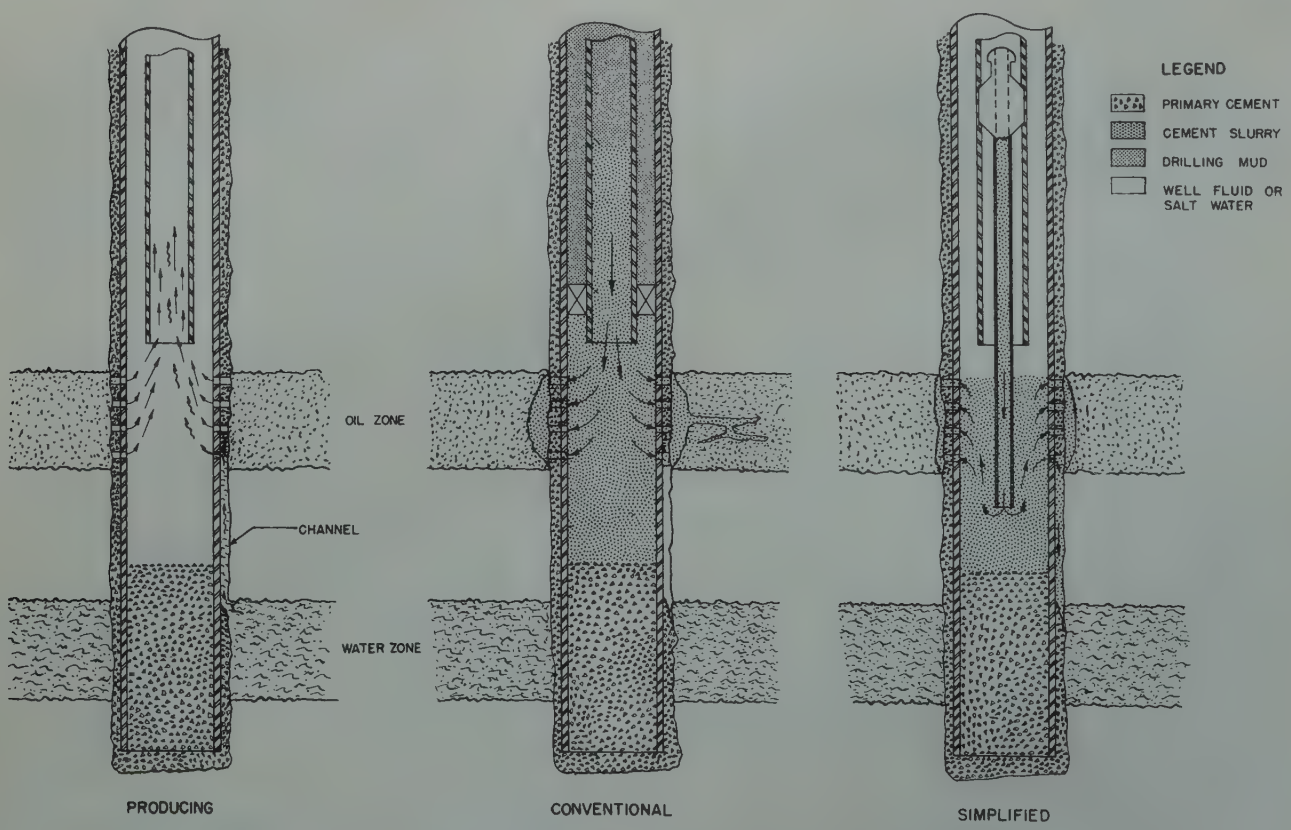

FIG. 1 — FILLING A CHANNEL BEHIND PRODUCTION CASING WITH CEMENT BY USING CONVENTIONAL AND LOW-PRESSURE SQUEEZE TECHNIQUE.

cementing without the use of mud will repair a channel in communication with the perforated interval when the channel is above or below the productive oil zone.

Squeeze-cementing is also often the means of controlling excessive gas and salt water production from an oil-producing zone. The low-pressure technique of squeeze-cementing entails the deposition of cement filter cake in each perforation hole. The conventional squeeze-cementing technique requires that the formation be ruptured or that a high pressure be applied so that the drilling mud in each perforation hole may be replaced with cement.

The fact that it is extremely difficult to create an individual fracture through each perforation hole, or to replace the drilling mud in each perforation hole with cement, explains the poor success ratio when drill-stem testing conventional squeeze-cementing jobs. Once the perforation holes have been sealed and the producing interval has been reperforated higher or lower, exclusion of gas or salt water is actually dependent on low vertical permeability within the formation due to shale, bentonite, or other barriers.

The formation of an effective impermeable layer of cement within the producing sand, which prevents the vertical migration of gas or salt water, is probably very rare. In considering the formation of an effective horizontal or bedding plane cement pancake, the following points are of interest:

1. Laboratory and field proof that numerous formation fractures occur at a high angle.[2]
2. Arc of cement pancake from perforation hole generally 140° to 270°, thereby reducing chance of obtaining 360° pancake.[1]
3. Ability to obtain fracture in desired location between gas or water and oil extremely limited.[3]

In those reservoirs where good vertical permeability is present and producing rates control gas- and water-oil ratios, conventional squeeze-cementing techniques have generally been unsuccessful. The new low-pressure squeeze-cementing technique would likewise be ineffective; however, it should be possible to restore production after each squeeze job, which is sometimes impossible after numerous conventional cement jobs.

To squeeze-cement a producing zone and reperforate a portion of this same zone by the conventional techniques, it is necessary to drill hard cement out of the casing. There is a growing feeling that the action of a drill bit may be detrimental to an otherwise successful cement job. The pounding of the bit against the casing while drilling out excess cement may fracture the small pieces of set cement in the perforation holes and in the channels, particularly if such cement is backed up with a cake of mud.

In the simplified technique, the tubing is left in place and excess cement is reverse-circulated from the casing to a point below the perforations, thus eliminating the drilling out of excess cement. This may be an added reason for a successful squeeze-cement job with this technique.

SURFACE EXPERIMENTS

It was considered that a relatively low-water-loss cement of retarded set time would be necessary if excess cement were to be reverse-circulated from the casing to a point below the perforations. A series of surface tests was initiated to determine if these predictions were correct and to determine which cements would be suitable. Test chambers were designed to simulate actual well conditions as closely as possible.

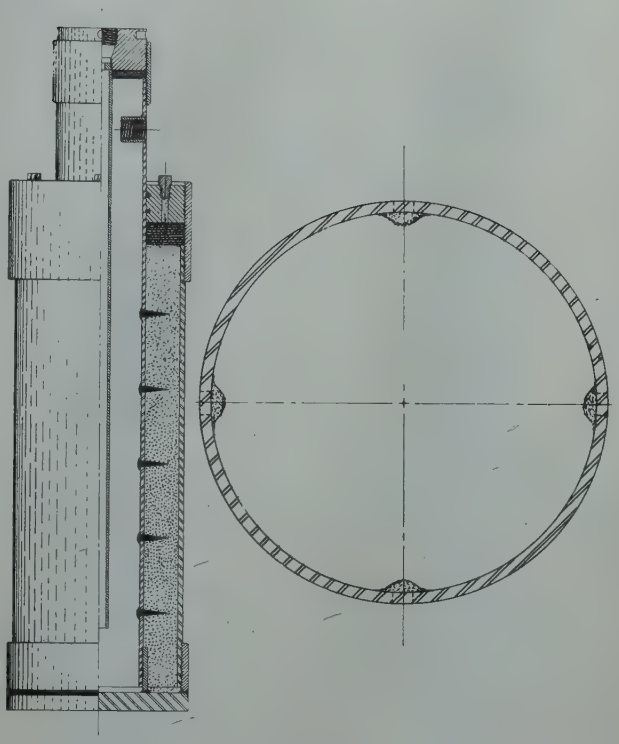

FIG. 2 — (left) SQUEEZE-CEMENTING TEST CHAMBER.

FIG. 3 — (right) CROSS SECTION OF CASING SHOWING CEMENT FILTER CAKES OVER EACH PERFORATION HOLE.

Each chamber shown in Fig. 2 consisted of a 7-in. OD casing nipple set concentrically inside a shorter 13⅜-in. OD casing nipple. Both ends of the larger nipple were sealed against the inner nipple by means of a sealed upper cap and a lower plate. The lower 1 ft of 7-in. OD nipple was blank and the next 2 ft were perforated with six ½-in. holes per ft. Above the sealing cap, a 2-in. regular side outlet was provided to allow attaching of a reversing line during cementing operations. A steel 7-in. OD cap was tapped to receive a regular cementing connection on the upper side and 1¼-in. wash pipe on the lower side. The 1¼-in. pipe extended below the perforation holes to simulate a small tubing extension. Small screen cones, 2½ in. long with a ½-in. diameter, were made of 30-mesh bronze screen wire to approximate the size and shape of jet perforation holes. The annular space between the 7-in. OD and 13⅜-in. OD nipples was filled with fine sand for each test.

The first test was performed with a conventional neat cement slurry having a water loss of about 650 cc per 30 minutes when taken against a sand bed in an API mud filter press. A maximum squeeze pressure of 1,000 psi was maintained for 30 minutes. At the end of this time, cement could not be reverse-circulated from the test chamber and was found to be in a tightly compacted state. Dehydration of all cement in the chamber was evident. As a result of this test, conventional neat cement slurry was considered unsatisfactory for this use, since it would not retain sufficient fluidity within the casing after squeeze-cementing.

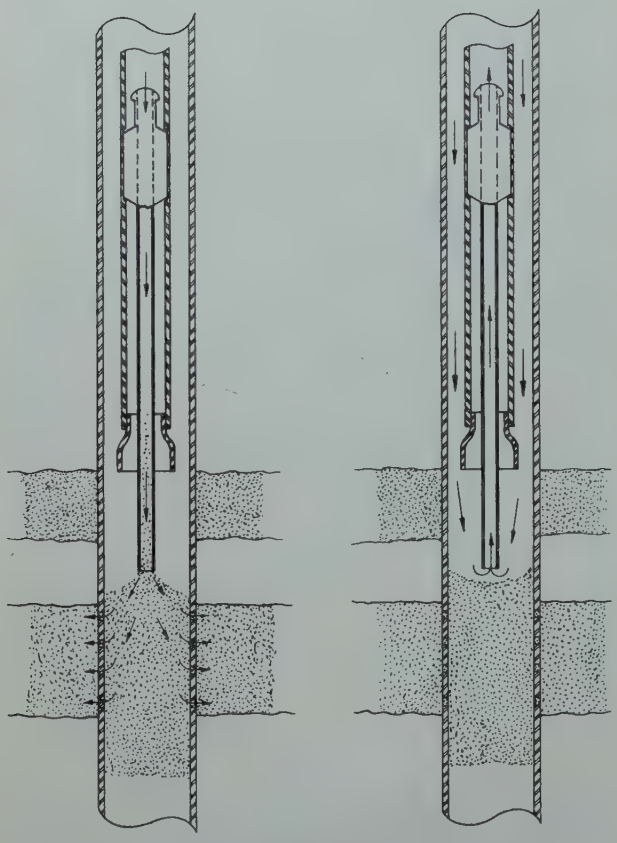

FIG. 4 — BASIC PROCEDURE FOR PLUGGING A NONCOMMERCIAL ZONE.

The remaining tests were performed with three cement slurries having a relatively low water loss. The water loss of the three cements, when taken against a sand bed in an API mud filter press, varied between 65 and 120 cc per 30 minutes. The slurry weights varied from 12 to 14.1 lbs per gal. Each cement was used in the test chamber with a squeeze pressure of 1,000 psi to 1,200 psi and was easily reverse-circulated from the chamber after pressure was maintained from 15 to 55 minutes.

Visual inspection of the test chamber showed cement filter cake formed in each perforation hole and extended into the 7-in. casing in shapes resembling rivet heads, as shown in Fig. 3. The cement filter cake protruding into the casing had been formed within a 15-minute interval while maintaining maximum squeeze pressure. The increase in size of the filter cake was extremely small when the time for maintaining this pressure was extended to 55 minutes. The amount of water used to reverse-circulate cement from the chamber was varied from 3 bbls to 60 bbls to determine if this cement filter cake could be eroded from inside the casing by the reversing fluid. The reversing rate was also varied, with no visible sign of filter cake erosion.

Each of the three cements was allowed to set in the test chamber after squeeze-cementing operations, and a pressure of 1,000 psi was applied into the annulus containing fine sand. Although thread leaks in the lower end of the chamber indicated pressure continuity through the annulus, each cemented hole maintained a satisfactory seal. The nodes of cement filter cake were mechanically removed from inside the 7-in. nipple prior to one pressure test to determine if these nodes were essential. The cemented perforations again held satisfactorily.

Since cement filter cake is permeable and in actual well operations a differential into the formation would exist because of the hydrostatic head of salt water above the perforations, it was necessary that a test be run to determine if the cement filter cake would remain permeable after setting. An API mud filter press was filled with cement and a cement filter cake formed. A water hose was then connected to the top of the press and water allowed to run through the cement filter cake. After the cement filter cake had set, generally from six to eight hours, the flow of water through the cake stopped and the cement, for all practical purposes, appeared to be impermeable.

Although the three cements with a relatively low water loss appeared to be satisfactory for this type of squeeze-cementing, it was decided to use only one of these cements for field work. Modified cement (normal Portland cement containing calcium lignosulfonate and bentonite) was selected because of its economy, availability, and the field personnel's greater familiarity with this cementing composition.[3]

SUBSURFACE EQUIPMENT FOR SIMPLIFIED SQUEEZE-CEMENTING

It was possible to reduce the cost of squeeze-cement-

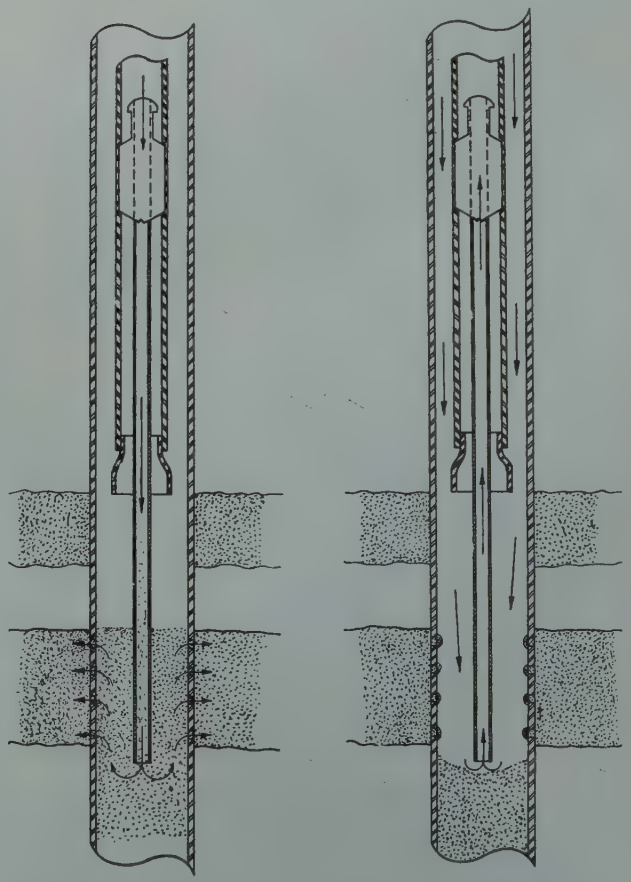

FIG. 5 — BASIC PROCEDURE FOR SQUEEZING OFF EXCESSIVE GAS OR WATER.

ing by increasing the success ratio, eliminating special squeeze tools, and decreasing the amount of cement used. Recompletion costs could be further reduced by eliminating the rig entirely or by reducing the setting time and "waiting-on-cement" time, as well as trip time necessary to use cement retainers and drill bits. Use of a cement with low water loss and added retarding agents which keep this cement fluid during the squeezing operations precludes a reduction of rig time during cement setting time and "waiting-on-cement" time, and emphasizes the need to eliminate the rig entirely.

It is possible to eliminate a rig while squeeze-cementing by completing a well with the proper tubing setting and by using a retrievable tubing extension. This tubing extension, made of 1-in. aluminum pipe, is suspended from a landing nipple near the lower extremity of the tubing during squeeze-cementing operations. The extension is lowered into place and retrieved with an 0.082-in. wireline; however, the wireline is not attached to the extension during cementing operations. The longest extension used to date is 1,000 ft; circulating pressures may become excessive if considerably longer extensions are used. Reverse-circulation with salt water, using the cementing pump, aids in running and retrieving long extensions without exceeding the strength of the small steel wireline.

All cementing with this new simplified method is accomplished by applying Bradenhead squeeze pressures. The basic procedures used in plugging a non-commercial zone or squeezing off excessive gas or water to allow reperforating lower or in the same interval are shown in Figs. 4 and 5. Cement is found approximately 1 ft below the bottom of the tubing extension setting after squeeze-cementing by either of the above procedures. Since squeezing pressures, cement volumes, and tubing settings are not varied for either technique, selection of the length of the tubing extension controls the top of the cement left in the casing and accordingly the amount of cased hole left vacant for reperforating.

By either technique, cement is displaced down the tubing and the well casing valve is closed prior to emergence of cement from the lower end of the tubing. This makes it necessary to force several barrels of salt water into the formation ahead of the cement. Should the permeability of the formation restrict this salt water displacement to a slow rate at the low pressures used, cement may be displaced around the tubing extension prior to squeezing, thus reducing the quantity of water to be displaced.

If a gas-lift well is completed in a manner to allow this method of cementing or if a well is set up in preparation for future gas lift as well as the simplified method of cementing, the landing nipple for the tubing extension is located above the lower retrievable gas-lift valve mandrel. This lower mandrel is generally one tubing joint above the production packer. The upper retrievable valve mandrels are located at the customary positions in the tubing to allow efficient gas-lifting, and contain dummy valves during cementing operations. The lower mandrel is left open to permit communication between tubing and casing and to by-pass the packer while squeezing. The tubing setup and direction of flow while cementing are shown in Fig. 6.

In gas wells, a production packer is used to keep excessive pressure off the casing while producing. A special circulating port is located between the landing nipple and the packer. The circulating port may be opened or closed with a wireline to permit communication between casing and tubing.

Wells may also be set up with a landing nipple which seats the tubing extension as well as a rod pump. A small pulling unit is used to remove and replace the pump and rods during remedial operations.

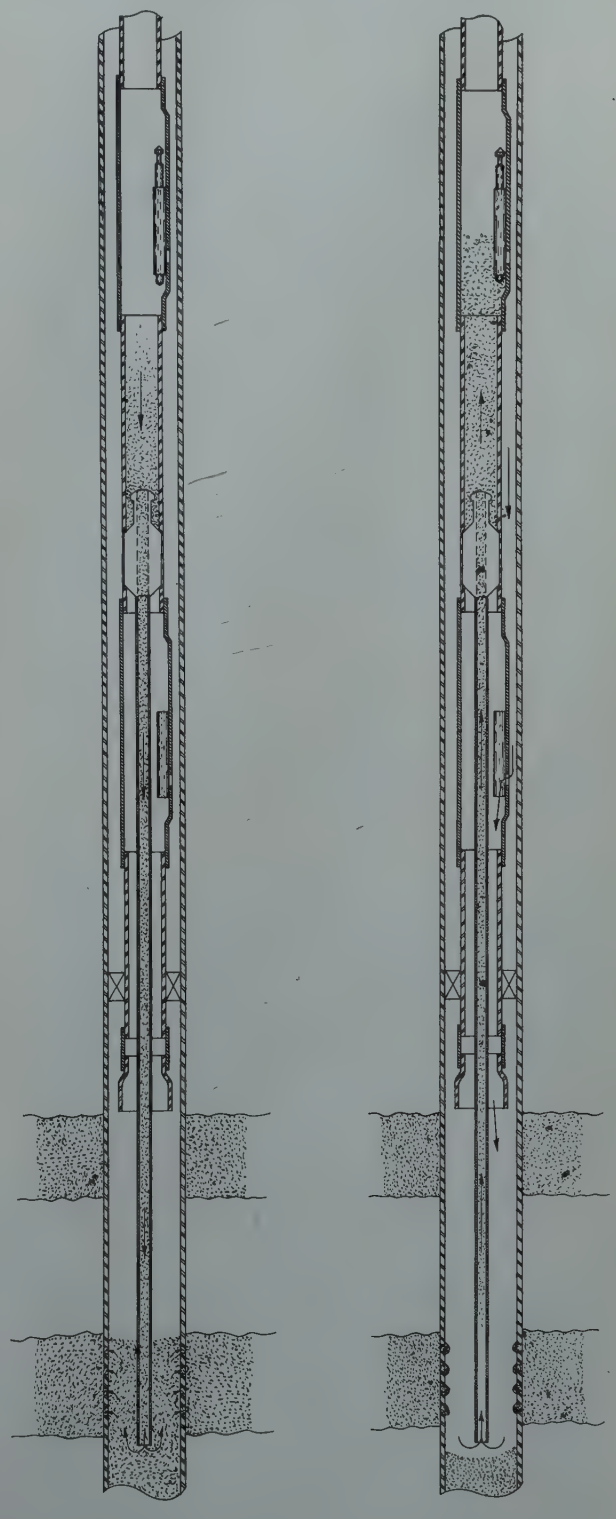

FIG. 6 — TUBING SETTING SHOWING GAS-LIFT EQUIPMENT, PRODUCTION PACKER, AND DIRECTION OF FLOW DURING SQUEEZING AND REVERSING.

To complete a well in preparation for the simplified method of cementing, the following conditions must be satisfied:

1. Tubing must be approximately full-opening to permit use of the tubing extension and tubing-type perforator.
2. Tubing mut be pressure-tight above landing nipple. Communication between tubing and casing must be provided below landing nipple.

FIELD RESULTS

The simplified method of squeeze-cementing without a rig, using low squeeze pressures and small volumes of modified cement, has been used in field work to seal off noncommercial intervals, allowing wells to be reperforated in the same, higher, or lower intervals. Surface squeeze pressures have varied between 1,200 and 2,500 psi, while the amount of cement left in place after cementing has varied between two and 15 sacks. The amount of slurry currently being mixed for each job ranges from 10 to 15 bbls. The magnitude of squeeze pressure has shown no effect upon the success of the cementing operations. As a test of a successful squeeze-cement job, wells have been gas-lifted, pumped, or swabbed dry after cementing, to place the full formation pressure against the cemented perforations.

One 3,700-ft well in East Texas was cemented with modified cement by using a surface squeeze pressure of 600 psi. The well had been completed with salt water and salt water was used as a workover fluid. A small pulling unit was used during this operation, since salt water could be used safely and since the cost was small. After squeezing, cement was reverse-circulated from the liner to a point 60 ft below the perforations. The workover fluid was swabbed from the well and no fluid was recovered from the cemented perforations. The well was then reperforated lower.

A 9,300-ft well in the Texas Gulf Coast was plugged with nine sacks of modified cement using the tubing extension. A maximum squeeze pressure of 1,700 psi was used. Upon perforating higher in the same sand, the well produced 25 per cent salt water. The success of the plugback job was questioned, and this well was squeezed in the conventional manner with a maximum and final pressure of 4,700 psi using 60 sacks of slow-set cement. Upon reperforating in the same zone, the well again produced salt water, proving the low-pressure squeeze technique to be as effective as the conventional technique. Later recompletion in a higher interval of the same sand eliminated water production.

Perforations in a 5,000-ft gas well in the Texas Gulf Coast were squeezed by this new technique, the cement job was tested, and the well was reperforated in a sand underlying the former producing interval. The well flowed with a 3,500-cu ft/bbl gas-oil ratio, causing doubt as to the effectiveness of the previous squeeze job. Perforations were squeezed in the conventional manner and the interval was reperforated. The well flowed with a high gas-oil ratio, again proving the simplified method of cementing to be as effective as the conventional method. Later reservoir analysis proved this high-ratio zone was not in communication with the upper gas zone.

The present trend toward small cement slurry volumes of about 10 bbls will allow lower squeeze pressures in the range of 1,000 to 1,200 psi. This lower squeeze pressure should extend the effective life of casing, while the Bradenhead squeeze technique exposes the tubing to a low pressure differential and allows a correspondingly longer useful life.

The elimination of a rig while cementing and performing other operations has brought about a substantial reduction in workover costs. A wireline workover involving squeeze-cementing and reperforating generally costs $1,200 to $2,000, depending on well conditions. However, the cost of this method is almost independent of depth, which is not true of conventional workovers. Use of the tubing extension and tubing-type perforator has reduced the cost of workovers performed with these tools by 40 to 60 per cent. Costs may also be reduced when rigs are used in reworking wells with salt water by using the low-pressure, low-volume method of cementing, since squeeze tools and rig time consumed while drilling cement are eliminated.

FRACTURED FORMATIONS

In the process of squeeze-cementing by the simplified method, the formation was accidentally fractured or opened in four wells, although low squeeze pressures were used. A dry test could not be obtained in one of these wells. This well had been squeezed with 1,800 psi maximum surface pressure, and excess cement was reverse-circulated from the well to a point below the perforations. Several cubic feet of cement fill-up was discovered in the casing below the perforations after the cement had set, indicating a cement flowback. This well was successfully repaired by a second squeeze job, using the simplified method, without rupturing the formation. One other well also exhibited a cement flowback.

When complete dehydration of the cement slurry is not obtained within a fracture, the fluid cement slurry tends to re-enter the well bore as the fracture closes after the squeeze pressure is released. Because of the low filtration rate of modified cement, the deposition of cement particles upon the face of the formation fracture is slower when this type cement slurry is used. It is necessary, therefore, to use a "hesitation" or stage squeeze to obtain a final squeeze pressure greater than the "breakdown" pressure without extending the fracture. The maximum squeeze pressure must be maintained for a longer period of time when a formation has been fractured to permit complete dehydration of cement within the fracture.

Two of the wells in which the formation was fractured did not exhibit a cement flowback. In both cases the maximum squeeze pressure was maintained for a longer period of time, and 1,000 psi pressure was placed on the well after cementing operations were complete. This action evidently maintained the cement in position until it was dehydrated or until its viscosity was too high to allow movement.

Formations with Low Permeability

The second and only other cementing failure occurred in a well which had been squeezed to a maximum pressure of 2,500 psi. This maximum pressure had been maintained for 10 minutes and cement was reverse-circulated from the casing to a point below the perforations. When this cement job did not stand up to a dry test, the well was again squeezed to 2,500 psi and the pressure was maintained for 20 minutes before reverse-circulating excess cement. After the second

squeeze-cement job, a dry test was obtained.

Examination of the electric log displayed a formation tight streak through the perforated interval. It was decided that insufficient time had been allowed for the deposition of cement filter cake within the perforation holes through the tight zone. High water-injection pressures during the second cement job and the success of this job seem to substantiate this decision.

FUTURE DEVELOPMENT WORK

Although field work to date has been gratifying, some minor problems have arisen as use of the simplified low-pressure squeeze-cementing technique has increased. The following problems are now being investigated, or will be studied in the near future:

1. Length of time squeeze pressure must be maintained to form satisfactory cement filter cake on low-permeability formation.
2. Method of treatment when a formation is unavoidably fractured. It may be necessary to discontinue the pumping of cement immediately. When allowing cement to set, pressure may be placed on the well. A recording gauge will be used to detect the dissipation of this pressure or to denote any buildup of pressure due to thermal expansion of well fluids.
3. Better field cement-mixing techniques with smaller surface cementing equipment.
4. Squeeze-cementing wells that have been completed with mud, have produced large quantities of fluid, and have been circulated and reworked with salt water. It must be determined if mud filter cake contained in the perforation holes after the original completion will be detrimental to a successful squeeze-cement job.
5. Method of reworking wells with a formation pressure gradient greater than 0.5 psi per ft without allowing drilling mud to contact the formation. This may be accomplished by lubricating the tubing extension into the tubing under pressure or by using a destructible plug at the lower end of the tubing as a seal while running the extension. Cement will then be forced into the well under pressure and excess cement will be reverse-circulated from the well with mud. The mud left in the well while cement is setting will be replaced with water prior to reperforating.

SUMMARY

Results obtained from laboratory studies and field use of the simplified cementing technique have led to the following conclusions:

1. Successful squeeze-cement jobs can be performed with low pressures and small volumes of cement if a clean fluid such as salt water is used as a completion and workover fluid. It is not necessary to fracture the formation while squeeze-cementing, nor is the surface squeeze pressure an indication of a successful cement job.
2. Hard or set cement need not be drilled from the casing after a squeeze job. The use of a cement slurry which remains fluid within the casing permits the casing to be cleaned after the squeeze-cement job by circulating all cement from the well to the depth desired. A low-water-loss cement should be used so that the slurry within the casing will remain fluid during squeeze-cementing operations.
3. The simplified low-pressure squeeze-cementing technique may be performed without rigs, special squeeze tools, or large cement pump trucks, thus making possible a large reduction in recompletion costs.
4. Developments in this method are promising and should be continued to provide better cement mixing with smaller equipment, more information concerning squeeze-cementing, and a means for handling wells having abnormal formation pressures.

REFERENCES

1. Howard, George C., and Fast, C. R.: "Squeeze Cementing Operations," *Trans.* AIME., (1950, 189, 53-64.
2. McGuire, William J., Harrison, Eugene, and Kieschnick, W. F., Jr.: "The Mechanics of Fracture Induction and Extension," presented at Petroleum Branch Fall Meeting, Dallas, Texas, October, 1953.
3. Morgan, B. E. and Dumbauld, G. K.: "Recent Developments in the Use of Bentonite in Cements," presented at Spring Meeting of Southwestern District, API, Fort Worth, Texas, March, 1953. ★ ★ ★

EFFECTIVENESS of GUN PERFORATING

T. O. ALLEN
MEMBER AIME
J. H. ATTERBURY, JR.

HUMBLE OIL & REFINING CO.
HOUSTON, TEXAS

T. P. 3740

ABSTRACT

Laboratory and field tests during the past five years indicated considerable variation in the penetrating power of commercially available gun perforators. Many of the guns which achieved inadequate penetration in these tests have since been improved. However, recent productivity tests indicated the possibility of inadequate penetration or, at least, ineffective penetration in some wells.

Laboratory experiments under simulated well conditions have demonstrated considerable plugging of the perforations, apparently as a result of factors associated with the shooting process and/or the drilling mud in the well at the time of perforating. The restrictions to flow per unit of hole depth caused by this plugging appears to be greater for jet perforators than for bullet guns of comparable diameter; however, because of the greater depth of penetration obtained with the jet guns, the total flow rates appear to be approximately equal. Limited testing with an experimental shaped charge suggests that less shot hole restriction and greater flow rates may result from larger-diameter perforations or other factors related to charge design.

INTRODUCTION

Gun perforating has been accepted for a number of years as a routine well completion method which is often preferred since it permits more selective operation of producing zones. Nevertheless, questions have continued to arise as to the effectiveness of the communication paths established between the productive formation and the interior of the casing. The basis for these questions has generally been failure to obtain anticipated fluid production rates through gun perforated completions in specific wells. These low productivities, together with the frequent recovery of bullets from well bores, were considered strong evidence of inadequate penetration.

Laboratory investigations of the penetration performance of many of the bullet guns available as late as 1948 gave support to these indications. Subsequent electrical analog studies[1, 2, 3] indicated that the depth of penetration required to provide productivities equivalent to open hole was beyond the capacity of most bullet perforators evaluated in the early laboratory penetration tests.

These results, together with the advent of the shaped charge in the field of oil well perforating, stimulated the interest of both oil operators and service companies in gun development. Improvements in gun design resulted in jet and bullet guns which appeared to be capable of providing sufficient penetration for most perforating jobs. However, some wells failed to yield satisfactory fluid production even after being perforated with the more powerful guns, again raising the question as to the effectiveness of the perforating operation. This fact, together with preliminary shooting into targets prepared with formation cores, indicated that factors associated with the perforating process and/or the fluids in the well bore at the time of shooting may reduce effective formation penetration and thereby decrease well productivity. These laboratory and field data prompted another phase in the investigation of the effectiveness of gun perforating: a program to determine the extent and seriousness of perforation plugging under simulated well conditions.

[1]References given at end of paper.

Manuscript received in the Petroleum Branch office August 5, 1953. Paper presented at the Petroleum Branch Fall Meeting in Dallas, Texas, Oct. 18-21, 1953.

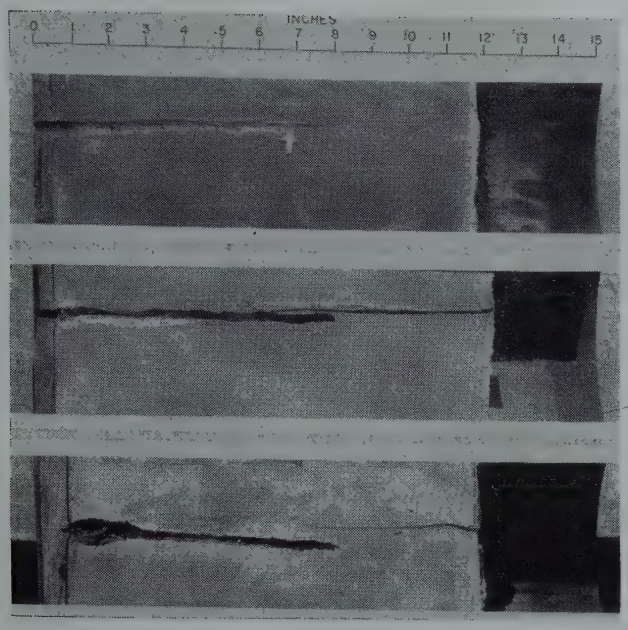

FIG. 1 — EXAMPLES OF JET PERFORATOR PENETRATION (STANDARD JET CHARGE FOR 4-IN. OD GUNS).

The object of this paper is, therefore, twofold: first, to review the analog and laboratory penetration investigations of the effectiveness of gun perforating, and second, to describe in detail the perforation plugging experiments now in progress.

REVIEW OF PREVIOUS INVESTIGATIONS

Penetration tests reported by Oliphant and Farris[4] in 1947 showed that the commercially available bullet perforators tested were capable of penetrating from zero to 2½ in. into the targets used in the experiment. These targets consisted of 5½-in., 17-lb, J-55 casing centrally located in an oil drum and backed up with a thin annular sheath of neat cement supported by either unconsolidated sand or concrete to represent formation.

Independent tests reported by Huber, Allen, and Abendroth[5] in 1950 confirmed these results, and presented additional information on improved bullet guns as well as jet perforators available at that time. These tests were performed in a pressure chamber with both gun and target submerged in cold water under pressures ranging from zero to 4,500 psi. The targets employed consisted of 0.435 in. of flattened N-80 steel casing supported by about 12 in. of neat cement having a tensile strength of 500 psi. A single-shot gun representing a 4-in. OD commercial perforator was fired into an individual target for each test. It may be noted from the results of these tests shown in Fig. 1 and 2 that the total penetrations are of the magnitude of 7½ in. for the shaped charges and 1 to 7 in. for 5 of the 10 bullet guns tested. Since the penetrations achieved by the other five bullet guns were less than 1 in., the results are not shown in the illustration.

Additional tests conducted on the surface with 4-in. OD and larger bullet guns with the same type targets indicated increased penetration with increased gun diameter. These results are illustrated in Fig. 3 for a premium-priced bullet gun. More recent penetration tests with a modified design of one of the bullet guns which achieved less than 1 in. of penetration in earlier tests indicate penetrations of 5⅞ in. for the 4⅛-in. OD gun, and 8 in. for the 5-7/16-in. OD gun.

The relative prductivity of wells with perforated casing has been treated mathematically by Muskat[6] and also through electric analog studies by McDowell and Muskat[1] and by Howard and Watson.[2,3] These data showed that the productivity for perforated casing completions could equal or exceed the productivity of open hole completions under idealized conditions represented in the analog studies. For example, a relative productivity equal to open hole is reached with perforations 6 in. deep in a 6-in. diameter well with a shot density of 5.5 holes per ft. using ½-in. diameter holes, or 6.5 holes per ft. using ¼-in. diameter holes.

Under the analog conditions the well diameter corresponds to the diameter of the hole drilled in the formation and the depth of the shot hole corresponds to the penetration into the formation. When comparing this optimum formation penetration of 6 in., or a total penetration of 7 to 8 in., including the casing and cement sheath, with the laboratory penetrations of zero to 2½ in. and zero to 7 in. reported above, it is obvious that most of the 4-in. and smaller bullet guns available as late as 1948 were incapable of the

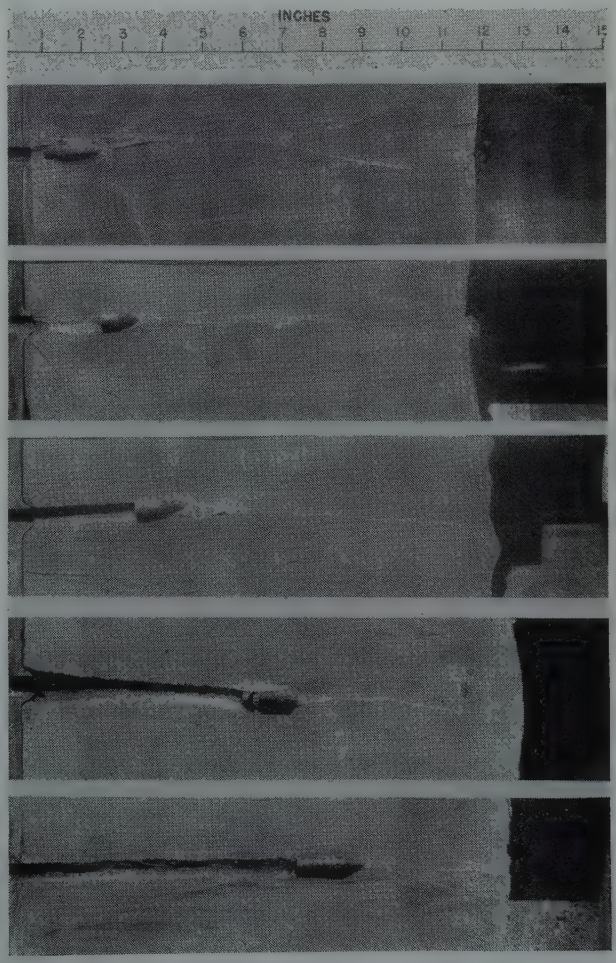

FIG. 2 — EXAMPLES OF PENETRATION FOR 4-IN. OD BULLET PERFORATORS.

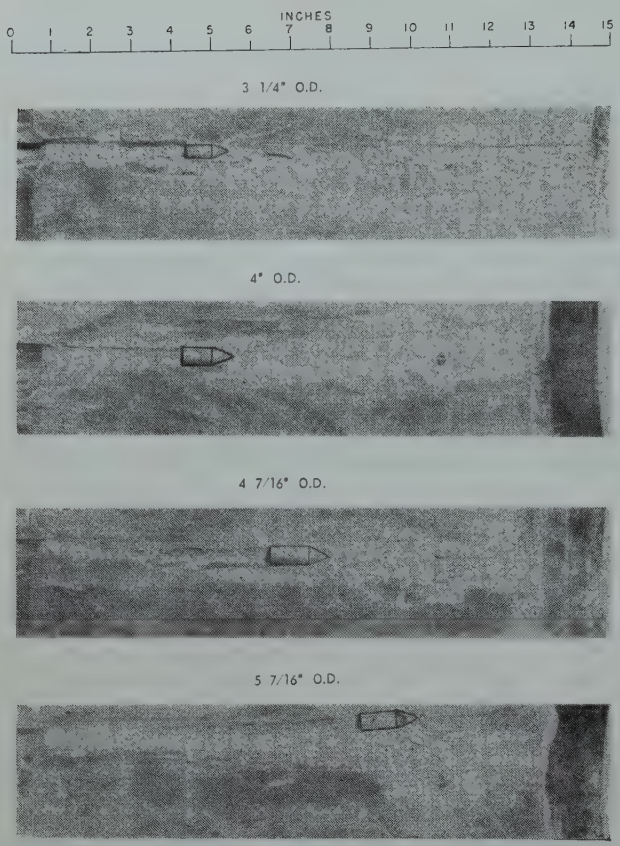

FIG. 3 — EXAMPLES OF PENETRATION FOR VARIOUS SIZES OF A PREMIUM PRICED BULLET GUN.

theoretically desired penetration. However, the 7½-in. penetration of the 21 gm shaped charges and that of the new or improved bullet guns appears satisfactory in a similar comparison.

An examination of the data presented by Lewelling[7] in 1952 regarding penetration into hard limestone cores showed significantly less penetration than was previously obtained with the same bullet gun fired into neat cement targets by other investigators; however, jet penetration was not reduced in the same magnitude by the hard limestone. Information obtained in the plugging investigations reported in the following section tends to support Lewelling's findings that bullet penetration is more adversely affected by hard formations than jet penetration.

INVESTIGATIONS OF PERFORATION PLUGGING

This investigation had as its objectives the determination of the effect of both the jet and bullet perforating processes on various types of formation, and how this effect is influenced by well conditions.

In simulating well conditions, the test well must be equipped with casing cemented adjacent to a formation which has controlled hydrocarbon and salt water saturations as well as reservoir temperature and pressure. The casing must be filled with a usual well completion fluid having the desired well temperature and pressure. In addition, the pressure differential between the formation and the well bore should be controlled during the shooting, well cleaning, and producing phases of the operation.

DESCRIPTION OF LABORATORY EQUIPMENT

The laboratory facilities which had been used for the competitive penetration tests reported by Huber, Allen, and Abendroth,[5] were expanded to accommodate testing under simulated well conditions. The schematic diagram in Fig. 4 shows the layout of test equipment employed. It may be noted that the test chamber in the center of the diagram contains an inner cylinder, or target, with a formation core cemented inside. The upper face of this target represents the well casing, and the single-shot test gun above the target is representative of a commercially available 4-in. OD bullet or jet gun. Both the target and gun are submerged in the mud being employed in the simulated well completion. The pressure control system on the right makes up a reservoir system for simulating formation pressure when used in series with the target, and provides the well fluid pressure when used in series with the test chamber. The hot water circulating system shown to the left of the test chamber in Fig. 4 supplies the heat required to maintain the desired well and reservoir temperature. The mud system shown directly above the hot water circulating system provides the equipment for mixing and handling the well fluid.

The mud system consists of a mixing tank, a portable ¾-hp mixer, and a positive displacement pump capable of handling fluids with a high viscosity and high solids content. The hot water circulating system in-

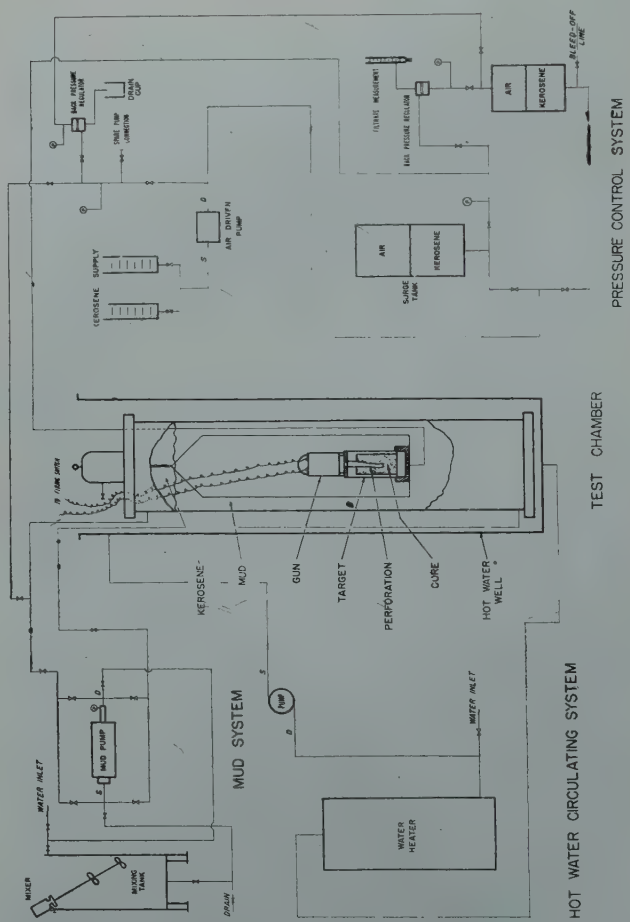

FIG. 4 — SCHEMATIC DIAGRAM OF GUN PERFORATOR TESTING SETUP.

cludes three thermostatically-controlled heaters, pumps, and a hot water well in which the test chamber is submerged. Temperatures up to 200°F can be maintained to within one to two degrees with this equipment. The pressure control system is comprised of an automatically-operated, air-driven pump, two back-pressure regulators, and sufficient additional instrumentation to maintain desired pressures and pressure differentials. The test chamber, constructed from 16-in. OD, 13½-in. ID, steel pipe, has an inside length of 100 in. between the two removable heads, which are equipped with O-ring seals.

The target, as stated previously, consists of a steel case with a core cemented inside. This case is made from 4½-in. OD, 16.6-lb drill pipe threaded on one end and with a mild steel plate representing the well casing welded on the other end. This plate is ⅜-in. thick for bullet targets and 1 in. thick for the jet targets. Since these tests were not designed primarily to compare penetrations, the added thickness of steel is used for the jet targets to insure against the perforation reaching too near the open face of the core.

Hydromite, a gypsum cement containing resin, is used for the cementing material rather than neat cement because of its greater tensile strength and excellent bonding characteristics. While experimenting with target design, neat cement was tried as the support material for the core, but it was found that its bonding characteristics were inferior to those of Hydromite. Berea sandstone cores were selected for use in these targets because of the availability and relative uniformity of this formation. The cores used were 3½-in. in diameter and 8 in. long, and cut parallel to the bedding plane.

Prior to fabricating the targets, these cores are processed to simulate oil and water saturations approaching those of a producing formation. This is done by drying, evacuating, saturating with 30,000 ppm salt water, and then flooding with kerosene until minimum water saturation is reached. The necessary weights are obtained to calculate porosity and oil saturation. The permeability to oil is measured at this final saturation.

A flow diagram of the equipment used in processing the cores is shown in Fig. 5. This apparatus and the other equipment in the core laboratory is, for the most part, standard laboratory equipment. Some of it is commercially available and part was built for this project.

Discussion of Tests and Test Procedure

The number of variable which might affect this investigation was recognized. Accordingly, the program was planned to first obtain basic data using the Berea sandstone cores, a low pH caustic-quebracho mud, and one set of pressure and temperature conditions, before extending the investigation to include work with other fluids, pressures, and formations. The first phase of testing is nearing completion with Berea sandstone cores with permeabilities in the range of 150 to 250 md, 2,000 psi mud pressure, 1,500 psi reservoir or formation pressure, 180°F well temperature, and caustic-quebracho mud with the following average properties:

Weight, lb/gal	9.5
Viscosity, cps	40
API Filtration Rate, cc	10.3
Initial gel, gm	5
10-min gel, gm	23
pH	7.5
Solids Content, Per Cent	19.7

Single shot test guns representing (a) a conventional 4-in. OD premium-priced bullet gun, (b) a jet gun with a standard 21-gm charge, and (c) a jet gun with an experimental 29-gm charge were used. The experimental charge was designed to give greater shot hole diameter at the expense of some penetration. It has been employed in only a limited number of tests.

To prepare for a typical test conducted under the conditions given above, the target and gun are assembled in a carrier and lowered into the test chamber which has been filled with drilling mud. The reservoir system and test chamber are then pressure tested at 1,500 psi and 2,000 psi, respectively. The chamber and its contents are heated to 180°F over a period of 15 to 18 hours. The reservoir and mud are then raised to test pressures, and the gun perforator is electrically fired, perforating the simulated casing, cementing material, and formation.

With a 500 psi pressure differential into the formation when the gun is fired, the mud follows the bullet or jet stream into the shot hole and a filter cake is laid down as mud filtrate invades the core. This filtration phase of the test corresponds to the period in a well completion between perforating and the time when the differential pressure into the formation is removed by swabbing or displacing the mud with lighter fluids.

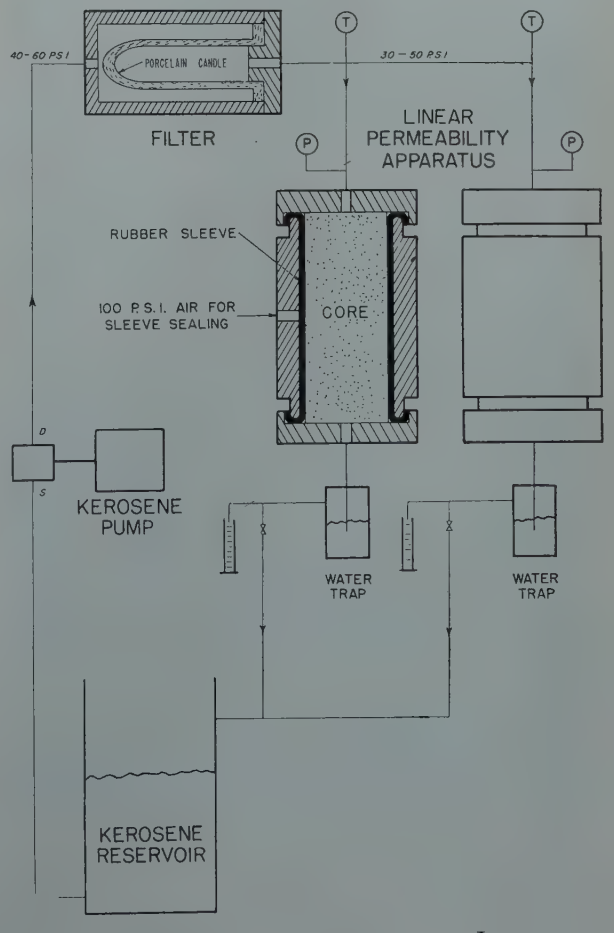

Fig. 5 — Flow Diagram—Permeability Laboratory.

The filtrate entering the core tends to build up the reservoir pressure to that of the mud, but the back-pressure regulator in the reservoir system releases the excess fluid, thereby maintaining a constant reservoir pressure. The volume of kerosene displaced by the filtrate entering the core is measured and the time recorded at prescribed intervals. The filtration phase is continued for a period of approximately 24 hours, the time which might be required on a deep well to come out of the hole with the gun, run the tubing in, and set the Christmas tree.

Following the filtration phase, the mud pressure is slowly reduced below the reservoir pressure to simulate bringing in a well. The purpose of this phase, in addition to simulating well conditions, is to determine the differential pressure required to initiate flow through the perforation.

After this differential has been determined, kerosene is back flowed through the target at a constant pressure differential of 100 to 300 psi. The object of this phase of the test is to flush the mud filtrate from the core with kerosene, simulating the initial production from a well, and to obtain a representative fluid flow rate through the perforation after the well has been cleaned. Within the accuracy of the control equipment, an essentially constant rate is normally attained after flowing 40 pore volumes or less through the core. Backflow is continued at this rate for an additional 40 or more pore volumes. After the target is removed from the well, it is cut open for visual inspection. Appropriate measurements and descriptions are recorded. Then the targets are photographed.

Evaluation of Data

The flow rate through a core of given dimensions depends on the pressure differential across the core, the viscosity of the fluid flowing, and the effective permeability of the formation to the fluid. When the core is cemented in a steel case and perforated as it is in these tests, the flow rate depends also on the diameter and depth of the shot hole, the degree of plugging which occurs, and the condition of the formation adjacent to the perforation.

The flow rate from the formation through the plugged perforation, measured in volume per unit time, reflects the combined influence of these factors. The effect of viscosity, pressure differential, and permeability can be determined by the application of Darcy's Law. The effect of the diameter and depth of the perforation on the flow rate was determined by drilling targets with various diameter holes to successive depths and measuring the flow rate at each depth.

Similar information could be obtained by setting up an electric analog of the target and perforations. However, such an investigation would assume equal formation permeability in all directions. Also, the flow rates obtained might not be as representative as the flow rates obtained with the drilled targets, where the formation bedding planes affect the flow perpendicular to the shot hole. The difference between the flow rate through a perforated hole of a given diameter and depth and the flow rate through the drilled hole of the same dimensions as the perforation and in the same type formation is considered in this paper to be the reduction in flow rate caused by both the perforation plugging and the alteration of the formation around the shot hole by the perforating process. For this to be valid the flow rates must first be corrected to the same viscosity, permeability, and pressure conditions by the application of Darcy's Law as noted above.

For convenience in evaluating the flow data taken in these tests, the flow rate through the core with both faces open to flow is taken as unity. The flow rates through the targets with one face open to flow and the opposite face cemented off, except for either a drilled hole or a perforated hole, are expressed as decimal fractions of this unit flow. These fractions, or ratios, are arbitrarily defined as the flow rate indices for a clean hole and a plugged perforation, respectively. They are designed by the symbols $\bar{q}_c$ and $\bar{q}_p$. Then $\bar{q}_c$ is a measure of the flow which should be obtained through the perforation with no restriction in or around the shot hole, and $\bar{q}_p$ is a measure of the actual flow rate obtained through the perforation.

To convert $\bar{q}_c$ and $\bar{q}_p$ to the corresponding flow rates in volume per unit time, such as cc per second or barrels per day, for a particular pressure, viscosity, and permeability, these indices must be multiplied by the flow rate through the core with both faces open to flow expressed in the desired units, either measured at the prescribed conditions or calculated from Darcy's Equation.

The reduction in flow rate in terms of these indices is, then $\bar{q}_c - \bar{q}_p$, and the per cent reduction, based on the flow rate which should be obtained through the given perforation, is as follows:

$$\text{Per Cent Reduction} = \left(1 - \frac{\bar{q}_p}{\bar{q}_c}\right) 100$$

Test Results

The results presented here are from 22 firing tests simulating individual well completions and conducted during the first phase of the program previously outlined. It should be pointed out that an additional 26 preliminary tests were conducted while experimenting with target design and equipment and in establishing a test procedure which would yield consistent results. A few subsequent tests have also been conducted with other fluids and pressures and Berea sandstone cores in a higher permeability range, but the results from this latter group of tests are too limited to establish a trend and are not reported at this time.

The results will be discussed in terms of (a) the physical characteristics of the perforation and plug, and (b) the flow rates obtained and calculated reductions in flow rates. The average diameter and depth of penetration obtained by each of the three perforators used are as follows:

	Hole Diameter — Inches	Penetration — Inches: Steel and Hydromite	Penetration — Inches: Core	Penetration — Inches: Total
a. Bullet	½	1⅛	1	2⅛
b. 21-gm Jet	¼	2	4¾	6¾
c. 29-gm Jet	½	2	3	5

Bullet penetration shown above was measured to the back of the bullet, and jet penetration was measured to a point ¾ of an inch from the bottom of the hole, since the jet hole usually has a very small diameter near the bottom.

TABLE 1 — FLOW DATA FOR TARGETS PERFORATED IN CAUSTIC QUEBRACHO MUD

Test No.	Perforator	Flow Rate Indices* $\bar{q}_c$	$\bar{q}_p$	Reduction in Flow Rate - % $\left(1 - \frac{\bar{q}_p}{\bar{q}_c}\right) 100$
1	4-in. OD Jet with 21-gm charge	1.22	0.39	68
2	4-in. OD Jet with 21-gm charge	1.20	0.44	63
3	4-in. OD Jet with 21-gm charge	1.45	0.39	73
4	4-in. OD Jet with 21-gm charge	1.39	0.43	69
5	4-in. OD Jet with 21-gm charge	1.34	0.53	60
6	4-in. OD Jet with 21-gm charge	1.20	0.75	37
7	4-in. OD Jet with 21-gm charge	0.82	0.40	52
8	4-in. OD Jet with 21-gm charge	1.54	0.35	77
9	4-in. OD Jet with 21-gm charge	1.45	0.32	78
10	4-in. OD Jet with 29-gm experimental charge	1.05	0.86	18
11	4-in. OD Jet with 29-gm experimental charge	1.16	0.88	24
12	4-in. OD Jet with 29-gm experimental charge	0.92	0.68	25
13	4-in. OD Premium Priced Bullet Gun	0.72	0.43	40
14	4-in. OD Premium Priced Bullet Gun	0.81	0.22	73
15	4-in. OD Premium Priced Bullet Gun	0.81	0.48	40
16	4-in. OD Premium Priced Bullet Gun	0.81	0.49	38
17	4-in. OD Premium Priced Bullet Gun	0.76	0.51	32
18	4-in. OD Premium Priced Bullet Gun	0.76	0.53	30
19	4-in. OD Premium Priced Bullet Gun	0.69	0.51	26
20	4-in. OD Premium Priced Bullet Gun	0.76	0.44	42
21	4-in. OD Premium Priced Bullet Gun	0.76	0.68	11
22	4-in. OD Premium Priced Bullet Gun	0.71	0.32	54

*The flow rate indices, $\bar{q}_p$ and $\bar{q}_c$, express the flow rates through the perforation and through a clean hole in the same formation drilled to the same dimensions as the perforation as decimal fractions of the flow rate which would be obtained through the unperforated core with both faces open to flow.

A comparison of these penetrations with those obtained in the steel and cement targets described in the first part of this paper shows that the 21-gm jet charge achieves approximately the same penetration in both targets, whereas the bullet penetration into the formation target is only about half that obtained in the neat cement targets. This suggests that penetration of hard formation with bullets may be limited; but, since Berea sandstone is considered only a medium hard formation, its confinement in a small diameter, heavy-walled target cylinder may possibly be a factor in reducing the bullet penetration.

The shot hole made by each of the guns used in these tests was filled with a plug which was not removed by backflowing, as illustrated in Fig. 6. The plug formed in the bullet perforation is relatively hard and dense, and consists principally of sand and mud solids. The plugs in the jet perforations also contain sand and mud solids, but, in addition, include a relatively large quantity of debris from the shaped charges.

When the 21-gm charge is used, this shaped charge debris makes up the bottom portion of an extremely hard, dense plug. With the 29-gm experimental charge, both the charge debris and mud solids are unevenly dispersed throughout a comparatively soft, sand plug. It appears that this distribution of the solids with the experimental charge may be a result of the large diameter perforation or possibly, the distribution of forces in and around the jet stream during the perforating operation.

Around the shot hole, which is filled by the plugs described, is a region of affected formation which appears to be composed of crushed and compacted sand grains held in place by the mud plugs. Microscopic examination does not indicate any glazing or fusing of this unconsolidated sand. Normally, there is little or no cracking of the core in the targets perforated with the jet guns; the bullet gun, however, produces hair-line cracks radiating outward from the bullet. The flow data calculated for each test is shown in Table 1.

A summary of this data is as follows:

Gun Employed in Firing Test Bullet	Bullet	21-Gm Jet	29-Gm Exp Jet
Number of Tests Averaged	10	9	3
Average Diameter and Depth of Formation Perforation, Inches	½ x 1	¼ x 4¾	½ x 3
Average Flow Rate Index, $\bar{q}_c$, for Clean Hole Drilled to the Same Dimension as Perforation	0.76	1.29	1.04
Average Flow Rate Index, $\bar{q}_p$, for Perforation	0.46	0.45	0.81
Average Reduction in Flow Rate, Per Cent	39	64	22

If the bullet perforator is taken as an example, these indices mean that if the permeability of the formation, viscosity of the fluid, and the pressure differential across the core are such that 1 bbl of fluid per day is produced through the core with both faces open to flow, then 0.76 B/D should be produced through a clean hole with the same dimensions as the perforation. But, because of the plugging, only a 0.46 B/D was produced. This corresponds to a flow rate 39 per cent less than that which should be obtained with no plugging.

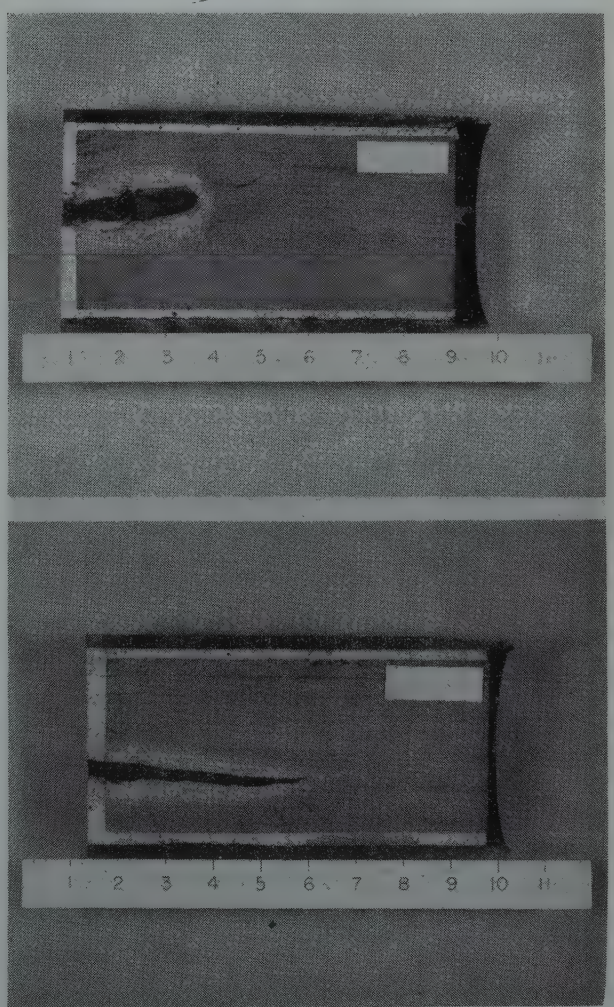

FIG. 6 — EXAMPLES OF FORMATION TARGETS PERFORATED IN THE PRESENCE OF MUD. TOP ILLUSTRATION DEMONSTRATES PERFORATION WITH 4-IN. OD PREMIUM PRICED BULLET GUN; BOTTOM ILLUSTRATION, WITH 4-IN. OD JET GUN WITH 21-GM CHARGE.

Though the jet perforators are penalized by ⅝-in. additional steel and ¼-in. additional Hydromite, the flow rate through the 21-gm jet perforation is approximately the same as that through the bullet perforation. This is indicated by a flow rate index of 0.45 as compared to 0.46. Also, the flow rate through the 29-gm experimental jet perforation is almost twice that achieved by either of the other perforators, as indicated by an index of 0.81. It should be pointed out that if the jets were not penalized by this additional steel and Hydromite, corresponding flow rates would no doubt be greater.

The average restriction per unit depth of penetration is greatest for the 21-gm jet as illustrated by the 64 per cent reduction in flow rate as compared to 39 per cent for the bullet gun and 22 per cent for the 29-gm experimental jet. It should be emphasized that these 29-gm charges are an experimental design not yet commercially available. Tests conducted with these charges have been limited, but the use of a charge design which produces a larger diameter hole appears to provide an approach to reducing the damaging effects of perforation plugging and obtaining greater well productivity.

Since the areal extent of the formation and the radial flow which occurs adjacent to the well is not duplicated in these tests, the percentage reductions in flow rate presented here cannot be directly applied to a well. However, since the pressure drop across a plugged perforation is large compared to the calculated pressure drop from the well bore to a drainage radius of 1,000 ft. for the same volume of flow, viscosity, and permeability, assuming four shots per ft. it appears that the percentage reductions give order of magnitude numbers which may be used in estimating the effectiveness of gun perforating under particular well conditions.

SUMMARY

Penetration

1. Gun perforators are currently available which are capable of providing sufficient penetration for most well perforating jobs, and, in many cases, penetration sufficient to provide productivities equivalent to or greater than open hole, based on previously mentioned analog studies.
2. The bullet perforating process is more adversely affected by heavy casing, hard cement, and hard formation than is the jet perforating process.

Plugging

1. When shooting in mud under conditions similar to those used in these tests, a plug which is not removed by backflowing is formed in the perforation, and the formation surrounding the shot hole is altered so that the flow rate through the perforation is restricted in varying degrees.
2. Total flow was approximately equal through perforations made with the 21-gm jet and with the premium-priced bullet perforator. The restriction per unit of hole depth was greater with the 21-gm jet than with the bullet perforator, however, the greater penetration obtained by the jet perforator resulted in equal flow through both types of perforations. The flow rate through the experimental jet perforation is almost twice that obtained with either of the other perforators. In considering flow rates, it is recognized that in penalizing the jet penetration with additional steel and Hydromite, the flow rates for these guns are also somewhat reduced.
3. One possible step toward increased productivity for perforated completions is the design of shaped charges which will give a larger diameter hole than the 21-gm charge and a deeper penetration than that obtained with the bullet gun. The 29-gm experimental charge used in these tests is a move in that direction; however, it is not yet known whether merely increasing hole size reduces plugging with jets, or whether the plugging effect may be a function of other factors related to charge design.

In addition to the problems recognized at the beginning of these investigations, many related problems have been uncovered which suggest that, in such an important operation as opening up pay horizons either in field development or wildcat operations, a great many more answers are needed than are now available.

The work presented in this paper covers only one phase of the problems associated with the effectiveness of gun perforating. To obtain sufficient information on this problem to satisfy the needs of the industry, extensive testing will be required under the various conditions which may occur in a well.

It is anticipated that additional work will be done by the authors to evalute the effectiveness of gun perforating, but the magnitude of the problem presents a program too lengthy for one company to complete. It is therefore hoped that this paper has not only stimulated interest in the program described, but will also encourage other companies to participate in similar work.

ACKNOWLEDGMENTS

The authors wish to express their appreciation for the cooperation and assistance from all service companies participating in the perforator penetration tests, and especially to Lane-Wells Co. and Welex Jet Services, Inc., for their assistance in connection with the perforator plugging experiment.

REFERENCES

1. Muskat, Morris, and McDowell, James M.: "The Effect on Well Productivity of Formation Penetration Beyond Perforated Casing," *Trans.* AIME, (1950), **189**, 309.
2. Howard, Robert A., and Watson, Marsh S., Jr.: "Relative Productivity of Perforated Casing," *Trans.* AIME, (1950), **189**, 179, 323.
3. Howard, Robert A., and Watson, Marsh S., Jr.: "Relative Productivity Index of Gun Perforated Completions as Affected by Depth of Penetration," *World Oil*, February 1, 1952, p. 166.
4. Oliphant, S. C., and Farris, R. Floyd: "A Study of Some Factors Affecting Gun Perforating," *Trans.* AIME, (1947), **170**, 225.
5. Huber, T. A., Allen, T. O., and Abendroth, G. F.: "Well Completion Practices," API Production Bulletin No. 236, (1950), p. 24.
6. Muskat, Morris: "The Effect of Casing Perforation on Well Productivity," *Petroleum Development and Technology*, (1943), **151**, 175.
7. Lewelling, Henry: "Experimental Evaluation of Well Perforation Methods as Applied to Hard Limestone," *Journal of Petroleum Technology*, June, 1952, p. 163.

★ ★ ★

SOME PRACTICAL ASPECTS of GRAVEL PACKING

C. J. RODGERS

GULF OIL CORP.
HOUSTON, TEXAS

T. P. 3741

ABSTRACT

The present day success of gravel packs to prevent or retard the migration of unconsolidated sands into the well bore is due to: (1) the use of a saline or non-aqueous, nonsolids drill fluid, (2) proper preparation of the well bore prior to gravel packing, and (3) pressure placement of the gravel.

The experience gained from the "pressure pack" method of gravel packing indicates that sand-free fluid production can be maintained for a length of time sufficient to make the operation economically attractive. Data pertaining to the first 15 wells so completed by Gulf indicate that for each dollar spent to effect the completion, there will be a return of more than $2.92.

The pressure pack technique of gravel packing is essentially the placing of gravel in and adjacent to the producing formations. This is done with fluid pressure and by the use of a drill fluid that will permit partial or complete loss of returns to the formation during placement. This technique was first intentionally used by Gulf in May, 1950, and since that time has been applied in more than 90 wells.

Other advantages claimed for this type of completion are that the pressure placement of the gravel has a scouring effect on the casing perforations, that additional drainage channels to the well bore are created, and that the possibility of shifting of the formations adjacent to the casing is minimized and possibly prevented.

INTRODUCTION

During the past few years, the use of gravel to prevent or retard the migration of unconsolidated sands into the well bore has met with a favorable degree of success. Numerous methods and techniques of "gravel packing" have been used, each having its own relative merits, and with varying results.

M. L. Cashion[1] in 1939 ably reviewed the history of gravel packing to that time. As stated in his paper, ". . . the idea of gravel packing wells is not new." During the period 1939 to 1949, very little if any progress or change in technique in this type of completion was made. However, it was noted in some cases that during the placement of gravel, if there was a loss of drill fluid to the formation, there was a corresponding loss of gravel to the formation.

Also, it was noted that in those gravel-packed completions (opposite casing perforations) that "sanded up," there was found to be an absence of gravel in the annular space between the liner and casing, although gravel had previously been placed in this space and no gravel had been removed from the well at the surface. These findings resulted in the placement of gravel with fluid pressure and by the use of a drill fluid that would permit partial or complete loss of returns to the formation during placement. Pressure placement of gravel became an accepted practice in late 1949 and early 1950.

Another fact brought to light that has contributed to the current success of gravel pack completions is that drilling fluids containing solids will to some extent cause plugging of the screening medium or blocking of the producing section. The removal of these solids by chemical action, mechanical action, or a combination of the

[1]References given at end of paper.

Manuscript received in the Petroleum Branch office July 29, 1953. Paper presented at the Petroleum Branch Fall Meeting in Dallas, Texas, Oct. 18-23, 1953.

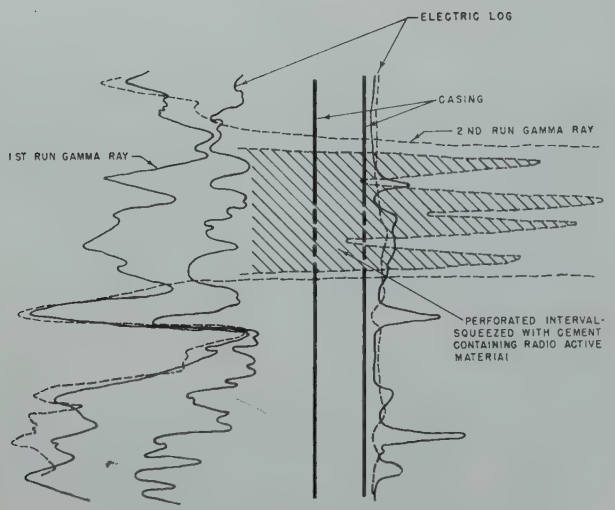
ELECTRIC LOG
CASING
2 ND RUN GAMMA RAY
1 ST RUN GAMMA RAY
PERFORATED INTERVAL-SQUEEZED WITH CEMENT CONTAINING RADIO ACTIVE MATERIAL

FIG. 1 — FORMATION PARTING CAUSED BY SQUEEZE CEMENTING.

two means, has been found to be essential for the success of any type of screening medium. The detrimental effects of fresh water or fresh water muds are also recognized and have resulted in their discontinuance in some cases. When fresh water mud is used in the filtrate, loss is considerably less than was the case a few years ago.

CURRENT PROCEDURE

The present day success of gravel packing in completion work is believed to be due primarily to: (1) the use of saline or non-aqueous, nonsolids drill fluid (normally salt water that is compatible with the formation fluids or oil), (2) proper preparation of the well bore prior to gravel packing; i.e., the removal of the original drill mud from the well bore and as much as possible from the sand face, and (3) pressure placement of the gravel.

Pressure placement of gravel may result in a parting of the stratified formations within the producing interval along bedding planes or other zones of weakness if sufficient pressure is applied. Fig. 1 illustrates the formation parting that resulted from squeeze cementing perforations in 5 in. OD casing in a well in the Thompsons field, Texas. The interval squeezed is a Frio sand section at a depth of approximately 5,300 ft. A gamma ray survey was conducted before and after squeeze cementing. A total of 173 sacks of cement containing a uniformly distributed radioactive material was forced through the casing perforations at a maximum and final surface gauge pressure of 4,700 psi (a 9.5 lb per gal mud was used as the drill fluid). Comparison of the two gamma ray curves indicates that the greatest increase in radioactivity is confined principally to the section opposite and adjacent to the perforated interval and that the formations within this section are parted as the increased radioactivity varies within this section.

REASONS FOR GRAVEL PACKING

It is reasoned that if the formations are pressure parted and gravel is forced into these induced cracks or fissures, the possibility of their being closed when the applied pressure is released will be eliminated. Also, these openings will provide additional drainage channels to the well bore. This will permit fluids to enter the well bore at lower velocities and, therefore, will tend to minimize the erosional effect of the fluid movement. The mechanical propping of the formations should provide added resistance to any tendency these formations may have to slough or shift, if there is a reduction in bottom hole pressure. The ability of the well to produce may also be improved by this parting and propping of the formations.

Numerous breaks in the exposed formations will be caused as the applied pressure is progressively increased. The breaking down and packing with gravel of these zones of weakness results in the mechanical consolidation of the producing interval, in the individual beds or layers having more strength to shear, and in a greater drainage area being opened to the well bore.

The use of the word "gravel" as pertains to gravel packing may be misleading. The individual grains are of such a size that the aggregate is usually considered to be a coarse sand. The grain size normally used for packing producing wells is 0.040 to 0.060 gauge (15-to-10 mesh) and for packing injection wells 0.060-to-0.090 gauge (10-to-8 mesh). Considerable laboratory work[2,3,4] has been done in order to determine the physical properties this gravel should have, including the sizes as stated above. Actual field testing in the reservoirs encountered in the Gulf Coast has substantiated the findings of the laboratory experiments. This gravel may be purchased from several supply firms and is packaged in sacks of 1 cu ft capacity.

ESSENTIALS FOR SUCCESS

The first well in the Gulf Coast District to be intentionally "pressure packed" by Gulf was a well at Sour Lake, Texas, in May, 1950. Since that time, several things have been found to be essential for the success of the operation. The formation pressure of the interval to be packed, or the differential to be caused by artificial lift equipment, or a combination of the two must be such that a sufficient volume of the drill fluid lost to the formation while gravel packing will be recovered and thus allow the entry of formation fluid to the well bore.

As gravel packing is usually a remedial measure, it has been necessary in most cases to place the gravel through perforations in the casing. These perforations should be of a size and density to prevent a tendency for the gravel to "bridge" opposite these holes inside the casing. In practice, it has been found that there is less tendency of the gravel to bridge when the perforations are 15/32 in. OD or larger and are of a density of at least six holes per foot. The ideal situation would be the complete removal of the casing opposite the producing section; i.e., the interval to be gravel packed. The economics of such an operation with the tools now available is subject to question, however. If the jet- or shaped-charge tools for the removal of a section of casing (now in the process of development and experimentation) are found to be adaptable, this possibility would be considered more favorably.

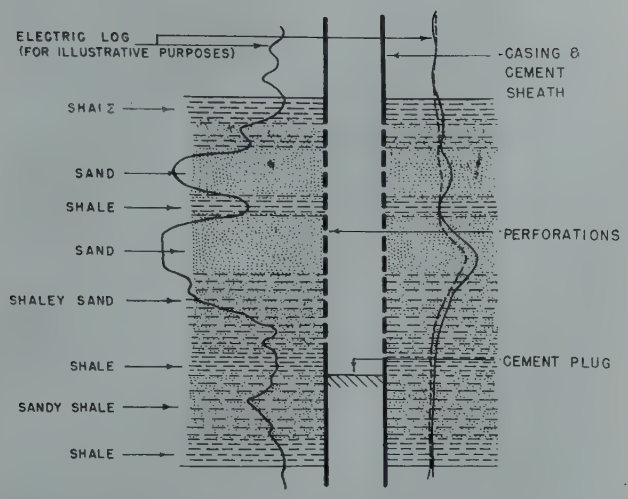

FIG. 2 — SECTION OF WELL BORE AND FORMATION TO BE GRAVEL PACKED.

TECHNIQUE

In order to describe the technique of gravel packing used by Gulf in the Gulf Coast District, sketches have been prepared (Figs. 2, 3, and 4). These sketches are of ideal conditions that may or may not be realized in practice. Fig. 2 illustrates the section of the well bore and formation to be gravel packed. Depicted is a well completion with the casing cemented through and opposite the producing sand body. The well casing and cement sheath have been perforated, allowing for drainage of fluids from the sand into the well bore. In this figure, the plug is near the bottom of the perforated interval. The sand face has been cleansed of foreign materials by swabbing, bailing, or washing. The electric log of this section of the hole has been superimposed on all sketches in order to illustrate the stratification of the sands and shales.

Fig. 3 shows the placing of the gravel. In this phase of the operation, a placement fluid (usually salt water) containing gravel is pumped down the tubing. The gravel is deposited in the well bore. By applying fluid pressures and reciprocating the tubing, gravel is forced through the perforations against the sand face, along bedding planes, and in any fractures that may exist or that may be caused to occur in the formation. The placement fluid is either lost to the sand body or returns to the surface through the annular space between the tubing and casing. During squeezing operations the fluid is lost to the formation. Gravel is placed in this manner until the well bore and formation have been "packed" to the desired fluid pressure. The basic idea involved is to pump gravel into or against the formation until the sand in the formation (reservoir) is mechanically impounded and results in a consolidated sand mass. This minimizes the possibility of sand movement into the bore hole.

BRADENHEAD SQUEEZING

The fluid pressure is applied in a manner that has commonly been referred to as "Bradenhead squeezing." The necessary surface equipment consists of a pack-off around the tubing or drill pipe at the well head (in this case a blowout preventer) that prevents or regulates the discharge of the circulating or placement fluid from the well bore. The squeeze pressure, caused by the circulating pump's attempting to force fluid in the tubing or drill pipe, is exerted on the tubing or drill pipe, the casing, and the formation. The maximum pressures that can be applied in this manner are limited to the bursting strength of the casing. For that reason this method of applying pressure is not applicable to high pressure work. Tools and methods will, no doubt, be designed and developed to remedy this situation. Several service companies claim to have such a tool available for use.

After placement of a quantity of gravel in the well bore to cause a fill-in above the top of the perforated interval, additional gravel is placed in the well bore. This is done so that after the screen liner is positioned (shown in Fig. 4), gravel fills the annular space between the liner and casing.

PLACING THE SCREEN LINER

Fig. 4 shows the screen liner in place with the packer sealed. This assembly has previously been run in on tubing or drill pipe attached to the packer by means of a setting tool. Wash pipe extends from the back pressure valve or set shoe inside the screen liner to the setting tool. This wash pipe permits the screen liner assembly to be washed down through the gravel fill-in in the well bore. In this washing down operation, the circulating fluid is pumped down the tubing or drill pipe, through the setting tool, the wash pipe, and out the set shoe. Then it is allowed to return to the surface through the annular space between the tubing and casing.

When the screen is positioned as desired, the setting tool is released from the packer by rotation. The setting tool assembly is raised a height sufficient to disengage the wash pipe from the set shoe and to allow the setting tool to disengage the packer. The setting tool is then lowered, and weight is applied to the packer to cause collapse and result in a seal to the casing. The

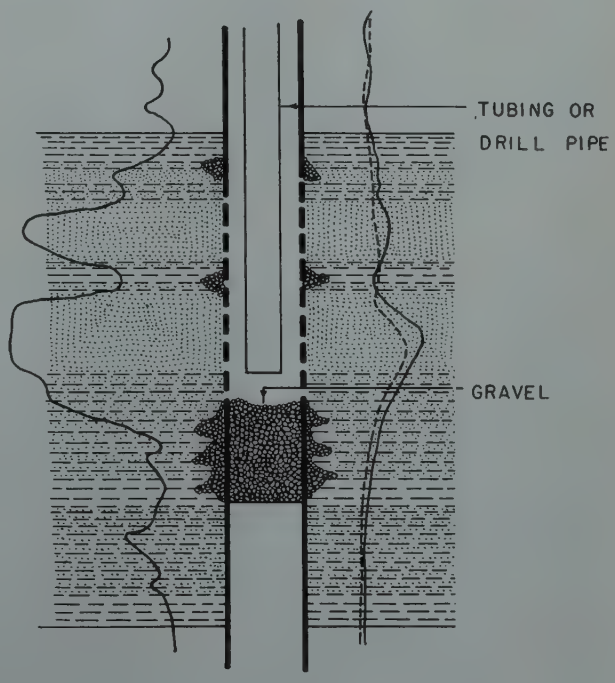

FIG. 3 — PLACING OF GRAVEL DURING THE GRAVEL PACKING OPERATION.

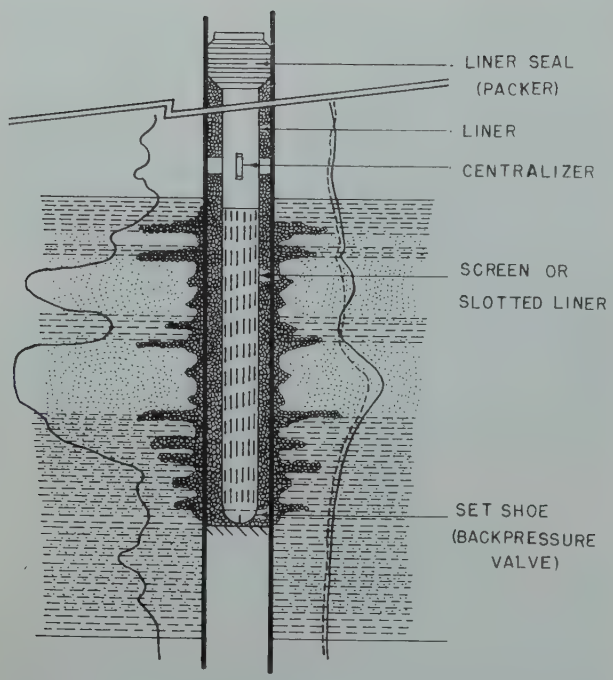

FIG. 4 — SCREEN LINER IN POSITION.

setting tool and wash pipe are pulled from the hole, leaving a gravel packed screen-liner setting as shown in Fig. 4. The customary tubing setting is made for completion.

IMPROVED METHODS

The above technique has been modified and improved and has resulted in the use of a gravel pack strainer assembly shown in Fig. 5. This assembly allows the completed interval, either open hole or perforated casing, to be pressure packed and the strainer setting made in one trip of the pipe. The assembly consists of a nose piece, slotted pipe, liner, setting tool and sleeves, and inserted wash pipe. The nose piece contains a flapper valve that is held in an open position by the wash pipe. Gravel is pumped down the tubing or drill pipe, through the wash pipe, and out the nose piece.

Fluid pressure is then applied and the gravel pack strainer assembly reciprocated by raising and lowering the tubing or drill pipe. These pressures cause the gravel to be pressure packed in and opposite the completed interval. The assembly is then washed into place by normal circulation.

Right-hand rotation of the tubing or drill pipe causes the setting tool to become disengaged from the setting sleeve. The tubing or drill pipe, the setting tool, and wash pipe are then pulled from the hole and the conventional tubing setting made. The flapper valve in the nose piece is allowed to close when the wash pipe is pulled.

CALCULATING MAXIMUM PRESSURE

The maximum pressure used in the placement of the gravel is arrived at by calculating the top hole gauge pressure necessary to exceed slightly the overburden pressure. By overburden pressure is meant "the calculated pressure at any given depth exerted by the theoretical weight of overlying formations as calculated from the average rock density."[5] The general opinion is that the overburden pressure gradient for formations along the Texas-Louisiana Gulf Coast is roughly 1 psi per ft of depth. The maximum desired gravel placement pressure (top hole gauge pressure) is equal to the pressure at the perforated interval (due to the weight of the overlying beds) minus the hydrostatic head of the fluid column plus 100 psi. The gravel pack squeeze pressure as calculated above is intended only as a basing point for present and future experimentation.

During the development or experimental phase of the work that preceded the adoption of the above technique, several innovations were tried. Some wells were packed with such volumes of gravel and at such pressures that it was possible to wash out the gravel inside of the casing before running in the screen-liner. In effect, a gravel pack that was self-supporting was placed adjacent to and in the producing interval. After positioning the screen-liner, the annular space (between the casing and screen-liner) was packed and the well completed in the conventional manner.

This procedure was desirable, as it allowed the completion to be made without disturbing the final pack. It soon became apparent, however, that in order to effect

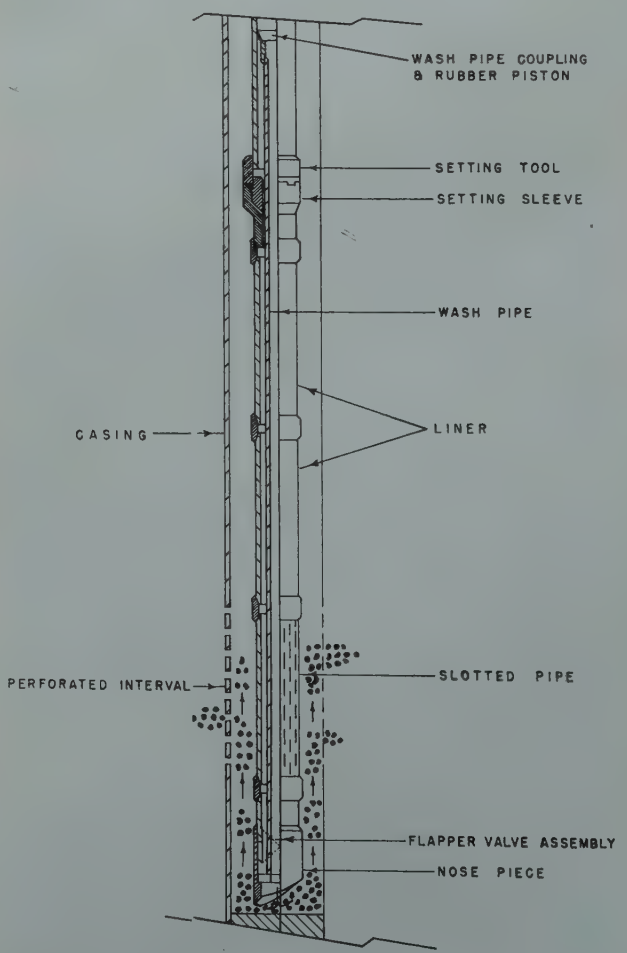

FIG. 5 — GRAVEL PACK STRAINER ASSEMBLY.

the self-supporting pack, it was usually necessary to repeat the squeezing and washing out operations until the gravel outside the casing was so arranged that it did not flow back into the well bore. This was both time consuming and expensive; therefore, on later wells the screen-liner was washed down through the gravel. As the wells produced satisfactorily this method of placement was adopted.

Strainers

Wire-wrapped screen and slotted pipe have been used as strainers. Both have performed satisfactorily. All but five of these settings (more than 90 have been made by Gulf) were made inside of casing opposite perforations. All of these inside strainers were either 2⅜ in. OD or 2⅞ in. OD. The casing size apparently does not limit the maximum size of the strainer that may be used to the degree that, prior to pressure packing, had been advocated; i.e., 2⅞ in. OD strainer inside of 7 in. OD casing, 2⅜ in. OD strainer inside of 5½ in. OD and 5 in. OD casing. Strainers of 2⅞ in. OD have been set inside of 5 in. OD casing opposite perforations of wells which have produced satisfactorily.

Kenneth E. Hill has stated that, "The thickness of gravel should be at least five gravel grain diameters."[3] This requirement is more than satisfied by the placement of a 2⅞ in. OD strainer inside of 5 in. OD casing, if the annular space between these two pipes is filled with 0.040-to-0.060 gauge gravel. However, 2⅜ in. OD strainer inside of 5 in. OD casing will allow an increase in annular volume of approximately 24 per cent more than that afforded by a 2⅞ in. OD strainer inside a 5 in. OD casing.

The reduction in cross sectional area of the strainer may be justified in order to provide more annular volume as a storage space for gravel. As a well is produced and fluid is removed from the reservoir, the gravel stored in the annulus is intended to provide replacement gravel to the pack, if this pack is disturbed by fluid movement or a reduction in bottom-hole pressure. Also, of no little importance is the fact that the 2⅜ in. OD strainer should be easier to "fish out" than a 2⅞ in. OD strainer. The smaller strainer would be more difficult to bail or wash out; however, if either strainer were to become sanded up, more extensive remedial measures probably should be undertaken.

Strainer Gauge Sizes

The gauge size of the strainer should be such that it will not pass the smallest gravel used in packing; e.g., when 0.040-to-0.060 gauge gravel is used, a strainer of gauge size less than 0.040 would be in order. Since allowance should be made for mechanical imperfection in the manufacture of the strainer and also for possible fracturing of the grains of gravel during placement, a 0.020-gauge strainer is normally used.

Table 1[6] is a compilation of several representative gravel pack completions in the Texas Gulf Coast. As will be noted from this datum, the sacks of gravel placed per foot of perforations varied from well to well even within the same field. For the wells listed, the maximum cubic feet of gravel placed per foot of perforations was 8.6, and the minimum was 1.4. The barrels of salt water used for the placement of this gravel varied in a like manner but were not necessarily in proportion to the cubic feet of gravel placed. For example, at one well a total of 8.0 cu ft of gravel was placed for each foot of perforations, and 46.2 bbls of water were required to place each cubic foot of gravel.

At another well, a total of 8.0 cu ft of gravel was also placed per foot of perforated interval, but only 18.0 bbls of water per cubic foot of gravel were required for placement. As shown, a maximum of 46.2 bbls of water was used to place a cubic foot of gravel, and a minimum of 3.6 bbls was used for a like purpose.

Satisfactory Results

The production performance of the wells that Gulf has gravel packed has been very satisfactory. A record of production tests of the first wells completed in this manner is given in Table 2. Before being gravel packed, all of these wells were off production due to being sanded up, or they had not been completed due to the well's inability to produce, which was caused by sanding.

As shown by Table 2, only two of the completions (of the 46 listed) were initial failures: a well at Goose Creek and one at Thompsons. The work at Goose Creek was performed according to the procedure outlined above; however, after it was packed, the well

TABLE I — GRAVEL PACK COMPLETION DATA

WELL DESIGNATION	SIZE CSG. OR LINER INS. O. D.	PROD. INTERVAL	FEET PERF.	TOTAL SKS. GRAVEL OUT	SKS. GRAVEL PER FOOT PERF.	WATER USED BBLS.	WATER PER SK. GRAVEL BBLS.	COST DOLLARS	POTENTIAL TEST OIL	METHOD PROD.
A	5 in.	7124-7131 ft.	7	28.5	4.1	411	14.4	2244	52	Pump
B	5½	7040-7064 ft.	24	34	1.4	285	8.8	1975	54	Pump
A	5 in.	4383-4400 ft.	17	51	3.0	1990	39.0	2867	7	Pump
B	5 in.	4875-4884 ft.	9	72	8.0	3331	46.2	3960	43	Pump
C	5½	4246-4273 ft.	27	100	3.7	925	9.3	4743	51.0	Pump
A	5 in.	3321-3350 ft.	29	69	2.4	854	12.4	3529	94	Pump
B	5½	3503-3517 ft.	14	109.5	7.8	393	3.6	5818	79	Pump
C	5½	3458-3490 ft.	32	45	1.4	534	11.9	2200	103	Flow
D	5½	3468-3486 ft.	18	41.5	2.3	1300	31.4	2551	112	Flow
E	5½	3370-3396 ft.	26	120	4.6	2500	20.4	4597	152	Flow
A	5½	2580-2592 ft.	12	103	8.6	2028	19.7	4006	35	Pump
A	5½	5280-5295 ft.	15	68	4.5	900	13.2	4067	88	Pump
B	5½	4494-4498 ft.	4	32	8	575	18.0	2058	56	Flow
C	5½	5442-5500 ft.	58	79	1.4	1555	19.7	4503	99	Pump

NOTE: Cost figures include cost to gravel pack well and run screen. Gravel pack costs include service charges and royalty fees. This does not include pulling old liner or running production string.

failed to produce any fluids. The well did not sand up. At Thompsons, well conditions prevented proper conditioning of the bore hole before packing, and the recoverable oil was believed to be such that large expenditures should not be made to remedy this situation. This well sanded up while being tested after gravel packing.

Two wells, both at Goose Creek, sanded up after having produced substantial volumes of oil. One of the wells produced 7,385 bbls of oil before sanding up and the other produced 6,867 bbls of oil before sanding up.

Another well, also at Goose Creek, sanded up approximately 11 months after being gravel packed and after an attempt was made to increase the rate of production by the injection of chemicals into the producing section. In this case, it is believed that the pack around the screen or casing was ruptured when an attempt was made to squeeze out the chemicals.

Histories of Gravel Packed Wells

Very little repair work to gravel pack completions has been necessary. At a Sour Lake well, the daily producing rate declined from the initial completion of 35 bbls of oil and 36 bbls of salt water to 6 bbls of oil and 25 bbls of salt water in an 11-month period, or after the well had produced approximately 4,543 bbls of oil. After the producing section was acidized with 450 gals. of inhibited hydrochloric acid, the daily produced volumes increased to 8 bbls of oil and 43 bbls of salt water, an increase of 20 bbls of fluid per day. This rate declined, however, and as shown by the last test made two months after having been acidized, the well was producing at a daily rate of 5 bbls of oil and 30 bbls of salt water.

The producing rate of a well at Goose Creek declined in 10 months time from 29 bbls of oil and zero barrels of salt water per day after it was gravel packed to 1 bbl of oil and zero bbls of salt water per day. It had produced 3,632 bbls of oil. The producing section was squeezed with a chemical mixture. After considerable difficulty was encountered over a two-week period while attempts were made to produce the well, it sanded up. The well bore was bailed clean, and after the fluid was pumped out of the casing, the well produced small volumes of dry gas. It was assumed that this section was depleted of oil, and the well was plugged back and completed in a higher sand.

REPACKING

Several repacking jobs have been performed and the over-all results from a production standpoint have been erratic. In some of these instances meager reservoir information was available, and when the rate of production declined, it was assumed that the original pack had

TABLE II — WELL PERFORMANCE — GRAVEL PACK COMPLETION

Field	Well Designation	Perforated Intervals	Tests				Cumulative Oil
			After Gravel Packing		Last Test		
Anahuac	B	7040-7064 ft	54 oil	17 water	5 oil	9 water	10,861
	A	7124-7131 ft	52 oil	78 water	17 oil	66 water	7,582
Big Creek	A	4074-4090 ft	57 oil	2 water	3 oil	0 water	11,084
	B	3970-3980 ft	20 oil	12 water	0 oil	4 water	4,559
			Plugged Back				
	C	4258-4268 ft	30 oil	10 water	21 oil	20 water	18,947
Fannett	A	5280-5295 ft	88 oil	15 water	12 oil	50 water	8,966
	B	4494-4498 ft	56 oil	1 water	21 oil	2 water	13,202
			C.I., High Input Ratio, Plugged Back				
	C	2318-2330 ft	91 oil	18 water	85 oil	77 water	12,869
	D	5482-5500 ft	99 oil	85 water	121 oil	60 water	51,980
Goose Creek	A	3234-3246 ft	94 oil	17 water	62 oil	93 water	65,386
	B	4100-4110 ft	2 oil	16 water	7 oil	0 water	3,734
	C	2184-2198 ft	Plugged Back, Did Not Produce Commercially				
	D	3074-3106 ft	106 oil	35 water			7,385
			Plugged Back				
	E	4423-4429 ft	79 oil	60 water	91 oil	97 water	36,012
	F	4237-4242 ft	68 oil	0 water	7 oil	6 water	7,753
			Regravel Packed; Unsuccessful, Plugged Back				
	G	3402-3412 ft	82 oil	123 water	8 oil	104 water	14,865
	H	4168-4182 ft	29 oil	0 water	1 oil	0 water	3,632
			Plugged Back				
	I	4323-4327 ft	125 oil	14 water	7 oil	370 water	6,571
	J	4360-4376 ft	14 oil	2 water	12 oil	0 water	13,781
	K	3366-3374 ft	76 oil	250 water	23 oil	163 water	23,276
	L	4221-4228 ft	13 oil	4 water	6 oil	0 water	2,112
	(Sold)						
Hankamer	D	3882-3898 ft	21 oil	65 water	18 oil	71 water	11,054
	B	4875-4848 ft	54 oil	162 water	43 oil	231 water	28,573
	E	4465-4473 ft	10 oil	19 water	9 oil	0 water	5,976
	F	4651-4667 ft	28 oil	23 water	8 oil	12 water	8,830
	G	3927-3938 ft	23 oil	91 water	16 oil	7 water	11,224
	A	4383-4400 ft	7 oil	20 water	10 oil	39 water	8,075
	C	4246-4273 ft	51 oil	52 water	46 oil	57 water	38,028
Pierce Junction	A	3934-3938 ft	88 oil	131 water	10 oil	200 water	5,016
	B	4010-4014 ft	66 oil	28 water	7 oil	2 water	11,113
	C	5210-5218 ft	94 oil	50 water	28 oil	23 water	31,861
South Liberty	B	3503-3517 ft	79 oil	20 water	2 oil	104 water	10,729
			Plugged and Abandoned				
	C	3458-3490 ft	103 oil	0 water	108 oil	0 water	57,049
	D	3468-3486 ft	112 oil	21 water	61 oil	113 water	47,582
	E	3370-3396 ft	121 oil	30 water	109 oil	0 water	50,140
	F	3318-3350 ft	101 oil	4 water	105 oil	0 water	46,158
	G	3450-3466 ft	103 oil	5 water	10 oil	23 water	14,100
Sour Lake	A	2580-2592 ft	35 oil	36 water	5 oil	30 water	6,459
			Plugged and Abandoned				
South Thompson	A	5370-5376 ft	120 oil	0 water	54 oil	109 water	34,658
	B	5364-5374 ft	37 oil	109 water	8 oil	75 water	10,684
Thompson	A	5315-5321 ft	115 oil	115 water	33 oil	0 water	9,807
	B	5260-5280 ft	13 oil	4 water	8 oil	1 water	10,178
	C	Unsuccessful	Plugged and Abandoned				
	D	5234-5255 ft 5283-5299 ft	64 oil	28 water	54 oil	16 water	49,999
	E	5312-5359 ft	109 oil	42 water	46 oil	125 water	51,052
West Bay	A	8999-9011 ft	283 oil	0 water	15 oil	0.5 water	2,617
			Plugged Back				

become plugged. Yet after repacking, in several cases the producing rate was not improved. It is now believed that these intervals were at or near depletion before the repacking work was performed. Repacking has been successfully applied in those wells that became sanded up either from erosion, corrosion of the setting, or shifting of the gravel pack after large fluid withdrawals.

The examples cited above illustrate the types of remedial measures attempted to date by Gulf on the initial gravel pack completion. It is probable that more work of this nature will be necessary in the future. In those cases where it is evident that the pack has become plugged, temporary relief may be obtained by the use of hydrofluoric acid or a combination of hydrofluoric acid and a surface tension reducing agent. It may be necessary to pull the inside screen and liner, bail the well in order to remove the plugging material, and re-gravel pack for completion.

Improvements Expected

In those cases where the wells have produced large volumes of fluids and there has been a drop in bottom-hole pressure that will permit shifting of the formation, it may be that such wells should be gravel packed again. This is also true where fluid movement has caused some shifting, and thereby caused damage to the gravel pack which permitted the well bore to become sanded up.

The mechanics of gravel pack completions are no doubt subject to numerous improvements. At the present time, the cost of this work, as shown by the data of Table 1[6], prohibits its application in known marginal wells. The gravel pack screen assembly was designed and developed to reduce this cost and has resulted in the elimination of one trip of the tubing or drill pipe and the cost of the liner packer. It is hoped that the completion cost can be reduced even more.

Pressure Packing

The experience gained from field applications of the pressure pack technique of gravel packing indicates that sand free, fluid production can be maintained for a length of time sufficient to make the operation economically attractive. Other advantages claimed, secondary in nature and difficult to verify, are that the pressure placement of the gravel has a scouring effect on the casing perforations, that additional drainage channels to the well bore are created, and that the possibility of shifting of the formations adjacent to the casing is minimized and possibly prevented.

The disadvantages of this technique are that large volumes of placement fluid are lost to the formation, and the gravel squeeze pressures may rupture the casing or break down the cement seal around the casing above or below the producing interval. In practice, it has been necessary in a few cases for the applied gravel squeeze pressure to be less than the desired maximum due to the estimated low bursting strength of the casing. There are no known instances in wells gravel packed by Gulf where the casing has been ruptured or the cement around the casing damaged because of the applied gravel squeeze pressures. The loss of placement fluid to the formation is a necessary evil for this type of completion and has not proved to be of a serious nature.

MONETARY VALUE

In order to place a monetary value on this type of completion, the following data pertaining to 15 of the first wells so completed by Gulf have been assembled.

Total cost to recomplete $143,841

This is the total job cost and includes all services and materials necessary to prepare the wells for packing; such as, pulling old screens, reperforating, cleaning out, gravel pack service charges, royalty fees, etc., in addition to the rig time costs actually required to gravel pack and restore the wells to a producing status.

Accumulated production resulting from these recompletions — oil 224,060 bbls.

The first of these wells was restored to production Oct. 10, 1950, the last Aug. 27, 1951, and the total barrels of oil produced since recompletion to May 1, 1953, is as shown above.

Daily production upon recompletion — oil 664 bbls

Present daily production — oil 214 bbls

Of the 15 wells selected for this compilation, eight are producing at this time, two were initial failures. Two wells have been abandoned, one has been plugged back, one was sold, and one well is now off production awaiting plug back operations.

The expenditure of $143,841 has made possible recovery of 224,060 bbls of oil to May 1, 1953, or a return of $2.92 for each dollar spent. Normal operating expenses have been deducted from the return figure stated above. Attention is brought to the fact that in some of these wells the gravel pack completion was made only after all other known sand control measures had failed. As eight of these wells are still producing, the ratio of return of $2.92 per dollar expended will increase with time.

ACKNOWLEDGMENT

The author wishes to express his appreciation to the Gulf Oil Corp. for the release of the data contained in this paper.

REFERENCES

1. Cashion, M. L.: "Application of Gravel Packs in the Completion of Wells," *Gulf Oil Corporation Report* (Oct., 1939).
2. Coberly, C. J.: "Selection of Screen Openings for Unconsolidated Sands," *API Drilling and Production Practice,* (1937) 189.
3. Hill, Kenneth E.: "Factors Affecting the Use of Gravel in Oil Wells," *API Drilling and Production Practice,* (1941) 134.
4. O'Shields, R. L., and Hawkins, M. F.: "The Full Hole Gravel Pack," *World Oil,* (Aug., 1951) **133,** No. 3, 185.
5. Howard, George C., and Fast, C. R.: "Squeeze Cementing Operations," *Trans.* AIME, (1950), **189,** 53.
6. LeGrand, W. H.: "Well Completion Techniques — Gravel Packing," *Gulf Oil Corporation Report,* (Sept., 1951).

★ ★ ★

HISTORY and PERFORMANCE of the COLDWATER OIL FIELD, MICHIGAN

C. R. CRISS
MEMBER AIME
R. L. McCORMICK

SOHIO PETROLEUM CO.
OKLAHOMA CITY, OKLA.

T. P. 3748

ABSTRACT

This paper summarizes the development and performance of the Coldwater Oil field, Isabella County, Mich. Production is obtained at a depth of 3750 ft from a dolomite reservoir, which is probably both Rogers City and Dundee. There appears to be no persistent barrier to vertical fluid movement between the Rogers City and Dundee, and both formations are believed to have a common original oil-water contact. No wells are open to production at the level of the Dundee.

The discovery of the field in 1944 was followed by the drilling of 81 producing wells and nine dry holes. By the end of 1952, the field had produced 12,763,000 bbl of oil, at which time 69 active wells were producing 3600 B/D oil and 21,000 B/D water.

The reservoir has an effective natural water drive, and bottom-hole pressure has declined 75 psi from an original pressure of 1453 psi. Oil is undersaturated at reservoir conditions with a solution GOR of 512 cu ft/bbl and a saturation pressure of 1190 psi.

INTRODUCTION

Although the Coldwater Field is now in its ninth year of production, it ranks seventh in cumulative recovery, and second in current daily oil production in the State. Following complete development of the field in 1946, it has consistently contributed approximately 11 per cent of Michigan's daily production.

Coldwater appears to have a greater pay thickness than most fields producing from the Rogers City formation in the west central part of the Michigan basin. Except as influenced by the extent of closure and the thickness of the oil column, reservoir performance is believed to be representative of Rogers City fields in this part of the basin. For this reason, it is felt that the following presentation of factual data for the field will be of general interest.

Manuscript received in the Petroleum Branch office Aug 17, 1953. Paper presented at the Petroleum Branch Fall Meeting in Dallas, Tex., Oct. 18-21, 1953.

Discussion of this and all following technical papers is invited. Discussion in writing (3 copies) may be sent to the offices of the Journal of Petroleum Technology. Any discussion offered after Dec. 31, 1954, should be in the form of a new paper.

HISTORY AND DEVELOPMENT

Discovery of the Coldwater field during Aug., 1944, followed favorable subsurface geological correlations and core tests drilled to a shallow stratigraphic marker horizon. The field is located in the west central part of the Michigan Basin in Coldwater Township (T16N-R6W), Isabella County. It is 60 miles west-northwest of Bay City, and near the geographic center of the southern peninsula of Michigan. The discovery well flowed 200 bbl of oil the first 24 hours from the Rogers City dolomite at a depth of approximately 3750 ft. Field production is principally from the Rogers City with a minor amount assumed to come from the underlying Dundee dolomite, although none of the wells are open to production at the level of the Dundee. Both the Rogers City and Dundee formations belong to the Devonian system (See Geologic Column-Fig. 1.)

In addition to Rogers City-Dundee oil production, sweet gas is produced from the Michigan Stray sand of the Mississippian system at a depth of 1400 ft. The gas reservoir has approximately the same areal extent as the underlying oil reservoir. Although gas production is an important feature of the Coldwater field, this report is concerned only with the oil reservoir.

The productive area is approximately 3200 acres. The pool is developed on a 40 acre spacing pattern with wells drilled in the center of the north half of 40 acre tracts, except for a few off-pattern wells drilled along

SYSTEM	FORMATION	LITHOLOGY	DEPTH
PLEISTOCENE	GLACIAL DRIFT	SAND, GRAVEL, CLAY	0-550
PENNSYLVANIAN	SAGINAW	GYPSUM RED CLAY SHALE, SANDSTONE	550-850
	PARMA	SANDSTONE	850-1000
MISSISSIPPIAN	BAYPORT	LIMESTONE: SOME SANDSTONE	1000-1100
	MICHIGAN	SHALE, ANHYDRITE & DOLOMITE SANDSTONE, LENSES (GAS)	1100-1500
	MARSHALL	WHITE SANDSTONE RED SANDSTONE	1500-1700
	COLDWATER	GRAY SHALE	1700-2500
MISSISSIPPIAN & DEVONIAN	SUNBURY-BEREA-BEDFORD & ANTRIM (UNDIFFERENTIATED)	BROWN SHALE	2500-3100
DEVONIAN	TRAVERSE GROUP	LIMESTONE LIMY SHALE IN LOWER PARTS	3100-3650
	BELL SHALE	GRAY SHALE, LIMY IN BASE	3650-3700
	ROGERS CITY	BROWN SECONDARY DOLOMITE	3700-3735
	DUNDEE	TAN PRIMARY DOLOMITE	3735-

FIG. 1 — GEOLOGIC COLUMN, COLDWATER FIELD.

the edge of the producing area. A total of 81 producing wells and nine dry holes have been drilled with development substantially completed by the end of 1946. Subsequent to 1946, seven producing wells and two dry holes were drilled on the extreme edges of the field.

Oil production rates have been regulated since discovery of the field. The total field allowable was 4600 B/D at the end of 1946 when development was substantially complete, and has varied up to 6700 B/D. Except as influenced by allowable changes, by the end of 1952 oil production had declined slowly to 3600 B/D and water production increased from 1800 B/D to 21,000 B/D. At this time cumulative production was 12,763,000 bbl of oil and 25,800,000 bbl of water, and there were 69 active producing wells.

Since the Rogers City-Dundee has an active water drive, oil production has been accompanied by steadily increasing water production rates. There has been a slight drop in reservoir pressure; however, it has remained above saturation pressure.

Daily oil and water production rates, cumulative oil production, number of producing wells and reservoir pressure are plotted versus time on Fig. 2.

COLDWATER OIL RESERVOIR

STRUCTURE

Fig. 3 shows the Rogers City structure to be an irregularly shaped, gently rounded dome. It is located 15 to 20 miles west of the center of the synclinal axis of the Michigan basin. Regional dip is to the northeast, and, the steepest dips of the Coldwater structure are found along the northeast side of the field with slightly lesser dips toward synclinal re-entrants along the north and south sides of the field. The structure has two axes, the major axes trending northwest-southeast, and the minor axes trending northeast-southwest.

PAY ZONES

Long standing usage by the oil industry of the term "Dundee," to include both the Rogers City and Dundee formations, has resulted in "Rogers City" being an unfamiliar term to many who are well acquainted with its contents and characteristics. This usage developed since, in many areas, the contact between these formations could not easily be determined from cable tool cuttings. With continuing oil development plus a few rotary cores in the Central Michigan basin and quarrying operations in outcrops on the rim of the basin, it

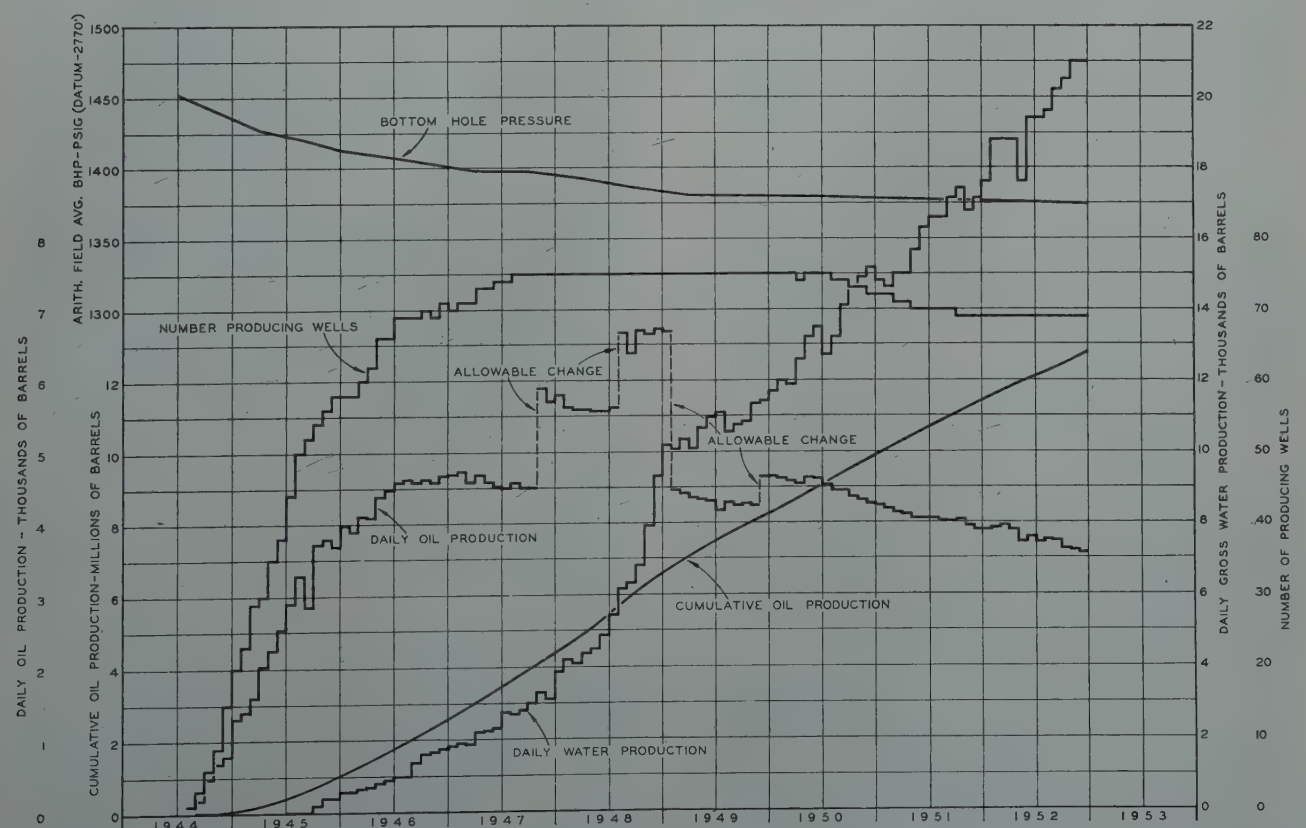

FIG. 2 — DEVELOPMENT, PRODUCTION RATES AND PERFORMANCE DATA, ROGERS CITY - DUNDEE RESERVOIR, COLDWATER FIELD.

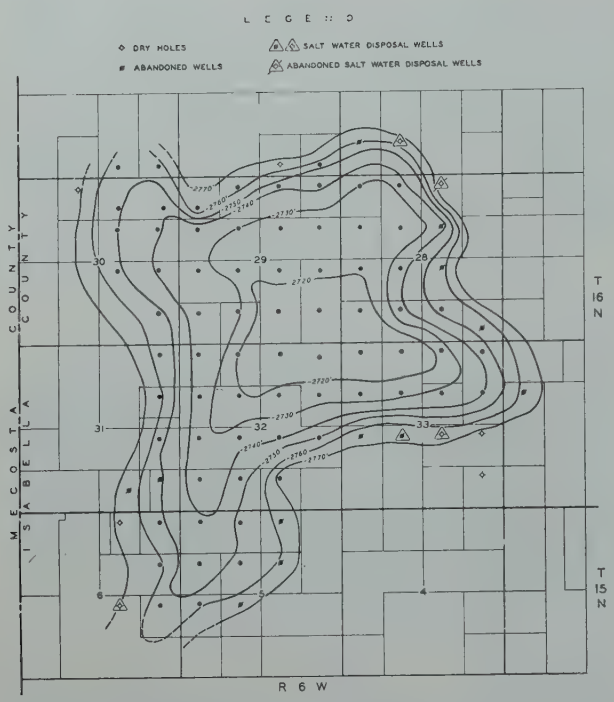

FIG. 3 — STRUCTURAL CONTOUR MAP OF TOP OF ROGERS CITY DOLOMITE, COLDWATER FIELD. CONTOUR INTERVAL, 10 FT.

became increasingly evident that the upper part of this section was separate with locally different characteristics.

The Rogers City is normally a fossiliferous marine limestone, locally altered to a secondary dolomite by brines with high magnesium chloride content moving upward through fractures from the underlying Dundee. At Coldwater the Rogers City is a secondary dolomite 30 to 35 ft thick. The movement of Dundee brine resulted in solution of fossils, recrystalization of minerals and enlargement of fractures. Consequently, the Rogers City contains numerous vugs, many of which are probably connected by erratic and random channels.

Dolomitization of the Rogers City appears to be related to structure in the Dundee and lateral migration of Dundee brines in the Rogers City probably is not extensive. This is suggested by the number of one well pools, some of which have produced large quantities of oil, and where tight non-productive Rogers City limestone has been encountered a short distance off structure.

The Dundee is regionally a porous and permeable primary dolomite. At Coldwater the Dundee is possibly 200 ft thick and has a finer and more uniform texture, and is lighter in color than the Rogers City. Although no wells are completed in the Dundee, the Dundee is believed to constitute approximately 15 per cent of the oil reservoir and to have had a maximum original oil column of 20 to 25 ft in the center of the field and an oil-water contact co-extensive with that found in the Rogers City on the flanks of the field. Cores taken from two wells indicated no barrier to vertical fluid movement at the Dundee-Rogers City contact although they might not be representative of the field.

Elsewhere in many of the Dundee fields, oil has been reported as occurring 30 to 50 ft "below the top of the Dundee." Probably, in some of these fields, the Rogers City is non-productive and the oil is encountered at the top of the Dundee.

Core data at Coldwater was limited to two wells cored with conventional barrels. Matrix porosity measurements average 4.2 per cent for 39 Rogers City core plugs, and 2.5 per cent for 16 Dundee core plugs. The contribution of vugs to the effective porosity in the Rogers City is unknown but probably is appreciable. The contribution of vugs to Dundee porosity is also unknown but probably is negligible, or at least much less than in Rogers City. Horizontal permeabilities ranged from zero to 1368 md and vertical permeabilities from zero to 62 md.

Forty-five ft were cored at one well with 84 per cent recovery and 48 ft cored at the other well with 83 per cent recovery. The lost section at both wells is presumed to have been vugular sections too fragile to have been preserved during coring.

Diamond coring, which was not practiced in Michigan until several years after development of Coldwater, has been successful in effecting practically complete recovery of Rogers City sections at other fields, presumably with sections very similar to that at Coldwater.

Electric logs of the Rogers City and the upper Dundee taken at two wells are shown in Fig. 4. Drill stem test data for the zones indicated on the electric log of Sohio-F. L. Hoffman No. 2 are listed in Table 1.

TABLE 1 — ROGERS CITY - DUNDEE DRILL STEM TESTS
SOHIO - F. L. HOFFMAN NO. 2

Test	A	B	C
Depth	3764-77	3780-90	3790-3800
Tool Open	12 min	7 min	60 min
Recovery:			
	(Flowed Oil)		
Oil	1000 ft	270 ft	15 ft
Water	90 ft	20 ft	540 ft
Mud	0	0	30 ft
Shut-in BHP	1410 psi	1430 psi	1410 psi

DRILLING AND COMPLETION PRACTICES

Most of the oil wells in the Coldwater Field were drilled with combination rotary and cable tools. The usual practice was to start with rotary tools and to set 10¾-in. casing through the Glacial Drift, which is approximately 550 ft thick in the Coldwater area. The hole was then drilled to a point in the Coldwater shale approximately 20 ft below the Marshall water sand. The Coldwater shale was competent and provided a safe casing point for cementing and deeper drilling. Seven in. casing was set through the Marshall at a depth of

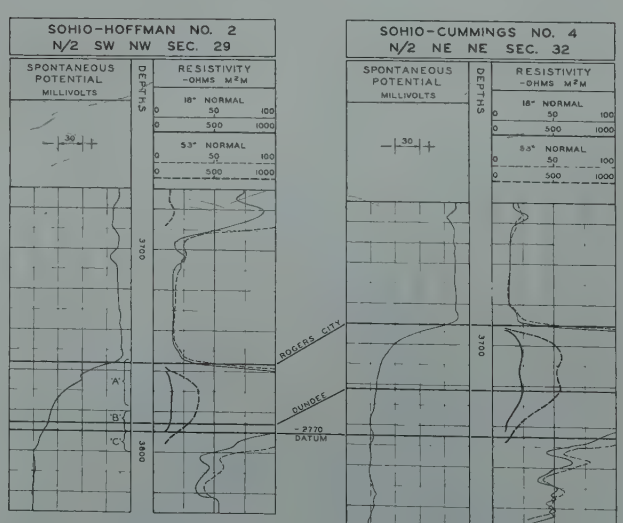

FIG. 4 — ELECTRICAL LOGS OF ROGERS CITY AND TOP OF DUNDEE FORMATION, COLDWATER FIELD.

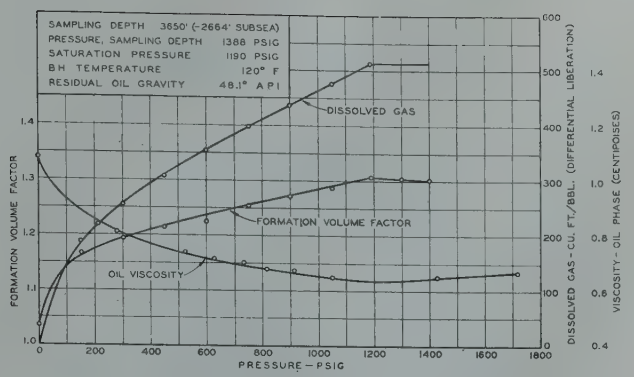
SAMPLING DEPTH 3650' (-2664' SUBSEA)
PRESSURE, SAMPLING DEPTH 1388 PSIG
SATURATION PRESSURE 1190 PSIG
BH TEMPERATURE 120° F
RESIDUAL OIL GRAVITY 48.1° API
DISSOLVED GAS
FORMATION VOLUME FACTOR
OIL VISCOSITY
FORMATION VOLUME FACTOR
DISSOLVED GAS - CU. FT./BBL. (DIFFERENTIAL LIBERATION)
VISCOSITY - OIL PHASE (CENTIPOISES)
PRESSURE - PSIG

FIG. 5 — BOTTOM HOLE SAMPLE ANALYSIS, COLDWATER FIELD.

1700 ft and cemented with sufficient fillup to protect the Michigan Stray gas sand at 1400 ft. Rotary tools were then replaced by standard rig and the hole was drilled dry on down to the top of the Rogers City where 5½-in. casing was set and cemented. An open-hole completion was then made by drilling the pay zone with cable tools strung through a lubricator. The pay was penetrated by stages until flowing tests through casing indicated satisfactory productivity. Penetration of the Rogers City zone averaged 11 ft.

Of a group of 55 wells, 45 were drilled by combination tools and 10 were drilled with rotary tools to the Rogers City. An intermediate 7-in. string was not set at the latter wells and the production string was stage cemented to protect the Michigan Stray gas sand. In two of the 10 wells drilled by rotary, pipe was set through the Rogers City and the wells completed by perforating the casing opposite the pay zone. Cable tools were moved in for completion after setting a production string on the top of the Rogers City in the remaining eight rotary holes.

One of the two rotary holes penetrating the Rogers City was drilled to a total depth of 5090 ft for an unsuccessful test of the Richfield zone of the Detroit River series. Due to completion method, electric logs and cores of the Rogers City were taken in only two wells.

Drilling time, from spud date to casing point, averaged 49 days for combination tools and 34 days for rotary tools. The 49 days for the combination tools includes time spent off bottom while moving out rotary tools, and waiting on and rigging up cable tools.

Except for penetrating the Glacial Drift at certain wells, no unusual drilling problems were encountered. Buried gravel beds in the Drift frequently caused lost circulation.

A number of wells were acidized upon completion but acid was used sparingly and only to obtain satisfactory productivity where the well-bore apparently penetrated a locally tight section. Certain wells were acidized subsequent to completion when performance indicated low productivity.

PRODUCTION PRACTICES AND PROBLEMS

By the end of 1952, 7,100,000 bbl of oil, or 56 per cent of the field recovery, had been produced by flowing wells, and there were 13 water-free flowing wells remaining. All wells flowed until a water cut of 5 to 10 per cent was reached. Paraffin deposition in the upper part of the tubing string at flowing wells necessitated frequent scraping with paraffin hooks. Plugging of chokes by loose paraffin required almost daily attention but was not a difficult problem. Very little trouble has been experienced with paraffin in flow lines.

Wells producing water have been pumped with conventional units and rods, with fuel provided from separator gas. Water production increased rapidly in most wells after its first appearance, and it has been necessary to handle large volumes of produced salt water. Temporary surface ponding of salt water was avoided due to danger of contamination of streams originating in the field and fresh water sands in the Glacial Drift. During the early life of the field, produced salt water was injected into dry holes beyond the productive limits and into a shallow water sand below the Glacial Drift. A field system using asbestos-cement pipe was eventually installed in which the water flowed by gravity to a central point and was then pumped to a concrete storage pit from which it flowed by gravity into dry holes deepened to lower zones for disposal.

RESERVOIR FLUIDS

As determined by analysis of a bottom-hole sample taken at 3650 ft the Rogers City reservoir oil at Coldwater has a saturation pressure of 1190 psi, a solution GOR (differential liberation) of 512 cu ft/bbl, and a formation volume factor of 1.306 at saturation pressure. The compressibility factor of the oil was 12.5×10^{-6} at 1400 psi. The reservoir temperature was 120° F. Data from this sample analysis are shown on Fig. 5.

Stock tank oil, produced water, and separator gas analyses are shown in Tables 2, 3, and 4.

TABLE 2 — STOCK TANK OIL ANALYSIS — COMPOSITE SAMPLE, ROGERS CITY RESERVOIR

Gravity	48.6° API
Pour Point	–30° F
Viscosity at 100° F	34 SSU
Salt	6.2 lbs/1000 bbl
Total Sulphur	0.23%
Sulphur as H_2S and Mercaptens	191.4 lbs/1000 bbl

TABLE 3 — PRODUCED WATER ANALYSIS — ROGERS CITY RESERVOIR

Specific Gravity 60/60	1.216	
pH	4.8	
Ion Analysis:		
SO_2	3	ppm
R_2O_3	4	ppm
Ca	30,410	ppm
Mg	5,260	ppm
Na	56,960	ppm
HCO_3	48	ppm
SO_4	154	ppm
Cl	158,390	ppm
TOTAL	251,229	ppm

TABLE 4 — AVERAGE SEPARATOR GAS SAMPLE ANALYSES (20 PSIG)

Component	Mol %
N_2	3.7
CO_2	0.1
C_1	52.8
C_2	24.0
C_3	13.4
nC_4	2.8
iC_4	1.7
nC_5	0.5
iC_5	0.5
C_6+	0.5
TOTAL	100.0

RESERVOIR PRESSURE

Bottom-hole pressure surveys taken at six-month intervals during the first five years of production indicate that the Rogers City reservoir has an effective water drive. The bottom-hole pressure curve plotted on Fig. 2 represents the arithmetical average of pressures observed at 14 centrally located wells. The average pressure

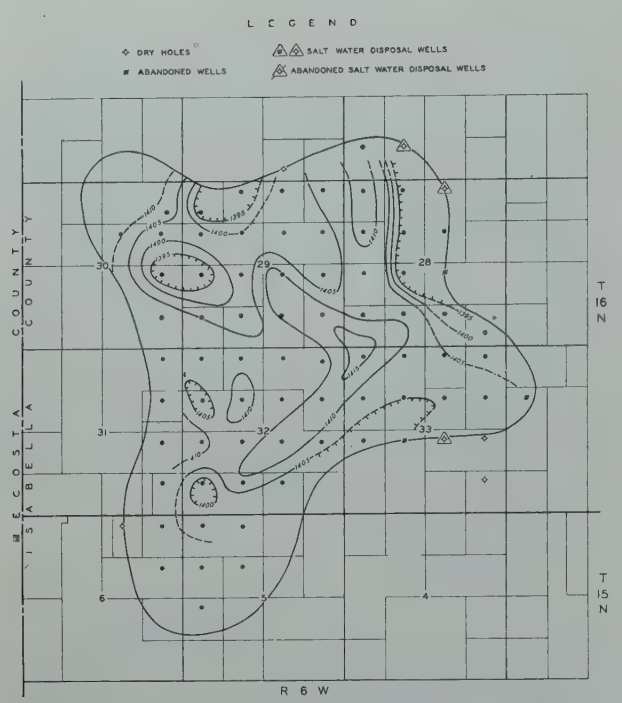

FIG. 6 — BOTTOM HOLE PRESSURE CONTOURS, AUG., 1946, COLDWATER FIELD. CONTOUR INTERVAL 5 PSI SUBSEA DATUM — 2770 FT.

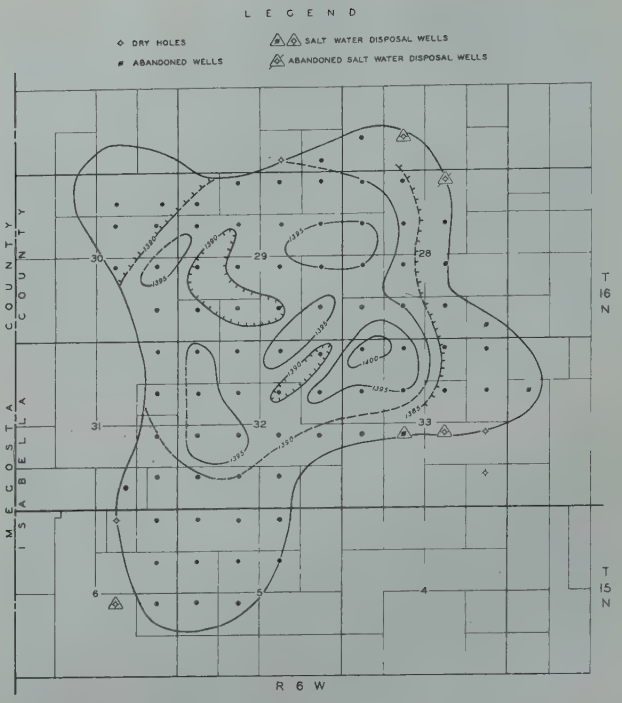

FIG. 7 — BOTTOM HOLE PRESSURE CONTOURS, MAR., 1948, COLDWATER FIELD, CONTOUR INTERVAL 5 PSI SUBSEA DATUM — 2770 FT.

of the 14-well group was within ± 3 psi of each of the areally weighted average pressures computed for surveys through 1948, each of which included from 40 to 50 wells. Pressures were taken only at flowing wells and, after 1948, calculation of areally weighted averages became unsatisfactory due to the gradually decreasing number of wells available for observation.

The bottom-hole pressure has dropped from 1453 psi initially to 1378 psi at the end of 1952. This drop appears to be insignificant and reflects, for the most part, readjustments of pressure within the pool necessary before the water drive could become effective. The pressure has stayed well above the bubble point and no free gas has been produced.

Bottom-hole pressure contour maps for Aug., 1946, and Mar., 1948, are shown on Figs. 6 and 7. The pressures are corrected to a datum of –2770 ft subsea which is the assumed original oil-water contact. These maps, which are contoured at 5 psi intervals, suggest slightly higher pressures near the center but little overall difference throughout the field.

WATER ENCROACHMENT

Since the field is possibly being produced by a combination of edge and bottom water drives, an investigation was made of encroachment independent of location upon structure. Assuming a uniform rise in the oil-water contact, appearance of water should correlate with relative elevation of the lowermost exposed pay section in the wells. Results of the investigation are shown in Fig. 8 which provides a comparison of the calculated rise in the water table versus appearance of water in the wells.

The appearance of water was determined as the date of reaching 10 per cent water cut. Subsea total depths for open hole completions, and the bottom of producing perforations for the two completions with pipe set through the pay, were plotted versus field cumulative recovery at the time the water cut at the plotted well reached 10 per cent.

The calculated rise in water table suggested by the line on Fig. 8, which is independent of observed water appearances, was obtained by assuming average acre-foot recoveries for the Rogers City and Dundee, and then finding the hypothetical number of acre-feet flooded, and the corresponding position of the rising water table which was assumed to remain horizontal.

The observed, or plotted data, are erratic and seem to establish a trend above the calculated position of the water table; however, at the end of 1952, one-third of the oil and two-thirds of the water were being produced by wells with total depths below –2750 ft, or well below either the calculated water table or the trend of plotted data. Obviously, the rising water table is neither horizontal, nor does it have sufficient definition to permit reliable estimation of the flooded-out volume of the reservoir at this stage of field depletion.

The principal utility of data on Fig. 8 is in attempting to analyze well performance and to relate seemingly

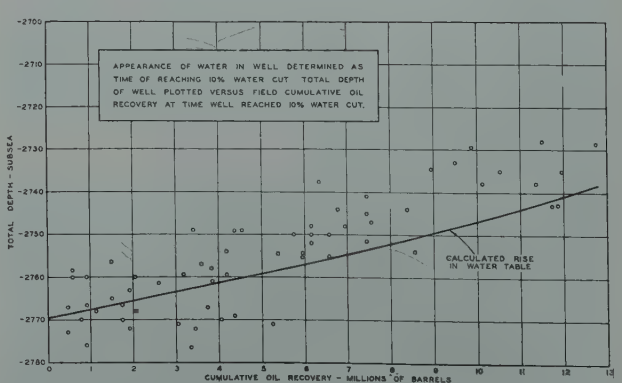
APPEARANCE OF WATER IN WELL DETERMINED AS TIME OF REACHING 10% WATER CUT. TOTAL DEPTH OF WELL PLOTTED VERSUS FIELD CUMULATIVE OIL RECOVERY AT TIME WELL REACHED 10% WATER CUT.
CALCULATED RISE IN WATER TABLE
TOTAL DEPTH - SUBSEA
CUMULATIVE OIL RECOVERY - MILLIONS OF BARRELS

FIG. 8 — RISE IN WATER TABLE, COLDWATER FIELD.

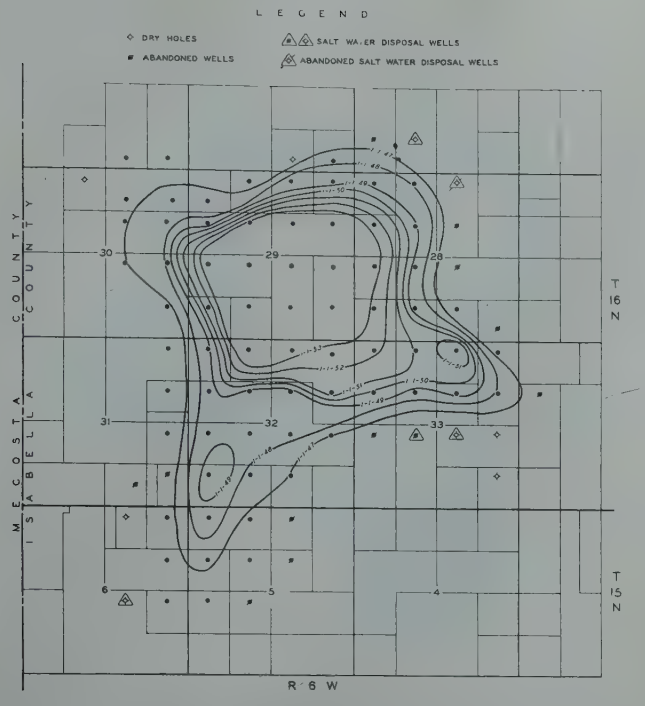

FIG. 9 — DATE OF FIRST WATER PRODUCTION AT WELLS, COLDWATER FIELD.

premature or late water appearance to such factors as structural position, total depths, effect of acidization, possible concentration of fractures, and isolated pay lenses. The wells appearing below the line on the lower left corner of Fig. 8 represent either late edge well completions or non-typical wells which may have penetrated pay lenses with porosity pinchouts updip and which had locally lower oil-water contacts than the main reservoir.

The majority of the wells fall above the line of calculated water table rise and indicate either one or more of the following:

1. A breakthrough in advance of the oil-water interface.
2. The transition zone between the water-free and flooded zones is on the order of 10 to 15 ft.
3. The principal routes of water invasion underline the center of the field.
4. The assumptions for calculating the rise are incorrect and the rise should be different than shown.

The authors feel the divergence between the trends probably results from a combination of the first three reasons. Since the Dundee is believed to be the aquifer and dolomitization of the Rogers City probably is confined to the vicinity of the structure, the total effect of water movement should be vertical. Probably there is a maze of permeable zones and intersecting fractures which could result in lateral movement over limited distances. The bottom-hole pressure maps shown on Figs. 6 and 7 indicate slightly higher pressure in the center of the field, suggesting better vertical communication in that area.

As to the fourth reason, it already has been shown that the assumption of a horizontal and definite oil-water contact cannot be justified.

Progressive water encroachment by years is shown on Fig. 9, which is contoured on the date of first water production. Fig. 9 shows a reasonably uniform pattern with contours approximating but not paralleling structural contours. Since total depth probably is the principal factor controlling first appearances of water, there is no necessary relationship between the water encroachment and the structure. The isolated closed contour in the SW/4 of Section 32 represents a well whose total depth is at a higher subsea elevation than any well south of the middle of Section 32, and where, as expected, water appeared later than at other wells in the area.

The closed contour in the NE/4 of Section 33 does not represent a similar situation since the total depth of the well enclosed by the contour is 7 ft lower subsea than the total depth of its west offset, which produced water earlier. Such irregularities may be related to proximity of vertical fractures to well bores, or to partial isolation by dense impermeable barriers which force the encroaching water into tortuous channels.

Figs. 10, 11, 12, and 13 are contoured on per cent water produced by each well at two-year intervals starting Jan., 1947. All of the wells included by the zero per cent contour were flowing at the date of the maps. Fig. 10 represents the encroachment status shortly after full development of the field. Figs. 11 and 12 show anomalies developing. The well in the SW/4 of Section 32 is the one which had the late water arrival mentioned in the preceeding paragraph.

The well two locations east, shown as making between 60 per cent and 80 per cent water on Fig. 12, is the lowest well in the field. It topped the Rogers City 2 ft below the oil-water contact for the rest of the field and its water-oil ratios have lagged behind those of other edge wells. It may be completed in an isolated pay lens which had a locally lower oil-water contact trapped by a porosity pinchout updip. Fig. 13 shows continued encroachment toward the center of the field, approximating but not paralleling structural contours.

RECOVERY EFFICIENCY

A reliable estimate of the recovery efficiency of the natural water drive at Coldwater would be desirable.

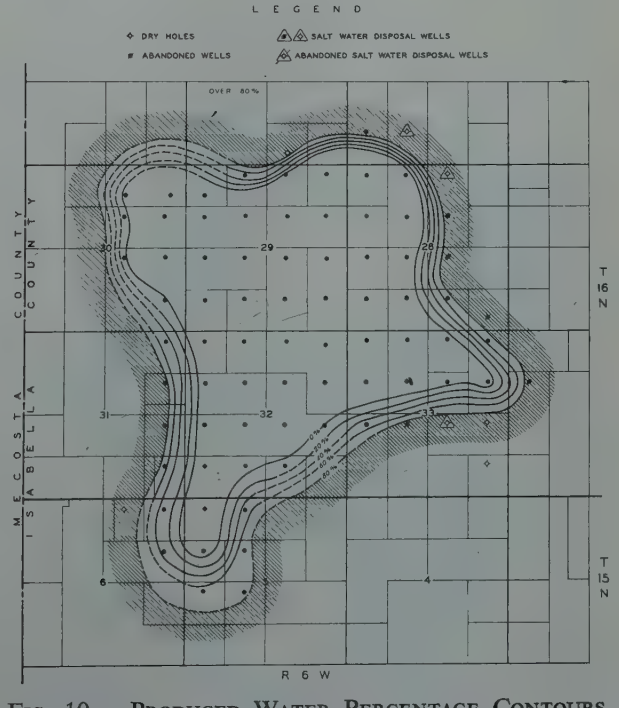

FIG. 10 — PRODUCED WATER PERCENTAGE CONTOURS, JAN., 1947, COLDWATER FIELD. CONTOUR INTERVAL 20 PER CENT.

FIG. 11 — PRODUCED WATER PERCENTAGE CONTOURS, JAN., 1949, COLDWATER FIELD. CONTOUR INTERVAL 20 PER CENT.

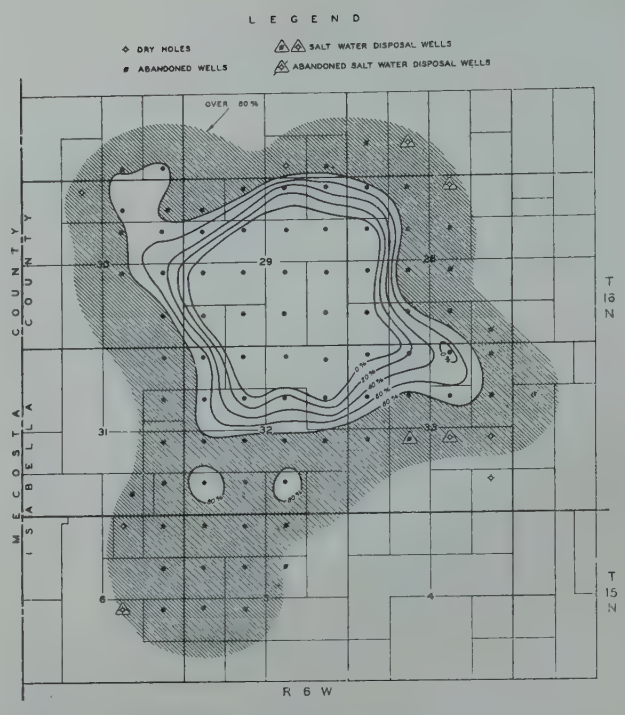

FIG. 12 — PRODUCED WATER PERCENTAGE CONTOURS, JAN., 1951, COLDWATER FIELD. CONTOUR INTERVAL 20 PER CENT.

Unfortunately, there are too many imponderables to permit an accurate estimate of total effective porosity and the original oil in place by volumetric calculations. Since the oil is undersaturated and the drop in reservoir pressure has been only on the order of 5 per cent, the change in density of the reservoir fluids has been too small to permit a satisfactory estimate of oil in place by means of material balance equations. However, well performance can be used to estimate the ultimate recovery for the field which can be related to the limited available core data to narrow the speculative ranges of recovery efficiency.

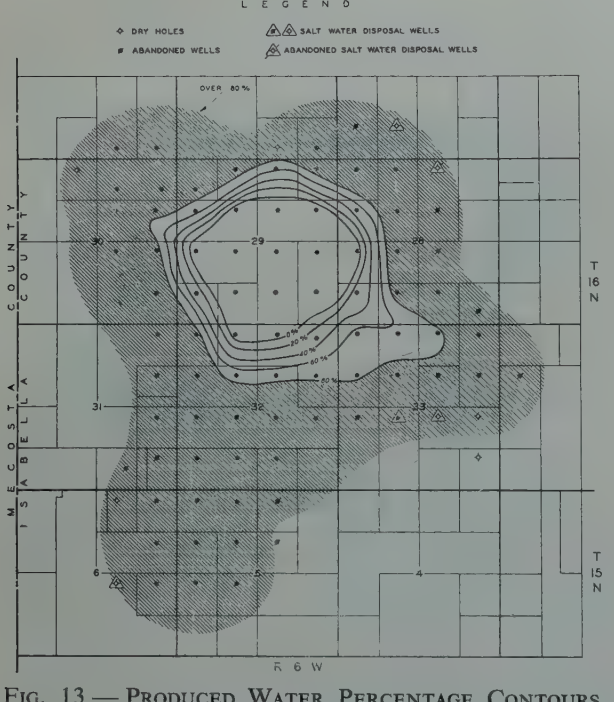

FIG. 13 — PRODUCED WATER PERCENTAGE CONTOURS, JAN., 1953, COLDWATER FIELD. CONTOUR INTERVAL 20 PER CENT.

The authors estimated the field ultimate recovery to be on the order of 17½ million bbl by use of individual well oil and water production trends where applicable and analogy based on structural position and gross pay volume for those wells making either no water, or having no discernable trend due to insufficient water production history. To enable calculation of the water-table rise shown on Fig. 8 in which cumulative recovery is related to reservoir volume flooded, the Rogers City was assumed to have a gross pay volume of 76,800 acre-ft and an average ultimate recovery of 215 bbl/acre-ft. The Dundee was assumed to have a gross pay volume of 13,200 acre-ft and an ultimate recovery of 75 bbl/acre-ft.

As a matter of interest, these acre-ft recoveries would be equivalent to 60 per cent recovery in the Rogers City if 7 per cent total effective porosity and 15 per cent original water saturation are assumed, and 65 per cent recovery in the Dundee if 2.5 per cent effective porosity and 20 per cent original water saturation are assumed.

The authors feel that, while recovery efficiency is speculative, the average ultimate acre-feet recovery can be resolved within reasonable accuracy from well performance.

ACKNOWLEDGMENTS

The authors wish to thank the Michigan Department of Conservation whose many cumulative contributions to field records have enabled the writing of this paper. They also wish to express their appreciation to the management of the Sohio Petroleum Co. for both the encouragement and permission to prepare and present this paper. ★ ★ ★

FILTRATION FROM MUD DURING DRILLING

C. K. FERGUSON
J. A. KLOTZ
JUNIOR MEMBERS AIME

CALIFORNIA RESEARCH CORP.
LA HABRA, CALIF.

T. P. 3749

ABSTRACT

This paper describes experimental investigations conducted at the California Research Corporation's model oil well.

The first part describes filter loss from several drilling muds through bore hole walls during mud circulation and drill string rotation. The effect of mud properties and drill string rotation with mud circulation is described. Filtration from a bore hole full of drilling mud, not circulating, but under pressure for extended time periods, is also discussed.

The second part describes filter loss to permeable formations from beneath a drilling bit where filter cake has no opportunity to develop appreciable thickness. If potential flow theory is applied to predict filtrate invasion from this hole bottom, large invasions are calculated. But model well experimentation shows that filtrate invasion from the hole bottom is controlled by mud particles that penetrate the formation ahead of the bit. This experimentation provides data to estimate the effect of mud particle penetration on fluid loss to formation.

The third part presents an estimate of mud filtration during drilling of a well.

INTRODUCTION

As oil wells are drilled by the rotary method, drilling mud circulates up the annulus between drill pipe and well wall. Drillers adjust mud density so that the pressure at the bottom of the mud column is several hundred psi greater than the pressure of reservoir fluid. As a result of this pressure difference, the liquid part of the mud filters into the rock around the bore and mud solids deposit as a filter cake on the well wall.

For many reasons the petroleum industry, within the past 20 years, has spent much money and energy to determine the volume of mud filtrate that enters rock around the well bore and dedicated much research effort to reduce this volume.

Among the reasons for attempts to determine the volume of mud filtrate and to reduce this volume are the following:

1. If filtrate damages the permeability of oil sand, the resultant damage to oil well productivity will depend on the distance that the filtrate invades the oil sand; reduction of filtrate volume may, therefore, increase well productivity.

2. Filtrate that penetrates shale sections may cause the shale to swell and to slough into the well bore. Uncontrolled sloughing may stick drill pipe. Reduction in filtrate volume may reduce drilling trouble.

3. Electric log resistivity curves are changed by invasion of a mud filtrate; the change depends on the depth to which filtrate invades. Knowledge of this depth is necessary before resistivity logs can be interpreted accurately.

For these reasons, specifications that place an upper limit to drilling mud filter loss are now written into almost all drilling programs. These specifications are based on API Recommended Practice 29, Standard Field Procedure for Testing Drilling Fluids,[1] which describes a static filtration test operated at 100 psi filtration pressure and at ambient temperature. Although this test is adequate for mud control, it cannot be used to compare filtration properties of different muds. Schremp and Johnson[2] showed, for example, that mud with a low API filter loss does not necessarily have low filter loss at bottom hole temperature and pressure. Also, no information has been available about the effect of bottom hole mechanics (mud circulation, drill string rotation, and bit action) on mud filtration.

This paper discusses filtration data measured in the California Research Corporation's model oil well, which models closely oil well bottom hole geometry and hydrodynamic conditions. The filtration processes that

[1]References given at end of paper.

Manuscript received in the Petroleum Branch office Aug. 6, 1953. Paper presented at the Petroleum Branch Fall Meeting at Dallas, Tex., Oct. 19-21, 1953.

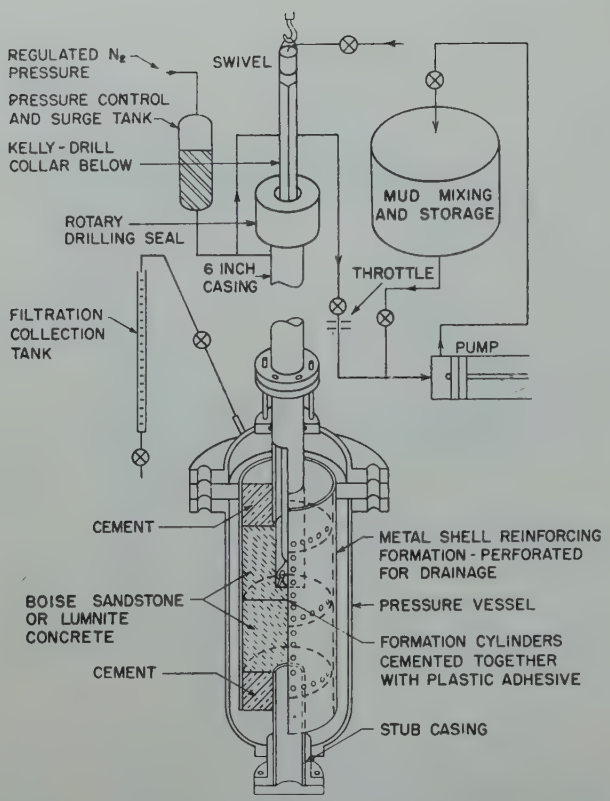

FIG. 1 — MODEL WELL PIPING AND EQUIPMENT

were studied are divided into three classes: (1) Static filtration — mud does not circulate, filtration rates are controlled by cake permeance; cake thickness increases and filtration rate decreases continually with time; (2) Dynamic filtration — drilling mud circulates past the surface of the filter cake; filtration rate is controlled by cake thickness; cake thickness and filtration rate become constant depending on mud circulation and on drill string rotation; (3) Filtration from beneath the bit while drilling — no filter cake forms beneath the bit; filtration is controlled by plugging of the formation ahead of the bit by mud particles.

Filtration beneath the bit is controlled by formation properties and drilling speed as well as by mud properties, whereas static and dynamic filtration are controlled almost entirely by mud properties. Experimental and analytical methods used to study filtration beneath the bit differ, therefore, from the methods used to study dynamic and static filtration.

Thus this paper is divided into three parts. Part I describes the model well equipment and methods used to measure static and dynamic filtration, and discusses these kinds of filtration; Part II discusses filtration beneath the bit; and Part III presents an illustrative estimate of total filtrate invasion.

PART I — FILTRATE INVASION THROUGH FILTER CAKE ON THE BORE WALL

APPARATUS AND METHODS

In the model well, where the measurements were made, bottom hole mechanics and hydraulics are approximated closely. A drill string may be rotated, a formation drilled, and mud circulated at rates and pressure differences that are close to those used in field wells. Changes in the filtration process that are caused by changes in bottom hole mechanics and hydraulics should be the same in field wells as those measured at the model well.

The model well has been described briefly in trade journals[3,4] and to supplement these descriptions, equipment used to measure static and dynamic filtration is described below. A description of the equipment used to measure filtration beneath a drilling bit is included in Part II of this paper.

Model Well

The model well consists of a sandstone formation, suspended inside a pressure vessel, and the equipment for conducting operations, with full scale tools, similar to those performed in field wells. Field well geometry and pressure differences are duplicated in the model well, but absolute pressures are not duplicated and no temperature control is provided. Fig. 1 shows the arrangement of equipment and piping.

Formation and Pressure Vessel

The model well formations that were used for static and dynamic filtration measurements were cast of Lumnite cement and sand. Lumnite cement is a blast furnace slag cement which is similar to Portland cement but reaches working strength within 24 hours. The sand ranged in size from 28 to 100 Tyler mesh. Each concrete formation was cast in the form of a cylinder, 10 ft long and 19 in. outside diameter, inside a perforated steel shell.

Reinforcing rings around the outside of the shell prestressed the concrete cylinder so it was able to withstand mud pressures in the well bore of 500 psi. Short sections, 4 ft long, of 6⅝-in. OD casing, called stub casings, were cast into each end of the cylinder. The formation was hung in a steel pressure vessel near the bottom of a 45-ft deep clearance hole. The 6⅝-in. casing, which extends from the top of the upper stub casing to the surface, together with the borehole in the formation constitutes a 45-ft well with 6 ft of exposed formation in which drilling and completion operations may be conducted.

Drilling Tools

The drilling equipment at the model well includes a short drill string that consists of a kelly and a drill collar. A standard 66-ft API derrick and an air-driven winch provide for raising and lowering the drill string. A 5½ by 14-in. mud pump, driven through a four-speed truck transmission, provides drilling mud circulation at flow rates between 20 and 350 gal/min.

Dynamic and static filtrations were run at a filtration pressure of 200 or 400 psi. Dynamic pressure was controlled by two ⅝-in. orifices and a 3-in. gate valve in series in the mud return line. At 100 gm/min, about 300 psi pressure drop occurred across the two orifices, and the gate valve controlled the remaining 100 psi pressure drop. Because the mud pump discharge rate was not uniform, mud pressure varied between about 390 and 410 psi despite a surge chamber in the line. During static filtration, mud pressure was maintained by nitrogen pressure applied through a regulator to the top of the mud pressure control tank.

A 10-in. rotary table rotates the drill string at 45, 90, 180, or 370 rpm. For all experiments reported here, the table rotated at either 45 or 90 rpm.

Standard oil field rock bits were used to drill the formations. No attempt was made, however, to standardize on one brand of rock bit or to differentiate between brands.

Test Procedure

After a new formation was cast and mounted in the pressure vessel, the formation was water saturated by a method similar to the standard laboratory evacuation and immersion method. The formation, pressure vessel, and adjacent piping were evacuated for about five hours with a mechanical pump; then, water under 60 psi line pressure was admitted to the pressure vessel. The completeness of saturation was checked by observing the compressibility of the system. One hundred psi air pressure was applied to the top of the mud pressure reservoir, and the volume of air remaining in the formation was estimated by observing the drop in liquid level in the mud pressure reservoir. For each new formation, residual air saturation was less than 2 per cent.

When saturation was complete, the formation was drilled with a 5¼ or 5⅝ rock bit. Because Lumnite cement seriously contaminates drilling mud, the formations were drilled with water as a drilling fluid. Except for beneath the bit filtration that is discussed in Part II of this paper, drilling was not considered part of the filtration experiment.

After drilling, water was drained from the well bore and mud circulation started. Mud circulation rates and circulation pressure were regulated by governing the pump speed and by adjusting the throttle valve. Then the filtrate line valve was opened to start filtrate collection. During dynamic filtration, the drill string rotated with the bit in the bottom stub casing so that the filtration reported here resembles filtration through the sides of a well bore just above the bit. At the end of dynamic filtration, the drill string was pulled, the master gate valve at the top of the casing string closed, and static filtration pressure was applied by admitting nitrogen to the top of the mud pressure tank.

Filtrate, or water forced out of the formation by filtrate, collected in calibrated gauge tanks. Filtrate volume was measured and recorded periodically: every 15 minutes at the start of dynamic filtration and hourly after the filtration rate decreased.

Filtration Hypotheses

Examination of drilling mud filtration reveals several paradoxes, and derivation is not possible of an exact theory that will describe either static or dynamic filtration. The first paradox is that static filtration follows part of the "classic" filtration theory but does not follow all of this theory. "Classic" filtration theory is considered here to be the theory outlined in chemical engineering texts[5] that may be summarized with the equation, Filtrate volume = constant • (time).$^{0.5}$

The second paradox is that equilibrium cake thickness during dynamic filtration is much less than predicted by comparison of the filtration forces, which deposit cake, and the hydraulic erosion forces, which remove cake.

A third paradox is that oil base muds exhibit substantial filter loss while they are circulating, but as soon as circulation stops, filtration stops; although no measurable filter cake is deposited. To reconcile these paradoxes, speculative ideas about mud filtration are presented in this section. In the next two sections dynamic and static filtration measurements made at the model well are discussed in the light of these ideas.

Static filtration of drilling mud in one respect follows the "classic" filtration law, but in another respect does not. As described in reference 5, this law states that the volume of filtrate collected will be proportional to the filter cake permeability and to the filtration pressure; the law also states that a plot of filtrate volume as a function of (time)$^{0.5}$ is a straight line as long as cake permeability and filtration pressure are constant.

For many muds, filtration at constant pressure results in a straight line plot of filtrate volume as a function of (time),$^{0.5}$ thus cake permeability appears constant for these muds. For these same muds, however, filtration is almost independent of filtration pressure. This independence indicates that cake permeability is not constant but that it decreases with increasing pressure. From one viewpoint, therefore, filter cake permeability is constant but from another viewpoint, cake permeability varies with pressure.

Fig. 2 shows calculated filtration for two filter cakes: one of nearly constant permeability (the bottom curve), and the other for a cake with a permeability that decreases with increasing pressure (the upper two curves). These calculations were made as follows: The filter cake was assumed to exist in thin layers. The permeability, k_i, of each layer was assumed to depend on the pressure gradient, p_i, in that layer at the time it was deposited, according to the equation,

$$k_i p_i^n = \text{constant} \quad . \quad . \quad . \quad . \quad . \quad . \quad . \quad . \quad . \quad . \quad . \quad (1)$$

As cake thickness increases, while total filtration pressure remains constant, p_i becomes smaller, and k_i larger, for each succeeding layer of filter cake.

For the lower curve of Fig. 2, the exponent "n" was assumed to be 0.2 so that cake permeability is almost independent of p_i. This curve is almost straight and is similar to the plot of filtration data for many muds. For the upper two curves, the exponent "n" was assumed to be 0.8 so that the product $(k_i\, p_i)$ is nearly constant; the 30-minute filtrate volume increases only

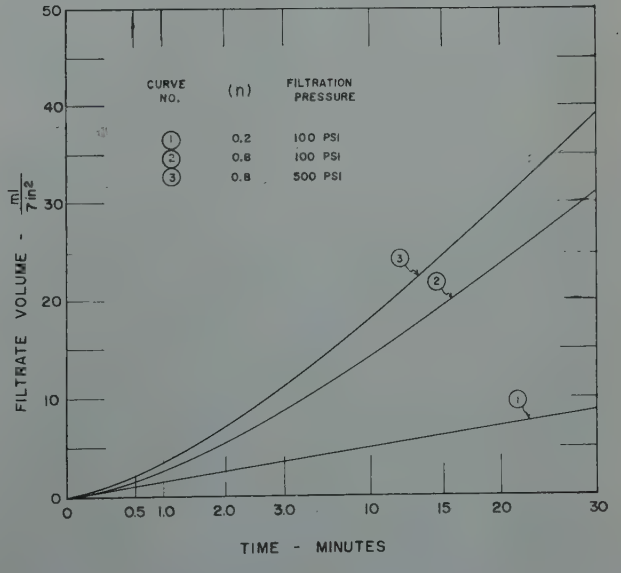

Fig. 2 — Calculated Filtration for Compressible Filter Cake. $k_i p_i^n$ = constant; at $p_i = 10^5$ psi/in., $k_i = 10^{-3}$ md.

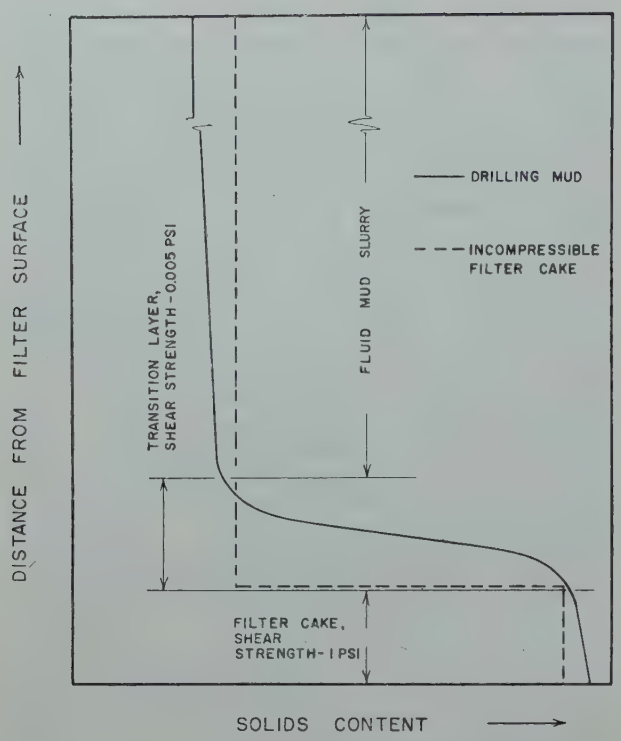

FIG. 3 — TRANSITION LAYER BETWEEN DRILLING MUD FILTER CAKE AND FLUID MUD.

25 per cent although filtration pressure is increased from 100 to 500 psi. This independence of filtrate volume from filtration pressure is observed in many muds. But the filtration data from these muds plot as straight lines, whereas the upper two curves of Fig. 2 are not straight.

The resistance offered by the low permeability filter cake may not, however, be the only resistance to removal of filtrate from the mud slurry. A portion of this resistance may be caused by gelation of the mud. This added resistance, increasing with time as mud gel strength increases, may reduce the volume of filtrate so that the volume-(time)$^{0.5}$ curve is bent back to approach a straight line even though the exponent, "*n*." of Equation (1) is near unity. The upper curves of Fig. 2 would be straightened, therefore, even though cake permeability was not constant. Because mud gelatin probably is little affected by pressure changes, the volume of filtrate will not change much as filtration pressure increases. This idea of added resistance, caused by mud gelation, to the removal of filtrate from the slurry is presented here as a possible explanation of the static filtration paradox.

This mud gelation hypothesis may also be used to explain partly the high filtration rates that are measured while mud is circulating. In a slurry that is filtering according to "classic" theory, the solid and liquid parts of the slurry move toward the filter cake at the same linear velocity. But in a slurry with gel strength, the liquid part of the slurry moves toward the filter cake at a higher velocity than the solid part; liquid flows with respect to solids throughout the entire slurry.

Because of this flow, filtration from a slurry with gel strength will be less than from a similar slurry with no gel strength, even though the two slurries have filter cakes with equal permeability. Conversely, filtration from a slurry with gel strength will be greater if the gel is continually broken by agitation than if the slurry filters statically. A larger volume of filtrate does flow from mud that is circulating than from mud that is static. This has been observed by Prokop[6] and Williams[7] as well as in the work reported here.

Prokop[6] discussed erosion of filter cake by flowing mud as a possible mechanism that limits the thickness of the filter cake. But for mud flow to erode filter cake on the well wall, hydrodynamic shear at the well wall must be about equal to the shear strength of the mud cake. For hydrodynamic shear to exceed the cake shear strength, which ranges between 0.3 and 15 psi, drilling fluid would have to circulate in typical holes under a pressure gradient of 3 to 150 psi/ft. Three psi/ft is 100 times greater than the hydrodynamic pressure gradients stated as typical by Beck, Nuss, and Dunn.[8] Apparently hydrodynamic shear is not great enough to erode mud cake.

A consequence of the relationship between gelation and filtration is that the surface of mud filter cake is not sharply defined. Fig. 3 shows the solids content as a function of distance from the filter surface for a classic incompressible filter cake and for a drilling mud filter cake. The interface between classic cake and slurry is defined sharply; the solids concentration increases abruptly from the slurry to the cake.

For mud, however, the interface between the slurry and cake has finite thickness. The solids content increases gradually from the slurry to the cake through a transition region that may be ⅛-in. thick. Fig. 3, as drawn here, is qualitative; the curves apply to no particular mud. But Grace[9] shows a similar curve that was plotted from measurements made on a filter cake of finely divided calcium carbonate.

This transition region influences dynamic filtration and may account for the apparent equilibrium filter cake thickness observed in dynamic filtration. Whereas shear strength of the cake is so high that hydrodynamic shear does not disturb it, shear strength of the upper part of the transition layer is only about 0.005 psi. This layer can be removed, therefore, by fluid flowing under a pressure gradient that is typical of mud flow.[8] During dynamic filtration, this transition layer is swept away continually and cake thickness is limited even though fluid shear does not erode the dense part of the cake.

The dynamic and static filtration data presented in this part of the paper do not permit quantitative evaluation of the hypotheses presented in the preceding paragraphs but the data will be discussed in the light of these hypotheses.

DYNAMIC FILTRATION

As long as drilling mud circulates or the drill string rotates, mud filters under dynamic conditions. Flowing mud continuously disrupts gelatin and erodes the low shear strength transition layer that exists between solid mud cake and fluid mud.

As filter cake becomes thicker, the filtration pressure gradient through the transition layer decreases until the pressure holding the transition layer against the cake is as low as the hydrodynamic wall shear tending to tear this layer from the cake. Eventually deposition and erosion become equal, and cake thickness and the rate of filtration through the cake become constant.

Dynamic filtration rates were measured for four drill-muds: a bentonite-barytes mud, an oil base mud, a lime-starch mud, and a tall oil emulsion mud. Figs. 4,

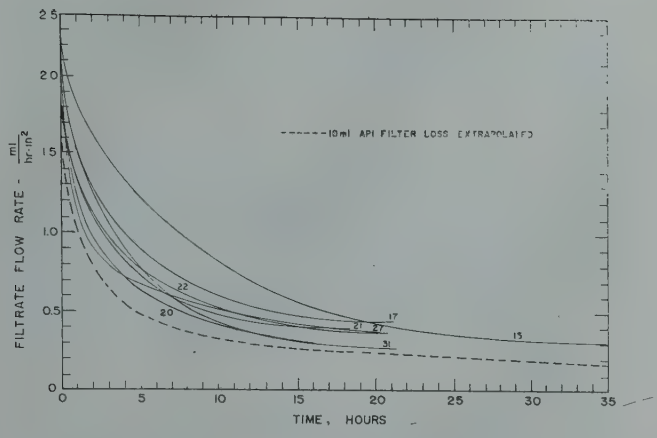

FIG. 4 — DYNAMIC FILTRATION FROM BENTONITE MUD; AVERAGE PROPERTIES:

API 30 min Filter Loss	10 ml
Density	73 pcf
Marsh Viscosity	43 sec

Filtration Pressure, 400 psi; Drill String Rotation, 45 rpm; Mud Velocity Between 4¼ OD Drill Collar and 5¾ Hole.

Run		Velocity
15	124 gal/min	3.37 ft/sec
17	94	2.56
20	83	2.26
21	130	3.54
22	113	3.08
27	111	3.02
31	109	2.97

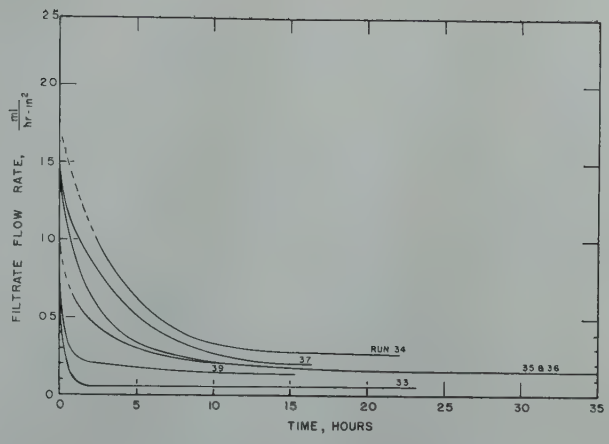

FIG. 5 — DYNAMIC FILTRATION FROM OIL BASE MUD; AVERAGE PROPERTIES:

API 30 min Filter Loss	0 ml
Marsh Viscosity	150 sec
Stormer Viscosity	80 cp
Density	70 pcf
Filtration Pressure, Runs 33-37	400 psi
Filtration Pressure, Run 39	200 psi

Drill String Rotation 90 rpm, Mud Velocity Between 4¼ OD Drill Collar and 5⅝ Hole.

Run		Velocity
33	37 gal/min	1.1 ft/sec
34	153	4.6
35	103	3.1
36	103	3.1
37	103	3.1
39	110	3.3

Drilled Hole With This Mud at Start of Test 39; See Part II for Discussion of Drilling Filtration.

5, 6, and 7 show dynamic rates as a function of time for these muds.

For each test, dynamic filtration rate starts high, about the same as the rate that would be predicted for static filtration. As dynamic filtration continues, the rate does not drop as rapidly as the static rate, and, after about 15 hours, the dynamic rate becomes constant or nearly constant, whereas static filtration rate continues to decrease.

The equilibrium dynamic filtration rates do not appear to be related to the extrapolated API filter loss for any of the muds. Moreover, muds with the lowest API filter loss, do not have the lowest equilibrium dynamic filtration rate. Fig. 8, which shows equilibrium filter rates as a function of mud velocity, illustrates the difference between the dynamic rates for different muds.

Dynamic filtration from the emulsion mud is greater than from the other muds but the API filter loss from this mud was only 4 ml, about the same as the filter loss from the lime-starch mud and less than one-half the filter-loss from bentonite mud. The oil base mud also has a higher equilibrium rate for lime-starch and bentonite muds; although the API loss for the oil base mud is zero.

For emulsion, lime-starch and oil base muds, equilibrium filter rate increases with increasing mud velocity; for bentonite mud all filtration was measured with mud circulating at velocities between 2¼ and 3½ ft/sec so change of filter rate with mud velocity is not apparent. The increases in filtration rate are predicted qualitatively by the ideas presented in the previous section. With increased mud circulation velocity, the filtration pressure gradient within the transition layer approaches the hydrodynamic gradient when the cake is thin. But for low circulation velocity, the filtration gradient does not approach the hydrodynamic gradient until the cake becomes thick. The thin equilibrium filter cake, at high mud velocity, results in high equilibrium filtration rate.

The high equilibrium filter rate for emulsion mud, however, is not explained by the speculative ideas presented. Emulsion mud filter cake has a low shear strength, 0.3 psi, that may be related in some way to the balance between erosion and filtration forces, but this relationship is obscure. Bentonite mud cake and emulsion cake are about equal in shear strength; yet, even though the API filter loss for bentonite is about three times the filter loss for emulsion mud, the equilibrium dynamic rate from emulsion mud is almost twice as great as the dynamic rate from bentonite mud.

The fact that dynamic filtration rates from bentonite and lime-starch muds are about equal also is difficult to explain. The filter loss from lime-starch mud is less than the filter loss from bentonite mud and the shear strength of lime-starch cake is greater. Both of these properties seem to point toward a lower equilibrium rate for lime-starch mud than for bentonite mud, but, as Fig. 8 shows, the rates are about equal.

STATIC FILTRATION

Whenever filtration occurs such that fluid mud remains quiet, the volume of the filtrate can be estimated by classic filtration theory;[5] filtration rate changes with time according to the equation:

$$\text{Rate} = \frac{\text{constant}}{(\text{time})^{0.5}}.$$

Mud filters statically both in wells when it is not circulating and in laboratory and field equipment used for measuring filter loss.

Fig. 9 shows filtration data for bentonite mud collected at the model well during a five-day static period. These data were collected after 21 hours of dynamic filtration so that the static cake was deposited over a dynamic filter cake. At the end of dynamic filtration, filtrate flowed through the cake on the wall at the rate of 0.44 ml/in² hour. Between the end of

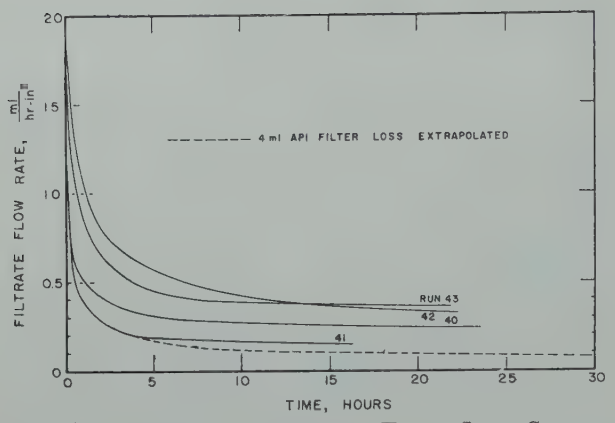

FIG. 6 — DYNAMIC FILTRATION FROM LIME-STARCH MUD; AVERAGE PROPERTIES:

API 30 min Filter Loss	4 ml
Marsh Viscosity	50 sec
Stormer Viscosity	25 cp
Density	75 pcf

Filtration Pressure 200 psi, Drill String Rotation 90 rpm, Mud Velocity Between 4¼ Drill Collar and 5¾ Hole:

Run		Velocity
40	92 gal/min	2.5 ft/sec
41	40.5	1.1
42	125	3.4
43	111	3.0

Drilled Hole With Mud at Start of Test 43; See Part II for Discussion of Drilling Filtration.

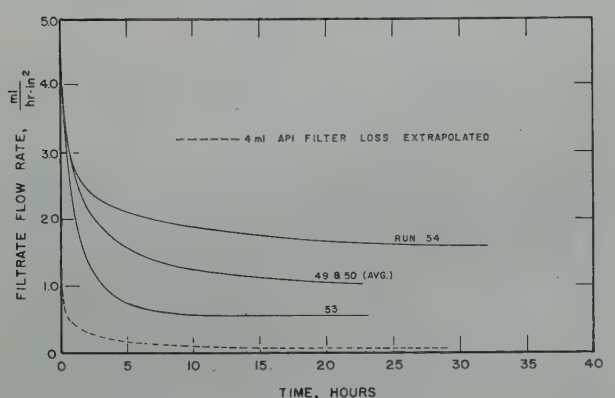

FIG. 7 — DYNAMIC FILTRATION FROM EMULSION MUD; AVERAGE PROPERTIES:

API 30 min Water Loss	4.0 ml
Marsh Viscosity	45 sec
Stormer Viscosity	17 cp
Density	70 pcf

Filtration Pressure 400 psi, Drill String Rotation 90 rpm, Mud Velocity Between 4¼ OD Drill Collar and 5½ in. Hole.

Run		Velocity
49 and 50	145 gal/min	5.0 ft/sec
53	62.5	2.1
54	286	9.6

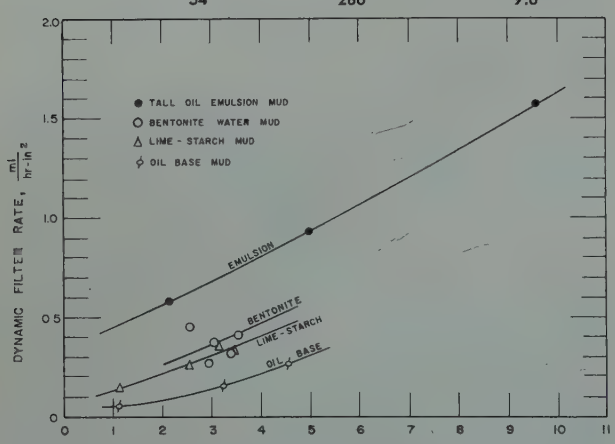

FIG. 8 — DEPENDENCE OF EQUILIBRIUM DYNAMIC FILTRATION RATE ON MUD FLOW VELOCITY AT 75°F

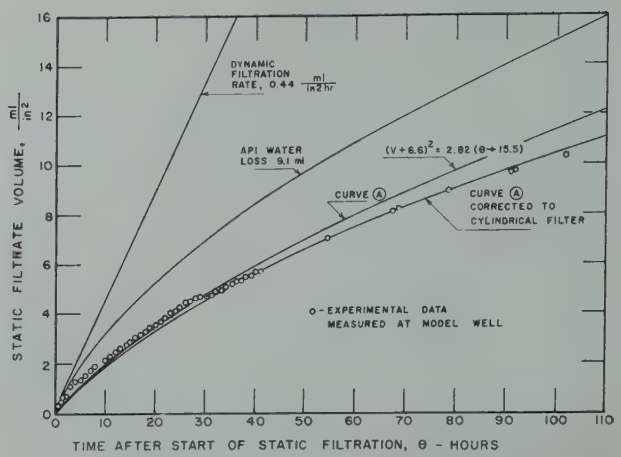
STATIC FILTRATE VOLUME, ml/in²
DYNAMIC FILTRATION RATE, 0.44 ml/in²hr
API WATER LOSS 9.1 ml
(V+6.6)² = 2.82 (θ+15.5)
CURVE (A)
CURVE (A) CORRECTED TO CYLINDRICAL FILTER
O - EXPERIMENTAL DATA MEASURED AT MODEL WELL
TIME AFTER START OF STATIC FILTRATION, θ - HOURS

FIG. 9 — STATIC FILTRATION FOR BENTONITE MUD — RUN 17 — MUD PROPERTIES:

API 30 min Filter Loss	9.1 ml
API Cake Thickness	0.12 in.
Marsh Viscosity	52 sec
Stormer Viscosity	27 cp
Density	72 pcf

Static Filtration After Dynamic Filtration With Equilibrium Rate of 0.44 ml/in.² hour. 4½ OD Slotted Liner in Hole During Static Filtration. Filtration Pressure 400 psi. Temperature 70-90°F.

dynamic filtration and the start of static filtration, the drill string was pulled and a 4½-in. OD slotted liner was run into the well.

Whenever a static filter cake is built upon a dynamic cake, or upon any filter media whose resistance to flow of filtrate is comparable to the resistance presented by the static cake, filtration volume can be described by a modification of the classic filtration equation. This equation is changed from:

$$V^2 = C\Theta \quad . \quad . \quad . \quad . \quad . \quad . \quad . \quad . \quad . \quad . \quad . \quad (2)$$

to the following modified form:

$$(V + V_o)^2 = C(\Theta + \Theta_o) \quad . \quad . \quad . \quad . \quad . \quad . \quad . \quad (3)$$

The resistance of the dynamic cake is represented[5] as the resistance of fictitious static filter cake that was deposited in Θ_o hours with a flow of V_o ml/sq in. of filtrate. This modified equation with $V_o = 6.6$ ml/sq in., $\Theta_o = 15.5$ hours and $C = 2.82$ ml/sq in. hour is plotted as curve (A) on Fig. 9.

The experimental static filtration data do not follow this modified equation for two reasons:

1. As the drill string, including a rock bit, was pulled and the liner run, part of the dynamic cake was scraped from the well bore so that part of the static cake deposited on a clean sand face and part on a dynamic cake;

2. The equation is derived for filtration through a plane filter whereas filtration in a well occurs on the inner surface of a cylinder.

The next three paragraphs explain qualitatively the deviation of experimental static filtration data from the modified classic equation that is observed for the first 30 hours of static filtration. This qualitative explanation shows that deviation can be attributed to partial removal of the dynamic cake by the bit as it is pulled and run.

The volume of filtrate that flows through the well wall after part of the wall has been scraped clean by a bit is given by the equation:

$$V = \propto V_s + (1 - \propto)V_u \quad . \quad . \quad . \quad . \quad . \quad . \quad . \quad (4)$$

V_s is the volume of filtrate that flows through the scraped portion of the well wall, V_u is the volume of filtrate through the unscraped portion, $\propto$ is the fraction of

the well wall that is scraped clean. V_s changes with time according to Equation (2), whereas V_u changes according to Equation (3). The total volume of filtrate, V, is:

$$V = \alpha(C\theta)^{1/2} + (1 - \alpha)\,[(C\theta + C\theta_o)^{1/2} - V_o]. \quad (5)$$

Exact numbers for α, C, θ_o V_o can be found to fit the experimental static filtration data of Fig. 9, but these numbers could not be applied to other filtration data. In order to discuss the effect of partial removal of the dynamic cake, therefore, α C, V_o, and θ_o have been assigned the following typical values:

$$\alpha = 0.5$$
$$C = 2.25 \text{ ml}^2/\text{in.}^4$$
$$\theta_o = 16 \text{ hours}$$
$$V_o = 6.0 \text{ ml/sq in.}$$

When these numbers are inserted into Equation 5, it becomes:

$$V = 0.75\,\theta^{1/2} + 0.75\,(\theta + 16)^{1/2} - 3.0 \quad . \quad (6)$$

Equation 6 describes exactly the volume of filtrate that will flow after one-half of the dynamic mud cake has been scraped away. The solid line on Fig. 10 shows how, according to Equation (6), V varies as a function of θ. This solid curve has the same form as the plot of measured static filtration data on Fig. 9. An equation of the form of Equation (3) may be calculated from three points of the solid curve of Fig. 10 just as Curve (A) was calculated from the measured filtration data. For example, if the following three points are taken from the solid curve of Fig. 10;

$\theta = 0$	$V = 0$
$\theta = 50$	$V = 8.35$
$\theta = 100$	$V = 12.6$

the calculated equation becomes:

$$V + 2.36 = 2.19\,(\theta + 2.56)^{1/2} \quad . \quad . \quad . \quad . \quad (7)$$

The plot of this equation, the dashed line on Fig. 10, follows the solid line closely, but falls below the solid line near the origin. Thus the simple Equation (7) deviates from the exact Equation (6) just as Curve (A) of Fig. 9 deviates from the measured filtration data between zero and 30 hours. Similarity of the measured

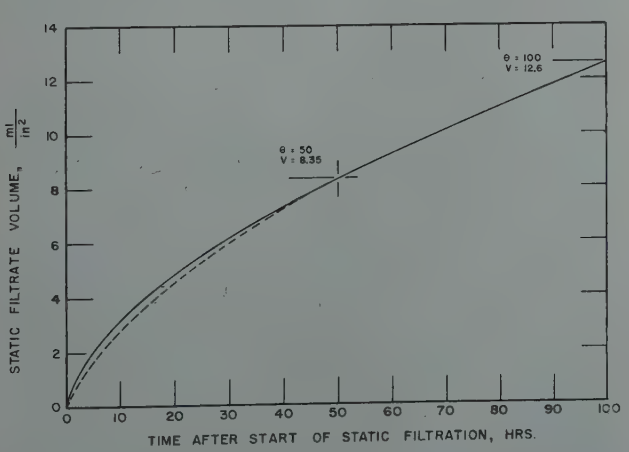

FIG. 10 — TYPICAL STATIC FILTRATION AFTER DYNAMIC FILTRATION CALCULATED FOR (1) 50 PER CENT OF FORMATION FACE CLEANED AS BIT IS PULLED (SOLID LINE) AND (2) CALCULATED FROM EQUATION 3 TO FIT THE SOLID LINE AT $\theta = 0$, 50, AND 100 HOURS (DASHED LINE).

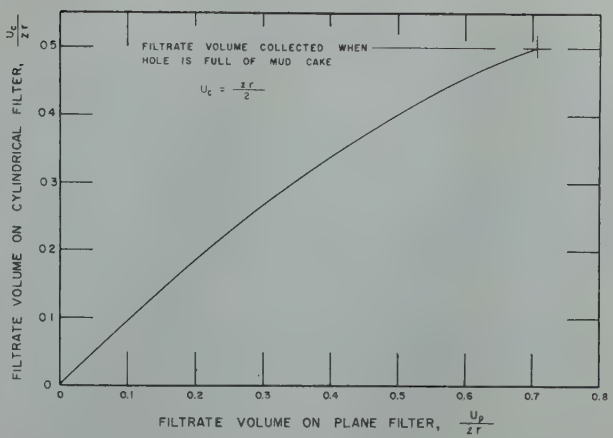

FIG. 11 — FILTRATION ON PLANE AND CYLINDRICAL SURFACES. V_c IS VOLUME OF FILTRATE COLLECTED ON CYLINDRICAL FILTER IN θ HOURS; V_p IS VOLUME COLLECTED ON PLANE FILTER IN THE SAME TIME; z IS THE RATIO OF FILTRATE VOLUME TO CAKE VOLUME; AND r IS THE WELL RADIUS.

deviation to the calculated deviation is evidence that the measured deviation is also caused by the bit scraping part of the dnamic cake from the well bore.

The discussion of the preceding paragraphs applies to filtration through a flat surface; whereas in a well, the filter surface (the well bore) is cylindrical. Fig. 11 presents a curve that may be used to determine from volumes measured on a plane filter the volume of filtrate that will flow through a cylindrical filter. On Fig. 11, V_c is the volume of filtrate that will collect on a cylindrical filter and V_p the volume of filtrate that will collect on a plane filter in the same time. The curve is derived from Darcy's law for the flow of fluid through a cylinder and from the assumption that filter cake volume is proportional to filtrate volume. Cake permeability was assumed constant, and the effect of mud gelation on filtration was neglected. From the derivation, V_c and V_p are related by the following equation:

$$(V_p/zr)^2 = (1/2 - V_c/zr)\quad [\log_e(1 - 2V_c/zr)] + V_c/zr \quad . \quad . \quad . \quad . \quad . \quad . \quad . \quad . \quad . \quad . \quad . \quad . \quad (8)$$

From this equation, V_c is plotted as a function of V_p on Fig. 11.

When the well bore becomes filled with filter cake, filtration will cease. At this time, the volume of mud cake collected on each square inch of well bore will be $(r/2)$, and the volume of filtrate collected will be $(zr/2)$.

Use of Fig. 11 is best shown by an example in which volume of filtrate collected on a plane filter is corrected to the volume collected in a cylinder. Assume the drilling mud to be a mud from which 10 ml of filtrate is collected during 30 minutes of filtration at bottom hole temperature and pressure in a filter cell of the same size as the standard API cell (7 sq in.). This mud filters statically for 150 hours in a 8-in. hole.

Then $V_p = 10$ ml $(1/7$ in.$^2)$ $(150/0.5)^{0.5} =$ 24.8 ml/sq in. at the end of 150 hours. For most water base muds, we observed that z is close to unity so that

$$V_p/zr = 6.2 \text{ ml/cu in.} = 0.38.$$

Then from Fig. 11 at $V_p/zr = 0.38$, $V_c/zr = 0.333$; and $V_c = 21.6$ ml/sq in. The correction from 24.8 to 21.6 is about 15 per cent.

PART II — FILTRATION FROM BENEATH A DRILLING BIT

Rotary drilling establishes an area beneath the bit where the formation is exposed to drilling mud at high pressure but is not protected by filter cake. Above the bit, filter cake is built which limits the penetration of filtrate into the formation. The properties of this cake — filter loss, thickness, toughness, penetration into formation, and pressure-temperature sensitivity have been studied for many years.

Part I of this paper describes a study of filtration through bore walls during drilling. Studies of filtration from beneath a drilling bit, however, have not been reported. Beneath the bit new formation is continually exposed as the bit chips and grinds the rock beneath it. Bit action and the mud stream prevent buildup of a mud cake that would limit flow of filtrate into the formation. Filter loss could be very high and radial penetration of filtrate from beneath the bit might be as great as the penetration of filtrate through the well walls above the bit.

Closely allied with bottom hole filtration is the movement of connate liquid that saturates rock in the path of the drilling bit. This connate liquid may be picked up into the mud stream, or it may be forced ahead of the bit through virgin formation.

The investigation described in this part of the paper was undertaken to study bottom hole filtration and movement of connate liquid ahead of the bit.

Limits of Filtration

The study of filtration from beneath a drilling bit consists of two parts: (1) measurement of the quantity of fluid that crosses the hole bottom, and (2) mathematical description of the flow path of this fluid. The quantity of fluid that flows depends on filtration pressure, mobility of the fluid in the formation, and on plugging of the formation immediately beneath the bit by mud particles. The flow path of the fluid depends on the ratio of the drilling velocity to the fluid flow velocity through the bottom of the hole.

This section describes the maximum flow of filtrate through the hole bottom and the radial distance this filtrate penetrates the formation. The "Results" section describes measurements made at the model well of radial penetration of filtrate from the hole bottom.

The maximum rate at which filtrate could flow beneath a drilling bit would be described by potential flow of a liquid from a disk source into an infinite, permeable formation. Fig. 12 (a) sketches the potential flow streamlines from beneath a stationary disk source. This potential flow field when combined with the downward hole motion, Fig. 12 (b), gives the resultant flow field shown in Fig. 12 (c). This resultant field is characterized by a depth of filtrate penetration, t, which is a function of the drilling rate, formation porosity and premeability to filtrate, flooding efficiency, pressure difference between hole and formation, and hole radius. For this theoretical discussion, the assumption is made that no filtrate passes through the hole wall.

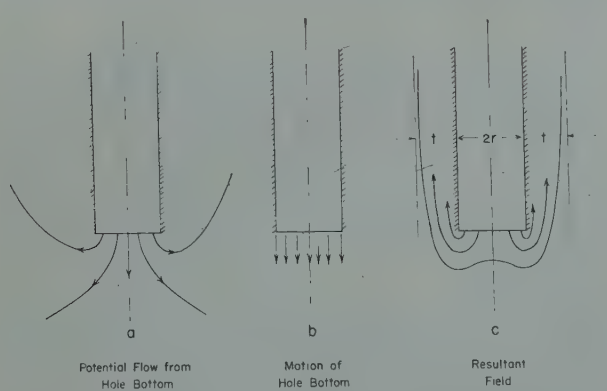

FIG. 12 — FLOW PATH OF FILTRATE FROM BOTTOM OF HOLE BENEATH DRILLING BIT.

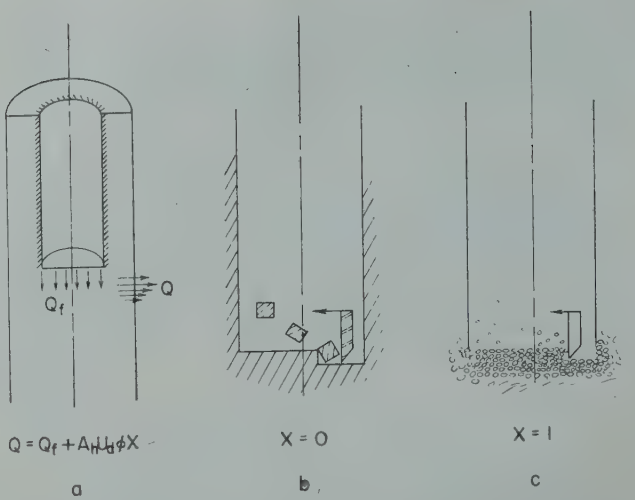

FIG. 13 — FILTRATE FLOW AND CONNATE WATER FLOW.
A. Q Is Total Fluid Through Cylinder, Part Connate Water, Part Filtrate. Q_f Is Filtrate Through Hole Bottom.
B. X = 0; All Connate Water Enters Mud Stream, No Connate Wate Flows Ahead of Bit.
C. X = 1; No Connate Water Enters Mud Stream.

Two methods may be used to estimate filtrate penetration. First, the problem was analyzed mathematically. An exact solution of the potential flow problem was not obtained but maximum and minimum limits of filtrate penetration were established. Second, the authors of this paper employed an electric analog of the drilling well system to determine the filtration rate predicted by potential flow theory. This analog is described in Appendix I. Maximum and minimum limits of filtration were calculated. The analytical lower limit agrees exactly with the minimum predicted by the electrical analog, and the upper limit lies well above the analog maximum.

Both analysis and analog predicted filtrate invasion of from one to 15 hole radii for normal drilling conditions. Such invasion was believed excessive because these studies neglected plugging by mud particles. Experimental data were needed, therefore, to determine if large filtrate invasion was probable.

In order to calculate theoretical limits, the assumption was made that an infinite formation was saturated with connate water of the same physical properties as filtrate. Connate water in the formation that lies in the path of the bit either may flow, with drilling mud filtrate, into the formation around the bit, or may enter the mud stream along with sand and chips. All of the fluid that flows through the formation, therefore, is not necessarily filtrate.

Fig. 13 (a) distinguishes between the volume rate of filtrate, Q_f, crossing the hole bottom, and the volume rate of liquid, Q, moving through the formation across a cylindrical surface whose axis is common with the bore. The relationship between Q and Q_f is given by

$$Q = Q_f + A_h \phi U_d X \quad . \quad . \quad . \quad . \quad . \quad . \quad . \quad . \quad (9)$$

where the symbols are defined in the nomenclature.

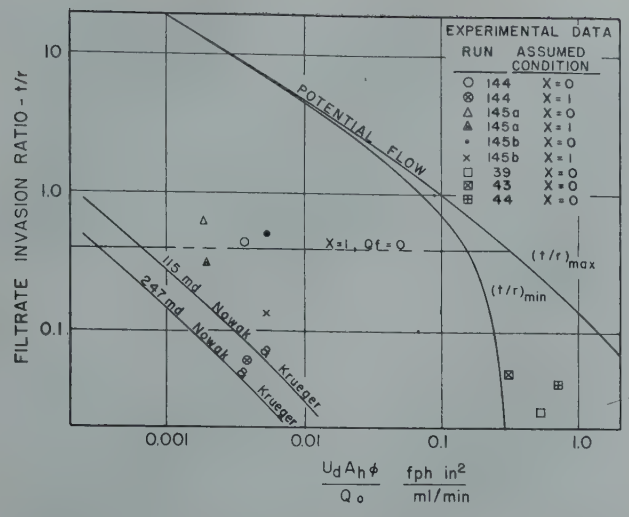

FIG. 14 — FILTRATE INVASION AS RESULT OF BENEATH THE BIT FILTRATION.

X is the fraction of connate liquid, volume $= A_h \phi U_d$, (within the formation that is drilled out by the bit) that is forced ahead of the hole bottom and not picked up by the mud stream with sand and chips.

If large chips are cut by the bit as shown in Fig. 13 (b), almost all the liquid within the pores of these chips will enter the mud stream and will not be forced into the formation below the hole bottom; then X will be small. If the bit drills be removing individual sand grains as shown in Fig. 13 (c), however, liquid within the pores between these grains can be forced ahead of the hole bottom by mud and will not enter the mud stream with the sand grains; then X will be near unity.

The distance that filtrate penetrates into the formation also depends upon the efficiency, E, of displacement of connate fluids within the formation around the hole. Thus,

$$Q_f = Q - A_h \phi U_d X = \pi(R^2 - r^2)\phi U_d E \quad . \quad (10)$$

where R is the radius of filtrate invasion and E is the fraction of connate fluids displaced by the advancing fluid front. From Equation (10), the ration of filtrate penetration depth, t, to hole radius, r, is obtained by substitution and rearrangement.

$$\frac{t}{r} = \left[1 - \frac{X}{E} + \frac{Q/E}{A_h \phi U_d}\right]^{0.5} - 1 \quad . \quad . \quad (11)$$

where $t = R - r$. In this equation, if $Q = Q_o$ (the flow rate predicted by electric analog) t/r is the theoretical maximum. In wells, Q may be less than Q_o because mud particles plug the formation beneath the bit and prevent filtrate and connate liquid from flowing at the rate predicted by potential theory.

Fig. 14 plots $(U_d A_h \phi / Q_o)$, E assumed equal unity, against filtrate invasion expressed as the ratio, t/r. Expressed in consistent units, the grouping $(U_d A_h \phi / Q_o)$ is dimensionless, but in Fig. 14, it is expressed in field units for convenient application. $(U_d A_h \phi / Q_o)$ is the ratio of formation pore drilling rate, $U_d A_h \phi$, to theoretical filtrate flow rate, Q_o For potential flow from well bottom into the formation, two limits of t/r may be calculated from Equation (11) in terms of $(U_d A_h \phi / Q_o)$ for assumed flooding efficiency of 100 per cent. They are $(t/r)_{max}$ for the condition $X = O$ and $(t/r)_{min}$ for $X = 1$. Both limits may be calculated using filtrate flow rates, Q_o, which are expressed from electric analog results as

$$Q_o \frac{\text{ml}}{\text{min}} = 0.792 \frac{k}{\mu} r P \quad . \quad . \quad . \quad . \quad (12)$$

The difference between $(t/r)_{max}$ and $(t/r)_{min}$ is connate water forced ahead of the bit from rock pore space drilled up by the bit. Curves of $(t/r)_{max}$ *and* $(t/r)_{min}$ are plotted on Fig. 14 as calculated from Equation (11) with $Q = Q_o$.

If no filtrate crossed the hole bottom, $Q_f = O$, and all connate water was forced ahead of the bit, $X = 1$, the experimental method would have measured this volume movement as filtration. As pseudo filtration, the calculated depth of invasion would be $t/r = 0.41$ and this invasion is plotted as a line on Fig. 14. When $(t/r)_{max} = 0.41$, then $(t/r)_{min} = 0$. For larger $(U_d A_h \phi / Q_o)$ the driving potential is not sufficient to cause a movement to $(t/r) = 0.41$ so that this line does not extend to the right of the potential flow curve.

EXPERIMENTAL METHOD

In order to utilize Equation (11) to predict filtrate invasion radially into formations from beneath a bit, experimental measurements of Q were needed. The equipment and test procedure used at the model well are described in this section.

Two types of formation were used. The first was made of Lumnite cement and sand; this type was the same as the formations used during dynamic and static filtration measurements. Permeability was about 10 md and porosity was 20 per cent. This formation could be used only with lime-starch and oil base muds because it contaminated clay-water mud. Also the material was soft, although of low permeability, and drilled rapidly with low bit weight.

The second type of formation was made of outcrop sandstone from Boise, Idaho. This sandstone is a uniform, not laminated, isotropic, feldspathic rock of about 500 md water permeability. Drilling conditions more representative of field operations were obtained with this formation. The sandstone formations were built of two sandstone cylinders 18 in. in diameter and 36 in. long. They were cemented together with plastic adhesive laid in a waffle pattern so that vertical permeability was infinite and radial permeability low across the joint. Lumnite cement-sand concrete bonded the stub casings above and below the sandstone cylinders.

Four different muds were used in six experimental runs: (1) field used clay-water mud treated with bentonite, barytes, quebracho, and phosphate; (2) bentonite-water gel mud free of contaminates or large solid par-

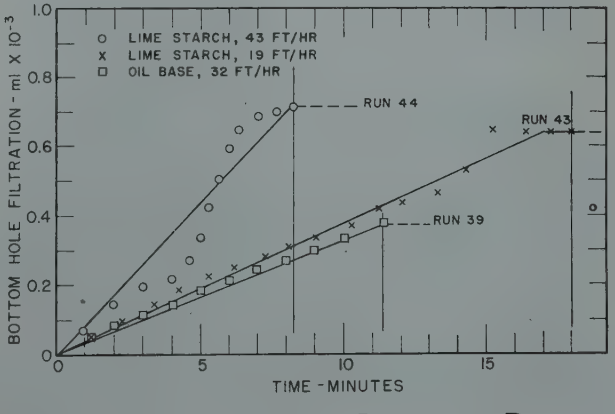

FIG. 15 — FILTRATION FROM BENEATH A DRILLING BIT FROM LIME-STARCH AND OIL BASE MUDS—LUMNITE CONCRETE FORMATION.

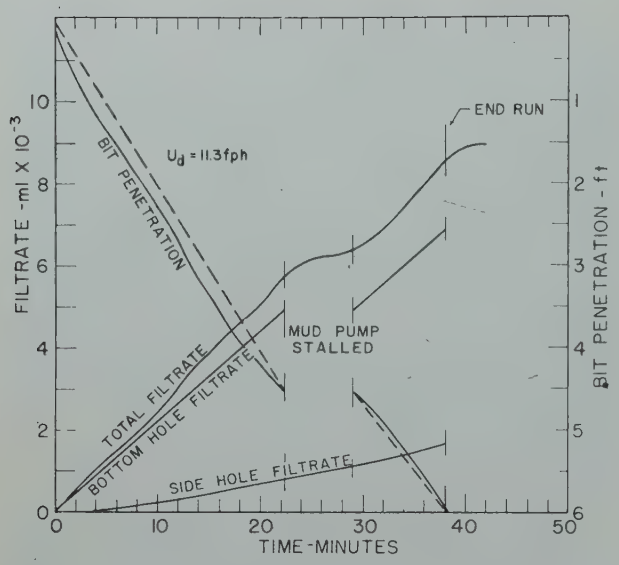

FIG. 16 — FILTRATION FROM BENEATH A DRILLING BIT FROM FIELD USED WATER BASE MUD — BOISE SANDSTONE FORMATION—RUN 144.

ticles; (3) lime-starch mud; and (4) oil base mud. Properties of these muds are listed in Table 1.

The procedure for saturating a formation was to evacuate it for 24 hours, flood with CO_2 to 60 psi, and again evacuate for 24 hours. Fresh water was then flooded into the formation to establish 100 per cent water saturation.

Before drilling, mud circulation was established at 100 gal./min and mud pressure set at 200 psi by applying nitrogen to the closed circulation system. Makeup mud came from the surge chamber as needed. The drill string, consisting of a 5¼ in. three cone roller bit, a 4¼ in. drill collar, and a kelly, rotated at 90 rpm during drilling. Weight on the bit was varied to maintain a constant drilling rate for each test. Drilling rates are listed in Table 1; they ranged from 6 to 43 ft/hour.

Filtrate was collected continuously and a gauge glass level read every 30 seconds. Filtrate volume as measured would be sensitive to temperature changes in the system, but measurements made every five minutes showed the temperature to be constant.

During each run, pump speed and mud pressure were recorded every five minutes. Mud samples were collected every five minutes, and density and Marsh Funnel viscosity measured. Mud properties showed no change except for a density increase caused by increased sand concentration.

TABLE 1

SUMMARY OF BOTTOM HOLE FILTRATION DATA

Run No.	Mud	Press. psi	Cir. Rate gpm	Bit Size n.	Rotary Speed rpm	Drill Speed fph	Formation Type	Formation Porosity ϕ	Formation Perm k md
144	Field (1)	200	100	5¼	90	11.3	(5)	24	550
145	Gel (2)	200	97	5¼	90	11.6	(5)	20	330
145	Gel (2)	200	97	5¼	90	6.2	(5)	20	506
39	Oil B (3)	200	110	5⅝	90	32	(6)	20	10
43	L-S (4)	200	100	5⅝	90	19	(6)	20	10
44	L-S (4)	200	105	5⅝	90	43	(6)	20	10

BOTTOM HOLE FILTRATION

Run No.	Model Well Test ml/min (7)	Model Well Theor Max ml/min (8)	Model Well % of Max	Field Well Test ml/min (9)	Field Well Theory ml/min (10)	Filtration Invasion Test $(t/r)_{max}$ (11)	Filtration Invasion Test $(t/r)_{min}$ (11)	Filtration Invasion Theory t/r (11)
144	219	18,350	1.2	216	15,560	0.454	0.06	9.8
145	216	10,980	1.9	211	9,340	0.510	0.13	8.1
145	150	16,910	0.9	148	14,320	0.638	0.29	14.3
39	31	358	8.5	28	303	0.027		0.35
43	36	358	9.9	32	303	0.050		0.27
44	85	358	23.4	61	303	0.043		0.41

(1) Field clay mud; 71.5 pcf, 40 sec Marsh, 10.1 ml 30 min API loss
(2) Bentonite Gel; 66 pcf, 53 sec Marsh, 10.5 ml 30 min API loss
(3) Oil Base; 70 pcf, 260 sec Marsh @ 70°F, 0.2 ml 30 min API loss
(4) Lime Starch; 75 pcf, 45 sec Marsh, 4.1 ml 30 min API loss
(5) Natural outcrop sandstone from Boise, Idaho
(6) Artificial, Lumnite cement bonded, sandstone
(7) Measured flow, Q, from outer surface of model well formations. $Q = Q_t$ if $X = 0$
(8) Calculated for potential flow conditions from electric analog, Q_o
(9) Test results corrected to constant pressure radius at 117 ft
(10) Same as (8) corrected to constant pressure radius at 117 ft
(11) Ratio of filtrate penetration distance to well radius

RESULTS

The experimental data are plotted in Fig. 15, 16, and 17. On all figures, the curve of bottom hole filtration was calculated by subtracting from the total measured filtration the estimated filtration through mud cake on the bore wall. Derivation of this estimation is given in Appendix II. The liquid volume plotted as bottom hole filtrate is, Q, the sum of Q_t, the volume of filtrate crossing the hole bottom, and of $A_h U_d \phi X$, the volume of connate water forced to move through formation ahead of the bit. Whether flow was filtrate or connate water could not be distinguished.

Runs 39, 43, and 44, plotted on Fig. 15, are characterized by rapid drilling in a tight formation with low filter loss muds. Runs 144 and 145 were made at lower, more representative drilling rates with clay water muds. During Run 144, the mud pump stopped automatically when crankcase oil pressure dropped below safe operating pressure. The run was continued after remedy, and the data are satisfactory despite the interruption.

The curve of total filtrate less side hole filtrate plots as a straight line with scatter of the data points about the straight line. The corrected points are plotted in Fig. 15 to show scatter; the greatest scatter is in Run 44 and is apparently a result of the high drilling velocity. The bottom hole filtrate curve of Run 144, Fig. 16, shows that the correction for side hole filtration accounted for all filtration during the time that drilling was interrupted. The same figure shows that the corrected bottom hole filtrate rate is the same before and after the interruption.

During Run 145, Fig. 17, the drilling speed was

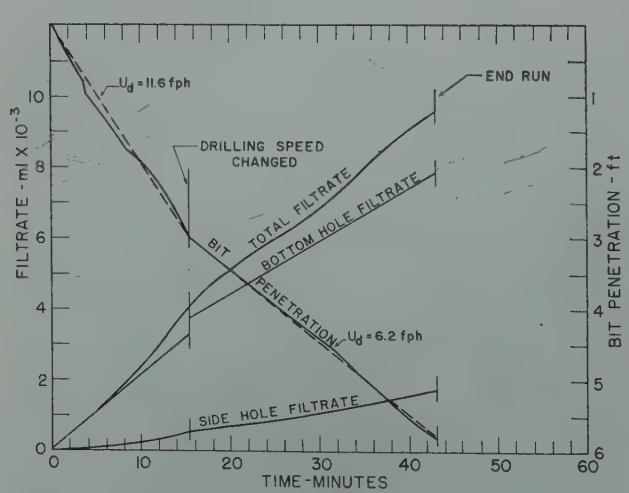

FIG. 17 — FILTRATION FROM BENEATH A DRILLING BIT FROM BENTONITE MUD (NO LARGE SOLIDS) — BOISE SANDSTONE FORMATION — RUN 145.

changed after drilling half way through the formation. No sudden change in the flow rate of total filtrate was observed. Consequently, the corrected bottom hole filtrate rate, drawn as the best straight line through the data, shows a discontinuity at the time drilling speed was reduced. Some of the discontinuity results from the drilling rate being faster than the average, 11.6 ft/hour, just before reducing drilling speed to 6.2 ft/hour.

The experimental conditions and measured data are tabulated in Table 1. The tabulated bottom hole filtrate rates were calculated with the assumption that all connate liquid within pore space in the rock drilled out is picked up into the drilling mud stream; $X = 0$. In Equation (9), this is equivalent to assuming that $Q = Q_f$. Experimentally, this assumption could not be verified, but the assumption of $Q = Q_f$ was made for two reasons.

First, use of this assumption expresses the largest possible filtrate invasion that can be calculated from the data, and thus the tabulated invasion may be too high but will not be too low

Second, the opposite assumption, that all connate water was forced ahead of the bit and was experimentally measured as filtrate, will lead, for the premium mud data, to the conclusion that no filtrate entered the formation.

If, for premium muds, flow rate of liquid from the drilled out formation ($U_d A_h \phi$) is subtracted from the measured filtrate rate, a negative filter rate results and even for $X = 1$ connate water enters the mud stream. Thus, the tabulated filtrate invasions, which are based on $X = 0$, predict maximum invasion of drilling fluid filtrate.

The invasion radius of bottom hole filtrate, shown in Table 1, was calculated with the assumption that filtrate flooded all of the connate fluid from the formation; the flooding efficiency, E, equalled unity. If the flooding efficiency is less, the invasion will be proportionately greater. Russell, Morgan, and Muskat[10] describe studies in which brines were flooded from sandstones by fresh water. They report that 80 per cent or more of the brine was displaced ahead of the advancing flood front at breakthrough.

Holmgren[11] describes water floods of sands saturated with 75 per cent oil and 25 per cent water. Displacement efficiency at breakthrough of the advancing flood front for this system is dependent upon viscosity ratios, and for μ_o/μ less than two the flood efficiency is about 45 per cent. For the experimental system in which all liquids were water, assumption of 100 per cent flooding efficiency is reasonable.

The experimental data plotted on Fig. 14 are plotted as t/r_{max} calculated from Equation (3) as

$$\left(\frac{t}{r}\right)_{max} = \left(1 + \frac{Q}{U_d A_h \phi}\right)^{1/2} - 1 \quad (13)$$

against the term

$$\frac{U_d A_h \phi}{Q_o}.$$

Q_o is the theoretical filtrate flow of Equation (12), and Q is the measured filtration flow from Table 1. The data for high speed drilling with premium drilling mud and the normal speed drilling with water-clay mud form two separated groups of data because of differences in formation permeability and drilling rate.

The clay water mud data, Runs 144 and 145, fall far short of the theoretical limit of filtration, thus indicating that particle bridging effectively controls water loss even at bottom-hole drilling conditions. Further, because of the proximity to $t/r = 0.41$ we suspect that the measured filtrate consists largely of displaced connate water.

The data on premium mud are above the theoretical $(t/r)_{min}$ and below the theoretical $(t/r)_{max}$. Filtrate flow is so small that the maximum filtrate invasion is of the order of 0.5 in. The measured flow, Q, may be the result of either filtration or connate water movement. At the high drilling rate and low formation permeability, however, the mud pressure was not high enough to move all of the connate water in the drilled formation. Even if no filtration occurred, $Q_f = 0$, only about 20 per cent of the connate water could flow ahead of the bit; the remainder would enter the mud stream.

Comparison To Other Experimental Data

Very little experimental data on filtrate penetration or invasion of liquid mud are available and applicable to bottom-hole drilling filtration. Nowak and Krueger[12] studied filtration through cores that were continuously surface scraped and against which a drilling mud stream jetted at high pressure. The data show that for field clay-water mud filtration was only about a tenth the rate calculated from potential flow theory through a 115 md core. The filtrate rate was not proportional to permeability, however, but was more nearly constant for a range of permeability from 15 to 247 md. This indicates that the flow was controlled primarily by plugging of the core with clay particles.

The Nowak and Krueger data can be used to calculate bottom-hole filtrate invasion for comparison, on Fig. 14, with the present data obtained under very different conditions. For their test conditions of 1000 psi differential pressure, 175°F temperature, 100 ft/min mud velocity, 115 md consolidated sandstone core, field clay-water mud, and both jetting and scraping the core face, Nowak and Krueger obtained a filtrate rate of 92 ml hourly/sq in. of flow surface. This is 0.70 cu ft of filtrate per hour.

If the same assumptions are made as were applied in calculating (t/r) from the present experimental data, namely that $X = 0$, the data of Nowak and Krueger plot as shown by solid lines in Fig. 14, even less filtrate penetration results than was measured in the model well drilling tests. If the model well data are calculated from Equation (11), however, (with $X = 1$) as

$$\left(\frac{t}{r}\right)_{min} = \left(\frac{Q}{U_d A_h \phi}\right)^{1/2} - 1 \quad . \quad . \quad (14)$$

than the model well data plot is shown by crosses on Fig. 14. Use of Equation (14) assumes that in the experimental equipment connate water was displaced by the advancing hole bottom. If this occurred, the Nowak and Krueger data should be compared to $(t/r)_{min}$ and in doing so on Fig. 14 a much closer agreement is observed.

The high temperature and pressure of the Nowak and Krueger tests might be expected to produce higher filtrate invasion than measured at the model well. This was not observed. Apparently the drilling operation contributes to higher filtration rates.

PART III — ESTIMATED FILTRATE INVASION

In this section, filtrate penetration into a permeable sand is estimated. The calculation shows how the data presented in this paper may be used and emphasizes the

difference in filtrate invasions that occur during dynamic and during static filtration.

Assume the estimate to be made of filtration in a sand at 7,000 ft and that total depth of the well is 7,500 ft. The hole will be drilled with a 7⅞-in. bit on 5-in. drill collars. An oil emulsion mud with the same properties as the fluid of Fig. 7 will circulate 170 gal./min, 2 ft/sec The schedule between the time the 7,000-ft sand is drilled and the time casing is cemented and mud filtration stops is shown in Table 2. Filtrate that flows into the formation from cement is not within the scope of this paper and is not considered in this estimation. Three kinds of filtration will be encountered: (1) filtration from beneath the bit, (2) dynamic filtration, (3) static filtration.

To estimate filtration from beneath the bit, refer to Equation (11) and Table 1. According to this equation, for $E = 1$

$$(t/r) = \left[1 - X + \frac{Q}{U_d A_h \phi}\right]^{0.5} - 1$$

Assume that the emulsion mud of this problem is similar to the field mud of Run 144 so that for a 5¼-in. hole, Q is 216 ml/min, and for a 7⅞ in. hole, Q is 455 ml/min. Then for an assumed porosity, $\phi = 20$ per cent, and assumed $X = 0.5$.

$$(t/r) = 0.92$$

and t, the invasion depth, is 3.5 in.

Dynamic filtration is estimated with the aid of Fig. 7. For Run 53, dynamic filtration reaches equilibrium at a rate of 0.6 ml/in.^{2} hour after about 10 hours. Integration of this curve shows 40 ml/sq in. of filtrate to flow in 50 hours at 75°F. Bottom hole temperature at 7,000 ft is about 200°F. At this temperature, auxiliary experiments show dynamic filtration will be about three times as great as at 75° so that 120 ml/sq in. will flow in 50 hours at 200°F. The depth to which this volume of filtrate will penetrate is estimated as follows:

Filtrate Volume = 120 ml/sq in. x (π x 7⅞) in. x 1 in. x 0.061 in.^{3}/ml. The volume of filtrate for each linear inch of hole is 176 in.^{3} This volume is related to R, the radial extent of filtrate invasion, as follows:

$$176 \text{ in.}^3 = \pi \left[R^2 - \left(\frac{7\frac{7}{8}}{2} + 3.5 \right)^2 \right] \text{ x 1 in. x 20 per cent}$$

From which $R = 18.4$ in.

During the round trip, mud is static and filtrate collects according to classic theory. A complication arises, however, because as the bit is pulled it probably scrapes part of the mud cake from the well bore. For this example assume that the bit cleans all filter cake from 25 per cent of the sand face each time it is pulled or run and that filter cake on the remaining 75 per cent of the sand face is not disturbed.

The API filter loss of this emulsion mud is 4 ml at room temperature; assume with the aid of the Schremp and Johnson paper[2], that this filter loss is increased to 7 ml at 200°F. The volume of filtrate that flows in 8 hours, through the well bore that is scraped clean may be estimated with the aid of Equation (2) as 4.0 ml/sq in.

The volume of filtrate that flows through the 75 per cent of the sand surface that is not scraped clean by the bit may be estimated with the aid of Equation (3). The parameters V_o and Θ_o are adjusted so that at the start of static filtration, filtration rate is the same as at the end of dynamic filtration. The average volume of filtrate is then 3.52 ml/sq in. and radial extent of invasion is 18.6 in.

For the second drilling stage, assume again that the bit, as it is run, cleans all filter cake from 25 per cent of the sand face. Then this area will collect 120 ml/in.^{2} hour of filtrate in 50 hours just as it did for the first drilling stage. For the 75 per cent of the sand face that was not scraped clean by the bit, assume dynamic filtration proceeds at the same rate that existed at the end of static filtration, 0.3 ml/sq in./hour; in 50 hours, 15 ml/sq in. of filtrate will collect through the unscraped area. Then the average filtrate volume that flows through each square inch of sand face is 41.2 ml; and this volume of filtrate extends the invasion radius to 21.1 in.

In the fifth step, static filtration continues for 12 hours while pipe is pulled, the well logged and pipe run again. During this time, an average of 2.94 ml will flow through each square inch of bore face and this filtrate will extend the invasion radius to 21.3 in.

During the two hours of circulation to clean the well before casing is run, dynamic filtration through the 25 per cent of the well bore area that was scraped clean by the bit results in flow of 10 ml/sq in. of filtrate. Dynamic filtration through the unscraped area at the equilibrium rate of 0.3 ml/in.^{2} hour results in flow of 0.6 ml/sq in. The average volume of filtrate is 2.9 ml/sq in.; this volume extends the invasion radius to 21.5 in.

After circulating mud to clean the hole, drill pipe is pulled and the casing run. During this time filtration is static. An average of 3.6 ml of filtrate flows through each square inch of well bore area and the invasion radius is extended to 21.5 in.

The volume of filtrate that flows for each of the completion operations and the depth to which filtrate invades at the end of these operations is summarized in Table 2.

The invasion radius reaches 85 per cent of its maximum extent before the first period of static filtration and more than 90 per cent of the total filtrate flows from mud that is circulating whereas less than 10 per cent of the filtrate flows from mud that is static. The data that are presented here show that this large volume of filtrate that flows under dynamic conditions cannot be predicted, even qualitatively, from the API filter loss test.

TABLE 2 — DRILLING SCHEDULE AND FILTRATE INVASION

Operation	Time	Filtrate Volume	Invasion Radius	Invaded Zone Thickness
	Hours	ml/in.^{2}	Inches	Inches
1. Drill through zone at 5 ft/hour			7.3	3.5
2. Drill below zone at 5 ft hour	50	120	18.4	14.6
3. Round trip to replace bit	8	3.5	18.6	14.8
4. Drill below zone at 5 ft/hour	50	61.5	21.1	17.3
5. Pull pipe, log well, run pipe	12	2.9	21.3	17.5
6. Condition hole to run casing				
a. Circulate drilling mud	2	2.9	21.5	17.7
b. Pull drill pipe	4			
7. Run casing	12	2.9	21.7	17.9
8. Cement casing, end of mud filtration				
Total Mud Filtration	138	192	21.7	17.9

SUMMARY

1. Filtration from drilling mud during the drilling of an oil well is of three kinds: (1) static filtration, while mud in the hole is quiet; (2) dynamic filtration, while mud in the hole circulates; and (3) beneath the bit filtration, where bit action prevents filter cake accumulation.

2. The filtrate flow rate for each of these three kinds of filtration was measured at the California Research

Corp. model well. The bottom hole mechanics of this well are similar to the bottom hole mechanics of a field well. Thus the effect of drilling rates and circulation rates on filtration could be observed.

3. Static filtration rate can be predicted by the "classic" filtration law ($V = C\Theta^{0.5}$), even though assumptions made in the derivation of this law are not strictly true for mud filtration.

4. Dynamic filtration rates are higher than static filtration rates. In the work reported here, dynamic filtration became constant after about 15 hours at rates that ranged from 0.05 to 1.5 ml/in.^{2} hour. Seventy to 90 per cent of the total volume of filtrate that enters permeable formations flows while the mud stream is circulating; only 10 to 30 per cent of the total volume of filtrate enters the formation during static filtration.

5. Liquid flow through the bottom of the hole beneath the bit during drilling causes fluid movement in the rock surrounding the hole bottom. The fluid that moves may be either invading filtrate or connate liquid displaced from rock broken by the drilling bit.

6. Movement of fluid through rock around the hole bottom was measured at the model well during drilling with clay water, lime-starch, oil base, and gel muds; drilling speeds ranged from 6 to 43 ft an hour.

7. The measured fluid movements were compared to maximum flow rates calculated from electric analog potential flow rates. The measured fluid movements, which represented possible filtrate invasions of from 0.04 to 0.64 well radii, were much smaller than the potential flow radii of from 0.3 to 14.3 well radii. Mud particle bridging and plugging apparently limit the flow of filtrate from mud stream to formation even beneath the bit where no mud cake exists.

8. At the model well, connate water in motion could not be distinguished from filtrate, but by comparing data with those collected by Nowak and Krueger, we conclude that much of the measured movement was due to displaced connate water and was not drilling mud filtrate.

NOMENCLATURE

A = Area in general
$A_h = \pi r^2$ area of hole bottom
C = Proportionality constant or static filtration constant
E = Flood efficiency, fraction of connate fluids displaced from pores by advancing fluid front
k = Permeability
k_f = Permeability of mud filter cake layer
L = Representative dimension that fixes scale of geometrically similar systems
L_m = Representative dimension of model that fixes model scale
n = Exponent
P = Pressure
p_i = Pressure gradient in filter cake layer at the time it is deposited
Q = Volume rate of liquid moving through the formation across any cylinder whose axis is common with the well bore
Q_c = Volume rate of filtrate crossing the hole bottom
Q_o = Volume rate of filtrate flow from hole bottom calculated from formation permeability and filtration pressure
q = API 30 minute water loss collected through a 7-sq in. filter
R = Radius of invasion of liquids
R_e = Electrical resistance
R_f = Electrical resistance in electric model of field well
R_W = Electrical resistance in electric model of model well
r = Well bore radius
r_c = Radius to inner surface of filter cake
$t = R - r$, depth of invasion of filtrate
U_d = Drilling rate
V = Filtrate volume
V_c = Volume of filtrate through a cylindrical filter
V_m = Volume of mud filter cake
V_o = Volume of fictitious filtrate that would deposit a static cake equal in resistance to the dynamic cake
V_p = Volume of filtrate through a plane filter of unit area
V_s = Volume of filtrate through the portion of the well bore that is scraped clean when the bit is pulled or run
V_u = Volume of filtrate through the part of the well bore that is not scraped clean when the bit is pulled or run
X = Fraction of connate water, within the formation drilled by the bit, that is forced ahead of the hole bottom and does not enter the mud stream with sand and chips
x = Distance drilled along axis of well bore
$z = V_c/V_m$, ratio of filtrate volume to mud cake volume
α = Fraction of the well bore that is scraped clean by the bit as pipe is pulled and run
Θ = Time measured from the start of static or dynamic filtration
Θ_1 = Time measured from the start of drilling
Θ_o = Time for the fictitious filtrate volume, V_o, to accumulate
μ = Viscosity, of water, unless designated
μ_o = Oil viscosity
ρ = Specific resistivity
τ = Time to drill to x, $(\Theta_b - r)$ is the time filtration has been in progress at location x
ϕ = Formation porosity

ACKNOWLEDGMENTS

The authors express their appreciation to W. T. Cardwell, Jr., and W. W. Garvin who originally conceived the investigation of beneath the bit filtration, developed our interest in this problem, and, by provocative discussions, helped us to arrive at the beneath the bit filtration results reported here.

REFERENCES

1. "Recommended Practice for Standard Field Procedure for Testing Drilling Fluids," API RP 29 (May, 1950) 3rd Ed.
2. Schremp, F. W., and Johnson, V. L.: "Drilling Fluid Filter Loss at High Temperatures and Pressures," *Trans.* AIME (1952), **195**, 157.
3. Stormont, D. H.: "Expermental Rig," *Oil and Gas Jour.* (Dec. 14, 1950), **49**, 61.
4. "Mystery Rig at La Habra," *Petroleum World,* (July, 1951) 48, No. 7, 28.
5. a) Brown and Associates; *Unit Operations,* John Wiley and Sons, New York (1950), p. 242.

b) Badger, W. L. and McCabe, W. L.: *Elements of Chemical Engineering*, McGraw-Hill Book Company, Inc., New York, 2nd Ed., (1936), p. 494.

c) Walker, W. H., Lewis, W. K., McAdams, W. H., and Gilliland, E. R.: *Principles of Chemical Engineering*, McGraw-Hill Book Company, Inc., New York, 3rd Ed., (1937), p. 342.

6. Prokop, C. L.: "Radial Filtration of Drilling Mud," *Trans.* AIME (1952), **195**, 5.
7. Williams, M.: "Radial Filtration of Drilling Mud," *Trans.* AIME (1940), **136**, 55.
8. Beck, R. W., Nuss, W. F., and Dunn, T. H.: "Flow Properties of Drilling Muds," *API Drilling and Production Practice* (1947), p. 9.
9. Grace, H. P., "Resistance and Compressibility of Filter Cakes, Part I," *Chem. Eng. Progress*, (June, 1953) **49**, 6, 303.
10. Russell, R. G., Morgan, F., and Muskat, M.: "Some Experiments on the Mobility of Interstitial Waters," *Trans.* AIME (1947), **170**, 51.
11. Holmgren, C. R.: "Some Results of Gas and Water Drives on a Long Core," *Trans.* AIME, (1949), **179**, 103.
12. Nowak, T. J., and Krueger, R. F.: "Effect of Mud Filtrate and Mud Particles on Permeability of Cores," *API Drilling and Production Practice* (1951), p. 164.

APPENDIX I — ELECTRIC ANALOG METHODS AND COMPUTATIONS

The maximum possible filtrate invasion into a uniform formation from beneath a drilling bit would occur if there were no filter cake resistance to flow of water. For this condition the flow of filtrate is described by Darcy's law and a potential flow field exists.

The analogy between incompressible fluid flow and current flow is given by the following equations:

$$\text{Fluid flow, } P = C\,\frac{1}{L}\,\frac{\mu}{k}\,Q$$

$$\text{Electricity, } Emf = C\,\frac{\rho}{L_m}\,I = R_e I$$

where symbols are given in the nomenclature. The constant of proportionality, C, is fixed by the system geometry. In the electrical system,

$$C = \frac{R_e L_m}{\rho}$$

which can be determined experimentally. With the constant, C, the pressure drop in the fluid flow, or prototype, system can then be calculated.

Two electrical models were used. One modeled the model well system and the other modeled a well in a reservoir of 117 ft drainage radius. Brass or copper surfaces were used for constant potential surfaces and a $CuSO_4$ solution was used for the electrolyte. Small, constant potential surfaces were platinized.

The electrical circuit was a Wheatstone bridge, one side of which contained a variable resistance and variable capacitance in parallel with each other and in series with the model. The bridge was resistance and capacitance balanced and the resistance then recorded.

No attempt was made to move the center electrode, or well bottom, during resistance measurements as the analog would then fail. The total resistance was determined at several levels in each model and, in the model well model, the hole was displaced from the vertical axis and, except when the boundaries were approached, only small effects, ±3 per cent, were observed.

Typical results for the model well model gave an average resistance, from six readings at six depths of drilled hole, of 351 ohms when the specific resistivity of the electrolyte was 2235 ohm-cm. The field well model had a resistance of 8500 ohm for an electrolyte of 3970 ohm-cm specific resistivity. Relative resistance of field and model well systems is computed as

$$R' = \frac{R_f (L/L_m)_w \rho_w}{R_w (L/L_m)_f \rho_f} = \frac{8500 \times \dfrac{5.25 \times 2.54}{2.06} \times 2235}{351 \times \dfrac{100}{1} \times 2970}$$

$$= 1.18$$

where R′ is the ratio of resistance to flow of fluid through the field well system to resistance to flow through the model well system. Despite the small outer radius of the model well formation, a good approximation to reservoir flow was obtained. R' is used to convert model well data to reservoir conditions.

The theoretical maximum flow of filtrate from beneath a drilling bit into a field well formation is,

$$Q_o = \frac{k\,L}{C}\,P$$

where $C = 0.329 \times 1.18 = 0.388$ if units are expressed as Q cc/sec, k darcy, μ cp, r' cm, and P atm. Then,

$$Q_o \frac{\text{ml}}{\text{min}} = 0.792 \left(\frac{k}{\mu}\right) rP \quad . \quad . \quad . \quad (15)$$

in which the well radius, r, has been substituted for the well diameter, which was the representative dimension.

APPENDIX II — SIDE HOLE FILTRATION

To obtain data on the bottom hole filtration and connate water movement, the experimentally measured volumes must be corrected by subtracting from them the side wall filtration. Side wall filtration is calculated from the condition

$$V = CA\Theta^{1/2}$$

For x, the distance drilled, and U_d, the drilling rate

$$\tau = \frac{x}{U_d}$$

and for an elemental area $2\pi r dx$ at some x

$$dV = 2\pi Cr dx(\Theta_d - \tau)^{1/2} = 2\pi Cr(\Theta_d - \tau)^{1/2} U_d d\tau$$

and

$$V = 2\pi C r U_d \int_o^{\Theta_d} (\Theta_d - \tau)^{1/2}\, d\tau = \frac{4}{3}\,\pi C r U_d \Theta_d^{3/2} \quad (16)$$

where

$$C = \frac{q \text{ ml}}{30^{1/2} \times 7}$$

The calculations carried out from Equation (16) are plotted in Fig. 16 and 17. For Run 145, Fig. 17, a 15 ml API water loss was used rather than the measure 10.5 ml in order to linearize the experimental data. Apparently erosion of mud cake due to circulation and drill string rotation was greater for gel mud than for solids-loaded field mud. ★ ★ ★

AN EXPERIMENTAL INVESTIGATION of the S.P. and RESISTIVITY PHENOMENA in DIRTY SANDS

M. R. J. WYLLIE
MEMBER AIME
P. F. SOUTHWICK

GULF RESEARCH & DEVELOPMENT CO.
PITTSBURGH, PA.

T. P. 3750

ABSTRACT

The importance of the so-called "dirty sand" or "conductive solids" problem in electric log interpretation was first stressed in a paper presented in 1949. Since that time the problem has been generally recognized as a most serious one. Several research papers bearing on the theory of the effects of clay contaminants on reservoir rock resistivities have appeared. These papers, while contributing to the theory of the problem, have not offered any practical solution.

In the present paper an experimental investigation has been made of the effects of ion-exchange materials on the electrical properties of natural and synthetic porous media. The method used to make synthetic dirty sands is entirely novel and has proved a valuable guide to a better understanding of the properties of dirty sands generally. The effects of ion-exchange materials on both the resistivity and self potential (S.P.) logs have been examined. From the data obtained it has been possible to formulate a simple, practical method whereby electrical logs of dirty sands can be qualitatively interpreted. The method is in all essentials identical to that presently in use for interpreting clean sands. New light has also been thrown on the significance of the term formation factor when it is applied to dirty sands.

INTRODUCTION

In 1949 a paper was presented[1] which showed that the presence of so-called "conductive solids" introduced considerable complexities into the analysis of the resistivities of dirty sands, i.e., permeable formations containing clay. The reduction of the self potential (S.P.) resulting from the presence of interlaminated shale or interstitial clay in permeable formations has been discussed by Doll.[2,3]

Noteworthy papers which dilate further upon the effects of shale and clay on the resistivity of permeable formations are those of deWitte,[4,5] Berg,[6] Wyllie,[7] and most recently, Winsauer and McCardell.[8] The last authors have endeavored to elucidate the chemistry of the resistivity phenomena in dirty sands in terms of an adsorption hypothesis. Specifically, they attribute the electrolytic conductivity of shales and clays within a permeable formation to an ionic double-layer effect and, for this reason, regard the term "conductive solids" as a misleading one.

Some consideration has been given to the effect of dirty sands on the S.P. by Wyllie[7] and by McCardell, Winsauer and Williams.[9]

Published work to date has cast light only on certain theoretical aspects of the problems created by the presence of clays and shales within permeable formations. One object of this paper is to describe experiments which serve to elucidate further the theory of the dirty sand problem and particularly the significance of the term "formation factor" as applied to dirty

[1]References given at end of paper.

Manuscript received in the Petroleum Branch office July 31, 1953. Paper presented at the Petroleum Branch Fall Meeting at Dallas, Tex., Oct. 18-21, 1953.

sands. A second and more important object is to present experimental data which bear on practical methods of overcoming the difficulty of interpreting electric logs of dirty sands.

STATEMENT OF PROBLEM

In a clean, permeable water sand, formation factor F[10] may be defined as

$$F = \frac{R_o}{R_w} \quad . \quad . \quad . \quad . \quad . \quad . \quad . \quad . \quad . \quad . \quad . \quad (1)$$

where R_o is the resistivity of the sand saturated with a fluid of resistivity, R_w. The value of F is a constant which is independent of the magnitude of R_w.

In a sand which contains clay aggregates or shale flakes, Equation (1) no longer holds. However, Equation (1) may be generalized and an apparent formation factor, F_a, defined so that

$$F_a = \frac{R_o}{R_w} \quad . \quad . \quad . \quad . \quad . \quad . \quad . \quad . \quad . \quad . \quad . \quad (2)$$

In Equation (2), F_a is not a constant independent of the magnitude of R_w unless the sand is free of clay contamination. For dirty sands it is found that F_a decreases as R_w increases.

The S.P. deflection recorded on an electric log opposite a thick permeable formation which contains clay is smaller than the S.P. deflection opposite an otherwise similar thick formation which contains no clay or shale.[3] By "otherwise similar formation" is here meant specifically a clean formation saturated with saline water identical to that which can be produced from the formation containing the clay.

Now it has been shown[11] that, as a reasonable approximation in many cases, the S.P. opposite a clean and thick permeable formation is related to the resistivities of the mud filtrate and interstitial water in the formation by the following relationship,

$$\text{S.P.} = kT \log \frac{R_{mf}}{R_w} \quad . \quad . \quad . \quad . \quad . \quad . \quad . \quad . \quad (3)$$

In Equation (3), k is a constant, T the temperature in °K and R_w the resistivity of the interstitial water in the formation. From Equation (3), if the S.P. is diminished because of the presence of shale and clay in the formation, the resistivity of the interstitial water computed will be increased. The abnormally large resistivity so computed may be designated R_{wa}, the apparent interstitial water resistivity.*

In practice, F_a is obtained by utilizing the resistivity of that portion of a permeable formation which lies immediately behind the mud filter cake in a borehole. The portion of sand behind the filter cake, in the case of a water sand, is believed to be fully flushed by mud filtrate. The resistivity of the flushed zone, R_{xo}, may be determined by logging.[12] For dirty water sands, therefore, an apparent formation factor may be obtained from the relationship R_{xo}/R_{mf}, while an apparent interstitial water resistivity, R_{wa}, may be calculated from Equation (3) by utilizing the S.P. read directly from the log.**

If $R_w < R_{mf}$, as is usually the case, the apparent formation factor obtained from the ratio R_{xo}/R_{mf} is smaller than one computed from the ratio R_o/R_w. On the other hand, the apparent interstitial water resistivity, R_{wa}, calculated from the recorded S.P. by the use of Equation (3) is greater than the true resistivity, R_w. Clearly, the product $(R_{xo}/R_{mf})R_{wa}$, when compared with the corresponding product $(R_o/R_w)R_w$, contains one term which is smaller and one which is larger than its counterpart. M. P. Tixier has suggested to the writers, with his customary intuition, that the product $(R_{xo}/R_{mf})R_{wa} = (R_o/R_w)R_w = R_o$, the resistivity of the dirty sand saturated with interstitial water. From *a priori* considerations such a conclusion is not obvious. Tixier's suggestion implies that the simultaneous experimental investigation of resistivity and S.P. phenomena in dirty sands should be profitable. It is this approach to the problem which has been followed below.

THEORETICAL MODEL

Consider the electrochemical cell which is set up between a shale stratum, a dirty sand containing saline water only (no hydrocarbons), and the mud in the borehole. It will be assumed, as outlined elsewhere,[7] that the presence of clay imparts to the pores of the sand an average fixed negative charge of activity, A. The magnitude of this charge is defined in terms of moles per thousand grams of physically mobile water in the sand. The negative charge is electrically counterbalanced by the presence of cations. These cations may be considered, for simplicity, to be sodium ions, but it may be noted that a portion of them are frequently divalent ions such as calcium.[7]* For the purpose of this discussion, it is immaterial how the negative charge on the clay lattice. It is convenient to emphasize here, howadsorption as suggested by McCardell et al,[9] but is more probably the consequence of charge deficiencies in the clay lattice. It is convenient to emphasize here, however, that the charged clay particles possess cation-exchange properties.

The total number of cations in the water contained within a dirty sand is greater than the number that would be anticipated on the basis of an analysis of a produced sample of the water. In the produced water, for reasons of electrical neutrality, one sodium ion would be found for each chloride ion, if hydrolysis is neglected and assuming, for simplicity, a sodium chloride solution. More generally the equivalents of positive and negative ions are equal.) Within the sand, sodium ions, which act as counterions to the charged clay particles, are also in solution. While these ions tend to congregate in the vicinity of charged surfaces and are not uniformly distributed, they may be considered effectively to increase the average concentration of sodium ions in the sand. This effect is most marked when the volume of mobile water is small by comparison with the volume of charged material distributed uniformly throughout the sand. The ionic distribution has been considered by McCardell et al, in more detail.[9]

*It seems worth emphasizing that because of the assumptions utilized to derive Equation (3), this equation may not be applied to dirty sands in order to compute a true interstitial water resistivity. In other words, the value of R_{WA} calculated for a dirty sand is not equal to Rw. That R_{WA} is itself of significance is a conclusion reached in the present paper. However, although R_{WA} may itself be useful, it is *not* the resistivity of the water which could be produced from the dirty sand. Attempts to apply Equation (3) to dirty sands by arbitrarily decreasing the value of the parameter (kT) have been made. Such methods are perfectly feasible and may enable Rw to be computed approximately. Nevertheless, they are entirely lacking in theoretical justification and, as such, may give rise to large errors if indiscriminately used.

**It is assumed that the formation is sufficiently thick so that the reduction of S.P. which results from geometrical effects[2] may be ignored. It is also assumed that streaming potential effects are negligible.

*The divalent ions are frequently replaced by sodium ions (by cation exchange) in the zone of filtrate invasion. Since sodium clays are more conductive than calcium or magnesium clays such exchange may, in extreme cases, still further complicate the interpretation of dirty sands. This possibility is not considered in the present paper.

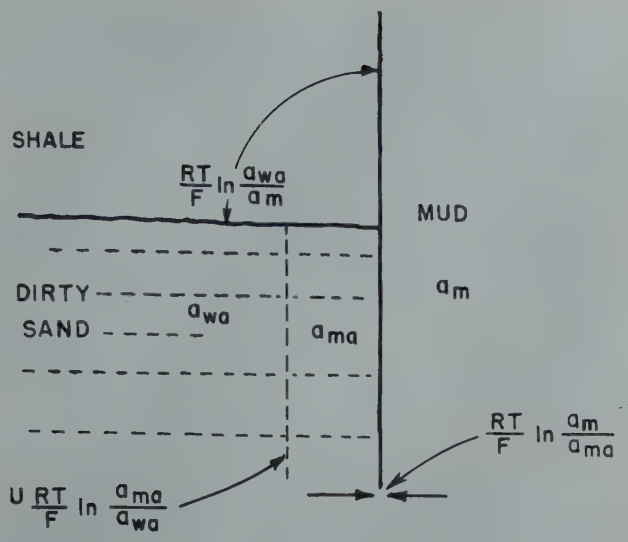

FIG. 1 — POTENTIAL DISTRIBUTION IN AN INVADED DIRTY SAND IN THE BOREHOLE.

The average cationic activity of the solution in the pores of the dirty sand may be written as a_{wa}, where a_w would be the activity measured on a sample of water produced from the sand. The potential across the shale between the dirty sand and mud will be

$$\frac{RT}{F} ln \frac{a_{wa}}{a_m} \quad . \quad . \quad . \quad . \quad . \quad . \quad . \quad . \quad (4)^*$$

as shown in Fig. 1. Here a_m is the cationic activity of the mud in the borehole.

Now if the dirty sand is invaded by mud filtrate from the borehole, the average cationic activity of the mud filtrate in the pores of the dirty sand will be increased by the presence of the cations which balance the negative charges on the clay particles in the sand. Let this average cationic activity of the mud filtrate in the invaded zone be a_{ma}.

Since there is a difference between the activities of the cations of the borehole mud and of the mud filtrate in the invaded zone, a Donnan potential[15] occurs across the interface borehole/invaded zone. The magnitude of this potential is

$$\frac{RT}{F} ln \frac{a_m}{a_{ma}} \quad . \quad . \quad . \quad . \quad . \quad . \quad . \quad . \quad (5)$$

For a clean sand this potential does not exist, since for a clean sand $a_m = a_{ma}$.

A liquid junction potential is also set up in the dirty sand between the mud filtrate which has penetrated into the sand and the interstitial water. The magnitude of this potential is approximately

$$U \frac{RT}{F} ln \frac{a_{ma}}{a_{wa}} \quad . \quad . \quad . \quad . \quad . \quad . \quad . \quad . \quad (6)$$

where $U = \frac{U_{Na} - U_{Cl}}{U_{Na} + U_{Cl}}$ and U_{Na}, U_{Cl} are the average mobilities of sodium and chloride ions in the interstices of the dirty sand. In Equation (6) cationic activities are written for mean activities. In moderately dirty sands this is probably a reasonable approximation.

*In Equations (4) to (9), RT/F preceding a logarithmic function has its customary thermodynamical significance, i.e., R is the gas constant, T the absolute temperature and F the Faraday.

The total potential of the chain, i.e., the S.P. that would be recorded, is the algebraic sum of the potentials in Equations (4), (5), and (6). It is approximately

$$\text{S.P.} = \frac{RT}{F} ln \frac{a_{wa}}{a_{ma}} + U \frac{RT}{F} ln \frac{a_{ma}}{a_{wa}} \quad . \quad (7)$$

Note that the actual activity of the mud does not appear in Equation (7). The mud in front of the dirty sand is negative with respect to that in front of the shale if $a_{wa} > a_{ma}$.

In the above derivation, certain simplifying assumptions have been made. These assumptions are believed to be quite compatible with the accuracy required in the practical solution of the problem. A more detailed thermodynamical discussion of the potentials across an imperfect, charged membrane, of which a dirty sand is a crude natural embodiment, has recently been presented by Scatchard.[13]

It may be noted also that the shale overlying the dirty sand has been considered to be a perfect cation-exchange membrane. Reasons for adopting this view have been presented in detail elsewhere.[7] These reasons are believed to override considerations based on laboratory data in cases where constant shale baselines are observed on logs.[14,9]

The earth train shown in Fig. 1 may be set up in the laboratory, but measurements on such a train are not readily made. It is more convenient to make potential measurements of part of the train and to derive the overall S.P. from these measurements by appropriate calculations.

If the potential is measured across a dirty sand saturated with saline water of activity, a_w, (measured on a sample) and invaded by a solution of external activity, a_m, the potential distribution is as follows:

$$a_m \,|\, a_{ma} \,|\, a_{wa} \,|\, a_w$$

Dirty Sand

Across the interface between a_m outside the dirty sand and a_{ma} inside the sand, the potential is

$$\frac{RT}{F} ln \frac{a_m}{a_{ma}}$$

The liquid junction potential between a_{ma} and a_{wa} inside the dirty sand may be written,

$$U \frac{RT}{F} ln \frac{a_{ma}}{a_{wa}}$$

Across the interface between a_{wa} inside the dirty sand and a_w outside, the potential is

$$\frac{RT}{F} ln \frac{a_{wa}}{a_w}$$

The overall potential, E, is the algebraic sum of the three potential components, i.e.,

$$E = \frac{RT}{F} ln \frac{a_m}{a_w} + \frac{RT}{F} ln \frac{a_{wa}}{a_{ma}} + U \frac{RT}{F} ln \frac{a_{ma}}{a_{wa}}. \quad (8)$$

A comparison of Equation (8) with Equation (7) reveals that the two equations differ only by the quantity $\frac{RT}{F} ln \frac{a_m}{a_w}$, the Nernst potential of a perfect cation-exchange membrane electrode. This quantity is readily calculable. Thus,

$$\text{S.P.} = E. - \frac{RT}{F} ln \frac{a_m}{a_w}$$

or, more conveniently, since $a_w > a_m$ in most cases and only numerical values are required,

$$\text{S.P.} = \frac{RT}{F} ln \frac{a_w}{a_m} + E \quad . \quad . \quad . \quad . \quad . \quad . \quad (9)$$

It may be noted that the derivation of Equation (9) is not dependent on assumptions made to calculate the liquid junction potential between the two saline solutions within the pores of the dirty sand. In the sign convention used, the term E has the same sign as $\frac{RT}{F} ln \frac{a_w}{a_m}$ for clean sands, but is of opposite sign for very dirty sands.

EXPERIMENTAL

Artificial Dirty Sands

Initial experiments were conducted with artificial dirty sands. There were three principal reasons for using artificial materials. One was the desire to magnify the effects which were to be studied by using very dirty sands. The second was to vary the dirtiness of a sand without changing the basic geometry of its solid constituents. The third was the desire to reproduce results. None of these aims can be realized with natural materials.

A very dirty natural sand is generally also almost completely impermeable. Again, natural variations make it highly probable that two specimens which differ in clay content, even if from the same formation, are texturally identical. A natural dirty specimen can be used only once, since the dispersion of clay minerals resulting from the use of saturating solutions of low salinity causes irreversible changes in its properties. Accordingly, use was made of the fact that synthetic cation-exchange materials are, in their electrochemical properties, closely analogous to natural clays.

The fact that the cation-exchange properties of synthetic cation-exchangers result from the presence of negative groups on their matrices and not from charge deficiency in the lattice or adsorption was considered, for initial experiments, to be of little moment. Further, if sulphonated polystyrene cation-exchangers are used, it is possible to obtain the material in the form of almost perfect spheres. In this event, Amberlite IR-120* was chosen and wet-sieved to 40-50 mesh U. S. Standard Screen Series.

Four artificial sands were prepared,

a. Composed entirely of Amberlite IR-120 spheres packed to a porosity of approximately 40 per cent.
b. Composed of a homogeneous mixture of Amberlite IR-120 spheres and 40-50 mesh glass spheres in the proportions 20 per cent by volume glass and 80 per cent by volume IR-120. The porosity of the mixture was again about 40 per cent.
c. Similar to b., but composed of 60 per cent by volume of glass and 40 per cent by volume of IR-120. The porosity of the mixture was again about 40 per cent.
d. Composed entirely of glass spheres packed to a porosity of about 40 per cent.

In order of listing, the four artificial sands grade from the equivalent of extremely dirty through very dirty and dirty, to perfectly clean, natural sands. In all cases, the superficial geometry of the solid particles composing the sand is similar; an aggregate of spheres of approximately 40 per cent porosity.

*Made by the Rohm and Haas Company of Philadelphia, who state it to be a nominal 8 per cent divinyl benzene crosslinked sulphonated polystyrene copolymer. For purposes of this investigation, it is closely analogous to Dow Chemical Company's Dowex 50 cation exchanger.

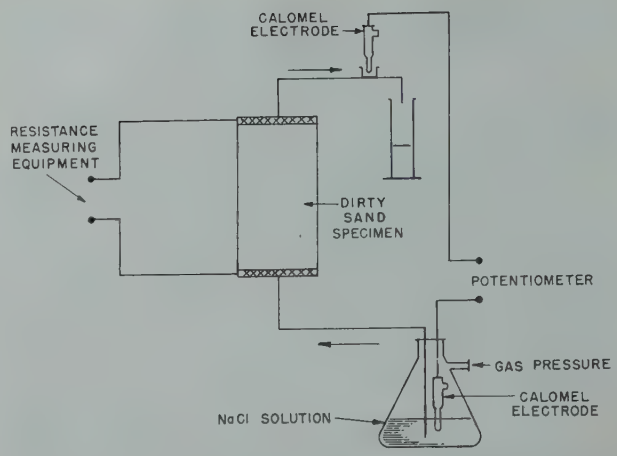

Fig. 2 — Schematic Illustrations of Apparatus for Measuring Resistivity of Dirty Sands as a Function of the Resistivity of NaCl Solutions Used to Saturate Them and for the Measurement of Liquid Junction Potentials Between Displacing and Displaced Saturating Solutions.

Natural Dirty Sands

Three natural dirty sands were also tested. These were selected at random from cores available and were: (a) Stevens Sand, Paloma, Calif.; (b) Yegua Sand, Hull field, Tex.; and (c) Kernco Sand, Fruitvale field, Calif.

Method of Measurement

A schematic representation of the apparatus used is shown in Fig. 2.

The specimens were packed in a glass tube (artificial dirty sands) or encased in Lucite (natural specimens). Each face of the specimens was in intimate contact with a platinized-platinum gauze screen. Leads from the screens were taken to a 1,000-cycle conductivity bridge. A specimen was first saturated with a solution of very low mean activity and its resistance measured. From this resistance the resistivity of the specimen was calculated. A second solution of mean activity twice that of the solution in the specimen was then forced by gas pressure into the specimen holder from the bottom, so as to displace the first solution from the specimen.

While the interface between the first and second solutions passed through the specimen, readings of the potential between two saturated calomel electrodes were made. Saturated KCl bridges were used. One calomel electrode and bridge was in the reservoir containing the second solution, the other in the line leading from the top of the specimen holder. A number of potential measurements were made with the interface stationary at different levels in the specimen. A stationary interface is necessary, particularly when solutions of very high resistivity are used, in order to avoid measuring a streaming potential in addition to the electrochemical potential between the two solutions. The potentials measured at different levels of the interface were generally very similar although not identical. The differences probably resulted from inhomogeneities in the specimens. The average of a number of readings obtained as an interface passed through a specimen was recorded.

After the potential measurements had been made, the KCl bridges were removed to obviate any contamination of the entering solution, and the second solution flowed until the resistance of the specimen became constant. The resistivity of the solution leaving the top of the core was also checked at this time to insure that it was identical to the resistivity of the solution entering at the bottom. A third solution of twice the mean activity of the second was then forced into the specimen from the bottom and the measuring procedure repeated. The sequence was continued until the mean activity of the last solution used approached that of a saturated solution.

The solutions used with all four artificial specimens and the three natural specimens were made from C.P. NaCl.

RESULTS

The principal experimental data obtained are conveniently summarized in Fig. 3 and 4. Fig. 3 shows the recorded potentials and Fig. 4 the conductivity data. For convenience, the potentials in Fig. 3 are recorded in the form of a Meyer-Sievers-Teorell[15] plot in which the potential (in millivolts) is plotted on a linear ordinate against $\frac{1}{a_2}$ (in moles^{-1}) as abscissa on a logarithmic scale. Here a_2 represents the mean activity of the more dilute NaCl solution used in the potential experiments. As noted above, the ratio $\frac{a_1}{a_2}$ of the mean activities of the two NaCl solutions employed for each displacement was maintained constant at a ratio of 2.0.

For purposes of comparison, theoretical curves are also shown on Fig. 3. These curves are calculated for a fixed charge $A = 1.0$ and varying ratios of the mobilities of the Na and Cl ions, U_{Na} and U_{Cl}, within the specimens. Since the Meyer-Sievers-Teorell theory neglects transfer of water and makes other approximations, Fig. 3 is principally designed to illustrate the similarity of the potential data obtained to analogous measurements on more conventional negatively-charged membranes.

In spite of the quantitative limitations of the Meyer-Sievers-Teorell theory, it will be seen that qualitatively the results obtained for both artificial and natural dirty sands are fully in accord with theoretical expectations. In all cases, as the activities of the NaCl solutions used increase, the potentials decrease. Only in very dilute solutions do the recorded potentials approach the limiting Nernst potential, 59.5 log a_1/a_2 millivolts, for a perfect negatively-charged membrane. In very concentrated solutions the potential approaches a lower potential limit, the liquid junction potential between the two NaCl solutions.

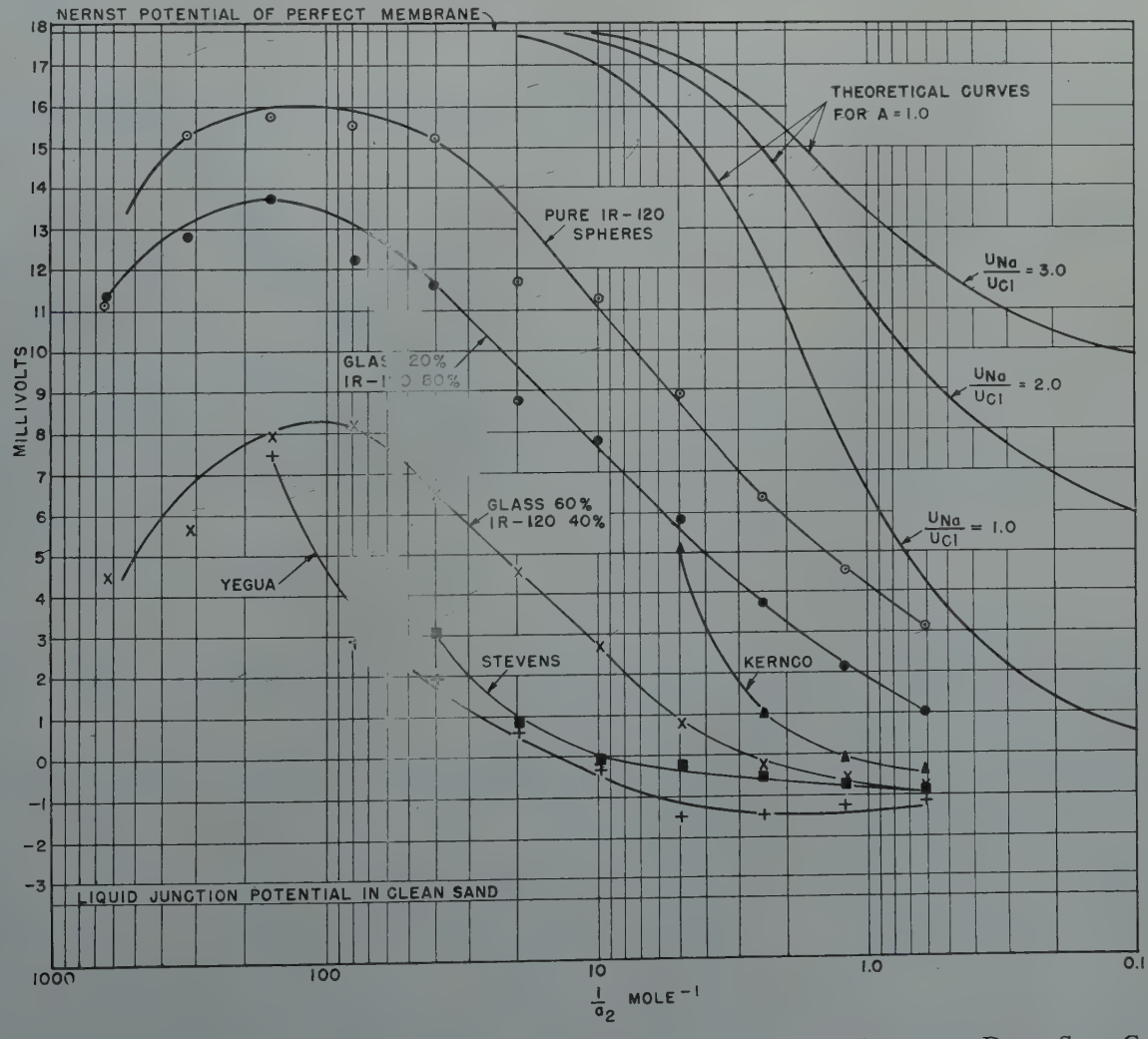

FIG. 3 — MEYER-SIEVERS-TEORELL PLOT OF POTENTIALS ACROSS NATURAL AND ARTIFICIAL DIRTY SAND CORES AS A FUNCTION OF a^1/a_2. SPECIMENS SEPARATING NaCl SOLUTIONS OF MEAN ACTIVITY RATIO $a^1/a_2 = 2.0$ IN ALL CASES.

It is of interest that in the case of the artificial dirty sands the recorded potentials increase to a maximum with decreasing NaCl activities and then, at very low activities of the solutions separated, tend to decrease once again. This phenomenon has been observed previously but is not yet fully understood.[13,16] The phenomenon is of no consequence in the present investigation since the activities at which it occurs are at least an order of magnitude smaller than those likely to be of practical significance in well logging operations.

According to the Meyer-Sievers-Teorell theory, the charge A can be determined by matching an experimental curve with a theoretical curve and finding the amount by which the experimental curve has to be transposed on Fig. 3 in order to be superimposed on a theoretical curve. Transposition to the right implies that A is less than unity, to left that A is greater than unity. It is apparent from Fig. 3 that in all cases the experimental curves refer to sands for which the charge A is considerably less than unity. Of the three natural dirty sands, the Kernco is the most dirty in terms of charge A. Even the Kernco sand has a smaller charge than either the artificial sand made from pure IR-120 spheres or that composed of a mixture of 20 per cent glass spheres and 80 per cent IR-120 spheres.

Fig. 4, which is plotted for convenience of presentation on a double logarithmic scale, shows the conductivity of the specimens as a function of the conductivity of the NaCl solutions used to saturate them. It will be seen that when the conductivities of the saturating solutions are large the plots in all cases tend to a slope of 45°, and that when the conductivities of the saturating solutions are small the curves bend away from the 45° line. A slope of 45°, which is exemplified by the data for the packing of glass spheres, indicates that a constant formation factor is being measured. The criterion for a constant formation factor is a constant ratio between the conductivities of specimen and solution which, on symmetrical double logarithmic paper, involves a slope of 45°.

Fig. 5 shows a linear plot of the conductivity data obtained for the artificial dirty sands.

From Fig. 5 it is apparent, as noted elsewhere,[7] that for saturating solutions having conductivities extending over a considerable range, a straight line can reasonably be drawn through the points representing the conductivities of the saturated specimens. Only as the conductivities of the saturating solutions tend to zero do lines through the plotted points diverge markedly from linearity. Divergence from linearity occurs at conductivities of the saturating solutions which are relatively large in the case of the specimen composed wholly of Amberlite IR-120 spheres, and at progressively lower conductivities as the quantity of IR-120 spheres in the artificial dirty sands decreases. For the specimen com-

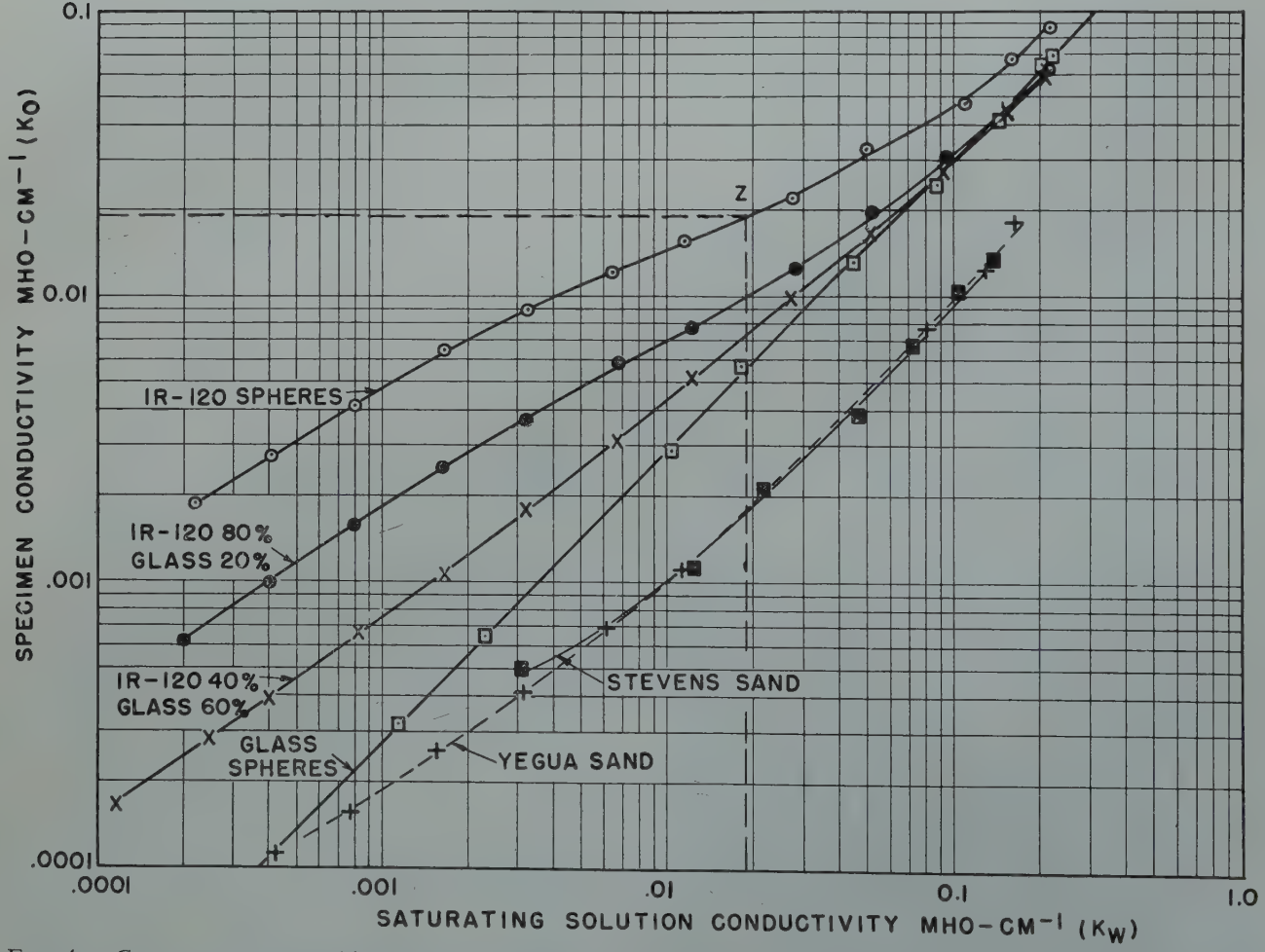

FIG. 4 — CONDUCTIVITIES OF NATURAL AND ARTIFICIAL DIRTY SAND SPECIMENS PLOTTED AS A FUNCTION OF SATURATING SOLUTION CONDUCTIVITY.

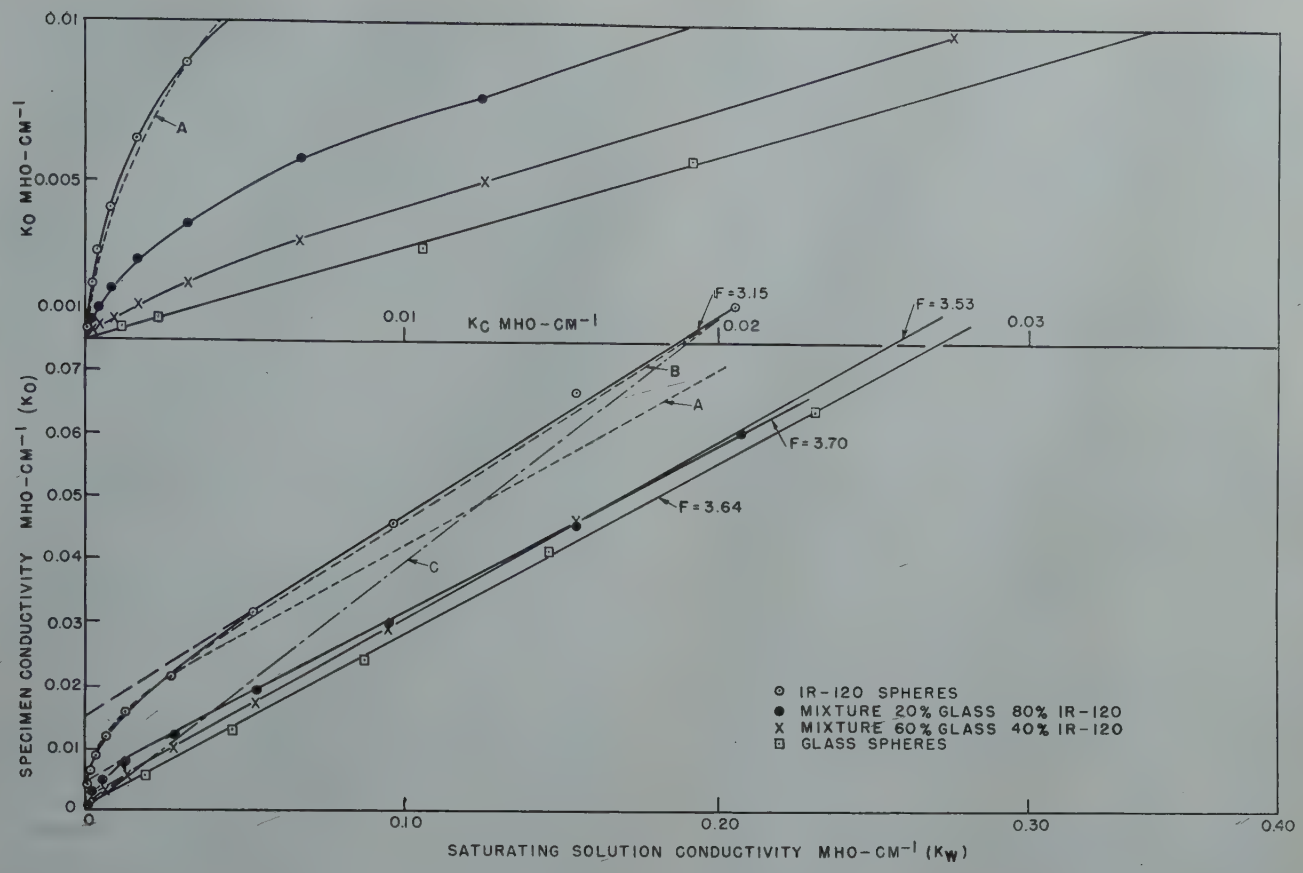

FIG. 5 — CONDUCTIVITIES OF PACKING OF SPHERES VERSUS CONDUCTIVITIES OF SATURATING SOLUTIONS.

posed of glass spheres only, as would be expected, a straight line is obtained which is independent of the conductivity of the saturating solution.

If the straight lines drawn through the point corresponding to saturating solutions with large conductivities are extended to cut the ordinate at $K_w = 0$, Fig. 5 shows that conductivities of the specimens so obtained decrease as the amount of Amberlite IR-120 in the artificial dirty sands decreases. The conductivities of the specimens saturated with a solution of zero conductivity are shown in Table 1.

Since formation factor, F, is given by

$$F = \frac{\text{Conductivity of saturating solution}}{\text{Conductivity of saturated specimen}}$$

it follows that the slope of the straight line through the points obtained for the packing of glass spheres is $\frac{1}{F}$.

If the specimen conductivities at $K_w = 0$ are ignored and the slopes of the straight line portions of the other curves are used to compute formation factors, the values listed in Table 1 are obtained.

In Fig. 7 the S.P. computed from Equation (9) is plotted on a linear scale against the conductivities of the specimens, K_o, on a logarithmic scale. The method used to calculate the S.P. data from the potentials measured experimentally is shown in detail in Table 2. In Table 2, column 5 gives the potentials actually measured between pairs of solutions whose mean activities are listed in column 1. Column 6 gives the cumulative potential measured against a solution of mean activity equal to 0.00625 m. The cumulative potential against any other solution is easily obtainable in an analogous manner.

DISCUSSION

THE TRUE FORMATION FACTOR OF DIRTY SANDS

For the relationship between the conductivity of a dirty sand, K_o, the conductivity of the fluid used to saturate it, K_w, and the "true formation factor," F, Patnode and Wyllie[1] suggested the following approximate expression,

$$K_o = \frac{K_w}{F} + K_f \quad . \quad . \quad . \quad . \quad . \quad . \quad . \quad . \quad . \quad (10)$$

In Equation (10), K_f is the conductivity of the conductive solids as distributed in the core. It was assumed that K_f was substantially constant and independent of the magnitude of K_w. The true formation factor, F, was defined as the formation factor that the sand would have if none of the solid materials in it were conductive. Essentially, F, on the basis of this definition, was intended to be the formation factor of the gross voids in a dirty sand, i.e., voids between grains of silica and other matrix minerals and shale or clay particles or aggregates.

It has subsequently been claimed[7,8] that K_f is apparently dependent on K_w, particularly at small values of K_w.

Consider first the conductivity data for the artificial specimens of dirty sand. It may be concluded, since in all cases the spheres of glass and IR-120 were packed

to a porosity of approximately 40 per cent, that the geometry of the gross voids of all these specimens was essentially the same. The specimen comprised of glass spheres represents one which contains no solid components capable of giving rise to electrolytic conductivity. The formation factor of this specimen is 3.64 and K_t is zero (Table 1).

The other extreme is represented by the aggregate of IR-120 spheres. The solid components of this specimen are all electrolytically conductive. If Equation (10) is correct, a plot of K_o against K_w on linear coordinates should yield, for this specimen, a straight line with slope $\frac{1}{3.64}$ and finite intercept on the K_o axis equal to K_t. Fig. 5 shows that these expectations are not realized. The plot of specimen conductivity against saturating solution conductivity is not a straight line. When the conductivity of the saturation solution exceeds about 0.03 mho-cm,$^{-1}$* a straight line through the plotted points appears justifiable. Of interest is the fact that the reciprocal of the slope of the straight line portion of the curve is only 3.15, considerably less than the 3.64 applicable to the voids between the IR-120 spheres. Table 1 reveals also that the value of K_t obtained on extrapolation is greatest for the specimen composed wholly of IR-120 spheres and decreases as the quantity of IR-120 spheres in the specimens decreases and the quantity of glass spheres increases. Considering the nature of the quantity K_t, these observations are in qualitative accord with Equation (10). The limiting formation factors, listed in Table 1, of the specimens composed of mixtures of IR-120 and glass spheres, exceed the formation factor of 3.15 applicable to the specimen composed of IR-120 spheres only. In one case the formation factor is 3.53 while in the other it is 3.70. Thus, one formation factor is less than the 3.64 applicable to a specimen composed of glass spheres while the other is greater. As will be shown below, the value of 3.70 is probably anomalous and indicative of the fact that the specimen was, in error, packed to a porosity which was less than 40 per cent.

Equation (10) is based on the assumption that the overall conductivity of a porous medium containing conductive solids such as Amberlite IR-120 is the sum of two components; the conductivity through the conductive solids and the conductivity through the solution filling the voids between the solids. The experimental data shown in Fig. 5 suggest that this assumption oversimplifies the true picture. It would appear that not only are there two conductivities in parallel as is assumed by Equation (10), but that, in addition, there is a component of conductivity in series with the two parallel conductivities. The series component may be of significant magnitude.

It is desirable now to consider the nature of the electrolytic conductivity shown by Amberlite IR-120. This conductivity is itself a dichotomy. Spheres of IR-120 are electrolytically conductive, even in the presence of water free from ionized solute, because of their exchangeable ions. The exchangeable ions (cations) are capable of carrying current. The conduction resulting from exchangeable ions may be considered, to a first approximation, as being independent of the ionic concentration of solutions in contact with the IR-120 spheres.

*i.e., resistivities less than 0.33 ohm-meters.

The IR-120 spheres themselves may best be visualized as porous sponges with sulphonic acid groups firmly bound at varying intervals along the surfaces of the pores. The sulphonic acid groups are electrically balanced by mobile (exchange) cations. When spheres of IR-120 are immersed in water free of solute, their pores contain only water and mobile cations. If the spheres are immersed in a solution containing anions and cations, some anions and cations from the solution will migrate into the water within the pores of the spheres. The concentration within the spheres of the immigrant ions will be controlled by a Donnan distribution.

At equilibrium the activity of the solute which has migrated into the pores of the IR-120 spheres must be equal to the activity of the solute in the solution in which the spheres are immersed. For a sodium chloride solution and for the IR-120 spheres in the sodium form, it follows that,

$$a_{Na(outside)} \times a_{Cl(outside)} = a_{Na(inside)} \times a_{Cl(inside)}$$

where a_{Na}, a_{Cl} represent activities of sodium and chloride ions. But the activity of sodium ions inside a sphere is much greater than that of chloride ions because of the high concentration of exchangeable sodium ions associated with the sulphonic acid groups. For IR-120 spheres the concentration of exchangeable sodium ions, in terms of the pore water, is about 7.0 molal; greater, in fact, than in a saturated solution of NaCl. Thus $a_{Na(inside)}$ is very large and $a_{Cl(inside)} = [a_{Na(outside)} \times a_{Cl(outside)}]/a_{Na(inside)}$ accordingly small unless the product $a_{Na(outside)} \times a_{Cl(outside)}$ is comparable to $a_{Na(inside)}$.

Since, for reasons of electrical neutrality, each chloride ion diffusing into an IR-120 sphere is accompanied by a sodium ion, it follows that the concentration of NaCl within a sphere is much smaller than the concentration outside. It follows, also, that the concentration of NaCl inside a sphere increases both absolutely and as a fraction of that in the external solution as the external solution concentration increases. Since the NaCl diffusing into a sphere supplements the conduction resulting from the exchangeable sodium ions already present, it follows also, that the specific conductivity of IR-120 is a function of the conductance of the NaCl solution in which the exchange resin spheres are immersed.

In summary then, the specific conductance of Amberlite IR-120 is the consequence of conduction by exchangeable sodium ions and conduction by sodium and chloride ions which have migrated into the pores of the resin spheres. The conduction by the exchangeable sodium ions may be regarded as being sensibly independent of the external NaCl concentration while the conduction of the immigrant sodium and chloride ions is a function of the external NaCl concentration. At low concentrations of the external NaCl solution the conductivity of IR-120 is almost entirely the result of conduction by exchangeable ions.

At medium and high NaCl concentrations the conduction by immigrant sodium and chloride ions becomes appreciable but is still small by comparison with the conduction of the exchangeable sodium ions. At an infinitely large external NaCl concentration, were such a concentration physically attainable, the immigrant NaCl content would be identical with the external NaCl content. Under such conditions the conductivity of IR-120 would be due entirely to the immigrant NaCl, the contribution of the exchangeable sodium ions being negligible by comparison.

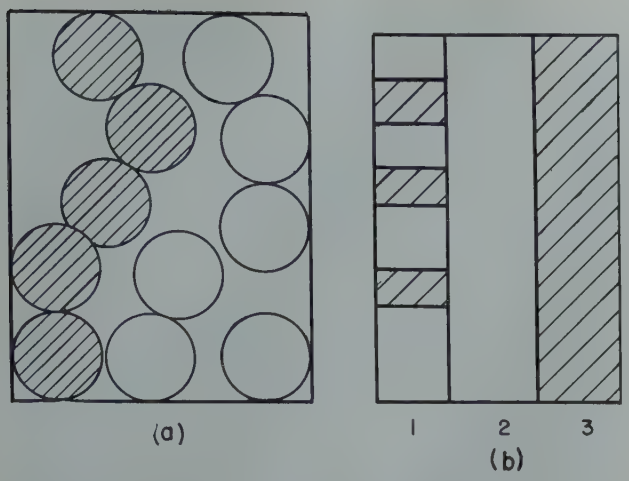

FIG. 6 — (A) MODEL OF CONDUCTING SOLID NETWORK COMPOSED OF SPHERES IN GOOD ELECTRICAL CONTACT (SHADED) AND IN POOR OR NON-EXISTENT CONTACT (UNSHADED). (B) SIMPLIFIED PICTURE OF THREE PARALLEL CONDUCTANCES USED FOR THE MATHEMATICAL DERIVATION PRESENTED IN TEXT.

Consider the arrangement of spheres shown in Fig. 6. The simplified packing reveals that there are spheres of two types. Shaded spheres are those that make contact with other spheres, and unshaded spheres are those which do not make such contacts. If the voids between the spheres are filled with a non-conducting fluid, it is immediately apparent that the overall conductivity of the packing will result from conduction through shaded spheres only. The unshaded spheres will be electrically isolated and unavailable for conduction.

On the other hand, if the voids are filled with a highly conducting fluid, all spheres will contribute to the overall conduction. In this case, conduction through unshaded as well as shaded spheres occurs, current now being able to pass in and out of the unshaded spheres via the conducting interstitial fluid.

If fluids of intermediate conductivity fill the voids, the unshaded spheres will contribute to the overall conductivity of the packing but their contribution will be small since the high resistance of the fluid linking them electrically will be of predominant importance. The spheres are essentially in series with the interstitial fluid, while their shaded counterparts are in parallel. The relative abundance of each type of sphere in any packing will clearly depend on such factors as the porosity of the packing and the size distribution of the spheres. In all cases, however, it seems probable that both types will exist. If this is so, it should be possible to represent the overall conductivity of a packing of IR-120 spheres by a model consisting of three components of conductivity in parallel.

These are:

1. A component consisting of solution and IR-120 spheres arranged in series. This component represents the passage of current through the unshaded spheres and the solution between them.
2. A component consisting of those IR-120 spheres which touch to form through-conducting paths (i.e., shaded spheres).
3. A component consisting of the conduction through the fluid-filled voids.

The three components of the model are shown diagrammatically on Fig. 6. Whether this simple model is an adequate representation of the physical facts can only be determined by comparing conclusions based on the model with the experimental data plotted on Fig. 5. For this purpose it is necessary to evaluate the relative contributions of the three components of conduction listed above when a packing of IR-120 spheres is saturated with solutions of varying conductivity.

If K_o is the overall specimen conductivity,

$$K_o = K_1 + K_2 + K_3$$

where K_1 is the conductivity of solution and IR-120 spheres in series, K_2 is the conductivity of IR-120 spheres in contact with one another throughout the packing and K_3 is the conductivity of the interstitial fluid network. Let K_R be the intrinsic specific conductance IR-120 when in equilibrium with a particular solution and K_w the conductivity of the interstitial solution, i.e., solution with which the IR-120 is at equilibrium. Then,

$$\frac{1}{K_1} = \frac{x}{K_w} + \frac{y}{K_R}$$

$$K_1 = \frac{K_R\ K_w}{xK_R + yK_w}$$

where x and y are dimensionless parameters descriptive of the arrangement of IR-120 spheres and interstitial water which are effectively in series.

$$K_2 = \frac{K_R}{z}$$

where z is a dimensionless parameter descriptive of the packing of the IR-120 spheres which are in contact with one another.

$$K_3 = \frac{K_w}{F}$$

where F is the formation factor of all the spheres as packed, i.e., 3.64 for a porosity of 40 per cent. Hence,

$$K_o = \frac{K_R\ K_w}{xK_R + yK_w} + \frac{K_w}{F} + \frac{K_R}{z} \quad . \quad . \quad (11)$$

When $K_w = 0$,

$$K_o = \frac{K_R}{z} \quad . \quad . \quad . \quad . \quad . \quad . \quad . \quad . \quad . \quad . \quad (12)$$

Thus, the value of K_o when K_w equals 0 gives K_R/z and is a measure both of the continuity of the IR-120 solid network and the specific conductance of the IR-120 when free from all immigrant (Donnan) solute.

If $K_w >> K_R$, ie., for solutions of high conductivity,

$$K_o \cong \frac{K_R}{y} + \frac{K_R}{z} + \frac{K_w}{F}$$

$$\cong K_R\left(\frac{1}{y} + \frac{1}{z}\right) + \frac{K_w}{F} \quad . \quad . \quad . \quad . \quad (13)$$

Thus, for values of K_w large by comparison with K_R, the plot of K_o against K_w should be a straight line with slope $1/F$ and with an extrapolated intercept at $K_w = 0$ of $K_R\ (1/y + 1/z)$ if K_R is independent of K_w. This is probably the case when highly crosslinked resinous materials are used which show little Donnan diffusion. For resins of moderate crosslinking, K_R is itself a function of K_w since, as described above, salt enters the pores of the IR-120 spheres and thereby increases their conductivity. The recent data of Pepper, Reichenberg and Hale[17] on the migration of solute from an external solution into ion-exchange resins of the same type as IR-120 shows that the ratio (salt concentration

inside/salt concentration outside) is almost proportional to the external salt concentration over a wide range of external salt concentrations. Thus, as a close approximation,

$$K_R \cong K_{Na} + \rho K_w^2$$

where K_{Na} = specific conductance of the resin due to exchangeable sodium ions,

$$\rho = \text{constant fraction} \propto \frac{\text{conductivity of NaCl inside a sphere}}{F_R K_w^2}$$

and

F_R = formation factor of the porous resin matrix of IR-120. Thus, Equation (12) may be rewritten,

$$K_o = \frac{K_{Na}}{z} \quad . \quad . \quad . \quad . \quad . \quad . \quad . \quad . \quad . \quad . \quad (14)$$

$K_w \to 0$

and Equation (13) becomes

$$K_o \cong K_{Na}\left(\frac{1}{y} + \frac{1}{z}\right) + \left[K_w\left\{\rho K_w\left(\frac{1}{y} + \frac{1}{z}\right) + \frac{1}{F}\right\}\right] \quad . \quad . \quad . \quad . \quad (15)$$

Thus, a plot of K_o against K_w for $K_w >> K_R$ will approximate a straight line of slope $1/F$ if ρ is small. If this line is extrapolated at the same slope to intercept the K_o axis it follows that for $K_w = 0$,

$$K_o \cong K_{Na}\left(\frac{1}{y} + \frac{1}{z}\right). \quad . \quad . \quad . \quad . \quad . \quad . \quad (16)$$

Qualitatively, the simple model is a reasonable fit with the experimental data shown in Fig. 5. Specifically it shows:

(a) That for large values of K_w the plot of K_w versus K_o is approximately a straight line with a slope which is somewhat greater than 1/F since the quantity $\rho K_w^2(1/y + 1/z)$ is not entirely negligible.

(b) That the approximate straight line relationship between K_w and K_o at large values of K_w, when extended by extrapolation to $K_w = 0$, gives a fictitious value of $K_o \cong K_{Na}(1/y + 1/z)$. This conductivity is the contribution of the resin to the total conductivity of the plug when the solution concentration is high and when no immigrant NaCl enters the IR-120 spheres.

(c) That the real conductivity K_o for $K_w = 0$ is K_{Na}/z. This conductivity is a measure both of the conduction resulting only from the exchangeable cations and of the electrical continuity of the spheres in the packing. By differentiating Equation (11), it is found that

$$\frac{dK_o}{dK_w} = \frac{xK_R^2}{(yK_w + xK_R)^2} + \frac{1}{F} \quad . \quad (17)$$

As $K_w \to 0$, Equation (17) reduces to

$$\frac{dK_o}{dK_w} = \frac{1}{x} + \frac{1}{F} \quad . \quad . \quad . \quad . \quad . \quad (18)$$

Hence, by measuring the slope of the plot of K_o versus K_w *as* $K_w \to 0$, it is possible, by utilizing Equation (18), to determine x if F is assumed to be 3.64 as shown in the experiments with the glass spheres. From the conductance of the plug in pure water, K_{Na}/z (Equation 14) is found, and by extrapolating as a straight line the relationship between K_o and K_w existing at large values of K_w to $K_w = 0$ a value of K_o is obtained which, from Equation (15), is approximately equal to $K_{Na}(1/y + 1/z)$. Thus, all the parameters necessary to solve Equation (11) for K_o in terms of K_w may be found.

The data for the packing of IR - 120 spheres when so treated yield $x = 0.2$, $K_{Na}/y = 0.01475$ mho-cm,$^{-1}$ $K_{Na}/z = 0.00025$ mho-cm.$^{-1}$ Utlizing these data, a relationship between K_o and K_w may be calculated. This relationship is plotted as the dotted line A on Fig. 5. The match between the calculated dotted line and the measured solid line is excellent over a range of K_w extending from zero to about 0.015 mho-cm.$^{-1}$ For $K_w > 0.015$ mho-cm,$^{-1}$ the dotted line falls below the solid line.

The data of Pepper, Reichenberg and Hale[17] show that up to about 0.1 N external salt concentration the uptake of salt by a sulphonated polystyrene ion-exchange resin with 8 per cent D.V.B. crosslinking is negligibly small. Thus for external conductivities less than a conductivity corresponding to 0.1 N NaCl solution the agreement between the dotted and solid lines would be expected to be good if the simple model considered above is reasonably accurate. For conductivities corresponding to solutions more concentrated than 0.1 N, the calculated conductivities of the packings of IR-120 spheres would be expected to fall below those measured since the calculated conductivities are based on a constant resin conductivity K_{Na}. The conductivity K_{Na} assumes that no NaCl diffuses into the pores of the IR-120 spheres. Since the conductivity of a 0.1 N NaCl solution is about 0.01 mho-cm,$^{-1}$ it will be seen that the calculated and measured conductivities diverge at a value of K_w which is in reasonable accord with theoretical expectations.

It follows that the difference between the calculated and measured values of K_o for values of K_w greater than about 0.01 mho-cm^{-1} represents the increasing contribution made by immigrant NaCl to the specific conductance of the IR-120 resin.

It is possible to compute approximately the contribution of the immigrant NaCl. For this purpose, the data of Pepper et al[17] were utilized to estimate the NaCl concentration in the IR-120 spheres and those of Bauman and Eichhorn[18] for Dowex 50 to estimate the matrix formation factor of a sphere. The data of Pepper et al show that the ratio (conductivity of NaCl inside a sphere/K_w^2) is about 0.05, while the data of Bauman and Eichhorn show that the diffusion constants inside and outside Dowex 50 spheres differ by a factor of five. Hence, the internal formation factor of a sphere is about five. Accordingly, the value of ρ is $0.05/5 = 0.01$. When the contribution to the specific conductivity made by immigrant NaCl is assessed, the dotted line marked B on Fig. 5 is obtained. The agreement between the calculated K_o versus K_w relationship and the measured relationship is now extremely good over the entire range of K_w. This agreement may be interpreted as lending support to the basic concepts embodied in the simple model shown in Fig. 6.

The replacement of IR - 120 spheres in a packing by glass spheres would be expected to reduce, on the basis of the above discussion, the contribution of the conductivities designated K_1 and K_2 above to the conductivity K_o. This expectation is confirmed by the data of Table 1.

The addition of glass spheres to the packings will alter

TABLE 1 — Limiting Formation Factors and Extrapolated Specimen Conductivities from Fig. 5

Specimen	Limiting Formation Factor	Specimen Conductivity at $K_C = 0$ mho-cm^{-1}
100% Glass Spheres	3.64	0
60% Glass + 40% IR-120 Spheres	3.53	0.0025
20% Glass + 80% IR-120 Spheres	3.70	0.005
100% IR-120 Spheres	3.15	0.15

the geometry of the IR - 120 spheres and thus alter the parameters y and z, descriptive of the IR - 120 geometry. That the addition of glass spheres will serve to increase both y and z may best be appreciated by noting the resemblance of the parameters y and z to conventional formation factors. A decrease in the quantity of IR - 120 spheres in the packings is then equivalent to a decrease in porosity and thus an increase in formation factor. Accordingly, y and z would be expected to increase as the quantity of IR - 120 in the packings decreases.

From this it follows from Equation (15) that the slope of the straight line portions of the K_o versus K_w plots would tend to $1/F$ with decreasing IR - 120 content, while the extrapolated intercepts on the K_o axis would tend to zero. Table 1 confirms these conclusions. The fact that in the one example the limiting formation factor, i.e., the reciprocal of the slope of the straight line portion of the K_o versus K_w plot, is 3.70 is almost certainly the result of the porosity of the mixed bed of IR - 120 and glass spheres being less than 40 per cent.

From the practical standpoint, Equation (15) is important. The equation reveals clearly the impossibility of deriving from simple measurements of K_o as a function of K_w the true formation factor F. However, for moderately large conductivities, K_w, the experimental data appear to give a straight line if K_o is plotted against K_w. The slope of this approximate straight line has been termed the limiting formation factor in Table 1. If this limiting formation factor be designated F', it follows from Equation (13) that

$$\frac{1}{F'} \cong \rho K_w \left(\frac{1}{y} + \frac{1}{z} \right) + \frac{1}{F} \quad . \quad . \quad (19)$$

Only if there is no Donnan diffusion of NaCl into the spheres of IR-120 ($\rho = 0$) will $1/F' = 1/F$. In general F' will be less than F.

The true formation factor, F, is clearly the formation factor which is of practical importance, particularly in relation to the problem of obtaining porosity information from electric log measurements. The formation factor, F', is related to the total fluid content in the specimens examined since some contribution to the overall conductivity is being made by NaCl in the fluid-filled pores within the IR - 120 spheres. Pores within IR - 120 spheres are of no practical importance since they would not be available for the storage of hydrocarbons. Only the space in the gross voids is important in this regard.

A method of obtaining true formation factor simply and directly is not indicated by the experiments carried out. It seems probable, however, that for most dirty sands sufficiently permeable to be of practical importance, the quantity $\rho K_w (1/y + 1/z)$ will be sufficiently small to justify the use of F' in place of F. This approximation seems justified when the uncertainties involved in relating the formation factors of even clean sands to porosity are recollected. The relationship between F_a (Equation 2) and porosity, for all values of K_w, is clearly very complex. Even if K_w is very large, F_a may still be inaccurate as the line C on Fig. 5 reveals. From Fig. 5 F_a, for $K_w = 0.2$ mho-cm,$^{-1}$ is only 2.58. Thus the popular "practical" method of measuring the formation factor of dirty sands by utilizing as saturating fluid a high conductivity salt solution is inherently unreliable.

The above conclusions are predicated on the assumption that the electrical effects of clays and shales in natural rocks are analogous to the electrical effects given by Amberlite IR - 120 spheres. Clearly, this assumption must be justified.

Three types of electrochemically-active materials in reservoir rocks can be distinguished theoretically:

1. Aggregates of clay and other fine-grained materials or small streaks of shale.*
2. Swelling-type clays of the montmorillonite type.
3. Non-swelling clays of the illite type:

(1) For this analysis the clay component of the clay-containing aggregates and shale streaks may be either a swelling or non-swelling type clay. The clay-containing particles are not composed only of clay. They may be visualized as consisting of a mixture of clay, silt and organic matter. The particles are saturated with water and this water may be regarded as analogous to the pore water of IR - 120 spheres. The clay-containing particles are similar to particles of a shale. A shale may be regarded as having a formation factor as Winsauer and McCardell[8] have demonstrated. Indeed, the data of these workers show that the conductivity of the shale varies with changes in the conductivity of the solution in which the shale is immersed. These data are precisely analogous to those applicable to IR - 120 spheres. A measurement of F' for a natural dirty sand would thus reflect not only the water content of the gross voids between all the solid constituents of the sand but would be affected also by the water content of the shale streaks or clay-containing aggregates.

(2) If swelling-type clays exist in a formation in pure unaggregated flakes, these would contain water and ions between lattice layers. For this type of dirty formation also, F' would be influenced by the water held by the clays.

(3) If a formation contains pure unaggregated non-swelling clay particles, no water can be considered to exist within the clay lattice itself. Water which can be removed from the clay structure by high temperature treatment need not be considered. Non-swelling clays of the type envisaged nevertheless have ion-exchange properties and show ionic-double layer conductivity as discussed by Winsauer and McCardell[8]. Formations containing such clays would show all the electrical effects of formations containing shale streaks or swelling clays. The non-swelling clays differ only by virtue of the fact that they have no internal water content. For such formations, $\rho = 0$. Thus, from Equation (19)

$$\frac{1}{F'} = \frac{1}{F} \quad . \quad . \quad . \quad . \quad . \quad . \quad . \quad (20)$$

Since most clay is believed to exist in natural dirty formations either as shale streaks or clay aggregates, it is suggested that the case discussed in (1) above is most applicable in practice.

Details of the actual mechanism of conduction in dirty sands are, however, of little practical importance.**

The Relationship Between Dirty Sand Resistivity and S.P.

From Fig. 7 it may be seen that a plot on semi-logarithmic coordinates of the conductivity of dirty sand specimens against S.P. gives rise to lines which, in many cases, are approximately straight. The slopes of the lines are closely similar to the slope of the straight line

*Gross laminations of sand and shale are specifically excluded.

**Note that the analysis made suggests a method of distinguishing various types of clay conductivity in rocks. If K_1 is large and K_2 small, the clay is disseminated. If K_2 is large and K_1 small, the clay probably exists as thin interbedded laminations.

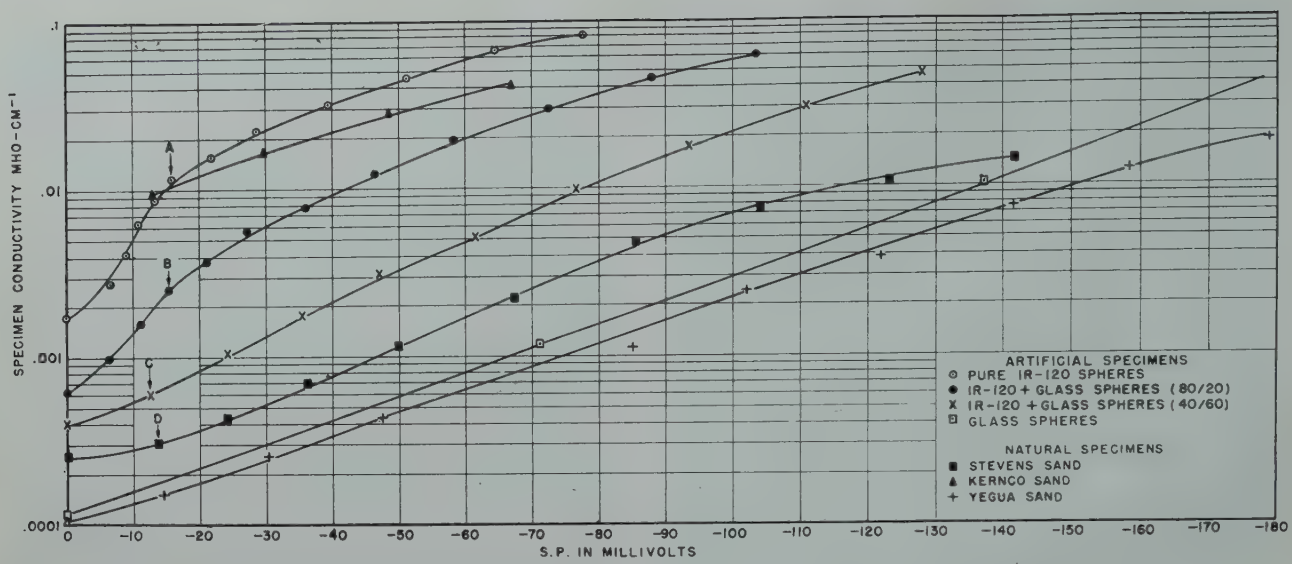

FIG. 7 — MEASURED CONDUCTIVITIES OF DIRTY SAND SPECIMENS AND CALCULATED S.P. DATA.

characteristic of a clean sand. In general, it appears from Figs. 3 and 7 that the straightness of the lines for dirty sand specimens and their similarity to the line for a clean sand increase as the content of electrochemically-active material in the dirty sands decreases.

In particular, specimens which contain a very high content of electrochemically-active material, such as the specimen composed only of IR - 120 spheres, give lines which approach linearity only after a certain limiting value of specimen conductivity is attained. The conductivity of a specimen is a function of the conductivity of the solution used for its saturation. Hence, only for solution conductivities above a certain limiting value is an approximately linear relationship obtained in Fig. 7. For the specimen composed of IR - 120 spheres approximate linearity commences at point A on Fig. 7. This point corresponds to a conductivity of saturating solution of 0.00659 mho-cm.$^{-1}$ Point B on Fig. 7 corresponds to 0.00166 mho-cm.$^{-1}$ In general, the limiting conductivity at which approximate linearity commences appears to decrease as the quantity of electrochemically-active material in a specimen decreases.

In Fig. 8 the ratio R_{xo}/R_o is plotted against S.P. The ratio R_{xo}/R_o is derived from Fig. 7. Here, $R_{xo} = 1/K_{xo}$ where K_{xo} is the limiting conductivity at which the lines of Fig. 7 become approximately linear and $R_o = 1/K_o$, where K_o is specimen conductivity. Column 10 of Table 2 illustrates the method of computation.

Fig. 8 shows that all the data points plotted fall within the limits $K = 56$ and $K = 80$ in the equation,

$$\text{S.P.} = K \log \frac{R_{xo}}{R_o} \quad . \quad . \quad . \quad . \quad . \quad . \quad . \quad (21)$$

If the data for the natural sands only are considered, the limits of K are 65 and 80. For a perfectly clean sand at the temperature at which the experiments were carried out, K is approximately 71. The data of Fig. 8 suggest that, as the quantity of electrochemically-active material in dirty sands decreases, the possible variation in K in Equation (21) decreases.

The approximate validity of Equation (21) undoubtedly stems from complex considerations. Nevertheless, a simple qualitative explanation may be based on the fact that the presence of ion-exchange materials in a porous body effectively increases the average ionic content of the solution in the pores of that body. The increase is principally the result of cations on exchange sites of the ion-exchange material.

From Equation (15) if, as an approximation, the quantity ρK_w^2 is considered small by comparison with K_{Na} and K_w (note that $0 < \rho < 1$ in all cases).

$$K_o = K_{Na}\left(\frac{1}{y}+\frac{1}{z}\right)+\frac{K_w}{F}$$

$$= \frac{1}{F}\left[K_{Na}F\left(\frac{1}{y}+\frac{1}{z}\right)+K_w\right]$$

$$K_{xo} = \frac{1}{F}\left[K_{Na}F\left(\frac{1}{y}+\frac{1}{z}\right)+K_{mf}\right]$$

$$\frac{K_o}{K_{xo}} = \frac{R_{xo}}{R_o} = \frac{K_{Na}F\left(\frac{1}{y}+\frac{1}{z}\right)+K_w}{K_{Na}F\left(\frac{1}{y}+\frac{1}{z}\right)+K_{mf}}$$

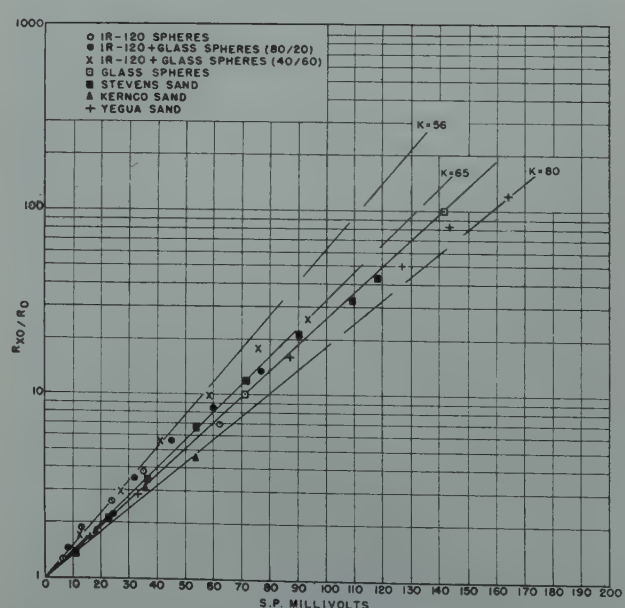

FIG. 8 — RATIO R_{xo}/R_o FOR NATURAL AND ARTIFICIAL DIRTY SANDS AS A FUNCTION OF S.P.

TABLE 2 — METHOD OF COMPUTING S.P. DATA FROM MEASURED POTENTIALS
(Stevens Sand Specimen)

1 Mean Activity of NaCl Soln. Moles	2 a_w/a_m	3 Temp. °C	4 $\frac{2.306RT}{F}\log\frac{a_w}{a_m}$	5 E* m.v.	6 E m.v.	7 S.P. m.v.	8 Specimen Conductivity K_o $\frac{}{\text{mho-cm}}-1$ x10^{-4} at 25°C	9 Solution Conductivity K_w $\frac{}{\text{mho-cm}}-1$ x10^{-4} at 25°C	10 $\frac{R_{xo}}{R_o}$	11 S.P. Based on K_{xo}
0.00625	1	26.4	0			0	2.54	8.45		
0.0125	2	26.8	− 17.9	+4.0	4.0	− 13.9	3.09=K_{xo}	16.0	1.0	0
0.025	4	29.7	− 36.2	+7.9	11.9	− 24.3	4.3	30.9	1.39	10.4
0.05	8	30.6	− 54.4	+6.4	18.3	− 36.1	6.95	63.5	2.16	22.2
0.10	16	25.5	− 71.4	+3.1	21.4	− 50.0	10.8	114	3.5	36.1
0.20	32	23.6	− 89.1	+0.3	21.7	− 67.4	21.0	219	6.7	53.5
0.40	64	24.6	−106.8	−0.3	21.4	− 85.4	37.8	467	12.0	71.5
0.8	128	25.2	−124.8	−0.6	20.8	−104.0	66.5	736	21.5	90.1
1.6	256	26.4	−143.1	−0.8	20.0	−123.1	103	1050	33.2	109.2
3.2	512	25.2	−160.9	−0.9	19.1	−141.8	134	1420	43.2	117.9

*Positive sign indicates that the solution of lesser activity is positive as measured.

But conductivities are approximately proportional to ionic activities. Therefore,

$$\frac{R_{xo}}{R_o} \cong \frac{\text{n(activity of exchangeable Na ions)} + \text{activity of Na and Cl ions in solution } K_w}{\text{n(activity of exchangeable Na ions)} + \text{activity of Na and Cl ions in solution } K_{mf}}$$

$$\text{where n} = \frac{F\left(\frac{1}{y}+\frac{1}{z}\right)}{F_R} = \text{constant}$$

This may be compared with the case where the porous body contains no ion-exchange material. Then,

$$\frac{K_o}{K_{xo}} = \frac{R_{xo}}{R_o} = \frac{F}{F}\,\frac{K_w}{K_{mf}} \cong$$

$$\frac{\text{activity of Na and Cl ions in solution } K_w}{\text{activity of Na and Cl ions in solution } K_{mf}}$$

For the case of a clean sand.

$$E = K \log \text{(activity ratio)}$$
$$\cong K \log \frac{R_{xo}}{R_o}$$

and, by analogy, a similar relationship for dirty sands is not, therefore, unexpected.

PRACTICAL APPLICATIONS

The experimental evidence suggests that Equation (21) may be a reasonable approximation if sands are moderately dirty and if the fluids they contain are not unduly resistive. The resistivity limitation appears to be of limited practical seriousness. The approximate linearity, shown in Fig. 7, which is the basis for Equation (21), commences, in the worst case, at a saturating solution conductivity of 0.00659 mho-cm^{-1} or 1.52 ohm-meters. For other specimens and particularly the natural dirty sands tested, the permissible resistivity was found to be considerably greater. In logging practice, if muds of about 1.0 ohm-meter or less are used, the resistivity of the saturating solutions in a formation should not be the factor limiting the applicability of Equation (21).

If the value of K in Equation (21) can be assumed, as an approximation, to be equal to the value (kT) in Equation (3), log interpretation of dirty sands can theoretically be carried out in the following manner.

WATER SANDS

From the measured cut-back S.P. opposite the dirty sand (assuming no bed-thickness effects) and Equation (21), R_{xo}/R_o, is calculated.

Then, R_{wa}, the apparent resistivity of the water in the dirty sand is found in the usual manner by dividing R_{mf}, the mud resistivity, by the ratio obtained from the S.P.,

$$\text{i.e., } R_{wa} = \frac{R_{mf}}{(R_{xo}/R_o)} = \frac{R_{mf} \cdot R_o}{R_{xo}}$$

The apparent formation factor, F_a, is found from the resistivity R_{xo}, read from a suitable log.

$$F_a = \frac{R_{xo}}{R_{mf}}$$

The resistivity of the water sand, if clean, is the product of the interstitial water resistivity and the formation factor. For a dirty sand this product is

$$F_a R_{wa} = \frac{R_{mf} \cdot R_o}{R_{xo}} \cdot \frac{R_{xo}}{R_{mf}} = R_o \quad . \quad . \quad . \quad . \quad (22)$$

Equation (22) shows that the product $F_a R_{wa}$ is equal to the true resistivity, R_o, of the dirty sand containing water. Equation (22) is, of course, only as accurate as the approximate nature of Equation (21) permits. Nevertheless, in many cases the available data suggest that Equations (21) and (22) may be used to assess whether or not a dirty sand is water bearing.

OIL SANDS

If a dirty sand contains oil, the relationship between resistivity and potential becomes more complex than for the case of sands saturated with water only. An approximate solution may be obtained on the assumption that the Donnan uptake of salt is negligibly small, i.e., ρK_w^2 is effectively zero. Then if R_t is the true resistivity of a dirty sand containing oil,

$$\frac{R_t}{F_a R_{wa}} \cong \frac{I}{I'} \quad . \quad . \quad . \quad . \quad . \quad . \quad . \quad (23)$$

were I is the resistivity index of the oil sand and I' the resistivity index of the zone invaded by mud filtrate and from which all oil has not been displaced.

It seems desirable, however, to determine by actual experiment the validity of Equation (23). Such experiments are now being carried out.

In all cases, however, it is apparent that if $R_t > F_a R_{wa}$, the dirty sand probably contains hydrocarbons. Thus the qualitative interpretation of dirty sands may be carried out in a manner precisely analogous to that used for a clean sand. It is well to bear in mind, however, that for very dirty sands, even though these are effectively oil saturated, the ratio $R_t/F_a R_{wa}$ may be quite small.

The quantities, apparent formation factor, F_a, and apparent interstitial water resistivity, R_{wa}, which may be computed for dirty sands are not in themselves physically meaningful. It appears that the product $F_a R_{wa}$ is of considerable utility in the semi-quantitative analysis of logs of dirty sands.

It remains, of course, for the experimental evidence reported above to be tested against actual field data.

Finally, it must be emphasized that *it is inherent in the procedures outlined that only information obtained from log records can be used. It is not permissible to utilize core analyses or measured water resistivities even in cases where such information is available.*

CONCLUSIONS

It is concluded,

1. That the true formation factor of a dirty sand (the formation factor applicable to the voids capable of containing oil) is not a quantity capable of simple measurement.

2. That the formation factor of a dirty sand derived from a series of formation factor measurements made using saturating solutions of varying conductivities may be a good approximation to the true formation factor of the sand, but, theoretically, must always be somewhat less than the true formation factor.

3. That as an approximation in moderately dirty sands and provided muds of resistivities of the order of 1 ohmmeter or less at formation temperature are utilized, the qualitative analysis of the electric logs of dirty sands may be carried out in precisely the same way as that utilized for logs of clean sands. In this procedure the apparent resistivity of the interstitial water in the dirty sand and the apparent formation factor of the dirty sand must both be obtained from log records. It is not permissible to utilize information based on analyses of produced water samples or cores (unless the core analyses can *exactly* reproduce the appropriate subsurface conditions).

ACKNOWLEDGMENT

The writers are indebted to their colleague, K. S. Spiegler, for his assistance in evaluating certain of the experimental data and to Paul D. Foote, executive vice president, Gulf Research & Development Co., for permission to publish this paper.

REFERENCES

1. Patnode, H. W., and Wyllie, M. R. J.: "The Presence of Conductive Solids in Reservoir Rock as a Factor in Electric Log Interpretation," *Trans.* AIME, (1950), **189**, 47.
2. Doll, H. G.: "The S.P. Log: Theoretical Analysis and Principles of Interpretation," *Trans.* AIME, (1948), **179**, 146.
3. Doll, H. G.: "The S.P. Log in Shaly Sands," *Trans.* AIME, (1950), **189**, 205.
4. de Witte, L.: "Resistivity and Saturation Distribution in Infiltrated Zones of Porous Formations," *Oil & Gas Jour.*, (1950), **49**, **12**, 246.
5. de Witte, L.: "Relations Between Resistivities and Fluid Contents of Porous Rocks," *Oil & Gas Jour.* (1950), **16**, 120.
6. Berg, J. W.: "Conductivity Studies of Aqueous Kaolin-NaCl Mixtures," *Producers Monthly*, (1952), **16**, 25.
7. Wyllie, M. R. J.: "Clay Technology in Well Log Interpretation," 1st National Conference on Clays and Clay Technology, Berkeley, Calif., July, 1952, (In press).
8. Winsauer, W. O., and McCardell, W. M.: "Ionic Double-Layer Conductivity in Reservoir Rock," *Trans.* AIME, (1953), **198**, 129.
9. McCardell, W. M., Winsauer, W. O., and Williams, M.: "Origin of the Electric Potential Observed in Well,' *Trans.* AIME, (1953), **198**, 41.
10. Archie, G. E.: "The Electrical Resistivity Log as an Aid in Determining Some Reservoir Characteristics," *Trans.* AIME, (1942), **146**, 54.
11. Wyllie, M. R. J.: "A Quantitative Analysis of the Electrochemical Component of the S.P. Curve," *Trans.* AIME, (1949), **186**, 17.
12. Doll, H. G.: "The Microlaterolog," *Trans.* AIME, (1953), **198**, 17.
13. Scatchard, G.: "Ion-Exchange Electrodes," *Jour. Am. Chem. Soc.*, (1953), **75**, 2883.
14. Wyllie, M. R. J.: "Some Electrochemical Properties of Shales," *Science*, (1948), **108**, 684.
15. Teorell, T.: "Transport Processes and Electrical Phenomena in Ionic Membranes," Chapter 9, *Progress in Biophysics and Biophysical Chemistry*, Edited by J. A. V. Butler and J. T. Randall, (1953), Academic Press, Inc., NY.
16. Wyllie, M. R. J. and Kanaan, Shirley L.: "Ion-Exchange Membranes II: Membrane Properties in Relation to Bi-ionic Potentials in Monovalent Ion Systems," *Jour. Phy. Chem.* (1954), **58**, 73.
17. Pepper, K. W., Reichenberg, D., and Hale, D. K.: "IV Swelling and Shrinking of Sulphonated Polystyrenes of Different Crosslinking," *Jour. Chem. Soc.* (1952), 213.
18. Bauman, W. C. and Eichhorn, J.: "Fundamental Properties of a Synthetic Cation Exchange Resin," *Jour. Am. Chem. Soc.* (1947), **69**, 2830. ★ ★ ★

DISPLACEMENT EXPERIMENTS in a CONSOLIDATED POROUS SYSTEM

J. S. LEVINE
MEMBER AIME

SHELL DEVELOPMENT CO.
HOUSTON, TEXAS

T. P. 3759

ABSTRACT

A series of four displacement experiments has been run in a large alundum core. Flow potential distribution in each liquid phase was measured continuously through oil-wet and water-wet capillary barriers, using a null-point pressure balance, and saturated distribution was determined from electrical resistivity measurements. A method has been devised for calculating the effective (and relative) permeability to each phase at any time and at any point in the flow system for the transient displacement process. Relative permeability points have been calculated and average curves drawn for oil displacing water and water displacing oil. The values of dynamic capillary pressure have also been determined. Data have been substituted into the generalized Buckley-Leverett fractional flow equation and a comparison between actual and theoretical breakthrough recoveries is shown.

This paper is publication No. 38, Exploration & Production Research Division, Shell Development Co., Houston, Tex.

[1]References given at end of paper.

Manuscript received in the Petroleum Branch office Aug. 3, 1953. Paper presented at the Petroleum Branch Fall Meeting in Dallas, Tex., Oct. 18-21, 1953.

Discussion of this and all following technical papers is invited. Discussion in writing (3 copies) may be sent to the offices of the Journal of Petroleum Technology. Any discussion offered after Dec. 31, 1954, should be in the form of a new paper.

INTRODUCTION

Displacement experiments have been performed in the laboratory for many years in an effort to determine the effect of a number of parameters on multiphase flow in porous materials. In the literature of petroleum technology, Wyckoff and Botset[1] were among the first to develop the relative permeability concept and to show experimentally that oil, gas, and water can flow simultaneously through a porous medium in a precise way governed by certain fluid properties, by the relative saturation of each fluid, and by characteristics of the medium itself. Somewhat later, Leverett[2] and Hassler, Brunner, and Deahl[11] developed some theoretical concepts of capillary behavior in porous materials.

The work of Buckley and Leverett[3] presented a theoretical analysis of immiscible liquid displacement based on the equation of continuity and the Darcy equation for viscous flow of each fluid. Subsequent investigators attempting to verify the Buckley-Leverett equation have, in general, deliberately neglected the capillary pressure term or have performed experiments in such a manner that it could be neglected.

Terwilliger, *et al*[4] in 1951, obtained agreement between theory and experiment for the constant rate displacement of water by gas in a long vertical sand column. Rapoport and Leas[5] have investigated the

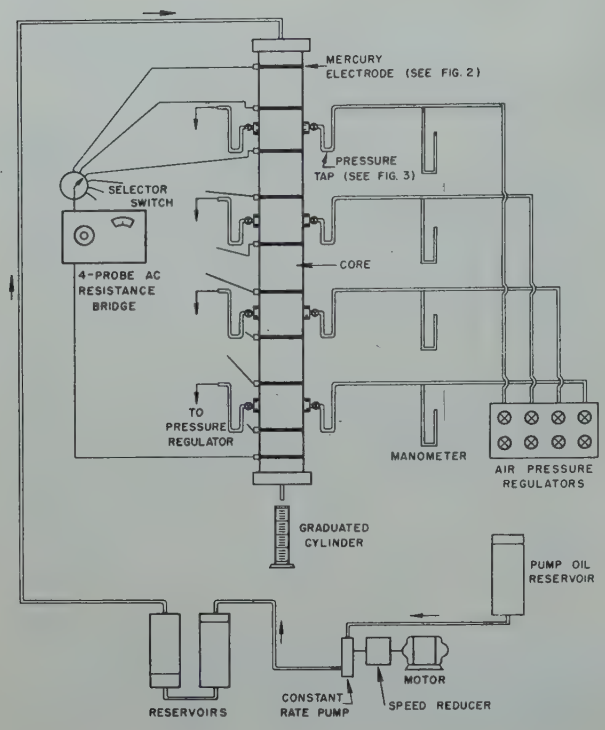

FIG. 1 — SCHEMATIC DIAGRAM OF APPARATUS.

properties of linear waterfloods in the laboratory and have shown that the recovery is related to a "scaling factor" containing the product of length of the system, velocity of the fluid, and viscosity of the fluid. The recovery becomes stabilized at certain values of the "scaling factor." They state that if the stabilized recovery is the same as that obtained by displacement through a capillary barrier, then the results of such experiments are applicable to the field.

Everett, Gooch, and Calhoun,[6] in studying the effect on recovery of liquid-liquid viscosity ratios and liquid-liquid miscibility, found the viscosity ratio to be the more significant parameter and concluded that viscous forces are more important than capillary forces with respect to recovery.

Welge[7] has shown a simplified method for computing recovery by gas or water drive based on the Buckley-Leverett equation. He postulates, however, that in the field the capillary pressure term may be neglected and, in the case of water flooding, the gravity term is normally negligible, too.

The effect of velocity on recovery has concerned several investigators. Earlougher[8] used radial flow through cores and found that as the fluid velocity increased the recovery increased. Rapoport and Leas[5] found the same effect for linear systems. However, Morse and Yuster,[9] and Holmgren[10] found that recovery was not materially affected by either pressure gradients or velocities in the systems which they studied.

Possibly no single parameter affecting the displacement mechanism has been studied more thoroughly than the relative permeability. Methods for measuring relative permeability have been developed by Hassler,[13,14] Morse, Terwilliger, and Yuster[12] and others. The measurement of relative permeability and factors affecting the measurement have received thorough investigation[15,16,17,18,19] in the past few years. The early work of Leverett and most of the other references cited have shown relative permeability to be independent of viscosity.

Odeh and Yuster[20] have recently presented data which indicate that the ratio of the oil permeability in a system containing water to the absolute permeability as measured with water may be greater than one and is a fraction of viscosity. Osoba, *et al*[18] and Geffen, *et al*[15] have shown that the relative permeability curves indicate a hysteresis and are, therefore, not unique functions of saturation but depend on the direction in which the saturation changes are made. Thus, the relative permeability is a function of the distribution of fluids in the system as well as of the amount of fluid.

The profusion of experimental work pertaining to fluid flow in porous media has revealed many details of the mechanism of multiphase flow. There did, however, appear to be a few gaps to justify further experimental work. In particular, no one has attempted to measure pressure distribution in each flowing phase during a displacement process in order to determine values of dynamic relative permeability and capillary pressure and to evaluate the effect of the interfacial forces. The work presented in this paper was undertaken in order to develop experimental techniques for measuring some of these parameters and to obtain a better understanding of the mechanism of displacement.

APPARATUS AND EQUIPMENT

All the experiments on which this paper is based were performed on a cylindrical alundum core having a total length of 53.9 cm and a cross-sectional area of 18.65 sq cm. The core had an average air permeability (extrapolated to infinite mean pressure) of 145 millidarcies and an average effective porosity of 25.1 per cent. A schematic diagram of the core and experimental set-up is shown in Fig. 1.

Ten small grooves, about 1/16-in. deep and 1/8-in. wide were machined around the circumference of the core at fixed points and were filled with powdered NaCl. A close-fitting lucite jacket was then bonded to the core at a pressure of 600 psi and a temperature of 200°C, after which holes were drilled into each salt groove. The salt was dissolved with water and these grooves then gave a continuous band around the core.

Before each experiment was started, the grooves were filled with mercury, which acted as electrodes, to give good surface contact with the pores of the core. The mercury was retained by means of platinum-tipped stainless steel screws which shouldered on thin gaskets and gave a good seal with the lucite. A detail of one of the mercury electrodes is shown in Fig. 2.

During an experiment, current was passed between the two electrodes near each end of the core. By means

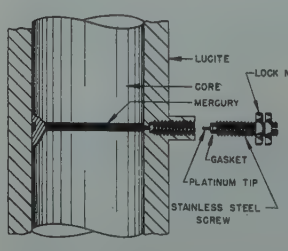

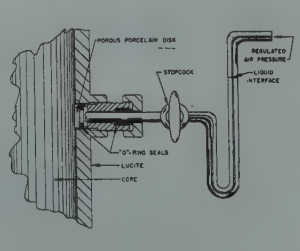

FIG. 2 (LEFT) — DETAIL OF MERCURY ELECTRODE.
FIG. 3 (RIGHT) — DETAIL OF PRESSURE TAP.

of a selector switch, the resistivity could be measured between any adjacent pair of electrodes with a 4-probe, 60-cycle a.c. resistance bridge. A resistivity-saturation curve was obtained on a separate piece of the core by measuring the resistance while the core was desaturated through a water-wet capillary membrane.[23] Resistance measurements made during any displacement experiment could then be converted to equivalent liquid saturations by means of the calibration curve. The saturation distribution throughout the column could be determined at any time.

The electrodes were spaced alternately at distances of 38 mm and 70 mm and the measured resistances obviously represented the average resistances over the respective intervals so that the saturations obtained were also average saturations. The saturation distribution was determined by drawing smooth curves through the points of average saturation plotted against the distance represented by the mid-point of the corresponding interval.

Fig. 3 shows the details of the pressure taps used to measure pressure in both oil and water at four equally spaced positions along the core. Pressure in the oil was measured through four porous porcelain disks which had been treated with G.E. "Dri-Film" in order to render them oleophilic. Pressure in the water was measured on the opposite side of the core through four porcelain disks which were normally hydrophilic. The disks were 1/2-in. in diameter and 1/10-in. thick. They were ground with plane faces so that they would make good contact with the core which was also milled plane at those places where the disks fit. A layer of Kleenex or diatomaceous earth was placed between the disk and core to offer better capillary contact with the wetting-phase liquid. The 0-ring seals insured that any oil or water flowing from the core and into the glass capillary tubing would flow through the oleophilic or hydrophilic disks respectively.

During an experiment, the liquid interfaces were continually maintained at the reference marks on the 1-mm diameter capillary tubes by means of regulated air pressure which could then be measured on external manometers. The air pressure necessary to keep the interface stationary is, therefore, equal to the pressure in the respective liquid at that position in the core. This method of measuring pressure was found to be very satisfactory. With experience, one could quickly adjust the pressure with volume changes of less than 0.2 cu mm. The 0-ring seals could easily be made leak-proof and any anomalies[21] in pressure measurement from this source are thought to be negligible.

All experiments were carried out in a thermostated cabinet at a temperature of 33°C ± 0.2°. The cabinet had plexiglas front panels through which control knobs were set to operate the pressure-tap stopcocks from the outside. A constant flow rate was maintained by means of Zenith Type "B" metering pumps. A special gearing arrangement and variable speed reducer allowed a wide range in pump output from 0.0005 to 0.20 cc/sec.

In order to reduce pump slippage to a minimum, only a high-viscosity oil (approximately 500 cp) was put through the pumps. This oil was then pumped into plexiglas reservoirs to displace the fluid to be flowed through the core. The reservoirs were in the cabinet to minimize volume changes due to temperature fluctuations.

DESCRIPTION OF FLUIDS USED

The water used in these experiments was an aqueous solution of 1-N NaCl to which had been added 1 per cent of formaldehyde to prevent bacteria formation; the term "water" in this paper always means a 1-N NaCl solution. A total of four runs will be reported. In three of the runs, the oil used was kerosene from which all the aromatics and unsaturates had been removed. In one run, the oil viscosity was increased by blending 25 per cent kerosene with 75 per cent mineral oil. Oil-water interfacial tension was about 39 dynes/cm determined by means of the pendent drop technique.

GENERAL PROCEDURE

Before each run, the core was thoroughly cleaned and dried and the air permeability measured in each interval over which resistance measurements were to be made by using the unfilled grooves as piezometer rings. The sectional permeabilities were found to vary about 20 per cent from the mean value.

The same general technique was followed in the four runs. First, the core was completely saturated under vacuum with the fluid to be displaced which was water in Runs 4, 5, and 7 and oil in Run 6. The porous disks which were to measure pressure in the displaced fluid were in place at the same time the core was saturated. The porous disks which were to measure pressure in the displacing fluid were saturated separately. They were put into place against the core after the core was saturated and before the displacement was started. The grooves were then filled with mercury. The core was mounted in the cabinet in a vertical position and the displacing fluid was forced into the top of the core and flowed vertically downward at a constant rate. The pressure tap stopcocks were opened and the liquid interfaces were continually kept at the reference marks (see Fig. 3). At frequent intervals (usually one-half hour), the manometer pressures, sectional resistivities, and volume of produced fluid were recorded. Readings were continued every half-hour to the time of breakthrough (24 to 48 hours) after which they were taken at less frequent intervals until no more of the displaced fluid was produced. Each displacement experiment lasted from 7 to 10 days.

EXPERIMENTAL RESULTS

Summary of Breakthrough and Final Recoveries

Table 1 summarizes some of the data of the four runs to be discussed in this report. Shown are the oil and water viscosities and densities, the total flow rates, and the saturation of displaced fluid at the time of breakthrough and at the end of production. It can be seen that for oil displacing water, a slightly higher breakthrough and total recovery are obtained for the higher flow rate (cf. Runs 4 and 5). At the same flow rate, the breakthrough and total recovery increases as the ratio of μ displacing/μ displaced increases (cf.

TABLE 1

Run No.	Displacing Liquid	Viscosity — cp*		Density — gm/cc*		Flow Rate cc/hour	Displaced Liquid Saturation Per Cent of Pore Volume	
		Oil	Water	Oil	Water		at Breakthrough	at End of Production
4	Oil	1.64	0.854	0.814	1.036	6.31	44.0	34.8
5	Oil	1.66	.854	.814	1.036	3.72	48.0	36.8
6	Water	1.48	.854	.782	1.036	6.21	39.2	29.6
7	Oil	19.30	.854	.859	1.036	3.71	29.2	16.8

*At 33°C.

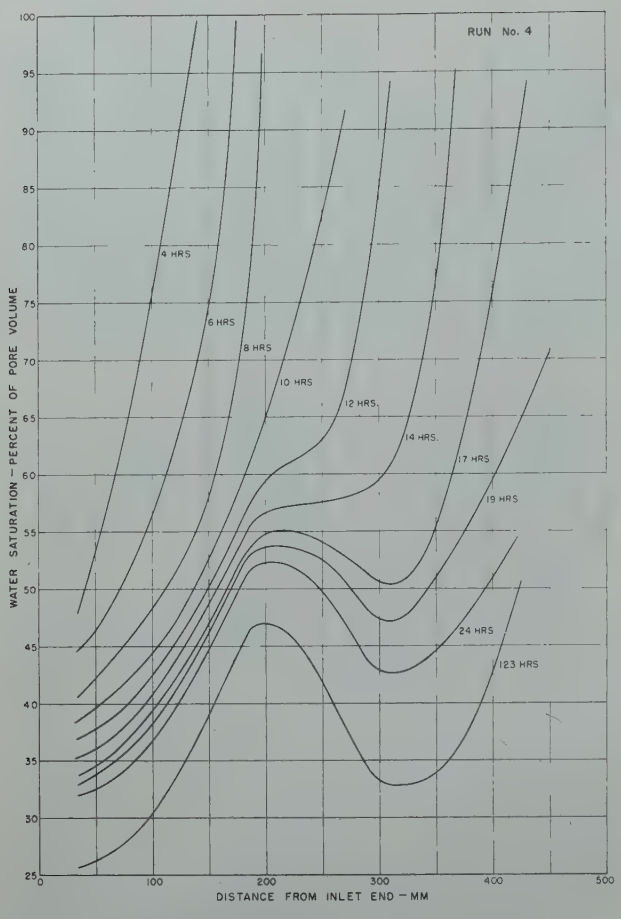

FIG. 4 — SATURATION DISTRIBUTION AT VARIOUS TIMES.

Runs 5 and 7). These results are in general agreement with the reported work of other investigators. In Run 6, where water displaced oil, the recoveries were higher than would have been anticipated from the low value of μ displacing/μ displaced.

SATURATION DISTRIBUTION AT VARIOUS TIMES

The values of water saturation were determined from the resistivity data and the saturations at various times were plotted as a function of distance from the inlet end of the core. A series of curves were obtained as shown in Fig. 4 where the saturation distributions are given for the displacement of water by oil in Run 4. The displacement is characterized by high saturation gradients for the first 10 hours with the distribution curve keeping the same general shape. After the flood front passes the approximate midpoint of the core and the water saturation reaches about 70 per cent there is an abrupt change in the gradient. This same general behavior was found in all four runs and is probably the result of a smaller average pore size (as indicated by a lower permeability) in the region between 170 to 300 mm.

FLOW-POTENTIAL DISTRIBUTION IN THE DISPLACING PHASE

In order to obtain the flow potential in each flowing phase, all pressure data were corrected to a datum plane corresponding to the bottom end of the core. The potentials were then plotted as a function of distance to give a series of curves as shown in Fig. 5 for the displacing (oil) phase of Run 4. It can be seen that the flow potential gradients in the displacing phase at a given distance decrease with time; the gradients are higher near the point of farthest penetration of the interface.

In Fig. 5, the potential lines are drawn only as far as pressure readings were obtained at the four pressure taps. Thus, at 10 hours, pressure readings were obtained at located at 79 mm and 192 mm, while those at 306 mm and 420 mm showed no pressure. At 12 hours, only the tap at 420 mm gave no reading. At 16 hours, pressure was obtained at all points of measurement. In Run 4, breakthrough occurred in about 22 hours, so that the 24-hour flow potential curve of Fig. 5 represents the distribution after breakthrough. It was found in all runs that the maximum flow potentials were reached in the displacing phase shortly after breakthrough and that they thereafter decreased to some lower equilibrium values. In every case, however, there was always a sharp potential drop near the end of the core.

FLOW-POTENTIAL DISTRIBUTION IN THE DISPLACED PHASE

Fig. 6 shows the flow-potential distribution in the displaced (water) phase at various times for Run 4. In this case, the gradients increase with time at a given distance. Since the displaced phase is continuous throughout the core — at least until such a low saturation is reached that the liquid film *may* be broken — pressure readings are obtained at all four taps for the duration of the experiment. Here the potential at the outflow face of the core must be zero and it can be seen that the curves approach zero in the vicinity of 539 mm.

The flow potentials in the displaced phase also decreased after breakthrough was reached. This is a condition necessary to the ultimate cessation of flow of the displaced phase, at which time the potential must be the same at all points. Actually this condition was never reached in any of the experiments. Even when the production of displaced fluid essentially ceased, there were still apparent slight saturation changes in the core (as indicated by resistivity measurements) which were sufficient to require a relatively high potential gradient.

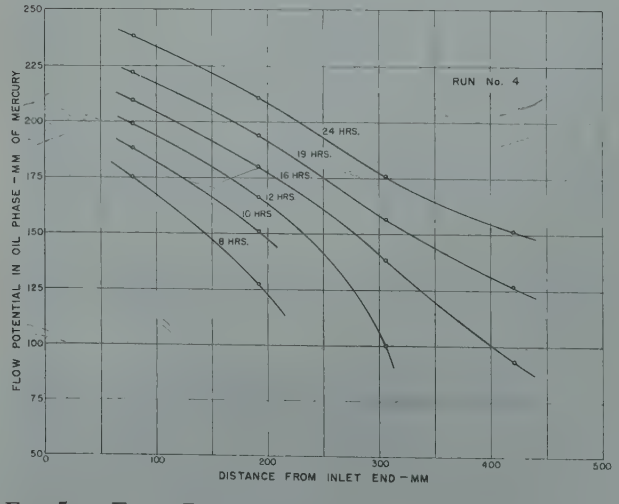

FIG. 5 — FLOW POTENTIAL DISTRIBUTION IN OIL PHASE AT VARIOUS TIMES.

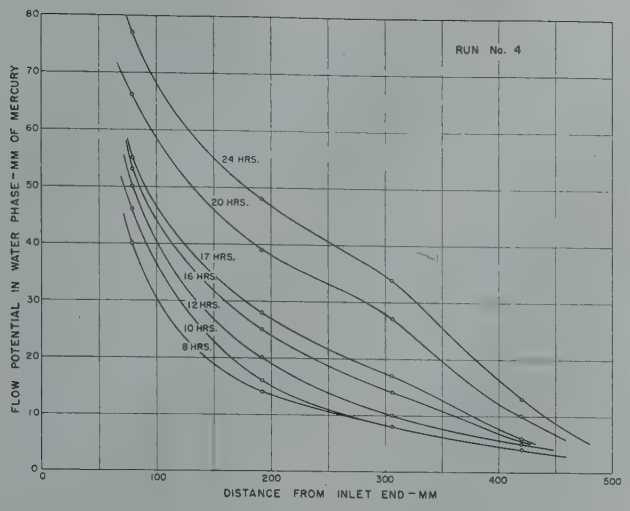

FIG. 6 — FLOW POTENTIAL DISTRIBUTION IN WATER PHASE AT VARIOUS TIMES.

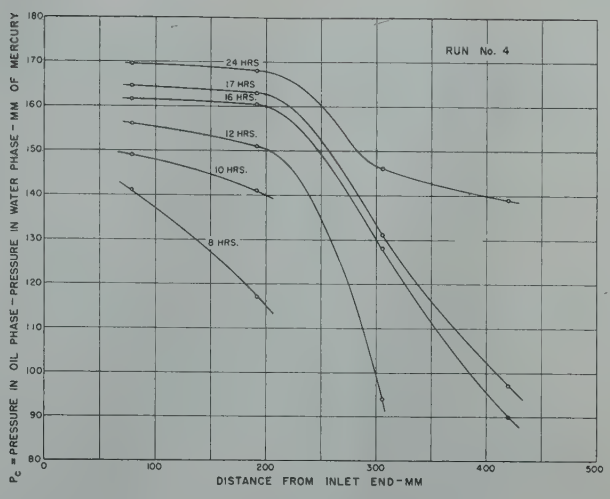
RUN No. 4
24 HRS.
17 HRS.
16 HRS.
12 HRS.
10 HRS.
8 HRS.
Pc = PRESSURE IN OIL PHASE - PRESSURE IN WATER PHASE - MM OF MERCURY
DISTANCE FROM INLET END - MM

FIG. 7 — VARIATION OF CAPILLARY PRESSURE DISTRIBUTION WITH TIME.

The greatest experimental difficulty in this work was encountered in determining the pressure in the displaced phase because of the problem of maintaining capillary contact at low liquid saturation. The present technique for measuring pressure — while essentially a zero volume displacement method — does require a small fluid movement across the barrier. When the saturation of displaced fluid in the core is low, even a slight fluid movement from the core must take place through relatively fine liquid filaments so that the position of the interface in the capillary manometers changes very slowly for any pressure unbalance. In those few instances where capillary contact was apparently lost between the porous disk and the core, it was found impractical to reestablish contact by forcing small volumes of fluid back into the core at that point.

DYNAMIC CAPILLARY PRESSURE MEASUREMENTS

In the same sense that all the pressure measurements essentially represent instantaneous values for a transient process, then the difference in pressure between displacing and displaced phase at any of the four points of measurement can be considered to represent a dynamic capillary pressure. Fig. 7 shows this capillary pressure as a function of distance at various times. After breakthrough, the capillary pressure distribution is characterized by two regions having a low gradient separated by a region having a high gradient. This latter region corresponds to the one showing the negative saturation gradients in Fig. 4. With the distance along the core always measured as positive downward and the capillary pressure always the difference in pressure between displacing and displaced phase, then the capillary pressure gradient was always found to be a negative value regardless of whether oil or water was the displacing medium.

Fig. 8 shows the dynamic capillary pressure plotted as a function of displaced phase saturation. The values can be obtained by combining Figs. 4 and 7. If the core were completely homogeneous and capillary pressure were uniquely a function of saturation, then the data should define a single curve in Fig. 8. As can be seen, three separate capillary pressure curves are actually obtained. This behavior repeated itself in all runs and is apparently the result of inhomogeneity of the core.

CALCULATION OF DYNAMIC RELATIVE PERMEABILITY

Figs. 4 to 8 have shown a portion of the data obtained during one experiment in which oil displaced water. A large amount of similar data was also obtained for three other runs which were varied as indicated in Table 1. One of the objectives of this investigation was to arrive at a method for calculating the dynamic relative permeability values for each phase during a transient displacement process.

The calculation of dynamic permeability at a particular time and at a given point in the system can be accomplished if one knows the instantaneous flow rate and flow potential gradient. According to the well-known Darcy equations:

$$k_o(t, Z) = -\frac{\mu_o q_o}{A\dfrac{\partial \phi_o}{\partial Z}} \quad . \quad . \quad . \quad . \quad . \quad . \quad . \quad . \quad (1)$$

$$k_w(t, Z) = -\frac{\mu_w q_w}{A\dfrac{\partial \phi_w}{\partial Z}} \quad . \quad . \quad . \quad . \quad . \quad . \quad . \quad . \quad (2)$$

where k_o and k_w = effective permeability to oil and water respectively in darcies
μ = viscosity in centipoises
A = cross-sectional area in cm^2
q = flow rate in cm^3/second
t = time in seconds
ϕ = flow potential in atmospheres
Z = distance in direction of flow in cm
subscripts $_o$ and $_w$ refer to oil and water respectively.

For the displacement of water by oil then, from the curves of Figs. 5 and 6, the values of $\partial\phi_o/\partial Z$ and $\partial\phi_w/\partial Z$ at a particular time and distance can be determined by graphical differentiation. The value of q_o at the same time and distance can be obtained from the equation:

$$q_o = q_{io} - c\int_0^Z \left(\frac{\partial S_o}{\partial t}\right) dZ \quad . \quad . \quad . \quad . \quad . \quad . \quad (3)$$

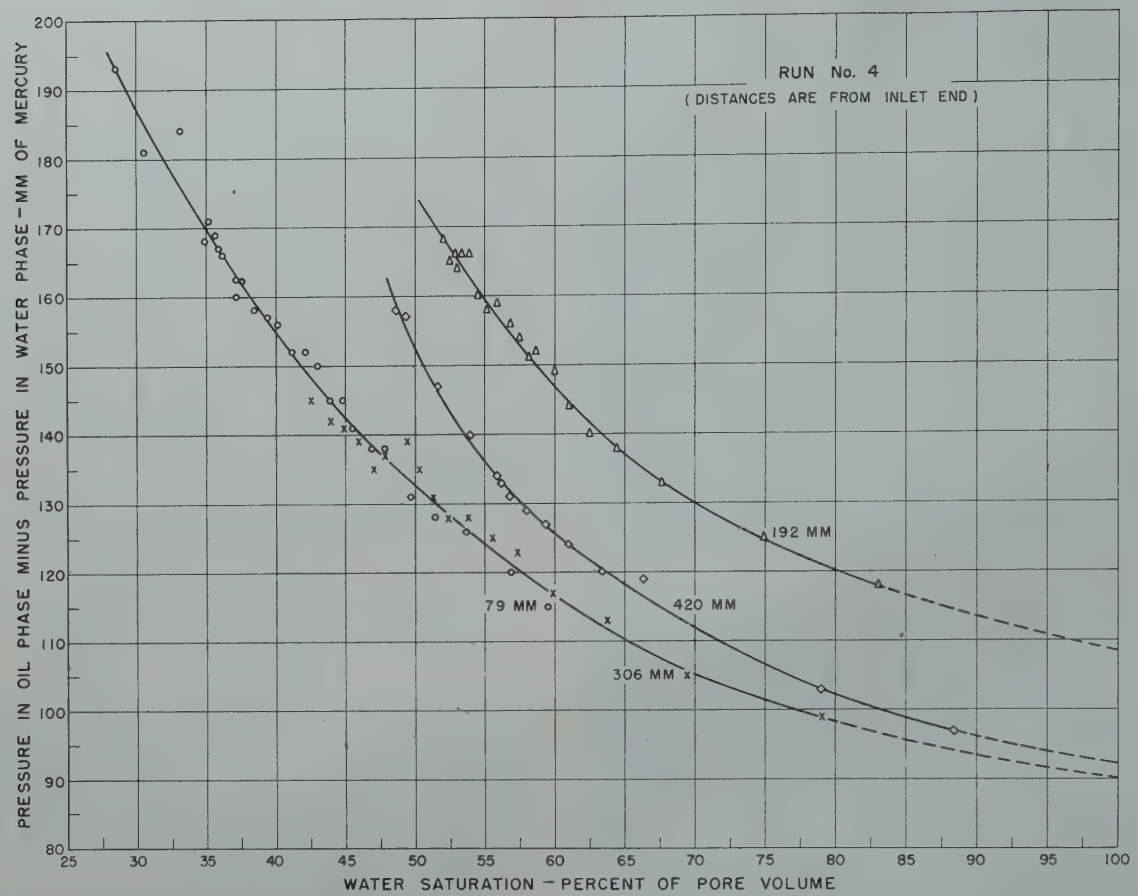

FIG. 8 — VARIATION OF CAPILLARY PRESSURE WITH SATURATION AT FOUR POSITIONS ALONG THE CORE.

where q_{i_o} = constant flow rate of oil into input end of core
S_o = fractional oil saturation in core
c = constant (cross-sectional area × fractional porosity)

From Fig. 4, a series of curves of oil saturation as a function of time for various fixed distances can be obtained. From the derivative of each curve at different times, another series of curves of $\partial S_o/\partial t$ as a function of distance can be plotted. The integral term in Equation (3) can then be evaluated by integrating the area under each curve to the desired distance. Thus, sufficient data are available to substitute into Equation (1) to calculate the oil permeability at a given saturation. Inasmuch as the oil and water can be considered incompressible, and the pore volume is completely filled with liquid, the rate at which oil accumulates in any part of the core is equal to the rate at which water is removed from the same part. Thus, the instantaneous water flow rate at any time and distance is numerically equal to the value of the constant times the integral term in Equation (3), and $k_w(t, Z)$ can be calculated from Equation (2). If the k_o and k_w values are divided by the absolute permeability of the core, two points of relative permeability as a function of saturation are then obtained. The entire procedure can then be repeated at any other time and distance.

Fig. 9 shows the points obtained using the above procedure on the data of Runs 4, 5, and 7, in all of which water was displaced by oil. It is apparent at once that there is considerable spread of the calculated points about some average value as indicated by the curves. If sufficient points are calculated, it seems reasonable to assume that average curves representing the true dynamic relative permeability can be obtained.

It is signifiicant to note that in Fig. 9 the values for relative permeability to oil for Run 7 are approximately the same as for Runs 4 and 5 even though the oil/water viscosity ratio was almost 12 times as great. This indicates that in this range, at least, the relative permeability is independent of viscosity.

The procedure outlined above was also repeated with the data of Run 6 in which water displaced oil from the core. The points fell closer to an average curve than did those of Fig. 9. In Fig. 10 are shown the average curves for the displacement of water by oil in Runs 4, 5, and 7, and the average curves for the displacement of oil by water in Run 6. They are plotted as a function of water saturation. A comparison of the curves will show the apparent effects of wettability on the flow characteristics. If the assumption is made that the porous material has an equal affinity for both oil and water, then the dotted oil curve should be a mirror image of the solid water curve and the solid oil curves should be a mirror image of the dotted water curve about the 50 per cent saturation line.

In other words, if all relative permeability values were plotted as a function of *displaced* phase saturation, only two curves should result if the assumption of equal affinity were correct. This is obviously not the case. The relative water permeability for a system in which water displaces oil is less than the relative oil permeability for a system in which oil displaces water for *the same saturation of displaced fluid*. From this, one may infer that in the porous solid used in these studies the solid

surface showed a greater affinity for water, so that, in general, water flowed in smaller pores than did oil at any given saturation. If, on the other hand, wettability is assumed to be indicated by the sign of the capillary pressure term, then the *displacing* fluid is always the *apparent* nonwetting fluid since the pressure in the displacing phase was always found to be greater than in the displaced phase.

Another fact that becomes apparent from Fig. 10 is that the displacing phase relative permeability goes to zero *only at zero saturation of displacing phase* in these dynamic displacement processes. In this respect, the relative permeability curves obtained by the method described differ from the usual equilibrium relative permeability curves in which the displacing fluid relative permeability becomes zero at saturations of that fluid greater than zero. Thus, the dotted oil curve and the solid water curve of Fig. 10 would more closely approximate values obtained by an equilibrium process. It becomes apparent then that to make reservoir calculations based on relative permeability data for, say, a water flooding process, relative permeability curves obtained by dynamic displacement of oil by water should be used.

CALCULATION OF THE BREAKTHROUGH RECOVERY

In order to calculate the breakthrough recovery, the theory and technique developed by Buckley and Leverett[3] have been applied. By using the generalized Darcy equations for each fluid, Equations (1) and (2), they have developed an equation which relates the fraction of one fluid in the flow stream to the viscous and capillary forces existing in the system. In our notation, this equation is:

$$F_1(S_1) = \frac{1 - \frac{k_2 A}{Q_t \mu_c}\left[\frac{g\Delta\rho}{b} + \frac{\partial P_c}{\partial Z}\right]}{1 + \frac{k_2 \mu_1}{k_1 \mu_2}} \quad . \quad . \quad . \quad (4)$$

where F_1 = fraction of displacing fluid in flow stream
S_1 = saturation of displacing fluid
k_2 = effective permeability in darcies
Q_t = total flow rate in cm³/second
P_c = pressure in displacing phase minus pressure in displaced phase in atmosphere
g = acceleration of gravity in cm/second²
$\Delta\rho$ = density of displaced phase minus density of displacing phase in gm/cm³
Z = distance in direction of flow in cm
b = 1.013 (10^6) dynes/cm²/atmosphere
subscripts 1 and 2 always refer to displacing and displaced phase respectively.

A method has already been indicated for calculating relative permeability as a function of saturation. Inasmuch as

$$k_1 = k_{r1} k \quad . \quad . \quad . \quad . \quad . \quad . \quad . \quad . \quad . \quad . \quad . \quad . \quad . \quad (5)$$

and

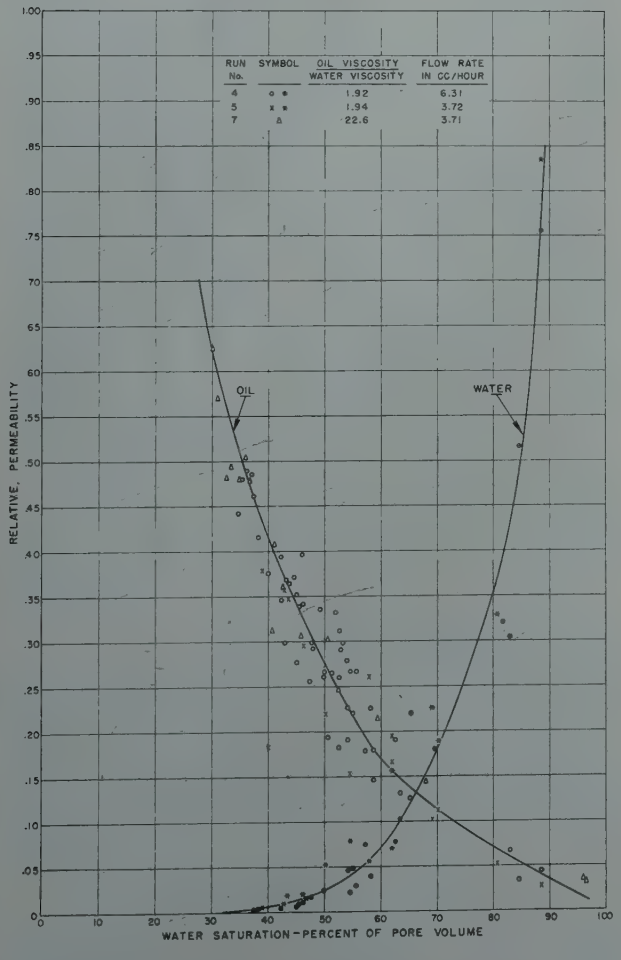

FIG. 9 — DYNAMIC RELATIVE PERMEABILITY CHARACTERISTICS FOR THE DISPLACEMENT OF WATER BY OIL.

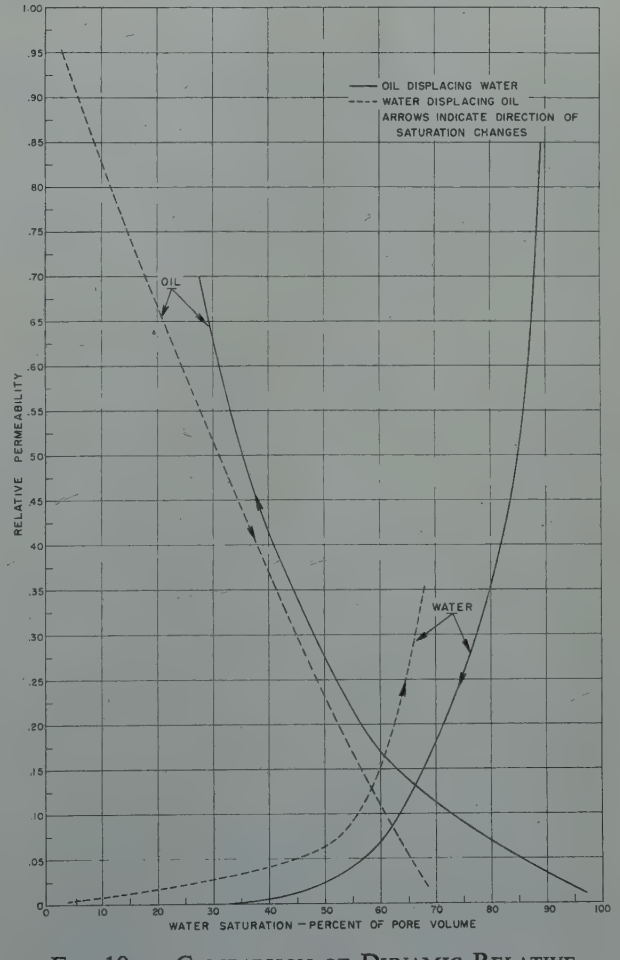

FIG. 10 — COMPARISON OF DYNAMIC RELATIVE PERMEABILITY CHARACTERISTICS FOR TWO TYPES OF DISPLACEMENT.

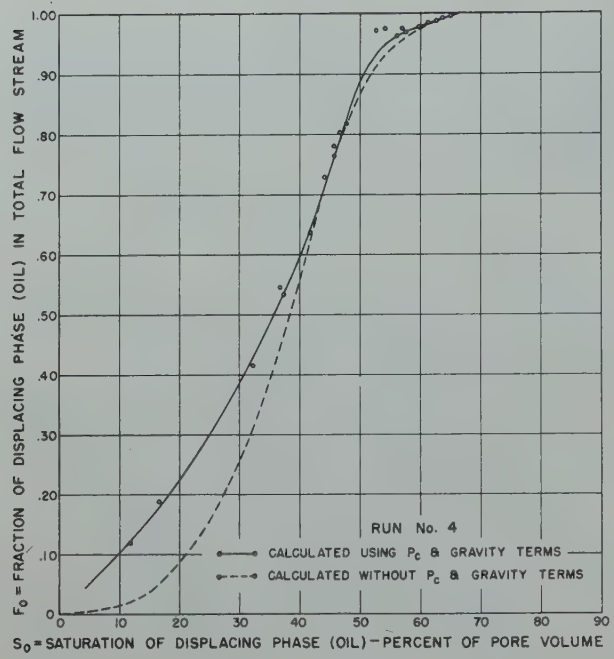
RUN No. 4
CALCULATED USING P_c & GRAVITY TERMS
CALCULATED WITHOUT P_c & GRAVITY TERMS
F_o = FRACTION OF DISPLACING PHASE (OIL) IN TOTAL FLOW STREAM
S_o = SATURATION OF DISPLACING PHASE (OIL) — PERCENT OF PORE VOLUME

FIG. 11 — COMPARISON OF F_o CURVES DETERMINED WITH AND WITHOUT CAPILLARITY AND GRAVITY TERMS FOR THE DISPLACEMENT OF WATER BY OIL.

$$k_o = k_r k \quad . \quad . \quad . \quad . \quad . \quad . \quad . \quad . \quad . \quad . \quad . \quad . \quad . \quad (6)$$

where k_r = relative permeability
k = absolute permeability in darcies,

the effective permeability can be obtained for each fluid at any saturation. All that remains for a determination of $F_1(S_1)$ from Equation (4) is an evaluation of the capillary pressure gradient $\partial P_c/\partial Z$. This can be determined from Fig. 7 by graphical differentiation at the desired distance and time. Thus, the fraction of displacing fluid in the flow stream can be calculated at all points of distance and time. This fraction has been

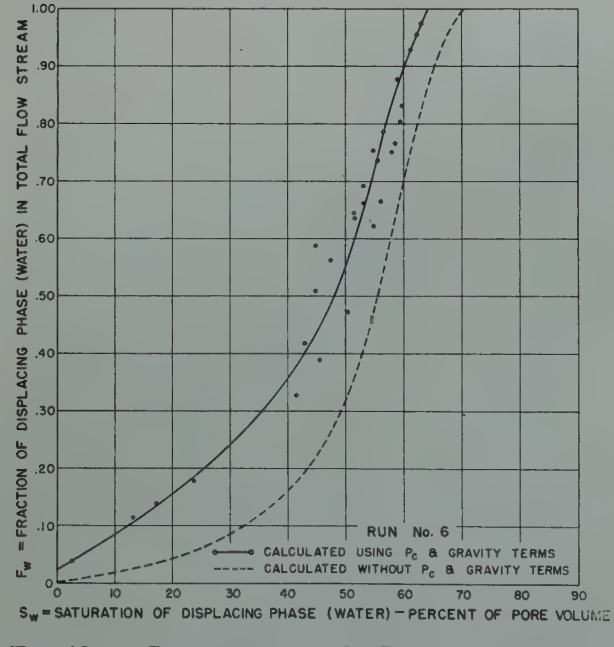
RUN No. 6
CALCULATED USING P_c & GRAVITY TERMS
CALCULATED WITHOUT P_c & GRAVITY TERMS
F_w = FRACTION OF DISPLACING PHASE (WATER) IN TOTAL FLOW STREAM
S_w = SATURATION OF DISPLACING PHASE (WATER) — PERCENT OF PORE VOLUME

FIG. 12 — COMPARISON OF F_w CURVES DETERMINED WITH AND WITHOUT CAPILLARITY AND GRAVITY TERMS FOR THE DISPLACEMENT OF OIL BY WATER.

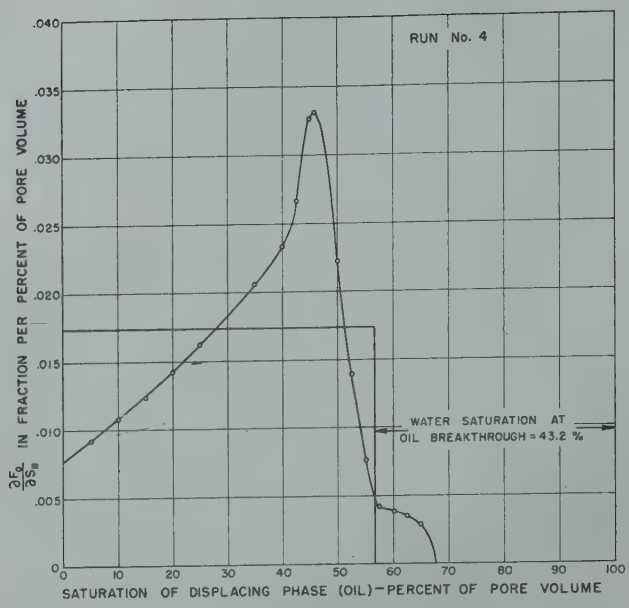
RUN No. 4
WATER SATURATION AT OIL BREAKTHROUGH = 43.2 %
$\frac{\partial F_o}{\partial S_o}$ IN FRACTION PER PERCENT OF PORE VOLUME
SATURATION OF DISPLACING PHASE (OIL) — PERCENT OF PORE VOLUME

FIG. 13 — CONSTRUCTION FOR CALCULATING BREAKTHROUGH RECOVERY FROM F_o CURVE.

calculated from the experimental data for the displacement of water by oil (Run 4) and the displacement of oil by water (Run 6) and is shown in Figs. 11 and 12, respectively, as a function of displacing phase saturation.

Also shown in each figure is the fraction calculated from Equation (4) with the capillary pressure and gravity term assumed equal to zero. It can be seen that the net effect of including the bracketed term is always to increase the F_1 value at any saturation. This means that the capillary pressure gradient always acts to decrease the recovery of displaced fluid. The effect is less pronounced in Run 4 than in Run 6.

Breakthrough recovery can be calculated from the theory by making use of what might be called the Buckley-Leverett construction (which has been explained in detail by Pirson).[22] Fig. 13 shows the $\partial F_o/\partial S_o$ versus S_o curve for Run 4. The horizontal line is drawn so that the area under it up to the intersection with the curve on the right is equal to the area under the curve up to that point. The vertical line is then drawn so that the area in the rectangle is equal to the total area under the curve. The average residual saturation of displaced fluid at the time of breakthrough is then equal to the difference between 100 and the displacing phase saturation indicated by the vertical line. For Run 4, the residual saturation at breakthrough is calculated to be 43.2 per cent. This compares with 44.0 per cent determined experimentally.

Fig. 14 shows the same construction for Run 6. In this case the oil saturation at water breakthrough was calculated to be 36.0 per cent which compares with an experimental value of 39.2 per cent. If the F_w curve which neglected capillary pressure and gravity had been used, the discrepancy would have been about six pore volume per cent greater. Table 2 shows a comparison

TABLE 2 — COMPARISON OF EXPERIMENTAL AND CALCULATED DISPLACED LIQUID SATURATION AT BREAKTHROUGH.

Run No.	Displaced Liquid Saturation at Breakthrough — Per Cent of Pore Volume	
	Experimental	Calculated from Data Using Eq. 4
4	44.0	43.2
5	48.0	44.5
6	39.2	36.0
7	29.2	32.5

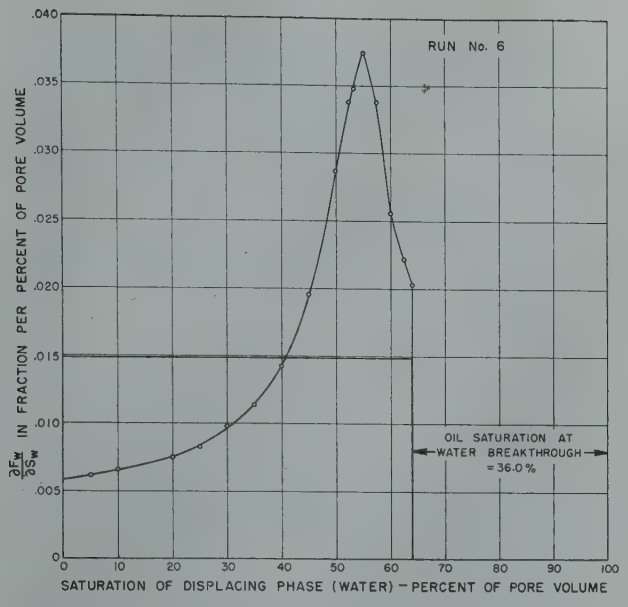
RUN No. 6
OIL SATURATION AT WATER BREAKTHROUGH = 36.0%
$\frac{\partial F_w}{\partial S_w}$ IN FRACTION PER PERCENT OF PORE VOLUME
SATURATION OF DISPLACING PHASE (WATER) – PERCENT OF PORE VOLUME

FIG. 14 — CONSTRUCTION FOR CALCULATING BREAKTHROUGH RECOVERY FROM F_w CURVE.

between the experimental and calculated displaced liquid saturations at breakthrough.

In the preceding calculation of F_1 for Runs 4 and 6, the value of $-[k_2A/Q_t\mu_2][(\partial P_c/\partial Z) + (g\Delta\rho/b)]$ was determined at various saturations for different positions of distance and time. Fig. 15 shows a plot of this term versus the displacing fluid saturation. It can be seen that the value for the entire term approaches a maximum at zero saturation and approaches zero at about 70 per cent saturation of displacing liquid. The function, however, is different depending on the type of displacement.

Fig. 16 shows the values of $\partial P_c/\partial Z$ at various saturations which were calculated from the curves of Fig. 15. It should be remembered that P_c is defined as the difference in pressure between displacing and displaced phases so that in Run 4, $P_c = P_o - P_w$, and in Run 6, $P_c = P_w - P_o$. It is readily apparent that even at the same flow rate, the capillary pressure gradient versus saturation curve for the displacement of water by oil is not the same as for the displacement of oil by water. Furthermore, where the flow rates differ for the same type of displacement, i.e., water by oil, it can be seen that $\partial P_c/\partial Z$ is a function of rate. The gradient curves converge at high displacing phase saturation so that the gradient is more sensitive near the flood front to a change in rate than in the region which has been more completely flooded.

The manner in which $\partial P_c/\partial Z$ varies as a function of Q_t will determine whether, in the laboratory at least, the recovery of displaced fluid will change as the total flow rate changes. Specifically, if the value of $([\partial P_c/\partial Z) + g\Delta\rho]$ is directly proportional to Q_t then the breakthrough recovery should be independent of rate. Thus it becomes necessary to know how the capillary pressure gradient varies with flow rate in order to predict whether changing the rate will change the recovery.

SUMMARY AND CONCLUSIONS

1. A series of four linear displacement experiments have been performed on an alundum core. Techniques were employed which allowed continuous measurements at various positions along the core of the saturation

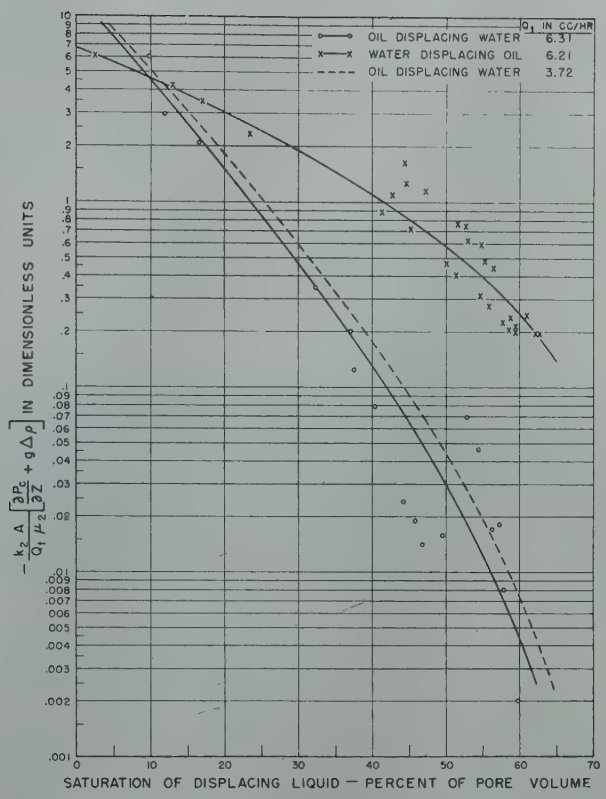
Q_t IN CC/HR
OIL DISPLACING WATER 6.31
WATER DISPLACING OIL 6.21
OIL DISPLACING WATER 3.72
$-\frac{k_2 A}{Q_t \mu_2}\left[\frac{\partial P_c}{\partial Z} + g\Delta\rho\right]$ IN DIMENSIONLESS UNITS
SATURATION OF DISPLACING LIQUID – PERCENT OF PORE VOLUME

FIG. 15 — VARIATION OF THE CAPILLARITY AND GRAVITY TERMS WITH FLOW RATE AND TYPE OF DISPLACEMENT.

distribution and pressure distribution in each flowing phase.

2. A method was developed for calculating the dynamic relative permeability as a function of saturation. The resulting curves for the displacement of

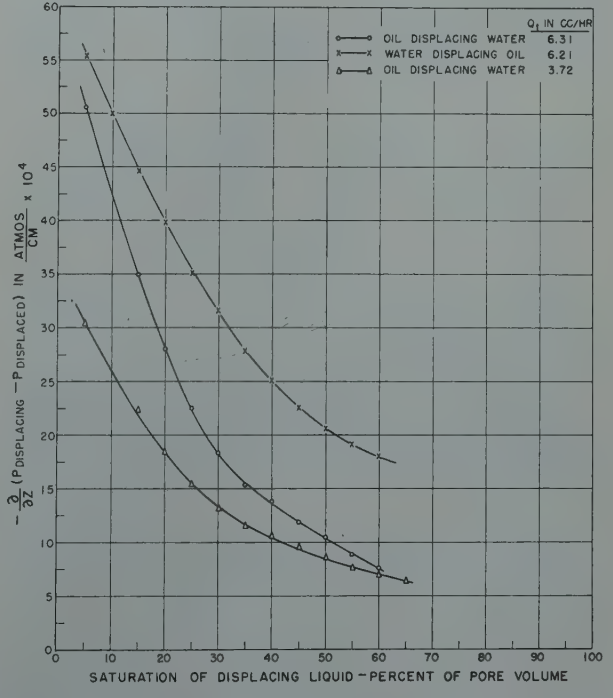
Q_t IN CC/HR
OIL DISPLACING WATER 6.31
WATER DISPLACING OIL 6.21
OIL DISPLACING WATER 3.72
$-\frac{\partial}{\partial Z}(P_{DISPLACING} - P_{DISPLACED})$ IN $\frac{ATMOS}{CM} \times 10^4$
SATURATION OF DISPLACING LIQUID – PERCENT OF PORE VOLUME

FIG. 16 — VARIATION OF THE CAPILLARY PRESSURE GRADIENT WITH FLOW RATE AND TYPE OF DISPLACEMENT.

water by oil and oil by water showed that relative permeability was not a unique function of saturation but depended on the direction of saturation change. It was shown that relative permeability was also not a unique function of *displaced* phase saturation. This is possibly the result of a difference in wettability of the porous system.

3. The displacing phase relative permeability goes to zero only at zero saturation of that phase in these dynamic displacement processes.

4. In the range studied, relative permeability appeared to be independent of viscosity.

5. The Buckley-Leverett fractional flow equation gives reasonable agreement between calculated and experimental breakthrough recoveries if the capillary pressure and gravity terms are retained. If capillary pressure is defined as the difference in pressure between displacing and displaced phases, then the experimental values of $\partial P_c/\partial Z$ were always negative. Thus, the net effect of including the capillarity term is to increase the value of the calculated fraction of displacing fluid in the flow stream at any saturation and to decrease the recovery of displaced fluid.

6. The capillary pressure gradient was calculated as a function of displacing phase saturation for the two types of displacement, and two different gradient curves were obtained for the same total flow rate. When the same type of displacement was involved, i.e., the displacement of oil by water, $\partial P_c/\partial Z$ was found to be a function of total flow rate.

ACKNOWLEDGMENT

The author wishes to thank M. O. Thaemar and R. D. Ward for performing a large part of the experimental work and for making many of the calculations reported in this paper. He also wishes to express his appreciation to C. H. Fay, W. R. Purcell, and C. S. Matthews of Shell Development Co. for their helpful comments, suggestions, and criticisms.

REFERENCES

1. Wyckoff, R. D., and Botset, H. G.: "Flow Through Unconsolidated Sands," *Physics* (Sept., 1936), 7.
2. Leverett, M. C.: "Capillary Behavior in Porous Solids," *Trans.* AIME (1941), **142**, 152.
3. Buckley, S. E., and Leverett, M. C.: "Mechanism of Fluid Displacement in Sands," *Trans.* AIME (1942), **146**, 117.
4. Terwilliger, P. L., Wilsey, L. E., Hall, H. N., Bridges, P. M., and Morse, R. A.: "An Experimental and Theoretical Investigation of Gravity Drainage Performance," *Trans.* AIME (1951), **192**, 285.
5. Rapoport, L. A., and Leas, W. J.: "Properties of Linear Waterfloods," *Trans.*, AIME (1953), **198**, 139.
6. Everett, J. P., Gooch, F. W., and Calhoun, J. C.: "Liquid-Liquid Displacement in Porous Media as Affected by the Liquid-Liquid Viscosity Ratio and the Liquid-Liquid Miscibility," *Trans.* AIME (1950), **189**.
7. Welge, H. J.: "A Simplified Method for Computing Oil Recovery by Gas or Water Drive," *Trans.* AIME (1952), **195**, 91.
8. Earlougher, R. C.: "Relation Between Velocity, Oil Saturation, and Flooding Efficiencies," *Trans.* AIME (1943), **151**.
9. Morse, R. A., and Yuster, S. T.: "Water Flood Tests on Long Cores," *Prod. Monthly* (Dec., 1946), Vol XI, No. 2.
10. Holmgren, C. R.: "Results of Gas and Water Drives on a Long Core," *Trans.* AIME (1949), **179**.
11. Hassler, G. L., Brunner, E., and Deahl, T. J.: "The Role of Capillarity in Oil Production," *Trans.* AIME (1944), **155**.
12. Morse, R. A., Terwilliger, P. L., and Yuster, S. T.: "Relative Permeability Measurements on Small Core Samples," *Prod. Monthly* (Aug., 1947).
13. Hassler, G. L., and Brunner, E.: "Measurement of Capillary Pressures in Small Core Samples," *Trans.* AIME (1945), **160**.
14. Hassler, G. L.: U. S. Patent No. 2,345,935 (April, 1944).
15. Geffen, T. M., Owens, W. W., Parrish, D. R., and Morse, R. A.: "Experimental Investigation of Factors Affecting Laboratory Relative Permeability Measurements," *Trans.* AIME (1951), **192**, 99.
16. Rapoport, L. A., and Leas, W. J.: "Relative Permeability to Liquid in Liquid-Gas Systems," *Trans.* AIME (1951), **192**, 83.
17. Caudle B. H., Slobod, R. L., and Brownscombe, E. R.: "Further Developments in the Laboratory Determination of Relative Permeability," *Trans.* AIME (1951), **192**, 145.
18. Osoba, J. S., Richardson, J. G., Kerver, J. K., Hafford, J. A., and Blair, P. M.: "Laboratory Measurements of Relative Permeability," *Trans.* AIME (1951), **192**, 47.
19. Richardson, J. G., Kerver, J. K., Hafford, J. A., and Osoba, J. S.: "Laboratory Determination of Relative Permeability," *Trans.* AIME (1952), **195**, 187.
20. Odeh, A. S., and Yuster, S. T.: "The Effect of Viscosity on Relative Permeability," AIME Paper No. 264-G, Los Angeles, Calif. (Feb., 1953).
21. Rose, W., and Greifer, B.: "Anomalies in the Measurement of Wetting Liquid Pressure Gradients," *Trans.* AIME (1950), **189**, 364.
22. Pirson, S. J.: *Elements of Oil Reservoir Engineering*, McGraw-Hill Book Co. (1950), 281-321.
23. Dunlap, H. F., Bilhartz, H. L., Shuler, E., and Bailey, C. R.: "The Relation Between Electrical Resistivity and Brine Saturation in Reservoir Rocks," *Trans.* AIME (1949), **186**, 259. ★ ★ ★

EQUILIBRIUM VAPORIZATION RATIOS for a RESERVOIR FLUID CONTAINING A HIGH CONCENTRATION of HYDROGEN SULFIDE

HAROLD VAGTBORG, JR.
MEMBER AIME

RESEARCH AND DEVELOPMENT LABORATORIES
THE PURE OIL CO.
CRYSTAL LAKE, ILLINOIS

T. P. 3760

ABSTRACT

Equilibrium vaporization ratios were obtained for light hydrocarbons, nitrogen, carbon dioxide, and hydrogen sulfide in a reservoir fluid containing 35 mole per cent hydrogen sulfide. The data cover the range from 700 to 2500 psia at 154°F.

The results of this study are compared with results obtained by other investigators on systems containing less hydrogen sulfide. When large amounts of hydrogen sulfide are present, the equilibrium vaporization ratios for ethane and heavier hydrocarbons are greater than the ratios for systems containing little or no hydrogen sulfide. Large amounts of hydrogen sulfide have the reverse effect on the ratios for methane.

Routine PVT studies were performed on the reservoir fluid including flash and differential liberations of the dissolved gas. The pressure-volume relationships of the saturated fluid were also determined.

It is shown that the use of published correlations on physical properties of reservoir fluids can lead to gross errors when applied to systems containing large amounts of hydrogen sulfide.

INTRODUCTION

Equilibrium vaporization ratios for various components in naturally occurring crude oil and condensate systems have been reported in the literature.[1,2,3,4] Recently, several papers have been published with emphasis on non-hydrocarbon components such as nitrogen, carbon dioxide and hydrogen sulfide.[5,6,7,8,9] The increased discovery of reservoir fluids having high concentrations of these non-hydrocarbon components, particularly hydrogen sulfide, has created a need for a further study of their phase behavior.

Equilibrium vaporization ratios are known to vary with pressure, temperature, and overall composition of the system.[10] It was anticipated that ratios for systems containing large amounts of hydrogen sulfide would differ from the ratios for systems containing small amounts of hydrogen sulfide. Therefore, the present work was undertaken in order to obtain reliable equilibrium vaporization ratios for the reservoir-fluid in question.

PROCEDURE

The procedure followed was evolved after considerable experimentation on methods of handling the very sour crude. It was found that drying agents (e.g. $CaCl_2$ and $CaSO_4$) absorbed an appreciable amount of hydrogen sulfide from the gas used to prepare the recombined samples. The concentration of hydrogen sulfide dropped as much as 10 mole per cent in a single pass through a 3-ft drying tube.

It was also found that when undried gas was agitated with mercury in the PVT cell, a black scum, believed to be mercuric sulfide, was formed and the hydrogen sulfide content of the gas dropped several mole per cent. Because composition changes during a run could not be tolerated, separation of the mercury and sour fluid was necessary. In order to effect this separation, a stainless steel piston, equipped with Teflon 0-rings, was placed in the PVT cell between the mercury and the sour fluid. This piston had to be constructed in three parts because

[1]References given at end of paper.

Manuscript received in the Petroleum Branch office Aug. 6, 1953. Paper presented at the Petroleum Branch Fall Meeting in Dallas, Tex., Oct. 18-21, 1953.

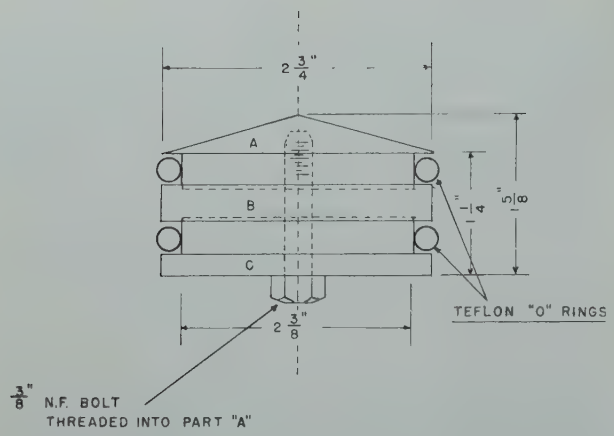

FIG. 1 — STAINLESS STEEL PISTON FOR USE WITH SOUR CRUDES IN RUSKA PVT CELL (ASSEMBLED).

the Teflon 0-rings would not stretch enough to pass over the piston to seat in the 0-ring grooves. The top of the piston was designed to conform with the top of the PVT cell, so that the liquids in the cell could be completely displaced. Fig. 1 shows the assembled piston.

The reservoir fluid used in this study was made by recombination of high pressure separator gas and liquid samples. These samples were recombined in the PVT cell according to the producing gas-oil ratio and were then agitated to equilibrium at the reservoir pressure of 2500 psia and reservoir temperature of 154°F.

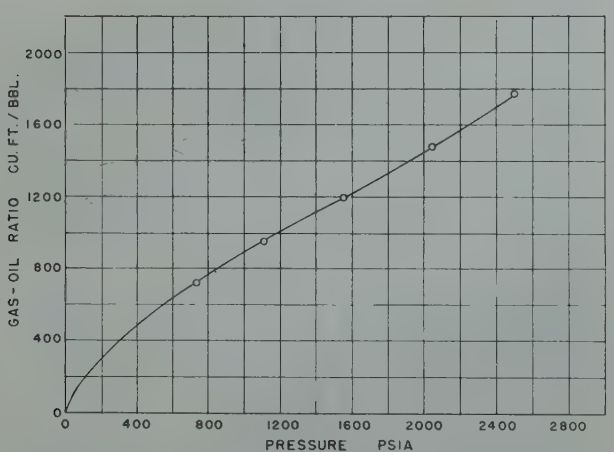

FIG. 2 — SOLUTION GAS-OIL RATIO VERSUS PRESSURE, BASED ON RESIDUAL OIL AT 60°F AND 14.7 PSIA.

TABLE 1 — GAS-OIL RATIOS AND VOLUME FACTORS OF RESERVOIR FLUID

Pressure psia	Gas-Oil Ratio in Solution Std. cu ft/bbl residual oil	Volume Factor $\left(\frac{V_s}{V_r}\right)$*
2745	—	1.884
2600	—	1.889
2545	—	1.891
2500	1772.0	1.894
2043	1478.3	1.762
1554	1197.0	1.637
1111	949.0	1.530
726	730.3	1.447

Gravity of Residual Oil — 34.0 API

*V_s = volume of saturated oil at the saturation pressure.
V_r = volume of residual oil at 60°F and 14.7 psia.

Any excess gas was displaced, leaving a sample with a bubble point of 2500 psia and 154°F.

Routine PVT data were obtained on this sample, including flash and differential gas liberations. The differential liberation consisted of a series of flash liberations at progressively lower pressures. Because of the large volume of gas required to make an accurate LTD analysis, it was necessary to take pressure decrements of approximately 500 psia. For this reason, it was possible to make only five successive flash liberations on the sample; of course, use of smaller pressure decrements would have approximated the true differential liberation more closely.

The procedure followed in performing the differential gas liberation was as follows: the pressure on a sample of saturated reservoir fluid, at reservoir temperature, was lowered below the bubble point pressure by withdrawing mercury from the bottom of the PVT cell. A gas phase was formed which was brought to equilibrium with the liquid phase by prolonged agitation. After equilibrium was attained, the gas phase was displaced from the cell at constant pressure; the pressure was maintained by injecting a volume of mercury equal to the volume of the gas displaced. When the cell was again liquid full, additional mercury was withdrawn; thus, a new gas phase was formed which was then agitated until it was at equilibrium with the coexisting liquid phase. This gas was then displaced at constant pressure.

This sequence was repeated until the cell contained a saturated liquid with a bubble point pressure of approximately 700 psia. The volume of the PVT cell, containing the stainless steel piston, was not large enough to allow expansion of the system to atmospheric pressure. Therefore, mercury was withdrawn from the bottom of the cell at this point, to form a gas phase

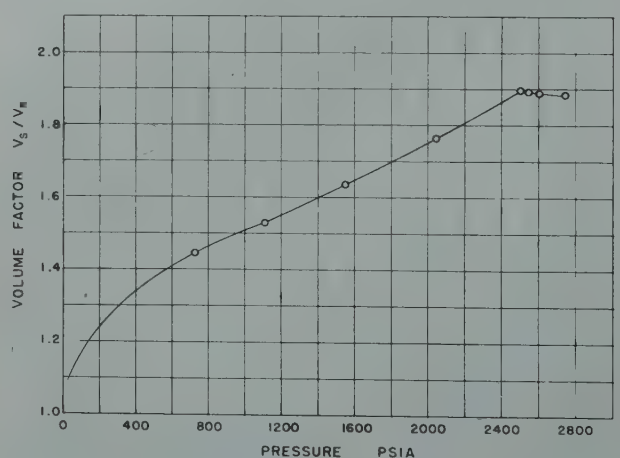

FIG. 3 — VOLUME FACTOR VERSUS PRESSURE, BASED ON RESIDUAL OIL AT 60°F AND 14.7 PSIA.

TABLE 2 — FLASH LIBERATION OF SATURATED RESERVOIR FLUID

Saturation pressure of fluid (psia)	2500
Separator gauge pressure	0
Solution gas-oil ratio, $\frac{\text{cu ft}}{\text{bbl residual oil}}$	1938
Stock tank API gravity at 60°F	32.6
Molecular wt, stock tank oil	201
Shrinkage factor, V_t/V_s*	0.5168
Formation volume factor, V_s/V_t	1.935
Specific gravity of flashed gas	1.031

*V_s = volume of saturated oil at the saturation pressure.
V_t = volume of stock tank oil at 60°F and 14.7 psia.

in the cell, and gas was released through the valve at the top of the cell until atmospheric pressure was reached. The residual oil was analyzed and its volume was determined.

From the volume of gas bled off at each pressure and the volume of residual oil, corrected to 60°F, the gas-oil ratios and volume factors were determined. The gas sample bled off at each liberation pressure was subjected to LTD analysis. The volume of each sample was determined by passing the gas into a 5-gal. carboy filled with saturated brine. A volume of brine equal to the gas volume entering the carboy was displaced and weighed.

Equilibrium vaporization ratios were calculated by mathematical recombination in the following manner: the volume and composition of the gas liberated at each pressure during the differential liberation were used to determine the number of moles of each component in each liberated gas volume. The composition, weight and molecular weight of the residual liquid remaining at the end of the gas liberation were also determined. From these data the number of moles of each component in the gas liberated in the pressure drop from 726 psia to atmospheric (the final pressure drop in the gas liberation process) was then added to the number of moles of the corresponding component in the liquid phase (residual oil). The summation gave the composition of the saturated liquid at 726 psia.

The composition of the equilibrium gas liberated at 726 psia was known, so a set of equilibrium vaporization ratios (at 726 psia) was calculated. The number of moles of each component in the gas liberated between 1111 and 726 psia was then added to the number of moles of that component in the saturated liquid at 726 psia. This gave the composition of the saturated liquid at 1111 psia. The composition of the equilibrium gas liberated at this pressure was known also, so a set of equilibrium vaporization ratios was calculated for 1111 psia. This process was followed until all of the gas was recombined with the residual oil.

DISCUSSION OF RESULTS

The results of the PVT study of the fluid under consideration are presented in Tables 1, 2, and 3 and Figs. 2, 3, and 4.

Table 1 and Fig. 2 present the gas-oil ratio data obtained for a differential liberation at 154°F. The gas solubility curve is similar to the curves usually obtained for ordinary crude oil systems. Only five points are presented because of the large pressure drops required to provide enough gas for accurate LTD analysis. The volume factors obtained from the differential liberation are presented in Fig. 3.

Table 2 presents the results of a flash liberation of the reservoir fluid to atmospheric pressure. No abnormal behavior was noted in this case.

Attempts were made to apply the bubble point — gas-oil ratio correlations of Standing[11] and Katz[12] to the present experimental data. Values of bubble point derived from these correlations were found to be over 100 per cent in error. Perhaps this is to be expected, since the correlations were not developed for this type of system.

The pressure-volume relations for the system are presented in Fig. 4 and Table 3.

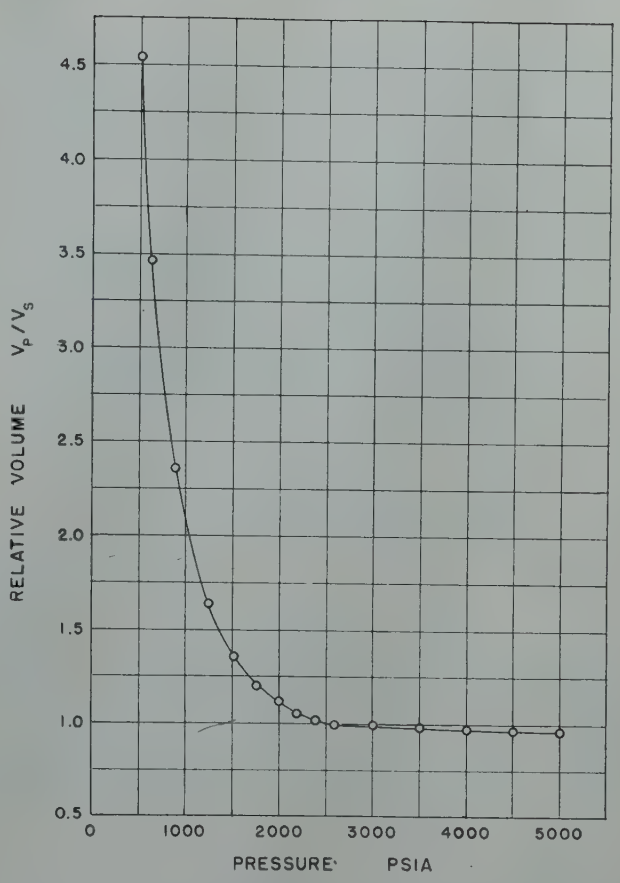

FIG. 4 — RELATIVE VOLUME OF RESERVOIR FLUID VERSUS PRESSURE AT 154°F.

TABLE 3 — PRESSURE-VOLUME RELATIONS FOR RESERVOIR FLUID AT 154°F

Pressure PSIA	Relative Volume $\frac{V_p^*}{V_s}$
5000	0.9594
4500	0.9667
4000	0.9750
3500	0.9826
3000	0.9915
2592	0.9998
2500	1.0000
2388	1.020
2180	1.063
1970	1.124
1750	1.215
1520	1.360
1245	1.635
890	2.368
648	3.470
518	4.548

*V_p = Combined volume of oil and gas at given pressure.
V_s = Volume of saturated fluid at saturation pressure.

The results of the LTD analysis of the gas samples taken during the gas liberation are given in Table 4 and Figs. 5a and 5b. The last two columns in Table 4 represent the composition of the total gas evolved in dropping the pressure from the given pressure down to atmospheric. Therefore, this gas was not in equilibrium with the residual oil at atmospheric pressure and K values could not be calculated for atmospheric pressure.

It will be noted that more points are presented on the methane, ethane, carbon dioxide, propane, and hydrogen sulfide curves than appear on those for the butanes and heavier components. Two separate pressure-

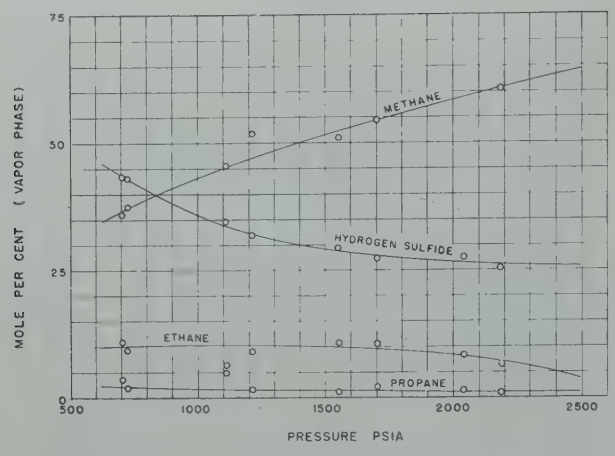

FIG. 5A — COMPOSITION OF LIBERATED GAS VERSUS PRESSURE.

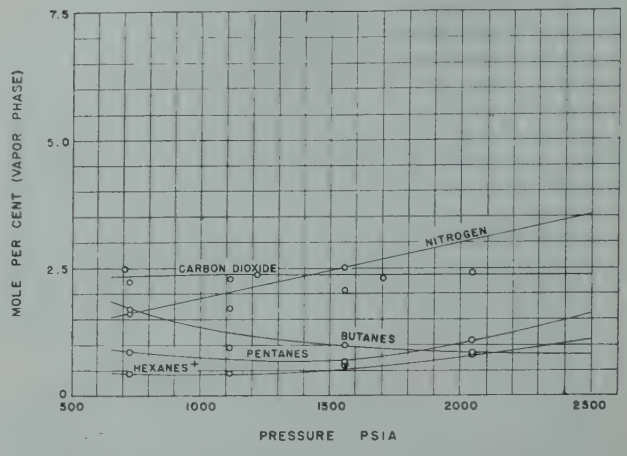

FIG. 5B — COMPOSITION OF LIBERATED GAS VERSUS PRESSURE.

TABLE 4 — COMPOSITION OF LIBERATED GAS*

	RUN NO. 1 PRESSURE PSIA					RUN NO. 2 PRESSURE PSIA				
Component	2187	1702	1215	705	705 - ATM	2043	1554	1111	726	726 - ATM
N_2						9.37	2.51	1.73	1.63	0.68
H_2S	25.6	27.7	32.3	43.9	59.5	27.69	29.58	34.71	43.38	69.48
CO_2	2.1	2.3	2.4	2.5	2.3	2.41	2.08	2.31	2.23	1.46
C_1	60.7	54.8	52.1	36.3	16.1	47.59	51.25	45.88	37.69	9.66
C_2	6.8	10.6	9.7	11.1	10.9	8.57	10.89	6.59	9.95	9.01
C_3	1.2	2.4	1.7	3.7	4.4	1.59	1.31	4.95	2.07	3.63
C_4						0.86	1.00	2.40	1.71	3.46
C_5						1.09	0.69	0.96	0.89	1.72
C_{6+}						0.83	0.69	0.47	0.45	0.90
Mol. Wt.						26.11	25.51	27.56	28.21	34.48
Sp. Gr.						0.901	0.881	0.952	0.974	1.19

*Experimental data. See Table 5 for smoothed data used in calculating equilibrium vaporization ratios.

composition determinations were made, the first of which showed scattered results for the heavier components because of the small concentrations present. A second determination was made on a considerably larger initial charge and these data were believed to be more accurate. The first determination verified the data of the second for the lighter components and for hydrogen sulfide, so both sets of points are presented in Figs. 5a and 5b for methane, ethane, carbon dioxide, propane and hydrogen sulfide. These data were smoothed in order to calculate the equilibrium vaporization ratios. The smoothed data are presented in Table 5. The second column in Table 5 represents the experimentally determined liquid composition at atmospheric pressure. All other liquid compositions in the table were calculated as described above. These calculated liquid compositions are plotted in Figs. 6a and 6b as a function of pressure.

The smoothed data were used to calculate equilibrium vaporization ratios K following the procedure outlined above. The calculated values are presented in Table 6 and Fig. 7. The solid lines drawn between 10 and 100 psia in Fig. 7 represent the ideal K's for each component, based on fugacities.[13] The data obtained here should approach these lines at low pressures. Therefore, the ideal K's were used as an aid in drawing the K curves for each component.

The K values for butanes and pentanes are quite scattered. This is undoubtedly a result of the fact that the concentrations of these components were of the same order of magnitude as the experimental accuracy. This was also the case for nitrogen; the nitrogen data are not presented in Fig. 7 because of their questionable accuracy.

The position of the K curves for butanes and pentanes was difficult to determine. The curves shown were based on the ideal K's at atmospheric pressure and the trends indicated by the other components of the system, as well as the experimental data.

An analysis of the procedures indicates several possible sources of error which should be considered. One of these is in the determination of the evolved gas volumes. Repeated experiments have shown that gas volumes can be reproduced within 20 cc by means of the brine displacement method. Since the gas volumes involved in this study were of the order of 3000 cc, the maximum error here should be somewhat under 1 per cent.

A second possible source of error is in the determination of the volume of residual oil following the differential gas liberation. This error was kept at a minimum by calibrating the PVT cell for liquid hang up previous to the study. The actual residual oil volume was determined by weighing the displaced liquid and then weighing a small sample in a pycnometer to determine its density. The total weight and density of the residual were used to determine the volume of residual oil. This volume was then corrected to 60°F.

A third source of error to be considered is the entrainment of liquid in the gas phase. Slow displacement from the PVT cell kept this at a minimum. At the end of the liberation no oil was noted on the water surface in the brine bottle. To prevent gas from dissolving to any large extent in the brine, the sample was transferred to the LTD apparatus immediately after the volume was determined. The results of the LTD analysis are believed to be accurate within one mole per cent.

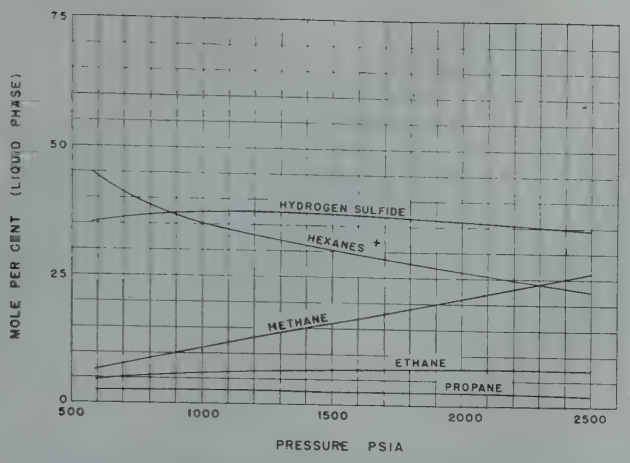

FIG. 6A — CALCULATED COMPOSITION OF SATURATED LIQUID VERSUS PRESSURE.

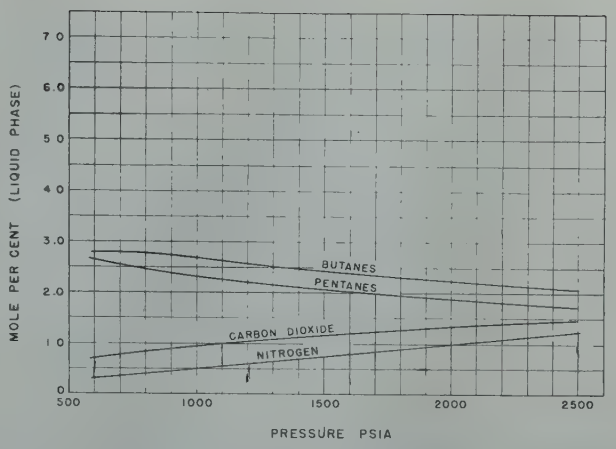

FIG. 6B — CALCULATED COMPOSITION OF SATURATED LIQUID VERSUS PRESSURE.

TABLE 5 — VAPOR-LIQUID COMPOSITION DURING LIBERATION OF DISSOLVED GAS FROM RESERVOIR FLUID, MOLE PER CENT

	PRESSURE PSIA										
	Atmospheric		726		1111		1554		2043		2500
Component	Liquid	Vapor	Liquid	Vapor	Liquid	Vapor	Liquid	Vapor	Liquid	Vapor	Liquid
C_1	0.00	13.80	7.787	37.58	12.10	45.86	16.843	53.23	21.723	56.73	26.121
C_2	0.00	9.50	5.361	10.15	6.05	10.49	6.677	9.94	7.127	8.08	7.247
C_3	1.37	4.00	2.854	2.06	2.74	2.04	2.641	1.60	2.497	1.45	2.366
C_4	2.00	3.45	2.818	1.71	2.66	1.34	2.473	1.00	2.270	0.84	2.090
C_5	3.63	1.70	2.541	0.88	2.30	0.74	2.081	0.68	1.888	1.04	1.782
C_{6+}	92.23	0.87	40.677	0.44	34.86	0.48	30.023	0.64	25.971	0.83	22.812
H_2S	0.77	64.55	36.761	43.28	37.70	34.60	37.267	29.06	36.135	25.72	34.827
CO_2	0.00	1.45	0.818	2.27	1.03	2.36	1.216	2.36	1.374	2.33	1.494
N_2	0.00	0.68	0.383	1.63	0.56	2.09	0.779	2.49	1.015	2.98	1.261

Atmospheric liquid compositions determined experimentally.
Vapor compositions are smoothed data from Fig. 5a and 5b.
Bubble point liquid (2500 psia) composition determined by extrapolation.

Considering these sources of error, it is believed that the data meet engineering requirements.

Fig. 8 gives a comparison of the results obtained here with the results of Jacoby and Rzasa. Jacoby and Rzasa worked with samples of crude oil containing five mole per cent hydrogen sulfide which they subjected to flash liberation. Their data, Fig. 5, were obtained at a temperature of approximately 150°F, compared with 154°F used in the present study. Since only one temperature was examined here, it was not possible to correct for the temperature difference of four to five degrees between the two studies. It is believed, however, that this difference should not affect the comparison appreciably. From the data given it appears that the higher concentration of hydrogen sulfide in the mixture studied here, raised the K values of the ethane and hydrogen sulfide and lowered those of methane. This effect may be partly the result of the high concentration of relatively volatile components in the mixture (ethane hydrogen sulfide, propane).

Fig. 9 shows a comparison of the results of this study with those of Katz and Hachmuth[2] for hydrocarbons. Here, too, the addition of hydrogen sulfide raised the equilibrium vaporization ratios of the ethane and heavier components.

TABLE 6 — EQUILIBRIUM VAPORIZATION RATIOS FOR RESERVOIR FLUID AT 145°F

	PRESSURE (PSIA)			
Component	726	1111	1554	2043
C_1	4.826	3.790	3.101	2.612
C_2	1.893	1.734	1.489	1.133
C_3	0.722	0.745	0.606	0.581
C_4	0.607	0.504	0.404	0.370
C_5	0.346	0.322	0.327	0.551
C_{6+}	0.011	0.014	0.021	0.032
H_2S	1.177	0.918	0.780	0.712
CO_2	2.775	2.291	1.941	1.696
N_2	4.256	3.732	3.196	2.936

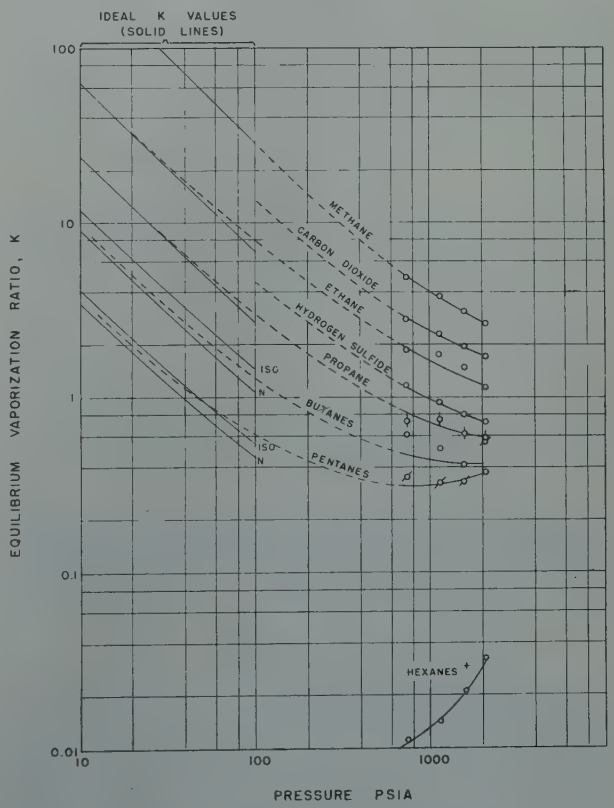

FIG. 7 — EQUILIBRIUM VAPORIZATION RATIOS VERSUS PRESSURE AT 154°F.

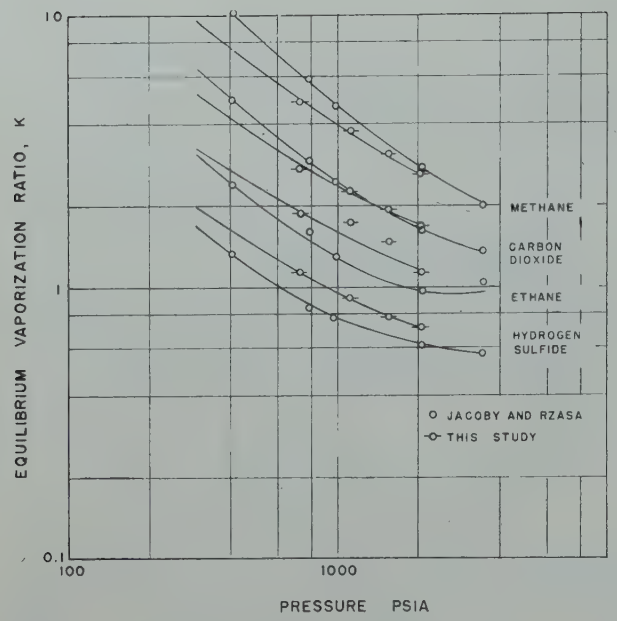

FIG. 8 — COMPARISON OF *K* VALUES FOR RESERVOIR FLUID AT 154°F WITH JACOBY AND RZASA'S DATA AT 150°F.

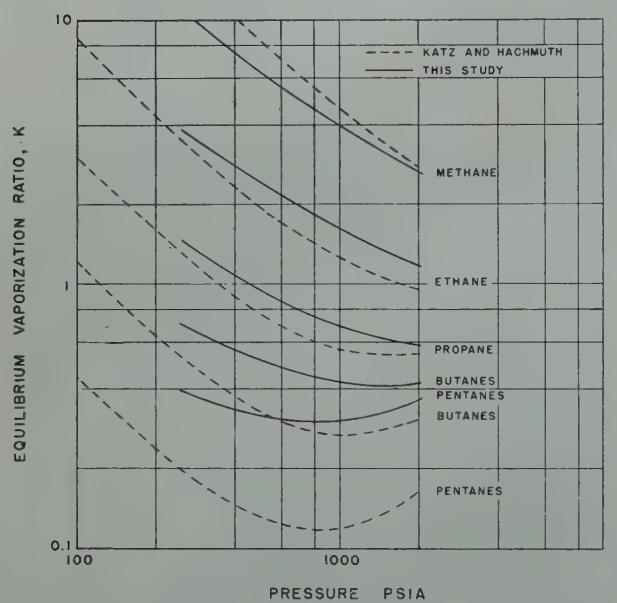

FIG. 9 — COMPARISON OF *K* VALUES FOR RESERVOIR FLUID WITH KATZ AND HACHMUTH'S DATA FOR HYDROCARBONS AT 154°F.

Reamer, Sage and Lacey's *K* values for the methane-hydrogen sulfide system[8] at 160°F fall between those of the present study and those of Jacoby and Rzasa.

CONCLUSION

Equilibrium vaporization ratios were obtained for a system containing 35 mole per cent hydrogen sulfide. The high concentration of hydrogen sulfide has a pronounced effect on the equilibrium vaporization ratios of the other components. It is recommended that in reservoir studies involving fluids of this nature experimental results be used exclusively. In the event these are not available, great care should be exercised in choosing *K* values.

ACKNOWLEDGMENT

The author wishes to thank the management of The Pure Oil Co. for permission to present this paper. Many thanks are also due the analytical group of the Research and Development Laboratories who performed the LTD analyses. The author also wishes to thank K. M. Watson for his valuable assistance in the interpretation of the data presented.

REFERENCES

1. Webber, C. E.: "Equilibrium Constants for Hydrocarbons in Adsorption Oil," *Trans.* AIME (1941), **142**, 192.
2. Katz, D. L., and Hachmuth, K. H.: "Vaporization Equilibrium Constants in a Crude Oil-Natural Gas System," *Ind. Eng. Chem.* (September, 1937), **29** (9), 1072.
3. Brown, G. G.: *Natural Gasoline Supply Men's Association Technical Manual* (Fifth Edition), (1948), pp. 63-71.
4. Roland, C. H., Smith, D. E., and Kaveler, H. H.: "Equilibrium Constants for a Gas Distillate System," *Oil and Gas Jour.* (March, 1941), **39** (46), 128.
5. Poettmann, F. H.: "Vaporization Characteristics of Carbon Dioxide in a Natural Gas-Crude Oil System," *Trans.* AIME (1951), **192**, 141.
6. Jacoby, R. H., and Rzasa, M. J.: "Equilibrium Vaporization Ratios for Nitrogen, Methane, Carbon Dioxide, Ethane and Hydrogen Sulfide in Absorber Oil-Natural Gas and Crude Oil-Natural Gas Systems," *Trans.* AIME (1952), **195**, 99.
7. Kay, W. B., and Brice, D. B.: "Liquid-Vapor Equilibrium Relations in Ethane-Hydrogen Sulfide System," *Ind. Eng. Chem.* (March, 1953), **45**, 615.
8. Reamer, H. H., Sage, B. H., and Lacey, W. N.: "Phase Equilibria in Hydrocarbon Systems — Volumetric and Phase Behavior of the Methane-Hydrogen Sulfide System," *Ind. Eng. Chem.* (April, 1951), **43**, 976.
9. Bierlein, J. A., and Kay, W. B.: "Phase Equilibrium Properties of System Carbon Dioxide-Hydrogen Sulfide," *Ind. Eng. Chem.* (March, 1953), **45**, 618.
10. Eilerts, K., and Smith, R. V.: *U. S. Bureau of Mines, R. I. 3642* (April, 1942).
11. Standing, M. B.: "A Pressure-Volume-Temperature Correlation for Mixtures of California Oils and Gases," *API Drilling and Production Practice* (1947), 275.
12. Katz, D. L.: "Prediction of the Shrinkage of Crude Oils," *API Drilling and Production Practice* (1942), 137.
13. Smith, K. A., and Smith, R. B.: "Vaporization Equilibrium Constant and Activity Coefficient Charts," *National Petroleum Publishing Co.* (1949).

★ ★ ★

THE CORROSION-METALLURGICAL ASPECTS of SUCKER RODS and their OIL WELL SERVICE PERFORMANCE

F. J. RADD
R. L. McGLASSON

CONTINENTAL OIL CO.
PONCA CITY, OKLAHOMA

T. P. 3758

ABSTRACT

The mechanisms of corrosion and corrosion fatigue damages to sucker rods are examined from a fundamental electrochemical viewpoint, and the relationships of sucker rod microstructures to these damaging effects are defined. The common corrosive agents in crude oil production and storage are discussed as to types of attacks that they cause. The variations of fatigue strength with alloy content, surface preparation, and stress ranges are analyzed. Finally, conclusions are drawn as to how microstructures largely influence and control sucker rod performance.

INTRODUCTION

Greater than 90 per cent of the crude oil produced by artificial lift methods is produced through sucker rod pumping systems. In the USA each year more than $14 million is spent for sucker rods in new and old pumping installations. It is important to make this investment a wise one.

Essentially, the sucker rod system is a long series of steel rods, operating under alternating stress loadings and under mechanical vibrations, which connect the surface power source with the subsurface pump. These rods often operate in a variety of corrosive media, including water, brines, carbon dioxide, hydrogen sulfide, and air.

Basically, this paper is concerned with the problem of the behavior of certain steels in various corrosive media under high and dynamic stress patterns. The main objective of this paper is to show how, once the stress effects and the corrosive environments are defined, one can still realize structural control and beneficial influence upon corrosion and corrosion fatigue.

FUNDAMENTAL DEFINITIONS AND ANALYSIS

In the corrosion and stress behavior of this solid state mixture of iron and iron carbide called steel, one must analyze upon what major factors does its service life depend and of what, exactly, is steel composed. The former question can be referred to two *external* factors and two *internal* factors. The two major *external* factors are:

1. the nature of the stress patterns — size and range of stresses present
2. the nature of the corrosion — erosion environment — the corrodent and/or wear involved

The two fundamental *internal* factors that govern the strength and useful life of a steel both in normal duty and in heavy-duty corrosion service are:

1. the nature of the steel volume properties
2. the nature of the steel surface properties

For the latter question normal steel is defined as a solid mixture of iron and iron carbide particles, generally with certain accidental and intentional elements present. (The amount of iron carbide present is determined by the carbon content of the steel.) These additional elements generally dissolve into either the iron (ferrite) or the iron carbide (cementite) components.

---

[1]References given at end of paper.

Manuscript received in the Petroleum Branch office Sept. 3, 1953. Paper presented at the Petroleum Branch Fall Meeting in Dallas, Tex., Oct. 18-21, 1953.

Publication space did not permit more metallographic data and examples to be printed. These examples may be seen in the AIME 1953 preprint of this paper or may be secured from the authors.

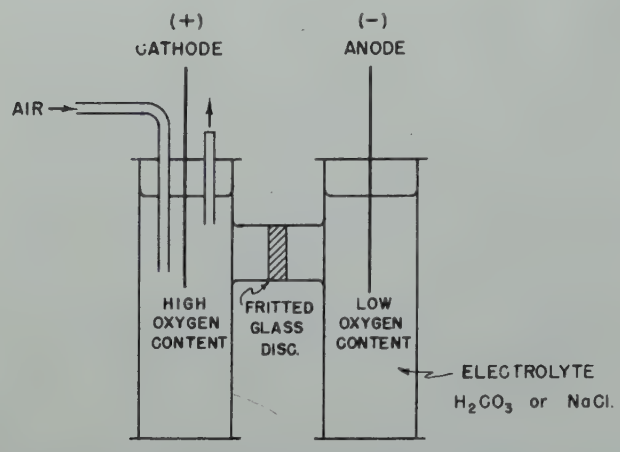

FIG. 1 — THE ELECTROCHEMICAL BASIS OF NORMAL RUSTING OF STEEL.

By changing the size, shape, distribution, number, and composition of the iron carbide particles and of the iron particles, the normal mechanical properties of steels can be changed to produce many desirable combinations. Nearly all the mechanical properties of a normal steel can be defined by changing the nature of the iron-iron carbide mixture or, in other words, its form, composition, and distribution. It is considered that by separating the major variables in this fashion their individual roles and then their various combinations of practical interest can first be assessed.

STRESS AND STRESS RANGES — HOW THEY AFFECT SERVICE LIFE

In the determination of the effects of certain alternating stresses upon air fatigue test specimen life, it is found that below a certain stress level the working life of a specimen is unlimited for all practical purposes. This stress level is called the endurance limit or the fatigue limit.

This limit defines for the given steel, with a certain surface condition and finish, the maximum loadings which may be given the steel in air and yet not experience failures within a reasonable and defined period of service life. An important point is that in corrosive environments there is no real endurance limit but only a steady decrease of the stress required to induce failure as the number of cycles is increased.

Several points of interest need to be underscored. One is that the air fatigue strength is approximately one-half of the air tensile strength value, assuming that the surface conditions and stress conditions of the engineering application and the test specimens are quite comparable.

The second is that corrosion exposures, such as to salt water or salt water and hydrogen sulfide, may bring nominal endurance limits to one-fifth and one-seventh of the tensile values, respectively. These data are, of course, approximations of the endurance limit decreases involved.

The third major point is that the increase of the tensile strength of the steels employed does not offer major hope of substantial improvement of working life. The final point is that one cannot expect any practical stress level to give, in a corrosive environment, an infinite fatigue life, as is inherent in the statement that corrosion is taking place.

Two important engineering considerations here are (1) since sucker rods are imperfect of surface finish and are not comparable to the fatigue test specimens, their performances should be, in fact, somewhat inferior to the experimentally determined values and (2) since a fatigue curve is not an absolute or final curve, but really is but one curve out of a statistical grouping or a family or band of curves, one must expect an endurance limit to be similarly subject to experimental scatter. These two criteria show that one can expect important positive or negative laboratory departures and even larger negative field departures from any non-statistical, single run endurance limit determination.

The effects of stress ranges and types of stresses present are summarized in the empirically established formulas given below:

Gerber's Law Criterion of Stress Range[1]

$$R = R_o\left(1 - \frac{M}{f}\right)^2 \quad . \quad . \quad . \quad . \quad . \quad . \quad . \quad . \quad . \quad . \quad . \quad (1)$$

R = safe range corresponding to mean stress M
R_o = safe range when $M = 0$
f = ultimate strength of the material

Moore's Statement of Nature of Stresses[2]

$$S_{max} = S_e\left(\frac{3}{2-r}\right) \quad . \quad . \quad . \quad . \quad . \quad . \quad . \quad . \quad . \quad . \quad . \quad (2)$$

If completely reversed stresses are not present in the fatigue test but only repeated cycles of pure tensile of compressive stresses, or tensile-compressive cycles partially reversed, then:

S_e = endurance limit for a given number of cycles for completely reversed stresses
r = ratio of minimum to maximum stress during a cycle, being a negative for completely or partially reversed stresses
S_{max} = endurance limit for this given number of cycles of this pattern of stresses

Strictly speaking, the above formulas apply to steels in air fatigue, but they should also in principle apply to corrosion fatigue. One may realize from these empirical formulas that air fatigue life is improved if the stress ranges are reduced and if the stresses are kept as pure and as unmixed as possible. Any design or operation variables that help in achieving these two points can be expected to help improve performance life.

The effects of frequency of stresses upon fatigue life are considered in a later section.

CORROSIVE AGENCIES

Four corrosive agencies are most commonly of major concern to oil field corrosion losses, being atmospheric oxygen, the dissolved acid gases of carbon dioxide and/or hydrogen sulfide, and the lower fatty acids.

ATMOSPHERIC CORROSION

Atmospheric oxygen, if permitted access to oil well brines or any suitable electrolyte, gives rise to oxygen concentration cells. The corrosion of a buried rusty nail or a rusty tin can or the exposed hull of a ship or the compartments of an oil tanker is of this type and mechanism. The origin of the electrochemical potentials involved here are from the differenences in oxygen content of the anode and of the cathode electrolyte regions, these being due to air accessibility differences.

Fig. 1 illustrates the origins and nature of this EMF. The larger the differences of the oxygen concentration levels at the two electrodes, the larger the produced

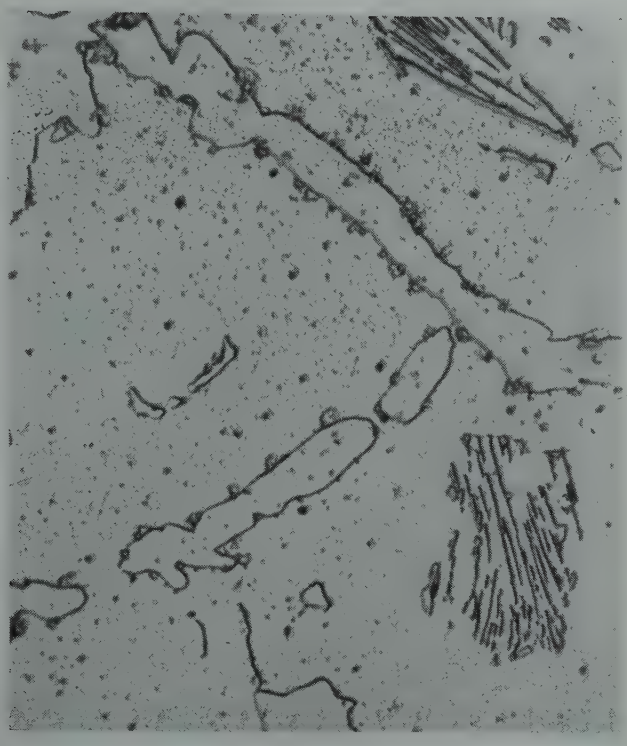

FIG. 2 — THE METALLOGRAPHIC STUDY OF RUST NUCLEATION ON STEEL. THIS SHOWS HOW THE RUST PARTICLES GROW ON THE IRON-IRON CARBIDE INTERFACE.

current will be and the greater the corrosion losses. The electrochemical reaction mechanisms of steel in sea water-oxygen exposures are summarized below:

1. $Fe^{+2} + 2OH = Fe(OH)_2$ (white)
2. $Fe^{+3} + 3OH = Fe(OH)_3$ (yellow-red)
   The reaction mixture is first bluish, then becomes greenish, and finally becomes yellow-brownish as more and more oxygen is absorbed.
3. $2\,Fe + 3O + H_2O = 2\,(FeO(OH)$
   (β—lepidocrocite)
4. $Fe + 3O = Fe_2O_3$ (haematite)
5. $Fe_3C = Fe_3C$ (undecomposed)

From these reactions it may be seen that ordinary rust is not a simple substance but is often a complex material. The sea water, marine, or brine variety is mainly β—lepidocrocite (FeO(OH) with iron carbide being entrapped undecomposed, often with a haematite undercoat film present. The important feature of the oxygen concentration cell is that it is chiefly due to an externally caused EMF. It may proceed somewhat independently of microstructural differences. The fact that it is still partly dependent on microstructure may be noted in that careful X-ray spectrometer and chemical analyses both reveal undecomposed, pyrophoric iron carbide present in ordinary steel rusts.

Evidently iron carbide has a significant role even in the atmospheric corrosion of steels, as may be studied in Fig. 2. Two roles appear for the iron carbide: first, it evidently helps to nucleate the first rust nuclei; then it produces with a given electrolyte an iron-iron carbide EMF which, upon an anodic region of the steel, is additive to the oxygen concentration cell EMF operative thereon. Using ASTM sea water as the electrolyte, the maximum oxygen concentration cell voltage observed with air saturation was greater than 260 mv and with oxygen bubbled in this was greater than 280 mv.

One interesting and significant aspect of the oxygen concentration cell involving iron or steel is that on its local cathodes in sea water or salt water a very tenaceous and protective film of homogeneous haematite is formed. The authors have found that this nonconductive film prevents further corrosion attack and is present in areas which are under cathodic protection. Furthermore, the authors have successfully electrochemically synthesized this desirable film on steels. It is believed that this film may have a direct beneficial action on the corrosion cracking improvement in mild steels under cathodic potential, as noted by R. N. Parkins.[3] As such, it implies that most substantial corrosion fatigue improvements may be accomplished upon steels in sea water and air by application of cathodic protection, even as to prevent or minimize paravane line failures and bridge wire deterioration and premature drill pipe failures. It would be applicable for stressed steels in these corrosive environments, either under constant or repeated stress.

Hydrogen Sulfide, Carbon Dioxide, and Lower Fatty Acid Attacks

The anaerobic corrosion attacks found in oil wells are generally due to these gases which form weak acids and the lower fatty acids in produced waters or brines. It is these electrolyte systems that shall be referred to in the remainder of this paper. Only the corrosion tendencies of the metal structures are considered, as the chemistry forms another subject paper.

Two factors tend to influence and control the corrosion behavior of steels in these environments. One is the degree of surface protection afforded by oil well paraffin deposition and the effects of polar compounds in the crude, since certain paraffin deposits can largely seal off the sucker rods from any extensive corrosion

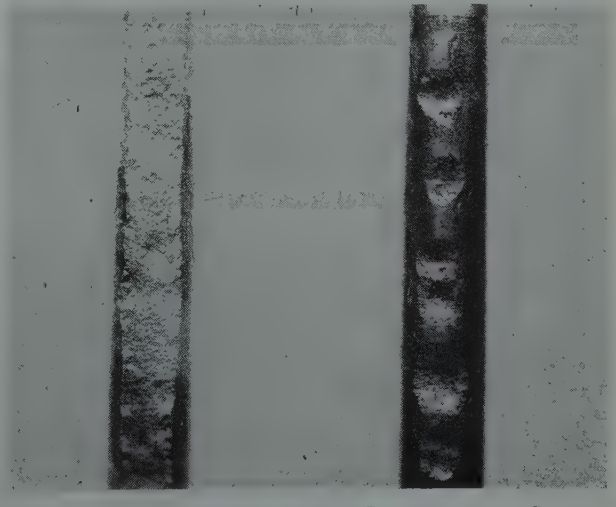

FIG. 3 — THE CHARACTERISTIC CORROSION OF SUCKER RODS, THE LEFT BEING A GENERAL OR UNIFORM ATTACK, AND THE RIGHT BEING A DEEP CONICAL PITTING. AN OIL WELL H_2S-BRINE CORRODENT AT APPROXIMATELY 120°F.

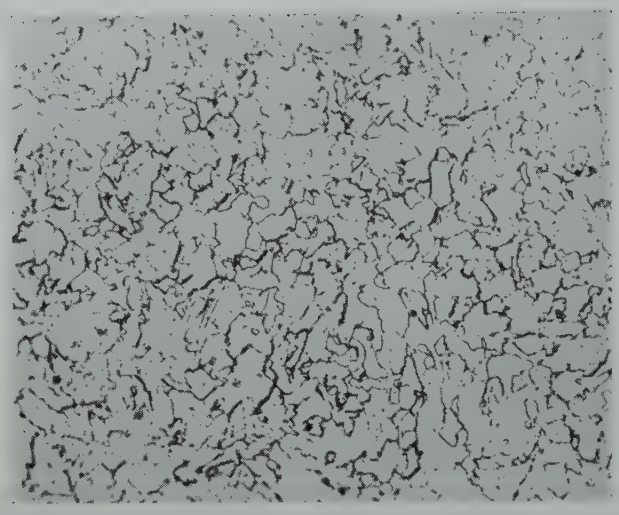

FIG. 4 — THE MICROSTRUCTURE OF THE UNIFORMLY CORRODED SUCKER ROD, 3.5 PER CENT NICKEL TYPE.

attacks and the polar compounds make the surface oil wet, thus excluding the corrosive water. The other is the amount of direct erosion or wear, which may largely determine the protectiveness of the corrosion by-products' films.

In Figs. 3, 4, and 5, one may see the effects of microstructure in sucker rod steels, in combination with wear, upon the character and extent of the corrosion attack in an H_2S-brine at approximately 120°F. It is strikingly interesting to note that, even in spite of a poor microstructure of the banded steel rod with the conical pits, the direct macrocorrosion of areas not subject to erosion wear was not accented.

There appears to be a strong difference of behavior of the hydrogen sulfide and the carbon dioxide attacks upon steels in oil well environments. In "sour" areas wherein hydrogen sulfide-brine electrolytes produce a black iron sulfide film, this insoluble sulfide film tends to be deposited and to be protective. In "sweet" oil areas wherein carbon dioxide-brine electrolytes occur, the corrosion by-product film is not observable and the solubility of the iron bicarbonate usually formed does not permit an insoluble by-product film. No major corrosion resistance may be expected in this type of service, assuming a given structure, unless the insoluble iron carbonate is formed and deposited. In a real sense, it is clear that the nature of the corrosion is, for a given steel and microstructure, the product of the environment, the steel structure, and the corrosion by-product behavior.

THE RELATIONSHIPS OF CORROSION AND MICROSTRUCTURES

From metallurgical studies of the corrosion pitting of the above specimens, we concluded that:

1. The corrosion attack was pearlite-accented and that certain of the pearlitic areas were more anodic in the ferrite-pearlite aggregate.
2. The iron-iron carbide potential was the agency helpful to and effective in the control of the attack. Preliminary potential measurements show that this EMF is greater than 250 mV and may be as high as 300 mV in 0.1 N NaOH at 73°F.

To demonstrate this point, it was found that in any similar series of steels arranged in order of carbon content the higher carbon steels were clearly cathodic to the lower carbon steels and that a 1.80 per cent Ni — 0.21 per cent C — 0.28 per cent Mo sucker rod (case-hardened) coupling was cathodic to the identical steel not carburized.

From the published data of S. M. Jones Co. on endurance limits of three popular sucker rod types,[4] a study was made of the relationships of the endurance limits of these three steels as a function of carbon content. A direct, linear, characteristic relationship was found between the carbon content and the endurance limit. While these endurance limits must be qualified by the previous considerations, the general relationship evident is considered interesting. It can be noted that the function of the nickel content here is to act as a ferrite strengthener and that its corrosion contribution with these small additions is to permit lower carbon contents to be used, and it cannot be held responsible for the corrosion fatigue improvements noted.

From the literature study, it was found that E. Heyn and O. Bauer[5] first studied the effects upon corrosion losses of carbon content and form. It was found that C. Chappell[6] demonstrated the increase of corrosion rates of steels wth increase of carbon content, showing that the corrosion losses decreased with this order: quenched, tempered, normalized, rolled, and annealed. Significant contributions on the above topics were made by H. Endo[7] and T. Matsushita and K. Nagasawa.[8]

In the work of T. Hoar and D. Havenhand,[9] massive cementite was considered to behave cathodically. F. Prange,[10] in a 1946 review article, made the observation that the iron-iron carbide potential could be considered as being relevant to the corrosion of steel. R. W. Manuel[11] has demonstrated experimentally the effect of certain carbide forms upon corrosion losses. He proved that the number and form and distribution of the iron carbide in steels are important to the accelerated, continuous corrosion of steels as affecting both the geometry of the corrosion and the weight loss rates.

Finally, the experimental data of C. Larrabee[12] show that, while phosphorus (primarily) and copper (sec-

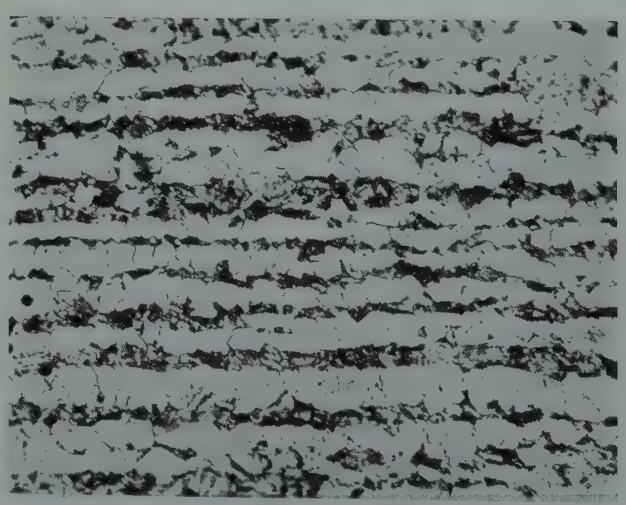

FIG. 5 — THE INJURIOUS MICROSTRUCTURE OF A BANDED NICKEL STEEL SUCKER ROD, 1.75 PER CENT NICKEL. THIS BANDED STRUCTURE WAS RESPONSIBLE FOR THE CONICAL, DEEP PITTING.

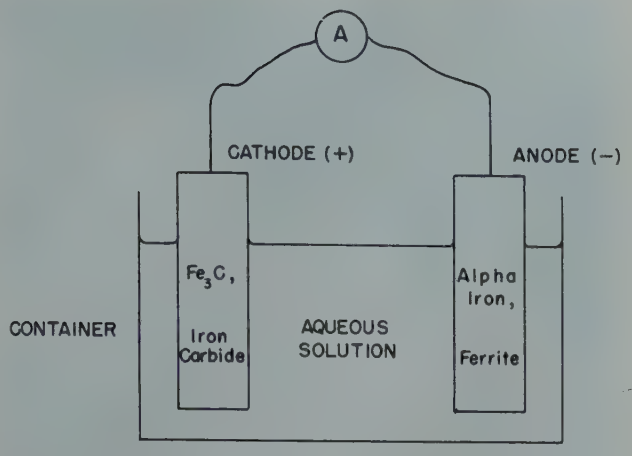

FIG. 6 — THE FUNDAMENTAL BASIS FOR THE ELECTROLYTIC MICRO CELL CORROSION OF STEEL. THIS CELL REPRESENTS ONE PAIR OF ELECTRODES PRESENT IN PEARLITE, SPHEROIDITE OR OTHER FERRITE-CARBIDE AGGREGATE.

ondarily) are atmospheric corrosion retardation agents, it is the carbon content of structural carbon or structural alloy steels that is the primary corrosion acceleration agency.

In the metallographic studies of 1.75 per cent Ni steel mentioned, the surface of the corroded steel was found to be preferentially attacked at the pearlite grains, some of which were found to be indented by the corrosion. The pearlite grains of different orientations were corroded to varying depths. This preferential attack of the pearlite grains was also observed shortly afterwards in oil well tubing and casing, where the pearlite, being more uniform, and the grain size, being much larger, made the observations more certain and accurate.

Consequently, the authors were led to consider that the corrosion of these normal steels was taking place through the formation of local microelectrolytic cells by having the iron carbide (cementite) platelets of these steels to function as one microelectrode, while the alpha iron (ferrite) platelets served as the other. Figs. 6, 7, and 8 afford a description of this electrochemical behavior of the normal microstructural elements and forms in normal steel as determined from our laboratory experiments and observations of field experience. It was observed that:

1. The corrosion of the pearlite was orientation dependent (as determined from the pearlite orientation in reference to the corrosion medium or, equivalently, to the number of cells active per unit area of exposed surface).
2. The corrosion of ferrite-carbide aggregates was not orientation dependent, giving rise to more uniform and severe corrosion activity, while the pearlitic corrosion tended to give restricted pitting action because of the poorly oriented grains.

These points can be clearly seen by examination of Fig. 9. It may be observed that the grain size found in a pearlitic steel is important, since it determines the magnitude and nature of the pearlitic corrosion pitting actions and so the local stress-raising effects.

HOW SUCKER RODS FAIL

One other point needs to be considered before the signifiicance of the iron-iron carbide potential and its orientation dependence in pearlite and orientation independence in spheroidite or globularized iron carbide forms can be assessed. *What is the mechanism of corrosion fatigue failures in sucker rods?*

Laboratory experience, from the macro and micro investigations of many failure specimens, shows that the initiation and the growth and development of a corrosion fatigue failure are essentially clearly intergranular until the stress levels reached on the remaining areas are so high that the normal tensile-type failure occurs. For approximately 60 to 90 per cent of the specimen area, the intergranular failure takes place with little or no local elongation. Then, transgranular or tensile failure takes place with slipping, warpage, and elongation of the grains being noted. These failure mechanisms can be observed by macrostructure studies alone.

These failures are quite similar to high-temperature failures in high-temperature alloys and in jet engine alloy blades. First, there is a chemical oxidation and reaction and penetration of the grain boundaries with a chemical deterioration and rupture of the grain boundaries. Then there is the normal transgranular tensile type failure (with perceptible elongation) when excessive stress levels are reached.

In the authors' judgment, in corrosion fatigue, the proportion of the intergranular to the transgranular fracture components depends upon the ratio of the stress level actually experienced to the yield stress level. It is, therefore, an index of the quality of design and its safety factor. The authors' data, therefore, force the conclusion that the condition of the grain boundaries and the chemical composition of the grain boundaries, as to possible electrochemical action, are important and even critical as to corrosion fatigue behavior. (The authors' data further imply that there does not exist in fact an "equi-cohesive" temperature for metals.) Fig. 10 illustrates a condition in the cor-

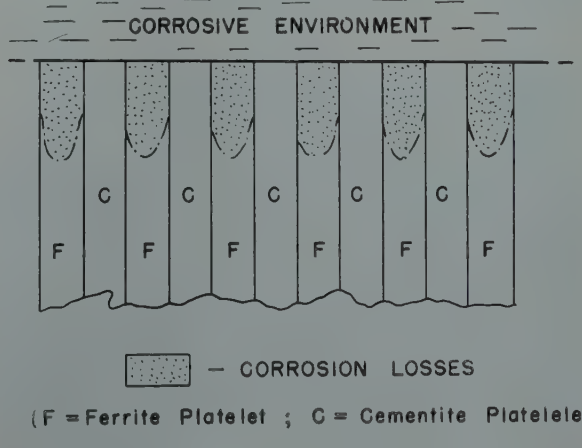

FIG. 7 — A BASIC MECHANISM IN THE CORROSION OF STEELS: THE ORIENTATION-DEPENDENT CORROSION OF PEARLITE (A STEEL MICROSTRUCTURAL FORM WITH ALTERNATING PLATELETS OF IRON AND IRON CARBIDE).

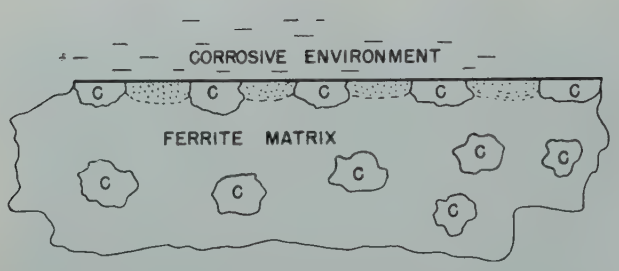

FIG. 8 — A BASIC MECHANISM IN THE CORROSION OF STEELS: SPHEROIDITE OR FERRITE-CARBIDE (PARTICLE SIZE AND DENSITY DEPENDENT, ORIENTATION INDEPENDENT) CORROSION.

rosion fatigue failure mechanism, found only in one mode, the electrochemically-produced one, of the general grain boundary oxidational failure mechanism in metals and alloys.

Fig. 11, included as a graphic example, illustrates the intergranular HF stress corrosion cracking of *K* monel. It is seen that in a grain boundary which possesses iron carbides there already exists on a micro-electrolytic cell basis an ample supply of local anodes and cathodes. The intergranular corrosion of certain 18 Cr-8 Ni stainless steels may be considered to be an analogous case. The authors believe that these grain boundary carbides in mild or low carbon steels are instrumental in corrosion fatigue work and are the primary agency in the lowering of the endurance limit with increased carbon content. The presence of iron carbide particles at the grain boundaries may have a multiple effect. Besides the electrochemical effects of dissimilar structures being present, the presence of a second phase at the grain boundaries also means the presence of severe microstresses. These microstresses may be expected to make the grain boundary even more anodic in these systems.

The results obtained in R. N. Parkins' work,[13] wherein he shows the improvement of stress corrosion cracking resistance of mild steels (0.07-0.22 per cent carbon) due to minimization of grain boundary cementite envelopes may be interpreted as being due to the focusing of anodic action upon the grain boundaries by the presence of grain boundary iron carbides.

THE DESIGN AND SELECTION OF SUCKER ROD STEELS

With the source of the microelectrolytic cell EMF being considered (the iron-iron carbide EMF) and with the nature of the failure being recognized as intergranular, it becomes relevant to examine the merits of various possible variations in microstructure.

First, the volume and the grain boundary resistance to deterioration should be made a maximum. With pearlitic steels, this implies a preference for reduction of corrosion pit notching through making the grain size as fine as is reasonably possible. It also implies that the carbides per unit grain boundary area be minimized.

Second, it appears evident that as low a carbon content is desirable as is consistent with necessary yields and elongation values.

Third, whatever the given carbon level, it should preferably be volume-distributed rather than grain boundary-distributed. This generally means a spheroidized carbide distribution rather than a pearlitic platelet distribution.

Fourth, it is clear that, while quenched and tempered structures have no built-in macro-corrosion resistance possible from orientation, it is quite possible to obtain some corrosion resistance based on orientation benefits from pearlite aggregates. But here a certain difficulty creeps in. The pearlite grains always have partial grain boundary cementite envelopes (Fig. 12). The pearlite grains are nucleated from grain boundary cementite particles so that it appears that the pearlite's macro-corrosion resistance can be obtained only at the expense of corrosion fatigue resistance (because of poor micro-corrosion resistance at the grain boundaries). This grain boundary cementite envelope effect works to minimize the pearlite orientation effects, since a poorly oriented grain may be protected initially by a coherent grain boundary cementite envelope.

The work of Dolan and Yen[14] on air fatigue indicates precisely this point, if the differences of the yield strengths of their steels can be assumed to be negligible. (Actually it appears more reasonable to express endurance limit in terms of yield strength than tensile strength.)

Several conclusions are possible from these reasonings: One is that Hopkinson's view,[15] that a slight increase of endurance limit should result with an increase of frequency of stress reversals, must be even more true for corrosion fatigue than for air fatigue. Since the electrochemical oxidation of the grain boundaries is a time dependent process, the lower the stress application frequency the larger the net effect of corrosion

FIG. 9 — AN EXAMPLE OF THE LOCAL MICRO NOTCHES DUE TO PREFERRED PEARLITE CORROSION REACTION.

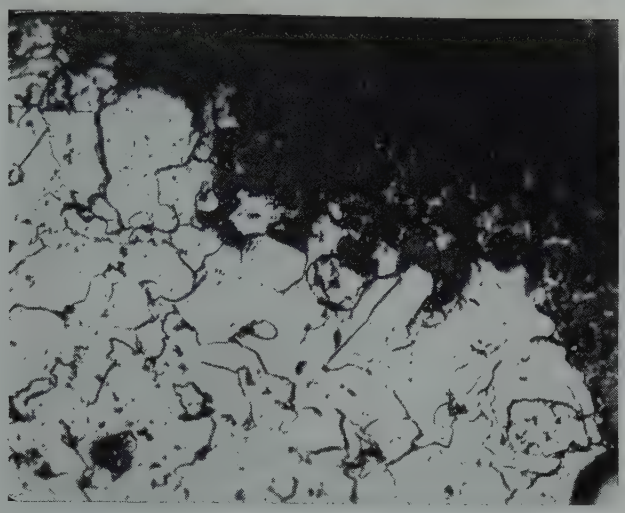

FIG. 10 — THE GRAIN BOUNDARY FAILURE PATH SHOWING GRAIN BOUNDARY CRACKING AND PARTING AND NOT SHOWING LOCAL GRAIN DEFORMATION.

penetration should be. But the effects of the frequency may not be structure-independent. An increase of frequency may be expected to give an effective increased life to grain boundaries that do have carbides and to have little or no effect upon grain boundaries that do not have carbides or other two-phase systems to give electrochemical differences.

MANUFACTURING VARIABLES AFFECTING SUCKER ROD PERFORMANCE

Several surface condition factors need to be underscored, as the final performance of the sucker rods is dependent upon both the surface and the volume properties of the finished sucker rod. First, the fact that increased surface roughness decreases the air fatigue life of steel is well established.

Second, the presence of mill scale, Fe_3O_4, is undesirable because it is very strongly cathodic to iron and causes strong local microelectrolytic cell action. The authors' results show that the EMF produced by the Fe_3O_4–Fe action is more than 0.82 volt in 0.1N HCl at 72°F. If the mill scale produced in manufacture is quite thick, there is both decarburization of the surface and severe grain boundary magnetite inclusion formation.

Both decarburization and inclusion formation tend to lower the corrosion fatigue life. The former factor, although improving corrosion resistance, tends to lower the net available cross section, while the latter forms a destructive corrosion system. If a pure ferrite film could be formed with a comparable or equal cross section, there should be a marked increase of corrosion fatigue life, as is implied by the reduction of iron-iron carbide cell density. Finally, any surface mechanical or chemical (electrochemical) injury can be expected to accent and intensify corrosion fatigue failures.

The Fe_3O_4-Fe potential referred to in the above paragraph refers to the hydrochloric acid-oxygen system, an aerobic system. In hydrogen sulfide-brine systems (anaerobic) the ferrite reacts rapidly to form an insoluble iron sulfide film. The effect of this film is apparently very desirable, since the mill scale, Fe_3O_4, does not in practice show corrosion acceleration with the iron sulfide. In hydrogen sulfide-brine oil well media, the FeS-Fe_3O_4 potentials are either quite small or are essentially negligible. (The carbon dioxide-brine cases are not defined for the Fe_3O_4 case; here, however, the Fe_3O_4 potentials are expected to be significant.) From the above it is apparent that the normally encountered decarburized steel surface layers, mainly ferrite with some residuals of Fe_3O_4 inclusions, act in certain applications as built-in corrosion inhibitors. These commercial ferrite films, within desirable limits, offer very interesting possibilities for use as desirable corrosion inhibitors for hydrogen sulfide-brine areas.

CONCLUSIONS

1. The performance and life of oil well sucker rods are microstructurally dependent and can be regulated by heat treatments. These variables are subject to manufacturing practice control. For optimum sucker rod service, the structure and carbon content as well as the alloy composition and design loads should be considered for maximum corrosion fatigue life. These should be considered in regards to the particular corrosive environment.

2. The corrosion fatigue life of sucker rods is carbide (carbon) content sensitive as well as carbide distribution sensitive. The grain boundary type of distribution is specifically undesirable. It is believed that the iron-iron carbide potential is the responsible and controlling agency.

3. Corrosion fatigue failures are mainly grain boundary oxidational reaction failures.

4. No external, electrolysis-producing currents are needed to give electrolytic action in steels for oil production service. The "built-in" microelectrolytic cells from microstructural variations provide ample voltages, under certain conditions, to give corrosion or corrosion fatigue attacks. The amount and form and distribution of the iron carbide help to control these.

5. It is pointed out that the iron-iron carbide potential is apparently of first-order significance even for normal rusting or atmospheric rusting. Atmospheric rusting

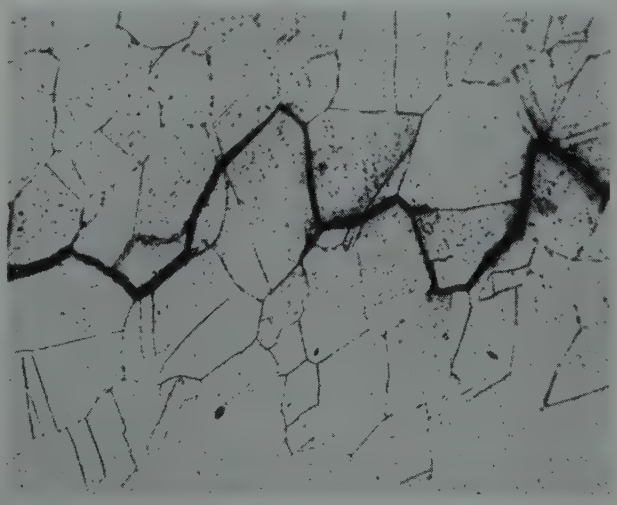

FIG. 11 — THE GRAIN BOUNDARY OXIDATIONAL FAILURE OF K MONEL DUE TO HF STRESS CORROSION CRACKING. THIS EXEMPLIFIES THE NATURE OF THE ORDINARY SUCKER ROD FAILURES.

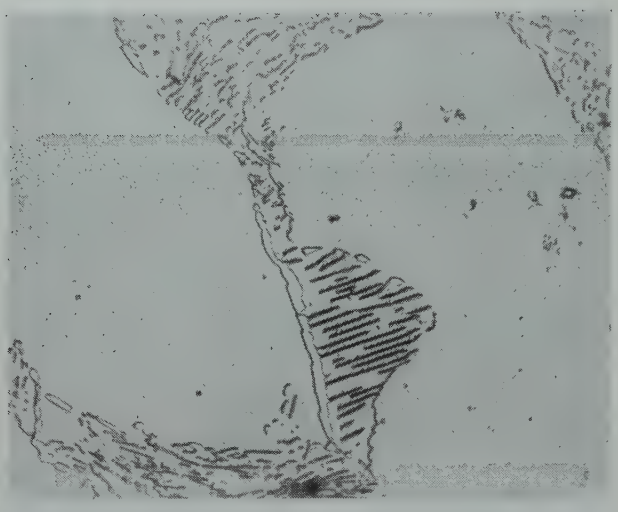

FIG. 12 — THE GRAIN BOUNDARY ENVELOPES OF MASSIVE IRON CARBIDES IN A HIGH PURITY STEEL.

appears to be nucleated at the ferrite-cementite (or iron-iron carbide) interface. In an anodic region of a steel in the atmospheric rusting process, the iron-iron carbide potential is apparently additive upon the oxygen concentration cell potential.

6. The sucker rod life, for a given stress pattern and surface, may be considered as being dependent upon both corrosion resistance and erosion resistance.* Where rod wear is not a problem and where corrosive service is encountered the lower carbon alloy steels of suitable yield strength levels and quenched and tempered structures would seem preferable. Where rod wear is a significant factor, the plain carbon and carbon-manganese rods (normalized condition) would tend to confer a desirable erosion resistance and a certain corrosion resistance, both of which should contribute to an improved corrosion fatigue life for this case. Finally, where neither wear nor corrosive conditions occur the low carbon alloy or the normalized plain carbon and carbon-manganese steels are indicated, with the former giving the longer life or the larger load-carrying capacity.

While corrosion fatigue capacity has been emphasized in this paper the final sucker rod behavior is, in certain cases, dependent on the corrosion-erosion fatigue behavior of sucker rod steels, with the erosion resistance increasing with increased carbon content and structural hardness.

*By erosion is meant rubbing and physical impingement losses.

ACKNOWLEDGMENTS

The authors wish to underline their sincere appreciation of the aid and encouragement given this study by D. A. Shock and to R. G. Edholm for his X-ray spectrometric determinations of β-lepidocrocite, haematite, and iron carbide in various rusts. To the management of Continental Oil Co. we are indebted for permission to publish the results of these investigations.

REFERENCES

*1. Gerber: *The Encyclopedia Britannica,* 14th Edition, **15**, 63.

2. Moore, H. F.: *Metals Handbook,* American Society for Metals (1948), 121.

3. Parkins, R. N.: "The Stress Corrosion Cracking of Mild Steels in Nitrate Solution," *Journal Iron Steel Institute* (London), (1952), **172**, 149.

4. S. M. Jones Co.: *Engineering Data Sheet,* Toledo, Ohio, 1950.

5. Heyn, E., Bauer, O.: *Stahl u. Eisen* (1908), **26, 2; (1910), **28**, 62.

6. Chappell, C.: *Stahl u. Eisen* (1912), **32, 832.

7. Endo, H.: *Science Rep.,* Tohoku University (1928), **17, 1245.

8. Matsushita, T., Nagasawa, K.: *Kinzoku-no-Kenkyu* (1937), **3, 92.

9. Hoar, T. P. Havenhand, D.: "Factors Influencing the Rate of Attack by Mild Steels by Typical Weak Acid Media," *Journal Iron Steel Institute* (London), (1936), **133**, 239.

10. Prange, F. "The Agents, Basic Causes, Control, and Prevention of Corrosion," *Oil and Gas Journal* (1946), **45**, (18), 88; (1946), **45**, (19), 88.

11. Manuel, R. W.: "The Effect of Carbide Structure on the Corrosion Resistance of Steel," *Corrosion* (1947), **3**, (9), 415.

12. Larrabee, C. P.: "Corrosion Resistance of High-Strength Low Alloy Steels as Influenced by Composition and Environment," *Corrosion* (1953), 8, (9), 259.

13. Parkins, R. N.: "Correspondence on Stress- Corrosion Cracking of Mild Steels," *Journal Iron Steel Institute* (London), (1953), **174**, (2), 140.

14. Dolan, T. J., Yen, C. S.: "Some Aspects of the Effect of Metallurgical Structure on Fatigue Strength and Notch Sensitivity of Steel," Proceedings ATSM (1948), **48**, 664.

*15. Hopkinson, *Proc. Roy. Soc.* (1911), **86**.

*Indicates references from 14th Edition, *Encyclopedia Britannica.*
Indicates references from summaries given in Mellor, J. W.: "A Comprehensive Treatise on Inorganic and Theoretical Chemistry" (1934), **13, (Fe, part 2).

★ ★ ★

OIL PRODUCTION after BREAKTHROUGH— as INFLUENCED by MOBILITY RATIO

A. B. DYES
B. H. CAUDLE
MEMBERS AIME
R. A. ERICKSON
JUNIOR MEMBER AIME

THE ATLANTIC REFINING CO.
DALLAS, TEX.

T. P. 3784

ABSTRACT

The study of the influence of fluid mobilities on the sweepout pattern resulting from the injection of gas or water has been extended to cover the production period which follows breakthrough of the injected material. Mobility ratios over the range common in field operations (0.1 to 17) were studied for several pattern floods (five-spot, staggered, and direct line drive). The experimental data required for these studies were obtained by the use of the x-ray shadowgraph technique using miscible oil phases of different viscosities in porous plate models of a reservoir element. From the shadowgraph pictures obtained before and after breakthrough of the injected fluid, flowing ratios at the producing well and cumulative volumes injected were calculated.

The method for applying such data in predicting field behavior is illustrated for a water flood of a five-spot. For this case a range of mobility ratios of 0.5 to 5.0 results in: (1) nearly complete (95 to 100 per cent) sweepout pattern efficiencies at abandonment conditions, (2) production after breakthrough being responsible for as much as one-third of the total recovery at the lower mobility ratios, and (3) a twofold variation in the operating life of the reservoir.

INTRODUCTION

In determining the merits of a secondary recovery operation, the fraction of the reservoir which is ultimately to be swept by the injected fluid is of major importance. Because of its significance a large amount of research has been applied to the study of areal sweepout efficiency. Muskat, Wyckoff and Botset[1,2] have presented the classic analysis of the pattern efficiency at breakthrough for several injection patterns in which the mobility of the fluids ahead of the injected phase front was equal to the mobility of the fluids behind the front. Aronofsky[3] has extended this analysis of recovery at breakthrough through numerical computations and by the stepwise use of the potentiometric model to include the effect of different fluid mobilities ahead of and behind the invasion front on the line drive performance. Fay and Prats[4] have also employed numerical computations to show the influence of one other condition of fluid mobilities on the five spot flood.

In a previous paper[5] a new method of attack on this problem which employed x-ray and porous plates was described. At that time experimental results were also presented which described the effect of fluid mobilities on the reservoir area contacted by the injected fluid at breakthrough for the five spot and direct line drive patterns.

Most of the literature pertaining to sweepout pattern efficiency has emphasized the pattern which is obtained at breakthrough of the injected phase. The increase in the sweepout pattern which occurs after breakthrough

---

[1]References given at end of paper.

Manuscript received in the Petroleum Branch office July 31, 1953. Paper presented at the Petroleum Branch Fall Meeting at Dallas, Tex., Oct. 19-21, 1953.

Discussion of this and all following technical papers is invited. Discussion in writing (3 copies) may be sent to the offices of the Journal of Petroleum Technology. Any discussion offered after Dec. 31, 1954, should be in the form of a new paper.

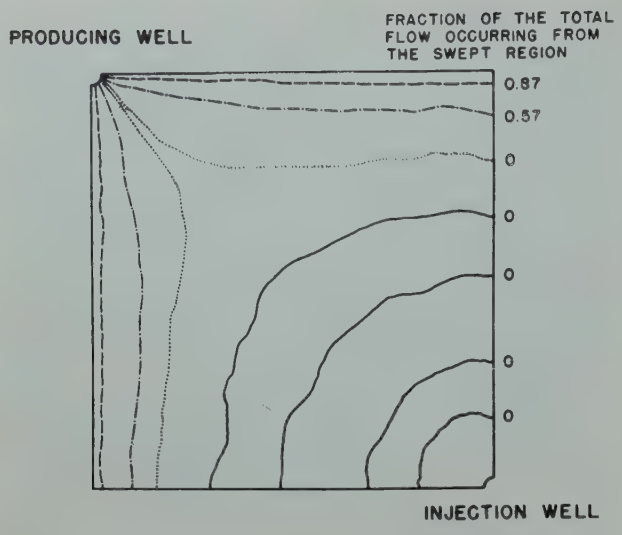

FIG. 1 — SWEEPOUT PATTERNS AT SUCCESSIVE TIMES DURING FLOOD OF A FIVE SPOT PATTERN AT MOBILITY RATIO OF 1.06.

and during the period of production of both displaced and displacing phase has been given little attention. Hurst[6] presented an analysis of production after breakthrough in a five spot flood for a limited case in which the mobility of the fluids in the swept and unswept regions were equal. Fay and Prats[4] added the recovery after breakthrough for the case in which the mobility of the fluids in the unswept region was one-fourth that in the swept region.

Because of the limited data available on the phase of production history after breakthrough and the emphasis which most of the literature has placed on recovery at breakthrough, the fraction of the reservoir considered in engineering studies for injection operations has perhaps often been taken as that reported for first breakthrough. To define accurately the economics of a flood and to make the proper choice of injection pattern to be employed, the reservoir engineer needs data concerning both the sweepout pattern at breakthrough and the continual enlargement of the pattern which occurs in the period of production following breakthrough. The development of the x-ray method provides the tool for studying the performance in both periods of production. This paper presents the results obtained by this method in studying the production performance before and after breakthrough for the five spot, staggered line drive, and direct line drive to cover the wide range of fluid mobilities generally encountered in field operations.

For floods in which no saturation gradient is present in the mobility of the fluids in either the swept or unswept region, the mobility ratio (M) of the system can be characterized by the ratio of the sum of the mobility of each phase flowing in the unswept region ahead of the front to the sum of the mobility of each phase flowing in the swept region behind the front.[5,9,10]

The mobility of a phase is expressed as its relative permeability divided by its viscosity. The mobility ratio can then be written as shown below.

$$M = \frac{\left(\frac{k_{r1}}{\mu_1} + \frac{k_{r2}}{\mu_2} \ldots\right)_{\text{unswept}}}{\left(\frac{k_{r1}}{\mu_1} + \frac{k_{r2}}{\mu_2} \ldots\right)_{\text{swept}}}$$

k_r = relative permeability
μ = viscosity, centipoise
numerical subscripts denote flowing phase 1, flowing phase 2, etc.

EXPERIMENTAL PROCEDURE

The use of the x-ray shadowgraph technique to study the recovery of oil resulting from the increase in the area contacted after the initial breakthrough of the invading phase consists of taking radiographs (x-ray pictures) of a porous model during a simulated flood employing the desired fluid mobilities. Since the injected fluid is rendered more strongly absorbent to x-rays than the reservoir fluid, most of the x-radiation passing through the swept portion of the model is absorbed and thus does not strike the x-ray film. On the other hand the x-radiation passes readily through the remainder of the model to strike and expose the film. Thus each radiograph taken during a flooding operation clearly shows the area which has been contacted by injected fluid at that time.

A Westinghouse medical x-ray unit having a maximum working potential of 80 kilovolts was used in these studies. A Fairchild x-ray roll film cassette with a sequence control was used in conjunction with the x-ray unit. This combination permits completely automatic operation, taking radiographs at predetermined intervals and recording the time at which each radiograph was exposed.

The models used for these experiments were cut from ¼-in. thick alundum plates. The surfaces were sealed with a ceramic type glaze. Fittings were fixed to the wells with a plastic adhesive. For all of the model results to be discussed here the injected and displaced phases were miscible in all proportions. Miscible fluids were used in obtaining a good control of the mobility ratio for a given experiment. This was possible since the displacement efficiency behind the invading front was near 100 per cent. The experimental results illustrated in Fig. 2 show a 98 per cent displacement efficiency behind the invading front. The relative permeability in the swept region in the models is essentially unity. Therefore, adjustment of the viscosity of the fluids in the unswept and swept regions gives the desired mobility ratios. Naphtha and mixtures of naphtha and mineral oil were used to obtain fluids with the desired viscosities. The injected fluid was forced into the models with a constant rate pump.

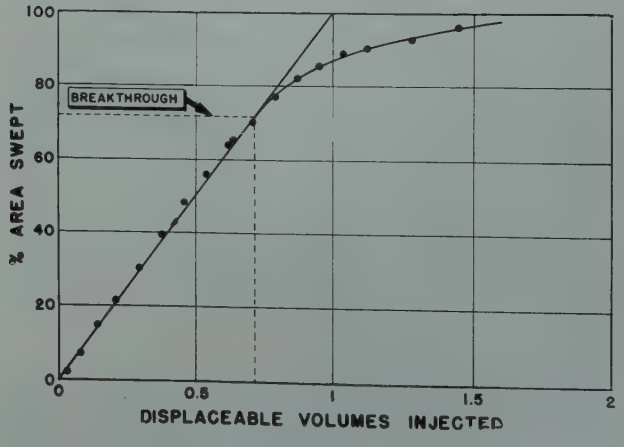

FIG. 2 — BASIC CURVE PLOTTED FROM DATA OBTAINED FROM FIG. 1.

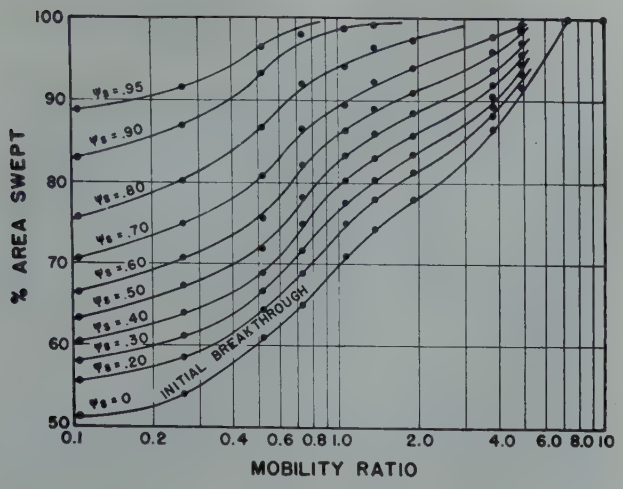

FIG. 3 — EFFECT OF MOBILITY RATIO ON OIL PRODUCTION FOR THE FIVE SPOT PATTERN.

The operational technique involved in these studies will be discussed for a five spot flood in which the mobility ratio was 1.06. The reservoir element represented by the porous model was one-quarter of a five spot pattern. The model was a 5-in. square, having the equivalent of one-quarter of an injection well at one corner and one-quarter of a producing well at the diagonal corner. The fluid viscosities were 1.33 cp for the injected phase and 1.25 cp for the displaced phase. Since the relative permeability to either of the phases is unity, the mobility ratio is 1.06.

In order to analyze the experimental data completely it is necessary to trace the area swept from each radiograph taken during a flood. Fig. 1 shows part of the set of tracings from which the fraction of reservoir area swept at the time of each radiograph is obtained. The increase in area contacted by injected fluid after breakthrough is apparent in this figure. The dotted line shows the position of the flooding front at initial breakthrough of injected fluid. Seventy per cent of the area of the model was swept at this time. The dashed line indicates the position of the flooding front at a later time when 96 per cent of the area had been contacted. The ratio of the flow of injected fluid produced to the total flow from the producing well at this time was 0.87. By the time abandonment conditions (arbitrarily considered as a ratio of 0.95) were reached the model was almost entirely swept.

From the complete set of tracings a basic curve is obtained by plotting the fraction of reservoir area swept versus the number of displaceable volumes which have been injected. The displaceable volume (D_v) is the product of the pore volume of the unit pattern and the displacement efficiency (the change in oil saturation which occurs in the swept region). This curve for the five spot flood being considered is shown in Fig. 2. The point at which this curve deviates from a straight line gives the areal sweepout efficiency at breakthrough of the injected phase. From this curve the information necessary for practical application of the data may be calculated. It can be shown from simple material balance considerations that the fraction of total flow occurring from the unswept region at any time after breakthrough is the slope of the curve at that point. For convenience in calculating water-oil ratios or gas-oil ratios from the laboratory data, the fraction of the total flow occurring from the swept region (Ψ_s) is reported.

The curves shown in Figs. 3 and 4 were obtained from similar flooding experiments on the five spot model. A range of mobility ratios from 0.105 to 17 was covered in this study. The data obtained at mobility ratios less than 0.5 must be considered as only approximate since the injected phase front at low mobility ratios becomes very irregular. These data at mobility ratios less than 0.5 can be considered to represent approximate extensions of the trend developed by the data obtained at higher mobility ratios.

A family of curves shown in Fig. 3 presents the area swept as a function of mobility ratio for increasing values of the fractional flow from the swept region and indicates the area of the reservoir which is contacted at abandonment conditions.

Fig. 4 shows the area swept as a function of mobility ratio and the number of displaceable volumes injected. This is used to predict the total volume of injected fluid necessary to produce a given quantity of oil. The breakthrough curve obtained with the miscible phases differs from that reported by Slobod and Caudle[6] in the region above a mobility ratio of 1. It is felt that this difference arises as a result of the previous data being obtained by the use of immiscible phases. The use of immiscible phases leads to difficulty in assigning a mobility ratio to the system since a small gradient in saturation is probably present behind the front, and this sometimes represents a large gradient in mobility. In addition, it is difficult to define accurately the relative permeability relationships of the model from the relative permeability relationships obtained on smaller samples. The use of miscible phases eliminates these difficulties and yields results which represent regions of uniform mobility and the influence of a known mobility ratio on flood pattern efficiency.

INFLUENCE OF MOBILITY RATIO ON DIRECT AND STAGGERED LINE DRIVE SYSTEMS

In addition to the work described above for the five spot pattern, results have also been obtained for the direct and staggered line drive flooding systems. For both of these systems the ratio of the distance between injection and producing lines to the distance between either producers or injectors was unity.

The results of these studies are shown in Figs. 5 to 8. These data can be used to predict reservoir performance in the manner to be discussed below for the five spot system.

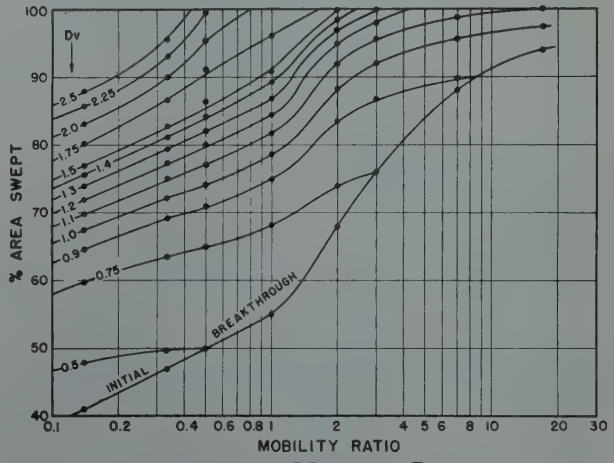

FIG. 4 — EFFECT OF MOBILITY RATIO ON THE DISPLACEABLE VOLUMES INJECTED FOR THE FIVE SPOT PATTERN.

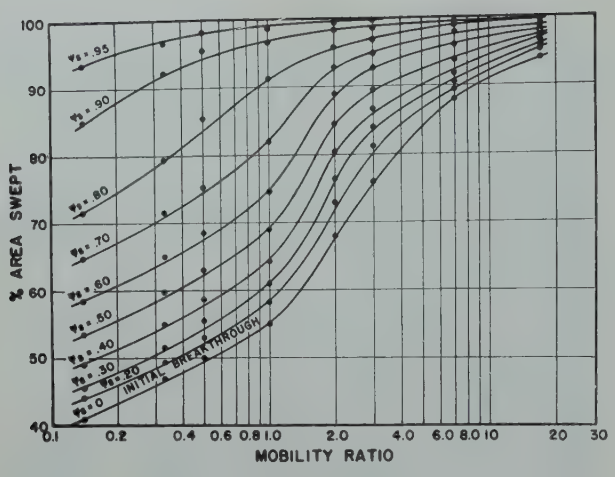

FIG. 5 — EFFECT OF MOBILITY RATIO ON OIL PRODUCTION FOR THE DIRECT LINE DRIVE (SQUARE PATTERN).

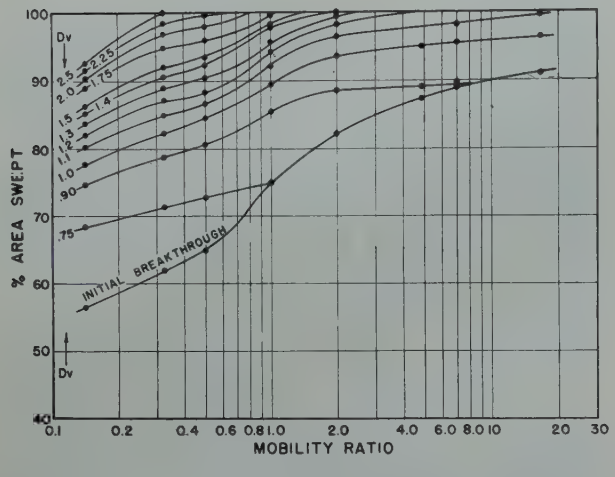

FIG. 6 — EFFECT OF MOBILITY RATIO ON THE DISPLACEABLE VOLUMES INJECTED FOR THE DIRECT LINE DRIVE (SQUARE PATTERN).

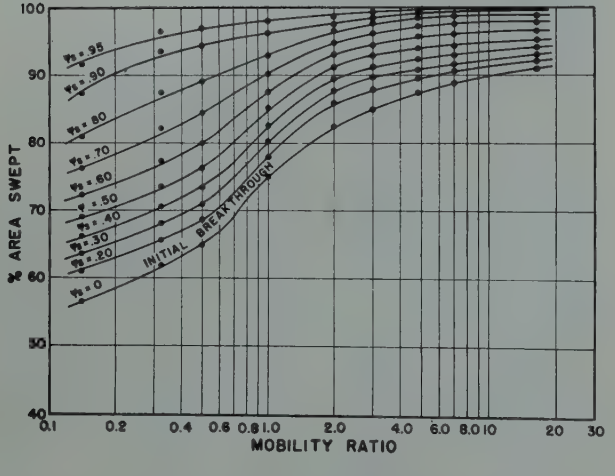

FIG. 7 — EFFECT OF MOBILITY RATIO ON OIL PRODUCTION FOR THE STAGGERED LINE DRIVE.

APPLICATION OF THE LABORATORY DATA TO RESERVOIR ANALYSIS

The data obtained from the laboratory models emphasizes the significant effect which mobility ratio can have on the oil production rate, the water or gas-oil ratio, the ultimate recovery, and the life of an injection operation. The information obtained represents conditions of the model in which the mobility ahead of the front and that behind the front was constant, in which the thickness and absolute permeability are uniform, in which no flow of the displaced phase occurs behind the front, and in which only one mobile phase is present in the unswept region.

These conditions in the model represent a steady-state injection operation and correspond to flooding operations above the bubble point and approximates floods conducted at gas saturations less than critical. The flooding of reservoirs containing high gas saturations and which are characterized by the formation of an "oil bank" is not being treated in this paper.

In practice a large amount of oil is generally thought to be produced from the region behind the front when gas is displacing oil and to a lesser degree when the injection phase is water. For water injection this continued oil production from the swept region frequently appears to be small and is sometimes neglected in engineering studies. In this case the curves presented in the paper can be used directly to describe the production after breakthrough.

EFFECT OF MOBILITY RATIO ON A WATER INJECTION OPERATION

From the basic laboratory results of Figs. 3 through 8 the influence of the mobility ratio on the production rate, producing ratio, cumulative recovery, quantity of injected fluid, and cycled fluid can be obtained for a wide range of mobility ratios. This might best be illustrated by applying these curves in showing the water flood performance of one five spot of an infinite array. Consider 40 acres to be flooded, having a thickness of 20 ft, a porosity of 20 per cent, an initial oil saturation of 70 per cent, an average saturation behind the front of 35 per cent, and an oil formation volume factor of 1.3. The displaceable volume of this five spot pattern would be 435,000 bbls. For an assumed constant injection rate of 200 bbls/day, the time required to inject one displaceable volume would be six years. The difference that could be encountered in field performance in flooding this pattern resulting from differences which might be encountered in mobility ratio for the case which assumes zero flow of oil from the swept region is illustrated in Figs. 9 and 10.

Fig. 9 illustrates the fact that low mobility ratios lead to early declines in the fraction of total flow which is proceeding from the unswept region and therefore result in a less favorable rate of oil recovery. The effect of less favorable rates of recovery at low mobility ratios on the life and cumulative oil recovery is shown in Fig. 10. Considering a 95 per cent water cut to be abandonment, the mobility ratio range of 0.5 to 5.0 would lead to a twofold difference in operating life.

The ultimate oil recovery, however, is near the same from 322,000 to 334,000 bbls. This corresponds to better than 96 per cent sweepout pattern efficiency for the five spot at abandonment conditions over the

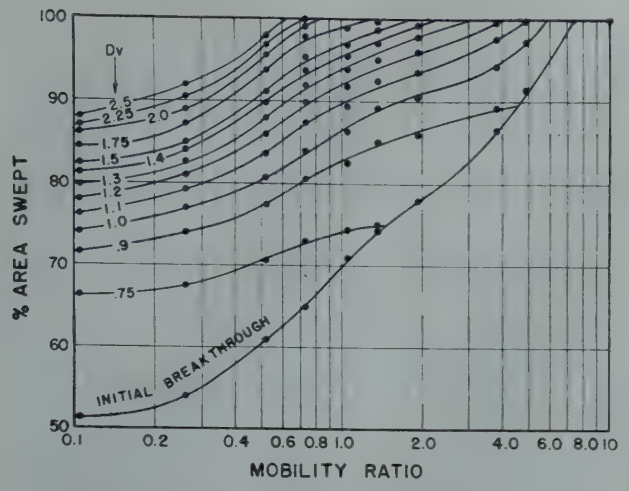

FIG. 8 — EFFECT OF MOBILITY RATIO ON THE DISPLACEMENT VOLUMES INJECTED FOR THE STAGGERED LINE DRIVE.

mobility ratio range of 0.5 to 5.0. At low mobility ratios up to one-half of the recoverable oil may be produced after breakthrough, as can be seen in Fig. 3.

In applying the data obtained on the laboratory models which was reported in terms of reservoir volume flow to the prediction of field performance, it is necessary to convert these data to stock tank conditions. For the case which assumes no oil flow behind the injection phase front, the following equations can be used to account for the formation volume factor of the oil and the solubility of the gas in the oil in expressing the above data in terms of oil rate, gas-oil ratio, water-oil ratio, etc. These equations are for the case in which oil is being displaced by water. Similar equations can be developed for gas cycling operations.

$$R_w = \frac{\Psi_s \beta_o}{1 - \Psi_s}$$

$$C_w = \frac{\Psi_s \beta_o}{1 + \Psi_s (\beta_o - 1)}$$

$$R_g = S$$

$$\Delta N = \frac{E_s V (\rho_{oi} - \rho_{os})}{\beta_o}$$

R_w = water-oil ratio, bbls/STB

β_o = oil formation volume factor, $\frac{\text{res bbls}}{\text{STB}}$

Ψ_s = fraction of total reservoir flow from swept region, $\frac{\text{res bbls}}{\text{res bbls}}$

C_w = water cut, water fraction of gross separator liquid

R_g = gas-oil ratio SCF/STB

S = solubility of gas in oil under reservoir conditions, SCF/STB

ΔN = oil production STB

E_s = fractional sweepout pattern efficiency

V = pore space of elemental pattern, bbls

ρ_{oi} = initial oil saturation, fractional pore space

ρ_{os} = oil saturation in swept region, fractional pore space

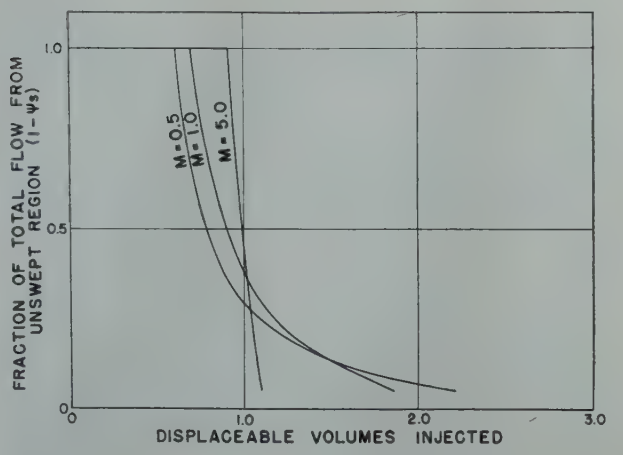

FIG. 9 — INFLUENCE OF MOBILITY RATIO ON OIL PRODUCTION FROM UNSWEPT REGIONS IN A FIVE SPOT PATTERN.

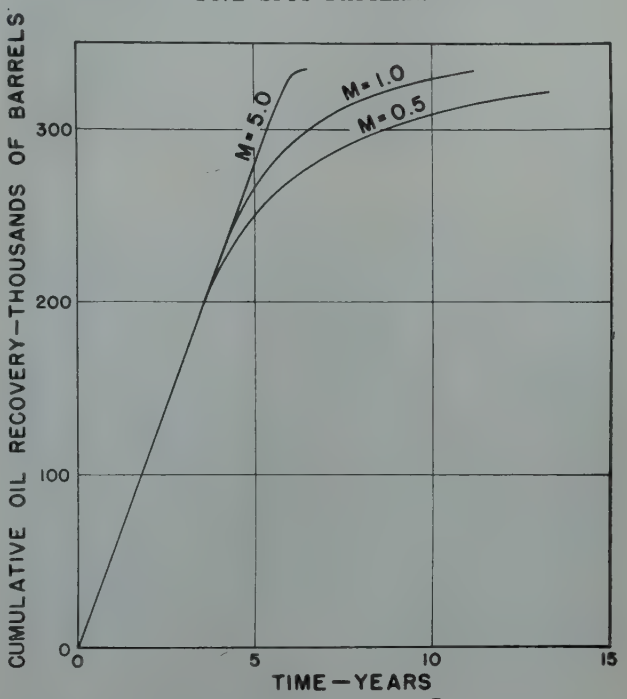

FIG. 10 — ILLUSTRATION OF THE INFLUENCE OF MOBILITY RATIO ON THE CUMULATIVE OIL RECOVERY FROM THE FLOOD OF ONE FIVE SPOT (40 ACRES, THICKNESS 20 FT, POROSITY 20 PER CENT, INITIAL OIL SATURATION 70 PER CENT, FINAL OIL SATURATION BEHIND THE FRONT 35 PER CENT, FORMATION VOLUME FACTOR OF 1.3).

APPLICATION OF LABORATORY DATA TO GAS INJECTION OPERATIONS

The saturation gradient which is believed to be present in operations involving the displacement of oil by gas complicates the simple application of the laboratory data to field performance by introducing such factors as: (1) a gradient in the fluid mobility behind the front, and (2) the flow and consequent production of oil from behind the front. In the laboratory floods it has been observed that the front remains radial during the encroachment into the first 15 to 25 per cent of the area of the model for all mobility ratios. This suggests that the mobility near the injection well has much less influence on the

sweepout pattern efficiency than that which is present near the front in the area in which flow ceases to be radial. Until a quantitative method is developed to consider properly the gradient in the fluid mobilities present in the reservoir, it is suggested that a series average of the fluid mobilities between the front and the injection well be used in defining the average mobility of this region. By this means the fluid mobility near the injection phase front is given more weight.

The application of relative permeability relationships to the displacement of oil by gas shows continued production of oil from areas after invasion by the gas. This production which occurs in the region behind the front must be considered in applying the data presented in this paper to the engineering calculations of field performance. No rapid and easy solution which accurately defines the oil flow from the swept region after breakthrough in a pattern flood as a function of the volume injected or areal sweepout efficiency can be presented at this time. The flow from this region can perhaps be approximated sufficiently well for engineering purposes by calculating the oil saturation in the swept region and the fraction of oil flow behind the front by the application of the method of Buckley and Leverett,[7,8] which was developed for a linear flow system.

Many factors influence the ultimate fraction of the reservoir to be swept by an injected phase at abandonment conditions. The information presented here shows the effect of one of the variables, that of mobility ratio. This is a property specific to a given flood and its influence must be considered by the reservoir engineers in arriving at an estimate of total oil to be recovered. The influence of other features of the reservoir, such as sand continuity, number of sand members present, permeability variations, irregular well pattern, and amount of oil beyond the boundary wells, etc., must also be considered by the reservoir engineer in arriving at an estimate of the fraction of the reservoir to be ultimately swept by the injected phase. For any given system, however, that estimate should include the performance following breakthrough and leading up to abandonment conditions.

CONCLUSIONS

The results of this study of the influence of the mobility ratio on the oil production after breakthrough lead to the following conclusions:

1. Over the wide range of mobility ratios which may be encountered in injection operations there can frequently be as much as 50 per cent of the ultimate oil recovery obtained after breakthrough.

2. Although high ultimate sweepout pattern efficiencies are obtained (85-100 per cent) for most mobility ratios encountered in field operations, the economic aspects of the rate of oil recovery and the total amount of fluid to be injected cause the higher mobility ratio floods to be much more favorable.

3. The inclusion of the production after breakthrough which results from a continual enlargement of the sweepout pattern is essential in making a comparison between different plans of operation.

4. The data presented here showing the contribution from the unswept region to the oil production after breakthrough can be combined with observed water flood behavior to give the engineer a means of gaining knowledge concerning the magnitude of oil flow behind an invasion front and knowledge of the possible influence of permeability stratification on the flood.

REFERENCES

1. Muskat, M.: "Flow of Homogeneous Fluids Through Porous Media," Chapter 9, McGraw Hill Book Co., Inc., (1937).
2. Wyckoff, R. D., Botset, H. G., and Muskat, M.: "Mechanics of Porous Flow Applied to Water Flooding Problems." *Trans.* AIME (1933), **103**, 219.
3. Aronofsky, J. S.: "Mobility Ratio — Its Influence on Flood Patterns During Water Encroachment," *Trans.* AIME (1952), **195**, 15.
4. Fay, C. H., and Prats, M.: "The Application of Numerical Methods of Cycling and Flooding Problems," *Proc. Third World Petroleum Congress,* Section II (1951), 555.
5. Slobod, R. L., and Caudle, B. H.: "X-Ray Shadowgraph studies of Areal Sweepout Efficiencies," *Trans.* AIME (1952), **195**, 265.
6. Hurst, W.: "Determination of Performance Curve in Five-Spot Water Flood," *Petroleum Engineer,* **25**, April (1953), pp. B-40-48.
7. Buckley, S. E., and Leverett, M. C.: "Mechanism of Fluid Displacement in Sands," *Trans.* AIME (1942), **146**, 149.
8. Kern, Loyd R.: "Displacement Mechanism in Multi-Well Systems," *Trans.* AIME (1952), **195**, 39.
9. Muskat, M.: "The Effect of Permeability Stratification in Complete Water Drive Systems," *Trans.* AIME (1950), **189**, 349.
10. Dyes, A. B., Comment to Paper by J. S. Aronofsky, *Trans.* AIME (1952), **195**, 15.

★★★

DRILLING MUD CONTROL in the SOUTHWEST LOUISIANA COASTAL AREA

C. R. CLAUS — MAGNOLIA PETROLEUM CO. LAKE CHARLES, LA.

G. A. STANDISH — MAGNOLIA PETROLEUM CO. HOUSTON, TEX.

T. P. 3783

ABSTRACT

Since March 1945, the Magnolia Petroleum Co. has drilled 39 wells in Southwest Coastal Louisiana. All wells were drilled within a comparatively small radius, but the area provides a large variety of problems. The deepest well drilled was 13,518 ft, and the total depth averaged 10,977 ft. Throughout this period drilling mud control and types of mud handled were: (1) phosphate, (2) red lime (late conversion), (3) red lime starch (early conversion), (4) red lime starch oil emulsion, (5) precision controlled low alkalinity-low lime content, and (6) gel muds for completion purposes.

Improvement has been obtained in effecting some or all of the following: (1) more rapid penetration, (2) reduction in drilling hazards, (3) better evaluation of cores and logs, and (4) better completions.

The geological sequence of zones penetrated range from recent sediments at the grass roots through the Frio section. Anticipation of high-pressure zones and incompetent formations entails precision control of drilling mud weights, and the unconsolidated nature of the various zones requires constant attention to the filtrate, viscosity, and gel strength values. In the Chalkley field, particularly, this combination of problems exists, where the formation pressures and overburden weight density values are in very close proximity. Design of casing and drilling mud programs must be modified to fit each well.

INTRODUCTION

Field and research work on drilling fluids has made constant progress, enabling operators to prospect progressively deeper horizons. Numerous papers have been written on the theoretical aspects of drilling fluid development, but in the field engineers have found it difficult to evaluate the role of specific mud constitutents when dealing in terms of thousand barrel mud systems. For that reason field data is somewhat lagging in technical report writing. However, applications of new techniques in the field have usually paralleled, and in numerous instances preceded, research work.

The information obtained by Magnolia Petroleum Co. in the course of drilling 39 wells within a comparatively small area in Southwest Coastal Louisiana provides an excellent opportunity of reviewing a specific example of drilling mud evolution. A large variety of problems has been coped with, the most important result being that every well was successfully drilled to its projected total depth. The discussion begins with the advent of deep drilling in this area in March, 1945, and is concluded with a resume of recent drilling operations in the Chalkley field.

The primary purpose of this paper is to describe the evolution in types of drilling fluids as it occurred and its application in the solution of various drilling problems. All of this information and experience resulted in the successful drilling of the three wells in the Chalkley field, where a combination of the most sound techniques was necessary in carrying drilling operations to the projected total depths. Other operators along with service company engineers have contributed considerably through the interchange of ideas and information to this paper, but the data and conclusions which are contained are based on first-hand observation of Magnolia Petroleum Company's drilling operations.

The 39 wells drilled by Magnolia Petroleum Co. average in depth 10,977 ft per well, while the maximum depth penetrated was 13,518 ft. The cost of drilling fluids have varied from $8,700 to $165,000, with the over-all drilling costs ranging from $74,000 to $543,000 per well. This wide variance illustrates the unpredictable nature of each well and the effects on over-all cost when high density muds are required to control

[1]References given at end of paper.

Manuscript received in the Petroleum Branch office Aug. 27, 1953. Paper presented at the Petroleum Branch Fall Meeting at Dallas, Tex., Oct. 18-21, 1953.

SERIES	GROUP	FAUNAL ZONES
RECENT	UNDIFFERENTIATED	
PLIOCENE	UNDIFFERENTIATED	
MIOCENE		Bigenerina humblei
		Amphistegina (B)
		Discorbis bolivarensis
		Siphonina davisi
		Planulina palmerae
		Abbeville assemblage
		Discorbis (large)
		Heterostegina sp.
		Bolivina perca
		Marginulina idiomorpha
		Marginulina vaginata
		Marginulina howei
		Camerina (A)
		Cibicides hazzardi
		Marginulina texana
		Hackberry assemblage
		Nodosaria blanpiedi
OLIGOCENE	VICKSBURG	

FIG. 1 — TENTATIVE STRATIGRAPHIC COLUMN OF CAMERON PARISH, LA.

abnormal pressures. The usual major potential sources of difficulty anticipated in drilling are loss of circulation, stuck pipe, blow-outs, salt water flows, formation sloughing, and crooked holes. The geological interpretations of coastal Louisiana are very complex, but an appreciation by mud engineers of the geological facts is important.

GEOLOGY

The stratigraphic section penetrated includes Recent, Pleistocene, Pliocene and Miocene deposits. This section consists of sand and shales interspersed with occasional thin shell beds and lime zones. The shales contain an abundance of mud-making constituents. The sands vary considerably in grain size and assortment and in degree of cementation. The lime and shell beds are not quite so prominent, but probably are responsible for a lot of the mud troubles because of the porous nature of the shell beds, which are found at any depth ranging from the grass roots to the maximum depths penetrated.

Difficulties are sometimes experienced in correlating from well to well, especially in the upper Miocene section which consists predominately of massive sands. Paleontological markers are used in defining the zones penetrated. These are listed in the geological section shown in Fig. 1.

The type of deposition varies. The lower Miocene is entirely marine, the upper Miocene is somewhat less than half marine, and the Pliocene and Recent are entirely continental deposits. Tectonic movements along hinge lines and upthrusts of salt masses have caused abnormal accumulation of sand in localized areas. When these sands occur as lenses, or are faulted against shale, abnormal pressures are often encountered. This is caused by the hydrocarbons and salt water contained in the shale deposits being forced by sheer overburden weight into available pore space where they had no subsequent path of escape.[1]

Structures in the area under discussion are the result of regional faulting and deepseated salt intrusions. Which of the two is responsible for the oil and gas accumulations in some of the fields under review is debatable, but it is not within the province of this paper to delve into that problem. It is sufficient to state that adequate structural relief has been found which could provide traps for the economic accumulations of hydrocarbons.

Geophysical methods, most reflection seismograph surveys and subsurface work, were responsible for discovering the anomalies. High pressure zones are found starting with the Planulina and Abbeville sections, with depth playing an important factor in the degree of pressure abnormality. Only those wells drilled on the crest of structures have completely penetrated the Abbeville section, as a tremendous thickening occurs on the flank downdip toward the Gulf of Mexico. The unpredictable depths at which prospective producing sands would be found beneath that zone on the coast have not yet warranted exploration efforts.

The tremendous role that the Abbeville section plays is best exemplified by the recent drilling in the Chalkley field. There only a very thin section was penetrated in the exploration of high-pressure-producing sands that are found below it in the Camerina and Cibicides Hazardi zones.

GEL-PHOSPHATE SYSTEMS

Prior to 1945 numerous shallow wells were drilled in Cameron Parish that did not require very close mud control. Deep-well drilling began in March, 1945, when the Lutcher A-1 was spudded in the Mud Lake area. The type mud customarily used at that time consisted of gel and native clay solids treated with phosphate and caustic-quebracho for viscosity and water loss control. Other chemicals were used, but mostly in a minor role, as retarding agents to phosphate deterioration. The time required to drill the Lutcher A-1 with this type mud to a total depth of 11,932 ft was 145 drilling days, with a drilling fluid material cost of approximately $33,000. Included in the 145 drilling days were eight days consumed in mud conditioning time that is not reflected in the cost of the drilling fluids. This mud conditioning time was caused by complications encountered in controlling rheological properties of the high density mud (16 lb/gal.), which was required to contain the abnormal formation pressures.

LIME-BASE MUDS

An advance in mud treatment occurred in early 1949. While drilling the Lutcher C-1 in the East Mud Lake field with a conventional phosphate mud at a depth of 11,012 ft, casing was set in anticipation of high pressure zones. Previously, difficulties in controlling mud properties at these depths and temperatures had been encountered. Therefore, in an effort to eliminate or reduce operational difficulties, the mud was converted to a high pH caustic-quebracho system and lime was employed to control gels and viscosities. This probably was the equivalent of our present concept of a lime-treated mud. Maximum mud weight was 13.2 lb/gal.

The well was then carried to a total depth of 11,707 ft without undue incident. At no time was there any trouble getting to bottom with drill pipe, logging tools or liner while using this type of mud. Drilling time was 95 days with a mud and chemical cost of $19,439. Also, it was concluded, and proved by subsequent drilling, that the hole would stand up for much longer periods of time with lime-treated or lime-base muds than with the previously employed systems.

The practice of using small lime additions in treating

red muds was short-lived, as control was found to be simplified by converting with excess lime, estimated at 4 to 12 lb/bbl, and continuing with large per tour treatments to maintain this value.[2] For a while it became a standard procedure for Magnolia to convert muds to lime base muds when drilling had reached approximately 8,000 ft.

Further simplification in mud control was the convenient expedient of converting muds at shallow depths when the percentage of solids was low, rather than at the 8,000 to 10,000 ft depth range. Surface casing in these wells in the subject area is usually set at 4,500 ft, which lends itself perfectly to a lime change-over at this point, while drilling cement, without the difficulty often encountered. This practice was started in March, 1949, and has become routine with conversion accomplished in several circulations. It has resulted in substantial savings in rig time and mud costs over the period.

OIL-EMULSION MUDS

Oil-emulsion muds were introduced in December, 1949, while drilling a directional hole on State of Louisiana Lease 1120 A-1 in the Holly Beach field. The hole tried to grab the drill pipe while drilling at 9,000 ft with a 3.5 cc water loss lime-base mud. The system was then emulsified with 10 per cent diesel oil which reduced the water loss to less than 1 cc. In 13 days 1,550 ft (9,390 ft - 10,940 ft) were drilled for an average of 119 ft/day, an outstanding record compared to straight hole drilling at equivalent depths where the previous fastest drilling rate was 84 ft/day. Sixty days were required to drill to 10,940 ft with a drilling fluid cost of only $16,422. Prior to this well the geologists had not given the "green light" to the use of oil in muds because of the uncertainty as to its effect on cuttings, core and electric log interpretations. Their objections have since been withdrawn, as with experience they have been able to differentiate between diesel oil and formation hydrocarbons.

Oil emulsion mud is being used quite often to speed drilling time. Its chief use, however, is in straight or directional holes where comparatively high filtrate loss of the muds or crooked hole conditions cause sloughing.[3] The volume percentage of oil has ranged as high as 16, but mud properties are easier to control when the oil content is around 10 per cent.

LIME TREATED MUDS

The development of methods for determining free lime content has been valuable to the mud engineer in controlling the lime systems.[4] As a direct result of mud control work in these wells Magnolia Laboratories was prompted to work on this problem. A method for determining the lime content and alkalinity level of drilling fluids has been developed and accepted for field use.[5] This method requires separate chemical titration of the drilling fluid and the drilling fluid filtrate.[6] As a result of this determination, it is no longer necessary to continue the practice of making heavy lime conversions or per tour treatments simply to be sure the lime concentration is sufficiently high. Reduced and more carefully considered additions are the rule.

The logical sequence in the treating evolution was the re-investigation of the commercial and practical aspects of reverting to moderately-high pH caustic-quebracho systems using lime only as a control agent.[7]

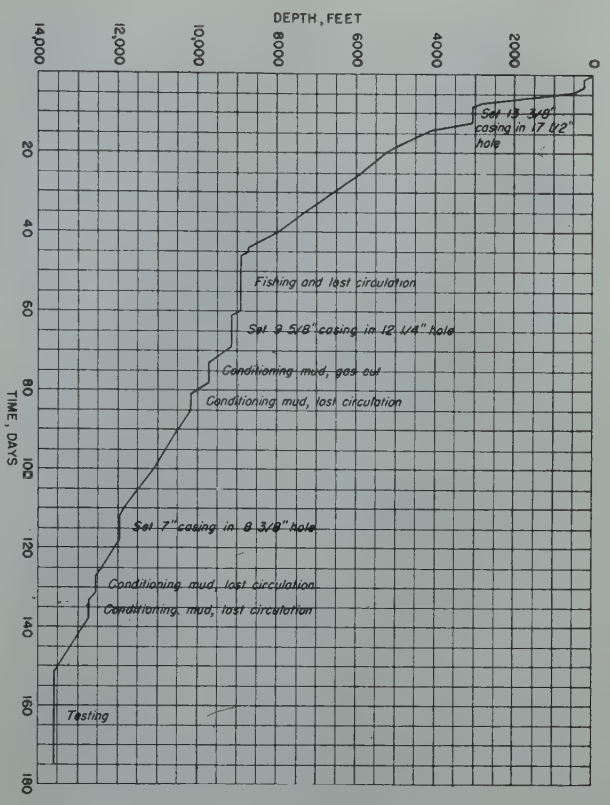

FIG. 2 — GRAPHIC DRILLING RATE, SWEETLAKE B-1, CHALKLEY FIELD.

The remarkable success of such controlled application is typified in the Sweetlake B-3 well in the Chalkley field. The initial conversion and a typical mud check along with a recommended per tour treatment for this type mud is shown in Table 1.

While lime base systems had definite advantages over phosphate-treated muds insofar as viscosity and gels were concerned, the inability to run logging and perforating instruments to bottom in the deeper wells was experienced. Maximum temperature recorded at 13,515 ft was 262°F. The average gradient is 1.4°/100 ft of depth. Conclusive evidence that the mud was actually forming a cement-like material was found. Excessive lime content in the presence of high alkalinities caused this. Lime-treated mud offered the best solution to the problem of drilling deep, hot holes.

It had been customary in deep wells where high-temperature gelation was likely to occur to prepare a

TABLE 1 — INITIAL CONVERSION, TOUR TREATMENT AND TYPICAL MUD PROPERTIES OF MUD USED ON THE SWEETLAKE B-3

	Initial Conversion, lb/bbl	Tour Treatment, lb
Caustic Soda	1	50
Quebracho	3	100
Lime	2	50
C M C	1	As needed to maintain filtrate below 5 cc

MUD PROPERTIES	
Weight, lb/gal.	17.8
Viscosity, Funnel, Sec.	53
Viscosity, Plastic. cp.	40
Yield value, lb/100 sq ft	8
Initial Gel., grams	0
10-minute gel, grams	1
pH	11.8
Filter loss, API, cc	4.8
Cake, 32nd in.	3
Lime, lb/bbl	0.5
Filtrate Analysis:	
Alkalinity, P	1.0
M	2.9
Chloride, ppm	1800

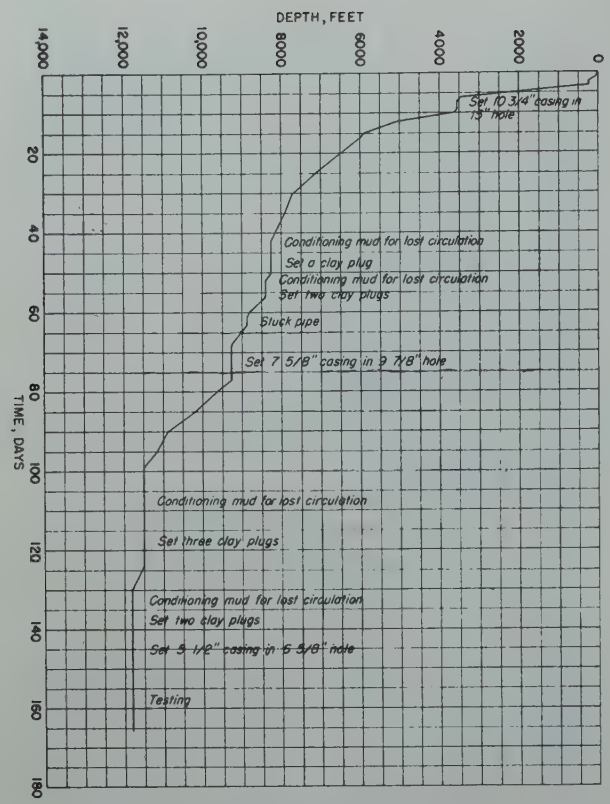

FIG. 3 — GRAPHIC DRILLING RATE, SWEETLAKE B-2, CHALKLEY FIELD.

low bentonite content behind the packer mud, weighted to the desired value. The only chemical used in this method is caustic soda, for pH control to minimize corrosion and also to accelerate the yield of the bentonite. A tremendous handicap encountered in this practice is the lack of tolerance for cement contamination, or the expense of having to revert to the original mud system if a cement squeeze job should become necessary. Rigtime and cost of materials to prepare an 18 lb/gal. mud for the B-3 well would have been, roughly, $8,000.

Field tests were conducted with both the lime-treated mud used in drilling and a laboratory-prepared low-percentage bentonite mud. At an elevated temperature over a 48-hour period the two muds checked closely in their ability to revert to fluidity. The well completion was made with the original mud, resulting, therefore, in the savings of the estimated $8,000. Another advantage of the lime treated system is in the obtention of higher resistivity values for better electric logging results. At 100°F the resistivity value of the lime base mud in Sweetlake B-1 and the lime treated mud in Sweetlake B-3 were 0.48 ohmmeter and 1.4 ohmmeter, respectively.

CHALKLEY FIELD

Probably the most difficult drilling in this area is in the Chalkley field, because of the proximity of formation pressures to overburden pressure. Sand objectives are not particularly deep compared with the average drilling depth of wells in South Louisiana, but depths are a relative matter where abnormal pressures and related hazards are concerned. Attesting to this fact is the high mortality rate of wells drilled below 10,000 ft in this field. At approximately 8,000 ft, pressures are abnormal. By the time 11,000 ft has been reached, formation pressures are near the rupture point of the overburden.

In Sweetlake B-1 the calculated static bottom hole pressure was 10,260 psi at 11,806 ft. This formation was penetrated with 17.5 lb/gal. mud which provided a differential of approximately 480 psi. The precarious nature of such a close differential is illustrated by the problem that faced the authors at the start of drilling the B-2 well. Geologists estimated that the high pressure zone would be encountered some 200 ft higher than B-1, which meant a 183 psi reduction of the 480 psi hydrostatic head differential using a 17.5 lb/gal. mud system. Therefore, 18 lb/gal. mud weight was recommended to compensate for the structural difference and to provide an added factor of safety for mechanical operations in the proposed reduced hole size. The rupture point of the overburden below 11,000 ft, however, was found to be slightly higher than the hydrostatic head equivalent of 17.8 lb/gal. mud, both during actual drilling in this well and in the subsequent drilling of the Sweetlake B-3. Equally important in the pressure consideration was attention to casing points, mud properties and drilling techniques in order to minimize the chances of causing any undue pressure surge against the hole. The actual casing and mud programs for the three wells drilled in the Chalkley field are shown in Table 2.

SWEETLAKE B-1 WELL

A brief history of the Sweetlake B-1 well is as follows: At 5,500 ft the mud was converted to a 10 per cent oil-emulsion, lime-base system. Mud weight was increased at approximately 8,600 ft from 12 to 13 lb/gal. because of gas cutting after trips. Lost circulation occurred at 8,889 ft and, as fibrous material was added, the shaker was by-passed and drilling was carried to 9,100 ft. There the casing was set while using 14 lb/gal. mud. The 9⅝-in. plug was drilled with 16.5 lb/gal. mud. Drilling continued without incident to the 7 in. casing point at 11,965 ft during which time the mud weight had been gradually increased to 17.5 lb/gal. In drilling out of the 7 in. casing to the 13,517 ft total depth, the weight varied between 17.5 to 17.7 lb/gal. The shale shaker was by-passed during the entire drilling operation from the 9⅝-in. casing point to the total depth to maintain a high concentration of lost circulation materials.

Viscosities could only be controlled through water additions which explains the $164,000 mud and chemical costs. Casing or liner was not set at total depth, for the well was completed through perforation 11,803-11,807 ft in the 7 in. casing as a gas-distillate producer. It had a shut-in tubing pressure of 8,695 psi. The serious danger of drilling the B-1 with the small hydrostatic pressure differential was only realized during testing operations in pipe.

TABLE 2 — CASING PROGRAMS USED IN THE CHALKLEY FIELD

	Sweetlake B-1		Sweetlake B-2		Sweetlake B-3	
	Size, in.	Depth, ft	Size, in.	Depth, ft	Size, in.	Depth, ft
Conductor	20	221	16	252	20	253
Surface	13⅜	3,011	10¾	3,505	13⅜	3,487
Intermediate	9⅝	9,119	7⅝	9,243	9⅝	9,063
Production	7	11,965	5½	11,740	7	11,198
Liner					5	10,931—11,943

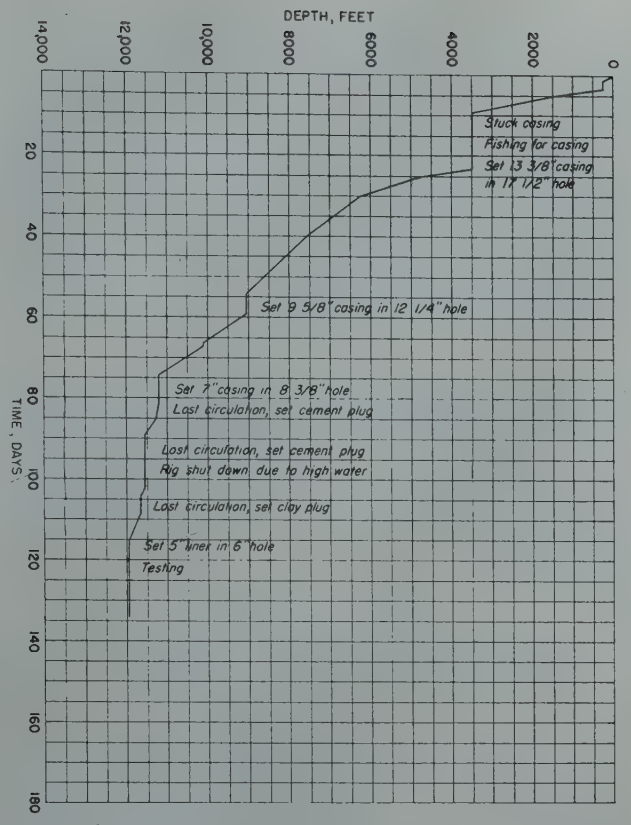

FIG. 4 — GRAPHIC DRILLING RATE, SWEETLAKE B-3, CHALKLEY FIELD.

SWEETLAKE B-2 WELL

A further curtailment in the casing program for B-2 became necessary, however. Because of a critical pipe shortage at the start of B-2, hole and pipe diameters were reduced from those employed in B-1. Again the plan was to drill substantially below the 9,119 ft casing point equivalent of B-1 and to case off most of the intermediate high pressure and heaving shale zones. Lost returns forced the casing to be set at 9,243 ft. First, 17 lb/gal. mud was used from that point; then 18 lb/gal. was in use by the time 10,000 ft had been reached. This was done in order to learn whether the formations would withstand this weight mud prior to drilling the 11,800 ft sand. Continued lost return difficulties at 11,800 ft forced the setting of 5½-in. casing after the high pressure sands were found beneath the gas-water contact.

Comparative analyses of both drilling and mud costs for the B-1 and B-2 wells show conclusively that the reduced hole size increased over-all drilling and mud costs. Cost of mud materials per foot was $12.20 and $12.63 for B-1 and B-2, respectively, while intangible drilling costs for the same wells were $34.29 and $36.29, respectively. Fig. 5 illustrates drilling rates at the various depths for all three wells.

SWEETLAKE B-3 WELL

Drilling costs for B-1 and B-2 were such that the economic feasibility of further developing the 11,800 ft sand was questioned. Only the possibility of encountering multiple sand reservoirs favored the drilling of B-3. Reduction in mud materials and drilling costs were mandatory in calculating a pay-out, and the design of the mud and casing programs to reduce these costs incorporated the following recommendations:

(1) Drill with mud weights compatible with both the competency of the formations and the abnormal pressure zones down to the 9,628 ft equivalent of B-1.

(2) Establish close casing point control by electric log, because every foot of hole cased would eliminate a future source of danger from shale sloughing or lost returns.

(3) Add a magnetic tracer material to the mud system at approximately 8,000 ft and maintain a proper concentration of this tracer to the total depth. In case of lost circulation, run a magnetic induction log to determine the exact point of mud loss by measuring variations in magnetic intensity; then spot time-setting clay cement in that zone to restore circulation.

(4) Set 7 in. casing at approximately 11,100 ft in anticipation of the two known high pressure zones found in the B-1 at 11,400 ft and 11,800 ft.

(5) Use a lime treated mud in drilling to the projected total depth and maintain this mud in a condition that would be satisfactory for completion purposes.

The above recommendations were followed with minor deviations in the drilling of the Sweetlake B-3 well. The result of this planning was that both the mud costs and intangible drilling costs were reduced approximately 31 per cent from those of the two previous wells. Drilling to the total depth required 89 days at a drilling and mud cost of $287,712 and $102,176, respectively. Although the same massive mud making shale formations were encountered in B-3, the lime treated mud did not result in any difficulty in viscosity control. In fact, the viscometric properties were very much better, as evidenced by the over-all reduction in mud costs. Table 3 reflects the percentage

TABLE 3 — PER CENT OF THE TOTAL COST OF THE MUD CONSTITUENTS USED IN DRILLING EACH WELL IN THE CHALKLEY FIELD

	Sweetlake B-1 per cent	Sweetlake B-2 per cent	Sweetlake B-3 per cent	Field Total per cent
Weighting Materials	73.10	69.90	81.44	74.23
Clays	1.22	1.10	0.91	1.09
Chemicals	11.01	9.23	6.91	9.05
Lost Circulation Materials	6.39	15.67	4.69	9.89
Water Loss Reducing Additives	8.38	4.10	6.05	5.74
	100.00	100.00	100.00	100.00

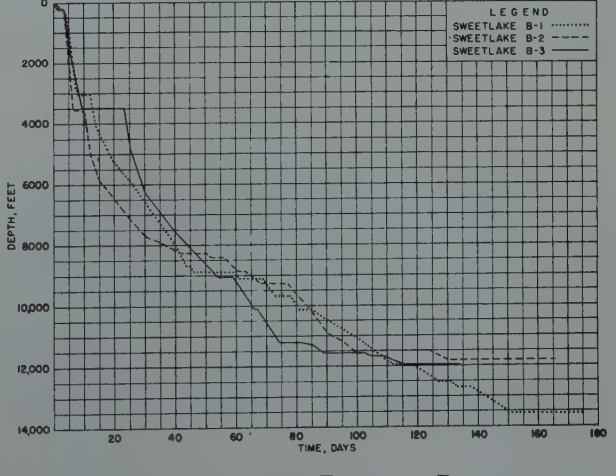

FIG. 5 — COMPARISON OF DRILLING RATES IN THE CHALKLEY FIELD.

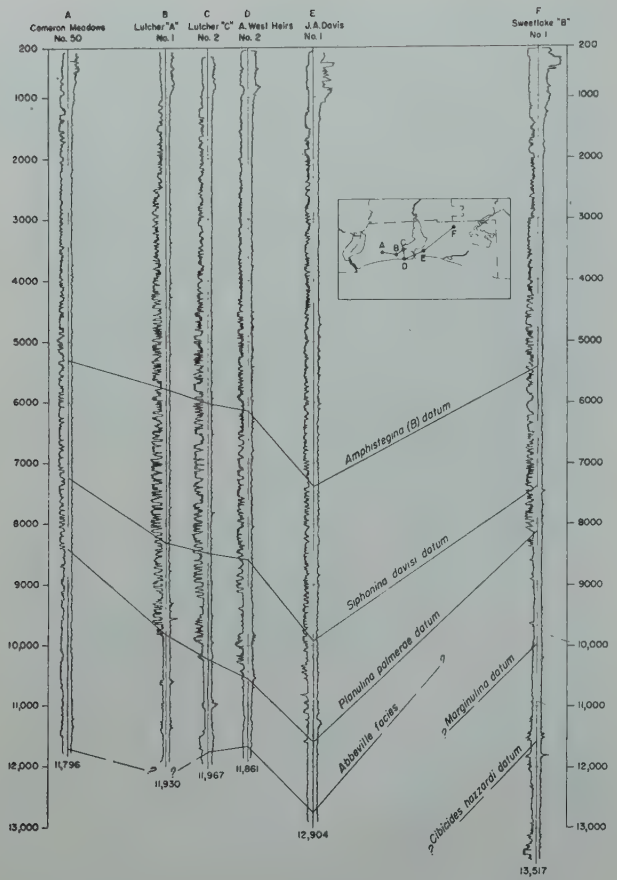

FIG. 6 — WEST-EAST CROSS SECTION OF SOUTHWEST COASTAL LOUISIANA.

of total costs of the mud constituents used in drilling the three wells in Chalkley field.

SUMMARY

Through experience gained in drilling wells since 1945 in Southwest Coastal Louisiana, field engineers and laboratory technicians have improved drilling mud control techniques. Within a small area many different problems were encountered that were successfully handled. Many kinds of mud systems were employed in drilling the wells, each of which has its merits. No one type can be satisfactorily used for all purposes. From an economical standpoint, the lime treated mud offers numerous advantages.

The knowledge accumulated during the period was applied in the planning and the concluding of the drilling of three wells in the Chalkley field, where the most severe drilling hazards of any of the fields under review were found. The experience gained in drilling the first two wells in that field enabled the drilling of Sweetlake B-3 well with a 31 per cent reduction in both drilling and drilling mud costs. Cost reduction is vitally necessary in any drilling operations, but it is particularly important in the development of structures where abnormally-pressured, relatively-thin producing sand zones are marginal in calculated pay-out.

ACKNOWLEDGMENT

Gratetul acknowledgment is made for the aid given by the personnel of the Petroleum Engineering, Geological, Production and Drilling Departments, and the Field Research Laboratories of the Magnolia Petroleum Co. Deserving special mention is A. L. Backlund.

REFERENCES

1. Dickinson, George: "Geological Aspects of Abnormal Reservoir Pressures in Gulf Coast Louisiana," *Bull. AAPG* (Feb., 1953), **37**, 418.
2. Lancaster, E. H., Jr., and Mitchell, M. E.: "Control of Conventional and Lime-Treated Muds in Southwest Texas," *Trans.* AIME (1949), **179**, 357.
3. Perkins, H. W.: "A Report on Oil-Emulsion Drilling Fluids," *Drilling and Production Practices, API* (1951), 351.
4. Battel, J. L., and Chaney, P. E.: "Lime-Base Muds," *Drilling and Production Practice, API* (1950), 99.
5. Nelson, M. D., and Watkins, J. E.: "Lime Content of Drilling Mud — Calculation Method," *Trans.* AIME (1950), **189**, 336.
6. "Principles of Drilling Mud Control," API and University of Texas Extension Bureau.
7. Watkins, T. E., and Nelson, M. D.: "Measuring and Interpreting High-Temperature Shear Strengths of Drilling Fluids," *Trans.* AIME (1953), **198**, 213.
8. Gray, G. R., Neznayko, M., and Gilkeson, P.W.: "Solidification of Lime-Treated Muds at High Temperatures," *Drilling and Production Practice, API* (1952), 73.
9. Watkins, T. E.: "A Drilling Fluid for Use in Drilling High-Temperature Formations," Paper No. 901-29-A, API preprint (1953). ★★★

MECHANICAL TREATMENT of WEIGHTED DRILLING MUDS

ROY A. BOBO
MEMBER AIME
R. S. HOCH

PHILLIPS PETROLEUM CO.
HOUSTON, TEX.

T. P. 3782

ABSTRACT

Maintenance of desirable plastic flow properties of weighted drilling muds may be greatly simplified by use of centrifugal classification to control the drilled solids content. The new application of a decanting type centrifuge to separate and reject the low density solids from the weighting material results in a drilling mud of greatly improved quality with lower values of yield and rigidity.

Its practicality and economy has been proven in field operation. The degree of separation of light and heavy solids is not limited by the machine, but by the particle size distribution of the solids in the mud. Removal of the low density component of drilling mud that makes chemical treatment necessary permits a marked reduction in chemicals.

The main uses of the centrifugal process are the treatment of muds while drilling, the reclaiming of discarded muds, cleaning up of workover muds, and the reduction in lime content of mud for completion.

INTRODUCTION

Drilling mud in any circulatory system is made viscous and difficult to pump by gradual accumulation of drilled solids which pass through the shale shaker and are continually reground. In a weighted mud containing a large proportion of barite by volume, the amount of drilled solids that may be tolerated is greatly reduced. Much effort has been expended to control by chemical treatment the effects of such solids. Though chemical treatment is quite effective, the time eventually comes at deeper depths after enough drilled solids have entered the system when a portion of the mud must be discarded and replaced with water and more weighting material. Once begun, this process is generally continued at frequent intervals with resultant high maintenance costs.

At the termination of drilling, mud highly contaminated with light solids and spent chemicals is poorly suited for completion operations.[1] It is likewise limited in utility for other drilling operations.

This investigation was conducted for the primary purpose of determining an acceptable mechanical means of removing the lightweight solids from weighted drilling muds in order to maintain viscosity at a minimum. A decanting type of centrifuge was selected from the various possible methods of mechanical separation.

The centrifugal process has been employed in this country for this purpose in central mud reclamation systems in California in earlier years. It also was used for treatment of weighted muds on the Gulf Coast.[2] In more recent years only sporadic attempts have been made to employ it in the field on weighted muds.

DISCUSSION OF PROCESS

Selection of Apparatus

Two factors favor mechanical procedure for the separation and removal of drilled solids or clays from the mud circulatory system. First, the greater specific gravity, 4.1 to 4.3, of the barite would promote more rapid settling than the clays whose specific gravity range is from 2.5 to 2.7. Second, the relative coarseness of the barite particles also facilitate faster settling of this phase.

A decanting type of centrifuge was preferred for this process over other possible methods for these reasons:

1. Requires no costly additives or excess dilution.
2. Centrifugal force affords greatly accelerated separation as compared to gravity.

[1]References given at end of paper.

Manuscript received in the Petroleum Branch office Aug. 28, 1953. Paper presented at the Petroleum Branch Fall Meeting at Dallas, Tex., Oct. 18-21.

3. More compact and greater portability.
4. Unaffected by fairly coarse material.

Requirements

In order to fulfill field needs, any centrifugal machine must meet the following:

1. Must make desired degree of separation between drilled solids and weighting material. Excess loss of barite cannot be tolerated.
2. Operation must be continuous and trouble free, with a minimum of operating personnel and maintenance.
3. Should be resistant to abrasion and corrosion.
4. Must operate with minimum of water dilution.

Description and Method of Operation

The centrifuge selected was of the conical decanting type. Its operating principle is illustrated in Fig. 1.

The mechanism shown in Fig. 3 consists essentially of a helical screw conveyor rotating inside a conical bowl, which also revolves in the same direction at a slightly higher speed. The speed of rotation of the bowl creates a high centrifugal force acting at right angles to the axis of rotation.

Diluted drilling mud enters the bowl through a stationary feed tube, as shown in Fig. 1, located in a hollow center shaft. The heavier barite particles, acted upon by centrifugal force, are thrown outward and deposited against the wall of the bowl. The clays and liquid, being of lower specific gravity, form a concentric inner layer in the bowl.

The barite deposited against the bowl is conveyed to the narrow end of the bowl by the pitch and the forward rotation of the helix relative to the bowl, where it is discharged through ports that are suitably located. The barite sludge is returned to the mud tank.

The clays and liquid referred to as effluent or underflow in this discussion are rejected through ports at the opposite end of the bowl.

FIELD RESULTS

Type of Separation Obtained

Field trial of the decanting type centrifuge demonstrated that any desired degree of separation could be effected, commensurate with the particle size distribution of the two solid phases in the system, by varying the rotating speed. This is illustrated diagrammatically in Fig. 2.

At a high rate of speed (point 1 on the curve), the centrifuge would reject all liquid with the effluent or overflow with all of the solids going to the underflow. At a reduced speed corresponding to point 2, a substantial portion of the clays would be rejected with the effluent, and the coarser clays and all of the barite would be returned with the underflow. At a further reduced speed (point 3), a still greater portion of the clays and some of the finer barite will be thrown out with the effluent. This latter point corresponds to the desired operating speed.

It can be visualized from Fig. 2 that an exceptionally high density of solids in the underflow is indicative of inefficient operation.

Table 1 is presented to show the effectiveness of separation that was secured when concentrating 12.5 lbs/gal. mud to 22 lbs/gal. This is best illustrated from the following summary, taken from the table:

Bowl Speed rpm	Per Cent of Total Clays Rejected	Per Cent of Total Barite Lost
1,470 - 1,500	73.7	9.44
1,736	67.6	4.88
2,070	66.4	0.09

Table 1 also substantiates the foregoing theory that density of the solids in the underflow decreases with increasing bowl speeds.

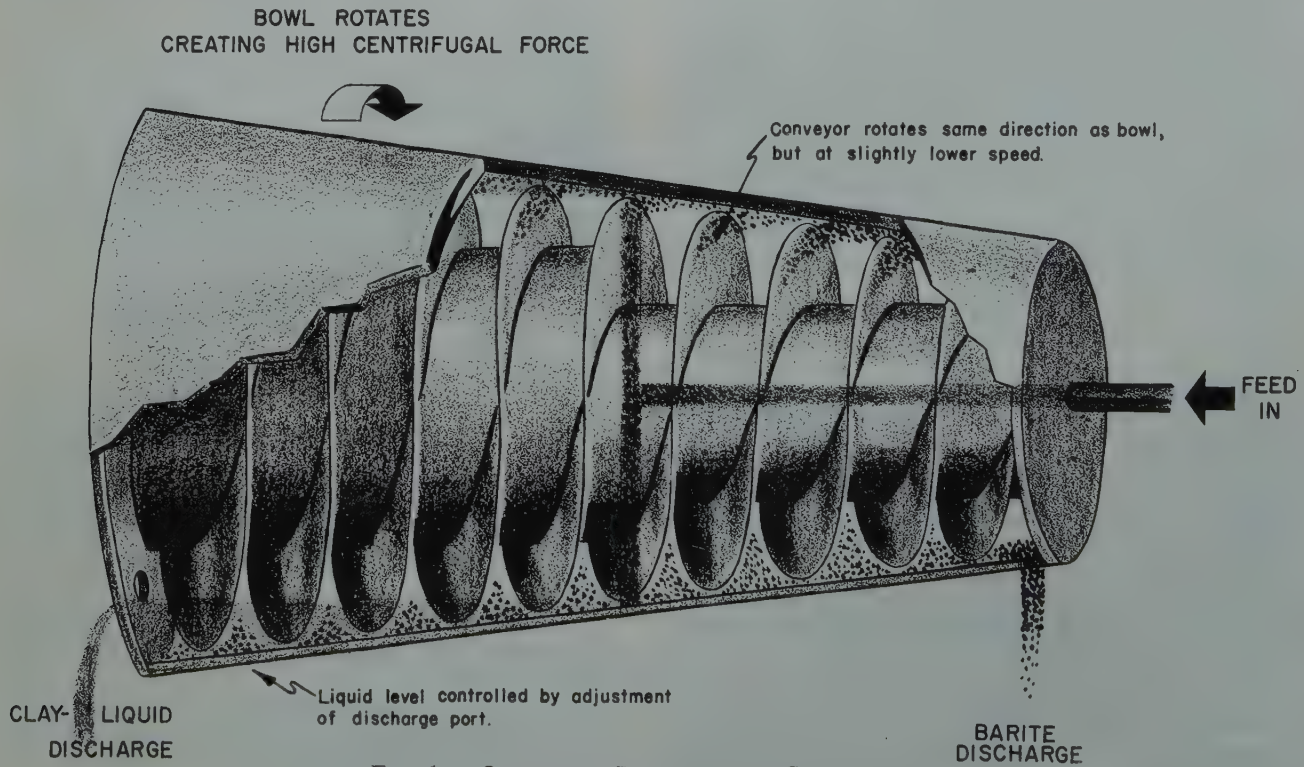
BOWL ROTATES
CREATING HIGH CENTRIFUGAL FORCE
Conveyor rotates same direction as bowl, but at slightly lower speed.
FEED IN
Liquid level controlled by adjustment of discharge port.
CLAY-LIQUID DISCHARGE
BARITE DISCHARGE

Fig. 1 — Operating Principle of Centrifuge.

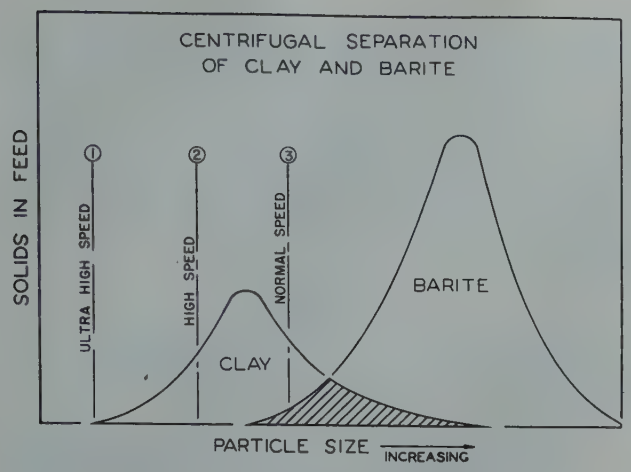

FIG. 2 — CHART, CENTRIFUGAL SEPARATION OF CLAY AND BARITE.

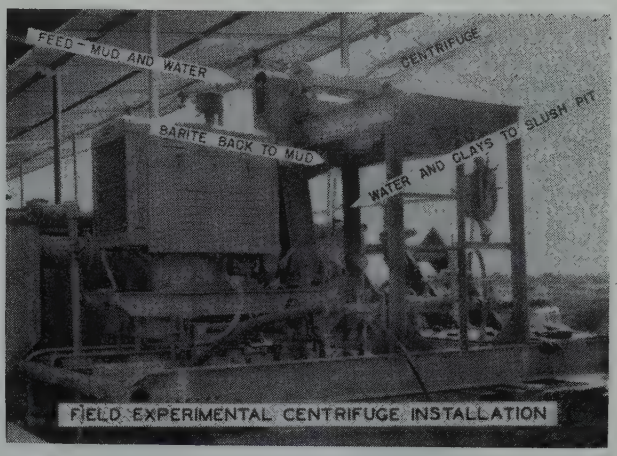
FEED — MUD AND WATER
CENTRIFUGE
BARITE BACK TO MUD
WATER AND CLAYS TO SLUSH PIT
FIELD EXPERIMENTAL CENTRIFUGE INSTALLATION

FIG. 3 — FIELD EXPERIMENTAL CENTRIFUGE INSTALLATION.

OPERATING FEATURES

The experimental gas-engine driven centrifuge installation is shown in Fig. 3. Mud to be processed was delivered to the centrifuge from a forward pit by a separately driven model 1L4 type CDQ Moyno pump. Water from a centrifugal pump was mixed with the mud. The feed thus mixed traversed 50 diameters of pipe in turbulent flow prior to entry into the centrifuge. Barite sludge from the centrifuge was jetted back to one of the mud pits. Rejected clays and water flowed by gravity to a waste pit.

No operational difficulty occurred when processing screened mud. Occasional shut-down resulted on reclamation of gelled mud due to plugging of the intake to a small supply pump with large clods, metallic objects, and other debris. However, the centrifuge handled all material that was fed to it without clogging and without difficulty. The machine was dismantled at the end of 1,000 hours of operation and no wear could be detected by micrometer measurement.

The capacity of a decanting type centrifuge is limited by the quantity of barite sludge than can be conveyed to the discharge end of the bowl. For this reason, mud having a density of 13 lb/gal. can be processed at a greater rate than 18 lb/gal. mud, the comparative throughput depending upon the relative amount of barite and coarse clays which are contained. A protective torque release prevents overloading.

A typical pumper's grind-out centrifuge was quite useful in estimating the relative solids content in both feed and effluent. This served as a rapid and effective test on the degree of separation being obtained.

EFFECT ON FLOW PROPERTIES OF THE MUD

By reducing the volume concentration of the drilled solids, centrifuging lowers both the yield and plastic viscosity of weighted drilling muds.

Fig. 4 shows how operating the centrifuge for one day affected the plastic flow properties of 15 lb/gal. drilling mud on a Chocolate Bayou well, in Brazoria County, Tex., drilling at 12,000 ft. At this time, the centrifuge was processing about one-fifth of the mud in the circulatory system per day. Note that the yield point was lowered from 17.7 to 10.0 lb/100 sq ft and the plastic viscosity was reduced from 37.8 to 33.8 cp. By chemical treatment alone, the yield value is the only component of resistance to flow that can be reduced appreciably.

OTHER EFFECTS OF CENTRIFUGING

One of the chief values of the centrifuge in the treatment of muds lies in the continual maintenance of minimum viscosities. It is generally acknowledged that good flow properties contribute to better bottom-hole-cleaning action and consequent increase in rate of penetration.

With a centrifuge, a marked reduction in chemicals that are required for maintenance will result. In the Chocolate Bayou well on which the decanting centrifuge was tried, the quantity of chemicals used after centrifuging was initiated were only one-fifth that used prior to installation. The centrifuge was used while drilling from 11,800 ft to 14,600 ft.

TABLE 1 — RESULTS OF OPERATING DECANTING TYPE CENTRIFUGE AT VARIOUS SPEEDS AND WITH DIFFERENT WATER RATES WHEN CONCENTRATING DRILLING MUD FROM 12½ TO 22 POUNDS PER GALLON

Test No.	Centrifuge r.p.m.	Mud Density lb/gal.	Feed* Mud B/D	Feed* Water B/D	Spec. Grav. of Solids Sludge	Spec. Grav. of Solids Effl.	Feed Solids lbs. per day Total	Feed Solids lbs. per day Sludge	Feed Solids lbs. per day Effl.	**CLAYS Volume b.p.d. Total	Volume b.p.d. Sludge	Volume b.p.d. Effl.	Weight lbs. per day Total	Weight lbs. per day Sludge	**CLAYS Effl.	**BARITE Volume b.p.d. Total	Volume b.p.d. Sludge	**BARITE Effl.	**BARITE Weight Total	**BARITE Weight Sludge	**BARITE Effl.
1	1486	12.46	249	814	3.76	2.78	50,404	29,368	21,036	30.1	8.7	21.7	22,000	5,840	18,320	24.1	21.9	2.0	28,400	23,500	2,640
2	1470	12.47	285	698	3.78	2.87	71,249	48,580	22,669	32.9	9.84	22.5	29,996	9,230	18,249	28.5	26.4	2.74	41,253	39,350	4,421
3	1500	12.51	308	582	3.80	2.81	77,129	50,825	26,304	35.5	9.06	27.3	32,857	9,098	22,227	30.1	26.0	3.17	44,272	41,727	4,077
4	1736	12.46	328	814	3.79	2.75	75,328	46,693	28,635	40.4	10.7	31.0	32,617	8,592	25,771	33.4	29.8	2.16	42,711	38,101	2,863
5	1736	12.56	350	698	3.74	2.72	89,093	62,868	26,225	42.5	15.2	25.0	38,577	13,139	24,390	35.0	36.2	1.18	50,516	49,729	4,458
6	2070	12.37	405	814	3.67	2.67	100,249	71,225	29,024	50.7	18.05	36.1	45,531	17,521	28,414	38.7	34.9	.48	54,936	53,704	610
7	2070	12.32	395	698	3.64	2.66	89,752	62,325	27,427	53.3	20.2	32.9	44,591	16,329	27,152	35.6	35.8	.20	47,160	46,620	274

*Subsequent tests demonstrated that water rates shown in table were all in excess of that required for operation. High water volumes will lower separating effectiveness of this type of machine.

**All volume and weight calculations were derived from individual measurements on feed, sludge, and effluent. Good, but not exact correlation was obtained as reflected in the tabulated results.

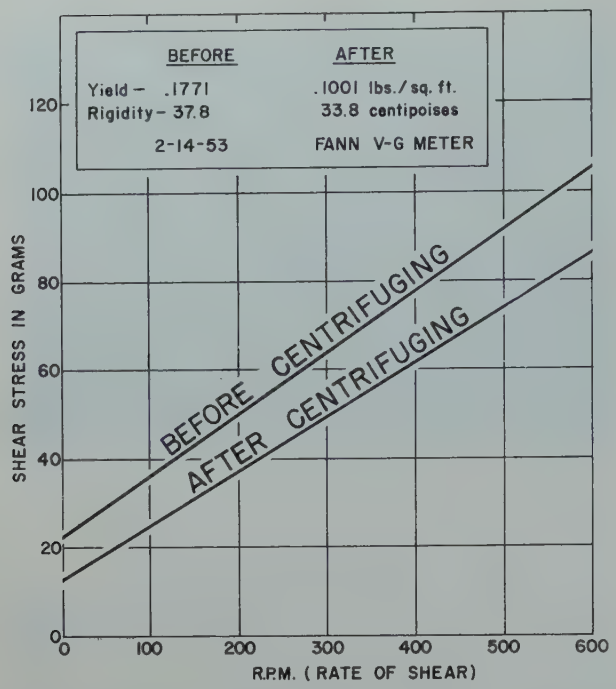

FIG. 4 — GRAPH SHOWING RESULTS OF 24 HOURS OF CENTRIFUGING 15 LB/GAL. DRILLING MUD ON PHILLIPS HOUSTON "T" NO. 1, CHOCOLATE BAYOU FIELD.

Much has been included in the literature on the effects of lime on high temperature gelation and high temperature solidification. Muds with high lime content will often solidify during drilling operations. Much more often, lime muds solidify when placed above the packer upon completion.

A centrifuge may be used to effectively remove a good portion of the active lime in a mud system upon completion. It may also make possible the drilling of deep wells without resorting to lime treatment.

Sand, being much coarser than other solid particles in the system, will readily settle in the first pit once the viscosity of the drilling fluid has been reduced by centrifuge action.

Upon completion of deep wells, the general practice is to abandon the contaminated mud remaining in the pits. A centrifuge may be used to clean-up, concentrate, and salvage a valuable portion of mud which otherwise would be discarded.

One phase of centrifuge performance that has not been evaluated, but which may be of importance, lies in the removal of "spent" chemicals from the mud. It is possible that part of the increase in viscosity which occurs with continued use of the mud is due to the accumulation of chemicals that have been added and whose effectiveness has been dissipated. By removing such chemicals the centrifuge will aid in maintaining low viscosity in weighted muds.

CONCLUSIONS

The practicality of a centrifuge for effecting substantial economies in drilling costs has been proved. The centrifuge will accomplish the following:

1. Maintain the desired flow properties of weighted drilling muds without resort to continual discarding and rebuilding substantial portions of the mud in the circulatory system;
2. Greatly reduce the quantity of chemicals required for treatment;
3. Reclaim and concentrate used muds to densities up to 24 lb/gal.

Properly installed and supervised, the machine will require little maintenance and attention.

Highly efficient separation may be obtained with the decanting type machine, resulting in low barite loss.

ACKNOWLEDGMENT

The authors wish to express their appreciation to the management of the Phillips Petroleum Co. for permission to publish this paper; to H. M. Barrett and his assistant, John Mesaros, of the Phillips Drilling Tools Division for field help in conducting tests from which Table 1 was prepared. Acknowledgment is also made to the Sharples Corp. and their representative, A. R. Greenlaw, for provision of the centrifuge used in this work.

REFERENCES

1. Gray, G. R., Neznayko, M., and Gilkeson, P. W.: "Some Factors Affecting the Solidification of Lime Treated Muds at High Temperatures," *Drilling and Production Practices,* API (1952), 73.
2. Cannon, G. E., and Sullins, R. S.: "Problems Encountered in Drilling Abnormal Formations" *Drilling and Production Practices,* API (1946), 29.

★★★

PRESSURE MAINTENANCE by GAS INJECTION in the BROOKHAVEN FIELD, MISSISSIPPI

J. B. JUSTUS
JUNIOR MEMBER AIME
R. W. CASSINGHAM
JUNIOR MEMBER AIME
C. R. BLOMBERG
W. H. ASHBY
MEMBERS AIME

THE CALIFORNIA CO.
BROOKHAVEN, MISS.

THE CALIFORNIA CO.
NEW ORLEANS, LA.

T. P. 3781

ABSTRACT

The Brookhaven field is one of several Basal Tuscaloosa reservoirs located in south-central Mississippi. It is a standstone reservoir, of erratic deposition and with several faults, having an approximate subsea depth of 9,800 ft. A large variation in permeability exists with a weighted average being 256 md. Estimated average interstitial water saturation is 45 per cent. The undersaturated reservoir fluid exhibits marked differences in physical properties with measured saturation pressures ranging from 733 to 2,255 psi.

Early rapid decline in reservoir pressure caused the operating interests to unitize the field and initiate a program of pressure maintenance by gas injection. At the time gas injection was commenced, the reservoir pressure had fallen to nearly half of the original pressure with only 4.5 per cent of the original oil in place produced. The reservoir pressure has since been maintained at approximately 2,750 psig, and cumulative production to date is 17 per cent of original oil in place. An analysis of field performance during gas injection is presented in detail.

The program of pressure maintenance by gas injection is considered to be a success, since the expected ultimate recovery has been increased and the current production rate is in excess of 2 per cent of original oil in place per year. Performance has been better, anticipated ultimate recovery is larger, and total production costs are lower than for a similar Basal Tuscaloosa reservoir nearby, even though that field appears to have a more effective natural water drive.

INTRODUCTION

The history of the Brookhaven Unit is a testimonial for unitization and for the application of engineering techniques in the operation of an oil field. The operating and royalty interests in this field have mutually benefited from their early recognition of the need for unitization and pressure maintenance and from the forthright manner in which these were accomplished. The tangible benefits accruing to the participants in the Unit are: (1) income from gasoline plant products, (2) reduced lifting and operating costs from those of competitive operation, (3) maintenance of high levels of current income by mitigation of the inevitable decline in production rates inherent to natural depletion, (4) an increase in ultimate recovery of about 40 per cent over natural depletion operations. This paper should properly be considered a progress report; however, the performance of the field after five years of pressure maintenance clearly indicates that the ultimate success of the project is assured.

LOCATION AND GEOLOGY

The Brookhaven field is located in south-central Mississippi, about six miles from the town of Brookhaven. Production at Brookhaven

[1]References given at end of paper.

Manuscript received in the Petroleum Branch office Aug. 3, 1953. Paper presented at the Petroleum Branch Fall Meeting at Dallas, Tex., Oct. 18-21, 1953.

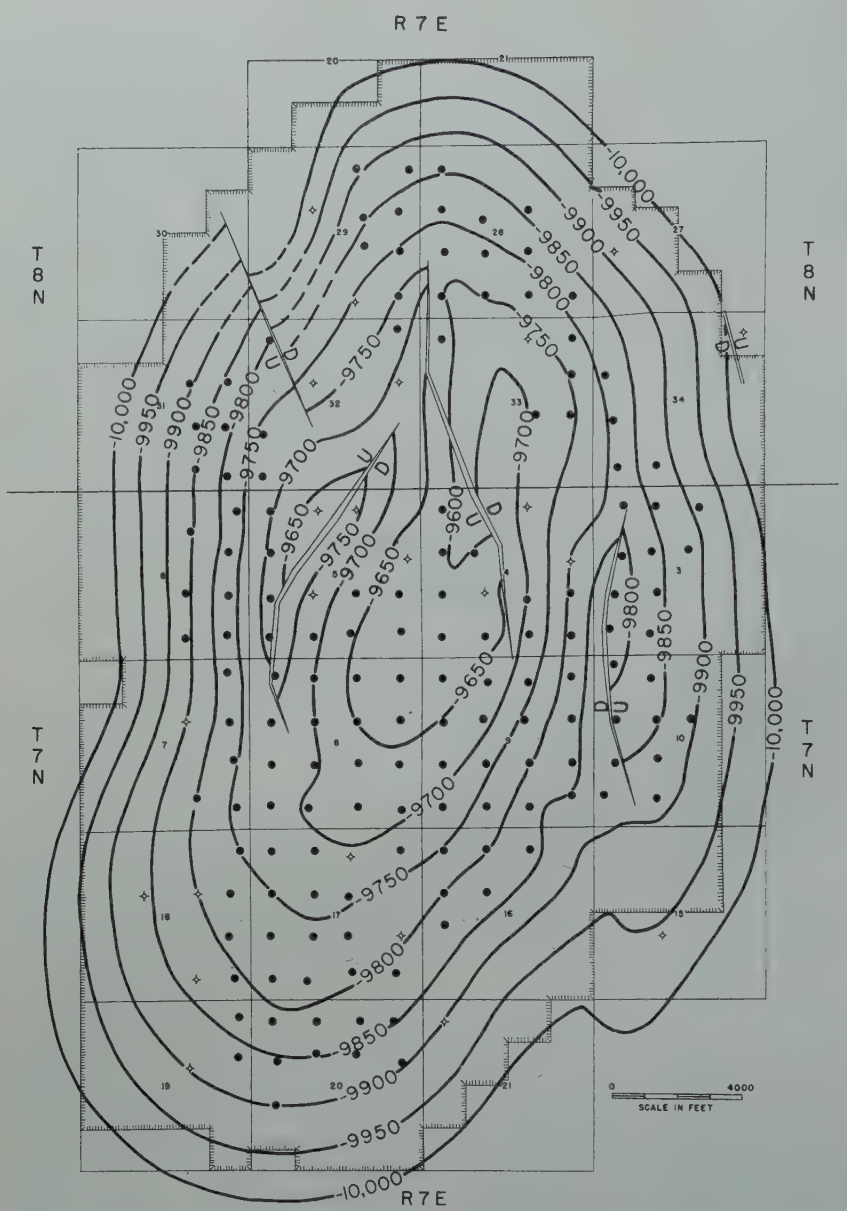

FIG 1 — STRUCTURE MAP OF THE BROOKHAVEN FIELD, LINCOLN COUNTY, MISS.

is from the Basal Tuscaloosa formation of Upper Cretaceous age. The average depth of the producing section is about 10,300 ft subsurface or 9,800 ft subsea.

Fig. 1 is the structure map of the field, drawn on top of the Basal Tuscaloosa formation. The proved closure is approximately 400 ft. Three faults trending north and south form a central graben area. The central of these faults occurs principally in a shaled out section of the field and is not of importance in the reservoir. The two faults along the east and west sides have sufficient throw to cause partial discontinuity within the reservoir. The erratic nature of the sand deposition is evidenced by two shaled out areas near the crest of the structure.

Production is from three separate zones in the Basal Tuscaloosa. These are the Pilot, Case and Smith zones. Fig. 2 shows two typical electric logs of the producing section with the general designation of these zones indicated. In the north and east portions of the field, the Smith and Case zones could not be readily segregated; therefore, these have been lumped together and called the Arrington zone. The Smith-Arrington zone has the greatest areal extent and is the major reservoir. Fig. 3 is the isopachous map of this zone. The Case zone has considerably less effective sand volume than the Smith, and the Pilot is relatively insignificant. Isopachous maps of these zones may be found in the literature.[1] The total effective sand volume is about 207,000 acre-ft, of which the Smith-Arrington zone comprises about 180,000 acre-ft and the Case zone 27,000 acre-ft.

DEVELOPMENT

The field was discovered by the drilling of The California Company's G. T. Smith No. 1. This well was completed as a small pumper in June, 1943. Two subsequent dry holes caused a period of inactivity until September, 1945, when Roeser and Pendleton's Leon Case No. 1 was completed as a good producer. This accelerated drilling activity and during 1946 and 1947 development was essentially completed on a 40-acre spacing. A total of 152 producers and 22 dry holes have been drilled in the field. Normal practice was to set about 1,100 ft of surface pipe and a production string of 7 or 5½-in. casing to total depth. The productive zones were then perforated. Many wells were initially completed in both the Case and Smith zones.

UNITIZATION

Early in the development period of the field frequent bottom hole pressure surveys were made. These surveys revealed that the reservoir pressure was declining at a very rapid rate. Only about 3,000 bbls of oil were produced per psi drop in reservoir pressure up to 1947. This clearly indicated that some form of pressure maintenance would be necessary to insure maximum recovery.

The operators held their first meeting in March, 1947. Plans were formulated for an engineering study of the reservoir. This study concluded that the limited natural water drive would not maintain pressure at a reasonable rate of production, so a program for unitization and pressure maintenance by gas injection was instigated. In June, 1948, only 15 months later, the unit agreements had been signed, a compressor plant built, a source of extraneous gas developed, and injection commenced in three wells. The California Co. is Unit operator.

Participation in production for both operating and royalty interests is based on the percentage of the total acre-feet of effective oil sand which underlies each tract. At the present time only one producing well in the field is not operated by the Unit. Approximately 98 per cent of the royalty interests have voluntarily signed the unit agreement.

The reservoir was originally undersaturated, and there was no extraneous source of gas in the field. Therefore, it was necessary to secure an outside source of gas to maintain pressure. A long-term contract was signed by the Unit with Southern Natural Gas Co. to supply the necessary make-up gas. Southern Natural laid a line from the Gwinville gas field, about 30 miles east of Brookhaven, to supply this gas. The contract guarantees a minimum purchase by the Unit of 11 MMcf per day for 12 years, and the average price is about 11 cents per Mcf. This gas is very dry, being composed of 97.5 mol per cent methane and 2.5 mol per cent carbon dioxide. A gasoline absorbtion plant was put in operation in June, 1949, together with a low pressure gas gathering system. These facilities are operated by the Unit.

RESERVOIR MATERIALS

The general drilling program included coring the Basal Tuscaloosa pay zones and analyses on cores from 140 wells were available. The average porosity of the Smith-Arrington zone is 26 per cent, and porosity of the Case zone is 24 per cent. The permeability of the Smith-Arrington zone ranges from 0 to 6,000 mds, and the arithmetic average is 340 mds. The arithmetic average permeability of the Case zone is 170 mds. Fig. 4 gives the permeability profile of a typical well. The permeability distribution as demonstrated by this typical profile would indicate that the coverage of injected gas may be very poor. However, layers of high permeability cannot be correlated from well to well, and it is postulated that this high degree of heterogeneity actually tends to improve the coverage by injected gas.

The average interstitial water saturation of the producing zone is estimated to be 45 per cent of the pore space. A transition zone with water saturation greater than 50 per cent occurs in the first 20-30 ft above the original oil-water contact.

Fig. 5 gives the two-phase, oil-gas, relative permeability data which have been used in the reservoir calculations. These curves represent the average of several laboratory investigations on Brookhaven cores and on similar Basal Tuscaloosa cores from neighboring fields.

The reservoir fluid was originally undersaturated, and there existed a unique condition with respect to fluid characteristics; that is, a variation in reservoir fluid properties within a more or less continuous reservoir. There were two very definite indications that this condition existed:

(1) Bottom hole sample analyses from seven wells at various locations within the field indicated a variation in saturation pressure from 733 psig to 2,255 psig.

(2) The gravity of the produced oil varied from 26° to about 40° API, and produced gas-oil ratios from 100 to over 500 cu ft/bbl.

For the purpose of making reservoir calculations, it was necessary to obtain data on the average fluid properties. This was accomplished by drawing a map of iso-saturation pressures, included as Fig. 6. The control for this map was obtained by plotting saturation pressure against both the produced tank oil gravity and GOR from the analyses of six wells sampled. (Fig. 7). Using this together with the well test data of produced gravity and GOR, a saturation pressure was estimated for each producing well not sampled. A weighted average saturation pressure of 1,439 psig was then estimated by planimetering this map.

The reservoir oil varies in viscosity from 0.6 to 1.9 cps. Fig. 8 gives the variation in formation volume factor and gas in solution with the saturation pressure. The formation volume factor of the original reservoir fluid varied from 1.155 to 1.375 and the gas solubility from 100 to over 500 cu ft/bbl. These curves have been extrapolated to calculated points at the current operating pressure. These points give the values of gas solubility and FVF of the saturated oil in the gas-swept formation under the assumption that injected gas goes in solution in the reservoir oil at the prevailing pressure, as discussed below.

PRESSURE PRODUCTION HISTORY

The pressure production history of the field is shown by Fig. 9. The reservoir pressure declined very rapidly from the original of 4,537 psig to slightly less than 2,800 psig in May, 1948, immediately prior to injection. The reservoir pressure has been maintained at between 2,700 and 2,800 psig by the gas injection program. The present distribution is shown by the iso-baric map of a pressure survey completed in October, 1952, Fig. 10. The two major faults and the two barren areas tend to restrict the over-all continuity of the reservoir. Therefore, to maintain

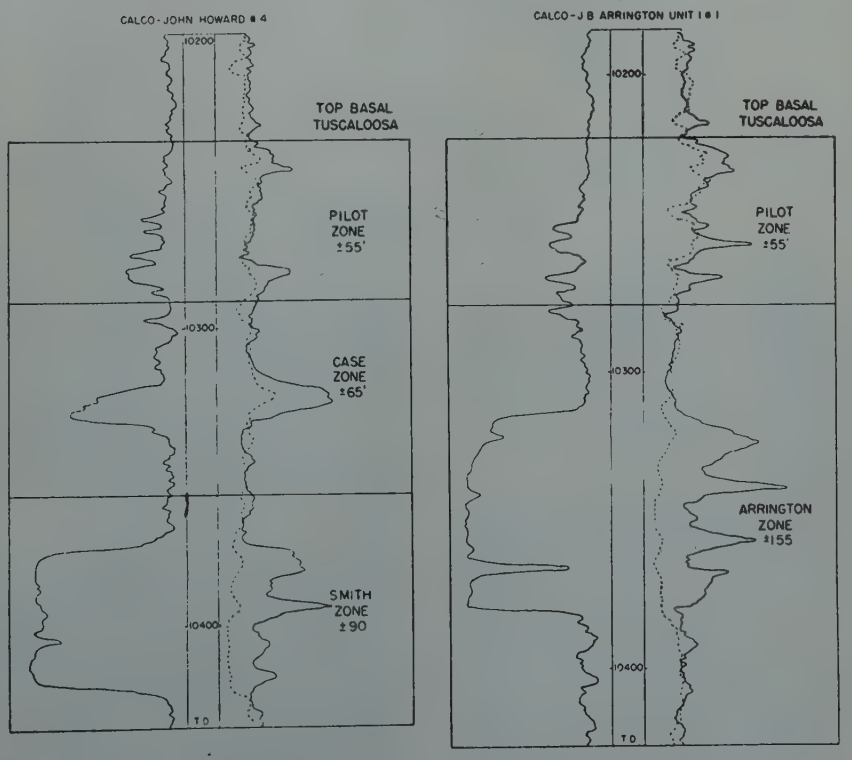

FIG. 2 — TYPICAL ELECTRIC LOGS OF PRODUCING ZONES IN BROOKHAVEN FIELD.

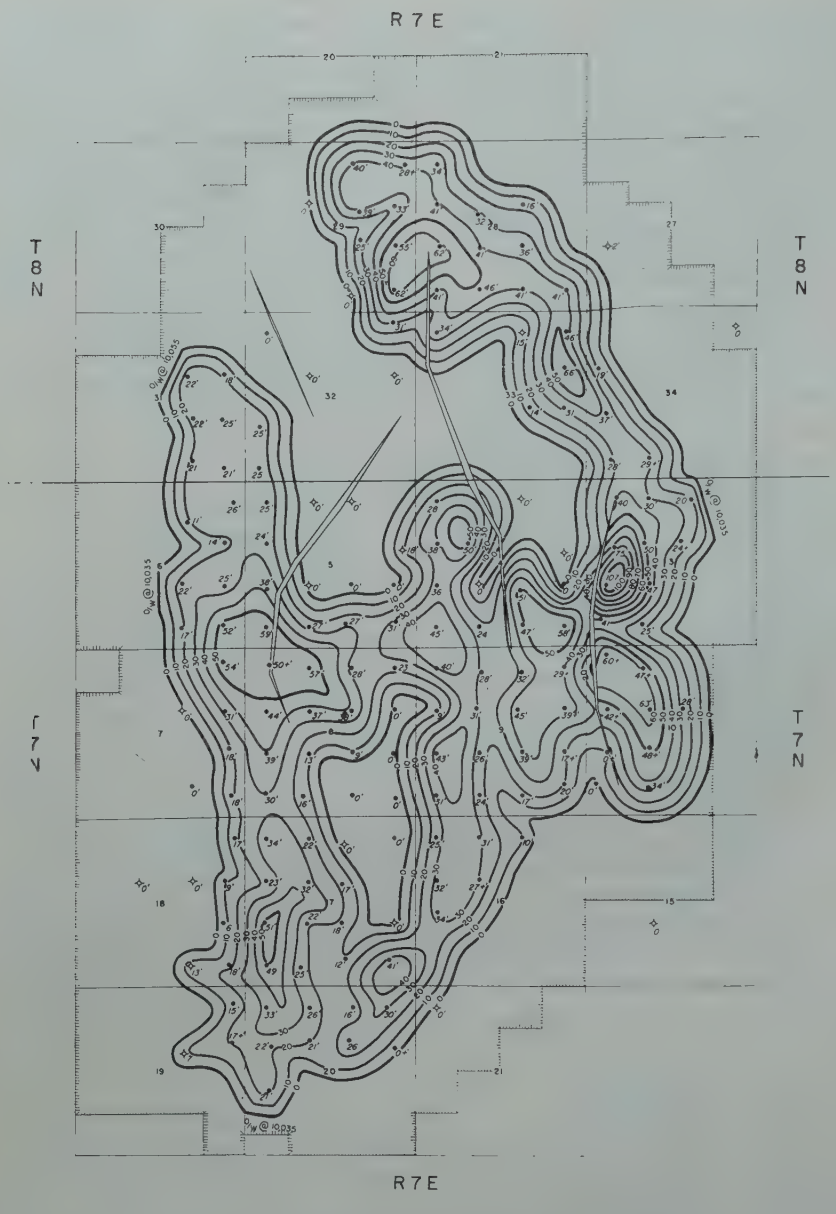

FIG. 3 — ISOPACH OF EFFECTIVE SAND, SMITH-ARRINGTON ZONE, BROOKHAVEN FIELD.

pressure in the entire reservoir, it has been necessary to inject in five dispersed areas. These areas are indicated on the isobaric maps. Presently, there are 12 injection wells, two in Block I, one in Block II, three in Block III, four in Block IV and two in Block V.

The production rate increased rapidly during the major development period, 1946 and 1947, and reached a maximum of slightly over 15,000 B/D in mid 1949. The production rate has declined somewhat from this maximum due principally to increasing gas-oil ratios and partially to water encroachment to edge wells. In recent months this decline has been arrested. The current production rate is approximately 12,000 B/D. This has been accomplished by installing additional compressor capacity, altering the stages of existing compressors and installing high pressure producing facilities in the field. The resulting increase in gas handling facilities permits the producing of wells after gas breakthrough.

The encroachment of edge water has imposed a secondary problem at Brookhaven. When water encroaches to a well the consequent lowering of the fluid level increases the lifting problem. This in itself is a serious problem, and at Brookhaven it is intensified by an apparent reduction in the total fluid productivity of the well. In most cases, there is as much as 50 or 60 per cent reduction in fluid productivity and in some cases complete plugging has occurred. In recent months, it has been found that these wells can be returned to a satisfactory producing status by the application of mud acid to increase fluid productivity and/or installation of gas lift valves to lift the necessary fluid volumes.

Currently about 37 MMcf per day is being injected. The initial gas gathering system was a 9 psig system. This sufficed as long as only solution gas was being produced, but after gas breakthrough occurred the volume of gas produced and tubing pressures increased. To handle this gas, 850 psig and 70 psig gathering systems have been installed. These systems are expanded as the gas front encroaches on additional wells. About 40 MMcf per day is currently being handled. Of this, 30 MMcf per day is compressed to 2,500 psig at the plant, including 11 to 13 MMcf per day of purchased gas, and about 10 MMcf per day is being compressed to 3,000 psig by three field compressors for direct discharge into injection wells. The plant processes about 18 MMcf per day of Unit gas and produces approximately 450 B/D of products. The cumulative gas injected through June, 1953, was about 39 billion cf. Fig. 11 shows the extent of the movement of injected gas from each of the five centers of injection as of Oct. 1, 1952.

The cumulative oil produced by the Unit wells through June, 1953, was 30,664,896 bbls. This represents about 17.5 per cent of the original oil in place, which was estimated to be 172.2 million bbls by volumetric calculations. Approximately 7.5 million bbls were produced prior to unitization and about 23 million bbls have been produced since the initiation of the gas injection program.

ANALYSIS OF PERFORMANCE

FACTORS AFFECTING PERFORMANCE

An analysis of the reservoir performance after five years of pressure maintenance by gas injection has been made. The purpose of this analysis was to determine how effective the gas injection program has been and from this estimate what the ultimate recovery will be. The analysis of the performance of this field is complicated by the following factors: (1) a wide variation in reservoir fluid properties, (2) a limited edgewater drive, (3) oper-

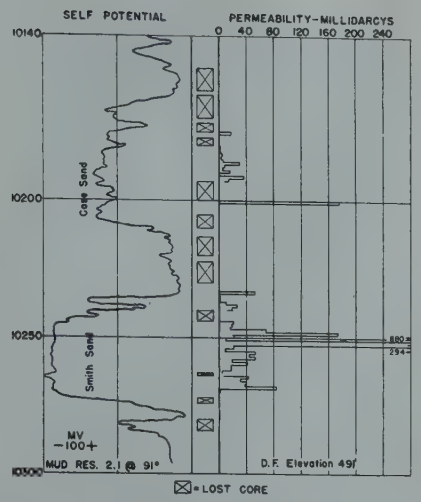

FIG. 4 — PERMEABILITY PROFILE OF A TYPICAL WELL, DANCIGER OIL AND REFINING CO. V. G. ALLEN NO. 2.

ating pressure considerably above the original saturation pressures of the reservoir oil, causing part of the injected gas to go into solution, (4) a tentative economic GOR limit for wells producing behind the gas front of 40,000/1, (5) a gravity gradient effective behind the gas front due to a slight formation dip, and (6) the geometry of the field.

In making an analysis of this type, there exists an inherent ambiguity. When oil is displaced, the resulting recovery can be attributed to: (1) high displacement efficiency from a small sand volume, or (2) low displacement efficiency from a large sand volume. In order to resolve this problem, it was necessary to employ both material balance and displacement type calculations to determine how much of the reservoir volume has been swept by gas and the recovery from this swept volume.

Due to its irregular geometry, the field is considered to be composed of five semi-independent reservoirs, as shown in Fig. 11. Gas is being injected in each of these Blocks. Because of this and the aforementioned complicating factors, a separate analysis has been made on each Block. For illustrative purposes only, the analysis of the Smith sand in Block IV is presented herein; this is believed to be representative of the field as a whole, because the performance of this Block during gas injection has been similar to the overall performance of the field. A detailed breakdown of production data from this Block and physical characteristics of the sand and reservoir fluids are given in Table 1. A brief summary of the analytical procedure employed is presented in the following paragraphs.

ANALYTIC PROCEDURE EMPLOYED

The Coverage Factor

"Coverage factor" is defined as the fraction of total effective sand behind the gas front which has been swept by gas. This should be distinguished from the "conformance factor" as presented by Patton,[3] which is the ratio of swept pore volume to the total reservoir pore volume. "Coverage factor" as herein used is a direct reflection of the reservoir performance at any stage of injection, whereas "conformance factor" by definition changes as the frontal position of the injected gas advances. First, the variation of the average free gas saturation with variation in coverage factor was calculated by material balance methods. Next, a relationship between coverage and average gas saturation was also established using Buckley-Leverett displacement type calculations.[4] The pair of values for these variables which satisfied both methods were accepted to be representative of reservoir performance.

The positions of iso-ratio lines, representing GOR's of 1,000/1, 5,000/1, 10,000/1, and 40,000/1, were estimated from the producing GOR's of the wells on Oct. 1, 1952 (the effective date of the analysis). These lines were superimposed upon a Smith sand isopachous map and the apparent reservoir volume enclosed by each was determined by planimetering. The position of the 1,000/1 GOR line was assumed to coincide with that of the gas front.

The Block under study was diagrammatically represented as in Fig. 12 where the Block is composed of two elements, B into which gas is being injected, and A into which edge water is encroaching. The boundary between B and A is the position of the gas front. By referring to the saturation pressure map, an average saturation pressure was determined for the fluids originally contained in each element. The physical properties of the reservoir fluids having these saturation pressures are given in Table 1. The hydrocarbon space in the gas-swept portions of element B contains free gas and saturated oil while the hydrocarbon space of the unswept portion of B contains undersaturated oil only. By material balance methods, the average free gas saturation in the swept portion of B was evaluated as a

TABLE 1 — SAND, PRODUCTION, AND FLUID DATA OF SMITH SAND, BLOCK IV, BROOKHAVEN FIELD

Sand Data:		
Porosity, ϕ	0.256	
Avg. Perm. K, md	256	
Interstitial water	0.45	
Total sand volume, acre-ft	55,445	
Sand volume enclosed by gas front, acre-ft	24,580	
Reservoir Temperature	250°F	
Production Data:	**Oil, Bbls**	**Gas, MCF**
Production prior to injection	2,404,263	
Production during injection period		
Wells ahead of gas front on 10-1-52	2,412,342	
Wells behind gas front on 10-1-52		
Prod. GOR's, GORs < GOR < 1000/1	1,852,466	802,131
1000/1 < GOR < 5000/1	436,497	1,105,748
5000/1 < GOR < 10,000/1	444,120	3,230,915
10,000/1 < GOR < 40,000/1	305,854	4,887,088
40,000/1 < GOR	2,035	195,517
Cumulative gas injected		14,008,782
Reservoir Fluid Data:	**Element B**	**Element A**
Beginning of injection,		
Reservoir pressure, 2,600 psig		
Saturation pressure	1,950	1,650
F.V.F. of oil, rvb/STB	1.304	1.273
Solution GOR, SCF/STB	433	....
On 10-1-52		
Reservoir pressure, 2,845 psig		
Saturation pressure, saturated oil	2,845	...
Undersaturated oil	1,950	1,650
F.V.F., saturated oil	1.402	....
Undersaturated oil	1.298	1.268
Solution GOR, saturated oil	647	...
Undersaturated oil	433	....
Gas conversion factor, rvb/MCF	1.2087	....
Viscosity @ 2,845 psig		
Saturated Oil, cp	0.540	
Gas, cp	0.019[7]	

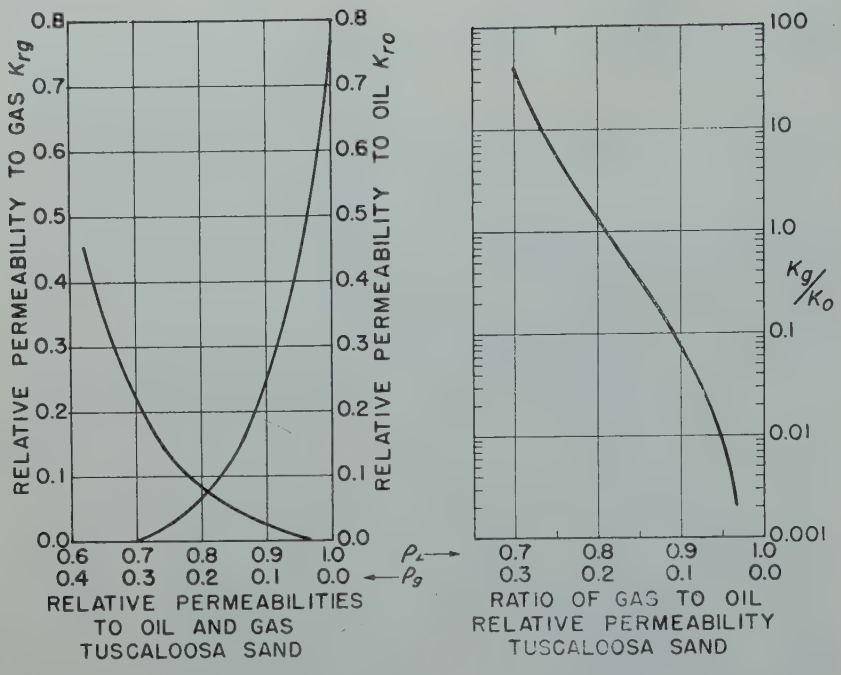

FIG. 5 — TWO-PHASE, OIL-GAS, RELATIVE PERMEABILITY DATA USED IN RESERVOIR CALCULATIONS.

function of the coverage factor, Fig. 13. The relationship of these variables may be expressed as,

1. $C_2\overline{P}_{g2} = \dfrac{(1-P_w)\ Q_{F2}V_2}{N_{b1}\beta_{b1}}$

For the case where no injected gas is assumed to go into solution, Q_{F2} is the net injected gas in the reservoir, or

2. (a) $Q_{F2} = Q_{I2} - Q_{P2} + R_{b1}\triangle n_{b2}$

For the case where the oil remaining in the gas swept portion of B is considered to be fully saturated, the free gas is given by,

2. (b) $Q_{F2} = \dfrac{(\beta'_{b2}-\beta_{b2})\ (Q_{I2}-Q_{P2}+R_{b1}\triangle n_{b2}) - (R_{b2}-R_{b1})\ [N_{b1}(\beta_{b1}-\beta_b) + \beta_{b2}\ (\triangle n_{b2}+\triangle n_{I2}+\triangle n_{x2})]}{\beta'_{b2}-\beta_{b2}-V_2\ (R_{b2}-R_{b1})}$

Where:

$\triangle n_{b2}$ = oil produced behind the gas front (cycled production).

$\triangle n_{I2}$ = Oil produced with its solution GOR from wells located behind the gas front.

$\triangle n_{x2}$ = Oil displaced from element B to element A.

(The remaining terms are defined in the legend at the end of this paper.)

By letting $\triangle n_{x2}$ have values progressively larger than zero, the curves, Fig. 13, were calculated. The two curves represent the limiting cases: (1) no injection gas goes into solution, and (2) the oil remaining in the swept pore volume is fully saturated at the prevailing pressure. It is believed that the latter is more representative of the actual situation.

In the normal Buckley-Leverett type displacement calculations where capillary pressure and gravity effects are ignored, the average gas saturation is solely a function of the volume of gas injected. However, if the gravity term in the equation is included,[5] the average gas saturation is also a function of the volumetric velocity, or flow rate. Since average distances between the iso-ratio lines could be measured on the flood map, application of a coverage factor resulted in reductions in the cross-sectional area available for transport. The flow rate resulting from any given injection rate is a function of the coverage factor. Consequently, the average free gas saturation in the swept pore volume could be evaluated as a function of the coverage factor.

Solving the Displacement Problem

In solving the displacement problem, a constant pressure of 2,845 psig was assumed. The average injection rate, in terms of reservoir gas volume, was calculated. Average volumetric velocities through each volume segment bounded by a pair of iso-ratio lines were determined by subtracting the cycled production from gross injection. For example, the reservoir volume produced with a ratio in excess of 10,000/1 was subtracted from the injected volume to find the fluid volume moving through that portion of the reservoir bounded by the 10,000/1 and 5,000/1 iso-ratio lines.

It was assumed that injected gas goes into solution at the gas front only. Having calculated the appropriate volumetric velocities for a given coverage factor, a series of fractional flow stream composition versus gas saturation curves were drawn. These were graphically differentiated and appropriate segments taken from each to construct the composite saturation distribution curve corresponding to a coverage factor of 0.55 given in Fig. 14. The discontinuities in the saturation distribution at the boundaries of the segments are the result of the assumption that the flow stream at an iso-ratio boundary is of constant fractional composition with respect to gas and liquid.

The average free gas saturation in each segment was directly calculated and from this the average free gas saturation in the entire gas swept portion of B determined. This procedure was repeated for various values of the coverage factor (Fig. 13). That coverage factor which yielded the same average free gas saturation in the swept portion of B using displacement theory and material balance methods was taken to be the most representative of the reservoir. It was found that an average free gas saturation of 15.3 per cent had been established in 55 per cent of the reservoir volume enclosed by the gas front.

Field Performance

Once a coverage factor had been established, a complete material balance solution on the Smith sand of Block IV was possible — including the cumulative net water influx during the period of gas injection. The oil production due to water encroach-

ment was related to the gross gas injected by the following procedure:

1. The variation of rate of water influx with time was calculated by a series of material balances, based on pressure and production data at various times during the injection period.
2. From the above and water production data, a plot of cumulative net influx versus time was made.
3. A plot of cumulative gas injected versus time was made from field data.
4. Cumulative net water influx was converted to stock tank oil and the desired relation was obtained by cross-plotting (2) and (3) above.

The difference between this curve and the actual performance curve for the Block is the performance of the gas injection program as illustrated in Fig. 15. The actual performance of the Block is described by the solid portion of Curve A. Curve C shows the oil recovery due to water encroachment and Curve B is the performance of the gas injection program as interpreted by the foregoing analysis.

Of interest is the degree with which the gas displacement performance as previously interpreted coincides with the theoretical performance of a comparable system. The theoretical performance may be readily calculated to any desired stage of depletion, and if applicable would permit estimates of the future performance of the Block to be made. Curves D and E are performance curves of this type and were calculated by the following methods.

Theoretical Performance

Electric model studies were made to determine the ultimate position of the gas front. They indicated that 71 per cent of the total Smith sand of Block IV would be enclosed by the ultimate front. Applying the previously established coverage factor to the pore volume enclosed by this front, the theoretical performance of Block IV was calculated, for the case of no production behind the front, after the method of Welge.[5] Curve D, on Fig. 15, describes the theoretical gas displacement performance of this case. The saturation distribution curve used in calculating this performance is the smooth curve in Fig. 14.

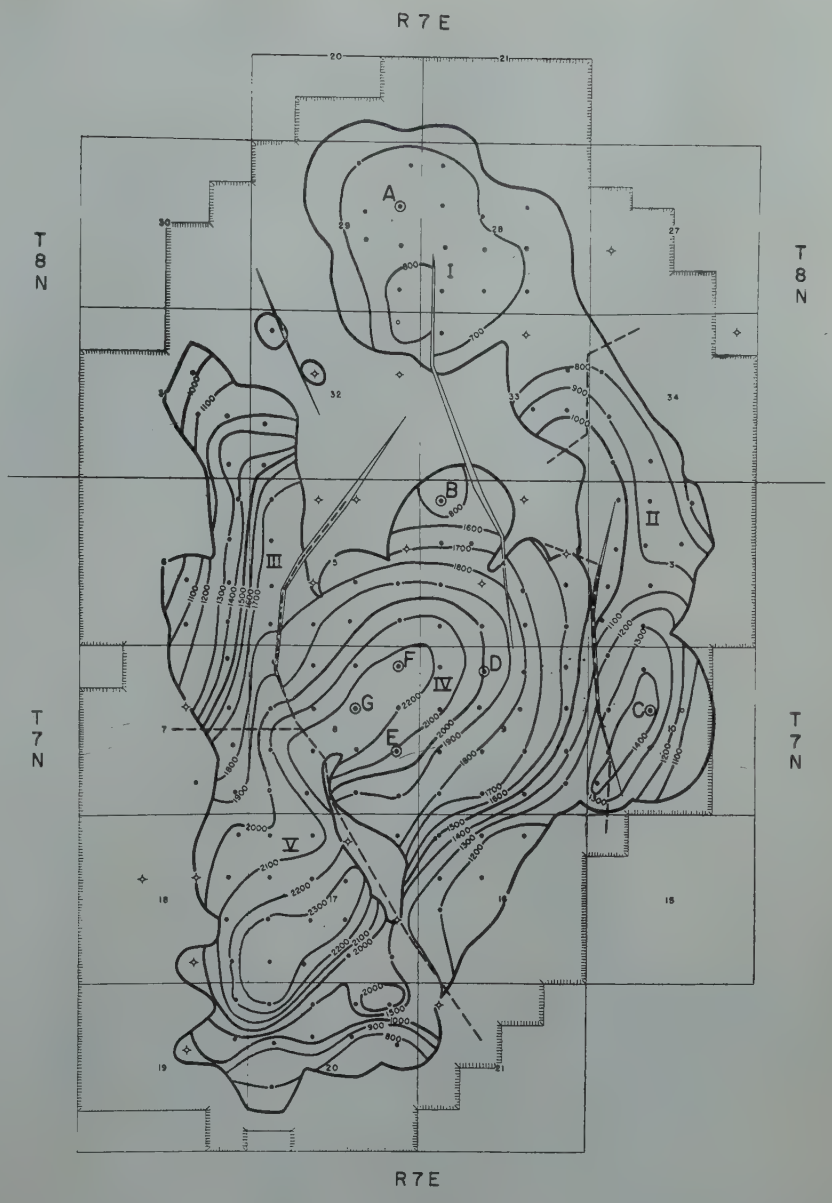

FIG. 6 — SATURATION PRESSURE MAP.

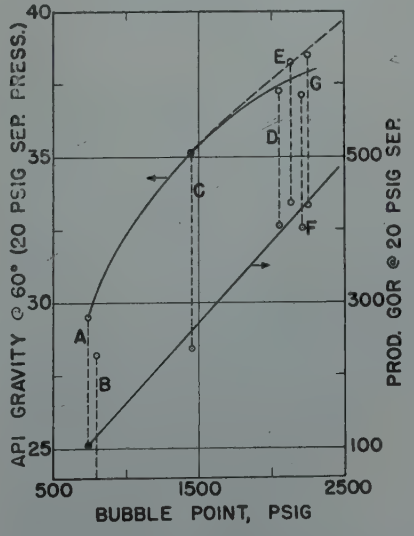

FIG. 7 — CORRELATION OF GRAVITY AND GOR VERSUS BUBBLE POINT OF BOTTOM HOLE SAMPLES.

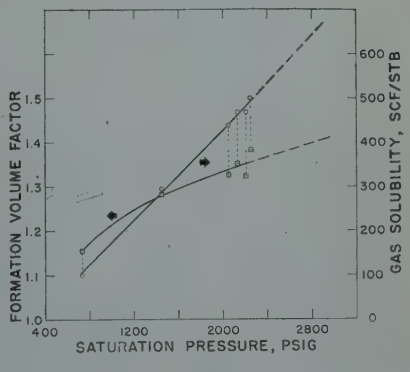

FIG. 8 — CORRELATION OF FORMATION VOLUME FACTOR AND GAS SOLUBILITY WITH SATURATION PRESSURE FOR SIX MEASURED BOTTOM-HOLE SAMPLES AT THEIR BUBBLE POINTS.

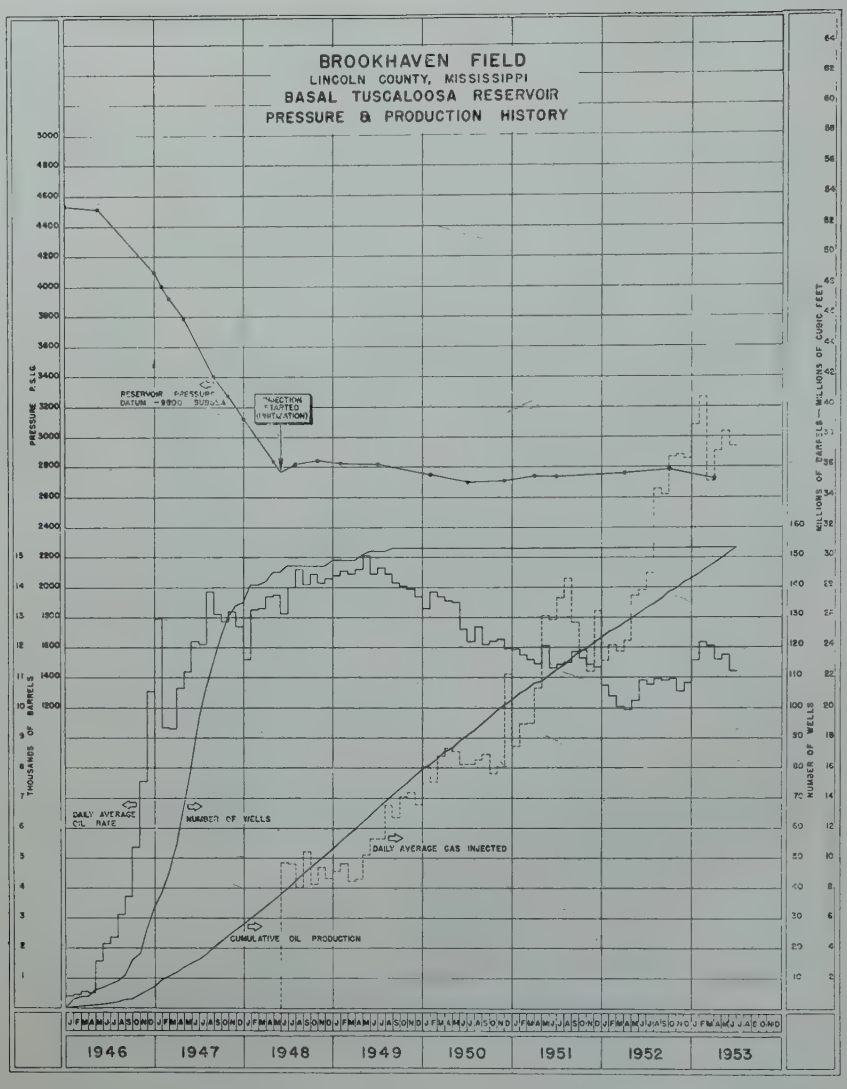

FIG. 9 — PRESSURE PRODUCTION HISTORY OF THE FIELD.

For the case where cycling occurs, the theoretical performance will not coincide with that indicated by Curve D because production behind the front will result in a more rapid increase in producing GOR. In order to calculate the behavior of a theoretical system representing an actual reservoir from which production is taken behind the advancing front of the displacing fluid, the plan or method of field operation must be known. Analysis of production data during the period of interest and the general principles guiding the operation of the field was, therefore, necessary. The plan followed to date at Brookhaven may be summarized as follows:

1. Those wells lying next to the boundaries of the Block have been produced continuously until their GOR's reached approximately 40,000/1. (with the exception of those wells lying near the edgewater boundary of the Block).
2. The interior wells have been produced until their GOR's reached 1,000/1. These wells have been shut-in, except for periodic testing, until their GOR's reached 5,000/1. After the producing GOR's reached 5,000/1, the wells have been opened and produced until their GOR's reached 40,000/1, consistent with the gas handling capacity of the plant. This procedure was adopted in an attempt to achieve a smooth gas front by reducing cusping into the producing wells. This cusping of gas into first line wells ahead of the gas front was indicated by the early behavior of the gas injection program.

Once established, this plan of operation was utilized with displacement theory to calculate the theoretical performance of the reservoir under cycling operations. The production, Table 1, was converted to reservoir volumes and average cycling rates determined. The procedure was to determine the injection volume necessary to cause the first ring of wells to produce with a ratio of 5,000/1 since this was the beginning of cycling.

The total reservoir volumes of the fluids produced with GOR's from 1,000/1 to 5,000/1, and 5,000/1 to 10,000/1, respectively, were divided by the time period during which cycling with these ratios took place. These rates were used to find that fractional part of the total flow stream which was produced behind the front. When the GOR of the first row of wells increased to 10,000/1, production in excess of this ratio became possible.

This procedure was repeated stepwise until production with ratios in excess of 40,000/1 became possible. The theoretical performance curve approximated in this manner is shown by Curve E in Fig. 15. The path taken by this curve depends upon the manner of operation of the field, since prior to breakthrough at the last row of wells any desired GOR may be achieved by judicious choice of producing wells. However, a mathematical consequence implied by the equations of Kern[6] is that if cycling occurs and all wells are produced to the same limiting GOR, the total amount of gas injected when the last row of wells produce with this GOR is the same as for the case without cycling. Consequently, the gas injection performance curves for the cycled and non-cycled cases join when the last row of wells produce with this ratio.

Estimated Gas Drive Production

If the coverage factor remains 0.55 and 39,303 acre-ft are ultimately enclosed by the 40,000/1 GOR line in this Block, an estimated 50 billion cu ft of gas will have been injected and 8.8 million stock tank bbls of oil will have been produced by gas drive. If the current rate of injection is maintained, it is estimated that the oil production due to water encroachment during the injection period will be 3.2 million STB. The total recovery from this Block during the gas injection period is, therefore, estimated to be 12 million STB, as shown by the extra-

polation of Curve A, Fig. 15. Since 2,404,263 STB of oil were produced prior to the initiation of gas injection, an estimated 31 per cent of the 46.45 million STB originally in place in this Block will have been recovered at the end of pressure maintenance. A total recovery of approximately 50 million bbls is estimated for the entire field.

The actual performance of the field indicates that the coverage factor has progressively increased to the present value of 0.55. Injection gas breakthrough to the first row of wells occurred after only a relatively small volume of gas had been injected. A coverage factor in the order of 0.40 was estimated at that time. Should future production provide data indicating that the coverage has continued on an increasing trend, it will be necessary to increase these recovery estimates.

The measurable performance of a reservoir is the combined result of all the producing mechanisms operable. Interpretation of performance data and delineation of production caused by each of these various mechanisms cannot be accomplished without resorting to the theory of each. Therefore, the interpretation of performance by gas displacement assumes that theoretical concepts and data used in applying these are valid. For example, if laboratory relative permeability measurements are not representative, the performance by gas displacement may be something other than that shown by Curve B. This paper merely attempts to point out that it is possible to interpret field data in the light of present theory. Also, that this interpretation reasonably agrees with the theoretical behavior of a hypothetical system having the parameters of the field.

GAS INJECTION VERSUS NATURAL DEPLETION

Fig. 16 shows a comparison of the calculated performance of the field under natural depletion with the performance estimated under gas injection operations. These estimates indicate that under pressure maintenance the ultimate recovery will be in the order of 50 million bbls or 250 bbls/acre-ft. This represents about 29 per cent of the original stock tank oil in place. The estimates of recovery by natural depletion indicate the ultimate recovery would be about 39 million bbls. However, the ultimate economic recovery under this method of operation is estimated to be 36 million bbls or about 21 per cent of the original oil in place. Under this method of operation, the decline in reservoir pressure would have required pumping from below 8,500 ft by 1957, and high lifting costs would have forced the abandonment of the field as uneconomic.

Fig. 17 is presented to show a comparison between the performance of Brookhaven, under gas injection, and a similar Basal Tuscaloosa reservoir which is being produced under natural depletion. This field, Mallalieu, is located about 12 miles from the Brookhaven field. The sand properties at Mallalieu are practically the same as those at Brookhaven, and the original reservoir oil was undersaturated. The principal difference between the two is that the Mallalieu west reservoir (for which the curve was drawn) is smaller than Brookhaven. The original stock tank oil in place was about 70 per cent of that at Brookhaven.

Actually, at Mallalieu production rates have declined to a point where pressure is being maintained above the bubble point by natural water drive. In spite of this, as shown by its performance curve, the production has rapidly declined to the present rate of only about 1 per cent per

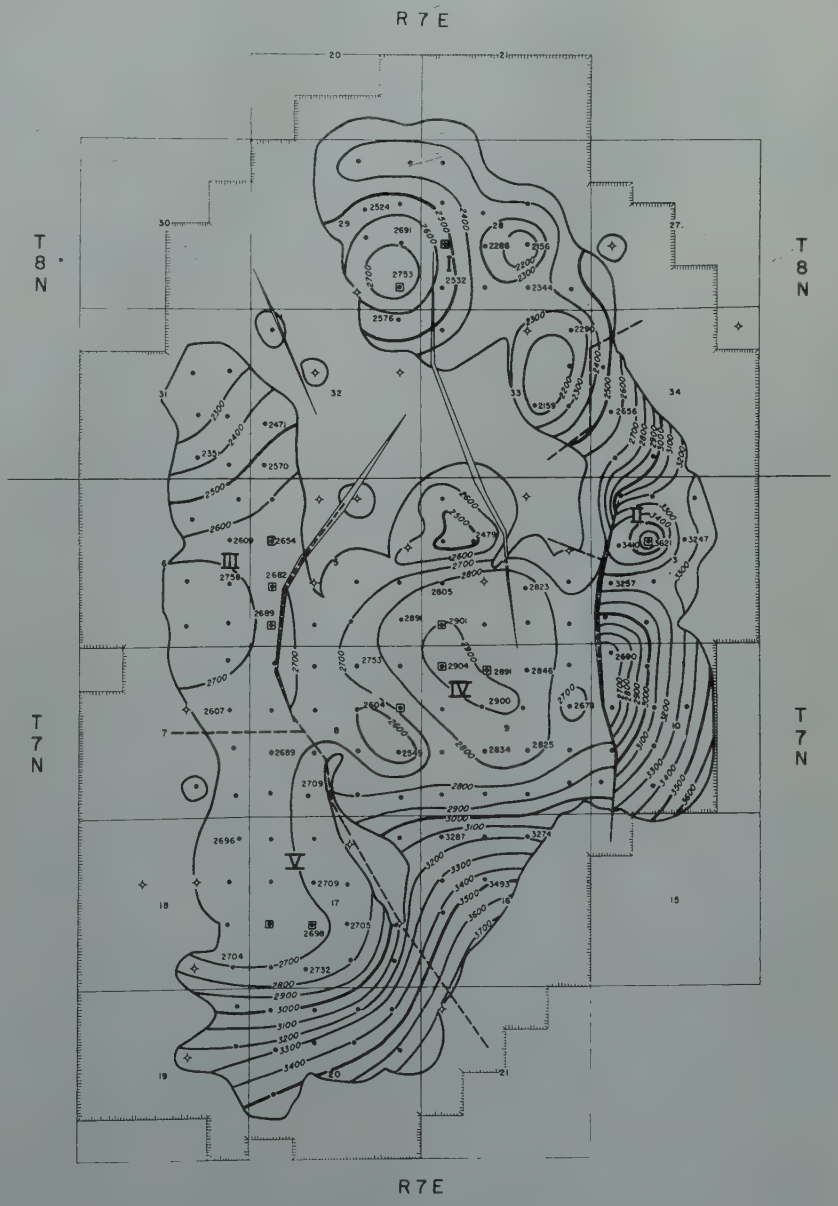

FIG. 10 — BOTTOM-HOLE PRESSURE MAP, OCTOBER, 1952. SUB SEA DATUM 9,800 FT.

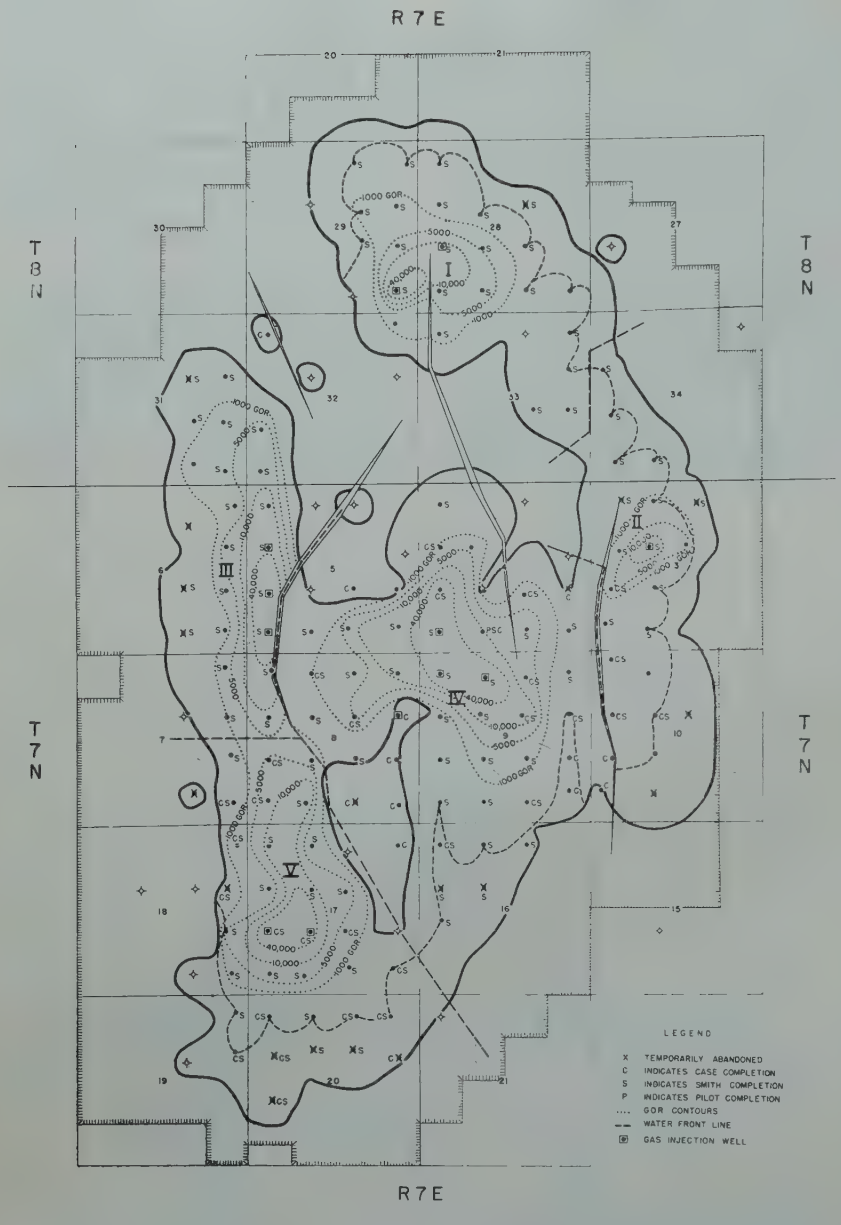

FIG. 11 — GAS AND WATER FLOODED AREAS.

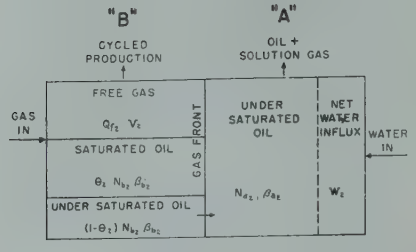

FIG. 12 — SCHEMATIC PRESENTATION OF BLOCK IV FOR MATERIAL BALANCE PURPOSES.

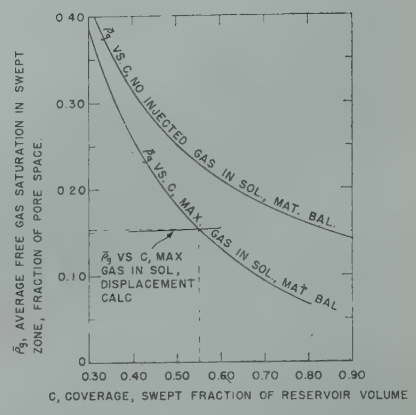
0.40
0.30
0.20
0.10
0
0.30 0.40 0.50 0.60 0.70 0.80 0.90
C, COVERAGE, SWEPT FRACTION OF RESERVOIR VOLUME
AVERAGE FREE GAS SATURATION IN SWEPT ZONE, FRACTION OF PORE SPACE.
VS. C, NO INJECTED GAS IN SOL., MAT. BAL.
VS C, MAX GAS IN SOL., MAT. BAL.
VS C, MAX GAS IN SOL., DISPLACEMENT CALC

FIG. 13 — VARIATION OF AVERAGE FREE GAS SATURATION IN THE GAS-SWEPT PORTION OF THE RESERVOIRS WITH THE COVERAGE FACTOR.
Dotted line shows agreement between material balance and displacement calculations for the case where the oil in the gas-swept reservoir volume is fully saturated.

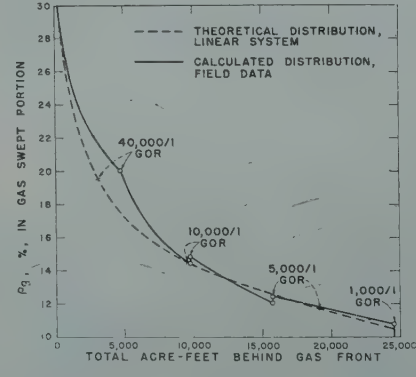

FIG. 14 — COMPARISON OF THE CALCULATED DISTRIBUTION IN THE GAS FLOODED REGION OF BLOCK IV WITH THE THEORETICAL SATURATION DISTRIBUTION RESULTING FROM GAS DISPLACEMENT IN AN IDEALIZED SYSTEM; NO PRODUCTION BEHIND THE GAS FRONT.

year of the original oil in place. An extremely long productive life will be necessary to recover a substantial part of the original reserve. The performance of Mallalieu is attributed principally to the fact that water encroachment to edge wells has caused their early abandonment. When water encroaches into a well, it is not physically possible to lift sufficient fluids from the low fluid levels to maintain economic production. The California Co. has found that lifting costs at Mallalieu are approximately one and one-half times those at Brookhaven, including the cost of purchased gas, which will have a resale value.

CONCLUSION

This paper has been presented as a progress report of five years of unitized pressure maintenance operations in the Brookhaven field. It should be stated that the performance during this period has been progressively better than the original predictions which furnished the basis for initiating the project. The overall economics have also been very satisfactory. Therefore, there is good basis for an optimistic outlook with regard to the future performance of the field.

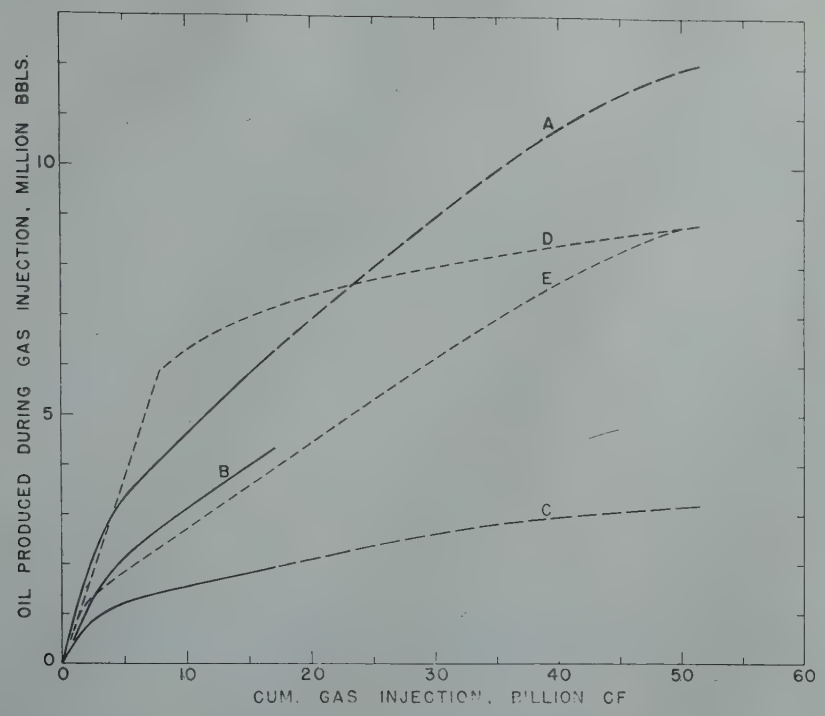

FIG. 15 — PERFORMANCE CURVES FOR THE SMITH SAND OF BLOCK IV.

A — Actual Performance, Measured Field Data.
B — Production Due to Gas Displacement.
C — Production Due to Water Encroachment.
D — Calculated Performance, No Cycled Production.
E — Calculated Performance, Production Behind Gas Front.

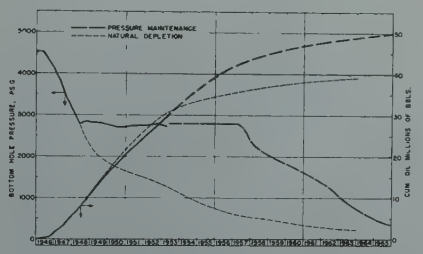

FIG. 16 — COMPARISON OF ESTIMATED CUMULATIVE OIL RECOVERY AND RESERVOIR PRESSURE DECLINE UNDER NATURAL DEPLETION AND PRESSURE MAINTENANCE OPERATIONS.

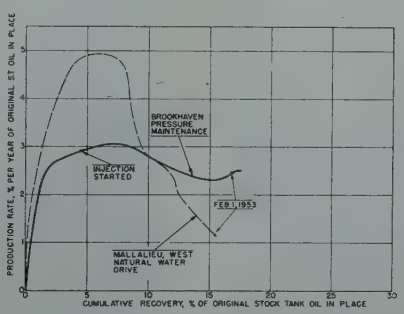
PRODUCTION RATE, % PER YEAR OF ORIGINAL ST OIL IN PLACE
BROOKHAVEN PRESSURE MAINTENANCE
INJECTION STARTED
FEB. 1953
MALLALIEU, WEST NATURAL WATER DRIVE
CUMULATIVE RECOVERY, % OF ORIGINAL STOCK TANK OIL IN PLACE

FIG. 17 — COMPARISON OF PERFORMANCE OF TWO SIMILAR BASAL TUSCALOOSA RESERVOIRS UNDER DIFFERENT PRODUCTION SCHEMES: (1) MALLALIEU, WEST RESERVOIR — NATURAL WATER DRIVE AND PRESSURE DECLINE CONTROLLED BY WITHDRAWAL RATES; AND (2) BROOKHAVEN — PRESSURE MAINTENANCE BY GAS INJECTION.

LEGEND

Numerical subscripts indicate different times.

Subscripts, a and b, refer to position relative to the location of the 1,000/1 GOR contour line.

Primes indicate different fluid systems; e.g. β_b, β_b'.

β = Formation volume factor, rvb/STB

R = Solution, GOR, SCF/STB

W = Net water influx into reservoir, bbls

C = Coverage, fraction of total hydrocarbon space swept behind the front.

N = Oil in place in one portion of reservoir, STB

$\triangle n$ = Incremental oil production from one portion of reservoir, STB

ϕ = Fractional porosity

Q_I = Cumulative gas injection, MCF

Q_F = Free gas in reservoir, MCF

Q_P = Total gas produced behind gas front, MCF

$\overline{P}_g$ = Average gas saturation behind front, swept zone

P_w = Connate water saturation, fraction of pore space

Θ = Fraction of reservoir oil behind front absorbing injected gas

V = Reservoir volume occupied by 1.0 MCF S.C. gas, rvb

ACKNOWLEDGMENT

The authors wish to thank the management of The California Co. and the other Brookhaven Unit operators for their permission to present this paper. ★★★

REFERENCES

1. Womack, R., Jr.: "Brookhaven Oil Field, Lincoln County, Miss." *Bull.* AAPG (1950), **34**, 1517.
2. Thomas, E. P.: "Mississippi Structures and Their Relation to Oil Accumulation," *Bull.* AAPG (1950), **34**, 1502.
3. Patton, E. C., Jr.: "Evaluation of Pressure Maintenance by Internal Gas Injection in Volumetrically Controlled Reservoirs," *Trans.* AIME (1947), **170**, 112.
4. Buckley, S. E., and Leverett, M. C.: "Mechanism of Fluid Displacement in Sands," *Trans.* AIME (1942), **146**, 107.
5. Welge, H. J.: "A Simplified Method for Computing Oil Recovery by Gas or Water Drive," *Trans.* AIME (1952), **195**, 91.
6. Kern, L. R.: "Displacement Mechanism in Multi-Well Systems," *Trans.* AIME (1952), **195**, 41.
7. Bicher, L. B., and Katz, D. L.: "Viscosity of Natural Gases," *Trans.* AIME (1944), **155**, 246.

DEVELOPMENT of an UNDERGROUND HEAT WAVE for OIL RECOVERY

BRUCE F. GRANT
STEFAN E. SZASZ
MEMBERS AIME

SINCLAIR RESEARCH LABORATORIES, INC.
TULSA, OKLA.

T. P. 3797

INTRODUCTION

During 1947, a Sinclair research team was assigned to investigate thermal methods of oil recovery. The assignment was recommended by a survey of possible research approaches to increase the amount of oil that ultimately can be recovered from oil producing reservoirs. The use of heat to stimulate oil production rates by the melting of paraffin deposited in well bores can be traced back to within one or two decades of the drilling of the Drake well.

The application of heat on a larger scale has been discussed by generations of oil producers. Shortly after the turn of the century, one intrepid operator is reported to have injected steam into a Pennsylvania property. After a few weeks, he apparently became discouraged and terminated his experiment. Subsequently, the literature contains references to several well-developed techniques for supplying heat to a producing well bore to melt paraffin or to reduce the viscosity of oil contained in the formation immediately around the well bore.[1,2,3,4] Some early references discuss procedures to furnish heat to the reservoir,[5,6] with the injection well as the heat source, thus obligating the process to maintain the entire rock mass at a temperature above that at which the desired improvement in oil recovery would occur.

Another approach to reservoir heating was reported by a group of Russian technologists in 1935.[7,8,9] They definitely demonstrated that combustion can occur within the porous structure of an oil-bearing sandstone. Their field experiments, however, relied less on combustion within the rock than on heat furnished by combustion of oil supplied to the injection well bore. Ignition of the air-oil mixtures in the well bore was found very difficult, and the field tests were carried on for only short periods of time. Publication of the Russian work spurred at least one independent operator in this country to try firing an air-gas injection well. on for only short periods of time.

Publication of the Russian work spurred at least one independent operator in this country to try firing an air-gas injection well. The Brundred Oil Corp. reportedly obtained combustion in the sand immediately around the injection well bore, but the experiment was abandoned because of interference with normal production schedules. Injection capacity of the experimental well was greatly reduced by firing. The well was reshot and pieces of sand showing partial fusing of the quartz matrix were recovered.

To the authors' knowledge no other field experiments utilizing combustion techniques for formation heating were undertaken prior to 1948, although the patent literature evidences continued interest in formation heating.[10,11]

CONCEPT OF COMBUSTION-SUPPORTED HEAT WAVE

The references cited were in agreement that heat applied to a reservoir would increase recovery, but there

---

[1]References given at end of paper.

Manuscript received in Petroleum Branch office Jan. 11, 1954. Paper presented at the AIME Annual Meeting in New York, N. Y., Feb. 13-17, 1954.

Discussion of this and all following technical papers is invited. Discussion in writing (3 copies) may be sent to the offices of the Journal of Petroleum Technology. Any discussion offered after Dec. 31, 1954, should be in the form of a new paper.

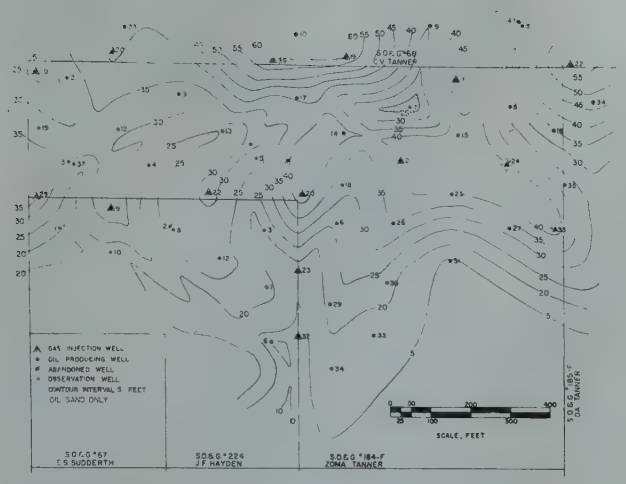

FIG. 1 — ISOPACHOUS MAP OF ZOMA TANNER PROPERTY, DELAWARE CHILDERS FIELD, NOWATA COUNTY, OKLA.

were few data as to the mechanism of the improvement or the temperature level required. The Sinclair team conducted exploratory work in the laboratory by subjecting groups of oil-saturated core samples separately to water (steam), nitrogen, and air drives over a range of temperatures up to 1,500°F. From these tests, the general conclusion was reached that temperatures of at least 700°F were necessary to approach maximum possible oil recovery. It was concluded that combustion techniques would be necessary to maintain temperatures of this magnitude. Yet, maintenance of high temperatures over the area that would be included within any reasonable well spacing was out of the question because of expected heat losses and fuel requirements.

Consideration of these factors led to the concept developed by Smith and Watson.[12] They proposed the creation of a high temperature zone in the reservoir rock around an injection well and the subsequent injection of cold gas to move the zone radially outward as a combustion-supported heat wave. Sensible heat of the rock behind the wave thus would be continually recovered and utilized to help heat "new" rock ahead of the wave. By keeping the width of the "hot" zone narrow, heat losses and fuel requirements would be minimized.

Laboratory experiments were conducted with sand packed columns saturated with crude oil and brine to develop techniques of propagating and controlling combustion and heat transfer waves. Details of some of the experiments have been given by Smith and Watson. After establishing the basic characteristics of heat wave propagation, calculations were made of the probable economic limits of the process. It was apparent that the use of air as the sole injection medium would require so great an energy consumption for compression to injection pressures as to limit commercial application to reservoirs having oil contents on the order of 1,200 bbls/acre-ft.

On the other hand, if oxygen requirements are held between 1.33 and 6.0 volume per cent, so that produced or "recycle" gas supplies 70 to 90 per cent of the total gas requirements, then compression costs of the process can be reduced in proportion to the pressure under which the produced gas can be delivered to the compressor. For example, if a 300 psi back pressure could be maintained in a field where 500 psi injection pressures were required, assuming well depths of 1,000 ft, 2½-acre five-spot development and permeability high enough to inject 250 MCF per well day, the process could be profitable with reservoir oil contents on the order of 250 bbls/acre-ft. A thermal recovery of 80 per cent of the oil in place is assumed.

Maintenance of high pressures on producing wells almost certainly would require unitized operation of pressure-depleted fields.

FIELD EXPERIMENTS ((1948-1951)

EXPERIMENTAL SITE

Early in 1948, it was decided that a field trial would be necessary to determine whether a combustion-supported heat wave could be started and maintained in a reservoir. Since a shallow unitized field was not readily available for the experimental work, the decision was made to proceed on any suitable property producing a "typical" crude from shallow depths. The purpose of the initial field tests would be to develop techniques for operating subsequent experiments aimed at commercial evaluation of the process.

Through the cooperation of Sinclair Oil & Gas Co., an experimental site was secured on the 80-acre Zoma Tanner farm, located in the NE/4 NW/4, Section 1, Township 26 North, Range 16 East, close to the south edge of the extreme eastern portion of the Delaware-Childers field, Nowata County, Okla. A 35° - 37° API crude oil is produced from the Bartlesville sandstone, which occurs at a depth of 600-620 ft over the experimental area. The geology, development, and oil production history of the eastern portion of the Delaware-Childers field has been comprehensively studied by Johnston and Riggs.[13]

Fig. 1 is a map of the Zoma Tanner property, with contours of oil-sand thickness, as taken from drillers' logs. Only the lower portion of the Bartlesville sand is oil saturated. The upper section is logged as "gas" sand. The 15-ft contour has been taken to be the edge of the productive area, as data from adjoining leases indicate the sand body thins abruptly along this line. The original development occurred between 1908

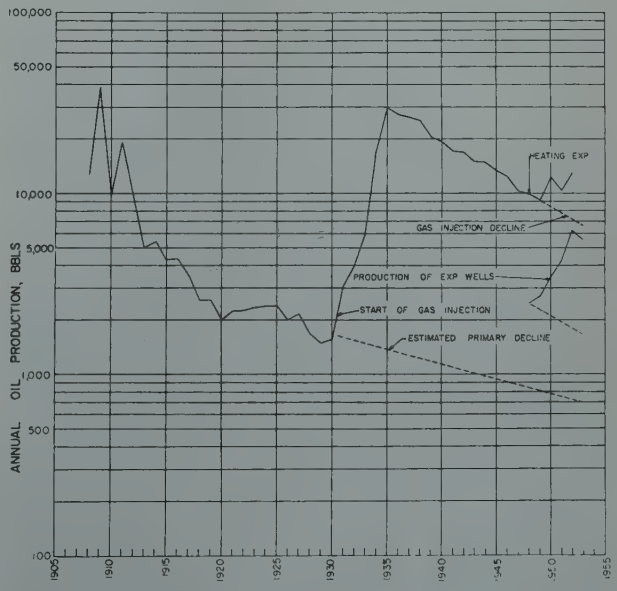

FIG. 2 — OIL PRODUCTION HISTORY OF ZOMA TANNER PROPERTY.

and 1912 when nine wells were drilled, eight of which were still producing in 1934 when gas injection was started on the property. Ten injection and 16 producing wells were drilled during the period from 1935-1938 to complete the secondary development. One producing well was converted to injection service in 1939. The oil production history of the property is presented in Fig. 2, and the effect of gas injected into adjoining leases is evident beginning in 1931. Reservoir and recovery data are tabulated below:

Production area, acres	60
Volume of oil productive sand, acre feet	1,893
Average permeability, md	145
Average porosity, percent	19.3
Assumed interstitial water content, percent of pore space	35
Assumed reservoir oil shrinkage, per cent	10.5
Calculated initial oil content, stock tank barrels	1,667,281
Primary production, 1908-1930 (inclusive), barrels	140,291
Primary production, percent of original oil	8.4
Production by gas injection, 1931-1947 (inclusive) barrels	277,103
Production by gas injection, per cent of original oil	16.6
Cumulative oil produced, 1908-1947 (inclusive), barrels	417,394
Cumulative oil produced, percent of original oil	25.0
Calculated oil content at end of 1947, barrels per acre-foot	660

Volumes of gas injected during the period 1934 to 1948 are not readily available. In general, injection rates were held to 15,000 cu ft per well per day. Daily oil production rates during June, 1948, averaged 1.1 bbl per well at an average estimated injected gas-oil ratio of 6,450 cu ft/bbl. No connate water has ever been produced with the oil in this portion of the field.

Preparation of Well 35

The first field experiments with thermal recovery were designed to develop techniques of "firing" a well, an operation which includes two separate steps: (1) burning fuel within the well bore to heat the sand around the well to temperatures sufficiently high to permit, (2) transferring combustion to the porous structure of the sand.

Injection well 35 on the Zoma Tanner lease was selected for these tests. The well had been completed as a producing well in 1937. The Bartlesville sand was logged in the depth interval 587 to 633 ft. The oil pay between 592 and 633 ft had been shot with 60 quarts of nitroglycerine. The well had been converted to injection service in 1949. In preparation for the tests, a bridge was placed at the top of the oil sand and the casing lowered by underreaming to this point, cemented, and the hole cleaned. Injection capacity of the well after cleaning was 310 MCF daily at 150 psi. The rig then was used to drill an observation well 20 ft west of well 35. The observation well was equipped with tubing set on a packer at the top of the oil sand. The annulus above the packer was loaded with mud. A thermocouple in a sealed quarter-inch thermowell was run inside the tubing string to a point below the packer.

For the first step of the firing procedure, a burner designed by Piros was installed in well 35. Although several types of well-bore burners were available, none of these completely fulfilled the postulated requirements for a well-bore burner which would operate with gaseous fuels under injection pressures up to 500 psi at heat release rates up to 500,000 Btu hourly with provision for wellhead control of burner ignition and of final combustion temperatures. Construction of the burner is shown in Fig. 3. Gas is injected through a ½-in. line, primary air through a concentric string of 2-in. tubing, and secondary air through the annulus between tubing and casing. The burner was placed at

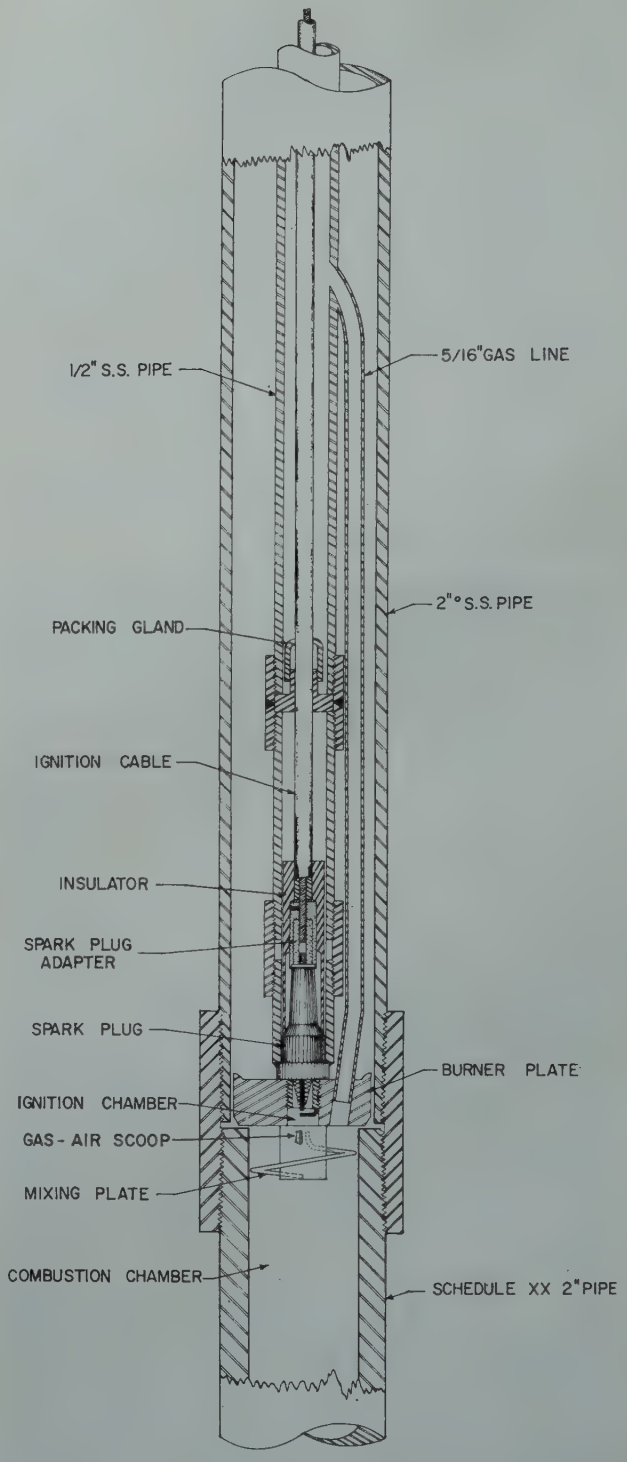

Fig. 3 — Piros Burner.

a depth of 600 ft so as not to injure the casing or impair the cement job around the casing shoe, and the hole was pressured with air in order to drive water and moisture from the well bore. Then, metered quantities of gas and primary and secondary air were injected, and the mixture was lighted by a high tension spark plug. As soon as the thermocouple below the tip of the burner indicated a rise in temperature, gas and air rates were adjusted to give maximum hourly heat release rates with flue gas temperatures between 1,200°F and 1,800°F under an operating pressure of 500 psi.

The step of transferring combustion to the heated

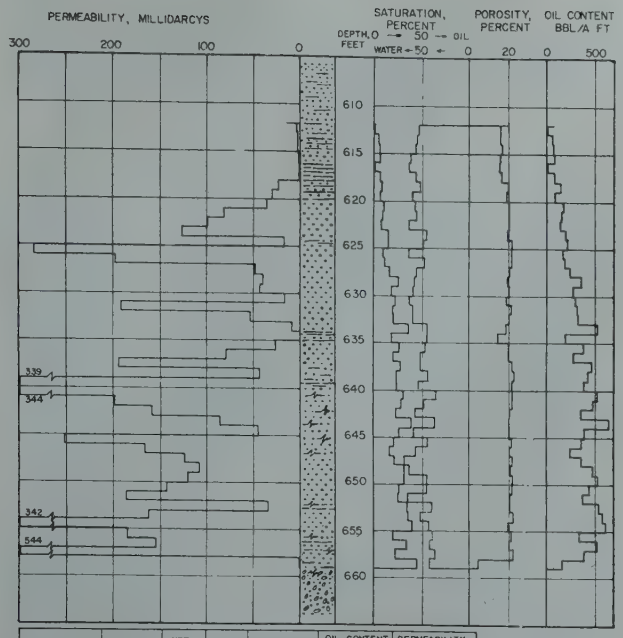

SAND	DEPTH, FEET FROM	TO	NET FT. OF SAND	AVG POR	AVG SAT OIL	AVG SAT WATER	OIL CONTENT AVG BBL/AFT	OIL CONTENT TOTAL BBL/A	PERMEABILITY AVG MD.	PERMEABILITY CAPACITY MD. FT
GAS SAND	612	628	16	19 25	7 10	56.61	111	1771	575	919 9
OIL SAND	628	659	31	20 77	25 88	51.69	407	12,67	1433	44416
SHALE	659	—	1	4 68	44 74	42 47	163	163	- 0 1	- 0 1

LEGEND
SAND
SHALE
CARBONIZED PLANT FRAG
CONGLOMERATE

FIG. 4 — CORE DATA, WELL 24-WEST.

sand immediately around the injection well bore was not difficult to accomplish provided the burner had been operated to transfer at least 50 million Btu to the 51-ft-thick sand. Several transfer techniques were used successfully, but all involved the injection of non-combustible gases. The simplest method was to shut off the fuel gas supply and to inject air alone. Injection well sand face temperature dropped sharply, but burning continued out into the formation as evidenced by the continuing presence of carbon dioxide in the gas produced from the observation well. The residual oil content of the formation supplied the necessary fuel during this step.

PROPAGATION OF HEAT WAVE INTO FORMATION

The next phase of the field experimentation was concerned with propagation of the combustion wave outward from well 35. The degree of combustion obtained with any given mixture of gases injected into well 35 was judged by the oxygen and carbon dioxide content of gas produced from the observation well and from the nearby producing wells. The limiting amounts of any one component of the mixture (air, recycle gas, or fuel gas) were explored by continuously varying the proportion of the component even to the point of losing combustion. These experiments confirmed the expected dependence of propagation rates on the oxygen-fuel ratio of the injected gases. For example, a mixture of air and produced gas having a hydrocarbon content equivalent to 80 Btu/cu ft and containing 6 per cent of oxygen caused the combustion to move from the injection to the observation well at a more rapid rate than was observed with any other mixture injected. However, as the oxygen content was increased beyond 6 per cent, forward travel of the combustion slowed; when the oxygen content of the injected gas (hydrocarbon content of 80 Btu) reached 12 per cent, the burning "flashed back" to the injection well bore. In subsequent tests, each time the proportions of oxygen to hydrocarbon came within the explosive range, as defined by Jones,[15] the combustion burned back toward the injection well.

In later experiments, it was found possible to get a "rich" mixture into the combustion zone by injecting alternate slugs of air and fuel without incurring excessive broadening of the zone through "burn-back." The amounts of each gas were proportioned to approach the stoichiometric proportions for complete combustion, while the volumes and timing of the separate injection cycles were adjusted to prevent complete mixing until the gases entered the combustion zone.

All of the experimental work at well 35 was aimed at developing operating methods which later could be utilized in a long-term test. The development of the fuel injection techniques was considered particularly necessary because with the injection of air alone to propagate the combustion wave, oxygen contents of gas produced from wells ahead of the wave had not been less than 5 per cent and had shown a tendency to increase with continued air injection. The same phenomenon had been oberved in laboratory tests and was invariably associated with a decline in peak temperature of the wave. Thus, it was felt that long-term operation with air injection could eventually extinguish combustion unless reliable techniques were developed for revivifying the combustion wave.

EXPERIMENTS WITH WELL 24 (1949-1953)

PRELIMINARY WORK

By 1949, the encouraging aspects of tests at well 35 led to a decision to prepare a well pattern for an extended test. Injection well 24 on the same lease was selected. An inverted seven-spot pattern is formed by well 24 and the six offset producing wells with an average distance of 300 ft from injection to producing wells. Well 24 had been drilled in 1934 and had been shot upon completion. Casing had been set at the top of

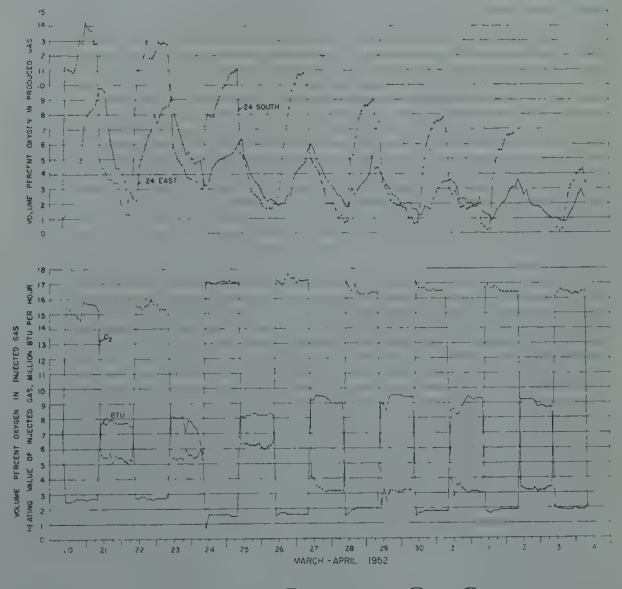

FIG. 5 — INJECTED AND PRODUCED GAS COMPOSITIONS DURING CYCLIC OPERATION TO FORM HEAT WAVE AT WELL 24-WEST.

the sand at a depth of 617 ft. In preparation for the tests, the well was cleaned, but not reshot. The casing point was not changed. After cleaning, air was injected into the well at a rate of 480 MCF daily at a pressure of 380 psi.

Four observation wells designated as 24-West, 24-North, 24-East, and 24-South were drilled as shown in Fig. 1, placing them on the corners of a square, 37.5 ft apart and 26.5 ft from well 24; they were cored using fresh water as the drilling fluid. Analysis showed the cores to be practically identical; the coregraph for well 24W is given in Fig. 4. In spite of an average dry air permeability of 140 md shown by the cores, none of the wells ever produced more than 15 per cent of the gas injected into well 24. Total oil production of the four wells was less than 1 bbl weekly, with 5 to 10 bbls of water. The low oil content of 407 bbls/acre-ft shown by the cores, and the low oil production are probably attributable to the close proximity of an operating gas injection well. Moreover, subsequent experience has shown that the fresh water used in coring severely impairs the ability of the cored well to produce gas on oil in this field.

Other preparatory work included rearranging gas and oil gathering lines to separate the six offset producing wells from the lease system. Gas sampling and metering connections were provided for the observation and producing wells. Thermowells were installed in the observation well.

A Piros burner was installed in the injection well and the burner was ignited on June 14, 1949. Injection pressures were much higher than indicated by the flow test. Combustion was transferred to the sand July 1, but pressures increased until on September 26, the test was discontinued. The well was opened and found to be filled with loose sand. Extensive cleaning was required, and the well was recased. On October 6, the burner was relighted, but after eight days of operation, the well bore became plugged. In the next two months, three successive cave-ins prevented continuous operation of the burner. On Jan. 11, 1950, the burner was lighted. After two weeks, combustion was transferred to the formation and operations continued until March 9, when the fire flashed back to the injection well bore as a result of attempts to inject mixtures in the explosive range. A hole was burned in the casing and the well was abandoned.

A replacement well drilled 6 ft southwest of well 24 was designated well 36. After completion, a mixture of air and produced gas having 6 per cent oxygen content was injected without any ignition device in the well. Immediate combustion occurred in the formation, as evidenced by the disappearance of oxygen from the produced gas. After 30 days of operation, injection pressure increased and it was decided to switch to straight air injection; however, only 12 hours after the switch, an explosion occurred in the well, collapsing the casing and causing the well to be abandoned.

Consequently, well 24W was prepared for injection, and recompleted by cementing the 53/16-in. casing at 617 ft and reaming the core hole to 5-in. diameter. An injection profile obtained with a spinner showed most of the injected gas to be entering the "gas sand" in the upper part of the sand. The depth interval from 617 to 628 ft was squeezed with 25 sacks of cement and the hole redrilled to a depth of 655 ft. From a second spinner survey, it was found that at injection rates below 250 MCF daily, by-passing to the upper sand still was evident; however, at rates of 500 MCF daily, the injected gas was uniformly distributed over the sand face. As operation would be at the higher rate, the completion was considered satisfactory.

Firing and Operation of 24-West Well

Although the remedial work was completed in April, 1951, firing of the well was delayed until the completion of the tests at well 35. On Dec. 27, 1951, well 24W was fired. The burner was operated until January 13, when the well was opened to clear an obstruction between the casing and 2-in. tubing which interfered with the flow of secondary air to the burner. On removing the burner, it was found that the mixing plate and combustion chamber had burned off. The well was cleaned, re-equipped, and the burner lighted on Jan. 23, 1952. Operation was continued with combustion in the well bore regulated to hold a temperature of 1,000°F at a point 6 in. below the burner outlet. By February 5, samples from observation wells contained less oxygen than the flue gas being injected, thus confirming that combustion was occurring in the formation.

Rather than drive the combustion away from the well bore, mixtures which would burn at well bore temperatures (1,000-1,200°F) were injected at the maximum possible rate to maintain combustion in and around the well bore. This operation was continued until March 20, when the injection of high air-fuel ratio mixtures for 24 hours was alternated with the injection of low ratio mixtures for 24 hours. In Fig. 5 are plotted the oxygen contents of injected gas during these cycles and of gas from East and South wells. Progressive smoothing of these latter curves occurred as combustion moved to, and became stable at, the forward edge of the heated area. The injection program of alternate days on high oxygen content gas was continued until April 9. At that time, the average oxygen content of gas produced from the six producing wells was 2 per cent. The injection well bore temperature had dropped from 1,000°F at the start of cyclic injection to 190°F on April 9. On this date, the continuous injection was started of an air-produced gas mixture containing 16 per cent oxygen and hydrocarbons equivalent to 40 Btu/cu ft. The subsequent changes in injection are summarized in Table 1, which also gives the quantities of gas, oxygen, and hydrocarbons injected to Nov. 28, 1953.

The columns in Table 1 which list the estimated oxygen consumed and the total heat generated were computed. At any given time, the weighted average oxygen content of the gas produced at the six "inner ring" producing wells (Wells 27, 25, 15, 8, and 16 on the Zoma Tanner, and well 35 on the Ida Tanner lease) was considered to represent the unburned portion of the oxygen injected during that time. It is realized that this assumption does not take into account the time delay between the injection and production of a unit volume of gas. The travel time, apparently, does not exceed two days to any of the wells and the time for a change in the combustion reaction to be reflected at the producing wells ranges up to a week. Considering the length of the test period, the simplification on a daily basis probably introduces only a negligible error in the estimate of total oxygen consumed. The quantity of heat generated was computed by assuming 500 Btu to be released for each standard cubic foot of oxygen consumed.

TABLE 1 — SUMMARY OF INJECTION TO SEVEN SPOT WELL PATTERN

Interval From	Interval To	Injection Mixture	Oxygen Content Percent	Heating Value Btu/CF	Approximate Injection rate MCFH	Time Interval Days	Gas Injected MCF	Oxygen Injected MCF	Fuel Injected Btu x 10^6
12-27-51	1-13-52	Air, nat. gas and prod. gas*	11	152	20	18	8,850	960.4	1,345.3
1-13-52	1-23-52	Shut down	0	0	0	10	0	0	0
1-23-52	2- 5-52	Air, nat. gas and prod. gas*	7	156	20	13	6,118	445.5	954.1
2- 5-52	3-20-52	Air and prod. gas**	9.5	135	40	44	43,562	4,043.5	5,893.8
3-20-52	4 -9-52	Air and prod. gas alternately	10	119	45	20	22,025	2,259.6	2,612.0
4- 9-52	4-13-52	Air and prod. gas	16	43	50	4	4,753	769.4	202.3
4-13-52	4-16-52	Air and prod. gas	17	34	50	3	3,537	603.9	119.2
4-16-52	7- 7-52	Air and prod. gas	16.5	42	47	82	93,449	15,598.6	3,888.1
7- 7-52	7-17-52	Air and prod. gas	17.5	28	45	10	10,724	1,885.6	303.4
7-17-52	10- 6-52	Air and prod. gas	18	21	40	81	76,945	14,734.1	1,611.6
10- 6-52	11- 5-52	Air	21	8	36	30	24,889	5,175.2	19.0
11- 5-52	11-18-52	Air and prod. gas	18	24	42	13	10,470	2,454.9	250.3
11-18-52	1- 5-53	Shut down	0	0	0	48	0	0	0
1- 5-53	1-12-53	Air and prod. gas	17	38	33	7	4,210	733.6	158.9
1-12-53	1-23-53	Air and nat. gas	20	10	24	11	6,725	1,294.0	66.4
1-23-53	3- 3-53	Air and nat. gas†	20.8	7	45	39	33,147	7,611.8	230.8
3- 3-53	4-28-53	Air and nat. gas	20.9	5	47	56	59,320	12,052.2	315.7
4-28-53	5-22-53	Air	21	0	47	24	26,357	5,543.7	0
5-22-53	6-14-53	Air and nat. gas	20.9	5	47	23	23,578	4,954.7	116.2
6-14-53	8-18-53	Air and nat. gas	20.9	5	32	65	45,212	9,480.5	242.2
8-18-53	11- 1-53	Air	21	5	30	75	50,667	10,597	0
11- 1-53	11-28-53	Air and nat. gas	20.5	17	30	27	19,829	4,153.6	333.3
			18.3	33		703	574,367	105,351.8	18,662.6

*Burner in operation
**Burner off, combustion in well bore and formation
†Injection changed from 24W to 24WA

The rates of oxygen injection and consumption are shown in Fig. 6 on a weekly basis. The cumulative heat generated by the oxygen consumed is plotted in Fig. 7 together with the Btu equivalent of all hydrocarbon gases injected.

Progress of Formation Heating

From June 14, 1949, to Mar. 11, 1950, well 24 was fired for only 173 days. North well was the first to show results: by December, 1949, its bottom-hole temperature had increased to 200°F, and the quantity of water produced by this well since its completion, increased with the bottom-hole temperature. In the spring of 1950, the following production sequence occurred: (1) a tight emulsion was produced for several weeks, followed by (2) the production of 40 bbls of 45° API distillate with less than normal amount of water, then, (3) production of a mixture of water and colloidal iron oxide having the appearance of thin red barn paint, and finally (4) a five-fold increase in gas production rate and the production of clear water with a trace of black residual oil having a gravity of 30° API. The corrosion of well bore equipment during stages (2) and (3) were so severe that plain steel tubing and thermowells were replaced at intervals as short as two weeks. In May, 1950, the lower joint of casing was corroded through. After installing a thermowell and gas sample line, the hole was bridged at the top of the sand and cemented.

By August, 1950, when experiments were discontinued on well 36, temperatures were as follows:

North well, 230°F; East well, 145°F; South well, 120°F; and West well, 180°F.

Sixteen months later, when injection in this area was resumed using West well, temperatures were as follows:

North well, 150°F; East well, 95°F; and South well, 95°F.

Formation temperatures 300 ft distant at the inner ring producing wells were unchanged from the normal 75°F. When South well temperatures reached 250°F in October, 1952, the same production sequence started as was observed when the heat wave reached the vicinity of North well. The "barn paint" stage was reached by South well in December, 1952, after 10 bbls of 42° API oil had been flowed from the well. Failure of the thermowell prevented measurement of well bore temperatures during this period. During January, 1953, the production of live steam from the well prevented repair work so the well was filled with mud. It is assumed that the combustion front then had passed the location of South well.

The same sequence of events occurred in East Well 24 weeks later than at South, leading to the assumption that the combustion front had passed the location of East well by July, 1953.

On Dec. 14, 1952, a cable-tool drilling rig was moved to a location designated as 24WA, 50 ft from West well in the direction of well 25. After cementing casing at 614.5 ft, a rotary coring rig was moved in and the hole cored from a depth of 601 ft (top of cement plug) to a depth of 670 ft. Air was used as the circulating medium to a depth of 654.5 ft, and coring was completed with water as the circulating medium. No trace of oil was visible on the pits during the entire coring operation. The location of the well obviously was behind the combustion front. All recovered core samples of the "oil" sand were red-brown in appearance. Clay inclusions, normally gray in color, were burned brick red. This was also true of the more

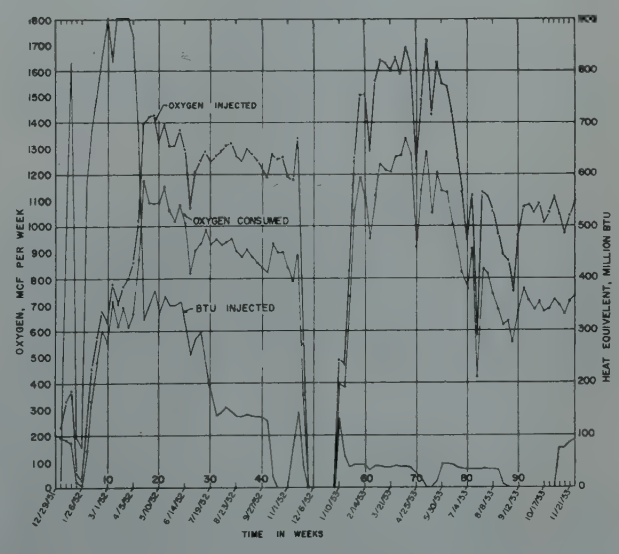

FIG. 6 — WEEKLY RATE OF OXYGEN INJECTED AND CONSUMED.

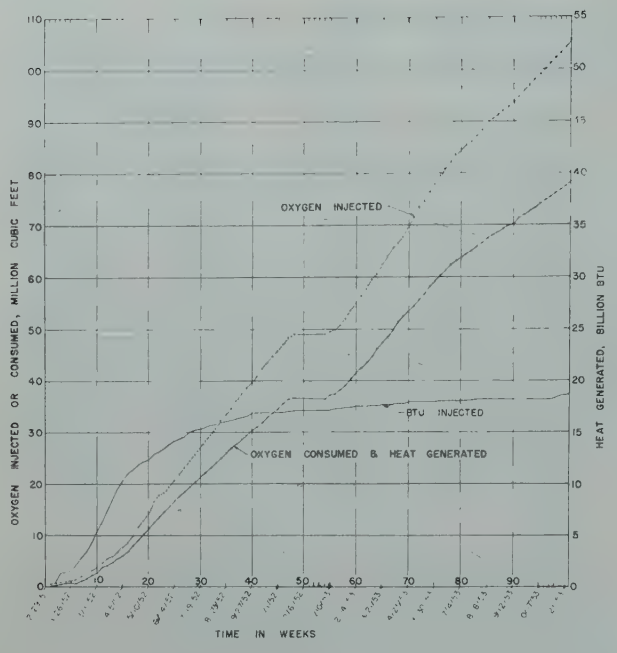

FIG. 7 — CUMULATIVE OXYGEN INJECTED AND HEAT GENERATED.

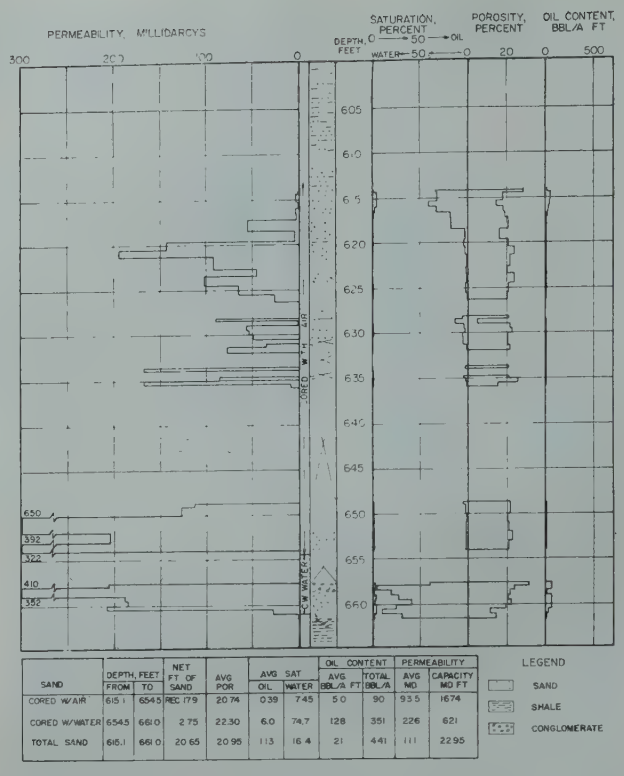

SAND	DEPTH, FEET FROM	DEPTH, FEET TO	NET FT OF SAND	AVG POR	AVG SAT OIL	AVG SAT WATER	OIL CONTENT AVG BBL/A FT	OIL CONTENT TOTAL BBL/A	PERMEABILITY AVG MD	PERMEABILITY CAPACITY MD FT
CORED W/AIR	615.1	654.5	REC 17.9	20.74	0.39	7.45	5.0	90	93.5	1674
CORED W/WATER	654.5	661.0	2.75	22.30	6.0	74.7	128	351	226	621
TOTAL SAND	615.1	661.0	20.65	20.95	1.13	16.4	21	441	111	2295

FIG. 8 — CORE DATA, WELL 24WA.

permeable beds of the "gas" sand. The coregraph of this well is plotted in Fig. 8.

Six other exploratory wells were drilled to define the extent of the heated area. Their locations are shown on Fig. 9. Core data are summarized in Table 2. The locations of wells 24WC and 24WG proved to be behind the combustion front in the trailing edge of the heat wave. The other four wells were drilled ahead of the heat wave. To illustrate the liquid contents ahead of the wave, the coregraph of well 24WB is shown on Fig. 10. By Dec. 1, 1953, well 24WD was producing in the "barn paint" stage and the combustion front was assumed to be at the location of this well and within a few feet of well 24WB. Well 24NA temperatures did not start to increase until January, 1954, and the assumption has been made that this well was located the same distance in front of the wave as was 24WB at the time it was drilled.

The outline of the area traversed by the heat wave to Dec. 1, 1953, is drawn on Fig. 9. The outline includes 0.92 acres and approximates an ellipse in shape. The major axis of the ellipse is along the line between wells 24W and 24WB with the center between wells 24W and 24WA.

EFFECT OF HEAT WAVE ON OIL PRODUCTION

The injection of gas at the relatively high rates (200 MCFD to 1,200 MCFD) required by the combustion experiments affected the oil production rates of the Zoma Tanner property and of each offsetting property. Fig. 2 is a plot of the annual oil production rates of the Zoma Tanner property. An extrapolation by the method of least squares of the exponential decline in production rate from 1938 to 1948 was used as the basis for computing an increased recovery of 16,563 bbls as a result of the experimental work. Similarly, in the period 1948-1953, 10,539 bbls have been gained on the Clyde Tanner property to the North; 3,445 bbls from the Ida Tanner property to the East; and 4,424 bbls from the J. F. Hayden property to the West. Total increased recovery is estimated at 34,971 bbls of oil.

Also plotted on Fig. 2 are the annual oil productions of the six producing wells in the experimental area. Based on the short period prior to the experiment during which the six wells were separately gaged, the 1948 production of the group would not have been more than 2,580 bbls. Extrapolating from this point by using the same percentage decline trend exhibited by the lease as a whole leads to the conclusion that 11,106 bbls or 67 per cent of the oil gained on the Zoma Tanner property have come from the six inner ring wells.

An accurate evaluation of the oil recovered that is directly attributable to the combustion-supported heat wave has not been made for the following reasons:

1. From the weekly rates of gas injected and produced within the pattern during 1952 and 1953, plotted in Fig. 11, it will be noted that the produced gas represents only 60 to 65 per cent of the injected gas. This is

TABLE 2 — SUMMARY OF OBSERVATION WELL DATA

Well	Date Coring Completed	Distance and Direction from West, ft	Coring Fluid	CORE DATA: Gas Sand Thickness ft	Gas Sand Porosity per cent	Gas Sand Permeability md	Gas Sand Oil Content bbl/acre ft	Oil Sand Thickness ft	Oil Sand Porosity per cent	Oil Sand Permeability md	Oil Sand Oil Content bbl/acre ft	Max. Temp. When Drilled °F	Temp. Dec. 1, 1953 °F
24WB	3- 3-53	170 SW	Air	25.15	17.0	51	56	29.7	21.2	160	524	78	200
24WC	4-27-53	100 SW	Air	20.9	20.9	97	25	24.1	23.0	211	8	650	340
24WD	7-24-53	100 NW	Water	14	18.2	50	102	35	21.0	147	464	140	235
24NA	7-15-53	125 NE	Water	17	16.6	98	84	20	19.9	101	562	78	78
24SA	2- 8-54	108 S SE	Water	19	19.3	125	149	23	21.1	179	499	90	
24WG	2-11-54	83 S	Water	29	18.7	73	10.5	24.1	20.4	233	6	530	

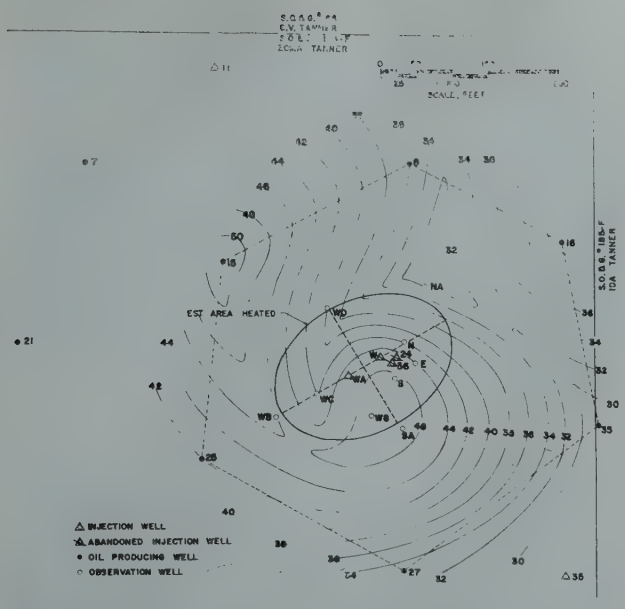

FIG. 9 — EXPERIMENTAL WELL PATTERN WITH OBSERVATION WELL LOCATIONS AND THICKNESS CONTOURS OF GROSS PERMEABLE SAND.

due, no doubt, to the fact that only a small amount of gas was injected outside the pattern, and, therefore, some gas injected within the pattern has found its way between the inner ring wells into the area outside the pattern. A similar phenomenon is to be expected for any oil which is moved.

2. Although gas was injected into all of the permeable formation, oil may have been moved and produced only from the oil sand and not from the upper gas sand.

3. The heat wave was reached only a relatively small portion of the pattern area. The oil removed from the sand behind the heat wave may have been recovered from the inner ring wells, driven out of the pattern area between the producing wells, burned, and/or stored within the pattern ahead of the heat wave as an increased oil content of the formation.

However, there are two encouraging factors at present which indicate that oil has been moved:

1. From the gas/oil ratios of the pattern wells plotted in Fig. 12, it is apparent that the upward trend in evidence during 1952 has been reversed during the last half of 1953. This probably reflects an increased oil content over the unheated area of the pattern, thereby changing the oil-gas relative permeability.

2. From the data shown below:

	Pattern Area	Heated Area
Surface area, acres	5.2	0.92
Net permeable sand, acre-feet	208.0	39.3
Oil containing sand, acre-feet	145.2	28.1
Average porosity, per cent	20.9	20.9
Estimated oil content, as of Dec. 31, 1951, based on 660 bbls/acre-ft oil content on Jan. 1, 1948; bbl	73,822	13,930
Oil produced, January, 1952-December, 1953; bbl	10,548	

The average oil content of the oil sand in the pattern area as of Jan. 1, 1952, was 509 bbl/acre-ft. However, the coregraphs of well 24WB (Fig. 10) and well 24NA show average oil contents of 524 and 562 bbls/acre-ft in spite of the fact that some oil has been produced between Jan. 1, 1952, and the time these wells were drilled. If the difference between the oil content of the pattern as of Jan. 1, 1952, and the oil produced in the 101 weeks of the experiment is considered distributed only over the unheated pattern area, the oil content would be 541 bbls/acre-ft, in good agreement with the data obtained from the two observation wells.

DISCUSSION OF THE HEAT WAVE

The basic facts about the generation and propogation of a combustion-supported heat wave through the formation are pretty well understood, and some experimental data have been derived from the field tests described in this paper. The well established facts may be summarized as follows:

1. There is a heat wave in the formation, in the sense that a high temperature zone moves outward from the injection well, with substantially lower temperatures prevailing in front as well as behind the high temperature zone.

2. The formation behind the high temperature zone has been practically stripped of its original oil content.

3. The peak temperature of the wave must have been slightly over 1,000°F throughout the permeable part of the formation and about 700°F in a shaly section separating the oil sand from the gas sand. This was established by microscopic examination of grains of ankerite in thin sections made from cores from wells 24WA and 24WC, and by comparison with grains of the same mineral in samples from well 24WB which had been subjected to controlled heating conditions in the laboratory.

4. Combustion is actually taking place in the formation, as evidenced by the low oxygen and high carbon dioxide content of the gas produced from the pattern. Whether the residual oxygen in the produced gas is due to by-passing of injected gas through the gas sand, where there is not enough residual fuel to burn all the oxygen, or to the fact that the ignition temperature

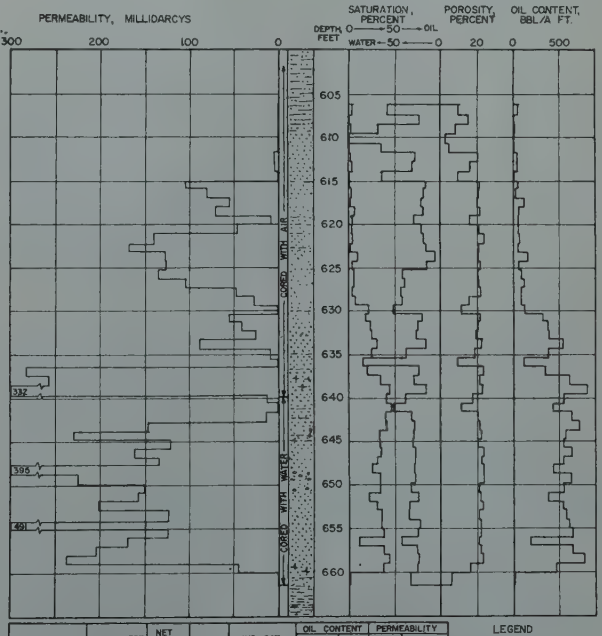

SAND	DEPTH, FEET FROM	DEPTH, FEET TO	NET FT. OF SAND	AVG. POR	AVG SAT OIL	AVG SAT WATER	OIL CONTENT AVG. BBL/A FT	OIL CONTENT TOTAL BBL/A	PERMEABILITY AVG. MD.	PERMEABILITY CAPACITY MD FT
GAS SAND	606.15	631.3	25.15	17.01	5.08	36.74	56	1401	51	1286.6
OIL SAND	631.3	661.0	29.70	21.15	31.80	30.61	524	15565	160	4760.6
SANDY LIMESTONE	661.0	661.6	0.60	6.12	0	31.08	0	0	-0.1	-0.1

FIG. 10 — CORE DATA, WELL 24WB.

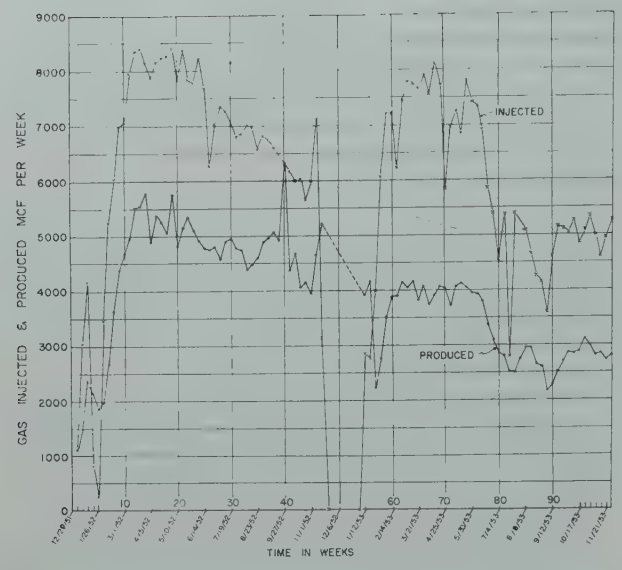

FIG. 11 — WEEKLY RATES OF GAS INJECTION AND PRODUCTION, EXPERIMENTAL WELL PATTERN.

was not reached for all components of the fuel could not be decided from these tests.

However, much detailed information is still lacking, to the point that it is not yet possible to calculate exactly what happens at every point and at every moment in the formation. The missing data concern primarily the heat exchange between the moving fluids and the stationary matrix, and the exact spot where, and extent to which, combustion in the formation occurs. Moreover, the temperature distribution along the wave is also unknown; it cannot be determined even from observation wells, because the drilling and existence of these wells distorts the wave in their vicinity. Temperatures measured in observation wells are always lower than they would be in absence of the well, because of the heat loss through the well bore.

Although heat losses to the over- and under burden are not known exactly, some indications were obtained from measuring temperature gradients just above the permeable formation when drilling wells 24WA and 24WC. The average value found was 5.17°F/ft. Assuming that heat loss to over- and under burden is a steady-state phenomenon occurring only from the heated area, and that gas injection and oxygen consumption were uniform throughout the 101-week test period, the following instantaneous heat balance can be set up:

heat generated = heat loss to over-and under burden + heat available to heat up new formation.

Using the following set of data:

— specific heat of injected gas = 0.02 Btu/scf/°F
— specific heat of matrix: 0.2 Btu/lb/°F
— density of matrix: 137 lb/cu ft
— average formation thickness: 42.7 ft
— average gas injection rate: 812 MCF/D
— average oxygen consumption rate: 111 MCF/D
— heat generated by oxygen consumption: 500 Btu/scf
— peak temperature of the wave: 1,000°F
— thermal conductivity of wet, compressed shale: 1.0 fph units

The heat loss to over- and under burden is found to be 248 Btu/sq ft/day, and the heat balance yields the differential equation.

$$55{,}500{,}000 = 248\,A + 1{,}082{,}000\,\frac{dA}{dt}$$

where A is the heated area at any time t. Integrating this equation

$$A = 224{,}000\,(1 - e^{-0.000229\,t})$$

or, for t = 707 days, A = 33,600 sq ft. The total area swept by the heat wave, including the area cooled down by the injected gas behind the wave, is then 42,880 sq ft or 0.983 acres, in excellent agreement with the area determined experimentally. It is true that the assumptions on which these calculations were based may be optimistic, but in the authors' opinion heat losses did not have a major influence on the propagation of the heat wave during this experiment.

SUMMARY AND CONCLUDING STATEMENT

The experimental work described in this paper has demonstrated the feasibility of creating and propogating a combustion-supported heat wave through an oil-bearing reservoir rock. Reliable techniques for firing an injection well and transferring combustion to the reservoir rock have been developed. The methods used to maintain wave continuity and temperature are described. Propagation of the heat wave has been continuous for a period of time sufficent to allow the statement that no undue difficulty will be encountered in moving a wave over the areas included in ordinary secondary recovery well spacing patterns.

Although it is realized that the work done this far is not complete and that much more remains to be done in the future in order to find precise answers to engineering problems such as heat loss, temperature distribution, well spacing and heat economy, the process looks promising from the viewpoint of recovery efficiency. Two facts must be considered in this respect: First the experiments so far have demonstrated practically complete depletion of the oil-bearing formation in the heated area, a result which cannot be approached by any recovery method now in use; and, second, laboratory results indicate that the oil present in the formation with the exception of a residual of the order

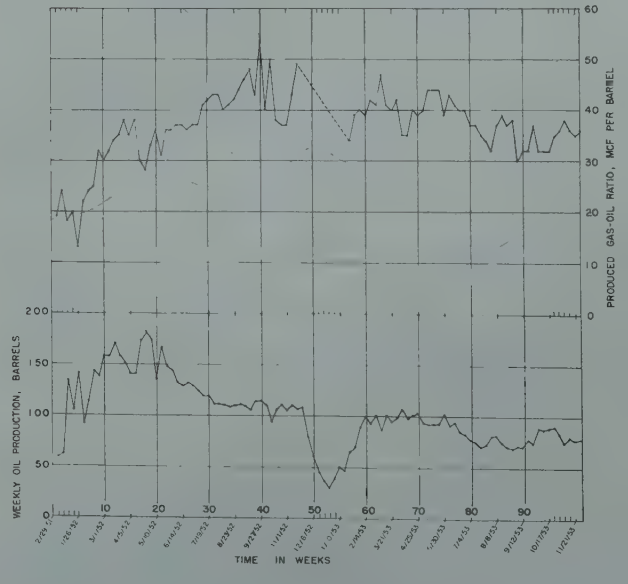

FIG. 12 — WEEKLY OIL PRODUCTION RATES AND PRODUCED GAS-OIL RATIOS, EXPERIMENTAL WELL PATTERN.

of 60 bbls/acre-ft, can be moved by the very front edge of the wave, before ignition temperatures are reached, and hence should be recoverable.

Since the experiments described in this paper were not conducted with economic efficiency in mind, it seems premature to draw conclusions as to the economic factors governing oil recovery by means of a combustion-supported heat wave. As an example, and as a subject for future study, it may be mentioned that recycling of gas produced at higher than atmospheric pressure would have a tremendous influence on the capacity of the compressor plant, and hence, through the compression costs, on the economy of the process.

ACKNOWLEDGMENTS

The authors are grateful to the managements of Sinclair Oil & Gas Co. and Sinclair Research Laboratories, Inc., for permission to publish these experimental data.

The authors wish to point out that their role is chiefly reportorial. Credit for the conception of the heat wave process and for conducting the substantiating experiments belongs to over a dozen members of the Company's Tulsa and Harvey Laboratories.

REFERENCES

1. Reistle, E. C., Jr: "Paraffin and Congealing-Oil Problems," *U. S. Bureau of Mines Bulletin 348* (1932), 89.
2. Howard, Frank A.: "Process for Distilling Crude Oil Underground," U. S. Patent 1,473,348 (Nov. 6, 1923). See also *National Petroleum News*, **16**, No. 4-5 (Feb. 27, 1954), 97.
3. "Shot Gun Shells Used in the Removal of Paraffin and Residue from Oil Wells," *The Producers Monthly*, 8 (April, 1944), 20.
4. Squires, F., and Merriam, E. S.: "A Burner for Underground Generation of Heat," *Producers Monthly*, **16** (May, 1952), 11.
5. Lindsly, B. E.: "Oil Recovery by Use of Heated Gas," *The Oil and Gas Jour.*, **27** (Dec. 20, 1928), 27.
6. Stovall, S. L.: "Recovery of Oil from Depleted Sands by Means of Dry Steam," *Oil Weekly*, **74** (Aug. 13, 1934), 17.
7. Sheinman, A. B., et al: "Gasification of Crude Oil Oil in Reservoir Sands," Neftyance Khozyaistva, 28 (April, 1935), English translation published in *Petroleum Engineer*, **10** (December, 1938) 27, and (February, 1939), 91.
8. Sheinman, A. B.: "Secondary Recovery and Underground Gasification of Oil Deposits," *Novosti Tekhniki*, **15** (1939), 30-3.
9. Lapuk, B. B.: "Heat Treatment of Oil Sands to Increase the Oil Yield," *Azerbaidzhanskoe Neftyance Khoz*, **12** (1939), 10-15.
10. Frey, F. E.: "Method of Recovery of Hydrocarbons" U. S. Patent 2382471 (Aug. 14, 1945).
11. Barton, P. D., and Dougherty, P. F.: "Method of Producing Petroleum," U. S. Patent 2390770 (Dec. 11, 1945).
12. Smith, Robert L., and Watson, Kenneth M.: "Oil Recovery Process," U. S. Patent 2642943 (June 23, 1953).
13. Johnston, Kenneth H., and Riggs, C. H.: "Secondary-Recovery Practices and Oil Reserves in the Eastern Part of the Delaware-Childers Field, Nowata County, Okla.," *U. S. Bureau of Mines Report of Investigation 4019* (December, 1946).
14. Piros, John J., et al: "Gas Burner and Method for Burning Gas in Oil and Gas Wells," U. S. Patent Application.
15. Jones, G. W., Kennedy, R. E., and Spolan, I.: "Effect of High Pressures on the Flammability of Natural Gas-Air-Nitrogen Mixtures." *U. S. Bureau of Mines Report of Investigation 4557* (November, 1949), Fig. 6.

DISCUSSION

H. J. RAMEY, JR.
JUNIOR MEMBER AIME

MAGNOLIA RESEARCH LABORATORIES
DALLAS, TEXAS

During the past few years, intense interest has been shown in the application of thermal energy to oil-bearing reservoirs as a means of increasing the percentage oil recovery. The paper by authors Grant and Szasz is another important contribution to the rather sparse literature in this field of oil recovery by thermal means. The authors have done a fine job of reporting the results from the work of the Sinclair Research Laboratories, Inc., on in-situ combustion experimentation. However, we feel that the authors have been unnecessarily restrictive in their conclusions about the appropriate composition of the injection gas stream and about some aspects of the economics of an in-situ combustion operation, particularly since their conclusions were based on only one experiment conducted under only one set of reservoir conditions. We are of the opinion that a number of field experiments must be conducted in different types of oil sands and under a variety of conditions before it will be possible to understand and evaluate all ramifications of this combustion process.

From the outset of our development work on this process, it has been apparent that, in addition to the use of air as the injection gas, the following schemes of operation might be appropriate under different circumstances:

1. Injection of Fuel Gas — In those cases where the fuel available from the in-place oil is insufficient for supporting combustion, it may be necessary to inject fuel gas. This operation would require careful control of oxygen and fuel gas contents of the injected gas stream so as to avoid mixtures in the explosive range. The injection of an explosive gas could result in an

underground explosion and destruction of the injection well.

2. Use of "Recycle" Produced Gases — Cycling of the produced gases, if discharged from the production wells at elevated pressure, would decrease compression costs but might require pumping larger volumes of gas because of its low oxygen concentration.

3. Oxygen Enrichment of the Injected Gas Stream — Enrichment of the injection gas stream with pure oxygen would offer the advantage of a lower (total gas) injection rate at a lower injection pressure. This type of operation might be important in fields of low effective gas permeability and the economics would depend to a great extent upon the cost of oxygen.

4. Addition of Catalysts to the Injected Gas Stream — The use of catalysts presents many advantages, among which is the selectivity of some catalysts which promote combustion toward carbon monoxide rather than carbon dioxide. This type of catalyst would effectively reduce oxygen requirements and result in lower compression costs.

5. Burning Less than the Full Areal Sweep Possible — As pointed out in our earlier publication, we believe a method of operation involving partial areal burning has considerable merit. This would involve first creating a region of hot sand. Then, combustion would be stopped and the heat contained in the burned region would be transferred to the unburned portions of the reservoir, resulting in an increase in formation temperature in the unburned region. In this method, oil production would be enhanced through a reduction in viscosity and an increase in gas pressure.

Any specific application of the in-situ combustion process would probably involve at least one or more of the above methods of operation, in various possible combinations. More important, such an analysis brings out a point which cannot be over-emphasized in considering the thermal recovery of oil: It will not be possible to stereotype the method of operation. On the other hand, this process will undoubtedly have to be designed and modified to meet the conditions for each and every reservoir. As an example, it may be necessary to prepare or condition a reservoir for gas injection before in-situ combustion can be applied.

Another critical factor which enters into the above five examples of operation involves fuel consumption. Our laboratory investigations have shown that the type of crude oil, the magnitudes of fluid saturations, and the formation characteristics (especially porosity and permeability) have important influences upon the amount of fuel available for combustion from within the formation. In the case of heavy crude oils, the fuel available to the combustion zone is usually plentiful, but in the case of light crude oils, the opposite appears to be true. Light crude oils have such high fluidity that they tend to move away from the combustion front too rapidly to leave adequate amounts of fuel for supporting combustion. Among several remedial steps, an obvious one is to inject a fuel gas with the oxygen-carrying gas in order to supplement the reservoir's low fuel supply. For any specific reservoir, suitable economic analysis will govern the choice of alternative methods of operation.

The Magnolia Petroleum Company's Field Research Laboratories have carried out numerous studies in the laboratory upon the thermal recovery of oil by in-situ combustion. In addition, one field test[1] has been completed and a second field test employing a five-spot well pattern is now in progress. Our work has been directed toward recovery of heavy viscous crude oils that defy economic production by the conventional secondary recovery methods: waterflooding and gas drive. As a result of this work, we do not agree with the authors' implications about the strong dependence of the process economics on restricted ranges of injected gas composition and reservoir oil content. In our opinion, a method of operation involving partial areal burning (method "5" above), with the possible use of oxygen enrichment and catalysts (methods "3" and "4"), will apply to a number of thermal recovery operations, especially for recovery of heavy crude oils.

In conclusion, it is gratifying to know of other investigations in the field of oil recovery by thermal methods. We reiterate that only after a number of actual field experiments on in-situ combustion have been completed can the process be evaluated and the economics of commercial applications be determined.

REFERENCE

1. Kuhn, C. S., and Koch, R. L.: "In-Situ Combustion — Newest Method of Increasing Oil Recovery," *Oil and Gas Jour.*, 52 (Aug. 10, 1953), 92.

AUTHORS' REPLY to H. J. RAMEY, JR.

In answering Ramey's discussion, we would like to point out that our initial approach to the problem of oil recovery has been apparently different from his. Our primary goal, even if it seems set somewhat high, was to recover substantially all of the oil left in the reservoir. Considerations of relative permeability and of mobility ratios seem to indicate that this is not possible by moving the oil in the liquid state; rather, the oil has to be vaporized in order to obtain substantially complete recovery.

As mentioned in our paper, we did not claim to have completely developed our recovery process for all possible reservoir conditions; we stated that more work has to be done before we know all engineering data.

The field test results presented in our paper afford a logical basis for engineering a recovery process which will move oil within the formation as a vapor.

Changing oil from non-mobile status to mobile status is essential. We have outlined one definite method for accomplishing this. It can be done economically by high pressure gas recycling with minimum air usage.

As regards the various alternatives offered by Ramey, they are of course possible, but they do not offer a definite single alternative to the method proposed in this paper. ★★★

A BLOTTER-TYPE ELECTROLYTIC MODEL DETERMINATION of AREAL SWEEPS in OIL RECOVERY by IN-SITU COMBUSTION

H. J. RAMEY, JR.
JUNIOR MEMBER AIME
G. W. NABOR

MAGNOLIA FIELD RESEARCH LABORATORIES
DALLAS, TEXAS

T. P. 3798

ABSTRACT

A blotter-type electrolytic model was utilized to prepare flow diagrams for a field test of the in-situ combustion process. It is pointed out that the areal sweep of a combustion pattern is similar to sweep patterns that would be developed at an infinite mobility ratio, which exists (approximately) across a combustion front because of the complete removal of liquids from the sand behind it.

The precision of the blotter method was tested by comparison with results obtained by other techniques and was found to be satisfactory. The blotter-type model will not furnish as much information as more elaborate and expensive potentiometric models, but its speed of operation and ease of construction make it a highly satisfactory tool to determine areal sweep patterns. A tabulation of sweep efficiency and mobility ratio is furnished for various well geometries.

INTRODUCTION

In connection with the first field experiment with the in-situ combustion method of oil recovery,[5] flow diagrams for the unique well geometry and boundary conditions involved in the subject test were developed. From these diagrams, information concerning the areal sweep and distribution of flow was obtained. A survey of the literature on potentiometric models, utilized to solve two-dimensional flow problems,[1,2,4,6,8,9,10] indicated that the information desired could be obtained by means of a blotter-type model by making certain modifications in the technique. The following discussion describes the application of the modified blotter-type electrolytic model to the solution of the problem of the flow of gases in an oil reservoir for an engineering appraisal of the progress of the combustion front during the first field experiment.

THEORY

Considerable information has been published on the theoretical aspects of electrical model techniques. One author stated that:[6]

> "The models are based on the observation that since the velocity of an ion in an electrolytic system is proportional to the potential gradient, just as the velocity of a fluid particle in a porous medium is proportional to the pressure gradient, the paths of the ions in the electrolytic systems must be similar to those of the fluid particles in a porous medium with the same geometry and equivalent boundary conditions."

This suggestion of a real analogy has been established repeatedly by comparisons of analytic derivations with model results.

The analogy between the movement of a combustion front and the model results is not as apparent, since the combustion process differs from water flooding and gas cycling in that the velocity of the burning front is different from the velocity of the injected fluid at the front in combustion. Analogy between electric current flow and movement of the burning front exists because the local velocity of the burning front is proportional to the air (mass) velocity at this point (assuming frontal temperatures are at least as high as the ignition temperature of the fuel).

Most model studies fall into one of two categories: (1) electron conduction, or (2) ionic conduction models. Examples of these are models which employ as flow media either a thin metal sheet, or a porous blotter saturated with an electrolyte, respectively. Of the two, the porous blotter model, an ionic conduction model, appears to be the most adaptable to the flow problem that results when using in-situ combustion. This problem requires that the mobility of the particles in the model be controlled analogous to the mobility of gas flowing through burned sand of high permeability to gas and then through oil sand of lower permeability to gas. Although the blotter model has heretofore been

[1]References given at end of paper.

Manuscript received in the Petroleum Branch office Jan. 29, 1954. Paper presented at the AIME Annual Meeting in New York City Feb. 13-17, 1954.

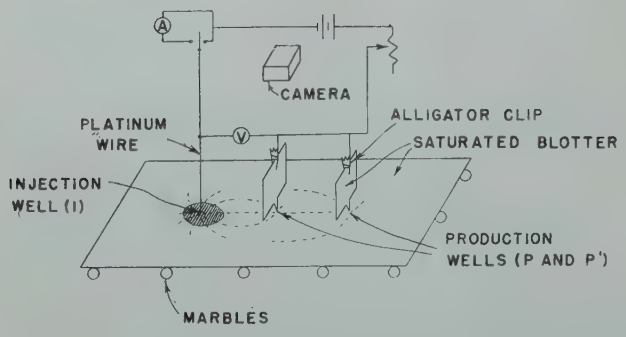

FIG. 1 — SCHEMATIC DIAGRAM OF APPARATUS.

employed solely for study of unit mobility ratio,* it was believed possible to study high mobility ratios by using paints[8] of relatively high conductivity to represent the burned sand. The model has the further advantage that it may be constructed of inexpensive apparatus and operated easily and rapidly. The main disadvantage of this type of model is that it is difficult** or perhaps even impossible to determine the flow streamlines and the potential distribution.

EXPERIMENTAL METHOD

A schematic diagram of the blotter model apparatus is shown in Fig. 1. A plane through a homogeneous oil reservoir is represented by a porous blotter saturated with an aqueous 0.2 N potassium sulfate solution containing about 12 ml of a saturated alcoholic solution of phenolphthalein per liter of salt solution. Direct current enters at the cathode, a 20-gage platinum wire which corresponds to the injection well, flows through the main blotter, and out the smaller blotters. The point of contact between the main and small blotter represents each production well. The voltage drop from the cathode to the point of contact between the main blotter and the nearest production blotter was controlled at 20 v/cm of distance between the contact points of the cathode wire and the anode blotter. Direct current was supplied by a variable output voltage d-c power supply rated at 300 v and 0.1 amps. The blotter was supported by glass marbles to minimize film conduction along the surface of the blotter. A camera, mounted above the plane of the blotter, could be used to record the progress of the ions as indicated by the color change.

The fundamental basis, or chemistry, of the blotter model operation has been well developed by other authors[6,9,10] and will, therefore, be only briefly reviewed here. In principle, the hydroxyl ions migrate from the injection well (cathode), represented by the platinum wire, through the saturated blotter and toward the production well (anode). These OH^- ions react with the penolphthalein indicator to form a red color which allows a record of the path of the ions with increasing time. Simultaneously, the hydrogen ions migrate in the opposite direction, and reduce the red color upon contact with the color front. Judicious choice of the size of the small production well blotter allows the OH^- ions to reach the point of contact between the small and large blotters representing the production well, before the H^+ ions move from the alligator clip supporting the small blotter to the contact point with the main blotter. Usually the production well blotters were constructed as a square with sides equal to the well spacing. It would be possible to have any number of producing wells by using additional contacting blotters.

The color front must move at a rate greater than the rate of diffusion of the ions in the saturated blotter to prevent a fuzzy appearance at the front. Generally, less than one hour was required to run a pattern with a 3 to 6 cm well spacing, the time depending upon the voltage gradient employed.

The infinite mobility ratio studies were accomplished by painting succeeding incremental frontal shapes with conductive silver paint,[8] and advancing the front by small increments. This technique was quite convenient inasmuch as the paint could be applied precisely and it dried rapidly. The progress of the fronts in infinite mobility ratio studies were not photographed, because the series of painted blotters furnished a permanent record which could be traced or copied for enlargement. An alternate method of operation was investigated which involved cutting metal templates to the shape of the succeeding fronts; this technique gave results comparable to the conductive paint method, but was far slower.

Model studies were run for an isolated two-spot well pattern for both the unit and infinite mobility ratios, an isolated three-spot well pattern for the infinite mobility ratio, and the combustion field test well pattern for both unit and infinite mobility ratios.

MOBILITY RATIO

Early in the development of the "in-situ" combustion oil recovery method, it appeared that the flow of gas in the combustion process might be somewhat analogous to the flow involved in gas injection and water flooding. However, the combustion process is unique in that the velocity of the burning sweep front is different from the velocity of the injected air at the combustion front. Analogy does exist, since the local

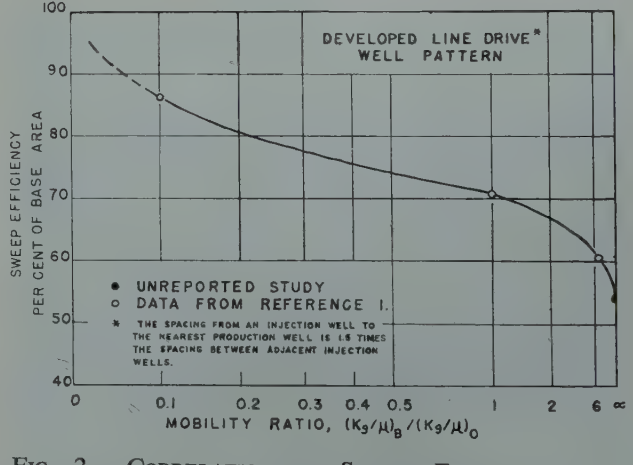

FIG. 2 — CORRELATION OF SWEEP EFFICIENCY AND MOBILITY RATIO FOR A DEVELOPED LINE DRIVE FLOW PATTERN.

*"Mobility ratio" is defined as the ratio of the mobility of the gas in the burned zone to the mobility of the gas in the unburned oil sand. Symbolically speaking, mobility ratio is $(k_g/\mu_g)_B/(k_g/\mu_g)_o$.

**Although flow streamlines are not determined directly from a blotter study, the flux of gas flow along an interface in the case of infinitely high mobility ratio can be calculated since the interfaces are isopotential surfaces. Flow streamlines necessarily are perpendicular to such an isopotential surface.[7]

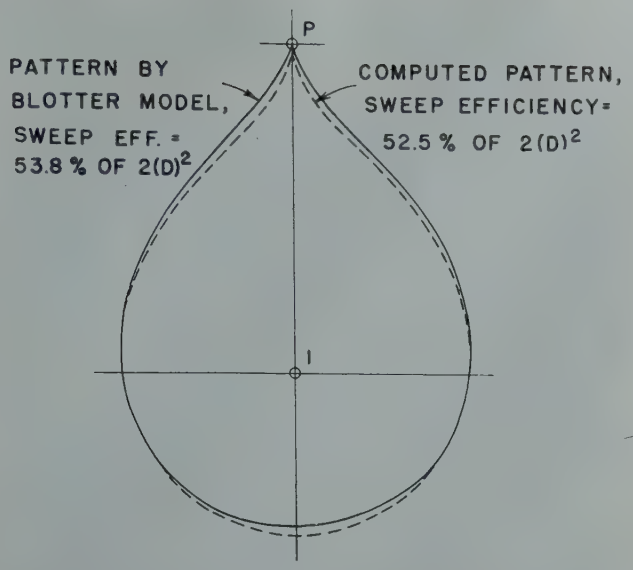

FIG. 3 — COMPARISON OF AREAL SWEEP AT BREAKTHROUGH FOR A COMPUTED AND EXPERIMENTAL ISOLATED TWO-SPOT PATTERN AT UNIT MOBILITY RATIO.

velocity of the burning front is proportional to the air mass velocity at the same point in question.

It was also visualized that the frontal interfaces in the combustion process would be somewhat unique in that the burned region would be at essentially constant pressure and result in an isopotential front. Since it was known that the mobilities in the regions behind and ahead of the front influenced the areal sweep,[1] flow diagrams were developed for the limiting case of the infinite mobility ratio, i.e., wherein the mobility of the gas flowing behind the front was infinitely greater than the mobility of the gas flowing ahead of the front. Results of earlier studies[1] coupled with the results from an unreported study indicate that the mobility ratio can have an extreme effect upon areal sweep efficiency. For example, in a developed line-drive well pattern, sweep efficiency decreases from 87 per cent to 61 per cent for a ratio increase from 0.1 to 10, but decreases only to 55 per cent as mobility ratios go to infinity. This is illustrated in Fig. 2.* If one considers the flow of hot combustion gases from the burned section of the reservoir into relatively cold and unburned oil sand, the mobility ratio during a combustion operation would vary but would normally be expected to be higher than 10. Consequently, in view of the precision possible with an electrolytic blotter model (which will be indicated in the next section), it appears that flow information obtained at an infinite mobility ratio can be applied to in-situ combustion and should give a conservative value for the theoretical sweep efficiency.

*These data were plotted on semi-arctangent coordinates which are very useful for plotting functions that approach a finite limit asymptotically as the variable approaches infinity. The arctangent scale is based upon the equation:

$$L = \frac{2}{\pi} L_{max} \arctan \frac{M}{0.120\pi}$$

L is the linear distance along the scale measured from the origin; L_{max} is the length of the scale from zero to infinity; M is the value of the variable plotted, the mobility ratio in the present case. The scale modulus, 0.120π, may be changed for best presentation of any particular set of data.

BLOTTER MODEL RESULTS

Initial experimental efforts were concerned with reproducing previously reported results[9,10] in order to establish the precision of the technique. Fig. 3 presents the maximum areal sweep for an isolated two-spot well pattern at unity mobility ratio determined by a blotter study as compared to the computed pattern.[6] The difference between the experimental pattern area sweep efficiency (53.8 per cent) and the computed pattern sweep (52.5 per cent) was 1.3 per cent.

Since no computed patterns were available at infinite mobility ratio, the blotter technique was tested against the results of a model study conducted in a tank-type potentiometric model, wherein succeeding frontal interfaces had been represented by bent strips of a metal conductor. A comparison is made in Fig. 4, which indicates that the difference between the blotter model pattern sweep (66.5 per cent) and the corresponding tank model study sweep (62.0 per cent) is 4.5 per cent. This was considered to be satisfactory agreement.

Fig. 5 presents the areal sweep diagram for the isolated two-spot well pattern at infinite mobility ratio. The sweep efficiency for this pattern was 27.7 per cent of the area represented by 2 (well spacing)², where the well spacing is the distance from the injection to the production well. This sweep efficiency is 24.8 per cent lower than the corresponding unit mobility "breakthrough" sweep of 52.5 per cent.

Fig. 6 presents the areal sweep diagram for a modified two-spot well pattern at unit mobility ratio, wherein the boundary conditions include the addition of a producing well located in-line and one well-spacing further from the first production well. This well pattern is the same as that employed in the field test of the in-situ combustion process reported in reference 5. The areal sweep efficiency was 46.1 per cent, which is 6.4 per cent lower than the isolated two-spot sweep of 52.5 per cent reported in Fig. 3.

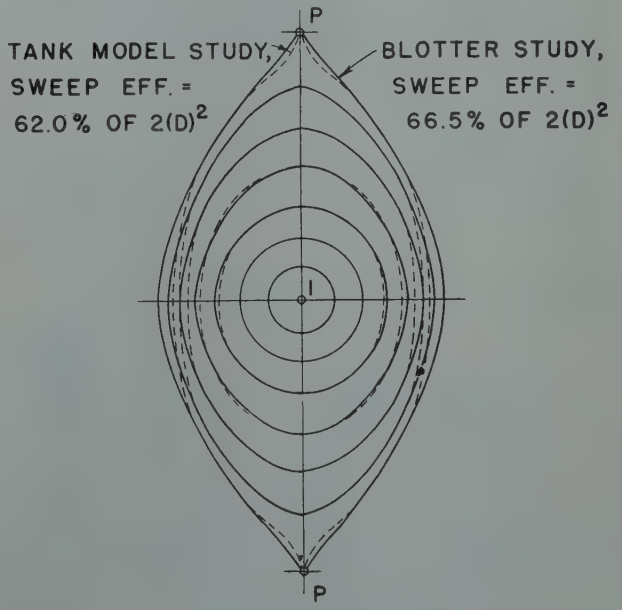

FIG. 4 — COMPARISON OF BLOTTER AND TANK MODEL EXPERIMENTAL AREAL SWEEP DIAGRAMS FOR AN ISOLATED, THREE-SPOT WELL PATTERN AT INFINITE MOBILITY RATIO.

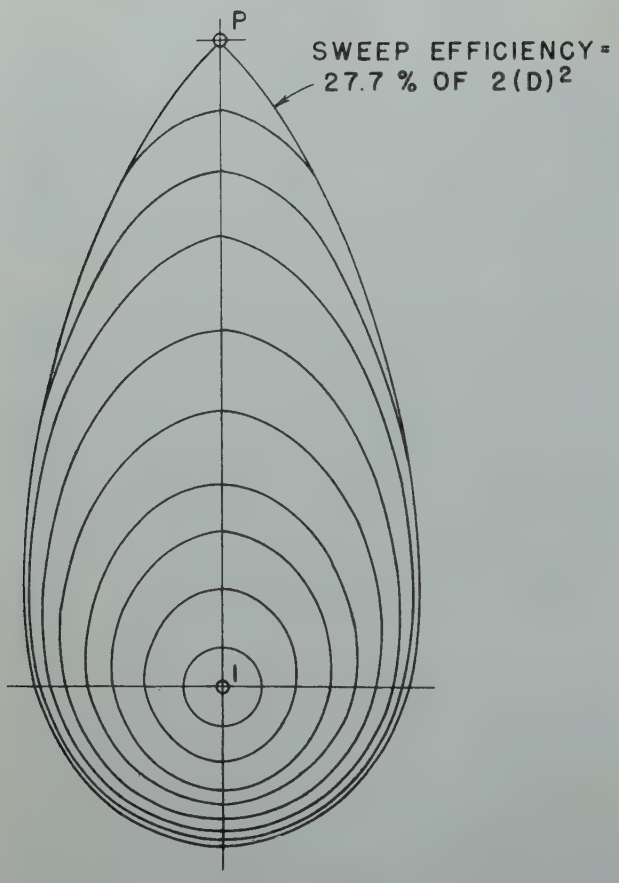

FIG. 5 — AREAL SWEEP DIAGRAM FOR AN ISOLATED, TWO-SPOT WELL PATTERN AT INFINITE MOBILITY RATIO.

Fig. 7 is a flow diagram for the same well pattern as shown in Fig 6, but presents the sweep patterns at infinite mobility ratio. The maximum sweep at breakthrough is 20 per cent, which is 26.1 per cent lower than the corresponding unit mobility ratio sweep of 46.1 per cent reported in Fig. 6, and 7.7 per cent lower than the corresponding sweep of 27.7 per cent for an isolated infinite mobility ratio two-spot pattern.

The foregoing results on areal sweep efficiencies are tabulated below, together with a comparison of the data plotted in Fig. 2 on a developed line drive pattern:

Mobility Ratio	Sweep Efficiencies for Various Well Patterns, Per Cent of Base Area					
	Developed Line-Drive	Isolated Two-Spot		Isolated Three-Spot		Combustion Three-Well Test Pattern
	Pot. Model	Calc	Blotter	Pot. Model	Blotter	Blotter
0.1	86.6					
1	70.8	52.5	53.8	78.5*		46.1
10	61.0					
∞	54.4		27.7	62.0	66.5	20.0

*Calculated value.

CONCLUSIONS

Clearly, the most important conclusion drawn from this study is that the heretofore unreported infinite mobility ratio is approximately a condition one might expect in some in-situ combustion operations. As such, flow diagrams could be quite important and also necessary in the estimation of areal sweeps involved in this type of operation.

Secondly, the blotter-technique may be utilized successfully to obtain high quality areal sweep information for the infinite mobility ratio, rapidly, and with relatively inexpensive apparatus. It is emphasized that other useful information such as flow streamlines and potential distribution may be obtained from more elaborate models. Additional work utilizing tank-type potentiometric models has been undertaken more recently in the study of two-dimensional flow problems as related to in-situ combustion.

In conclusion, it is emphasized that the areal sweep efficiencies reported in this paper in connection with the in-situ combustion oil recovery process cannot be taken in the same sense that areal sweep efficiencies are applied to water flooding to predict ultimate oil recoveries. One main goal of the combustion recovery process is to enhance oil production by means of a reduction in oil viscosity through increased formation temperature. It is conceivable that this beneficial effect could result from burning less than the maximum possible sweep. Further, there is only the result of one actual field test of the new recovery process upon which to base the use of this highly idealized approach to the problem of predicting the effect of burning upon an actual oil reservoir.

ACKNOWLEDGMENT

Acknowledgment is hereby made to the management of the Field Research Laboratories, Magnolia Petroleum Co., for permission to publish this investigation. The writers are further grateful to Rodman Jenkins

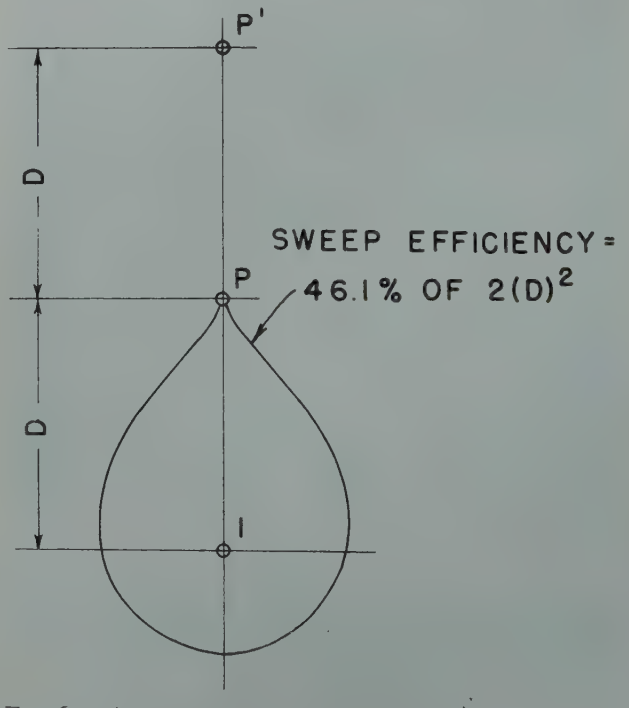

FIG. 6 — AREAL SWEEP AT BREAKTHROUGH FOR A MODIFIED TWO-SPOT PATTERN AT UNIT MOBILITY RATIO ILLUSTRATING EFFECT OF AN ADJACENT PRODUCING WELL.

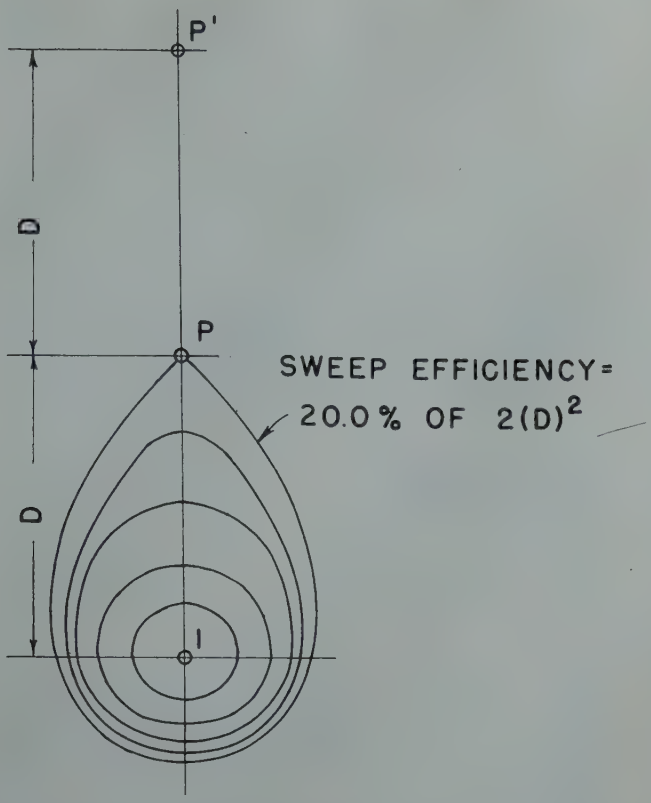

FIG. 7 — AREAL SWEEP DIAGRAM FOR A MODIFIED TWO-SPOT PATTERN AT INFINITE MOBILITY RATIO ILLUSTRATING EFFECT OF ADJACENT PRODUCING WELL.

and William L. Wahl for many helpful suggestions in carrying out the model study and preparation of this manuscript.

REFERENCES

1. Aronofsky, J. S.: "Mobility Ratio — Its Influence on Flood Patterns During Water Encroachment." *Trans.* AIME (1952), **195**, 15.
2. Botset, H. G.: "The Electrolytic Model and Its Application to the Study of Recovery Problems." *Trans.* AIME (1946), **165**, 15.
3. Brunetti, C., and Curtis, R. W.: *Printed Circuit Techniques,* NBS Circ. 468, USDC (Nov. 15, 1947).
4. Horner, W. L., and Bruce, W. A.: *Secondary Recovery of Oil in the U. S.* (1950), 195.
5. Kuhn, C. S., and Koch, R. L.: "In-Situ Combustion — Newest Method of Increasing Oil Recovery," *Oil and Gas Jour.* (Aug., 1953), **204**, 92.
6. Muskat, M.: *The Flow of Homogeneous Fluids Through Porous Media,* (Sec. Pr.), J. W. Edwards, Inc., Ann Arbor (1946).
7. Phillips, H. B.: *Vector Analysis,* John Wiley and Sons, Inc., New York (1944).
8. Swearingen, J. S.: "Predicting Wet-Gas Recovery in Recycling Operations," *Oil Weekly* (1939), **96**, 30.
9. Wyckoff, R. D., Botset, H. G., and Muskat, M.: "The Mechanics of Porous Flow Applied to Water-Flooding Problems," *Trans.* AIME (1933), **103**, 219.
10. Wyckoff, R. D., and Botset, H. G.: "An Experimental Study of the Motion of Particles in Systems of Complex Potential Distribution," *Physics,* (1934), **5**, 265.

NOMENCLATURE

$(k_g)_B$ = effective permeability of burned sand to gas, millidarcys
$(k_g)_O$ = effective permeability of unburned oil sand to gas, millidarcys
$(\mu_g)_B$ = viscosity of gas in burned sand, centipoise
$(\mu_g)_O$ = viscosity of gas in unburned oil sand, centipoise
D = well spacing, feet
I = injection well
M = mobility ratio, $(k_g/\mu_g)_B \div (k_g/\mu_g)_O$
P, P' = production well ★★★

THE EFFECT of SURFACE and INTERFACIAL TENSIONS on the RECOVERY of OIL by WATER FLOODING

HARVEY T. KENNEDY
ERASMO T. GUERRERO
MEMBERS AIME

A&M COLLEGE OF TEXAS
COLLEGE STATION, TEX.

T. P. 3796

ABSTRACT

In this investigation, the effects of the surface tension of brine and the interfacial tension between oil and brine on the recovery of oil by water flooding of Woodbine sand were studied. Variation of the surface forces was obtained by the addition of small amounts of commercially available chemicals, which did not appreciably change the surface tension of the oil.

Fourteen surface-active agents, which were found to be effective in lowering the surface and interfacial tensions, were further investigated to determine the extent of their adsorption by the Woodbine Sand cores. It was found that adsorption was sufficient in all cases to prevent any substantial concentration of chemical at the flood front. The flow system was, therefore, brought to equilibrium with definite concentrations in the flood water by circulation before each test. The data thus have no relation to the results obtainable by using the chemicals in full-scale water floods, but should be helpful in predicting the performance of surface-active chemicals which are not lost by adsorption, if such can be found.

Flow tests were made on various concentrations of six chemicals selected from the 14 investigated for surface activity and adsorption, with and without the presence of gas in the core. It was found that lowering the interfacial tension had a tendency toward reducing the recovery of oil and that the reduction of the surface tension of the brine had little or no effect. A substantial beneficial effect, however, resulted from the presence of gas in the cores.

INTRODUCTION

The movement and distribution of crude oil in a porous medium are governed by such factors as surface and interfacial tensions, viscosity of the oil, pore size configuration, and wetting characteristics of the medium. The knowledge of the part played by each of these factors is limited. If the oil is assumed to be distributed in droplets whose movement is restricted only by the pore openings, the following equation may be applied:

$$\triangle P = 2\Upsilon(1/r_1 - 1/r_2) \quad . \quad . \quad . \quad . \quad . \quad . \quad . \quad . \quad (1)$$

In this equation $\triangle P$ is the pressure drop necessary to force an oil droplet through the construction, Υ is the oil-brine interfacial tension, r_1 is the radius of curvature at the forward and smaller end of the deformed droplet, and r_2 is the larger radius. This equation neglects the effects of viscosity, as a static or near static condition is assumed. It would apply equally well for a bubble of gas in liquid if Υ were taken as the surface tension of the liquid. This relation shows that droplets can be more easily displaced if the interfacial tension is decreased.

The displacement of oil from the surface of a sand particle may also be considered from the basis of selective wetting assuming that the oil droplets are smaller than the pore constructions and that the sand surfaces may be considered as planes. A relation of the forces involved can be derived from Dupre's equation to give:

$$W_{os} = \Upsilon_{ow}\,(1 + \text{Cos}\,\theta) \quad . \quad . \quad . \quad . \quad . \quad . \quad . \quad . \quad (2)$$

where

W_{os} = Work of adhesion between the sand and the oil
Υ_{ow} = Oil-water interfacial tension
θ = Contact angle
Υ_{os} = Oil-solid interfacial tension

This equation would indicate that the displacement of oil from a sand surface is more readily obtained when the water-oil interfacial tension is reduced provided the contact angle remains constant. Evidently, however, the values of Cos θ may vary along with the water-oil interfacial tension due to changes in the other surfaces of the system.

The above theoretical considerations suggest that perhaps even the static behavior of a dispersed oil phase in a porous medium is considerably more complex than may be inferred by the simple systems

[1]References given at end of paper.

Manuscript received in the Petroleum Branch office July 31, 1953. Paper presented at the Petroleum Branch Fall Meeting at Dallas Oct. 19-21, 1953.

presented. In the present investigation, therefore, the effect of brine-gas surface tension and water-oil interfacial tension upon the recovery of oil by water flooding for a system was determined empirically.

Many chemicals which affect the surface forces of the phases present in reservoirs have been added or proposed for addition to flood waters. Nutting[1,2] and Beckstrom and Van Tuyl[3] employed inorganic acids, bases, and salts. Most of these solutions showed no appreciable difference in recovery when compared to a normal water flood except for the dilute solutions of salts formed by the reaction of a strong base and a weak acid. They claimed that this type was effective in increasing the recovery of oil by water flooding.

In the early 1930's work was begun at the Pennsylvania State College on the use of wetting agents to increase oil recovery. In 1934 this[4] laboratory reported increased oil recoveries in waterflooding experiments amounting to as much as 15 per cent by using wetting agents such as sodium sulfo-resinoleate, oleo-glyceryl-sulfates, Gardinol WA, Mapromal Special and Igepon T. In 1936 further tests[4] showed that 4 per cent additional oil could be recovered using Igepon T in the water after normal flooding to the point where no more oil was produced. Further experiments[4] were carried on in 1937, using Ninal No. 555.

In 1947 Terwilliger and Yuster[5] published results that disagreed with the work previously performed. These investigators performed waterflood experiments using both water-soluble and oil-soluble surface-active chemicals. Their results showed that no additional recovery could be obtained by adding these agents to the flood water. Furthermore, their results indicated an excessive amount of adsorption occurring in the case of every chemical tested.

Based on encouraging laboratory tests Breston and Johnson,[6] conducted four field tests with wetting agents and reported favorable results. They claimed increases in production over a limited period of time in excess of 20 per cent.

Laboratory and field tests performed by Morgan, Prusick, and Torrey[7] resulted in their concluding that clear-cut benefits could be obtained by the use of surface-active agents in waterflooding operations.

More recently work has been done on the use of surface-active agents in waterflood operations by Moore and Blum[8] and Caro, Calhoun, and Nielsen.[9] The former did their work with Alundum and Yates sandstone cores and concluded from experimental and theoretical evidence that no increase in oil recovery should be expected from water-wet sands by the use of surface-active agents in the flood water. They did find, however, that some additional recovery could be expected in oil-wet sands.

Caro, Calhoun, and Nielsen[9] did their work on Bradford, Allegheny, and Berea sandstone cores. Their data show additional recoveries due to the wetting agent solutions ranging from a fraction of a per cent up to approximately 7 per cent.

In the present work no agent was found effective in lowering interfacial or surface tensions which was not highly adsorbed on the surface of the sand grains which make up the reservoir rocks. This adsorption has been shown to be a major factor in preventing the movement of chemical at the flood front where it is needed. Although adsorption is mentioned in a few of the investigations cited, it has not been eliminated or corrected for in any of them. Consequently, it appears that in none of the tests reported in the literature cited was there an actual reduction in the surface or interfacial tensions at the flood front. In the present work, this difficulty was overcome by first bringing to equilibrium the fluids and sand surfaces.

DESCRIPTION OF MATERIALS

Cores

In this work two outcrop Woodbine Sand cores, approximately 2-ft long and 2-in. square, were used. Based on microscopic examination the sandstone appeared to be composed chiefly of medium to fine silica grains, iron oxide particles, and clayey materials. The general core data obtained on these cores are shown in Table 1.

Oil, Gas and Brine

The crude oil used for these experiments was obtained from the East Texas oil field and had not been subjected to any type of chemical treatment. As received at the laboratory this oil had a gravity of 39.9° API. For the flow tests this crude oil was saturated with a gas having the composition shown in Table 2.

Synthetic East Texas field brine was used for most of the tests. It was prepared using distilled water and all the components of the East Texas brine except the sodium bicarbonate. This latter component was excluded because in the initial tests it tended to precipitate on the sand grains. The compositions of East Texas field brine and brine used in the tests are shown in Table 3.

Surface-Active Chemicals

Fourteen surface-active chemicals were used in this work. The chemicals by number, trade name, and ionic activity are shown in Table 4. The chemical constitution and properties of these chemicals can be found in the technical literature.

DESCRIPTION OF EQUIPMENT AND PROCEDURE

Density

As part of the supplementary data required in this work, it was necessary to determine the effect of pressure on the densities of saturated and undersaturated East Texas crude oil and synthetic East Texas brine. In the case of oil this was accomplished with the aid of a calibrated metal bomb with a capacity of 262.5 cc.

TABLE 1 — GENERAL CORE DATA

Property	Core A	Core B
Pore volume, cc	517	513
Porosity, percent	38.9	38.4
Air Permeability, md.	3,370	3,700
Brine Permeability, md.	3,021	2,300

TABLE 2 — GAS ANALYSIS

Component	An Analysis of East Texas Gas, mol per cent	Gas Used, mol per cent
Methane	38.05	38.05
Ethane	15.40	15.40
Propane	25.70	46.55
Butane	13.75	
Pentane	7.10	

TABLE 3 — BRINE COMPOSITION

Component	East Texas Brine, PPM	Brine Used, PPM
$NaHCO_3$	756	
NaCl	61,840	61,840
$MgCl_2$	1,095	1,095
$CaSO_4$	407	407
$CaCl_2$	3,552	3,552

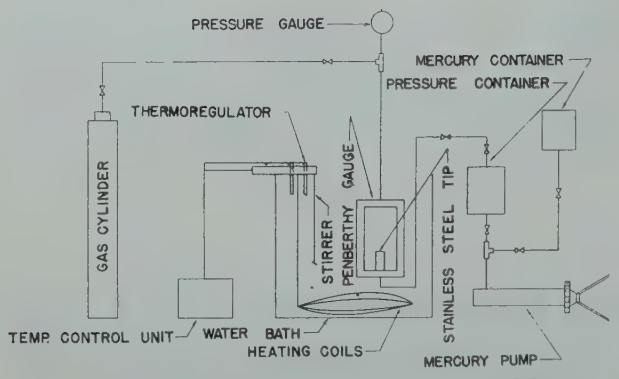

FIG. 1 — FLOW DIAGRAM OF APPARATUS FOR MEASURING SURFACE AND INTERFACIAL TENSIONS.

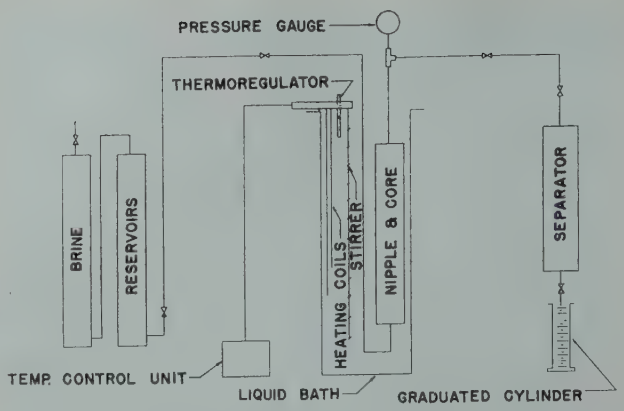

FIG. 2 — FLOW DIAGRAM OF WATER FLOODING APPARATUS.

In determining the effect of pressure on the density of saturated and undersaturated synthetic East Texas brine at 146°F, the only experimental point obtained was that for atmospheric pressure. The remaining data on brine at 146°F, the only experimental point obtained was value and the data of Dodson and Standing[10] which were used to correct the water compressibility constants at different pressures for gas in solution and salinity.

SURFACE AND INTERFACIAL TENSIONS

Surface and interfacial tensions were measured both at atmospheric pressure and 77°F and at higher pressures and 146°F. At atmospheric pressure surface and interfacial tensions were measured with a duNouy interfacial tensiometer. At higher pressures and 146°F the drop weight method was used. The apparatus used is shown diagrammatically in Fig. 1. Both in the measurement of surface and interfacial tensions the recommendations of Hocott[11] in regard to the size of tips were followed.

ADSORPTION

The preliminary adsorption tests on chemicals were performed under atmospheric conditions of temperature and pressure. The equipment used in these tests consisted chiefly of vertical glass tubes 40- to 50-in. long and having an internal diameter of approximately ½ in.

Twenty-five gm samples of unconsolidated Woodbine Sand were placed in each glass column on top of a very small plug of glass wool, used to keep the fine sand from flowing out of the columns. Brine solutions containing a concentration of the chemical to be tested for adsorption were next flowed through this sand. The volume of the effluent was measured and periodically samples of the effluent were taken and checked for chemical content with the duNouy tensiometer. When the effluent gave the same interfacial tension reading against fresh oil as the injected solution, the sand was considered saturated with the chemical at that concentration. The extent of adsorption was calculated from the volume and chemical concentration of the solution passed through the sand.

TABLE 4 — INDEX FOR CHEMICALS

Chemical	Trade Name	Classification as to ionic activity
1	Sterox SE	Non-ionic
2	Span 20	Non-ionic
3	Antarox A-400	Non-ionic
4	Pluronic L-64	Non-ionic
5	Antarox A-200	Non-ionic
6	Ethomid HT/60	Non-ionic
7	Ethomeen S/20	Cationic
8	Ethofat 242/60	Non-ionic
9	Brij 35	Non-ionic
10	Triton X-155	Non-ionic
11	Triton X-100	Non-ionic
12	Ethomid HT/15	Non-ionic
13	Renex	Non-ionic
14	Sterox SK	Non-ionic

FLOW TESTS

In preparation for the flow tests cores were cut to size, coated with Bakelite resin, and set in a section of steel pipe with Wood's metal.

The dead spaces at the ends of the core were measured by determining the weight of the assembly when the spaces were filled with brine and when empty.

Before a flow test was performed, the core was saturated with oil by displacing water with oil in a vertically downward direction. The water displaced from the system was collected in the lower portion of a separator and later measured to determine the amount of oil saturation in the core.

In test runs involving a surface-active agent the chemical was usually placed in the water used to saturate the core. In some of the tests made with oil containing no gas it was dissolved in the oil contained in the system. Circulation of the oil through the initially brine-saturated core for a period of 48 to 72 hours distributed the chemical between the sand, oil, and water. Samples of oil and brine from the system were then obtained and placed against fresh brine and fresh oil respectively. Their interfacial tensions were then measured after a period of 24 hours to determine the equilibrium concentration of chemical in each phase.

Fig. 2 shows the flow diagram of the apparatus used for water flooding. Gas pressure on top of the brine was used to force the flood through the vertical core from bottom to top. The oil flooded out of the core was collected in the upper portion of the separator and later measured with a mercury pump. The rate of flow of the flood was adjusted manually to 600 ± 25 cc/hour with the needle valve on the outlet.

In flow tests where surface-active chemicals were present, their concentration was measured and an amount sufficient to give an equal concentration in the flood water was added. The amount of water used in each flood was 10 pore volumes.

Floods were performed at 1,000, 250, and 125 psig. In the case of the latter two pressures both oil and free gas were present. For these floods production was obtained by pressure depletion from 1,000 to 250 or 125 psig over a period of two hours. A free gas phase

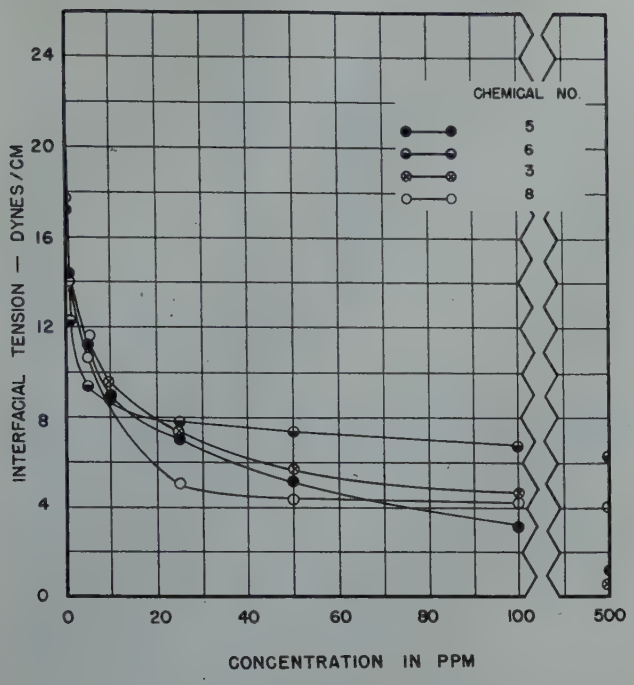

FIG. 3 — THE EFFECT OF VARIOUS CHEMICALS AND THEIR CONCENTRATION ON THE INTERFACIAL TENSION BETWEEN EAST TEXAS CRUDE OIL AND SYNTHETIC EAST TEXAS BRINE AT 77°F AND ATMOSPHERIC PRESSURE.

was formed amounting normally to 25 to 30 per cent of the pore volume.

During these tests six different chemicals were used. To avoid contamination after the use of each chemical, it was necessary to wash the entire system including the core with carbon tetrachloride and water until the washings showed no trace of chemical.

DISCUSSION OF RESULTS

The effect of various chemicals on the interfacial tension between brine and crude oil at atmospheric pressure and 77°F is shown in Fig. 3. These plots show that the chemicals used are very effective in lowering the interfacial tension nearly to a minimum with 10 ppm or less concentration.

ADSORPTION

Fig. 4 shows the adsorption curves for five of the surface-active chemicals tested. In these tests, the sand adsorbed the chemical from solution in the water and in the absence of oil. Later six of the 14 chemicals were selected for use in the flow experiments. It was noticed that some of these chemicals were adsorbed to a lesser degree by the sand grains when the temperature and pressure were increased and an oil phase was present in addition to the water. Table 5 shows the comparison of the adsorption of five surface-active chemicals in the presence and absence of oil and under different conditions of pressure and temperature. It will be noticed that particularly Chemicals 3, 4, and 6 show considerably less adsorption for the sand-brine-oil system at 1,000 psig and 146°F than for the sand-water system at atmospheric pressure and temperature. However, in spite of the much lower adsorption under reservoir conditions and in the presence of oil, it was still prohibitive in magnitude.

TABLE 5 — THE ADSORPTION OF SURFACE-ACTIVE CHEMICALS ON WOODBINE SAND

Chemical	Concentration in Brine, ppm	Adsorption: Sand-Water System at Atm Pres and Temp lb/acre-ft	Adsorption: Sand-Water-Oil System at 1,000 psig and 146°F lb/acre ft
1	100	21,800	15,800
2	10	1,797	1,690
3	250	21,800	2,260
4	75	7,610	1,580
6	25	10,900	1,308

All of the data thus far discussed were supplemental to the waterflooding experiments, which had as their principle objective the determination of the effect of surface and interfacial tensions on the recovery of crude oil by water flooding. It was felt that any other variables affected, such as wettability, would be different for various surface-active chemicals and thus would average out.

Fig. 5 shows the effect of interfacial tension on the recovery of East Texas crude oil by water flooding. As can be noted from the plot, the data for this curve were obtained by using the six chemicals mentioned above. Table 6 in the appendix shows complete data regarding the use of these chemicals in the 17 flow tests plotted in Fig. 5. These tests were not performed in any specific pattern. It can be noted in Table 6 that the two first runs did not involve any chemical. These two were followed by two runs involving high chemical concentrations. This random order should eliminate the effects of any minor changes occurring in the core with time.

Except for the points representing interfacial tensions below 6.5 dynes/cm all of the data for this curve were obtained using undersaturated oil at 1,000 psig having a bubble point of 755 psia. The points for interfacial

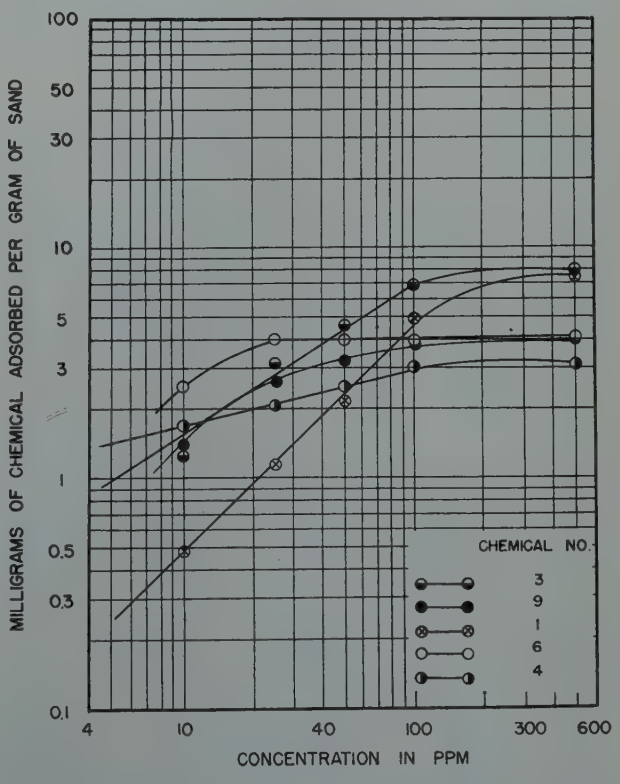

FIG. 4 — THE EFFECT OF CONCENTRATION ON THE ADSORPTION OF SURFACE-ACTIVE CHEMICALS ON UNCONSOLIDATED WOODBINE SAND UNDER ATMOSPHERIC CONDITIONS.

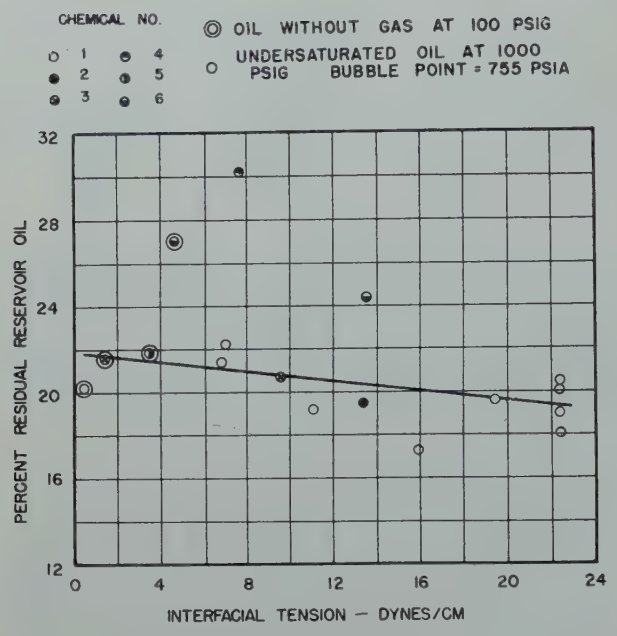

FIG. 5 — THE EFFECT OF INTERFACIAL TENSION ON THE RECOVERY OF EAST TEXAS CRUDE OIL BY WATER FLOODING AT 146°F.

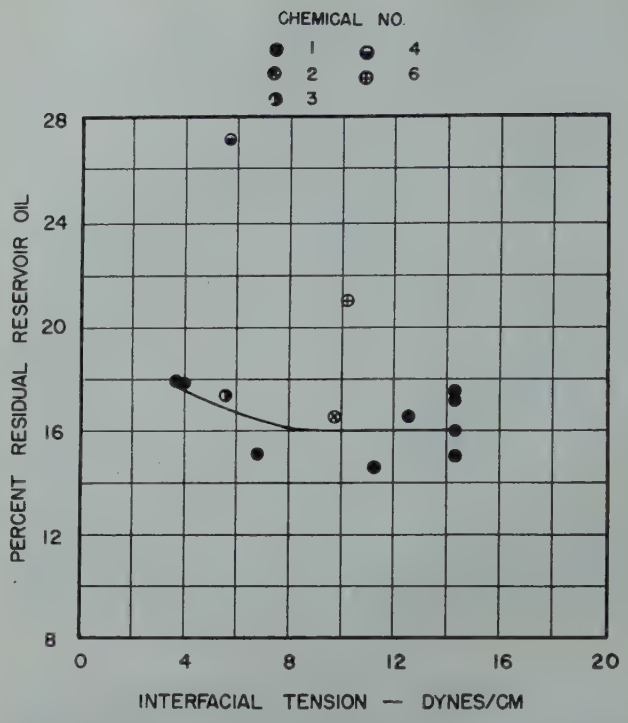

FIG. 6 — THE EFFECT OF INTERFACIAL TENSION UPON THE RECOVERY OF GAS-SATURATED EAST TEXAS CRUDE OIL BY WATER FLOODING FOLLOWING ORIGINAL WATERFLOOD AT 1,000 PSIG AND PRODUCTION BY PRESSURE DEPLETION TO 125 PSIG AT 146°F.

tension values below 6.5 dynes/cm were obtained using oil containing no gas in solution. By using gas-free oil it was possible to lower the oil-brine interfacial tension to 0.4 dynes/cm. The removal of the gas from solution increases the viscosity of the oil from 1 to 5 cp. These values of viscosity were taken from the data of Craze and Buckley[12] and Beal.[13] However, according to the work of Heath[14] the change in viscosity would not affect the recovery as the final water-oil ratios of these tests exceeded 2,000.

It can readily be seen in Fig. 5 that the percentage of residual oil decreases slightly as the interfacial tension is increased. Within the range tested, 0.4 to 22.3 dynes/cm interfacial tension, the difference in percent residual oil is only slightly greater than 2 per cent. At 22.3 dynes/cm interfacial tension it can be seen that the reproducibility is about 2.5 per cent to 3.0 per cent. Thus the effect of interfacial tension upon the recovery of crude oil by water flooding was not much greater than the order of magnitude of the error of measurement.

It will be noticed that the curve of Fig. 5 was drawn without considering the data for Chemicals 4 and 6 which show residuals above 24 per cent. These two chemicals had a tendency to change the wettability of the cores. This was supported in two ways. First, 4 to 6 per cent more water was removed in the oil floods involving these chemicals than in the preceding runs. This indicated partial wetting of the sand by the oil and consequently larger initial oil saturations as a result of the greater amount of water removed. When droplets of the oil used in runs involving these chemicals were tested by the sessile drop method using brine from the same run, partial wetting of the silica by the oil was indicated.

After each water flood performed at 1,000 psig, the pressure was dropped to 125 psig and a second water flood was performed at the lower pressure. This was to determine whether or not the presence of a gas-

TABLE 6 — WATER FLOODING TESTS INVOLVING TWO PHASES, SYNTHETIC EAST TEXAS BRINE AND UNDER-SATURATED EAST TEXAS OIL AT 146°F AND 1,000 PSIG BUBBLE POINT — 755 PSIA

Test No.	Core Used	Per Cent Orig. Oil Sat.	Chem. Used	Equilibrium PPM in Brine	Chem. PPM in Oil	Distribution Grams on Core	γ_{o-w} ** dynes/cm	Per cent Resid Res Oil	Per cent Resid 60°F and 14.7 psia
1	A	72.5	None	0	0	0	22.3	18.0	14.8
2	A	75.6	None	0	0	0	22.3	20.4	16.7
3	A	71.7	1	100	5,500	14.1	7.0	22.2	18.2
4	A	68.7	1	120	6,500	24.1	6.8	21.4	17.6
5	A	66.4	None*	0	0	0	22.3	18.9	15.5
6	A	67.4	1	.5	20	1.48	15.8	17.2	14.1
7	A	67.0	1	3	150	11.8	11.0	19.1	15.7
8	A	57.1	1	150	8,200	30.5	0.4	20.2	19.5
9	A	68.3	1	.02	1	0.5	19.3	19.6	16.1
10	B	71.8	None	0	0	0	22.3	20.6	16.9
11	B	68.8	2	10	130	1.5	13.3	19.3	15.9
12	B	71.4	3	250	250	2.02	9.5	20.8	17.1
13	B	66.9	3	400	400	13.30	1.4	21.7	20.7
14	B	73.1	4	75	50	1.40	7.8	30.4	24.9
15	A	68.7	5	90	90	4.84	3.4	21.9	20.9
16	A	70.0	6	25	25	1.16	13.6	24.3	19.8
17	A	72.3	6	100	100	383	4.3	27.1	25.9

*Chemical from previous run was removed with CCl_4 and fresh brine.
**Oil-water interfacial tension.
FVF determined from the tests above = 1.22
FVF reported for the East Texas Field oil = 1.23
γ_{o-w} Oil-Water interfacial tension

TABLE 7 — WATER FLOODING TESTS INVOLVING THREE PHASES; EAST TEXAS SYNTHETIC BRINE, EAST TEXAS GAS-SATURATED OIL, AND NATURAL GAS TEMP = 146°F PRESSURE = 125 PSIG

Test No.	Core Used	Per cent Orig Oil Sat.	Per cent Orig. Gas Sat.	Equilibrium		Chem Distribution		γ_{w-o} dynes/cm	γ_{w-g} dynes/cm	Per cent Resid Oil at 125 psig	Per cent Resid Oil at Stnd Cond
				Chem Used	PPM in Brine	PPM in Oil	Grs on Core				
1	A	16.2	28.0	None	0	0	0	14.3	60.6	16.0	14.4
2	A	18.3	28.2	None	0	0	0	14.3	60.6	17.5	15.9
3	A	19.9	25.1	1	100	5,500	14.1	4.0	33.4	17.8	16.0
4	A	19.2	24.0	1	120	6,500	24.1	3.7	31.1	17.9	16.2
5	A	17.0	22.6	1	0	0	0	14.3	60.6	15.0	13.7
6	A	15.4	22.1	1	.5	20	1.48	11.2	51.7	14.6	13.3
7	A	17.1	22.5	1	3	150	11.8	6.8	45.2	15.1	13.8
8	A	17.6	22.8	1	.02	1	0.5	12.3	59.4	16.4	15.0
9	B	18.5	26.5	0	0	0	0	14.3	60.6	17.7	16.1
10	B	17.4	25.8	2	10	150	1.5	9.9	56.5	16.4	15.0
11	B	18.7	25.6	3	250	250	2.02	5.8	47.7	17.4	15.9
12	B	27.7	27.9	4	75	50	1.40	5.5	35.8	26.7	24.4
13	A	21.8	27.0	6	25	25	1.16	10.3	52.4	20.9	19.1

FVF determined from the above tests = 1.095
γ_{o-w} Oil-Water interfacial tension
γ_{w-g} Water-Gas surface tension

liquid interface along with the oil-brine interface would tend to lower the residual oil saturation. Normally the additional recovery amounted to only 1 to 2 per cent. And as Figs. 6 and 7 show a reduction of the surface and/or the interfacial tension resulted in only small effects upon the recovery. In these plots as in Fig. 5, the reproducibility is about 3 per cent. Again the curves were drawn without any consideration to the data of Chemicals 4 and 6.

Figs. 8 and 9 show the effect of surface and interfacial tensions upon the recovery of oil by water flooding following production by pressure depletion from 1,000 to 250 psig at a temperature of 146°F. These curves show that a reduction of the surface and interfacial tensions under these conditions does not affect the production of oil by water flooding within experimental error. Although the residual saturations varied from 8 per cent to 21.8 per cent, this does not represent the errors in the method employed, since considerable variations in the wetting properties of the chemicals and the gas saturations before flooding were involved.

As was seen in connection with Fig. 5, the wetting properties are of primary importance in determining residuals. As will be seen later, the gas saturation before flooding is likewise an important variable. Thus, it will be noticed that two runs are shown for an interfacial tension value of 7.6 dynes/cm and a surface tension value of 47 dynes/cm. Run 6 has a 12.3 per cent residual whereas Run 5 has an 8 per cent residual. The two runs differed in the gas saturation present at the beginning of the water floods due, perhaps, to a slight difference in the rate of pressure depletion. The gas saturation for the 8 per cent residual oil run was 18.9 per cent and for the 12.3 per cent residual oil run 24.4 per cent. In addition to this variation, it will be noticed that here, as well as in the other plots discussed above, the data for Chemical 4 shows much less recovery than that for the other chemicals.

Fig. 10 shows the effect of the gas saturation, before water flooding, just mentioned. The close grouping of points about the curve indicates that the gas satura-

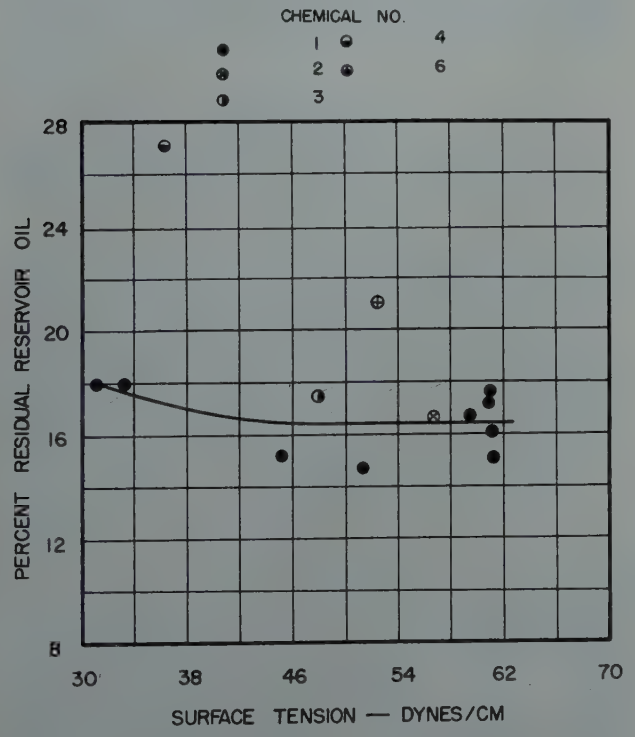

FIG. 7 — THE EFFECT OF BRINE-GAS SURFACE TENSION UPON THE RECOVERY OF GAS-SATURATED EAST TEXAS CRUDE OIL BY WATER FLOODING FOLLOWING ORIGINAL WATER FLOOD AT 1,000 PSIG AND PRODUCTION BY PRESSURE DEPLETION TO 125 PSIG AT 146°F.

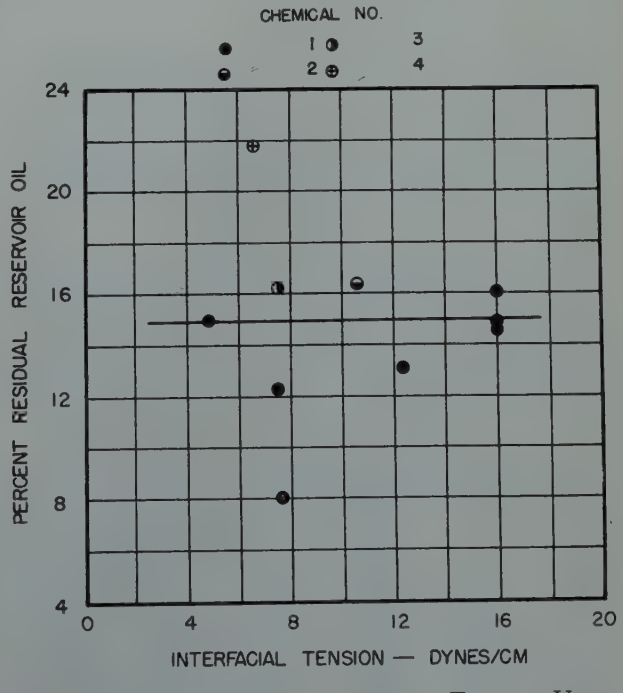

FIG. 8 — THE EFFECT OF INTERFACIAL TENSION UPON THE RECOVERY OF GAS-SATURATED EAST TEXAS CRUDE OIL BY WATERFLOODING FOLLOWING PRODUCTION BY PRESSURE DEPLETION FROM 1,000 PSIG TO 250 PSIG AT 146°F.

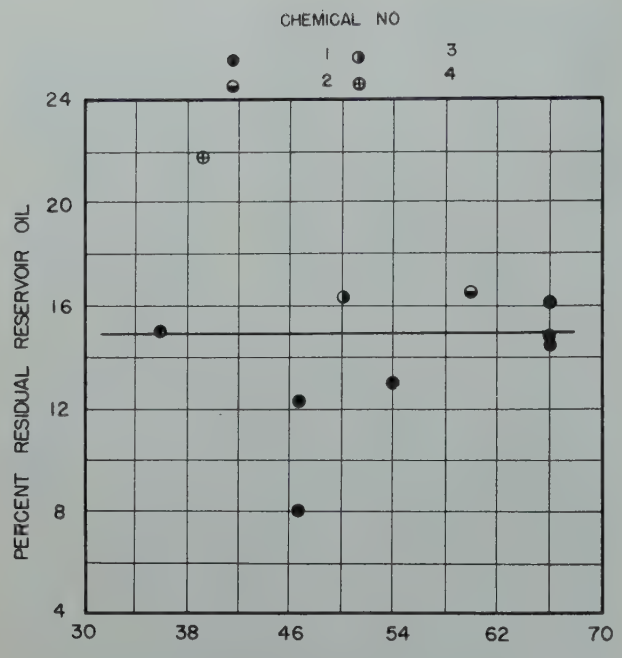

FIG. 9 — THE EFFECT OF BRINE-GAS SURFACE TENSION UPON THE RECOVERY OF GAS-SATURATED EAST TEXAS CRUDE OIL BY WATER FLOODING PRODUCTION BY PRESSURE DEPLETION FROM 1,000 PSIG TO 250 PSIG AT 146°F.

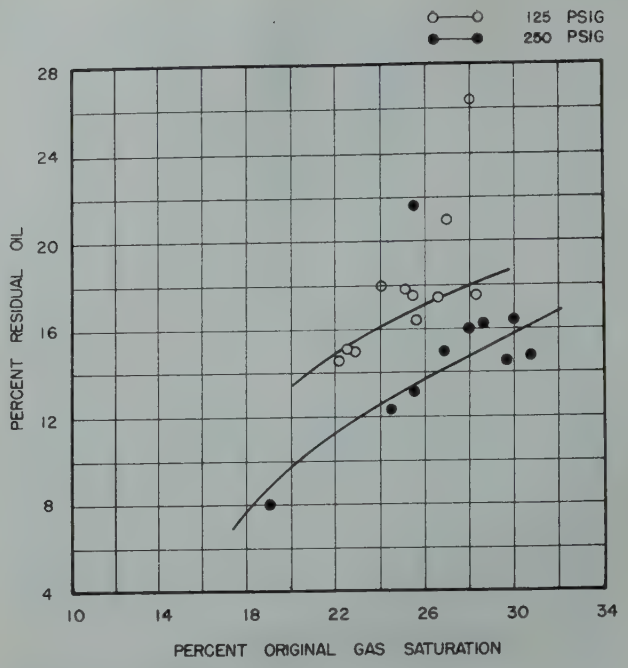

FIG. 10 — THE EFFECT OF ORIGINAL GAS SATURATION ON THE RECOVERY OF GAS-SATURATED EAST TEXAS CRUDE OIL BY WATER FLOODING AT 146°F.

tion is a more important variable than the surface and interfacial tensions of the liquids. It is seen from Fig. 10 that within the range tested the percentage of residual oil decreases as the percentage of initial gas saturation decreases. Here again, the data for those chemicals which tended to make the sand oil-wet were not considered in plotting the curves.

The data from Figs. 5, 6, and 8 are re-plotted in Fig. 11 using as ordinate the stock tank oil equivalent to the reservoir oil residuals previously plotted, by using the formation volume factors given in Tables 6, 7, and 8 of the appendix. These data show that approximately 3 to 4 per cent more recovery can be obtained if gas is present in the porous medium.

Fig. 12 is plotted in a similar manner as Fig. 11 using the data of Figs. 7 and 9. Here it is seen that a greater recovery was obtained by a single water flood following pressure depletion than was obtained for a water flood performed on a core which had been previously waterflooded at a pressure above the bubble point and pressure depleted.

No agreement can be seen between the results of this investigation and the theoretical predictions made by water flooding a core which has been previously that if the oil phase is distributed as droplets in the porous medium, the recovery of the oil should be increased by decreasing the interfacial tensions between the liquids. In the tests described, a slight contrary effect of less production, or no effect at all, is observed. This may signify that the oil does not occur as segregated droplets, as commonly assumed.

CONCLUSIONS

The data obtained from this study support the following conclusions as applied to the conditions under which the investigation was made.

1. Reduction of the interfacial tension between oil and brine reduces slightly the recovery of oil by water flooding above the bubble point.

2. At pressures below the bubble point, in the presence of gas, reduction of interfacial and surface tensions of the liquids has a small or negligible effect on recovery. However, the presence of gas, regardless of the surface and interfacial tensions, exerts a substantial beneficial effect on the recovery.

3. No appreciable additional oil can be obtained by water flooding a core which has been previously

TABLE 8 — WATER FLOODING TESTS INVOLVING THREE PHASES: EAST TEXAS SYNTHETIC BRINE, EAST TEXAS GAS-SATURATED OIL, AND NATURAL GAS TEMP = 146°F PRESSURE = 250 PSIG

Test No.	Core Used	Per cent Orig. Oil Sat.	Per cent Orig. Gas Sat.	Equilibrium		Chem. Distribution		γ_{w-o} dynes/cm	γ_{w-g} dynes/cm	Per cent Resid Oil at 250 psig	Per cent Resid Oil at Stnd Cond
				Chem. Used	PPM in Brine	PPM in Oil	Grs on Core				
1	A	42.2	29.6	None	0	0	0	16.0	63.8	14.5	13.1
2	A	43.1	30.6	None	0	0	0	16.0	63.8	14.7	13.2
3	A	38.7	26.8	1	100	5,500	14.1	4.8	35.7	15.0	13.5
4	A	39.8	25.4	1	0.5	20	1.48	12.3	54.0	13.1	11.8
5	A	39.4	18.9	1	3	150	11.8	7.7	46.4	8.0	7.2
6	A	38.0	24.4	1	3	150	11.8	7.7	46.4	12.3	11.1
7	B	38.2	27.9	None	0	0	0	16.0	63.8	16.1	14.5
8	B	38.3	30.0	2	10	150	1.5	10.5	59.1	16.6	14.9
9	B	38.7	28.3	3	250	250	2.02	7.6	49.9	16.3	14.7
10	B	37.2	25.5	4	75	50	1.40	6.4	38.9	21.6	19.5

FVF determined from the above tests = 1.11

γ_{o-w} Oil-Water interfacial tension

γ_{w-g} Water-Gas surface tension

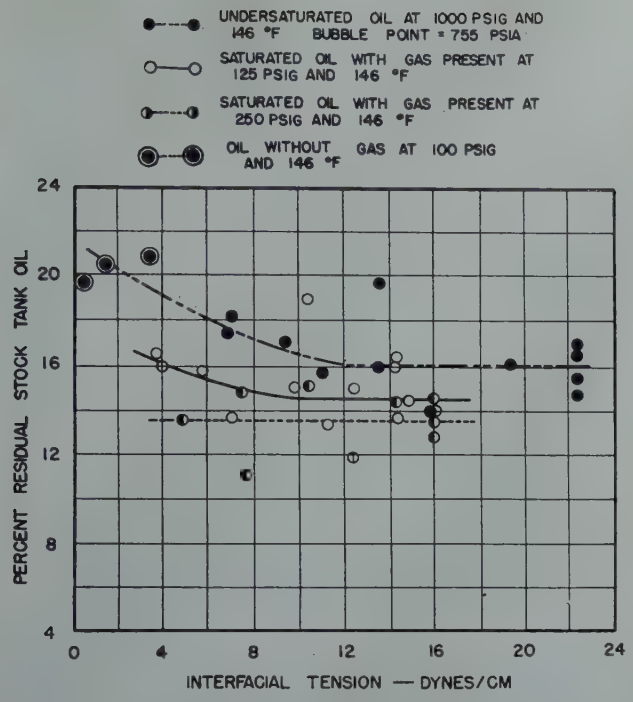
UNDERSATURATED OIL AT 1000 PSIG AND 146 °F BUBBLE POINT = 755 PSIA
SATURATED OIL WITH GAS PRESENT AT 125 PSIG AND 146 °F
SATURATED OIL WITH GAS PRESENT AT 250 PSIG AND 146 °F
OIL WITHOUT GAS AT 100 PSIG AND 146 °F
PERCENT RESIDUAL STOCK TANK OIL
INTERFACIAL TENSION — DYNES/CM

FIG. 11 — A COMPARISON OF RECOVERIES OBTAINED FROM WATERFLOODING EXPERIMENTS WITH VARYING INTERFACIAL TENSIONS

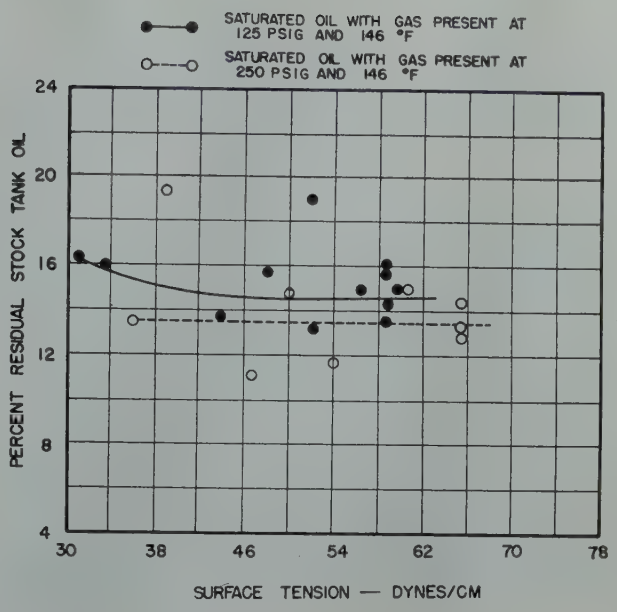
SATURATED OIL WITH GAS PRESENT AT 125 PSIG AND 146 °F
SATURATED OIL WITH GAS PRESENT AT 250 PSIG AND 146 °F
PERCENT RESIDUAL STOCK TANK OIL
SURFACE TENSION — DYNES/CM

FIG. 12 — A COMPARISON OF THE RECOVERIES OBTAINED FROM WATERFLOODING EXPERIMENTS WITH VARYING BRINE-GAS SURFACE TENSION.

waterflooded above the bubble point and pressure depleted.

4. The adsorption of some surface-active chemicals on Woodbine sand is considerably less in a sand-brine-oil system under reservoir conditions than in a sand-brine system under atmospheric conditions. However, all of the chemicals tested are adsorbed in prohibitive quantities.

5. Surface-active agents that change the wettability of a sand from water-wet to oil-wet may reduce the recovery of oil by water flooding as much as 8 per cent.

ACKNOWLEDGMENT

The work performed in this investigation was sponsored by the Magnolia Petroleum Co. through its fellowship funds and by the Texas Engineering Experiment Station through its Project 203. The writers are grateful to these sponsors for their financial contributions without which this work would not have been possible. Thanks are due to the Magnolia Petroleum Co. Field Research Laboratories in suggesting some of the chemicals investigated.

REFERENCES

1. Nutting, P. G.: "Chemical Problems in the Water Driving of Petroleum from Oil Sands," *Ind. Eng. Chem.* (1952), **17**, 1035-36.
2. Nutting, P. G.: "Soda Ash Process for Petroleum Recovery," *Oil and Gas Jour.* (1927), **25** (45), 76, 150.
3. Beckstrom, B. C., and Van Tuyl, F. M.: "Flooding Oil Sands with Alkaline Solutions," *Bull.* AAPG, (1927) **11**, 223-237.
4. Calhoun, J. C., Stahl, C. D., Preston, F. W., and Nielsen, R. F.: "A Review of Laboratory Experiments on Wetting Agents for Water Flooding," *Producers Monthly* (Nov., 1951), **16** (1), 15-23.
5. Terwilliger, P. L., and Yuster, S. T.: "Chemical Agents in Water Flooding," *Oil Weekly* (1947), **126** (1), 54-6.
6. Breston, J. N., and Johnson, W. E.: "Experiments with Wetting Agents in the Bradford Field," *Producers Monthly* (1951), **16** (1), 24.
7. Morgan, L. O., Prusick, J. H., and Torrey, P. D.: "Application of Surface Chemistry to Oil Recovery, Proceedings Fourth Oil Recovery Conference, TPRC (May 8-9, 1952), *Bulletin No. 17, 78.*
8. Moore, T. F., and Blum, H. A.: "Importance of Wettability in Surface-Active Agent Waterflooding," *Oil and Gas Jour.* (1952), **51** (31), 108-111.
9. Caro, R. A., Calhoun, J. C., Jr., and Nielsen, R. F.: "Experiments Show Under What Conditions Surface-Active Agents Increase Oil Recovery," *Oil and Gas Journ.* (1952), **51** (34) 62-3 (86-7).
10. Dodson, C. R., and Standing, M. B.: "Pressure-Volume-Temperature and Solubility Relations for Natural Gas-Water Mixtures," *Drilling and Production Practice,* API (1944), 173-9.
11. Hocott, C. R.: "Interfacial Tension Between Water and Oil Under Reservoir Conditions," *Trans.* AIME (1938-1939), **127** and **132**, 184.
12. Craze, R. C., and Buckley, S. E.: *Drilling and Production Practice,* API (1945), 144.
13. Beal, C.: "The Viscosity of Air, Water, Natural Gas, Crude Oil, and its Associated Gasses at Oil Field Temperatures and Pressures," *Trans.* AIME (1946), **165**, 94.
14. Heath, W. A.: "Influence of Viscosity of Crude Oil on Secondary Recovery," *Secondary Recovery of Oil in the United States,* Second Edition, API (1950), 228-32.

PLUGGING OFF WATER in FRACTURED FORMATIONS

GEORGE C. HOWARD
P. P. SCOTT, JR.
MEMBERS AIME

STANOLIND OIL AND GAS CO.
TULSA, OKLA.

T. P. 3799

ABSTRACT

A field remedial procedure utilizing a kerosene-cement slurry as a water plug-off agent in fractured formations was evaluated both in the laboratory and in the field. This procedure has proved to be capable of effectively shutting off water without causing permanent impairment of the oil production. Success was attributed to the fact that an immobile cement slurry, when placed in a water-producing strata, will set and form an impermeable barrier; whereas when placed in an oil-producing section the cement will retain a relatively high permeability and may be removed by acidizing.

INTRODUCTION

One of the most perplexing problems facing the oil industry is the selective exclusion of water production from oil or gas-producing wells. This problem has been studied by many investigators in an attempt to develop a material that is not only capable of reducing water production but is also capable of being selective in that it will not impair oil production in either fractured or intergranular type reservoirs. A study of these two types of formations indicated that two distinct types of materials for controlling water production might be required — a completely liquid plugging agent for intergranular formations and a semi-liquid or slurry type plugging agent for fractured formations. This paper is limited to the control of water production from fractured formations.

[1]References given at end of paper.

Manuscript received in the Petroleum Branch office Sept. 23, 1953. Paper presented at the Petroleum Branch Fall Meeting in Dallas, Oct. 19-21, 1953.

Discussion of this and all following technical papers is invited. Discussion in writing (3 copies) may be sent to the offices of the Journal of Petroleum Technology. Any discussion offered after Dec. 31, 1954, should be in the form of a new paper.

THEORY

A common source of water in the vicinity of oil bearing rock reservoirs is water which previously has entered and, because of its higher density, generally lies near the bottom of the formation. When the deepest point of penetration of a well into such an oil and water-bearing formation is above the level of the water, and the dynamical gradients due to the flow of oil overbalance the difference in densities between oil and water, water production becomes a problem. Then the water level rises in the shape of a cone and is produced from the lower depths.

Other investigators[1,2,3,4] have developed theories which define the pressure gradients and contours of this cone in a homogeneous formation and have shown that the placement of a plug in the bottom of a well is only slightly effective in temporarily reducing the flow of water.

Assuming that the manner of flow of bottom water from fractured formations to a well is generally similar to the flow in homogeneous formations, then it would be expected that some form of coning, perhaps of less symmetry, would also occur. Then, because of the similarity of the manner of flow of water, placement of a vertical plug in a fractured formation would also probably be ineffectual for controlling water production. However, as has been shown by electric model flow study,[4] the placing of a plug in a well and an impermeable horizontal streak in the formation might prove to be a means for materially reducing or even eliminating water production in a fractured formation.

An indication of the difference in effectiveness between horizontal and vertical plugs based on theory developed from study of the flow of water and oil in rock reservoirs is depicted in Fig. 1. These curves show the expected

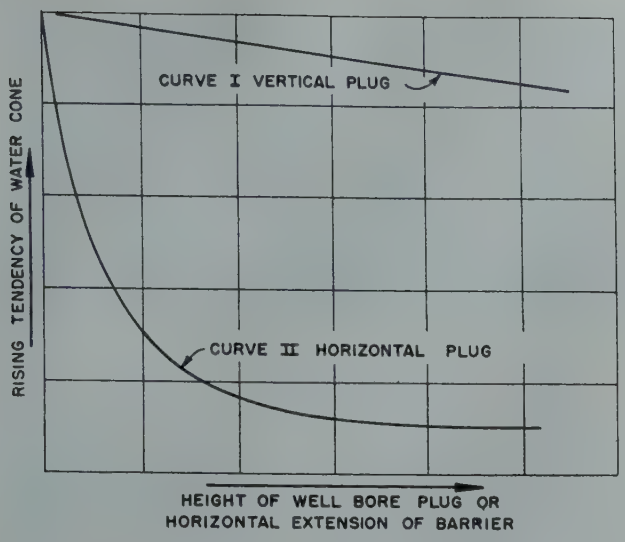
CURVE I VERTICAL PLUG
CURVE II HORIZONTAL PLUG
RISING TENDENCY OF WATER CONE
HEIGHT OF WELL BORE PLUG OR
HORIZONTAL EXTENSION OF BARRIER

FIG. 1 — EFFICIENCY OF HORIZONTAL VERSUS VERTICAL BARRIERS TO CONTROL WATER CONING.

effect on the rising tendency of a water cone of changing the pressure gradient by increasing the height of a vertical plug (Curve I) and increasing the horizontal penetration of an impermeable barrier (Curve II).

From this analysis it may be noted that as the height of the vertical plug is increased, water production is reduced only slightly; whereas, as the penetration of the horizontal plug is increased, water production is reduced at a rapid rate.

Further indication of the effectiveness of horizontal plugs in fractured zones was found in an analysis of a number of plugback operations in a West Texas field. As may be seen by the data in Table 1, the frequency of success in reducing water production was greater where the plug was forced into the formation.

LABORATORY EXPERIMENTATION

The theoretical study, confirmed by field data, indicated that if a plug or barrier were injected into a water cone in sufficient volume to form a penetrating horizontal barrier, water influx due to coning could be controlled. In such a technique there would exist a danger of displacing some of the plugging material into the oil zone and subsequently impairing oil production. To overcome this possibility, a study was initiated to develop a plugging material that would have the following characteristics:

1. Be capable of being pumped and placed in deep wells.
2. Set and develop sufficient strength to resist backflow of water in a water-bearing fractured medium.
3. Fail to set or be easily removable from an oil-bearing formation.

A number of materials offering possibilities of meeting the requirements set forth above were evaluated in a series of tests both in the laboratory and in shallow wells drilled into sandstone outcrops.

LABORATORY TESTS

Initial screening of all materials considered for selective control of water production was accomplished by using the apparatus shown in Fig. 2. This apparatus consisted essentially of a fluid reservoir connected to two simulated fractured limestone formations, one saturated with oil, the other with water. The plugging materials were injected into both the oil and water-saturated simulated formations and the displacement pressure observed. After the barriers were set, the pressure differential that could be imposed without leakage and the pressure at which failure occurred were measured. If, after placement of the barrier in the oil zone, the rate of flow of oil was reduced, remedial measures were undertaken to restore the original permeability.

SHALLOW WELL TESTS

Shallow well tests were conducted in wells drilled approximately 15 ft into a sandstone outcrop. Casing was set in the upper 10 ft, and the open hole section shot with 6 to 10 lbs of an explosive for the purpose of providing fractures surrounding the well bore. The general procedure in this series of tests was as follows:

1. An oil or water permeability of the open hole portion of the shallow well was determined by injection.
2. Two to 5 bbls of the plugging agent were squeezed into the open hole portion of the well and allowed to set.
3. That portion of the plug in the well bore was drilled and the well cleaned to original total depth.
4. An oil or water permeability of the open hole portion of the well bore after plugging operations was determined.

For wells simulating fractured water zones:

5. Water was injected into the well for approximately eight hours. Permeability was determined at regular intervals during water injection.
6. Well was allowed to stand 24 hours.
7. Water injectivity test was conducted to determine the ability of the well bore to withstand water injection pressures.

For wells simulating fractured oil zones:

8. Where applicable, remedial measures were undertaken to restore original oil permeability of blocked zone.

TABLE 1 — WEST TEXAS FIELD PLUGBACK OPERATIONS

Well No.	Top Producing Formation	TD	Top Water Entry	Top Plug	Production Before BOPD	Production Before BWPD	Production After BOPD	Production After BWPD	Plug Material	Estimated Penetration	Remarks
1	4,520	4,813	4,803	4,798	117	22	125	21	Plastic	0	Unsatisfactory job.
2	4,520	4,823	....	4,800	8	10	61	52	Sand and Plastic	0	Unsatisfactory job. Acidized after plugback. Used blanket.
3	4,490	4,795	....	4,785	63	291	173	66	Plastic	0	Satisfactory job. No plastic lost to formation.
4	4,590	4,822	....	4,775	62	330	158	15	Cement	0	Satisfactory job.
5	4,512	4,806	4,797	4,797	129	51	105	39	Plastic	1 ft to 1¼ ft	Satisfactory job.
6	4,468	4,808	4,790	4,800	....	350	150	160	Plastic	½ ft to 1 ft	Water plug-off job satisfactory.
7	4,468	4,800	4,785	4,772	152	163	160	33	Cement	2 ft to 3 ft	Satisfactory job.
8	4,495	4,807	4,792	4,780	....	150	15	0	Cement	3 ft to 4 ft	Water plug-off job satisfactory.

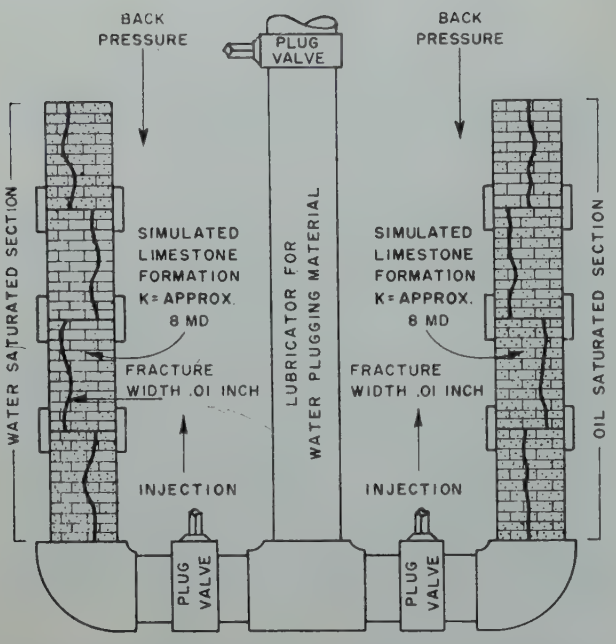

FIG. 2 — LABORATORY APPARATUS FOR TESTING WATER PLUGGING MATERIALS FOR FRACTURED FORMATIONS.

9. Oil permeability of open hole portion of well was measured to determine effectiveness of remedial procedure.

TEST RESULTS

Of 17 materials tested in the laboratory, only slurries of kerosene-cement, agricultural limestone-cement-water, and gilsonite-cement-water appeared sufficiently promising to warrant further tests in shallow wells.

Results of the tests with kerosene-cement slurries indicated that connate water present in oil-bearing formations might cause small particles of set cement to form; however, the plugging effect was not appreciable. Unset cement which lodged in the oil-bearing rock was readily removable with acid. Acid had no effect on the permeability of set cement in the simulated water zones. The results of shallow well tests on each of the three materials are included in Table 2.

To prevent backflow of the kerosene-cement after placement, it was found necessary to encourage removal of the kerosene from the slurry by imposing a high final squeeze pressure. The removal of kerosene formed an immobile barrier which was hydrated by the injection of water. Formation water would serve this purpose in oil and water-bearing zones.

Agricultural limestone-cement-water slurries were displaced into the open hole portion of the well and allowed to set. This material after its initial set was found to have a permeability of approximately 10 md. That portion of the slurry which was placed in the oil-producing zone was removed by acidizing. The relatively low permeability of this type barrier, while not completely effective in shutting off the water production, did restrict water by imposing a low permeability barrier about the well bore. In field treating operations care would have to be exercised to prevent the acid from entering the water zone and removing the plugging agent.

Gilsonite-cement-water slurries which were allowed to set in the water or oil zones were found to have a permeability of approximately 10 md. The presence of an oil-soluble material such as gilsonite in the cement permitted the disintegration of any portion of the cement placed in the oil bearing zone by flowing oil through the barrier.

A review of the results of the laboratory and shallow well tests indicated that of the materials tested, slurries of kerosene and cement offered the best possibility of forming a barrier that would be *selective* in that it would shut off water production yet fail to set in an oil-producing zone. If such a barrier material should inadvertently become lodged in an oil-producing zone, it could be effectively removed by acid.

FIELD TESTS

Based on the results of the laboratory and shallow well tests described above, eight tests were conducted in two fields in West Texas and one field in Wyoming to evaluate the selective plugging method of excluding water production. The basic well data and results of these field tests are tabulated in Table 3.

FACTORS AFFECTING SUCCESS

These tests emphasized a number of factors which could affect the success of future applications of kerosene-cement slurries. For example, in the first field test which was conducted in the Torchlight field, Wyo., the kerosene-cement slurry was not selective in shutting off only water. The total water production was reduced from 326 to 8 BWPD; however, the oil production was also reduced from 23 to 14 BOPD. It is believed that the reduction in oil production was a result of the kerosene-cement slurry by-passing the packer and penetrating the oil-producing zone and not being completely removed by acidizing following the job. The presence of *unset* cement above the packer indicated that the oil pay may have been squeezed with kerosene-cement slurry.

Later acidizing operations in the oil zone with only 500 gal. of acid failed not only to remove all of the cement, but also apparently resulted in the setting of the remaining cement-kerosene slurry in the productive section of the pay. This operation illustrated that a sufficient volume of acid should be used on the first stage, for once the cement has set it has practically no permeability and thus will not respond to further acidizing.

Wells A, B, C, D

The workover on Well B in the Midland Farms field, Tex., was not considered successful because oil production dropped from 88 BOPD to 16 BOPD. The water production was, however, reduced from 170 to 12 BWPD. It is possible that the packer was set too high in this well, and in order to regain the lost oil pro-

TABLE 2 — RESULTS OF SHALLOW WELL TESTS

	Kerosene-Cement		Agricultural Limestone-Cement-Water	Gilsonite-Cement-Water
	Well No. 1 (Water)	Well No. 2 (Oil)	(Oil)	(Oil)
Water or Oil Injection Rate before Shooting, GPM at 250 psi	19.4	16.3	0.4	2.0
Water or Oil Injection Rate after Shooting, GPM at 250 psi	88	73	16	12.0
Oil Injection Rate after Plugging Operation, GPM at 250 psi	....	28.2	0.6	1.1
Water Injection Rate after Plugging Operation, GPM at 250 psi (initial)	18.3	....	0.5	0.4
(24-hour)	0	....	0.4	0.2
Oil Injection Rate after Acidization, GPM at 250 psi	....	75	55	10.0

TABLE 3 — SUMMARY OF FIELD TESTS OF KEROSENE-CEMENT SQUEEZES SELECTIVE WATER PLUG-OFF JOBS

	Torchlight Field, Wyo.	Midland Farms Field, Tex.							Goldsmith Field, Tex.
	Well A	Well B	Well C	Well D	Well E		Well F	Well G	Well H
Producing Formation	Madison	Grayburg	Grayburg	Grayburg	Grayburg		Grayburg	Grayburg	Clearfork
Total Depth	3,680 ft	4,890 ft	5,048 ft	4,890 ft	4,900 ft		4,917 ft	4,861 ft	6,292 ft
Casing Seat	3,442 ft	4,719 ft	4,650 ft	4,724 ft	4,720 ft		4,777 ft	4,671 ft	6,154 ft
Prior Plugback Depths	3,571 ft	None	5,029 ft	None	None		4,877 ft	None	None
Production Before Squeeze	5/4/51; Pump 23 BOPD and 326 BWPD	2/1/52; Pump 88 BOPD and 170 BWPD on potential test	2/11/52; swb. No oil and 250 BWPD (below 4,973 ft)	2/14/52; swb. No oil and 280 BWPD (below 4,847 ft	3/16/52; swb. No oil and 360 BWPD (below 4,862 ft)		4/22/52; swb. 25 BOPD and 104 BWPD	7/7/52; 0 BOPD and 150 BWPD (below 4,786 ft)	2/16/52; swb. No oil and 360 BWPD (below 6,262 ft)
Date Kerosene-Cement Squeeze	5/24/51	2/9/52	2/9/52	2/20/52	3/17/52	4/3/52	5/5/52	7/14/52	2/17/52
Amount of Acid Used Ahead of Kerosene-Cement Squeeze	Oil used	1,000 gal. 15 percent	1,000 gal. 15 percent	1,000 gal. 15 percent	—	1,000 gal. 15 percent	1,000 gal. 15 percent	1,000 gal. 15 percent	2,000 gal. 15 percent
Plugback Depth of this Workover	3,544 ft	4,851 ft	5,000 ft	4,844 ft	4,856 ft	4,824 ft	4,872 ft	4,824 ft	6,260 ft
Amount of Cement and Kerosene Used	348 sx cement 3,480 gal. kerosene	250 sx cement 2,500 gal. kerosene	250 sx cement 3,000 gal. kerosene	350 sx cement 3,500 gal. kerosene	230 sx cement 2,500 gal. kerosene	250 sx cement 2,500 gal. kerosene	250 sx cement 2,500 gal. kerosene	78 sx cement 780 gal. kerosene	115 sx cement 1,150 gal. kerosene
Amount of Cement Circulated Out	20 bbl	2 bbl	1 bbl	Could not circulate	—	6 bbl	11 bbl	Could not circulate	Could not circulate
Maximum Squeeze Pressure	2,600 psi	1,500 psi	1,200 psi	1,700 psi	2,800 psi	2,900 psi	2,400 psi	3,000 psi	4,000 psi
Acid Treatment After Squeeze	500 gal. 15 percent	19,000 gal. in three stages using oil-soluble plugging material and jellied acid as staging agents	Not reacidized	20,000 gal. in three stages using oil-soluble plugging material and jellied acid as staging agents	Not reacidized	22,000 gal. in three stages using oil-soluble plugging agent as a staging agent	8,000 gal. in two stages using oil-soluble plugging agent as a staging agent	14,000 gal. in two stages using oil-soluble agent as a staging agent	12,000 gal. with a $CaCl_2$ blanket ahead of the acid
Production After Squeeze and Reacidization	6/5/52; pump 14 BOPD and 9 BWPD	2/16/62; pump 16 BOPD and 12 BWPD	3/12/52; pump 99 BOPD and 63 BWPD on repotential	4/15/52; pump 285 BOPD and no water on potential test	3/26/52; swb. 200 BWPD and 18 BOPD 1st Stage	6/23/52; pump 15 BOPD and 1 BWPD	6/9/52; pump 102 BOPD and 50 BWPD on repotential test	8/11/52; pump 12 BOPD and 124 BWPD	3/7/52; flow 83 BOPD and no water on potential test
Success of Squeeze	Successful	Unsuccessful	Successful	Successful	Unsuccessful	Successful	Successful	Unsuccessful	Successful

duction the packer and cement plug would have had to have been drilled out to the bottom of the oil pay.

Well C in the Midland Farms field was deepened in an effort to increase its producing capacity. Prior to the workover, the well produced approximately 5 BOPD and 6 BWPD. The production resulting from the deepening was no oil and 250 BWPD. After the kerosene-cement squeeze job, the potential of the well was determined by tests to be 99 BOPD and 63 BWPD. This squeeze job was considered successful in selectively plugging off the water production. This well was not re-acidized after the kerosene-cement squeeze job.

The squeeze job on Well D in the Midland Farms field was considered successful, for the water production was reduced from 280 BWPD to no water production. The potential of the well was determined by tests after the squeeze job at 285 BOPD.

Wells E, F, G, H

To shut off effectively the water production of Well E, Midland Farms field, it was necessary to perform two kerosene-cement squeeze jobs. The lower producing section of this well was producing no oil and 360 BWPD before the workover. After the first squeeze job, the total open hole production of the well was 18 BOPD and 200 BWPD as determined by swab test. This squeeze was not considered successful for the water production was not decreased appreciably. A second squeeze performed directly above the first squeeze job successfully shut off the water production. After the well was acidized with 22,000 gal. of 15 per cent regular acid in three stages using an oil-soluble temporary plugging agent, the well production averaged 15 BOPD and 1 BWPD.

Prior to the remedial workover on Well F in the Midland Farms field the total open hole production of the well was 25 BOPD and 104 BWPD. A plastic plugback job on the lower section was not successful. After the plastic plug was drilled out to total depth, a packer was set 5 ft above the initial plugback depth and the well squeezed with a kerosene-cement slurry. The well swabbed dry after the squeeze, but by stimulating the production with 8,000 gal. of 15 per cent regular acid in two stages with an oil-soluble temporary plugging agent in gelled acid, the potential of the well was found to be 102 BOPD and 50 BWPD. The kerosene-cement squeeze job on this well was considered a success.

The zone 4,786 to 4,861 ft of Well G in the Midland Farms field produced 1 bbl of oil per hour on a swab test after the well was drilled to total depth. After acidizing this zone with 10,000 gal. of 15 per cent acid to stimulate the oil production, this zone swabbed 100 per cent water or 150 BWPD. The squeeze with a kerosene-cement slurry below 4,824 ft eliminated the water production; however, no increase in oil production was noted. Acidizing the formation with 14,000 gal. of 15 per cent HCl acid from 4,671 to 4,804 ft

to obtain oil production resulted in an average production of 12 BOPD and 124 BWPD.

After acidizing the lower producing section of Well H of the Goldsmith Clearfork, Tex., this section produced no oil and 360 bbls of water per day. A kerosene-cement squeeze job performed on this section resulted in the elimination of the water production. After the well was acidized with 12,000 gal. of 15 per cent acid, the well produced 83 BOPD and no water on a potential test. Therefore, this workover was considered successful.

Summary of Tests

A Tabulation

Of the eight wells used to evaluate the kerosene-cement-water selective plugging method, six responded to the treatment and resulted in a 550 BOPD increase and 1,367 BWPD decrease. Of the two wells that were reported as unsuccessful, both resulted in a decrease in water production, but in one instance the oil production was also adversely affected and in the second well the decrease in water production was not considered adequate.

In summary, it may be seen that the success of kerosene-cement squeeze operations is dependent upon the use of an adequate amount of cement placed as low in the well bore as is practicable. A barrier thus placed has less chance of impairing oil zone permeability. Approximately 20 sacks of cement per foot of open hole was found satisfactory and has been recommended as a standard treating volume (Fig. 3A).

Another consideration affecting the success of this type remedial procedure is that the kerosene-cement slurry must contact water only in water-producing sections. There is the possibility the kerosene-cement slurry might enter the water zone and be diverted upward into the oil-producing sector through a fracture pattern existing in the formation surrounding the well, or the plugging agent might pass through a portion of the oil-producing formation already invaded by the water cone.

The possibility also exists that the kerosene-cement slurry might be displaced into a well bore filled with water and then become contaminated with water to such an extent that the slurry would lose its selective characteristics. Therefore, it was found advisable to precede the slurry with 10 to 20 bbls of oil. In this manner water could be forced ahead of the oil cushion so that only cement placed in the water-producing zone would later be exposed to formation water and set (Fig. 3B).

Use of Oil

The successful exclusion of water from the oil zone during the treating operation dictates that no water and preferably only oil should be used where pressure must be applied above the packer to prevent by-passing of the kerosene-cement slurry. A lost circulation recovery material, if used, should be completely oil-soluble. Such a procedure should greatly enhance the possibility of effecting a good water shut-off without endangering oil production.

Selectively acidizing oil-producing strata with enough acid to remove completely any cement present in the strata was found necessary to restore impaired oil production (Fig. 3C).

Water and oil production following a remedial job of this type is generally characterized by a relatively

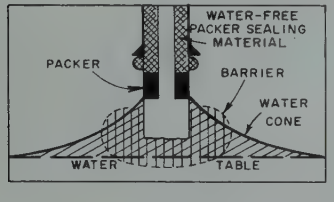

USE ADEQUATE VOLUME OF PLUGGING AGENT TO FORM BARRIER 20 SKS / FOOT

FIGURE 3A

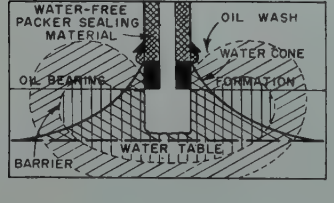

OIL WASH AHEAD OF SELECTIVE PLUGGING AGENT TO INSURE THAT IF PLUGGING AGENT IS PLACED IN OIL ZONE IT WILL BE WATER FREE

FIGURE 3B

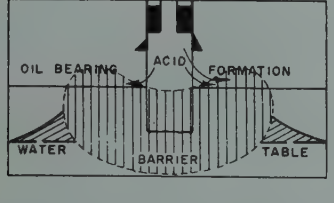

ACIDIZE OIL BEARING ZONE IF PRODUCTION IS IMPAIRED. BARRIER PERMEABLE IN OIL ZONE IMPERMEABLE IN WATER ZONE

FIGURE 3C

FIG. 3 — RECOMMENDED PRACTICES FOR KEROSENE CEMENT PLUGGING OPERATIONS.

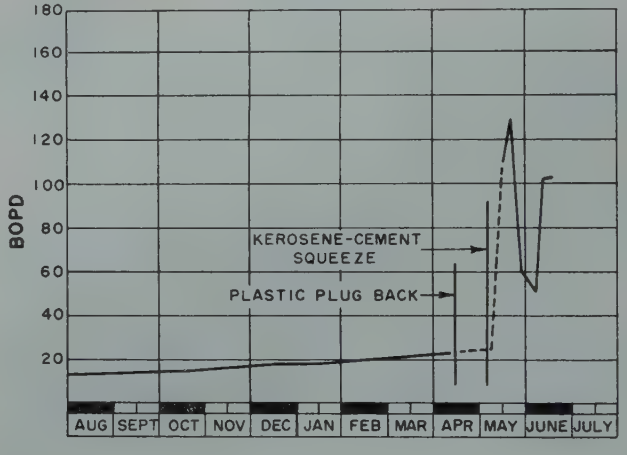

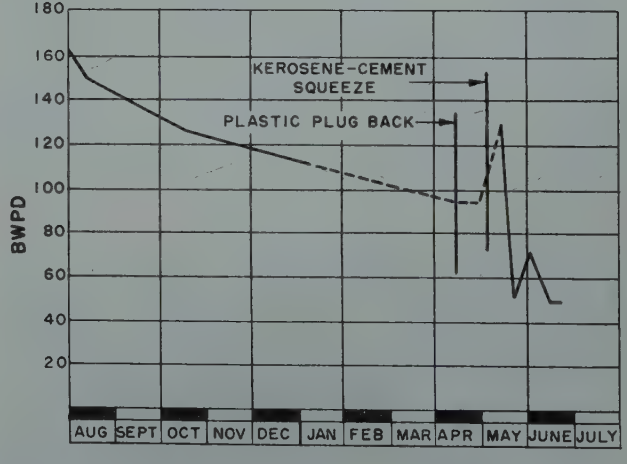

FIG. 4 — PRODUCTION DATA FOR WELL F, MIDLAND FARMS FIELD, TEX.

high water production decreasing in a few days to a very low producing rate. This, coupled with initial production of unset cement and kerosene from the oil zone, is taken as evidence that this material remains unset in the oil zone and gradually sets in the water zone as the well produces water. A typical plot of production data before and after treatment is illustrated in Fig. 4.

Since the slurry of kerosene-cement is dependent upon the re-invasion of the water through the immobilized or "dehydrated" cement, the danger of cementing the workover equipment in the hole is minimized by using these materials.

A suggested kerosene squeeze cementing procedure based on the information obtained from laboratory and field tests is presented in the Appendix.

CONCLUSIONS

Based on the results of laboratory and field tests described in this report, it is concluded that:

1. Kerosene-cement squeeze operations are effective for excluding water production from fractured formations.

2. Following a kerosene-cement squeeze operation, the oil section should be acidized if production tests indicate that oil production has been reduced.

3. Kerosene-cement squeeze operations reduce the danger of cementing the workover equipment in the well.

APPENDIX

Procedures for Kerosene-Cement Squeeze

A. Pre-Squeeze Operations

1. Determine the top and bottom of the major water entry.

2. Use two cementing trucks (one connected to the casing and the other to the tubing).

3. Twenty sacks of cement per foot of hole section squeezed is recommended unless field experience has shown that more or less cement is required to accomplish the job.

4. The squeezing of more than 10-ft of hole is unnecessary. Generally, if the oil is located immediately above the water, the packer should be set 5 to 10 ft below the water-oil contact; if the oil is located 5 to 10 ft above the water zone, the packer may be set at the top of the water entry. If more than 10 ft of hole is open below the point selected for the packer setting, the well should be plugged back inside the well to within approximately 10 ft of the packer setting before squeezing in order to minimize the amount of material required to do the job.

B. Formation Breakdown Operations

1. Circulate the hole with oil and spot a suitable packer sealing material (containing no water and completely soluble in oil) in the annulus on top of the packer. Use a sufficient quantity of packer seal to fill the open hole section above the packer, plus the quantity estimated to be necessary to maintain pressure and prevent by-passing during the formation breakdown and treating operations.

2. Break down the formation with oil. In event the formation cannot be broken down with oil, and the formation is known to be acid-reactive, acid may be used provided the spent acid is displaced away from the well bore with at least 20 bbls of oil.

C. Squeeze Cementing Operations.

1. Precede the cement and kerosene with a minimum of 20 bbls of oil.

2. Use the number of sacks of cement determined in A-4 above mixed in kerosene to a slurry weight of 12.4 lbs/gal.

3. Start mixing and displacing cement. The cement should be displaced down the tubing at as rapid a rate as practicable using a minimum of 5 bbls of oil on top of the cement slurry as the displacing medium.

4. Maintain adequate pressure in the casing to prevent the plugging agent by-passing the packer.

5. When the cement reaches the formation, continue pumping at as fast a rate as practicable until all but 5 bbls of slurry have been injected into the formation.

6. Shut down the pumps and wait five minutes.

7. Resume pumping at a very slow rate (¼ BPM or slower).

8. If a final squeeze pressure has not been obtained by the time 2 bbls have been displaced since pumping was resumed, repeat steps C-6 and C-7.

9. Hold the final squeeze pressure for five minutes to be sure that the slurry has been completely immobilized.

10. Reverse circulate the excess slurry and packer seal to the surface. (If reverse circulation cannot be accomplished, 1¼-in. OD flush joint tubing may be run inside the squeezing string and the excess cement displaced to the surface with water-free oil.)

11. Inject 20 bbls of oil into the producing zone above the packer.

D. Testing Operations

1. Pull the tubing and packer, run pumping equipment, and produce well.

2. If the daily production after seven days indicates that the oil section has been partially plugged, acidize this zone using sufficient acid to remove the plugging material in the oil zone.

ACKNOWLEDGMENT

Appreciation is expressed to Stanolind Oil and Gas Co. for permission to publish this paper.

REFERENCES

1. Muskat, M.: "Flow of Homogeneous Fluids through Porous Media," McGraw-Hill Book Co., Inc. (1937) 480-506.
2. Muskat, M.: "The Performance of Bottom Water-Drive Reservoirs," *Trans.* AIME (1947), 170, 81-111.
3. Muskat, M.: "Physical Principles of Oil Production," McGraw-Hill Book Co., Inc. (1939), 226-236.
4. Muskat, M., and Wyckoff, R. D.: "An Approximate Theory of Water-Coning in Oil Production," *Trans.* AIME (1935), 114, 144-163.
5. Teague, J. V.: "Economics of Controlling Water Produced with Oil," *Oil and Gas Jour.* (Nov. 14, 1940).
6. Torrey, Paul D.: "Selective Exclusion of Fluid from Wells," *Drilling and Production Practices,* API, 205.

★★★

A CONTRIBUTION to ELECTRICAL LOG INTERPRETATION in SHALY SANDS

A. POUPON — SCHLUMBERGER WELL SURVEYING CORP. RIDGEFIELD, CONN.

M. E. LOY, MEMBER AIME — SCHLUMBERGER WELL SURVEYING CORP. LOS ANGELES, CALIF.

M. P. TIXIER, MEMBER AIME — SCHLUMBERGER WELL SURVEYING CORP. HOUSTON, TEX.

T. P. 3800

ABSTRACT

Simple qualitative methods are explained for identifying those shaly sands in a well that are most likely to contain oil. A need for more precise measurement of the variables that enter shaly sand analysis is indicated. Field examples are given to illustrate the methods.

A theoretical discussion of the quantitative interpretation of shaly sands is given as a basis for discussion and as a guide for the future. While not generally capable of practical application at the present time because of the lack of sufficient accuracy of the electric log data, these methods may become more feasible in the future as the result of the improved logging methods now being introduced.

INTRODUCTION

Experience has shown that for porous formations containing only a negligible amount of clayey material, reliable information on the fluid saturation and porosity of the reservoir rocks can usually be derived from the electrical logs. The interpretation is based on empirical formulae relating the true resistivity of a porous formation to its lithologic character, to the resistivity of the interstitial water, and to the proportions of water and hydrocarbons in the pores.[1] If the resistivity of the interstitial water is not known, its approximate value can be derived from the SP curve.[2,3] The porosity can usually be determined to a good approximation from a MicroLog, or a MicroLaterolog.[4,5]

When the reservoir rocks contain an appreciable percentage of clayey material, an additional factor is introduced into the analysis. In a clean formation, the matrix is an electrical insulator, so that the ability of the formation to conduct current is due only to the conductivity of the electrolytes in the pores; in a shaly formation, the shale constitutes a part of the rock matrix able to conduct current, and influences the resistivity of the formation. On the other hand, the spontaneous emf's and the circulation of the SP currents are also responsive to the presence of the shaly material. All other factors being the same, the deflection of the SP curve opposite a shaly permeable formation is smaller than the deflection which would be observed if the formation were clean. The effects of the presence of shale on the resistivity and on the SP curves in a shaly formation are functions of the amount, of the specific resistivity, and of the geometrical distribution of the shaly material within the formation.

The presence of shale therefore constitutes an important complication in electrical log interpretation. It is easy to realize, for example, that the presence of a large amount of clayey material in a sand may have such a predominant effect that the resistivity of the sand will not change very much, whether the pores are entirely filled with connate water, or contain a high saturation of hydrocarbons.

Important research projects have been undertaken to investigate the influence of shales and to find a way to allow for this influence in the interpretation of a log. The problem of the SP in shaly sands was analyzed mathematically by H. G. Doll[6,7] for the case of sands with shale laminations. Formulae expressing the resistivity of shaly formations were proposed by Patnode and Wyllie[8] and de Witte.[9] Other quite interesting theoretical and experimental results have been published by various authors.[10,11,12,13,14]

The purpose of the present paper is to discuss an approach to electrical log interpretation in shaly sands. This approach is based partly on some of the theoretical and experimental data available in the literature and partly on observations made on actual field logs.

Comparatively simple methods for qualitative and semi-quantitative analysis are described. These methods depend principally upon information provided by the electrical logs.

---

[1]References given at end of paper.

Manuscript received in the Petroleum Branch office Sept. 28, 1953. Paper presented at the Petroleum Branch Fall Meeting in Dallas, Oct. 19-21, 1953.

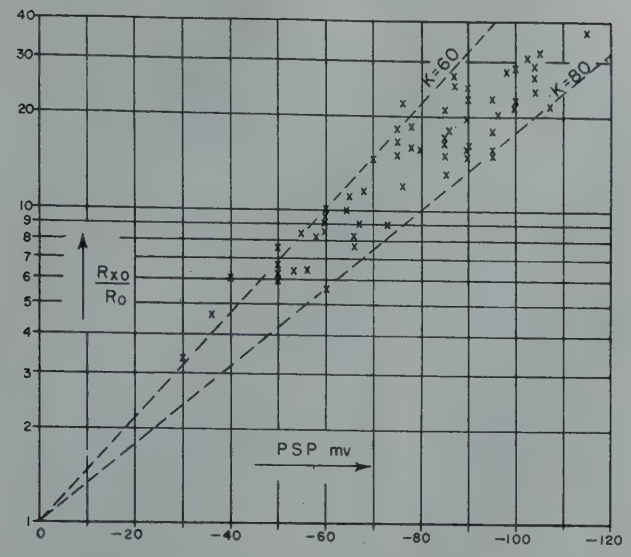

FIG. 1 — A PLOT OF R_{xo}/R_o VERSUS PSP FOR A GROUP OF SHALY WATER SANDS OF THE SHALLOW WILCOX, MISS. (FOR A 100 PER CENT WATER SAND $R_o = R_t$).

QUALITATIVE INTERPRETATION

SP DEFLECTION IN SHALY WATER SANDS

The study of a number of electrical logs has shown that in 100 per cent water saturated shaly sands, the Pseudo-Static SP is given, to a good approximation, by:

$$PSP = -K \log \frac{R_{xo}}{R_o} \quad . \quad . \quad . \quad . \quad . \quad . \quad . \quad (1)$$

where K is the same coefficient as in the formula

$$SSP = -K \log \frac{R_{mf}}{R_w} \quad . \quad . \quad . \quad . \quad . \quad . \quad . \quad (2)$$

In these equations SSP and PSP are respectively the deflections of the SP curve for a *thick* clean sand and a *thick* shaly sand*; R_{xo}, resistivity of the invaded zone; R_o, resistivity of 100 per cent water saturated sands, whether clean or shaly; R_{mf}, resistivity of the mud filtrate; and R_w, resistivity of the connate water.**

Fig. 1 shows for one of the wells studied the plot of PSP in abscissa against R_{xo}/R_o in ordinate, on a semi-log grid. (R_{xo} values derived from a MicroLog; R_o values derived from an Electrical Survey — Induction Log.) As seen on the figure, most of the experimental points plot between the straight lines PSP $= -60 \log R_{xo}/R_o$ and PSP $= -80 \log R_{xo}/R_o$, and PSP in this case can be expressed approximately by a single relation between the different variables.†

$$PSP = -70 \log \frac{R_{xo}}{R_o}$$

Log experience, although still limited, has shown that the relationship (1) PSP $= -K \log R_{xo}/R_o$ seems to exist both in water sands with laminated shales and in water sands with dispersed clays.

SHALY SANDS WITH LAMINATED SHALES

For water sands with laminated shales the above relationship (1) between PSP, R_o and R_{xo} was expected as a consequence of the results established through mathematical developments by H. G. Doll‡ (equation 15).

Let R_t^s be the resistivity of the clean sand streaks. R_t (harmonic average of the true resistivity of the shaly sand) is related to p (proportion of shale laminations), to R_{sh} (resistivity of the shale laminations), and to R_t^s by the equation;‡

$$\frac{1}{R_t} = \frac{p}{R_{sh}} + \frac{1-p}{R_t^s}$$

The resistivity R_t^s of the clean sand streaks is given to a good approximation by:

$$R_t^s = \frac{F R_w}{S^2},$$

where F is the formation factor of the clean sand streaks, and S the connate water saturation.

Then:

$$\frac{1}{R_t} = \frac{p}{R_{sh}} + \frac{(1-p)\, S^2}{F R_w} \quad . \quad . \quad . \quad . \quad . \quad (3)$$

Similarly R_{xo} is given by:

$$\frac{1}{R_{xo}} = \frac{p}{R_{sh}} + \frac{(1-p)\, S_{xo}^2}{F R_{mf}} \quad . \quad . \quad . \quad . \quad (4)$$

where S_{xo} is the mud filtrate saturation in the invaded zone.

Taking into account these two relationships (3) and (4), it can be shown that Doll's equation (15), using the notations adopted in this paper, can be transformed into:

$$\propto = \frac{\log \dfrac{R_t}{R_{xo}}}{\log \dfrac{R_w}{R_{mf}} + 2 \log \dfrac{S_{xo}}{S}} \quad . \quad . \quad . \quad . \quad (5)$$

where $\propto$, the SP reduction factor, is defined as PSP/SSP.

Inasmuch as

$$\left\{ \begin{array}{l} \propto = \dfrac{PSP}{SSP} \\ \text{and } SSP \cong -K \log \dfrac{R_{mf}}{R_w} \end{array} \right.$$

the above formula (5) becomes:

$$PSP = -K \log \frac{R_{xo}}{R_t} - 2 \propto K \log \frac{S_{xo}}{S} \quad . \quad (6)$$

It is seen readily that, for a 100 per cent water saturated shaly sand, $S_{xo} = S = 1$, $R_t = R_o$, and formula (6) reduces to PSP $= -K \log R_{xo}/R_o$, i.e. to formula (1).

If the shaly sand contains oil or gas, S_{xo} will be greater than S, since in the invaded zone the mud filtrate will replace some of the oil or gas in addition to the connate water. Then $\log S_{xo}/S$ will be positive, and the term $-2 \propto K \log S_{xo}/S$ will be negative. Therefore, for a series of shaly sands in a given well, if values of PSP are plotted against values of R_{xo}/R_t on a semi-log grid, it appears that for sands with shale laminations containing only water, the corresponding

*Except as otherwise specified, for the sake of simplicity, PSP and SSP are used in the equations and graphs of this paper as equivalent to their electrochemical components. This assumes that under usual field conditions other possible components, such as that due to electrofiltration, are comparatively small or negligible.

**See table of "Definitions of Terms and Symbols" for a more complete definition of symbols.

†In a sand with 100 per cent water saturation, $R_o = R_t$.

‡Preferably the thickness of the laminations should be smaller than the resolution of the logging devices which measure R_{xo} and R_t. In practice that condition is always satisfied for R_t. When such is not the case for R_{xo}, it is acceptable to take the harmonic average of the R_{xo} values derived from the micro device (see "Definition of Symbols" at the end of the present paper, footnotes* and **).

points will fall on or near a straight line PSP $= -K$ log R_{xo}/R_o; for sands with shale laminations containing oil and/or gas, the corresponding points will fall *below* this straight line (Fig. 2), i.e., fall in the range of lower values of R_{xo}/R_t for a given PSP value.

According to equation (6), lines of constant saturation will all go through the point with coordinates $R_{xo}/R_t = 1$, PSP $= 0$, and will diverge in a fan shaped manner. *It follows then that points close to the line PSP $= -K$ log R_{xo}/R_t may correspond to oil production only if the SP reduction factor $\propto$ is a small fraction, but will most probably correspond to a water production if the SP reduction factor $\propto$ tends toward unity.*

Sands with Dispersed Clays

In a sand with dispersed clays, if no oil or gas is present, the pores are filled with a mixture of conductive solids and connate water. According to de Witte[9] the average resistivity R_z of that mixture is given by:

$$\frac{1}{R_z} = \frac{q}{R_c} + \frac{1-q}{R_w} \quad . \quad . \quad . \quad . \quad . \quad . \quad . \quad . \quad (7)$$

q being the proportion of the total porosity occupied by the conductive solids, and R_c their resistivity.

The resistivity R_o of the sand is

$$R_o = F_z R_z \quad . \quad . \quad . \quad . \quad . \quad . \quad . \quad . \quad . \quad . \quad (8)$$

where F_z is the formation factor corresponding to the total porosity.

Similarly, in the flushed zone of the sand the resistivity R_{zo} of the mixture of conductive solids and mud filtrate in the pores is given by:

$$\frac{1}{R_{zo}} = \frac{q}{R_c} + \frac{1-q}{R_{mf}} \quad . \quad . \quad . \quad . \quad . \quad . \quad . \quad (9)$$

and the resistivity R_{xo} of the flushed zone is

$$R_{xo} = F_z R_{zo} \quad . \quad . \quad . \quad . \quad . \quad . \quad . \quad . \quad . \quad (10)$$

In usual field conditions R_c can be assumed to have roughly the same value in the invaded zone and in the non-invaded part of the formation, and the above equations (7) to (10) are likely to be good approximations.

If the above values of R_{xo} and R_o are introduced into formula (1), PSP $= -K$ log R_{xo}/R_o, it becomes:

$$\text{PSP} = -K \log \frac{R_{zo}}{R_z} \quad . \quad . \quad . \quad . \quad . \quad . \quad . \quad . \quad (11)$$

Formula (11) indicates that the PSP has the same value as if the two mixtures electrolyte-dispersed clays were replaced by two homogeneous electrolytes having resistivities R_z and R_{zo} respectively.

It seems logical to expect this result to hold true in the case of sands containing oil and/or gas. In that case, according to de Witte:

$$R_t = \frac{F_z R_z}{S_z^2} \text{ or } R_z = \frac{R_t S_z^2}{F_z}$$

where S_z is the saturation of the conductive mixture (dispersed clays — connate water) in the total pore space. Similarly R_{zo} is given by

$$R_{zo} = \frac{R_{xo} S_{zo}^2}{F_z}$$

where S_{zo} is the saturation in the invaded zone of the total porosity with the mixture mud filtrate-dispersed clays.

Using these expressions for R_z and R_{zo} in formula (11), it is found that

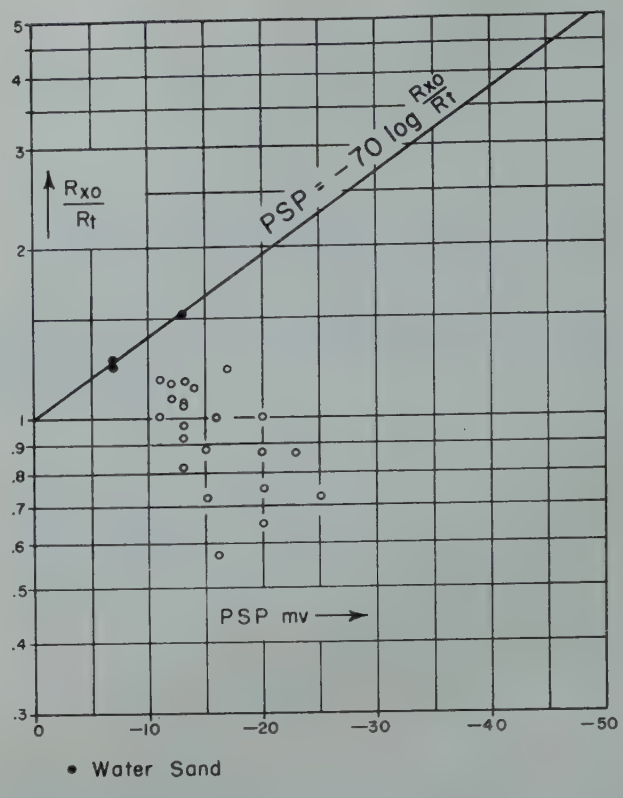

Fig. 2 — An Example of Qualitative Interpretation of Shaly Sands. R_{xo}/R_t Is Plotted Against PSP for a Group of Shaly Sands in a California Well. The Water Sands Lie on or Near the Line SP $= -70$ Log R_{xo}/R_t, Whereas the Oil Producing Sands Tend to Fall Well Below it.

$$\text{PSP} = -K \log \frac{R_{xo}}{R_t} - 2K \log \frac{S_{zo}}{S_z} \quad . \quad . \quad (12)$$

Formula (12), which applies to sands with dispersed clays, is similar to formula (6) derived from H. G. Doll's study of sands with laminated shales.

Accordingly, the same method of qualitative interpretation, plotting PSP against R_{xo}/R_t, can be used both for sands containing shale laminations and for sands containing dispersed clays, and, as a consequence, to shaly sands containing both laminated shales and dispersed clays.

For dispersed clays, as for laminated shales, the lines for constant values of S, connate water saturation in the effective pore space, will go through the point $R_{xo}/R_t = 1$, PSP $= 0$, and will diverge in a fan shaped manner. *Accordingly, in both types of shaly sands, points close to the line PSP $= -K$ log R_{xo}/R_t may correspond to oil production only if the SP reduction factor $\propto$ is a small fraction, but will most probably correspond to water production if the SP reduction factor tends toward unity.*

The factors required for the application of the qualitative method of interpretation described above are PSP, R_{xo}, and R_t. These factors can be determined from the electrical logs (SP curve for PSP, MicroLog, or Micro-Laterolog for R_{xo}, resistivity curves for R_t) without the need for additional data, except that it would be

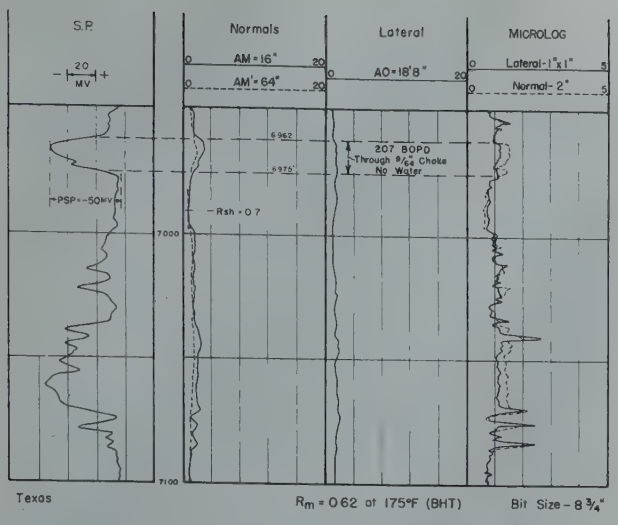

FIG. 3 — SHALY OIL SAND — FRIO SERIES, SOUTH TEXAS.

helpful to know $\propto$, or at least its approximate value, in view of its influence as stated above.

Fig. 2 shows a plot of PSP against R_{xo}/R_t for a California well. The black discs correspond to water producing formations. The open circles correspond to oil sands producing collectively 310 BOPD with a 29 per cent water cut.

SIMPLIFIED APPROACH

In a *clean* sand the formation factor F can be derived to a good approximation from R_{xo}/R_{mf}. Furthermore, an approximate value of the connate water resistivity can be derived from the Static SP through the formula

$$SSP = -K \log \frac{R_{mf}}{R_w}$$

and the value of the connate water saturation can be estimated from the comparison of R_t to $F\ R_w$ (in a clean sand $F\ R_w$ is equal to R_o).

In a *shaly* sand the formation factor and the connate water resistivity cannot be derived readily from the value of R_{xo} and from the Pseudo-Static SP. Let us designate F_a and R_{wa} respectively an "apparent formation factor," equal to R_{xo}/R_{mf}, and an "apparent connate water resistivity," given by $PSP = -K \log R_{mf}/R_{wa}$.

Considering, for example, the case of a sand with dispersed clays, if in the first member of equation (12), PSP is replaced by $-K \log R_{mf}/R_{wa}$, the following relationship is obtained.

$$-K \log \frac{R_{mf}}{R_{wa}} = -K \log \frac{R_{xo}}{R_t} - 2K \log \frac{S_{xo}}{S_z}$$

This can be transformed to

$$2 \log \frac{S_{xo}}{S_z} = \log \left[\frac{R_t}{\frac{R_{xo}}{R_{mf}} \times R_{wa}} \right] = \log \frac{R_t}{F_a R_{wa}}$$

It thus appears that if $R_t = F_a R_{wa}$, S_{xo} is about equal to S_z, and the chances are that the sand contains no hydrocarbons. If R_t is substantially greater than $F_a R_{wa}$, S_{xo} will be greater than S_z, which indicates that the sand contains oil. A very similar derivation can be made for the case of sands with shale laminations.

This approach provides for a quick and convenient method of qualitative analysis: it becomes sufficient to determine F_a and R_{wa} from the log, as F and R_w are determined in the case of clean sands, and to compare $F_a R_{wa}$ to the actual value of R_t. *The formulae indicate that when the SP reduction factor $\propto$ is a small fraction, it is possible to have oil or gas production even if R_t is not much greater than $F_a R_{wa}$; whereas if the SP reduction factor tends to unity, oil production is to be expected only if R_t is substantially greater than $F_a R_{wa}$.*

This conclusion regarding $F_a R_{wa}$ and R_t parallels that previously developed for R_{xo}/R_t and PSP.

REMARK

It often happens that the exact value of R_w, resistivity of connate water, is known from direct measurements on samples. In the application of the simplified method, the value to be introduced, of course, is the *apparent value* R_{wa}, as defined above, and not the *true value* R_w. Likewise, the *apparent formation factor* F_a must be used, even though information on F is available from core analysis.

FIELD EXAMPLE

Fig. 3 illustrates an electric log and MicroLog of the Frio series. Before considering the electric logs themselves, the following data are tabulated here.

$R_m = 0.62$ at 175°F (BHT)

$R_w = 0.06$ at BHT — from measurements made on drill stem test water

The section tested was from 6,962 ft to 6,975 ft. The following values are derived from the electric log and MicroLog:

PSP = — 50 mv

$R_{sh} = 0.7$

$R_t = 2.0$ — from long normal

$R_{xo} = 2.0$ — from MicroLog readings using SWSC Document No. 5

We have

$$\frac{R_{xo}}{R_t} = \frac{2.0}{2.0} = 1.$$

Point A on Fig. 4 corresponds to the above data for R_{xo}/R_t and PSP. The line for $PSP = -K \log R_{xo}/R_t$ has been drawn using $K = 80$, a value deduced from the tabulated and other known data.

With the logging techniques used in this example the values for R_{xo} and R_t are not obtained with great accuracy. Assuming possible maximum errors of $\pm$ 20 per cent for both R_{xo} and R_t, the ratio R_{xo}/R_t will be found to vary between

$$\frac{2.0 \times 1.2}{2.0 \times 0.8} = 1.5 \text{ and } \frac{2.0 \times 0.8}{2.0 \times 1.2} = 0.66.$$

The upper and lower lines of the rectangle surrounding point A represent these limits.

Furthermore, it is possible that for this sand the SP is not completely developed and an increase of 5 mv (negative) may be necessary to bring the SP value to represent the PSP. Consequently the right side of the rectangle has been drawn to correspond to a limit of — 55 mv. It may also be necessary to substract from the SP a few millivolts due to electrofiltration, since the abscissa of Fig. 3 should in fact be only the electrochemical component of the PSP. Tentatively we are estimating that a maximum electrofiltration potential E_f

of − 15 mv might exist for this sand and, consequently, the left side of the rectangle has been drawn to correspond to a limit of − 35 mv.

The rectangle shows the possible positions for point A. Obviously, all the rectangle falls below and at some distance from the line PSP = − 80 log R_{xo}/R_t. For this reason the bed under investigation should be an oil or gas sand, and the possible errors that might be made in the selection and use of the basic data should not change the interpretation. This sand is producing 207 B/D of oil through 9/64-in. choke, with no water.

If we use the technique described under "Simplified Approach," we find $F_a = 4.5$ and $R_{wa} = 0.11$ (with $K = 80$), giving $F_aR_{wa} = 0.47$. Inasmuch as $R_t = 2.0$, the product F_aR_{wa} is much smaller than R_t, indicating the presence of oil. A similar discussion of the possible errors could be made also for that technique.

DISCUSSION OF RESULTS

We have seen that to make qualitative interpretations we need at least three parameters: R_{xo}, R_t, and PSP.

To refine the accuracy of R_{xo}, improved MicroLog devices are being studied. In addition, the Micro-Laterolog, which is under active development, promises further improvement in obtaining R_{xo}, especially in formations of low porosity.

With the conventional electric log made up of normals and laterals, the errors that can be made in R_t, especially for thin sands, are such that the interpretation can be seriously affected. To improve the accuracy of R_t in many instances some other type of log will be necessary. It appears today that a solution for this will come from the Induction Log, which is well suited for this purpose because it can measure accurately the average conductivity of shaly sands even as thin as four or five feet.

The quantity PSP appearing in equations (6) and (12) and the various graphs should, as previously noted, more properly be the electrochemical component of the Pseudo-Static SP. The approximation made by taking PSP as such is satisfactory under usual field conditions, when R_{mf} and the differential pressure are not too high, in which case the electrofiltration emf, E_f, is small and negligible. In some cases, however, E_f may represent a considerable part of the PSP (for example, when fresh muds are used in highly shaly sands), and in equations (6) and (12) and in the various graphs PSP should be replaced by PSP − E_f, since it is not permissible anymore to neglect E_f.

One possible way to determine an approximate value of E_f is to measure PSP, R_{xo}, and R_o, on a sand known to be 100 per cent water saturated, then derive E_f from equation

$$\text{PSP} - E_f = -K \log \frac{R_{xo}}{R_o},$$

taking for K the theoretical value as given in reference 3. However, it seems preferable to attempt that method only when the ratio R_{mf}/R_w is small.

In addition, research efforts are being devoted to methods for possible direct measurement of E_f in the hole.

QUANTITATIVE INTERPRETATION

As already seen from the discussion in the previous section of the paper, the different data that enter into the various relations for the interpretation cannot all be determined with sufficient accuracy in most cases to permit an accurate quantitative analysis, at least with the means available at the present time. It may be, therefore, premature to expect a practical use of quantitative techniques in the interpretation of shaly sands. Nevertheless, a discussion of quantitative methods of interpretation, even though more theoretical than practical, seems justified for the following reasons:

1) Quantitative analysis might be permissible in some favorable cases such as thick sands only moderately shaly. Furthermore, as the techniques improve, and as the various data can be obtained with more accuracy, the instances where quantitative interpretation will be possible should become more numerous.*

(2) The charts that will be given are interesting for the analysis of the problem. They should permit a better understanding of the behavior of the various electric logs in shaly sands. This should help to identify the particular data and techniques whose refinement will contribute the most to improved quantitative interpretation.

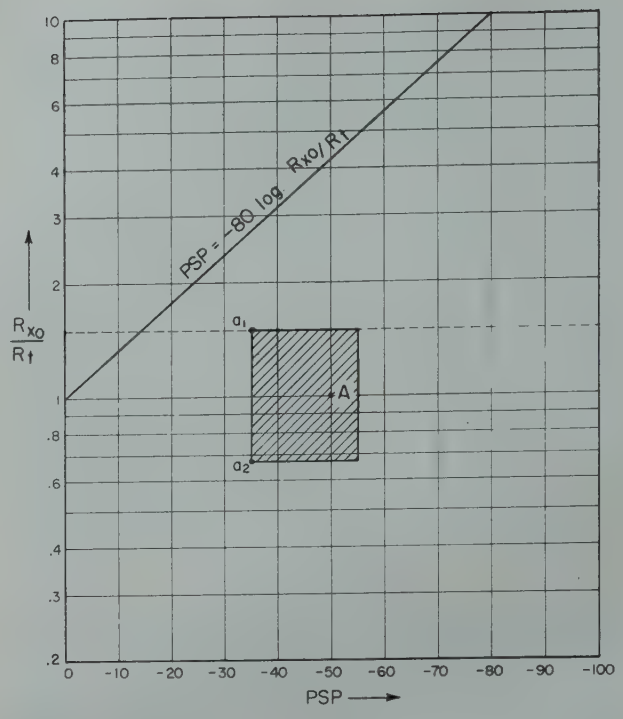

FIG. 4 — POINT A REPRESENTS A PLOT OF R_{xo}/R_t VERSUS P SP FOR THE SHALY SAND 6,962 FT — 6,975 FT OF FIG. 3. THE SURROUNDING RECTANGLE REPRESENTS THE POSSIBLE POSITIONS OF A RESULTING FROM ERRORS IN THE DATA. THE RECTANGLE IS WELL BELOW THE LINE P SP = − 80 LOG R_{xo}/R_t, INDICATING PROBABLE OIL AND/OR GAS. MAXIMUM AND MINIMUM POSSIBLE WATER SATURATIONS ARE REPRESENTED BY POINTS A_1 AND A_2.

SANDS WITH LAMINATED SHALES

Taking into account equations (3), (4), and (5), equation (6) can also be written:

*This is particularly true when improved methods of logging such as Induction Logging, MicroLogging, Laterolog, etc., are used.

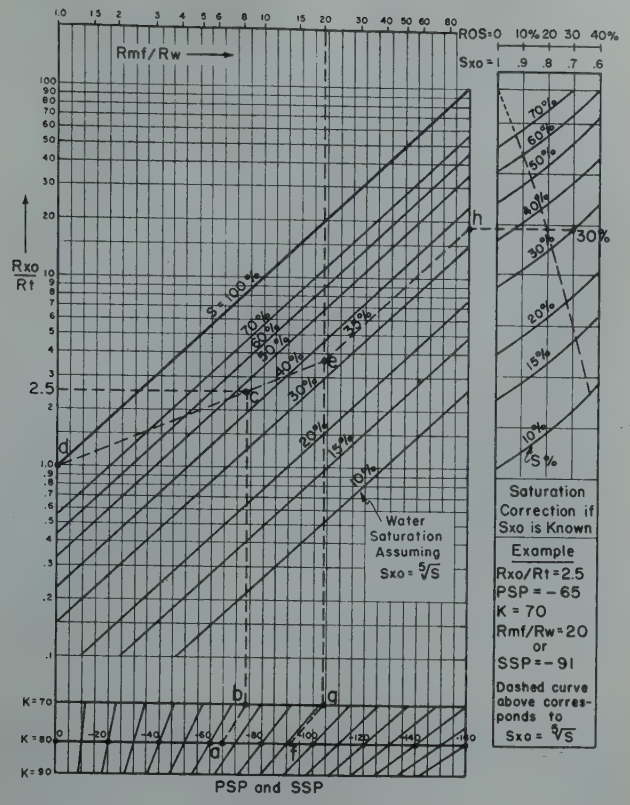

FIG. 5 — CHART FOR FINDING THE WATER SATURATION S OF SHALY SANDS.

$$\alpha = \frac{\log \dfrac{R_t}{R_{xo}}}{\log \left(\dfrac{\dfrac{R_t}{R_{xo}} - p \dfrac{R_t}{R_{sh}}}{1 - p \dfrac{R_t}{R_{sh}}} \right)} \quad . \quad . \quad . \quad . \quad (6')$$

These three equations (3), (4), and (6), or (6'), provide a basis for quantitative interpretation. The logs give R_t, R_{xo}, PSP and α, and the equations can be solved for p, F, and S, provided that R_w and R_{mf} are known, and that an approximate value can be assumed for S_{xo}. It seems reasonable to assume that R_{sh}, resistivity of the shale laminations, is equal, to a good approximation, to the resistivity of the thick shales above and below the shaly sand under investigation.

SANDS WITH DISPERSED CLAYS

As already seen, in the case of sands with dispersed clays we can assume the relationships:

$$\begin{cases} \text{PSP} = -K \log \dfrac{R_{xo}}{R_t} - 2K \log \dfrac{S_{zo}}{S_z} \\ R_t = \dfrac{F_z R_z}{S_z^2} \\ R_{xo} = \dfrac{F_z R_{zo}}{S_{zo}^2} \end{cases}$$

It is necessary to replace R_z and R_{zo} by their expressions as functions of the physical parameters that we seek to determine. The system of equations to be solved then becomes:

$$\begin{cases} \text{PSP} = -K \log \dfrac{R_{xo}}{R_t} - 2K \log \dfrac{S_{zo}}{S_z} \quad . \quad (12) \\ \dfrac{1}{R_t} = \dfrac{S_z}{F_z} \left[\dfrac{q}{R_c} + \dfrac{S_z - q}{R_w} \right] \quad . \quad . \quad (13) \\ \dfrac{1}{R_{xo}} = \dfrac{S_{zo}}{F_z} \left[\dfrac{q}{R_c} + \dfrac{S_{zo} - q}{R_{mf}} \right] \quad . \quad . \quad (14) \end{cases}$$

PSP, R_t and R_{xo} having been determined from the logs, it will be possible to make a quantitative interpretation, that is to determine q, F_z, and S_z provided R_w and R_{mf} are known and approximate values of S_{zo} and R_c can be assumed.

Although R_c is not exactly a constant[14] it is likely that an average value can be used for a given geological area, and it would thus be sufficient to have only a few determinations of R_c. Unfortunately it is difficult to measure R_c, and, to the authors' knowledge, no practical method to make such measurements is currently available.

In some favorable cases the study of electrical logs can permit an approximate determination of R_c. If, for example, in an electric log showing a series of 100 per cent water saturated sands containing dispersed clays, it is found that, as a well marked trend, the diminutions in the negative deflection of the SP curve (which indicates increases in clay content), correspond to decreases in the R_{xo} values, it can be concluded that R_c is smaller than the resistivity R_{mf} of the mud filtrate, assuming that the total porosity is unchanged. If several such logs run with different mud resistivities are available, it will be possible to arrive at an approximate value of R_c.

Similar plottings of SP deflections against R_o values seem to indicate that R_c is usually substantially greater than R_w.

In the Shallow Wilcox of Louisiana and Mississippi it has been found that R_c is probably of the order of .6 ohm, whereas the thick shale beds have an average resistivity of about 1.2 ohms.

For either type of shaly sand, after the system of equations has been solved and the formation factor determined, the porosity can then be calculated using one of the relationships currently in use.

APPLICATIONS

Many shaly sands were analyzed using both sets of equations for laminated shales and for dispersed clays. Inasmuch as the basic parameters R_{xo}, R_t and PSP were not known with the necessary accuracy, the values derived for water saturation S and effective porosity ϕ were not exact; but it was found in most cases that these values calculated independently using the two systems were about the same.

The equations for sands with laminated shales lend themselves conveniently to the construction of two rather simple charts giving solutions for water saturation S and effective porosity ϕ. Since experience seems to indicate that the systems of equations for both classes of shaly sands yield about the same results for these two parameters, it seems permissible to use these same charts for both classes of shaly sands.

Fig. 5 shows a chart for the determination of the water saturation. It gives a rigorous solution of the laminated shale relation (6). The following example

shows how to use the chart. Let $K = 70$, $R_{xo}/R_t = 2.5$, PSP $= -65$, $R_{mf}/R_w = 20$ or SSP $= -91$. Through point a corresponding to PSP $= -65$ on line for $K = 80$ draw a slanting line to the intersection b with horizontal line for $K = 70$. Point c is at the intersection of vertical line bc and horizontal line of ordinate $R_{xo}/R_t = 2.5$. Draw a straight line from d (SP $= 0$, $R_{xo}/R_t = 1$) through c to the intersection with the vertical line corresponding to $R_{mf}/R_w = 20$. If R_{mf}/R_w is not known, enter SSP (-91 mv in present example) in f and draw slanting line fg. At point e, read by interpolation $S = 35$ per cent. The S scale on left-hand part of the chart assumes that S_{xo} is equal to $\sqrt[5]{S}$. If S_{xo} is thought to have another value, use right-hand part of the chart as shown on example assuming $S_{xo} = .7$ (or residual oil saturation ROS $= 30$ per cent: draw line eh parallel to the S lines and from h a horizontal line to the intersection with the vertical line for $S_{xo} = .7$, and read $S = 30$ per cent.

For completeness, a chart of porosity is also given in Fig. 6. This chart gives the solution of relations (3), (4), and (6), with only a small systematic error which has been tolerated for the sake of simplicity. To use this chart one first locates the intersection of the proper R_{xo}/R_t and α lines in the bottom part of the chart, and then goes vertically to the applicable line of R_{xo}/R_{mf} (which is F_a). From this point one goes horizontally to the right and reads the porosity corresponding to the estimated residual oil saturation. The shaly sand represented by point A of Fig. 4 is used on the chart as an illustration, giving an effective porosity of approximately 36 per cent.

Incidentally, this chart shows quite clearly that very low values for R_{xo}/R_{mf} (apparent formation factor F_a) can be quite valid, and result from the influence of the shale content as represented by the quantitative relations from which the chart was computed.

In addition to the parameters R_{xo}, R_t and PSP, it is necessary to know R_w (or α) and S_{xo}. Often it is possible to find in the neighborhood of the shaly sand under study a clean sand giving a fully developed SP curve, and this value can be used to compute R_w from the relation SSP $- E_f = -K \log R_{mf}/R_w$. As mentioned previously, the electrofiltration potentials are often small enough to be neglected in the use of this equation. If no clean sand can be found, R_w must be obtained from direct measurements, or derived from statistics for the same type of formation.

S_{xo} is usually inferred from the statistical study of the residual oil in core analysis. As reported by various authors, it is believed that the residual oil saturation is usually in the range 10 to 30 per cent.

Finally, for sands with shale laminations, p, the proportion of shale, can be computed using the formula

$$p = \frac{\dfrac{R_t}{R_{xo}} \quad \dfrac{S^2}{S_{xo}^2} \quad \dfrac{R_{mf}}{R_w} \quad -1}{\dfrac{S^2}{S_{xo}^2} \quad \dfrac{R_{mf}}{R_w} \quad -1} \times \frac{R_{sh}}{R_t}.$$

CONCLUSION

Methods have been suggested for the qualitative interpretation of shaly sands, which are based on theoretical and experimental data published by other investigators, and on results derived from the examination of field logs. Furthermore, a quantitative analysis has been presented.

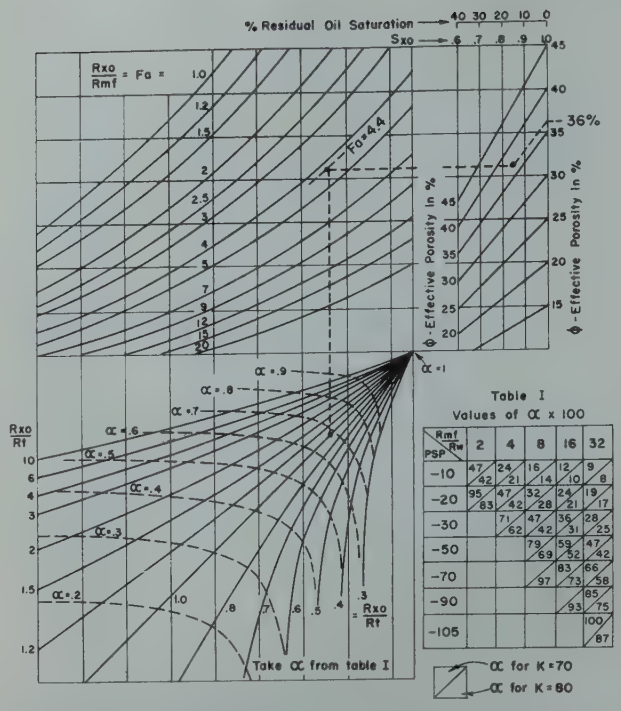

FIG. 6 — CHART FOR FINDING THE EFFECTIVE POROSITY, ϕ, OF SHALY SANDS. USE OF THE CHART IS ILLUSTRATED FOR SHALY SAND CORRESPONDING TO POINT A OF FIG 4.

A plot of R_{xo}/R_t vs PSP on semi-log paper yields interesting qualitative information concerning the presence or absence of hydrocarbons in a shaly sand. Furthermore, it has been shown that the presence of hydrocarbons in shaly sands can often be recognized qualitatively by comparing R_t, true resistivity of the bed, to the product of F_a, an apparent formation factor given by the MicroLog, and R_{wa}, an apparent connate water resistivity derived from the SP curve.

For a valid application of the methods, improved accuracy is definitely necessary in the determination of the electrical parameters involved.

DEFINITION OF TERMS AND SYMBOLS

SSP — Static SP — The Static SP is the deflection of the SP curve which is obtained when a *clean* formation is thick enough that the influence of bed thickness, mud column and invasion are negligible. The SSP is equal to the total emf generating the spontaneous currents.*

PSP — Pseudo-Static SP — Same definition as for Static SP, but applied to the case of a *shaly* formation.*

α — SP Reduction Factor — ratio of the PSP opposite a *shaly* formation to the value of the SSP which would obtain if the formation were *clean*, all *other conditions being the same*. In a series of sands, either shaly or clean, α may be taken as the ratio of the SP deflection opposite a shaly sand to the SP deflection opposite a clean sand, provided both sands are thick enough, contain connate water of the same resistivities and are drilled with muds of the same resistivities.*

R_t — true resistivity of a given formation. In the case of a sand containing laminated shales, this value is

*See also footnote regarding PSP and SSP, page 28.

related to a bulk of material which is very large with respect to the thickness of each sand and shale bed. R_t, in this case, is therefore the harmonic average* of the resistivities of the individual sand and shale beds.

R_{xo} = resistivity of the invaded zone immediately adjacent to the bore hole.**

R_o = resistivity of 100 per cent water saturated sands, whether clean or shaly.

R_{sh} = resistivity of shale laminations.

R_c = resistivity of the dispersed clays.†

R_w = resistivity of connate water.

R_{mf} = resistivity of mud filtrate.

R_z = resistivity of the mixture of dispersed clays and connate water in the non-invaded part of a porous formation.‡

R_{zo} = resistivity of the mixture of dispersed clays and mud filtrate in the invaded part of a formation immediately adjacent to the bore hole.

ϕ = effective porosity, space per unit volume of formation occupied by fluids.

ϕ_z = total porosity, space per unit volume of formation occupied by fluids and dispersed clays.

F = formation factor of a clean sand.

F_z = in the case of a sand containing dispersed clays, formation factor corresponding to the total porosity.

p = proportion of shale in a sand containing shale laminations.

q = in a sand containing dispersed clays, proportion of the total porosity occupied by these clays.

S = connate water saturation in the effective pore space (pore space occupied by fluids).

S_{xo} = mud filtrate saturation in the *effective* pore space for the part of the invaded zone immediately adjacent to the bore hole.

S_z = in sands containing dispersed clays, proportion of *total porosity* occupied by the mixture connate water-dispersed clays.

S_{zo} = proportion of total porosity occupied by the mixture mud filtrate-dispersed clays in the part of the invaded zone immediately adjacent to the bore hole.

ROS = residual oil saturation in the effective pore space for the invaded zone.

*If a formation is constituted of beds 1, 2, ... n, with thicknesses respectively equal to $e_1, e_2, \ldots e_n$, and resistivities respectively equal to $R_1, R_2, \ldots R_n$, the harmonic average is given by:

$$\frac{e_1 + e_2 + \ldots\ldots + e_n}{R_{\text{harmonic average}}} = \frac{e_1}{R_1} + \frac{e_2}{R_2} \ldots\ldots + \frac{e_n}{R_n}$$

whereas the arithmetic average would be:

$$\frac{e_1R_1 + e_2R_2 + \ldots\ldots + e_nR_n}{e_1 + e_2 + \ldots\ldots + e_n}$$

Any system of resistivity measurement in a bore hole (normal, lateral, Laterolog, Induction Log) ... gives the harmonic average of the resistivities of the individual beds included within the bulk of material involved in the measurement.

**The values recorded with the MicroLog, or the MicroLaterolog, are related to much smaller volumes of material than those measured with the normal, lateral, Laterolog, or Induction Log. In order to compare both kinds of measurements, the values given by the MicroLog, or MicroLaterolog, should be averaged (harmonic average) over the same intervals for which the values of R_t are taken.

†R_c is introduced as a convenient factor for the discussion, without any implication regarding the actual nature of the conductivity of the dispersed clays.
Experimental data indicate that for practical purposes in usual field conditions R_c can be assumed to have roughly the same value in the invaded zone and in the non-invaded part of a porous formation.
In a given zone R_c is not necessarily equal to the resistivity of the laminated shales.

‡The subscript z relates to mixtures of electrolyte and dispersed clays.

ACKNOWLEDGMENTS

The authors are indebted to H. G. Doll and L. Allaud for their valuable suggestions.

They wish also to express appreciation for discussions held with A. A. Perebinossoff and C. Rosoff.

Acknowledgments are also due to M. Martin, K. S. Kunz, R. P. Alger, C. F. Gallagher, H. F. Schwede and C. W. Bailey for their efficient assistance in the preparation of this paper.

The authors wish to express their appreciation to the oil companies who provided data for this study and released the examples used to illustrate this paper.

REFERENCES

1. Archie, G. E.: "The Electrical Resistivity Log as an Aid in Determining Some Reservoir Characteristics," *Trans.*, AIME (1942), **146**, 54.
2. Tixier M. P.: "Electric-Log Analysis in the Rocky Mountains," *Oil and Gas Jour.* (June 23, 1949), **48**, 143.
3. Wyllie, M. R. J.: "A Quantitative Analysis of the Electrochemical Component of the SP Curve," *Trans.*, AIME (1949), **186**, 17.
4. Doll, H. G.: "The MicroLog — A New Electrical Method for Detailed Determination of Permeable Beds, *Trans.*, AIME (1950), **189**, 155.
5. Doll, H. G.: The MicroLaterolog, *Trans.*, AIME (1953), **195**, 17.
6. Doll, H. G.: The SP Log: "Theoretical Analysis and Principles of Interpretation," *Trans.*, AIME (1948), **179**, 146.
7. Doll, H. G.: "The SP Log in Shaly Sands," *Trans.*, AIME (1950), **189**, 205.
8. Patnode, H. W., Wyllie, M. R. J.: "The Presence of Conductive Solids in Reservoir Rocks as a Factor in Electric Log Interpretation," *Trans.*, AIME (1950), **189**, 47.
9. de Witte, L.: "Relations Between Resistivities and Fluid Contents of Porous Rocks, *Oil and Gas Jour.* (Aug. 25, 1950), **49**, 120.
10. de Witte, L.: "Experimental Studies on the Characteristics of the Electrochemical Potential Encountered in Drill Holes," AIME Meeting, Los Angeles (October, 1950).
11. Berg, J. W., Jr.: "Conductivity Study of Aqueous Kaolin NaCl Mixtures," *Producers Monthly* (January, 1952), **16**, 36.
12. Wyllie, M. R. J.: "Clay Technology in Well Log Interpretation," National Conference of Clays and Clay Technology, University of California (July, 1952).
13. McCardel, William, Winsauer, W. O., and Williams, M.: "Origin of Electric Potential Observed in Wells," *Trans.*, AIME (1953), **195**, 41.
14. Winsauer, W. O., and McCardell, W. M.: "Ionic Double Layer Conductivity in Reservoir Rock," *Trans.*, AIME (1953), **195**, 129.
15. Winsauer, W. O., Shearin, H. M., Jr., Masson, P. H., and Williams, M.: "Resistivity of Brine-Saturated Sands in Relation to Pore Geometry," *Bulletin*, AAPG; (1952), **36**, 253. ★★★

A TEN-POUND CEMENT SLURRY for OIL WELLS

HENRY F. COFFER
J. J. REYNOLDS

ROSCOE C. CLARK, JR.
MEMBERS AIME

CONTINENTAL OIL CO.
PONCA CITY, OKLA.

THE WESTERN CO.
MIDLAND, TEX.

T. P. 3801

ABSTRACT

A cement slurry lightweight additive has been adapted in the Conoco laboratories for use in oil well cements. This additive makes possible the use of air to lighten oil well cement slurries. Specifically, the additive consists of small clay bubbles of air having sufficient strength to resist crushing by bottom hole pressures. Clay bubble cement slurry weights can be safely reduced to 10 lbs/gal. In addition, the clay bubbles tend to act as lost circulation materials and to provide a cement texture which should produce good perforating characteristics. Clay bubble cement is relatively impermeable.

INTRODUCTION

In many areas in Oklahoma, Texas, Wyoming, and California, difficulties are experienced during casing cementing operations with lost returns caused by the high density of the cement slurries. Wells in these areas are ordinarily drilled with 9 to 11 lbs/gal. drilling mud while neat cement slurries may range in densities from 14.5 to 17 lbs/gal. In these areas, cement slurry weights are at present being successfully reduced to around 12 lbs/gal. (under bottom-hole conditions) by the use of additives in the cement. Since the use of additives will decrease the strength which the cement will develop, the amount of additives which can be used must be based on the minimum cement strength which is acceptable; and thus the maximum slurry weight can be reduced. At present, the minimum tensile strength generally acceptable is 50 lbs/sq in. cured for 24 hours under bottom-hole temperature. This figure is based on laboratory tests[1] and on a large number of cement jobs which have been conducted using cement which will not develop more than 50 psi tensile strength in 24 hours under bottom-hole conditions.

Two additives are now in use for decreasing cement slurry weights. These are expanded perlite and/or bentonite. The density of both of these materials is greater than that of the cement slurry; however, large quantities of water may be added with these materials without producing a slurry which will settle out of suspension. It is these large quantities of water which contribute to the reduction in the slurry weight. The minimum slurry weight at present obtainable with expanded perlite and/or bentonite is approximately 12 lbs/gal. using a standard Portland cement slurry. In many areas, this weight reduction is insufficient; and returns are still lost during casing cementing operations. In many cases, the pay formation itself is fractured; and a considerable quantity of this cement is lost to the pay zone. It is therefore believed that if cement slurry weights can be reduced to as low as 10 lbs/gal., two advantages will accrue:

1. The lighter densities (10 to 12 lbs/gal.) should mitigate or eliminate lost returns during casing cementing operations.
2. Cement slurries above 12 lbs/gal. (the present minimum limit) should develop considerably more strength than is now being obtained. A tensile strength of 100 psi is desirable.[1]

It is the object of this paper to describe a cement slurry having a weight of 10 lbs/gal. and capable of

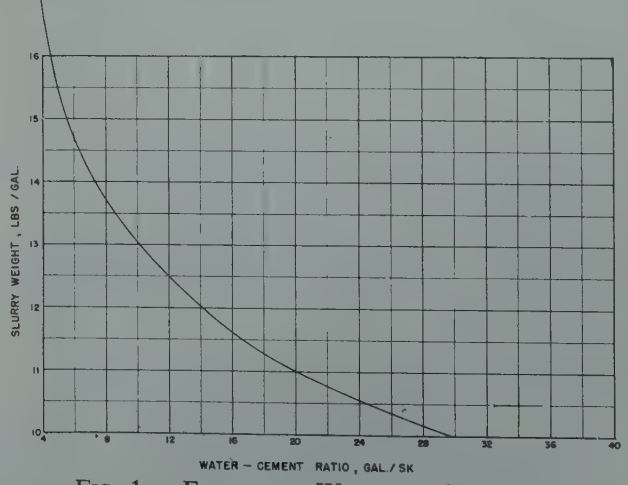

FIG. 1 — EFFECT OF WATER ON REDUCING SLURRY WEIGHTS.

[1]References given at end of paper.

Manuscript received in the Petroleum Branch office Jan. 15, 1954. Paper presented at the Annual AIME Meeting in New York, N. Y., Feb. 13-17, 1954.

FIG. 2 — CLAY BUBBLES.

developing a tensile strength of at least 50 lbs/sq in. in 24 hours under bottom-hole conditions.

PROCEDURE

LABORATORY EVALUATION

It was felt that it would be difficult to reduce cement slurry weights to less than 12 lbs/gal. by the use of additional water or by the use of additives which would permit the addition of more water. The curve presented in Fig. 1 illustrates the quantities of water which would have to be added to a slurry in order to reduce slurry weights to various values. From this curve, it can be seen that almost 30 gals. of water per sack of cement would have to be used in order to reduce the slurry weight to a figure of 10 lbs/gal. Since this is more than twice the amount of water which can now be added without seriously impairing the cement strength, it is believed impractical to attempt to reduce slurry weights to 10 lbs/gal. by the use of additional water. The easiest method for reducing slurry weights is by the entrapment of air in the slurry. This, however, is impracticable in oil well cements unless the air is contained in a bubble of material which will be able to withstand bottom-hole pressures without collapsing.

The search for an inexpensive material of this type resulted in a laboratory trial of an additive consisting of clay bubbles (Fig. 2), that is, small spheres of clay containing a pocket of air in the center. These clay bubbles were found to be very effective for reducing slurry weights without the high losses in strength usually encountered. The curves in Fig. 3 illustrate the tensile strengths obtainable with the clay bubbles versus the slurry weight of the clay bubble cement slurry. Curves are also presented showing the results of laboratory tests conducted to determine the strength versus slurry weight of expanded perlite and bentonite slurries* in order

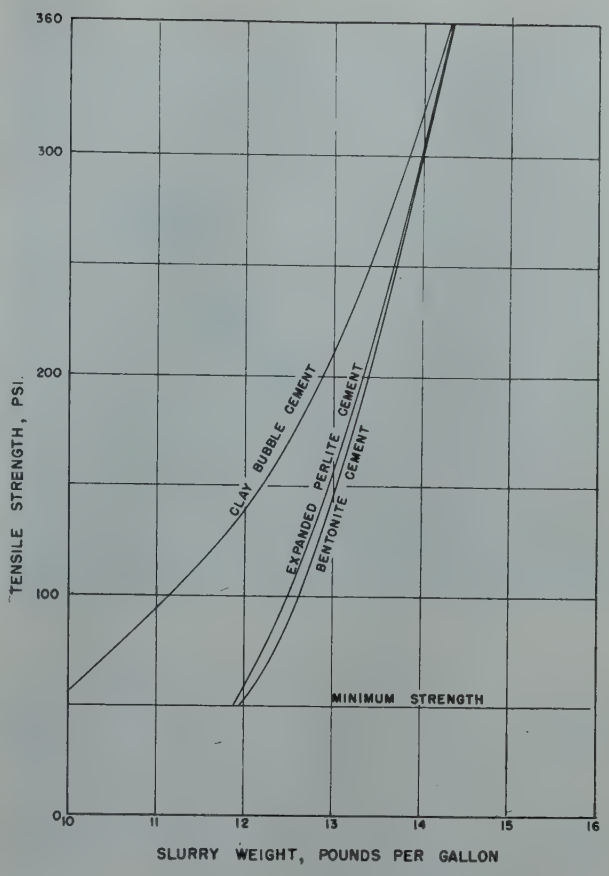

FIG. 3 — LIGHT WEIGHT CEMENT TENSILE STRENGTHS AND SLURRY WEIGHTS.

to compare the effectiveness of the three additives. All slurry weight measurements were made under 5,000 psi pressure, and all cement specimens were cured for 24 hours at 100°F under 5,000 psi pressure prior to measuring their strengths.

Slurry weight measurements were made at atmospheric pressure and at 5,000 psi pressure. These measurements were made by determining the weight and volume of samples of the slurries in a pycnometer at each of the above two pressures. All cement slurry strength developments reported were determined by curing the samples in an autoclave at 5,000 psi pressure and at a temperature of 100°F for 24 hours.

As a result of the air pockets contained in the clay bubbles, clay bubble cement is quite porous, as may be seen from the picture of a cross section of the cement in Fig. 4. The permeability of the clay bubble cement, however, is essentially the same as that of neat cement, all samples tested measuring less than .05 of a millidarcy.

When first tested, the clay bubbles were found to absorb large quantities of water under pressure. It was found that most of this water intake could be eliminated by the addition to the slurry of additives made up of long chain molecules which would not seriously affect the strength development of the cement. The addition of clay particles such as bentonite was found to be effective in preventing water intake in bubbles made up of certain clays. Clay bubble slurries still increase slightly in density when pressure is applied to the slurry. This is probably due to compression of the air clinging to the outside of the bubbles. The density increase is very little; however, it should be taken into consideration when calculat-

*The same cement was used for all tests.

FIG. 4 — CROSS SECTION OF CLAY BUBBLE CEMENT.

ing the slurry weights desired at the bottom of the hole. For example, if a 10-lb slurry is desired at the bottom of the hole, it would have to be mixed to a slurry weight of 9 lbs/gal. at the surface.

The results of standard API RP10B thickening time tests for a cement slurry with and without clay bubbles indicated that clay bubbles will not affect the pumpability times of Portland cements.

Considering the cost of clay bubble slurries, the curves in Fig. 5 illustrate the average cost of cement slurries in dollars per cubic foot of slurry for various slurry weights of the clay bubble cement,* expanded perlite cement, and bentonite cement. From the Fig. 5, it can be seen that the clay bubble cement slurries are more expensive than bentonite slurries and less expensive than neat or expanded perlite slurries.

FUTURE WORK

Field tests are planned for the near future using this cement. Pilot tests are still underway, however, to determine the most effective type of raw clay which can be used for making bubbles and to determine the most effective manufacturing methods. Although clay bubbles are at present very effective for reducing cement slurry weights, indications are that clay bubbles can be made still more effective in oil well cements.

DISCUSSION

Clay bubbles are not yet available in large quantities; however efforts are being made to obtain this material as soon as possible.

Clay bubble cement, in addition to being practicable at slurry weights of 10 to 12 lbs/gal., will develop considerably more strength than expanded perlite or bentonite cements at slurry weights greater than 12 lbs/gal. Being made of small particles, clay bubbles should tend to prevent the loss of cement slurries into zones of lost circulation should returns be lost during a cementing operation.

The porous nature of the cement should produce good perforating characteristics by reducing the degree of cracking and shattering of the cement and by increasing the penetrability of bullets or shaped charges.

*Estimated cost.

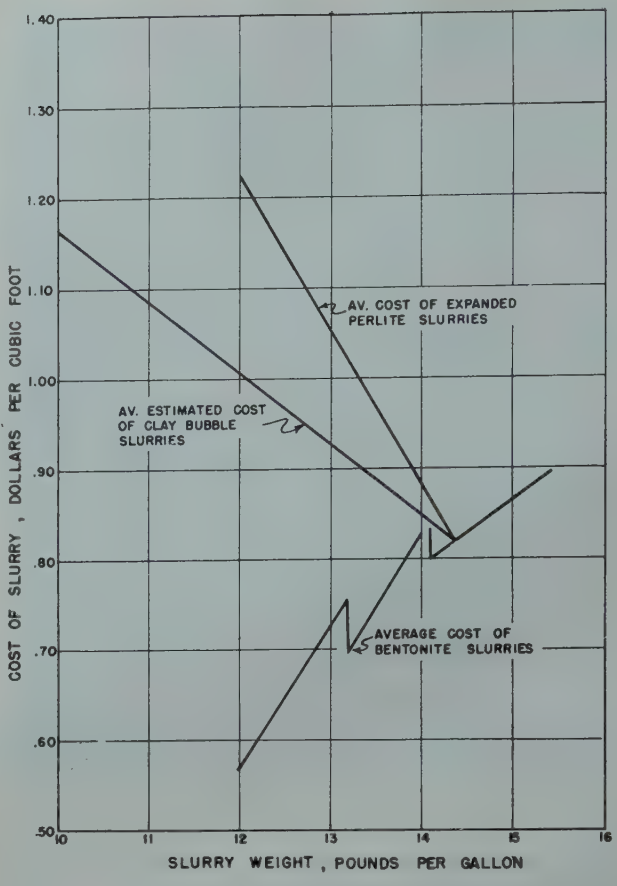

FIG. 5 — COST OF LIGHTWEIGHT CEMENT SLURRIES.

CONCLUSIONS

Based on the results of laboratory and field tests, it is concluded that:

1. When mixed with Portland cement, clay bubbles will produce a cement slurry which has a density of 10 lbs/gal. and which will develop adequate strength for casing cementing operations.
2. Clay bubble cements exhibit a low permeability.
3. Density for density clay bubble cement will develop more strength than any cement presently available.
4. Clay bubbles do not affect the pumpability times of Portland cements.
5. Because of its texture, clay bubble cement should exhibit good perforating characteristics.
6. The use of clay bubble cement should lead to the use of cement slurries having densities designed for the specific job at a cost not more than that being paid for current light weight slurries.

ACKNOWLEDGMENTS

The authors wish to express their appreciation to the Kanium Corp. for furnishing test samples, and to the management of Continental Oil Co. for permission to publish this paper.

REFERENCES

1. Clark, Roscoe C., Jr.: "Requirements of Casing Cement for Segregating Fluid Bearing Formations," *Oil and Gas Jour.* (Apr. 20, 1953).
2. "Making Bubbles from Clay," Article, *Chemical Engineering,* December, 1952.

★★★

RESISTIVITY LOGGING in THIN BEDS

LEENDERT DE WITTE | CONTINENTAL OIL CO.
PONCA CITY, OKLA.

T. P. 3803

ABSTRACT

Conventional resistivity logs consisting of a short normal, a long normal, and one or more long lateral curves do not give data that allow a complete quantitative interpretation in beds thinner than 20 ft. Reservoir rocks usually exhibit zones of continuous homogeneity of quite limited thickness where the long lateral curves become useless because of adjacent bed effects and boundary phenomena. If the beds are 12 ft or thicker, the short and long normals may be used for qualitative interpretation, which can be streamlined by the application of simplified departure curves. For beds of a thickness less than twice the long normal spacing, this procedure breaks down.

The combination of the limestone curve, the laterolog or guard electrode log, and the microlaterolog permit quantitative interpretation for beds that are at least 10 ft thick, provided the mud resistivity and the hole diameter are known with sufficient accuracy.

For beds thinner than 10 ft, combinations of the microlaterolog with short spaced laterologs and pseudo laterologs appear to be promising. Interpretation of these curves again requires the application of simplified departure curves. Resolution of various possible combinations was analyzed using departure curve data calculated on the Whirlwind I computer at the Massachusetts Institute of Technology.

A field example is shown using the microlaterolog-microlog combination, and the combination of a 6-in. modified laterolog plus a 6-in. pseudo laterolog.

INTRODUCTION

For the purpose of quantitative interpretation of resistivity logs in porous formations, we want to obtain two essential quantities from the logs, namely, the true resistivity of the undisturbed formation, R_t, and the resistivity of the part of the formation invaded by mud filtrate, R_i. The apparent resistivities of all conventional logging devices are functions of these two parameters and are also influenced by a third unknown parameter, the diameter of the invaded zone, d_i.

It has been shown[1] that from the normal curves alone it is impossible to arrive at a unique solution for the three unknowns, R_t, R_i, and d_i. In very thick homogeneous beds, if invasion is not too deep, we can obtain a fair approximation to R_t from the long lateral curves and then use the two normal curves to find R_i and d_i. Even under the most favorable conditions, the resolution of this system is not very good. The short normal does not give a reasonable approximation to R_i unless invasion is very deep ($d_i > 16$ hole diameters). For very deep invasion, however, the long laterals no longer approximate R_t.

For bed thickness between 20 and 40 ft, the long laterals are affected appreciably by the adjacent beds; and the curves are distorted by boundary anomalies to the extent that they lose their quantitative usefulness in most cases. For the same bed thicknesses, the normal curves still function reasonably well.

Although it is impossible to find unique solutions for R_i and R_t using the normal curves alone, we can obtain a reasonable approximation for the ratio R_i/R_t through the use of simplified departure curves. This fact was brought to our attention by A. J. de Witte, geologist with Continental Oil Co. As the magnitude of R_i/R_t is a major clue to the presence of oil in formations, this method can be used to good advantage for qualitative analysis and will be discussed in somewhat greater detail.

With the aid of suitable bed thickness corrections, the analysis of the normal curves may be used for bed thicknesses larger than 12 ft. For thinner beds, the method rapidly loses its resolution; and we have to resort to different types of resistivity logs if we want to attempt to analyze the curves quantitatively.

The inadequacy of conventional resistivity curves in thin beds is far more serious than generally realized. Fig. 1 shows a conventional E. S. with a 16-in. and 64-in. normal and a 16-ft lateral through a section of Lansing-Kansas City lime, in comparison to a guard electrode survey through the same section in a neighboring well. The porous zones, which show up as low resistivity breaks on the guard electrode log, are completely masked by adjacent bed effects and boundary anomalies on the conventional curves. Even the short normal shows most of the porous zones only as vague deflections and in many cases fails to register their

[1]References given at end of paper.

Manuscript received in the Petroleum Branch office Sept. 14, 1953. Paper presented at the Petroleum Branch Fall Meeting in Dallas Oct. 19-21, 1953.

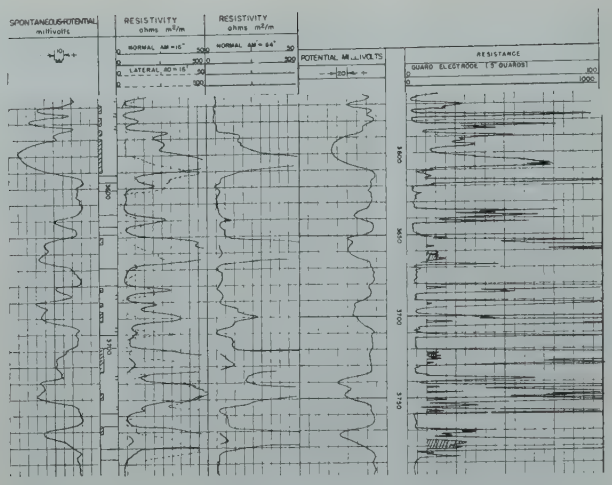

FIG. 1 — A CONVENTIONAL ELECTRIC LOG SURVEY THROUGH A SECTION OF LANSING-KANSAS CITY LIME. AND A GUARD ELECTRODE LOG THROUGH THE SAME SECTION.

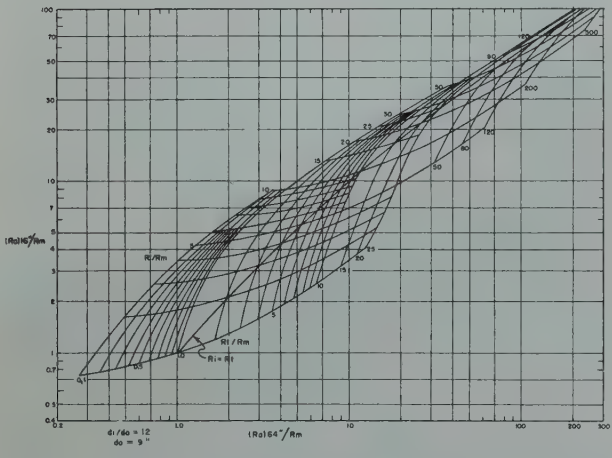

FIG. 2 — SIMPLIFIED DEPARTURE CURVES — 16-IN. AND 64-IN. NORMAL DEVICES.

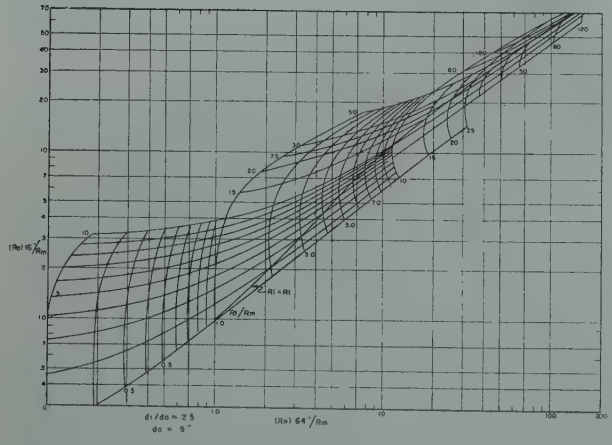

FIG. 3 — SIMPLIFIED DEPARTURE CURVES — 16-IN. AND 64-IN. NORMAL DEVICES.

presence completely. It is obviously out of the question to make a quantitative analysis for the porous producing horizons from the conventional curves in cases like this.

SIMPLIFIED DEPARTURE CURVES FOR THE NORMAL DEVICES

As stated before, the normal curves cannot give unique solutions for R_i, R_t, and d_i. If, however, we assume a certain value of d_i, then two normal apparent resistivities suffice to determine R_i and R_t. These determinations are most easily carried out with the help of simplified departure curves of the type shown in Figs. 2 and 3. Each graph is made up for a certain hole diameter and a given value of d_i/d_o. After measuring the apparent resistivities for the 16-in. normal and 64-in. normal from the logs, we find a value for R_i/R_m and R_t/R_m from each chart corresponding to each assumed value of d_i/d_o (where d_o is the hole diameter).

Fig. 4 shows a conventional E. S. through the Sussex sand in a well in the Meadow Creek field, Wyo. We notice that the long lateral curve is distorted while the normals appear to give reliable deflections, especially in the center portion of the bed (3,550-67).

The mud resistivity, R_m, at formation temperature is 2.0 ohmmeters. The hole diameter is 9 in. The apparent resistivities of the 16-in. normal and the 64-in. normal are respectively: $(R_a)16 = 28\Omega m$; $(R_a)64 = 18.5\Omega m$. This gives $(R_a)16/R_m = 14$ and $(R_a)64/R_m = 9.25$.

For simplified departure curves as shown in Figs. 2 and 3, we obtain the following possible answers:

d_i/d_o	R_i/R_m	R_t/R_m	R_i/R_t
12	15.5	3.7	4.19
5	18.0	6.0	3.00
2.5	26.0	6.2	4.2

The ratio of R_i/R_t is indicative of the fluid content of the formation. Various methods have been described to calculate the water saturation from this ratio.[2,3]

Continental Oil Co. at present uses a set of nomographs based on analysis of the SP curve and on the equations 20 and 22 given in Ref. 3. The value of the SP curve for the sand under analysis is 34 mv. The connate water resistivity for the Sussex sand is $0.3\Omega m$ at formation temperature. This gives a K_t factor of 41.3 in the equation $SP = K_t \log R_{mf}/R_w$.* Corrected to 77°F., the K factor becomes $K_{77} = 40.3$.

Using the nomograph for $K_{77} = 40$ shown in Fig. 5, we find the following values for the water saturation S_w:

R_i/R_t	S_w
4.19	100 per cent
3.0	70 per cent
4.2	100 per cent

The above S_w values, obtained for assumed d_i/d_o ratios ranging from 2.5 to 12, show that in all probability the sand contains only water. Although by this procedure, we do not arrive at a unique quantitative answer, the qualitative distinction between oil and water bearing formations can be made in most cases, where the beds are thick and homogeneous enough for the normal curves to give reliable deflections.

*The coefficient K_t used in this equation is equal to the product αK in the Schlumberger terminology where K is the SP coefficient for a clean sand and α is the ratio of pseudo static SP of a shaly sand to the static SP of a clean sand (for the same values of R_{mf} and R_w).

A similar procedure of interpretation using simplified departure curves could be worked out for other conventional curves, say a short normal and one long lateral. In most cases this would require correcting the long laterals for bed thickness effects as may be done by the use of the maximum-minimum formulae.[4] These corrections, however, all neglect the influence of the drill hole and of invasion; and they are, therefore, not very accurate. In view of the much larger number of lateral spacings in use than the number of standard normal spacings, it is far more practical to use a simplified departure curve system for the normals in areas where two normal curves are run.

DETERMINATION OF INVADED ZONE RESISTIVITY FROM THE MICROLATEROLOG

A more direct approach to the determination of R_1 and R_t in thin sands can be made by measuring the invaded zone resistivity directly with a microlaterolog.[5]

To find R_1 the reading of the microlaterolog has to be corrected somewhat to take the presence of mudcake into account. To do this, one or two microlog curves are used and mudcake corrections are made with the aid of suitable departure curves.[5]

The determination of R_1 from the microlaterolog assumes that the invaded zone has a fairly constant resistivity from the boreface out to its diffuse contact with the undisturbed formation. Evidence in support of this assumption has been given by experimental work on resistivity distributions in invaded zones of porous formations.[6]

Fig. 6 shows a microlaterolog and conventional microlog through the Shannon sand in the West Sussex field, Johnson County, Wyo. In the section from 2,773-2,776, the microlaterolog apparent resistivity is approximately 15 ohmmeters. Both the microinverse and the micronormal curves read 9.2 ohmmeters. The values of R_m and R_{mc} were measured as 1.6 and 1.79 ohmmeters (corrected to formation temperature). This gives R_1 ½-in./R_{mc} = 5.15; R_2-in./R_{mc} = 5.15; and R_{mLL}/R_{mc} = 8.4. This gives for the mudcake thickness (MCT) = .12 in. Using R_{mLL}/R_{mc} = 8.4 and MCT = .12 in., we find from the departure curves for the 9/16-9/16-9/16 microlaterolog, that R_1/R_{mc} = 9.5 or R_1 = 17 Ω_m.

THE LATEROLOG-LIMESTONE CURVE COMBINATION

If R_1 is determined from the microlaterolog, we have two remaining unknowns, namely, the extent of invasion (described by the invasion diameter d_1) and the true resistivity R_t. Theoretically any two additional apparent resistivity readings which are not influenced by adjacent bed effects or distorted by boundary phenomena, should give us sufficient information to solve for d_1 and R_t. A further criterion is that the current patterns of the two devices are sufficiently different so that the registered apparent resistivities are related to the unknown quantities by dissimilar (and therefore independent) equations.

For beds thicker than 10 ft the combination of the laterolog[7] and the limestone device fulfills in most cases the above conditions.

The solution of the two simultaneous equations given by the relations between the laterolog and limestone curve apparent resistivities and d_1 and R_t can be represented graphically by simplified departure curves. The departure curve charts can be made up for given values

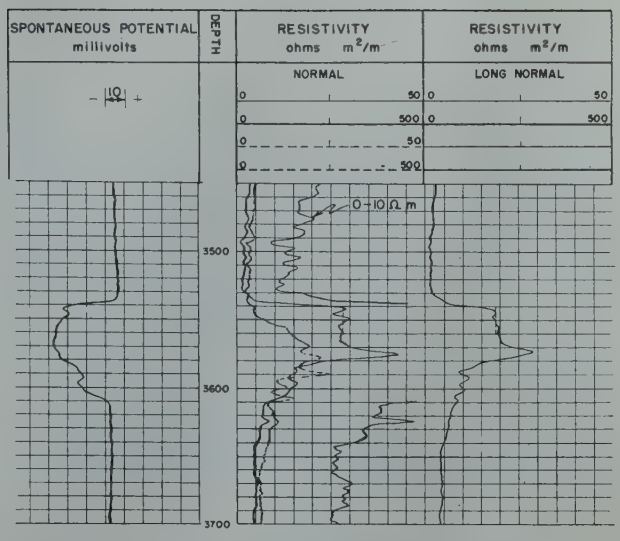

FIG. 4 — A CONVENTIONAL ELECTRIC SURVEY, SUSSEX SAND, MEADOW CREEK FIELD, WYO.

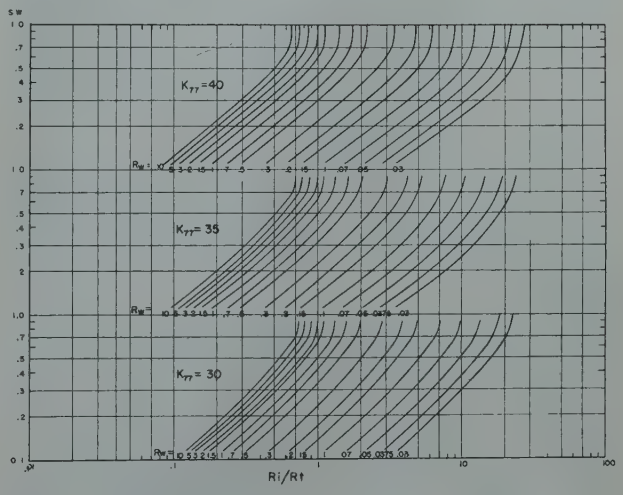

FIG. 5 — NOMOGRAPH FOR SATURATION CALCULATIONS.

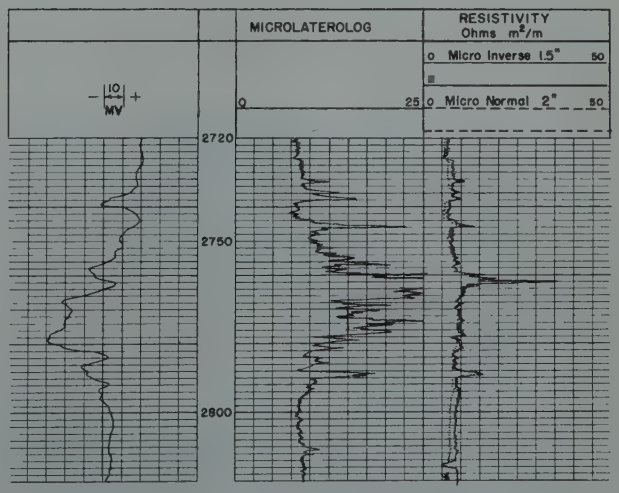

FIG. 6 — MICROLATEROLOG AND CONVENTIONAL MICROLOG, SHANNON SAND, WEST SUSSEX FIELD, WYO.

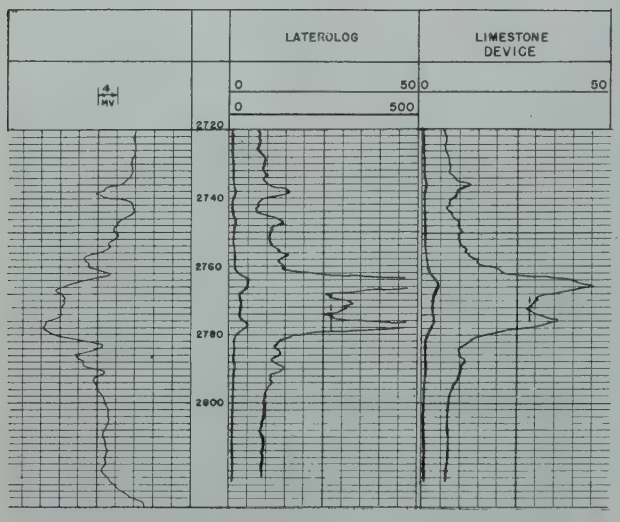

FIG. 7 — 16-IN. LATEROLOG — 7-IN. AND 37-IN. LIMESTONE CURVE, SHANNON SAND, WEST SUSSEX FIELD, WYO.

of R_i/R_m. The abscissa carries the ratio of the laterolog apparent resistivity to R_m (R_{LL}/R_m), while the ordinate carries the ratio of the limestone curve apparent resistivity to the mud resistivity (R_{Ls}/R_m). The departure curves are plotted as two families of curves: one set representing constant values of R_t/R_m, while the other set represents given values of d_i/d_o.

In this form the charts are completely direct reading: a set of values of R_{LL}/R_m and R_{Ls}/R_m obtained from the logs, determines the position of a point on the departure curve chart. By visual interpolation, we easily obtain the values of R_t/R_m and d_i/d_o corresponding to this point.

Fig. 7 is a copy of a 16-in. laterolog-7 and a 37-in. limestone curve through the same section of Shannon sand that was shown in Fig. 6.

We shall apply a simplified departure curve analysis to the same zone for which R_i was found from the microlaterolog (2,772-76). Although the readings are taken in this 3-ft zone, the immediately adjacent beds have resistivities that differ by a sufficiently small amount, so that for practical purposes adjacent bed effects can be neglected.

The laterolog apparent resistivity in this zone is

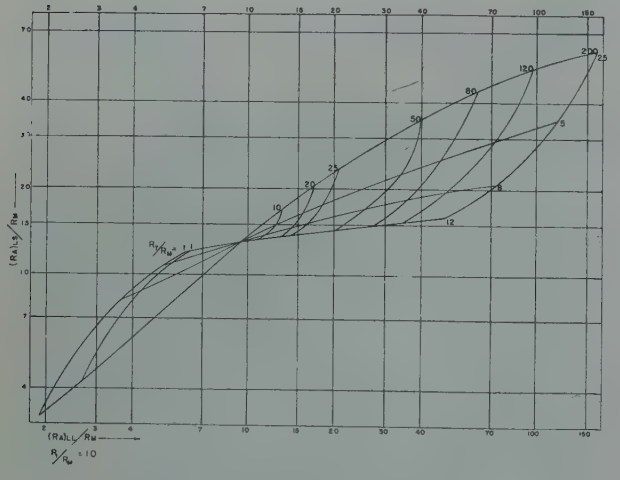

FIG. 8 — SIMPLIFIED DEPARTURE CURVE FOR LATEROLOG LIMESTONE CURVE COMBINATION.

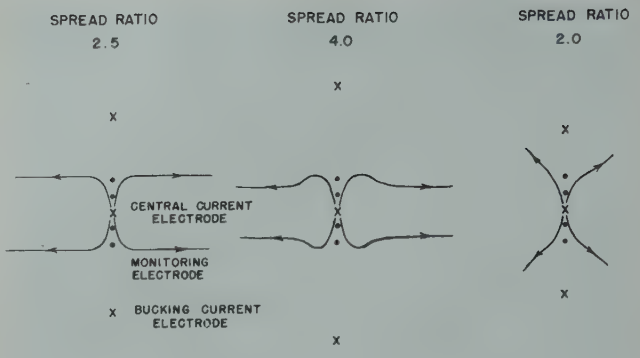

FIG. 9 — THE EFFECT OF SPREAD RATIOS.

approximately $27\Omega m$ while $R_{Ls} = 28.5\Omega m$. The mud resistivity at formation temperature is $1.6\Omega m$. This gives $R_{LL}/R_m = 16.9$ and $R_{Ls}/R_m = 17.8$. The foregoing microlaterolog and analysis gave $R_i = 17\Omega m$ or $R_i/R_m = 10.6$.

We select a departure curve chart for $R_i/R_m = 10$ for a close enough approximation. The chart is shown in Fig. 8. Using the R_{LL}/R_m and R_{Ls}/R_m values gives $R_t/R_m = 23$.

The resulting ratio R_i/R_t is .46. Using this value we can make a nomograph interpretation of the oil saturation of the sand if the water resistivity and the K_{77} value are known.

This example illustrates the feasibility of the limestone curve — laterolog method in beds of medium thickness. For beds thinner than 10 ft with adjacent beds of strongly contrasting resistivities, the limestone curve can no longer be relied upon.

Other drawbacks are the fact that the limestone curve deflection is quite sensitive to hole diameter variations and rapidly loses resolution in beds of high resistivity because of its well known ceiling effect. When using the limestone curve-laterolog system, the hole size must be close to bit size or a caliper survey must be run. In beds where $R_i/R_m > 100$, the ceiling effect of the limestone curve causes the resolution of the limestone curve — laterolog interpretation to disappear.

MODIFIED LATEROLOGS

The limestone curve-laterolog combination is a somewhat unbalanced system, as its applicability is limited in all cases by the limestone curve (the laterolog has less adjacent bed effects, is fairly independent of hole diameter variations, and has no ceiling effect.

It is logical, therefore, to look for a device with an intermediate radius of investigation but with other properties comparative to those of the laterolog to take the place of the limestone curve.

The radius of investigation of a laterolog can be controlled by the extent of focusing of the central current sheet. It was shown by Doll[7] that, if the ratio of the bucking current electrode spread to the monitoring electrodes spacing is equal to 2.5 the central current sheet has boundaries which are roughly perpendicular to the axis of the sonde. The above ratio is normally referred to as "spread-ratio." If the spread-ratio is larger than 2.5, the boundaries of the central current sheet converge for some distance outward from the sonde. This makes the cross-section to current increase less rapidly with radial distance from the sonde than in the case of the current sheet with parallel boundaries and increases the radius of investigation. For spread

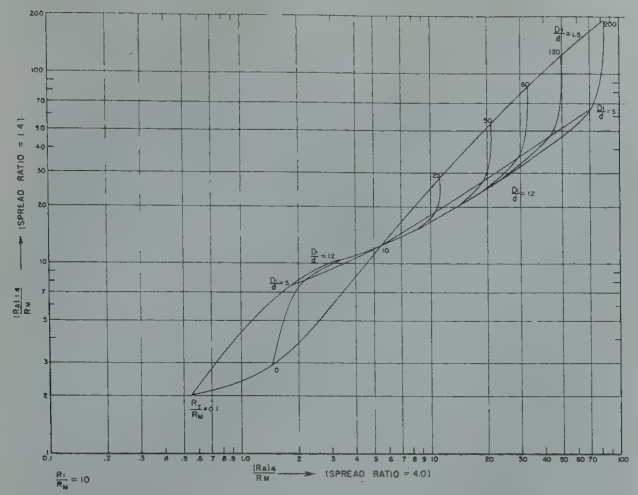

FIG. 10 — SIMPLIFIED DEFARTURE CURVE FOR LATEROLOGS OF DIFFERENT SPREAD RATIOS.

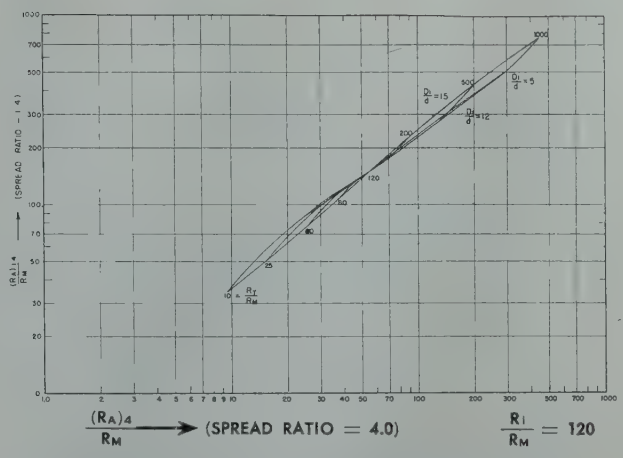

FIG. 11 — SIMPLIFIED DEPARTURE CURVE FOR LATEROLOGS OF DIFFERENT SPREAD RATIOS.

ratios smaller than 2.5, the boundaries of the current sheet diverge and the radius of investigation is smaller than in the case of the current sheet with initially parallel boundaries. Fig. 9 shows schematically the current distributions for laterolog systems with different spread ratios.

If we combine a laterolog with a spread ratio of 4.0 or larger with another arrangement with spread ratio of 2.0 or smaller, we might expect two detailed curves with essentially different current patterns from which d_i and R_t can be determined once R_i has been found from the microlaterolog. In regions of fairly low formation, resistivities ($<$ 20 times the mud resistivity) this is indeed possible. In formations of higher resistivity, the resolution of the method vanishes rapidly. This is due to the fact that at the boreface the current lines of the central current sheet refract towards the normal (to the boreface). The larger the contrast between the formation resistivity and the mud resistivity, the stronger the refraction towards the normal. This causes the boundaries of the current sheet after refraction to become essentially parallel, regardless of whether they started out diverging or converging. If the configuration of the current sheet within the formations becomes very similar for the two devices, then we cease to have two independent equations from which we can solve for d_i and R_t.

The above behavior can be very well illustrated with the use of simplified departure curves. Fig. 10 shows a departure curve chart for a combination of a laterolog with spread-ratio of 1.4 and an arrangement with spread-ratio 4.0 for $R_i/R_m = 10$. From the two laterolog measurements, R_t/R_m can be determined with good accuracy in this case. Fig. 11 shows a chart for $R_i/R_m = 120$. We see that in this case no useful information at all regarding R_t/R_m can be obtained from the combination of two laterologs with different spread ratios.

PSEUDO LATEROLOG — LATEROLOG COMBINATIONS

The problem that remains, is to find a combination of focused resistivity logs that have characteristically different current patterns in beds of relatively high resistivities. An important step in this direction was made by the introduction of Schlumberger's pseudo-laterolog. The pseudo-laterolog has the same electrode arrangement (central current electrode, monitoring span and bucking current electrodes) as the laterolog, except that the return current electrodes have been moved close to the rest of the electrode assembly. The proximity of the return current electrodes causes the bucking current to become ineffective at a short distance from the sonde. The focused current beam starts diverging at a relatively short distance beyond the boreface. Fig. 12 shows the electrode assembly and approximate current patterns of a typical pesudo-laterolog.

As a criterion of performance in high resistivity beds, we can use the resolution of the simplified departure curves for $R_i/R_m = 120$. Fig. 13 shows the departure curves for the original Schlumberger pseudo-laterolog plotted versus the standard 16-in. laterolog for $R_i/R_m = 120$. We notice that the resolution for the determination of R_t/R_m is quite good where $R_t > R_i$. When $R_t << R_i$, the resolution becomes definitely very small. Shown, also, on Fig. 13 is the electrode arrange-

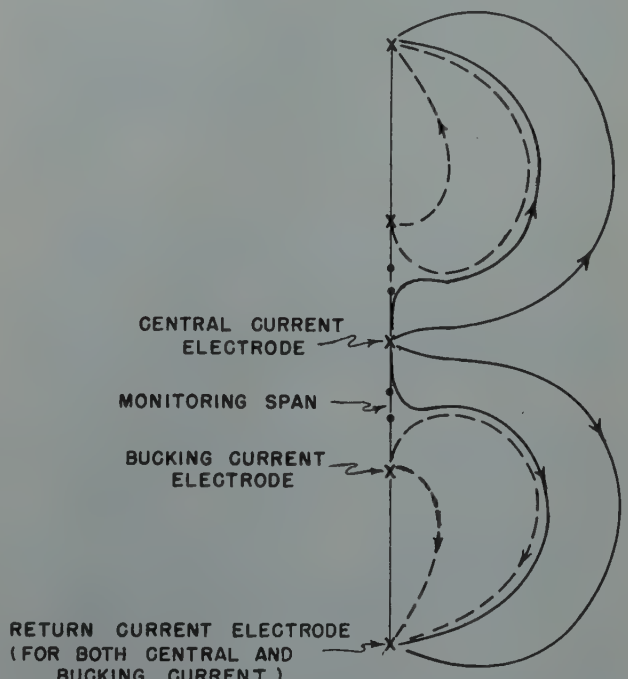
CENTRAL CURRENT ELECTRODE
MONITORING SPAN
BUCKING CURRENT ELECTRODE
RETURN CURRENT ELECTRODE (FOR BOTH CENTRAL AND BUCKING CURRENT)

FIG. 12 — ELECTRODE ASSEMBLY AND CURRENT PATTERN FOR PSEUDO-LATEROLOG.

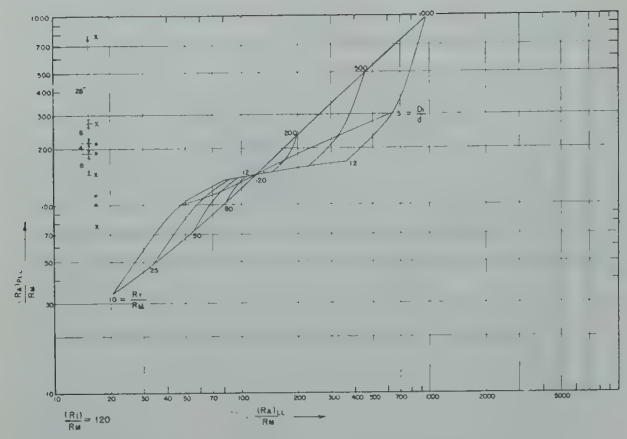

FIG. 13 — SIMPLIFIED DEPARTURE CURVE FOR PROTOTYPE PSEUDO-LATEROLOG COMBINED WITH LATEROLOG.

ment of the prototype pseudo-laterolog. One disadvantage of this arrangement is that the total spread of the central current after divergence covers a span of 96 in. This means that in thin beds the current distribution will be distorted to a considerable extent by the effects of the adjacent beds. Particularly if we have a thin conductive bed, such as a porous zone in limestone, surrounded by dense beds of high resistivity, the dense adjacent beds will limit the divergence of the central current quite drastically. Under such conditions, the departure curves calculated for infinitely thick beds no longer apply.

The best way to reduce the adjacent bed effects on the pseudo-laterolog is to make the spread and spacing as small as possible. After computations of typical departure curves for various spacings, spread ratios, and return current spreads, an experimental sonde was made combining a pseudo-laterolog with 6-in. spacing, a spread ratio of 2 and a return current spread of 28 in., with a laterolog of 6-in. spacing a 28-in. spread (spread ratio 4.67). Fig. 14 shows the electrode arrangement for this combination. Although the number of field tests of this device to date has been quite small, it is believed that satisfactory results can be obtained with it in most cases where the horizons to be analyzed are more than 5 ft thick.

FIELD EXAMPLE OF SHORT-SPACED PSEUDO LATEROLOG-LATEROLOG COMBINATION

The system of short-spaced laterolog and pseudo-laterolog curves was tried out in a section of relatively thin-bedded sandstones and shales of the Canyon formation in the West Flowers field, Stonewall County, Tex.

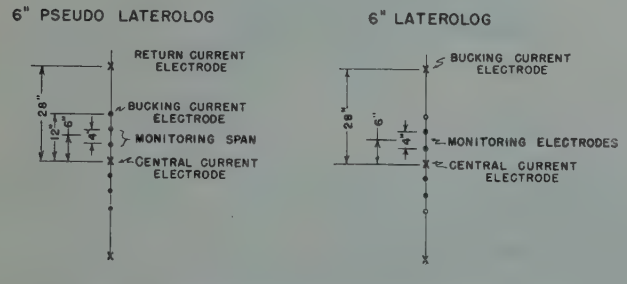

FIG. 14 — ELECTRODE ARRANGEMENT FOR MODIFIED PSEUDO-LATEROLOG AND LATEROLOG.

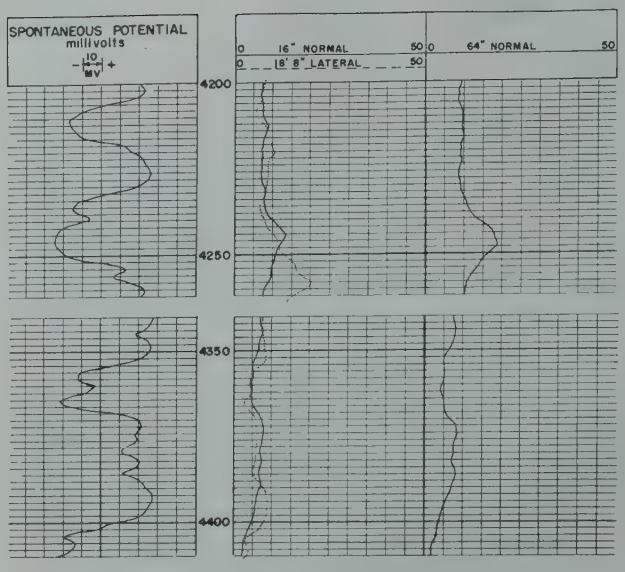

FIG. 15 — CONVENTIONAL ELECTRIC LOG, CANYON FORMATION, STONEWALL COUNTY, TEX.

Fig. 15 shows a conventional electrical log through the sections that were studied.

Figs. 16 and 17 show the microlaterolog-microlog and the laterolog-pseudo laterolog combinations through the same sections.

Invaded zone and true resistivities were determined for four zones. Assuming that the lower zone is 100 per cent water saturated, approximate water saturations for the upper two zones were calculated from Archie's formula. Table 1 gives the pertinent data of the analysis.

Fig. 18 shows the simplified departure curves for $R_i/R_m = 30$ which were used for the determination of the R_t/R_m values. The effects of the drill hole on the apparent resistivities of the laterolog and pseudo-laterolog are small enough so that we can use the chart for $R_i/R_m = 30$ for cases where R_i/R_m is approximately of that magnitude, after a proportional adjustment of the observed apparent resistivites. The adjustment is made by simply multiplying the observed apparent resistivities of the laterolog and pseudo-laterolog by the ratio of the R_i/R_m value indicated on the chart ($R_i/R_m = 30$) over the calculated R_i/R_m value. For example, the apparent resistivity ratios R_{LL}/R_m and R_{pLL}/R_m for the zone at 4,231-4,237 listed in Table 1 were multiplied by 30/27.7, and the resulting R_t/R_m is multiplied by 27.7/30.

Departure curve charts are made up for the following R_i/R_m values: 1, 5, 10, 20, 30, 50, 80, 120, 200, and

TABLE 1

Zone Feet	R_1 1/2"	R_2"	R_{mc}	R_1 1/2"/R_{mc}	R_2"/R_{mc}	MCT	R_{mLL}*	R_{mLL}/R_{mc}
4,402-4,406	1.5	1.95	.98	1.53	2	.6	4.7	4.8
4,362-4,366	1.5	2	.98	1.53	2.05	.6	6.0	6.1
4,353-4,358	2	2.4	.98	2.04	2.44	.37	6.8	6.95
4,231-4,237	1.9	2.4	.98	1.94	2.44	.4	7.5	7.65

Zone Feet	R_i/R_{mc}	R_i/R_m	R_{LL}*	R_{pLL}*	R_{LL}/R_m	R_{pLL}/R_m	R_t/R_m	R_t	S_w
4,402-4,406	6.8	19.6	.9	3.0	2.65	8.9	5.2	1.8	1.0
4,362-4,366	11	31.7	1.3	4.5	3.82	13.2	8.45	2.9	.79
4,353-4,358	8.5	24.5	1.45	4.7	4.26	13.8	10.3	3.5	.71
4,231-4,237	9.6	27.7	2.3	6.95	6.76	20.4	14.0	4.8	.61

*The notations R_{mLL}, R_{LL}, and R_{pLL} are used respectively for the apparent resistivities of the microlaterolog, 6-in. laterolog, and 6-in. pseudo-laterolog.

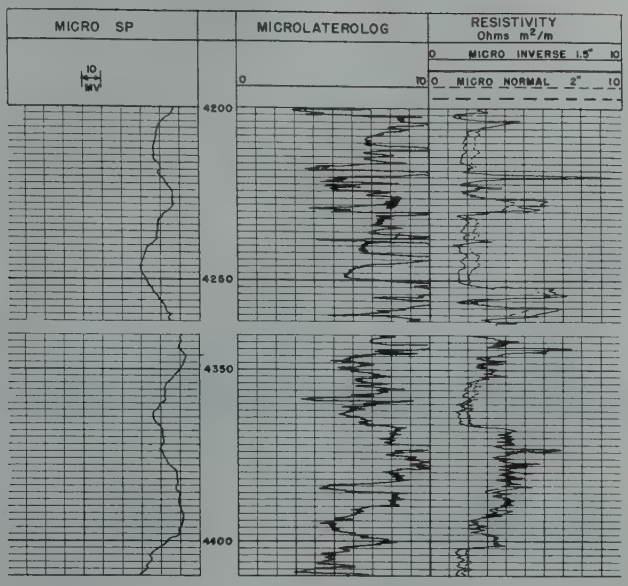

FIG. 16 — MICROLATEROLOG-MICROLOG, CANYON FORMATION, STONEWALL COUNTY, TEX.

500. The chart for the nearest R_i/R_m value to that calculated for a particular zone is selected, and the apparent resistivities are adjusted in the above manner for the determination of R_t/R_m. Graphical interpolation is used to find the R_t/R_m values corresponding to points falling between the curves on a particular chart.

In Figs. 15 through 17, the zones at 4,353-58 and 4,362-66 appear to be in the capillary transition zone at the oil-water contact and are expected to produce with a large water cut. The zone at 4,231-37 is probably at the irreducible water saturation and should produce clean oil.

CONCLUSIONS

From the work done to date, it appears to be feasible to obtain fairly accurate values of invaded bone resistivities and true resistivities in thin bedded sandstone formations by using a microlaterolog-microlog and short-spaced pseudo laterolog-laterolog combination. The resolution of the method is greatest if $R_t > R_i$. If $R_i >> R_t$, the accuracy of the method becomes very poor. For thin bed logging, it appears, therefore, advisable to keep the resistivity of the drilling mud as low as possible. In regions of very saline connate water, the mud resistivity should be held at two to four times the resistivity of the connate water, which will still make it possible to register a useful SP curve on an amplified scale. In areas of fresh connate water, we can make the mud resistivity two to four times smaller than the connate water resistivity and reverse the polarity of the SP curve.

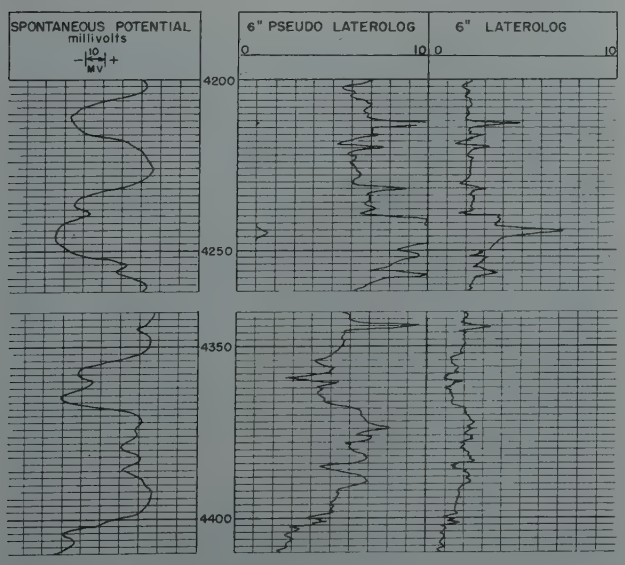

FIG. 17 — PSEUDO-LATEROLOG AND LATEROLOG, CANYON FORMATION, STONEWALL COUNTY, TEX.

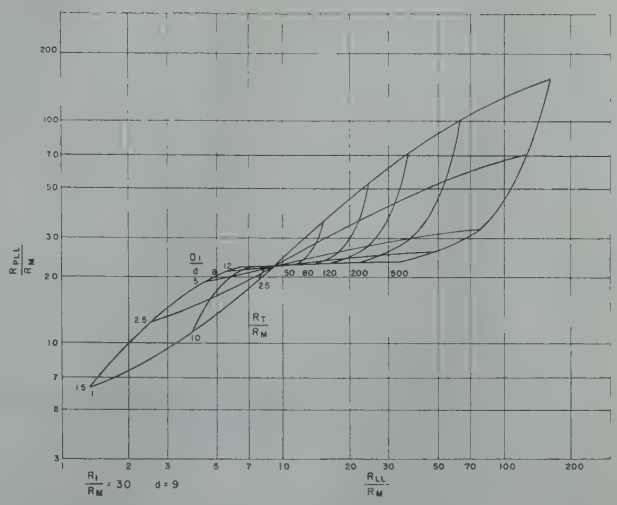

FIG. 18 — SIMPLIFIED DEPARTURE CURVES FOR 6-IN. LATEROLOG AND PSEUDO-LATEROLOG.

ACKNOWLEDGMENTS

The author wants to express his gratitude to the management of Continental Oil Co. for permission to publish this article, to Miss Elayne Chousis, Mrs. B. L. Erickson, and Miss E. A. Wells, who helped in the preparation of the simplified departure curves, and to the Engineering Department of Schlumberger Well Surveying Corp., who constructed the special laterolog-pseudo laterolog sonde and made the experimental surveys discussed in this paper.

REFERENCES

1. de Witte, L.: "Simplified Departure Curves and the Effects of the Equivalence Principle in Resistivity Logging," *Oil and Gas Jour.* (Feb. 11, 1952).
2. Tixier, M. P.: "Electric Log Anslysis in the Rocky Mountains," *Oil and Gas Jour.* (June 23, 1949).
3. de Witte, L.: "Relations Between Resistivities and Fluid Contents of Porous Rocks," *Oil and Gas Jour.* (Aug. 24, 1950).
4. Schlumberger Well Surveying Corp.: Document No. 4, "Interpretation Handbook for Resistivity Logs," pp. 24-31 and 82-90.
5. Doll, H. G.: "The Microlaterolog," *Trans.* AIME (1953), **198**, 17.
6. de Witte, L.: "Resistivity and Saturation Distribution in Infiltrated Zones of Porous Formations," *Oil and Gas Jour.* (July 27, 1950).
7. Doll, H. G.:"The Laterolog: A New Resistivity Logging Method with Electrodes Using an Automatic Focusing System," *Trans.* AIME (1951), **192**, 305.

★★★

A STUDY of DISPLACEMENTS in MICROSCOPIC CAPILLARIES

CHARLES C. TEMPLETON
JUNIOR MEMBER AIME

SHELL DEVELOPMENT CO.
HOUSTON, TEXAS

T. P. 3804

ABSTRACT

Any explanation of the nature of multiphase fluid flow through porous media must ultimately involve a knowledge of the mechanism of such flow through the individual pores of the medium. To provide quantitative information of the latter type, a study was made of gas-liquid and liquid-liquid displacements in single uniform Pyrex capillaries with diameters as small as 4 microns.

Quantitative observation of air-liquid displacements with zero contact angle indicates the adequacy of a model based on Poiseuille's Law and the independence of capillary pressure and interfacial velocity. Consequently, this work discounts previous claims that flow is abnormally retarded in very small capillaries.

For the displacement of a very viscous oil by water in a capillary initially filled with water, flow is faster than predicted by the above model. This behavior is probably due to the existence of a thin annular film of water between the oil column and the capillary wall as postulated by Yuster.

INTRODUCTION

The need for experimental observation of the microscopic nature of multiphase fluid flow, to further the understanding of the results of macroscopic flow investigations, has been previously recognized. Chatenever and Calhoun[1] in connection with the API Project 47B have extensively studied the flow of fluids through layers of glass or lucite spheres between glass or lucite plates. Lowman[2] prepared an interesting film concerning flow in a single capillary, using an apparatus which made a moving interface appear stationary in the field of a microscope.

The purpose of the present investigation was to determine what contribution might be made to this field by comprehensive *quantitative* observation of gas-liquid and liquid-liquid displacements in single capillaries of uniform, very small diameter. The techniques used are similar to those of Lowman but incorporate improvements necessary for quantitative work. Quantitative observations must begin with fluids of simple chemical composition to provide a basis for analyzing the more complex behavior that may be expected with natural reservoir fluids. However, some qualitative observations on systems involving crude oils are presented.

Experiments of this sort involve the observation of the velocity of the interface separating two fluids, and have been performed in horizontal or vertical capillaries by several investigators.[3,4,5,6,7,8] The most general treatment of their mechanics, by Brittin,[9] involves forces due to capillarity, viscous resistance, gravity, an "end-drag" effect, and the rate of change of momentum of the capillary contents.

Since the range of pore diameters of interest in petroleum reservoirs is about 0.1 to 100 microns, it was desired to perform these experiments in the smallest capillaries possible, to ascertain whether capillary diameter had any effect on the existing theory based on data from larger capillaries.* It was also important to be able more systematically to vary the direction and rate of displacement than was done by previous investigators. Finally, to concentrate attention on viscous and capillary forces by eliminating gravity as a parameter, this study involves only horizontal capillaries. The work of Eley and Pepper[7] with a "large" (0.766-mm diameter) horizontal capillary is the previous investigation which is most similar to the present method of quantitative observation. Here capillaries with diameters as small as 4 microns will be studied.

[1]References given at end of paper.

Manuscript received in the Petroleum Branch office July 31, 1953. Paper presented at the Petroleum Branch Fall Meeting in Dallas Oct. 19-21, 1953.

*Even single-phase flow in very small capillaries has not been investigated as extensively as one might imagine from the universal acceptance of Poiseuille's law. Bingham,[10] in reproducing Poiseuille's data, indicates that only five measurements were made in capillaries of about 13 microns diameter, and that the other capillaries had bores of 29 microns or greater. The most comprehensive study was that of Bulkley,[11] who used glass capillaries of about 11 microns diameter.

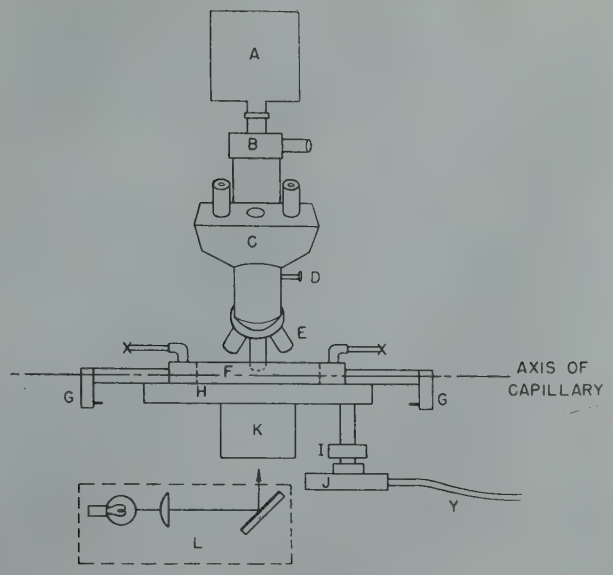

LEGEND

A —— CAMERA
B —— BEAM SPLITTER
C —— BINOCULAR HEAD
D —— SLIDE FOR QUICK-SHIFT BETWEEN BINOCULAR AND CAMERA-BEAM SPLITTER SYSTEMS
E —— OBJECTIVES
F —— CELL CONTAINING CAPILLARY
G —— LIMIT MICROSWITCHES AND CELL HOLDER
H —— MECHANICAL STAGE
I —— MANUAL KNOB FOR STAGE MOVEMENT PERPENDICULAR TO PLANE OF ILLUSTRATION
J —— GEARED DRIVE FOR STAGE MOVEMENT ALONG AXIS OF CAPILLARY
K —— CONDENSER
L —— BUILT-IN ILLUMINATION SYSTEM
X —— FLEXIBLE HOSE CONNECTIONS TO PRESSURE SYSTEM
Y —— FLEXIBLE SHAFT TO MOTOR DRIVE UNIT

FIG. 1 — GENERAL ARRANGEMENT OF APPARATUS.

APPARATUS AND TECHNIQUES

The general arrangement of the Leitz Ortholux microscope and its associated apparatus is sketched in Fig. 1.

Fig. 2 illustrates the capillary cell (Type I) used in the first several months of the study. The lower stainless steel block at each end contains a fluid reservoir and an inclined hole to receive the end of the capillary. Since the capillary is sealed to the block only at the external end of the hole, the fluid contacts glass and steel but no cementing material. The upper steel block receives a brass elbow which permits connection to a pressure system employing Nullmatic regulators. A pressure-tight seal is obtained by placing a rubber gasket between the two blocks and screwing them together. Only one block has pressure applied to it at any one time; the other is always at atmospheric pressure. Either mercury or oil manometers were used.

About an hour is required for mounting a capillary in the cell. The end-blocks are cleaned with boiling ethanol and dried. A section of capillary (about 12 cm long) is cut; its length is measured with the aid of a stereoscopic microscope. A reference mark is placed on the capillary with fingernail polish, and its location measured with respect to the ends. This allows subsequent calibration of a Veeder-Root counter (geared to the stage-drive) in terms of capillary position for any given run. The capillary is inserted into both end-blocks, and is fastened down in a straight position on the bottom plate with small pieces of drafting tape. Dekhotinsky cement or paraffin is then used to make a dam around the capillary and to seal the capillary gas-tight into the end blocks. The pool surrounding the capillary is filled with immersion oil.

With the Type I cell, no provision was made for temperature control; the temperature of each displacement was read from a thermometer mounted on the mechanical stage. On the basis of some auxiliary measurements with a thermocouple, it was concluded that the true temperature of the capillary was known within $\pm$ 0.1°C.

During the later part of the study a new cell (Type II) was used, in which the temperature could be maintained at 30.00° $\pm$ 0.1°C. This cell differs from the Type I cell only in having a hollow set of all-metal cell walls for the circulation of thermostated water.

The capillaries were prepared from Pyrex glass by an apparatus developed in conjunction with this study.[12] It employs a modification of the method of Shereshefsky[13] with the replacement of gas heating by electrical heating. Capillaries are drawn immediately before mounting to keep them as clean as possible. Before drawing, the tubing stock is cleaned with acid-dichromate solution, rinsed with distilled water, baked dry, and sealed to permit storage.

Diameters of capillaries are measured with a 12.5 $\times$ filar micrometer eyepiece. By taking the average of seven to 10 measurements, a length may be determined to $\pm$ 0.1 μ with a 22 $\times$ oil-immersion objective. The use of immersion oil removes the necessity of applying corrections to these measurements.[14]

QUALITATIVE EXPERIMENTS

The appearance of oil-water-Pyrex systems under the microscope depends on the refraction indexes involved. Air slugs are quite dark, water slugs somewhat lighter, and oil slugs are clear. Boundaries of oil against glass are practically invisible, but boundaries of water against glass are quite sharp. A water torus (doughnut) was observed to be a fairly stable configuration.

It was established early that velocities of the order of 1 cm/min (46.2 ft/day), which exceed the range to be expected in a reservoir except perhaps near the well, do not in general lead to appreciable interfacial deformation in *freshly prepared* systems. In a 30-micron-diameter capillary, a water-air interface had the same geometry at rest and traveling at 3 cm/min as did a water-refined hydrocarbon fraction interface at rest and moving at 2 cm/min. In a latter part of this paper photographic measurements show that for fresh Pyrex-air-liquid systems in which the static contact angle is zero the static and dynamic angles are the same to within 1 per cent in cos Θ. Photographic measurements on a Pyrex-air-methylene iodide system showed the range of hysteresis to be about 7 per cent of the cosine of the static angle ($\Theta^\circ = 52^\circ$).

Most of the air-liquid systems observed did not change their behavior very rapidly upon aging over a few days. However, the behavior of liquid-liquid systems tended to become considerably more complicated after aging, the situation being more involved for mixtures than for pure liquids. Thus, when alternate slugs of distilled water and a mixed "oil" (90 per cent kerosene, 10 per

cent ∝-monochloronapthalene) were set in motion, the advancing end of the water slug flattended in agreement with the conventional pattern of contact angle hysteresis.[15]

Crude-oil samples from several fields were displaced with water. For each crude, a single crude-water interface was created in a 5-micron-diameter capillary, which had initially been filled with water. The interface was immediately displaced in each direction at about 1 cm/min. If the interface was initially stable, it was then maintained as nearly as possible at a fixed position in the capillary for about 3 hours, by continual adjustment of the applied pressure. The "aged" interface was then displaced in each direction at 1 cm/min. for another check on its stability.

Some of the crude-oil-water systems examined showed a 15 to 20 per cent decrease in capillary pressure over a 3-hour period. When this occurred for a Benton field, Illinois crude which had been exposed to the atmosphere for 6 months, it was thought to indicate the presence of surface-active agents formed by oxidation. However, the decline also was observed for a fresh crude sample from the KMA field, Wichita County, Tex.

As for interfacial instability, crude-water interfaces broke up during the initial displacements for fresh sample from the Luke field, Okla., and the Fox-Graham field, Okla. The Benton field, Ill., crude interface with water showed instability only after the 3-hour aging period. The crude-water interfaces for fresh samples from the Mercy field, Tex., and the KMA field, Tex., showed no appreciable instability during the entire test. Displacements at comparable velocities of water-oil interfaces for some pure hydrocarbons and some refined hydrocarbon mixtures, covering a viscosity range from 0.6 to 12 cp, have not revealed interfacial instability. All the crudes had velocities within this range at the temperature of the observations. Thus, the effect appears to be more dependent upon the chemical nature of the fluids rather than upon their physical properties.

The interfacial break-up always followed a characteristic pattern, which is illustrated in Fig. 3. It has been observed only when water displaces oil. As the water-oil interface begins to move, the center part of the interface tends to lag as in Fig. 3-b. Soon the wetting phase begins to advance along the wall on one or both sides, giving the situations shown in Fig. 3 (c, d, e). As soon as flow stops, the distorted interfacial region readjusts into slugs and tori.

Fig. 4 describes an air displacement of Benton crude, followed by a water flood, which allows an estimate of the thickness of the oil film left on the wall during the displacement of the oil by air. An air slug separated water and crude columns in a 36.7-micron-diameter capillary as indicated in Fig. 4-a. The capillary had been initially filled with water. Photographs of the water-air and air-oil interfaces at rest are shown, respectively, in Fig. 4 (b and c). During the initial entry of the oil there was no change in the appearance of the air-oil interface.

However, when the direction of displacement was reversed, after a time the water-air interface changed into a combination of water-oil interface and an oil-air interface (Fig. 4-d). This apparently indicated that an oil film was left behind the air-oil interface, and that this film was collected into an oil slug by the advancing water-air interface. (Because the capillary was initially filled with water, there probably was also a water film between the oil film and the wall.) After the air slug had traveled farther, the oil slug disintegrated into the situation portrayed in Fig. 4-e. Here there is essentially a water-air interface with an oil "sack" attached to it. As displacement continued, additional oil was apparently picked up from the wall, causing the oil "sack" to grow into the "sausage" shown in Fig. 4-f. From the distances traveled and the dimensions of the capillary, it was estimated that the thickness of the oil film was about 0.012 micron. The complex shape of the oil "sack" suggests rigid film formation, which has been observed at crude-oil-water interfaces with aging.[16]

QUANTITATIVE OBSERVATION OF DISPLACEMENTS

Definitions and Theory

Consider a horizontal capillary of length l and of uniform radius r, containing a wetting-phase column (fluid 1) separated by a single interface from a nonwetting-phase column (fluid 2). The viscosities are μ_1 and μ_2. x is the length of capillary occupied by wetting phase; $l-x$ is occupied by the nonwetting phase. $v = dx/dt$ is the velocity of the interface.

P_t is the pressure at the nonwetting phase end of the capillary minus that at the wetting phase end. P_c is the capillary pressure. P_c°, the static capillary pressure, is equal to the particular value of P_t that maintains the interface stationary. Θ and Θ° are the dynamic and static contact angles, respectively.

From the fundamental equation of capillarity,

$$P_c = \frac{2\gamma \cos \Theta}{r} \quad . \quad . \quad . \quad . \quad . \quad . \quad . \quad . \quad . \quad (1)$$

where γ is the interfacial tension for a liquid-liquid system, or the surface tension for an air-liquid system.

Fig. 2 — Capillary Cell, Type 1.

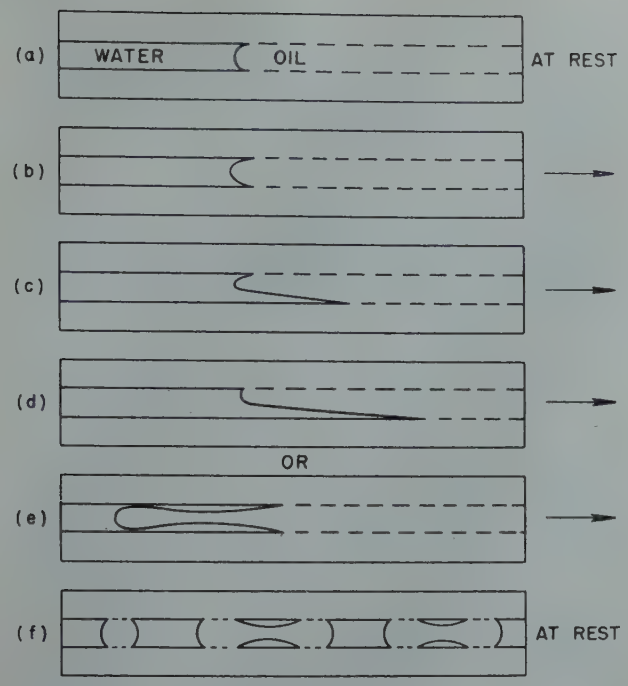

FIG. 3 — MECHANISM OF BREAK-UP OF A WATER-OIL INTERFACE DURING A WATER FLOOD.

Let a "boundary tension" be defined as

$$T = \frac{P_c \cdot r}{2} = \gamma \cos \Theta \quad . \quad . \quad . \quad . \quad . \quad . \quad . \quad (2)$$

for the expression of both static (T°) and dynamic (T) results.

The following assumptions will be made for evaluating the data: (1) Poiseuille flow, since the Reynolds numbers are low. (2) The fluids are incompressible. (3) Displacement is perfect at the interface. (4) Capillary hysteresis is absent; i.e., $P_c = P^\circ_c$, since in any of the systems to be studied, the static, advancing, and receding contact angles appeared to be identical to within 1 per cent in cos Θ. From the above it may be shown that

$$P^\circ_c - P_t = [8v/r^2]\,[(\mu_{1eff} - \mu_{2eff})\,x + \mu_{2eff} \cdot l]\,, \quad (3)$$

where the subscripts distinguish effective viscosities determined from displacement data from the values determined in conventional viscometers (μ_1 and μ_2).

P_t is maintained constant during a displacement. Measurements are made of the times t at which the interface passes certain positions x. When possible, photographs are made of the interface, both stationary and moving, for the measurement of Θ and Θ°. Velocity values are calculated from the observed (x,t) data by the approximation of setting $v = (x_i - x_j)/(t_i - t_j)$ at $x = (x_i + x_j)/2$. P°_c is measured with the interface at various points. The surface or interfacial tensions of the fluids are measured either by the pendent-drop apparatus or the duNouy tensiometer.

All quantities in Equation (3) are known except μ_{1eff} and μ_{2eff}. Let

$$G = \left(\frac{r^2}{8}\right)(P^\circ_c - P_t) \quad . \quad . \quad . \quad . \quad . \quad . \quad . \quad (4)$$

which is constant for a given displacement; then

$$G/v = (\mu_{1eff} - \mu_{2eff})\,x + \mu_{2eff} \cdot l \quad . \quad . \quad . \quad . \quad (5)$$

Hence a plot of G/v versus x should be linear, and μ_{1eff} and μ_{2eff} can be determined from the slope and intercept. When either viscosity gets much greater than the other, the smaller effective viscosity is subject to a large propagated error in this graphical method. Thus for an air-liquid displacement the handbook value of air viscosity is substituted for μ_{2eff} in Equation (3), and a value of μ_{1eff} can be calculated numerically from each (x, t, v) point.

LIQUIDS USED IN QUANTITATIVE EXPERIMENTS

Distilled water was used in these displacements. The benzene (Baker) was C.P. grade, the *n-cetane* (Du Pont) was "practical" grade or better. Nujol (heavy mineral oil, U.S.P.) was sold by Stanco, Inc. Refined hydrocarbon "Cut No. 3" was a mixture of 65 per cent from a boiling range of 356°-405° and 35 per cent from a boiling range of 391°-477°C.

RESULTS FOR AIR-LIQUID DISPLACEMENTS IN 25 TO 35 MICRON INNER DIAMETER CAPILLARIES

Table 1 presents typical data gathered from the application of these methods to displacements in Pyrex capillaries with inner diameters between 25 and 35 microns. With water and two refined hydrocarbon fractions (Cut No. 3 and Nujol), the viscosities range from about 1 to 140 cp. Each capillary is assigned a number; each displacement in that capillary is designated by adding a letter.

TABLE 1 — TYPICAL AIR-LIQUID DISPLACEMENTS; 25- TO 35-MICRON I.D. (TYPE II CELL IF MARKED WITH ASTERISK; OTHERWISE TYPE I CELL)

A Constants and Static Behavior

Run No.	Capillary Diameter cm	Surface Tenson γ dynes/cm	T°/γ	cos Θ° (From Photographs)
Water				
37A,B	28.65×10^{-4}	71.82	991	0.99
Refined Hydrocarbon Cut No. 3				
36A,B,C	29.52	31.2	.979	1.00
*44A,B,C,D	29.98	30.76	1.026	.99
*45A,B,C,D	28.20	30.76	.997	.99
Nujol				
*42A,B,C,D,	31.37	31.6	.959	1 00
*43A,B,C,D	31.64	31.15	.984	.98
*46A,B,C,D	28.17	31.15	1.008	1.00

B. Dynamic Behavior

Run No.	Temperature °C	$(P^\circ_c - P_t)/P^\circ_c$	cos Θ (From Photographs	μ_1 poise	μ_{1eff}/μ_1
Water					
37A	25.90	— .051	0.99	.00876	.977
37B	25.85	.050	.99	.00877	1.124
Refined Hydrocarbon Cut No. 3					
36A	24.60	5.348	1.00	.479	.981
36B	24.71	—4.775	1.00	.476	.960
36C	24.89	5.173	1.00	.471	.958
*44A	30.00	—6.872	.99	.364	.984
*44B	30.00	7.298	.98	.364	1.029
*44C	30.00	—5.298	.96	.364	.992
*44D	30.00	9.423	....	.364	1.031
*45A	30.00	—3.065	.99	.364	1.062
*45B	30.00	5.105	.98	.364	1.020
*45C	30.00	—5.140	....	.364	1.059
*45D	30.00	7.143	.98	.364	1.055
Nujol					
*42A	27.40	—8.249	1.00	1.237	1.058
*42B	27.40	10.327	1.00	1.237	1.059
*42C	27.40	—9.293	1.00	1.237	1.054
*42D	27.40	13.008	1.00	1.237	.047
*43A	30.07	10.146	.99	1.048	.996
*43B	30.09	—8.068	.99	1.046	.967
*43C	30.09	11.255	.99	1.046	.965
*43D	30.09	—9.255	.99	1.046	.944
*46A	30.00	—4.314	1.00	1.055	1.044
*46B	30.00	6.345	1.00	1.055	1.050
*46C	30.00	—5.484	1.00	1.055	1.028
*46D	30.00	7.468	1.00	1.055	1.043

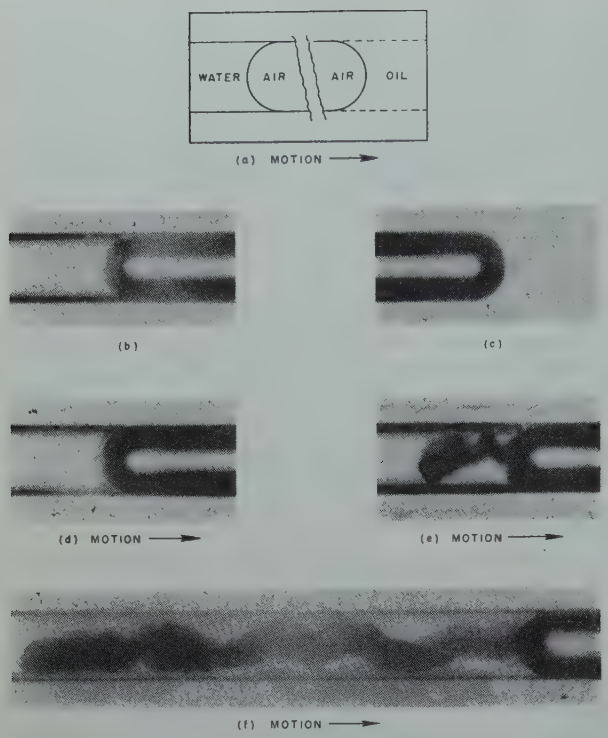

FIG. 4 — AIR DISPLACEMENT OF BENTON CRUDE FOLLOWED BY WATER FLOOD WHICH COLLECTS OIL FILM FROM WALL.

In three-fourths of the air-liquid systems studied, P_c° along the capillary for each case was constant to within ± 1 per cent of the average value. For any run, P_c° has been taken as the average of the values at the ends of all the runs in the particular capillary.

Part *A* of Table 1 summarizes the static behavior as value of T°/γ; values of cos θ° obtained from enlarged photographs are given in the final column. The actual agreement may be judged from the fact that the average of the T°/γ values is 0.992, while that of the actual cos θ° entries is 0.993.

Part *B* of Table 1 describes the dynamic observations. The quantity $(P_c^\circ - P_t)/P_c^\circ$ seems to be the most convenient means for representing the magnitude of the forces and pressures involved. If $P_c^\circ = P_c$, then this pressure ratio is equal to the ratio of viscous pressure (work) to capillary pressure (work). Further, the ratio is positive for a wetting-phase flood and negative for a nonwetting-phase flood.

The first result to be noted is that the static and dynamic contact angles have been experimentally shown to be the same, and equal to zero, within a reasonable experimental error. This was the basis for assuming that $P_c = P_c^\circ$ in the theoretical discussion, although this equality also requires that γ be unchanged by interfacial motion.

If the model adequately describes the experimental behavior, then μ_{1eff}/μ_1 is expected to be unity. Actually, the average of the μ_{1eff}/μ_1 values in Table 1 is 1.019. Although the extreme values are 0.944 and 1.124, the average deviation from the mean is only 0.038. A study of Table 1, Part *B* will show that there is no apparent systematic relation between μ_{1eff}/μ_1 and any of the following:

1) the direction of displacement or sign of $(P_c^\circ - P_t)/P_c^\circ$;

2) the ratio of viscous pressure to capillary pressure [magnitude of $(P_c^\circ - P_t)/P_c^\circ$];

3) the liquid viscosity; or

4) the surface tension.

Hence we may conclude that our model is adequate for describing air-liquid displacements, in capillaries of 30 microns inner diameter, within a random error of about ± 4 per cent.

RESULTS FOR AIR-LIQUID DISPLACEMENTS IN 3 TO 7 MICRON INNER DIAMETER CAPILLARIES

Table 2 describes 12 runs in the Type II cell for three capillaries, with diameters between 6 and 7 microns with a refined hydrocarbon fraction of about 36 cp viscosity. Here the T°/γ values average 0.958; no direct photographic measurement of cos θ° was feasible in capillaries this small. The μ_{1eff}/μ_1 values average 1.007, with an average deviation from the mean of 0.065. This average dynamic behavior is very close to what was theoretically expected.

The present techniques were also applied to five other liquids in capillaries whose diameters were between 3 and 7 microns in the Type I cell. The viscosities of these liquids ranged from 0.6 to 160 cp. A total of 26 air-liquid displacements in nine different capillaries was observed. For these data, T°/γ averaged 0.957, while the average of μ_{1eff}/μ_1 was 0.930. Even though μ_{1eff}/μ_1 was somewhat lower than expected (these measurements were made in the beginning of the study when the techniques may not have been fully developed), these data nonetheless demonstrated the lack of any systematic relation between μ_{1eff}/μ_1 and $(P_c^\circ - P_t)/P_c^\circ$, μ_1, or γ in these smaller capillaries. For later comparison with water-Nujol results, it should be stated that four air-Nujol displacements in two capillaries (with diameters of 4.99 and 5.52 microns, respectively) gave an average μ_{1eff}/μ_1 of 0.935 ± 0.009.

Bulkley[11] investigated the flow of several liquids in glass capillaries of about 11 microns inner diameter.

TABLE 2 — AIR-OIL DISPLACEMENTS, 6- to 7-MICRON I.D., TYPE II CELL. OIL IS "REFINED HYDROCARBON CUT NO. 3."

A. Constants and Static Behavior

Run No.	Capillary Diameter cm	Surface Tension γ dynes/cm	T°/γ
47A,B,C,D	6.177×10^{-4}	30.76	0.963
49A,C,D,F	6.370	30.76	.937
50A,B,C,D	6.604	30.76	.975

B. Dynamic Behavior (All runs at 30.00°C; $\mu_1 = 0.3642$ poise)

Run No.	$(P^\circ_c - P_t)/P^\circ_c$	μ_{1eff}/μ_1
47A	−5.907	1.063
47B	7.907	1.060
47C	−6.943	1.053
47D	8.943	1.061
49A	−6.683	.909
49C	−7.595	.913
49D	2.803	.916
49F	2.841	.921
50A	−6.991	1.123
50B	9.024	1.070
50C	−7.729	1.001
50D	9.707	.994

From his flow data and the conventionally measured viscosities of the fluids, he calculated radius values which he compared with radius values measured according to the visual technique of Shereshefsky.[13] The average of his visual values, for a given capillary, was 2.1 per cent lower than the average of his calculated values; i.e., flow was faster than indicated by the visually measured radius and the viscosity. Bulkley concluded that the effects are within the range of experimental error. The recent claims of Henniker[17,18] that flow in very small capillaries is slower than predicted by Poiseuille's law and conventionally measured viscosities has been effectively rebutted by Bulkley.[19]

From Equation (3) it may be seen that, when μ_{2eff} is much less than μ_{1eff}, μ_{1eff} is proportional to r^2. T° is directly proportional to r from Equation (2). If for Table 2 all the deviations of μ_{1eff}/μ_1 from unity were attributed to a mistake in the visual radius measurement (which seems possible because of the approximate agreement between μ_{1eff}/μ_1 values for runs in a given capillary), the following errors in r result:

	Systematic	Random
Static (T°/γ)	−4%	±2%
Dynamic (μ_{1eff}/μ_1)	<1%	±4%

Since Bulkley's results could have been caused by a −2.1 per cent systematic error in the visual diameter measurement technique, such an error might be inherent in this method.

These quantitative measurements cover only cases for which the air-liquid-solid contact angle is zero. It appears that this angle is zero for water or simple hydrocarbon mixtures. The techniques might well be applied to systems such as air-methylene iodide-Pyrex for which this angle is greater than zero.

QUANTITATIVE STUDY OF OIL-WATER DISPLACEMENTS

The results of a study of oil-water displacements will almost certainly be affected by whether the capillary is initially filled with oil or water. A few results will now be presented for the "water-in-first" case. If these data are interpreted according to the present theory ($P_c = P_c^\circ$), oils of high viscosity show μ_{eff}/μ values definitely less than unity. The same oils gave μ_{eff}/μ values of about unity for the air-oil case. Thus Table 3 contrasts the results obtained with the Type I cell for the benzene-water and Nujol-water systems in Pyrex capillaries with diameters between 4 and 6 microns. Here the effective viscosities of both water and oil have been determined by the graphical method. For these water-oil systems P_c° in a given capillary was generally constant to about ±2 per cent, rather than the ±1 per cent range encountered in air-liquid systems.

In 5-micron-diameter capillaries, the only evidence for the assumption of $P_c - P^\circ$ is that the contact angle *visually* appeared to be the same during oil and water floods, and that the interface remained stationary at a well-defined static capillary pressure. However, photographic measurements of the dynamic and static contact angles for the same oil-water systems in 30-micron-diameter capillaries show that $\theta = \theta^\circ$ within 1 per cent of the cosine.

For the benzene-water case, only ranges or average values of the various quantities have been recorded. Within an average deviation of about 10 per cent, our model seems to describe water-oil displacements adequately when the capillary is initially filled with the wetting liquid and the viscosities of the two liquids are not greatly different.

In the Nujol-water case it may be stated that the wide variation of the μ_{1eff}/μ_1 values has little physical significance because, when $\mu_1 << \mu_2$, μ_{1eff} is affected greatly by small errors in the measured quantities. In fact, if μ_{1eff} is set equal to μ_1, and μ_{2eff} is calculated numerically, all the μ_{2eff}/μ_2 values still remain between 0.486 and 0.613. Gillespie,[20] in studying slug flow in the water-castor oil system in 40 to 60 micron-diameter capillaries, observed the equivalent of these low effective viscosities for the oil phase.

The interpretation of the reduced μ_{2eff}/μ_2 values is that there is probably a thin annular film of water between the oil column and the capillary wall. Yuster[21] has derived an expression for the relative permeabilities in a uniform capillary in which this distribution of fluids prevails. His Equation (24) for the relative permeability to oil, with our notation for the viscosities, is

$$K_{ro} = 2S_o(1 - S_o)\frac{\mu_2}{\mu_1} + S_o^2, \quad . \quad . \quad . \quad . \quad . \quad (6)$$

where S_o is the oil saturation. If ϵ is the ratio of the thickness of the water film to the radius of the capillary, then

$$S_o = \frac{\pi(r - \epsilon r)^2}{\pi r^2} = (1 - \epsilon)^2 \quad . \quad . \quad . \quad . \quad . \quad (7)$$

Further, it may be shown* that

$$K_{ro} = (\mu_2/\mu_{2eff})(1 - \epsilon)^2 \quad . \quad . \quad . \quad . \quad . \quad . \quad . \quad (8)$$

By combining Equations (6), (7), and (8), we obtain

$$\frac{\mu_2}{\mu_{2eff}} = 2\epsilon(2 - \epsilon)\frac{\mu_2}{\mu_1} + (1 - \epsilon)^2 \quad . \quad . \quad . \quad (9)$$

If Equation (9) is applied to the Nujol data of Table 3, the calculated water-film thicknesses all lie between 28 and 44 Å. These values are reasonable both in terms of molecular dimensions and the limit of resolution of the microscope.

It should be emphasized that, although these results

TABLE 3 — OIL-WATER DISPLACEMENTS (TYPE I CELL)
"WATER-IN-FIRST"

Run No.	$\frac{P_c^\circ - P_r}{P_c^\circ}$	$\frac{\mu_2}{\mu_1}$	(Water) (μ_{1eff}/μ_1)	(Oil) (μ_{2eff}/μ_2)
Benzene-Water				
29 runs in eight capillaries	Range: −0.609 to 0.632	Range: 0.665 to 0.681	Avg.: 0.997 Avg. Dev.: ±.105	Avg.: 0.939 Avg. Dev.: ±.092
Nujol-Water				
10A	3.452	165.	1.12	.485
10B	−3.081	155.	4.07	.477
13A	3.912	176.	−.56	.493
13B	−3.728	176.	−.55	.530
14A	3.548	173.	7.89	.566
14B	−3.136	173.	12.02	.550

Capillary Diameters:
Benzene-Water Range: 4.42×10^{-4} to 6.16×10^{-4} cm
Nujol-Water 10A-B 4.97×10^{-4} cm
13A-B 5.79
14A-B 5.16

*K_{ro} is the ratio of the actual oil flow rate during the displacement, Q_{actual}, to the flow rate to be expected in the same capillary when *completely* filled with oil, Q, with the same potential gradient (dP/dx) in both cases. By Poiseuille's law: $Q = (\pi r^4/8\mu_2)(dP/dx)$. Further, $Q_{actual} = \pi r^2(1 - \epsilon)^2 v$, where v is the interfacial velocity. Our calculations essentially define μ_{2eff} by the relation $dp/dx = 8v\mu_{2eff}/r^2$. Combination of these relationships yields Equation (8).

confirm the possibility of a relative permeability to oil greater than unity for *the case of a uniform capillary,* they in no way prove the existence of such an effect in actual cores. At most they might suggest the possibility of its occurrence in a core. However, most flow data rule against this possibility. There might be value nonetheless in more extensive checking of the generally accepted independence of relative permeability and viscosity in oil-water systems with oil viscosities of several poises.

REFERENCES

1. Chatenever, A, and Calhoun, J. C.: "Visual Examinations of Fluid Behavior in Porous Media, Part I," *Trans.* AIME (1952), **195**, 149-168.
2. Lowman, Q.: *Microscopic Studies of Capillary Flow,* a film based upon "A Microscopic Study of the Flow of Oil, Water and Air in Small Capillaries," M. S. Thesis, The Pennsylvania State College (1950).
3. Washburn, E. W.: "The Dynamics of Capillary Flow," *Phys. Rev.* (1921), **17**, 273.
4. Peak, R. L., and McLean, D. A.: "Capillary Penetration of Fibrous Materials," *Ind. Eng. Chem. Anal. Ed.* (1934), **6**, 85.
5. Rense, W. A.: "Rate of Rise of Water in Capillary Tubes," *Journ. Applied Phys.* (1944), **15**, 436.
6. LeGrand, E. J., and Rense, W. A.: "Data on Rate of Capillary Rise," *Journ. Applied Phys.* (1945), **16**, 843.
7. Eley, D. D., and Pepper, D. C.: "A Dynamical Determination of Adhesion Tension," *Trans. Faraday Soc.* (1946), **42**, 697.
8. Ligenza, J. R., and Bernstein, R. B.: "The Rate of Rise of Liquids in Fine Vertical Capillaries," *Journ. Am. Chem. Soc.* (1951), **73**, 4636.
9. Brittin, W. E.: "Liquid Rise in a Capillary Tube," *Journ. Applied Phys.* (1946), **17**, 37.
10. Bingham, E. C.: "Fluidity and Plasticity," McGraw-Hill Book Co., New York (1922).
11. Bulkley, R.: "Viscous Flow and Surface Films," *Journ. Research Nat. Bur. Stand.* (1931), **6**, 89.
12. Templeton, C. C.: "Drawing of Small Uniform Glass Capillaries by Electrical Heating," *Rev. Sci. Inst.* (1953), **24**, 880.
13. Shereshefsky, J. L.: "A Study of Vapor Pressures in Small Capillaries, Part I — Water Vapor (A) Soft Glass Capillaries," *Journ. Am. Chem. Soc.* (1928), **50**, 2966.
14. Shereshefsky, J. L., and Carter, C. P.: "Liquid-Vapor Equilibrium in Microscopic Capillaries, I — Aqueous System," *Journ. Am. Chem. Soc.* (1950), **72**, 3682.
15. Bikerman, J. J.: "Surface Chemistry for Industrial Research," Academic Press, Inc., New York (1948), 338.
16. Bartell, F. E., and Niederhauser, D. O.: "Fundamental Research on Occurrence and Recovery of Petroleum, 1946-47," API (1949), 57-80.
17. Henniker, J. C.: "The Depth of the Surface Zone of a Liquid," *Rev. Mod. Phys.* (1949), **21**, 332.
18. Henniker, J. C.: "Retardation of Flow in Narrow Capillaries," *Journ. Colloid Sci.* (1952), **7**, 443.
19. Bulkley, R.: "Retardation of Flow in Narrow Capillaries," *Journ. Colloid Sci.* (1953), **8**, 485.
20. Gillespie, C. B.: "Slug Flow in Capillary Tubes," Thesis for Master of Petroleum Engineering, University of Oklahoma (1952).
21. Yuster, S. T.: "Theoretical Considerations of Multiphase Flow in Idealized Capillary Systems," *Proceedings Third World Petroleum Congress,* E. J. Brill, Leiden (1951), Sec. II, 437. ★★★

RESERVOIR FRACTURING — A METHOD of OIL RECOVERY from EXTREMELY LOW PERMEABILITY FORMATIONS

L. E. WILSEY
ASSOCIATE MEMBER AIME

W. G. BEARDEN
JUNIOR MEMBER AIME

STANOLIND OIL AND GAS CO.
TULSA, OKLA.

T. P. 3878

ABSTRACT

This paper presents results of analysis of the effect of fracturing on initial flow rates and on ultimate recoveries from low capacity oil formations. This analysis shows that even in formations of permeability as low as 0.1 md, large fracture treatments can yield oil recoveries and production rates approaching those of high permeability formations. Field production information is shown which supports the analytical work.

INTRODUCTION

Often hydrocarbon bearing formations are discovered which, while they are known to contain large quantities of oil, will not produce at commercially attractive rates without special well stimulation. Attempts to solve this problem led to the development of such techniques as underreaming, shooting, acidizing, and recently hydraulic fracturing. These methods of stimulation have been highly successful in many fields. All of these treatments, however, affect only the pay section near the well bore and therefore owe their success to circumventing and overcoming local permeability reduction about the well bore.

It has been the belief that in treating wells to stimulate production in which there is no permeability reduction near the well, the maximum possible production rate increase would be of the order of two or fourfold. Hence, it has been concluded that fracture treatment of uniformly low capacity (permeability times thickness) formations could meet with but limited success.

It is the purpose of this paper to show that the use of fracture treatments much larger than usually used can yield commercially attractive producing rates and high recoveries even in formations of permeability less than 0.1 of a md.

PROCEDURE

In order to illustrate the effects of fracturing, an analytical study of some hypothetical systems was made in which one factor at a time was varied to show what is important in recovering oil from fractured wells. It was assumed that a horizontal fracture of relatively high fluid-carrying capacity extended from a well bore. The presence of such a fracture will cause a marked influence on the flow pattern and pressure distribution in the formations, with the net effect being to reduce tremendously the resistance to flow into the well bore.

A diagram of the resulting flow pattern and pressure distribution is illustrated in Fig. 1. Immediately after production commences, the principal flow of fluid is vertically from the formation flanking the fracture, into the fracture, and then into the well. After sufficient oil and gas have been produced to lower the pressure in the formation adjacent the fracture, oil and gas will begin to flow in a radial manner into the fracture from the formations beyond the end of the fracture.

In calculating the performance under such conditions, the material balance or conservation of matter equation and equations of flow were solved simultaneously by a stepwise method of calculation. Flow rates were found by determining the pressure distribution, as illustrated

Manuscript received in the Petroleum Branch office Sept. 24, 1953.
Paper presented at the Petroleum Branch Fall Meeting in Dallas, Oct. 19-21, 1953.

Discussion of this and all following technical papers is invited. Discussion in writing (3 copies) may be sent to the offices of the Journal of Petroleum Technology. Any discussion offered after Dec. 31, 1954, should be in the form of a new paper.

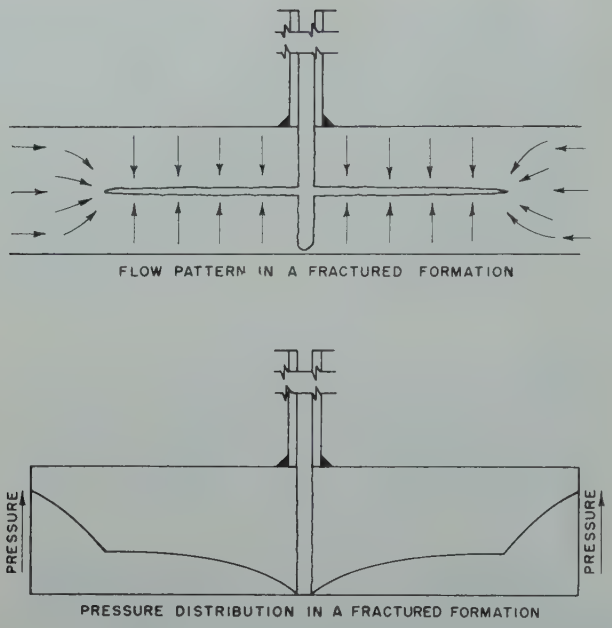

FIG. 1 — EFFECT OF FRACTURING ON FLOW PATTERNS AND PRESSURE DISTRIBUTIONS.

in Fig. 1, at each average reservoir pressure. Linear flow into the fracture from the formation was found by using volumetrically weighted average pressure of the reservoir rock flanking the fracture; radial flow into the fracture was found from the pressure at the extremity of the fracture and at the limit of the drainage area.

From these calculations the flow rates and time to reach a particular stage of depletion could be determined. The ultimate recovery was found by calculating the pressure when the flow rate had declined to the assumed abandonment rate. The recovery factor was fixed as the sum of the oil produced from the formation methods would likely have very little if any water yond the end of the fracture divided by the total oil in place in the assumed drainage area of the well.

In this study only volumetric or depletion drive reservoirs were considered since a reservoir too tight to produce satisfactorily without special well stimulation methods would likely have very little if any water influx. No attempt was made to stimulate any particular well or reservoir, but instead, arbitrary values of oil in place per foot of thickness, abandonment, producing rate, producing bottom hole pressure, crude characteristics, etc., were chosen. These arbitrary characteristics are listed in the Appendix.

RESULTS AND DISCUSSION

The recovery of oil from a fractured well is affected by the characteristics of the formation and the fracture in a rather complex manner in that the same recovery can result from several different combinations of rock and fracture characteristics. Therefore, in order to show the effect on recovery, each factor is discussed separately.

EFFECT OF FORMATION PERMEABILITY ON ULTIMATE RECOVERY

As this study was directed toward recoveries from extremely low permeability formations, the first factor investigated was the effect of permeability on the ultimate recovery from a fractured well. The results of this analysis are shown on Fig. 2 which is a plot of recovery factor versus permeability. The "maximum recovery" indicated on this and subsequent figures is the recovery which would result if the well were produced to an abandonment rate of 10 BOPD with a 100 psi well bore pressure. This "maximum recovery" is a theoretical recovery which serves as a reference to show how nearly complete is the recovery from a particular part of the reservoir.

The results of this analysis show that recovery continually decreases as the permeability decreases. Fig. 2, however, shows that with a 625-ft fracture, this decrease in recovery is not as large as might be expected, particularly from the formations flanking the fracture. The range of permeability used in preparing this figure may at first seem unusually low since it has been the general practice of geologists and engineers to neglect very low permeabilities and not even measure them below about 0.1 to 0.05 md. However, formations of permeability below this are known to exist and do contain oil which can be recovered by proper fracture treatment. Even for permeabilities of the order of .001 of a md, very high recoveries are obtained from the formations flanking the fracture; hence, if a large proportion of the oil in place is in the formation flanking the fracture, the permeability below which recovery is negligible is extremely low.

The high recoveries in very low permeability formations shown on Fig. 2 result from changing the flow pattern in much of the drainage area. Instead of requiring all of the fluids to converge on the well through the low permeability formations, much of the fluid flows only a short distance vertically in the tight

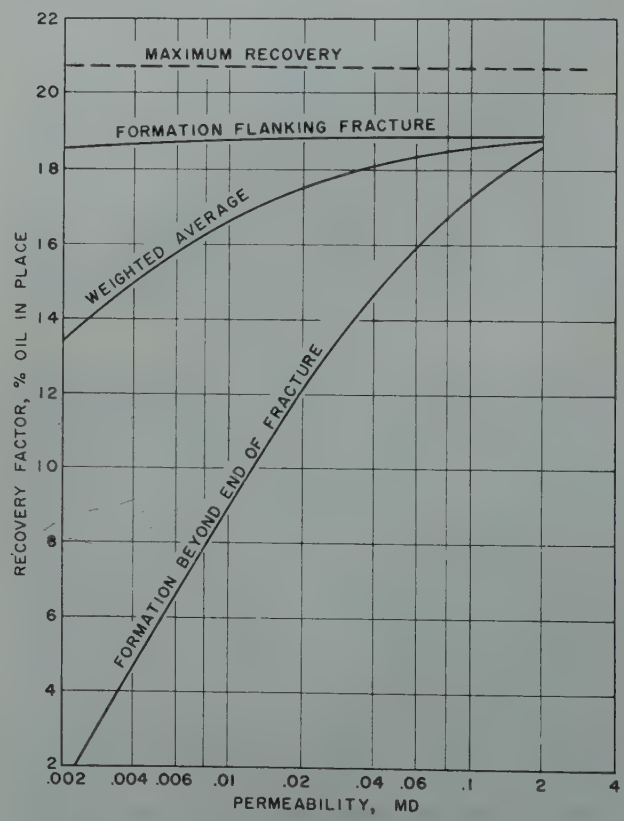

FIG. 2 — EFFECT OF FORMATION PERMEABILITY ON ULTIMATE RECOVERY.

Formation thickness = 30 ft. Fracture carrying capacity = 30 md-ft. Radius of fracture = 625 ft. Abandonment rate = 10 BOPD. Well bore pressure at abandonment = 100 psi. Normal relative permeability and crude characteristics as indicated in Appendix.

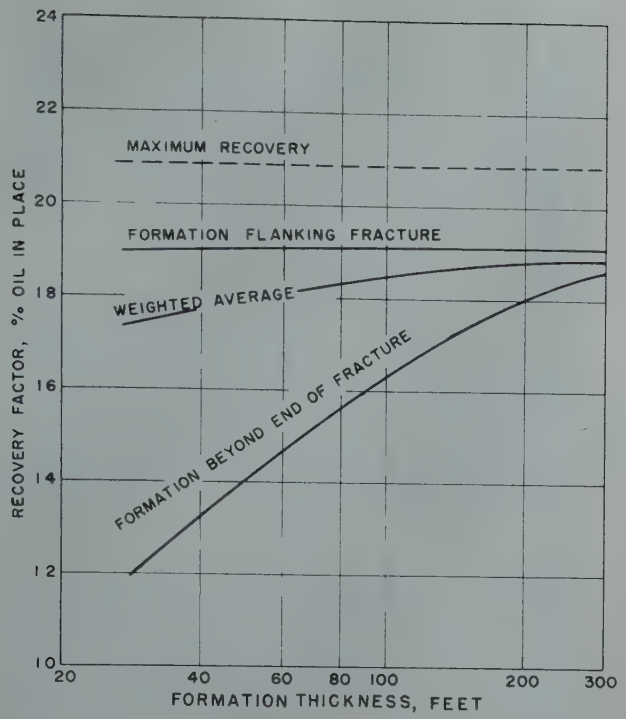

FIG. 3 — EFFECT OF FORMATION THICKNESS ON ULTIMATE RECOVERY.

Formation permeability = .02 md. Fracture carrying capacity = 30 md-ft. Radius of fracture = 625 ft. Abandonment rate = 10 BOPD. Well bore pressure at abandonment = 100 psi. Normal relative permeability and crude characteristics as indicated in Appendix.

formation to a high capacity or low resistance avenue to the well.

EFFECT OF FORMATION THICKNESS ON ULTIMATE RECOVERY

Fig. 3 presents the results of an analysis of the effect of formation thickness on ultimate recovery. This figure shows that the recovery both from the formations flanking the fracture and from the zone of radial flow beyond the end of the fracture increases as the thickness of the formation increases. This is due to the decrease in the per foot abandonment producing rate with increasing formation thickness. For example, if the abandonment producing rate is 10 BOPD, a well drilled in a 10-ft formation will result in some recovery which is dependent on fluid and formation characteristics. If the abandonment producing rate for this well could be reduced to 1 BOPD, other factors being equal, a higher recovery would result.

A well completed in a 100-ft formation with a 10 BOPD abandonment rate is equivalent to 10 wells with 1 BOPD abandonment rates, each producing from 10-ft formations but producing through a common well bore. Actually, Fig. 3 indicates that even though the recovery from the formation flanking the fracture increases with thickness, this increase is of very small magnitude. This means that in very low permeability formations, essentially complete recovery of the oil contained in the rocks flanking the fracture is obtained at all reasonable formation thicknesses.

Throughout this paper an abandonment rate of 10 BOPD is used. This abandonment rate is arbitrary, but lowering it merely serves to make the difference between the recovery from the formation beyond the end of the fracture, the formation flanking the fracture, and the "maximum recovery" less. Conversely raising the abandonment rate would serve to increase these differences.

EFFECT OF FRACTURE CHARACTERISTICS ON ULTIMATE RECOVERY

To determine the effect of fracture characteristics on ultimate recovery, calculations of the recovery were made when the producing rate had declined to an assumed abandonment rate of 10 BOPD. Cumulative production expressed as a percent of the oil in place was then plotted against the assumed radius of fracture. Fig. 4 of this paper presents the results of this analysis for three different values of the fracture flow capacity.

Fig. 4 shows that for any given carrying capacity of the fracture, the recovery increases rapidly with increases in radius of the fracture. Moreover, when the fracture radius approaches the well spacing, the recovery approaches the maximum possible in a volumetric reservoir. This follows from the fact that most of the total pressure drop occurs beyond the end of the fracture; therefore, at the time of abandonment, all the reservoir rock flanking the fracture is substantially at the well bore pressure. Hence, as more of the total reservoir flanks the fracture, the higher will be the recovery.

Fig. 5 is a cross plot of the data presented in Fig. 4 with the recovery factor plotted against the fracture flow capacity for three different fracture radii. Fig. 5 illustrates that when the fluid-carrying capacity of the fracture is of low magnitude, say 30 md-ft, the recovery for any given radius of fracture increases rapidly with small increases in fracture capacity. However, when the fracture-carrying capacity is high (in the order of 200 md-ft), large increases in fracture capacity result in only small increases in recovery. This is due to the decrease of the fraction of the total pressure drop occurring in the fracture with increases in fracture capacity. This, in turn, causes less change in recovery.

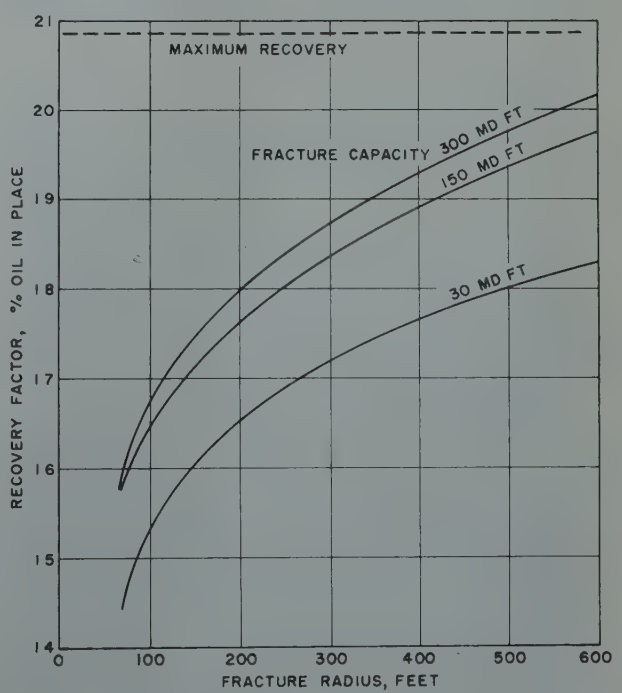

FIG. 4 — EFFECT OF FRACTURE CHARACTERISTICS ON ULTIMATE RECOVERY.

Formation permeability = 0.2 md. Abandonment rate = 10 BOPD. Well bore pressure at abandonment = 100 psi. Normal relative permeability and crude characteristics as indicated in Appendix.

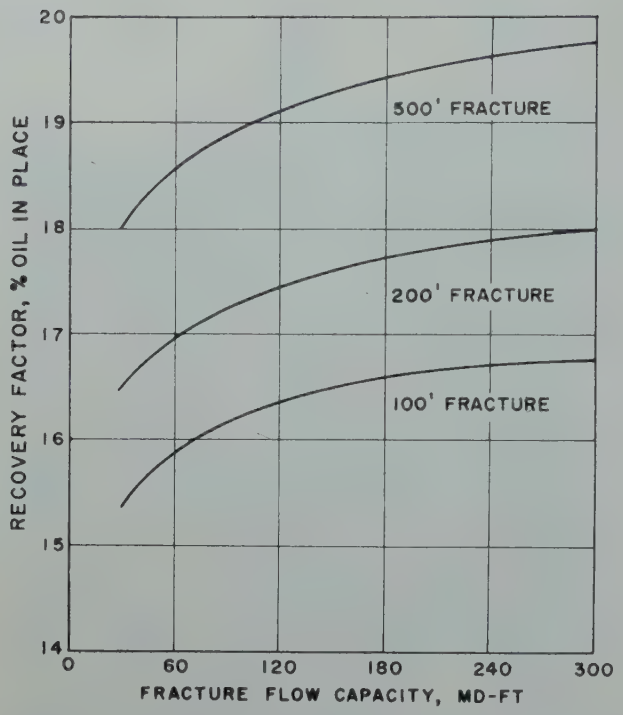

FIG. 5 — EFFECT OF FRACTURE FLOW CAPACITY ON ULTIMATE RECOVERY.

Formation permeability = 0.2 md. Abandonment rate = 10 BOPD. Well bore pressure at abandonment = 100 psi. Normal relative permeability and crude characteristics as shown in Appendix.

Undoubtedly, many factors influence the values of the fracture flow capacity; the formation itself to a large part determines the capacity. In general, laboratory tests indicate that increases in propping agent size and concentration will result in increased flow capacity. The magnitude of the fracture flow capacity was found to vary from 10 md-ft to several thousand md-ft, depending on well conditions.

EFFECT OF FRACTURE CHARACTERISTICS ON INITIAL POTENTIAL

The preceding results have indicated that formations of permeability considerably below what is considered commercially productive can produce substantial quantities of oil if a long radius fracture is made. In order that it be economically feasible to recover this oil, relatively high initial producing rates must be obtainable since, in addition to the normal drilling costs, a considerable expense is incurred in creating a long radius of fracture. Therefore, the effects of fractures on initial producing rates were studied.

The effect of fracture characteristics on initial potential is illustrated on Fig. 6 which is a plot of productivity index versus cumulative recovery plotted on a logarithmic scale. Illustrated on this plot are nine conditions which might result from fracturing a formation.

This figure illustrates that the initial potential or productivity index of a well is not sufficient to evaluate a deeply penetrating fracture treatment. If the capacity of the fracture is large compared to the capacity of the formation, the initial potential of a well is a measure of the fracture flow capacity and very little else. This may be observed by comparing the initial potentials resulting from a 150 md-ft fracture capacity with those resulting from a 30 md-ft fracture capacity. From Fig. 6 it may be seen that if the fracture capacity is 150 md-ft, the initial productivity index is approximately 0.27 regardless of the fracture radius; if, on the other hand, the fracture capacity is 30 md-ft, the initial productivity index is only 0.06 which again is not influenced by the fracture radius. The second purpose of Fig. 6 is to illustrate that the length of time a well can maintain a high initial productivity is directly related to the length of the fracture, i.e., the longer the fracture, the longer the period of high productivity.

RADIUS OF FRACTURE REQUIRED

Figs. 2 to 6 have shown that the low recoveries in very low permeability formations are caused by the radial nature of flow into wells which can largely be overcome by making a deeply penetrating fracture to reduce the flow in the formation to essentially linear flow. Under these conditions of linear flow, high recoveries can be obtained despite low matrix permeability as the pressure in the formation flanking the fracture may be reduced to a low value at reasonably high producing rates.

Figs. 2 and 6 have also shown, however, that as the permeability or capacity of the formation increases, the increase in ultimate recovery from fracturing uniformly permeable formations becomes smaller. Uniformly permeable formations of high capacity allow the average reservoir pressure to be reduced to a low value at commercial producing rates without the aid of fracturing.

From the above discussion, it may be seen that the radius of fracture required to obtain high recoveries in formations of uniform permeability is dependent upon the formation capacity. If the formation capacity is extremely low, substantial recovery can only be obtained from that portion of the formation flanking the reservoir fracture. Therefore, for all practical purposes, recovery from low capacity formations is directly influenced by the areal extent of the fracture.

Well spacing influences the radius of fracture required only to the extent that the same fraction of the reservoir

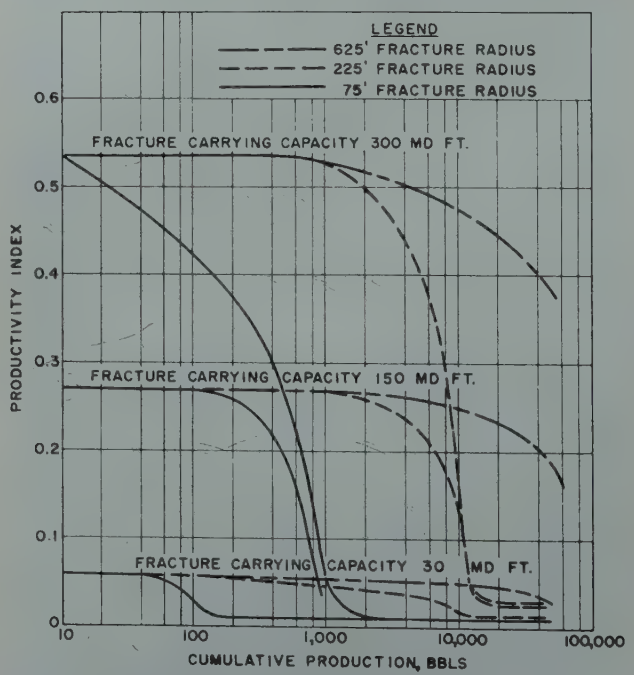

FIG. 6 — INFLUENCE OF FRACTURE CHARACTERISTICS ON INITIAL POTENTIAL.

Formation thickness = 30 ft. Formation permeability = 0.2 md. Oil in place = 400 bbls/acre-ft. Normal relative permeability and crude characteristics as indicated in Appendix.

rock can be flanked by several shorter fractures extending from closely spaced wells instead of by one long fracture from a well on wider spacing. If, for example, a certain recovery can be obtained from one well on 40-acre spacing which contains a fracture of 196,000 sq ft areal extent (fracture radius = 500 ft), the same recovery for the 40 acres under consideration may be obtained from four wells, each well containing a fracture of 196,000/4 or 49,000 sq ft areal extent. In the latter instance, the radius of fracture required in each of the four wells to result in the same recovery from the 40-acre block is only 250 ft.

The relationship between formation fluid capacity, well spacing, and radius of fracture is illustrated on Fig. 7 which is a plot of formation capacity versus recovery to an assumed abandonment producing rate of 10 BOPD. From this figure, it may be observed that as the formation capacity decreases, the radius of fracture required to attain the same recovery increases.

For example, if the formation capacity is 60 md-ft, wells on 40-acre spacing with no fractures yield a recovery of 19 per cent; if the formation capacity is 40 md-ft, 75-ft fractures on 40-acre spacing, or 37-ft fractures in wells on 10-acre spacing, are required to yield a recovery of 19 per cent. Similarly, if the formation capacity is only 6 md-ft, 625-ft fractures on 40-acre spacing, or 312-ft fractures on 10-acre spacing, are required to result in a 19 per cent recovery.

Thus, in general, the radius of fracture required to obtain a given recovery in a uniform permeability formation is dependent upon the formation capacity and the well spacing; the lower the capacity, the longer the fracture and the closer the well spacing, the shorter the fracture.

In applying the information from Fig. 7, allowance must be made for differences between the reservoir where it is being applied and the system assumed in this study. If a more viscous crude is encountered than the one used in this study, the beneficial effects of making a large fracture will continue at higher capacities, *kh*, than indicated in this figure. For example, the same increase in recovery by making a 225-ft fracture, as is shown on Fig. 7 for a 10 md-ft capacity formation, would occur in a 100 md-ft formation if the reservoir contained a crude with a viscosity of 10 cp instead of about 1 cp viscosity as is used in this study.

Similarly, but to a lesser degree, the gas in solution, the reservoir volume factor of the crude oil, and the relative permeability characteristics of the formation also tend to change formation capacity where the highly beneficial effects of deeply penetrating fractures begin. Thus, Fig. 7 must be used as a qualitative guide in selecting reservoirs for large volume, deeply penetrating fracture treatments rather than an inflexible yardstick.

When considering large fracture treatments, allowance must also be made for precipitation of solids or semisolids from the produced fluids. Little is known about the exact causes of this precipitation; however, often waters are produced which contain dissolved salts which may precipitate as a result of lowering the pressure in the vicinity of the well. Also, in formations of low permeability, some crudes have a tendency to plug the rocks. If the plugging resulting from reducing pressure occurs throughout the reservoir, the effect will be the same as discussed in regard to recovery of highly viscous oil; namely, plugging of the formations throughout tends to increase the capacity, *kh*, where deeply penetrating fractures are needed. If lack of ability of a well to produce is the result of local precipitation or

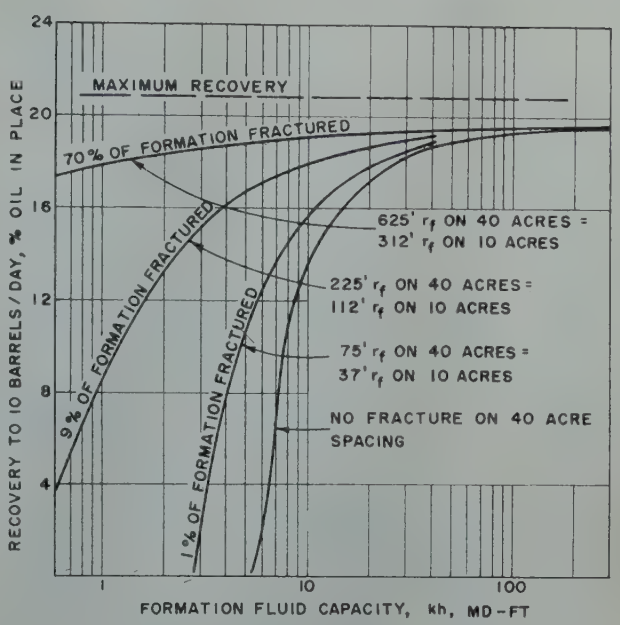

FIG. 7 — RECOVERIES FROM FRACTURED WELLS.

Oil in place = 400 bbls/acre-ft. Fracture carrying capacity = 30 md-ft. Normal relative permeability and crude characteristics as indicated in the Appendix.

accumulation of solids entrained in the fluids near the well bore rather than low capacity *kh*, large increases in production and recovery will result if fractures are long enough to penetrate beyond the zone of reduced permeability. However, if the plugging is due to accumulation of material from the reservoir fluid, more plugging can be expected as all fluids produced must converge and flow through the bottleneck formed by the rocks flanking the fracture plus those forming the well. If a deeply penetrating fracture is made, the increase in area through which the fluids must flow is increased tremendously. A 625-ft fracture in a 30-ft formation exposes over 52,000 times as much area as is exposed in a 6-in well bore. Thus, when considering the fracture radius required, deeply penetrating fractures have the added advantage that where solids accumulate at the well bore, production increases can be expected to be sustained for a much longer time.

TREATMENT REQUIREMENTS FOR LONG FRACTURES

The preceding portions of this paper have illustrated that commercially attractive producing rates and recoveries can be obtained from oil bearing formations of extremely low permeability, provided fractures of large areal extent may be created in the productive zone. To complete this analysis of reservoir fracturing, a study was made to determine the treating techniques and materials required to create fractures of this size by hydraulic fracturing.

In this study of treatment requirements, data were collected from several hundred fracturing jobs and analyzed as to pump rates, pressures, volume and viscosity of fracturing fluid, production rate increases, etc. From theoretical considerations and these data, it was concluded that a reasonable estimate of the radius of fracture could be obtained from the following formula:

$$r_f = C\left[Q\sqrt{\frac{\mu t}{K}} \right]^{1/2} \quad . \quad . \quad . \quad . \quad . \quad . \quad . \quad . \quad . \quad (1)$$

Where r_f = radius of fracture, feet

Q = injection rate, gallons per minute

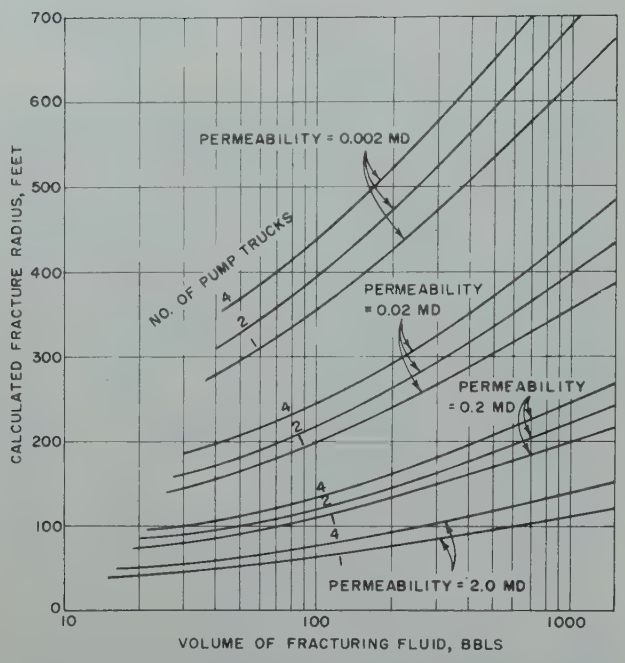
CALCULATED FRACTURE RADIUS, FEET
VOLUME OF FRACTURING FLUID, BBLS
PERMEABILITY = 0.002 MD
NO. OF PUMP TRUCKS
PERMEABILITY = 0.02 MD
PERMEABILITY = 0.2 MD
PERMEABILITY = 2.0 MD

FIG. 8 — FRACTURES CREATED BY HYDRAULIC FRACTURING TREATMENTS IN LOW PERMEABILITY FORMATIONS. Well depth = 4,000 ft (C = 0.15). Fracturing fluid viscosity = 200 cp.

μ = fracturing fluid viscosity, cp

t = pumping time while fracturing, minutes

K = formation permeability, darcys

C = a constant which depends upon the confining stress and rock characteristics

In brief, this equation indicates that the higher the fracturing fluid viscosity and the larger the volume of fluid (product of injection rate Q and pumping time t), the larger will be the fracture created; permeability inversely affects the fracture radius, that is, the lower the permeability the larger the fracture. The constant C involves an inverse function of the confining stress, reservoir pressure, rock strength and porosity and may be determined by analysis of field conditions. Actually, the study indicated that the absolute value of the constant C is not essential as it does not vary widely under most treating conditions. For example, the value of the constant C for a 2,000-ft well was found to be 0.16 and for a 10,000-ft well was found to be 0.11.

In actual practice it is often sufficient to utilize the values as commonly measured on conventional viscosimeters for the viscosity term (μ) in Equation (1). Some fracturing fluids, however are characterized by low viscosity and yet exhibit low fluid loss properties due to suspended solid or semi-solid particles. This low fluid loss causes the fluid to behave as one of much higher viscosity, which, in turn, causes larger fractures than would be expected. In such instances the viscosity value used in Equation (1) may be adjusted upwards to account for low fluid characteristics; however, as the purpose of this equation is merely to illustrate that large fractures can be created, it is sufficient to consider any fluid loss characteristics as a safety factor.

Equation (1) allows the fracture radius to be estimated for any given set of treating conditions and also allows the determination of the materials and techniques required to create long fractures. To determine if it is feasible to create fractures of the size discussed in this paper, a hypothetical set of conditions were assumed and substituted in Equation (1). For this analysis, the well depth was assumed equal to 4,000 ft ($C = 0.15$) and the fracturing fluid viscosity was assumed equal to 200 cp which is typical of the viscous oils commonly used in fracturing treatments. The injection rates were expressed as an equivalent number of pump trucks from computed values of friction losses through 2½-in. EUE tubing, pump rates and surface pump pressures. The injection rates from these computations were as follows:

No. of Pump Trucks	Rate Bbls/Min.	Surface Pressure, psi
1	1.75	1,500
2	2.70	1,900
4	4.05	2,400

The pumping time t in Equation (1) was varied from 50 to 500 minutes. The permeability of the formation to be fractured was varied from 0.002 md to 2.0 md.

The results of these calculations are shown on Fig. 8 which is a plot of volume of fracturing fluid versus fracture radius. From this figure, it may be seen that the tighter the formation the larger the fracture created under any given set of treating conditions. Also, illustrated on Fig. 8 is the increase in fracture radius with increasing injection rates (pump trucks) and fracturing fluid volumes. Finally, Fig. 8 illustrates that fractures of the size needed in very low permeability formations are well within the reach of present day treating practices.

EXAMPLES OF FRACTURING RESULTS

To illustrate the effect of large radius of fractures in tight formations, the following examples are given.

Wells "A" and "B" were open hole completions producing from a tight formation. The formation was a 125-ft lime with a permeability of about 1/3 of a md. Both wells had been acidized when initially completed but the rate of production after several years had declined to about 2 BOPD and it was decided to treat the wells to stimulate production.

Well "A" was treated with a small volume hydraulic fracture treatment. This treatment consisted of 1,250 gals. of gelled hydrocarbon containing about 1/6 of a pound of sand per gallon of gel. Initial production

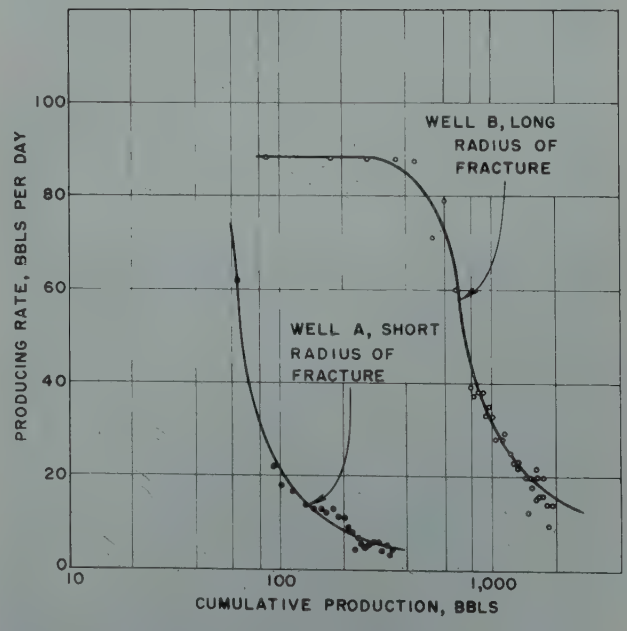

FIG. 9 — PRODUCTION RATE DECLINE FOLLOWING FRACTURE TREATMENT.

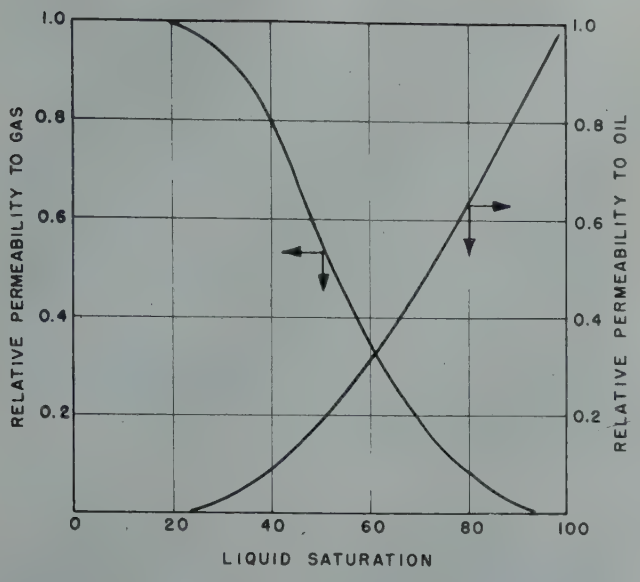

FIG. 10 — ASSUMED RELATIVE PERMEABILITY CHARACTERISTICS.

after treatment was high but rapidly declined as indicated on Fig. 9.

Well "B" was treated with 8,400 gals. of No. 5 fuel oil containing approximately 1 lb of sand per gallon of fuel oil. When this well was placed on production, a high rate of production was maintained for several days and then production declined as shown on Fig. 9.

Productivity index tests were not run on these wells. However, on the assumption that a constant bottom hole pressure was maintained following the time when the wells were again placed on production, production rate is a direct measure of productivity index; therefore, it can be reasoned that Fig. 9 is substantially equivalent to Fig. 6. The economic abandonment rate of these wells was approximately 2 BOPD.

In summary, the results of the study presented in this paper indicate that, though a formation is of very low permeability, substantial recovery at commercially attractive rates can be obtained by making a long radius fracture. These findings mean that in the search for oil, less attention need be given to the permeability of reservoir rocks; it is necessary only to find saturated

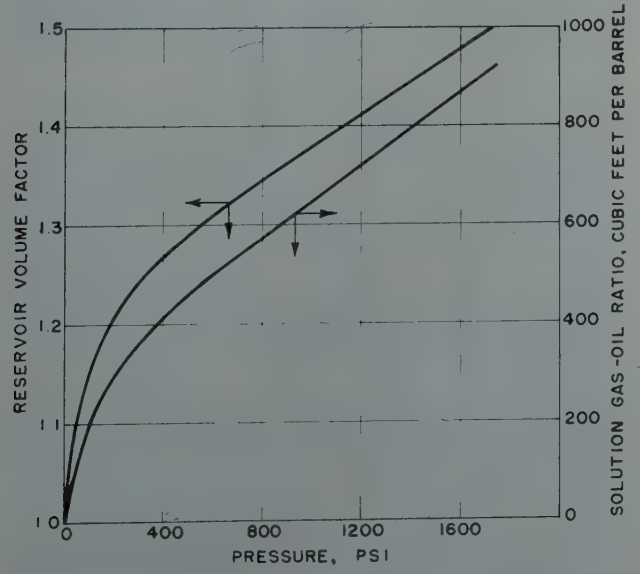

FIG. 11 — ASSUMED CRUDE CHARACTERISTICS.

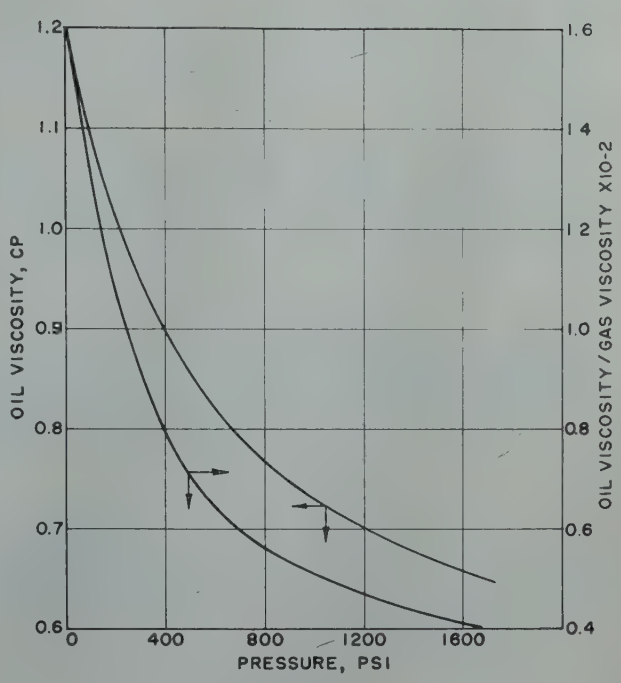

FIG. 12 — ASSUMED RESERVOIR VISCOSITIES.

pore space of sufficient quantity. If sufficient permeability does not exist in the reservoir rock for production at commercial rates, the oil can still be recovered at attractive rates of production by creating a long radius fracture.

CONCLUSIONS

1. The formation permeability below which commercially attractive producing rates and recovery cannot be obtained is extremely low, provided at least one deeply penetrating fracture is created in every continuous reservoir penetrated by a well.

2. In order to increase substantially commercial recovery from extremely tight formations (capacity less than about 50 md-ft), it is necessary to make a sufficiently long fracture such that an appreciable part of the reservoir rock flanks the fracture.

3. Fractures of the length necessary to increase recovery in low permeability formations may be created by present day treating techniques.

4. Very long fractures in tight formations in addition to increasing recovery, will permit relatively high rates of production over most of the well's producing life.

5. Initial potential tests do not indicate the effectiveness of deeply penetrating fractures. They indicate the fracture flow capacity but not the penetration.

ACKNOWLEDGMENT

Acknowledgment is made to the management of the Stanolind Oil and Gas Co. for permission to publish the results of this investigation.

APPENDIX

In order to determine the effect of reservoir fracturing on recovery, certain crude and rock characteristics were assumed. These characteristics given as Figs. 10, 11, and 12, were not chosen to simulate any particular reservoir but were intended to permit evaluation of the relative importance of the variables affecting recovery from fractured wells. Oil in place was arbitrarily set at 400 bbls/acre-ft. ★★★

INTERRELATION of RESISTIVITY and POTENTIAL of SHALY RESERVOIR ROCK

F. M. PERKINS, JR.
JUNIOR MEMBER AIME
H. R. BRANNON, JR.
W. O. WINSAUER
JUNIOR MEMBER AIME

HUMBLE OIL AND REFINING CO.
HOUSTON, TEXAS

T. P. 3877

ABSTRACT

Both the abnormal resistivity exhibited by shaly reservoir materials and their potential are due to adsorption of ions. Interrelationships between the two have been derived and verified by laboratory results. These relations which have resulted from this work may be used in a qualitative manner to estimate whether or not a particular shaly reservoir contains hydrocarbons, and also to estimate the porosity of shaly sands.

INTRODUCTION

In spite of the progress which has been made in the last decade toward a better understanding and utilization of the electric log, there remain a number of problems in the interpretation of the log. One of these which is often troublesome is that of divining the nature of the fluids in sandstones or carbonate rocks which contain appreciable amounts of shale.

It was shown by Patnode and Wyllie[1] in 1949 that shaly rocks exhibit an abnormally low resistivity when saturated with solutions of low ionic concentrations. This phenomenon has been demonstrated to be due to the adsorptive properties of shale or clay in the rock.[2]

In estimating the fluid content of shaly sands or carbonates from the electric log, it is desirable and sometimes necessary to correct for the abnormally low resistivity. A similar correction is likewise often necessary if attempts are made to estimate the porosity of a stratum from resistivity measurements. The correction may be made from data obtained on core samples and from information on salinity of interstitial water. Cores, however, are not always available. Moreover, even if cores are at hand, their examination is time-consuming. It would be most desirable, therefore, to make corrections of this nature from the log itself. Since both the abnormal resistivity and the potential[3] are consequences of the adsorption of ions on shale, it should be possible to utilize the potential curve to give better interpretation of resistivity data obtained in logging shaly materials. The work described in following sections was directed toward this end.

THEORY

Relation of Resistivity of Shaly Reservoir Rock to Adsorptive Properties

In discussing the effect which the presence of shale or clay exerts on the resistivity of a reservoir rock, it is convenient to make use of the *resistivity factor*.[4,5] This quantity has been defined as the ratio of the resistivity of the rock when it is completely saturated with an electrolyte to the resistivity of the electrolyte itself.

When the rock, such as a clean sand or carbonate, is free of shale the resistivity factor is virtually independent of the ionic concentration of the electrolyte used to saturate the sample, so that

$$F = R_o/R_w = \text{constant for a clean rock} \quad . \quad . \quad (1)$$

where F is the resistivity factor,

R_o is the resistivity of the rock saturated with electrolyte, and

R_w is the resistivity of the electrolyte.

When the rock contains argillaceous material, the resistivity factor as defined above is no longer independent of the concentration of the electrolyte used to saturate the rock, but decreases as the ionic concentration of the electrolyte decreases.

In explanation of this behavior, it is instructive to consider a sample of shaly porous rock placed in contact with a large volume of a dilute electrolyte. The sample is considered to become saturated with the electrolyte, and to attain equilibrium with it. As a result of adsorption by the shale surfaces within the rock, there is a greater concentration of ions in the solution adjacent to the shale particles in the interstices of the sample than there is in the external solution with which the

[1]References given at end of paper.

Manuscript received in the Petroleum Branch office Sept. 2, 1953. Paper presented at the Petroleum Branch Fall Meeting in Dallas Oct. 19-21, 1953.

rock is in contact. For brevity, the solution within the pores of the rock may be termed the "interstitial solution" and that external to the rock and in equilibrium with it the "equilibrium solution."

As ordinarily determined, the resistivity factor is the ratio of the resistivity of the saturated rock to the resistivity of the *equilibrium solution*. It is this factor which decreases for a shaly sample as the electrolyte concentration decreases. On the other hand, it may be assumed that the ratio of sample resistivity to resistivity of *interstitial solution* does not vary with concentration of the electrolyte if the internal dimensions do not change, or that

$$F_o = \frac{R_o}{R_{wi}} = \text{constant for any particular rock} \quad (2)$$

where R_{wi} is the resistivity of the interstitial solution, and

F_o is the resistivity factor.

The distinction between use of the resistivity of the interstitial solution, on the one hand, and that of the equilibrium solution, on the other, in determining the resistivity factor makes it necessary to redefine the resistivity factor, F_o, as the ratio of sample resistivity to resistivity of *interstitial solution,* and to introduce the apparent resistivity factor, F, as the ratio of resistivity of sample to that of the equilibrium solution.

Even for very shaly sands or carbonates F approaches F_o as the equilibrium solution becomes more concentrated, indicating that the concentrations of interstitial and equilibrium solutions differ little at high electrolyte concentration.

By eliminating the resistivity of the sample, R_o, between Equations (1) and (2), the following equation is obtained:

$$F = F_o \frac{R_{wi}}{R_w} \quad . \quad . \quad . \quad . \quad . \quad . \quad . \quad . \quad . \quad . \quad . \quad (3)$$

The conductivity of the solution in the pores of an argillaceous rock may be considered as the sum of the conductivity of the equilibrium solution, $\frac{1}{R_w}$, and an excess double-layer conductivity, $\frac{1}{Z}$, or

$$\frac{1}{R_{wi}} = \frac{1}{R_w} + \frac{1}{Z} \quad . \quad . \quad . \quad . \quad . \quad . \quad . \quad (4)$$

Combining Equation (4) with (3), there results

$$\frac{F_o - F}{F} = \frac{R_w}{Z} \quad . \quad . \quad . \quad . \quad . \quad . \quad . \quad . \quad . \quad (5)$$

The charge on clay surfaces within the rock imparted by adsorbed negative ions or other phenomena results in an increased concentration of positive contra-ions in the interstitial solution. This increase may be approximated for univalent ions by

$$\Delta n = A\sigma \quad . \quad . \quad . \quad . \quad . \quad . \quad . \quad . \quad . \quad . \quad . \quad (6)$$

where Δn is the increase in positive ion concentration,

σ is the charge density on the clay surface, and

A is a constant.

The added conductivity that results from these positive ions, neglecting any changes in negative ion concentration in the interstitial solution, is given by

$$\frac{1}{Z} = A'\sigma\mu_1 \quad . \quad . \quad . \quad . \quad . \quad . \quad . \quad . \quad . \quad (7)$$

where μ_1 is the mobility of the positive ion, and

A' is a constant.

The conductivity of the equilibrium solution, expressed in terms of concentration of univalent ions and ionic mobilities, is given by

$$\frac{1}{R_w} = en(\mu_1 + \mu_2) \quad . \quad . \quad . \quad . \quad . \quad . \quad . \quad (8)$$

where n is the ionic concentration in the equilibrium solution, respectively, and e is the ionic charge.

Substituting Equations (7) and (8) into Equation (5), there results

$$\frac{n}{\sigma}\frac{(F_o - F)}{F} = \frac{A'\mu_1}{e(\mu_1 + \mu_2)} \quad . \quad . \quad . \quad . \quad . \quad (9)$$

Writing Equation (9) for two solutions of different ionic concentrations, n_1 and n_2, with the assumption that the ratio $\frac{\mu_1}{\mu_1 + \mu_2}$ does not vary with concentration,

$$\left(\frac{F_o - F_2}{F_2}\right)\left(\frac{F_1}{F_o - F_1}\right) = \frac{\sigma_2}{\sigma_1}\frac{n_1}{n_2} \quad . \quad . \quad . \quad (10)$$

This relation alone does not permit computation of the extent of abnormality, since σ cannot be measured directly. The quantity σ, however, can be related to the potential, as shown in the following section.

Relation of Mounce Potential to Adsorptive Properties

It has been shown in a recent publication[3] that the Mounce potential, observed when a sample of shaly material is interposed between solutions of different ionic concentrations, is the sum of three potentials — two so-called phase boundary potentials, and a diffusion potential. The latter component is usually of minor importance in shaly materials. The Mounce potential is the principal component of the potential recorded by the electric log.[4]

In the work on the Mounce potential to which reference is made above, the phase boundary potential is related to a quantity termed n_o, which reflects the amount of adsorption of negative ions by the shale. The quantity n_o is expressed as a charge density per unit volume, and is related to σ, the surface charge density of Equation (10), by a constant of proportionality for any particular sample.

In some of the previous work on the potential it has been necessary to assume, to avoid complexities in mathematics, that n_o is constant for a given rock sample, even though it has been realized that n_o is a function of concentration of the electrolyte. For the present purpose n_o and its counterpart σ are considered to be functions of concentration.

An analytical solution for the phase boundary potential and the diffusion potential, allowing for a variation of n_o with concentration, requires a knowledge of proper boundary conditions, which are determined by the geometry of the rock, and of a functional relation between n_o and concentration. These difficulties, as well as that introduced by the nonlinearity of the differential equation that results, present obstacles to a rigorous analytical approach.

To circumvent these difficulties, another approach may be made. The Mounce potential, $\Delta\Phi$, can be described by

$$\Delta\Phi = g(n_1, n_2, \sigma_1, \sigma_2) \quad . \quad . \quad . \quad . \quad . \quad . \quad . \quad (11)$$

The potential existing between a charged rock surface and the equilibrium solution is also completely determined by the surface charge and solution concentration, so that

$$\Delta\Phi = f(\Phi_{s_1}, \Phi_{s_2}, \Phi_d) \quad . \quad . \quad . \quad . \quad . \quad . \quad . \quad . \quad (12)$$

where Φ_{s_1}, Φ_{s_2} are, respectively, surface potentials at concentrations n_1 and n_2, and

$\Phi_d = 0.2 \ln \frac{n_1}{n_2}$, the normal diffusion potential for NaCl.

As a trial solution, the Mounce potential is considered to be a linear function of the surface and diffusion potentials, giving

$$\Delta\Phi = \Phi_{s_1} - \Phi_{s_1} + \Phi_d \quad . \quad . \quad . \quad . \quad . \quad . \quad . \quad . \quad (13)$$

An equation for the surface potential of a flat charged plate is available from Verwey and Overbeek.[7] For the conditions described in the reference, the potential is given by

$$\sin h \frac{\Phi_s}{2} = \sigma \left[\frac{\pi}{2nDkT}\right]^{1/2} \quad . \quad . \quad . \quad . \quad . \quad (14)$$

where Φ_s is the surface potential in units of $\frac{kT}{\epsilon}$ referred to the equilibrium solution,

k is Boltzmann's constant,
D is the dielectric constant,
n is the concentration of ions in the equilibrium solution,
T is the temperature in °K,
σ is the surface charge/cm.^{2}, and
ϵ is the charge on an electron.

Substituting Equation (14) into (13), with the approximation that

$$e^{-\Phi_s/2} >> e^{\Phi_s/2},$$

there results

$$\Delta\Phi = 2 \ln \frac{\sigma_1}{\sigma_2} + 0.8 \ln \frac{n_2}{n_1} \quad . \quad . \quad . \quad . \quad . \quad (15)$$

The approximation is necessary only to bring Equation (14) into a form having an explicit solution for $\frac{\sigma_1}{\sigma_2}$.

Equation (13) is an assumed form of solution to Equation (12). It cannot be verified experimentally by potential determinations alone, but elimination between Equations (15) and (10) of terms containing the surface charge does provide an expression for the Mounce potential and the resistivity factor containing measurable quantities.

Relation Between Potential and Resistivity Factor

Simultaneous solution of Equations (15) and (10) yields

$$\ln\left[\frac{(F_o - F_2)}{F_2} \frac{F_1}{(F_o - F_1)}\right] = \frac{-\Delta\Phi}{2} - 0.6 \ln \frac{n_2}{n_1} \quad (16)$$

with F_2, F_1, $\Delta\Phi$, n_1, and n_2 having values that may be determined experimentally.

Other solutions containing similar terms might also be chosen. The only criteria for selection are that the equations contain useful quantities and be subject to experimental verification. One other such equation can be obtained as follows:

Equation (3) may be written in the form

$$\frac{F_o}{F} = \frac{\rho}{\rho_1} = \frac{\overline{\mu_1}\,\overline{n_1} + \overline{\mu_2}\,\overline{n_2}}{n(\mu_1 + \mu_2)} \quad . \quad . \quad . \quad . \quad (3a)$$

where n_1 and n_2 are the positive and negative ion concentrations in the core, the bar denoting an average taken to satisfy Equation (3a), and μ_1 and μ_2 are the ionic mobilities in the core, similarly averaged.

The concentration of positive ions, n_1, and negative ions, n_2, may be related to the equilibrium concentration, n, by Boltzmann's distribution equations

$$n_1 = \overline{ne^{-\Phi b}}$$
$$n_2 = \overline{ne^{\Phi b}} \quad . \quad . \quad . \quad . \quad . \quad . \quad . \quad . \quad . \quad . \quad . \quad . \quad (17)$$

where Φb is the potential in the core referred to the equilibrium solution in units of kT/ϵ.

Substituting Equation (17) in (3a) gives

$$\frac{F_o}{F} = \frac{\overline{\mu_1 e^{-\Phi b}} + \overline{\mu_2 e^{\Phi b}}}{\mu_1 + \mu_2} \quad . \quad . \quad . \quad . \quad . \quad . \quad (18)$$

If it be assumed, for convenience in computations, that $\overline{e^{\Phi b}}$ is negligible and that the ratio $\frac{\overline{\mu_1}}{\mu_1 + \mu_2}$ does not vary with concentration, then

$$\frac{F_o}{F} = \text{constant } \overline{e^{-\Phi b}} \quad . \quad . \quad . \quad . \quad . \quad . \quad (19)$$

When F is taken at two different ionic concentrations, F_o may be eliminated to give

$$\frac{F_2}{F_1} = \frac{\overline{e^{-\Phi b1}}}{\overline{e^{-\Phi b2}}} \quad . \quad . \quad . \quad . \quad . \quad . \quad . \quad . \quad . \quad (20)$$

It is again necessary to assume a form of the solution to an equation in order to relate the resistivity factor to the Mounce potential. A convenient choice is that

$$\ln \frac{F_2}{F_1} = \ln \overline{e^{-\Phi b1}} - \ln \overline{e^{-\Phi b2}} = \Delta\Phi \quad . \quad . \quad (21)$$

where $\Delta\Phi$ is the Mounce potential.

Because of the methods employed to obtain Equations (16) and (21) the usefulness of the equations can only be determined by application to experimental data. The above equations have been used to correlate experimental data, and the results are presented in the following section.

EXPERIMENTAL

Procedure

In order to test experimentally the relations given by Equations (16) and (21), determinations were made of the apparent resistivity factors and Mounce potentials given by shaly sands from several different strata and localities. No shaly carbonates were examined.

Small cylindrical plugs, 1-in. in diameter and averaging about 1-in. in length, were cut from well cores. The axis of each cylinder was parallel to the bedding plane. The samples were extracted with organic solvents, air-dried, and saturated with 5N sodium chloride solution. Each sample was then placed in a Hassler type core holder, and 5N sodium chloride solution was passed through the core until the resistivity, as determined by a four electrode alternating-current measuring system, was constant. Successively more dilute salt solutions were passed through the core, and resistivity measurements were made until equilibrium was attained at each concentration, as shown by constancy of resistivity.

Mounce potential measurements were made on each sample after all resistivity determinations had been completed. For this purpose, solutions of the desired concentrations were placed in contact with the ends of the sample, and readings were taken after the potential became constant.

TABLE 1 — EXPERIMENTAL RESISTIVITY FACTOR DATA

Concentration of Equilibrium Solution eq./liter n	Sample S-1 Formation: Frio Source: Kleberg Co., Texas Depth: 6,000 ft Porosity: 23 % F	Sample R-1 Formation: McElroy Source: Live Oak Co., Texas Depth: 4,560 ft Porosity: 26.8% F	Sample S-2 Formation: Frio Source: Kleberg Co., Texas Depth: 6,000 ft Porosity: 18.3% F	Sample W-2B Formation: Wilcox Source: McMullen Co., Texas Depth: 6,860 ft Porosity: 18.2% F	Sample KD-1 Formation: Frio Source: Brooks Co., Texas Depth: 6,165 ft Porosity: 15.5% F	Sample P-1 Formation: Frio Source: Kennedy Co., Texas Depth: 8,100 ft Porosity: 20.0% F	Sample P-A Formation: Spraberry Source: Upton Co., Texas Depth: 7,000 ft Porosity: 13.6% F	Sample 8 Formation: Stevens Source: Elk Hills California Depth: 7,500 ft Porosity: 17.6% F
5.0	15.3	9.7	20.0	21.1	30.4	21.8	44.7	26.0
1.0	----	----	----	----	----	15.7	40.7	19.7
0.97	13.5	8.7	16.1	20.0	26.0	----	----	----
0.31		7.8	----	----	21.8	----	----	----
0.138	9.7	----	10.2	...	----	----	----	----
0.1	...	----	----	----	----	7.65	36.4	10.0
0.087	----	5.9	----	...	14.5	----	----	----
0.06	----	----	----	13.5	----	----	----	----
0.025	6.3	3.1	4.6	----	----	----	----	----
0.01	----	----	----	8.0	4.8	2.26	28.2	4.10
0.006	3.6	----	----	----	----	----	...	----
0.005	----	----	1.3	6.6	3.2	1.45	24.5	3.15

RESULTS

Sample description and source, data on porosity, and apparent resistivity factors at various electrolyte concentrations are given in Table 1. Table 2 presents data on Mounce potentials of the same samples.

Since the concentrations of solutions used in determining the apparent resistivity factors and the Mounce potentials generally differed somewhat, it was necessary to interpolate in order to obtain data for testing Equations (16) and (21).

Table 3 shows interpolated values of apparent resistivity factor and of potential for each sample at different pairs of values for electrolyte concentrations.

Tabulated in this table are the values of F_o computed by use of Equation (16). As criteria of the manner in which the equation agrees with the experimental data, the computed values of F_o should be (1) reasonably constant as computed from different pairs of electrolyte concentrations, and (2) equal to or slightly greater than the values of resistivity factor determined by use of 5N solution. Although F_o computed from Equation (16), gives a reasonably good check of the equation, the calculated values are not entirely independent of electrolyte concentration. However, slight modification of the coefficient of the concentration term in Equation (16) from 0.6 to 0.5 results in a more satisfactory fit of the data. It is interesting to note that this is equivalent to omitting the diffusion potential. So modified, the equation becomes

$$-2ln\left(\frac{F_o-F_2}{F_2}\right)\left(\frac{F_1}{F_o-F_1}\right)=\Delta\Phi+ln\frac{n_2}{n_1}. \quad (22)$$

Values of F_o computed by the above equation are also shown in Table 3. The consistency of these data indicates that Equation (22) is preferable for estimation of the resistivity factor.

A comparison of Equation (21) with experimental data is shown in Fig. 1. In this figure the Mounce potential is plotted against the logarithm of F_2/F_1. As shown in this figure, the experimental data are in excellent agreement with Equation (21).

Both Equations (22) and (21) relate Mounce potential to the resistivity of the sample. It may be noted that these equations can be combined by eliminating the Mounce potential to yield a very simple relation. When this is done and the solution resistivities are substituted for the solution concentrations, the following equation results

$$\frac{F_o-F_2}{F_o-F_1}=\left(\frac{R_{o_2}}{R_{o_1}}\right)^{0.6}. \quad (23)$$

The above equation was tested by solving for F_o at various values of electrolyte concentrations. In order that the values of F_o, computed from Equation (23), may be compared with the resistivity factors determined from Equation (16) and (22), they are also tabulated in Table 3. The average values of F_o computed by use of Equation (23) are in good agreement with those obtained by use of Equation (22).

It is possible to make an additional indirect check on Equations (22) and (23) by using the values of F_o computed from them to calculate the porosity by use of the relation[8]

$$F_o=0.62\phi^{-2.15}. \quad (24)$$

where ϕ is the porosity, expressed as a fraction.

The porosities so computed can then be compared with the measured porosities. A comparison is shown in Table 4 of the measured porosities with those calculated from Equation (24) using average values of F_o obtained by employing, respectively, Equations (22) and (23).

APPLICATION TO ELECTRIC LOG INTERPRETATION

Of the various problems which arise in the interpretation of electric logs of shaly rocks, perhaps the most important is that of estimating whether or not a particular stratum contains oil or gas. Another problem

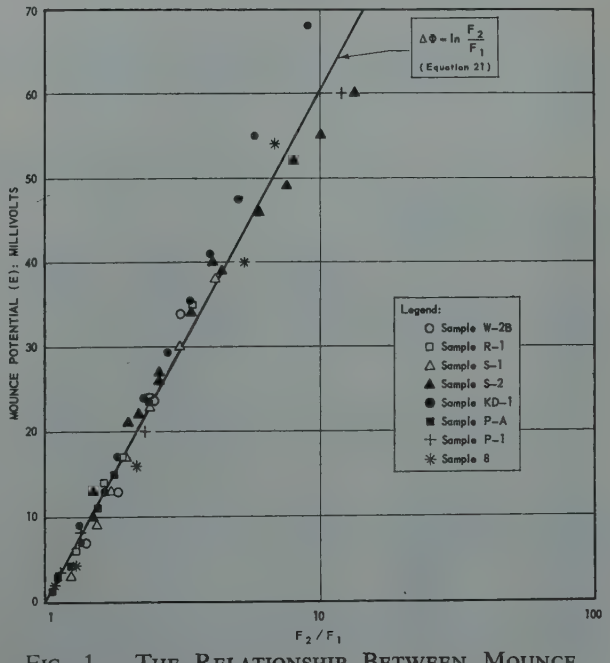

FIG. 1 — THE RELATIONSHIP BETWEEN MOUNCE POTENTIAL AND THE RESISTIVITY FACTOR RATIO.

which is often encountered is that of estimating the porosity.

The approach to the first problem, that of deciding whether a shaly zone may contain hydrocarbons, consists of first estimating the resistivity of the stratum filled only with formation water and of then comparing this resistivity with the resistivity indicated by the electric log. If the latter is significantly higher, it is logical to assume the presence of oil or gas.

To estimate the resistivity which the shaly zone would have if completely saturated with formation water, Equation (21) may be applied. For this purpose, the term $\Delta\Phi$ must be expressed in terms of the potential read from the electric log, referred either to a shale base line or to the value for a clean sand or carbonate in the immediate vicinity of the bed of interest.

If a clean sand is used as a reference for the potential, it is necessary to know (1) the resistivity of the mud filtrate, (2) the resistivity of the formation water, (3) the resistivity of the invaded zone, and (4) the difference in potential read opposite the clean sand and the bed of interest. If the shale base line is used as a reference, it is not necessary to know the resistivity of the formation water or of the mud filtrate.

Laboratory results have indicated[3,9] that the Mounce potential of shales may be considered virtually independent of the character of the shale at relatively low electrolyte concentrations. It is possible that the maximum electrolyte concentration under which this condition prevails depends upon the particular shale; tentatively, it may be assumed that the upper limit is possibly in the range of 25,000-100,000 ppm sodium chloride. Assuming that the Mounce potential under these conditions is not dependent upon the type of shale

$$E_{shale} = \frac{kT}{\epsilon} \ln \frac{n_2}{n_1} \quad . \quad . \quad . \quad . \quad . \quad . \quad . \quad . \quad (25)$$

where E_{shale} is the Mounce potential across the shale in mv.

If the above equation is combined with Equation (21) so that the resulting equation contains the difference in potential between the shale base line and the shaly bed under consideration, then

$$E = \frac{kT}{\epsilon} \ln \frac{n_2}{n_1} \cdot \frac{F_1}{F_2} \quad . \quad . \quad . \quad . \quad . \quad . \quad . \quad (26)$$

where E is the difference in potential in millivolts between the shale and the shaly bed on the potential curve.

When the solution resistivities are substituted for concentrations, and the logarithm and temperature are changed to conform with common electric log usage, the equation becomes

$$E = 0.11(460 + T) \log_{10} \frac{R_{xo}}{R_o} \quad . \quad . \quad . \quad . \quad . \quad . \quad (27)$$

where T is temperature in °F.,

R_{xo} is, in this case, resistivity of the invaded zone, and

R_o is, in this case, resistivity of the bed completely saturated with formation water.

The assumption that the log potential is equivalent to the Mounce potential tacitly implies that there is a negligible effect due to any streaming potential, that the salt in the drilling mud filtrate and formation water is sodium chloride, and that geometrical corrections of the type discussed by Doll[10] are not significant.

In practice, R_{xo} must be determined from an electrode configuration which has close spacing, such as that of a "microlog" tool.

In estimating the porosity of a shaly bed, the most direct method utilizes Equations (23) and (24). The latter equation requires the use of the true resistivity factor, which is obtained from the former equation.

In applying Equation (23), F_1 is designated as the apparent resistivity factor of the invaded zone, which has resistivity R_{xo}. These quantities are determined from log resistivity measurements made with close electrode spacing and from a knowledge of the mud filtrate resistivity at formation temperature. F_2 is designated as the apparent resistivity factor of the uninvaded zone, and R_o is the resistivity of this zone when it is completely saturated with formation water. If the zone is known to contain no hydrocarbons, R_o may be estimated from log measurements. In the case in which there is no positive knowledge of the fluid content, R_o may be estimated by use of Equation (27), as described in foregoing paragraphs. To compute F_2, it is necessary to know the resistivity of formation water and to utilize R_o.

Although it is apparent that the relations discussed in this report may be useful in the interpretation of the electric log, it must be emphasized that they are subject to limitations. First, as in the case of any relations proposed as aids to log interpretations, they must be proved by actual usage under a wide variety of conditions. Second, the data they require are subject to errors in measurement. In consequence, it is necessary

TABLE 2 — EXPERIMENTAL MOUNCE POTENTIAL DATA

Concentration Test Solution eq. /liter n_1	Concentration Reference Solution eq. /liter n_2	Sample S-1 E, mv.	Sample R-1 E, mv.	Sample S-2 E, mv.	Sample W-2B E, mv.	Sample KD-1 E, mv.	Sample P-1 E, mv.	Sample P-A E, mv.	Sample 8 E, mv.
0.001	1.5	---	---	---	60	---	---	---	---
0.002	1.5	51	---	72	52	83	---	---	---
0.005	1.5	38	60	60	34	68	60	15	54
0.01	1.5	30	45	51	24	56	---	11	40
0.02	1.5	---	34	---	---	42	---	---	---
0.05	1.5	17	22	27	10	27	---	---	---
0.1	1.5	---	14	18	---	18	20	4	16
0.2	1.5	4	10	10	---	10	---	---	---
0.5	1.5	---	---	---	---	---	---	3	---
1.0	1.5	---	---	0.5	---	---	3	1	2
0.001	0.128	---	---	---	---	74	---	---	---
0.002	0.128	---	---	---	---	64	---	---	---
0.005	0.128	---	---	---	---	48	---	---	---
0.01	0.128	---	---	---	---	36	---	---	---
0.02	0.128	---	---	---	---	25	---	---	---
0.05	0.128	---	---	---	---	11	---	---	---
0.2	0.128	---	---	---	---	−5	---	---	---
0.005	0.1	---	---	45	---	---	---	---	---
0.02	0.1	---	---	25	---	---	---	---	---
1.75	0.1	---	---	−16	---	---	---	---	---
5.0	0.1	---	---	−19	---	---	---	---	---

TABLE 3 — RESISTIVITY FACTORS COMPUTED FROM MOUNCE POTENTIAL AND RESISTIVITY DATA

Sample No.	Solution Concentrations eq./liter n_1	n_2	Apparent Resistivity Factors F_1 (with n_1)	F_2 (with n_2)	Mounce Potential E, mv.	Computed Resistivity Factors F Eq. (16)	F Eq. (22)	F Eq. (23)
S-1	0.005	1.5	3.3	13.9	36.5	14.7	15.3	15.7
S-1	0.01	1.5	4.4	13.9	29.0	14.8	15.5	15.9
S-1	0.04	1.5	7.2	13.9	17.0	15.1	15.9	16.4
S-1	0.1	1.5	9.1	13.9	11.0	15.4	16.1	16.6
S-1	0.3	1.5	11.3	13.9	5.0	15.8	16.6	17.0
S-1	....	5.0	....	15.3	Average (F_o)	15.2	15.9	16.3
R-1	0.025	1.5	3.0	9.2	28.0	10.3	11.1	11.5
R-1	0.04	1.5	4.0	9.2	21.0	10.3	11.0	11.4
R-1	0.06	1.5	4.8	9.2	16.5	10.2	10.9	11.3
R-1	0.1	1.5	5.8	9.2	11.5	10.3	10.8	11.2
R-1	0.2	1.5	7.6	9.2	5.0	9.9	10.2	10.6
R-1	....	5.0	....	9.7	Average (F_o)	10.2	10.8	11.2
S-2	0.005	0.1	1.3	9.1	45.0	16.3	23.4	22.8
S-2	0.02	0.1	4.0	9.1	21.0	16.0	19.8	21.6
S-2	0.005	1.5	1.3	17.4	60.0	19.9	22.4	23.2
S-2	0.06	1.5	7.3	17.4	24.0	20.0	21.6	23.2
S-2	0.1	1.5	9.1	17.4	17.5	20.4	21.9	23.1
S-2	....	5.0	....	20.0	Average (F_o)	18.5	21.8	22.8
W-2B	0.005	1.5	6.6	20.4	34.0	21.1	21.8	22.4
W-2B	0.01	1.5	8.1	20.4	24.0	21.5	22.2	22.7
W-2B	0.02	1.5	10.0	20.4	17.0	21.7	22.4	23.0
W-2B	0.1	1.5	15.1	20.4	6.5	22.0	22.7	23.2
W-2B	0.2	1.5	16.9	20.4	2.5	22.1	22.8	23.2
W-2B	....	5.0	....	21.1	Average (F_o)	21.7	22.4	22.9
KD-1	0.005	0.128	3.2	16.3	47.5	21.4	24.9	28.6
KD-1	0.06	0.128	12.0	16.3	9.0	27.6	31.6	37.0
KD-1	0.005	1.5	3.2	27.6	68.0	29.6	31.4	34.1
KD-1	0.06	1.5	12.0	27.6	24.0	31.4	33.9	36.4
KD-1	0.1	1.5	15.0	27.6	17.5	32.0	34.0	36.2
KD-1	....	5.0	....	30.4	Average (F_o)	28.2	31.2	34.4
P-1	0.005	1.5	1.45	17.5	60.0	20.0	22.2	22.8
P-1	0.01	1.5	2.26	17.5	44.0	20.5	23.4	23.0
P-1	0.10	1.5	7.65	17.5	20.0	21.8	24.2	25.0
P-1	....	5.0	....	21.8	Average (F_o)	20.8	23.3	23.6
P-A	0.005	1.5	24.5	43.0	15.0	43.8	44.5	45.0
P-A	0.01	1.5	28.2	43.0	11.0	44.0	44.7	45.0
P-A	0.10	1.5	36.4	43.0	4.0	44.2	45.6	45.7
P-A	....	5.0	....	44.7	Average (F_o)	44.0	44.9	45.2
8	0.005	1.5	3.15	21.5	54.0	23.0	24.6	25.8
8	0.01	1.5	4.10	21.5	40.0	23.6	26.0	26.4
8	0.10	1.5	10.0	21.5	16.0	26.6	29.4	29.2
8	....	5.0	....	26.0	Average (F_o)	24.4	26.6	27.1

to apply these relations with caution, and it is desirable not to condemn any stratum as being non-productive solely on the basis of results obtained by their use.

CONCLUSIONS

1. The adsorptive characteristics of shaly reservoir materials can be used to relate the Mounce potential and abnormal conductivity of these materials. The relations so derived have been verified by laboratory results.

2. The relations resulting from this work may be used qualitatively to estimate whether or not a particular shaly stratum contains oil or gas.

3. These relations may be also used in the estimation of porosity of shaly sands.

ACKNOWLEDGMENT

The authors wish to express their appreciation to G. G. Priest for obtaining the experimental data on some of the samples used in this report.

REFERENCES

TABLE 4

Sample No.	Measured Porosity Per Cent	Computed Porosity, Per Cent Equation (22)	Equation (23)
S-1	23.0	22.2	21.8
R-1	26.8	26.5	26.0
S-2	18.3	19.2	18.8
W-2B	19.2	18.8	18.7
KD-1	15.5	16.2	15.4
P-1	20.0	19.0	18.8
P-A	13.6	13.9	13.8
8	17.6	17.8	17.5

1. Patnode, H. W., and Wyllie, M. R. J.: "The Presence of Conductive Solids in Reservoir Rock as a Factor in Electric Log Interpretation," *Trans.* AIME (1950), **189**, 47.

2. Winsauer, W. O., and McCardell, W. M.: "Ionic Double-Layer Conductivity in Reservoir Rock," *Trans.* AIME (1953), **198**, 129.

3. McCardell, W. M., Winsauer, W. O., and Williams, M.: "Origin of the Electric Potential Observed in Wells," *Trans.* AIME (1953), **198**, 41.

4. Sundberg, K.: "Effect of Impregnating Waters on Electrical Conductivity of Soils and Rocks," *Trans.* AIME, Geophysical Prospecting (1932), **367**.

5. Archie, G. E.: "The Electrical Resistivity Log as an Aid in Determining Some Reservoir Characteristics," *Trans.* AIME (1942), **146**, 54.

6. Mounce, W. D., and Rust, W. M.: "Natural Potentials in Well Logging," *Trans.* AIME (1944), **155**, 47.

7. Verwey, E. J. W., and Overbeek, J. T. G.: *Theory of the Stability of Lyophobic Colloids,* Elsevier, New York (1948).

8. Winsauer, W. O., Shearin, H. M., Masson, P. H., and Williams, M.: "Resistivity of Brine-Saturated Sands in Relation to Pore Geometry," *Bull.* AAPG (1952), **36**, 253.

9. Wyllie, M. R. J.: "Clay Techonology in Well Log Interpretation," presented at National Conference on Clays and Clay Technology, Berkeley, Calif., July, 1952.

10. Doll, H. G.: "The S. P. Log: Theoretical Analysis and Principles of Interpretation," *Trans.* AIME (1949), **179**, 146.

★★★

A METHOD for DETERMINATION of AVERAGE PRESSURE in a BOUNDED RESERVOIR

C. S. MATTHEWS
MEMBER AIME
SHELL DEVELOPMENT CO.
HOUSTON, TEXAS

F. BRONS
SHELL OIL CO.
HOUSTON, TEXAS

P. HAZEBROEK
B.P.M.
THE HAGUE

T. P. 3876

ABSTRACT

A method has been developed for calculating the average pressure in a bounded reservoir. The reservoir is first divided into the individual drainage volumes of each well, by using the criterion that at steady state each individual drainage volume is proportional to a well's production rate. The average pressure in each drainage volume is then calculated by a method developed in the report. By volumetrically averaging these individual drainage volume pressures, the average pressure in the entire reservoir is obtained.

To calculate the average pressure in each drainage volume, a correction is applied to the ordinary extrapolated pressure, i.e., the pressure obtained by extrapolating to infinite time the linear portion of the graph of closed-in pressure versus $\log[\Delta t/(t + \Delta t)]$, *where* Δt *is the closed-in time and* t *the production time. The correction, which is a function of the production time, is presented in graphical form for different shapes of the drainage area (horizontal cross section of the drainage volume).*

INTRODUCTION

It is important to be able to find the volumetric average pressure in a reservoir so that the size of the reservoir may be determined from material balance calculations. It is also desirable to be able to find the approximate distribution of pressure within a reservoir for detection of fluid movement. The purpose of this paper is to present a method for calculating both the average reservoir pressure and the approximate distribution of pressure within a bounded reservoir — that is, a reservoir with no water drive.

In reservoirs where the pressure builds up rapidly after wells are shut in, the determination of average pressure generally poses little problem, for one often need only average the final buildup pressures. It is when pressure buildup is slow that difficulties arise. For practical and economical reasons, the time allowable for closing in wells is limited. If at the maximum allowable closed-in time the pressure has not reached a constant value (and this is more often the case than is generally realized), calculation of average pressure presents difficulties.

One method which has been used in the past for obtaining an "average" pressure involves the extrapolation to infinite closed-in time of curves of pressure as a function of closed-in time. Contour maps of these extrapolated pressures are used in arriving at an average pressure. In some cases wells are shut in for arbitrary lengths of time, and contours of these arbitrary shut-in pressures are used for calculation. All these methods are somewhat arbitrary and suffer from lack of fundamental theoretical basis. For example, no precise meaning can be given either to the extrapolated or to the arbitrary shut-in pressure. Furthermore, there seems to be no reason why either set of pressures should be contourable. It was because of the vagueness of these old methods and their lack of a sound theoretical basis that the present method for determining average reservoir pressure was developed.

SYMBOLS

A = drainage area of a well, cm^2
A_j = drainage area of well j, cm^2
A_t = total drainage area of all wells in a reservoir, cm^2
c = coefficient of compressibility of fluid at reservoir temperature, atm^{-1}
f = hydrocarbon-filled porosity, fraction
h = net thickness of formation, cm
k = permeability of formation, darcy
p = pressure at a well, atm
p_o = initial reservoir pressure, atm
p^* = pressure obtained by straight-line extrapolation of linear portion of plot of p versus $\log[\Delta t/(t + \Delta t)]$
$\bar{p}$ = volumetric average pressure inside drainage volume of a well
q = volume flow rate at a well, cc/sec at prevailing reservoir conditions
q_t = total volumetric flow rate from a reservoir, cc/sec at prevailing reservoir conditions
r_w = radius of well bore, cm
$T = kt/f\mu cA$
t = corrected time of production of a well, seconds, defined by

Publication No. 37, Exploration & Production Research Division, Shell Development Co., Houston, Tex.
[1]References given at end of paper.
Manuscript received in the Petroleum Branch office Aug. 4, 1953. Paper presented at the Petroleum Branch Fall Meeting in Dallas, Oct. 19-21, 1953.

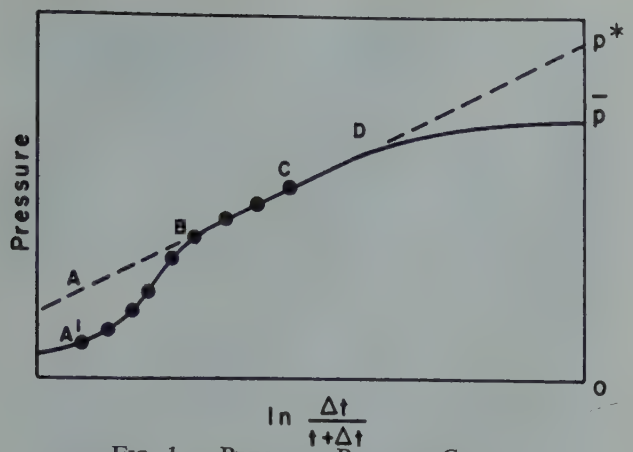

FIG. 1 — PRESSURE BUILDUP CURVE.

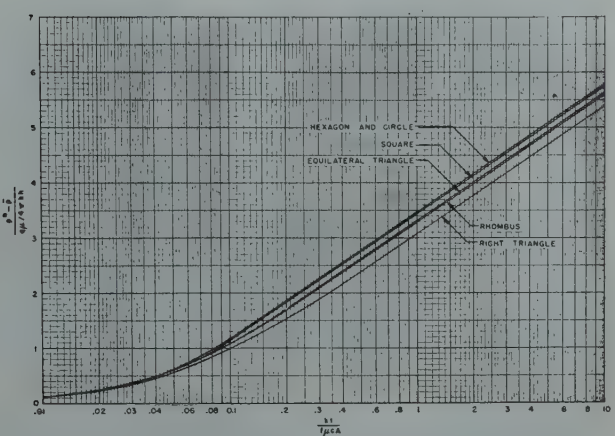

FIG. 2 — PRESSURE FUNCTION FOR ONE WELL IN CENTER OF EQUILATERAL FIGURES.

$t = \dfrac{\text{total fluid produced}}{\text{rate of production just before shutting in}}$

Δt = closed-in time of a well, seconds

v_j = drainage volume of a well j, cc of matrix and pores

v_t = total volume of reservoir, cc of matrix and pores

μ = viscosity at reservoir conditions, cp

log = logarithm to base 10

ln = logarithm to base e

$ln\,\gamma = 0.5772$

Ei = exponential integral: $Ei(-x) = -\int_x^\infty \dfrac{e^{-u}}{u}\,du$

ASSUMPTIONS

It is assumed that the reservoir is horizontal, homogeneous, isotropic, and of uniform thickness. The fluid is assumed to be in a single phase of small and constant compressibility and constant viscosity. However, it is believed that the method developed herein may be applied with good approximation to many bounded reservoirs and fluids encountered in practice, even though they do not strictly obey these assumptions. The presence of a zone of altered permeability immediately around the well bore does not affect the determination of average pressure by this method.

ONE WELL IN A HOMOGENEOUS BOUNDED RESERVOIR

By methods similar to those used by other authors,[2,3,4] it is shown in Appendix I that the pressure-buildup behavior of a single well in the center of a circular reservoir is given by an equation of the form

$$p = p_o + \frac{q\mu}{4\pi kh}\left\{ ln\,\frac{\Delta t}{t+\Delta t} + Y(t+\Delta t) - Y(\Delta t)\right\} \quad . \quad . \quad (1)$$

Equation (1) is plotted in Fig. 1 as line $ABCD\bar{p}$. Because of disturbing effects of flow into casing and tubing after a well is shut in, the initial portion of the curve is normally observed to be curved, as $A'B$. After the effects of inflow die out the buildup plot becomes linear, as along BCD, and then finally flattens toward the average reservoir pressure $\bar{p}$. Now if the observed linear portion BC is extrapolated to the point where $ln[\Delta t/(t+\Delta t)] = O$ (i.e., to infinite closed-in time), a pressure p^* is obtained. Generally p^* has no practical meaning, but knowledge of its value enables calculation of the average pressure $\bar{p}$ in the bounded reservoir. For this purpose the quantity $(p^* - \bar{p})/(q\mu/4\pi kh)$ is introduced as shown in Fig. 2 and derived in Appendix I.

For a given production time in a circular reservoir the value of $(p^* - \bar{p})/(q\mu/4\pi kh)$ can be read from Fig. 2, and after p^* and $q\mu/4\pi kh$ are obtained from the pressure-buildup curve, $\bar{p}$ may be calculated. An example of this will be shown later.

It is also possible to derive values for the function $(p^* - \bar{p})/(q\mu/4\pi kh)$ for boundaries of shapes other than circular and for various positions of the well within by use of the method of images. The general

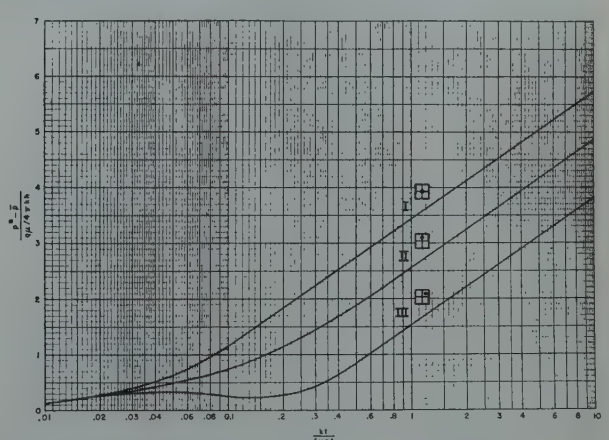

FIG. 3 — PRESSURE FUNCTION FOR DIFFERENT WELL LOCATIONS IN A SQUARE BOUNDARY.

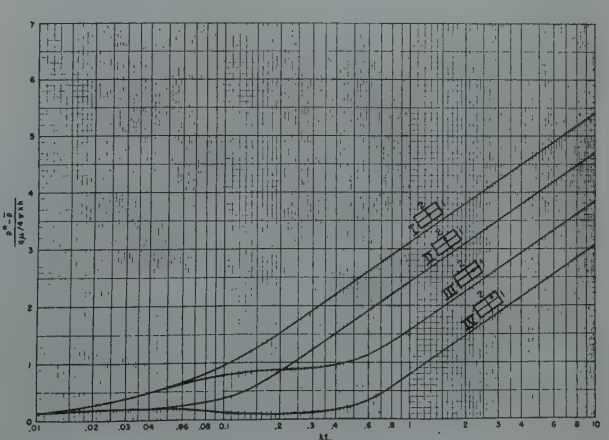

FIG. 4 — PRESSURE FUNCTION FOR DIFFERENT WELL LOCATIONS IN A 2:1 RECTANGULAR BOUNDARY.

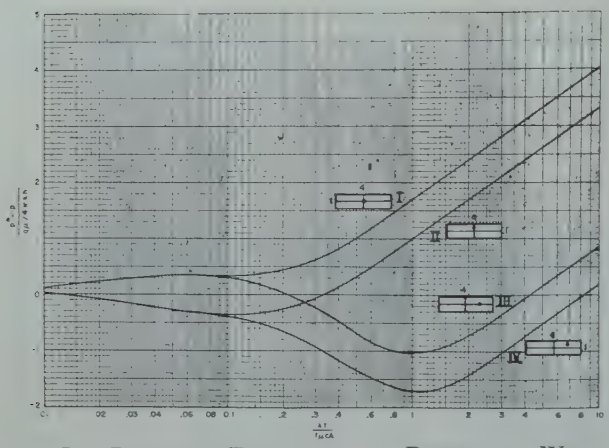

FIG. 5 — PRESSURE FUNCTION FOR DIFFERENT WELL LOCATIONS IN A 4:1 RECTANGULAR BOUNDARY.

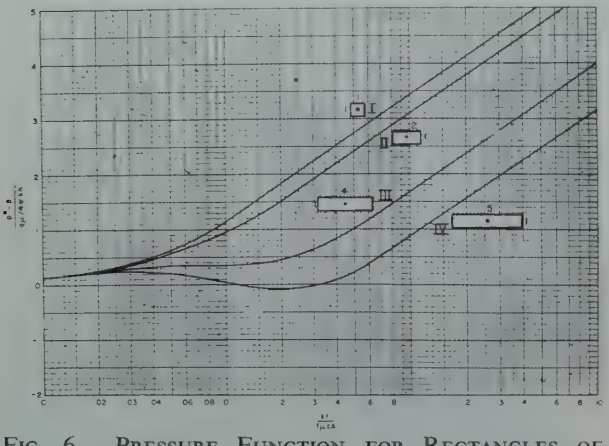

FIG. 6 — PRESSURE FUNCTION FOR RECTANGLES OF VARIOUS SHAPES.

features of the method are given in Appendix II, and the results in Figs. 2 to 8. The application of the results is discussed in the next section. With slight modification Figs. 2 to 8 could also be applied according to the method discussed by Miller, Dyes, and Hutchinson.[3]

The quantity $(p^* - \overline{p})/(q\mu/4\pi kh)$ may be called the pressure correction function. It may be seen from Fig. 2 that when a well is symmetrically located inside symmetrical boundaries, the exact shape of the boundaries has little effect on this function. Thus the curves differ but little, regardless of whether the outer boundaries are in the form of a hexagon, square, rhombus, equilateral triangle, right triangle, or circle. This result gives at least some basis for the often used assumption that the behavior of a circular drainage area may be used to represent the behavior of a square drainage area.

There is a considerable effect of well asymmetry with respect to boundaries as shown by Curves II and III in Fig. 3, and Curves II, III, and IV in Figs. 4 and 5. In these figures the position of the well is indicated by a dot. In general the more asymmetric a well's position with respect to its boundaries, the lower the position of its curve on the graph.

In Fig. 6 the effect of the shape of a rectangular boundary on the pressure correction function is shown. The more asymmetric the shape of the rectangle, the lower the position of its curve on the graph.

In Figs. 5, 6, 7, and 8 the pressure correction function takes on negative values at certain times. In these regions the extrapolated pressure p^* is less than the average pressure $\overline{p}$. This happens because the pressure build-up curve has more than one "hump" in a reservoir of such shape. An illustrative pressure build-up curve for which $p^* - \overline{p}$ is negative is shown by Curve 1, Fig. 9. Curve 2 is the more normal type. These curves are easily obtained by appropriate superposition of the pressure correction function according to Equation (B-3) of Appendix II. It will not often be possible to observe this sort of behavior in practice, however, because only seldom do we have one-well reservoirs. In a multi-well reservoir, well interference effects will tend to mask any such behavior.

BOUNDED RESERVOIRS CONTAINING MORE THAN ONE WELL

In the preceding section a discussion was given of the function $(p^* - p)/(q\mu/4\pi kh)$ for one well inside a boundary. In this section there will be indicated a method of subdividing a reservoir containing more than one well so that the preceding results may be applied.

If there is production at a constant rate from a bounded reservoir containing a fluid of constant compressibility and drained by a single well, after a certain time the rate of pressure decrease, $\partial p/\partial t$, becomes constant at every point and a steady state is reached.[1] Now consider several wells draining from the same reservoir. Since we can superpose the effects of the several wells to get the resultant pressure effect, we will find, after some production time, in this multiwell reservoir, that the rate of pressure decline also becomes constant and equal everywhere. In addition, the volume of the reservoir drained by each well becomes constant.

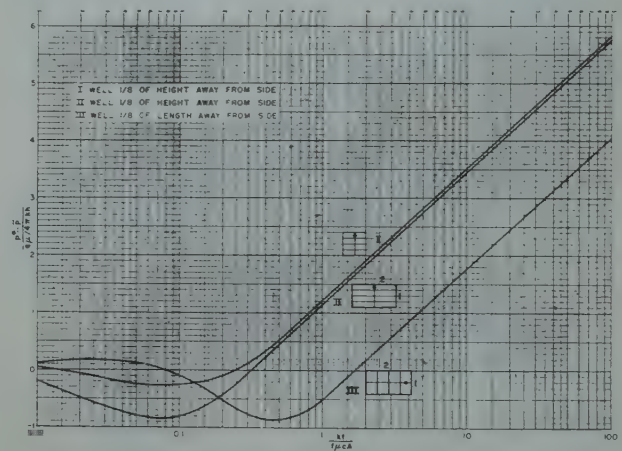

FIG. 7 — PRESSURE FUNCTION IN A SQUARE AND 2:1 RECTANGLE.

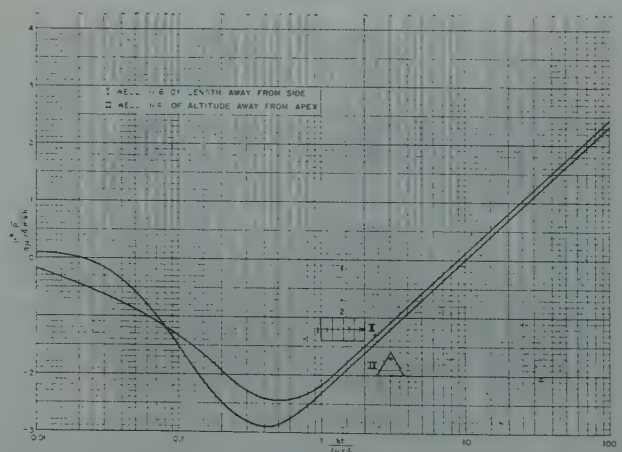

FIG. 8 — PRESSURE FUNCTION IN A 2:1 RECTANGLE AND AN EQUILATERAL TRIANGLE.

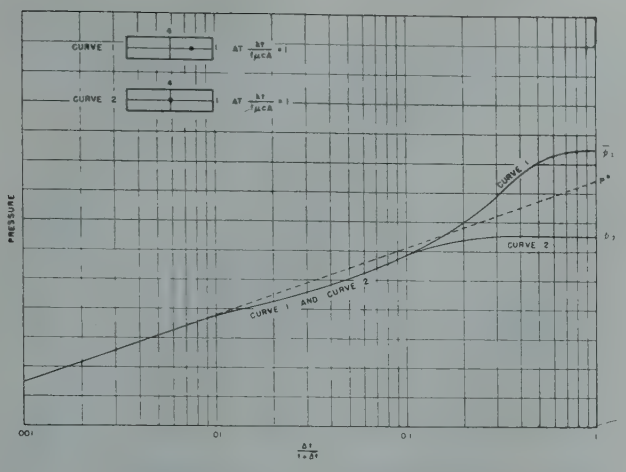

FIG. 9 — ILLUSTRATIVE PRESSURE-BUILDUP CURVES.

In Appendix III, it is shown that the rate of pressure decline approaches a value q/cfv in any drainage volume. Thus for any two wells j and k in the reservoir at the steady state when $\partial p/\partial t$ is constant,

$$\frac{q_j}{fv_j} = \frac{q_k}{fv_k} \quad . \quad . \quad . \quad . \quad . \quad . \quad . \quad . \quad . \quad . \quad (2)$$

Thus at steady state the drainage volumes in a bounded reservoir are proportional to the rates of withdrawal from each drainage volume. From this it can easily be seen that a well producing at rate q_j from a reservoir of total volume v_t drained by wells with a total rate of off-take q_t, has a relative drainage volume at steady state given by

$$\frac{v_j}{v_t} = \frac{q_j}{q_t} \quad . \quad . \quad . \quad . \quad . \quad . \quad . \quad . \quad . \quad . \quad (3)$$

This equation may be used to estimate the drainage volume of each well in the bounded reservoir at steady state. Thus, after determining the average pressure in each of these volumes by use of pressure build-up data and the $p^* - \bar{p}$ curves (details of the method are discussed below), the over-all volumetric average may be easily computed with the aid of (3). Although Equation (3) applies strictly at steady state only, it will be shown below that it also furnishes a satisfactory approximation for purposes of determining average reservoir pressure at times prior to steady state.

After steady state is reached the drainage volumes remain constant as long as the rates of withdrawal remain constant. If any one rate is altered, a transient stage is introduced throughout the reservoir. Only after the reservoir has been drained for a certain time by the changed rates will the drainage volumes become constant again at the new steady state. However, it is believed that for purposes of approximating average reservoir pressure the drainage volume may generally be calculated with sufficient accuracy from Equation (3) regardless of production time.

Results from additional work, as yet unpublished, have suggested that the shape of the drainage areas may be estimated as follows: (1) Draw a line between the well in question and adjacent wells. Locate the position of the drainage boundary along these lines at distances d_i from well i, where

$$\frac{d_i}{d_{ij}} = \frac{q_i}{q_i + q_j} \quad . \quad . \quad . \quad . \quad . \quad . \quad . \quad . \quad (4)$$

d_{ij} being the distance from well i to well j, and q_i and q_j the production rates of wells i and j. (2) Sketch in all drainage areas and check to determine whether they satisfy Equation (3). If they do not, adjust the drainage areas until they do. If the drainage area of a strong producer must pass between that of two other wells in order to satisfy (3), in general it will tend to pass between the drainage areas of poor producers or will tend to finger toward a sparsely drilled section.

In order to test these methods, the true average reservoir pressure was computed from the amount of production for several simulated multiwell reservoirs of simple shape. The true average was then compared with the average pressure obtained by use of the correction charts in Figs. 2 to 8. In each case the drainage volume of each well in the multiwell reservoir

TABLE 1 — AVERAGE PRESSURE IN A SIMULATED FOUR-WELL RESERVOIR

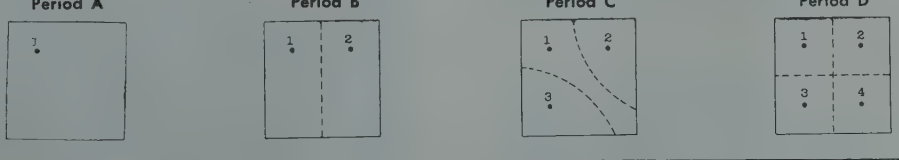

	$kt_3/f\mu cA_t$	$kt_4/f\mu cA_t$	$kt_1/f\mu cA_t$	$kt_2/f\mu cA_t$	Computed from Charts $\bar{p}_1$ atm	$\bar{p}_2$ atm	$\bar{p}_3$ atm	$\bar{p}_4$ atm	$\bar{p}$ atm	True $\bar{p}$ atm	Error atm
Period A	0				250				250	250	0
	.1	0			246.23				246.23	246.23	0
Period B	.2	.1			238.45	238.96			238.71	238.69	+ .02
	.5	.4			215.44	216.07			215.75	216.07	− .32
	.7	.6	0		200.96	200.96			200.96	200.99	− .03
Period C	.72	.62	.02		198.16	192.49	205.03		198.56	198.73	− .17
	.8	.7	.1		190.22	185.90	191.57		189.23	189.68	− .45
	1	.9	.3	0	167.87	165.47	166.22		166.52	167.06	− .54
Period D	1.01	.91	.31	.01	160.15	163.45	164.14	174.25	165.50	165.55	− .05
	1.25	1.15	.55	.25	128.70	129.33	129.36	130.02	129.35	129.36	− .01
	1.5	1.4	.8	.5	91.60	91.66	91.66	91.69	91.63	91.66	− .03
	1.75	1.65	1.05	.75	53.93	53.96	53.96	53.96	53.95	53.96	− .01
	2	1.9	1.3	1	16.26	16.26	16.23	16.23	16.25	16.26	− .01

NOTES: $q\mu/4\pi kh = 3$ atm in each well. All wells produce at the same rate but for different times. Drainage areas during each period are estimated using Equation (3). Then drainage boundaries are sketched in, as above. The following models were then selected to simulate the effect of these boundaries during each period:
A) One well draining the square — curve III, Fig. 3.
B) Two wells draining the square — curve III, Fig. 4 for each well.
C) Three wells draining the square — curve I, Fig. 3 for wells 2 and 3; and curve III, Fig. 4 for well 1.
D) Four wells draining the square — curve I, Fig. 3 for each well.

TABLE 2 — DETERMINATION OF DRAINAGE AREA

(1)	(2)		(3)	(4)	(5)	(6)	(7)
Well	Average Rate January 1950 tank bbl/day	res. bbl/day	v_j/v_t	Net Sand ft	$\frac{v_j}{v_t h_j}$ ft x 10^3	A_j/A_t	fv_j cc
1	39	47	.156	58	2.69	.205	1.76×10^{11}
2	33	40	.132	51	2.59	.198	1.49×10^{11}
3	28	34	.113	68	1.66	.126	1.28×10^{11}
4	151	181	.599	97	6.17	.471	6.77×10^{11}
		302	1.000		13.11	1.000	

v_t, volume of matrix and pores in reservoir estimated to be 1.00×10^{13} cc
Porosity = .174, interstitial water = .35
Net hydrocarbon-filled volume = $.174(1 - .35)\ 1.00 \times 10^{13}$
$= 1.13 \times 10^{12}$
$= fv_t$
and $fv_j = 1.13 \times 10^{12}\ (v_j/v_t)$

was obtained from Equation (3). The pressures p^* were obtained by the method of images given in Appendix II. A typical result is shown in Table 1.

Four periods are considered in Table 1. In period A, only well 1 is producing. At the end of 0.1 unit of dimensionless time, well 2 begins producing and period B begins. In period C, three wells produce and in period D, all four wells produce for times indicated in Table 1. At each value of time the value of p^* at each well was computed using the method of images discussed in Appendix II. Then, using Figs. 3 and 4, as indicated at the bottom of the table, values of $\bar{p}$ were obtained for each well and the over-all value for average pressure computed using Equation (3). The true value of $\overline{p}$ was obtained from the known cumulative production. Although transients were introduced every time a new well began producing, excellent agreement was obtained between observed and computed values for average pressure. These results (and others) are believed to justify use of Equation (3) for pressure estimation purposes even when the reservoir is known to be in a transient stage.

This example also indicates that the proposed method is accurate even though considerable regional migration may have occurred before a well is drilled. A theoretical analysis indicates that the proposed method should be exact when a steady state is reached and that the magnitude of the numerical error should, in general, be small in the transient period, as noted in this example.

It seems pertinent to note at this point that the average drainage volume pressure may vary over a bounded reservoir in a completely random manner. Drainage volumes of high average pressure may be mixed in any manner with drainage volumes of low average pressure. It is believed that the method of volumetric averaging suggested in this section is both simpler and sounder theoretically than a method based on "contouring" of well pressures.

APPLICATION OF THE METHOD

Determination of Drainage Boundaries

A map of the example field is shown in Fig. 10. Average production rates the month before shutting in are given in Table 2. From these rates the relative drainage volumes, v_j/v_t, shown in column (3) were computed using Equation (3). To compute the drainage areas it was assumed that the average thickness of each drainage volume was proportional to the thickness at the well, and that the constant of proportionality was the same for all areas. It may then be shown that

$$\frac{A_j}{A_t} = \left(\frac{v_j}{v_t}\,\frac{1}{h_j}\right) \div \left(\sum \frac{v_j}{v_t}\,\frac{1}{h_j}\right). \quad (5)$$

Thus, column (5) in Table 2 was obtained by dividing the items in column (3) by those in column (4). Column (6) was obtained by dividing column (5) by the sum of column (5) according to Equation (5).

TABLE 3 — DETERMINATION OF AVERAGE PRESSURE

Well	p^* psia	$\frac{q\mu}{4\pi kh}$ atm	q at res. cond. cc/sec	$\frac{kh}{\mu}$ darcy-cm/cp	fv_j cc x 10^{-11}	C atm^{-1}	Total Production tank bbl
1	3877	1.594	86	4.29	1.76	2×10^{-4}	4480
2	3858	.1870	74	31.5	1.49	2×10^{-4}	5640
3	3932	3.051	63	1.643	1.28	2×10^{-4}	1930
4	3787	2.047	330	12.83	6.77	2×10^{-4}	10,800

Well	t sec x 10^{-6}	$\frac{kt}{f\mu cA}$	Model	$\frac{p^* - \overline{p}}{q\mu/4\pi kh}$	$p^* - \overline{p}$ psi	$\overline{p}$ psia	v_j/v_t	Volumetric Avg. Press.
1	9.94	1.21	2:1	1.76	41	3836	.156	
2	14.77	15.6	2:1	4.27	12	3846	.132	
3	5.96	.383	4:1	.11	5	3927	.113	
4	6.17	.585	2:1	1.90	57	3730	.599	
								3784

After the relative areas A_j/A_t were obtained, the drainage boundaries were sketched in and adjusted, as shown in Fig. 10, until each area was of the correct proportion.

Also shown in Table 2 are the quantities fv_j. These quantities are obtained by estimating a value for the total hydrocarbon-filled pore volume, fv_t, and multiplying this quantity by v_j/v_t. After the pore volume is obtained from a material balance analysis (which is usually the end object of determining the average pressure) these values may be refined.

Determination of Dimensionless Production Time

The essential steps in determining $kt/f\mu cA$ are shown in Table 3. One of the buildup curves is shown in Fig. 11. By straight-line extrapolation on the semi-log plot, a value of p^* was obtained for this well. Values of p^* obtained in the same way from other buildup curves are shown in Table 3. Values for the corrected production time t were obtained, as suggested by Horner,[2] by dividing the total amount of fluid production by the rate of production just before shutting in. After computing the slope of the straight-line section of each buildup curve, values of $q\mu/4\pi kh$ in atmospheres were obtained from

$$\frac{q\mu}{4\pi kh},\ \text{atm} = \frac{\text{slope, psi}}{14.7\ (2.303)}.$$

From all these quantities, values for $kt/f\mu cA$ were calculated by noting that

FIG. 10 — RESERVOIR MAP.

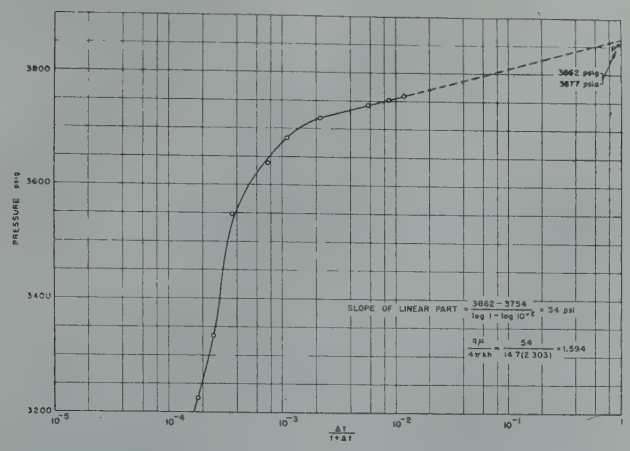

FIG. 11 — PRESSURE BUILDUP CURVE, WELL NO. 1.

$$\frac{kt}{f\mu cA} = \frac{kh}{\mu}\left(\frac{1}{fv_1}\right)\frac{1}{c}(t) \ .$$

The next step is to select models whose shapes are most like those of each drainage area. It is believed that applicable models may be obtained in most instances by finding the rectangular figure with the length to width ratio about that of the irregular area, and with similar well placement in the rectangular area. The most critical point in the selection is the relative nearness of the well to the closest side. This should be relatively the same in the model as in the real figure. The divergence between the shapes some distance from the well should affect the results very little.

In the example case, drainage area 1 was considered to be like a 2:1 rectangle lying on its long side, with the well on the central long axis, but not on the central short axis, as indicated in Table 3. Drainage area 2 was considered as a 2:1 rectangle standing on its short edge. Drainage area 3 was taken as a 4:1 rectangle on its short edge with the well off center as indicated in Table 3. For drainage area 4, the long tip at the bottom left was considered to be partially balanced by the thinning to the top, and this area was also considered as a 2:1 rectangle on end.

After the model for each drainage area was selected, values for $(p^* - \overline{p})/(q\mu/4\pi kh)$ were read from the appropriate curve at the correct dimensionless time. Values of $\overline{p}$ were then obtained and, using the values of v_1/v_t, volumetrically averaged to give an over-all average reservoir pressure of 3,784 psia.

DISCUSSION AND CONCLUSIONS

An important question is "How does one take into account drainage volumes in which there are no pressure data?" To answer this question, it is suggested that a plot of average pressure against relative drainage volume may allow the missing pressures to be estimated. Such a plot has a theoretical basis if the reservoir is reasonably homogeneous and the shape of each drainage boundary is roughly equivalent in its effect on pressure behavior. To obtain the average reservoir pressure when the permeability variation, horizontalwise, is great, enough representative wells should be surveyed to allow a representative volumetric average to be taken on surveyed wells alone.

In conclusion, it may be stated that the method developed in this study is simply and easily applied when pressure-buildup data are available. It is believed that the method may be applied with good approximation to many bounded reservoirs which are met in practice. The suggested method of volumetric averaging of individual drainage zone pressures is believed simpler and of sounder theoretical basis than the older method of averaging based on contours of well pressure.

REFERENCES

1. Brownscombe, E. R., and Collins, Francis: "Pressure Distribution in Unsaturated Oil Reservoirs," *Trans.* AIME (1950), 189, 371.
2. Horner, D. R.: "Pressure Build-up in Wells," *Proceedings* of the Third World Petroleum Congress, Section II, E. J. Brill, Leiden (1951).
3. Miller, C. C., Dyes, A. B., and Hutchinson, C. A., Jr.: "The Estimation of Permeability and Reservoir Pressure from Bottom Hole Pressure Build-up Characteristics," *Trans.* AIME (1950), 189, 91.
4. Muskat, M.: *The Flow of Homogeneous Fluids Through Porous Media,* McGraw-Hill, New York (1937), 657.

APPENDIX I

PRESSURE-BUILDUP BEHAVIOR IN A CIRCULAR RESERVOIR

Muskat[4] has given the following equation for the relation between the pressure in a well at the center of a circular reservoir and the production time:

$$p = p_o + \frac{q\mu}{4\pi kh}\left\{\frac{3}{2} - 2\,ln\,\frac{R_b}{r_w} - \frac{r_w^2}{R_b^2} - \frac{4kt}{f\mu cR_b^2} + 4\sum\frac{Jo\left[\frac{x_n r_w}{R_b}\right]\exp\left[-\frac{x_n^2 kt}{f\mu cR_b^2}\right]}{x_n^2 J_o^2(x_n)}\right\}, \quad (A\text{-}1)$$

where r_w and R_b are the well-bore and boundary radii respectively and the x_n are the roots of $J_1(x_n) = 0$. Now this equation may be rewritten

$$p = p_o + \frac{q\mu}{4\pi kh}\left[ln\,\frac{\gamma f\mu cr_w^2}{4kt} + Y(t)\right], \quad (A\text{-}2)$$

where

$$Y(t) = \frac{3}{2} - 2\,ln\,\frac{R_b}{r_w} - \frac{r_w^2}{R_b^2} - \frac{4kt}{f\mu cR_b^2} + 4\sum\frac{Jo\left[\frac{x_n r_w}{R_b}\right]\exp\left[-\frac{x_n^2 kt}{f\mu cR_b^2}\right]}{x_n^2 J_o^2(x_n)} - ln\,\frac{\gamma f\mu cr_w^2}{4kt} \quad (A\text{-}3)$$

Let the well produce at rate q for time t and then be closed in for time Δt. Then the pressure at time $t + \Delta t$ may be written

$$p = p_o + \frac{q\mu}{4\pi kh}\left[ln\,\frac{\gamma f\mu cr_w^2}{4k(t+\Delta t)} + Y(t+\Delta t) - ln\,\frac{\gamma f\mu cr_w^2}{4k\Delta t} - Y(\Delta t)\right]$$

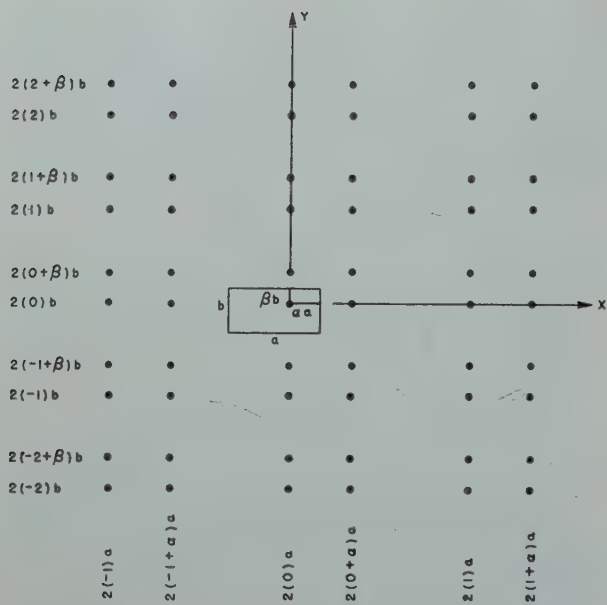

FIG. 12 — IMAGES OF WELL INSIDE RECTANGLE

$$= p_o + \frac{q\mu}{4\pi kh}\left[ln\frac{\Delta t}{t+\Delta t} + Y(t+\Delta t) - Y(\Delta t)\right] \quad . . . . (A\text{-}4)$$

Now when Δt is small, $Y(t+\Delta t) \cong Y(t)$ = a constant during the closed-in interval Δt. Also $Y(\Delta t) \cong 0$ for small Δt (this is by no means obvious, but can be shown numerically to be true).[a] Therefore, Equation (A-4) may be written for small Δt

$$p = p_o + \frac{q\mu}{4\pi kh}\left[ln\frac{\Delta t}{t+\Delta t} + Y(t)\right]. \quad . . . (A\text{-}5)$$

It may be seen from Equation (A-5) that a plot of closed-in pressure versus $ln[\Delta t/(t+\Delta t)]$ will be linear for small Δt. If such a plot is made and the linear portion is extrapolated to the point where $ln[\Delta t/(t+\Delta t)] = 0$, a pressure p^* is obtained:

$$p^* = p_o + \frac{q\mu}{4\pi kh}Y(t) \quad . . . . (A\text{-}6)$$

It can easily be shown that for a fluid of small and constant compressibility,

$$p_o - \overline{p} = \frac{qt}{cfhA} = \frac{q\mu}{4\pi kh}\cdot\frac{4\pi kt}{f\mu cA} \quad . . . (A\text{-}7)$$

Thus, we may write

$$p^* - \overline{p} = \frac{q\mu}{4\pi kh}\left[\frac{4\pi kt}{f\mu cA} + Y(t)\right]; \quad . . . (A\text{-}8)$$

and setting $T = kt/f\mu cA$ where $A = \pi R_b^2$,

$$\frac{p^* - \overline{p}}{q\mu/4\pi kh} = 4\pi T + Y(t) \quad . . . . . . (A\text{-}9)$$

$$= 4\pi T + \frac{3}{2} - ln\frac{R_b^2}{r_w^2} - \frac{r_w^2}{R_b^2} - 4\pi T$$

[a]For very small Δt, the term $\ln(\gamma f\mu c r_w^2/4k\Delta t)$ in $Y(\Delta t)$ should be replaced by its corresponding Ei function.

$$+ 4\sum\frac{Jo\left[\frac{x_n r_w}{R_b}\right]\exp\left[-x_n^2\pi T\right]}{x_n^2 J_o^2(x_n)}$$

$$- ln\frac{\gamma f\mu c r_w^2}{4kt} \quad . . . (A\text{-}10)$$

Grouping the logarithm terms together and noting that for large R_b, $r_w^2/R_b^2 \cong 0$ and $J_o(x_n r_w/R_b) \cong 1$,

$$\frac{p^* - \overline{p}}{q\mu/4\pi kh} = \frac{3}{2} + ln\frac{4\pi T}{\gamma} + 4\sum\frac{\exp(-x_n^2\pi T)}{x_n^2 J_o^2(x_n)}$$

$$= F(T) \quad . . . . . . (A\text{-}11)$$

Values of $(p^* - \overline{p})/(q\mu/4\pi kh)$ calculated from Equation (A-11) are shown in Fig. 2. For values of $kt/f\mu cA \geqslant 0.1$, the series terms are negligible as shown by the linearity of the log plot in Fig. 2. For values of $kt/f\mu cA \leqslant 0.05$ we have

$$\frac{p^* - \overline{p}}{q\mu/4\pi kh} \cong 4\pi T = \frac{4\pi kt}{f\mu cA}.$$

For extremely small values of T (not shown in Fig. 2), Equation (A-11) does not apply, but must be modified by inclusion of the factor $J_o(x_n r_w/R_b)$ in the series, and by substitution of the Ei function for $ln(\gamma f\mu c r_w^2/4kt)$.

APPENDIX II

PRESSURE-BUILDUP BEHAVIOR IN NONCIRCULAR BOUNDARIES

FORMAL SOLUTION

It is possible to determine the pressure behavior inside bounded reservoirs which have the shape of simple polygons by the method of images. Fig. 12, for example, shows part of the infinite image net required to simulate the conditions of zero flow across the outer boundary in a rectangle. Similar nets can be developed for many other polygons. Using these sets of images, the solution to our problem consists of the following steps:

1) the summation of the pressure influence of each well in the infinite net on the pressure at the sink, and, from this, the obtention of p^*;

2) calculation of the average pressure, $\overline{p}$, in the drainage volume;

3) the relating of the average pressure $\overline{p}$ to the extrapolated pressure, p^*.

If we consider each well as a point sink, then the summation of the pressure influence at our real well of each well in the infinite net is given by

$$p = p_o + \frac{q\mu}{4\pi kh}\left\{Ei\left[-\frac{f\mu c r_w^2}{4kt}\right] + \sum_{i=1}^{\infty} Ei\left[-\frac{f\mu c a_i^2}{4kt}\right]\right\} \quad . . . (B\text{-}1)$$

where a_i is the distance of the ith image well from the well in question.

Suppose that after producing for time t the well is closed in for time Δt. Then the pressure in the well is given by

$$p = p_o + \frac{q\mu}{4\pi kh}\left\{\mathrm{Ei}\left[-\frac{f\mu c r_w^2}{4k\,(t+\Delta t)}\right] - \mathrm{Ei}\left[-\frac{f\mu c r_w^2}{4k\Delta t}\right] + \sum_{i=1}^{\infty}\mathrm{Ei}\left[-\frac{f\mu c a_i^2}{4k\,(t+\Delta t)}\right] - \sum_{i=1}^{\infty}\mathrm{Ei}\left[-\frac{f\mu c a_i^2}{4k\Delta t}\right]\right\} \quad . \quad . \quad . \quad . \quad \text{(B-2)}$$

For values of Δt large enough that $f\mu c r_w^2/4k\Delta t < 0.01$ we may closely approximate $\mathrm{Ei}\,[-f\mu c r_w^2/4k\,(t+\Delta t)]$ by $\ln\,[\gamma f\mu c r_w^2/4k\,(t+\Delta t)]$, and $\mathrm{Ei}\,[-f\mu c r_w^2/4k\Delta t]$ by $\ln\,[\gamma f\mu c r_w^2/4k\Delta t]$. Thus, Equation (B-2) may be closely approximated as

$$p = p_o + \frac{q\mu}{4\pi kh}\left\{\ln\frac{\Delta t}{t+\Delta t} + \sum_{i=1}^{\infty}\mathrm{Ei}\left[-\frac{f\mu c a_i^2}{4k\,(t+\Delta t)}\right] - \sum_{i=1}^{\infty}\mathrm{Ei}\left[-\frac{f\mu c a_i^2}{4k\Delta t}\right]\right\} \quad . \quad . \quad . \quad . \quad \text{(B-3)}$$

which is of the same form as Equation (A-4). When Δt is small and the closed-in pressure p is linear with $\log\,[\Delta t/(t+\Delta t)]$ we may write

$$p = p_o + \frac{q\mu}{4\pi kh}\left\{\ln\frac{\Delta t}{t+\Delta t} + \sum_{i=1}^{\infty}\mathrm{Ei}\left[-\frac{f\mu c a_i^2}{4kt}\right]\right\} \quad . \quad . \quad . \quad \text{(B-4)}$$

Therefore, if the linear portion of the graph of closed-in pressure versus $\log\,[\Delta t/(t+\Delta t)]$ is extrapolated to $\log\,[\Delta t/(t+\Delta t)] = 0$, a pressure p^* will be obtained, where

$$p^* = p_o + \frac{q\mu}{4\pi kh}\sum_{i=1}^{\infty}\mathrm{Ei}\left[-\frac{f\mu c a_i^2}{4kt}\right] \quad . \quad . \quad \text{(B-5)}$$

Since

$$\overline{p} = p_o - \frac{q\mu}{4\pi kh}\left[\frac{4\pi kt}{f\mu cA}\right], \quad . \quad . \quad . \quad . \quad . \quad . \quad \text{(B-6)}$$

we have

$$\frac{p^* - p}{q\mu/4\pi kh} = \frac{4\pi kt}{f\mu cA} + \sum_{i=1}^{\infty}\mathrm{Ei}\left[-\frac{f\mu c a_i^2}{4kt}\right] \quad . \quad . \quad \text{(B-7)}$$

This is the desired relationship between extrapolated pressure and average pressure.

Evaluation of the Solution

It is convenient for purposes of summation of (B-7) to introduce the symbols T for $kt/f\mu cA$, $F(T)$ for $(p^* - \overline{p})/(q\mu/4\pi kh)$, and $a_{m,n}$ for a_i. Then

$$F(T) = \frac{p^* - \overline{p}}{q\mu/4\pi kh} = 4\pi T + \sum_{m,n=-\infty}^{\infty}{}' \mathrm{Ei}\left[\frac{a_{m,n}^2}{-4AT}\right]. \quad \text{(B-8)}$$

In this expression $a_{m,n}^2$ is the square of the distance of any image well (x,y) from the real well at the origin

$$a_{m,n}^2 = x^2 + y^2 \ .$$

The prime on the summation indicates that the term where $a_{m,n} = 0$ is to be omitted. For any rectangular case, as shown in Fig. 12, the images are at the positions $(2ma, 2nb)$, $[2(m+\alpha)a, 2nb]$, $[2ma, 2(n+\beta)b]$, and $[2(m+\alpha)a, 2(n+\beta)b]$, where m and n take all integral values from $-\infty$ to $+\infty$. Similar image patterns were worked out for all the cases shown in Figs. 2 to 8.

For small values of T the series of Ei terms converges very rapidly. For larger values it is necessary to develop an alternate expansion as follows:

$$F(T) = 4\pi T - \sum_{m,n=-\infty}^{\infty}{}' \int_{\frac{a_{m,n}^2}{4AT}}^{\infty}\frac{e^{-u}}{u}\,du \quad . \quad . \quad \text{(B-9)}$$

$$= 4\pi T - \sum_{-\infty}^{\infty}{}' \int_{1/\pi T_o}^{\infty}\frac{e^{-\pi x a_{m,n}^2/4A}}{x}\,dx \quad . \quad . \quad \text{(B-10)}$$

$$= 4\pi T - \int_{1/\pi T}^{\infty}\frac{dx}{x}\left\{\sum_{-\infty}^{\infty}{}' e^{-\pi x a_{m,n}^2/4A}\right\}. \quad \text{(B-11)}$$

$$= 4\pi T - \int_{1/\pi T_o}^{\infty}\frac{dx}{x}\left\{\sum_{-\infty}^{\infty}{}' e^{-\pi x a_{m,n}^2/4A}\right\} - \int_{1/\pi T}^{1/\pi T_o}\frac{dx}{x}\left\{\sum_{-\infty}^{\infty}{}' e^{-\pi x a_{m,n}^2/4A}\right\}. \quad \text{(B-12)}$$

so that

$$F(T) = 4\pi T + F(T_o) - 4\pi T_o - \int_{1/\pi T}^{1/\pi T_o}\frac{dx}{x}\cdot \left\{\sum_{-\infty}^{\infty}{}' e^{-\pi x a_{m,n}^2/4A}\right\} \quad . \quad . \quad . \quad \text{(B-13)}$$

Inserting values of $a_{m,n}^2$ for the rectangle and factoring, we have

$$F(T) = 4\pi T - 4\pi T_o + F(T_o) - \int_{1/\pi T}^{1/\pi T_o}\frac{dx}{x}\cdot \left\{\left[\sum_{m=-\infty}^{\infty} e^{-m^2\pi x/\lambda} + \sum_{m=-\infty}^{\infty} e^{-(m+\alpha)^2\pi x/\lambda}\right]\right.$$

$$\left.\left[\sum_{n=-\infty}^{\infty} e^{-n^2\pi x\lambda} + \sum_{n=-\infty}^{\infty} e^{-(n+\beta)^2\pi x\lambda}\right] - 1\right\}, \quad . \quad \text{(B-14)}$$

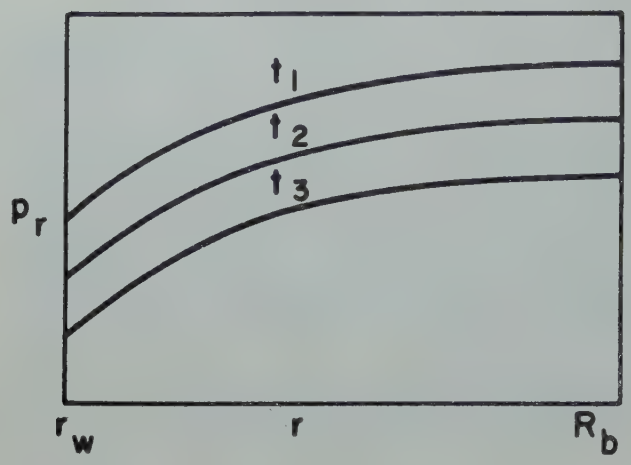

FIG. 13 — PRESSURE BEHAVIOR AT STEADY STATE IN A CYLINDRICAL RESERVOIR.

where $\lambda = b/a$ in Fig. 12. Now it can be shown* that for any variable w

$$\sum_{m=-\infty}^{\infty} e^{-(m+\alpha)^2 \pi w} = \frac{1}{\sqrt{w}} \sum_{m=-\infty}^{\infty} e^{-(m^2 \pi/w) - 2m\alpha\pi i} \quad \text{(B-15)}$$

Using this identity and letting $u = \pi/x$, we have

$$F(T) = 4\pi T - 4\pi T_o + F(T_o) + \ln\frac{T}{T_o} + \int_{\pi^2 T}^{\pi^2 T_o} \frac{du}{\pi} \left[\sum_{m=-\infty}^{\infty} e^{-m^2 \lambda u} (1 + e^{-2m\alpha\pi i}) \right] \left[\sum_{n=-\infty}^{\infty} e^{-n^2 u/\lambda} (1 + e^{-2n\beta\pi i}) \right] \quad \text{(B-16)}$$

Expanding the exponentials in terms of sines and cosines and noting that certain functions are even functions, we get

$$F(T) = 4\pi T - 4\pi T_o + F(T_o) + \ln\frac{T}{T_o} + \frac{1}{\pi} \int_{\pi^2 T}^{\pi^2 T_o} \left[2 + 2 \sum_{m=1}^{\infty} e^{-m^2 \lambda u} (1 + \cos 2m\alpha\pi) \right] \left[2 + 2 \sum_{n=1}^{\infty} e^{-n^2 u/\lambda} (1 + \cos 2n\beta\pi) \right] du \quad \text{(B-17)}$$

Using this equation, $(p^* - \overline{p})/(q\mu/4\pi kh)$ may be evaluated quite rapidly at large values of T. For small values of T, Equation (B-8) is used.

*The identity can be proved by noting that

$$\sum_{m=-\infty}^{\infty} e^{-(m+\alpha)^2 \pi w} = e^{-\alpha^2 \pi w} \Theta_3(i\alpha\pi w : w),$$

and

$$\sum_{m=-\infty}^{\infty} e^{-(m^2 \pi/w) - 2m\alpha\pi i} = \Theta_3(-\pi\alpha : 1/w),$$

where Θ_3 is a theta function. See, for example, H. and B. S. Jeffreys, *Methods of Mathematical Physics*, Cambridge (1950), page 683. The relationship (B-15) follows immediately from the identity

$$\Theta_3(z:w) = w^{-1/2} e^{-z^2/\pi w} \Theta_3(iz/w : 1/w).$$

The results obtained for rectangles of various shapes by use of Equations (B-8) and (B-17) are given in Figs. 2 to 8. Expressions similar to these were worked out and evaluated in a like manner for all other geometrical shapes shown in these figures.

APPENDIX III

VALUE OF $\partial p/\partial t$ AT STEADY STATE

First of all it is pertinent to define what is meant by steady state for a compressible fluid inside closed boundaries. Consider, for example, a regular cylindrical drainage volume drained by a central well producing at constant rate. Then using the results of Muskat[4] we write for the pressure at any radius r, inside the boundary radius R_b of a reservoir containing a fluid of small and constant compressibility

$$p_r = p_o - \frac{q\mu}{4\pi kh} \left\{ -\frac{3}{2} + 2\ln\frac{R_b}{r} + \frac{r^2}{R_b^2} + \frac{4kt}{f\mu c R_b^2} - 4 \sum \frac{J_o\left[\frac{x_n r}{R_b}\right] \exp\left[-\frac{x_n^2 kt}{f\mu c R_b^2}\right]}{x_n^2 J_o^2(x_n)} \right\}, \quad \text{(C-1)}$$

where x_n are the roots of the Bessel function $J(x_n) = 0$. For large values of time, t, the series terms are negligible and Equation (C-1) becomes

$$p_r = p_o - \frac{q\mu}{4\pi kh} \left\{ -\frac{3}{2} + 2\ln\frac{R_b}{r} + \frac{r^2}{R_b^2} + \frac{4kt}{f\mu c R_b^2} \right\} \quad \text{(C-2)}$$

Then,

$$\frac{\partial p_r}{\partial t} = -\frac{q\mu}{4\pi kh} \cdot \frac{4k}{f\mu c R_b^2} = -\frac{q}{cfh\pi R_b^2} = \frac{-q}{cfv}, \quad \text{(C-3)}$$

where fv is the pore volume in the cylinder. Equation (C-3) shows that for large time the change in pressure with time is a constant for all radii for all successive values of time. Thus, the curves of pressure versus radial distance are parallel for all successive times, as shown in Fig. 13. In this state the pressure gradient and therefore the flow rate are constant with time at all points in the reservoir. It is this state which is called steady state.

For a reservoir of any shape the average pressure $\overline{p}$ is given by the following equation when c is small and constant:

$$\overline{p} = p_o - \frac{qt}{cfhA}, \quad \text{(C-4)}$$

so that

$$\frac{\partial \overline{p}}{\partial t} = -\frac{q}{cfhA} = -\frac{q}{cfv}. \quad \text{(C-5)}$$

Thus, the rate of change of average pressure with time is a constant at constant q and c for a reservoir of any shape. In a cylindrical reservoir, at large time, the rate of change of pressure at any point with time, as given by (C-3), is the same as the rate of change of average pressure with time, as given by (C-5). It can be shown by the image summation method of Appendix II that this is also true for reservoirs of the simple

shapes treated there. In other words, at large time for these reservoirs

$$\frac{\partial p}{\partial t} = \frac{\partial \overline{p}}{\partial t} \quad \ldots\ldots\ldots \quad \text{(C-6)}$$

where p is the pressure at any point in the reservoir. It seems reasonable to assume that all reservoirs will approach a steady state such that (C-6) is true. Accepting this, we have for large t when q and c are constant

$$\frac{\partial p}{\partial t} = \frac{\partial p}{\partial t} = -\frac{q}{cfv}, \quad \ldots\ldots \quad \text{(C-7)}$$

where q is the production rate of fluid of constant compressibility c from the reservoir of total pore volume fv. It seems reasonable to define steady state for any bounded reservoir by Equation (C-7), if c is small and constant.

Next we wish to consider bounded reservoirs containing more than one well. Now the solution for the pressure behavior in a multiwell reservoir can be obtained (under the assumptions made in this paper) by superposing the solutions for the behavior of the individual wells in the reservoir. It follows from this that if $\partial p/\partial t$ becomes constant in a single-well reservoir, it will also become constant in a multiwell reservoir. Furthermore, if $\partial p/\partial t$ is constant, all pressure gradients will be constant and all flowlines will be invariant. Each flowing well will have a definite flowline boundary defined by the fact that inside this drainage boundary fluid will flow toward the well in question, while outside the boundary fluid will flow to other wells. Flowline boundaries of this type will define a drainage volume for each well in the reservoir.

At steady state when the drainage boundaries do not move, the rate of change of average pressure with time inside any drainage volume fv_j is given by

$$\frac{\partial \overline{p}_j}{\partial t} = -\frac{q_j}{cfv_j} \quad \ldots\ldots\ldots \quad \text{(C-8)}$$

We have shown that at steady state $\partial p/\partial t$ becomes constant and equal everywhere in a multiwell reservoir. Therefore, the rate of change of pressure at any point must be equal to the rate of change of average pressure, or

$$\frac{\partial p_j}{\partial t} = \frac{\partial \overline{p}_j}{\partial t}, \quad \ldots\ldots\ldots \quad \text{(C-9)}$$

where p_j is the pressure at any point in drainage volume j. Also, for drainage volume k

$$\frac{\partial p_k}{\partial t} = \frac{\partial p_k}{\partial t} = -\frac{q_k}{cfv_k} \quad \ldots\ldots\ldots \quad \text{(C-10)}$$

Since

$$\frac{\partial p_j}{\partial t} = \frac{\partial p_k}{\partial t}, \quad \ldots\ldots\ldots \quad \text{(C-11)}$$

we have

$$\frac{q_j}{fv_j} = \frac{q_k}{fv_k} \quad \ldots\ldots\ldots \quad \text{(C-12)}$$

Therefore, for a total rate of offtake q_t from a reservoir of volume v_t, we have

$$\frac{v_j}{v_t} = \frac{q_j}{q_t} \quad \ldots\ldots\ldots \quad \text{(C-13)}$$

★★★

ESTIMATED EFFECT of VERTICAL FRACTURES on SECONDARY RECOVERY

PAUL B. CRAWFORD
MEMBER AIME
R. E. COLLINS*

TEXAS PETROLEUM RESEARCH COMMITTEE
A & M COLLEGE OF TEXAS
COLLEGE STATION, TEXAS

T. P. 3879

ABSTRACT

Potentiometric model studies have been made of ertically fractured reservoirs. All fractures originated at he well and extended into the reservoir for various distances. Studies were made to determine the areal sweep efficiencies for line-drive patterns. The areal sweep efficiency for the unfractured system studied was 70.6 per cent. It was found that if the vertical fracture was parallel with the direction of flood, the areal sweep efficiency may be considerably reduced, approaching zero in some instances. If the fracture was at right angles to the direction of flood, the areal sweep efficiency may be greater than that for the unfractured system. The sweep efficiency depends on the length and orientation of the fracture and direction of the flood. It is concluded that considerable effort should be made to determine the nature and direction of fractures before initiating a flooding program. Such information is required if the maximum sweep efficiency is to be obtained and channeling is to be reduced to a minimum.

INTRODUCTION

The recent development and application of fracturing techniques to petroleum reservoirs has served to focus considerable attention on the effect such fractures may have on secondary oil recoveries. The opinion has been expressed that fracturing may not alter appreciably the water flooding possibilities. Others have thought that channeling may occur and that the creation of fractures may serve to substantially reduce the possibilities of conducting a successful water flood in the reservoir

The purpose of this study was to obtain quantitative estimates of the effect of vertical fractures on the areal sweep efficiencies of line-drive flooding patterns. In presenting this work on vertical fractures, it is not to be inferred that the present fracturing techniques result in producing a vertical fracture. The types of fracture which are created are not known with certainty in every case. Some are believed to be horizontal, others inclined along bedding planes, and some data indicate vertical fracturing. Each fracture will probably exert a different influence on the sweep efficiency of the secondary recovery program; consequently each fractured well should perhaps be considered as a separate problem, requiring a careful analysis.

Preliminary work on the effect of fractures on producing capacity of a well indicated that for practical purposes many fractures may be treated as having a nearly infinite permeability This assumption appears to be valid in some instances where the permeability of the fracture is only 10 or 100 times greater than the permeability of the matrix. It is known to depend on the type, orientation and length of the fracture. In realization that fractures of only 0.01 in. width have calculated permeabilities near 5,000 darcys, it is believed that many fractures may be considered as of near infinite permeability without incurring serious error. Primarily for this reason this study was made with fracture analogs of very great permeability compared to the matrix.

FRACTURED SYSTEM ANALOG

The pattern sweep efficiencies reported here were obtained with the aid of a potentiometric model. The application of this type model for solving reservoir problems has been described in the literature.[1,2,3] The electrolyte reservoir was 20 in. wide by 30 in. long by approximately ½ in. deep. The liquid depth was constant, which corresponded to a constant permeability-feet product from the injection to the production well. The electrolyte reservoir was built to correspond to a unit in the line-drive pattern shown in Fig. 1. This figure shows part of an infinite array of wells having alternate rows of fractured and unfractured wells. The area within the dashed rectangle shows the area generally studied in the model.

In using the model to represent a fractured system, a thin strip of copper was soldered to the well or wells and the length and orientation of the strip was made to conform to the vertical fracture under consideration.

[1]References given at end of paper.

Manuscript received in the Petroleum Branch office July 31, 1953. Paper presented at the Petroleum Branch Fall Meeting at Dallas, Oct. 19-21, 1953.

*Present address: Stanolind Oil and Gas Co. Tulsa.

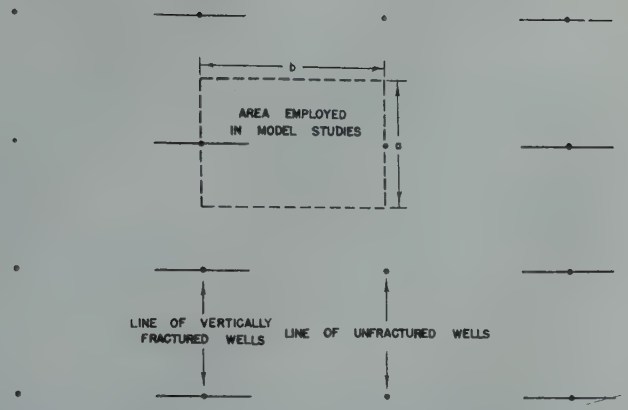

FIG. 1 — INFINITE ARRAY OF WELLS AS TREATED IN MODEL STUDIES.

PATTERN SWEEP EFFICIENCIES

VERTICAL FRACTURES PARALLEL TO DIRECTION OF FLOOD

The first types of fractures studied were those where the fractures originated at one well and extended directly toward the opposite well. This is shown in Fig. 2, where the streamlines and isopotentials for a particular vertically fractured system are indicated. The length of the fracture is 12.9 per cent of the distance to the opposite well. The isopotentials are numbered 0, 5, 10, etc. The streamlines are not numbered but are of approximately equal carrying capacity. It will be noted on Fig. 2 that a very low potential gradient existed about the fractured well.

The first isopotential represents only 5 per cent of the applied potential. At the unfractured well it will be noted that 40 per cent of the potential drop occurs within a very close distance to the well. Substantially radial flow was found to exist near the unfractured well. Of particular interest, perhaps, is the location of the 50 per cent or dividing isopotential line. This line which may be related to the approximate drainage radius during the final stages of primary depletion, is seen to be located very near the unfractured well.

Fig. 3 shows the flood fronts at breakthrough for the system described above. The flood fronts are shown for two conditions: (a) flooding from the fractured to the unfractured well, and (b) flooding from the unfractured to the fractured well. The areal sweep efficiency was found to be 63.8 per cent of the total area inclosed within the rectangle. The sweep efficiency was the same for conditions (a) and (b) above. The shape of the fronts differed, but the swept area was the same. The sweep efficiency of near 63 per cent is that which occurs at breakthrough, i.e., when the injected water first reaches the producing well. The production of water and oil to a high water-oil ratio would permit an increase in sweep efficiency over that shown. It is desired to point out that these studies were made at a mobility ratio of one.

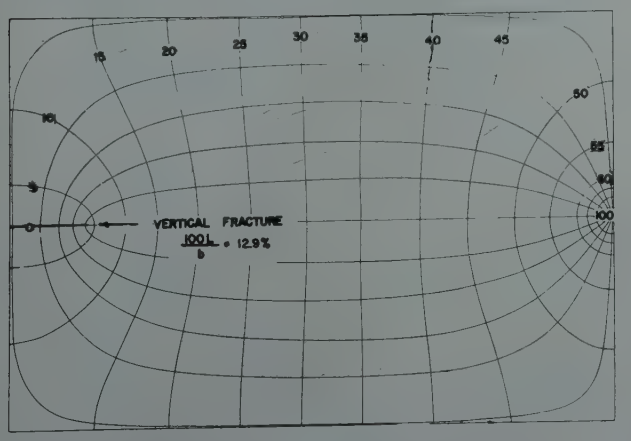

FIG. 2 — STREAMLINES AND ISOPOTENTIALS FOR A VERTICALLY FRACTURED SYSTEM (FRACTURE PARALLEL TO DIRECTION OF FLOOD).

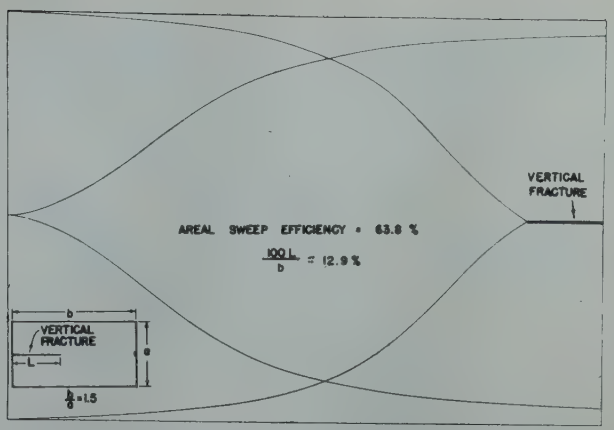

FIG. 3 — FLOOD FRONTS AT BREAKTHROUGH FOR A VERTICALLY FRACTURED SYSTEM.

A composite of flood fronts at breakthrough for vertically fractured systems having fractures of different lengths is shown in Fig. 4. The flow is from the unfractured well to the fractured well. Curve I shows the sweep efficiency when neither well was fractured; the sweep efficiency was 70.6 per cent. Curve III shows the sweep efficiency for the system in which the fracture length was 26.3 per cent of the distance between input and output wells, the corresponding sweep efficiency was 50.3 per cent. For Curves IV and V the fracture lengths were 36.1 and 44.6 per cent; the corresponding sweep efficiencies were 40.9 and 33.4 per cent respectively. It is perhaps obvious that the pattern sweep efficiency would be reduced to zero if the fracture connected the input and output wells.

Fig. 5 shows a composite of the flood fronts at breakthrough where the above fractured systems were considered to be flooded, in the reverse direction, i.e. from the fractured to the unfractured well. These flood fronts are shown to provide a comparison between the shapes

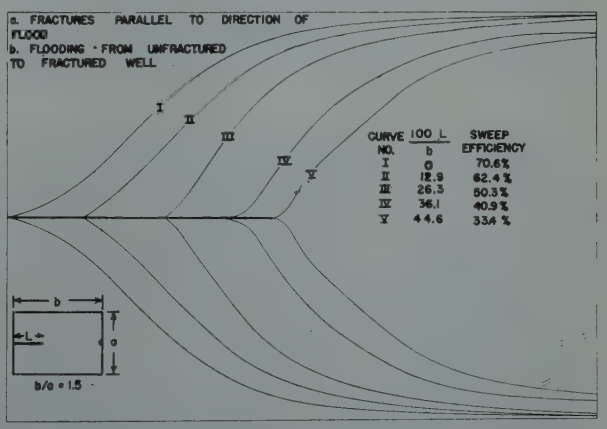

FIG. 4 — FLOOD FRONTS AT BREAKTHROUGH FOR VERTICALLY FRACTURED SYSTEMS.

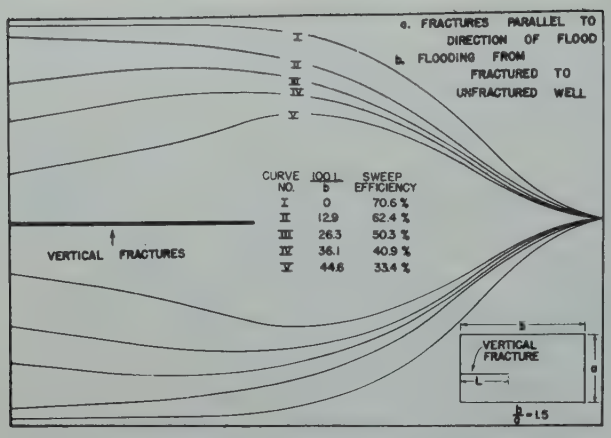

FIG. 5 — FLOOD FRONTS AT BREAKTHROUGH FOR VERTICALLY FRACTURED SYSTEMS.

of the water-swept areas. It will be noted in this figure that the very long fractures produced a spearhead shape. As the fracture lengths were reduced, the shape of the flood fronts approached those of the unfractured system.

Fig. 6 shows a plot of the areal sweep efficiency versus fracture length where the flood is conducted parallel to the fracture. It will be noted that the sweep efficiency is seen to decrease as the fracture length increases. If the fracture extends half the distance between wells, a sweep efficiency of only 28 per cent may be expected. However, if an analysis of the fracture system indicated the possibility that such a fracture exists then studies should be made to consider the possibility of utilizing the fracture to increase the areal sweep efficiency. Means of accomplishing this are discussed below.

VERTICAL FRACTURES PERPENDICULAR TO DIRECTION OF FLOOD

Following the above work studies were made where the vertical fractures were perpendicular to the direction of flood. In this case the fracture (copper strip) was positioned along one end of the model. The opposite well was considered unfractured. Fig. 7 shows the streamlines and isopotentials for such a system. The fracture is 47.5 per cent of the distance between adjacent input wells. The isopotentials are shown 5, 10, 15, etc. The streamlines are not numbered but are of approximately equal carrying capacity. It will be noted on the figure that a very low pressure gradient existed near the fractured well. The 50 per cent isopotential was located very near the unfractured well. Figs. 2 and 7 and others prepared during the course of this work indicate the possibility of some fractured wells being able to drain large areas under favorable conditions.

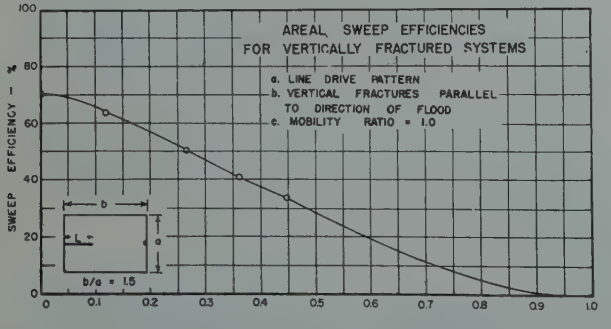

FIG. 6 — AREAL SWEEP EFFICIENCIES FOR VERTICALLY FRACTURED SYSTEMS.

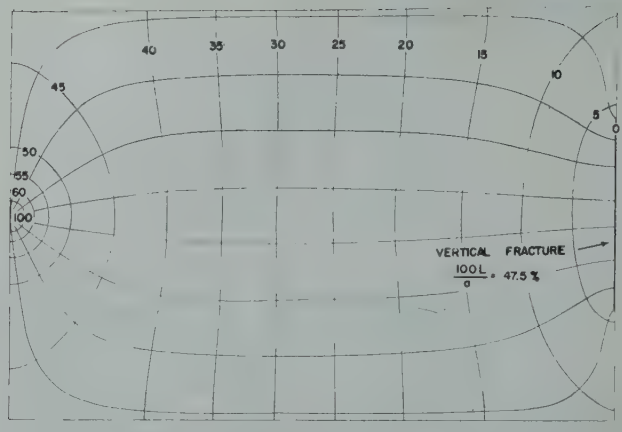

FIG. 7 — STREAMLINES AND ISOPOTENTIALS FOR A VERTICALLY FRACTURED SYSTEM (FRACTURE PERPENDICULAR TO DIRECTION OF FLOOD).

Fig. 8 shows the flood fronts at breakthrough for the fractured system shown in Fig. 7. The front on the right shows the flood front at breakthrough with the fractured well as the input well, and the front on the left shows the flood front when flooding in the reverse direction. The areal sweep efficiency was 84 per cent in each case. It will be noted that the nose of the flood front advancing toward the fracture was fairly blunt or rounded in comparison with the sharp nose advancing toward the unfractured well. This was due principally to the difference in flow conditions in these regions. Near the central portion of the fracture the flow and voltage gradient were nearly linear. Approximately radial flow existed near the unfractured well.

Fig. 9 is a composite of the flood fronts at breakthrough for vertically fractured systems in which the fracture is perpendicular to the direction of flood, and flooding is toward the fractured wells. Curve I shows the sweep efficiency for the unfractured system. Curves II, III, and IV show the flood fronts when the fracture length was 23.8, 47.5, and 95.0 per cent; the corresponding sweep efficiencies were 78.0, 84.0, and 87.5 per cent, respectively. It will be noted in this figure that as the fracture length increased the nose at breakthrough became progressively more rounded.

Fig. 10 shows the flood fronts at breakthrough for the same system as described by Fig. 9 except that the flooding is from the fractured to the unfractured well. The sweep efficiencies are identical with those having corresponding fractures shown in Fig. 9.

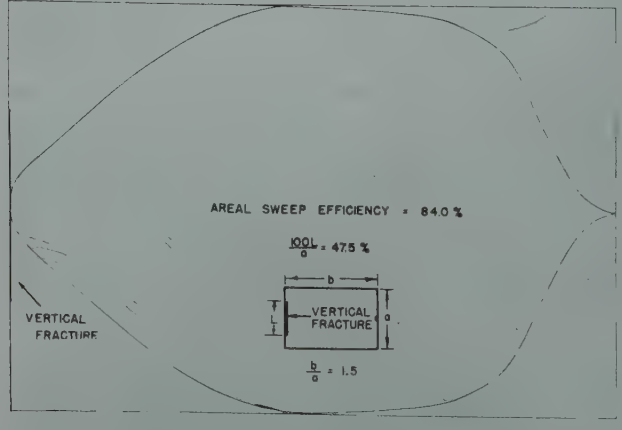

FIG. 8 — FLOOD FRONTS AT BREAKTHROUGH FOR A VERTICALLY FRACTURED SYSTEM.

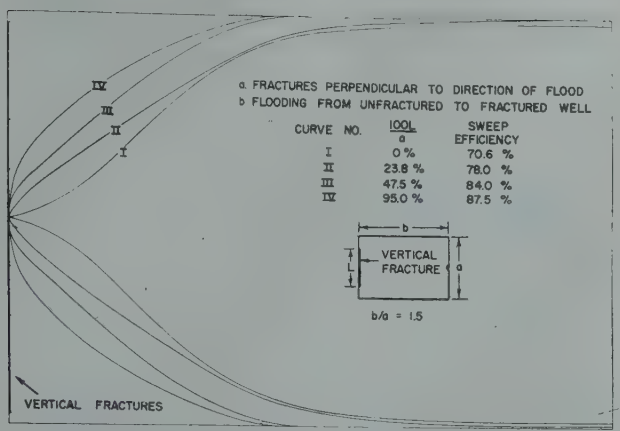
a. FRACTURES PERPENDICULAR TO DIRECTION OF FLOOD
b FLOODING FROM UNFRACTURED TO FRACTURED WELL
CURVE NO. 100L/a SWEEP EFFICIENCY
I 0 % 70.6 %
II 23.8 % 78.0 %
III 47.5 % 84.0 %
IV 95.0 % 87.5 %
VERTICAL FRACTURE
b/a = 1.5
VERTICAL FRACTURES

FIG. 9 — FLOOD FRONTS AT BREAKTHROUGH FOR VERTICALLY FRACTURED SYSTEMS.

Fig. 11 is a plot of areal sweep efficiency versus fracture length for vertically fractured systems in which the fracture is perpendicular to the direction of flood. These data were obtained for the line-drive pattern shown using a mobility ratio of one. It will be noted that as the length of fracture increased the areal sweep efficiency increased up to fracture lengths of about 80 per cent. At fracture lengths near 100 per cent, the sweep efficiency was slightly less than 90 per cent.

The above studies indicated the possible merit which might come about as a result of exploiting a vertically fractured system.

Other studies were made in which fractures existed at each well. These included fractures of the type shown in Fig. 12 where there were equal and opposite parallel vertical fractures. Fig. 12 shows the flood fronts at breakthrough for a specific case. The fractures were 23.5 per cent of the distance between adjacent input wells. An areal sweep efficiency of 80 per cent was observed. Fig. 13 is a plot of the areal sweep efficiency versus fracture length for systems having equal and opposite parallel vertical fractures. This figure indicates that such vertical fractures may permit very high sweep efficiencies to be obtained, approaching 100 per cent as the fracture length ratios approach unity. For fractures extending half the distance between adjacent input wells, sweep efficiencies of near 90 per cent may be expected.

A pattern was studied where two vertical fractures existed at one well. The fractures, which were at right angles, formed the cross configuration shown in Fig.

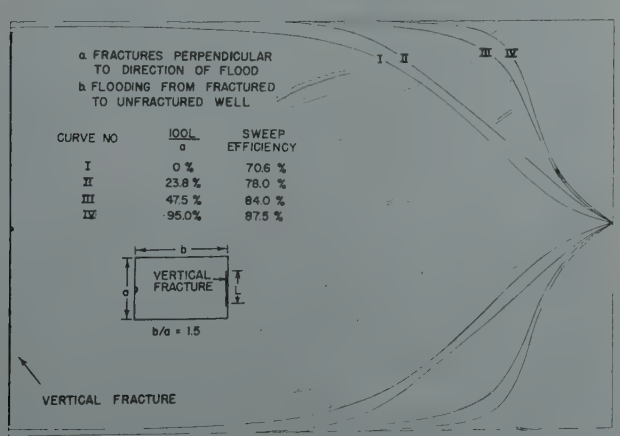
a. FRACTURES PERPENDICULAR TO DIRECTION OF FLOOD
b. FLOODING FROM FRACTURED TO UNFRACTURED WELL
CURVE NO 100L/a SWEEP EFFICIENCY
I 0 % 70.6 %
II 23.8 % 78.0 %
III 47.5 % 84.0 %
IV 95.0% 87.5 %
VERTICAL FRACTURE
b/a = 1.5
VERTICAL FRACTURE

FIG. 10 — FLOOD FRONTS AT BREAKTHROUGH FOR VERTICALLY FRACTURED SYSTEMS.

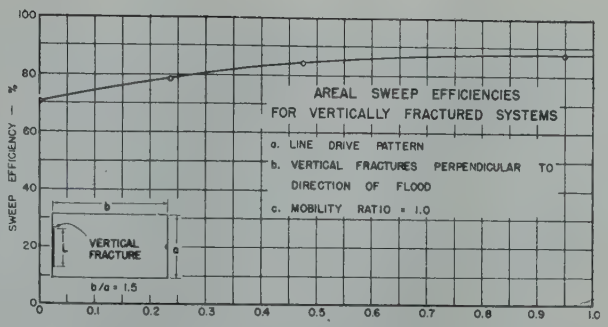
AREAL SWEEP EFFICIENCIES FOR VERTICALLY FRACTURED SYSTEMS
a. LINE DRIVE PATTERN
b. VERTICAL FRACTURES PERPENDICULAR TO DIRECTION OF FLOOD
c. MOBILITY RATIO = 1.0
SWEEP EFFICIENCY — %
VERTICAL FRACTURE
b/a = 1.5

FIG. 11 — AREAL SWEEP EFFICIENCIES FOR VERTICALLY FRACTURED SYSTEMS.

14. In this case the length of the fracture was the same in each direction. The fracture length was 23.5 per cent of the distance between adjacent input wells or 15.7 per cent of the distance between input and output wells. This fracture pattern is of considerable interest in that it indicates how a second vertical fracture might be made to partially offset the deleterious effects of a first fracture. If only the fracture parallel to flow had been present, Fig. 6 indicates that a sweep efficiency near 61 per cent would have been obtained. If a second fracture could be created so that a cross was formed then the sweep efficiency might be increased to the 68.7 per cent shown on Fig. 14. These data tend to emphasize the significance vertical fracturing may have on areal sweep efficiencies of some secondary recovery programs.

A study was made to determine the areal sweep efficiency of the four well system shown in Fig. 15. It will be noted on this figure that the two wells on the left have vertical fractures extending directly toward the unfractured wells on the right. The length of these fractures was 23.5 per cent of the distance "b" shown in prior figures. The injection and production wells are labeled in the figure. The potential difference was the same between each set of input and output wells which corresponds to carrying the same pressure at each injection well in the reservoir. Under this condition the model study indicated that these particular fractured wells would take fluid 4.94 times the rate of the unfractured wells.

Fig. 15 shows that breakthrough will occur first between the two unfractured wells. When this occurs the invading fluid will have advanced only about half the distance between the unfractured wells. The swept area at breakthrough was 55.2 per cent. Several studies

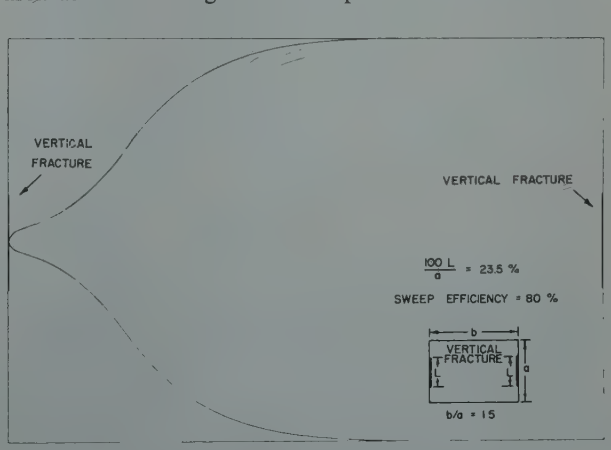

FIG. 12 — FLOOD FRONTS AT BREAKTHROUGH FOR PARALLEL VERTICAL FRACTURES.

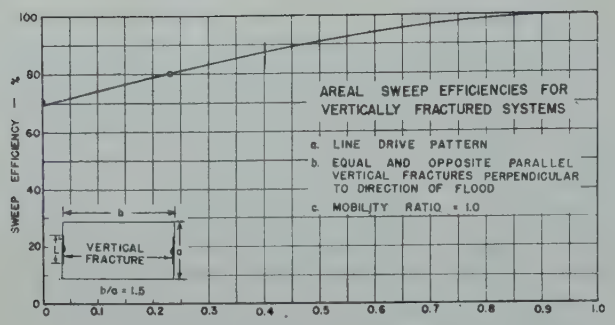
AREAL SWEEP EFFICIENCIES FOR VERTICALLY FRACTURED SYSTEMS
a. LINE DRIVE PATTERN
b. EQUAL AND OPPOSITE PARALLEL VERTICAL FRACTURES PERPENDICULAR TO DIRECTION OF FLOOD
c. MOBILITY RATIO = 1.0
SWEEP EFFICIENCY - %
VERTICAL FRACTURE
b/a = 1.5

FIG. 13 — AREAL SWEEP EFFICIENCIES FOR VERTICALLY FRACTURED SYSTEMS.

were made of the well pattern shown in Fig. 15, and it appears entirely possible to achieve a considerably higher sweep efficiency by proper adjustment of the injection and production rates.

DISCUSSION AND CONCLUSION

The work reported here constitutes a part of the research program sponsored by the Texas Petroleum Research Committee on a study of fractured and heterogeneous reservoirs.

Potentiometric model studies have been made of the areal sweep efficiencies of vertically fractured, line-drive patterns at a mobility ratio of one. In every case the fractures originated at the well and extended into the reservoir for various distances. The areal sweep efficiency was found to vary from near 0 to 100 per cent, depending on the length and orientation of the fracture and direction of the water flood.

A decrease in areal sweep efficiency was obtained where the fracture was parallel to the direction of the flood. If the fracture extended half the distance between wells a sweep efficiency near 28 per cent might be expected for the particular pattern studied here.

An increase in areal sweep efficiency was obtained where the fracture was perpendicular to the direction of flood. Very high sweep efficiencies were obtained for the case of equal and opposite parallel vertical fractures. In this case theoretical areal sweep efficiencies near 100 per cent may be approached. For a given vertically fractured system a 90-degree change in the direction of the flood may alter appreciably the oil recovered at breakthrough.

It is suggested that a study be made of fractured

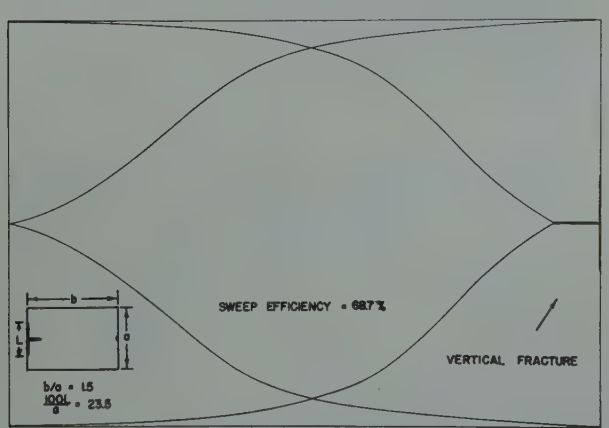

FIG. 14 — FLOOD FRONTS AT BREAKTHROUGH FOR A SYSTEM OF MULTIPLE VERTICAL FRACTURES.

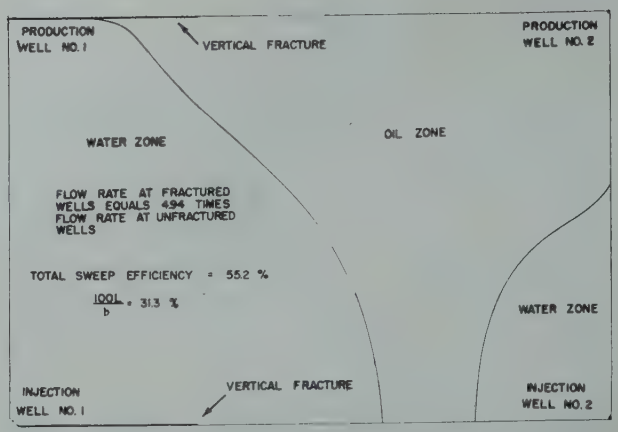
PRODUCTION WELL NO. 1
VERTICAL FRACTURE
PRODUCTION WELL NO. 2
WATER ZONE
OIL ZONE
FLOW RATE AT FRACTURED WELLS EQUALS 4.94 TIMES FLOW RATE AT UNFRACTURED WELLS
TOTAL SWEEP EFFICIENCY = 55.2 %
100L/b = 31.3 %
WATER ZONE
INJECTION WELL NO. 1
VERTICAL FRACTURE
INJECTION WELL NO. 2

FIG. 15 — FLOOD FRONTS AT BREAKTHROUGH FOR A VERTICALLY FRACTURED SYSTEM.

wells to determine the nature of the fractures prior to initiating a secondary recovery program. If a flooding scheme cannot be devised whereby the fractures are utilized to increase the sweep efficiency, then some consideration should be given to remedial measures.

The possible advantages which might accrue from the development of a directionally controlled vertical fracturing technique are indicated.

ACKNOWLEDGMENT

The authors wish to acknowledge the aid and encouragement of Robert L. Whiting, acting director of Texas Petroleum Research Committee, in conducting this study. Appreciation is expressed to the Texas Petroleum Research Committee for permission to publish the paper.

REFERENCES

1. Horner, W. L., and Bruce, W. A.: "Electrical Model Studies of Secondary Recovery," *Secondary Recovery of Oil in the United States,* Second Edition, API (1950), 195.
2. Lee, B. D.: "Potentiometric Model Studies of Fluid Flow in Petroleum Reservoirs," *Trans.* AIME (1948), 174, 41.
3. Muskat, Morris: "The Theory of Potentiometric Models," *Trans.* AIME (1949), 179, 216.

DISCUSSION BY AUTHORS

The data and results which are presented in this paper were obtained on a potentiometric analyzer of a type which has been used in the past in some instances to estimate sweep efficiencies for water flooding programs.

The model as operated here shows the sweep efficiencies which would be expected if a uniform homogeneous reservoir consisting of an infinite array of the studied patterns could be operated at steady-state conditions. It is further required that the mobility ratio be one and that gravitational effects be entirely neglected. The indicated results shown in the paper apply only in such proportion as the flow in the reservoir corresponds to that in the model. Subsequent data which have been obtained on the effect of vertical and elliptical fractures on the five spot pattern efficiency indicate that each fractured pattern is unique and will require a special study. ★★★

COMPARISON of METHODS for ANALYZING a WATER DRIVE FIELD, TORCHLIGHT TENSLEEP RESERVOIR, WYOMING

F. M. STEWART
MEMBER AIME
F. H. CALLAWAY
R. E. GLADFELTER
JUNIOR MEMBERS AIME

STANOLIND OIL AND GAS CO.
TULSA, OKLA.

T. P. 3889

ABSTRACT

In this paper oil initially in place is calculated by the various methods commonly used for analysis of water drive fields using data available as time progresses. Rate and pressure are predicted by means of the same methods using data available at the end of two years' history. These predictions are then compared with subsequent performance permitting an evaluation of the methods, which are Modified Schilthuis, Simplified Hurst, van Everdingen et al (1952), and the Electric Analyzer.

INTRODUCTION

Several variations of the material balance equation, differing in the term used to evaluate water influx, are in common use for estimating oil in place, predicting rate and volume of water influx, and forecasting producing rates and reservoir pressure in water drive reservoirs. The electric analyzer with an electrical network set up to simulate the oil reservoir and aquifer and their contained fluids may be used for the same purpose.

Examples of the application of one or another of these methods have appeared in the literature. The accuracy and reliability of the material balance for calculating oil in place have been covered.[1] However, there have been few articles in which more than one method has been applied to an actual field allowing a comparison. It is felt that a field example, simple in nature, where the Modified Schilthuis, Simplified Hurst, van Everdingen et al (1952), and the Electric Analyzer have been applied would be of benefit in providing an evaluation of these methods as to their comparative usefulness and reliability in calculating initial oil in place and predicting performance.

The Torchlight Tensleep reservoir is a small field in a large aquifer. The reservoir oil is greatly undersaturated, having a bubble point of only 55 psi and 2 cu ft/bbl of gas in solution. Changes in the reservoir volume factor in the range of pressures encountered are small, meaning little error in converting production to reservoir conditions. The pressure has declined from 1,618 psi initially to 137 psi during the first four and one-half years. Water production has been negligible. For Torchlight, the material balance equation as discussed later is considerably simplified by the omission of terms having to do with free gas. Thus with simpler equations, less variables to consider, the large pressure drop, the absence of a gas phase, and rapid pressure-rate adjustments, which mean an unusual amount of history in a short time, the reservoir appears suitable for comparing the methods listed above.

GENERAL INFORMATION ON THE FIELD

The Torchlight field is located on the eastern side of the Big Horn Basin, Big Horn County, Wyo., approximately 3 miles east of the town of Basin. The Tensleep reservoir was discovered in September, 1947. It lies at a depth of about 3,000 ft and produces oil of 35° API gravity. A total of five wells have been completed in the Tensleep, but only four are now producing. The reservoir is well defined in areal extent in that a total of 13 wells have penetrated the Ten-

[1]References given at end of paper.

Manuscript received in Petroleum Branch offices Sept. 24, 1953. Paper presented at Petroleum Branch Fall Meeting in Dallas, Oct. 19-21, 1953.

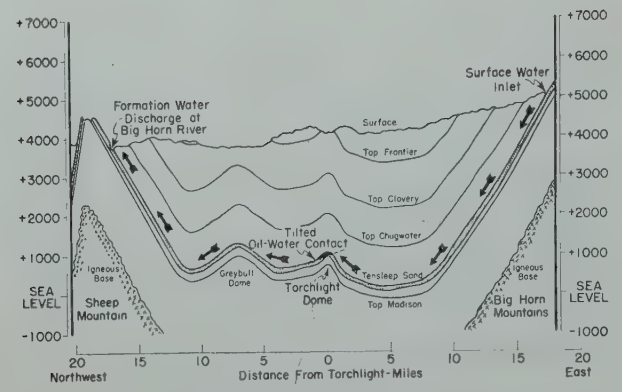

FIG. 1 — GENERALIZED CROSS-SECTION, SHEEP MOUNTAIN-TORCHLIGHT-BIG HORN MOUNTAINS.

sleep. Several of these wells lie outside the productive limits of the Tensleep reservoir.

The water drive recovery mechanism is usually associated with formations of wide areal extent having continuous permeability over a large area in the vicinity of the reservoir. The Tensleep is a "blanket" sand fitting this description.

The Tensleep outcrops in the Big Horn Mountains approximately 15 miles east of the field at elevations of roughly 5,000 to 6,500 ft above sea level, although a few creeks cross it at slightly lower elevations. It also is exposed where the Big Horn River cuts through Sheep Mountain some 17 miles northwest of the field. The elevation of the Tensleep where it is cut by the river is about 3,740 ft.

With intake of surface water into the formation outcrop at high elevations along the west edge of the Big Horn Mountains and discharge from the exposure along the river at much lower elevations, movement of water through the formation occurs. This is accompanied by a dynamic pressure gradient toward the point of water discharge. These conditions are illustrated in the regional cross-section, Fig. 1.

The original pressure of 1,618 psi at plus 1,000-ft datum at Torchlight is about 200 psi above that which would be expected from the surface elevation of 4,075 ft at the field and a fresh water gradient of .433 psi/ft of depth. The water table at Torchlight is tilted 140 ft from southeast to northwest through a distance across the productive area of about ⅞ of a mile. This tilt is equivalent to a differential of about 20 ft of water head or 9 psi over the same distance. This conversion may be made by use of Hubbert's[2] equation

$$\frac{\partial h}{\partial x} = \frac{\partial z}{\partial x}\,\frac{\rho_w - \rho_o}{\rho_w}$$

In this equation, $\frac{\partial h}{\partial x}$ is the rate of increase of total head of water along the interface in the x direction, $\frac{\partial z}{\partial x}$ is the tilt or slope of the oil-water interface in the same direction, and ρ_w and ρ_o are the densities of the water and oil, respectively, at reservoir conditions.

The map, Fig. 2, shows the anticlinal structure of the field, the shape of the oil reservoir, and the intersection of the oil-water contact with the top and base of the pay. No faults are evident in the vicinity of the field. The characteristics of the reservoir rock and fluids are tabulated below.

Productive Area	220 acres
Net Thickness of Pay	31 ft
Porosity	17 per cent
Connate Water Saturation	10 per cent
Permeability from Cores	204 mds
Permeability from PI's	87 mds
Initial Pressure	1,618 psi
Reservoir Temperature	100°F
Bubble Point	55 psi
Gas in Solution	2 cu ft /bbl
Reservoir Volume Factor at Bubble Point	1.0225
Viscosity of Oil	3.5 cps
Viscosity of Water	.60 cps
Compressibility of Reservoir Oil	7.7×10^{-6} vol /vol /psi
Compressibility of Reservoir Water	3.1×10^{-6} vol /vol /psi
Compressibility of Reservoir Rock	6.6×10^{-7} pore vol /bulk vol /psi

Of particular significance are the unusually low bubble point, solution ratio, and volume factor.

Production and pressure history of the field are shown by the lighter lines in the lower part of Fig. 3. In general, oil production increased rapidly to a peak within a few months after discovery followed by a period of rapidly decreasing rate as reservoir pressure and well capacity declined. Production rate was then reduced below capacity during 1949 and reservoir pressure responded by increasing rapidly. Production was increased in February, 1950, and since mid-1950 has been at well capacity. Withdrawals during this latter period are directly related to and controlled by the rate of water influx.

EVALUATION OF METHODS

The most common methods used to calculate oil in place and to analyze the performance of a water drive field have been applied to the Torchlight Tensleep reservoir.

By pore-volume, using the data in the table, initial oil in place was calculated to be 6.1 million bbls. Core data were available on seven wells, six of them located within the productive limits. In view of the number of wells drilled to the Tensleep defining the productive area and the extensive core coverage, the pore-volume estimate is believed to be fairly accurate, probably with less than 10 per cent error.

In all other methods of evaluating oil in place, the material balance equation is used. Assuming that all physical properties of the reservoir fluids are known, that pressure and production statistics of reasonable accuracy are available, and that a reasonable evaluation of the gas-cap volume ratio (if a gas cap exists) could be made, the only two unknowns in the equation are N, the original stock tank oil in place, and W, the cumulative water encroachment.

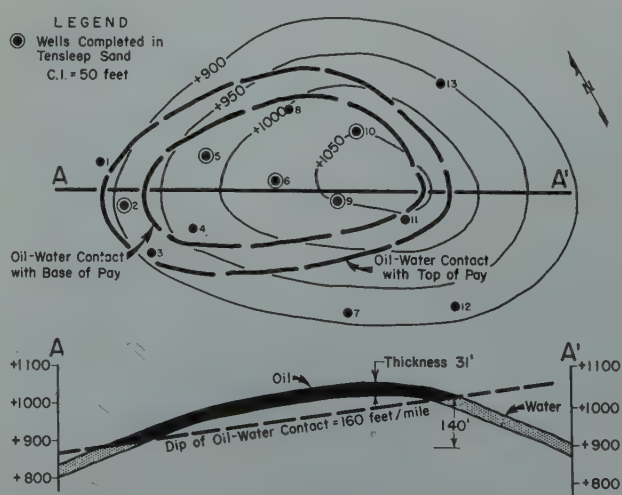

FIG. 2 — STRUCTURE AND CROSS-SECTION, TORCHLIGHT TENSLEEP RESERVOIR.

The methods differ only in the manner in which W is evaluated, and all require the simultaneous solution for the most likely values of the two unknowns, usually arrived at by the method of least squares.

The material balance equation may be written as follows, using nomenclature listed in a later section:

$$n\beta + [n\ (r_n - S) - N(S_o - S)]\,a + w - N(\beta - \beta_o) - m\,N\,\beta_o\left(\frac{a}{a_o} - 1\right) = W \quad . \quad (1)$$

At Torchlight, in spite of the large pressure drop which has occurred, pressure has never declined to the bubble point of 55 psi. Since no free gas has existed, $r_n = S$; $S_o = S$; and $m = 0$. The material balance may be simplified and rearranged to

$$N\ (\beta - \beta_o) = n\beta + w - W \quad . \quad . \quad . \quad . \quad . \quad . \quad . \quad . \quad (2)$$

As long as the pressure remains above the bubble point the difference in reservoir volume factors $(\beta - \beta_o)$ may be replaced by $C\beta_o(P_o - P)$. Thus the equation as applicable to Torchlight is

$$N\beta_o C\ (P_o - P) = n\beta + w - W \quad . \quad . \quad . \quad . \quad . \quad . \quad . \quad (3)$$

Regardless of how W is determined, solution for N is inversely proportional to the compressibility factor used. Where undersaturated crudes are involved, serious error in the calculation of N can result by neglecting rock compressibility.[3] In this case, $C = 7.7 \times 10^{-6}$. However, effective compressibility, C_e, including connate water and rock compressibilities, is equal to $C + (C_w \times$ vol connate water/vol oil$) + ($Cr $\times$ vol rock/vol oil$) = 12.4 \times 10^{-6}$ vol/vol of oil/psi. Calculated N using the compressibility factor for oil but neglecting connate water and rock compressibilities would be 12.4/7.7 or 1.61 times greater than the actual N, assuming all other data including W are accurately known.

Examination of the equation also shows that at pressures near original a small error in pressure measurements could make a very great error in the N determined. As $(P_o - P)$ becomes greater, errors in pressure measurements become less significant.

Methods of analysis applied to Torchlight are as follows:

Modified Schilthuis
Simplified Hurst
van Everdingen, et al (1952)
Electric Analyzer

With the first three, oil initially in place was calculated from cumulative data available at successive times. Using data available at the end of two years' history (November, 1949) and average calculated oil in place as of that date, future rate and pressure performance were predicted by each method. The predictions were then compared with subsequent performance, permitting an evaluation of the methods. Similar predictions and comparison were made using the electric analyzer and pore-volume oil in place.

For the predictions in each case, the production rate was maintained at 500 B/D as long as wells had the capacity to produce that amount, and capacity thereafter. The capacity of the wells was evaluated using a composite PI of 3.2 from field data and minimum producing bottom hole pressure of 15 psi. These conditions conform closely with the actual. Water production was assumed to remain at roughly 2 per cent, which also agrees closely with the actual.

MODIFIED SCHILTHUIS METHOD[4,5]

In this method water influx is related to pressure and time by means of a constant as follows:

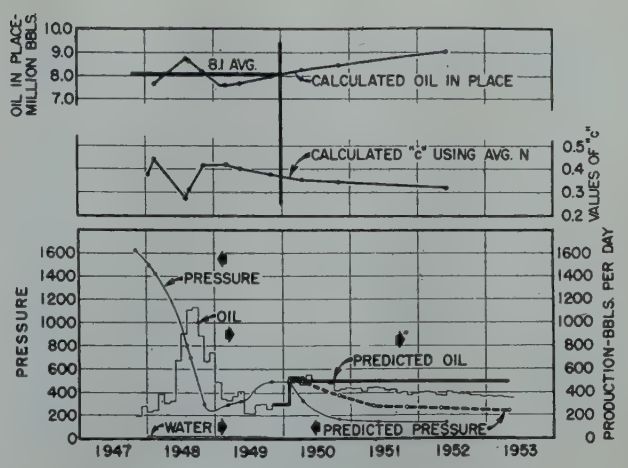

FIG. 3 — MODIFIED SCHILTHUIS METHOD, CALCULATED N AT SUCCESSIVE TIMES AND PREDICTIONS FROM NOVEMBER, 1949, COMPARED WITH ACTUAL PERFORMANCE.

$$N\beta_o C_e(P_o - P) = n\beta + w - c\,\Sigma_o^{\Theta}\,\Delta P \Delta\Theta \quad . \quad . \quad (4)$$

Assumptions are that steady state conditions exist and that rate of water influx into the reservoir at any time is proportional to the difference between the initial pressure (P_o) and the field pressure (P), and to the area exposed to water encroachment on the field's boundary. The proportionality constant, c, includes the formation permeability, water viscosity, and area of encroachment on the field's boundary.

Fig. 3 shows the calculated oil in place, N, from the Modified Schilthuis method using reservoir data cumulative to the time of the points plotted. When water is replacing a high percentage of withdrawals after the initial large pressure drop, N is continually increasing. Using the average N of 8.1 million bbls determined from the first two years' history, the proportionality constant, c, has been calculated and is found to be steadily decreasing. Obviously, predictions of reservoir pressure and influx rate based on this method and using a constant c will be in error.

Predictions of rate and pressure made using data available as of November, 1949, N of 8.1 million bbls, and c of .38, appear on Fig. 3. Compared to subsequent history, also shown on Fig. 3, a large degree of error is evident.

If pore-volume N of 6.1 million bbls had been used, values of calculated c would decrease from 1.12 to .423 from the first point to November, 1949, and predictions would have been just as much or more in error.

The direction of the error in predictions is as expected because this method does not take into account the gradually lengthening travel path of the encroaching water. Although it is simple and easily applied, its application is limited because of neglecting transient conditions. Transient conditions cause a lower water pressure gradient, a gradually decreasing encroachment rate, and consequently lower reservoir pressure with time than would be expected under the steady state assumption.

SIMPLIFIED HURST METHOD[5]

This method is similar to the previous one but introduces logarithm of time into the denominator of the W expression to approximate the actual variation in $(P_o - P)$ with time when the field is producing at constant rate.

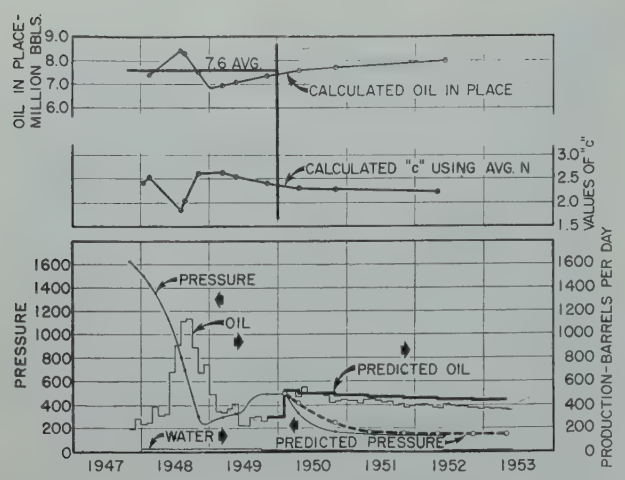

FIG. 4 — SIMPLIFIED HURST METHOD, CALCULATED N AT SUCCESSIVE TIMES AND PREDICTIONS FROM NOVEMBER, 1949, COMPARED WITH ACTUAL PERFORMANCE.

$$N\beta_o C_e (P_o - P) = n\beta + w - c\Sigma_o^{\Theta} \Delta P \Delta\Theta / \log \Theta \quad . \quad (5)$$

The proportionality constant, c, is a different number than the one in the previous equation.

Oil in place was again calculated using cumulative data at various times and appears on Fig. 4. As in the previous case the calculated N is increasing after the initial large pressure drop; however, values of N are consistently closer to the pore-volume determination of 6.1 million bbls. Conversely, c, determined using an average N of 7.6 million bbls calculated for the first two years, is decreasing. However, values for both are more consistent than those calculated using the Modified Schilthuis method.

Predictions of rate and pressure using N of 7.6 million bbls, c of 2.38, and other data as of November, 1949, appear on Fig. 4. The predicted pressure falls off more rapidly than by the previous method and the capacity of wells declines below 500 B/D as the pressure decreases. These predictions are closer to the actual rate and pressure behavior subsequently observed than similar predictions for the preceding method, but considerable error is still apparent. This is expected from comparison of the trends of the calculated c's using single values for N as shown on Figs. 3 and 4.

If pore-volume N of 6.1 million bbls had been used, calculated c would have decreased from 4.71 to 2.60 for successive times up to November, 1949, and no improvement in the accuracy of predictions would have resulted. Little more engineering time is involved in application of this method than in the preceding one.

VAN EVERDINGEN, ET AL (1952) METHOD[6]

A new method for calculating oil in place was introduced in 1952 by van Everdingen, Timmerman and McMahon. It combines the material balance equation with the water influx equation of van Everdingen and Hurst (1949).[8] For Torchlight, the combined equation resolves to

$$N\beta_o C_e (P_o - P) = n\beta + w - B\Sigma\Delta p Q_T \quad . \quad (6)$$

B is a proportionality factor to convert reduced units into barrels and is different from the factors in the previous methods; Δp is the successive pressure drop occurring during successive time intervals of equal duration, psi; and Q_T is a dimensionless function of production time in reduced units T and the ratio of aquifer radius to oil reservoir radius. Values of Q_T as a function of T for an infinite aquifer are given in Table 1 of Reference 8. The procedure for obtaining the summation of $\Delta p Q_T$ for various times is covered in Reference 6.

As in the other methods there are only two unknowns in the above equation, namely N and the proportionality factor (B in this case). These may be determined by the least squares method if two or more of the equations can be written, i.e., if data are available for at least two time intervals. However, in order to find the correct values of $\Delta p Q_T$ it is necessary to determine T, which may be approximated from the equation

$$T = \frac{kt}{f\mu C_a r_b^2} \quad . \quad . \quad . \quad . \quad . \quad . \quad . \quad . \quad . \quad (7)$$

For Torchlight, using the values for porosity, permeability, viscosity of water, and combined compressibility of water and rock derived from the data in the table, $T = 477$ for the 1,643 days (four and one-half years) the field produced to May, 1952, and $\Delta T = 53$, for half-year intervals.

N and B have been calculated by the least squares method using cumulative data at the end of successive half-year intervals. If the correct time conversion were used, basic assumptions hold, and other data were reliable, values of N and B would not change. Fig. 5 shows values of N calculated for $\Delta T = 5$, 10, 40, and 60. Obviously, the correct value for ΔT must lie between 5 and 10 and possibly very close to 5, at which successive values of N are more consistent.

N corresponding to $\Delta T = 5$ is 6.1 million bbls which is in agreement with that calculated by pore volume. However, if time had been taken to determine N for values of $\Delta T = 6$ or 7, slightly larger values of N would have resulted as can be seen by interpolation between the curves.

Using N of 6.1 million, B of 23.26, and values of Q_T for $\Delta T = 5$, rates were predicted from November, 1949, as shown on Fig. 5. A close check with actual performance is noted. Pressure values similarly would be fairly close to the actual, however, they are not plotted. The above values of N and ΔT were derived from information available through May, 1953. Referring to Fig. 5 again, it is highly unlikely that information available in November, 1949, would have been reliable enough to obtain a reasonable value for ΔT. Therefore, although a reasonably accurate forecast from November, 1949, was made using cumulative data through May, 1953, to fix the values of N and ΔT, a reasonable forecast would have been unlikely based only on data available to November, 1949.

OTHER MATHEMATICAL METHODS

There are two other mathematical methods of calculating water influx, other than those discussed above, which have appeared in the literature. These are called Hurst (1943)[7] and van Everdingen and Hurst (1949)[8] methods. In both, the water influx is determined independently of the material balance. Water influx is equal to a constant, which can be calculated from data normally available on the field, times a step function which is read from published charts or tables. In both, the constant is equivalent to the B in the van Everdingen, et al (1952) method. In the van Everdingen and Hurst (1949) method, T is calculated according to Equation 7. For Torchlight, the calculated ΔT for a half-year period is 53, compared to the more representative value of 5 which was found in the preceding

section to give the most consistent values for N. The proportionality constant was calculated to be 66.9 compared to B of 23.26. If the directly calculated values of 53 for ΔT and 66.9 for the proportionality constant had been used without any adjustment, the water influx determined obviously would be greatly in error.

The van Everdingen et al (1952) method, of course, was developed using the 1949 work as a basis and represents an improvement in that the correct T is approximated, and most probable N and B are determined from solution of simultaneous equations. Since the van Everdingen et al (1952) method is simply an improvement over the other two procedures, applications of the Hurst (1943) and van Everdingen and Hurst (1949) methods to Torchlight are not included.

In brief review of the mathematical methods already discussed, it is readily noted that the methods differ in allowance made for transients in the aquifer. The Modified Schilthuis method is simple but neglects these transients. The Simplified Hurst method requires little more engineering time, makes some allowance for the transient, and gives closer results. The van Everdingen et al (1952) method holds closely providing the basic data are reasonably accurate, the aquifer is fairly uniform in thickness, permeability, porosity, and its size is known, the character of the fluids in the aquifer does not change, and no other fields common to the aquifer have an appreciable effect on behavior of the field in question; however, much more engineering time is involved, especially in arriving at the correct value for T.

ELECTRIC ANALYZER[9,10]

The mathematical methods are somewhat laborious, which usually means the person making the analysis is limited to a single set of rock and fluid characteristics. With an electric analyzer, different combinations of these properties and other pertinent factors, such as size of aquifer and changes in the properties of the aquifer with distance, may be taken into account. Presumably all these factors could be adjusted until past performance were duplicated. This is an apparent advantage in the analysis of water drive performance with the analyzer compared to mathematical methods.

The pressure history of the Torchlight field up to

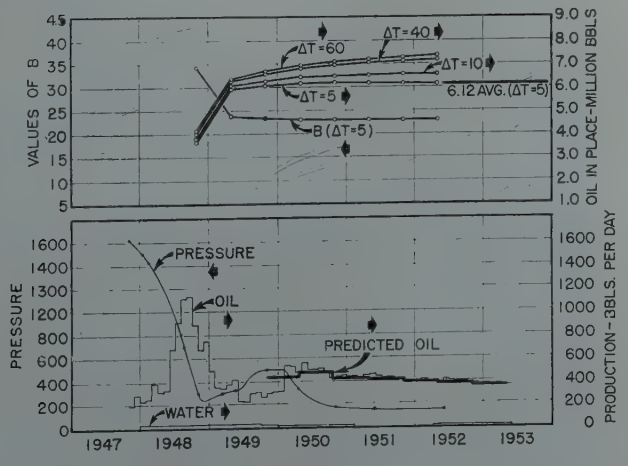

FIG. 5 — VAN EVERDINGEN ET AL (1952) METHOD, CALCULATED N AT SUCCESSIVE TIMES FOR VARIOUS VALUES OF ΔT AND PREDICTION FROM NOVEMBER, 1949, COMPARED WITH ACTUAL PERFORMANCE.

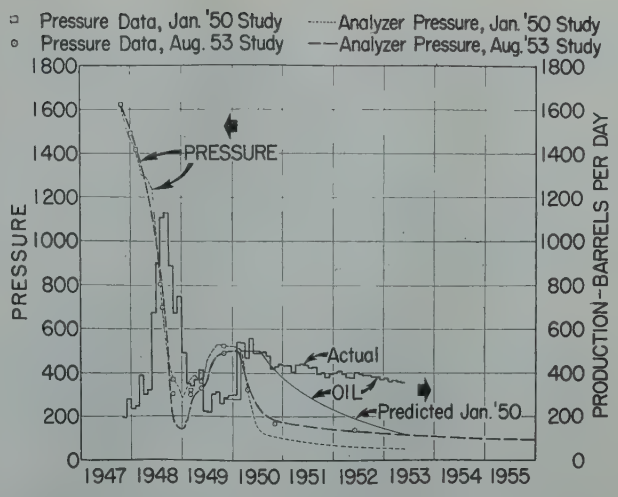

FIG. 6 — ELECTRIC ANALYZER STUDIES OF JANUARY, 1950, AND AUGUST, 1953, AND ACTUAL PERFORMANCE.

November, 1949, was matched on the electric analyzer by using 6.1 million bbls oil in place and by considering an aquifer acting only on the eastern edge of the reservoir. The latter assumption was made because water production and pressure gradients existing within the oil reservoir were interpreted at that time to mean that water encroachment was occurring principally on that side. At the time, it was found that the field performance could be reasonably duplicated with an aquifer extending 2.2 miles; however, the data could have been fitted equally well with an unlimited aquifer. At the time of this first analyzer study, geological data alone were not believed conclusive evidence that the aquifer was continuous past the 2.2-mile radius. Because the drop in pressure which had occurred was much more severe than at any other Tensleep reservoir in the Big Horn Basin, and since a large Tensleep field in the northern part of the Basin had practically no water influx at all, the use of the limited aquifer did not seem unreasonable.

Future pressure predictions were made with the 2.2-mile aquifer assuming a withdrawal rate of 500 B/D as long as the wells could make that amount, and capacity production thereafter. These predictions deviated appreciably from subsequent field performance as shown on Fig. 6. This, of course, was disturbing since a reasonable fit of past performance had been obtained.

A second analyzer study was conducted using data available through the first part of 1953 and using 6.1 million bbls oil in place. Several of the field pressure points used in the previous study were changed to eliminate the effect of water influx on pressure build-up during the shut-in period (these are shown by the circular points. The results of this study are shown on Fig. 6. The performance up to this time indicated that an aquifer of at least 5 miles radius was required to obtain an agreement between field performance and the analyzer representation. However, it was found that past performance could be duplicated with either an infinite aquifer or an aquifer of radius 5 miles. Therefore, at this time, from pressure performance history alone, it is not possible to further define the size of the aquifer, that is, determine how much greater than 5 miles its radius may be.

As seen from the behavior in Fig. 6 the size of the aquifer is one of the critical parameters governing future performance. The reliability of future predictions

depends on the size of aquifer assumed; however, the limits within which future pressure trends must fall can be determined. If an aquifer just large enough to match past performance is used the pressure predictions will give a lower limit of the future reservoir pressure curve. If an infinite aquifer is used in predicting future pressure performance, an upper limit of the reservoir pressure curve will be obtained. An infinite aquifer was used to obtain the analyzer pressure curve and prediction for the second study.

It is advisable to examine available geological information about the aquifer, its extent, continuity, etc. From recent geological data on the Big Horn Basin there is now good evidence, as described earlier, that an aquifer of essentially unlimited extent adjoins the Torchlight field. Therefore, the predictions using the infinite aquifer are considered more nearly correct.

It was found that the pressure history of the Torchlight field up to the first part of 1953 could be reasonably duplicated on the analyzer using oil in place values varying from 3.8 to 7.5 million bbls and varying slightly the aquifer properties. This means that reliable values of oil in place and aquifer size for Torchlight cannot be found simultaneously, which is in accordance with expectations since only a very small portion of the withdrawals is replaced by expansion of the oil.

CONCLUSIONS

The following conclusions are made on application of the various methods of analyzing a water drive field to the Torchlight Tensleep reservoir — a small oil reservoir in which pressure has been maintained above the bubble point by an effective water drive:

1. With the exception of pore-volume calculation of oil in place, no method gave either a reliable determination of oil in place or reliable prediction of producing rate and reservoir pressure using data available the first two years; however, using later data reasonable results for both oil in place and performance prediction were obtained by the van Everdingen et al (1952) method once reduced time, T, could be accurately determined.

2. In methods using the material balance, accuracy in determining oil in place and predicting producing rate and pressure is directly influenced by the allowance made in the water influx term for transient conditions in the aquifer. Consequently, in application to Torchlight, results by the Modified Schilthuis method were seriously in error; by the Simplified Hurst method, appreciably in error but somewhat better; by the van Everdingen et al (1952) method, fairly reasonable after reduced time, T, could be accurately determined.

3. The performance prediction made in 1950 with the Electric Analyzer was not reliable due to lack of definition as to the extent of the aquifer. The performance prediction prepared in August, 1953, is subject to the same basic limitation; however, the uncertainty of the prediction is much less as a result of the additional performance history.

ACKNOWLEDGMENTS

The authors wish to thank Robert Lewis and C. A. Bickel for their work in conducting the last electric analyzer study, L. E. Wilsey for his helpful suggestions on the analyzer work, and the management of Stanolind Oil and Gas Co. for permission to prepare and publish this paper.

NOMENCLATURE

N = Oil in place, stock tank bbls.
W = Cumulative water influx, bbls.
n = Oil produced, stock tank bbls.
w = Water produced, bbls.
β = Reservoir volume of 1 unit of stock tank oil and its dissolved gas at pressure P.
C = Compressibility of reservoir oil above its bubble point, vol/vol/psi.
C_w = Compressibility of water, vol/vol/psi.
C_r = Compressibility of reservoir rock, pore vol/bulk vol/psi.
C_e = Effective compressibility, vol/vol of oil/psi, for the reservoir computed from C, C_w, and C_r.
C_a = Combined compressibility of aquifer.
P = Reservoir pressure, psi.
r_n = Average gas oil ratio, cu ft/bbl, from P_o to P.
S = Gas in solution at pressure P, cu ft/bbl.
α = Reservoir volume of 1 unit of gas at standard conditions, when subjected to pressure P and reservoir temperature.
m = Fraction of reservoir volume originally occupied by gas.
Θ = Time from date of initial production, days.
f = Porosity, fraction.
μ = Viscosity of water, cp.
r_b^2 = Square of radius of oil reservoir, sq cm.
t = Time in days during which pressure drop has been operative.
k = Permeability in darcys.
T = Reduced time as defined by Equation 7.
$_o$ = Subscript denoting initial conditions.
Δ = Incremental change.

REFERENCES

1. Muskat, Morris: *Physical Principles of Oil Production,* McGraw-Hill, New York (1949), Chapter 9.
2. Hubbert, M. King: "Entrapment of Petroleum Under Hydrodynamic Conditions" *Bulletin* of AAPG (August, 1953), **37**, 1987.
3. Hall, H. N.: "Compressibility of Reservoir Rocks," *Trans.* AIME (1953), **198**, 309.
4. Schilthuis, R. J.: "Active Oil and Reservoir Energy," *Trans.* AIME (1936), **118**, 37.
5. Pirson, S. J.: *Elements of Reservoir Engineering,* McGraw-Hill, New York (1950), Chapter 7.
6. van Everdingen, A. F., Timmerman, E. H., and McMahon, J. J.: "Application of the Material Balance Equation to a Partial Water Drive Reservoir," *Trans.* AIME (1953), **198**, 51.
7. Hurst, W.: "Water Influx into a Reservoir and its Application to the Equation of Volumetric Balance," *Trans.* AIME (1943), **151**, 57.
8. van Everdingen, A. F., and Hurst, W.: "The Application of the Laplace Transformation to Flow Problems in Reservoirs," *Trans.* AIME (1949), **186**, 305.
9. Bruce, W. A.: "An Electrical Device for Analyzing Oil-reservoir Behavior," *Trans.* AIME (1943), **151**, 112.
10. Schaefer, Henry: "Extending the Application of Electric Analogy in Oil-reservoir Studies," *Trans.* AIME (1947), **170**, 62. ★★★

A MAGNETIC SUSCEPTIBILITY METHOD for the DETERMINATION of LIQUID SATURATION in POROUS MATERIALS

J. W. WHALEN

MAGNOLIA FIELD RESEARCH LABORATORIES
DALLAS, TEX.

T. P. 3893

ABSTRACT

The design, operation and evaluation of an instrumental method for the determination of fluid saturation in porous materials during multiphase flow studies is described. The presence of a magnetic tracer comprising approximately 20 per cent by weight of the aqueous phase is necessary in the utilization of this method.

The results of two-phase relative permeability studies on two samples of porous media are presented. The realizable accuracy of the magnetic susceptibility apparatus in fluid saturation determination is estimated to be 2 saturation per cent. The response characteristics of the instrument, together with its simplicity of operation and maintenance are sufficient to recommend its use in routine laboratory studies.

INTRODUCTION

The problem of fluid saturation determination in laboratory multiphase flow studies characterizing oil recovery processes is one which has been given exhaustive study. Briefly the requirements which are considered essential for a method serving this purpose are: (1) that the measurement be made external to the porous rock sample under study with no interruption of the fluid flow pattern, (2) the saturation indication must be independent of fluid distribution in the volume scanned by the measuring device, (3) the sensing element should have a small field of definition enabling several independent measurements to be made along the length of a core sample, and (4) the properties of the fluid phases should not be too greatly influenced by required tracer substances.

Several methods of saturation determination have found acceptance as meeting most of the above requirements. These include resistivity,[1] X-Ray absorption,[2,3,4] radiotracers,[5,6,7] and neutron[8] diffraction. The merits of these techniques have been discussed elsewhere in detail and will not be considered here. It may, however, be pointed out that the elaborate instrumentation required by the methods mentioned above, with the exception of the resistivity method (which is undesirable from other standpoints) encourages the development of methods of saturation determination which, while meeting the requirements listed, are simple to operate and maintain.

It is the purpose of this paper to describe the instrumentation and evaluation of a technique for the determination of fluid saturation which combines relative simplicity with an accuracy and applicability comparable with methods now in practice.

DESCRIPTION OF THE METHOD

If the magnetic susceptibility of one of the fluid phases contained within a porous material is sufficiently greater than that of the remaining phases, the fluid content of the material with respect to that phase may be determined by an induction measurement. This may be accomplished by measuring the induced voltage in the secondary of a transformer which contains the porous sample and its interstitial fluids as a portion of the magnetic flux path. Since the fluids used in multiphase flow studies involving petroleum reservoir samples possess uniformly low magnetic susceptibilities, the use of a magnetic tracer in one of the fluid phases is required.

In view of the relatively high paramagnetic susceptibility of salts of the transition elements, together with their high water solubility, these compounds become logical choices as tracer materials. Cobaltous chloride, having a specific magnetic susceptibility of 17.5×10^{-6} cgs electromagnetic units, was used as the tracer material throughout this work, in a concentration of approximately 20 per cent by weight in the aqueous phase.

MAGNETIC SUSCEPTIBILITY APPARATUS

Basically, the magnetic susceptibility apparatus consists of a transformer serving as the detecting head, a

[1]References given at end of paper.

Manuscript received in the Petroleum Branch office Jan. 15, 1954. Paper presented at the AIME Annual Meeting in New York City, Feb. 13-17, 1954.

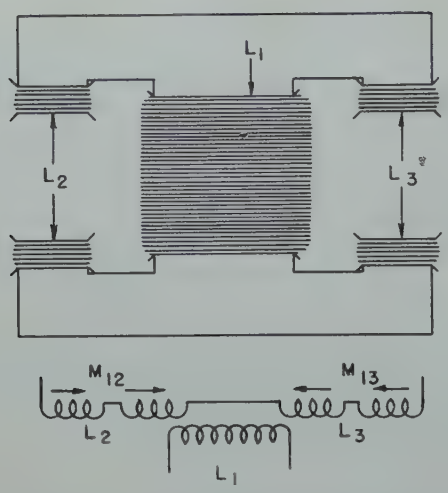

L_1 PRIMARY 780 TURNS NO.30 COPPER WIRE
L_2, L_3, EACH COIL 400 TURNS NO.35 COPPER WIRE

FIG. 1 — DETAIL OF TRANSFORMER HEAD FOR MAGNETIC SUSCEPTIBILITY MEASUREMENT OF CORE SATURATION.

nulling circuit for obtaining a zero signal prior to introducing the core sample and its interstitial fluids into the flux path of the transformer, a metering circuit for observation of the transformer response, and a stable power supply serving the transformer and nulling circuit.

The transformer used in this work was constructed with balanced secondary coils in an effort to eliminate the effects on the mutual inductance of temperature, stray electrostatic and electromagnetic fields, and humidity. Two air gaps were symmetrically located with respect to a central member around which the primary coil was wound. Secondary coils were wound about each arm of the air gap and the two secondaries were connected in series opposition. The transformer core was built up with 0.005-in. thick Conpernick* laminations insulated from one another by a baked-on coat of transformer dope except at a grounding point on each lamination. Details of the transformer construction are shown in Fig. 1.

The residual unbalance voltage from the two secondaries, resulting from an inability to wind the two sets of secondary coils so as to exactly cancel the opposing induced voltages, was matched with a voltage of equal amplitude and opposite phase from the nulling circuit. Amplitude control was accomplished by means of a helipot setting, and phase control was obtained from an inductive-capacitive network. A schematic circuit diagram is shown in Fig. 2.

A Southwestern Industrial Electronic Co. Model M oscillator having a frequency stability of 0.1 per cent and an amplitude stability of 1 per cent was used to supply power to the transformer and nulling circuit. The output voltage level at 1,000 cps was maintained at 20 volts throughout this work.

The amplification and metering circuit consisted of a Hewlett-Packard Model 450-A amplifier operating at 40 db gain, a 1,000-cps band-pass filter and a Hewlett-Packard Model 400-C vacuum tube voltmeter. The magnitude of the amplified readings was such that the 0.3-volt scale of the voltmeter was used for most signals. The voltmeter scale could be read with a precision of 1 per cent of full scale.

*Conpernick is the trade name of a high magnetic permeability alloy produced and distributed by Westinghouse Electric Co.

TABLE 1 — POROSITY OF SAND PACKS: COMPARISON OF POROSITY VALUES CALCULATED FROM GEOMETRY OF PACK WITH POROSITY VALUES MEASURED USING THE MAGNETIC TRACER.

Sand Mesh Size	Calculated Porosity %	Measured Porosity %
35-45	40.4	40.2
20-25	39.6	39.8

In order to ascertain that the sensitivity of the magnetic susceptibility apparatus remained constant throughout protracted studies, an iron-Lucite powder mixture was molded into a plug of the same dimension as the mounted core samples used in this work and readings were obtained on this standard during the multiphase flow experiments. The standard contained 75 micrograms of iron per 100 gms of Lucite powder.

INSTRUMENT CHARACTERISTICS

A series of tests was carried out to determine the utility of the magnetic susceptibility apparatus in liquid saturation determination. Various concentrations of cobaltous chloride solution were prepared by successive dilution of a 17 per cent (by weight) cobaltous chloride stock solution. These solutions, contained in a hollow Lucite cylinder, were placed in the transformer air gap and the voltmeter deflection noted for each solution. The response of the induced voltage in the transformer to the quantity of paramagnetic material present in the air gap is shown in Fig. 3. As a further check, the porosities of two sand packs were determined from the magnetic susceptibility reading. A comparison between the porosity value calculated from the sand density and geometry of the container and that found experimentally is shown in Table 1.

In considering what volume of a core sample placed in the transformer air gap is "scanned" by the measuring apparatus, the flux density in various portions of the magnetic field and the variation in flux density from point to point under various distributions of the tracer liquid is of interest. The flux density pattern was obtained using as a probe a small steel ball approximately 0.1 in. in diameter. The field strength was taken to be proportional to the voltmeter reading and isomagnetic lines were constructed in two planes as shown in Figs. 4 and 5.

The effect of tracer liquid distribution in the magnetic field of the measuring transformer on the induced voltage was determined as follows. A hollow Lucite cylinder was placed in the transformer air gap and tracer liquid added in increments. The voltmeter deflection was noted for each increment. In the first portion of this study added volume increments advanced the

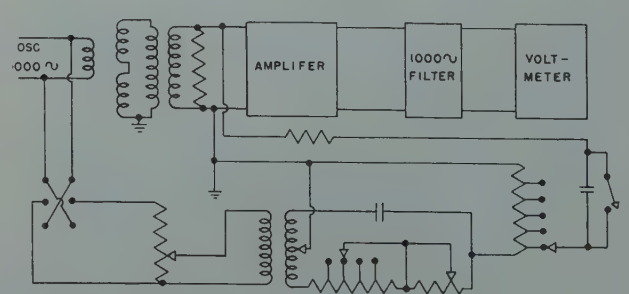

FIG. 2 — SCHEMATIC CIRCUIT DIAGRAM FOR MAGNETIC SUSCEPTIBILITY APPARATUS NULLING CIRCUIT.

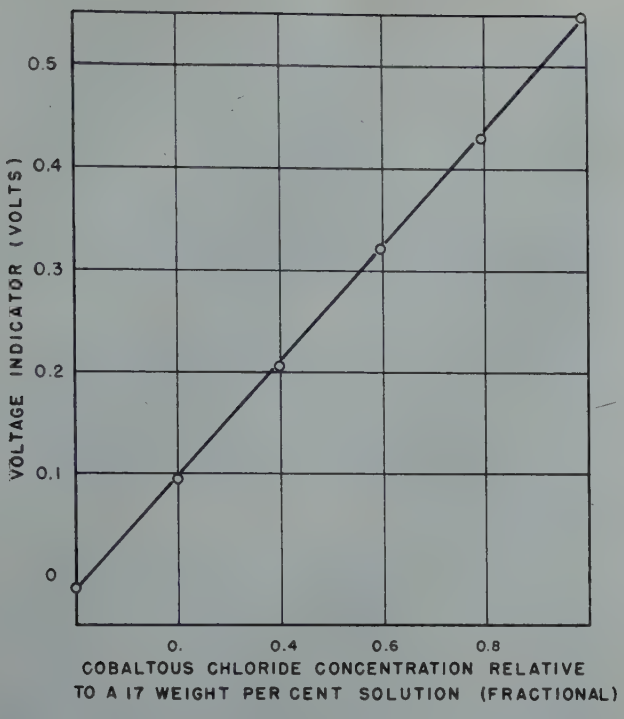

FIG. 3 — RESPONSE CHARACTERISTICS OF THE MAGNETIC SUSCEPTIBILITY APPARATUS.

air-liquid interface from a point beyond the influence of the magnetic field toward the air gap center of the transformer. Measurements were halted when the air-liquid interface reached the air gap center. In the second portion of the study, starting with no tracer liquid in the magnetic field, the air-liquid interface receded from the air gap center with each addition of liquid. Measurements were halted when further additions of liquid produced no change in the voltmeter indication.

These data are presented in Fig. 6 as a magnetic susceptibility profile of the fluid-filled hollow cylinder for two concentrations of tracer solution. Solutions containing 17 and 7 per cent (by weight) cobaltous chloride were used in this study, corresponding to a reduction in the saturation of a core sample from 100 per cent to 41 per cent with respect to the aqueous phase.

RELATIVE PERMEABILITY APPARATUS AND PROCEDURE

Dynamic two liquid-phase flow studies were carried out using two positive displacement pumps to deliver the required flow rates. Standard 250 ml volumetric pump barrels were equipped with a synchronous motor drive, two stages of gear reduction and a quick-change lathe gear box. Using this arrangement it was possible to obtain 63 different discharge rates varying from 0.15 to 18 cc/hour. Each of these flow rates could be increased by a factor of 6.25 by reversing the sprockets on the chain drive mechanism linking the transmission and feed screw.

Core samples 3 in. in length and 1 in. in diameter were extracted with a constant boiling mixture of methanol and benzene (40 per cent methanol) and molded in Lucite. A number of flow channels were drilled through the plastic mount into one end of the mounted sample in the manner illustrated in Fig. 7.

Separate channels were drilled for the oil and aqueous phases, although, to avoid complication only a single set is shown in the schematic drawing. The oil and aqueous phases were thus in contact only through interfaces of capillary dimensions. The necessity of a mixing section preceding the core sample under study, with the attendant difficulty and uncertainty of maintaining capillary contact between the sections, was thus avoided. In this manner, it was possible to measure separate pressure drops in the oil and aqueous phases at the extremeties of the core sample in the flow lines. A Lucite butt-piece containing sealed-in Saran flow lines was cemented to the mounted sample. Saran flow lines, Lucite reservoirs and glass stopcocks were used throughout the flow system in view of the highly corrosive nature of the tracer solution.

The pressure drop across the core sample was measured in each of the liquid phases using Moore Products Differential Pressure Transmitters. These instruments operate on a pneumatic null-balance principle and have a volumetric displacement, when completely liquid filled, of less than 0.05 cc. This small volume change is due to an uncertainty in relocation of the null position following a change in differential pressure.

Since the null position of the magnetic susceptibility apparatus was found to be dependent on the position of the transformer head relative to its surroundings, it was necessary to move the core sample and attached flow lines into the field of the transformer rather than moving the transformer itself. The core sample was held rigidly in a Lucite framework which fitted closely in grooves machined in flat Lucite stock. These guides were fastened securely to the framework of the transformer mounting.

In practice an initial voltmeter reading, obtained with the dry mounted core sample in the transformer gap, and a reading obtained after the core sample was saturated with the tracer liquid served as the basis from which further saturation values were obtained. The nature of the calibration curve, Fig. 3, and the data in Table 1 were presumed to verify the linear nature of the voltmeter response to the quantity of paramagnetic liquid in the air gap. A null was obtained on the voltmeter each time before the core sample was moved into the transformer field. Throughout these studies the criterion of flow equilibrium was chosen as the stability of differential pressure across the core sample.

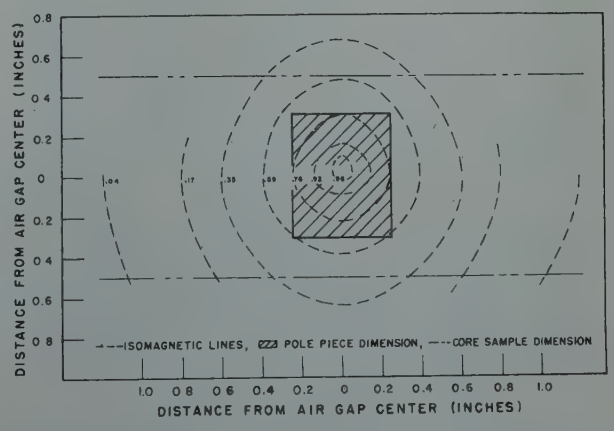

FIG. 4 — ISOMAGNETIC LINES AT THE AIR GAP CENTER IN A PLANE PERPENDICULAR TO THE PLANE OF THE TRANSFORMER.

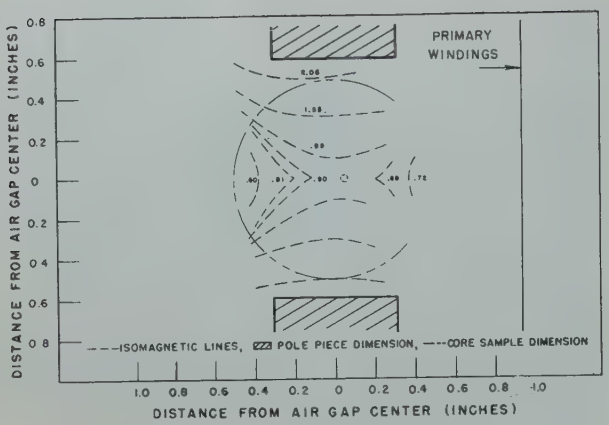
PRIMARY WINDINGS
DISTANCE FROM AIR GAP CENTER (INCHES)
DISTANCE FROM AIR GAP CENTER (INCHES)
---ISOMAGNETIC LINES, POLE PIECE DIMENSION, ---CORE SAMPLE DIMENSION

FIG. 5 — ISOMAGNETIC LINES IN THE AIR GAP CENTER IN A PLANE CONTAINING THE TRANSFORMER.

The results of relative permeability studies on two core samples using the magnetic susceptibility apparatus for liquid saturation determination are reported herein. Pertinent data concerning these samples are given in Table 2. K_g is the single phase gas permeability uncorrected for slip effects, K_w is the single phase permeability to distilled water and k_{aq} is the single phase permeability to the tracer solution. The two phases used in this study were the mutually saturated liquids Soltrol "C" and the magnetic tracer solution. In each case the single aqueous-phase permeability was determined prior to two-phase flow studies. The relative permeability to each phase was determined at a number of points during both the aqueous-phase desaturation and the forced aqueous-phase imbibition. A total of three desaturation-imbibition cycles was completed on the sandstone core sample. A single cycle was run with the alundum sample. The two-phase dynamic flow studies are reported in the form of relative permeability curves in Figs. 8 and 9.

DISCUSSION

The performance of the magnetic susceptibility apparatus in the determination of liquid saturation when that liquid is uniformly distributed throughout the magnetic field is considered to be satisfactory. The graphical results shown in Fig. 3, where voltage indication was plotted versus relative concentration of tracer solution show excellent linearity. The maximum deviation from linearity was found to be 1.1 saturation per cent. All deviations were negative; the indicated saturation being lower than the value required by a linear calibration curve. Aside from this consideration the deviations are no greater than would be expected from the precision of the apparatus and are well within the limits currently considered acceptable for fluid saturation measurements.

The magnetic field studies presented in Figs. 4 and 5 indicate an adequate flux density concentration directly between the pole pieces of the magnet. The slight asymmetry of the isomagnetic lines about the air gap in Fig. 4 is due to flux leakage back to the transformer primary. This condition could, of course, be eliminated with no loss in sensitivity by constructing a transformer with a greater distance between the primary and the air gap. The flux leakage effects, however, contribute less to the non-uniformity of the magnetic field in the region occupied by a core sample than does the effect of the transformer pole piece area in concentrating flux lines near the center of the core sample. In addition, leakage effects would be expected to diminsh as reference planes nearer the transformer pole faces were selected.

TABLE 2 — PROPERTIES OF POROUS SAMPLES

Sample	Porosity (%)	Single-Phase Permeability (md) K_g	K_w	K_{aq}	Voltmeter Reading Dry Mounted Core
Alundum	25.3	133	110	109	− 0.024
Aris Sand Outcrop	27.8	1080	....	1040	+ 0.083

From Fig. 5 it will be noted that a very minor portion (about 15 per cent) of the cross sectional area of the sample lies in a relatively low flux density portion of the magnetic field. Furthermore, in practice the distribution of tracer liquid throughout a portion of the field of the measuring transformer will tend to reduce the asymmetry of the field indicated by the pointwise study.

On the basis of these magnetic field studies it would appear that the distribution of liquid in the field of the measuring transformer can contribute significantly to the magnetic field strength only when the liquid distribution is varied along the length of a sample. In general, the variation in saturation encountered along a short core sample during multiphase flow studies is not large; seldom does it amount to more than 5 saturation per cent.

The magnetic susceptibility profile presented in Fig. 6 shows that the voltage decline is not appreciable until a point 0.75 in. from the center of the test cylinder is reached. The voltage indication is shown to be 43 per cent of the maximum reading when the transformer air gap is centered over the end of the test cylinder. The comparison between the magnetic susceptibility method and the low energy radiotracer method reported by Josendal, Sandiford, and Wilson[7] is quite good. These authors report a count decline over approximately ⅝-in. at the end of the test cylinder used in their work. Their data, however, indicate a slight decline, approximately 10 per cent, in the indicated activity over the ½ in. of the cylinder length preceding this region. Further indications from

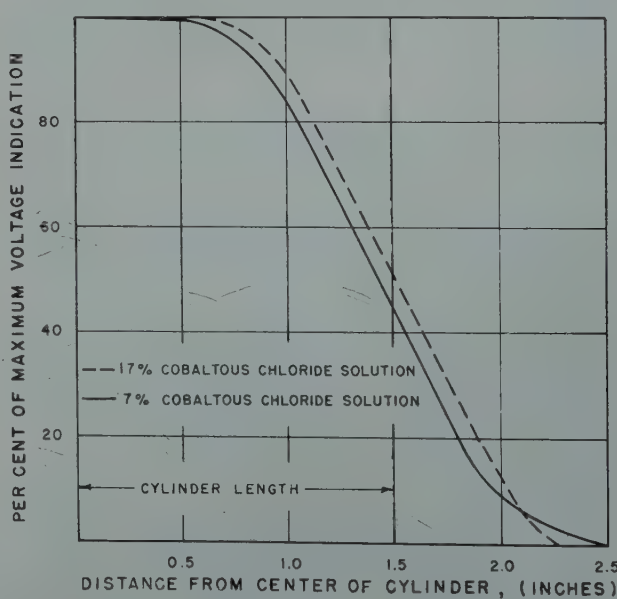
PER CENT OF MAXIMUM VOLTAGE INDICATION
17% COBALTOUS CHLORIDE SOLUTION
7% COBALTOUS CHLORIDE SOLUTION
CYLINDER LENGTH
DISTANCE FROM CENTER OF CYLINDER, (INCHES)

FIG. 6 — MAGNETIC SUSCEPTIBILITY PROFILE OF LIQUID FILLED HOLLOW CYLINDER.

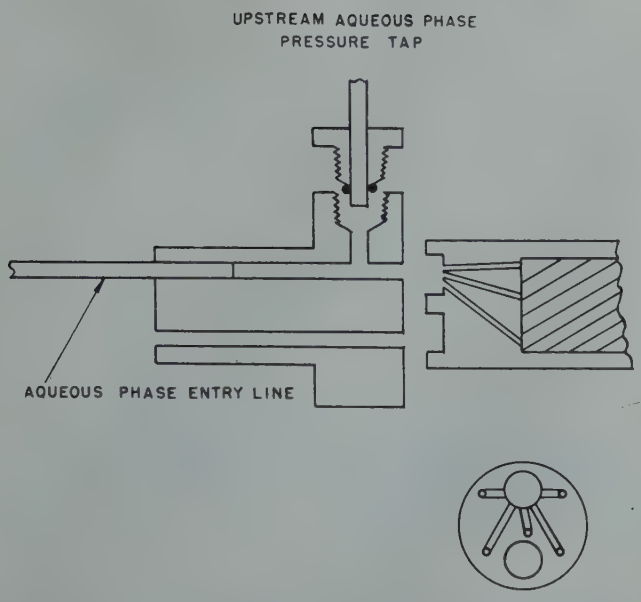

FIG. 7 — DIAGRAM OF TWO PHASE FLUID DISTRIBUTION HEAD.

their data show an activity decline to approximately 60 per cent of the initial activity at the end of the test cylinder.

In the magnetic susceptibility method, the slight spreading of the magnetic field of the measuring transformer as the quantity of magnetical material is increased introduces a factor not encountered in the radioactivity method. The dependence of field definition on the core sample saturation is not great, however, and may be no greater than the effect of self absorption, which is also saturation dependent, encountered in the use of radiotracers. The inability of the low energy radiotracer technique to define the end of the cylinder more exactly is somewhat surprising in that a better definition would be expected than for the magnetic susceptibility method.

On the basis of magnetic field studies reported it appears that the magnetic susceptibility method compares favorably with the radiotracer technique when low energy tracers are used. It should be emphasized that the radiotracer method and the magnetic susceptibility method for the external determination of saturation are the only volumetric methods reported to date. The resistivity method requires independent calibration for each core sample.[1] Linear absorption methods such as X-ray or gamma-ray absorption have been questioned[9,10] as to the uniqueness of their saturation indication when the core sample is undergoing successive saturation-desaturation experiments.

The simplicity of the magnetic susceptibility method is illustrated adequately by the schematic diagram shown in Fig. 2. With the present model of the transformer head, a slight drift in the voltage required to null the residual transformer unbalance necessitated nulling the instrument prior to each reading. Operation of the apparatus under conditions of controlled temperature and humidity was found to have no influence on the zero drift. The greatest utility of the magnetic susceptibility method would appear to be found in routine work where saturation profiles are not required. The data shown in Fig. 6 indicate that core samples as short as 1.5 in. could be used successfully. In the case of short core samples, saturation gradients due to fluid introduction and loss of capillary pressure at the output end of the sample are limiting factors.

The multiphase flow data reported herein using the magnetic susceptibility apparatus in the determination of liquid saturation are intended as a demonstration of the utility of the instrument. There are, however, several points of unusual behavior which warrant discussion. Relative permeability hysteresis was quite pronounced in the case of the alundum sample investigated and was accompanied by an inversion in the sign of the dynamic capillary pressure.* During the aqueous-phase desaturation portion of the flow cycle the dynamic capillary pressure exhibited a slight decrease with decreasing aqueous phase saturation, the absolute value at each point being lower than the corresponding value of the static capillary pressure. During the forced aqueous-phase imbibition portion of the flow cycle the pressure drop in the aqueous-phase was greater than that in the oil phase. Aqueous-phase permeabilities were greater at a given saturation in the imbibition (i.e., imbibition with respect to the aqueous phase) than those obtained in the desaturation portion of the flow cycle. Oil phase permeabilities, while exhibiting hysteresis effects, were normal in behavior. This behavior, together with the low oil-phase permeability at minimum aqueous-phase saturation, may be an indication of oil-wet surface properties for the particular alundum sample investigated. Low values of the dynamic capillary pressure as compared to static capillary pressure and apparent reversal of wetting properties of the two liquid-phases have been noted by other workers.[7]

Hysteresis was also noted in the relative permeability relationships for the natural sandstone core sample. In this case, however, aqueous-phase permeabilities decreased during the aqueous-phase imbibition portion of the flow cycle from those obtained during the first portion of the flow cycle. Dynamic capillary pressures were constant during any half flow cycle within the ability of the pressure sensing devices to resolve the small pressure differences between the oil and aqueous phases. Two repetitions of the flow cycle produced relative permeability values which are considered con-

*For the purposes of this paper the difference in pressure loss across the core sample in the oil and aqueous phases under equilibrium flow conditions is referred to as the dynamic capillary pressure. For a water-wetted porous material the dynamic capillary pressure is referred to as being positive in sign.

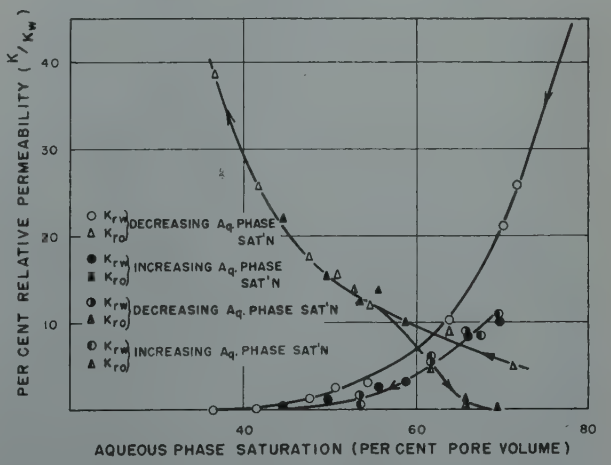

FIG. 8 — RELATIVE PERMEABILITY VERSUS AQUEOUS PHASE SATURATION SANDSTONE CORE SAMPLE NO. 2703.

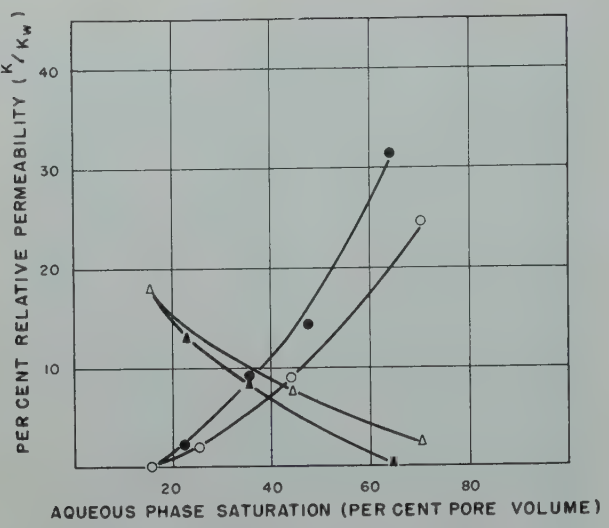

FIG. 9 — RELATIVE PERMEABILITY VERSUS AQUEOUS PHASE SATURATION ALUNDUM SAMPLE NO. 1427.

stant within the precision of the flow apparatus and magnetic susceptibility measurement. A slight decrease in the dynamic capillary pressure was noted during flow cycles following the initial aqueous-phase desaturation-imbibition cycle. There were, however, no corresponding differences in the relative permeability versus saturation relationships.

Use of the fluid distribution head illustrated in Fig. 7 makes possible the attainment of uniform saturation at a very short distance from the input end of the core sample. Microscopic examination indicated that less than ½ in. is required for "mixing" in the core sample. Maintenance of the required dynamic capillary pressure between the input phases should remove the possibility of "slug" flow encountered when the two fluids are introduced at the same pressure into a mixing head. Resolution of the change in sign of the dynamic capillary pressure in the case of the alundum sample is considered as further evidence that the distribution head functioned as anticipated.

In many cases the necessity for using a highly concentrated cobaltous chloride brine solution as the aqueous phase rather than a solution matching formation water in its composition may impose limitations on the applicability of the method. The natural sandstone sample used for relative permeability studies showed essentially no reduction in aqueous phase permeability from the air permeability value as shown in Table 2. In general, few complications should be encountered from swelling of the clay matrix using the tracer solution. The extent of changes introduced in the surface properties of natural core samples and the effects of such changes on the flow characteristics of the sample are not known at this time.

A more serious limitation on the use of the magnetic susceptibility apparatus concerns the use of core samples containing appreciable amounts of ferromagnetic materials. The Aris sandstone sample contained approximately the maximum amount of native magnetic materials which can be tolerated. The unbalance voltage indication for the dry unmounted core sample was 0.083 volts, approximately 30 per cent of the reading obtained when the sample was saturated with the tracer liquid. X-ray analysis of the core material indicated the presence of 0.7 per cent goethite.

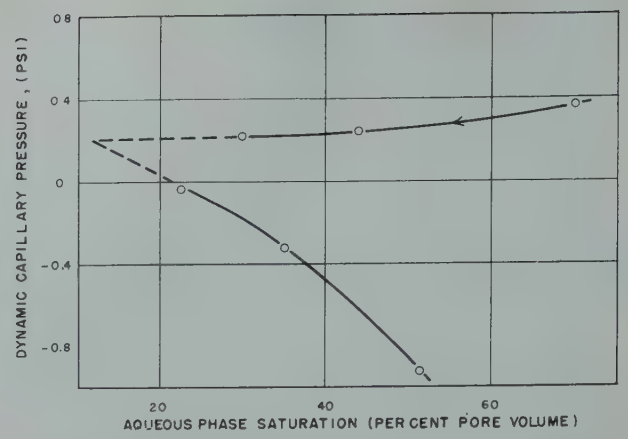

FIG. 10 — DYNAMIC CAPILLARY PRESSURE VERSUS AQUEOUS PHASE SATURATION ALUNDUM CORE SAMPLE NO. 1427.

CONCLUSIONS

A novel method of determining liquid saturation in a core sample using a magnetic tracer in the aqueous phase has been developed. The method is simple to operate and maintain and compares favorably with techniques currently practiced in the industry.

The utility of the method in the determination of liquid saturation values during oil-water relative permeability studies has been demonstrated. The method should be particularly applicable for routine studies.

ACKNOWLEDGMENT

Acknowledgment is made to the Magnolia Petroleum Co. for permission to publish the results of this work and to P. P. Reichertz who suggested the application of magnetic susceptibility techniques to the problem of fluid saturation determination in porous materials. Special thanks are due to C. W. Zimmerman for the construction of the transformer head used in these studies and for suggestions concerning the nulling circuit. The technical assistance of Karl Brockman, who performed much of the developmental work, is appreciated.

REFERENCES

1. Morse, R. A., Terwilliger, P. L., and Yuster, S. T.: *Producers Monthly* (1949), **11**, 19.
2. Boyer, R. L., Morgan, F., and Muskat, M.: *Trans.* AIME (1947), **170**, 15.
3. Morgan, F., McDowell, J. M., and Doty, E. C.: *Trans.* AIME (1950), **189**, 183.
4. Laird, A. D. K., and Putnam, J. A.: *Trans.* AIME (1951), **195**, 65.
5. Russell, R. G., Morgan, F., and Muskat, M.: *Trans.* AIME (1947), **170**, 51.
6. Coomber, S. E., and Tiratsoo, E. N.: *J. Inst. Pet.* (1950), **36**, 543.
7. Josendal, V. A., Sandiford, B. B., and Wilson, J. W.: *Trans.* AIME (1952), **195**, 65.
8. Brunner, E., and Mardock, E. S.: *Trans.* AIME (1946), **165**, 133.
9. Lipson, L. B.: *Trans.* AIME (1951), **192**, 375.
10. Geffen, T. M., and Gladfelter, R. E.: *Trans.* AIME (1952), **195**, 332. ★★★

USE of RADIOACTIVE IODINE as a TRACER in WATER-FLOODING OPERATIONS

J. WADE WATKINS
MEMBER AIME
BUREAU OF MINES
BARTLESVILLE, OKLA.

E. S. MARDOCK
MEMBER AIME
WELL SURVEYS, INC.
TULSA, OKLA.

T. P. 3894

ABSTRACT

The accurate evaluation of reservoir-performance characteristics in the secondary recovery of petroleum by water flooding requires use of a water tracer that may be injected into water-input wells and detected at oil-production wells to supplement data obtained from core analyses, wellhead tests, and subsurface measurements. Radioactive iodine has been used successfully as a water tracer in field tests to determine: (1) relative rates and patterns of flow of injected water between water-input and oil-production wells and (2) zones of excessive water entry into oil-production wells.

Laboratory evaluations of potential water tracers, previous tracer studies, the value of using a radioactive tracer, general field procedures, and the use of surface and subsurface instruments for the detection of the emitted gamma radiation, are summarized. Data from the field tests are presented graphically and discussed in detail.

It is concluded that the radioactive-tracer method, using radioactive iodine, may be used successfully to measure either the relative rates and patterns of flow or zones of excessive water entry into wells under conditions of comparatively rapid transit time between wells.

INTRODUCTION

Extensive use is made of data obtained from core analyses, wellhead tests, fluid characteristics, and subsurface measurements in evaluating the sweep efficiency of water injected into oil sands for the recovery of oil. Theoretical flow rates and patterns may be calculated from those data using radial-flow formulas, if it is assumed that the physical conditions in the productive formation are homogeneous. Unfortunately, homogeneous conditions rarely, if ever, exist in oil-productive formations. The use of a tracer that may be injected into an oil sand and detected quantitatively, or even qualitatively, at offsetting oil-production wells provides basic data that may be used in determining more accurately the subsurface rates and patterns of flow of injected water between wells than is possible by theoretical calculations based on assumed conditions. Consideration of the data obtained by using a water tracer assists in the application of remedial measures to water-input wells, such as plugging of channels, or selective plugging of highly permeable zones, thereby effecting a more uniform flood and a greater ultimate oil recovery.

A water tracer should have the following characteristics: (1) low adsorption on solid reservoir material; (2) high solubility in water; (3) low or negligible solubility in crude petroleum; (4) a wide range of solubility of compounds that may be formed by chemical reactions with ions present in reservoir rocks or waters; (5) high detectability in low concentrations by portable apparatus; and (6) general availability at low cost. Additional desirable characteristics are that the tracer should be nonhazardous in nature under normal working conditions and quantitatively detectable in the well bore, as well as at the surface.

Review of Previous Tracer Studies

The need for a water tracer has been recognized for many years. As far back as 1906, Dole[1] described the use of fluorescein in flow-rate studies made in France in 1901. In 1921, Ambrose[2] discussed in detail the use of organic and inorganic dyes, chlorides, nitrates, and other anions, lithium salts, and the Slichter electrical

[1]References given at end of paper.

Manuscript received in Petroleum Branch office Jan. 11, 1954. Paper presented at Annual AIME Meeting in New York City, Feb. 13-17, 1954.

method for tracing the underground flow of oil-field waters. More recently, several articles on the use of water tracers in oil production have been published. Sturm and Johnson[3] presented the results of field tests in Pennsylvania oil fields in which fluorescein, chlorides, and surface-active agents were employed as water tracers. Carpenter and others[4] discussed several field tests in Mid-Continent oil fields in which boron, as borax and boric acid, was used as a tracer. Quite recently, Garst and Wood[5] presented the results of experimental field tests in which stable (not radioactive) copper and iodide salts were used as flood-water tracers. In 1945, Plummer[6] discussed the general subject of water tracers, including many of those previously mentioned, as well as radioactive tracers.

Archibald[7] reported the results of surface flow tests made in 1949 in which radioactive iodine was used as a tracer in field tests. In 1950, Coomber and Tiratsoo[8] published the results of laboratory flow tests in which radioactive iodine was used as a tracer in the oil phase in laboratory flow tests. Several patents have been issued that bear on the injection of radioactive materials into water-input and oil-production wells for various purposes, such as those issued to French[9] in 1947, describing the use of a radioactive gas, and Hinson[10] in 1951, describing the use of radioactive gases, liquids, and solids for determining flow rates and patterns of fluids injected into subsurface strata. A patent also has been issued to Bond and Savoy[11] bearing on the use of acetylene as a tracer gas in both gas and water-injection operations.

Despite the attention evidenced in the subject by the above-cited references, nothing has been published concerning the successful or attempted use of radioactive water tracers in field secondary-recovery operations.

LABORATORY EVALUATION OF TRACERS

In July, 1947, a water-tracer study was started in the Bartlesville laboratories of the Bureau of Mines, but the study was temporarily discontinued in January, 1948. Several tracer substances were considered during this period, and field tests were made using the ammonium ion as a tracer. The results, however, were unsatisfactory because of the high concentration of ammonium ion in many produced waters. Laboratory tests were made with fluorides with inconclusive results. At the time the study was discontinued, the expressed opinion of the chemist in charge of the work was that radioactive tracers appeared to offer the greatest promise.

A radiochemical laboratory was completed, and the tracer study was resumed in 1951. Numerous selected substances were tested to determine their adsorption characteristics by passing "slugs" of the material in water through long, consolidated sandstone cores, sealed in plastic, and measuring quantitatively the tracer in the effluent fluid. Substances for tests were selected primarily on the basis of the solubility of their common compounds and secondarily on the basis of expected low adsorption characteristics. Fluorescent dyes were among the tracers tested and, like several other substances, were found to be highly adsorbed in the cores. It was concluded that fluorescent dyes, such as fluorescein, were useful for tracers only when it was known or suspected that channels or fractures existed between wells. One of the materials selected as a potential water tracer was iodine as the iodide ion. All of the laboratory evaluation tests were made with stable rather than radioactive isotopes, and standard methods of quantitative analysis were used.

It was believed that radioactive tracers would be superior to stable ones because: (1) they may be easily detected in low concentrations; (2) they may be detected by subsurface instruments if the emitted radiation is gamma or hard beta; and (3) the necessary radiation-detection equipment may be made portable.

Consequently, instruments were assembled, and the necessary permission was obtained from the Atomic Energy Commission to make field tests using radioactive iodine (iodine 131) as a water tracer.

GENERAL FIELD PROCEDURES

All field radioactive-tracer tests described herein were made by the Bureau of Mines in cooperation with Well Surveys, Inc., Tulsa. Under the existing cooperative agreement the Bureau of Mines has procured and injected the radioactive iodine used as the water tracer and made all surface measurements of radioactivity. Well Surveys, Inc., has made all subsurface gamma-ray and neutron logs and radioactivity input-profile logs on water-input wells.

Before a location was selected for a field tracer test, all available information concerning the wells and reservoir characteristics and performance was evaluated. Injection rates and pressures on water-input wells were examined to determine anomalous conditions thereby indicated, such as abnormally high injection rates or low injection pressures.

The first step in the field tests was to obtain a water-input profile on the well selected for tracer injection by the use of the Well Surveys, Inc., radioactivity input-profile method. If caliper measurements were not available on the holes used in the tracer tests, those measurements were made (especially if the sand had been shot) as part of the profile measurement and to assist in the interpretation of radioactivity logs.

Standard gamma-ray and neutron logs were made on the input well as well as on all production wells at which the tracer might appear, using conventional gamma-ray and neutron ionization-chamber instruments. This equipment is the same as that used commercially by the licensees of Well Surveys, Inc. These logs correlated the lithology of the formation with core-analysis data and provided the necessary background information for the tracer surveys.

If the data available indicate that the water is passing rapidly from the input to the production wells, it may be advisable to make a dye-tracer test before injecting the radioactive tracer. The purpose of this test in the Bureau of Mines field work was to determine the approximate transit time from the water-input well to the production wells. This information permitted scheduling arrival of the gamma-ray logging crew at a time that would permit locating the subsurface logging instrument in the borehole of the production well at which the tracer first appeared without excessive waiting. Also, the positive appearance of dye tracer at production wells confirmed the existence of channels and simplified calculation of the quantity of tracer needed and the optimum injection time of the tracer slug.

Both the dye tracer and the radioactive iodine tracer were injected into the head of the input well while normal injection rates and pressures were maintained.

The injection device employed a chamber containing a free-floating piston, which was moved hydraulically, confining all contamination to the chamber and piping manifold. The usual injection rate of tracer was about 3.8 liters (1 gal.) in 15 minutes.

Radioactivity of the fluids produced from all production wells at which the tracer might appear was continuously monitored by the use of gamma-sensitive Geiger-Mueller tubes inserted vertically into each wellhead or lead line. The tubes, made in the Bureau of Mines radiochemical laboratory at Bartlesville, were 1¼-in. in diameter, had an effective bismuth cathode length of about 12 in., and were filled with an argon-ethyl formate gas mixture. The tubes were equipped with a standard 1½-in. pipe-thread adapter that permitted screwing them directly into a pipe fitting. The output pulse from each tube went into a counting-rate meter, and the signal from the counting-rate meter was fed into a strip-chart recorder. Thus, a continuous recording was made of the radioactivity background of produced fluids at production wellheads.

Liquid samples were taken at random intervals from each of the wellheads until the recorded radioactivity increased significantly above background. Thereafter, samples were taken at frequent intervals. The radioactivity of the water separated from the liquid samples was measured with a conventional dipping-type Geiger-Mueller tube and scaler to provide more accurate measurements.

Before the anticipated time for the tracer to reach the borehole of the first production well the subsurface gamma-ray logging instrument was positioned opposite the productive formation in that well. Numerous gamma-ray logs of the well borehole were made as the radioactive tracer was produced into the hole with water. In this manner, the zones through which the water was moving most freely were clearly defined.

POTENTIAL HEALTH HAZARDS FROM THE USE OF RADIOACTIVE MATERIAL

Although some hazard to health always is present when radioactive material is used, careful and proper handling techniques and rigid personnel monitoring reduced the potential health hazard in field operations to a negligible level. The greatest concentration of radioactive material handled was at the water-input well. As soon as the tracer entered the input well, it was diluted to a great extent before its reappearance.

The use of proper techniques, adequate shielding, film badges and pocket chambers, and constant monitoring with survey meters guarded field personnel against overexposure to radiation. The quantities of radioactive iodine handled in laboratory and field tests ranged from 1 to 250 millicuries. In no field test made was the radiation level of containers in which produced brine carrying radioactive tracer was stored, above tolerance.*

The maximum permissible level of iodine 131 in the body, with maximum concentration in the thyroid, is given by the National Bureau of Standards[12] as 0.3 microcurie, and the maximum permissible level in liquid media for continuous exposure as 3×10^{-5} microcuries/ml. No hazardous concentration of iodine 131 was available for human or livestock consumption in any of the field tests, as produced brine containing greater than the cited permissible concentrations was routinely diluted in surface storage ponds to a low level of concentration. Although the contamination of surface equipment by radioactive iodine was guarded against, the short half-life (eight days) was considered an advantage from the standpoint of the rapid decay of active material. However, the comparatively short half-life limits the use of radioactive iodine as a flood-water tracer to situations when passage of injected water between wells may be expected within about four half-lives, or four to five weeks.

*Tolerance dose usually is expressed as 0.3 roetgen equivalent physical per week, or 7.5 milliroentgen equivalent physical per hour, based on a 40-hour work week.

RESULTS OF FIELD TRACER TESTS

Test A

Field tracer test A was made on an inverted five-spot where excessive water was produced at two wells and an undesirably high ratio of water to oil was produced at the other two wells. Production data indicated that there was a direct channel from southwest to northeast, connecting the input well with the two production wells having the highest water-oil ratios. Fluorescein was injected into the input well to confirm the presence of this channel and to establish transit time between wells. No fluorescence was detected, however, in water from any of the production wells over a period of two weeks. Radioactive tracer tests then were made by injecting radioactive iodine in quantities of 1, 25, and about 85 millicuries* in three successive tests to determine the optimum quantity of tracer material needed.

Slight increases in the radioactivity of water produced from one of the wells were observed in each of the three tests. However, these increases were small, of short duration, and were not proportional to the quantities of radioactive material injected. In no instance was it possible to get the gamma-ray logging instrument into a well soon enough to detect any significant increase in the radioactivity of the water entering the well. One of the production wells in the inverted five-spot had not been reworked when the flood was started and did not have pipe cemented at the top of the production formation, and the pipe was not continuous throughout the borehole. It was concluded that most of the tracer was lost through that well to upper, permeable formations, through which the water was escaping from the immediate vicinity. Figures on fluids injected and produced tended to confirm this conclusion. Injectivity-index data obtained indicated that the loss of water may have been caused in part by operation of the project at pressures high enough to increase the bypassing potential between wells.

Test B

Field tracer test B was made in Nowata County, Okla., on a water-flooding project that was near the economic limit of production by conventional water flooding. Production was from the Bartlesville sand, which in the area of the test is 510** ft deep. The wells involved in the test were completed with about 45 ft of oil sand exposed.

*One millicurie is equal to 3.7×10^7 disintegrations per second. All activity values given in this paper are corrected for decay to injection time.

**All depths given are from the surface.

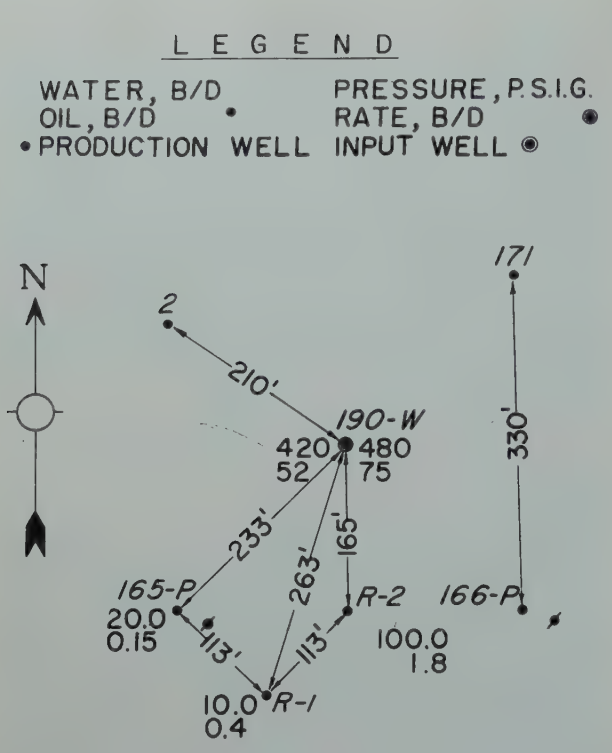

FIG. 1 — LOCATIONS OF WELLS IN FIELD RADIOACTIVE-TRACER TEST B, NOWATA COUNTY, OKLA.

Fig. 1 shows the locations of, and distances between, wells involved in the test and pertinent wellhead data. Well R-2 had been drilled a few months earlier, midway between two water-input wells, and Well R-1 midway between a water-input and an oil-production well to determine the residual-oil saturation of the sand. As indicated on Fig. 1, the daily production from Well R-1 at the time of the tests was 10.0 bbls of water and 0.4 bbl of oil, or a water-oil ratio of 25:1; from Well R-2, 100.0 bbls of water and 1.8 bbls of oil, or a water-oil ratio of 56:1; and from Well 165-P, 20.0 bbls of water and 0.15 bbl of oil, or a water-oil ratio of 130:1. The excessive water production from wells R-1 and R-2 suggested that there was channeling of water from water-input Well 190-W. Flow-rate tests were made on Well 190-W by the operating company, using anchor packers to isolate the zones tested. The results of those tests indicated that most of the injected water was leaving the well at a depth of approximately 520 ft. As 2-in. tubing was cemented in that well, it was not possible to obtain gamma-ray logs or to make radioactivity input profiles of the well with the equipment then available. However, subsequent input-profile tests by the operating company confirmed the information obtained from the flow-rate tests.

A solution containing 8 oz of fluorescein was injected into input Well 190-W over a period of 15 minutes in about 0.36 bbl of water. Dye was detected in the water produced from Well R-2 after about 11 hours, or after the injection of approximately 16 bbls of water into Well 190-W and the production of approximately 28 bbls of liquid from Well R-2. No fluorescence was detected in the water produced from wells R-1 and 165-P. Production of the dye at Well R-2 confirmed the presence of the suspected channel between wells.

A solution containing approximately 87 millicuries of iodine 131 was injected into input Well 190-W over a period of 15 minutes in about 1 bbl of injection water. The rate of water injection into Well 190-W had been increased since the dye-tracer test. Increased radioactivity was detected in the well bore of Well R-2 2¾ hours after tracer injection, during which time 11 bbls of water was injected into Well 190-W. From the height of the radioactive liquid in the well tubing when the first log was made, it appeared that the tracer had reached the well bore after an elapsed time of about two hours. Increased radioactivity was detected at the surface in the liquid produced from Well R-2 4½ hours after tracer injection, during which time about 19 bbls of water was injected.

The increased radioactivity of water produced into Well R-2, as compared to the gamma-ray background, is shown in Fig. 2. As indicated, the recorded increase in gamma radiation, after three hours and 15 minutes (log 2) showed that water was coming into the hole in quantity at a depth of 520 ft. Radioactivity was high from 497 to about 520 ft, declined, and was high again from about 491 to 494 ft, or just under the pipe seat.

Subsequent logs made at 30-minute intervals (logs 3 and 4) showed that the activity of the water produced into the hole at a depth of 520 ft decreased while that of the water produced at about 491 ft increased. Also, in the later logs it was shown that the principal zones of water entry within the 497 to 520-ft zone were at about 506 and 514 ft. Log 5, made the following day, showed that a greater zone of activity was present behind the pipe, at about 487 ft, than at any other point in the well. This indicates that the upper zone of transmission may have been at that vertical point and that some residual radioactivity was present because of partial adsorption.

From the time that increased radioactivity was detected in water produced from Well R-2, the radioactivity of samples of water obtained at that wellhead increased sharply and reached a peak at about seven hours after tracer injection, as shown in the plot of radioactivity in Fig. 3. Radioactivity of the produced water decreased rapidly during the next three hours, and more gradually thereafter. Samples of the water

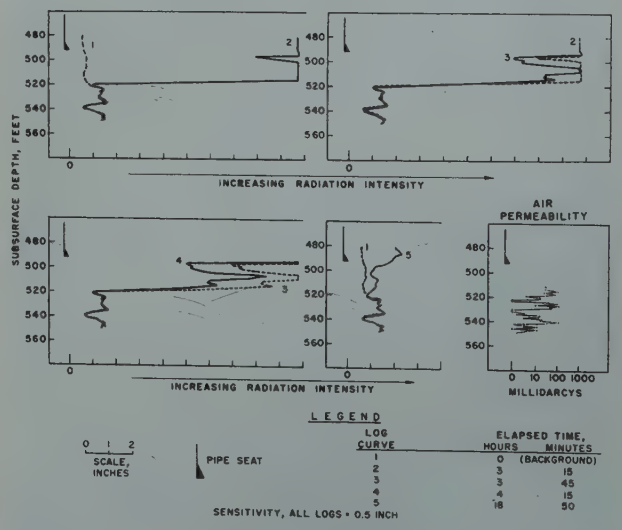

FIG. 2 — GAMMA-RAY BACKGROUND, WATER-PRODUCTION, AND AIR-PERMEABILITY LOGS, PRODUCTION WELL R-2, FIELD RADIOACTIVE-TRACER TEST B, NOWATA COUNTY, OKLA.

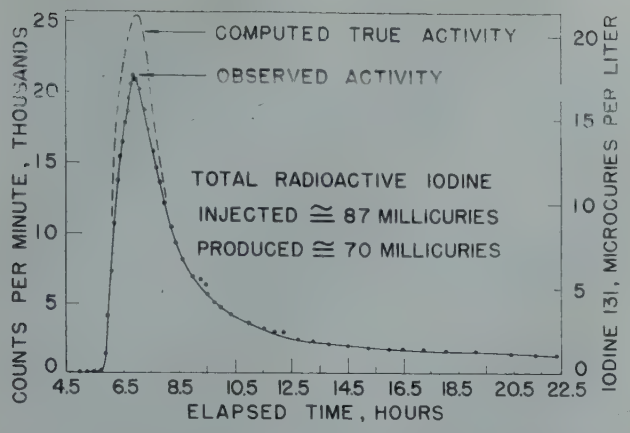

FIG. 3 — RADIOACTIVITY ABOVE BACKGROUND OF WATER FROM PRODUCTION WELL R-2, FIELD RADIOACTIVE-TRACER TEST B, NOWATA COUNTY, OKLA.

produced from Well R-2 still had some significant activity above background 12 days after tracer injection.

All determinations of the radioactivity of produced water were made by counting liquid samples, using a conventional scaling unit and a bismuth-cathode tube having a high sensitivity to the gamma radiation from iodine 131. Integration of the activity detected in water produced from Well R-2 showed that approximately 70 millicuries, or about 80 per cent of the total iodine injected entered that well. The higher observed radioactivity values determined on samples of produced water, as shown on Fig. 3 from about 11,000 to 21,000 counts per minute, were subject to error because the resolving time of the counter did not permit counting all of the pulses in that range. Corrections made for counts missed, based on the known resolving time of the counter, were added to the observed radioactivity and plotted as shown to indicate the true radioactivity of the samples.

A slight increase in radioactivity of the water produced from Well R-1 was detected about 72 hours after tracer injection; however, the peak was low in magnitude, and the rate of radioactivity decrease was much more rapid than that of the water from Well R-2. No significant increases in radioactivity were detected in the water produced from any of the other four wells likely to have been affected. At the time R-1 was relogged, several hours after the slight radioactivity increase was observed, the radioactivity had declined in the sand section to a point where no increase above background was detectable.

The data obtained show that water was transmitted directly from input Well 190-W to production Well R-2 through one or two channels at a depth of about 520 ft. Water also was being produced into the well from behind the pipe, at the pipe seat, possibly through a zone at a depth of about 487 ft. The production of the water from two zones into the production well suggested the presence of a vertical fracture in the formation between the wells. Knowledge of such a fracture would be important in planning remedial work, such as selective plugging. The fact that some tracer was found in water from Well R-1 indicates that the channel from 190-W to R-2 may have been continuous, either from 190-W to R-1 over a distance of 263 ft, or from 190-W to R-1 via R-2 over a distance of about 278 ft.

TEST C

The third field radioactive-tracer test was made on an inverted, elongated, irregular five-spot in a shoestring field in Anderson County, Kans., where oil was produced from a Bartlesville sandstone. The top of the production formation ranged in depth from 774 to 791 ft, and sand thicknesses ranged from 25 to 42 ft in the immediate vicinity. The locations of, and distances between, wells affected by the test and pertinent wellhead data are shown in Fig. 4. Production Well G-17 was drilled as a core-test well and later was utilized as a production well. Production wells H-16 and F-16 were old wells; H-14 and F-14 and input Well G-15 were new wells. Excessive water was being produced at wells H-16 and F-16 and, to a lesser extent, at wells H-14 and F-14.

The rate of water production at Well H-16 alone was greater than the rate of injection into input Well G-15; therefore, this input well alone could not be considered responsible for the excessive water production. Wellhead injectivity-index tests were made and pressure-decline rates were determined on several water-input wells in the general area. The results of those tests indicated that the performance of Well G-15 was abnormal and that this well might be the major cause of the high water-production rate at Well H-16, as well as at the surrounding wells. The fact that Well G-17, almost in a direct line between input Well G-15 and Well H-16, did not produce water in appreciable quantity led to the conclusion that a channel, or zone of very high permeability existed between wells.

A dye-tracer test was made to confirm the existence of such a zone and to establish transit time between wells. A solution containing 8 ozs of fluorescein was injected into input Well G-15 over a period of 15 minutes, with approximately 0.7 bbl of water. Liquid samples were obtained from all five production wells each two hours for the next three 24-hour periods and each day for the following week, and the separated water was examined for fluorescence. The first fluorescence was detected in water produced from Well H-16 58 hours after tracer injection, during which time about 162 bbls of water had been injected into Well G-15 and about 261 bbls of liquid had been produced from Well H-16. The fluorescence of the water had a peak intensity of 0.5 ppm and was present for at least two weeks. The first fluorescence was detected in water produced from Well F-16 after about seven days at a

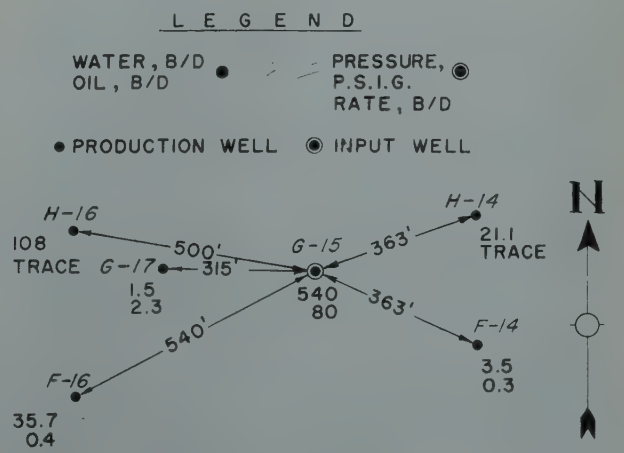

FIG 4 — LOCATION OF WELLS ON FIELD RADIOACTIVE-TRACER TEST C, ANDERSON COUNTY, KANS.

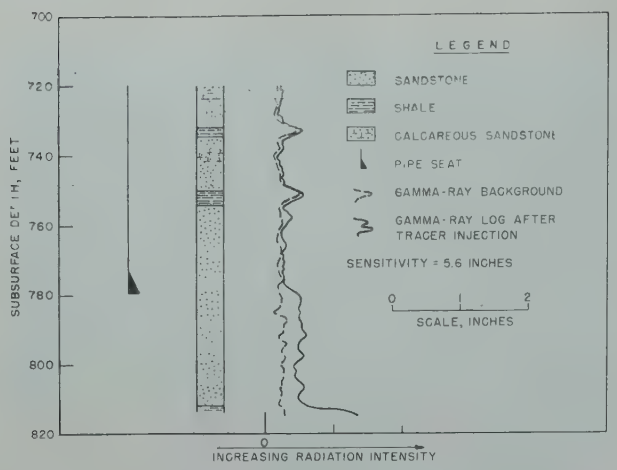

FIG. 5 — LITHOLOGY, GAMMA-RAY BACKGROUND, AND INPUT-PROFILE LOGS, WATER-INPUT WELL G-15, FIELD RADIOACTIVE-TRACER TEST C, ANDERSON COUNTY, KANS.

maximum concentration of less than 0.5 ppm and fluorescence in that water decreased rapidly. No fluorescence was detected in water produced from wells H-14, F-14, and G-17.

After completion of the dye-tracer tests, standard gamma-ray and neutron logs were made on all wells involved in the tracer test. A radioactivity input profile also was determined on input Well G-15. The lithology of the hole as interpreted from standard gamma-ray and neutron logs and a log of the input profile are shown in Fig. 5. Increased radioactivity at the principal points of exit of water from the well bore is shown as compared to the gamma-ray background caused by naturally radioactive material in the formation. Although upper sections of the formation are shown to be taking some water, the principal point of water exit is shown to be at the bottom of the hole, or from about 811 to 814 ft. Minor zones of water exit were indicated at about 798 and 807 ft.

After the input profile was determined, a solution containing 44 millicuries of iodine 131 was injected into input Well G-15 over a period of 15 minutes with approximately 0.8 bbl of water. The injection rate into Well G-15 at that time was 88 bbls daily, as compared to 67 bbls daily at the time of the dye-tracer test.

Wells H-16, F-16, and H-14 were monitored continuously in the manner previously described to determine the radioactivity of produced fluids during the next eight days. No instruments were available for use in wells F-14 and G-17. However, little water was produced at those wells during the tracer test. Liquid samples were taken from all wellheads at random intervals until the radioactivity of the produced fluids increased significantly above background; thereafter samples were taken regularly at frequent intervals. At no time during the tests was any significant increase in radioactivity noticed in the water produced from wells F-14 and G-17.

Gamma-ray logs reproduced in Fig. 6 illustrate the rate of production of the tracer into Well H-16, as indicated by increases in radioactivity above background. The first increase in radioactivity of produced water at the surface was observed about 32 hours after tracer injection. Transit time of the fluid from the well bore to the surface was calculated to be about two hours and 48 minutes; consequently, the first entry of radioactive water into the well bore probably occurred after about 29 hours. However, the first log showing entry of radioactive material into the well bore was not made until 49 hours and 20 minutes after tracer injection. The difference in transit time between wells with dye and radioactive tracers in this instance, as well as in test B, is believed to have been caused primarily by increases in injection rates and secondarily by partial adsorption of the fluorescent dye.

The zones of water entry into Well H-16 on the first log made after tracer injection (log 2) were at 815 ft and at 823 ft. As shown in logs 3, 4, and 5, the radioactivity at 815 ft decreased, and the radioactivity of the water coming into the hole at the 823-ft level and at about 829 ft increased. These data show that water was entering the hole through three zones, two of which were within 9 ft of the bottom of the well.

The first log of Well F-16, after surface detection of a radioactivity increase, was made 118 hours and 30 minutes after tracer injection. Surface radioactivity recordings indicated that the radioactive tracer was present about 10 hours earlier. Although some slight indications of increased radioactivity were logged at depth intervals of 792-4 and 803-6 ft, repeated logs on this well showed that the greatest amount of the tracer material entering the well was coming in at the bottom, or at about 830 ft as shown in Fig. 7.

The radioactivity of the fluids produced from wells F-16, H-16, and H-14, as recorded at the surface, is illustrated in Fig. 8. The first increase in recorded radioactivity of fluids from Well H-16 occurred about 32 hours, and a peak of activity was reached about 46 hours after tracer injection. A second well-defined peak was recorded 78 hours, and a third, lower peak about 108 hours after tracer injection. The appearance of these peaks of activity at the surface correlates fairly well with the maximum intensity of detected subsurface radioactivity from the three zones of maximum production.

Again, in the recorded radioactivity of Well F-16, three peaks of less magnitude may be seen. The first occurred after 108 hours, the second after 132 hours, and the third after 170 hours' elapsed time.

Although the recorded radioactivity of fluids produced from Well H-14 also shows three peaks, anomalies are exhibited as follows: (1) the peaks are in

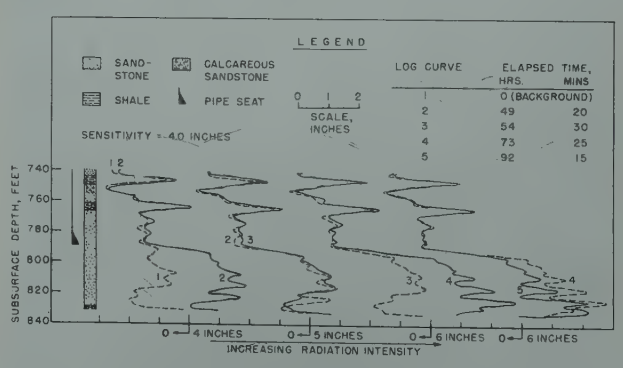

FIG. 6 — LITHOLOGY, GAMMA-RAY BACKGROUND, AND WATER-PRODUCTION LOGS, PRODUCTION WELL H-16, FIELD RADIOACTIVE-TRACER TEST C, ANDERSON COUNTY, KANS.

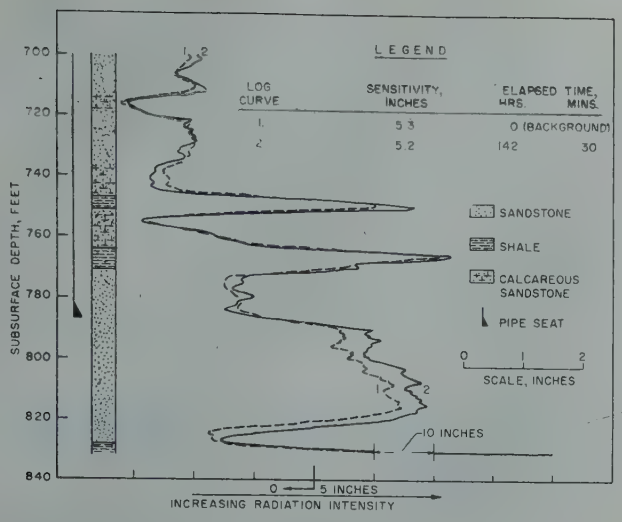

FIG. 7 — LITHOLOGY, GAMMA-RAY BACKGROUND, AND WATER-PRODUCTION LOGS, PRODUCTION WELL F-16, FIELD RADIOACTIVE-TRACER TEST C, ANDERSON COUNTY, KANS.

reverse order of magnitude to those obtained on records of the radioactivity of water produced from other wells; (2) the maximum activity recorded was much higher than that on the other two wells; and (3) the decrease of radioactivity in each instance was quite rapid.

The first peak was recorded after 134 hours, the second after 158 hours, and the third after 182 hours' elapsed time. The high magnitude and short duration of the activity recorded suggests that concentrated slugs of radioactive water were produced at intervals from three highly permeable zones. It is conceivable that the production of tracer slugs of increasing magnitude might occur if the zones of transmission had different permeabilities and thicknesses. It was not possible to obtain subsurface radioactivity logs in this well after the appearance at the surface of increased radioactivity.

Conclusions drawn from the third field test follow: (1) excessive water production in the wells considered was caused by the rapid travel of injection water through highly permeable zones, sand-shale contacts, or fractures near the bottoms of the completed wells; (2) the zones were continuous between wells and the zone of maximum water transmission was shown at or near the bottoms of the wells, with other zones indicated within 10 ft of the bottoms; (3) plugging back of wells, or selective plugging of the "loose" zones should materially decrease water production and increase oil production on the property; and (4) the peaks of surface recorded radioactivity were caused by the production of water, in varying quantities, through three zones of high permeability or channels having different capacities for water transmission.

CONCLUSIONS

General conclusions concerning the practicability of using a radioactive water tracer and the particular advantage of using radioactive iodine may be drawn from the results of the field tests performed to date, as follows:

(1) The radioactive water-tracer method is considered to be superior to a method using a stable tracer

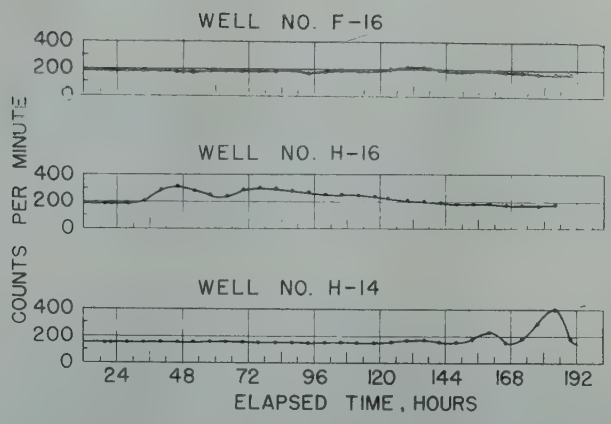

FIG. 8 — RECORDED RADIOACTIVITY OF WATER FROM PRODUCTION WELLS, FIELD RADIOACTIVE-TRACER TEST C, ANDERSON COUNTY, KANS.

because the radioactive method may be used successfully:

(a) To locate vertically channels or highly permeable zones extending between wells within an oil-productive formation; and

(b) To define horizontally the areas of greatest comparative permeability to water within a field or lease.

(2) Radioactive iodine is a satisfactory tracer material to use in the method because it has most of the characteristics of an ideal water tracer, namely:

(a) The loss of iodine, as iodide, through adsorption on reservoir solids is low as compared to other potential tracer substances;

(b) Iodide remains preferentially soluble in water and insoluble in oil during the progress of a tracer test;

(c) The possibility of an insoluble iodine compound being formed and precipitated in the oil-productive formation with consequent loss of tracer material is remote;

(d) The cost of using radioactive iodine as a tracer in the quantities normally required is not prohibitive;

(e) Radioactive iodine is readily and routinely available through the Atomic Energy Commission if adequate facilities for handling and personnel monitoring are available by the user; and

(f) Radioactive iodine, because of the intensity of the emitted gamma radiation, is easily detectable in small concentrations, both on the surface and in bore holes, by the use of standard, portable instruments.

(3) The short half life of artificially radioactive elements gives them a great advantage over the long-lived naturally radioactive elements previously considered for this and similar tracer applications because:

(a) The formations are not permanently contaminated and accordingly standard radioactivity well logs may be run on the wells involved in a tracer survey after a relatively short waiting period, and

(b) The personnel hazard is greatly reduced because any contamination of surface equipment re-

maining following decontamination procedures will decay to the vanishing point.

(4) The only disadvantage of using radioactive iodine as a water tracer is the very short half-life which limits its use to conditions where the transit time of injected water between wells is no longer than four to five weeks. It is believed that other radioactive isotopes may be used for conditions of longer transit times.

ACKNOWLEDGMENT

The authors are grateful to the following persons for constructive criticism of, and suggestions pertaining to, this paper: J. H. Buck and R. K. Schumacher, Well Surveys, Inc., and D. B. Taliaferro and R. Vincent Smith, Bureau of Mines. The cooperation of supervisory and field personnel of the Deep Rock Oil Corp. and Sinclair Research Laboratories, Inc., in providing properties, facilities, and data for the study, especially is acknowledged.

REFERENCES

1. Dole, R. B.: "Use of Fluorescein in the Study of Underground Waters," Water Supply Paper 160, U. S. Geological Survey, (1906) 76.
2. Ambrose, A. W.: "Underground Conditions in Oil Fields," *Bull.* 195, Bureau of Mines, (1921) 106.
3. Sturm, P. W., and Johnson, W. E.: "Field Experiments with Chemical Tracers in Flood Waters," *Producers Monthly* (December, 1950) **15**, 11.
4. Carpenter, P. G., Morgan, T. D., and Parsons, E. D.: "Boron Compounds Used as Water-Flood Tracers," *World Oil* (April, 1953) **136**, No. 5, 214.
5. Garst, A. W., and Wood, B. B.: "Field Tests of Copper and Iodide Salts as Water Flood Tracers," presented, Seventh Tri-Sectional Meeting, Amer. Chem. Soc., Bartlesville, Okla., Oct. 17, 1953.
6. Plummer, F. B.: "Tracing Flow of Fluids and Gases Beneath Ground," *Oil and Gas Jour.*, (Sept. 29, 1945) **44**, No. 21, 141.
7. Archibald, R. S.: "Radioactive Tracers in Flow Tests," *Jour. Boston Soc. Civil Eng.*, (1950) **37**, 49.
8. Coomber, S. E., and Tiratsoo, E. N.: "The Application of Radioactive Tracer Techniques to the Study of the Movement of Oil in Sands," *J. Inst. Pet.*, (September, 1950) **36**, 543.
9. French, R. W., Jr.: "Method for Determining Fluid Conductance of Earth Layers," U. S. Letters Patent 2,429,577, Oct. 21, 1947.
10. Hinson, H. H.: "Method of Determining Path, Rate of Flow, Etc., in Earth Strata," U. S. Letters Patent 2,560, 510, July 10, 1951.
11. Bond, Donald C., and Savoy, Michael: "Method of Studying Earth Formations Employing Acetylene as a Tracer Gas," U. S. Letters Patent 2,589,219, Mar. 18, 1952.
12. "Maximum Permissible Amounts of Radioisotopes in the Human Body and Maximum Permissible Concentrations in Air and Water," Handbook 52, National Bureau of Standards (1953). ★ ★ ★

SOLUTION of the EQUATIONS of UNSTEADY STATE TWO-PHASE FLOW in OIL RESERVOIRS

W. J. WEST
W. W. GARVIN
CALIFORNIA RESEARCH CORP.
LA HABRA, CALIF.

J. W. SHELDON
SCIENTIFIC COMPUTING SERVICE
INTERNATIONAL BUSINESS MACHINES CORP.
NEW YORK, N. Y.

T. P. 3892

ABSTRACT

One of the most important problems of reservoir mechanics is the prediction of the behavior of a gas and oil producing reservoir for a variety of production programs. In the absence of a knowledge of the behavior of even idealized systems, it has been difficult, if not impossible, to determine which production program would yield maximum economic recovery. The problem was formulated mathematically many years ago, but a solution of the equations had never been obtained because of their extreme complexity. The solution of the problem became possible, however, with the advent of modern computing machines.

This paper describes a digital method of solving the problem and discusses some of the results which have been obtained to date. The IBM Type 701 Electronic Data Processing Machines located at IBM's New York Scientific Computing Service were used successfully to perform the computations.

The flow of gas and oil through a reservoir can be described mathematically by two second-order, nonlinear partial differential equations which must be solved simultaneously. All derivatives were replaced by finite differences to bring the equations into a form suitable for digital calculations. A number of finite difference formulations were investigated and one form was found which resulted in stable, convergent solutions. This form was used to obtain solutions for both radial and linear systems producing by solution gas drive.

The results presented in this paper are: (a) saturation profile within the hypothetical reservoir vs. time, (b) pressure profile within the hypothetical reservoir vs. time, (c) gas-oil ratio vs. cumulative recovery, and (d) ultimate recovery. The saturation profile clearly shows the effect of critical gas saturation. The saturation near the wellbore drops quickly to the critical gas saturation and remains essentially at that value until the remainder of the reservoir also has dropped to the critical gas saturation. The pressure profile shows a smooth variation of pressure across the reservoir. The gas-oil ratio drops slightly during the early stage of production until the critical gas saturation is reached, rises rapidly from then on and eventually passes through a sharp maximum just before the economic limit of production is reached. For the radial example presented in this paper, the average oil saturation of the reservoir at a time corresponding to the limit of economic production was 56.5 per cent and the ultimate recovery was 6.86 per cent. The difference between change in saturation and ultimate recovery is caused by shrinkage of the oil phase.

The solution time with the 701 Computer is sufficiently short to permit an economically feasible investigation of the effects of variation of the many parameters which describe an oil reservoir. In particular, the ultimate recovery for various systems can be determined as a function of rock and fluid properties, of well spacing, and of production rate.

INTRODUCTION

The effective planning for maximum economic depletion of oil reservoirs is one of the major problems confronting oil producers. The most important part of the planning is prediction of the response of the oil reservoir to a particular production program. The production program can be selected by imposing certain controls available to the operator. Some of these controls are: (a) well spacing, (b) production rate, (c) time

[1]References given at end of paper.

Manuscript received in the Petroleum Branch office Aug. 6, 1953. Paper presented at Petroleum Branch Fall Meeting in Dallas, Oct. 19-21, 1953.

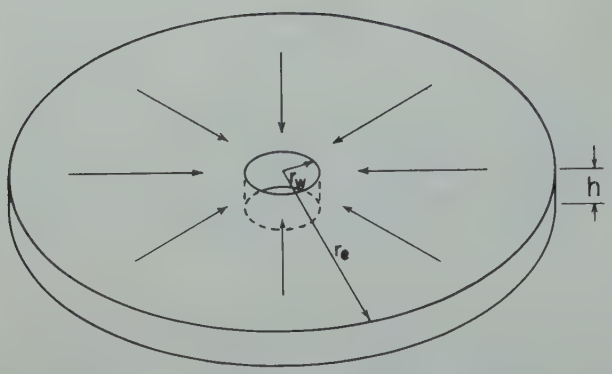

FIG. 1 — GEOMETRY OF RADIAL SYSTEM.

and kind of fluid injection programs, and (d) well completion and well rejuvenation practices. These four controls affect the distribution of the fluids within the reservoir during production. If the values of saturation and pressure of gas and oil throughout a reservoir could be predicted as a function of time for any production program, the one particular program could be selected that would give the maximum economic recovery of oil for a given reservoir.

The response of any one reservoir will depend on the physical properties of the reservoir and these properties can vary considerably from one oil field to another. The physical properties affecting oil recovery are viscosity and density of fluids as a function of temperature and pressure, porosity and permeability of the formation, relative permeability of the formation to each phase as a function of saturation, interfacial tension between phases, and reservoir dip. The problem is to find the controls that would give the maximum economic recovery for each reservoir with its particular physical properties. One method of determining the optimum controls would be to produce repeatedly a particular reservoir, restoring it to its original state after each run, and then selecting the controls giving maximum economic recovery. Such a method, however, is not only impractical but is impossible and other methods of solution of the problem must be sought. The best method for solving the problem is the mathematical method, whereby many solutions can be obtained for hypothetical reservoirs under a variety of different physical conditions and production programs. A major difficulty in the mathematical approach lies in the fact that the phases (such as gas and oil) within the reservoir interact with each other during the production period to such an extent that an analytical solution, at present, is not feasible. With the advent of modern computing machines, however, numerical solutions to the problem became possible.

The problem must first of all be somewhat idealized before the mathematical method can be applied. A typical oil reservoir with irregular boundaries and irregularly spaced wells constitutes a formidable problem for the mathematical approach. It is best to consider at first the simultaneous flow of gas and oil from a radial system as shown in Fig. 1. The quantity r_w is the radius of the well, r_e is its effective drainage radius, and h is the thickness of the producing sand. The idealized reservoir is considered to be composed of a number of such identical units spaced a distance $2r_e$ between centers. This is a fair approximation to a five spot pattern. Specifically, the term "two-phase flow problem" as used in this paper refers to the study of simultaneous flow of gas and oil within the system shown in Fig. 1 subject to the conditions that no fluid crosses the outer boundary and that either the oil production rate or the pressure at the wellbore is a prescribed function of time.

The first attempt to obtain solutions of the two-phase flow problem by numerical integration of the equations was made by Muskat in 1936.[1] As automatic electronic computers were nonexistent at the time, the tedious calculations were performed with a desk calculator. The time required per solution was prohibitive from an economic point of view and precluded a thorough investigation of the effects of all the pertinent parameters. At a later date[2] (1949) Muskat pointed out that his method was crude and that the results had to be subjected to considerable smoothing, guided only by physical intuition.

The next advance was made by Terwilliger et al in 1951.[3] IBM punched card equipment was used to solve a gravity drainage problem but many of the nonlinear features of the two-phase flow equations were neglected.

Bruce et al in 1953[4] investigated the problem of linear and radial unsteady-state gas flow through porous media. They considered only the nonlinearity introduced by the dependence of gas density on pressure as given by Boyle's Law (which holds rigorously only in the low-pressure region) and neglected the variation of gas viscosity with pressure. Their results cannot be applied to oil reservoirs because of the interaction between the gas and liquid phases.

Several years ago, a study of the application of computing machines to production problems was initiated at the California Research Corp. The results of this study showed that either an analog or a digital method could be employed for solution of the two-phase flow problem. The analog method required construction of a special computer because no existing analog computer installation, to our knowledge, contained the proper proportion of components. The digital method required a computer of extremely high speed and large memory capacity. Such a digital computer was developed and made available to industry by the International Business Machines Corp. in April, 1953. These computers are called the Type 701 Electronic Data Processing Machines.

Between April 8 and May 13, the two-phase flow problem was coded for digital solution and a number of problems were successfully run on IBM's Type 701 Computer. This paper presents a general discussion of the two-phase flow problem, the digital method of solution, and some of the results obtained to date. The use of the method to determine optimum controls for producing an oil field is not presented at this time.

FUNDAMENTAL EQUATIONS

The fundamental equations that describe two-phase fluid flow in porous media are Darcy's law for each phase and an equation of continuity for each component. These equations contain coefficients that specify the physical properties of the fluids and coefficients that specify the ability of the porous material to transmit the fluids. The forces driving the fluids included in these equations are the expansion force of the compressed fluids, the force of capillarity, and the force

of gravity. It can be shown (Appendix I) that the fundamental equations can be combined to give the two following equations (in dimensionless form*) as the general equations of two-phase flow in porous media:

$$\nabla \cdot [A(\rho, p)\ \nabla p + C(\rho, p)\ \nabla \rho - E(\rho, p)\mathrm{g}] = \frac{\partial}{\partial T}[-\gamma_1(p) \cdot \rho + \gamma_2(p)] \quad . \quad . \quad . \quad (1)$$

$$\nabla \cdot [B(\rho, p)\ \nabla p + D(\rho, p)\ \nabla \rho - F(\rho, p)\mathrm{g}] = \frac{\partial}{\partial T}[\gamma_3(p) \cdot \rho]. \quad . \quad . \quad . \quad . \quad . \quad . \quad . \quad . \quad (2)$$

The dependent variables in Equations 1 and 2 are the relative pressure, p, and the saturation of the oil phase, ρ. The independent variables are the dimensionless space coordinates and dimensionless time, T.

$A(\rho, p)$, $B(\rho, p)$, $C(\rho, p)$, $D(\rho, p)$, $E(\rho, p)$, and $F(\rho, p)$ are coefficients which depend on both pressure and saturation. These coefficients are given in Appendix I in terms of rock and fluid properties.

Coefficients $\gamma_1(p)$, $\gamma_2(p)$, $\gamma_3(p)$, are functions only of pressure and are given in Appendix I in terms of the gas density, liquid density, and gas in oil solubility.

Equations 1 and 2 can be described as second order, nonlinear, partial differential equations. An analytical solution to these equations does not exist at present, and does not seem likely because of their inherent complexity. Numerical solutions, however, are possible by use of large capacity, high speed computing machines. The first successful solutions to these equations were obtained for horizontal flow under the assumption that the force terms caused by capillarity can be neglected. For these conditions and for linear flow, Equations 1 and 2 become:

$$\frac{\partial}{\partial x}\left[A(\rho, p)\frac{\partial p}{\partial x}\right] = \frac{\partial}{\partial T}\left[-\gamma_1(p) \cdot \rho + \gamma_2(p)\right]. \quad (3)$$

$$\frac{\partial}{\partial x}\left[B(\rho, p)\frac{\partial p}{\partial x}\right] = \frac{\partial}{\partial T}\left[\gamma_3(p) \cdot \rho\right]. \quad . \quad . \quad . \quad . \quad . \quad (4)$$

The variable x is the dimensionless linear distance defined by $x = \frac{x'}{L}$ where x' is actual linear distance and L is length of system.

For radial flow, Equations 1 and 2 become:

$$\frac{1}{r}\frac{\partial}{\partial r}\left[A(\rho, p)r\frac{\partial p}{\partial r}\right] = \frac{\partial}{\partial T}\left[-\gamma_1(p) \cdot \rho + \gamma_2(p)\right] \quad . \quad (5)$$

$$\frac{1}{r}\frac{\partial}{\partial r}\left[B(\rho, p)r\frac{\partial p}{\partial r}\right] = \frac{\partial}{\partial T}\left[\gamma_3(p) \cdot \rho\right] \quad . \quad . \quad (6)$$

The variable r is the dimensionless radial distance defined by $r = \frac{r'}{r_e}$ where r' is the actual radial distance and r_e is radius of the outer boundary.

For purposes of computation, the logarithmic transformation $u = ln\ r$ was made for radial flow. With this transformation, Equations 5 and 6 become

$$\frac{\partial}{\partial u}\left[A(\rho, p)\frac{\partial p}{\partial u}\right] = e^{2u}\frac{\partial}{\partial T}\left[-\gamma_1(p) \cdot \rho + \gamma_2(p)\right] \quad . \quad (7)$$

$$\frac{\partial}{\partial u}\left[B(\rho, p)\frac{\partial p}{\partial u}\right] = e^{2u}\frac{\partial}{\partial T}\left[\gamma_3(p) \cdot \rho\right] \quad . \quad . \quad . \quad (8)$$

Equations 7 and 8 can be made the same as Equations 3 and 4 for linear flow by separately setting $u = x$ and $exp\ 2u = 1$.

DISCUSSION OF NUMERICAL METHOD

The solution of the nonlinear partial differential equations, Equations 7 and 8, was performed by the replacement of all derivatives by finite differences.[5] No criteria exist at present for determining a unique set of finite differences resulting in a stable solution that will converge to the exact solution as the finite differences approach zero. Methods exist, however, for testing whether a particular finite difference formulation for linear equations will be stable and converge to the correct solution. In view of the nonlinear nature of two-phase flow equations, a linearized approximation was obtained upon which the finite difference formulations were tested. The particular finite difference formulation presented in this report was the only finite difference form found which when tested on the linearized form gave stable solutions converging to the exact solution as the finite differences approached zero. The possibility exists that other finite difference formulations which were not investigated could also give satisfactory solutions.

It was not known that the finite difference form that satisfied stability and convergence requirements on the linearized equations would give stable, convergent solutions to the nonlinear equations until solutions of the nonlinear equations had been obtained on the IBM 701 Computer.

The finite difference grid is shown in Fig. 2. It is to be noted that this grid differs from conventional ones in the following two respects: (a) the pressure and saturation are calculated at alternate space points, and (b) the values of pressure and saturation for a new time line are computed from the results obtained at the two previous time lines. The numbering system for the space points is shown in Fig. 3.

The finite difference representation of the derivatives reduced the partial differential equations to a set of nonlinear algebraic equations which had to be solved

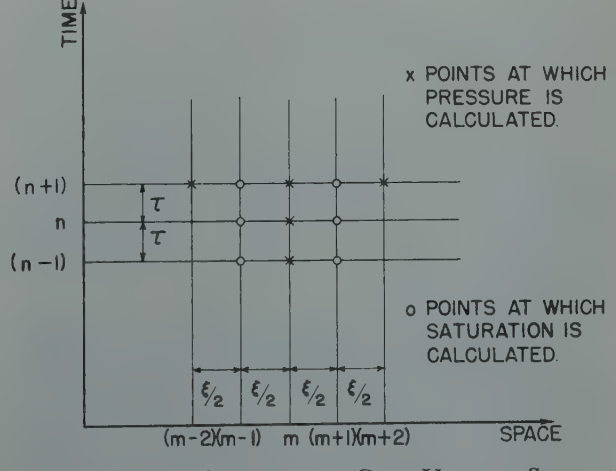

FIG. 2 — FINITE DIFFERENCE GRID USED IN SETTING UP FINITE DIFFERENCE EQUATIONS.

*See Nomenclature at end of paper.

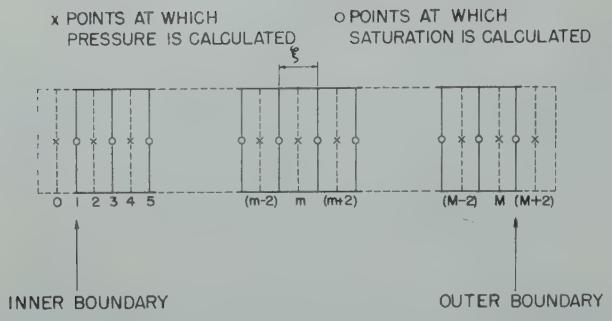
x POINTS AT WHICH PRESSURE IS CALCULATED
o POINTS AT WHICH SATURATION IS CALCULATED
0 1 2 3 4 5
(m-2) m (m+2)
(M-2) M (M+2)
INNER BOUNDARY
OUTER BOUNDARY

FIG. 3 — SPACE DIVISION REPRESENTATION IN U-SPACE.

simultaneously at every time step. This solution was accomplished by an interative procedure which converged rapidly. A detailed discussion of the numerical method is presented in Appendix II.

The fundamental empirical data used in the calculations were: (a) viscosities of gas and oil phases as a function of pressure, (b) formation volume factors of the gas and oil-phases as a function of pressure, (c) solubility of the gas in the oil-phase as a function of pressure, and (d) relative permeability of the oil and gas phases as a function of oil saturation. These are the usual functions used in reservoir mechanics. For purposes of calculation, it was found convenient to combine the empirical data into the dimensionless functions α_1, α_2, α_3 γ_1, γ_2, and γ_3 as defined in Appendix I. The gas and oil relative permeabilities σ_1 and σ_2, already are in dimensionless form. These functions, in turn, were represented by suitable polynomials because the polynomial representation of empirical data is more advantageous in digital computation than the use of tables. It was found that four terms at the most in each polynomial were required to represent the functions, derived from the empirical data, with satisfactory accuracy.

The boundary conditions used in the calculations were as follows: (a) the flow rate was zero at the outer boundary and (b) either the oil production rate or the pressure at inner boundary was a prescribed function of time. These conditions are sufficient to determine the problem.

RESULTS

Representative solutions of the two-phase flow problem are shown in Figs. 4, 5, 6, and 7 for radial and linear systems. The phases considered are gas and oil and the production mechanism is solution-gas drive. The data describing the fundamental rock and fluid properties used in these examples are given in Figs. 10 through 12. The basic data for the fluids is typical of a 40° API oil and associated gas. The relative permeability curves represent typical laboratory data. The porous medium was assumed to be homogeneous throughout the reservoir.

The solutions were obtained in terms of dimensionless variables and dimensionless parameters. This makes it possible to obtain several specific solutions in terms of actual variables and parameters from one dimensionless solution because the conversion factors between dimensionless quantities and actual quantities contain many reservoir parameters such as porosity, specific permeability, dimensions of the system, initial pressure and fluid properties at initial pressure. For instance, from Appendix I, the relations between dimensionless time, T, and real time, t, and dimensionless production rate, Q, and oil production rate, q, are given by:

Radial System	Linear System
$T = \dfrac{\gamma_g^{\kappa}(p_i)\, K P_i}{r_e^2 \phi\, \mu_g(p_i)\, \gamma_o^{\circ}(p_i)} \cdot t$	$T = \dfrac{\gamma_g^{\kappa}(p_i)\, K P_i}{L^2 \phi u_g(p_i) \gamma_o^{\circ}(p_i)} \cdot t$
$Q = \dfrac{\mu_g(p_i)}{2\pi h P_i K \gamma_g^{\kappa}(p_i)} \cdot q$	$Q = \dfrac{L\, \mu_g(p_i)}{A\, K P_i\, \gamma_g^{\kappa}(p_i)} \cdot q$

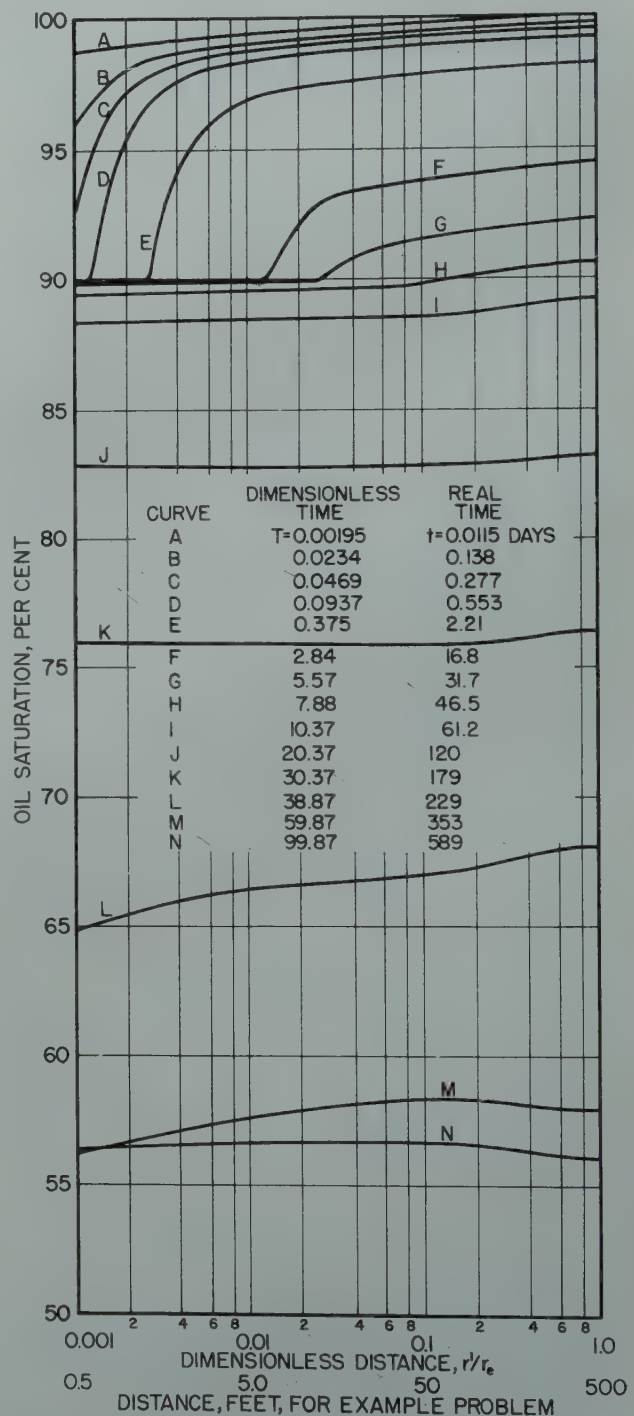

FIG. 4 — CALCULATED OIL SATURATION PROFILE HISTORY OF HYPOTHETICAL SOLUTION-GAS DRIVE RADIAL FLOW SYSTEM.

It can be seen from these relations that a given value of T and Q may correspond to many values of t and q, depending on the properties of the system under consideration. New solutions must be obtained, however, whenever (a) the shapes of the α, γ, or σ functions are changed, (b) the production rate is changed while keeping the reservoir parameters constant, and (c) the ratio of drainage radius to well radius is changed.

Figs. 4 through 7 are plotted in terms of dimensionless variables and also in terms of real variables pertaining to the following conditions:

$\gamma_g^g(p_i)/\mu_g(p_i) = 8.69$ gm/cu cm-cp
$K = 0.020$ Darcys (20 md)
$P_i = 340$ atmospheres (5,000 psia)
$r_e = 15{,}240$ cm (500 ft)
$r_w = 15.2$ cm (0.5 ft)
$\phi = 0.30$
$\gamma_o^o(p_i) = 0.432$ gms/cu cm
$h = 3{,}048$ cm (100 ft)
$A = 929$ sq cm (1 sq ft)
$L = 3{,}048$ cm (100 ft)
$q = 792$ gms/sec (522 B/D) (radial system)
$q = 0.126$ gms/sec (.0830 B/D) (linear system)

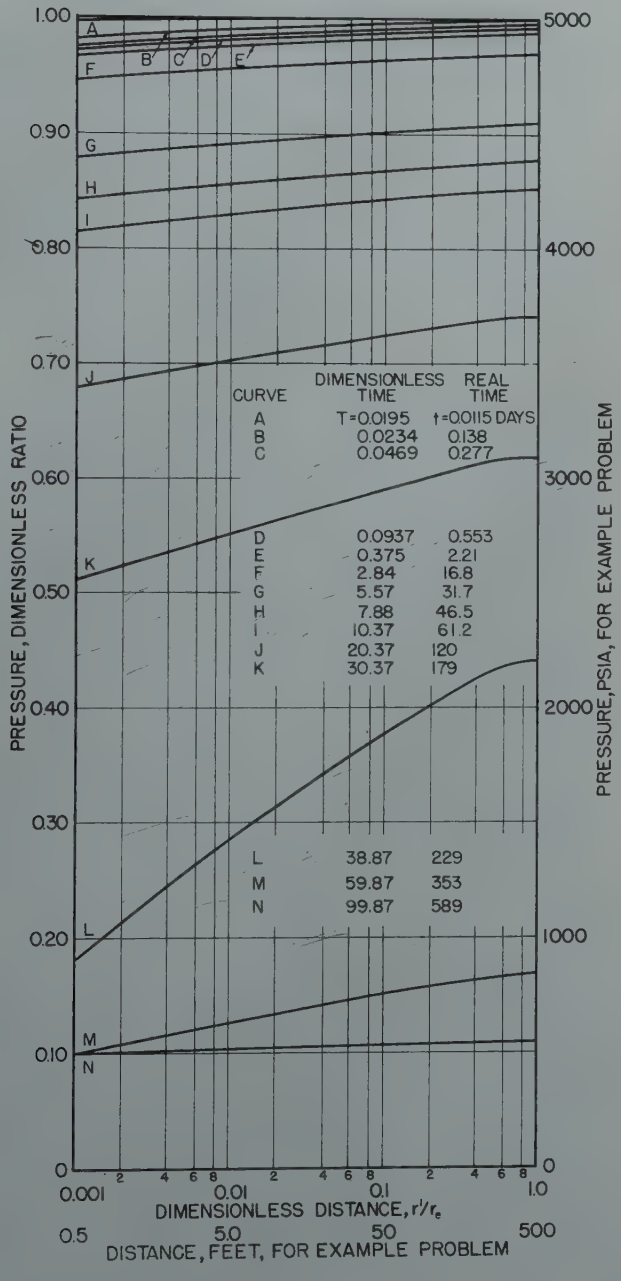
PRESSURE, DIMENSIONLESS RATIO
PRESSURE, PSIA, FOR EXAMPLE PROBLEM
DIMENSIONLESS DISTANCE, r/r_e
DISTANCE, FEET, FOR EXAMPLE PROBLEM
CURVE | DIMENSIONLESS TIME | REAL TIME
A | T=0.0195 | t=0.0115 DAYS
B | 0.0234 | 0.138
C | 0.0469 | 0.277
D | 0.0937 | 0.553
E | 0.375 | 2.21
F | 2.84 | 16.8
G | 5.57 | 31.7
H | 7.88 | 46.5
I | 10.37 | 61.2
J | 20.37 | 120
K | 30.37 | 179
L | 38.87 | 229
M | 59.87 | 353
N | 99.87 | 589

FIG. 5 — CALCULATED PRESSURE PROFILE HISTORY OF HYPOTHETICAL SOLUTION-GAS DRIVE RADIAL FLOW SYSTEM.

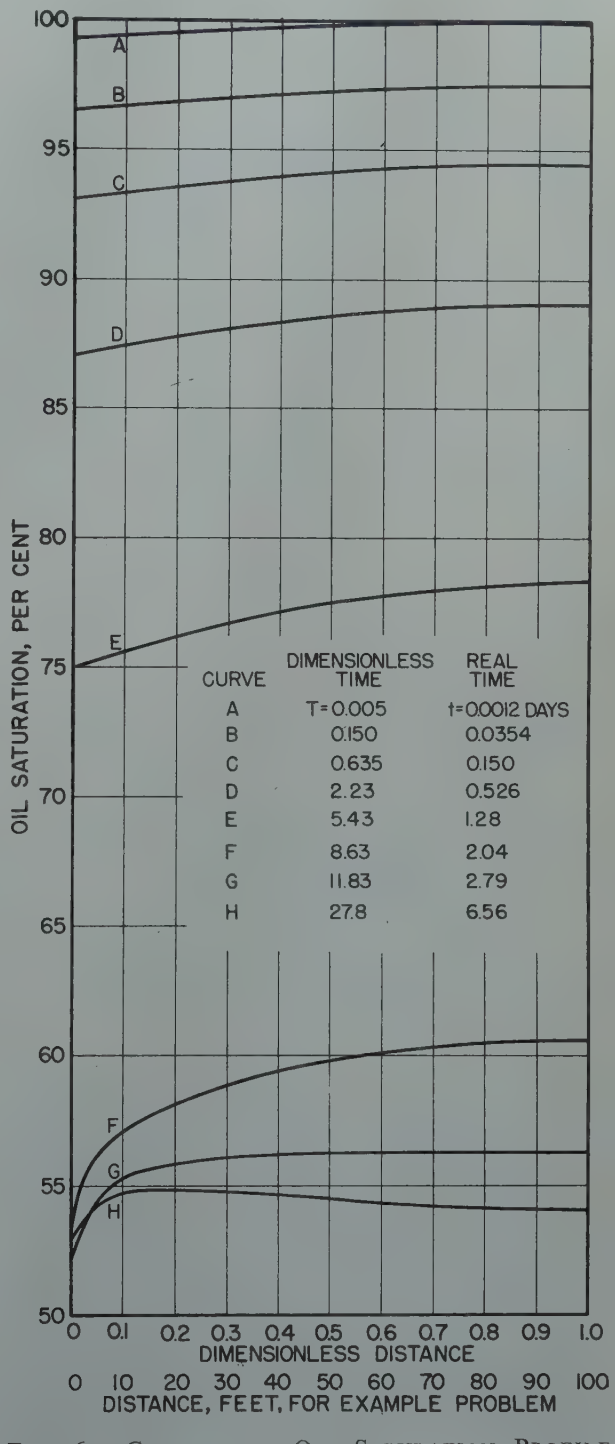
OIL SATURATION, PER CENT
DIMENSIONLESS DISTANCE
DISTANCE, FEET, FOR EXAMPLE PROBLEM
CURVE | DIMENSIONLESS TIME | REAL TIME
A | T=0.005 | t=0.0012 DAYS
B | 0.150 | 0.0354
C | 0.635 | 0.150
D | 2.23 | 0.526
E | 5.43 | 1.28
F | 8.63 | 2.04
G | 11.83 | 2.79
H | 27.8 | 6.56

FIG. 6 — CALCULATED OIL SATURATION PROFILE HISTORY OF HYPOTHETICAL SOLUTION-GAS DRIVE LINEAR FLOW SYSTEM.

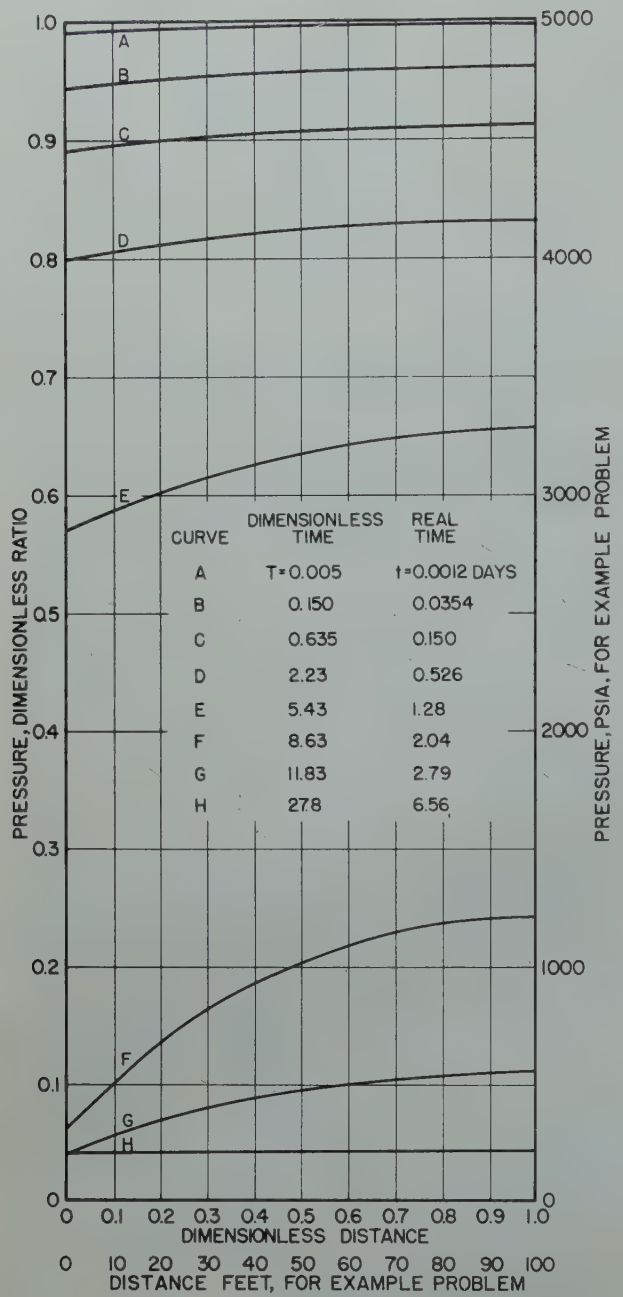

FIG. 7 — CALCULATED PRESSURE PROFILE HISTORY OF HYPOTHETICAL SOLUTION-GAS DRIVE LINEAR FLOW SYSTEM.

In the examples shown, the initial oil saturation was selected to be 100 per cent throughout the reservoir and the initial pressure was uniform.

As pointed out in the preceding section, the production rate can be any prescribed function of the time, as long as the pressure at the wellbore exceeds zero. For the examples shown, the production rate was held constant at the values given above until the pressure at the outflow face had fallen to a terminal pressure which was 10 per cent of the initial pressure for the radial system and 4 per cent of the initial pressure for the linear system. After that time, the pressure at the outflow face was held constant and the production rate allowed to decline as determined by the system. The calculations were terminated when the production rate had fallen to some low value. For the radial system, this was taken to be about 6 B/D.

A striking feature of the performance of the radial system is the combined effect of the critical gas saturation and of convergence at the wellbore. It is seen in Fig. 4 that the saturation at the wellbore drops quickly to the critical gas saturation (in about 0.5 days) and remains nearly at this value until the rest of the reservoir is below the critical gas saturation. This is achieved after approximately 46 days. As is seen in Fig. 4, a knee is formed which progresses into the formation with decreasing amplitude. In the period between 46 and 179 days, the saturation throughout the reservoir is nearly uniform. From then on, a saturation gradient again begins to develop around the wellbore until the terminal pressure is reached at approximately 237 days. For the remainder of the production life, the saturation profile tends toward uniformity. It is interesting to note (a) that the saturation at the wellbore increases slightly toward the end of production and (b) that the saturation exhibits a slight maximum toward the end of the production life about 100 ft from the wellbore.

During the early production period (up to about 61 days) the pressure distribution throughout the reservoir is nearly uniform with a drawdown of only about 200 psi. As the saturation near the wellbore decreases, the pressure gradient near the wellbore must increase so as to maintain the prescribed production rate. This gradient continues to increase until the pressure at the wellbore reaches the terminal presure. At that time, the drawdown is about 1,300 psi. From then on, the pressure distribution flattens out until the entire reservoir is at the terminal pressure. The drawdown was 40 psi when the calculations were terminated at 589 days and the production rate at that time had decreased to 6.3 B/D. It is interesting to note that the pressure distribution curves are quite smooth, even though the saturation distribution is irregular because of the effects of the critical gas saturation.

Even though the average saturation of the reservoir was 56.5 per cent when the economic limit was reached, the ultimate stock tank oil recovery for this particular example was only 6.86 per cent of that originally in place. The saturation decline shown on Fig. 4 was caused mainly by shrinkage of the oil as the dissolved gas was expelled and not by oil production.

The gas-oil ratio as a function of cumulative recovery is shown in Fig. 8. This curve is typical of the behavior of wells producing by solution gas drive in that the gas-oil ratio decreases at first until the saturation in the reservoir falls below the critical gas saturation, increases from then on, reaches a maximum and then declines sharply. A graph of average reservoir pressure vs. cumulative recovery is shown in Fig. 9.

A comparison was made of the results of these detailed calculations with results of calculations* using the approximate solution-gas drive depletion theory.[6] This approximate theory is used extensively to predict the performance of solution-gas drive reservoirs. This theory, however, is based on the assumption that no pressure or saturation gradients exist within the reservoir, which implies that fluids are removed from the reservoir with no flow between different points in the reservoir. Results of the approximate calculation also have been plotted on Figs. 8 and 9.

*This equation was integrated numerically by T. D. Mueller of the California Research Corp. We are indebted to J. S. Aronofsky of Magnolia Petroleum Co. for suggesting that we include a discussion of the approximate theory with the exact transient theory.

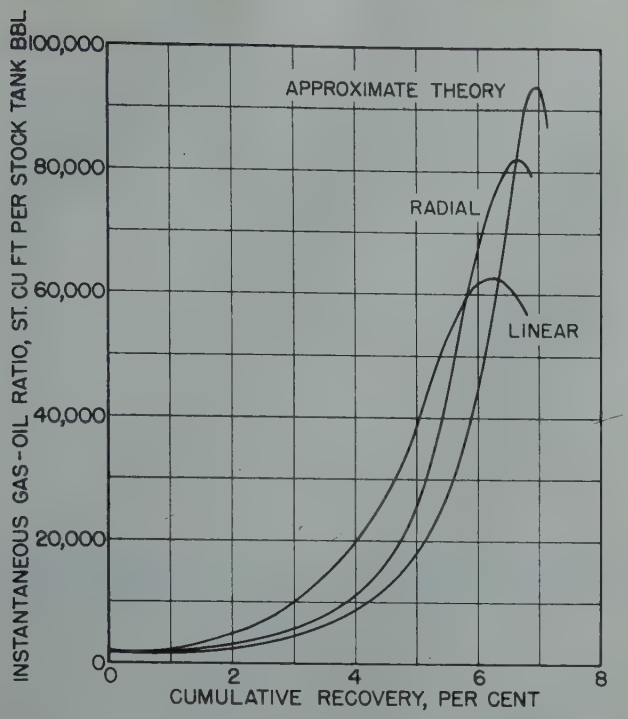

FIG. 8 — CALCULATED GAS-OIL RATIO HISTORIES OF HYPOTHETICAL SOLUTION-GAS DRIVE RADIAL AND LINEAR FLOW SYSTEMS. CALCULATED GAS-OIL RATIO HISTORY FROM APPROXIMATE SOLUTION-GAS DRIVE THEORY.

On Fig. 8, the gas-oil ratio behavior of the approximate analysis has two distinct characteristics that differ from the gas-oil ratio behavior of the detailed analyses. (1) The initial producing gas-oil ratio declines linearly with cumulative production until the reservoir gas saturation exceeds the critical gas saturation. The gas-oil ratio of the detailed analyses decline slightly initially with cumulative production, but then rise much sooner than the gas-oil ratio of the approximate analysis. (2) The maximum gas-oil ratio obtained in the approximate solution is greater than that obtained in the detailed solutions.

On Fig. 9, the average pressure behavior of the approximate solution is always higher than that of the detailed solutions when compared at the same cumulative recovery. At the terminal pressure of 500 psia the approximate solution shows a cumulative recovery of 7.12 per cent, which is 4 per cent more stock tank oil than that recovered at the same terminal pressure with the radial solution.

The saturation and pressure distributions for the linear flow example are shown in Figs. 6 and 7. The linear system does not exhibit the constriction effects which were observed in the radial system. Also, the effects of the critical gas saturation are not as readily apparent. The knee in the saturation curves, which was so prominent in the radial system, does not appear in this particular linear flow example. The cumulative oil recovery for this system was 6.80 per cent at an average reservoir terminal pressure of 200 psia.

The problem was coded for the computer in such a way that any number of cells (space divisions) up to 48 could be used.* In general, the higher the production rate, the greater should be the number of cells to keep the truncation error below a specified level. The truncation errors in both space and time were investigated by running identical problems with 12, 24, and 48 cells and with three different time step schedules. This method was used to determine the optimum number of space and time divisions. The optimum number was 12 for linear flow and 24 for radial flow. It is to be emphasized that all the curves which resulted from the digital calculations were drawn without smoothing. The fact that stable solutions were obtained confirmed the results of the preliminary investigation concerning the selection of the finite difference form to be employed.

The errors in digital computations of this type may result from three causes, (1) round-off error, (2) machine error, and (3) truncation error. Round-off error was known to be small because the 701 Computer carries 10-digit numbers. Machine errors were checked by having the computer calculate at each time increment a reservoir mass balance check. The total products produced were compared to the original products less the products remaining in the reservoir. These two quantities agreed to within one-thousandths of 1 per cent or less. This small difference was caused by the small round-off error. The machine was considered to be operating correctly if the difference of these two quantities was below this value. The truncation error was controlled by appropriate selection of space and time divisions as discussed above. Other errors in these particular solutions could have arisen in the Newton method (see Appendix II) employed to solve the non-

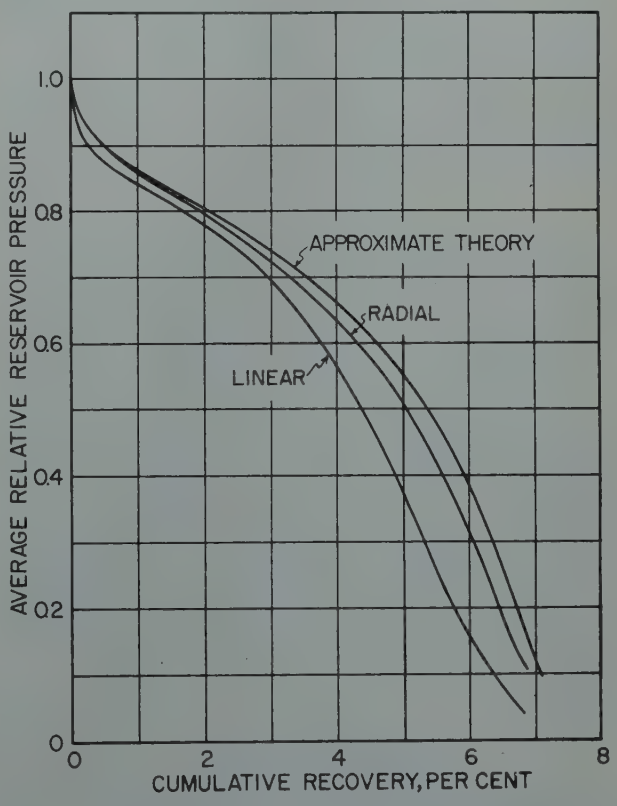

FIG. 9 — CALCULATED AVERAGE PRESSURE HISTORIES OF HYPOTHETICAL SOLUTION-GAS DRIVE RADIAL AND LINEAR FLOW SYSTEMS. CALCULATED AVERAGE PRESSURE HISTORY FROM APPROXIMATE SOLUTION-GAS DRIVE THEORY.

*Calculations with 48 cells used all of the electro-static storage of the 701 Computer. If a greater number of cells is desired, the magnetic storage must be used in addition, which results in a slower computing speed.

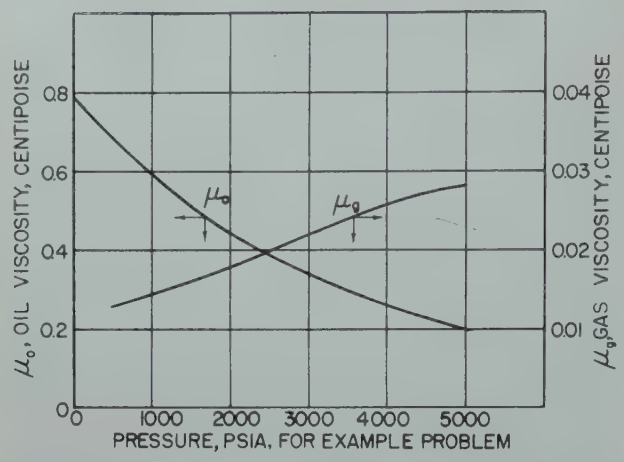

FIG. 10 — VISCOSITY OF GAS AND OIL PHASES CONTAINED IN HYPOTHETICAL RESERVOIRS AS A FUNCTION OF PRESSURE.

linear algebraic equations. In this method, which requires an iterative procedure, seven iterations for the first time step and four iterations for all succeeding time steps were found sufficient to keep the error of this method to the same order as the round-off error.

The total solution time depends on (a) the number of space divisions, (b) the number of iterations per time step, and (c) the total number of time steps. For the 701 Computer, this time in seconds can be expressed roughly by 0.1 times the number of iterations per time step times the total number of cells times the total number of time steps. For the radial flow example presented in this paper, four iterations, 24 cells, and 200 time steps were used, giving a solution time of 32 minutes. A conservative estimate indicates that one man with a desk calculator working a normal workweek would require about 20 years to perform the same calculations barring mistakes and training of replacements.

CONCLUSIONS

It has been shown that the problem of transient two-phase flow through porous media can be solved successfully on a large digital computer. The comparatively short solution time makes it economically feasible to investigate rigorously the effects of many combinations of rock and fluid properties, of well spacing, and of production rate on ultimate recovery. The method presented in this paper is equally applicable to other situations more complex than the one which has been considered. For instance, the effects of capillary pressure and of gravity can be investigated without adding appreciably to the complexity of the problem. Two- and three-dimensional two-phase flow also could be considered. The development of digital computers has provided means for solving many of the hitherto unsolved problems of reservoir behavior.

APPENDIX I

DERIVATION OF TWO-PHASE FLOW EQUATIONS

Darcy's law for the gas and oil phases can be written as:

$$v_g = -\frac{k_g}{\mu_g}\left[\nabla P_g - \gamma_g^g G\right] \quad . \quad . \quad . \quad . \quad . \quad (9)$$

$$v_o = -\frac{k_o}{\mu_o}\left[\nabla P_o - (\gamma_o^o + \gamma_o^g) G\right] \quad . \quad . \quad (10)$$

where subscripts $_g$ and $_o$ refer to the gas and oil phases, and the superscripts ^{g} and ^{o} refer to the gas and oil components. The pressures in the gas and oil phases are related through the capillary pressure function

$$P_o - P_g = P_c(\rho). \quad . \quad . \quad . \quad . \quad . \quad (11)$$

The equations of continuity for the gas and oil components are:

$$\nabla \cdot [\gamma_g^g \mathbf{v}_g + \gamma_o^g \mathbf{v}_o] = -\phi \frac{\partial}{\partial t}\left[\gamma_g^g(1-\rho) + \gamma_o^g \rho\right] \quad (12)$$

$$\nabla \cdot [\gamma_o^o \mathbf{v}_o] = -\phi \frac{\partial}{\partial t}\left[\gamma_o^o \rho\right] \quad . \quad . \quad . \quad . \quad . \quad . \quad (13)$$

Substituting Equations 9 and 10 in Equations 12 and 13 and eliminating P_o by Equation 11 and dropping the subscript on P_g, the following equations are obtained:

$$\nabla \cdot \left[\left(\frac{\gamma_g^g k_g}{\mu_g} + \frac{\gamma_o^g k_o}{\mu_o}\right)\nabla P + \frac{\gamma_o^g k_o}{\mu_o}\frac{\partial P_c}{\partial \rho}\nabla \rho - \left\{\frac{\gamma_g^g k_g}{\mu_g}\gamma_g^g + \frac{\gamma_o^g k_o}{\mu_o}(\gamma_o^o + \gamma_o^g)\right\} G\right] = \phi \frac{\partial}{\partial t}\left[\gamma_g^g(1-\rho) + \gamma_o^g \rho\right] \quad . \quad . \quad . \quad (14)$$

$$\nabla \cdot \left[\frac{\gamma_o^o k_o}{\mu_o}\nabla P + \frac{\gamma_o^o k_o}{\mu_o}\frac{\partial P_c}{\partial \rho}\nabla \rho - \frac{\gamma_o^o k_o}{\mu_o}(\gamma_o^o + \gamma_o^g) G\right] = \phi \frac{\partial}{\partial t}\left[\gamma_o^o \rho\right] \quad . \quad . \quad . \quad . \quad . \quad (15)$$

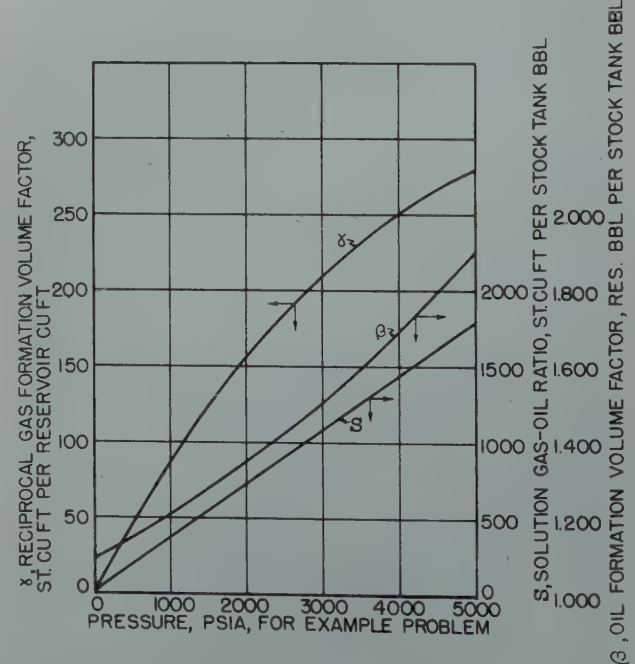

FIG. 11 — PRESSURE - VOLUME - TEMPERATURE CHARACTERISTICS OF FLUIDS CONTAINED IN HYPOTHETICAL RESERVOIRS.

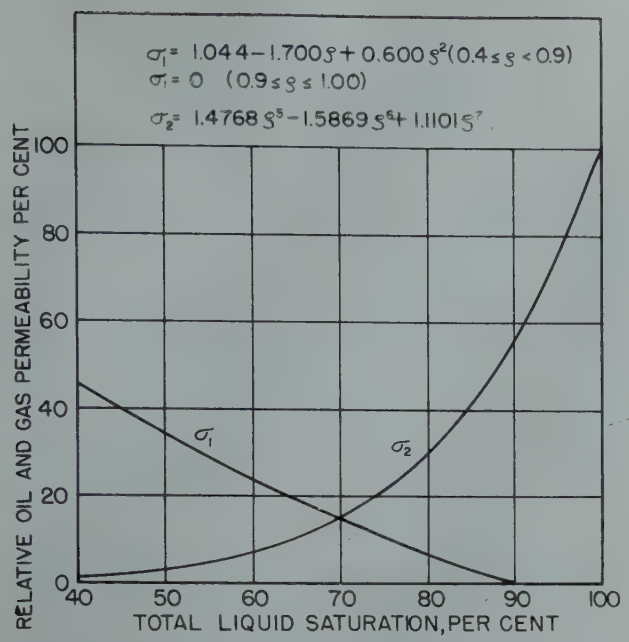

FIG. 12 — OIL AND GAS RELATIVE PERMEABILITIES OF THE RESERVOIR ROCK AS A FUNCTION OF OIL SATURATION AND CORRESPONDING POLYNOMIAL REPRESENTATIONS USED IN CALCULATIONS.

Defining the following dimensionless variables:

$$p = \frac{P}{P_i} \qquad \gamma_1(p) = \frac{\gamma_g^g - \gamma_o^g}{\gamma_o^o(p_i)}$$

$$\alpha_1(p) = \frac{\gamma_g^g}{\mu_g} \Big/ \frac{\gamma_g^g(p_i)}{\mu_g(p_i)} \qquad \gamma_2(p) = \frac{\gamma_o^g}{\gamma_o^o(p_i)}$$

$$\alpha_2(p) = \frac{\gamma_o^g}{\mu_o} \Big/ \frac{\gamma_g^g(p_i)}{\mu_g(p_i)} \qquad \gamma_3(p) = \frac{\gamma_o^o}{\gamma_o^o(p_i)}$$

$$\alpha_3(p) = \frac{\gamma_o^o}{\mu_o} \Big/ \frac{\gamma_g^g(p_i)}{\mu_g(p_i)} \qquad \gamma_4(p) = \gamma_g - \gamma + \gamma_2$$

$$g = \frac{\gamma_o^o(p_i)\, L}{P_i} \cdot G$$

$$\sigma_1(\rho) = \frac{k_g(\rho)}{K} \qquad T = \frac{\gamma_g^g(p_i)\, K P_i}{L^2 \phi \mu_g(p_i)\, \gamma_o^o(p_i)} \cdot t$$

$$\sigma_2(\rho) = \frac{k_o(\rho)}{K} \qquad Q = \frac{L\, \mu_g(p_i)}{A\, K P_i \gamma_2^g(p_i)} \cdot q$$

Equations 14 and 15 can be written as

$$\nabla \cdot \left[(\alpha_1\sigma_1 + \alpha_2\sigma_2)\, \nabla p + \left(\alpha_2\sigma_2 \frac{\partial p_c}{\partial \rho} \right) \nabla \rho - (\alpha_1\sigma_1\gamma_2 + \alpha_2\sigma_2\gamma_4)\, g \right] = \frac{\partial}{\partial T} \left[-\gamma_1 \cdot \rho + \gamma_2 \right] \quad (16)$$

$$\nabla \cdot \left[(\alpha_3\sigma_2)\, \nabla p + \left(\alpha_3\sigma_2 \frac{\partial p_c}{\partial \rho} \right) \nabla \rho - (\alpha_3\sigma_2\gamma_4)\, g \right] = \frac{\partial}{\partial T} \left[\gamma_3 \cdot \rho \right] . \quad (17)$$

The quantity L is a characteristic length of the system. For linear systems L was chosen as the length of the system, and for radial systems L was chosen as the radius of the outer boundary of the system.

For fluid systems with components of constant composition, the density functions γ_g^g, γ_o^g, and γ_o^o can be defined in terms of formation volume factors and solubility.

$$\gamma_o^o(p) = \gamma_o^o(p_i) \frac{\beta(p_i)}{\beta}$$

$$\gamma_g^g(p) = \gamma_g^g(p_i) \frac{\gamma}{\gamma(p_i)}$$

$$\gamma_o^g(p) = \frac{\gamma_g^g(p_i)}{\gamma(p_i)} \frac{S}{\beta\, 5.615}$$

where β is oil formation volume factor

$1/\gamma$ is gas formation volume factor, and

S is solubility in cu ft/bbl.

Equations 16 and 17 can be further simplified by letting

$$A(\rho, p) = \alpha_1\sigma_1 + \alpha_2\sigma_2$$

$$B(\rho, p) = \alpha_3\sigma_2$$

$$C(\rho, p) = \alpha_2\sigma_2 \frac{\partial p_c}{\partial \rho}$$

$$D(\rho, p) = \alpha_3\sigma_2 \frac{\partial p_c}{\partial \rho}$$

$$E(\rho, p) = \alpha_1\sigma_1\gamma_2 + \alpha_2\sigma_2\gamma_4$$

$$F(\rho, p) = \alpha_3\sigma_2\gamma_4$$

The final equations then become:

$$\nabla \cdot [A(\rho, p)\, \nabla p + C(\rho, p)\, \nabla \rho - E(\rho, p)\, g] = \frac{\partial}{\partial T} \left[-\gamma_1(p) \cdot \rho + \gamma_2(p) \right] . \quad (18)$$

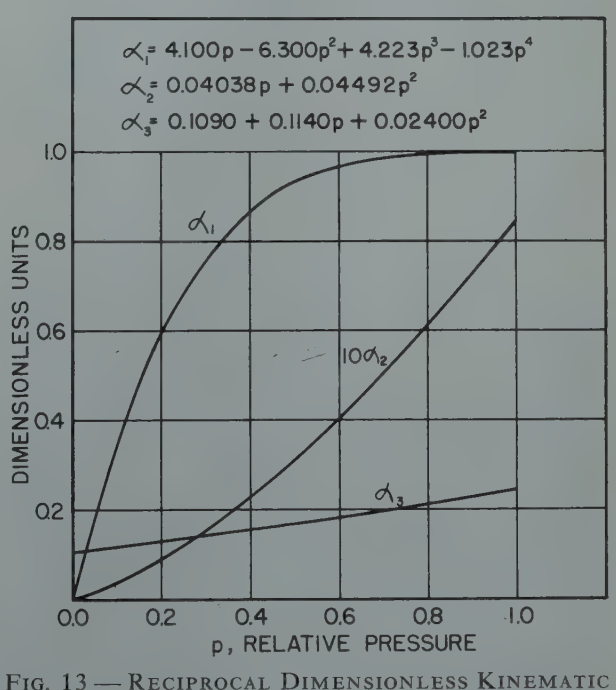

FIG. 13 — RECIPROCAL DIMENSIONLESS KINEMATIC VISCOSITIES DEFINED IN APPENDIX *I* AS A FUNCTION OF RELATIVE RESERVOIR PRESSURE AND CORRESPONDING POLYNOMIAL REPRESENTATIONS USED IN CALCULATIONS.

$$\nabla \cdot [B(\rho, p)\ \nabla p + D(\rho, p)\ \nabla \rho - F(\rho, p)\ g] = \frac{\partial}{\partial T}\left[\gamma_3(p)\cdot\rho\right] \quad . \quad . \quad . \quad . \quad . \quad (19)$$

which are Equations 1 and 2 of the text.

APPENDIX II

NUMERICAL METHOD OF SOLUTION

The finite difference forms that gave successful solutions of Equations 7 and 8 are as follows:

$$[A_{m+1}\ \Delta p_m - A_{m-1}\ \Delta p_{m-2}]_{n+1} = \frac{e^{2u_m}\xi^2}{\tau}\left[\frac{3}{2}(-\gamma_1\cdot\rho+\gamma_2)_{m,\ n+1} - 2(-\gamma_1\cdot\rho+\gamma_2)_{m,\ n} + \frac{1}{2}(-\gamma_1\cdot\rho+\gamma_2)_{m,\ n-1}\right] \quad . \quad . \quad (20)$$

$$[B_{m+1}\Delta p_m - B_{m-1}\Delta p_{m-2}]_{n+1} = \frac{e^{2u_m}\xi^2}{\tau}\left[\frac{3}{2}(\gamma_3\cdot\rho)_{m,\ n+1} - 2(\gamma_3\cdot\rho)_{m,\ n} + \frac{1}{2}(\gamma_3\cdot\rho)_{m,\ n-1}\right] \quad . \quad . \quad . \quad (21)$$

where:

$$\Delta p_{m-2} = p_m - p_{m-2}$$

$$\Delta p_m = p_{m+2} - p_m$$

$$u_m = ln\frac{r_w}{r_e} + (m-1)\frac{\xi}{2}$$

The symbols m and n are integers and ξ and τ are the lengths of the finite differences in u and T. The different quantities are evaluated at the space and time points designated by the subscripts m, n.

The values of p and ρ are calculated at time line $(n+1)\tau$ using values of p and ρ previously calculated for time lines $n\tau$ and $(n-1)\tau$. The finite difference grid is shown in Fig. 2. Values of pressure are calculated at points of even m, and values of saturation are calculated at points of odd m. Equations 20 and 21 are centered at the points m(even), n + 1.

Equations 20 and 21 cannot be used for starting the problem because when $n = 0$, values of p and ρ at $T = -\tau$ are needed and the problem is not defined for negative times. To get around this difficulty, the coefficients $+3/2$, -2, and $1/2$ appearing in Equations 20 and 21 are replaced by $+1$, -1, and 0, respectively. As this is a cruder approximation than Equations 20 and 21, a very small value of τ was used for the first time step. The value of τ was increased progressively as the solution advanced.*

Fig. 3 is a schematic representation of the space division of the u dimension. A region bounded by two solid lines in Fig. 3, a distance ξ apart, is called a unit cell. The unit cell corresponds to a region around a well bounded by two concentric rings. If the unit cells are all equal in u-space as shown in Fig. 3, the volumes of unit-cells in r-space increase exponentially with distance from the well.

Equations 20 and 21 must be satisfied in each unit cell. It is seen, however, from Fig. 3, that the set of equations at m contains the values of pressure in the two adjacent unit cells and also the values of the saturation at the boundaries between cell m and its two adjacent cells. Thus, the M/2 sets of Equations 20 and 21 written for m = 2, 4, 6, . . . M, with the equations representing the boundary conditions, must be solved simultaneously for the values of p and ρ at each new time step.

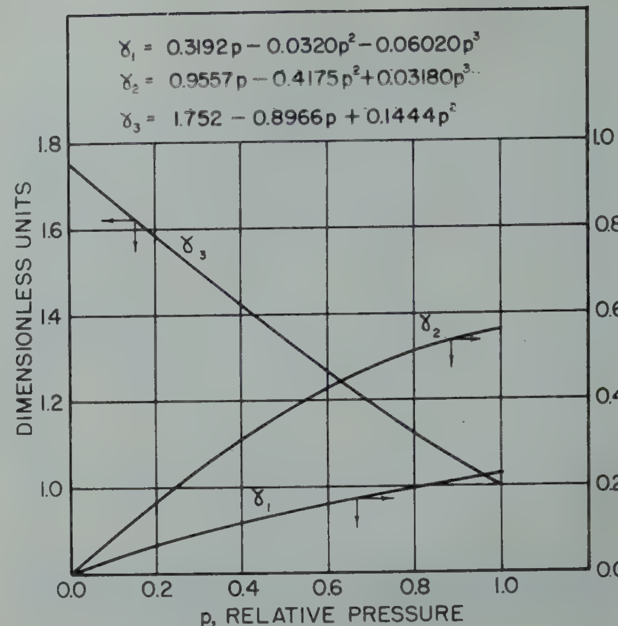

FIG. 14 — DIMENSIONLESS DENSITY FUNCTIONS DEFINED IN APPENDIX *I* AS A FUNCTION OF RELATIVE RESERVOIR PRESSURE AND CORRESPONDING POLYNOMIAL REPRESENTATIONS USED IN CALCULATIONS.

The boundary condition at the wellbore, m = 1, is that the oil flow rate is a prescribed function of the time. The oil flow rate at the outflow boundary is given by:

$$Q_1 = -\frac{B_1\Delta p_0}{\xi} = f(t) \quad . \quad . \quad . \quad . \quad . \quad (22)$$

At the outer boundary, m = M + 1, the condition is imposed that no fluid crosses this boundary. This condition requires that the pressure gradient at the outer boundary be zero which implies that:

$$p_{M+2} = p_M \quad . \quad . \quad . \quad . \quad . \quad (23)$$

An additional equation is required to determine the saturation at m = M + 1 with this boundary condition. This equation is obtained by carrying out the space differentiation in Equations 7 and 8, setting $\partial p/\partial u = 0$, and then eliminating $\partial^2 p/\partial u^2$ between the two equations. The result is:

$$B\frac{\partial}{\partial T}\left[-\gamma_1\cdot\rho+\gamma_2\right] = A\frac{\partial}{\partial T}\left[\gamma_3\cdot\rho\right] \quad . \quad (24)$$

In finite difference form, Equation 24 is as follows:

$$B_{M+1,\ n+1}\left[\frac{3}{2}(-\gamma_1\cdot\rho+\gamma_2)_{M+1,\ n+1} - 2(-\gamma_1\cdot\rho+\gamma_2)_{M+1,\ n} + \frac{1}{2}(-\gamma_1\cdot\rho+\gamma_2)_{M+1,\ n-1}\right] = A_{M+1,\ n+1}\left[\frac{3}{2}(\gamma_3\cdot\rho)_{M+1,\ n+1} - 2(\gamma_3\cdot\rho)_{M+1,\ n} + \frac{1}{2}(\gamma_3\cdot\rho)_{M+1,\ n-1}\right] \quad . \quad . \quad . \quad . \quad (25)$$

*Equations 20 and 21 as shown apply for equal time steps and have to be modified slightly if the successive time steps are unequal.

It is to be emphasized that Equation 24 does not introduce any additional physical constraints but is a consequence of Equations 7, 8, and 23. It may appear at first that Equation 24 would automatically be included in the general equations set up for each cell. The general equations, however, were centered at the midpoint of each cell while Equation 24 is equivalent to Equations 7 and 8 centered at the outer boundary of the last cell. Therefore, Equation 24 is independent.

If p_M is substituted for p_{M+2}, the number of equations to be solved simultaneously for each time step is $M + 2$ for $M/2$ cells because there are two equations per cell plus two for the two boundary conditions, Equations 22 and 25. The unknowns are the saturations at the boundaries of each cell and the pressures at the center points of each cell and at $m = 0$. The number of unknown values of saturation for a new time step is $(M/2) + 1$, and the number of unknown values of pressure for a new time step also is $(M/2) + 1$. Therefore, the total number of unknowns is $M + 2$. The number of equations equals the number of unknowns and the $M + 2$ values of pressure and saturation can be solved for each new time line from the $M + 2$ equations. These equations are nonlinear algebraic equations and special methods must be used for their solution.

Newton's method[7] was used to obtain solutions to the $M + 2$ algebraic equations. This method is as follows: Suppose it is desired to find the value of x satisfying the equation:

$$g(x) = C \quad . \quad . \quad . \quad . \quad . \quad (26)$$

where $g(x)$ is some function of x and C is a constant. Let the function $f(x)$ be defined as:

$$f(x) = g(x) - C = O \quad . \quad . \quad . \quad (27)$$

Expansion of $f(x)$ in a Taylor's Series around the point x_o keeping only first order terms is as follows:

$$f(x_o + \delta x_o) = f(x_o) + \frac{\partial f}{\partial x}(x_o)\,\delta x_o = O \quad . \quad . \quad (28)$$

where x_o is the first guess of x to satisfy equation $f(x) = 0$ and δx_o is a first approximation of the amount x_o differs from the true value of x satisfying equation $f(x) = 0$. δx_o is obtained from Equation 28 and a second guess x_1 is then tried where

$$x_1 = x_o + \delta x_o \quad . \quad . \quad . \quad . \quad . \quad (29)$$

The process is repeated until δx_i decreases to a satisfactorily low value. This method was extended to apply to a system of $M + 2$ unknowns.

When this method was applied to Equations 20 and 21, 22 and 25, the unknowns in the new equations became $(\delta p_m)_i$ and $(\delta \rho_m)_i$ which are the corrections to be added to the i^{th} guesses. These new equations have the following form:

$$[C_{m-1}\delta p_{m-2} + D_{m-1}\delta \rho_{m-1} + E_{m-1}\delta p_m + F_{m-1}\delta \rho_{m+1} + G_{m-1}\delta p_{m+2}]_i = [H_{m-1}]_i \quad . \quad . \quad . \quad (30)$$

$$[C_m\delta p_{m-2} + D_m\delta \rho_{m-1} + E_m\delta p_m + F_m\delta \rho_{m+1} + G_m\delta p_{m+2}]_i = [H_m]_i \quad . \quad . \quad . \quad . \quad . \quad . \quad . \quad . \quad . \quad (31)$$

where Equation 30 corresponds to Equation 20 which represents gas flow, and Equation 31 corresponds to Equation 21 which represents oil flow. Newton's method applied to the equations representing the boundary conditions gives:

$$[E_o\delta p_o + F_o\delta \rho_1 + G_o\delta p_2]_i = [H_o]_i \quad . \quad . \quad . \quad (32)$$

$$[C_{M+1}\delta p_M + D_{M+1}\delta \rho_{M+1}]_i = [H_{M+1}]_i \quad . \quad . \quad (33)$$

where Equation 32 corresponds to Equation 22 which represents the boundary condition at the outflow boundary, and Equation 33 corresponds to Equation 25 which represents boundary condition at the outer boundary. The coefficients appearing in Equations 30 through 33 are defined in Appendix III.

In matrix notation, the set of simultaneous Equations 30 through 33 is as follows:

$$\begin{bmatrix}
E_o & F_o & G_o & & & & & & \\
C_1 & D_1 & E_1 & F_1 & G_1 & & & & \\
C_2 & D_2 & E_2 & F_2 & G_2 & & & & \\
 & & C_3 & D_3 & E_3 & F_3 & G_3 & & \\
 & & C_4 & D_4 & E_4 & F_4 & G_4 & & \\
 & & . & . & . & . & . & & \\
 & & & . & . & . & . & . & \\
 & & & & . & . & . & . & \\
 & & & & & C_{M-1} & D_{M-1} & (E_{M-1} + G_{M-1}) & F_{M-1} \\
 & & & & & C_M & D_M & (E_M + G_M) & F_M \\
 & & & & & & & C_{M+1} & D_{M+1}
\end{bmatrix}_i
\begin{bmatrix}
\delta p_o \\ \delta p_1 \\ \delta p_2 \\ \delta p_3 \\ \delta p_4 \\ . \\ . \\ . \\ \delta p_{M-1} \\ \delta p_M \\ \delta p_{M+1}
\end{bmatrix}_i
=
\begin{bmatrix}
H_o \\ H_1 \\ H_2 \\ H_3 \\ H_4 \\ . \\ . \\ . \\ H_{M-1} \\ H_M \\ H_{M+1}
\end{bmatrix}_i \quad . \quad (34)$$

This set of simultaneous equations was solved by first triangularizing the matrix, i.e., the equations were combined so that the matrix elements below the main diagonal of the square matrix were reduced to zero, and the values of the δp's and $\delta \rho$'s then were obtained by back substitution.

The first guess for the values of p and ρ at $(n+1)\tau$ was obtained by linear extrapolation of the values at $n\tau$ and $(n-1)\tau$. The coefficients appearing in Equation 34 were calculated for the values of p and ρ thus obtained and the correction to the first guess was calculated by solving the simultaneous Equations 34. The corrections were added to the first guess and the coefficients in the matrix were recalculated for the corrected values of p and ρ and new corrections to p and ρ were obtained by again solving the simultaneous Equations 34. This process was repeated until the $(\delta p_m)_i$ and $(\delta \rho_m)_i$ were below a specified value. The $(p_m)_i$ and $(\rho_m)_i$ were then the values of pressure and saturation for that particular time line. To calculate the values for the next time line, the values of $p_{m,n+1}$ and $\rho_{m,n+1}$ were transferred to $p_{m,n}$ and $\rho_{m,n}$, and values of $p_{m,n}$ and $\rho_{m,n}$ transferred to $p_{m,n-1}$ and $\rho_{m,n-1}$, and the solution to Equations 34 was then repeated as discussed above. The solution to the problem advanced one time step at a time until the desired terminal conditions were reached.

APPENDIX III

DEFINITION OF COEFFICIENTS IN EQUATIONS 30-33

The following coefficients are evaluated only for even m.

$$C_{m-1} = \left[A_{m-1} - \frac{\Delta p_{m-2}}{2}\left(\frac{\partial A}{\partial p}\right)_{m-1} \right]_{n+1}$$

$$D_{m-1} = -\left[\Delta p_{m-2}\left(\frac{\partial A}{\partial \rho}\right)_{m-1} - \frac{\xi^2 e^{2um}}{\tau}\ \frac{3}{4}\ (\gamma_1)_m \right]_{n+1}$$

$$E_{m-1} = -\left[A_{m+1} + A_{m-1} - \frac{\Delta p_m}{2}\left(\frac{\partial A}{\partial p}\right)_{m+1} + \frac{\Delta p_{m-2}}{2}\left(\frac{\partial A}{\partial p}\right)_{m-1} + \frac{e^{2um}\xi^2}{\tau}\ \frac{3}{2}\left\{ -\left(\frac{\partial \gamma_1}{\partial p}\right)_m \cdot p_m + \left(\frac{\partial \gamma_2}{\partial p}\right)_m \right\} \right]_{n+1};$$

$$F_{m-1} = \left[\Delta p_m \left(\frac{\partial A}{\partial \rho}\right)_{m+1} + \frac{e^{2um}\xi^2}{\tau}\ \frac{3}{4}\ (\gamma_1)_m \right]_{n+1};\quad G_{m-1} = \left[A_{m+1} + \frac{\Delta p_m}{2}\left(\frac{\partial A}{\partial p}\right)_{m+1} \right]_{n+1}$$

$$H_{m-1} = \left[A_{m-1}\Delta p_{m-2} - A_{m+1}\Delta p_m \right]_{n-1} + \frac{e^{2um}\xi^2}{\tau}\left[-\frac{3}{2}\left(-\gamma_1 \cdot \rho + \gamma_2\right)_{m,n+1} - 2\left(-\gamma_1 \cdot \rho + \gamma_2\right)_{m,n} + \frac{1}{2}\left(-\gamma_1 \cdot \rho + \gamma_2\right)_{m,n-1} \right]$$

$$C_m = \left[B_{m-1} - \frac{\Delta p_{m-2}}{2}\left(\frac{\partial B}{\partial p}\right)_{m-1} \right]_{n+1}$$

$$D_m = -\left[\Delta p_{m-2}\left(\frac{\partial B}{\partial \rho}\right)_{m-1} + \frac{e^{2um}\xi^2}{\tau}\ \frac{3}{4}\ (\gamma_3)_m \right]_{n+1}$$

$$E_m = -\left[B_{m+1} + B_{m-1} - \frac{\Delta p_m}{2}\left(\frac{\partial B}{\partial p}\right)_{m+1} + \frac{\Delta p_{m-2}}{2}\left(\frac{\partial B}{\partial p}\right)_{m-1} + \frac{e^{2um}\xi^2}{\tau}\ \frac{3}{2}\left(\frac{\partial \gamma_3}{\partial p}\right)_m \cdot \rho_m \right]_{n+1}$$

$$F_m = \left[\Delta p_m \left(\frac{\partial B}{\partial \rho}\right)_{m+1} - \frac{e^{2um}\xi^2}{\tau}\ \frac{3}{4}\ (\gamma_3)_m \right]_{n+1}$$

$$G_m = \left[B_{m+1} + \frac{\Delta p_m}{2}\left(\frac{\partial B}{\partial p}\right)_{m+1} \right]_{n+1}$$

$$H_m = \left[B_{m-1}\Delta p_{m-2} - B_{m+1}\Delta p_m \right]_{n+1} + \frac{e^{2um}\xi^2}{\tau}\left[\frac{3}{2}\left(\gamma_3 \cdot \rho\right)_{m,n+1} - 2\left(\gamma_3 \cdot \rho\right)_{m,n} + \frac{1}{2}\left(\gamma_3 \cdot \rho\right)_{m,n-1} \right]$$

$$F_0 = \left[\frac{\Delta p_0}{2}\left(\frac{\partial B}{\partial p}\right)_1 - B_1 \right]_{n+1}$$

$$F_0 = \left[\Delta p_0 \left(\frac{\partial B}{\partial \rho}\right)_1 \right]_{n+1}$$

$$G_0 = \left[\frac{\Delta p_0}{2}\left(\frac{\partial B}{\partial p}\right)_1 + B_1 \right]_{n+1}$$

$$H_0 = -\left[Q_1 \xi + B_1 \Delta p_0 \right]$$

$$C_{M-1} = \left[\frac{3}{2}\left\{ B\left(-\frac{\partial \gamma_1}{\partial p} \cdot \rho + \frac{\partial \gamma_2}{\partial p} \right) + \frac{\partial B}{\partial p}\left(-\gamma_1 \cdot \rho + \gamma_2 \right) - A\frac{\partial \gamma_3}{\partial p} \cdot \rho + \frac{\partial A}{\partial p}\gamma_3 \cdot \rho \right\}_{M+1,\,n+1} - \left(\frac{\partial B}{\partial p}\right)_{M+1,\,n+1}\left\{ 2\left(-\gamma_1 \cdot \rho + \gamma_2\right)_{M+1,\,n} - \frac{1}{2}\left(-\gamma_1 \cdot \rho + \gamma_2\right)_{M+1,\,n-1} \right\} + \left(\frac{\partial A}{\partial p}\right)_{M+1,\,n+1}\left\{ 2\left(\gamma_3 \cdot \rho\right)_{M+1,\,n} - \frac{1}{2}\left(\gamma_3 \cdot \rho\right)_{M+1,\,n-1} \right\} \right]$$

$$D_{M+1} = \left[\frac{3}{2}\left\{ B\left(-\gamma_1\right) + \frac{\partial B}{\partial \rho}\left(-\gamma_1 \cdot \rho + \gamma_2\right) - A\left(\gamma_3\right) + \frac{\partial A}{\partial \rho}\left(\gamma_3 \cdot \rho\right) \right\}_{M+1,\,n+1} - \left(\frac{\partial B}{\partial \rho}\right)_{M+1,\,n+1}\left\{ 2\left(-\gamma_1 \cdot \rho + \gamma_2\right)_{M+1,\,n} - \frac{1}{2}\left(-\gamma_1 \cdot \rho + \gamma_2\right)_{M+1,\,n-1} \right\} + \left(\frac{\partial A}{\partial \rho}\right)_{M+1,\,n+1}\left\{ 2\left(\gamma_3 \cdot \rho\right)_{M+1,\,n} - \frac{1}{2}\left(\gamma_3 \cdot \rho\right)_{M+1,\,n-1} \right\} \right]$$

$$H_{M+1} = \left[\frac{3}{2}\left\{ -B\left(-\gamma_1 \cdot \rho + \gamma_2\right) + A\left(\gamma_3 \cdot \rho\right) \right\}_{M+1,\,n+1} + B_{M+1,\,n+1}\left\{ 2\left(-\gamma_1 \cdot \rho + \gamma_2\right)_{M+1,\,n} - \frac{1}{2}\left(-\gamma_1 \cdot \rho + \gamma_2\right)_{M+1,\,n-1} \right\} - A_{M+1,\,n+1}\left\{ 2\left(\gamma_3 \cdot \rho\right)_{M+1,\,n} - \frac{1}{2}\left(\gamma_3 \cdot \rho\right)_{M+1,\,n-1} \right\} \right]$$

NOMENCLATURE

$A(\rho, p), B(\rho, p) \ldots F(\rho, p)$ = coefficients in fundamental fluid flow equations, contain parameters describing rock and fluid properties.

$C_m, D_m \ldots H_m$ = coefficients in nonlinear algebraic equations, defined in Appendix III.

A = cross sectional area of linear system

$\mathbf{G}$ = gravitation acceleration vector

g = dimensionless gravitational acceleration vector (see Appendix I)

h = thickness of producing formation

K = specific permeability of producing formation

k_g = effective permeability to gas phase, function of oil saturation

k_o = effective permeability to oil phase, function of oil saturation

L = length of linear system

M = twice number of divisions in u space

m = integer, $\ln \frac{r_w}{r_e} + (m\text{-}1)\frac{\xi}{2}$ = position in u space

n = integer, $n\tau$ = position in T space

P_g = absolute pressure of gas phase

P_o = absolute pressure of oil phase

P_i = absolute pressure at start of problem

P_c = capillary pressure between gas and oil phases

p = dimensionless pressure, $p = \frac{P}{P_i}$

Q = dimensionless oil production rate

q = oil production rate

r' = actual radial distance

r = dimensionless radial distance, $r = r'/r_e$

r_e = radius of outer boundary of radial system

r_w = radius of the producing well

S = gas solubility in oil phase

T = dimensionless time for computations

t = real time

u = space variable used for calculations, $u = \ln r$

$\mathbf{v}_g$ = vector gas phase macroscopic velocity

$\mathbf{v}_o$ = vector oil phase macroscopic velocity

x' = actual linear distance

x = dimensionless linear distance, $x = \frac{x'}{L}$

$\alpha_1, \alpha_2, \alpha_3$ = dimensionless reciprocal kinematic viscosities, defined in Appendix I

β = oil phase formation volume factor

γ = reciprocal gas phase formation volume factor

γ_g^g = density of gas in gas phase, mass of free gas per unit gas phase volume

γ_o^g = density of gas in oil phase, mass of dissolved gas per unit oil phase volume

γ_o^o = density of oil in oil phase, mass of oil per unit oil phase volume

$\gamma_1, \gamma_2, \gamma_3$ = dimensionless fluid densities, defined in Appendix I

μ_g = viscosity of gas phase

μ_o = viscosity of oil phase

ξ = length of finite difference in u space

ρ = saturation of oil phase, fraction of pore volume

σ_1 = relative permeability of gas phase

σ_2 = relative permeability of oil phase

τ = length of finite difference in T space

ϕ = porosity of medium

∇ = differential vector operator

ACKNOWLEDGMENTS

Valuable suggestions about stability were given by L. H. Thomas, IBM Pure Science Department. Detailed coding of the problem for the IBM Type 701 Electronic Data Processing Machines was performed by K. Eisemann and Mrs. L. Lee, IBM Scientific Computing Service. W. T. Cardwell, Jr., of California Research, La Habra Laboratory, initiated the project at the La Habra Laboratory dealing with the application of computers to problems associated with two-phase flow.

REFERENCES

1. Muskat, Morris, and Meres, M. W.: "The Flow of Heterogeneous Fluids through Porous Media," Physics (1936), **7**, 346.
2. Muskat, Morris: "Application of Computing Machinery to Research of the Oil Industry," *Proceedings of a Second Symposium on Large Scale Digital Calculating Machinery,* Harvard University Press (1951), 399.
3. Terwilliger, P. L., Wilsey, L. E., Hall, H. N., Bridges, P. M., and Morse, R. A.: "An Experimental and Theoretical Investigation of Gravity Drainage Performance," *Trans.* AIME (1951), **192**, 285.
4. Bruce, G. H., Peaceman, D. W., Rachford, H. H., Rice, J. P.: "Calculations of Unsteady-State Gas Flow through Porous Media," *Trans.* AIME (1953), **198**, 79.
5. Milne, W. E.: *Numerical Solution of Differential Equations,* John Wiley and Sons, Inc., New York, (1953).
6. Muskat, M.: *Physical Principles of Oil Production,* McGraw-Hill Book Co., New York, (1949), 409.
7. Willers, F. A.: *Practical Analysis,* Dover Publications, Inc., New York, (1947), 218. ★★★

STUDY of UNDERSATURATION during REPRESSURING and SUPERSATURATION during FLOW of OIL to WELLS

RALPH V. HIGGINS
MEMBER AIME

BUREAU OF MINES
SAN FRANCISCO, CALIF.

T. P. 3891

ABSTRACT

This paper concerns the magnitude of the amount of supersaturation that occurs in an underground reservoir during the flow of oil and gas to wells and to the amount of undersaturation that occurs during repressuring of an oil reservoir where some effective permeability to gas exists.

The study is based on earlier laboratory findings of other investigators on the rate of diffusion of gas in oil as a function of the depth of oil. Utilizing these relationships and the principles of reservoir mechanics, a quantitative estimate of undersaturation and supersaturation was calculated. The results showed that the diffusion of the gas is rapid enough that for all practical purposes no supersaturation exists during the flow of oil to wells or undersaturation during repressuring in reservoir sands having some effective permeability to gas.

The reason diffusion of the gas virtually keeps the oil saturated is the long time required in radial flow for oil to reach the well and the slow rate at which pressure in reservoirs is increased during repressuring.

INTRODUCTION

Knowledge of the phase relationships during flow of gas and oil in an underground reservoir is essential to operating the reservoir in the most efficient manner. In material-balance calculations and in fluid-flow studies, the oil is assumed to contain all the gas that it will dissolve at given temperature and pressure. Pressure-volume-temperature relationships are normally obtained in the laboratory using "bottom-hole" or combined samples of the reservoir fluids. In such laboratory determinations equilibrium is obtained between the oil and gas in the pressure cells by mechanical agitation. During the flow of oil and gas in reservoirs, however, no comparable agitation occurs to mix thoroughly these fluids to aid in effecting equilibrium between the two phases.

During repressuring of a partly depleted underground reservoir, the gas is usually injected into the reservoir faster than the oil can absorb it; consequently, the oil is undersaturated. On the other hand, as the oil flows through the reservoir to the wells during producing operations the pressure decreases faster than the gas in solution can diffuse through the oil to the gas phase. The oil therefore is supersaturated with gas. Where the oil is undersaturated, gas diffuses away from the gas-oil interface, and where it is supersaturated the gas diffuses toward the interface. In either case the gas moves from a higher to a lower saturation.

This report contains the results of a study of the factors influencing the degree of nonequilibrium of the phase relations of oil and gas in porous mediums during the flow of oil through reservoirs to wells and also during the injection of gas into partially depleted sands. Data from an underground reservoir are presented and the degree of supersaturation during the flow of the oil through the reservoir to the well is approximated. Also data from another reservoir are used and the degree of undersaturation during the repressuring operation is calculated.

In addition, the flow rates of oil in laboratory experiments and in underground reservoirs are compared, as data from the laboratory are often used to interpret events in the reservoir, and the rates of flow influence appreciably the degree of nonequilibrium.

Much of the contents of this report was prepared in 1943; but, because of other activities during and since the war, the manuscript was left untouched until 1952, when it was decided to include an estimate of the amount of undersaturation during repressuring as well as supersaturation during flow.

---

[1]References given at end of paper.

Manuscript received in the Petroleum Branch office Aug. 17, 1953. Paper presented at the Pacific Petroleum Chapter Fall Meeting in Los Angeles, Calif., Oct. 1-2, 1953.

UNDERSATURATION DURING REPRESSURING

After a reservoir has been partly depleted of its oil by expansion of the dissolved gas the oil in the upper part of the zone may drain downward and fill the space vacated by the oil that flowed from the bottom of the zone to the wells. If the oil moves downward readily, gravity drainage is very active. Lacey[1] in 1933 published calculations of the rate of gas diffusion for a virgin reservoir or where the oil had drained thoroughly enough to completely fill (no free gas) all the pores of the sand below the gas cap. In one of his examples, in which the depth of the liquid-filled sand was 10 ft, the time " required (after pressure above the oil body has been increased) for dissolving half the amount of gas which would eventually dissolve due to the increase in pressure" was 33 years. This is a rather long time.

Interpretations of the experiments of Muskat, Wyckoff, Botset, and Meres[2] indicate that during the expulsion of oil by dissolved gas, part of the liberated gas accumulates in the pores as the oil is forced to the well. The accumulated gas in the pores allows most of the gas that is liberated later, with reduction in pressure, to move readily through the gas phase without forcing appreciable oil to the wells. As a consequence, much oil is left behind in the pores, and the effective permeability to the gas through the pores at this stage is very high and to oil very low.

Repressuring Operations

During repressuring operations the effective permeability to gas allows the gas to move freely through the pores, unless gravity has been so effective as to displace the gas associated with the oil from the pores. If such efficient drainage to the bottom of the formation should occur, the oil at the bottom would be able to move equally as rapidly to wells as it moved to the bottom of the formation, owing to gravity or augmented by the piston-like action of the gas injected for repressuring. The mechanism would be somewhat similar to oil and gas in a tank without any porous mediums. This would result in an unusually high recovery.

Probably the greater part of the oil remains in the pores of most reservoir sands after depletion by the expansion of the dissolved gas, as the usual recovery from field reservoirs depleted by expansion of dissolved gas is less than 25 per cent of the oil in place, whereas when gravity drainage is active the recovery is much greater. Even when gravity drainage is active it is doubtful if the upward movement of the gas and downward flow of the oil are such as to completely displace the gas with oil from the pores of the lower part of the reservoir. Accordingly, only the more common condition in which some effective permeability to gas exists throughout the reservoir before repressuring is considered in this report.

As the pressure in a reservoir is raised by gas injection, the oil not in immediate contact with the gas-oil interface becomes undersaturated because the gas does not diffuse through the oil fast enough to completely saturate the oil to the equivalent concentration of the gas in the oil at the gas-oil interface. The more the oil becomes undersaturated with gas, the more rapidly the gas diffuses, and finally a condition is reached where the degree of undersaturation remains unchanged. At this point the rate of diffusion of the gas through the liquid balances with the rate of change in saturation at the interface as the pressure increases.

Quantitative Relationship

The quantitative relationship between the quantity of gas entering an interface and diffusing through an oil as related to the depth of the oil, time interval, and diffusion constant has been presented by Pomeroy, et al.[3] These investigators measured the rate of solution of methane in gasoline and proved experimentally that the following equation is valid. It represents the relation of the rate of solution of a gas in a quiescent liquid when the liquid is 50 or more per cent saturated with the gas.

$$Q = C_s AL\left[1 - \frac{8}{\pi^2} e^{-Dt\left(\frac{\pi}{2L}\right)^2}\right] \quad . \quad (1)$$

where

Q = total quantity of gas which has diffused into the liquid, cubic feet.

C_s = saturation concentration, cubic feet of gas per cubic foot of solution.

A = area at right angles to direction of flow, square feet.

L = depth of the liquid, feet.

D = diffusion constant, square feet per second.

t = time, seconds.

e = base of natural logarithms.

If Equation (1) is divided by $C_s AL$ it becomes

$$f = \frac{Q}{C_s AL} = \left[1 - \frac{8}{\pi^2} e^{-Dt\left(\frac{\pi}{2L}\right)^2}\right] \quad . \quad (2)$$

where f is the saturation fraction — ratio of the quantity of gas in solution to the quantity of gas that would be in solution if the oil were completely saturated.

An examination of Equation (2) shows that the time required for the oil to become completely saturated is very long compared to the time required for a slightly undersaturated oil to become less undersaturated. It is doubtful if complete saturation is reached in the flow of oil and gas mixtures through porous mediums, but the approach to complete saturation is so close that complete saturation may be assumed by the petroleum engineer.

The required value of f necessary to cause the rate of diffusion of gas in the liquid to equal the rate at which the gas is to be absorbed, owing to the increasing pressure, is a measure of the degree of undersaturation existing during repressuring. Using the physical properties of a sample of oil from Elk Hills field, Calif., the degree of undersaturation has been calculated as follows:

The rate of change in undersaturation is obtained in convenient form by differentiating Equation (2) with respect to t:

$$df/dt = \left[\frac{8}{\pi^2} e^{-Dt\left(\frac{\pi}{2L}\right)^2}\right] D\left(\frac{\pi}{2L}\right)^2 \quad . \quad (2a)$$

or

$$df/dt = (1-f)\ D\left(\frac{\pi}{2L}\right)^2 \quad . \quad . \quad . \quad . \quad . \quad . \quad (3)$$

Degree of Undersaturation

By means of this equation the degree of undersaturation, $1-f$, can be approximated with respect to the diffusion of gas into oil with increasing pressure.

The term df/dt is the rate at which gas is being absorbed because of the degree of undersaturation, $1-f$. When df/dt is made equal to the rate at which gas is provided by the increasing pressure, the degree of undersaturation, $1-f$, which will maintain the gas output (owing to increased pressure) and input (owing to absorption) in balance, can be calculated.

The $\frac{df}{dt}$ for the increasing gas pressure is calculated as follows:

$$\Delta f = \frac{F\Delta p}{C_s} \quad . \quad . \quad . \quad . \quad . \quad . \quad . \quad . \quad . \quad . \quad . \quad (4)$$

C_s = cubic feet of gas per cubic foot of solution when the oil is 100 per cent saturated at the pressure p.

F = cubic feet of gas which dissolves in a cubic foot of oil for each increase of 1 psi in pressure. F varies with the pressure but may be assumed constant through a narrow pressure range.

According to Fig. 3B of a report by Cook and Shea,[4] F is about 0.022 for Elk Hills, Calif., crude oil between the limits of 600 to 1,500 lbs/sq in. Then

$$\frac{\Delta f}{\Delta t} = \frac{0.022\Delta p}{C_s \Delta t} \quad . \quad . \quad . \quad . \quad . \quad . \quad . \quad . \quad (5)$$

$$\frac{df}{dt} = \frac{0.022}{C_s} \frac{dp}{dt} \quad . \quad . \quad . \quad . \quad . \quad . \quad . \quad (6)$$

Equating the member of this equation at the right with the member of Equation (3) at the right and solving for $1-f$ results in the degree of undersaturation that will keep in balance the rate of gas absorption and the rate at which gas is brought to the gas-oil interface. Thus, in the illustrated example that follows, the pressure in the formation is assumed to increase 2 lbs/24 hours; therefore, dp/dt is 2/86,400, or the rate of pressure change per second. The maximum thickness, L, of an oil film in pores of the sand was assumed to be 9.8×10^{-4} ft, which is 0.03 cm. The average thickness of the oil film is much less but use of the maximum thickness results in a conservative estimate of the degree of undersaturation.

The effect of pore size on the thickness of the oil film is discussed in detail in the section of the report entitled "Pore Shape and Flow Characteristics." The value of D, the diffusion constant, is 1.9×10^{-8} sq ft/sec and is the value determined by Hill and Lacey[5] in their experimental work. The foregoing value of D is about that measured for Ventura crude oil at 86°F and it would be considerably more at reservoir temperature. The use of the smaller value, however, results in more undersaturation and is, therefore, a conservative value to use. According to Fig. 3B in the foregoing report by Cook and Shea, C_s at 700 lbs/sq in. is about 15 cu ft/cu ft of solution. Using these values in Equations (3) and (7)

$$\frac{0.022}{15} \times \frac{2}{86{,}400} = (1-f)\ 1.9 \times 10^{-8} \left(\frac{3.14}{2 \times 9.8 \times 10^{-4}} \right)^2$$

Solving for the degree of undersaturation, $1-f = 6.9 \times 10^{-7}$ or the per cent undersaturation is 100 $(1-f)$ or 0.000069 or 6.9×10^{-5} per cent. Thus with the pressure increasing at the rate of 2 lbs/day, undersaturation is practically nil. This results from the thin oil film and the appreciable time.

Discussion of Equation

The foregoing method of approximating the undersaturation has been based on an equation that has been tested experimentally. However, in using this equation the analogy is not perfect, as Equation (1) is based on a fixed saturation at the gas-oil interface instead of a slowly changing one. In an unpublished manuscript on the subject prepared in 1942, the writer treated supersaturation quantitatively and undersaturation qualitatively. R. H. Olds, one of the reviewers of the paper, suggested an equation and included its derivation for treating supersaturation so as to accurately account for the slowly changing saturation at the oil-gas interface. By a change in sign in the fore part of Olds' derivation, because of the inward diffusion of gas during undersaturation instead of its outward diffusion during supersaturation, and by proceeding in an analogous manner with the derivation, the same equation is obtained for undersaturation as for supersaturation. The derivations for both undersaturation and supersaturation are presented later in the report.

The degree of undersaturation when the slow change in the gas saturation at the oil-gas interface is included is

$$\text{per cent undersaturation} = \frac{100\,L^2}{3Dp} \frac{dp}{dt} = 5.6 \times 10^{-5}$$

Thus both methods of estimating the degree of undersaturation result in about the same negligible amount of undersaturation.

SUPERSATURATION DURING FLOW

As oil moves through reservoir sands to wells, with decreasing pressure, part of the gas in the oil phase exceeds that required to saturate the oil at the decreased pressure. The excess gas diffuses to the oil-gas interface at a rate depending in part on the rate at which the pressure decreases. Because the gas does not diffuse rapidly enough from the oil to maintain the same gas saturation in the oil as exists at the gas-oil interface, some supersaturation exists. Marked difference exists between this supersaturation and a supercooled liquid such as water, commonly mentioned in school textbooks on physics and chemistry. The property of the latter system is such that a small, sharp surface can cause instantaneous formation of ice and raising of the temperature to that of freezing ice. In the supersaturated oil considered in this report no comparable instantaneous lowering of the gas concentration to that at the gas-oil interface occurs. The gas diffuses according to the unsteady-state equations for the diffusion of dissolved gases through liquids. The prefix super is used because the quantity of gas in solution exceeds that at the gas-oil interface.

In the radial flow of oil to wells, the rate of pressure change with time depends on the distance from the well, and this rate of change can be approximated by using the radial flow equation for oil and differentiating with respect to t. Thus:

$$\frac{p - p_w}{p_e - p_w} = \frac{ln \frac{r}{r_w}}{ln \frac{r_e}{r_w}} \quad . \quad . \quad . \quad . \quad . \quad (8)$$

where

p = pressure at the radius r from the axis of the well, pounds per square inch absolute.

p_w = the back pressure at wall of well, pounds per square inch absolute.

p_e = pressure at the outer boundary, r_e, pounds per square inch absolute.

r_w = radius of well, feet.

r_e = radius of external pressure boundary, feet.

r = any radius, feet.

ln = natural logarithm.

These equations are for an incompressible liquid, and therefore the results are not as accurate as if those for two phase flow had been used.
The differential equation is

$$\frac{dp}{dt} = \frac{p_e - p_w}{ln \frac{r_e}{r_w}} \frac{1}{r} \frac{dr}{dt} \quad . \quad . \quad . \quad . \quad (9)$$

The term dr/dt is the velocity, and for radial flow of oil through porous mediums

$$\frac{dr}{dt} = \frac{Q}{2\pi r\ h\ m\ w} \quad . \quad . \quad . \quad . \quad . \quad (10)$$

where

Q = flow rate, cubic feet per second.

h = sand thickness, feet.

m = porosity of the sand, fraction.

w = pore space through which the advancing oil front moves, fraction.

By means of Equation (10) by m and w, the velocity is corrected for the presence of the sand, interstitial water, and immobile oil.

Substituting the value of dr/dt from Equation (10) for dr/dt in Equation (9) results in

$$\frac{dp}{dt} = \frac{p_e - p_w}{ln \frac{r_e}{r_w}} \frac{Q}{2\pi r^2\ h\ m\ w} \quad . \quad . \quad . \quad (11)$$

the relation for the rate of change of pressure with time along a radial flow line.

When an oil is supersaturated with gas, the gas diffuses from the oil; consequently, df/dt is negative instead of positive because the saturation fraction is decreasing. When the change in sign for df/dt is made in Equation (3), it becomes

$$\frac{df}{dt} = (f - 1)\ D \left(\frac{\pi}{2L}\right)^2 \quad . \quad . \quad . \quad (11a)$$

Equation (11a), relating the rate of change of saturation with time to the degree of supersaturation, the diffusion constant, and the depth from which the oil diffuses; Equation (11), representing the rate of pressure change; and Equation (6), relating the rate of change of saturation with pressure, were used to estimate the degree of supersaturation along a radial flow line in the reservoir of the Kettleman Hills field.

The constants in Equation (6) are for the crude oil in Elk Hills reservoir. When the constants for Kettleman Hills crude oil between the limits of 600 to 1,000 psia are substituted Equation (7) becomes

$$\frac{df}{dt} = \frac{0.043}{C_{s_r}} \frac{dp}{dt} \quad . \quad . \quad . \quad . \quad . \quad . \quad (12)$$

where C_{s_r} = cubic feet of gas per cubic foot of solution

when the oil is 100 per cent saturated at a pressure, p, a radial distance, r, from the well axis. Combining of (11a), (11), and (12) then gives the degree of supersaturation along a radial flow line:

$$f - 1 = \frac{0.043}{C_{s_r}} \frac{Q}{2\pi r^2\ h\ m\ w} \frac{(2L)^2}{D\pi^2} \frac{p_e - p_w}{ln \frac{r_e}{r_w}} \quad . \quad (13)$$

In the radial flow of an oil through reservoir sands to a well, the maximum pressure drop per unit of time or per unit distance exists at the well wall; consequently, the supersaturation that exists should be a maximum at the well wall and appreciably less a few feet away. By means of Equation (13), the amount of supersaturation at the well wall of a Kettleman Hills well has been approximated. For this approximation the following values of some of the terms in Equation (13) were assumed to be reasonable from the meager data that are available.

C_{s_r} = 21 cu ft of gas/cu ft of oil at r_w, where p = 600 psi

$Q = 1.3 \times 10^{-2}$ cu ft/sec, which 200 B/D

r = 0.25 ft for this particular problem

h = 312 ft

m = 0.15

w = 0.20

$L = 9.8 \times 10^{-4}$ ft, which is 0.03 cm (The pore size is probably much less)

$D = 1.9 \times 10^{-8}$ ft^2/sec, which is 2×10^{-6} cm^2/sec

p_e = 1,000 psia

p_w = 600 psia

r_e = 200 ft

r_w = 0.25 ft

When the foregoing values are substituted in Equation (13) the result is 0.0087 or 0.87 per cent supersaturation. Hence the supersaturation at the well wall where the greatest amount exists is small and is much less a short distance away from the well wall, therefore supersaturation may be neglected in most engineering studies.

Substituting the foregoing values and using Equation (11) and Olds' equation, the per cent supersaturation is 0.60, which is somewhat less than that obtained by the use of Equation (13).

Laboratory experiments also indicate that the degree of supersaturation at the usual rates of oil production in field practice is very small. Stewart et al[6] have shown that the degree of supersaturation decreases markedly with the decreasing production rate of oil and gas from cores and "extrapolation of the laboratory data indicates very little supersaturation will exist under most field conditions."

Derivation of Equation for Changing Gas Saturation

The derivation of the Olds' equation, which accounts for the changing gas saturation at the gas-oil interface, is as follows:

Consider a thin layer of oil which has been saturated with a single component gas and is now in dynamic equilibrium with a slowly and uniformly decreasing gas pressure at the gas-oil interface. The pressure has been decreased sufficiently to eliminate any transient effects associated with initial lowering of the gas pressure.

The differential equation relating the variables as given in texts is

$$\frac{\partial C}{\partial t} = D \frac{\partial^2 C}{\partial 1^2}, \quad \ldots \quad (a)$$

where

C = concentration of gas in solution.

t = time.

D = diffusion constant, and

1 = depth of oil measured from gas-oil interface.

A linear relation between the gas pressure and the saturation pressure (Henry's law) is assumed, then

$$C = b\ p, \quad \ldots \quad (b)$$

where p = pressure and b = solubility constant. Then at the oil-liquid interface,

$$\frac{dC_o}{dt} = b \frac{dp}{dt}, \quad \ldots \quad (c)$$

where C_o = concentration of gas in the oil phase at the gas-oil interface.

After sufficient time has elapsed to permit decay of transient effects associated with the initial lowering of pressure, a steady decline in pressure will produce a corresponding steady decline in concentration throughout the liquid. Then it may be assumed that the time rate of change of concentration at any depth in the liquid is the same as that at the gas-oil interface. Hence,

$$\frac{\partial^2 C}{\partial 1^2} = \frac{b}{D} \frac{dp}{dt} \quad \ldots \quad (d)$$

The integration Equation (d) with respect to 1 and the insertion of the boundary conditions, $C = C_o$ when $1 = 0$, and $\partial C/\partial 1 = 0$ when $1 = L$, yields

$$C = C_o - \frac{b\ L}{D} \frac{dp}{dt} 1 + \frac{b}{2\ D} \frac{dp}{dt} 1^2 \quad \ldots \quad (e)$$

This equation gives the gas concentration for any depth of oil and an examination of the equation will show that the gas concentration increases as the distance from the gas-oil interface increases.

The degree of supersaturation is calculated as follows:

$$\text{Per cent supersaturation} = 100 \frac{Q - Q_o}{Q_o}, \quad \ldots \quad (f)$$

where Q_o = the quantity of gas in solution corresponding to a uniform concentration C_o throughout the liquid. The quantity of gas in solution in the liquid is

$$Q = \int_0^L AC\ dl, \quad \ldots \quad (g)$$

where A = area normal to flow by diffusion and 1 = depth of oil measured from the gas-liquid interface. Then per cent supersaturation

$$= 100 \frac{\int_0^L A\ C\ dl - \int_0^L A\ C_o\ dl}{\int_0^L A\ C_o\ dl}, \quad \ldots \quad (h)$$

$$= -100 \frac{L^2}{3DP} \frac{dp}{dt}, \quad \ldots \quad (i)$$

which is Olds' equation for supersaturation.

Equation (i) is independent of the concentration and solubility of the gas in the liquid as a consequence of the assumption of Henry's law in the derivation

If Equation (e) is applied to the data pertaining to Fig. 8 of the article by Gurney and Lurie,[7] the same results as are shown in their figure will be obtained at any time except for the initial 8-minute period. To obtain the same results, temperature is substituted for concentration and thermal diffusivity for the diffusion constant in Equation (e).

Thus the validity and method of derivation of Equation (e) are proven by data which have been obtained by the use of the Fourier series. Incidentally, the curves of Gurney and Lurie also can be applied to determine the variation of gas saturation with depth.

PORE SHAPES AND FLOW CHARACTERISTICS

The equations in the foregoing section are based on linear diffusion from a mass of oil having a uniform cross sectional area A and length L and a volume represented by AL. Because of the shape of the pores and the mechanics of flow of gas and oil in porous mediums, simple linear diffusion seldom takes place. It will be shown that the value of L used in the report results in the gas diffusing at a slower rate in a pore than actually occurs. As a result, the degree of super or undersaturation calculated in the report would be less if an attempt were made to choose a factor to alter L to a length which would approach accurately the equivalent of what is happening in a pore.

The cross sectional area of the pores resulting from the cubic and rhombohedral packing of uniform spheres are similar to two triangles placed base to base. According to the results of experiments by Wyckoff and Botset,[8] probably the first bubbles accumulate at the base of the triangles in the flow stream, because the permeability of porous mediums decreases rapidly at first without the efflux of appreciable free gas from the sand face. During this initial period the permeability is decreased more than would be expected by the volume increase of gas in the pores of the sand. Therefore the bubbles of gas must occupy positions which offer considerable resistance to the flow of the oil phase.

Bubbles that accumulate in the flow stream require much of the oil phase to pass around the bubble, decreasing the over-all time required for gas to diffuse from the oil phase to the bubble. Also, gas from a bubble at the base of the triangles would have only to diffuse half the distance to the extremities of the pore than if it were in the apex of one triangle. Thus the factors indicate that, where there is some effective permeability to gas, the use of the distance between the apexes of the triangles is conservative.

Length L used in the illustrative examples is the distance between the apexes of triangles formed by the cubic packing of uniform spheres having diameters (0.03 cm) equivalent to the openings in a No. 48-mesh screen (Tyler). The mean length L should be much less for the Kettleman Hills formation containing sands of different grain sizes mixed and cemented as to give an average permeability of the order of 250 md. The cubic packing of uniform spheres 0.03 cm in diameter result in porous mediums having a permeability greater than 24,000 md. Therefore, the choice of $L = 0.03$ cm for the illustrative example pertaining to Kettleman Hills is thought to be conservative, in that a shorter length would result in still less supersaturation.

The use of $L = 0.03$ cm in the calculations results in extremely low value for undersaturation during repressuring and in very low value for supersaturation a short distance from the well wall. If $L = 1$ in. and where the pressure in the reservoir is changing at the rate of 2 psi/24 hours, the under or supersaturation would be only 0.5 per cent. Accordingly, the use of $L = 0.03$ cm is not critical.

In some reservoirs containing undersaturated oils there may be a transient period before gas accumulates immediately following reduction in pressure below that of the bubble point.[9] In the radial flow of oil to wells, however, the time element for any unstable condition to come to equilibrium is very long.

TIME ELEMENT IN LINEAR AND RADIAL FLOW

Many experiments are conveniently performed in the laboratory to study the flow behavior of oil in field reservoirs. As time is important in the diffusion of gas through oil, the example calculations, which follow, are presented to show that in the radial flow of oil through underground reservoirs to wells much more time is required than in linear flow of oil through laboratory cores.

The time required for a globule of oil to move through the formation from a point 100 ft from the well axis to the well was calculated by integrating the Differential Equation (10). The integrated equation is

$$t = \frac{\pi h m w}{Q}(r^2 - r_w^2) \quad . \quad . \quad . \quad . \quad . \quad . \quad (14)$$

Substitute the following in Equation (14):

$r = 100$ ft, the distance from the well axis
$h = 312$ ft, the thickness of the formation
$m = 0.15$, the porosity
$w = 0.20$, the fraction of the pore space occupied by moving oil front
$Q = 1.3 \times 10^{-2}$ cu ft/sec (200 B/D), the flow rate of oil

The result is 22.6×10^6 seconds or 262 days, the time for a globule of oil to travel from a point 100 ft from the well axis to the well wall.

In a linear core having the same permeability, the same pressure drop from entrance to exit, and the same velocity at the outlet face as the condition in the foregoing field example, the time required for a particle of oil to travel the length of the core is much less than for the corresponding length in radial flow.

The velocity in the reservoir at any place in radial flow of oil is

$$v_r = \frac{K}{u} \frac{p_w - p_e}{r \ln \frac{r_e}{r_w}} \quad . \quad . \quad . \quad . \quad . \quad . \quad . \quad . \quad (15)$$

where v_r is the velocity at any radius r, K is the permeability, and u is the viscosity of the oil.

The corresponding equation for velocity in linear flow is

$$v = \frac{K}{u} \frac{p_i - p_o}{n} \quad . \quad . \quad . \quad . \quad . \quad . \quad . \quad (16)$$

where v is the velocity of the oil in the channel, p_i is the inlet pressure, p_o is the outlet pressure, and n is the length of the channel.

The velocity of the oil at the sand face in the well and at the outlet of the core are identical. The radius r_w of the well is 0.25 ft and $p_i - p_o = p_e - p_w$. Then the division of Equation (15) by Equation (16) and substitution of 0.25 for r_w, results in

$$\ln \frac{r_e}{0.25} = \frac{n}{0.25} \quad . \quad . \quad . \quad . \quad . \quad . \quad . \quad (17)$$

Table 1, based on Equation (17), shows the comparative distances for linear and radial flow systems for equal pressure drops and the same velocities at the outlet face. The data show the much greater distance required for radial as compared to linear flow. For example, when r_e is 100 ft in the radial system, the length of the linear core is 1.5 ft.

TABLE 1 — RELATION BETWEEN DISTANCES IN LINEAR AND RADIAL FLOW.

Length of linear channel, n, feet	Distance from well axis to outer boundary in radial flow, r_e, feet
0.5	1.8
1.25	37
1.50	100
1.75	274
2.00	745
2.50	5,500

In the example given in the first part of this section a radial distance of 100 ft was used and the time required for an oil globule to reach the wall was 262 days. In that example in which the time interval was 262 days, the velocity dr/dt at the well wall, r = 0.25, is found to be 8.9×10^{-4} ft/sec.

In the linear flow of a homogeneous liquid, the velocity at all points in the core is the same as at the outlet; therefore the time required for an oil particle, having the same properties as the oil in the radial flow example, to travel from the inlet to the outlet of a linear channel 1.5 ft long is $1.5/(8.9 \times 10^{-4})$ or 1,690 seconds or 28 minutes. This is appreciably different from the 262 days in the radial flow example and is a factor to consider in making any laboratory experiments to determine the amount of supersaturation of gas in oil contained in reservoirs about wells.

CONCLUSION

This study has been made to estimate the degree of non equilibrium between oil and gas in an underground reservoir during the flow of oil and gas to a well and during repressuring operations. According to the experiments of Wyckoff and Botset, when the pressure on the oil is reduced below the bubble point in an underground reservoir by the movement of oil to wells, gas accumulates in the pores of the formation. During repressuring operations, the oil at the gas-oil interface in the pores instantaneously becomes com-

pletely saturated at the new pressure resulting from the gas injection. The gas diffuses from the interfaces into the oil.

Equations relating the depth of oil, the concentration of the gas in solution, and the time for the gas to diffuse were developed and applied. The results show hat the degree of undersaturation of the oil with gas would be negligible in systems of the type considered. This conclusion arises from the small quantity of oil through which gas diffuses in pores where some effective permeability to gas exists and the long time required to increase the pressure in a large reservoir by gas injection.

The corresponding situation exists in a reservoir during the flow of oil through reservoir sands to wells, even to the long time available for the gas to diffuse. An example is presented which shows that 262 days would be required for an oil particle to move 100 ft radially through an oil reservoir to a well when oil is flowing into a well at a rate comparable to that in many fields. Consequently, gas has appreciable time in which to diffuse.

In laboratory flow tests the oil seems to move very slowly through the cores, but when compared to flow rates in underground reservoirs the movement is fast. For example, it was found that a laboratory core 1.5 ft long offered the same resistance to linear flow as that presented to radial flow through 100 ft of a selected underground reservoir. With the same velocity of flow at the outlet face of the core as at the well face, the calculated time required for the oil to move through the core was 28 minutes, compared to 262 days for the oil to travel the radial distance of 100 ft in the selected underground reservoir.

This time difference in the laboratory and field is a factor to consider in making any laboratory experiments to determine the degree of nonequilibrium of gas in oil contained in reservoirs about wells as the longer the time, the less the supersaturation during flow and the less the undersaturation during repressuring.

The general conclusion may be made that, in pores of those underground reservoirs which have some effective permeability to gas, virtually complete equilibrium between oil and gas can be assumed for most reservoir engineering investigations using pressure, volume, and temperature data, because the slow rate of flow in underground reservoirs and the short distance through which gas has to diffuse allows enough time for the gas virtually to saturate the oil completely.

In other words, for the purpose of this report, it is assumed that the more common condition in partly depleted, solution-gas-drive reservoirs will be one of an existing effective permeability to gas (also in sections of other reservoirs where this condition exists) and that the gas will be distributed in the oil zone such that the depth of the oil through which gas diffuses during conditions of phase nonequilibrium will not exceed the average pore diameter. For the examples treated in the report, the average pore diameter is considered to be equal or less than 0.03 cm (the opening in a 48-mesh screen) and this value is used as the depth of diffusion L. In other systems where L may appreciably exceed this value, the results presented in this report would be altered accordingly. The equations presented can be used to calculate the magnitude of the alterations. In one such calculation L was chosen to be 1 in. and the rate of pressure change in the reservoir 2 psi per 24 hours. The super- or undersaturation was of the order of 0.5 per cent, therefore, the use of $L = 0.03$ cm is not critical, except at or near the well wall.

If appreciable super- or undersaturation is found to exist in reservoirs that fulfill the conditions in this report, then some other factor than diffusion and Wyckoff and Botset's principles of fluid flow must be operative.

ACKNOWLEDGMENTS

The investigation was conducted under the supervision of R. A. Cattell, chief, Petroleum and Natural Gas Branch, Bureau of Mines, Washington, D. C., and G. B. Shea, chief, Fuels Technology Division, Region III, Bureau of Mines, San Francisco, Calif.

Thanks are extended to the following: V. J. Berry, Jr., Stanolind Oil & Gas Co; Michael J. Rzasa, Cities Service Research and Development; and Harvey T. Kennedy, R. L. Whiting, Paul B. Crawford, A&M College of Texas; E. M. Tignor, John F. Noonan, James L. Moore, C. Kenneth Eilerts, Alton B. Cook, R. V. Smith, G. L. Gates, F. G. Miller, and especially C. Q. Cupps, Bureau of Mines, for their helpful suggestions and criticisms in preparing the report.

REFERENCES

1. Lacey, William N.: "Practical Benefits of Pressure Maintenance in Petroleum Production," API Production *Bull.* (1933), **210**, 18.
2. Muskat, M., Wyckoff, R. D., Botset, H. G., and Meres, M. W.: "Flow of Gas-Liquid Mixtures Through Sands," *Trans.* AIME (1937), **123**, 247.
3. Pomeroy, Richard D., Lacey, William N., Scudder, Nathan F., and Stapp, Frederick P.: "Rate of Solution of Methane in Quiescent Liquid Hydrocarbons," *Ind. Eng. Chem.* (September, 1933), 1015.
4. Cook, Alton B., and Shea, G. B.: "Special Studies of Reservoir Oils in Naval Petroleum Reserve No. 1, Elk Hills field, California." Bureau of Mines Report of Investigations 4054 (1947).
5. Hill, E. S., and Lacey, W. N.: "Rate of Solution of Methane in Quiescent Liquid Hydrocarbons," *Ind. Eng. Chem.* (December, 1934), **2**, 1325.
6. Stewart, C. R., Craig, F. F., Jr., and Morse, R. A.: "Determination of Limestone Performance Characteristics by Model Flow Tests," *Trans.* AIME (1953), **198**, 98.
7. Gurney, H. P., and Lurie, J.: "Charts for Estimating Temperature Distributions in Heating or Cooling Solid Shapes," *Ind. Eng. Chem.* (November, 1923), 1172.
8. Wyckoff, R. D., and Botset, H. G.: "Flow Through Unconsolidated Sands," *Physics* (1936), 325-345.
9. Kennedy, H. T., and Olson, C. R.: "Bubble Formation in Supersaturated Hydrocarbon Mixtures," *Trans.* AIME (1952), **195**, 271-278. ★★★

GAS HYDRATES of HYDROGEN SULFIDE-METHANE MIXTURES

LESLIE J. NOAKER
DONALD L. KATZ
MEMBER AIME

UNIVERSITY OF MICHIGAN
ANN ARBOR, MICH.

T. P. 3895

ABSTRACT

Experimental data are presented for hydrate formation conditions for mixtures of hydrogen sulfide and methane. Vapor-solid equilibrium constants for hydrogen sulfide are also presented. Equilibrium constants, defined here as the ratio of the mole fraction of hydrogen sulfide in the vapor phase (dry basis) to the mole fraction of hydrogen sulfide in the solid phase (dry basis), were calculated using the vapor-solid equilibrium constants for methane presented in an earlier paper. The conditions at which a natural gas will form gas hydrates with water may be computed from its composition, when hydrogen sulfide is present in addition to carbon dioxide and the paraffin hydrocarbons.

INTRODUCTION

Many gases are known to form solid hydrates in the presence of liquid water at temperatures above 32°F. This hydrate formation is of importance to the natural gas industry inasmuch as most of the constituents found in natural gases will form hydrates. The attention of the industry was called to hydrates by Hammerschmidt[10] in 1934. A number of papers have been written giving the temperatures and pressures at which these hydrates will form[3,4,5,6,7,8,10,13,14,15,18,19] and a bibliography on the subject has been compiled[13]. Deaton and Frost[4,5,6,7,8] report work for various pure gases and for some natural gases. Katz and co-workers[3,4,13,14,18,19] have reported data for various gases at high pressure. They developed a method of predicting conditions for hydrate formation from equilibrium constants[3,19] and from gas gravity.[11] The effects of anti-freeze agents on the formation of hydrogen sulfide hydrate were reported by Bond and Nelson.[2] The hydrogen sulfide-water system, including hydrate, has been the subject of recent investigation by Sage and co-workers.[17]

Mixtures of hydrates behave as solid solutions and an equilibrium exists between the vapor phase and the solid phase that appears to be comparable to the equilibrium between vapor and liquid phases.[3,19] By means of the vapor-solid equilibrium constants which have been published for methane, ethane, propane, isobutane,[3] and carbon dioxide[10] it is possible to determine the temperature and pressure at which hydrates will form for a specific gas mixture when water is present.

Hydrogen sulfide which is frequently found in natural gases has a very strong tendency to form hydrate and must enter the solid solution when present in a natural gas forming a hydrate. To determine the effect of hydrogen sulfide when computing the conditions for gas hydrate formation, it is necessary to have the equilibrium constant giving the ratio of the concentration of hydrogen sulfide in the gas phase to the concentration in the solid phase. This paper presents data on hydrate formation for mixtures of hydrogen sulfide and methane and presents the equilibrium constants which were calculated from these data.

EXPERIMENTAL PROCEDURE

The apparatus used to determine the conditions of hydrate formation for the methane-hydrogen sulfide system was similar to that employed by previous investigators.[3,18,19] A charge gas cylinder was used to supply the hydrogen sulfide-methane mixtures, called the charge gas, and to supply the pressure up to 1,000 psia. This

[1]References given at end of paper.

Manuscript received in the Petroleum Branch office on Mar. 3, 1954.

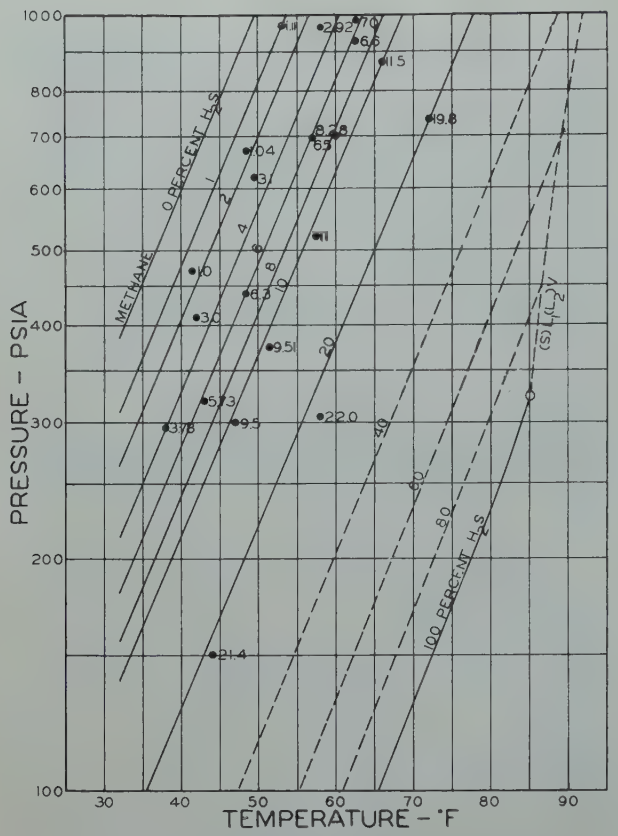

FIG. 1 — HYDRATE FORMATION CONDITIONS FOR HYDROGEN SULFIDE-METHANE MIXTURES.

cylinder was filled by introducing hydrogen sulfide gas to some pressure below the vapor pressure, and then introducing methane to a total pressure of approximately 1,200 psia. The cylinder was allowed to stand 24 hours or more to allow complete mixing by diffusion. This charge gas was analyzed to determine its composition by the Tutwiler method.[1] It involves a direct titration with standard iodine solution of a fixed volume of gas mixture, then calculating the hydrogen sulfide content from the amount of iodine solution used.

The hydrate cell had glass windows and was immersed in a constant temperature water bath. The cell was continuously rocked to agitate its contents. In charging, the hydrate cell was filled with water and the charge gas was introduced into the cell without agitation, displacing the water until 10.5 cc of water remained. The pressure in the cell was then set at the desired value by introducing additional charge gas.

The bath was cooled to some 5°F below the expected hydrate formation temperature by the addition of ice. As the cell was rocked the hydrate would form with an accompanying drop in pressure as observed by a calibrated Bourdon tube gage. The temperature, measured by a thermometer in the bath, was increased by the addition of hot water until the hydrate began to melt and the pressure to increase.

The temperature was then increased more slowly until almost all of the hydrate had disappeared. The hydrate was present as flakes adhering to the wet glass walls of the cell, so it was observed easily. The bath temperature was then reduced about a degree to cause hydrate to form again. The temperature was again allowed to rise very slowly, about 1.0°F per hour, and observations made until no more hydrate was present and no noticeable change in pressure could be observed. These two conditions would occur at substantially the same temperature.

The temperature and pressure at which the hydrate disappeared are reported as the hydrate formation conditions for the composition of the gas in the vapor phase, Table 1. Again lowering the bath temperature around 0.5°F would cause hydrate to reform, so it is felt that the formation temperature is known at least within 0.5°F. Charge gas was then introduced to produce a higher pressure and the procedure was repeated. In this manner, several points were obtained with each composition of charge gas.

The composition of the vapor phase at hydrate formation conditions was obtained experimentally by direct analysis using the Tutwiler method.[1] After purging the delivery lines a sample of vapor was drawn off, dried with magnesium perchlorate, warmed to room temperature, and analyzed in the Tutwiler apparatus. The composition of the gas phase was estimated for those points in which it was not obtained experimentally. Solubility data for hydrogen sulfide[20] and for natural gas[9] in water are available.

The methane was supplied through the courtesy of the Phillips Petroleum Co. with reported purity of better than 99 per cent. The hydrogen sulfide was reported to be 99.9 per cent pure.

PHASE BEHAVIOR

The data for the various mixtures were plotted on Fig. 1 and cross-plotted on Fig. 2. Fig. 1 shows the pressure-temperature relations for hydrate formation in the three component system hydrogen sulfide-methane-water. The three phase equilibrium, water-rich liquid (L_1), hydrate (S), and vapor (V) for the system methane-water[14] is represented by the line labelled 0 per cent H_2S. The similar equilibrium for hydrogen sulfide-water is shown by the line labelled 100 per cent H_2S.[2,15] The intermediate lines labelled with the per cent hydrogen sulfide in the vapor (dry basis) represent the three phase equilibrium L_1 and V saturated with S, that is, the conditions at which hydrate just begins to form, for the three component system hydrogen sulfide-methane-water at the indicated vapor phase compositions.

The S,L_1,V curve for hydrogen sulfide-water terminates at 324.7 psia and 85.1°F. At this point a fourth phase,

TABLE 1 — CONDITIONS FOR HYDRATE FORMATION WITH HYDROGEN SULFIDE-METHANE-WATER MIXTURES

Temp. °F	Press. psia	Mol % H_2S in Charge Gas	Expr. Mol % H_2S in Vapor Phase	Calc. Mol % H_2S in Vapor Phase
60.0	700	11.6	8.23	7.0
52.0	375		9.51	9.0
48.5	440	7.15		6.3
57.0	695			6.5
62.5	985			7.0
43.0	320		5.73	6.5
62.5	925		6.6	7.0
42.0	410	3.11		3.0
49.5	620			3.1
58.0	965		2.92	2.95
38.0	295		3.78	3.9
41.5	470	1.09		1.0
48.5	670			1.04
53.0	970		1.11	1.06
58.0	305	22.2		22.0
72.0	735		19.8	21.0
44.0	150		21.4	22.0
47.0	300	12.5		9.5
57.5	520			11.0
66.0	870		11.5	11.5

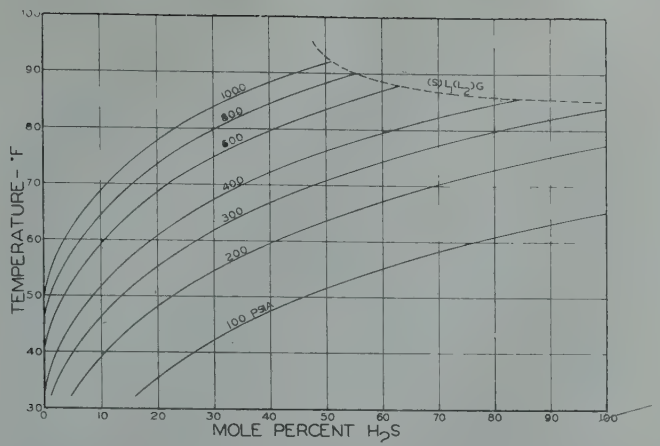

FIG. 2 — HYDRATE FORMATION CONDITIONS FOR HYDROGEN SULFIDE-METHANE MIXTURES.

the hydrogen sulfide-rich liquid (L_2) appears and the system becomes invariant. The addition of another component, methane, causes this S,L_1,L_2,V equilibrium to gain one degree of freedom and move out into the three component diagram as a single line upon which terminate the lines representing the three component L_1, V, S equilibria. On Fig. 1 this four phase line is labelled (S), L_1, (L_2), V to indicate that it represents L_1 and V saturated with S and L_2. The location of the (S), L_1, (L_2), V line was estimated using the data for the hydrogen sulfide-methane system available in the literature[16] and assuming that the presence of water has little effect on the vapor-liquid equilibrium in this system.

EQUILIBRIUM CONSTANTS

The vapor-solid equilibrium constants for hydrogen sulfide, defined as the mole fraction of hydrogen sulfide in the vapor (dry basis) divided by the mole fraction of hydrogen sulfide in the solid (dry basis), were calculated using the equilibrium constants for methane[3] and the hydrate formation conditions for gas mixtures. The hydrate formation corresponds to the dew point in vapor-liquid equilibrium. Accordingly, $\Sigma x = \Sigma y/k = 1.0$ where x and y are the mole fraction of the constituent (dry basis) in the solid phase and vapor phase respectively, and K is the vapor-solid equilibrium constant. The smoothed equilibrium constants are plotted on Fig. 3. The fact that K for a vapor containing only hydrogen sulfide would be unity was used in extrapolating the K values to 1.0. These equilibrium constants can be used along with the charts for other gases[2,18] in computing hydrate formation conditions for natural gases containing hydrogen sulfide.

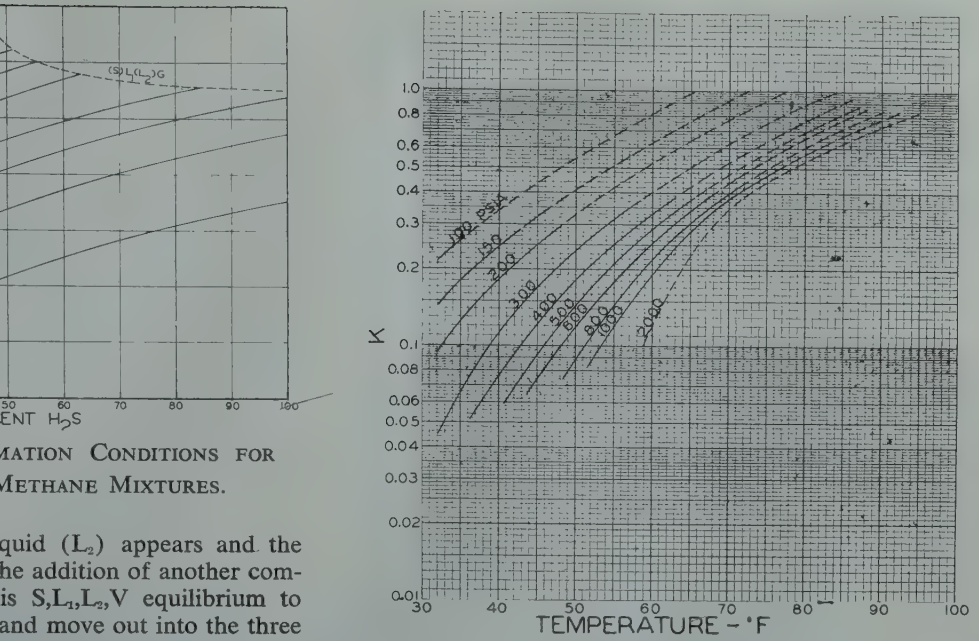

FIG. 3 — VAPOR-SOLID EQUILIBRIUM CONSTANTS FOR HYDROGEN SULFIDE.

ACKNOWLEDGMENT

The research was made possible by a fellowship supported by the Standard Oil Co. of California. The previous work on this subject done by J. D. Hembree was of considerable help. The pure methane supplied by the Phillips Petroleum Co. was appreciated.

REFERENCES

1. Altieri, V. J.: "Gas Analysis and Testing of Gaseous Materials," American Gas Association, New York, N. Y. (1945).
2. Bond, D. C., and Nelson, B. R.: AIME Pub. No. 2450 (1948).
3. Carson, D. B., and Katz, D. L.: "Natural Gas Hydrates," *Trans.* AIME (1942), **146**, 150.
4. Chinworth, H. E., and Katz, D. L., *Refr. Eng.*, (1947), 359-62, **54**.
5. Deaton, W. M., and Frost, E. M., Am. Gas Assoc., Nat. Gas. Dept. *Proc.* (1937), 23-31.
6. Deaton, W. M., and Frost, E. M.: Ibid. (1938), 112-9.
7. Deaton, W. M., and Frost, E. M.: Ibid. (1940), 122-8.
8. Deaton, W. M., and Frost, E. M.: *Oil and Gas Jour.* (1946), **45**, No. 12, 170-8.
9. Dodson, C. R., and Standing, M. B.: *Drilling and Production Practice,* API (1944), 173.
10. Hammerschmidt, E. G.: *Ind. Eng. Chem.* (1934), **26**, 851.
11. Katz, D. L.: *Trans.* AIME (1945), **160**, 140.
12. Katz, D. L., and Rzasa, M. J.: "Physical Behavior of Hydrocarbons Under Pressure," J. W. Edwards, Inc. (1946), Ann Arbor, Mich.
13. Katz, D. L., Kobayashi, R., Withrow, H. J., Williams, G. B.: Proc. Nat. Gasoline Assn. of America (1951), 27-31.
14. Kobayashi, R., and Katz, D. L.: *Trans.* AIME (1949), **186**, 66.
15. Reamer, H. H., Sage, B. H., and Lacey, W. N.: *Ind. Eng. Chem.* (1951), **43**, 976-81.
16. Roberts, O. L., Brownscombe, E. R., and Howe, L. S.: *Oil and Gas Jour.* (1940), **39**, No. 30, 37.
17. Selleck, F. T., Carmichael, L. T., and Sage, B. H.: *Ind. Eng. Chem.* (1952), **44**, 2219-26.
18. Unruh, C. H., and Katz, D. L.: *Trans.* AIME (1949), **186**, 83.
19. Wilcox, W. I., Carson, D. B., and Katz, D. L.: *Ind. Eng. Chem.* (1941), **33**, 662-5.
20. Wright, R. H., and Maass, O.: *Can. J. Res.* (1932), **6**.

★★★

PRODUCTION of WATER-DRIVEN RESERVOIRS below their BUBBLE POINT

A. B. DYES
MEMBER AIME

THE ATLANTIC REFINING CO.
DALLAS, TEX.

T. P. 3918

ABSTRACT

In the operation of a water-driven reservoir, a free gas saturation can be established by maintaining production rates fast enough to cause the reservoir pressure to decline below the bubble point. The benefit of such a procedure on the displacement efficiency of the oil by water is illustrated for two types of sandstone samples from one reservoir. Those rock samples showing the poorest recovery to water drive in the absence of a free gas saturation give the most improvement in the presence of a free gas saturation. Employing one type of reservoir fluid (low shrinkage) the benefit of evolved gas on oil displacement is calculated at several reservoir pressures below the bubble point. This demonstrates the presence of an optimum pressure for water displacement which is several hundred pounds per square inch below the bubble point. Displacement of oil at the optimum pressures results in the removal of 7 to 12 per cent more oil than would be obtained by displacement at the bubble point pressure. In some instances this magnitude of increase may be worthy of consideration in establishing the maximum efficient rate of production from many water-driven fields.

INTRODUCTION

For many years the belief that the use of gas could be combined with that of water to result in a better recovery operation than the use of either of these phases alone has been prevalent in the oil industry. This is evidenced by the several field trials which have employed the injection of gas and water in combination.[1,2,3,4] In most cases the small amount of any additional recovery, in combination with the limited knowledge available on the older reservoirs, has left uncertain the influence of gas on recovery in these earlier attempts to combine the use of gas with water.

Research studies in recent years have demonstrated through laboratory floods the magnitude of the benefit of the presence of gas on the displacement of oil from sandstones by water.[5,6,7,8,9,10,11] In addition, studies of the distributions of the phases which are present during the displacement process have developed concepts concerning the mechanism by which this benefit is obtained.[11,12] It now remains for the engineer to incorporate these findings into the general technology of reservoir operations.

It is the purpose of this paper to illustrate that the production of a water-driven reservoir at pressures below the bubble point is one such operation whereby improved oil displacement efficiency can be obtained as a result of gas evolution. The establishment of a gas saturation by evolution of dissolved gas was one of the techniques used by several investigators in the laboratory studies. The possibility of obtaining the benefit of gas evolution in water-driven reservoirs by producing at pressures less than the bubble point has also been pointed out previously.[11]

The desirability of this operation has undoubtedly

[1]References given at end of paper.

Manuscript received in Petroleum Branch office Aug. 2, 1954. Paper presented at Petroleum Branch Fall Meeting in San Antonio, Oct. 17-20, 1954.

Discussion of this and all following technical papers is invited. Discussion in writing (3 copies) may be sent to the offices of the Journal of Petroleum Technology. Any discussion offered after Dec. 31, 1954, should be in the form of a new paper.

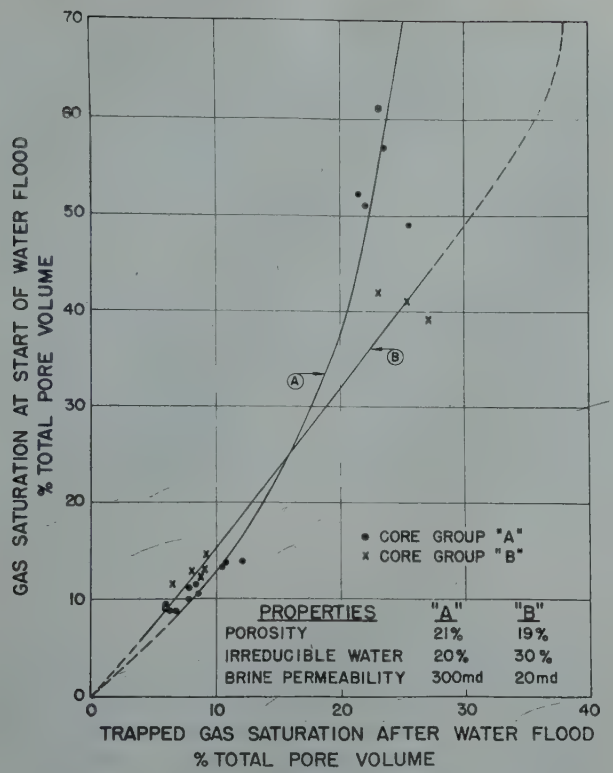
GAS SATURATION AT START OF WATER FLOOD
% TOTAL PORE VOLUME
TRAPPED GAS SATURATION AFTER WATER FLOOD
% TOTAL PORE VOLUME
• CORE GROUP "A"
x CORE GROUP "B"
PROPERTIES "A" "B"
POROSITY 21% 19%
IRREDUCIBLE WATER 20% 30%
BRINE PERMEABILITY 300md 20md

FIG. 1 — RELATION BETWEEN INITIAL AND RESIDUAL GAS SATURATION FOR TWO SANDSTONE CORE GROUPS.

been considered by many engineers. However, it is proper at this time to illustrate the magnitude of the improvement in oil displacement efficiency to be obtained by producing water-driven reservoirs below the bubble point pressure and to stimulate consideration of this subject. It is also pertinent to the establishment of a sound maximum efficient rate of production for a given field to emphasize that the optimum pressure for maximum oil displacement in water-driven reservoirs is not at the bubble point as has often been considered to be the case in establishing rates of production. If we are to take advantage of the maximum benefit of gas evolution on oil recovery, the desirability of producing water-driven reservoirs at pressures several hundred pounds per square inch less than the bubble point for those cases in which the well productivity and rock and fluid properties are suitable must be emphasized.

EXPERIMENTAL DATA

When a mobile gas saturation is present in the rock prior to water flooding, the flow of oil ahead of the invading water will generally reduce the gas to an immobile saturation in the oil bank region. The benefit of gas on the displacement of oil by water then results from the immobile gas saturation present at the water displacing front. Since the residual gas saturation has been shown to be a function of the initial gas saturation,[11] the measurement of the influence of various residual gas saturations on the efficiency of the oil displacement by water is necessary for each specific reservoir.

For the reservoir employed as an illustration in this paper, these data were obtained on small core samples. Historically, the use of small cores in flooding experiments has presented difficulties in maintaining desired accuracy in saturation determinations and in specifying the appropriate laboratory flood conditions to give results applicable to field behavior. The development of equipment and laboratory techniques utilizing small cores for this purpose (1 in. length, .87 in. diameter) has progressed in our laboratory to the point that data obtained in this manner for conventional waterflooding is as reliable as that obtained through the measurement of relative permeability curves by the capillary pressure method. The latter is commonly used in making flood studies.

The small core flooding equipment was used in measuring the benefit of the presence of gas on the water displacement of oil. The cores were carried through the following sequence of operations: (1) irreducible water in the presence of oil was established by restored state techniques, (2) an initial gas saturation was established by gas injection, (3) the oil and gas saturations were reduced to residual by a waterflood, and (4) the value of the residual gas saturation was determined by material balance at the conclusion of the flood. The oil saturation remaining at a water-oil ratio of 100:1 was taken to be residual oil and is referred to as such throughout this discussion.

In this type study, it is essential that the free gas saturation present in the oil bank not be dissolved under the pressure gradients employed. The floods were conducted at low pressure gradients across the cores of a few pounds per square inch generally between 1 and 5 psi, and a negligible amount of gas was dissolved. However, the rates of flooding were high enough to minimize end effects. The phases employed were brine, a light oil (tri-isobutylene) and air.

The relation between initial and residual gas saturations for two of the different groups of rock properties is illustrated in Fig. 1. Measurements on five cores in Group A and three cores in Group B were obtained. At low gas saturations there is little difference in the relationship between the initial and residual gas saturations for the two core groups. However, at high initial gas saturations the two core groups show a difference. It would be expected that high initial gas saturations

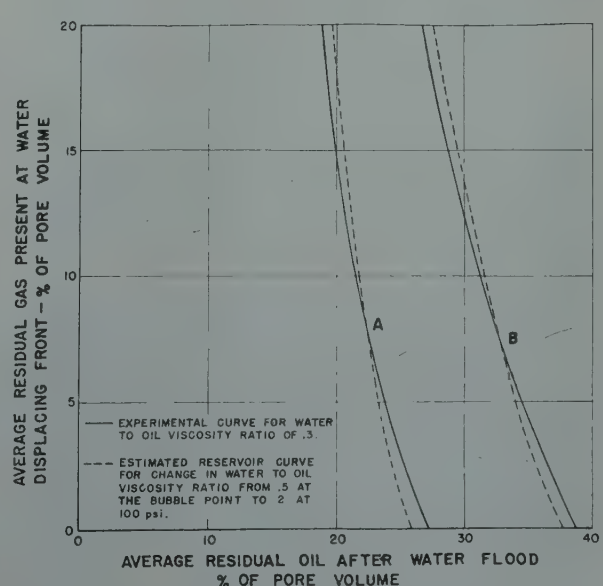
AVERAGE RESIDUAL GAS PRESENT AT WATER DISPLACING FRONT – % OF PORE VOLUME
AVERAGE RESIDUAL OIL AFTER WATER FLOOD
% OF PORE VOLUME
A
B
EXPERIMENTAL CURVE FOR WATER TO OIL VISCOSITY RATIO OF .3.
ESTIMATED RESERVOIR CURVE FOR CHANGE IN WATER TO OIL VISCOSITY RATIO FROM .5 AT THE BUBBLE POINT TO 2 AT 100 psi.

FIG. 2 — INFLUENCE OF RESIDUAL GAS ON THE RESIDUAL OIL AT END OF WATER FLOOD.

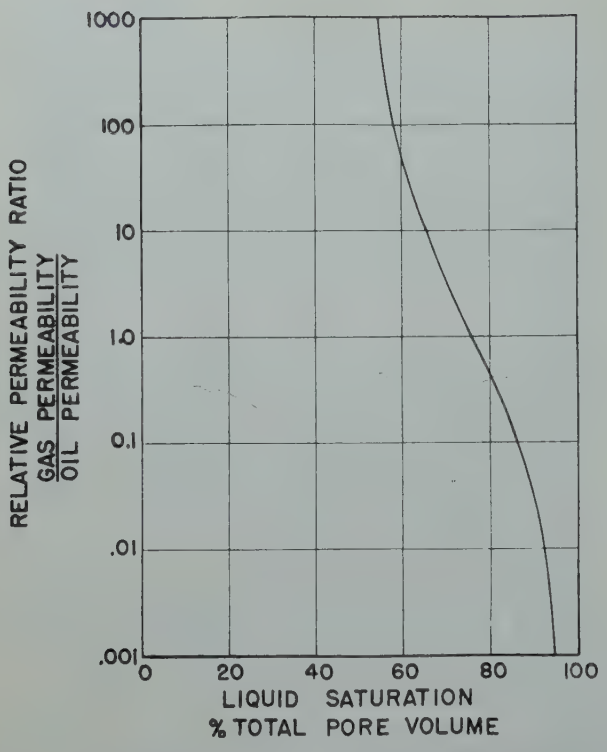

FIG. 3 — RELATIVE GAS-OIL PERMEABILITY RATIO FOR BOTH CORE GROUPS.

would result in higher residual gas saturations in core Group B than in core Group A. This would be expected since the two groups show a marked difference in the residual oil saturation to a waterflood. Both gas and oil act as a nonwetting phase during the water flood, consequently the maximum residual gas saturation would be expected to be the same as the residual oil saturation which is obtained in the absence of gas. The relationship between initial and residual gas saturations of Fig. 2 appears to extrapolate to the values of the residual oil saturations of 26 per cent for core Group A and 37 per cent for core Group B.

The influence of various gas saturations on the average residual oil saturation is illustrated in Fig. 2. The average curves are shown for the two core groups representing five cores in Group A and three cores in Group B. At low gas saturations the reduction in oil saturation is nearly equal to the residual gas saturation present. Also, it appears that the cores showing the poorest displacement of oil by water in the absence of a gas saturation also show the most benefit to the presence of gas.

These experimental data were obtained for a water-to-oil viscosity ratio of 0.3. For the specific reservoir under study this viscosity ratio is 0.5 at the bubble point pressure and declines to 0.2 at 100 psi. In the calculations which illustrate the influence of the gas saturation established under this pressure decline on the oil displacement efficiency by water, it is necessary to consider the reduction in the oil displacement efficiency which results from the lower viscosity ratios. When the change in the viscosity ratio is large, laboratory floods would be required at several viscosity ratios.

For the reservoir under study, floods were conducted at a zero gas saturation for one other viscosity ratio (0.7). The change in residual oil of 2 pore per cent was too small to justify extensive additional flooding tests at other ratios and at other gas saturations. The flooding data at the two viscosity ratios were used to estimate by interpolation and extrapolation the change in residual oil which results from the change in the viscosity ratio from 0.5 to 0.2 which occurs during the pressure decline in the reservoir. This is shown as the dashed curve in Fig. 2. The residual oil saturation differs from that of the experimental curve obtained at a viscosity ratio of 0.3 by only 1 pore per cent. The pressure-volume-temperature relationships of the reservoir fluid in the sample case illustrated here are summarized in Table 1. This fluid could be classified as one of low shrinkage. The reservoir is considered to be saturated initially. The experimental relative permeability relationships of the oil-gas system were obtained by the capillary pressure method.[13] These relationships for the two core groups are shown in Fig. 3.

CALCULATION PROCEDURE

In illustrating the benefit of gas on the oil displacement efficiency by water during production of a water-drive reservoir below the bubble point, a simplification in the calculation procedure will be employed. This simplification will assume that the reservoir is depleted by solution gas drive to various pressures, followed by water displacement of the oil at each of these pressures.

The method presented by Muskat[14] for the calculation of solution gas drive behavior was employed in obtaining the recovery and gas saturation resulting from this production mechanism at each of the several pressures. The residual oil left after the water flood at each of these pressures was taken for the appropriate condition from the data of Fig. 2. While the experimental data represents the influence of injected gas, it has been shown that the influence of either injected or evolved gas is approximately the same.[11]

In practice, the pressure decline below the bubble point in a water-driven reservoir is continuously influenced by the water encroachment. The exact solution to a specific case would involve the analysis of the gas distribution present in the reservoir throughout its pressure decline history and the analysis of the influence of that gas distribution on the oil displacement. In illustrating the presence of an optimum pressure and approximate magnitude of the effect of this optimum pressure for utilizing the benefit of gas evolution on the oil displacement efficiency, the above-mentioned simplification appears justified. The influence of this type operation on the displacement efficiency is illustrated for two of the types of rock material present within the reservoir under study since the average behavior of many reservoirs may fall between these two examples. For any given reservoir it is necessary to develop an

TABLE 1 — FLUID PROPERTIES

Pressure psig	Viscosity c.p.	Formation Volume Factor Res. bbl /STB (flash)	Formation Volume Factor Res. bbl Residual bbl (differential)	Gas Solubility SCF /STB
2,186 (Bubble Point)	.74	1.284	1.334	438
2,000	.78	1.257	1.317	406
1,500	.91	1.195	1.275	311
1,000	1.07	1.142	1.230	212
500	1.24	1.092	1.183	109
100	1.51	1.054	1.141	23

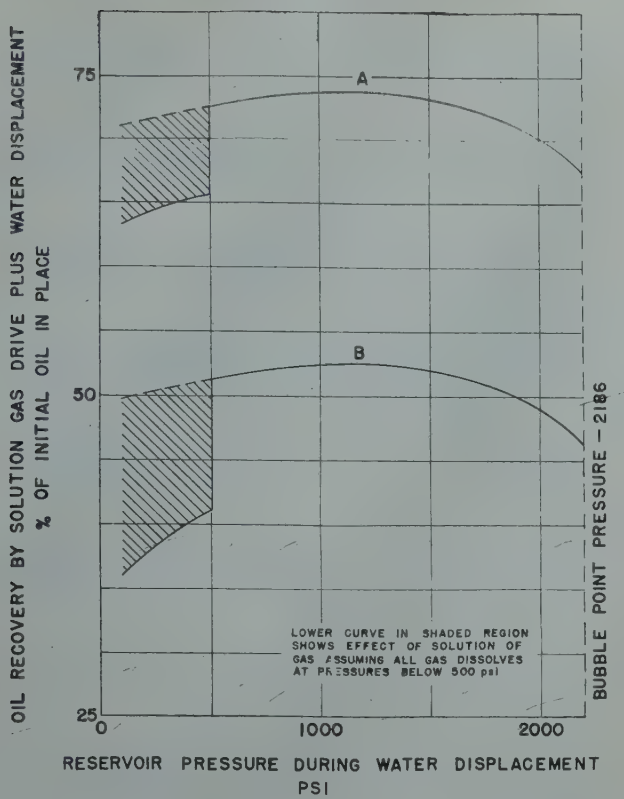

FIG. 4 — CALCULATED OIL RECOVERY BY PRODUCTION UNDER SOLUTION GAS DRIVE PLUS THAT BY WATER DISPLACEMENT.

analysis specific to that reservoir and its individual pressure decline history. The rock samples used here are from a Wilcox Sand reservoir.

BENEFIT OF GAS

The benefit of gas evolution on the oil displacement efficiency by water in water-driven reservoirs producing below the bubble point pressure is illustrated in Fig. 4 and summarized in Table 2. This is illustrated by showing the total oil recovery to be obtained by a solution gas drive to each given pressure, plus the oil recovery to be obtained by water displacement at each given pressure.

The curves of Fig. 4 illustrate that a significant improvement in oil recovery is obtained during the first few hundred pounds per square inch decline of the reservoir pressure below the bubble point. They also illustrate the presence of an optimum pressure for the displacement of the oil by water in the presence of evolved solution gas. At the optimum pressure (about 900 psi below the bubble point) a 7 to 12 per cent increase in recovery is obtained over that which would result from a flood at the bubble point pressure. At low pressures the shrinkage of the oil and the increased oil viscosity are sufficient to result in a lower total oil recovery even though the presence of a gas saturation is exerting a beneficial effect in reducing the residual oil saturation.

The effect of the gas saturation is illustrated in the lower pressure region of Fig. 4 by assuming that the gas is re-dissolved. This re-solution of the gas may frequently happen late in the life of a partial water drive when the reservoir voidage rates have declined low enough to permit some re-pressuring of the reservoir. At pressures less than 500 psi, the standard cubic feet of free gas present in the reservoir are low enough to require only small pressure increases to cause re-solution of all of the gas. The benefit of gas on the oil displacement by water is also frequently lost in low pressure water injection operations as a result of re-solution of the gas under the injection pressure gradients normally employed.

While the illustration of the benefit of gas was obtained for a fluid of low shrinkage, the qualitative influence of other fluids can be speculated upon. A higher shrinkage oil would show an optimum pressure for displacement by water which is nearer the bubble point pressure; the broad pressure region showing little change in recovery would be compressed and the difference between the maximum and minimum recovery shown in Fig. 4 would be enlarged.

In the foregoing discussion the benefit of gas on the displacement of oil in the volume of a reservoir con-

TABLE 2 — CALCULATED RECOVERY BY SOLUTION GAS DRIVE PLUS THAT OBTAINED BY WATER DISPLACEMENT

Pressure, psig	2,186		2,000		1,800		1,400		1,000		600		200		100	
Core Group	A	B	A	B	A	B	A	B	A	B	A	B	A	B	A	
Solution Gas Drive Recovery Per Cent Initial Oil	0	0	3.5	3.1	7.1	7.3	10.9	12.5	13.0	14.7	14.3	16.0	15.3	17.8	15.9	18.5
Gas Saturation Present at Start of Waterflood Fractional P.V.	0	0	0.38	.031	.075	.068	126	.120	.162	.153	.193	.181	.224	.212	.235	.222
Oil Saturation Present at Start of Waterflood Fractional P.V.	0.800	0.700	.762	.669	.725	.632	.674	.580	.638	.547	.607	.519	.576	.488	.565	.478
Residual Gas Saturation Fractional P.V.	0	0	.036	.027	.063	.049	.098	.081	.117	.100	.133	.117	148	.136	152	.141
Residual Oil Saturation After Waterflood Fractional P.V.	0.258	0.376	.239	.356	.228	.342	.217	.325	.212	.315	.208	.308	.205	.300	.204	.298
Oil Recovery During Waterflood Per Cent Initial Oil	67.7	46.2	66.8	45.7	64.9	43.3	62.0	39.4	59.9	37.2	58.1	35.0	56.0	32.5	55.1	31.4
Total Oil Recovery of Solution Gas Drive Plus Waterflood Per Cent Initial Oil	67.7	46.2	70.3	48.8	71.9	50.6	72.9	51.9	72.9	51.9	72.4	51.0	71.3	50.3	70.9	49.9
Connate Water Per Cent Pore Volume	20	30														

tacted by the invading water has been illustrated. However, the evolution of gas may frequently cause a greater percentage loss in the relative permeability to oil than to water (at low gas saturations the water saturation in the invaded region is little affected). This relative permeability change reduces the mobility of the unswept region with respect to the mobility of the swept region and this may adversely affect the sweepout pattern.

In injection operations it has been shown that the amount of oil recovered prior to breakthrough of the displacing phase as well as the ultimate sweepout pattern attained by continued production after breakthrough are adversely affected by reductions in mobility ratio.[16] It would also be expected that the sweepout pattern developed by natural water encroachment would also be adversely affected by reductions in the mobility ratio. The effect of gas evolution on the sweepout pattern must be considered for each reservoir. In some instances, particularly with high viscosity oils, the loss in oil recovery resulting from the reduction in the volume of the reservoir to be invaded at the lower mobility ratios may be greater than the additional recovery resulting from an increased oil displacement efficiency obtained in the region contacted by the water.

CONCLUSIONS

The studies of the influence of a gas saturation on the displacement of oil by water reported by several investigations and the analysis related to the production of water-driven reservoirs below their bubble point pressure presented here lead to the following conclusions:

1. The optimum pressure for the displacement of oil by water in some water-driven reservoir is not at or above the bubble point pressure as has perhaps often been assumed in establishing the maximum efficient rate of production from a field but may be several hundred pounds per square inch below this point.

2. The increase in the oil displacement efficiency of 7 to 12 per cent which may sometimes be obtained by the displacement of oil at the optimum pressure rather than at the bubble point as illustrated here, while not large, is sufficient to warrant consideration in planning reservoir operations.

3. The results to be expected by production of a water-driven reservoir below the bubble point must be analyzed for each given reservoir. Consideration must be given to the effect of any gas segregation, mobility changes, reservoir inhomogeneities, etc., on the oil recovery in determining whether or not production below the bubble point is desirable for the specific reservoir.

REFERENCES

1. Booth, A. E.: "Gas Injection as an Aid to Waterflooding," *Producers Monthly* (November, 1937), 2.
2. Torrey, Paul D.: "A Review of Some Important Water Injection Projects," API *Drilling and Production Practice* (1951), 286.
3. Breston, Joseph N.: "Injection of Natural Gas Before and During Waterflooding," *Producers Monthly* (June, 1952), **16**, 16.
4. Calhoun, John C., Jr.: "The Injection of Gas as an Aid in Waterflooding," *Producers Monthly* (February, 1953), **17**, 32.
5. Krutter, Harry, and Day, Robert J.: "Air Drive Experiments on Long Horizontal Consolidated Cores," *Jour. of Petroleum Tech.* (November, 1943), T. P. 1627.
6. Breston, Joseph N., and Hughes, R. V.: "Long Core Experiments with Brine Floods Following Depletion with Gas Drive," *Producers Monthly* (December, 1948), **13**, 14.
7. Pfister, R. J.: "More Oil from Spent Water Drives by Intermittent Air or Gas Injection," *Producers Monthly* (September, 1947), **11**, 10.
8. Holmgren, C. R.: "Some Results of Gas and Water-Drives on a Long Core," *Trans,* AIME (1949), **179**, 103.
9. Dykstra, Herman, and Parsons, R. L.: "The Prediction of Oil Recovery by Waterflood," *Secondary Recovery of Oil in the United States,* API, 2nd Ed. (1950), 160.
10. Schiffman, Louis, and Breston, Joseph N.: "The Effect of Gas on Recovery When Waterflooding Long Cores," *Producers Monthly* (January, 1950), **14**, 11.
11. Holmgren, C. R., and Morse, R. A.: "Effect of Free Gas Saturation on Oil Recovery by Waterflooding," *Trans.* AIME (1951), **192**, 135.
12. Wilson, D. A., and Geffen, T. M.: "Fluid Distributions in Porous Systems," Motion Picture from the Stanolind Oil and Gas Co.
13. Brownscombe, E. R., and Slobod, R. L., and Caudle, B. H.: "Laboratory Determination of Relative Permeability," *Oil and Gas Jour.,* Part I (Feb. 9, 1950), **48**, 68; Part II (Feb. 16, 1950), **48**, 98.
14. Muskat, M.: "The Production Histories of Oil Producing Gas Drive Reservoirs," *Journal of Applied Physics* (March, 1945), **16**, 147.
15. Dyes, A. B., Caudle, B. H., Erickson, R. A.: "Oil Production After Breakthrough — As Influenced by Mobility Ratio," (April, 1954), **6**, 27.

★★★

THE PHASE and VOLUMETRIC BEHAVIOR of NATURAL GASES at LOW TEMPERATURES and HIGH PRESSURES

P. C. DAVIS — ETHYL CORP. BATON ROUGE, LA.
A. F. BERTUZZI — PHILLIPS PETROLEUM CO. BARTLESVILLE, OKLA.
T. L. GORE — STANDARD OIL CO. (IND.) KANSAS CITY, MO.
F. KURATA — UNIVERSITY OF KANSAS LAWRENCE, KANS.

T. P. 3917

ABSTRACT

The phase and volumetric properties of 10 very volatile mixtures are presented for temperatures from −200°F to above the critical points. These mixtures consisted of natural gases and of mixtures of natural gases with methane and nitrogen. Existing correlations of compressibility factors have been extended to apply to these mixtures. Existing correlations of critical pressures and temperatures do not apply to these mixtures. Methods have been developed for estimating critical temperatures of these mixtures to ± 4°F and critical pressures to ± 5 per cent. These methods apply to other volatile and very volatile mixtures.

The results of this work are particularly applicable to the separation of nitrogen from hydrocarbons by low-temperature distillation.

INTRODUCTION

Knowledge of the low-temperature phase and volumetric properties of natural gases and of other mixtures of the light hydrocarbons is becoming increasingly important as interest in low-temperature separation processes increases. Low-temperature distillation has been used to separate ethane and ethylene from natural gas and from refinery gases for petrochemical uses. Removal of nitrogen from natural gas by low-temperature distillation has been proposed[7,20] as a means of increasing the capacity of existing gas transmission lines and of improving the marketability of the gas.

Further application of low-temperature separation processes has been retarded by lack of data on the phase and volumetric behavior of mixtures at low-temperatures and at high pressures. This paper presents the results of determination of the phase and volumetric properties of 10 very volatile mixtures at temperatures from −200°F to above the critical point. These mixtures consisted of natural gases with methane and nitrogen. Generalized methods are presented for estimating the critical temperatures, critical pressures, and the densities of such mixtures.

Manuscript received in Petroleum Branch offices Feb. 15, 1954. Paper presented at Petroleum Branch Fall Meeting in San Antonio, Oct. 17-20, 1954.

[1]References given at end of paper.

EXPERIMENTAL APPARATUS AND PROCEDURES

The apparatus and the experimental procedures have been described in an earlier paper[13]. The method consists of displacing the mixture from a reservoir which is maintained at constant temperature and pressure into an agitated glass equilibrium cell which is maintained at constant temperature. The liquid level within the glass equilibrium cell was visually observed, and the pressure was measured to within ± 3 psi with a calibrated Bourdon gage.

COMPOSITIONS OF MIXTURES STUDIED

The compositions of the mixtures studied are summarized in Table 1. The measured properties included in Table 1 will be discussed later in this paper. The sources of these gases are described below:

Gas "A-1" was obtained from the Phillips Petroleum Co. Its composition was reported in connection with earlier work.[22] The properties of this gas were reported in an earlier paper.[13]

Gases "A-2, A-3, A-4" were prepared by mixing nitrogen with gas "A-1."

Gas "AB-1" was prepared by mixing methane with gas "A-1." The properties of this gas were reported in an earlier paper.[13]

Gases "AB-2" and "AB-3" were prepared by mixing nitrogen with gas "AB-1."

Gas "B" was obtained by W. W. Bodle of J. F. Pritchard & Co. from the primary separator of a well in western Kansas.

Gas "C" was obtained from a Cities Service Co. pipeline at Lawrence, Kans.

Gas "D" was prepared by mixing gas "AB" with gas "C."

TABLE 1 — PROPERTIES OF GASES STUDIED

Gas	A-1	A-2	A-3	A-4	AB-1	AB-2	AB-3	B	C	D
Carbon Dioxide, Mole %	1.20	1.09	1.00	0.91	0.44	0.30	0.20	0.13	0.20	0.25
Helium	....	....	....	....	....	....	....	1.00	0.60	0.31
Nitrogen	....	8.84	16.11	24.41	....	11.30	24.00	11.46	13.50	7.05
Methane	90.89	82.86	76.25	68.70	96.68	85.80	73.64	76.65	75.15	85.32
Ethane	4.40	4.01	3.69	3.33	1.60	1.50	1.20	5.51	6.10	4.11
Propane	1.91	1.74	1.60	1.44	0.70	0.60	0.53	3.35	3.27	1.98
i-Butane	0.33	0.30	0.28	0.30	0.14	0.12	0.10	0.35	0.38	0.37
n-Butane	0.60	0.55	0.51	0.40	0.20	0.18	0.15	0.90	0.60	0.39
i-Pentane	0.21	0.19	0.18	0.16	0.07	0.06	0.05	0.17	)	
n-Pentane	0.13	0.12	0.11	0.10	0.05	0.04	0.04	0.15	0.20	0.22
Hexanes	0.15	0.14	0.12	0.11	0.05	0.04	0.04	0.33)	)	
Heptanes +	0.18	0.16	0.15	0.14	0.07	0.06	0.05			
Critical Pressure psia	925	955	968	973	765	790	815	1,143	1,107	918
Critical Temp., °R	381	368	356	340	359	343	329	376	370	364
Critical Density, gm/ml	0.230	0.242	0.279	0.311	0.183	0.220	0.225	0.266	0.270	0.270
Mol. Av. Crit. Press.	676	659	646	631	674	653	630	644	644	658
Mol. Av. Crit. Temp.	369	356	346	334	353	339	322	358	354	354
Wt. Av. Crit. Temp.	409	386	368	349	370	344	320	397	380	379
Mol Av. Mol. Wt.	18.40	19.25	19.94	20.75	16.90	18.11	19.56	20.02	19.98	18.60
Wt. Av. Equiv. Mol. Wt. (W)	22.26	21.47	20.80	20.22	18.54	18.00	17.62	22.85	21.25	20.19
Mol. Av. B. P. $(\overline{B})$ °R	218	211	205	199	207	199	191	213	210	209

Volumetric Behavior

The volumetric data of this study were determined by metering gas into the test cell from a reservoir at temperatures from 100 to 110° F and at pressures from 750 to 1,300 psi gage. The densities of the gases in the reservoir were calculated from the correlation of Standing and Katz.[26] This correlation has been shown[3] to be accurate to approximately 1 per cent for dry gases containing up to 7.5 per cent nitrogen, within the pressure and temperature ranges mentioned above. The correlation has not been tested for high concentrations of nitrogen, but the success in calculating the compositions of mixtures of gases "A" and "AB" with nitrogen indicates that it is probably correct within 2 per cent.

The density of liquid propane at 32°F was determined by this experimental method. The result was 0.529 gm/ml compared with a published[27] value of 0.5304 gm/ml. Other data indicate the reasonableness of the results of this investigation. For example, the compressibility factors of gas "AB" agreed with those of pure methane[8] to less than 1 per cent at a reduced temperature of 1.10 and at reduced pressures up to 0.6. It is believed that the compressibility factors are correct within 2 per cent as far as the experimental determinations are concerned; uncertainty in the correlation of Standing and Katz increases the over-all uncertainty to approximately 4 per cent.

The volumetric data were calculated as compressibility factors (PV/RT). Large errors in compressibility factors at very low densities were avoided by extrapolating the factors obtained at higher densities to unit compressibility factors at zero pressure. The compressibility charts thus prepared were cross plotted to obtain compressibility factors at even values of reduced temperature. These compressibility factors are summarized in Table 2.

The volumes used in calculating the compressibility factors are the volumes of the entire mixtures. In many cases both liquid and vapor are present. Standing and Katz[26] showed that compressibility factors of mixtures may be correlated with reduced temperatures and pressures even when two phases are present. The compressibility factors shown in Table 2 were averaged at each reduced pressure and temperature to obtain the average compressibility factors chart which is shown in Fig. 1. Values from the correlation of Standing and Katz are included in Fig. 1 for comparison. Fairly good agreement is indicated by this comparison. The standard deviations of the compressibility factors are shown in Table 2 which shows that the mean compressibility chart can be used with a standard deviation less than 2 per cent at reduced pressures greater than 0.40 and compressibility factors greater than 0.8. It can be used with a standard deviation less than 5 per cent at reduced pressures greater than 0.4 and compressibility factors greater than 0.6. Errors are large where large amounts of liquid are present if the density of this liquid is much greater than the density of the vapor.

Although the average compressibility factors can be used with small error, subject to the limitations mentioned above, it is recommended that compressibility factors from Table 2 be used. The compressibility factors used should be those of the gas which most closely resembles the gas in question. These compressibility charts can then be combined with the zero-pressure specific heat data for the individual components to obtain thermodynamic functions such as enthalpy and entropy for natural gases and for other mixtures of nitrogen and the light hydrocarbons.

Phase Equilibria

Previous Work

Limited low-temperature equilibrium data are available for hydrocarbons and for mixtures of hydrocarbons with nitrogen and helium.[1,2,5,9,10,11,13,14,17,28] Most of these data are for binary systems, and the data of Stutzman and Brown[28] are the only data on a natural gas. Since the completion of this study, Bloomer and Parent[2] and Cines, et. al.[5] have published complete phase equilibrium data on the methane-nitrogen system.

There are extensive published critical data for systems containing hydrocarbons. However, the only published critical point data on systems having critical temperatures below the ice point are the methane-ethane data of Ruhemann[23], the nitrogen-methane data

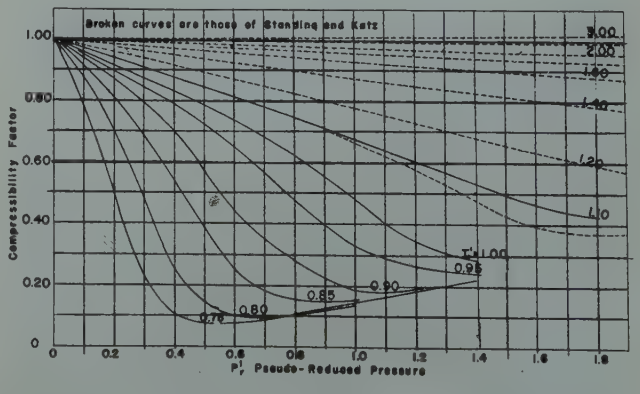

FIG. 1 — MEAN COMPRESSIBILITY FACTORS.

of Bloomer and Parent,[2] and Cines, et. al.,[5] and the data of Eilerts et. al.[9] on a gas-condensate system. These data alone are not sufficient for estimation of the critical points of the very volatile systems of engineering interest. While publication of complete data on the nitrogen-methane system has eased this problem, additional data on more complex systems are required.

Experimental Phase Diagrams

As described earlier in this paper the experimental phase data were obtained as volume per cent liquid versus pressure at various constant temperatures. The isotherms for gas "A-4" are shown in Fig. 2. This chart was cross-plotted to obtain a plot of pressure versus temperature at constant volume per cent liquid. These plots are shown in Fig. 3 for mixtures "A-4" and "C". The bubble-points of all mixtures studied are tabulated in Table 3. The critical point of each mixture was determined as the point at which all constant per cent liquid lines converged. This point could be determined to within about ± 1°F.

The phase diagrams of these mixtures are typical of hydrocarbon mixtures having a preponderance of the most volatile component. There is a large region above the critical point in which two phases can exist. All of the mixtures studied have a large region of "retrograde condensation" in which condensation can occur with increase in temperature or with decrease in pressure. The addition of nitrogen increased the critical pressures of the mixtures.

The vapor-liquid equilibria of hydrocarbon mixtures are commonly expressed in terms of the equilibrium vaporization ratios (K's) of the individual components. These K's may be obtained from the bubble-point dew-point data of binary mixtures, but they cannot in general be obtained in this way for multi-component mixtures. Thus the data obtained in this investigation cannot be directly used to obtain K's, however, any proposed set of K's can be checked against the bubble-point data. In order that this may be done with greater accuracy, the bubble-points of those mixtures are tabulated in Table 3. The use of the dew-point curves for this purpose is not recommended since these curves are much less accurate. The relative accuracy of the bubble-point and dew-point curves is indicated in Fig. 2.

It has been shown in an earlier paper[13] that the bubble-points of the gases which contain no nitrogen ("A-1 and AB-1") may be estimated accurately from the M. W. Kellogg Equilibrium constants,[16] even at temperatures approaching the critical temperature. This

TABLE 2 — COMPRESSIBILITY FACTORS OF GASES STUDIED

Gas	A-1	A-2	A-3	A-4	AB-1	AB-2	AB-3	B	C	D	AV	σ
Pr′						Tr′ = 1.10						
0.20	0.936	0.939	0.940	0.937	0.944		0.945	0.930	0.937		0.939	0.005
0.40	0.877	0.880	0.878	0.876	0.902		0.896	0.870	0.880		0.882	0.011
0.60	0.808	0.811	0.807	0.807	0.832		0.839	0.804	0.806		0.814	0.013
0.80	0.742	0.748	0.740	0.741	0.745		0.774	0.744	0.736		0.746	0.012
1.00	0.679	0.687	0.667	0.677	0.650		0.687	0.690	0.673		0.676	0.013
1.20	0.602	0.617	0.596	0.607	0.540		0.598	0.630	0.610		0.600	0.027
1.40	0.510	0.543	0.524	0.546			0.530	0.572	0.555		0.540	0.021
1.60	0.398	0.468	0.464	0.483				0.504	0.494		0.468	0.040
1.80			0.403	0.421				0.450	0.434		0.427	0.020
						Tr′ = 1.00						
0.20	0.911	0.920	0.912	0.905	0.940	0.924	0.911	0.910	0.910	0.917	0.916	0.010
0.40	0.829	0.837	0.825	0.810	0.880	0.845	0.829	0.828	0.820	0.830	0.833	0.019
0.60	0.741	0.742	0.733	0.713	0.782	0.750	0.736	0.740	0.720	0.735	0.738	0.019
0.80	0.627	0.622	0.622	0.616	0.639	0.618	0.610	0.646	0.617	0.621	0.624	0.011
1.00	0.480	0.460	0.490	0.508	0.396	0.427	0.436	0.550	0.509	0.485	0.474	0.046
1.20	0.290	0.322	0.347	0.396		0.286	0.280	0.452	0.411	0.340	0.347	0.061
1.40		0.240	0.247	0.290				0.370	0.337	0.250	0.289	0.054
1.60								0.302	0.302			
1.80								0.262	0.222			
						Tr′ = 0.95						
0.20	0.895	0.910	0.896	0.894	0.912	0.915	0.890	0.894	0.888	0.903	0.900	0.010
0.40	0.790	0.800	0.780	0.810	0.805	0.809	0.774	0.790	0.772	0.781	0.791	0.014
0.60	0.663	0.660	0.649	0.712	0.660	0.644	0.636	0.680	0.638	0.643	0.658	0.025
0.80	0.462	0.460	0.620	0.615	0.320	0.395	0.418	0.554	0.486	0.444	0.477	0.030
1.00		0.250	0.490	0.507		0.150	0.212	0.513	0.340	0.280	0.343	0.142
1.20		0.170	0.348	0.396				0.303	0.270	0.201	0.281	0.086
1.40		0.205	0.248	0.290				0.254	0.240	0.201	0.240	0.033
1.60								0.260	0.230		0.245	
1.80								0.294			0.294	
						Tr′ = 0.90						
0.20	0.871	0.880	0.877	0.855	0.870	0.899	0.860	0.855	0.850	0.873	0.869	0.015
0.40	0.721	0.720	0.694	0.699	0.688	0.715	0.690	0.702	0.688	0.706	0.702	0.013
0.60	0.490	0.479	0.470	0.511	0.200	0.389	0.421	0.538	0.505	0.490	0.449	0.098
0.80		0.190	0.245	0.311				0.390	0.329	0.248	0.286	0.071
1.00		0.134	0.160	0.168				0.284	0.211	0.162	0.187	0.055
1.20								0.235	0.180	0.185	0.200	
1.40									0.188	0.221	0.205	
1.60									0.204		0.204	
						Tr′ = 0.85						
0.20	0.846	0.802	0.786	0.780		0.828	0.821	0.810	0.800	0.820	0.810	0.021
0.40	0.590	0.580	0.501	0.551		0.537	0.502	0.601	0.538	0.501	0.544	0.039
0.60		0.182	0.230	0.320			0.156	0.360	0.302	0.210	0.251	0.076
0.80			0.110	0.127				0.176	0.202	0.160	0.155	0.037
1.00			0.150					0.139	0.173	0.170	0.158	0.016
1.20												
1.40												
1.60												
						Tr′ = 0.80						
0.20	0.802	0.701	0.632	0.675			0.741		0.729	0.710	0.713	0.053
0.40		0.216	0.238	0.325			0.169		0.351	0.206	0.251	0.072
0.60		0.069	0.087	0.103					0.152	0.099	0.102	0.031
0.80			0.091						0.130	0.120	0.114	
1.00			0.128							0.151	0.139	
1.20										0.188	0.188	
1.40										0.220	0.220	
						Tr′ = 0.75						
0.20	0.650	0.431	0.400						0.605	0.448	0.507	0.113
0.40		0.050	0.067						0.189	0.102	0.102	0.062
0.60		0.081	0.057						0.108	0.082	0.082	0.021
0.80			0.091						0.130	0.109	0.110	
1.00			0.148							0.140	0.140	
1.20										0.179	0.179	
1.40										0.210	0.210	

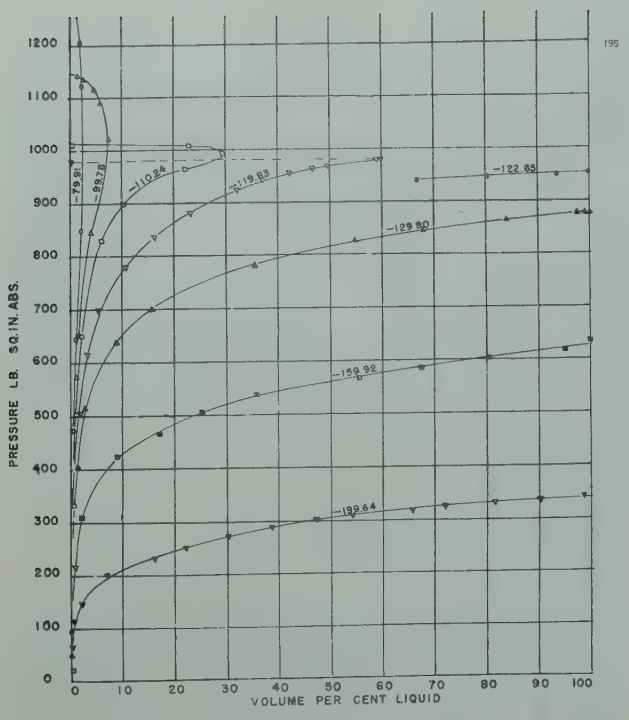

FIG. 2 — EXPERIMENTAL ISOTHERMS OF MIXTURE "A-4."

is essentially a check of the K's for methane since there is only a small amount of less volatile components. It has not been possible to satisfactorily calculate the bubble-points of the gases containing nitrogen. Brown and Stutzmann[4] have presented a set of average K's for nitrogen but it is necessary to apply a large correction factor for application to systems containing hydrocarbons, and this correction factor has not yet been correlated.

The phase diagrams of gases "C and D" show a marked effect of small amounts of helium upon the bubble point. Gas "C" at –200°F required a pressure increase of 50 psi to compress the last 2 per cent of the vapor, even though the mixture contained only 0.6 per cent helium. This effect is marked only at low temperatures, presumably due to the fact that the K for helium goes through a maximum as temperature is decreased.[11] Kay[15] has reported a similar phase diagram for the system hydrogen-naphtha.

CORRELATION OF CRITICAL TEMPERATURES

A number of different correlations have been proposed[8,18,21,25,30] for estimating the critical temperatures of hydrocarbon mixtures. The critical temperature of a mixture of N components is in general a function of $N-1$ composition variables, but it has been found possible to correlate the critical temperatures of hydrocarbon mixtures with only a few variables. The critical temperatures of many mixtures are nearly equal to the weight average critical temperatures, ${}_{m}T'_{c}$, of these mixtures. Kurata and Katz[18] succeeded in correlating the critical temperatures of hydrocarbon mixtures studied up to 1942 using the molal average critical temperature, T'_{c}, and the average molecular weight, with a special treatment for gases containing methane. Organick[21] correlated both critical temperatures and critical pressures as a single function of the molal average boiling point, $\overline{B}$, and the weight average molecular weight, W.

The method which was found most satisfactory for volatile mixtures and for the very volatile mixtures of this study consisted of applying a set of corrections to ${}_{m}T'_{c}$, the weight average critical temperature. Existing data for binary mixtures shows that ${}_{m}T'_{c}$ approximates the true critical temperature, T_{c}. The deviation is greatest at nearly-equal weight fractions of the two components and can be approximated by

$$T_{c} - {}_{m}T'_{c} = A_{1,2}\, m_1\, m_2 \quad . \quad . \quad . \quad . \quad (1)$$

where m_1 and m_2 are the weight fractions of components 1 and 2, respectively. The constant $A_{1,2}$ is characteristic of the particular binary mixture. Equation (1) was extended to complex mixtures by the equation

$$T_{c} - {}_{m}T'_{c} = A_{1,2}\, m_1\, m_2 + A_{1,3}\, m_1\, m_3 + \quad . \quad . \quad .$$
$$+ A_{2,3}\, m_2\, m_3 + A_{2,4}\, m_2\, m_4 + \quad . \quad . \quad . \quad . \quad . \quad .$$
$$+ \quad . \quad . \quad . \quad . \quad . \quad . \quad . \quad . \quad . \quad . \quad . \quad (2)$$

where a term is included for each possible binary system.

The constants for Equation (2) were derived from existing data where these data were available. Since complete binary data were not available, it was necessary to obtain more constants by interpolation and extrapolation from the available binary data. Other constants were obtained by trial-and-error methods from data on complex mixtures. The values thus obtained are shown in Table 4. The use of Equation (2) is demonstrated by Example 1.

The critical temperatures estimated by use of Equation (2) are compared in Table 5 with the experimental values and with the values calculated by the method of Kurata and Katz. The method of Kurata and Katz predicts critical temperatures which are much too high for mixtures which contain large amounts of methane, and it breaks down completely for mixtures containing nitrogen. Equation (2) predicts critical temperatures for the mixtures studied with an error of approximately 4° R or 1 per cent. Its use is recommended for mixtures containing no significant amounts of components less volatile than the heptanes. The method of Kurata and Katz[18] is recommended for these less-volatile mixtures.

A number of the constants of Equation (2) were obtained from data on complex mixtures and are subject to considerable error. As new data on binary mixtures become available, new constants should be calculated to replace these values.

TABLE 3 — BUBBLE-POINT PRESSURES OF GASES STUDIED

GAS	A-1	A-2	A-3	A-4	AB-1	AB-2	AB-3	B	C	D
Critical Temperature, °F	−79	−92	−104	−120	−101	−117	−131	−84	−90	−96
Critical Pressure, psia	925	955	968	973	765	790	815	1,143	1,107	918
−200°F	114	200	255	337	115	220	318		520	320
−180	178	284	369	471	183	321	434		535	371
−160	270	407	507	622	286	447	580	622	623	463
−140	396	555	664	780	425	608	764	766	750	594
−120	547	720	831	973 +	595	765	852*	912	891	745
−100	731	882	996*	1,052*	772*	861*		1,041	1,040	893
−80	912	1,044*	1,172*		907*			1,164*	1,180*	1,011*
−60	1,072*	1,195*						1,248*	1,280*	
−40	1,204*									

* Upper Dew Point
\+ Critical Point

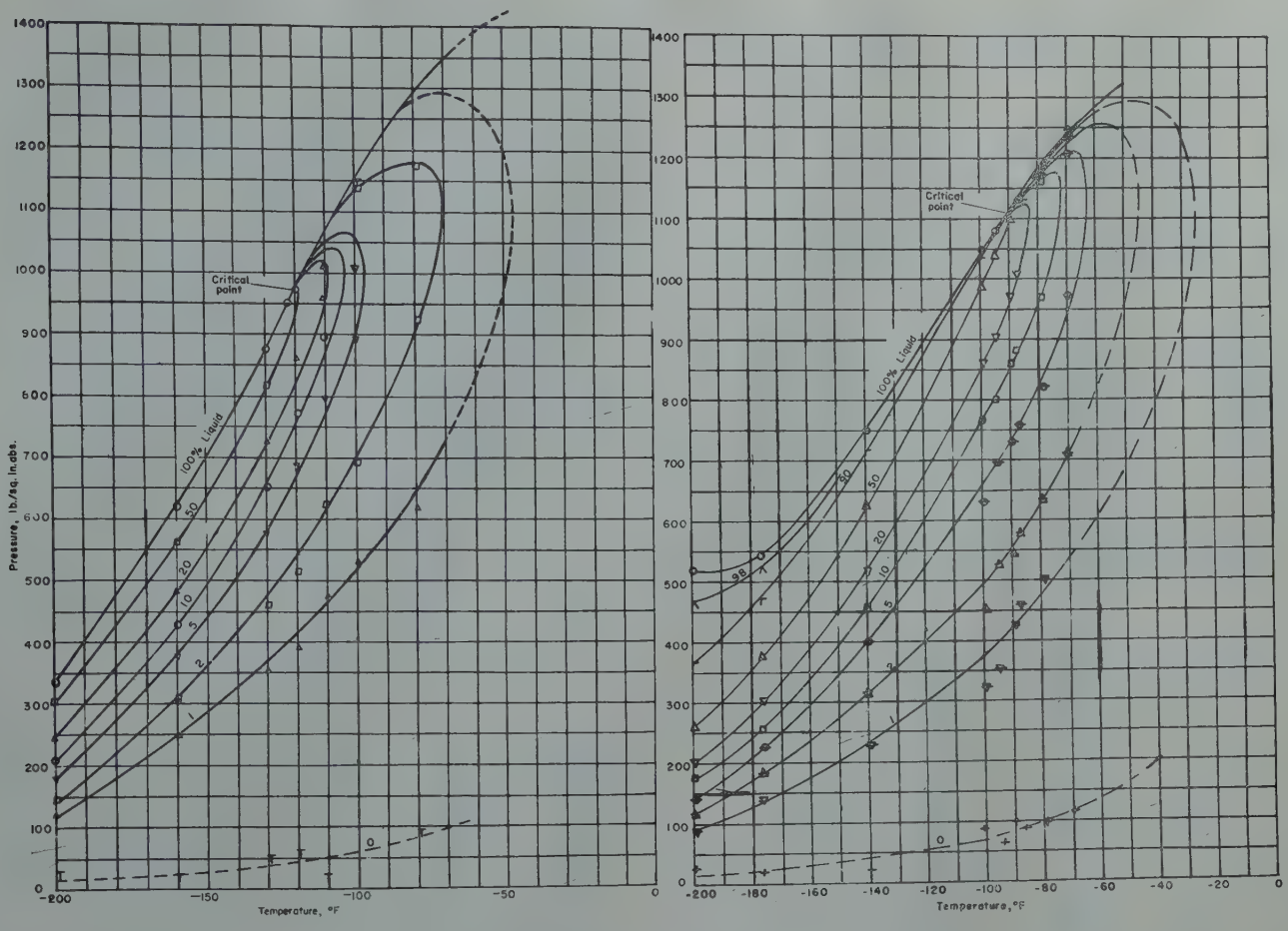

FIG. 3 — PRESSURE-TEMPERATURE DIAGRAMS FOR MIXTURES "A-4" AND "C."

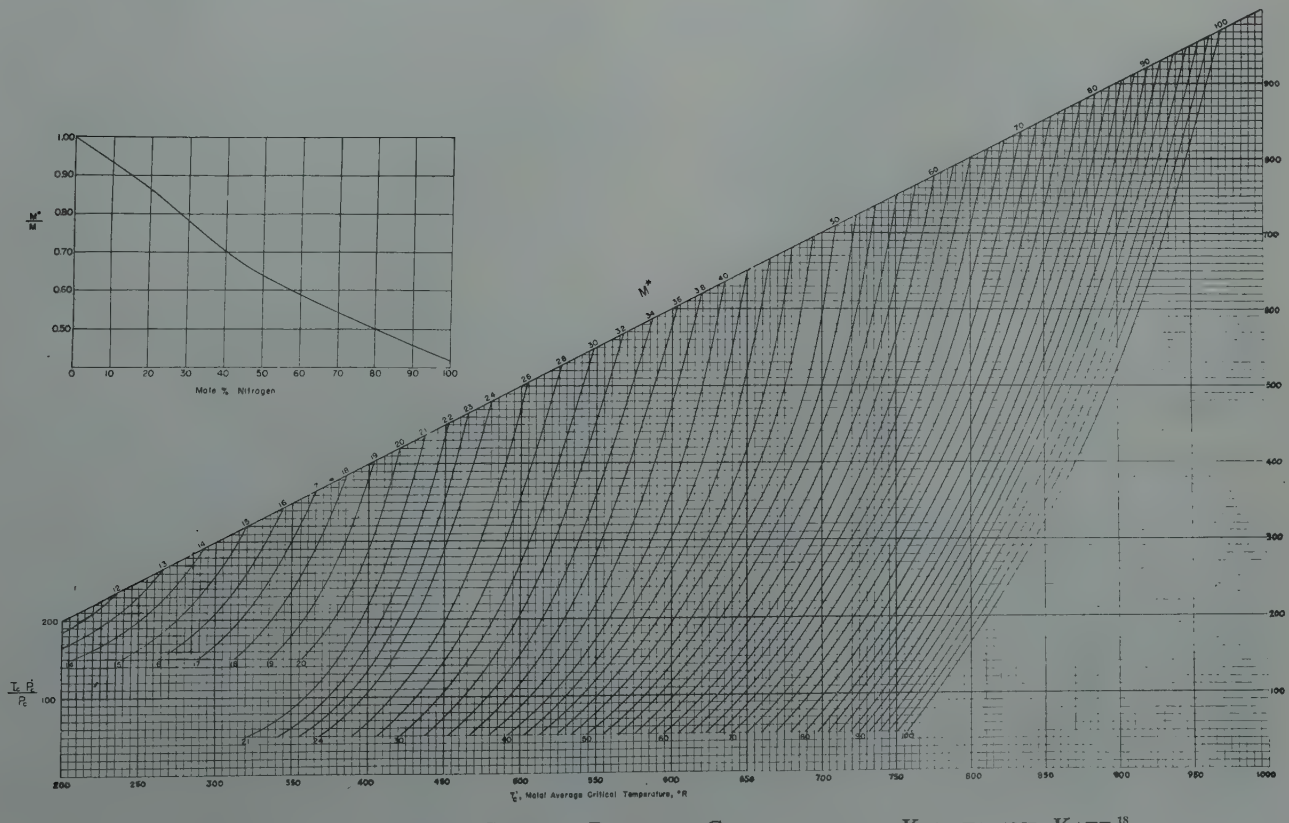

FIG. 4 — MODIFICATION OF CRITICAL PRESSURE CORRELATION OF KURATA AND KATZ.[18]

TABLE 4 — CONSTANTS FOR EQUATION (2)

	N_2	C_1	C_2	C_3	C_4	C_5	C_6	C_7
N_2	0							
C_1	$37+95(N_2)-150$	0						
C_2	$+25$	$-400(C_1)^3$	0					
C_3	0	-30	0					
C_4	-100	-180	-27	$+10$	0			
C_5	-300	-150	-50	-30	0	0		
C_6	-500	-400	-50	-50	0	-25	0	
C_7	-600	-400	-100	-50	-10	-100	0	0
C_8	-600	-400	-150	-50	-10	-100	0	0

Example 1 — Estimation of Critical Temp. of Gas "A-3" Using Equation (2)

	x	M	xM	m	T_c °R	$_mT_c$
Carbon Dioxide	0.010	44.01	0.44	0.022	548	12.0
Nitrogen	0.161	28.02	4.52	0.226	227	51.3
Methane	0.762	16.04	12.22	0.611	343.4	209.7
Ethane	0.037	30.07	1.11	0.056	550	30.6
Propane	0.016	44.09	0.71	0.036	666	24.0
Butanes	0.008	58.12	0.46	0.023	766	17.6
Pentanes	0.003	72.15	0.22	0.011	847	9.3
Hexanes	0.001	86.17	0.09	0.004	914	3.7
Heptanes	0.002	114.22*	0.23	0.011	1,025	11.3
	1,000	M =	20.00	1.000	$_mT_c'$ =	370°R

*Properties of normal octane are used for this gas. For larger amounts of heavy ends, it would be important to experimentally determine the average molecular weight and to use corresponding properties.

		m	A (From Table 4)		mA	
	C_1	0.611	58		34.8	
	C_2	0.056	25		1.4	
N_2	C_3	0.036	0		0	
	C_4	0.023	-100		-2.3	
	C_5	0.011	-300		-3.3	
	C_6	0.004	-500		-2.0	
	C_7	0.011	-600		-6.6	
			0.226	x	19.8 =	+ 4.5°R
	C_2	0.056	-241		-13.5	
	C_3	0.036	-30		-1.1	
C_1	C_4	0.023	-180		-4.1	
	C_5	0.011	-150		-1.6	
	C_6	0.004	-400		-1.6	
	C_7	0.011	-400		-4.4	
			0.611	x	-26.3 =	-16.1°R
	C_3	0.036	0		0	
C_2	C_4	0.023	-27		-0.6	
	C_5	0.011	-50		-0.6	
	C_6	0.004	-50		-0.2	
	C_7	0.011	-150		-1.6	
			0.056	x	-3.0 =	-0.2°R
	C_4	0.023	10		0.2	
C_3	C_5	0.011	-30		-0.3	
	C_6	0.004	-50		-0.2	
	C_7	0.011	-50		-1.1	
			0.036	x	-1.4 =	-0.05°R

Further effects may be neglected for this mixture.

Estimated T_c = 370 + 4.5 - 16.1 − 0.2 − 0.05 = 358°R

Experimental T_c = 356°R

error = + 2°R

TABLE 5 — COMPARISON OF ESTIMATED AND EXPERIMENTAL CRITICAL TEMPERATURES

Mixture	Expt. T_c, °R	Error, °F Equation 2	Error, °F[18]
	Very Volatile Mixtures		
A-1	381	− 5	+ 34
A-2	368	− 1	+ 72
A-3	356	0	
A-4	339	+ 6	+ 141
AB-1	359	+ 3	+ 25
AB-2	343	− 2	
AB-3	329	0	
B	378	+ 1	
C	365	− 3	
D	364	− 3	
	Standard Deviation	3.6	

Mixture	Expt. T_c, °R	Error, °R Equation 2	Error, °R[18]
	Volatile Mixtures		
S-1 (18)	515	− 6	+ 5
S-3 (18)	569	+ 11	+ 3
S-4 (18)	569	+ 6	0
S-5 (18)	630	+ 25	− 3
T-1 (18)	514	− 11	− 3
T-3 (18)	525	− 6	+ 3
T-4 (18)	550	+ 4	+ 3
T-5 (18)	649	+ 26	+ 2
B-1 (18)	538	+ 5	− 8
B-2 (18)	576	− 11	+ 10
B-3 (18)	602	− 17	− 3
B-4 (18)	610	− 12	− 5
A (31)	559	− 1	− 14
B (31)	555	+ 9	0
	Standard Deviation	14.0	6.6

CORRELATION OF CRITICAL PRESSURES

Estimating critical pressures is more difficult than estimating critical temperatures. The critical temperatures of mixtures are roughly approximated by the weighted average of the critical temperatures of the components, but critical pressures are often many times the average critical pressures. Several methods of estimating critical pressures have been proposed.[8,13,21,25,30] None of these methods has been tested for mixtures containing very large amounts of methane or for mixtures containing significant amounts of nitrogen.

The critical pressures of the mixtures studied during this investigation were correlated by a modification of the method of Kurata and Katz.[18] The original correlation was a plot of $T_c P'_c/P_c$ versus T'_c with M as a parameter. The correlation was extrapolated into the low temperature region, since there were at that time no data on the critical behavior of very volatile complex mixtures. This correlation was modified in the low temperature region (below $T'_c = 400°R$) in order to fit the data of this study. An arbitrary correlating

Helium seems to increase the critical pressures above that predicted by Fig. 4 by about 100 psi for each 1 per cent helium content.

Example 2 — Estimation of Critical Pressure of Gas "A-3"

	X	T_c	$_xT_c$	P_c	$_xP_c$
Carbon Dioxide	0.010	548	5.5	1,070	10.7
Nitrogen	0.161	227	36.7	491	79.2
Methane	0.762	343.4	261.5	673	512.8
Ethane	0.037	550	20.4	712	26.3
Propane	0.016	666	10.7	617	9.9
Butanes	0.008	766	5.9	551	4.4
Petanes	0.003	847	2.5	485	1.5
Hexanes	0.001	914	0.9	435	0.4
Heptanes	0.002	1,025	2.0	362	0.7
		T'_c = 347		P'_c = 646	

From Example 1 M = 20.00

Fig. 4 by about 100 psi for each 1 per cent helium content.

Using estimated T_c of Example 1

$$\frac{T_c P'_c}{P_c} = \frac{358 \times 646}{P_c} = 233$$

Estimated P_c = 992 psia

Experimental P_c = 968 psia

error = + 24 psi

Using experimental T_c, estimated $P_c = \frac{356 \times 646}{233} = 988$ psia

error = + 20 psi

TABLE 6 — COMPARISON OF ESTIMATED AND EXPERIMENTAL CRITICAL PRESSURES

Gas	Exptl. P_c psia	Error Fig. 4 psi	Error[18] psi
	Very Volatile Mixtures		
A-1	925	+ 1	+ 150
A-2	955	+ 15	
A-3	968	+ 6	
A-4	973	− 20	+ 3,453
AB-1	765	− 9	+ 20
AB-2	790	+ 21	
AB-3	815	+ 7	
8	1,143	− 80	+ 1,057
C	1,107	− 100	
D	918	− 18	
	Standard Deviation	64.2	

Gas	Exptl. P_c psia	Error, Fig. 4 psi	Error[18] psi
S-2 (18)	2,387	+ 227	+ 227
S-3 (18)	2,574	+ 56	+ 56
S-4 (18)	2,537	+ 3	+ 3
S-5 (18)	2,615	+ 65	+ 65
T-1 (18)	2,605	+ 35	+ 35
T-3 (18)	2,675	− 65	− 65
T-4 (18)	2,730	+ 60	+ 60
T-5 (18)	2,900	+ 10	+ 10
B-1 (18)	1,826	+ 14	+ 14
B-2 (18)	1,797	− 9	− 9
B-3 (18)	1,796	+ 4	+ 4
B-4 (18)	1,706	+ 4	+ 4
A (31)	1,994	+ 6	+ 6
B (31)	1,987	− 7	− 7
	Standard Deviation	75	75

variable, M^*, was substituted for the molecular weight, in order to adapt the correlation for gases containing nitrogen. The ratio M^*/M was plotted versus mole per cent nitrogen. When no nitrogen is present, M^*, is equal to M. Fig. 4 shows the modified correlation. This correlation is identical with the original correlation of Kurata and Katz for gases which contain no nitrogen and for which T'_c is greater than 400° R.

The critical pressures estimated from Fig. 4 are compared in Table 6 with the experimental values and with the values estimated from the original correlation of Kurata and Katz. Table 6 shows that the original correlation gives fair agreement with the data for gases containing very large amounts of methane but is unsatisfactory for gases containing nitrogen. Fig. 4 agrees with the critical pressures of the gases studied to within about 5 per cent. If the helium-bearing gases are not included the agreement is within about 2 per cent.

NOMENCLATURE

x_1 = Mole fraction of component 1
m_1 = Weight fraction of component 1
T_c = True critical temperature, °R
${}_1T_c$ = Critical temperature of component 1, °R
P_c = True critical pressure, psia
M = Molecular weight of a pure component, molal average molecular weight of a mixture
T'_c = Molal average critical temperature, °R
${}_mT'_c$ = Weight average critical temperature, °R
P'_c = Molal average critical pressure, psia
M^* = A correlating variable used in Fig. 4
$A_{1,2}$ = A correlating variable, defined by Equation (2)
B = Molal average normal boiling point, °R
W = Weight average molecular weight

ACKNOWLEDGMENT

Financial aid supplied by the University of Kansas Industrial Fellowship Committee Project No. RF 222 and by the University of Kansas Fund for Research Project No. 17 made this work possible.

REFERENCES

1. Atack, Evans, and McCormack (given by Ruhemann, M.): "The Separation of Gases," 2nd Edition, London: Oxford University Press, 1949.
2. Bloomer, O. T., and Parent, J. D.: "Physical-Chemical Properties of Methane-Nitrogen Mixtures," *Institute of Gas Technology Research Bulletin*, Chicago, Ill. (April, 1952).
3. Brown, G. G., Katz, D. L., Oberfell, G. G., and Alden, R. C.: *Natural Gasoline and the Volatile Hydrocarbons*, Midwest Printing Co., Tulsa, Okla., 1948.
4. Brown, G. M., and Stutzmann, L. F.: *Chem. Eng. Progress* (1949), **45**, 142.
5. Cines, M. R., Roach, J. T., Hogan, R. J., and Roland, C. H.: *Chem. Eng. Prog. Symposium Series* (1953), **49**, No. 6, 1.
6. Davis, P. C., Gore, T. L., and Kurata, Fred: *Ind. Eng. Chem.* (1951), **43**, 1826.
7. Deschner, W. W., and Bodle, W. W.: *Oil and Gas Jour.* (1948), **46**, No. 50, 76; No. 51, 92, 112.
8. Edmister, W. C., and Pollock, W. C.: *Chem. Eng. Progress 44* (1948), 905.
9. Eilerts, C. K., Barr, V. L., Mullins, N. B., and Hanna, Betty: *The Pet. Eng.* (1948) **20**, 502.
10. Fastowsky, V. G., and Gonikberg, M. G.: *Acta Physiochim* (U.R.S.S.) (1940), **12**, 485.
11. Fedoritenko, A., and Ruhemann, M.: *Jour. Tech. Phys.* (U.R.S.S.) (1937), **4**, 36.
12. Gonikberg, M. G., and Fastowsky, V. G.: *Acta Physiochim* (U.R.S.S.) (1940), **12**, 67.
13. Gore, T. L., Davis, P. C., and Kurata, F.: *Trans.* AIME (1952), **195**, 279.
14. Guter, M., Newitt, D. M., and Ruhemann, M.: *Proc. Roy. Soc.* (London) (1940), **176A**, 140.
15. Kay, W. B.: *Chem. Rev.* (1943), **29**, 501.
16. M. W. Kellogg Equilibrium Constants, New York: 1950.
17. Kharakhorin, F. F.: *Foreign Petroleum Tech.* (1941), **9**, 411.
18. Kurata, F., and Katz, D. L.: *Trans.* AIChE (1942), **38**, 995.
19. McKay, R. A., Reamer, H. H., Sage, B. H., and Lacey, W. N.: *Ind. Eng. Chem.* (1951), **43**, 2112.
20. Mullins, P. V., and Wilson, R. W.: *Am. Gas. Assoc. Proc.* (1948), **30**, 601.
21. Organick, E. I.: *Chem. Eng. Prog. Symposium Series* (1953), **49**, No. 6, 81.
22. Poettmann, F. H.: *Trans.* AIME (1951), **192**, 141.
23. Ruhemann, M.: *Proc. Roy. Soc.* (London) (1939), **171A**, 121.
24. Scheffer, F. E. C.: *K. Akad. Wet. Versl. van Vergad* (1913), **22**, 427.
25. Smith, R. L., and Watson, K. M.: *Ind. Eng. Chem.* (1937), **29**, 1408.
26. Standing, M. B., and Katz, D. L.: *Trans.* AIME (1942), **146**, 140.
27. Stearns, W. V., and George, E. G.: *Ind. Eng. Chem.* (1943) **35**, 602.
28. Stutzman, L. F., and Brown, G. M.: *Chem. Eng. Progress* (1949), **45**, 139.
29. Vaughn, W. E., and Collins, F. C.: *Ind. Eng. Chem.* (1942), **34**, 885.
30. Mayfield, F. D.: *Ind. Eng. Chem.* (1942), **34**, 843.
31. Hanson, G. H., and Brown, G. G.: *Ind. Eng. Chem.* (1945), **37**, 821. ★★★

THE MECHANICS of FRACTURE INDUCTION and EXTENSION

EUGENE HARRISON
W. F. KIESCHNICK, JR.
JR. MEMBER AIME
W. J. McGUIRE
MEMBER AIME

THE ATLANTIC REFINING CO.
DALLAS, TEX.

T. P. 3916

ABSTRACT

This paper concerns the induction and extension of fractures into rock formations as involved in drilling, completing, and production stimulating operations on wells. Conclusions concerning formation breakdown are derived from (1) a review and extension of published analyses relating to mechanical theories of rock stress and the state of stress in the earth's crust and (2) a correlation of field data from fracturing operations.

Conclusions concerning the mechanics of fracture extension, which indicate the relationship between fracture dimensions and rock properties, depth, and volume of injected fluid, are tentative and largely establish limits of relationships. These conclusions are derived from stress calculations, limited field data, and laboratory experimental studies. The experimental work involves the study of the stresses at the fracture boundaries and the geometry of pressurized fractures by means of photo-elastic modeling methods.

Results of this investigation indicate that a large majority of pressure induced wellbore fractures are vertical, particularly in deeper wells; and variations in the pressures necessary to create and extend fractures can be explained largely on a basis of established rock properties. It is also shown that variations due to tectonic forces should usually be expected to be slight. Other results indicate that during that extension of fractures rather large fracture volumes are temporarily created by the parting of the formation.

Manuscript received in Petroleum Branch office July 31, 1953. Paper presented at Petroleum Branch Fall Meeting in Dallas, Oct. 18-21, 1953.

[1]References given at end of paper.

INTRODUCTION

The purpose of this paper is to present the results of calculations and laboratory experiments concerning the mechanics of fracture induction and extension with a view to broadening existing knowledge relating to these phenomena. It is believed that continued progress in developing knowledge of this type is important to the further development of techniques for drilling and completing wells.

When a wellbore is subjected to sufficiently high pressure, fracturing of the formation surrounding the well occurs. This phenomenon is a common cause of lost circulation during drilling operations, is a deliberately planned factor in most squeeze cementing operations, and is the controlling factor in many productivity stimulation operations. The exploitation of formation fracturing in recent years has been particularly impressive in sand-viscous fluid well stimulation treatments which were first introduced to the industry by the Stanolind research group[1, 2, 3] several years ago.

The borehole fracturing phenomenon has been analyzed mathematically by application of the principles defining the elastic and inelastic behavior of thick-walled cylinders of homogeneous, isotropic, and impermeable material.[4, 5, 6] This basic argument is re-presented in this paper along with new considerations which strengthen it.

In addition to these arguments relating to fracture induction some calculations and experimental results relating to the mechanics of fracture extension are presented. Since the nature of the pressure induced fracture at distances from the well is of great importance in considerations of well stimulation procedures there appears to be a need for an integrated approach which deals with the mechanics of fracture extension as well as with wellbore rupture.

It is believed that the mechanisms presented in this paper are consistent with recent developments in the field of applied mechanics and material strength as well as with geologic concepts of the state of stress in the earth's crust. It is particularly interesting to note that the mechanism of fracture extension presented here is in agreement with the observations and concept of igneous dike formation presented by Anderson.[7] It is recognized that the results, particularly with respect to fracture extension, are incomplete and need further development; however, they are believed to be useful conceptually and as a basis for further work.

INDUCTION OF FRACTURES IN BOREHOLES

Discussions relating to this subject frequently concern the orientation of pressure induced formation fractures. Scott et al[8], at least by implication, have argued for frequent horizontal fracturing on the basis of laboratory and correlated field data. Squeeze cementing operations are often planned in the belief that horizontal "pancakes" of cement are squeezed between bedding planes in this operation. Walker[5], on the other hand, has argued that squeeze cementing results most frequently in vertical fracturing. Another argument[9] implies that the orientation of the fractures is dependent upon the pre-existing joint or fault system and that thus the pressure induced opening may have a configuration corresponding to the rock's natural fracture system.

From a statistical point of view there is a paucity of published direct evidence relating to induced fracture orientation. However, some interesting cases have been reported in the literature. Only a few cases involving deep wells are available. Teplitz and Hassebroek[10] presented the now well known case involving a core from a Continental Oil Co. well in the Corpus Christi, Tex., area. In this well, cores taken from a sidetracked hole through a formation which had been previously squeezed with cement showed vertical fracture zones filled with cement. Walker[5] reports a case in which a Stanolind well was drilled to 9,523 ft where 9⅝-in casing was set and 3⅞-in rathole was drilled into the formation below. A cement squeeze operation was performed after which the rathole and an additional foot of section was cored. The core recovered had vertical fracture zones filled with cement. Only one case known to the authors is reported as an example of horizontal fracturing in a deep well. Torrey is credited by Walker[5] as describing a case of coring a sidetracked hole adjacent to the squeezed original hole in Louisiana in which horizontal fractures filled with cement were found. No treatment pressures were given in this account.

Clark et al[11] have reported some fracturing experiments in holes from 4 to 15 ft in depth. Several horizontal fractures and one vertical fracture were observed.

This paper seeks to examine the fracturing phenomenon as a problem in applied mechanics. The assumption made to facilitate that examination is the behavior of rock under the influence of applied forces can, if the directions and magnitudes of those forces are known, be predicted on the basis of generalized rock properties such as modulus of elasticity and Poisson's ratio, as determined in the laboratory and listed in engineering handbooks. The study was further simplified by assuming that the fractured rock is homogeneous and isotropic. It is recognized that reservoir rocks are neither homogeneous, isotropic, nor impermeable and that a completely rigorous analysis of fracture mechanics should be based upon analytical expressions which would take into account these factors. However, it is argued that insofar as the homogeneity is concerned, the rock of a given formation usually possesses about the same degree of inhomogeneity as many materials of construction which lend themselves to stress analysis.[12] Further, the simplified analysis for the case of thick-walled cylinders of homogeneous impermeable elastic material has been extended qualitatively to the practical case by examining mathematically in a special case the effect of permeability and porosity. It is believed that by this device the analysis has produced realistic conclusions which apply in a general manner to the actual case in the field.

The Tensile Strength of Rock

Although the thick pipe formula predicts that thick-walled cylinders will rupture when the applied internal pressure equals the tensile strength of the material, it has been observed that thick-walled cylinders of rock on a laboratory scale frequently require rupturing pressures which are far in excess of the generally accepted values of rock tensile strength. This peculiar behavior of small brittle models has been observed by others[13] and is explained by Weibull's statistical theory of material strength.[14] This theory indicates that the results of standard tensile tests in which the specimens are pulled apart, and results of cylinder rupturing tests, should not be expected to agree unless large bored cylinders are employed. As is indicated in Fig. 1, a graph of bursting pressure versus hole diameter for thick cylinders of Austin limestone, a marked relationship between hole diameter and rupturing pressure has been noted.

It is concluded that cylinders of rock do obey the thick pipe formula and that the values of rock tensile

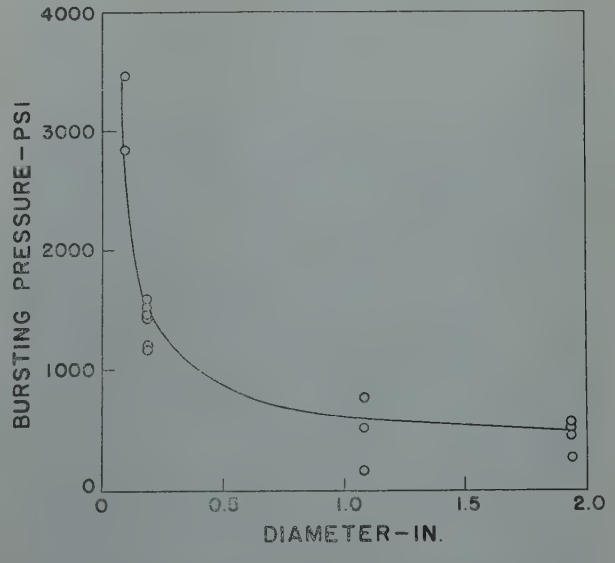

Fig. 1 — Graph of Bursting Pressure vs Hole Diameter for Thickwalled Cylinders of Limestones.

strength as listed in materials handbooks (approximately 500 psi for sandstone and limestone)* reflect the effective strength of rock cylinders of wellbore dimensions with sufficient reliability for the purpose of this investigation.

The State of Stress in the Earth's Crust

In order to determine the magnitudes of the stresses which resist wellbore fracturing it is first necessary to determine the condition of stress at depths in the earth's crust. If we designate as *principal stresses* those stresses which are normal to planes in which there is no shear, the state of stress at any point in the earth's crust can be defined in terms of the principal stresses, σ_z along the vertical Z axis, σ_x and σ_y along the horizontal X and Y axes.

In the absence of external forces, the cause of stress at any point is the weight of the overlying mass. Saturated sedimentary rocks weigh approximately 144 lbs/cu ft.[15] Then, assuming a level surface, the vertical stress at any point is expressed by the equation,

$$\sigma_z = 1.0\,h \text{ psi}^{**} \quad . \quad . \quad . \quad . \quad . \quad . \quad . \quad . \quad . \quad (1)$$

where h is the depth in feet. Under the influence of this vertical stress the rock tends to expand laterally, but is constrained from doing so by the surrounding material. This tendency induces a horizontal stress which, in the ideal situation, is equal in all horizontal directions. In the elastic zones of the earth's crust the relationship between the vertical stress and the induced horizontal stresses should be governed by the elastic laws and be expressed by the equation,

$$\sigma_x = \sigma_y = \sigma_H = \frac{\mu}{1-\mu}\,\sigma_z \quad . \quad . \quad . \quad . \quad . \quad . \quad . \quad (2)$$

Since Poisson's ratio, μ, for sedimentary rocks ranges between 0.18 and 0.27,[16] the horizontal compressive stress lies in the range between 0.22 and 0.37 psi/ft.

The relationship between the stresses in much of the earth's crust is governed by nonelastic properties, the shear strength, cohesiveness, and frictional resistance to deformation. It has been shown that this relationship is approximated by the equation,

$$\frac{\sigma_z}{\sigma_H} = \left(f + \sqrt{1+f^2}\right)^2 \quad . \quad . \quad . \quad . \quad . \quad . \quad . \quad (3)$$

where f is the coefficient of internal friction of the rock.[17]

This condition in which the relationship between the principal stresses is governed by other than the material's elastic properties is often called the plastic state of stress. To generalize, the strong sedimentary rocks have coefficients of internal friction in the vicinity of 0.7 while the coefficient for softer shales, clays and loosely consolidated sands lies in the vicinity of 0.3.[17] These weaker formations exist in the so-called plastic state of stress below relatively shallow depths and possess values of horizontal stress which are greater than 0.37 psi/ft of depth. In the absence of external forces the horizontal stresses are always less than the vertical stress.

Before this consideration of the effect of earth stresses on wellbore rupture is concluded, cognizance should be taken of the not uncommon belief that the competent formations of the earth's crust support the overburden in such a way as to lessen the vertical stress in underlying formations. Hubbert's[18] analysis of the strength of the earth indicates that the effective strengths of formations of reservoir size are negligible. Others,[19] investigating the strengths of natural arches, have found that in order to support even moderate loads over geologic time, arches must rise almost as high as they span. Therefore, it appears that in all cases the vertical stress is expressed by Equation 1.

A possible alternative picture of the state of stress in the earth's crust is one in which through geologic time the principal stresses have entered into a state of hydrostatic equilibrium. If this were the case every direction would be the direction of a principal stress and there would be no shear on any plane. As Hubbert[20] has indicated, this picture is inconsistent with the fact that normal faulting, generally recognized as a manifestation of shear, is occurring in many areas at the present time.

The State of Stress Around Boreholes

The presence of a vertical borehole in a rock formation results in a local zone of high stress in its vicinity. It has been shown[21] that the tangential stress on the periphery of the hole is equal to twice the homogeneous compressive stress which exists at great distances from it. Fracturing on a vertical plane cannot occur until that tangential stress passes from compression to tension. Thus, the pressure required to rupture the borehole vertically is expressed by the equation,

$$p_i = 2\sigma_H + S_t = \frac{2\mu}{1-\mu}\,\sigma_z + S_t \quad . \quad . \quad . \quad (4)$$

which assumes that the borehole will rupture according to the thick pipe formula.

Substituting the value of σ_z from Equation 1 and using 0 to 500 psi as the range of tensile strengths, we find that in competent sandstones and limestones the pressure necessary to induce vertical fracturing should lie between,

$$(\mu = 0.18),\ p_i = .44h$$
$$(\mu = 0.37),\ p_i = .74h + 500 \quad . \quad . \quad . \quad . \quad (5)$$

Up to this point no account has been taken of the loss of fluid into the formation. The thick pipe concept of borehole rupture assumes that the walls of the borehole are impermeable which is frequently not the case. However, it is shown in the Appendix that fluid loss does not invalidate the conclusions of this analysis. It is shown that the loss of fluid into the formation decreases slightly the pressure required to produce vertical fractures.

Up to this point the wellbore has been treated as a thick-walled cylinder in order to determine analytically the pressures required to produce vertical fracturing. There has appeared no analytical tool for the determination of the pressure required to produce horizontal fracturing. However, the lower limit of the pressure necessary to produce relative vertical displacement at the wellbore can be determined by assuming the existence of a thin horizontal layer of permeable material or of a naturally occurring horizontal fracture which is capable of delivering fluid at high pressure to distances from the wellbore. Vertical relative displacement at the wellbore will be accompanied by some bending of the displaced rock. However, the amount of bend-

*This statement is not meant to deny the existence of stronger sedimentary rocks. One sample of sandstone manifested a tensile strength of 1,500 psi both in conventional tensile tests and in cylinder bursting tests.

**Compressive stress is positive.

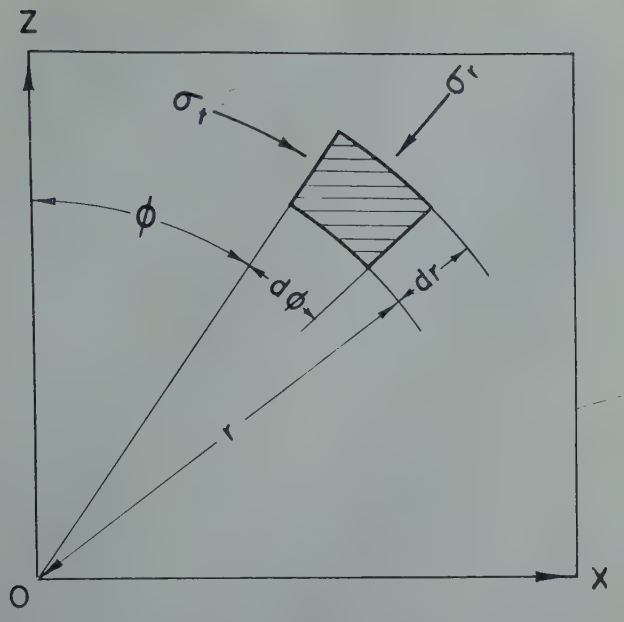

FIG. 2 — STRESSED ELEMENT OF THE EARTH'S CRUST REPRESENTED ON POLAR COORDINATES.

ing, and hence the pressure required to produce it, can be made insignificant if the area over which the vertical displacement takes place is large. Then, in the lower limiting case, horizontal parting can take place when,

$$p_i = \sigma_z \quad . \quad . \quad . \quad . \quad . \quad . \quad . \quad . \quad . \quad . \quad (6)$$

The approximate maximum depth at which horizontal fracturing should occur in the absence of special external forces can be determined from equations 4 and 6 by setting,

$$\frac{2\mu}{1-\mu}\,\sigma_z + S_t < \sigma_z$$

Using the vertical stress gradient of 1 psi/ft and assuming 0.25 as Poisson's ratio the maximum depth is found as 3,300 ft for a tensile strength (S_t) of 1,000 psi.

THE EFFECTS OF JOINTS AND FAULTS NEAR THE WELLBORE ON BOREHOLE RUPTURE

Bugbee[9] has postulated that, "the pressure required to break down rock formations in a well is dependent primarily upon the presence of a fracture, fault or joint system and secondarily, etc. . . .".

It can be assumed that, as is the case with naturally occurring horizontal fractures, a fracture into which fluid can be injected readily will open when the applied pressure equals the compressive stress normal to it.

It has been shown[17] that the general stress system in the elastic zone of the earth's crust can be expressed in polar coordinates as illustrated in Fig. 2 by the following two equations:

$$\left.\begin{aligned} \sigma_r &= \tfrac{1}{2}\,\frac{\sigma_z}{1-\mu}\,[1 + (1-2\mu)\cos 2\phi] \\ \sigma_t &= \tfrac{1}{2}\,\frac{\sigma_z}{1-\mu}\,[1 - (1-2\mu)\cos 2\phi] \end{aligned}\right\} \quad . . \quad (7)$$

Let an open fracture inclined at an angle ϕ with the vertical cut the borehole. The compressive stress normal to it and thus the pressure required to widen it is expressed by Equation 7 for σ_t. The pressure required to induce a vertical fracture in a nonfractured location is expressed by Equation 5. Equating p_i to σ_t from equations 4 and 7 and solving for ϕ we find that,

$$\cos 2\phi = \frac{1-4\mu}{1-2\mu} - \frac{2(1-\mu)\,S_t}{(1-2\mu)\,\sigma_z} \quad . \quad . \quad (8)$$

Assuming 0.25 as Poisson's ratio, 0.1 for the ratio of S_t/σ_z and solving the above equation for the angle at which opening of the existing fracture is equally likely as opening a new vertical fracture, it is seen that the naturally occurring fracture will be opened preferentially if it makes an angle of about 50° or less with the vertical.

Faults which make angles of 30° or less with the vertical should widen at applied pressures equal to $\sigma_z/2$ (to overcome resisting normal stress) while open vertical joints should open at pressures of $\sigma_z/3$. Thus, it appears that cases in which no breakdown pressure is observed in a fracturing operation can be explained sometimes as Bugbee postulates on the basis of the occurrence of such open fracture systems intersecting the wellbore.

However, if the naturally occurring fracture were tightly closed or filled with secondary deposits so that, though it possessed a negligible tensile strength, fluid could not be readily injected into it, the pressure required to open it would be twice the normal stress σ_t expressed in Equation 7,

$$p_i = \frac{\sigma_z}{1-\mu}\left[1 - (1-2\mu)\cos 2\phi\right] \quad . \quad . \quad (9)$$

because of the stress concentrating effect of the borehole. Equating 9 with 6 it is found that the pre-existent fracture would be opened when

$$\cos 2\phi \leq 1 - \frac{(1-\mu)S_t}{(1-2\mu)\sigma_z} \quad . \quad . \quad . \quad . \quad (10)$$

It can be seen that as the vertical stress increases with depth, ϕ approaches zero. Then the tightly closed or cemented fracture would not be opened in preference to a new vertical fracture except at shallow depths unless it were almost vertical.

In the case of the existing formation fracture occurring away from the wellbore the authors would argue that the wellbore fracture would be initiated as described earlier. Then as the new fracture intersects the existing fracture it would "turn" to extend the existing fracture if the angle from vertical were small enough, or it would continue in its original orientation if the angle were too large. The analysis above to predict the critical angles is essentially applicable to predicting this case.

THE EFFECT OF TECTONIC FORCES ON WELLBORE RUPTURES

Up to this point it has been assumed that the horizontal principal stresses in the earth's crust are equal and are a function of the overburden load and material properties, assuming the rock to be in elastic or so-called plastic equilibrium. This is termed the idealized state of earth stress.

Actually the earth's crust is stable over a wide range of stress relationships.[22] This stable region is bounded by the conditions of faulting. One of the limits of stability is the condition of normal faulting which is approximately coincident with the idealized state. That

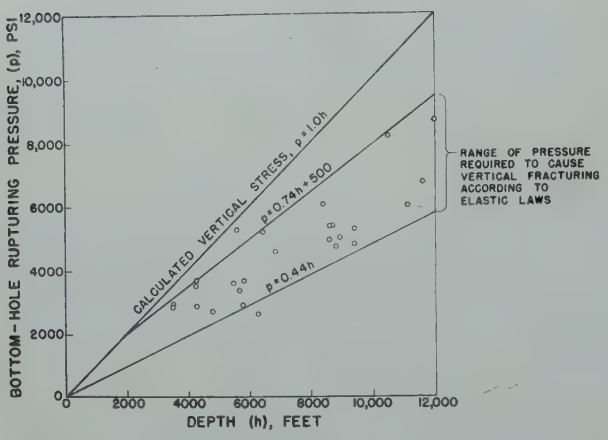

FIG. 3 — BREAKDOWN PRESSURE VS DEPTH FROM 27 WELLBORE FRACTURING OPERATIONS IN THE PERMIAN BASIN.

is, when one of the horizontal stresses is decreased below the ideal value, normal faulting occurs and continues until the stress relationship is returned to the idealized state. The stable region is also limited by the conditions of transcurrent and thrust faulting. These types of faulting return the stress conditions only to their respective limits of stability, in which instances one or both horizontal stresses would exceed the vertical stress.

The widespread prevalence of normal faulting argues that much of the earth's crust exists in a state of stress which is near the idealized state. Therefore, fracturing pressure should usually be predicted by Equation 4.

Miles and Topping have shown that an increase in horizontal stress in one direction would result in a decrease in the pressure required to induce vertical fractures. Obviously an increase in stress on both horizontal axes would result in an increase in the pressure required to induce vertical fractures.

Interpretation of Data From the Field

On the basis of the above arguments the orientation of borehole fractures should be indicated by rupturing pressures if tensile strengths are of conventional value. Fig. 3 is a graph of bottom hole rupturing pressure versus depth for 27 wells in the Permian Basin of West Texas and New Mexico. These data were obtained during well stimulation operations which involved fracturing of the various limestones in that region.* It can be seen that most of the data points fall in the region predicted by Equation 5. Fig. 4 is a graph of rupturing pressure versus depth from wells in some lightly consolidated sands of the Texas and Louisiana Gulf Coast during squeeze cementing operations. These formations being of recent geologic origin would be expected to exist in the plastic state of stress. Then the horizontal stresses and, as a result, the rupturing pressures should be higher than those which occur at corresponding depths in the Permian Basin. It can be seen from Fig. 4 that most of the rupturing pressures are in excess of those predicted by Equation 5 but are less than the estimated overburden load.

Although a study of formation breakdown pressures lends credence to the belief that pressure induced formation fractures are vertical, there are a few instances where extremely high breakdown pressures are observed. With few exceptions this behavior appears to be limited to cased and perforated wells. Unfortunately, without detailed knowledge of the dimensions of the perforations and, if they are plugged, the degree to which the plugging is effective, as well as knowledge of the stresses imposed on the formation by the cement sheath, the breakdown pressure for cased holes is non-analytical. Therefore, more precise information concerning the orientation of the fractures which emanate from cased and perforated holes must be sought from a study of fracture extension mechanics.

*Breakdown pressures were recorded during acidizing operations.

FRACTURE EXTENSION

Objectives and General Approach

Broadly, the studies relating to fracture extension fall into two closely related categories: (1) Calculation of the fluid pressure** required to extend a newly created fracture as a function of rock properties, and (2) Development of relationships between fluid pressure,** rock properties, and the dimensions and volume of the fracture system. The studies to calculate the pressure required to extend fractures were largely pointed to developing evidence relating to prediction of fracture orientation. In this regard a relationship between the extending pressure and resisting stresses would permit inferences from field injection pressure data regarding whether fractures were vertical or horizontal. Briefly, the problem here was to consider three factors: (1) the tensile stress at the ends of the fracture resulting from the injected fluid pressure tending to extend the fracture, (2) the tensile strength of the rock at the ends of the fracture which resists fracture extension, and (3) the compressive stress at the ends of the fracture resulting from horizontal formation stresses and tending to resist fracture extension. When (1) is large enough, the combined effects of (2) and (3) would be overcome and the fracture would spread. Treating rock as an elastic material, attempts to formulate this problem mathematically were unsuccessful.

**Bottom-hole injection pressure if pressure drop in fracture is negligible.

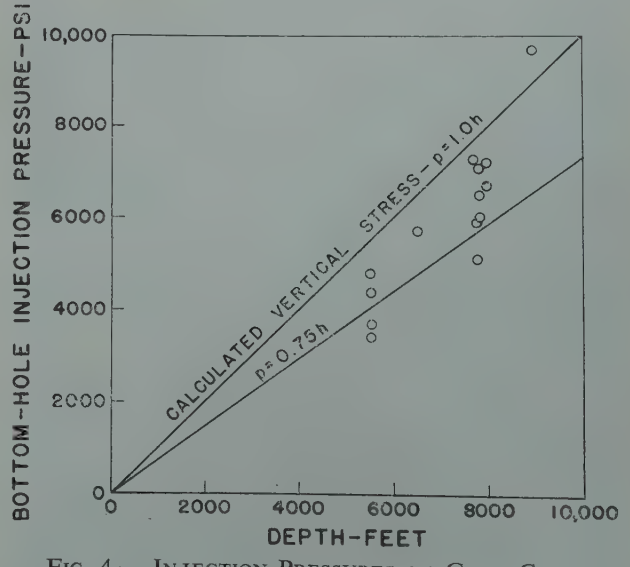

FIG. 4 — INJECTION PRESSURES ON GULF COAST WELLS.

Sneddon[23] had formulated an expression relating the stress in the vicinity of a fracture with the internal pressure but his solution became nonanalytical at the leading edges of the fracture. Accordingly, an empirical study was devised in which photoelastic stress studies were conducted with a model of an earth element containing a fracture. The photoelastic method involving polarized light and a photoelastic material has been well described by others[24,25] and basically serves merely as a method to observe directly stress patterns that are too complicated to calculate analytically.

The studies to develop a relationship between fluid pressure, rock properties, and dimensions of the fracture were pointed mainly at the problem of designing well stimulation treatments. Results of this work are presently being considered along with considerations of effect of fluid loss and the effect of fractures upon well productivity to develop conclusions relating to optimum treatment size and composition. The main factors considered here have been fracture dimensions and volume. This study utilized the same scaled down model which was involved in the photoelastic studies except that its photoelastic property was not exploited and observations were made visually and by camera of the model fracture's shape and dimensions. Actually the model data in this case were only used to corroborate mathematically derived relationships available from the literature.

General Assumptions and Definitions

Only vertical fractures were analyzed in this work although the basic relationships could be applied to the case of a horizontal fracture. It was assumed throughout that rock behaves as an elastic material. The effect of permeability and porosity on fracture extending pressure was assumed to be negligible. If a fracture were initiated in an extensive and relatively homogeneous formation it should be propagated in one plane and extend from the point of origin to approximately equal distances in all directions in the fracture plane. There should be a slight preference for propagation toward the earth's surface since the horizontal compressive stress decreases in this direction. However, this tendency would be partially balanced by a corresponding decrease in fluid head and was not considered in the analysis. Fractures radiating from opposite sides of a wellbore would be expected since the initiation of a fracture on one side would result in an additional tensile stress upon the opposite side.

The type of fracture described above, roughly taking the shape of a vertical "pancake," will be referred to as an *unrestricted* fracture.

If it is postulated that the pressure required to extend a fracture is a linear function of the least stress which resists fracturing, then a vertical fracture in a sandstone or limestone formation which is bounded by shales usually should terminate at the shale interfaces since shales usually possess higher horizontal stresses than do the more competent formations. Such a fracture will be termed a *restricted* fracture. If the shale were a brittle one with properties much like those of the pay, then the vertical propagation of the fracture would probably not stop at the shale. On the other extreme, for example, a soft clay-like shale would probably be in hydrostatic equilibrium and would surely stop the vertical propagation of a fracture. The authors are presently attempting to secure direct field evidence from radioactivity tracer studies to gain more insight into the effect of horizontal discontinuities such as shale beds on vertical fracture propagation.

Neither type of fracture described above lends itself directly to study by photoelastic experiments. To study either type directly would require experimental stress analysis on three dimensional models,* a type of investigation which is beyond the scope of our facilities. However, a two-dimensional model* could be studied with ease and a mathematical transformation used to apply the results of the study to the cases of interest.

Pressure Required to Extend a Fracture in a Two-Dimensional Model

The photoelastic fracture models were fabricated from gelatin, a material which has been used successfully by others[20,27] in earth stress modeling experiments. No attempt was made to obtain exact similitude between model and prototype. Rather, the goal was to model a fracture in a medium which could be considered infinite relative to the size of the fracture and develop a general formula (applicable to all materials in the elastic range) for the internal pressure necessary to extend such a fracture against an external resisting stress. Since the borehole diameter is small in comparison to fracture length it would have no effect on the stress at the fracture ends and was eliminated from the experimental models to simplify fabrication. The models were supported on a horizontal sheet of plate glass in a vertically arranged polariscope. Internal pressure was applied by injecting a viscous mineral oil into the fracture through a plexiglas cover plate, while external stress was imposed through bars connected to a weight and pulley system.

The experimental procedure consisted of progressively increasing the pressure while observing the fringe order (the fringe order is directly proportional to stress) at the fracture ends. Fig. 5 shows the type of fringe pattern obtained. The fringe pattern represents the stress pattern. Experimental runs were made for several magnitudes of external stress. Upon substituting the data from these experiments into the photoelastic equation** it was found that the stress at the ends of the fracture was defined by the equation,

$$\sigma = 2(p_i - 1.5\sigma_H). \quad . \quad . \quad . \quad . \quad . \quad . \quad . \quad (11)$$

Caution was exercised in obtaining data for Equation 11 to insure that the elastic range had not been exceeded and that the straight line function between fringe order and stress was applicable. Particular notice was given to the magnitude of pressure necessary to change the stress at the fracture ends from compression to tension ($p_i = 1.5\sigma_H$).

After the stress at the fracture ends passes from compression to tension, it has only to overcome the material tensile strength for the fracture to be extended. Thus the pressure necessary to extend a two-dimensional fracture is found from Equation 11 by replacing σ with the tensile strength (S_t) giving,

$$p_i = 1.5\sigma_H + \frac{S_t}{2} \quad . \quad . \quad . \quad . \quad . \quad . \quad . \quad (12)$$

*The dimensional order of a model refers to the number of directions in which properties vary. In a two-dimensional model stress varies in but one plane.

**See Appendix.

If the material being fractured remains elastic until the fracture is on the verge of being extended Equation 12 will apply. Such was observed to be the case for gelatin. Since rock also exhibits little inelastic action prior to rupture, reservoir materials should behave in like manner.

Pressure Required to Extend Unrestricted Fractures

Sneddon[23] has shown that the stress at a point in the vicinity of an unrestricted fracture could be obtained by a simple transformation of the expression for the stress at the corresponding point in the vicinity of a two-dimensional model.

According to Sneddon, the normal stress along the axis of a fracture in a two-dimensional model can be expressed by,

$$\sigma = (\delta - 1)\left(p - \frac{\delta}{\delta - 1}\sigma_H\right) \quad . \quad . \quad . \quad (13)$$

where the parameter, δ, varies with position. By the photoelastic method of stress analysis it was found that δ had a value of 3 at the leading edges of the model fracture. The value of the stress normal to the axis of the unrestricted fracture can be found by Sneddon's transformation by multiplying δ by $\frac{2}{\pi}$. Then for the unrestricted fracture, the tangential stress at the leading edge is found to be,

$$\sigma = \left(\frac{2}{\pi}\delta - 1\right)\left[p - \frac{\frac{2}{\pi}\delta}{\frac{2}{\pi}\delta - 1}\sigma_H\right] \quad (14)$$

The pressure necessary to extend the fracture is given by the equation,

$$p_i = 2.09\sigma_H + \frac{S_t}{0.92} \quad . \quad . \quad . \quad . \quad . \quad . \quad . \quad (15)$$

For practical purposes this equation may be written as,

$$p_i = 2\sigma_H + S_t. \quad . \quad . \quad . \quad . \quad . \quad . \quad . \quad . \quad . \quad (16)$$

Pressure Required to Extend Restricted Fractures

Two extremes in configuration can be conceived for the restricted fracture. If the frictional resistance to lateral displacement at the top and bottom of the formation (at the shale break, for example) were negligible, the restricted fracture would correspond directly to the model which was studied in the laboratory. However, if this frictional resistance were large the top and bottom of the fracture would remain closed. The restricted fracture would then have a shape such as that generated by a lens rolling on its edge. The fracture would be expected to terminate at each end in a semicircular front. This latter configuration appears to be the most likely in view of the magnitude of the frictional resistances involved. Therefore, it is tentatively assumed that the pressure required to extend the restricted fracture is the same as that required to extend the unrestricted fracture.

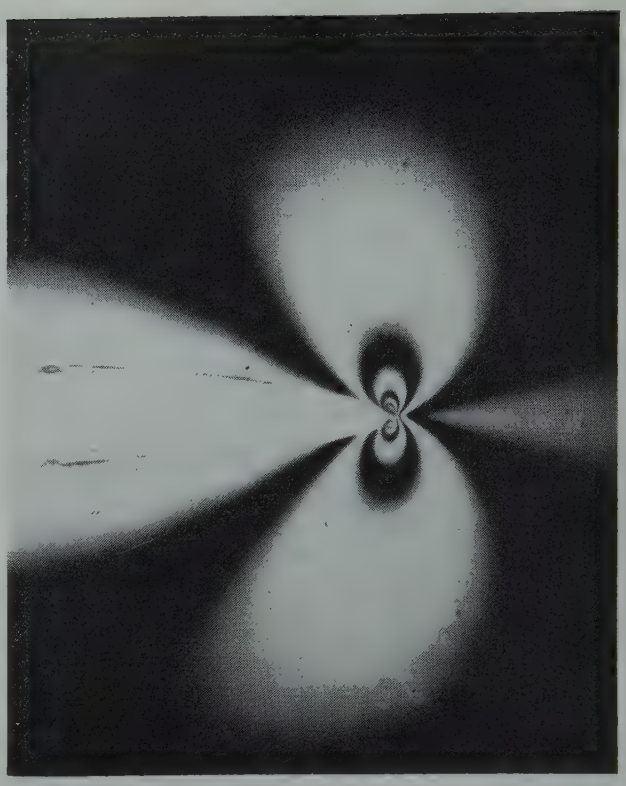

Fig. 5 — Photograph of Fringe Pattern Showing Stress Distribution at the End of a Fracture in a Gelatin Model.

Fracture Geometry and Dimensions

From mathematical analyses made by Westergaard[28] and Sneddon[29] it can be shown that a fracture in a two-dimensional system will have an elliptical cross-section whose maximum width is given by the formula,

$$w = \frac{4(1 - \mu^2)\,(p_i - \sigma_H)^l}{E} \quad . \quad . \quad . \quad . \quad (17)$$

However, in the derivation of this equation it was assumed that the strain parallel to the vertical axis of the fracture was constant (plane strain). In the model studies the vertical stress was held constant (plane stress). The fracture width formula assuming plane stress is,

$$w = \frac{4(p_i - \sigma_H)^l}{E} \quad . \quad . \quad . \quad . \quad . \quad . \quad . \quad (18)$$

This equation is found by replacing μ and E in Equation 17 by $\overline{\mu}$ and $\overline{E}$ where,

$$\overline{\mu} = \frac{\mu}{1 + \mu}$$

$$\overline{E} = \frac{E(1 + 2\mu)}{(1 + \mu)^2}$$

From Sneddon's analysis of an internally pressurized circular crack corresponding to an unrestricted fracture it can be shown that its configuration will be an oblate spheroid (elliptical cross-section) whose maximum width is given by the formula,

$$w = \frac{8(1 - \mu^2)\,(p - \sigma_H)^l}{\pi E} \quad . \quad . \quad . \quad . \quad (19)$$

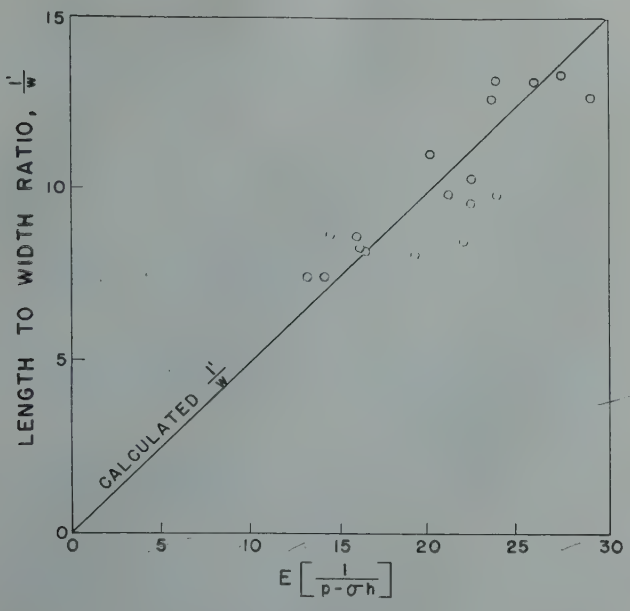

FIG. 6—CORRELATION OF OBSERVED FRACTURE LENGTH-TO-WIDTH RATIOS AS A FUNCTION OF APPLIED LOADS COMPARED TO CALCULATE RELATIONSHIP.

Since these mathematical expressions included a number of assumptions experimental corroboration was believed necessary and a number of model experiments were made. These experiments substantiated the predicted width (Equation 11) for the fracture in the model. The models used were identical to those used in the photoelastic study. The same apparatus was also employed for applying internal pressure and external stress. For convenience in comparing experimental data with theoretical values, Equation 18 was put in the form,

$$\frac{l'}{w} = \frac{E}{2(p - \sigma_H)},$$

where, l' = total length = $2l$.

The ratio of $\frac{l'}{w}$ was obtained from photographs of pressurized fractures taken while the corresponding internal pressure and external stress were recorded. The modulus of elasticity was obtained by use of the method described by Farquharson and Hennes.[26] Fig. 6 is a plot of experimental values of $\frac{l'}{w}$ versus $\frac{E}{p_i - \sigma_H}$.

The theoretical prediction that an internally pressurized fracture would have an elliptical cross-section was also proved by use of the two-dimensional model. The outline of a pressurized fracture was traced from a photograph and compared to an ellipse having equal corresponding axes. The two figures were for all practical purposes congruent.

FRACTURE VOLUME AND EXTENT

The conclusion that the cross-sections of pressurized fractures are elliptical and that fracture shapes can be related to material properties should prove of immediate practical interest. Such a relationship provides a means of estimating the widths and the lengths of the fractures which are obtained during fracturing operations.

The unrestricted fracture such as might be obtained in the fracture treatment of a thick and homogeneous formation should be a spheroid with a minor axis equal to w and a radius l which are related by Equation 19 given above. The volume* of such a spheroid is expressed by the equation,

$$V = 2/3\pi w l^2 \quad . \quad . \quad . \quad . \quad . \quad . \quad . \quad . \quad . \quad (20)$$

Combining equations 19 and 20 and solving for length it is found that,

$$1 = \sqrt[3]{\frac{3VE}{16(p_i - \sigma_H)}} \quad . \quad . \quad . \quad . \quad . \quad . \quad (21)$$

Using the following dimensions and values:

l = feet — $E = 3\text{x}10^6$
V = gallons — w = inches
$(p_i - \sigma_H) = 1/3$ psi/ft — $\mu = 0.25$ . . (22)

$$1 = 60.9\sqrt[3]{\frac{V}{h}}\, w = 9\text{x}10^{-4}\, V^{1/3}\, h^{2/3}.$$

The restricted fracture does not lend itself as readily to analysis. Slight lateral displacements may take place at the top and bottom of such a fracture. However, if it is assumed that such displacement is negligible it follows that the vertical section of the restricted fracture is elliptical. Also, if the fracture is very long with respect to its height, a vertical section perpendicular to the main axis of the fracture and taken well back from its end will correspond directly to the modelled fracture which was studied in the laboratory. Therefore, it appears likely that Equation 17 can be used to approximate the width of the restricted fracture by substituting one-half fracture height (one-half formation thickness) for l in the equation. Then the volume of the restricted fracture is approximated by,

$$V = \frac{(1 - \mu^2)\ (p_i - \sigma_H)}{E}\, \pi h l' \quad . \quad . \quad . \quad . \quad (23)$$

where l' is the total length of the fracture. The facilitating assumption that the cross-section is constant appears reasonable since, in the case of the restricted fracture, the vertical dimension controls fracture width.

FIELD DATA

The bottom hole injection pressures from 31 fractured wells** in the Permian Basin were obtained for comparison to pressures as predicted by the theory of fracture extension. Fig. 7 is a graph of injection pressure as a function of depth showing these data as compared to predicted fracture extension pressure. The range of predicted extension pressures reflects the assumption that Poisson's ratio for limestone varies between 0.18 and 0.27 and that tensile strength varies from negligible to 500 psi. It can be seen that with two exceptions the injection pressures fall within the range predicted.

All the data points may be explained on the basis of vertical fracturing while none fall on or above the 45° line representing vertical stress which must be

*In this development it is assumed that there is no loss of fracturing fluid to the formation. The fluid loss could be calculated and taken into account in order to calculate the total amount of fluid to be injected to obtain a fracture of a given length.

**Fractured by injection of acid.

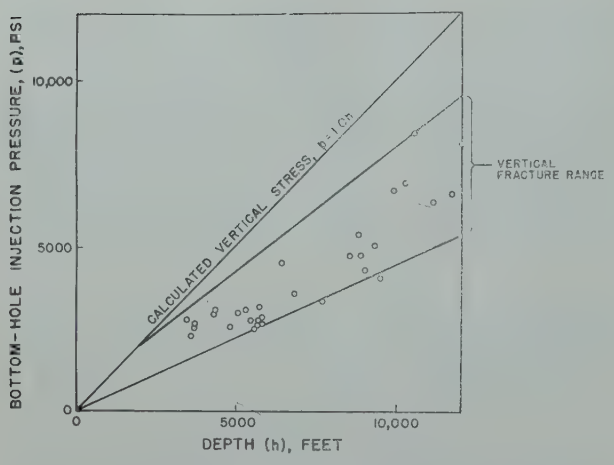

FIG. 7 — BOTTOM-HOLE INJECTION PRESSURES DURING FRACTURE EXTENSION AS A FUNCTION OF DEPTH COMPARED TO PREDICTED VALUES.

overcome to open a pre-existing horizontal fracture. Furthermore, as was shown previously a pressure of twice the external resisting stress plus the material tensile strength is necessary to extend an unrestricted fracture where there is no pre-existent fracture. On this basis the injection pressure would have to be twice the magnitude of the overburden stress in order to indicate the induction and extension of a horizontal fracture.

Injection pressures of the magnitude predicted for unrestricted fractures are probably the rule for the following reasons:

1. All fractures are unrestricted at first.

2. The leading edge of a fracture probably remains semicircular or some variation thereof.

3. The frictional resistance to shear on the planes between the fractured medium and adjoining shales raises the pressure requirements above that of a two-dimensional fracture.

CONCLUSIONS

1. The competent formations of the earth's crust even when arched lack sufficient strength to alleviate the load from underlying formations, and the overburden load may be taken as approximately equal to 1 psi/ft of depth.

2. Hard, well consolidated rocks can be considered as existing in the elastic state of stress to the depths penetrated in present oil well operations. As a result, as indicated by theory and data from the field, such formations usually possess horizontal stresses in the neighborhood of 0.33 psi/ft of depth.*

3. The soft shales and unconsolidated sands most frequently found in the Texas and Louisiana Gulf Coast area can be considered to exist in the plastic state of stress and to possess horizontal stresses in excess of 0.33 psi/ft of depth.

4. Pressure induced wellbore fractures may be horizontal when the bottom hole fracturing pressure has exceeded the overburden load of about 1 psi/ft of depth. However, this seldom occurs below 3,000-4,000 ft except possibly in the infrequent case of abnormally high horizontal stresses.

5. Vertical or nearly vertical fractures are obtained at bottom hole pressures below the overburden load and frequently below 0.7 psi/ft of depth.

6. Fluid loss to the matrix during the injection of a fracturing fluid alters only slightly the pressure required to fracture a wellbore vertically. (The tendency is to reduce the required pressure.)

7. Hydraulically induced wellbore fractures are comparatively wide. During the latter part of a large-volume treatment widths near 1 in may be expected, particularly in deeper wells.

8. The bottom hole injection pressure** at which a fracture extends indicates its orientation. In general, a vertical or near vertical fracture will be extended at a pressure which is approximately two-thirds the calculated overburden stress, or less. If the extension pressure is equal to or greater than the overburden stress a horizontal fracture is indicated.

9. The relationships involving fracture extent, width, and volume, although not quantitatively precise, give some insight as to the magnitude of fracture dimensions and offer an approximate basis for the design of well stimulation treatments.

The practical implications of these conclusions deserve some comment. Conclusions 2 and 3 suggest that in the case in which a consolidated sand is bounded by nonbrittle shales, the vertical extent of vertical fractures would be limited by the shale because of the greater horizontal stresses in the shale. These conclusions also might explain the difference in the nature of lost circulation problems between the Gulf Coast and West Texas, for example. Relatively high mud weights are probably tolerable in Gulf Coast operations because of high compressive stresses resisting fracture, whereas in West Texas relatively low horizontal compressive stresses and already existing fractures offer relatively little resistance to fracture induction and extension. Shale flow into the hole in the Gulf Coast area might be explained by the relatively high horizontal stresses existing in it being greater than the mud hydrostatic pressure. Conclusion 5 argues that squeeze cementing cannot be counted upon to result in horizontal pancakes. It might also explain frequent cases of well stimulation treatments fracturing to water. Fracture volume estimations from relationships presented are consistent with observations of volumes pumped into formations and may explain large lost circulation losses without postulating subterranean caverns.

APPENDIX

I. PHOTOELASTIC EXPERIMENTAL DETAILS

Gelatin was chosen as the photoelastic modeling material to represent the earth for the following reasons: (1) It has a high optical sensitivity; (2) The stress-strain and stress-fringe relation is linear nearly

*An exception to this would be expected when horizontal stresses are significantly influenced by tectonic forces. For example, in areas of active thrust faulting the horizontal stresses would be greater than the vertical stress. At least in the Gulf Coast and West Texas-New Mexico areas and probably in the Oklahoma area, areas familiar to the authors, such extremely high horizontal stresses are believed to be very infrequent.

**This observation would be obscured in the case of very high viscosity fluids flowing in a fracture, e.g. partially dehydrated cement slurry in a squeeze cementing operation.

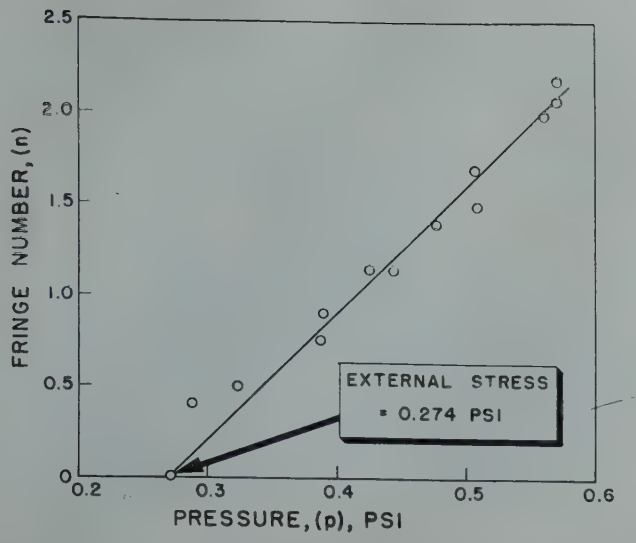

FIG. 8 — FRINGE ORDER VS APPLIED PRESSURE IN MODEL FRACTURE USED TO DEVELOP CORRELATION BETWEEN STRESS AT FRACTURE ENDS WITH APPLIED PRESSURE.

to the breaking point; (3) It affords ease in model fabrication; and (4) It has been used successfully by others in earth stress modeling experiments.[26,27]

A regular high grade food gelatin was used and a mixture containing approximately 14 per cent gelatin and 15 per cent glycerin was found to give best results. Models were made in the form of 10-in square plates of ½-in thickness. The molds consisted of ½-in thick wooden frames to which were clamped top and bottom plates of plate glass. Cellophane was stretched on the inside of the glass plates to facilitate removal of the models. Gelatin was poured at 130°F through an opening in the frame. To negate gravitational effects on the model, the polariscope components were arranged vertically with a horizontal plate glass support for the model (Fig. 8).

If fractures were extended from opposite sides of a wellbore they could be thought of as constituting a single fracture. This is the type of fracture modeled. For ease of fabrication the borehole was eliminated since it would have no effect on the stress at the fracture ends provided the fracture length were large relative to the hole diameter. Fractures were initiated mechanically in the gelatin models and further extended by applying internal pressure to simulate a hydraulically induced two-dimensional fracture. Pressure application was effected by injecting a viscous mineral oil through an opening in a plexiglas cover plate and into the fracture. Steady flow was maintained by forcing the oil from a tank with a constant air pressure controlled by a Nullmatic pressure regulator. The oil flowed into the fracture and then out between the model and adjacent plates. Internal pressure could be maintained because of the pressure drop as the oil flowed from the fracture to the model edge. The oil flow on each side also reduced the friction between the model and adjoining plates to an insignificant force. An air probe leading into the fracture through the cover plate registered the internal pressure on a water monometer. The air-oil interface in the air probe was regulated by a second Nullmatic pressure regulator so that an air bubble was maintained on the end of the probe within the fracture. With this device, the pressure within the fracture could be determined with an accuracy of ± 4 mm water. External edge stresses were imposed through bars connected to a weight and pulley system.

The lengths of the fractures studied were from 1 to 2 in. It was found from the size of the stress field around internally pressurized fractures whose lengths fell near this range that the overall model dimensions could be considered infinite relative to the fracture length.

The fringe order (n) at a point is the number of fringes which pass through it during the application of a system of loads and is related to the state of stress by a factor (F) termed the model fringe value. This factor (F) was found by imposing unidirectional stresses on a model and noting the fringe order.

The experimental procedure consisted of progressively increasing the pressure while observing the fringe order at the fracture ends with the aid of a magnifying glass. Fig. 5 shows the type of fringe pattern obtained. Experimental runs were made for several magnitudes of external stress. Fig. 7 is a graph of fringe order (n) versus pressure for a biaxial external stress of 0.274 psi.

II. PHOTOELASTIC EQUATIONS

The fringe order as a function of pressure from Fig. 8 may be expressed as,

$$n = m\,(p_i - \sigma_H) \quad . \quad . \quad . \quad . \quad . \quad . \quad . \quad . \quad . \quad (a)$$

where, m = slope of fringe order versus pressure curve,
p_i = internal pressure.
σ_H = external stress.

The photoelastic equation[21] is given as,

$$\sigma_1 - \sigma_2 = 2\,F\,n \quad . \quad . \quad . \quad . \quad . \quad . \quad . \quad . \quad . \quad (b)$$

where σ_1 = maximum principal stress,
σ_2 = minimum principal stress,
F = model fringe value.

Since at the fracture wall the normal stress (compressive) is equal to internal pressure, $(-p_i)$ can be substituted for σ_2. Then by substituting for the value of n from Equation (a) there results the expression

$$\sigma_1 = (2\,F\,m - 1)\left(p_i - \frac{2\,F\,m}{2\,F\,m - 1}\,\sigma_H\right) \quad . \quad . \quad . \quad (c)$$

relating tensile stress (σ_1) at the end of a fracture to internal pressure and external stress. It appears at first examination that σ_1 depends on the model fringe value. However, since m is inversely proportional to F the effect is cancelled. Substituting representative values as determined experimentally into Equation (c) gives

$$\sigma_1 = 2\,(p_i - 1.5\,\sigma_H) \quad . \quad . \quad . \quad . \quad . \quad . \quad . \quad (d)$$

For a fracture to extend, σ_1 must become greater than the tensile strength S_t of the fracture medium. Thus the necessary pressure is found from Equation (d) as

$$p_i = 1.5\,\sigma_H + \frac{S_t}{2} \quad . \quad . \quad . \quad . \quad . \quad . \quad . \quad . \quad (e)$$

III. BOREHOLE RUPTURE AS AFFECTED BY FLUID LOSS

The effect of fluid loss on the pressure necessary to initiate a fracture in a permeable formation may be analyzed by determining its effect on the tangential stress in a thick-walled cylinder. This cylinder may be considered as representing a borehole in the earth's

crust. In the general case the outer radius is undefined but is very large with respect to the inner radius. A definite outer boundary and steady state fluid loss are assumed to facilitate analysis. Fig. 9 shows an element of the cylinder and the stresses and pressures involved. It is assumed that the porosity consists of numerous pockets interconnected by channels.

Summing the forces on this element in the radial direction and simplifying the resulting equation gives

$$\sigma_t - \sigma_r - r\frac{d\sigma_r}{dr} + \frac{1-\sqrt{}}{\sqrt{}} r\frac{dp}{dr} = 0 \quad . \quad . \quad . \quad (f)$$

where $\sqrt{}$ = ratio of new solid areas to gross area on a surface of tensile failure.

If it is assumed that the stress in the vertical direction remains constant as σ_r and σ_t are changed (plane stress) then the equations[21]

$$\sigma_r = \frac{E}{1-\mu^2}\left(\frac{dU}{dr} + \mu\frac{U}{r}\right) \quad . \quad . \quad . \quad . \quad (g)$$

$$\sigma_t = \frac{E}{1-\mu^2}\left(\frac{U}{r} + \mu\frac{dU}{dr}\right)$$

may be used to get σ_r and σ_t in terms of displacement (U). Furthermore, by obtaining $\frac{dp}{dr}$ from Darcy's law Equation (f) may be written,

$$\frac{d^2U}{dr^2} + \frac{1}{r}\frac{dU}{dr} - \frac{U}{r^2} - \frac{\psi}{r} = 0 \quad . \quad . \quad . \quad . \quad . \quad (h)$$

$$\text{where } \psi = \frac{(1-\sqrt{})\,(1-\mu^2)\,(p_i - p_o)}{\sqrt{}\,E\,ln\,b/a}$$

a,b = inside and outside radii,
p_i,p_o = internal and external pressures.

The solution to Equation (h) is

$$U = A_r + \frac{B}{r} - \psi\frac{r\,ln\,r}{2} \quad . \quad . \quad . \quad . \quad . \quad . \quad . \quad (i)$$

The equation for (U) contains two constants (A and B) which may be evaluated by substitution into Equations (g) and imposing the boundary conditions:

1. $r = a, \sigma_r = -p_i$
2. $r = b, \sigma_r = 0.$

Then the maximum tangential stress is found to exist at $\sqrt{} = a$ and is expressed by

$$\left[\sigma_t\right]_{max} = p_i\frac{a^2+b^2}{b^2-a^2} + \frac{(1-\sqrt{})\,(1+\mu)\,b^2}{\sqrt{}\,(b^2-a^2)}\,p_i$$

$$+ \frac{(1-\sqrt{})\,(1-\mu)\,p_i}{2\sqrt{}\,ln\,b/a} \quad . \quad . \quad . \quad . \quad . \quad (j)$$

Up to this point the stress was considered as existing only in the solid portion of the rock. This was necessary when making the initial force balance in order to differentiate between pressure and stress. Now, in order to express the results in a form which is consistent with the usual way of expressing the intensity of stress in rock, it is necessary to convert to a gross area basis. This is done by multiplying by the factor, $\sqrt{}$, which gives

$$\left[\sigma_t\right]_{max} = p_i\,(\sqrt{})\left(\frac{a^2+b^2}{b^2-a^2}\right)$$

$$+ \frac{(1-\sqrt{})\,(1+\mu)\,b^2}{b^2-a^2}p_i + \frac{(1-\sqrt{})\,(1-\mu)\,p_i}{2\,ln\,b/a} \quad (k)$$

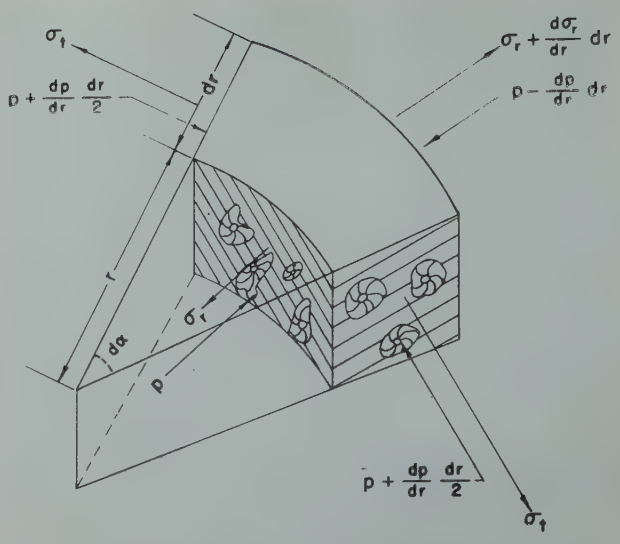

FIG. 9—ELEMENT FROM THICKWALL POROUS CYLINDER USED IN FLUID LOSS ANALYSIS.

As b becomes very large relative to a, Equation (k) reduces to essentially,

$$\left[\sigma_t\right]_{max} = (1 + \mu - \mu\sqrt{})\,p_i \quad . \quad . \quad . \quad (l)$$

Thus it is seen that fluid loss does slightly reduce the pressure necessary to create a vertical fracture.

If the problem is assumed to be one of plane strain instead of plane stress, the solution may be obtained by replacing μ by $\bar{\mu}$ where

$$\bar{\mu} = \frac{\mu}{1-\mu}.$$

Making this substitution in Equation (1) gives

$$\left[\sigma_t\right]_{max} = \left(\frac{1-\mu\sqrt{}}{1-\mu}\right)p_i \quad . \quad . \quad . \quad . \quad . \quad (m)$$

Neither the plane stress nor plane strain solution truly represent the stress picture when a formation is being fractured. The actual stress would have a value somewhere between what would be predicted by the two solutions. However, since the numerical difference between equations (1) and (m) is small, either one will differ from the true solution only slightly.

The effect of leak-off on the pressure required for the induction of a horizontal fracture may be analyzed in the following manner. Rewriting the stress equations at $r = a$ for the case of plane strain for the radial and tangential stress on a gross area basis we have,

$$\sigma_r = -\sqrt{}\,p_i,$$

$$\sigma_t = \left(\frac{1-\mu\sqrt{}}{1-\mu}\right)p_i.$$

Substituting these values of stress into the equation for vertical stress[21]

$$\sigma_z = \mu\,(\sigma_r + \sigma_t) \quad . \quad . \quad . \quad . \quad . \quad . \quad . \quad . \quad . \quad (n)$$

gives

$$\sigma'_z = \frac{\mu\,(1-\sqrt{})}{1-\mu}\,p \quad . \quad . \quad . \quad . \quad . \quad . \quad . \quad . \quad (o)$$

which is that part of the vertical stress which must be imposed such that no vertical displacement takes place. If it is assumed that pressure is applied to a

porous medium between two impermeable boundaries, then the vertical stress between the medium and a boundary, due to internal pressure alone, will be

$$\sigma''_z = (1 - \sqrt{}) p_i \quad . \quad . \quad . \quad . \quad . \quad . \quad . \quad . \quad (p)$$

The total vertical stress tending to cause failure across a horizontal plane is found as,

$$\sigma'_z + \sigma''_z = \left(\frac{1 - \sqrt{}}{1 - \mu}\right) p_i \quad . \quad . \quad . \quad . \quad . \quad (q)$$

It should be noted that these equations are developed without regard to the dimensions of the system. Therefore, the conclusions from them apply to extremely thin zones of high permeability which are bounded by impermeable layers just as well as to thick zones. On the basis of this analysis, it is concluded that such inhomogeneities do not alter the orientation of pressure induced fractures.

NOMENCLATURE

a,b = Internal and external radii
E = Modulus of elasticity
F = Model fringe value
f = Coefficient of internal friction
h = Depth in feet
l = Fracture length measured from borehole to end
l' = Fracture length measured from end to end
m = Slope
n = Fringe order
p_i p_o = Internal and external pressure
S_t = Tensile strength
U = Displacement
w = Fracture width
X,Y,Z = Cartesian coordinates
$\sqrt{}$ = Ratio of new solid area to gross area on a surface tensile failure
δ = Dimensionless constant
Θ, r, Φ = Spherical coordinates
μ = Poisson's ratio
σ = Stress
$\sigma_x, \sigma_y, \sigma_z$ = Stress in Cartesian coordinate system
σ_H = Stress in horizontal direction
σ_r, σ_t = Radial and tangential stress
σ_1, σ_2 = Principal stress
ψ = Dimensionless term related to fluid flow in a radial system

REFERENCES

1. Clark, J. B.: "A Hydraulic Process for Increasing the Productivity of Wells," *Trans.* AIME, **186** (1949).
2. Hassebroek, W. E.: "Applications and Results of the Hydrafac Process," *World Oil,* (Feb. 1, 1951), 132, 133.
3. Grossman, W. L.: "Hydrafac Operations in the Spraberry Production, West Texas," *Jour. Pet. Tech.* (Nov., 1951), Sec. III, 9.
4. Miles, A. J., and Topping, A. D.: "Stresses Around a Deep Well," *Trans.* AIME, **179** (1949).
5. Walker, A. W.: "Squeeze Cementing," *World Oil* (Sept., 1949), **129,** 87.
6. Topping, A. D.: "Wall Collapse in Oil Wells as Result of Rock Stresses," *World Oil* (July, 1949), **129,** 112.
7. Anderson, E. M.: "The Dynamics of Faulting and Dyke Formation," Oliver and Boyd, Edinburgh and London, 1942.
8. Scott, P. P., Bearden, Wm. G., and Howard, G. D.: "Rock Rupture as Affected by Fluid Properties," *Trans.* AIME, **198** (1953).
9. Bugbee, J. M.: Discussion of Reference 8, ibid. (1953), 123.
10. Teplitz, A. J., and Hassebroek, W. E.: "An Investigation of Oil Well Cementing," *API Drilling and Production Practice* (1946), 95.
11. Clark, J. B., Fast, C. R., and Howard, G. C.: "A Multiple Fracturing Process for Increasing the Productivity of Wells," *API Drilling and Production Practice* (1952), 104.
12. Wuerker, R. G.: "The Status of Testing Strength of Rock," *Mining Engineering* (Nov., 1953), 1107.
13. Peterson, R. E.: "An Investigation of Stress Concentration by Means of Plaster-of-Paris Specimens," *Mechanical Engineering* (1926), **48,** 1449.
14. Weibull, W.: "A Survey of Statistical Effects in the Field of Material Failure," *Applied Mechanics Review* (Nov., 1952), **5,** 449.
15. Jakosky, J.: "Densities of Earth Materials," *Exploration Geophysics,* Times Mirror Press, Los Angeles (1946), 156.
16. Birch, F., Schairer, J. F., Spicer, H. C.: *Handbook of Physical Constants,* Geological Society American Special Papers 36 (Jan., 1942), 76.
17. Fenner, R.: "Untersuchungen zur Erkentnis des Gebirgsdrucks," (Studies on the Determination of Stresses in the Earth), *Gluckauf* (Aug. 13, 1938), **74,** 681.
18. Hubbert, M. K.: "Strength of the Earth," *Bulletin* AAPG (Nov., 1945), **29,** 1630.
19. Shoemaker, R. P.: "A Review of Rock Pressure Problems," *Quarterly of the Colorado School of Mines* (1951), **46,** 133.
20. Hubbert, M. K.: Discussion of Reference 7, ibid. (1953), 112.
21. Timoshenko, S.: *Strength of Materials* (1951), Part II, D. Van Nostrand Co., Inc.
22. Hafner, W.: "Stress Distributions and Faulting," *Bulletin* GSA (April, 1951), **62,** 373.
23. Sneddon, I. N.: "The Distribution of Stress in the Neighborhood of a Crack in an Elastic Solid," *Proceedings of the Royal Society* (A), (1946), **187,** 229.
24. Frocht, M. M.: *Photoelasticity,* John Wiley and Sons (1949), Volume 1.
25. Hetenyl, M., et al: *Handbook of Experimental Stress Analysis,* John Wiley and Sons (1950).
26. Farquharson, F. B., and Hennes, R. G.: "Gelatin Models for Photoelastic Analysis in Earth Masses," *Civil Engineering* (April, 1940), 10.
27. Cuykendall, T. R.: "Gelatin Photoelastic Models," *Cornell Engineer* (Dec., 1940), 8.
28. Westergaard, H. M.: "Bearing Pressure and Cracks," *Jour. of Applied Mech.* (1939), **6,** A49.
29. Sneddon, I. N., and Elliott, A. A.: "The Opening of a Griffith Crack Under Internal Pressure," *Quarterly of Applied Math.* (1946), IV, 262.

★★★

VISCOSITY of HYDROCARBON GASES under PRESSURE

NORMAN L. CARR*
ILLINOIS INSTITUTE OF TECHNOLOGY
CHICAGO, ILL.

RIKI KOBAYASHI
MEMBER AIME
THE RICE INSTITUTE
HOUSTON, TEX.

DAVID B. BURROWS
MEMBER AIME
CONTINENTAL OIL CO.
PONCA CITY, OKLA.

T. P. 3915

ABSTRACT

The viscosity of hydrocarbon mixtures, whether in the gas or liquid phase, is a function of pressure, temperature, and phase composition. This paper presents methods for the prediction of the viscosity of the gas or less dense fluid phase over the practical range of pressure, temperature, and phase compositions encountered in surface and subsurface petroleum production operations. The correlation necessary to predict the effect of pressure on viscosities is presented in Part I. Serious discrepancies in high pressure gas viscosity data in the literature are discussed.

The application of the correlation to predict absolute viscosities is discussed in Part II. Auxiliary correlations are presented to enable calculations of viscosities from a knowledge of the pressure, temperature, and gravity of the gas phase.

INTRODUCTION

A knowledge of the viscosity of hydrocarbon fluids is needed to study the dynamical or flow behavior of these mixtures through pipes, porous media, or more generally wherever transport of momentum occurs in fluid motion. Since flow is predominantly in the laminar region in petroleum reservoirs, the influence of fluid viscosity on this flow is especially important.

As early as 1894, Onnes[1] and Onnes and de Haas[2] noted that the viscosities of homologs under corresponding states could be correlated. The theorem of corresponding states has been further developed and applied to the viscosity of pure, nonpolar gases under pressure by Comings, Mayland, and Egly.[3] It was demonstrated that the viscosity ratio could be expressed rather closely as a function of reduced pressures and temperatures, i.e.:

$$\mu/\mu_1 = f(T_R, P_R) \quad . \quad . \quad . \quad . \quad . \quad . \quad . \quad . \quad (1)$$

where:

$$T_R = \frac{\text{temperature, absolute units}}{\text{critical temperature, absolute units}}$$

$$P_R = \frac{\text{pressure, absolute units}}{\text{critical pressure, absolute units}}$$

μ = viscosity of gas at reduced temperature T_R and reduced pressure P_R

μ_1 = viscosity of gas at atmospheric pressure and at temperature T_R

Serious discrepancies in the viscosity of pure hydrocarbon gases at high pressures have been called to our attention by Comings, Mayland, and Egly. They made a careful analysis of the following methods commonly used to measure gas viscosities:

1. Oscillating disc viscometer[4,5]
2. Rolling ball viscometer[6,7]
3. Capillary tube viscometer[1,2]

On the basis of their analysis of the problem and their experimental data on the viscosities of methane, ethylene, carbon dioxide, and propane, they preferentially selected data obtained by the capillary tube viscometer to develop their viscosity correlation. Since then a need has existed to verify the experimental technique of Comings, Mayland, and Egly for the determination of viscosities at high pressure; to extend the data to mixtures of hydrocarbons; and to extend the range of their correlation to include higher pressures.

Using the correlation procedure of Comings, Mayland, and Egly, the prediction of gas viscosities is resolved into the correlation of the effect of pressure, temperature, and composition on the viscosity of hydrocarbons and their mixtures and the prediction of viscosities of mixtures of hydrocarbons and other natural gas components at one atmosphere pressure.

Manuscript received in Petroleum Branch Offices Oct. 18, 1953. Paper presented at Petroleum Branch Fall Meeting in Dallas, Oct. 18-21, 1953.

[1]References given at end of paper.

*Present address: Pure Oil Co., Crystal Lake, Ill.

PART I

CORRELATION of the EFFECT of PRESSURE, TEMPERATURE, and COMPOSITION on the VISCOSITY of HYDROCARBONS and their MIXTURES

BY NORMAN L. CARR

METHODS OF DETERMINING GAS VISCOSITY

The coefficient of viscosity, μ, may be defined as the ratio of the unit shear stress acting at a point in a fluid which is necessary to maintain a unit velocity gradient perpendicular to the plane of shear. Viscosity, the shear modulus for the fluid, is somewhat analogous to the resistance to shear in solids. Only in the laminar region can the viscosity be defined simply as:

$$\mu = w/du/dy \quad . \quad . \quad . \quad . \quad . \quad . \quad (2)$$

where: w = shear stress per unit area

du/dy = velocity gradient perpendicular to the plane of shear

The relationship between pressure drop and flow of fluids through a smooth-walled, cylindrical, straight tube may be expressed simply by means of the well known Poiseuille's law,[9] provided laminar flow prevails in the tube and end effects can be made negligible. Reynolds number,[10] the criterion of dynamc similarity, may be used to define the region of laminar and turbulent flow in smooth-walled cylindrical, straight tubes. Since the flow relations encountered in the oscillating disc viscometer and the rolling ball viscometer are complicated, they provide means of determining viscosities by comparative methods. The rolling ball viscometer was designed primarily to measure the viscosities of liquid where laminar flow can easily be obtained. For gas viscosity determinations, it is difficult, if not impossible to conduct experimental measurements entirely in the laminar region using a rolling ball viscometer. If the condition of flow in the tube is laminar, then the viscosity is nearly linear in time of roll multiplied by a buoyancy factor which takes into account the density of the rolling ball and the gas.[11] If the condition of flow is turbulent (this in itself is difficult to define in a rolling ball viscometer), then the rolling ball viscometer must be calibrated for turbulence. Comings, Mayland, and Egly list the difficulties and uncertainties attending such calibrations. On the basis of their analysis, they concluded that: (1) the rolling ball viscometer has been misused in the determination of the viscosity of gases at high pressures and (2) the rolling ball viscometer is not a suitable instrument for the study of the viscosity of gases under pressure.

On the other hand, experimental determinations of gas viscosities may be made entirely in the laminar region by means of a capillary tube viscometer. Rankine[12,13] developed the theory of a capillary tube viscometer and constructed an instrument for low pressure studies. Comings, Mayland, and Egly adapted the Rankine viscometer for high pressure studies and determined viscosities for carbon dioxide, methane, and ethylene up to 2,500 psia. The viscosity of propane was determined to 615 psia.

Basic viscosity data for methane and three multicomponent gas mixtures have recently been obtained[14,15,16] up to 10,000 psia and 220°F. The experimental technique used in the accumulation of these data involves the capillary tube or Rankine type viscometer.

Fig. 1 shows a comparison of the curves for the viscosity of methane at 86°F and 203°F determined by means of the capillary tube viscometer and by means of a rolling ball viscometer. A comparison of the viscosity data for propane is shown in Fig. 2. Invariably, the values of viscosities obtained by the rolling ball viscometer fall above those obtained by the capillary tube viscometer. The influence of pressure on the discrepancies may be studied in the light of the influence of pressure on the dimensionless Reynolds number[10] defined as:

$$\text{Re No.} = \frac{DV\rho}{\mu} \quad . \quad . \quad . \quad . \quad . \quad . \quad . \quad . \quad (3)$$

where

D = diameter or effective diameter of the channel through which flow occurs

V = mean velocity of flow

ρ = density of fluid

μ = viscosity of fluid

Since the ratio ρ/μ increases very rapidly with increased pressure, high Reynolds numbers and hence turbulence is favored by high pressures for a given instrument. Figs. 1 and 2 indicate a rise in the discrepancies with increased pressures. The Reynolds number may be shown to reach a maximum with respect to pressure for some isotherms so that the degree of turbulence in the rolling ball viscometer may also reach a maximum value with respect to pressure. These points of consistency are demonstrated in Figs. 1 and 2.

The Benedict, Webb, and Rubin Equation of State[20] has been applied in an analogy to predict the effect of pressure on the viscosity of methane, nitrogen, and two complex mixtures. The results of the computations indicated close agreement between the computed and experimental values. The results for methane are presented in Fig. 5.

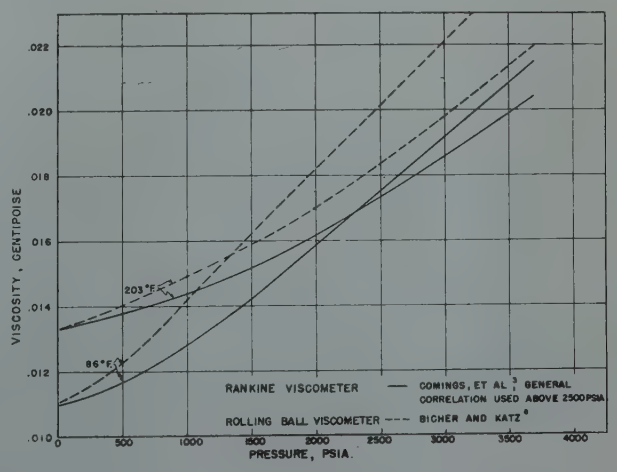

FIG. 1 — COMPARISON OF METHANE VISCOSITY DATA.

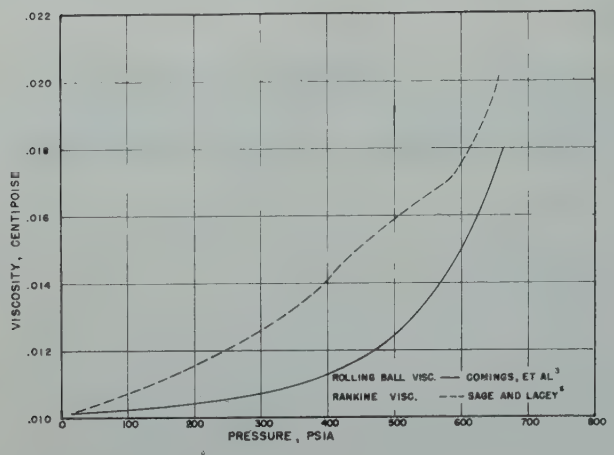

FIG. 2 — COMPARISON OF PROPANE VISCOSITY DATA AT 220°F.

CORRELATION OF GAS VISCOSITY DATA

Table 1 gives the composition of the gas mixtures on which viscosity determinations were made. In addition, viscosity determinations were made on pure methane. These data and the data previously obtained by Comings, Mayland, and Egly and by Michels and Gibson[17] on nitrogen have been correlated as functions of reduced pressures and temperatures. Fig. 3 presents the final correlation of μ/μ_1 as functions of pseudoreduced pressure for various values of pseudoreduced temperatures. The viscosity ratios for pseudoreduced pressures below 1.0 have been obtained from the work of Comings, Mayland, and Egly. Fig. 4, a crossplot of Fig. 3, may be used to interpolate between the isotherms of Fig. 3. For mixtures of hydrocarbons, the pseudocritical concept of Kay[18] is applied. Thus, in place of the critical temperature in Equation (1) the pseudocritical temperature,

$$pT_c = \sum_{i=1}^{n} x_i T_{ci} \quad . \quad . \quad . \quad . \quad . \quad . \quad . \quad (4)$$

and the pseudocritical pressure,

TABLE 1 — COMPOSITION OF GAS MIXTURES USED IN VISCOSITY RATIO CORRELATION

A. HIGH ETHANE CONTENT GAS

Component	Mol Per Cent	
N_2	0.6	
CH_4	73.4	Gas Gravity = .6844
C_2H_6	25.6	
C_3H_6	0.2	
C_3H_8	0.2	

B. HIGH NITROGEN CONTENT NATURAL GAS

He	0.8	
N_2	15.8	
CH_4	73.1	
C_2H_6	6.1	Gas Gravity = .6903
C_3H_8	3.4	
i - C_4H_{10}	0.2	
n - C_4H_{10}	0.6	

C. LOW ETHANE CONTENT GAS

N_2	0.3	
CH_4	95.6	Gas Gravity = .5776
C_2H_6	3.6	
C_3H_8	0.5	

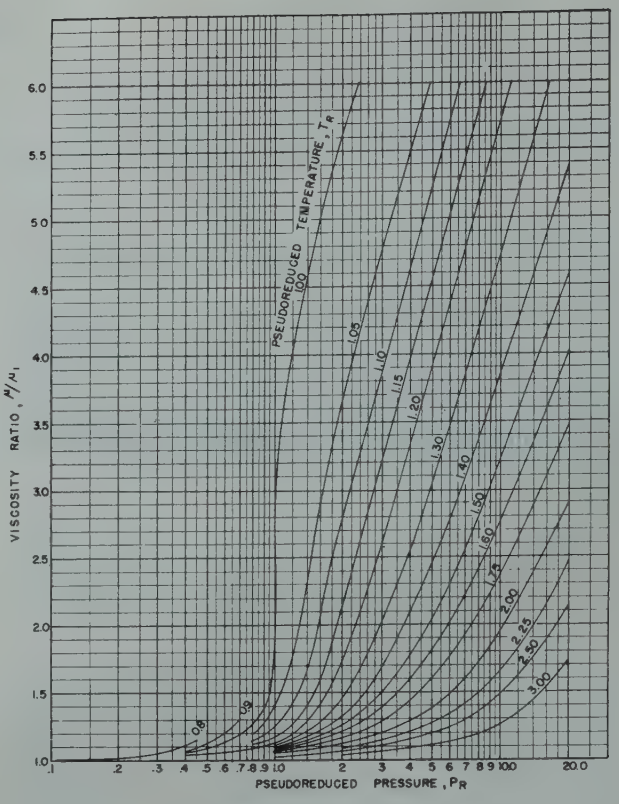

FIG. 3 — VISCOSITY RATIO VS PSEUDOREDUCED PRESSURE.

$$pP_c = \sum_{i=1}^{n} x_i P_{ci} \quad . \quad . \quad . \quad . \quad . \quad . \quad (5)$$

were used. In the above equations:

x_i = mol fraction of component i in the mixture

T_{ci} = critical temperature of component i, absolute scale

P_{ci} = critical pressure of component i, absolute scale

The average deviation of the predicted viscosity ratio from experimental points used in the correlation was found to be approximately 1.5 per cent. The maximum deviation occurred at reduced pressures in excess of 10 for the high nitrogen content gas mixture. The maximum deviation was 5.4 per cent.

The success with which the viscosity ratios may be correlated as unique functions of reduced temperatures and pressures is intimately related to the success with which the volumetric behavior of the pure components and mixtures can be correlated as a unique function of reduced temperatures and pressures. Thus, in the region near $T_R = 1$ and $P_R = 1$ where correlation of volumetric properties becomes difficult, the representation of viscosity ratios may be expected to have the greatest uncertainty. On the other hand, in the region of high reduced temperatures, the accuracy of representing viscosity ratios of hydrocarbon mixtures in general may be expected to be good. It should be emphasized that Figs. 3 and 4 apply to the viscosity of a single phase mixture, more particularly to the gas or less dense phase. Phase equilibria calculations may be necessary to insure the existence of a single phase or to obtain the composition of the equilibrium gas phase.

PART II

APPLICATION of CORRELATION to the PREDICTION of VISCOSITIES of NATURAL GAS MIXTURES

BY NOMAN L. CARR, RIKI KOBAYASHI, AND DAVID BURROWS

The usefulness of Figs. 3 and 4 in predicting the viscosities of complex hydrocarbon mixtures is dependent on the prediction of the atmospheric viscosities of mixtures by relatively simple means. Methods for the prediction of the atmospheric viscosities of natural gases which have been developed by past workers[21,22] are discussed.

VISCOSITY AT ONE ATMOSPHERE PRESSURE BY INTERPOLATION OF PURE COMPONENT VISCOSITIES

Fig. 6 is a plot of viscosity versus molecular weight which is essentially the plot proposed by Bicher and Katz[21] to determine the viscosity of hydrocarbon gas mixtures at atmospheric pressure. It was developed from the viscosities of natural mixtures containing a moderate amount of isomers. Bicher and Katz observed that the viscosities of methane-propane mixtures at one atmosphere pressure read from a plot of viscosity versus molecular weight checked the experimental values obtained by Trautz and Sorg.[23] Fig. 9 shows this comparison graphically for the methane-propane system. The agreement in all cases over the concentration range is within 1 per cent. Either the molecular weight or gas gravity may be applied to Fig. 6 to determine the atmospheric viscosities. Throughout this paper the gas gravity is defined as:

$$G = \frac{\text{Density of Gas at } 60°\text{F, } 14.7 \text{ psia}}{\text{Density of Air at } 60°\text{F, } 14.7 \text{ psia}} \quad . \quad . \quad (6)$$

Nonhydrocarbon components occur quite frequently in natural mixtures of hydrocarbons. The atmospheric viscosities of some of the more common nonhydrocarbon components are plotted on Fig. 7. The molecular weight-viscosity relationship of these components cannot be expected to correlate with the hydrocarbons, since the kinetic behavior of these molecules differs considerably from hydrocarbons of the same molecular weight. The viscosity of i-butane, n-butane, n-octane, and n-nonane, which were computed by the method of Hirschfelder,[24,25] are also plotted on Fig. 7. The values for n-decane were obtained by extrapolation. The viscosity of i-butane is shown to be higher than that of n-butane, whereas Sage, Yale, and Lacey[30] report the viscosity of n-butane to be greater than that of i-butane.

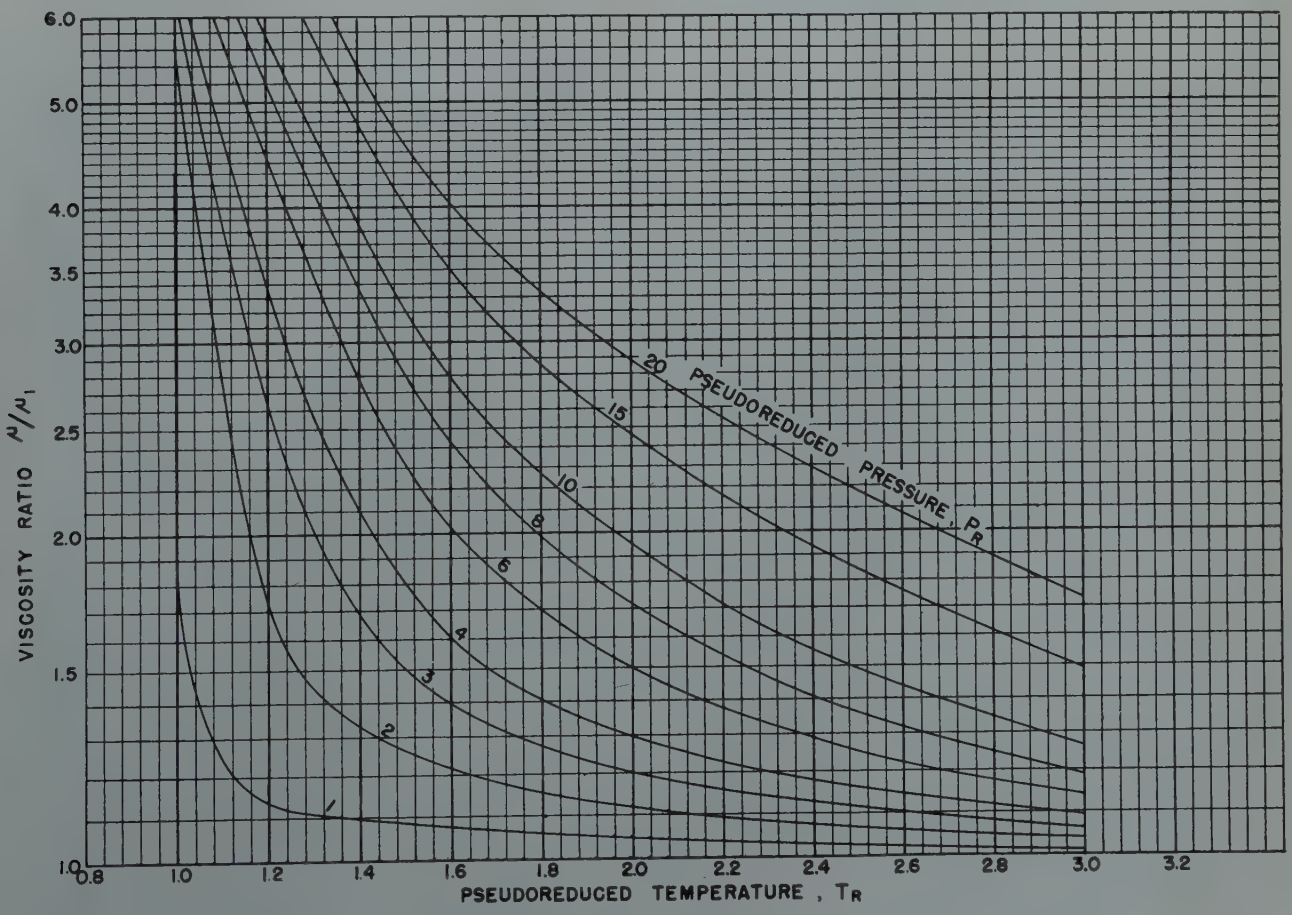

FIG. 4 — VISCOSITY RATIO VS PSEUDOREDUCED TEMPERATURE.

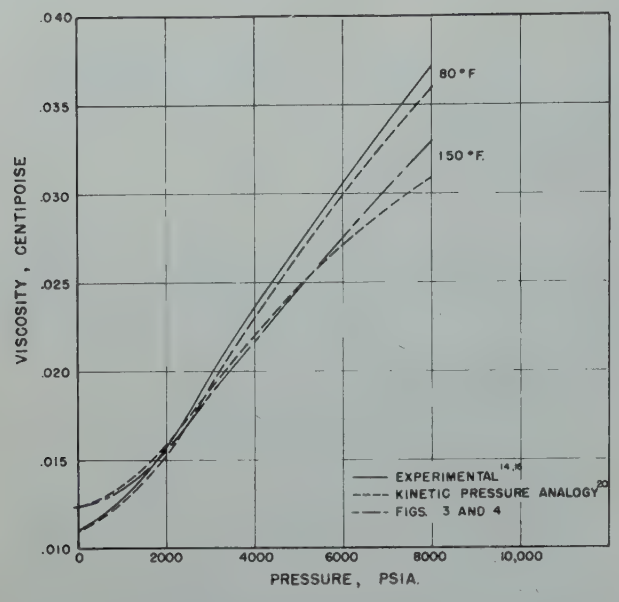

FIG. 5 — COMPARISON OF EXPERIMENTAL VISCOSITIES OF METHANE WITH KINETIC THEORY CALCULATIONS.

Fig. 10 presents the viscosity of nitrogen-ethane and carbon dioxide-propane mixtures at one atmosphere. Both lines show a nearly linear relationship of the effect of concentration on viscosity. Insert plots on Fig. 6 show corrections to the hydrocarbon viscosity values which may be applied to account for the presence of hydrogen sulfide, nitrogen, and carbon dioxide. A linear effect of concentration has been assumed to apply over the concentration range from 0 to 15 mol per cent of nonhydrocarbons. The insert plots were obtained from the viscosity of the pure components and Fig. 6. The presence of each of the nonhydrocarbons is to increase the viscosity of the hydrocarbon mixtures.

The accuracy with which the viscosities of mixtures of methane and higher molecular weight hydrocarbons at one atmosphere may be predicted from Fig. 6 is not known with certainty, since experimental data are unavailable. Methods used to calculate viscosities seem to indicate that Fig. 6 may be extended to complex mixtures involving components heavier than propane.

CALCULATION OF VISCOSITY AT LOW PRESSURE

Herning and Zipperer[22] proposed the following mixture rule for the viscosity of a mixture of gaseous components:

$$\mu_m = \frac{\sum_{i=1}^{n} \mu_i x_i \sqrt{M_i}}{\sum_{i=1}^{n} x_i \sqrt{M_i}} \quad \ldots \ldots \quad (7)$$

in which: μ_i = viscosity of component i

μ_m = viscosity of mixture

x_i = mol fraction of component i

M_i = molecular weight of component i

Equation (7) affords a simple and reliable means

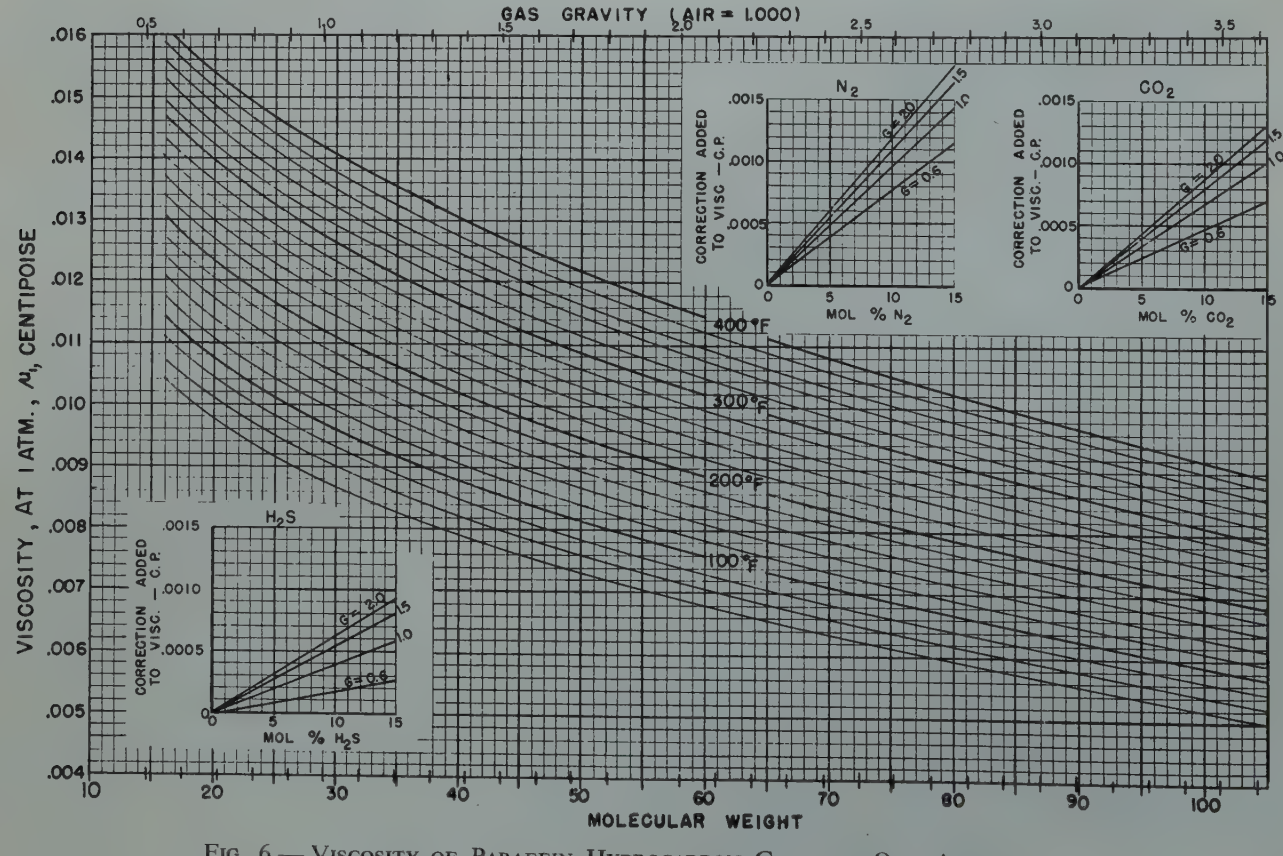

FIG. 6 — VISCOSITY OF PARAFFIN HYDROCARBON GASES AT ONE ATMOSPHERE.

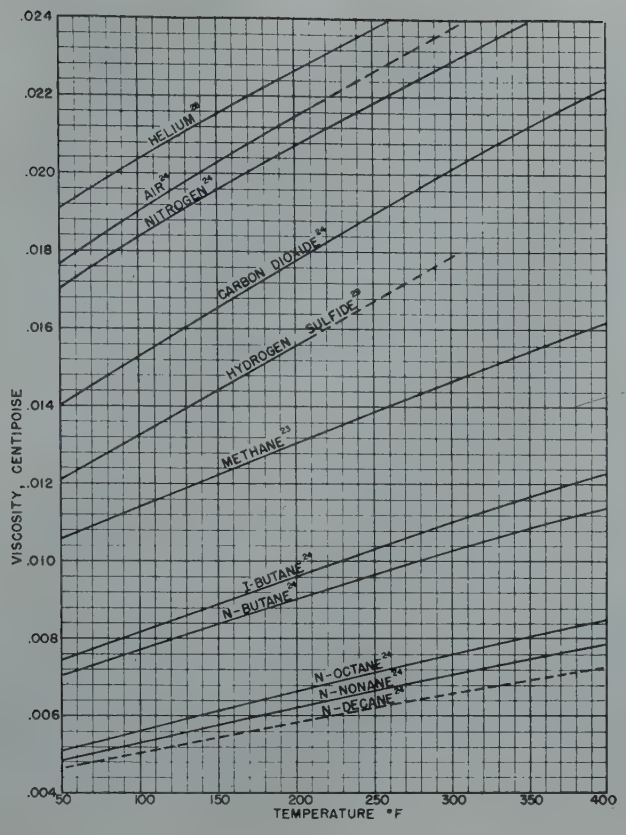

FIG. 7 — VISCOSITY OF NATURAL GASES AT LOW PRESSURES.

for calculating the viscosity of natural gas mixtures whose analyses are known. This equation was applied to synthetic mixtures and compared with the results obtained from Fig. 6. For both binary and complex mixtures, the calculated values were found to be in close accord with Fig. 6. Table 2 shows comparison of some of the mixtures calculated.

CALCULATIONS BASED ON MOLECULAR THEORY

Outstanding theoretical work has been published by Hirschfelder et al[24,25] on the viscosity and other transport properties of gases. Basic equations and procedures for calculating the temperature dependence of viscosity for 45 pure gases are given.[24] Curtiss and Hirschfelder developed relations to calculate the viscosities of mixtures at low pressures. Their relations have been applied to binary, ternary, and multicomponent systems with amazing accuracy. This calculation of viscosity, which is based upon molecular theory, probably gives the most accurate means of computing temperature and composition dependence of viscosity. The computational methods of Hirschfelder et al have been adapted to graphical and nomographic solutions by Bromley and Wilke.[26]

PSEUDOCRITICAL PRESSURES AND TEMPERATURES OF NATURAL GASES

In order to obtain the effect of pressure on viscosity from Fig. 6, it is necessary to know the pseudoreduced pressure and temperature of the mixture. If the gas analysis is known, the pseudocriticals used to compute the pseudoreduced pressure and temperature may be computed using Equations (4) and (5).

Katz[27] showed that the pseudocritical temperatures and pressures of natural gases could be correlated with gas gravity. The pseudocritical gas gravity relation for various gas streams from a given gas field showed an even higher degree of correlation. The correlation obtained by Bicher and Katz,[8] Fig. 8, may be used to obtain the pseudocritical pressure and temperature and thence the pseudoreduced pressure and temperature of natural gases. Again, insert plots are provided to indicate the direction and magnitude of errors introduced in the pseudocritical predictions by the presence of nonhydrocarbon constituents. These corrections are hypothetical in nature and assume that the hydrocarbon distribution remains unaffected by the presence of the nonhydrocarbons. This assumption is, of course, open to question.

PROCEDURE TO DETERMINE GAS VISCOSITIES OF NATURAL GASES FROM GAS GRAVITY

The gas viscosities of naturally occurring gases may be obtained in the following manner:

1. From the experimental specific gravity of the gas phase, determine the pseudocritical temperature and pressure from Fig. 8. Corrections to these pseudocritical properties for the presence of the nonhydrocarbon gases (CO_2, N_2, and H_2S) should be made if they are present in concentrations greater than 5 mol per cent. As mentioned previously, if the compositions of the gas phase are available, the calculated pseudocriticals are recommended over this procedure.

2. Divide the known pressure (psia) by the pseudocritical pressure to obtain the pseudoreduced pressure. In like manner, divide the known temperature (°*R*) by the pseudocritical temperature to obtain the pseudoreduced temperature.

3. From the pseudoreduced temperature and pressure, obtain the corresponding viscosity ratio from Figs. 3 and 4.

4. Obtain the viscosity of the gas at one atmosphere from Fig. 6 and convert the viscosity ratio to the absolute gas viscosity. Corrections of the atmospheric viscosities for the presence of high contents of nonhydrocarbon gases may be made from the insert plots in Fig. 6.

TABLE 2 — COMPARISON OF EXPERIMENTAL AND CALCULATED VISCOSITY AT ONE ATMOSPHERE

Gas	Temp. °F	Experimental	Calculated by Mixture Rule[22]	Per Cent Dev.	Fig. 6	Per Cent Dev.
A*	79	.01040	.01055	+ 1.44	.01042	+ 0.19
	150	.01180	.01185	+ 0.42	.01158	— 1.86
B*	150	.01326	.01333	+ 1.29	.01299	— 2.04
	200	.01420	.01419	— 0.07	.01375	— 3.17
50%C_1-50%C_3**	68	.00906	.00911	+ .55	.00908	+ .22
	392	.01386	.01382	— .29	.01391	+ .36
50% C_1-50% C_2**	68	.00984	.00983	— .10	.00981	— .30
	392	.01496	.01490	— .40	.01480	— 1.07
50% C_2-50% C_3**	68	.00854	.00865	+ .12	.00855	+ 1.17
	392	.01326	.01322	— .30	.01320	— .45

*See Table 1 for composition
**Mol Per Cent

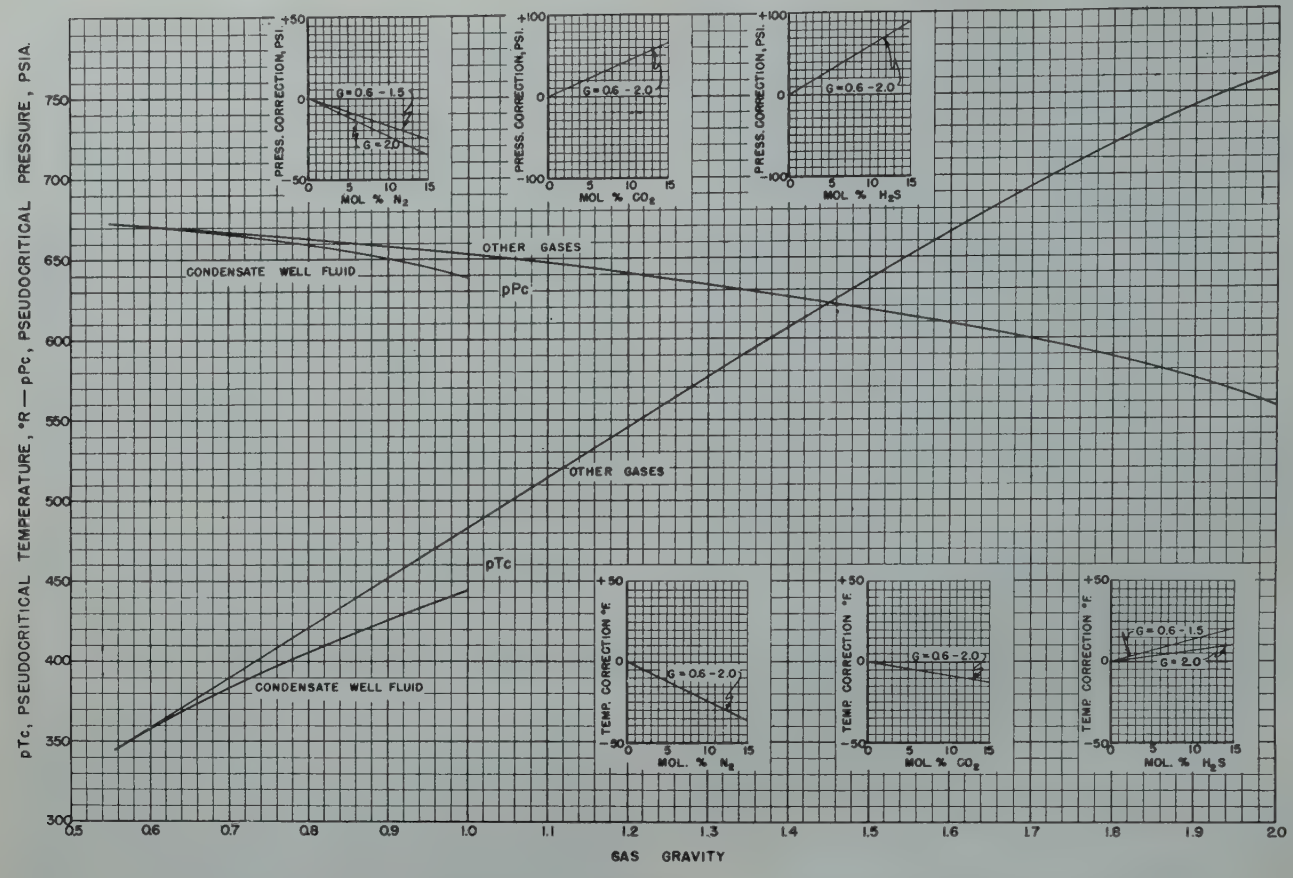

FIG. 8 — PREDICTION OF PSEUDOCRITICAL PRESSURE AND TEMPERATURE FROM GAS GRAVITY.

EXAMPLE CALCULATION

The following example calculation is presented to illustrate the use of the correlation to obtain gas viscosities from reservoir fluid data. The gas used in this illustration was collected during one displacement operation in the stepwise pressure reduction during the analysis of a bottom-hole sample. This procedure is followed to simulate differential liberation of gas from a reservoir fluid. The reservoir temperature was 195°F, and the test pressure was 1,800 psig (1,815 psia). The gravity of the liberated gas was determined by the use of a tared glass weighing balloon. The gas gravity was found to be .7018 (air = 1.000). The calculations proceed in the following manner:

1. Molecular weight = $(.7018 \times 28.95) = 20.31$
2. From which:
   Pseudocritical pressure = 667 (Fig. 8)
   Pseudocritical temperature = 390 (Fig. 8)
   Pseudoreduced pressure = $1{,}815/667 = 2.721$
   Pseudoreduced temperature = $(460 + 195)/390 = 1.679$
3. From Figs. 3 and 4:
   $\mu/\mu_1 = 1.28$
4. From Fig. 6:
   Viscosity at one atmosphere (μ_1) = .01223 cp
5. Therefore:
   The viscosity at 1,800 psig and 195°F = $1.28 \times .01223 = .01565$ cp

This and other points computed in the same manner from gas specific gravity measurements are plotted in Fig. 11. Viscosity values which were calculated using compositions obtained by mass spectrometer fractional analyses from which pseudocritical pressures and temperatures were obtained by the use of Equations (4) and (5) are also presented on the same plot. It is seen that the viscosity values computed from the fractional analyses (which is considered the most accurate method) and those obtained from gas gravity measurements are in close agreement.

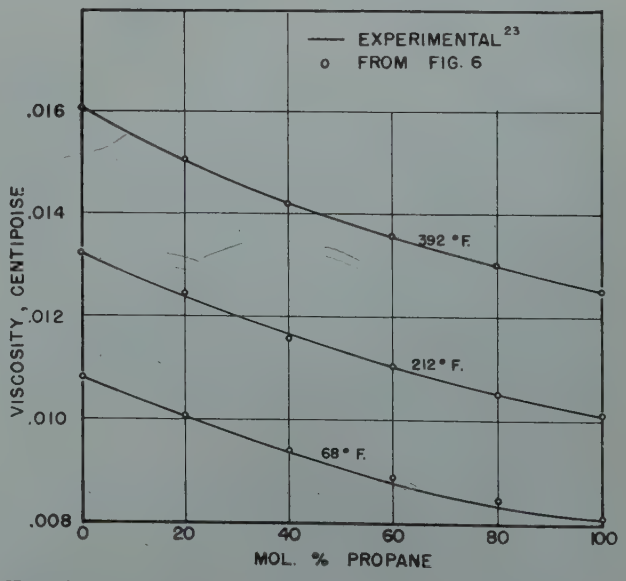

FIG. 9 — VISCOSITY OF METHANE-PROPANE MIXTURES AT ONE ATMOSPHERE: EXPERIMENTAL VS FIG. 6.

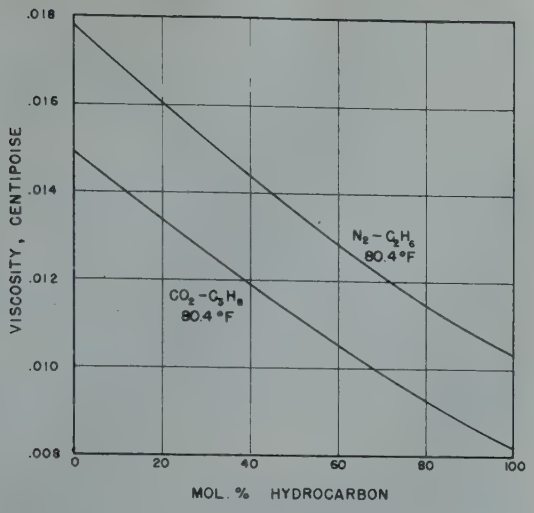

FIG. 10 — VISCOSITY OF NITROGEN-ETHANE AND CARBON DIOXIDE-PROPANE MIXTURE AT ONE ATMOSPHERE.

Additional analyses were performed on experimental data obtained from five separate reservoir fluid samples to check the two methods of obtaining pseudocritical pressures and temperatures. The deviation in gas viscosities did not exceed 3 per cent.

CONCLUSIONS

A correlation of the effect of pressure, temperature, and composition on the viscosity of hydrocarbons at pressures greater than 14.7 psia is presented. The correlation employs the theorem of corresponding states and may be expected to apply wherever this theorem accurately describes the volumetric behavior of the mixtures in question. The viscosity of complex hydrocarbon gas mixtures at one atmosphere may be computed from the gas analysis and almost as accurately from the gas gravity. Reliable viscosities of complex hydrocarbon gas mixtures at a given pressure and temperature may be rapidly calculated from a knowledge of gas gravity only.

ACKNOWLEDGMENTS

The authors wish to express their appreciation to R. E. Peck of the Illinois Institute of Technology for his helpful suggestions and criticisms and to the management of Continental Oil Co. for permission to publish this paper.

REFERENCES

1. Onnes, H. K.: "The Coefficient of Viscosity for Fluids in Corresponding States," *K. Akad. Wet., versl. van vergad.* (1894), **2**, 126.

2. Onnes, H. K., and de Haas, M.: "On the Coefficient of Viscosity of Liquids in Corresponding States According to Calculations by M. de Haas," *Ibid.* (1894), **3**, 62.

3. Comings, E. W., Mayland, B. J., and Egly, R. S.: "The Viscosity of Gases at High Pressures," *University of Illinois Engineering Experiment Station Bulletin No. 354* (1944), **42**.

4. Mason, S., and Maass, O.: "Measurement of the Viscosity in the Critical Region," *Canadian Journal of Research* (1940), **18B**, 128.

5. Naldreth, S. N., and Maass, O.: "The Viscosity of Carbon Dioxide in the Critical Region," *Ibid.* (1940), **18B**, 322.

6. Sage, B. H., and Lacey, W. N.: "Effect of Pressure Upon Viscosity of Methane and Two Natural Gases," *Trans. AIME* (1938), **127**, 118.

7. Hubbard, R. M., and Brown, G. G.: "Viscosity of n-Pentane," *Ind. Eng. Chem.* (1943), **35**, 1276.

8. Bicher, L. B., and Katz, D. L.: "Viscosities of the Methane-Propane System," Ibid. (1943), **35**, 754.

9. Poiseuille, J.: *Memoires des Savants Etrangers* (1846), **9**, 433.

10. Reynolds, O.: "An Experimental Investigation of the Circumstances Which Determine Whether the Motion of Water Shall Be Direct or Sinous and of the Law of Resistance in Parallel Channels," *Phil. Trans. Roy. Soc.* (London), (1883), **174**, 935.

11. Smith, A. S., and Brown, G. G.: "Correlating Fluid Viscosity," *Ind. Eng. Chem.* (1943), **35**, 705.

12. Rankine, A. O.: "On a Method of Determining the Viscosity of Gases," *Proc. Roy. Soc.* (1910), **83A**, 265.

13. Rankine, A. O.: "A Simple Viscometer for Gases," *J. Sci. Instr.* (1924), **1**, 105.

14. Carr, N. L.: "The Viscosity of Gas Mixtures at

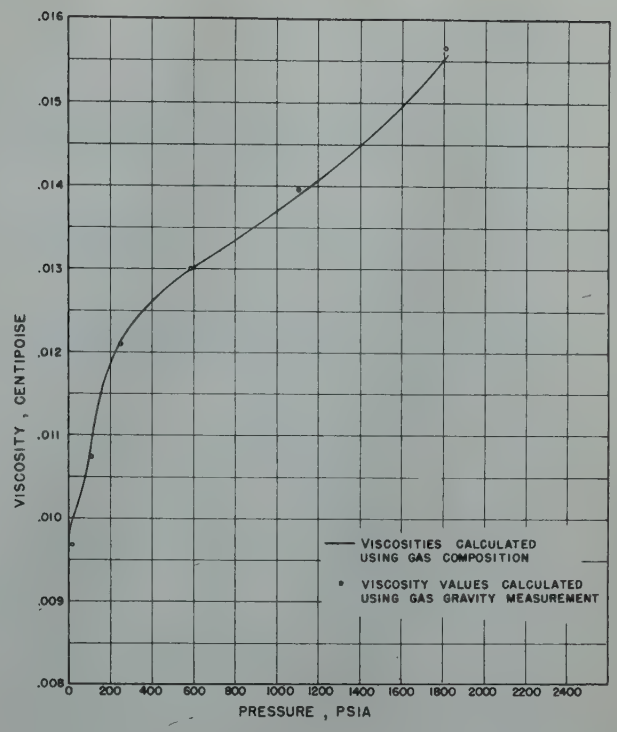

FIG. 11 — COMPARISON OF GAS VISCOSITIES OBTAINED USING LIBERATED GAS COMPOSITION AND GAS GRAVITY MEASUREMENTS.

High Pressures," Ph.D Thesis, Illinois Institute of Technology (1952).

15. Carr, N. L., Parent, J. D., and Peck, R. E.: "The Viscosity of Gases and Gas Mixtures at High Pressures," Paper Presented at the AIChE Regional Meeting in San Francisco, Sept. 13-16, 1953.

16. Carr, N. L.: "Viscosities of Natural Gas Components and Mixtures," *Institute of Gas Technology Research Bulletin No. 23,* June, 1953.

17. Michels, A., and Gibson, R. O.: "The Measurement of the Viscosity of Gases at High Pressures, the Viscosity of Nitrogen at 1,000 Atmospheres," *Proc. Roy. Soc.* (1931), **134A**, 288.

18. Kay, W. B.: "Density of Hydrocarbon Gases and Vapors," *Ind. Eng. Chem.* (1936), **28**, 1014.

19. Smith, K. A., and Watson, K. M.: "High Pressure Vapor-Liquid Equilibria, Activity Coefficients for Ideal Systems," *Chem. Eng. Progress* (1949), **45**, 494.

20. Benedict, M., Webb, G. B., and Rubin, L. C.: "An Emperical Equation for Thermal Properties of Light Hydrocarbons and Their Mixtures," *Chem. Eng. Prog.* (1951), **47**, 419.

21. Bicher, L. B., and Katz, D. L.: "Viscosity of Natural Gases," *Trans.* AIME (1944), **155**, 246.

22. Herning, F., and Zipperer, L.: "Calculation of the Viscosity of Technical Gas Mixtures from the Viscosity of the Individual Gases," *Gas und Wasserjoch* (1936), **79**, 49.

23. Trautz, M., and Sorg, K. G.: "Viscosity of Hydrogen, Methane, Ethane, Propane, and Their Binaries," *Ann. Physik* (1931), **10**, 81.

24. Hirschfelder, J. O., Bird, R. B., and Spotz, E. L.: "Viscosity and Other Properties of Gases and Gas Mixtures," *Trans. AIME* (1949), **71**, 921.

25. Curtis, C. F., and Hirschfelder, J. O.: "The Transport Properties of Multicomponent Systems of Gases," *J. of Chem. Phys.* (1948), **16**, 968.

26. Bromley, L. A., and Wilke, C. R.: "Viscosity Behavior of Gases," *Ind. Eng. Chem.* (1951), **43**, 1641.

27. Katz, D. L.: "High Pressure Gas Measurement," *Refiner and Natural Gasoline Manufacturer* (June, 1942).

28. N.B.S.-NACA Tables of Thermal Properties of Gases.

29. Rankine, A. O., and Smith, C. J.: "On the Viscosities and Molecular Dimensions of Methane, Sulphuretted Hydrogen, and Cyanogen," *London, Edinburgh, and Dublin Philosophical Magazine and Journal of Science* (1921), **42**, 615.

30. Sage, B. H., Yale, W. D., and Lacey, W. N.: "Effect of Pressure on Viscosity of n-Butane and i-Butane," *Ind. Eng. Chem.* (1939), **31**, 223.

★★★

OPTIMUM SAND CONCENTRATIONS in WELL TREATMENTS

PETER DEHLINGER — A&M COLLEGE OF TEXAS, COLLEGE STATION, TEX.
W. H. BROWNE — BATTELLE MEMORIAL INSTITUTE, COLUMBUS, OHIO
C. O. BUNDRANT, MEMBER AIME — THE WESTERN CO., MIDLAND, TEX.

T. P. 3929

ABSTRACT

Brief laboratory investigations are described which attempt to determine optimum sand concentrations in gel-sand and oil-sand[1] well-treatments. The investigations apply to the case where sand acts as a propping agent in formation fractures. Both analytically and experimentally it is demonstrated that optimum sand concentrations can be defined. It is difficult to translate laboratory results to field treatments, however, since the relative distribution of sand and fluid in fractures may not be the same as injected. This is because fluid may penetrate the furtherest narrow portions of fractures, which would not pass sand. Optimum concentration of a monolayer of Ottawa sand in fractures of 0.025-in. width at the usual range of pressures encountered in treatments appears to be about ½ to 2 lb/gal. of gel.

An investigation of abrasion of rock-walls by sand in treatments, described in the Appendix, shows that such abrasion is not probable in significant amounts.

INTRODUCTION

Experience in the Spraberry formation of West Texas, as well as in other formations, has shown that sand is a necessary and vital part of gel-sand and oil-sand treatments. Many observers of treatments have also concluded that there seems to be an optimum range of sand concentration for these injections. Brief laboratory investigations were made at Battelle Memorial Institute to study flow in fractures with different sand concentrations. To investigate the existence and range of optimum concentrations in the laboratory, however, necessitates knowledge of the mechanism by which the sand aids in increasing subsequent production.

The action of sand in fractures is usually thought to be either that of a propping agent, thus providing a greater effective formation permeability; that of an abrasive in eroding fill material in fractures; or that of an abrasive eroding rock-wall irregularities along fracture surfaces. Investigations described in the Appendix show that sand does not appear to erode rock-wall materials appreciably. In a subsequent paper it is reasoned, at least for the Spraberry formation of West Texas, that the primary action of sand is not in removing fill materials in fractures. In this formation, and probably others, too, the main effect of sand appears to be that of a propping agent.

Both analytical and experimental investigations were made for the case of a monolayer of sand acting as a propper, in which sand concentrations were determined that would, after treatment, permit flow of the maximum quantities of oil from the formation into a well. If too few sand grains are injected into fractures in which the bottom hole pressure has decreased appreciably below the original formation pressure, the confining pressure in the formation may become relatively large, thus compress the rock-walls around the sand grains, essentially close fractures, and so decrease the subsequent flow of oil. Similarly, if too much sand is used, the flow of oil will be impeded by the volume of sand present.

THEORY

Although an analytical approach to determining optimum sand concentrations involves gross assumptions,

Discussion of this and all following technical papers is invited. Discussion in writing (3 copies) may be sent to the offices of the Journal of Petroleum Technology. Any discussion offered after Dec. 31, 1954, should be in the form of a new paper.

Manuscript received in Petroleum Branch offices on Apr. 1, 1954. Paper presented at Petroleum Branch Fall Meeting in San Antonio on Oct. 17-20, 1954.

[1]Reference given at end of paper.

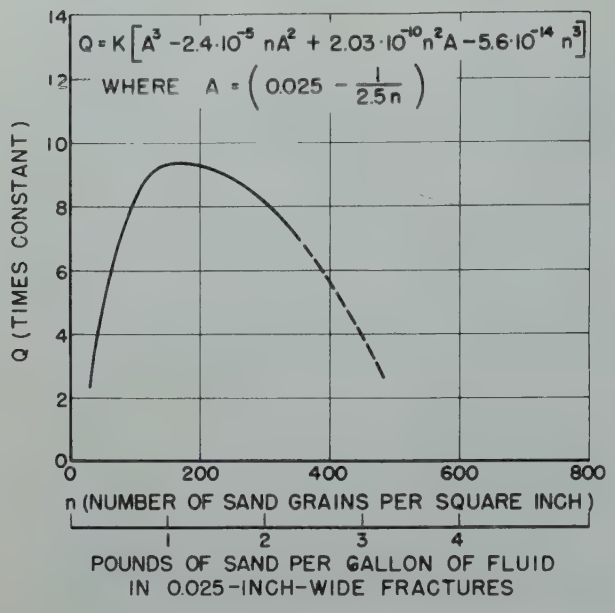
Q = K [A³ -2.4·10⁻⁵ nA² + 2.03·10⁻¹⁰ n²A -5.6·10⁻¹⁴ n³]
WHERE A = (0.025 - 1/2.5n)
Q (TIMES CONSTANT)
n (NUMBER OF SAND GRAINS PER SQUARE INCH)
POUNDS OF SAND PER GALLON OF FLUID IN 0.025-INCH-WIDE FRACTURES

FIG. 1 — CALCULATED RELATION BETWEEN FLOW RATE AND SAND CONCENTRATION FOR SPHERES 0.0025-IN. IN DIAMETER.

it may nevertheless indicate reasonable flow velocities for various sand concentrations. It is assumed for this analysis that sand particles are spherical in shape, uniform in size, the sand is distributed uniformly in fractures, and because of the greater hardness of the sand than that of nearly all formations encountered in treatments, the sand particles are, in effect, rigid. Most of the deformation encountered in a fracture would be expected to occur in the rock-wall contacting the sand. Consequently, as the confining pressure in a formation tends to close fractures around each sand grain, the area of contact between the rigid sand spheres and rock-wall increases.

The forces acting in a formation fracture are:

$$F_c = F_f + NF_s \quad . \quad . \quad . \quad . \quad . \quad . \quad . \quad . \quad . \quad (1)$$

where F_c is the force, due to overlying rocks and regional stresses, tending to close fractures,
F_f is the force of formation fluid, tending to keep fractures open,
F_s is the force each sand grain exerts on the formation, tending to keep fractures open,
N is the number of sand grains.

In terms of pressures,

$$P_c - P_f = MF_s \quad . \quad . \quad . \quad . \quad . \quad . \quad . \quad . \quad . \quad (2)$$

where P_c is the confining pressure in a formation, tending to close fractures,
P_f is the formation pressure,
M is the number of sand grains per sq in. of fracture surface.

Just prior to fracturing, F_s can be equated with the strength of the formation:

$$MF_s = anS_t$$

where a is the area of contact between sand grain and formation,
n is the minimum number of sand grains per sq in. of fracture surface required to prevent crushing in the wall-rock, and
S_t is the strength of the formation.

Equation (2) then becomes:

$$P_c - P_f = anS_t \quad . \quad . \quad . \quad . \quad . \quad . \quad . \quad . \quad . \quad (3)$$

The area of contact of two portions of a spherical sand grain with the rock-wall, assuming the wall to be deformed around the sphere, is approximately:

$$a = 2\pi Dh = \pi D(D\text{-}W)$$

in the region where $W > \frac{D}{2}$, and

D is the diameter of sand grain,
W is the width of fracture, and

$$h = \frac{D\text{-}W}{2}$$

Equation (3) becomes:

$$P_c - P_f = \pi nD(D\text{-}W)\, S_t \quad . \quad . \quad . \quad . \quad . \quad . \quad (4)$$

By assuming relevant values for a given formation and inserting them into Equation (4), n can be determined as a function of fracture width W. For the Spraberry formation, typical values at the bottom of a well may be approximately:

P_c = 2,500 psi (horizontal confining pressure)
P_f = 1,900 psi (bottom hole pressure)
S_t = 20,000 psi (strength of formation)
D = 0.025 in.

Then Equation (4) reduces to:

$$W = 0.025 - \left(\frac{1}{2.5n}\right) \quad . \quad . \quad . \quad . \quad . \quad . \quad . \quad (5)$$

The relationship between flow rate and width between two parallel plates for laminar motion in the viscous range is[1]:

$$Q \sim W^3$$

where Q is the flow rate.

Sand between parallel plates decreases the volume open to flow by the volume of sand present, however. The flow is further complicated by the drag of fluid around each sand grain, although the extent of this drag is difficult to estimate. For low velocity flow in the viscous range, the drag will be small. If it can be assumed, to a rough approximation, that the flow rate varies directly as the volume available to flow between spheres in the fractures, then:

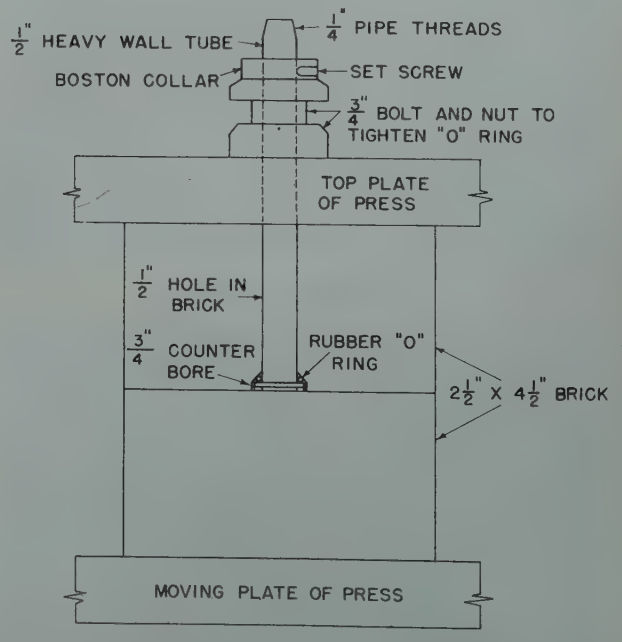

FIG. 2 — DIAGRAM OF CERAMIC-BRICK TESTING APPARATUS.

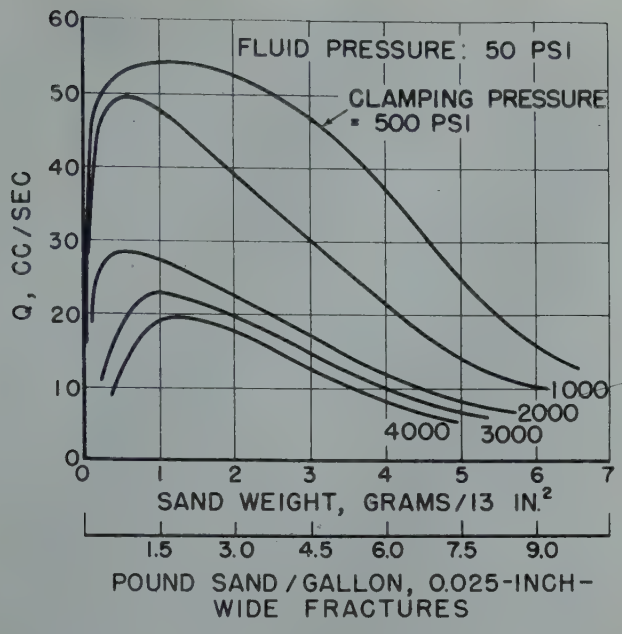

FIG. 3 — FLOW RATE OF SAE 10 MOTOR OIL AS FUNCTION OF SAND CONCENTRATION BETWEEN POROUS, SEMIHARD, CERAMIC BRICKS.

$$W_1 = W - n\left(\frac{\pi D^2}{6}\right) \quad . \quad . \quad . \quad . \quad . \quad . \quad . \quad (7)$$

where W_1 is the effective fracture width or the volume per sq in. of fracture surface open to flow.

Using this new effective fracture width in Equation (6), an equation in form:

$$\frac{Q}{K_1} = K_2 W_1^3 =$$

$$K_2\left(\quad W^3 - \tfrac{1}{2}\pi n D^3 W^2 + 1/12\,(\pi^3 n^2 D^6 W) - \right.$$

$$\left. \frac{1}{216}\,(\pi^3 n^3 D^9) \quad \right) \quad . \quad . \quad . \quad . \quad . \quad . \quad . \quad . \quad . \quad . \quad . \quad (8)$$

is obtained,

where K_1 is a constant of proportionality, and
K_2 is a quantity indicating the effect of fluid drag.

For no drag, $K_2 = 1$; for drag, $K_2 < 1$.

Inserting Equation (5) into (8) gives, for conditions assumed in Equation (5), the equation shown and illustrated graphically on Fig. 1. Because of the assumptions involved, this equation is not reliable at the higher sand concentrations, although it appears more reasonable for the vicinity of the maximum of the curve.

Fig. 1 shows flow rate into a well as a function of the number of sand grains per unit fracture surface. The abscissa of this curve also shows sand concentrations in pounds per gallon of gel or oil for uniform fractures of 0.025 in. width. This curve may, in general, approach conditions near the bottom of a well in the Spraberry formation, where it would indicate minimum sand concentration before some crushing occurs in the wall-rocks.

The curve suggests that a maximum flow of oil may be anticipated in a well. For the assumed conditions, the maximum flow may be near 1¼ lbs of sand per gallon of fluid.

EXPERIMENTS

The test procedure was to place various monolayers of concentrations of sand between two ceramic bricks and determine fluid pressures required to obtain specific flow rates of SAE 10 motor oil along the interface between the bricks. Two different types of ceramic refractory bricks, both 3 x 4½ in. on a side, were used. The first set of bricks was quite impervious and hard. The second set was softer and more porous. In each test two bricks of the same type were clamped together between jaws of a hydraulic press, as illustrated in Fig. 2. A center hole through the top brick permitted injection of fluid to the interface between the bricks.

Sand weights of ⅛, ½, 1, 2, 4, and 6 gm were distributed evenly over the area of brick surface. Tests were made at specific flow rates of oil: 11, 18, 25, 37, and 50 cc/sec. The fluid injection pressures applied were those required to obtain the constant flow rates. In some instances these pressures ranged up to 10,000 psi, but they were generally lower. Pressures used to clamp the bricks together ranged from 500 to 4,000 psi and were varied at intervals of 500 psi.

Ottawa sand was used that passed a 20 but not 30 mesh screen. Thus, grains of reasonably uniform size, approximately 0.025-in. diameter, were used. In most tests the distribution of sand grains remained uniform during fluid injection. At higher sand concentrations there was some tendency for the injected fluid to redistribute the grains and open one or more channels, resulting in spurious flow rates. At lower sand concentrations, however, few channels formed so that the more reliable data were obtained at the lower concentrations.

Fluid pressures were obtained from a 150-ton capacity Watson-Stillman Press which has a maximum ram velocity of 1½ in./sec. Clamping pressures on the interface containing sand were obtained with a 2-ton hydraulic jack. Because it was easier to vary pressures

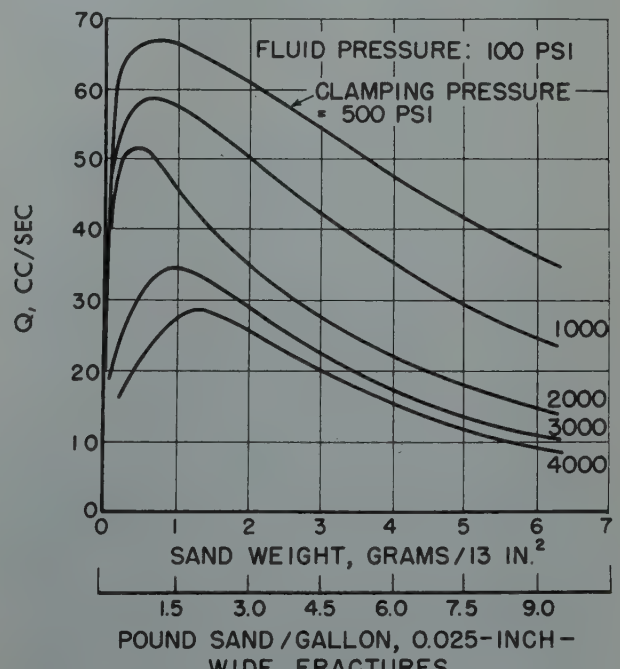

FIG. 4 — FLOW RATE OF SAE 10 MOTOR OIL AS FUNCTION OF SAND CONCENTRATION BETWEEN POROUS, SEMIHARD, CERAMIC BRICKS.

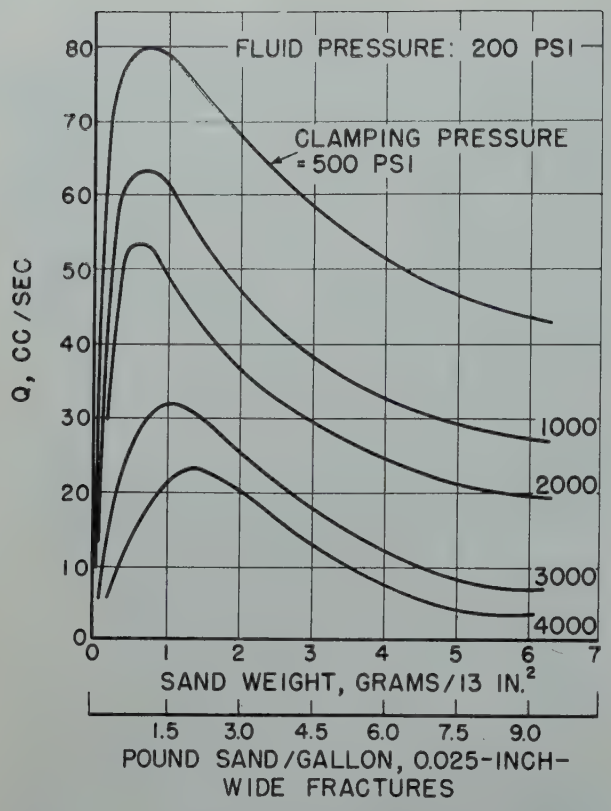

FIG. 5 — FLOW RATE OF SAE 10 MOTOR OIL AS FUNCTION OF SAND CONCENTRATION BETWEEN POROUS, SEMIHARD, CERAMIC BRICKS.

rather than flow velocities with this equipment, basic measurements were made by recording injection pressures as functions of clamping loads for specific sand concentrations and flow rates. Curves of the basic data were cross-plotted to show fluid pressure as a function of sand concentrations for specific flow rates and clamping pressures. Neither of these sets of basic curves is presented in this paper. Figs. 3 through 6 are further cross-plots, showing the desired flow rates as functions of sand concentration for specific injection and clamping pressures in the softer bricks.

Figs. 3 through 6 indicate that there are sand concentrations that permit a maximum flow of oil and that this maximum varies with clamping pressure and, possibly, fluid pressure. Very similar curves, with maxima shifted slightly toward larger sand concentrations, were obtained with the harder, less porous, bricks. The hardness of a formation thus has a minor effect on optimum sand concentrations: the harder formations would require slightly larger amounts of sand to permit maximum flow at comparable pressures. It is noteworthy that the general shapes of the experimental curves are similar to the analytical one shown on Fig. 1, although the experimental results indicate somewhat lower optimum concentrations. Whereas optimum concentrations for 0.025-in. wide fractures and specified pressures were calculated to be about 1¼ lbs/gal. of fluid, the laboratory results indicate optimum concentrations closer to ½ or 1 lb/gal. for comparable pressures. A significant difference between these curves is that the sand content in Fig. 1 refers to the minimum amount necessary to prevent crushing in fractures, whereas in Figs. 3 through 6 the concentrations may be both greater and less than this amount.

Fig. 7 shows maximum flow rates of SAE 10 oil, as obtained from the maxima of Figs. 3 through 6 and similar curves (not shown) for the harder bricks, for various clamping pressures as functions of sand concentration. Within the experimental error, these curves appear to be independent of flow pressure. Magnitudes of maxima flow rates were found to be about the same in both the harder and softer bricks for comparable pressures. However, the maxima were shifted toward higher sand concentrations in the harder bricks, as indicated in Fig. 7.

In correlating these laboratory data with field conditions, fluid pressures in the laboratory correspond approximately to the difference in formation and bottom hole pressures, and clamping pressures to the pressure tending to close the formation fractures (see section on "Theory"). In most formations encountered, these pressures would correspond to laboratory injection pressures up to about 1,000 psi and clamping pressures up to about 3,000 psi, or more in some instances. In the Spraberry formation, applicable fluid pressures would probably be less than 600 psi and clamping pressures well below 1,000 psi.

Although tests with bricks suggest that for specific pressure conditions optimum sand concentrations can be determined in fractures of formations of given hardness, care must be exercised in translating these laboratory results to field conditions. To apply laboratory results directly to concentrations injected implies that all sand travels as far in fractures as does the fluid and remains mixed in a constant ratio with the fluid. Unfortunately, little information is available on the relative penetrability of sand with respect to fluid.

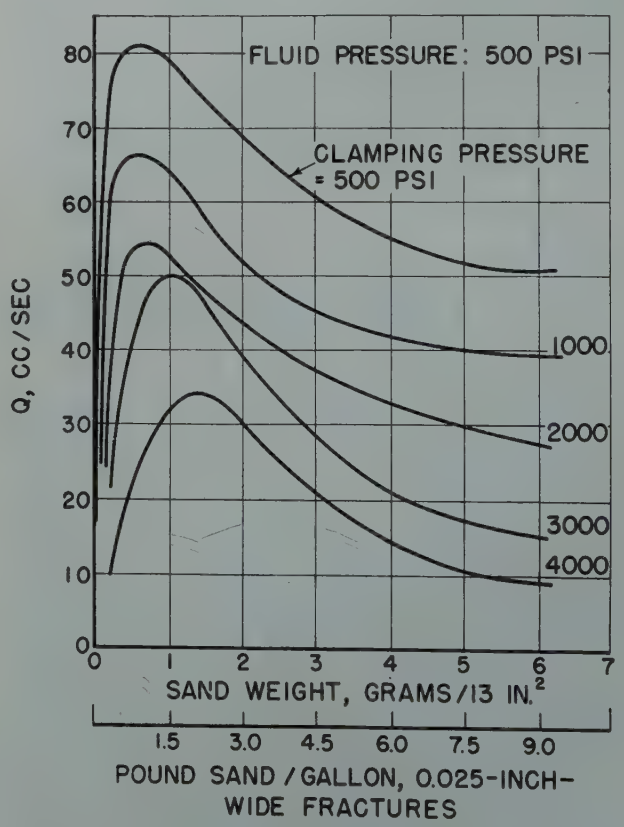

FIG. 6 — FLOW RATE OF SAE 10 MOTOR OIL AS FUNCTION OF SAND CONCENTRATION BETWEEN POROUS, SEMIHARD, CERAMIC BRICKS.

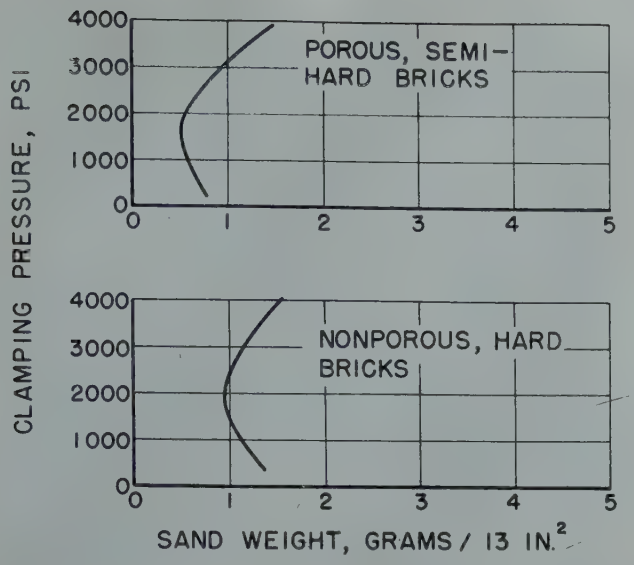

FIG. 7 — TYPICAL CURVES OF MAXIMUM FLOW RATE OF SAE 10 MOTOR OIL, FOR DIFFERENT CLAMPING PRESSURES AND SAND CONCENTRATIONS, WITH TWO DIFFERENT TYPES OF CERAMIC BRICKS.

However, as the fluid probably travels further than sand in narrow fractures, actual concentrations in fractures will probably be greater near the well than in the injected mixture.

Figs. 3 through 6 indicate that flow velocity is not particularly sensitive to sand concentration. Thus, although concentration for effective flow should not be less than a certain minimum, optimum concentrations can be exceeded appreciably without a significant reduction in flow. As there may be a tendency for the formation to creep, i.e., to close fractures long after the sand has been injected, it would seem advisable to use more than the apparent optimum concentration.

CONCLUSIONS

It is concluded that optimum sand concentrations do exist for treatments of fractured formations where the sand acts as a propping agent, and that this optimum does not seem to be very sensitive. For Ottawa sand this apparent optimum concentration, in fractures 0.025-in. wide, may be between ½ and 2 lbs/gal. of fluid. Effective optimum concentrations in treatments, allowing for creep in the fractures in the course of time, may be somewhat greater. The optimum concentration is a function of the formation pressure, bottom hole pressure, hardness of formation, formation confining pressure, and viscosity of oil.

In converting laboratory sand concentrations to field application, the relative penetration of fractures by sand and fluid as the fracture width narrows must be estimated. Where desirable sand concentrations in fractures can be inferred, effective injection concentrations might be estimated to obtain such mixtures in fractures. For example, if the desired amount of sand in fractures, allowing for a moderate excess is 2 lbs/gal. and if the sand is assumed to spread over only half the volume occupied by fluid, then the proper injected mixture might be 1 lb/gal.

APPENDIX

Since the possibility of sand eroding rock-walls in well treatments has been raised on occasions, a number of qualitative laboratory tests were made at Battelle to determine the likelihood of this action. Initial tests for abrasion were made on fractured surfaces of Spraberry cores. Similar tests were made with relatively soft transparent Lucite discs.

TEST PROCEDURE

The same press was used as in the tests with ceramic bricks. A fractured Spraberry core, usually 3½ in. in diameter, was clamped between plates of the press (Fig. 8) by a 20-ton hydraulic jack. In contrast to the previously described tests, a gel-sand was injected in the abrasion tests. The gel-sand consisted of 85 gm of aluminum soap and ¼ lb of sand/gal. of kerosene. This fluid was injected into the fracture surface at specific pressures through a hole in the top half of the core. The flow rate of the fluid ejected from the fracture surface was measured. This fluid was injected at various pressures, some at high enough pressures to rupture the cores. Generally, injection pressures were sufficiently lower than clamping loads to permit injection and flow of sand and gel through the original core fracture. A fairly rounded lake sand was used which had an average diameter of 0.018 in. Sand was injected uniformly over the interface in these tests, but careful examinations of the rock surfaces indicated that the sand did not erode any of the rock materials significantly.

A number of similar tests were made with Lucite discs to determine whether the softer material could be abraded more readily. In the tests it was also attempted to evaluate abrasion both parallel and perpendicular to the direction of flow. In one set of tests, two flat Lucite discs, 1 in. thick and 4 in. in diameter, were used (as shown in Fig. 9, except that the interface between the discs is flat). They were placed in the same apparatus used for the rock cores and ceramic

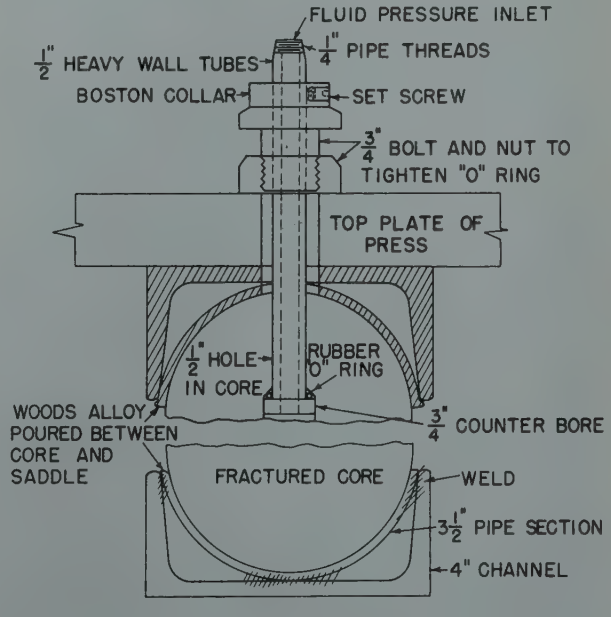

FIG. 8 — DIAGRAM OF FRACTURED-CORE TESTING APPARATUS.

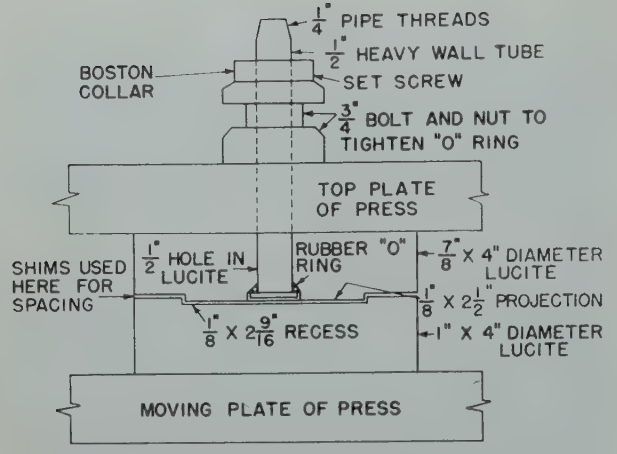
1/4" PIPE THREADS
1/2" HEAVY WALL TUBE
BOSTON COLLAR
SET SCREW
3/4" BOLT AND NUT TO TIGHTEN "O" RING
TOP PLATE OF PRESS
SHIMS USED HERE FOR SPACING
1/2" HOLE IN LUCITE
RUBBER "O" RING
7/8" X 4" DIAMETER LUCITE
1/8" X 2 1/2" PROJECTION
1/8" X 2 9/16" RECESS
1" X 4" DIAMETER LUCITE
MOVING PLATE OF PRESS

FIG. 9 — DIAGRAM OF RECESSED LUCITE-DISK TESTING APPARATUS.

bricks. In other tests, Lucite discs with a cylindrical recess (Fig. 9) were used to evaluate abrasion in different flow directions.

The Lucite discs were separated by three shim spacers of various thicknesses, located radially at 120°. The spacer thickness was varied, with different discs used for each set of spacers, from 0.010 to 0.033 in. Clamping pressures exceeded fluid pressures in these tests so that the spacers would not be removed during injection, yet this pressure difference was not so large as to cause indentations on the discs. Fluid pressures ranged up to 400 psi, the maximum available with this testing arrangement.

TEST RESULTS

Since Spraberry cores were not abraded appreciably, most of the results pertain to Lucite. When spacers of 0.017 in. or less were used, sand was filtered at the inlet hole of the top disc, but was not injected into the interface between the discs; only gel was ejected from the disc interface then. When spacers of 0.018 in. and larger were used, sand and gel were ejected from the interface between the discs. When a low injection velocity was applied, corresponding to a pressure of 30 psi, the discs were not abraded. At a fluid pressure of 400 psi varying degrees of abrasions were observed on the lower disc. Abrasion was greatest with the 0.018-in. spacers, the diameter of the sand grains, and was progressively less as the spacing was increased. At the higher injection pressures a deep erosion pit was created in the lower disc just around the region of the inlet recess. For the 0.018-in. spacer this pit was found to extend over approximately 90° and was about 1/32-in. deep and ⅛-in. long. Less pronounced erosion pits were observed for larger shim spacers. With 0.025-in. spacers, the pit was barely noticeable. Beyond the abraded pit, sand produced radial scratches when spacers were 0.018 or 0.019-in. thick. When larger spacers were used, such abrasion marks were not observed.

Lucite discs with a recess were used to investigate erosion as a function of flow direction. The injected fluid made two right angle turns between the discs before extrusion. The upper disc mates the lower one except for a 1/32-in. clearance on the projected parts of the cups (Fig. 9). Three 1/32-in. diameter pins were placed at the edges of the recess at 120° to provide equal circumferencial spacing of the discs. Although abrasion was pronounced toward the center of the lower disc when an 0.018-in. spacer was used at a fluid pressure of 200 psi, only slight abrasion was observed near the outer edge of the lower disc. No abrasion was observed along the vertical walls of the recess, presumably because the spacing there was greater than the sand grain diameter. Larger shim spacers resulted in even less abrasion.

Since abrasion was found to be most pronounced when the fracture width was approximately equal to the sand grain diameter, the discs in Fig. 9 were modified in further tests. The three pins were removed and the upper disc was placed in contact with one end of the recess of the lower disc, so that spacing between the recesses varied from 0 to 1/16-in. When 0.018-in. shims were used, nearly all the gel-sand was ejected from the wider side of the recess, so that no abrasion was observed along the vertical portion of the recess. Time did not permit further modification of these test procedures.

CONCLUSIONS FROM ABRASION TESTS

The brief investigations with the Spraberry cores and the Lucite discs have indicated that:

1. No evidence for abrasion was observed on fracture surfaces of Spraberry cores. Greater sand concentrations could have resulted in some abrasion, but probably not in significant amounts.
2. Abrasion of Lucite by sand in gel is significant only when the spacing between the discs is nearly equal to the sand grain diameter. Too small a spacing results in filling the inlet area with sand, passing only fluid between the discs, while too large a spacing allows the sand to pass between films of fluid without scratching the surfaces.
3. Maximum abrasion also appears to require a high flow velocity and normal incidence of sand striking a surface; i.e., where the sand has a blasting effect. Greater sand concentrations would probably also result in some increased abrasion.

Translating these laboratory results to application in the field indicates that:

1. Except in the softest and least consolidated formations, abrasion of wall rock by sand in treatments appears to be of minor importance. In those portions of formation fractures where widths equal the sand grain diameter there might be some local abrasion.
2. Where fracture widths are less than the sand grain diameters, it appears that sand would plug the inlet to the fracture. This means that fractures will have to be widened to at least the sand grain diameter before an injection with sand is possible.

ACKNOWLEDGMENTS

Permission by The Western Co. to publish these results is gratefully acknowledged. Members of a Steering Committee at the Battelle Memorial Institute, formed to guide this and similar investigations, have provided valuable and significant suggestions.

REFERENCE

1. Streeter, V. L.: *Fluid Mechanics*, McGraw-Hill (1951), 150.

★★★

MEASUREMENT of RESISTANCE to FLOW of FLUIDS in NATURAL GAS WELLS

R. V. SMITH*
MEMBER AIME
R. H. WILLIAMS**
E. J. DEWEES

BUREAU OF MINES
BARTLESVILLE, OKLA.

T. P. 3928

ABSTRACT

Before this paper was presented, the terms "f" and "$\sqrt{1/f}$" in flow equations had been called "friction coefficient" and "friction factor," respectively. However, many authors have used the names for the terms interchangeably, with the result that considerable confusion has existed in the literature on flow of fluids. In an effort to establish a clear and concise terminology for these terms, the authors have designated f as "resistance coefficient" and $\sqrt{1/f}$ as "transmission factor."

Transmission factors for the flow strings of gas wells were determined by tests on wells in six fields of Oklahoma, Texas, and Louisiana. Data were collected on 14 gas wells while gas was flowing through 1¼, 2, 2½, and 3-in. tubing and 5½ and 7-in. casing. The transmission factors developed from these data were found to follow the resistance equation published by Nikuradse[1] for turbulent flow in "rough" pipes with an average absolute roughness of 0.000,65 in. This average absolute roughness is believed to be representative generally of the flow strings of gas wells with the exception of those that have been exposed to corrosion or other conditions causing undue roughness. Also, use of an absolute roughness of 0.000,65 in. probably will result in transmission factors that are more representative of gas-well conditions than those in common use today, provided that the transmission factors are calculated by the methods outlined in this report. The authors believe that use of these transmission factors will permit calculation of more accurate subsurface pressures in gas wells than those in use today.

*Present address: Phillips Petroleum Co., Bartlesville, Okla.
**Present address: Carter Oil Co., St. Elmo, Ill.
Paper received in Petroleum Branch offices on Apr. 28, 1954.
[1]References are given at the end of the paper.

INTRODUCTION

Engineers use transmission factors in flow equations to compute subsurface pressures in flowing gas wells from measured wellhead pressures. These subsurface pressures are necessary for determining the productivity of gas wells from "back-pressure" tests. The methods of calculating pressures in flowing gas wells, as outlined by Rawlins and Schellhardt[2] in *Bureau of Mines Monograph 7*, are based on the transmission factors in the well-known Weymouth formula[3]. Natural gas engineers have realized that errors introduced by using transmission factors as given by the Weymouth formula are relatively unimportant in testing low-capacity gas wells; but they also know that such factors are important considerations in testing large-capacity wells. Accordingly, the research described in this report was undertaken to fulfill the need for more accurate means of calculating subsurface pressures in gas wells.

This report is part of the Bureau's study of the flow of natural gas through pipe and commercial pipelines. Several of the conclusions regarding flow in the flow strings of gas wells were influenced by the results of the study of flow in horizontal pipelines. These instances are mentioned in the text of this report.

METHODS OF COMPUTING TRANSMISSION FACTORS

Methods and procedures for computing transmission factors for turbulent flow in circular pipes from test data taken on gas wells have been derived and explained in detail in a paper by Smith[4]. As these methods were used to calculate the transmission factors presented in this report, a summary is included. Starting with

an energy balance over a differential length of pipe and defining the resistance coefficient, f, by the equation:

$$\text{frictional resistance} = dF = \frac{4fU^2dL}{2gD} \quad . \quad . \quad . \quad (1)$$

The following vertical-flow equation was derived by integration of the energy balance over the length of pipe considered:

$$144\int_{P_w}^{P_s} vdP = L_s + \frac{Q^2G^2(V_w^2 - V_s^2)}{2.551{,}5 \times 10^9 d^4} + \frac{fQ^2G^2}{53.157 \times 10^6 d^5}\int_0^L v^2 dL \quad . \quad . \quad . \quad . \quad . \quad . \quad (2)$$

The subscripts s and w refer to conditions at depth L and at the wellhead, respectively. Line integral signs were used because the values of specific volume required for the integration are a function of the temperature and compressibility as well as of the pressure and the relation between temperature and pressure is not specified by the terms of the integral.

As Equation (2) does not contain assumptions that define the path of the flow process of the fluid, it is considered general for the flow of fluids in wells.

The authors have found that Equation (2)* was particularly useful and reliable in evaluating the resistance coefficient, f, for gas wells. Pressures and temperatures must be measured in the flowing column of gas at enough depths in the well to permit accurate evaluation of the two integrals in Equation (2). As the flow mechanism in a well is essentially a weight-lifting process with frictional effects, the specific-gravity term G must convert the volume of gas into the weight of the total fluid lifted in the flow. Consequently, the specific-gravity term must be representative of the hydrocarbon liquid and gases produced during the flow. If the well produces water as a result of the condensation of water vapor that entered the well from the reservoir, a separate energy balance can be approximated for the water whereby the deficiency in energy supplied by the water toward lifting itself can be subtracted from the available energy of the gas. However, the effect of water condensed from vapor was found to be small, probably being less than the experimental errors in determining transmission factors for gas wells.

The application of Equation (2) to test data on gas wells measured with subsurface instruments requires a high degree of pressure and flow-rate stabilization of the reservoir surrounding the well. Measurement of pressures and temperatures at several depths in the well simultaneously is impossible with existing equipment and changes in pressures or flow rate before measurements at all depths have been completed will result in errors in the application of Equation (2) to flow test data.

To develop an equation similar to those commonly used in problems of flow in horizontal pipelines, Smith[4] integrated the energy balance equation for a finite length of pipe with an "effective" compressibility factor and an "effective" temperature to arrive at the following equation:

$$Q = 19{,}686\,\frac{(1)}{(ZT)}\sqrt{\frac{1}{f}}\sqrt{d^5\left(\frac{P_s^2 - e^s P_w^2}{e^s - 1}\right)} \quad . \quad (3)$$

Equation (3) is based on the assumptions that the temperature in a well is constant at an "effective" value, that the change in kinetic energy is negligible, and that the compressibility of the fluid in the well can be approximated by a constant "effective" value. The latter assumption is equivalent to assuming that the ideal-gas laws hold for the gas in a well but with a different value assigned to the gas constant in the ideal-gas equation. The accuracy of Equation (3) for determining transmission factors is limited because average effective compressibilities and temperatures must be estimated. However, subsurface pressure and temperature gages could not be run through the 1¼-in. tubing and against several of the higher flow rates in 2, 2½, and 3-in. tubing to provide data for Equation (2). In these instances, Equation (3) was used to compute transmission factors. Flow tests, when possible, were conducted to meet the requirements of Equation (2) because it will provide transmission factors of greater accuracy than Equation (3).

Exact methods of estimating the average effective compressibilities and temperatures for use in Equation (3) to describe adequately the behavior of a column of flowing gas are not known. However, reasonably accurate estimates of these factors can be made from prior knowledge of well behavior or the behavior of similar wells. Usually, the average effective temperature is an arithmetic average of the wellhead temperature and the subsurface temperature at the desired depth, providing temperature is a straight-line function of depth. Otherwise, an integrated average is used. The average effective compressibility is taken at the effective temperature and the estimated average pressure.

All transmission factors given in this report are based on pressure measurements between a depth of 50 ft and lower depths in the flow string. This was done to eliminate the effects of wellhead fittings on the resulting transmission factors.

REYNOLDS NUMBERS FOR FLOW IN GAS WELLS

The Reynolds number, a dimensionless ratio commonly used to characterize the conditions of fluid flow in circular pipes, is given in the literature as:

$$R = \frac{DUS}{\mu}$$

The above relationship has been expressed by Biddison[5] in natural gas engineering terms as:

$$R = 13.23 \times 10^{-6}\,\frac{QG}{\mu d} \quad . \quad . \quad . \quad . \quad (4)$$

The viscosity of the fluid in a flowing gas well varies from the bottom of the well to the top because of the change in viscosity with pressure and temperature. Consequently, the Reynolds number varies also, although in most flowing gas wells the variation is small. In this paper, all Reynolds numbers were computed by means of Equation (4) for the midpoint of the pipe under consideration to provide a standard basis for comparison. Values of the viscosities of the gases were taken from charts published by Bicher and Katz[6] and converted to the proper units for use in Equation (4).

*Equation (2) states that the available energy from the flow process equals the energy required to lift the fluid plus the energy involved in the kinetic energy change plus the energy required to overcome friction. The maximum observed energy involved in the kinetic change for all of the wells studied was 0.2 per cent of the total available energy. Consequently, the kinetic energy term in flow equations for gas wells can be neglected for all practical purposes.

EXPERIMENTAL PROCEDURE

After a well had been selected for testing, it was started producing at a flow rate high enough to cause a pressure drop along the flow string that would provide pressure data for accurate determinations of transmission factors. The lowest flow rates practicable for transmission-factor determinations varied from 2 MMcf/24 hours in 2-in. tubing to about 7 MMcf/24 hours in 7-in. casing. After the desired flow rate had been obtained, the rate of gas production was measured with an orifice meter and calculated for 20-minute intervals. The specific gravity of the produced gas was measured at each test flow rate. If the well produced hydrocarbon liquid and water, the rate of production was determined by measuring the accumulation of liquid in the separator over a particular time interval. Liquid water was measured by draining the water from the separator into a calibrated container at regular intervals of time depending upon the rate of water accumulation. Simultaneously with the rate measurements, the wellhead pressures, both tubinghead and casinghead, were measured by means of a piston gage at regular intervals of, usually, not longer than 20 minutes.

After both wellhead pressure measurements and rate determinations indicated that a satisfactory stable flow had been reached, pressures and temperatures at depths ranging from 50 ft below the wellhead to within 50 ft of the bottom of the flow string were measured with subsurface pressure and temperature gages. The flow rate against which the subsurface gages could be run was severely limited in tubing by two factors. First, the presence of the gages in the flow stream would decrease the flow rate to a slight degree depending principally upon the flow rate. Second, at the higher rates of flow, the gas stream would lift the gages in the tubing. After the subsurface pressures and temperatures were measured, the producing rate of the well was changed and the experimental procedure repeated.

Selection of Test Wells

Test wells were selected primarily to obtain transmission factors for flow strings in common use in gas wells. Although 1¼-in. tubing is not commonly used for flow strings in gas wells, this size tubing was included in the study because it is used to remove liquids from gas wells. Flow strings of casing alone, without tubing, are in general use in the Panhandle gas field of Texas.

Wells selected for testing in the study of transmission factors had to meet several important requirements regarding equipment, condition of the flow string, and the production of formation water. The required wellhead equipment included suitable connections for the measurement of pressures and, except in the case of the 1¼-in. tubing, "full opening" wellhead valves so that subsurface-pressure and temperature gages could be lowered into the well. Flow strings coated with drilling mud or mud from the producing formation would be unsuitable for the determination of transmission factors. A coating of mud or cement would not only decrease the pipe diameter but would also change materially the roughness of the internal surface. Flow strings that have been subjected to corrosion have roughness characteristics that are unusual and, for this reason, should not be included in a summary of transmission factors for normal gas wells.

The presence of liquid formation water in the flowing gas causes pressure losses other than that involved in the passage of the gas past the pipe surface. However, a certain amount of water is condensed from the water vapor contained in the reservoir gas (reservoir gas is in equilibrium with the connate water of the reservoir) as the gas flows up the flow string of a well, so the presence of some water in the flow string of a gas well cannot be avoided. No well was selected for test that produced salt water, as the liquid water complicates the determination of transmission factors.

Flow and Pressure Stabilization

Although transmission factors may be determined for the flow strings of wells that stabilize slowly, such tests are unduly time consuming. Equation (2) requires a constant value for the rate of flow in addition to constant wellhead and subsurface pressures. As subsurface pressures at successive depths in the well could not be measured simultaneously, a constant flow rate was required for the period of time necessary for the pressure measurements. However, the ideal conditions outlined above are seldom if ever attained in gas-well testing; as a result, the procedure followed was a compromise between ideal conditions and a degree of stabilization that could be reached in a reasonable time. When possible, the test well was maintained at the desired rate of production overnight before the transmission-factor data were taken. Normally, changes in flow rate during testing were small; after a major change in rate, the well under test was allowed to flow 12 to 16 hours. Usually the stabilization of a well was considered to be satisfactory when any change in wellhead pressure was within 0.1 to 0.3 psi in a 20-minute interval and at the same time there was no observable change in the flow rate, as indicated by the orifice meter.

Measurement of Subsurface Pressures and Temperatures

In measuring subsurface pressures and temperatures, a pressure gage and a temperature gage were run in the well as a unit. No pressure measurements were made without a corresponding temperature measurement. The gages were run first to a depth of 50 ft in the well and allowed to remain there until complete temperature equilibrium was reached. Then the gages were lowered to successive depths in the flow string. Pressures and temperatures were measured at eight depths in wells with about 3,000 ft of flow string and at 10 or 11 depths in wells with longer flow strings. The lowest depth at which measurements were taken was 50 to 100 ft above the highest opening in the flow string. At each "stop" or depth, the wellhead pressures (both tubing and casing) were measured to 0.1 psi with a calibrated piston gage.

The pressure and temperature deflections of the gages were recorded on polished-aluminum foil charts with Permopivot phonograph needles that made lines less than 0.001 in. in width. Deflections on the charts were measured to 0.001 in. and estimated to 0.000,1 in. with a comparator microscope and converted to corresponding pressures and temperatures by the methods published by Smith and Dewees[7] and Smith, Dewees, and Williams[8].

In addition to the techniques described above, the accuracy of the pressure gages in field usage was de-

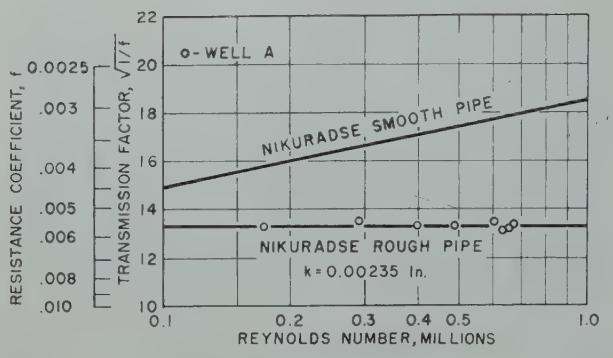

FIG. 1 — EXPERIMENTAL TRANSMISSION FACTORS DETERMINED FOR 1¼-IN. TUBING (ID—1.380 IN.); PANHANDLE FIELD, MOORE COUNTY, TEX.

termined after each series of transmission-factor determinations by shutting in the well and measuring pressures in the shut-in column of gas. These measured pressures were subsequently compared with pressures computed for the same depths by the method published by Rzasa and Katz[9]. In the dry-gas wells in the Panhandle field, Tex., where reservoir pressures varied from 270 to 380 psia, the difference between calculated and measured subsurface pressures averaged 0.25 psi for 19 determinations. The corresponding difference for wells in a Louisiana field averaged 1.3 psi for 10 determinations for pressures ranging from 1,500 to 1,600 psia. This comparison method of determining gage accuracy in these wells that produced appreciable quantities of hydrocarbon liquids gave differences that could be explained only by errors in the method of computing pressures.

Transmission factors reported for the 1¼-in. tubing and at several flow rates through the 2, 2½, and 3-in. tubing where it was impossible to run subsurface gages were computed with Equation (3), the integrated equation. In these cases, the subsurface pressures at the lower end of the tubing were calculated from wellhead pressure measurements on the static column of gas in the annular space between the tubing and casing by a modification of the method of Rzasa and Katz[9].

GAS MEASUREMENT

The rate of gas production was measured with standard orifice meters and computed to a pressure base of 14.4 psia and 60° F in accordance with *Gas Measurement Committee Report No. 2,* issued by the American Gas Association, with a correction of volume for the compressibility of the gas at meter conditions. The static element of the orifice meter was calibrated with a piston gage, and the differential element was compared with a water manometer at several differential pressures over the range of the orifice meter. Calibration corrections were applied to the static and differential pressures in the flow computations. Orifice-meter readings and observations of the temperature of the gas flowing through the meter were taken at 20-minute intervals after stabilization of well pressures, and the resulting flow rates were averaged for calculating transmission factors. The specific gravity of the gas was measured with a gas-gravity balance several times during each test period.

RESULTS OF TESTS TO DETERMINE TRANSMISSION FACTORS

Tests to determine transmission factors for the flow of natural gas in circular flow strings in wells were completed for 1¼, 2, 2½, and 3-in. tubing and 5½ and 7-in. casing. The resulting transmission factors, with corresponding Reynolds numbers are illustrated in Figs. 1 to 6, inclusive. In addition, the Nikuradse[10] resistance equation for turbulent flow in smooth pipes is shown by a diagonal line in each figure. This equation is:

$$\sqrt{1/f} = 4 \log R\sqrt{f} - 0.4 \quad . \quad . \quad . \quad . \quad . \quad (5)$$

Although Equation (5) appears to be a straight line on the semilogarithmic coordinates of Figs. 1 to 7, the line actually is slightly curved. The Nikuradse smooth-pipe curve, Equation (5), is shown on the illustrations, because many investigators in the field of fluid mechanics believe that the Nikuradse resistance equation for flow in smooth pipes represents the highest value of the transmission factor at a given Reynolds number for any type of pipe surface. The line at a constant value of the transmission factor drawn through the developed data points represents the Nikuradse resistance equation[1] for turbulent flow in *rough pipes,* which is

$$\sqrt{1/f} = 4 \log \left(\frac{7.4r}{k} \right) . \quad . \quad . \quad . \quad . \quad . \quad (6)$$

The relative roughness used to determine the position of the line was the average of the absolute roughness value for each datum point divided by the pipe radius and was calculated by Equation (6). In Nikuradse's experimental work the absolute roughness was considered to be the diameter of the uniform sand grains glued to the test-pipe interior. By using various sizes of uniform sand, Nikuradse measured transmission factors for a 30-fold variation in the ratio of sand-grain diameter to pipe radius. These experiments enabled Nikuradse to arrive at Equation (6) for turbulent flow in rough pipe. Equation (6) is significant in that it does not contain the Reynolds number, which means that the fluid viscosity has no influence on the flow or the transmission factor.

TRANSMISSION FACTORS FOR 1¼-IN. TUBING

The transmission factors illustrated in Fig. 1 were determined for a string of 1¼-in. tubing (2.4 lb/ft, EUE) that had been installed in a gas well in the Panhandle field in Moore County, Tex. As mentioned previously, although 1¼-in. tubing is seldom used as a flow string in gas wells, these transmission factors are included in this report because 1¼-in. tubing is used widely as "siphon strings" to remove water from gas wells. However, this particular well did not produce water, and the tubing had not been used for gas or water production. This circumstance may have resulted in an abnormal pipe-surface condition with the resultant unusually high absolute roughness measurement for the tubing shown in Table 1.

As illustrated in Fig. 1, the transmission factors were relatively constant and independent of Reynolds number over the entire range of data from 173,000 to 671,000 and can be represented closely by the Nikuradse equation for flow in rough pipe with an average relative roughness of 0.003,40. The corresponding aver-

TABLE 1 — SUMMARY OF RELATIVE AND ABSOLUTE ROUGHNESS VALUES FOR GAS-WELL FLOW STRINGS COMPUTED BY THE NIKURADSE ROUGH-PIPE EQUATION

Pipe size, in.	Internal diameter, in.	Wells included	Relative roughness, k/r	Absolute roughness, k, in.
1¼-in. tubing	1.380	A	0.003,40	0.002,35*
2-in. tubing	1.995	B, C	.000,534	.000,532
2½-in. tubing	2.441	D, E, F	.000,530	.000,647
3-in. tubing	2.992	G, H	.000,565	.000,846
3-in. tubing	2.992	I	.006,12	.009,15*
5½-in. casing	5.012	J, K, L	.000,292	.000,732
7-in. casing	6.336	M	.000,103	.000,325
7-in. casing	6.398	N	.000,260	.000,831

*Excluded from average. Average = 0.000,65 in.

age absolute roughness is 0.002,35 in. The relatively small diameter of the 1¼-in. tubing prevented the measurement of pressures and temperatures in the tubing with subsurface gages. Consequently, data were taken and calculated by the methods explained in the discussion of Equation (3).

Transmission Factors for 2-in. Tubing

The transmission factors determined for the 2-in. tubing (4.7 lb/ft, EUE) of two gas wells in Leon County, Tex., are illustrated in Fig. 2. These wells produced hydrocarbon liquid that varied from 1.4 to 6.8 bbl/MMcf of separator gas. Usually, the higher hydrocarbon liquid-gas ratios were observed at the lower flow rates. These wells produced, with the hydrocarbon liquid, relatively small quantities of fresh water which probably entered the wellbore in the vapor state. Neither the past history of the wells nor inspection of well equipment at the time of testing gave any indication that the well equipment had been subject to corrosion.

The transmission factors for 2-in. tubing, illustrated in Fig. 2, were constant and independent of Reynolds number or fluid viscosity over the experimental range of Reynolds numbers from 0.567 to 4.48 million. The straight line through these transmission factors is the Nikuradse rough-pipe equation for a relative roughness of 0.000,534 or an absolute roughness of 0.000,532 in. The accuracy of the data as indicated by the spread of points about the line is probably within the range of experimental error. The first two points for each well in Fig. 2 are the averages of data developed from five successive measurements of pressures with subsurface gages at depths of 300-ft intervals. (Actual depths were 4,000, 4,700, 5,000, 5,300, and 5,600 ft). The first two transmission factors for each well were calculated by Equation (2), the line-integral method. The remaining data were calculated by means of Equation (3) from surface measurement of pressures. The measurement of pressures and temperatures in 2-in. tubing with subsurface gages at flow rates greater than 3.5 MMcf/24 hours was considered to be unsafe, as determined from previous experience.

Transmission Factors for 2½-in. Tubing

The transmission factors determined for the 2½-in. tubing (6.50 lb/ft, EUE) of three gas wells are given in Fig. 3. Wells D and E were in Bossier Parish, La., and Well F was in Caddo County, Okla. Wells D and E produced small quantities of fresh water and hydrocarbon liquid that varied from 1.2 to 3.1 bbl/MMcf of separator gas depending upon the test rate. Before the tests, the operator exposed metal coupons in the flow stream of these wells for 18 to 34 days and concluded that corrosive conditions were absent in one well and "slight" in the other. Well F produced gas with only traces of water and hydrocarbon liquid, and the well equipment was thought to be free from the effects of corrosion.

The transmission factors illustrated for 2½-in. tubing in Fig. 3 were constant within the range of experimental error and were independent of the Reynolds number. At Reynolds numbers of 0.824 and 0.832 million, two data points were about 0.8 and 1.8 units, respectively, lower than the average line through the transmission factors. The relative and absolute roughness values for the two points were excluded from the average for all the data. At these lower Reynolds numbers, the pressure loss due to friction in the 2½-in. tubing was low compared to the accuracy of the subsurface-pressure gage causing the probable error in transmission factors to be high at the lower Reynolds numbers. Consequently, the low values of the transmission factors at Reynolds numbers of 0.824 and 0.832 million are believed to be caused by errors in pressure measurement and do not indicate a trend in the data. The average relative roughness was 0.000,530, and the average absolute roughness was 0.000,647 in. for the 2½-in. tubing in the three wells. Transmission factors for Well F were calculated from surface measurement of pressures by Equation (3).

Transmission Factors for 3-in. Tubing

Transmission factors were calculated for the flow of gas through 3-in. tubing (9.30 lb/ft, EUE) from test data taken on three gas wells in Jackson County, Tex., and are illustrated in Fig. 4. These wells produced small quantities of fresh water and hydrocarbon liquid with ratios that varied from 0.4 to 1.5 bbl/MMcf of separator gas, depending upon the flow rate.

The transmission factors for the 3-in. tubing fall into two groups, as shown on Fig. 4. Data for Wells G and H are in reasonable agreement and have an average relative roughness of 0.000,565 and an average absolute roughness of 0.000,846 in. as calculated by the Nikuradse equation for flow in rough pipes. The low value of the transmission factor for a Reynolds number of 1.28 million was caused probably by errors in pressure measurement. This point was excluded from the average roughness values. Transmission factors for Well I are much lower in value than those for Wells G and H. As this difference was consistent and beyond the probable range of experimental errors, a separate set of roughness values was calculated by the Nikuradse equation for flow in rough pipes. The average relative roughness for Well I was 0.006,12 and the average absolute roughness 0.009,15 in.

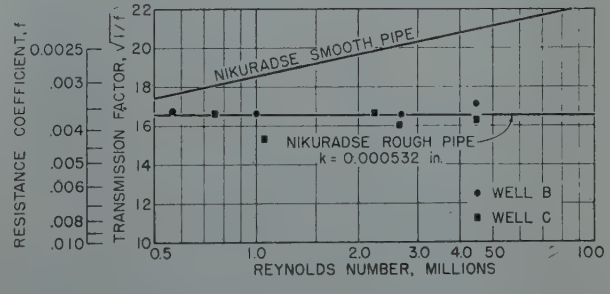

FIG. 2 — EXPERIMENTAL TRANSMISSION FACTORS DETERMINED FOR 2-IN. TUBING (ID—1.995 IN.); LEON COUNTY, TEX.

As the roughness values for the tubing in Well I were in the order of 10 times the magnitude of those for Wells G and H, the operator ran a tubular caliper survey of the tubing in Well I and found that the tubing surface was rougher than usual and that the pits had depths from 8 to 14 per cent of the wall thickness in places. These independent measurements of roughness with a tubular caliper confirm qualitatively the conclusions drawn from the flow tests that the tubing of Well I had an absolute roughness greater than that of Wells G and H.

Transmission Factors for 5½-in. Casing

Flow tests were conducted on three wells with 5½-in. casing (14.0 lb/ft, plain end) to determine the transmission factors shown in Fig. 5. All of these wells were in the Panhandle field in Hartley County, Tex. Although these wells were not equipped with separators, it was believed they produced gas that was relatively free of water and liquid hydrocarbons.

The transmission factors for the 5½-in. casing, as illustrated in Fig. 5, show a trend that differs slightly from that for the various sizes of tubing discussed previously or for the 7-in. casing discussed in the following section. While no definite reason can be assigned for the change, water movement up the flow string may have caused this trend. From experience with tests on short lengths of horizontal pipes, similar trends were observed when water accumulated on the pipe surface.

Relative roughness and absolute roughness values were computed from the transmission factors. Roughness values for five of the 13 transmission factors were excluded in computing the average relative roughness of 0.000,292 and the average absolute roughness of 0.000,732 in. as calculated by the Nikuradse equation for flow in rough pipes. The Nikuradse rough-pipe equation for 5½-in. casing with an absolute roughness of 0.000,732 in. is illustrated in Fig. 5, where the line passes through the experimental data but is not especially indicative of the apparent trend of the data.

Transmission Factors for 7-in. Casing

The transmission factors determined from experimental data on a well with 7-in. casing (24 lb/ft, plain end) and a well with 7-in. casing (22 lb/ft, plain end) are illustrated in Fig. 6. Well M was in Moore County and Well N in Hartley County in the Panhandle field, Tex. Neither well was equipped with a separator, but both wells were believed to produce gas relatively free of water and liquid hydrocarbons.

The average relative roughness and average absolute roughness for Well M were 0.000,103 and 0.000,325 in., respectively, and the values for Well N were 0.000,260 and 0.000,831 in., respectively. Because of this approximately 2.5-fold spread in values, equations of the Nikuradse type for flow in rough pipe with different relative roughness values for both sets of values are shown in Fig. 6. With regard to Well M (Fig. 6), values for two points at the lower Reynolds numbers were excluded from the average absolute roughness of 0.000,325 in. for the well. Except for these two points, the data are in reasonable agreement with the rough-pipe equation, as shown on Fig. 6. The data for Well N, as illustrated in Fig. 6, indicate that the rough-pipe equation for an absolute roughness of 0.000,831 in.

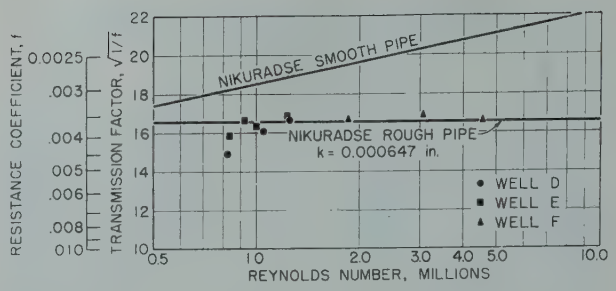

FIG. 3 — EXPERIMENTAL TRANSMISSION FACTORS DETERMINED FOR 2½-IN. TUBING (ID—2.441 IN.); WELLS D AND E, BOSSIER PARISH, LA.; WELL F, CADDO COUNTY, OKLA.

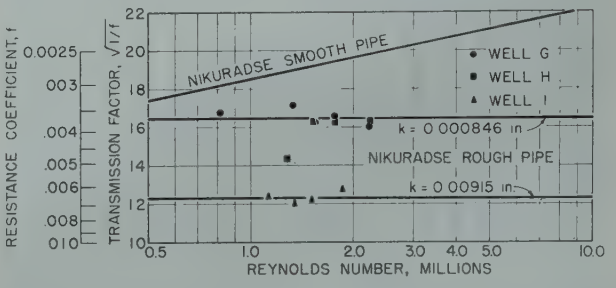

FIG. 4 — EXPERIMENTAL TRANSMISSION FACTORS DETERMINED FOR 3-IN. TUBING (ID—2.992 IN.); JACKSON COUNTY, TEX.

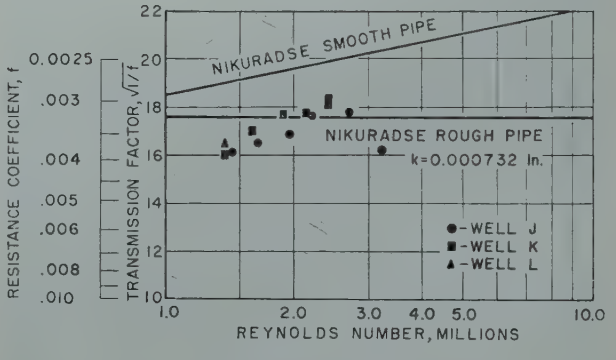

FIG. 5 — EXPERIMENTAL TRANSMISSION FACTORS DETERMINED FOR 5½-IN. CASING (ID—5.012 IN.); PANHANDLE FIELD, HARTLEY COUNTY, TEX.

represents the experimental points within the accuracy of the experimental methods, except for the point at the lowest Reynolds number, which was excluded from the average roughness value.

CORRELATION OF RESULTS

Several means of correlating the results of the study of transmission factors for the flow strings in gas wells were tried, and the conclusion was reached that the Nikuradse equations for flow in smooth pipe and for flow in rough pipe provided one of the best and least complicated methods of correlation. One of the trial methods for correlation was based on the Colebrook[11] equation, which relates the transmission factor to Reynolds number and relative roughness of the pipe sur-

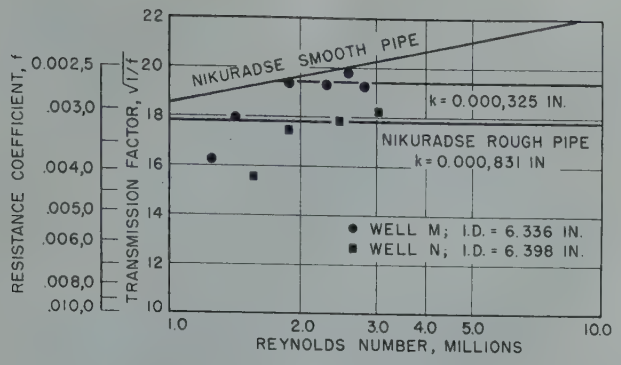

FIG. 6 — EXPERIMENTAL TRANSMISSION FACTORS DETERMINED FOR 7-IN. CASING; PANHANDLE FIELD, HARTLEY AND MOORE COUNTIES, TEX.

face. Colebrook's equation, in units consistent with the foregoing equations, is:

$$\sqrt{1/f} = -4 \log\left(\frac{k}{7.4r} + \frac{1.255}{R}\sqrt{1/f}\right) \quad . \quad . \quad (7)$$

At the lower Reynolds numbers, the Colebrook equation for a given relative roughness is asymptotic to the Nikuradse smooth-pipe equation; and, at the higher Reynolds numbers, it is asymptotic to the rough-pipe equation. In between the two extremes of Reynolds numbers—the transition region—the Colebrook equation forms a smooth curve. None of the data presented in Figs. 1 to 6, inclusive, show a transition region of the type indicated by the Colebrook equation. In addition, experiments conducted by the Bureau of Mines on short lengths of horizontal commercial pipe do not confirm the Colebrook transition relationship. For these reasons, the Nikuradse equations were used for correlating the transmission factors for the flow strings of gas wells. However, the data presented in this report were not taken with the degree of experimental accuracy necessary to justify a rejection of the Colebrook relationship.

A summary of the relative roughness and absolute roughness values as calculated with the Nikuradse equation for flow in rough pipes (Equation 6) is given in Table 1. The relative roughness values vary from a maximum of 0.006,12 for the 3-in. tubing in Well I to 0.000,103 for the 7-in. casing in Well M. Obviously, the relative roughness values for the flow strings of Wells A and I are high, as they are in the order of 6 to 11 fold greater than the next highest value observed (for Wells G and H). If the relative roughness values for Wells A and I are excluded, the values vary from 0.000,103 to 0.000,565—a 5.5-fold variation. These considerations lead to the conclusion that the relative roughness is not constant for the various flow strings.

If the absolute roughness, as shown in the last column of Table 1, is considered and the values for Wells A and I are excluded, the variation in absolute roughness is from 0.000,325 to 0.000,846 in.—a 2.6-fold variation. If the apparently low absolute roughness for Well M is neglected temporarily, the spread is then from 0.000,532 to 0.000,846 in.—a 1.6-fold variation. The relatively small variation in absolute roughness as compared to the variation in relative roughness permits the calculation of an average value of 0.000,65 in., which includes the value for Well M but not the values for Wells A and I.

The average absolute roughness of 0.000,65 in. for the flow strings of gas wells can be used to calculate transmission factors for all sizes of flow strings in gas wells, as is illustrated in Fig. 7, where transmission factor and Reynolds number are the coordinates. The horizontal lines numbered 1 to 5 represent the Nikuradse rough-pipe equation with an absolute roughness of 0.000,65 in. for 2, 2½, and 3-in. tubing and 5½-in. 14 lb/ft and 7-in. 24 lb/ft casing, respectively. These lines representing a constant transmission factor independent of Reynolds number are extended to the lower Reynolds numbers until they meet the line representing the Nikuradse equation for turbulent flow in smooth pipes. Transmission factors for Reynolds numbers less than that at the intersection of the curves for the rough-pipe and the smooth-pipe equations are taken from the smooth-pipe curve at the proper Reynolds number. For example, line 2, representing transmission factors for 2½-in. tubing, meets the smooth-pipe curve at a Reynolds number of 290,000. The transmission factor for 2½-in. tubing at Reynolds numbers above 290,000 is constant at 16.57. Below a Reynolds number of 290,000 the transmission factor is assumed to vary with Reynolds number and should be taken from the Nikuradse curve for flow in smooth pipe—at a Reynolds number of 200,000 the transmission factor for 2½-in. tubing would be 15.98.

The procedure outlined above for estimating transmission factors for the flow strings of gas wells obviously ignores the transition region between smooth turbulent flow and rough turbulent flow that undoubtedly exists for commercial pipe. The transition region occurs at relatively low flow rates for the flow strings of gas wells, so very little error would be introduced in the calculation of pressures at depths below the surface in gas wells. However, it must be stressed that the reported average absolute roughness of 0.000,65 in. does not apply equally to all flow strings in gas wells, but the authors believe that this absolute roughness value will give transmission factors that are more representative of gas-well conditions than those in common use today.

The average absolute roughness of 0.000,65 in. proposed for gas wells in this report agrees very well with an average value of 0.000,6 in. reported by Cullender and Binckley[12]. They calculated their absolute rough-

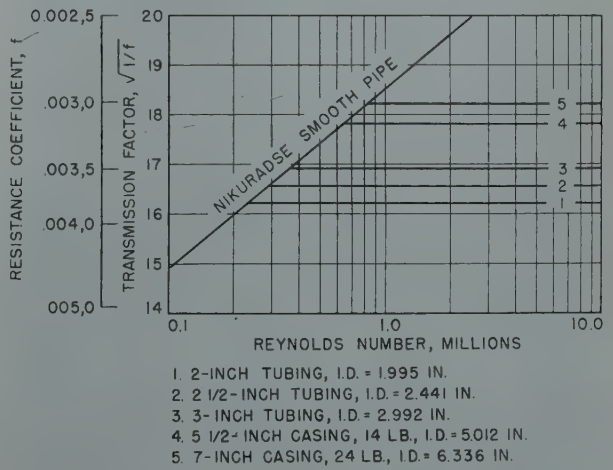

FIG. 7 — TRANSMISSION FACTORS FOR CIRCULAR FLOW STRINGS COMPUTED WITH THE NIKURADSE ROUGH-PIPE EQUATION; ABSOLUTE ROUGHNESS = 0.000,65 IN

ness by the Colebrook equation from published data on horizontal pipelines and experimental data obtained on 13 gas wells in the Panhandle and Hugoton fields. Although absolute roughness values computed with the Nikuradse equation for flow in rough pipe are slightly greater than corresponding values computed by the Colebrook equation, the results reported herein and those of Cullender and Binckley are in close agreement.

SUMMARY

A study of the experimental data taken on flow tests conducted on 14 gas wells in Oklahoma, Texas, and Louisiana shows that the transmission factors for the flow strings of these gas wells may be correlated by means of the Nikuradse[10] Equation (5) for turbulent flow of fluids in smooth pipe and the Nikuradse[1] Equation (6) for turbulent flow in rough pipes. Most of the transmission factors presented in this report can be represented by the Nikuradse equation for flow in rough pipe, using a relative roughness which varies with the size of the pipe. However, the absolute roughness as calculated from the relative roughness was found to be fairly constant at an average value of 0.000,65 in. for 12 of the 14 wells tested.

The average value of 0.000,65 in. for the absolute roughness may be used with the Nikuradse Equation (6) for the flow of fluids in commercial pipe to calculate transmission factors for the flow strings of gas wells providing the proper Reynolds number restrictions are observed. The Nikuradse resistance equation for flow in rough pipe for the average absolute roughness of 0.000,65 in. and a given pipe radius will meet the Nikuradse equation for flow in smooth pipe at a certain Reynolds number. For flow at Reynolds numbers less than the Reynolds number at the intersection, the pipe may be considered "smooth," and the transmission factor is determined by the Reynolds number and the smooth-pipe equation. For flow at Reynolds numbers greater than the Reynolds number at the intersection, the relative roughness of the pipe may be considered to be the only variable influencing the transmission factor; therefore, the transmission factor may be calculated from the pipe radius, the average absolute roughness of 0.000,65 in. and the equation for flow in rough pipes.

Transmission factors calculated by the methods outlined in this report are believed to be representative of the flow strings of gas wells and may be used in calculating subsurface pressures in flowing gas wells from measured wellhead pressures.

ACKNOWLEDGMENTS

The study by the Bureau of Mines of the productivity of gas wells is being carried on in cooperation with the American Gas Association. The assistance given by E. L. Rawlins, chairman, Gas-Well Deliveries Subcommittee of the Operating Section, American Gas Association, is gratefully acknowledged.

The authors express their appreciation to the managements of Lone Star Producing Co., Magnolia Petroleum Co., Phillips Petroleum Co., and Union Producing Co. for permission to conduct tests on their wells and to their respective field personnel for making arrangements for the tests.

The authors acknowledge the assistance and suggestions offered in the preparation of this paper by: C. W. Binckley of Phillips Petroleum Co., and J. W. Ferguson of Continental Oil Co.; and C. J. Wilhelm, C. K. Eilerts, R. V. Higgins, and E. M. Tignor of the Bureau of Mines.

SYMBOLS USED IN EQUATIONS

D = internal diameter of pipe, feet
d = internal diameter of pipe, inches
e = natural logarithm base = 2.718,28+
f = resistance coefficient, dimensionless
$\sqrt{\frac{1}{f}}$ = transmission factor, dimensionless
G = specific gravity of fluid, air = 1.0
g = acceleration of gravity (conversion factor)
k = absolute roughness, inches (height from peak to valley of a hypothetical uniform roughness profile)
$\frac{k}{r}$ = relative roughness, ratio
L = depth of flowing column of fluid, feet
L_s = energy required to lift 1 lb of the fluid from a depth L in the well, foot-pound (as 1 lb of fluid is under consideration L_s is numerically equal to L)
P = pressure, psia
P_s = subsurface pressure at depth L in the well, psia
P_w = wellhead pressure, psia
Q = volume rate of flow, cubic feet per 24 hours (pressure base = 14.4 psia and temperature base = 60° F)
R = Reynolds number, dimensionless
r = radius of pipe, inches
S = density of fluid, pounds per cubic foot
s = exponent of e in Equation (3) = $0.037,504 \frac{GL}{TZ}$
T = effective temperature, °F absolute
U = average linear velocity, feet per second
v = specific volume, cubic feet per pound
Z = effective compressibility of gas, dimensionless
μ = viscosity of fluid, pounds per second foot
log is to base 10

REFERENCES

1. Nikuradse, J.: Stromungsgesetze in Rauhen Rohren. V.D.I. Forschungsheft No. 361 (August 1933). Translation, *Pet. Eng.*, **11** (March, May, June, July, August, 1940).
2. Rawlins, E. L., and Schellhardt, M. A.: *Bureau of Mines Monograph 7* (1936).
3. Weymouth, T. R.: *Trans. ASME*, **34** (1913), 185.
4. Smith, R. V.: *Trans., AIME*, **189** (1950), 73.
5. Biddison, P. M.: American Gas Association, Proceedings, Nat. Gas Section (1941), 51.
6. Bicher, L. B., and Katz, D. L.: *J. Pet. Tech., 6* (July 1943).
7. Smith, R. V., and Dewees, E. J.: *Oil and Gas Jour.*, **47** (Dec. 9, 1948), 85.
8. Smith, R. V., Dewees, E. J., and Williams, R. H.: *Pet. Eng.*, Drilling and Producing Edition, **23** (Jan. 1951), B7-12.
9. Rzasa, M. J., and Katz, D. L.: *Pet. Eng.*, Reference Annual, **16** (1945), 148.
10. Nikuradse, J.: V.D.I. Forschungsheft No. 356 (October, 1932).
11. Colebrook, C. F.: *J. Inst. Civil Engr.* (London), **11** (1938-1939), 133.
12. Cullender, M. H., and Binckley, C. W.: Exhibit presented to the Railroad Commission of Texas, Hearing of Nov. 9, 1950, Amarillo, Tex. ★★★

THE PUMPABILITY of CLAY-WATER DRILLING FLUIDS

I. HAVENAAR | KONINKLIJKE/SHELL LABORATORIUM AMSTERDAM, THE HAGUE

T. P. 3930

ABSTRACT

Various methods have been proposed in the literature to calculate the pressure losses in drill-pipe and bit-nozzles, i.e., those parts of the mud-circuit where the largest pressure-losses occur. Very few data, however, are available to check the validity of these proposals.

Presented in this paper are the results of pumping experiments with clay-water drilling fluids of different specific gravities and different laminar flow-properties (differential viscosity and Bingham yield value), using pipes of different diameters. In addition, a series of measurements on bit-nozzles is discussed.

Two main conclusions may be drawn from this work for the flow through pipes.

1. In the laminar flow region pressure losses can be calculated from the differential viscosity and Bingham yield value of the mud.

2. In the turbulent flow region pressure losses can be calculated with good approximation from a viscosity term which is determined by the volume fraction of the dispersed phase. Calculations making use of laminar flow properties may lead to erroneous results. The effect of temperature on the pressure losses in the case of turbulent flow can be calculated from the change in viscosity of the dispersing medium, i.e., water.

The main conclusions determined for the flow through bit-nozzles are that for flow conditions prevailing in the field, the pressure-drops in bit-nozzles are independent of the laminar flow properties of the mud. They are solely determined by the density of the mud and the geometry of the nozzle.

Manuscript received in Petroleum Branch offices on July 8, 1954. Paper presented at Petroleum Branch Fall Meeting in San Antonio Oct. 17-20, 1954.

[1]References given at end of paper.

INTRODUCTION

The last decades have witnessed a steady increase in the depth of oil wells. This is illustrated by the increase in the drilling depth record in the USA from 8,046 ft in 1927 to 21,482 ft in 1953. This increasing depth, together with the experience that high rates of mud circulation and high fluid velocities in the bit-nozzles enhance the rate of drilling, has emphasized the importance of selecting suitable mud-pumps when starting the drilling of a deep borehole.

For such a selection it is necessary to be able to calculate the pumping pressures necessary to obtain the required circulation rates. The main part of the pressure-losses in the mud circuit occur in the drill pipe and the bit-nozzles. Various methods have been proposed in the literature to calculate the pressure-losses in the drill pipe[1,2,3,4]. These methods do not all lead to the same results, and at the time this investigation was started insufficient basic data were available to check their validity. Moreover, to our knowledge, no data are available at all on the effect, if any, of the flow-properties of the mud on the pressure-losses in bit-nozzles.

The work described in this paper was carried out to collect basic data on the subject. It is to be considered as a continuation of Van Olphen's work in this field[5,6].

FLOW BEHAVIOR OF MUDS

Various authors[5,7,8] have shown that clay water-muds approximately behave as Bingham fluids; the main part of the curve relating the rate of shear D to the shearing stress τ can be represented by the formula $\tau - \tau_B = nD$.

Laminar Flow in Pipes

For laminar flow of a Newtonian fluid through a pipe, the Poiseuille equation is valid:

$$Q = \frac{\pi R^4}{8\eta l} P \quad . \quad . \quad . \quad . \quad . \quad . \quad . \quad . \quad . \quad . \quad (1)$$

The corresponding formula for a Bingham fluid is the Bingham-Buckingham equation:

$$Q = \frac{\pi R^4}{8nl} \left\{ P - \frac{4}{3} p_o \left(1 - \frac{p_o^3}{4P^3}\right) \right\} \quad . \quad (2)$$

$$\text{where } p_o = \frac{2l\tau_B}{R} \quad . \quad . \quad . \quad . \quad . \quad . \quad . \quad . \quad . \quad . \quad (3)$$

The flow is characterized by the presence of a plug in the center of the pipe. When P becomes large as compared with p_o (which is normally the case), Equation (2) becomes:

$$Q = \frac{\pi R^4}{8nl} \left\{ P - \frac{4}{3} p_o \right\} . \quad . \quad . \quad . \quad . \quad (4)$$

When comparing Equation (4) with Equation (1) it may be seen that the viscosity η in Equation (1) has been replaced by the term:

$$n + \frac{\pi R^3 \tau_B}{3Q} = n + \frac{R}{3V} \tau_B$$

which term is called the apparent viscosity (η_a).

The Onset of Turbulence

For Newtonian fluids, flow becomes turbulent when

$$Re\text{-number} = \frac{2RV\rho}{\eta} = 2000\text{-}3000.$$

According to Binder and Busher[9] the flow of Bingham fluids becomes turbulent when

$$\frac{2RV\rho}{\eta_a} = \frac{2RV\rho}{n + \frac{R}{3V} \tau_B} = 2000\text{-}3000$$

McMillen[10] introduces a Re-number in which R is replaced by δ, the distance from the wall. Instead of η he uses the apparent viscosity corresponding with the rate of shear prevailing at this distance δ. When this Re-number exceeds the value 2,000 to 3,000 at any point of the tube, flow becomes turbulent at that point. According to this theory turbulence begins somewhere between the wall and the plug.

Hedstrom[11] assumes that laminar flow begins when the calculated laminar flow-curve crosses the calculated turbulent flow-curve. The latter curve is computed with Equation (5) assuming that the turbulent viscosity is equal to the differential viscosity. For the calculation of the critical rate of flow he uses two dimensionless quantities *viz.* $Re = \frac{2RV\rho}{n}$ and $S = \frac{2R\tau_B}{nV}$.

It is shown that the critical Re-number depends on the value of S. A graph is given in Hedstrom's paper from which Re_{cr} may be derived when S is known.

Turbulent Flow

When flow is turbulent, the relation between pressure and volume rate of flow in circular pipes reads for Newtonian fluids:

$$P = f \frac{l\rho Q^2}{\pi^2 R^5} \quad . \quad . \quad . \quad . \quad . \quad . \quad . \quad . \quad . \quad (5)$$

In this formula f is a dimensionless quantity, called the friction-factor, which is a function of Re-number and roughness of the pipe.

It is generally agreed that Equation (5) should also be used for the calculation of pressure-losses in the case of Bingham-fluids. Of importance is the question which viscosity-value should be substituted in the Re-number, in order to find the right value for f.

The opinions as to which value should be taken for this turbulent viscosity (η_t) are widely divergent. According to Caldwell and Babbitt,[5] η_t is equal to the viscosity of the dispersing medium. The pressure drop calculations given by Koch[4] are based on this assumption.

In a pamphlet issued by Hughes Tool Co.[2] graphs are given which are based on the assumption that drilling-muds have a turbulent viscosity of 3 cp. Dunn, Nuss and Beck[3] are of the opinion that the relation $\eta_t = 1/3.2n$ holds true. Hedstrom[11] found indications that $\eta_t = n$, whereas Van Olphen[6] found $\eta_t = 1.5\, n$.

Pressure-Losses in Bit-Nozzles

In the case of Newtonian fluids the pressure-drop, when forcing a fluid through a stricture, is given by:

$$\triangle P = \frac{\rho Q^2 (1 - \beta^4)}{2C^2 A^2} \quad . \quad . \quad . \quad . \quad . \quad . \quad . \quad (6)$$

To our knowledge, no data exist on the influence of the Bingham yield value and differential viscosity on the value of C (coefficient of discharge). Usually C is considered to be independent of the fluid properties and is given a constant value.

Summarizing the above, there seems to exist no unanimity for Bingham fluids as regards: (a) criteria for the onset of turbulent flow; (b) the magnitude of the turbulent viscosity, and (c) the influence of the flow-properties on the pressure-losses in bit-nozzles. The experiments described in this paper were intended to shed more light on these points.

EXPERIMENTAL PROCEDURE

Flow Experiments on Pipes and Nozzles

The muds were pumped through pipes of 8 m length and of different diameter (1, 2 or 3 cm) by means of a small mud-pump (maximum capacity 100 gal./min).

Experiments on smaller pipes (diameter of 0.6 and 0.8 cm and a length of 1 m) were carried out with the aid of a 10 gal pressure vessel to which the various pipes could be attached. By means of compressed air the mud was forced through the pipes.

The pressure drops in the pipes were measured with either a mercury or a Bourdon type manometer at a sufficient distance from beginning and end of the tubes to avoid the influence of end effects.

In the experiments on nozzles the mud was pumped through a nozzle of 0.4 cm diameter by means of the above mud-pump. Recovery of kinetic energy of the fluid was avoided by placing a wide vessel behind the nozzle, in which the kinetic energy was transformed into heat.

Measurement of Differential Viscosity and Bingham Yield Value

For the determination of these flow-properties use was made of two rotational viscometers, which both had a small clearance between cup and rotor, the Stormer viscometer as modified by Van Olphen [5], and a motor-driven viscometer *. An important advantage of the latter is that the pre-treatment of the mud can be continued until no further structural break-down of the mud occurs.

SURVEY OF EXPERIMENTS

A first series of tests covered the whole flow-curve viz. laminar flow, the onset of turbulence and turbulent flow.

It comprised the following experiments:

(a) Clay water muds with a density of 1.31 gm/cm³ (10.9 lb/gal.) and different rheological properties were pumped through a pipe of 2 cm diameter.

(b) Muds with a density of 1.69 gm/cm³ (14.1 lb/gal.) and different rheological properties were pumped through pipes of 1 and 2 cm diameter. These muds are prepared from the former muds by loading with barytes.

The rheological properties were varied by adding flocculating or peptising agents (e.g. NaCl, quadraphos).

A second series of experiments more especially dealt with the turbulent part of the flow-curve:

(a) Experiments with two bentonite muds loaded with barytes with densities of 1.26 gm/cm³ (10.5 lb/gal.) and 1.55 gm/cm³ (12.9 lb/gal.) in which the influence of temperature on the turbulent visocity η_t was investigated.

(b) Experiments with clay-water muds of different densities, viz. from 1.10 gm/cm³ (9.2 lb/gal.) to 1.40 gm/cm³ (11.7 lb/gal.), in which the influence of the rate of flow and pipe diameter on η_t was studied. These experiments further served the purpose of investigating the relation, if any, between the differential viscosity and η_t and between the volume fraction of dispersed phase and η_t.

(c) Experiments with muds containing 6 per cent bentonite, loaded with barytes with densities from 1.15 gm/cm³ (9.6 lb/gal.) to 1.75 gm/cm³ (14.6 lb/gal.).

(d) Finally, the η_t-values of some field muds were determined, viz.: a clay-water mud with a density of 1.17 gm/cm³ (9.8 lb/gal.), treated with flocgel (a modified starch); a saturated salt water mud with a density of 1.37 gm/cm³ (11.4 lb/gal.), also treated with flocgel, and a red mud with a density of 1.30 gm/cm³ (10.9 lb/gal.).

A third series of experiments dealt with the pressure drops in bit-nozzles. The muds from the first series were also used here.

In all cases the *f-Re* relations, valid for the various pipes, and the *C-Re* relations for the nozzles were determined with the aid of water. These measurements were repeated regularly during the above experiments in order to trace possible changes in these relations.

DISCUSSION OF RESULTS

Experiments Covering the Whole Flow-Curve

By way of example the results obtained with the muds having a density of 1.31 gm/cm³, pumped through a pipe of 2 cm diameter are presented in Fig. 1.

The Laminar Flow Region

If the two rotational viscometers provide the right values for the differential viscosity and the Bingham yield value of the mud, the pressure losses calculated by means of the Bingham-Buckingham Equation (2) should correspond with those actually observed.

*Developed by H. C. Darley: Shell Development Co.'s Exploration and Production Research Div., Houston, Tex.

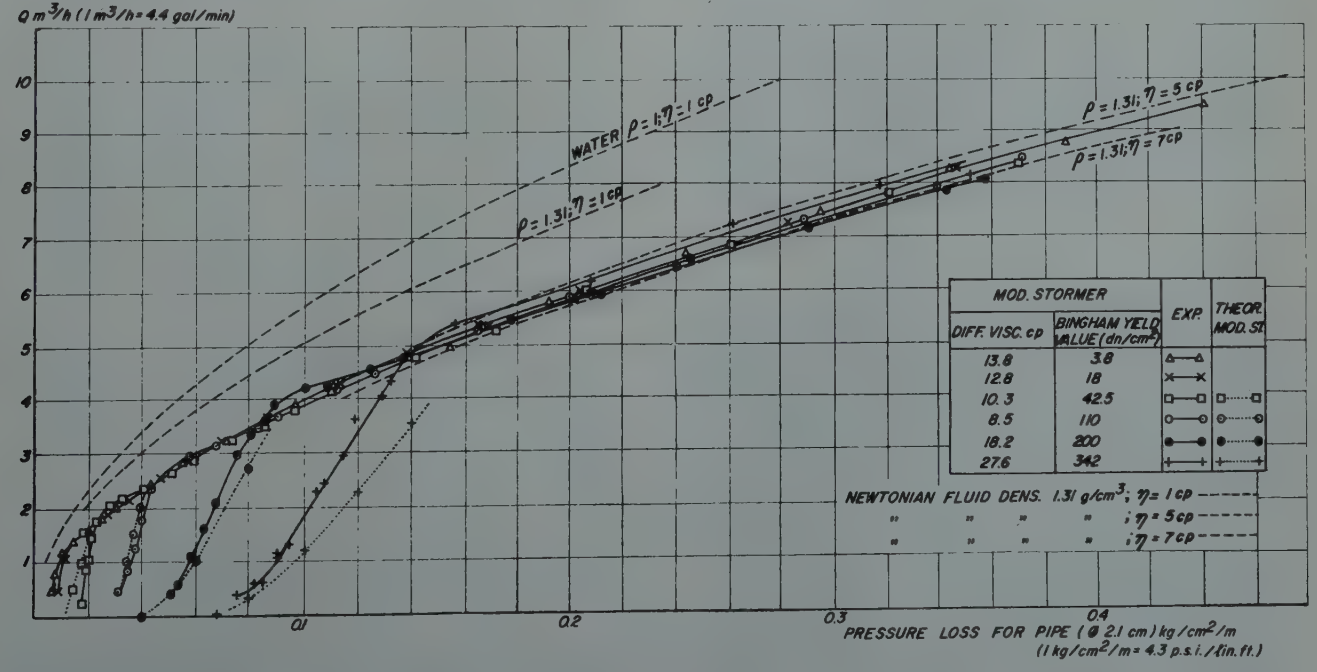
Q m³/h (1 m³/h = 4.4 gal/min)
WATER ρ = 1; η = 1 cp
ρ = 1.31; η = 1 cp
ρ = 1.31; η = 5 cp
ρ = 1.31; η = 7 cp
MOD. STORMER
DIFF. VISC. cp
BINGHAM YIELD VALUE (dn/cm²)
EXP.
THEOR. MOD. ST.
13.8 3.8
12.8 18
10.3 42.5
8.5 110
18.2 200
27.6 342
NEWTONIAN FLUID DENS. 1.31 g/cm³; η = 1 cp
η = 5 cp
η = 7 cp
PRESSURE LOSS FOR PIPE (Ø 2.1 cm) kg/cm²/m
(1 kg/cm²/m = 4.3 p.s.i./lin.ft.)

FIG. 1 — PRESSURE LOSS-VOLUME RATE OF FLOW DATA FOR A MUD WITH VARYING RHEOLOGICAL PROPERTIES; MUD DENSITY 1.31 GM/CM³; PIPE DIAMETER 2.1 CM.

TABLE 1 — COMPARISON OF LAMINAR FLOW-PROPERTIES WITH THE TURBULENT VISCOSITY

Density of mud g/cm³	Pipe diameter cm	τ_B dn/cm² Modified Stormer viscometer	τ_B dn/cm² Motor driven viscometer	τ_B dn/cm² Pipe	n cp. Modified Stormer viscometer	n cp. Motor driven viscometer	n cp. Pipe	η_t at 20°C in cp.
1.31	2.1	3.8	10.6	15.5	13.8	10.9	9.3	5.7
1.31	2.1	18.5	16.0	28.3	13.0	11.8	6.9	6.1
1.31	2.1	42.5	....	65	10.3	....	6.8	6.4
1.31	2.1	112	126	121	9.3	19.8	8.6	6.3
1.31	2.1	200	....	189	18.2	....	15.5	6.0
1.31	2.1	342	....	325	26.0	....	16.8	5.8
1.69	2.1	35	45	39	31.0	15.0	19.3	9.5
1.69	2.1	172	209	206	28.0	16.0	14.0	8.4
1.69	2.1	288	....	280	51.0	....	18.0	8.0
1.69	1.0	30	31	96	27.0	14.7	13.1	9.1
1.69	1.0	107	114	192	23.7	14.9	12.9	8.7
1.69	1.0	258	265	420	49.5	28.0	18.9	9.4

In the case of muds of 1.31 gm/cm³ density and of not too high yield values (e.g. lower than 200 dn/cm²) the agreement is reasonable (Fig. 1). However, for higher Bingham yield values substantial deviations may occur (e.g. 20 per cent). The deviations are even more pronounced with the muds of 1.69 gm/cm³ density (sometimes 50 per cent). In most cases the calculated pressures are higher than the observed pressures. This is mainly caused by the fact that the viscometers give higher values for n than correspond with pipe flow data. This is illustrated in Table 1, where τ_B and n derived from pipe-flow data (with Equation 4) are compared with the viscometer values.

These deviations are probably connected with the influence of agitation on the flow-properties (thixotropy). This agitation is strongest in the pumping experiments. The deviations are smallest at low τ_B-values because then the influence of agitation is smallest. The motor-driven viscometer gave better results at higher τ_B-values than the modified Stormer viscometer, probably because with the former viscometer a longer pretreatment was given to the mud.

The Onset of Turbulence

From the flow-curves a critical rate of flow may be derived at which turbulence begins (cf Fig. 1). To check the validity of the various criteria for predicting the critical rate of flow Re-numbers have been calculated according to the various methods proposed in the literature. For these calculations the Bingham yield value and the differential viscosity derived from the laminar part of the pipe flow curve have been used. The critical Re-numbers as defined by Binder and Busher and by McMillen should have a value of 2,000 to 3,000, whereas the critical value of Hedstrom's Re-number is dependent on the value of $S\ (= \frac{2R\tau_B}{nV})$.

In Table 2 the values for Re_{cr}, derived from the flow-curves are compared with those postulated by the above authors. It is seen that Binder and Busher's method predicts the onset of turbulence with reasonable accuracy. In the case of muds with a density of 1.31 gm/cm³, Re_{cr} is somewhat low, but the transition region is rather large and the lowest possible Q_{cr} value has been used in the calculation. Hedstrom's method also appears to provide a reasonable criterion for determining whether flow is laminar or turbulent.

Finally, it appears that McMillen's method is not suitable in the cases investigated here: the value of his Re_{cr} is considerably lower than 2,000 to 3,000. This means that the critical rate of flow as predicted by McMillen would be too high. The reason possibly is that these muds do not behave exactly as Bingham fluids.

The Turbulent Flow Region

By means of Equation (5), the friction factor f corresponding with the rate of flow Q could be calculated from the turbulent part of the flow curves. From this friction factor and the relationship between f and Re as determined with water, a Re-number $\frac{2Q\rho}{\pi\eta_t R}$ was derived, which was used for computing the turbulent viscosity η_t. All experiments were carried out with smooth pipes, which closely follow the Blasius equation. The experiments indicated that η_t is independent of the rate of flow.

In Table 1 the values of the turbulent viscosity of the muds are compared with their differential viscosities and Bingham yield values as measured with the viscometers and derived from pipe flow data. The η_t-values in this table have been calculated from the observed η_t-values and the temperature at which the experiments were carried out according to a method described in the next section.

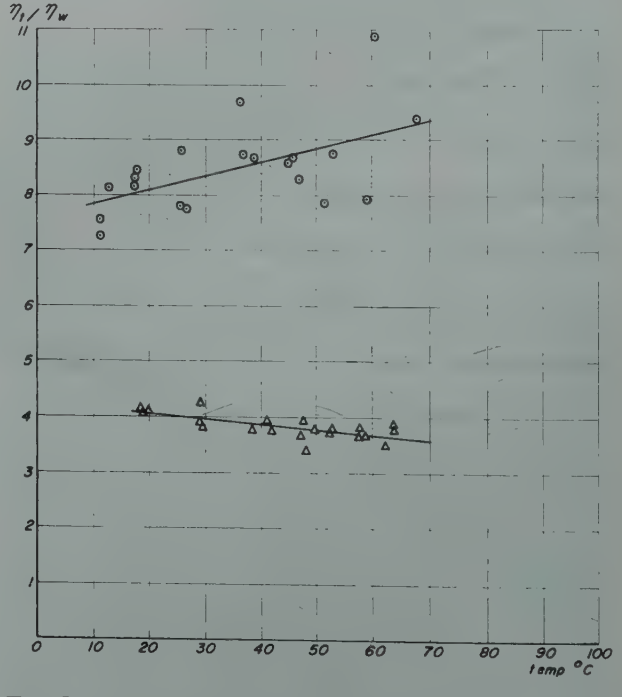

FIG. 2 — INFLUENCE OF TEMPERATURE ON η_t/η_w BENTONITE-BARYTES MUD WITH A DENSITY OF 1.26 GM/CM³△. BENTONITE-BARYTES MUD WITH A DENSITY OF 1.55 GM/CM³⊙.

TABLE 2 — COMPARISON BETWEEN SOME METHODS OF CALCULATING THE ONSET OF TURBULENCE

Mud density gm/cm³	Pipe diameter cm	τ_B pipe dn/cm²	η_{pipe} cp	Q_{cr} gal/min	Binder and Busher[9] Re_{cr} from curves	Binder and Busher[9] Re_{cr} expect.	McMillen[10] Re_{cr} from curves	McMillen[10] Re_{cr} expect.	Hedstrom[11] Re_{cr} from $\frac{2Q_{cr}\rho}{n\pi R}$	Hedstrom[11] Re_{cr} via $S = \frac{2R\tau_B}{nV}$
1.31	2.1	28.3	6.9	4.4	1150	2000-3000	174	2000-3000	3210	4500
		15.5	9.3	5.3	1770		464		2850	2500
		65	6.8	7.7	1690		240		5670	6000
		121	8.6	9.9	1560		407		5820	7000
		189	15.5	13.6	1620		261		4420	4500
		325	16.8	15.8	1420		200		4740	6000
1.69	2.1	39	19.3	7.5	1650	2000-3000	490	2000-3000	2500	2450
		206	14.0	13.6	2050		314		6300	5300
		280	18.0	17.6	2330		388		6320	4500
1.69	1.0	96	13.1	3.5	2625	2000-3000	827	2000-3000	3760	2400
		192	12.9	4.0	2470		616		4300	2750
		420	18.9	5.6	1505		514		4080	2900

Table 1 clearly illustrates that η_t is not influenced by the degree of flocculation of the mud (the variation in τ_B and n was effected by adding flocculating or peptising agents).

With respect to the magnitude of η_t it may be remarked that η_t is higher than the viscosity of the dispersing medium and lower than the differential viscosity.

The table further shows that $\frac{n}{\eta_t}$ is not a constant as assumed by Dunn et al. This point is further illustrated in Table 3 A and B.

The Turbulent Viscosity

When comparing the turbulent viscosites of the two muds investigated with the viscosity of water at the corresponding temperature, it appears that their quotient is practically independent of temperature. This is illustrated in Fig. 2. In the one case $\frac{\eta_t}{\eta_w}$ slightly increases, in the other case it slightly decreases with temperature. If there is any influence of t on $\frac{\eta_t}{\eta_w}$, this is so small that it may be neglected for practical purposes. This fact may be used for calculating η_t at any temperature, when its value at one temperature is known.

TABLE 3A — QUOTIENT $\frac{n}{\eta_t}$ FOR DIFFERENT CLAY-WATER MUDS

Mud density gm/cm³	τ_B dn/cm² Motor driven viscom-eter	n cp Modified Stormer viscom-eter	n cp Motor driven viscom-eter	η_t cp at 20°C	$\frac{n}{\eta_t}$ Modified Stormer viscom-eter	$\frac{n}{\eta_t}$ Motor driven viscom-eter
1.31	3.8	13.8	10.9	5.7	2.4	1.9
1.31	112	9.3	19.8	6.3	1.5	3.1
1.31	200	18.2		6.0	3.0	
1.69	35	31.0	15.0	9.5	3.1	1.6
1.69	30	27.0	14.7	9.1	3.0	1.6
1.69	258	49.5	28.0	9.4	5.3	3.1
1.10	0	3.0	3.3	2.0	1.5	1.7
1.10	8	4.3	5.0	2.25	1.9	2.2
1.20	20	6.6	5.2	3.9	1.7	1.3
1.20	20	6.6	5.2	3.2	2.1	1.6
1.40	35	21.8	17.1	9.7	2.2	1.8
1.15	30	13.5	11.1	3.0	4.5	3.7
1.15	30	13.5	11.1	4.2	3.2	2.7
1.54	50	16.4	14.4	8.0	2.0	1.8
1.54	80	19.8	19.3	8.3	2.4	2.3
1.18	7.5	5.3	6.4	3.7	1.4	1.7
1.31	33	27.4	19.3	13.1	2.1	1.5

TABLE 3B — SOME $\frac{n}{\eta_t}$ VALUES FOUND BY DUNN ET AL. ON 2-IN. TUBING

Mud No.	n cp	η_t cp	$\frac{n}{\eta_t}$
1	30	9.0	3.3
2	10.2	4.8	2.1
3	17.1	8.1	2.1
4	26.1	7.1	3.7
5	39.0	12.6	3.3
6	15.9	2.5	6.4
7	5.1	2.7	1.9

All experiments described have not been carried out at the same temperature. If necessary, the results of these experiments will be compared on the basis of

$$\frac{\eta_t}{\eta_w}.$$

In Fig. 3 the results of pumping experiments with clay-water muds at different rates of flow are presented. It appears that η_t is independent of the rate of flow. Measurements on the barytes-loaded bentonite muds confirmed this observation.

The results of experiments on the bentonite muds with barytes and pipes of different diameter are presented in Fig. 4. No significant influence of pipe diameter on η_t/η_w was observed. This was again confirmed by measurements on the clay-water muds without barytes.

In the section on turbulent flow it was noted that n/η_t is not a constant. To further illustrate this a series of n/η_t-values, representative for our experiments have been collected in Table 3A. The η_t-values at 20°C and the n-values at room temperature are given. The table shows large variation in n/η_t-values. The quotient n/η_t has also been calculated for some data given by Dunn et al. (Table 3B). The figures again show a considerable spread. From this it may be concluded that methods

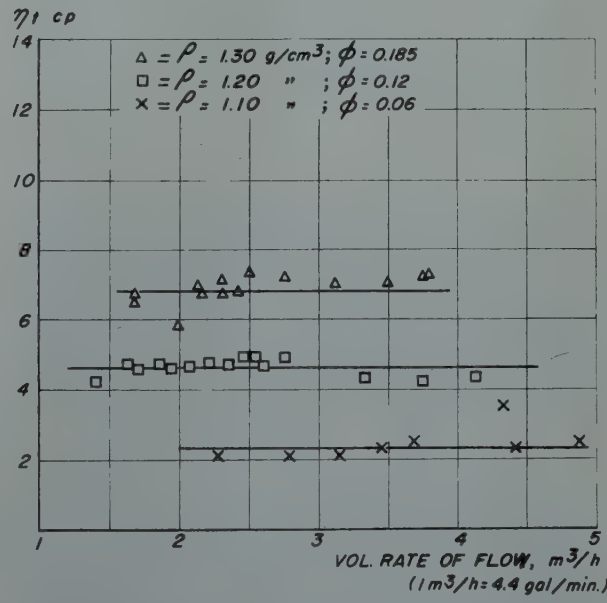

FIG. 3 — THE INFLUENCE OF RATE OF FLOW ON THE TURBULENT VISCOSITY OF CLAY WATER MUDS (PIPE DIAMETER 1.0 CM).

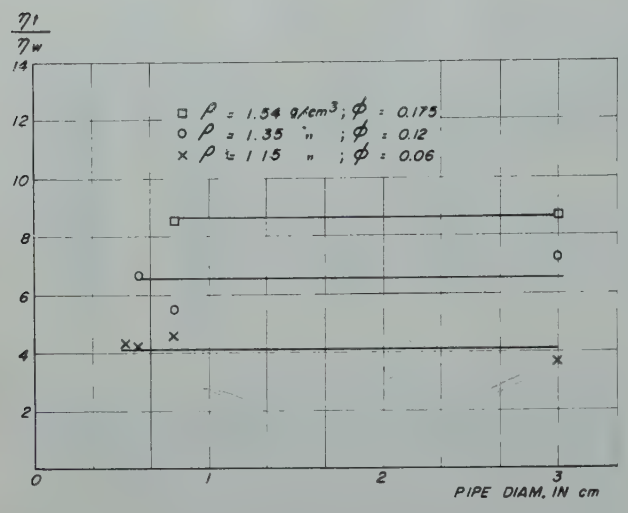

FIG. 4 — INFLUENCE OF PIPE DIAMETER ON η_t/η_w FOR MUDS PREPARED FROM BENTONITE AND BARYTES.

based on the assumption that n/η_t is a constant may lead to erroneous results.

In Fig. 5 the influence of the volume fraction of dispersed phase ϕ* on $\frac{\eta_t}{\eta_w}$ is shown for clay water muds and bentonite muds loaded with barytes. As explained earlier, the position of the points in this graph is not influenced by the degree of flocculation of the mud. Each point represents the average of in total *ca.* 40 measurements on three or four pipes of different diameter. The standard deviation in such a group of measurements varies from 10 to 25 per cent.

It appears that the η_t/η_w-values of the bentonite-barytes muds are higher than those for the other muds. However, no value deviates more than 30 per cent from the average η_t/η_w-values of the two types of muds.

The results of measurements on field muds are also presented in Fig. 5. For the case of the saturated salt water mud the viscosity of a saturated salt solution (2.2 cp at 20°C) has been used instead of η_w. The best straight line through all the points follows the equation:

$$\frac{\eta_t}{\eta_w} = 46.5\,\varphi \quad . \quad . \quad . \quad . \quad . \quad . \quad . \quad . \quad . \quad (7)$$

The field mud with a φ-value of 0.185 shows a deviation of 43 per cent, whereas the η_t-values of all other muds deviate less than 40 per cent from the line. It should be borne in mind that the pressure losses vary as the fourth root of the η_t-value. This means that when using Equation 7 to predict η_t/η_w, the pressure-losses may be calculated with an accuracy of ± 10 per cent approximately. The relation between f and Re has to be known for these calculations. Probably for drill pipes the Blasius equation ($f = 0.079\,Re^{-1/4}$) may be used, because usually their surface will be smooth, as a result of the polishing action of the mud.

Though not perfect, the above method of predicting η_t from φ is more accurate than methods which use the differential viscosity for this purpose.

EXPERIMENTS WITH BIT-NOZZLES

By way of example the relation between C and Re as determined with water is presented in Fig. 6 for one of the nozzles used in these experiments. It appears that C decreases with increasing Re-number to become practically constant at a Re-number of 150,000.

From the steep part of the C-Re-curve and the C-values obtained via Equation (6) from pumping experiments with muds, the η_t-values of these muds could be derived. The C-Re relation at high Re-numbers could not be used because it gives too inaccurate values of η_t. It appeared that the η_t-values thus obtained are independent of rate of flow and of the laminar flow-properties of the mud.

An average value of 1.75 cp was obtained for muds with a density of 1.31 gm/cm³ and of 1.9 cp for muds with a density of 1.69 gm/cm³. In Fig. 6 the C-values of a mud with a density of 1.31 gm/cm³ are plotted against a Re-number computed with an η_t-value of 1.75, which illustrates that the points so obtained fall on the

*100 m³ water/hour through four ¾-in. nozzles already corresponds with a Re-number of 100,000.

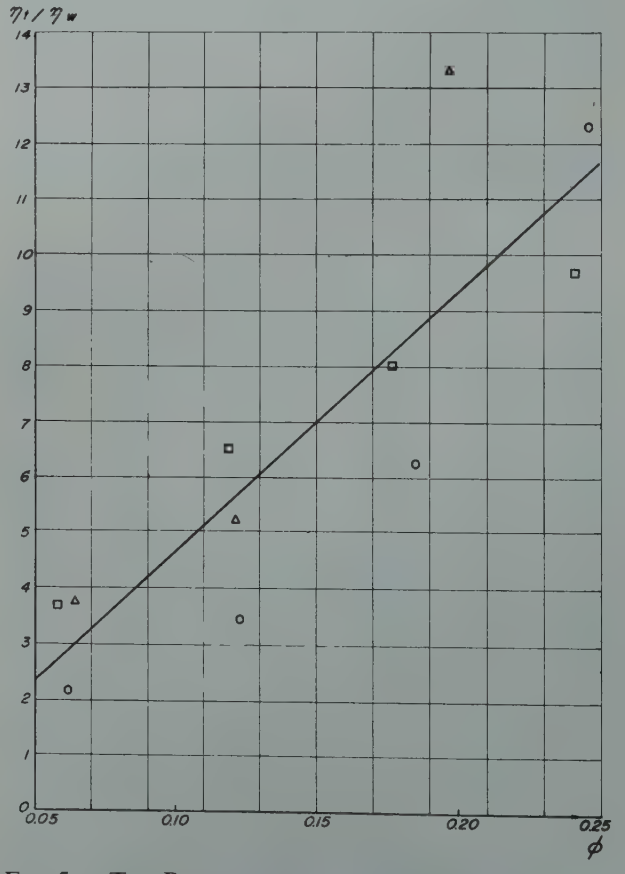

FIG. 5 — THE RELATION BETWEEN η_t/η_w AND THE VOLUME FRACTION OF DISPERSED PHASE ϕ; CLAY MUDS ○; BENTONITE-BARYTES MUDS □; FIELD MUDS △.

* ϕ can be calculated from the equation $A + (1 - \phi) \cdot \rho_{fl} = \rho_m$ where ϕ = volume fraction of dispersed phase, A = grams of dispersed phase per ml mud (= grams dry weight of 1 ml mud minus grams dissolved salts per ml mud), ρ_{fl} = density of medium and ρ_m is density of mud. A and ρ_m can be determined experimentally. In the case of water base muds, ρ_{fl} is unity. Dissolved salts do not contribute to ϕ, but they affect η_m (the viscosity of the medium) and ρ_{fl}. In this case, η_m and ρ_{fl} have to be determined or may be derived from tables.

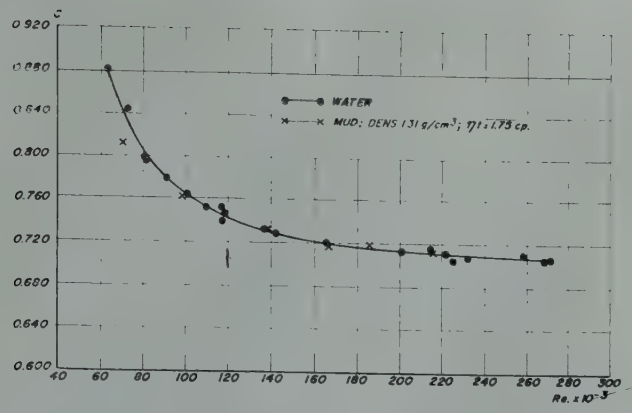

FIG. 6 — NOZZLE EXPERIMENTS; *C-Re* RELATIONSHIPS FOR MUD AND WATER.

waterline. In the field the flat part of the *C-Re* curve is of importance*. This means that under field conditions the *C*-value for a mud is the same as that for water. Its magnitude is only determined by the geometry of the nozzle. If the nozzle has been designed well[12], it has a coefficient of discharge which lies between 0.9 and 1.0.

CONCLUSIONS

1. When clay-water muds are pumped through pipes, pressure losses in the laminar flow region may be calculated — though not very accurately — from the differential viscosity of the muds as measured with rotational viscometers (The data obtained with the motor-driven viscometer were found to be better suited for the purpose than those found with the modified Stormer viscometer).

2. The criterion of Binder and Busher[9] or that of Hedstrom[11] may be used to calculate whether the flow of a clay-water mud in a pipe is laminar or turbulent. McMillen's[10] criterion is not suitable for clay-water muds in that it gives too high values for the critical rate of flow.

3. The turbulent viscosity of a clay-water drilling mud is not influenced by: (a) the degree of flocculation of the mud; (b) the rate of flow; and (c) the diameter of the pipe.

4. The quotient of the turbulent viscosity of a clay-water mud and the viscosity of water at the same temperature is practicially independent of temperature.

5. This quotient may be predicted with reasonable accuracy from the volume fraction of dispersed phase.

6. The turbulent viscosity of a clay-water mud is not equal to the viscosity of the dispersing medium[8], nor to the differential viscosity of this mud[11].

7. The quotient of the differential viscosity and the turbulent viscosity is not a constant[3,6]. The use of such a relation to calculate pressure-losses may lead to erroneous results.

8. For flow conditions prevailing in the field, the pressure-losses in the bit-nozzles are independent of the laminar flow properties of the mud; they are solely determined by the density of the mud and the geometry of the nozzle.

ACKNOWLEDGMENT

The author wishes to thank J. van Heiningen and L. J. Klinkenberg for valuable discussions on the subject, and to A. Luyt, R. Eype and W. A. M. van der Wielen for carrying out the experimental work. He further expresses his appreciation to the management of the N. V. De Bataafsche Petroleum Maatschappij, The Hague, Netherlands for permission to publish this paper.

LIST OF SYMBOLS

β = ratio of nozzle diameter to tube diameter
Φ (ϕ) = volume fraction of dispersed phase
η = dynamic viscosity in poises
η_a = apparent viscosity in poises
η_m = viscosity of dispersing medium in poises
η_w = viscosity of water in poises
η_t = turbulent viscosity of mud in poises
η_t/η_w = quotient of η_t and η_w at the same temperature
ρ = density gm/cm³
τ = shear stress dn/cm²
τ_o, τ_B = gel strength and Bingham yield value dn/cm²
A = cross sectional area of nozzle in cm²
C = coefficient of discharge, dimensionless
D = rate of shear second⁻¹
l = length of tube in cm
n = differential viscosity in poises
P or ΔP = pressure drop over pipe or nozzle in dn/cm²
Q = volume rate of flow in cm³/sec
R = tube radius in cm
Re = Reynolds' number
Re_{cr} = critical Reynolds' number
t = temperature in degrees centigrade
V = linear rate of flow cm/sec

REFERENCES

1. Pigott, R. J. S.: "Mud Flow in Drilling," *Drilling and Production Practices,* API (1941), 91.
2. Hughes Tool Co. Bulletin 1A, *Hydraulics in Rotary Drilling* (Revised Edition: April, 1954).
3. Dunn, T. H., Nuss, W. F., and Beck, R. W.: "Flow Properties of Drilling Mud," *Drilling and Production Practices,* API, (1947) 9.
4. Koch, W. M.: "Fluid Mechanics of the Drilling String," *J. Pet. Tech.,* (April, 1953) **5**, 9.
5. Olphen, H. van: "Pumpability, Rheological Properties and Viscometry of Drilling Fluids," *J. Inst. Pet.* (1950) **36**, 223.
6. Olphen, H. van: *Thesis Delft 1951.*
7. Evans, P., and Reid, A.: "Drilling Mud, Its Manufacture and Testing," *Trans.* Mining Geol. Inst. India, (1936) **32**, 1.
8. Caldwell, D. H., and Babbitt, H. E.: "Flow of Muds, Sludges and Suspensions in Circular Pipe," *Ind. Eng. Chem.,* (1941) **33**, (2), 249.
9. Binder, R. C., and Busher, J. E.: "Study of Flow of Plastics through Pipes," *J. Applied Mechanics,* (1946) **13**, (2), A-101.
10. McMillen, Elliott L.: "Simplified Pressure-Loss Calculations for Plastic Flow," *Chem. Eng. Progr.,* (1948), **44**, (7), 537.
11. Hedstrom, B. O. A.: "Flow of Plastic Materials in Pipes," *Ind. Eng. Chem.,* (1952), 44, 651.
12. Eckel, J. R., and Bielstein, W. J.: "Nozzle Design" *World Oil* (February, 1952) 118; (March, 1952) 115.

★★★

THE ROLE of BUBBLE FORMATION in OIL RECOVERY by SOLUTION GAS DRIVES in LIMESTONES

C. R. STEWART
MEMBER AIME

E. B. HUNT, JR.
F. N. SCHNEIDER
T. M. GEFFEN
V. J. BERRY, JR.
JUNIOR MEMBERS AIME

STANOLIND OIL AND GAS CO.
TULSA, OKLA.

T. P. 3962

ABSTRACT

Laboratory data show that the gas-oil ratio performance of non-uniform porosity limestones produced by solution gas drive is sensitive to producing rate and to fluid properties. Non-uniform porosity limestones are those for which laboratory solution and external gas drive tests yield considerably different relative permeability ratio characteristics.

The oil recovery performance by solution gas drive depends directly on the number of gas bubbles formed. Laboratory rates of pressure decline, which are 100 to 10,000 times greater than normal field rates, cause the formation of an unusually large number of gas bubbles. This results in abnormally high oil recovery efficiencies. Since it is impractical to reproduce the number of bubbles formed under field conditions, laboratory solution gas drive data on non-uniform porosity limestones are therefore not directly applicable to field operations. However, certain laboratory data can be used to make a conservative estimate of field performance.

The concepts presented in this paper indicate the possibility that increased field oil recoveries may be obtained from non-uniform porosity limestones by rapidly reducing reservoir pressure for a short interval of time. It has yet to be established that significant improvements in oil recovery from such reservoirs can be realized by varying the pressure decline rate within limits possible in the field. However, the possibility that recovery may be increased in this manner warrants further study.

INTRODUCTION

Limestone reservoir rocks can be divided into two general classes according to the nature of their pore space. One class has a comparatively uniform pore system composed mainly of voids between grains of the rock (intergranular type porosity). The other class, in addition to having intergranular porosity, has a secondary pore system composed of combinations of solution cavities, fractures, etc., and is considered to have non-uniform porosity.

It has been shown in a previous publication[1] that the laboratory measured gas-oil flow behavior of uniform type porosity limestones is essentially the same for a test simulating a field solution gas drive as for one simulating an external gas drive. For non-uniform porosity type limestones a significant difference in gas-oil flow behavior was found. More efficient behavior was

Manuscript received in Petroleum Branch office on Sept. 8, 1954. Paper presented at Petroleum Branch Fall Meeting in San Antonio, Oct. 17-20, 1954.

[1]References given at end of paper.

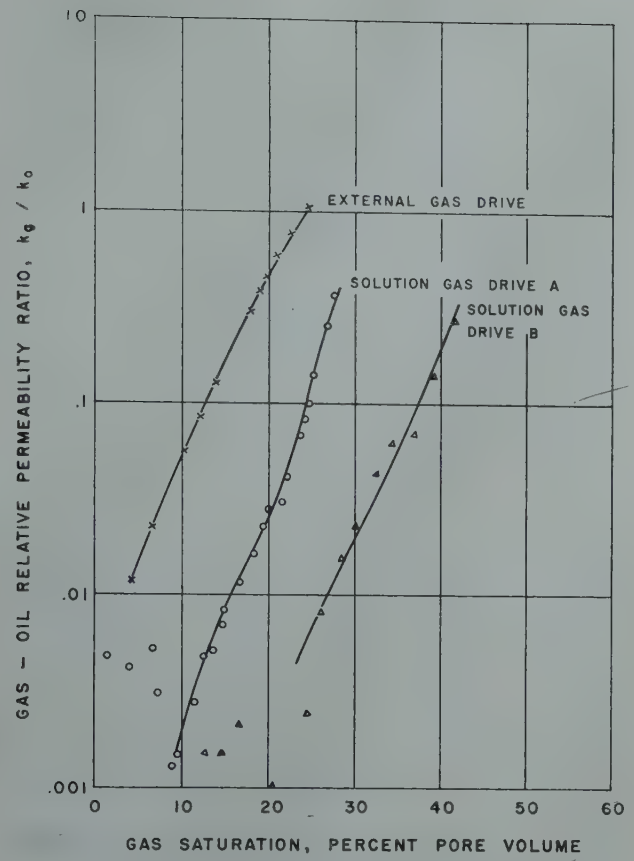

FIG. 1—RELATIVE PERMEABILITY CHARACTERISTICS OF WEST TEXAS REEF LIMESTONE CORE.

Permeability = 21 mds: Porosity = 20 per cent.
Curve A: Methane and C_{10}-C_{12}, bubble point pressure = 200 psig.
Curve B: Nitrogen and C_{10}-C_{12}, bubble point pressure = 1,000 psig.

observed during a solution gas drive test. This difference in oil displacement behavior was attributed to the complex nature of the pore space and to the fact that the source of gas in the two displacement operations is not the same. That is, in a solution gas drive the gas is evolved from oil within the pores of the rock itself, while in an external drive the gas is injected from an outside source.

Experimental work beyond that previously published shows that the laboratory solution gas drive behavior of non-uniform porosity limestones is not unique. Differences in oil recovery up to twofold, at the same flowing gas-oil ratio, were found by varying the test conditions. A variation in results on uniform porosity type rocks was also observed. However, the variation in flow behavior of one core under different test conditions was small and of the same magnitude as the observed differences between results of identical tests on separate cores of the same rock material.

For the non-uniform porosity limestones, the laboratory solution gas drive relative permeability characteristics were found to be affected by: (1) rate of pressure decline, (2) original bubble point pressure of the gas-oil solution, (3) oil viscosity, and (4) gas solubility characteristics.

Two examples of the variation observed on non-uniform porosity limestones are shown in Figs. 1 and 2. The data in Fig. 1 were measured on a West Texas reef sample and those in Fig. 2 on a Mid-Continent limestone sample. The data for test B in each figure were obtained using a gas-oil solution having an initial bubble point pressure of 1,000 psi. The initial bubble point pressure for tests A was 200 psi. In addition, the pressure decline rates for tests B were faster than for tests A.

The data of Figs. 1 and 2 are quite typical of those obtained on non-uniform porosity limestones, and no satisfactory explanation has been heretofore published. The purpose of the studies reported in this paper was therefore: (1) to determine the reason for the observed variation in results of laboratory solution gas drive tests; (2) to design a laboratory test which would provide data for predicting field performance; and (3) to determine if special production practices in certain oil fields could result in improvements in oil recovery. The answer to the first question has been obtained. These studies offer only an insight into the possible means for answering the second and third questions.

FORMATION OF GAS SATURATION IN POROUS MEDIA

During all laboratory solution gas drive tests it has been observed that the oil is in a supersaturated state.[1] That is, the oil contains more dissolved gas than would be predicted from PVT relationships. In terms of pressure, the degree of supersaturation is expressed as the difference between the bubble point pressure of the oil and the actual pressure. Some degree of supersaturation is always observed to exist throughout the entire pressure depletion life of solution gas drive tests. It is noted, in fact, that the supersaturation history of a test actually is closely related to the measured flow behavior. In general, the higher the degree of supersaturation, the greater is the displacement efficiency of oil by gas.

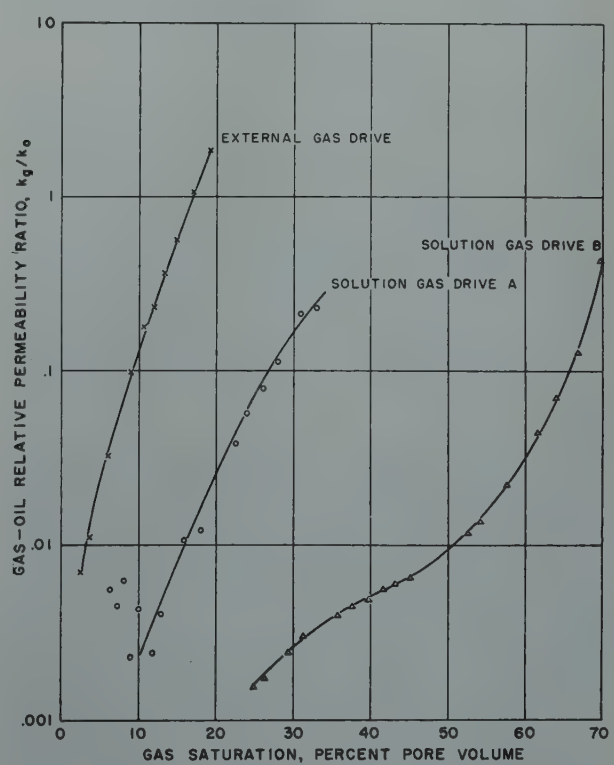

FIG. 2—RELATIVE PERMEABILITY CHARACTERISTICS OF MID-CONTINENT LIMESTONE CORE.

Permeability = 1 md: Porosity = 30 per cent.
Curve A: Methane and C_{10}-C_{12}, bubble point pressure = 200 psig.
Curve B: Methane and C_{10}-C_{12}, bubble point pressure = 1,000 psig.

By experience, it is known that supersaturation results in the formation of bubbles in a gas-oil solution. One might conclude, therefore, that the manner in which bubbles form and subsequently grow controls the displacement of oil during any solution gas drive. Since not all rocks exhibit unusual laboratory solution gas drive performance, the pore geometry probably also plays an important role.

A study of results such as are presented by Figs. 1 and 2, and visual studies of non-uniform porosity limestones indicate that only a part of the total gas saturation is responsible for the observed gas-oil ratio performance. This implies that part of the porosity of these non-uniform rocks does not contribute to gas permeability. Nevertheless, if the saturation existing only in the conductive regions could be correlated with the flowing gas-oil ratios, it is believed that the differences exhibited in solution drive behavior would be resolved into one basic flow relationship. At present no way of obtaining such a correlation is apparent for naturally occurring rocks.

The above considerations indicate the influence of (a) the formation of gas bubbles, and (b) the displacement of oil by expanding gas bubbles on depletion characteristics of non-uniform porosity rocks.

Formation of Gas Bubbles

Kennedy and Olson[2] have shown that the rate at which gas bubbles form in a gas-oil solution is a function of the supersaturation. This in turn depends on the rate of pressure reduction. The higher the supersaturation, the greater is the rate at which gas bubbles form. Since in laboratory solution gas drive tests the supersaturation histories were different, it was logical to conclude that the oil displacement behavior was affected by the rate of bubble formation, and hence by the number of gas bubbles formed.

Information in the literature[3,4,5], together with data obtained at the Stanolind Research Center on gas bubble formation, were used to predict the total number of bubbles which might form under various rates of pressure decline. Although the details of this study are beyond the scope of this paper and will be covered in a future publication[6], an example of the results can be shown here. The predictions were made using different assumptions than were made by Kennedy and Olson[2]. Nevertheless, the agreement with their predictions on the number of bubbles formed is satisfactory, considering that both methods give only order of magnitude values.

The theoretical supersaturation history as well as the cumulative number of bubbles formed are shown in Fig. 3 for a gas-oil solution undergoing constant rates of pressure decline of 1,000, 100, 10, 1, and 0.1 psi per day. These rates of pressure decline cover the range of importance in field and laboratory solution gas drives. It must be emphasized that the results of Fig. 3 apply only to a specific system. However, the effect of rate of pressure decline on the number of bubbles formed is the same for all systems; namely, an increase in the rate of pressure decline by a factor of 10 results in about 10 times as many bubbles being formed.

The significant information shown in Fig. 3 is that the higher the rate of pressure decline, the greater is the total number of bubbles formed in a system. Also, essentially all of the bubbles are formed throughout a relatively short time interval during the pressure depletion life. From Fig. 3 it can be estimated that in usual laboratory tests the number of bubbles formed is 100 to 10,000 times greater than the number formed under normal field conditions.

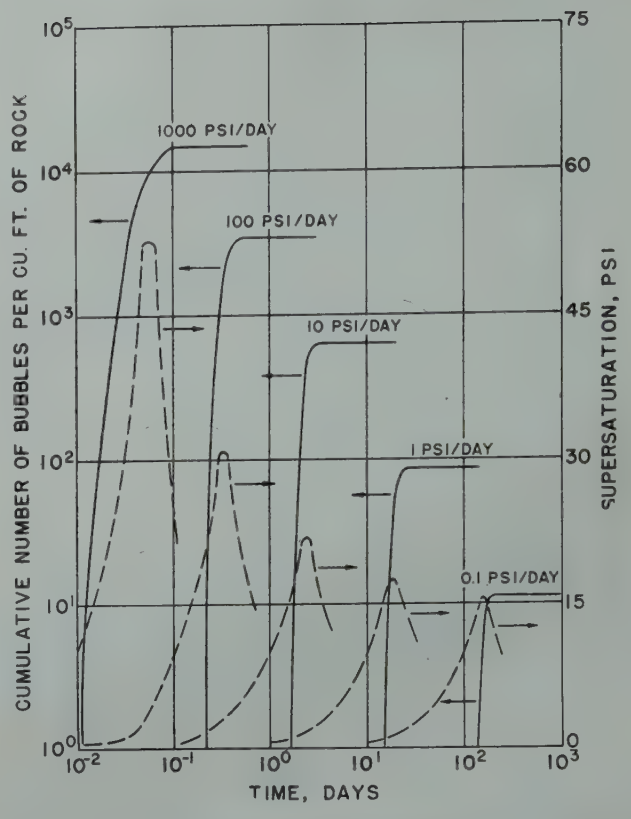

Fig. 3 — Calculated Supersaturation and Bubble Formation History With Varying Rates of Pressure Decline.

Values shown apply to a hypothetical system; however, the relative values apply to any system, e.g., a 10-fold increase in rate of pressure decline results in a 10-fold increase in the number of bubbles formed.

Displacement of Oil by Expanding Gas Bubbles

It is reasoned that the number of gas bubbles formed during the pressure depletion of a gas-oil solution in a porous material will have an effect on the oil displacement behavior. In this type of recovery method, oil is pushed out of a pore by the evolution of a gas bubble within this pore or by the intrusion of gas from another pore.

A gas bubble grows in two ways; namely, by the addition of gas which diffuses from adjacent oil and by expansion due to pressure reduction. As it grows it will invade the network of pores which offers the least resistance. This bubble will unite with others, eventually forming a continuous gas phase which extends to the exit of the porous body. After this occurs, gas flowing in this connected network of pores will be less effective in displacing oil from other pores. However, isolated gas bubbles will still be present, and will continue to displace oil with the maximum efficiency until they join the continuous gas phase. The more bubbles present, the greater will be the displacement of oil from regions not invaded by the conductive gas saturation. Figs. 1 and 2 provide examples showing the

effect of the number of bubbles on recovery. The approximate number of bubbles formed in each of these tests has been calculated using methods referred to in the previous section. The calculations show that about 10 times as many bubbles were formed in the B tests as were formed in the A tests reported in each of the figures. This is in agreement with the concepts outlined above.

The amount by which bubble formation and the growth of bubbles affects flow behavior in a solution gas drive on uniform porosity type rocks has been found to be small, except in the early stages of depletion. In this type of rock all of the pores act as fluid conductors as well as fluid storage spaces. Displacement of oil from a specific pore or from a group of pores does not require the formation of a gas bubble in it. The reason is that gas evolved upstream can enter and thereby displace oil from any pore.

This is not the situation in non-uniform porous materials as is suggested above. In these, some pores act as fluid conductors as well as storage spaces while others are essentially storage spaces. In other words, comparison of the oil recovery performances calculated from laboratory solution and external gas drives indicates the presence of pore space which is not entered by an immiscible, non-wetting, displacing fluid (such as gas) during an external drive. These pores, or clusters of pores, have capillary pressure-saturation characteristics which are different from the "conductor" pores comprising the rest of the pore space. Recovery of oil from these "storage" pores by an external gas drive can be accomplished only at high gas-oil ratios. However, in this type of pore, or cluster of pores, the formation of a gas bubble during a solution gas drive can result in the displacement and recovery of this oil when the system is producing at a relatively low gas-oil ratio.

The above discussion explains why a laboratory solution drive recovers more oil than does an external gas drive at comparable flowing gas-oil ratios. It also offers an explanation for the variations in oil recovery observed in solution gas drives. To summarize, recovery of oil from these storage pores can only result from the formation of bubbles therein. If the number of bubbles formed during a solution drive varies, the recovery of oil from these pores will vary also. Where the volume of these pores comprises a high percentage of the total volume of the rock, these variations will be significant.

It was shown previously that at field rates of pressure decline the number of gas bubbles formed is small compared to the number formed in laboratory tests. This can be taken qualitatively to mean that laboratory solution gas drive tests will yield a higher oil displacement efficiency from a non-uniform limestone rock than should be expected in the field.

To confirm further the ideas expressed above, several solution drive tests were conducted under special conditions. The following section describes apparatus and general experimental techniques used in these tests. A description of the special test conditions employed is given in a later section, together with a discussion of the objectives of the experiments and of the results obtained.

DESCRIPTION OF APPARATUS AND PROCEDURE

The core samples used in this work were selected from producing sections in oil reservoirs and also from outcrop formations. All samples were cylindrical in shape and ranged from 2½ to 4½ in. in diameter. These samples varied from 6 to 11 in. in length with one exception. This exception was a specially prepared 6 ft long core. The apparatus and technique of mounting and testing these samples from 6 to 11 in. long have been described in a previous publication.[3]

The 6 ft long core sample was prepared from a piece of Cordova shellstone which outcrops near Austin, Tex. This core sample had a uniform diameter of 4½ in. for 5 ft of length. The diameter was then reduced uniformly over a 3 in. long section, and the remaining 9 in. of the core were shaped into a square cross section, 1 in. on a side. The core was prepared in this manner to minimize effects of boundary conditions on flow test results. In the flow tests this reduced section formed the downstream end of the core. At a point 1 ft from the downstream end of the core a small diameter tube was attached for pressure measurement. Fluid gathering plates were attached to each end of the rock and the assembly was surrounded by a thermosetting plastic. The plastic-sealed core was then placed in a steel cell, and the space between the inside of the cell and the outside of the core was pressured to 400 psi.

The technique of saturating the 6 ft long Cordova shellstone core differed from that used on the smaller samples. The large core was first saturated with a gas-free relatively pure hydrocarbon in the range of C_{10}-C_{12}. Next, methane gas was injected and oil produced until the average gas saturation reached approximately 30 per cent pore space. The injection pressures were very close to the bubble point pressure of the methane-C_{10}-C_{12} solution to be used in the flow tests. After flow was terminated, methane gas was injected into the core through a regulator set to operate at the intended bubble point pressure. After various intervals of time the core was shut off from the methane supply, and the gas phase pressure change with time was observed. When the gas phase pressure drop became negligible for an interval of several hours, the residual oil was considered to be substantially at equilibrium with the gas present.

The gas phase was then removed by the injection of 200 psi bubble point oil, first at an injection pressure slightly above the bubble point pressure, then later at an injection pressure of 300 psi. The extent of liquid saturation was determined by both material balance and fluid compressibility checks. It was found that 2 pore volumes of oil were sufficient to remove the gas and thus completely saturate the core.

In addition to the previously described apparatus[1], a special constant rate pump was used in the tests where a constant rate of pressure decrease or increase was used. This pump was powered by a constant speed electric motor working through a machine lathe gear train. The pump was connected to a back pressure regulator. Depending on the manner of connecting the pump, the pressure could be either increased or decreased at a constant rate.

RESULTS AND DISCUSSION

Short Core Tests

The usual laboratory solution gas drive test involves a pressure depletion time of hours compared with years for an actual reservoir. The laboratory pressure decline rates are accordingly orders of magnitude greater than field rates. Under such conditions the number of gas bubbles formed in a laboratory test is likewise much greater than the number formed in the reservoir.

The most direct method for reducing the number of bubbles formed during laboratory tests is to use slower rates of depletion. However, it is impractical from the standpoint of time alone to perform laboratory tests at field rates. There is also another serious objection to reducing laboratory depletion rates. A decrease in the rate of pressure decline also means a decrease in the pressure drop across the system and an increase in the "end effect," or liquid pile-up at the downstream end of the core. If this end effect is appreciable, it becomes impossible to obtain reliable gas-oil relative permeability data. These two factors militate against the direct laboratory measurement of correct solution drive gas-oil relative permeability characteristics. Nevertheless, laboratory tests described in the following paragraphs have been made to show the effect of bubble formation on oil recovery efficiency. These tests actually allowed measurement of the amount of oil produced solely as a result of the formation and growth of gas bubbles in the storage pores of a non-uniform porosity limestone sample.

Two nearly identical tests were performed on a single reservoir sample. The main feature of each test was the execution of a solution gas drive after the initial establishment of a high gas saturation (the necessity for the gas saturation will be explained later). The two solution gas drives were performed at greatly different rates, so that in one test few, if any, bubbles would be formed, whereas in the other test, many bubbles would be formed.

In order to form essentially no bubbles during a depletion test, it is sufficient to maintain supersaturation at a low value, such as 15 psi or less. The amount of supersaturation which will exist in a core subjected to a given rate of pressure decline depends, of course, on how fast the dissolved gas can diffuse out into the connected gas phase. Since it was desired to use reasonable rates of pressure decline in the tests, it was therefore necessary first to establish a high gas saturation prior to the solution gas drive.

Fig. 4 is an example of results of diffusion tests on a sample of non-uniform porosity limestone. Although these data were not actually obtained on the Reef sample, they serve as an excellent example of the characteristics of such rocks. As can be seen from Fig. 4, at high gas saturations the maximum rate of pressure decline which can be maintained without exceeding a given degree of supersaturation increases rapidly with increasing gas saturation. A solution gas drive in which no bubbles are formed cannot, therefore, be carried out at reasonable laboratory rates unless a high gas saturation is first established.

A further reason for initially driving the cores to a high gas saturation was to insure that any oil produced during the subsequent depletion test could come only from pores not normally emptied during an external gas drive, i.e., from the storage pores. Actually, the

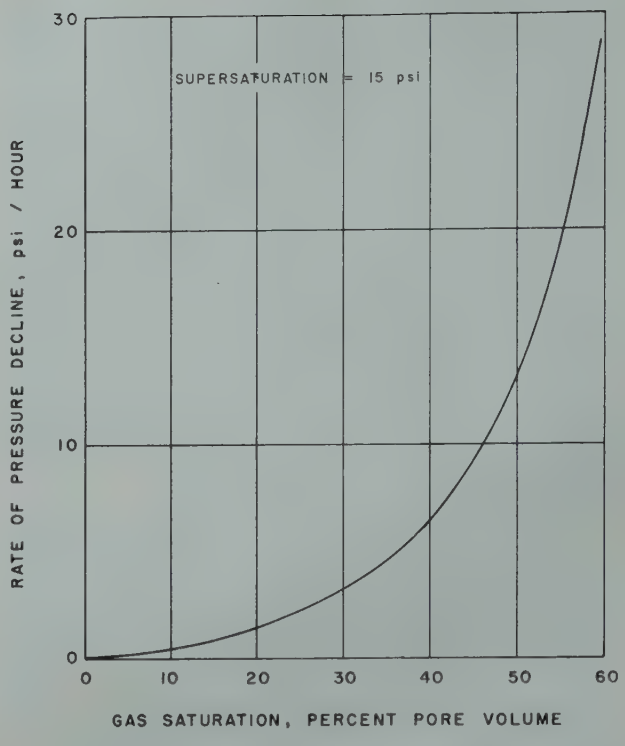

FIG. 4 — RELATIONSHIP BETWEEN PRESSURE DECLINE RATE AND GAS SATURATION WITHOUT BUBBLE FORMATION FOR CORDOVA SHELLSTONE.

Methane and C_{10}-C_{12}.

solution drives were also followed by final external gas drives to recover any newly released oil which might have been held back by end effect during the depletion process.

The two nearly identical experiments were performed on a single sample of the previously mentioned Reef limestone. In each of the two tests, the sample was saturated with gas-free C_{10}-C_{12}. Following this, the initial external gas drive was applied with a pressure differential sufficiently high to overcome end effect. This drive was terminated at 57 per cent pore space average gas saturation. After establishing the gas saturation, the core was pressured to 1,000 psig with gas until the residual oil was substantially at equilibrium at this pressure. At this point the core was depressured at a controlled rate of pressure decline. At the end of the pressure depletion a final external gas drive was applied at the same pressure conditions as were used for the initial external drive.

The two series of experiments were identical except for the rate of pressure decline during the depletion process. The two rates used during the solution drives were 38 and 2,100 psi per hour. The 38 psi per hour rate was chosen on the basis of a calculation which indicated that the degree of supersaturation attained at this rate would not exceed 15 psi, and thus no bubbles would form. The 2,100 psi per hour rate was the maximum rate attainable. A special bubble formation calculation indicated that even at the existing high gas saturation (57 per cent), many bubbles would be formed at this rate of pressure decline.

The results of these tests are given in Fig. 5. The data are presented as the flowing gas-oil ratio for the external drives versus the oil recovery as per cent pore

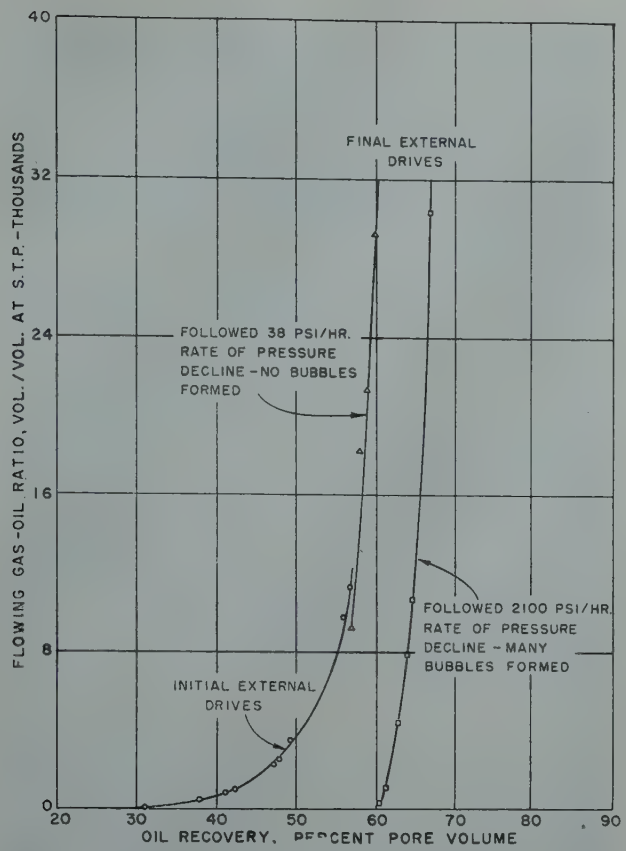
FLOWING GAS-OIL RATIO, VOL./VOL. AT S.T.P.-THOUSANDS
OIL RECOVERY, PERCENT PORE VOLUME
FINAL EXTERNAL DRIVES
FOLLOWED 38 PSI/HR. RATE OF PRESSURE DECLINE - NO BUBBLES FORMED
FOLLOWED 2100 PSI/HR. RATE OF PRESSURE DECLINE - MANY BUBBLES FORMED
INITIAL EXTERNAL DRIVES

FIG. 5 — FLOWING GAS-OIL RATIO PERFORMANCE FOR REEF LIMESTONE CORE.

Permeability = 21 mds: Porosity = 20 per cent.

space. The effect of bubble formation on oil recovery for this non-uniform porosity limestone sample can be measured by comparing the performance of the two final external gas drives. The shift to the right for the gas drive which followed the rapid rate of pressure decline shows the increase in oil recovery due to bubble formation. This increase is appreciable in spite of the initial high gas saturation. The gas drive following the slow rate of pressure decline shows no significant increase in oil recovery. Identical tests on a sandstone core sample (uniform porosity) showed no effect of bubble formation on oil recovery.

The significant difference between the limestone core tests, therefore, is the increased oil recovery resulting from the formation of a large number of bubbles during the 2,100 psi per hour pressure decline solution gas drive. *For the other case, where very few bubbles were formed, the performance is a continuation of the normal external gas drive behavior.* On the basis of the above results, there is reason to believe that similar behavior should be observed at lower gas saturations. This would mean that in the field, where a small number of bubbles are formed, the oil recovery performance under a solution gas drive might approach that predicted from the flow characteristics measured in the laboratory by an external gas drive.

LONG CORE TESTS

The preceding tests substantiate the theory concerning the role of bubble formation on the recovery of oil from non-uniform porosity limestones. However, a field begins its producing history with no gas saturation, and the previous tests began with a connected gas saturation initially much greater even than the final gas saturation in a depleted reservoir. This difference is believed to be irrelevant with respect to the conclusions already reached. On the other hand, the actual establishment of the initial flowing gas saturation in a reservoir is a complex process. To bridge this gap between field conditions and the tests described to this point, experiments have been made in which no initial gas saturation was present, and in which bubble formation rates approached those for reservoir conditions.

The first consideration in selecting the operating conditions for such a test was to decide on the minimum practical rate of pressure decline. Obviously, a rate of 0.1 to 1 psi per day was unsatisfactory from the time standpoint alone. A decline rate of 10 psi per day was selected. This value was not considered too high, and it probably represents the maximum rate under which a reservoir might be produced even for a short interval of time.

The selection of a 10 psi per day rate of pressure decline presented a real problem with regard to end effect. At such a low rate of decline the pressure drop across a core is usually negligible, and end effect renders gas-oil relative permeability data meaningless. However, by a special core design this difficulty could be obviated. By increasing the flow resistance of the system, it was possible to operate at higher differential pressures with the same rate of pressure decline. The increase in the flow resistance of the system was accomplished in two ways. First a practical maximum length of core was used; namely, 6 ft. Secondly, addi-

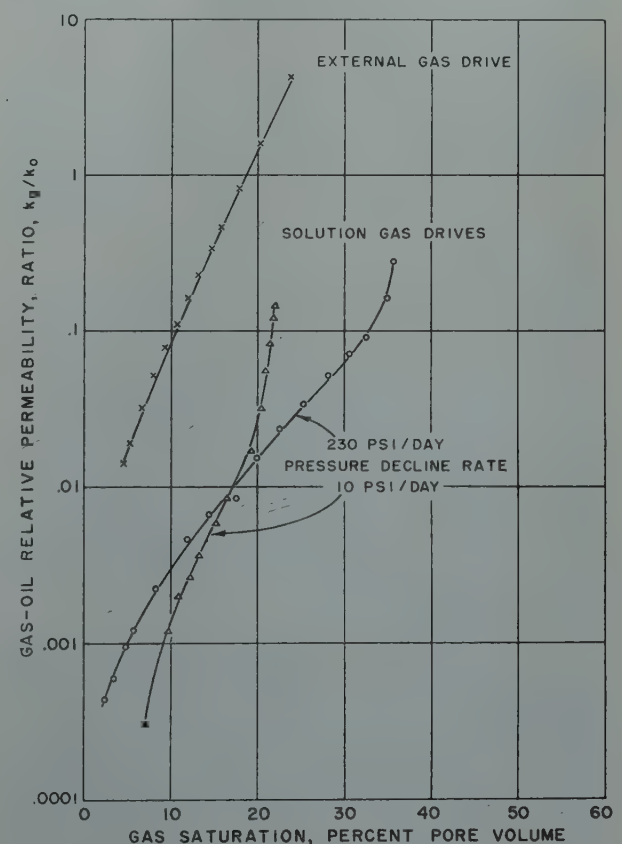

FIG. 6—RELATIVE PERMEABILITY CHARACTERISTICS OF CORDOVA SHELLSTONE.

Permeability = 200 mds: Porosity = 25 per cent.
Solution gas drives used a 200 psig bubble point solution of methane and C_{10}-C_{12}.

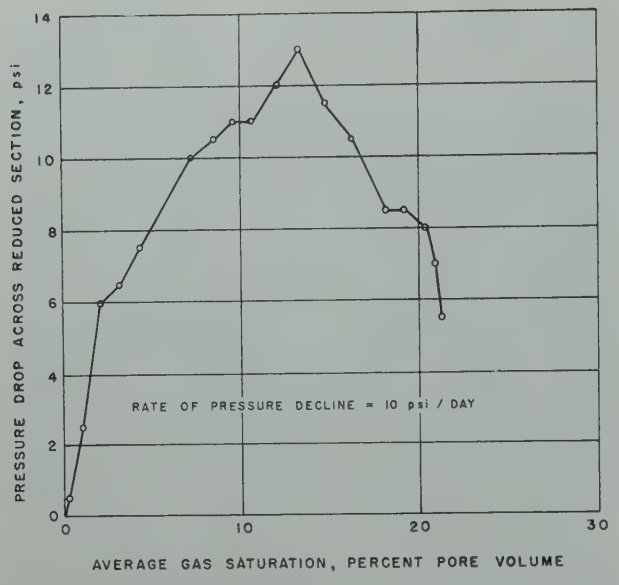

FIG. 7 — PRESSURE DROP PERFORMANCE ACROSS REDUCED SECTION OF CORDOVA SHELLSTONE.

tional resistance without a change in important capillary characteristics was obtained by reducing the cross-sectional area of the downstream end of the core. Because it was impractical to obtain an oil field core of the desired size, an outcrop (Cordova shellstone), was selected for these tests. The manner in which the core was shaped has already been described.

An external gas drive and two solution gas drives at widely different rates of pressure decline were performed on this large core sample. The results of these tests are presented by Figs. 6 through 8. Fig. 6 shows for these three tests the relationship between the gas-oil relative permeability ratio, k_g/k_o, and the gas saturation in per cent pore space. The divergence noted between the laboratory external and solution gas drives indicates that this rock has a non-uniform porosity.

The rates of pressure decline for the two solution gas drive runs were 10 psi per day and 230 psi per day. The reliability of the k_g/k_o data from the standpoint of end effect can be evaluated from the history of the pressure drop across the reduced section of the core and from gas-oil capillary pressure data. Capillary pressure characteristics indicated that end effect would be negligible as long as the pressure drop across the reduced section exceeded 1 psi. Fig. 7 presents the pressure drop history for the 10 psi per day run and shows that the test was not detrimentally influenced by end effect. The amount of end effect was, of course, even less with the fast decline rate.

The results of the two individual solution gas drive tests show a difference in recovery efficiency. At pressure depletion, the 10 psi per day decline rate test resulted in an oil recovery of 22 per cent pore space. This may be contrasted with the 36 per cent recovery achieved in the test carried out at the higher rate. This 64 per cent increase in oil recovery is attributed to an increase in the number of bubbles formed during the faster run.

Fig. 8 shows the wide variation in supersaturation which existed for the two individual solution gas drive tests. A calculation of the number of bubbles formed indicates that at the fast rate of pressure decline there were about 100 times more bubbles than at the slower rate. The effect which this increased number of bubbles had on the efficiency of oil recovery was not apparent until an average gas saturation of approximately 17 per cent pore space was reached. Beyond this saturation the difference in oil displacement efficiency for the two tests increased as depicted by the position of the separate k_g/k_o curves.

The increased number of bubbles formed during the rapid decline test does not explain the relative positions of the two solution drive curves of Fig. 6 in the range from 0 to 17 per cent gas saturation. Their relative positions can, however, be explained by visualizing the variation in extent of the connected gas saturation as a function of time. Since the pressure is always lowest at the downstream end of the core, the gas phase develops to a greater extent and becomes connected first in this part of the system. The connected portion of the gas phase then progresses upstream. This will result in the measurement of higher k_g/k_o values at a given average gas saturation than would exist if the connected portion of the gas phase was distributed uniformly throughout the core. This is also evident, at low gas saturations, in Figs. 1 and 2.

The differences in the depletion rates and the measured pressure drops across the system for the two runs of Fig. 6 show that the above explanation is probably correct. For the test carried out with a pressure decline rate equal to 10 psi per day there was no measurable pressure drop (0.5 psi could have been detected) across

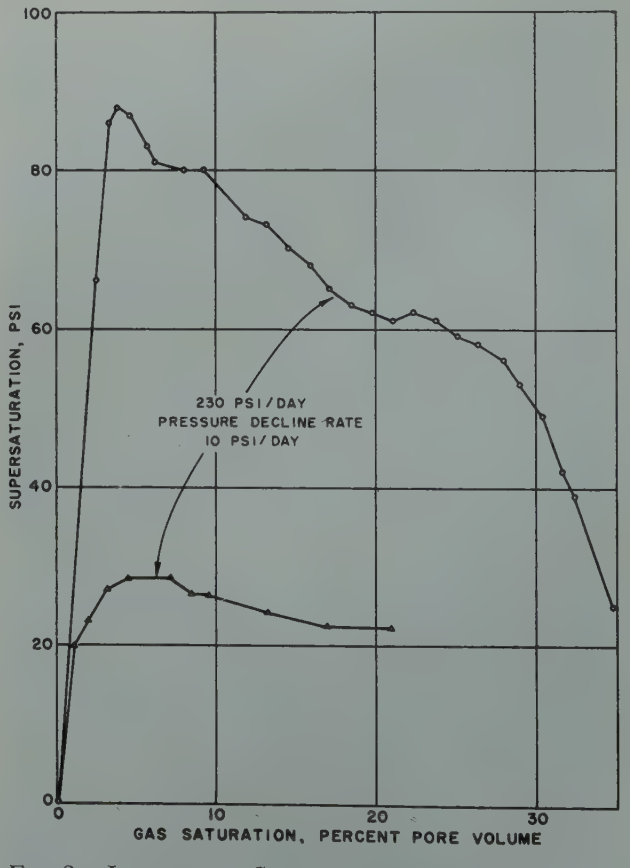

FIG. 8—LABORATORY SUPERSATURATION PERFORMANCE OF CORDOVA SHELLSTONE.

Initial bubble point pressure in each test was 200 psig using a solution of methane and C_{10}-C_{12}.

the 4½ in. diameter section, and a maximum pressure drop across the reduced section of 12 psi. For the fast rate of pressure decline the pressure drops were 4 to 6 psi and 200 psi, respectively. This indicates a definite possibility of progressive gas phase development during the fast pressure decline test. If the rate of progression of conductive gas saturation had been the same in the two tests, it can be reasoned that the measured relative permeability curve for the faster test would be to the right of the curve for the slower test throughout the entire range of gas saturation.

Significance of Study in Regard To Reservoir Performance

One objective of this study was to design a laboratory test which would give results applicable to the prediction of field solution gas drive performance. Fig. 3 shows that the number of bubbles formed under field rates of pressure decline (0.1 to 1 psi per day) would be less than 100 bubbles per cubic foot of reservoir rock. The exact number of bubbles would depend upon the rock and the fluids involved. Nevertheless, the value is an order of magnitude less than the number of bubbles calculated to have been formed in the 10 psi per day test discussed above.

On this basis it may be concluded that the results obtained from the above test do not represent normal field solution gas drive performance. It may be concluded from the above tests, however, that a decrease in the rate of pressure decline (at least throughout the range investigated in the laboratory) results in a lower efficiency of oil displacement from non-uniform porosity limestones. It may be proposed again that a limiting value on reservoir performance would be that predicted by the laboratory external k_g/k_o relationship, with the possibility that the field solution drive behavior would be somewhat more efficient. At least, the use of the external gas drive characteristics should give a conservative estimate of reservoir solution drive behavior.

In laboratory solution gas drives on non-uniform porosity limestones, oil recovery efficiency is seen to be improved appreciably by increasing rates of pressure decline. In the field the usual rates of pressure decline are 100 to 10,000 times slower than are practical in the laboratory. It has yet to be established that significant differences in oil recoveries from non-uniform porosity limestone reservoirs can be realized by varying the pressure decline rate within this lower range.

However, we cannot discount the possibility that unconventional production practices might be devised to yield recoveries approaching those obtainable in the laboratory. To achieve this goal would require a pressure decline rate of at least several psi per day. Nevertheless, it is possible that such a rate would need to be maintained for only a few days. The reason is that at any particular rate of pressure decline, the majority of bubbles are formed in a short time. For example, at about 10 psi per day pressure decline rate nearly all the gas bubbles are formed within three days. Of course, the most suitable time to subject the reservoir to such a fast decline rate would be when the reservoir pressure is near the bubble point. At this stage of depletion the gas-oil ratio is low, permitting maximum liquid withdrawal rates. Since the productivity of the wells would control pressure decline, the use of deep penetrating fractures would probably be indicated. Although these latter conclusions must, at present, be classed as speculative, their significance is great enough to demand further study.

CONCLUSIONS

1. The laboratory solution gas drive oil recovery efficiency of non-uniform porosity limestones increases with an increase in the number of gas bubbles formed. Pressure decline rate is the important factor in establishing the number of gas bubbles formed.

2. No practical test is available to measure in the laboratory the solution gas drive oil recovery performance at field rates of pressure decline. It is postulated that laboratory external gas drive data can be used to make a conservative prediction of field solution gas drive performance for non-uniform porosity limestone reservoirs.

3. The concepts presented in this paper indicate the possibility that increased field oil recoveries may be obtained from non-uniform porosity limestones by rapidly reducing reservoir pressure for a short interval of time. It has yet to be established that significant improvements in oil recovery from such reservoirs can be realized by varying the pressure decline rate within limits possible in the field. However, the possibility that recovery may be increased in this manner warrants further study.

ACKNOWLEDGMENT

The authors wish to express their appreciation to Herman Teel for his assistance in gathering the data for this paper.

REFERENCES

1. Stewart, C. R., Craig, F. F., Jr., and Morse, R. A.: "Determination of Limestone Performance Characteristics by Model Flow Tests," *Trans.* AIME, (1953) **198**, 93.
2. Kennedy, H. T., and Olson, C. R.: "Bubble Formation in Supersaturated Hydrocarbon Mixtures," *Trans.* AIME, (1952) **195**, 271.
3. Bernath, L.: "Theory of Bubble Formation in Liquids," *Ind. Eng. Chem.*, (1952) **44**, 1310.
4. Epstein, P. S., and Plesset, M. S.: "On the Stability of Gas Bubbles in Liquid-Gas Solution," *Jour. Chem. Phys.*, (1950) **18**, 1505.
5. Wood, J. W., Jr.: "Bubble Formation in Rangely Field, Colorado," M. S. Thesis, Texas A. and M. College, (unpublished).
6. Hunt, E. B., Jr., and Berry, V. J., Jr.: "The Evolution of Gas from Liquids Flowing through Porous Media," Paper to be presented at AIChE Meeting, Houston, May 1-4, 1955. ★★★

A NEW TOOL for PERFORATING CASING below TUBING

BLAKE M. CALDWELL
HARROLD D. OWEN
MEMBERS AIME

WELEX JET SERVICES, INC.
FORT WORTH, TEX.

T. P. 3961

ABSTRACT

The continued use of permanent-type well completion has pointed up the need for more powerful through-tubing perforating equipment. A new expendable shaped charge perforator has been developed in which the charges are run through the tubing in a vertical position and then opened out to a horizontal position when at the desired shooting zone. The performance of this new tool is comparable to that of conventional casing type perforators.

This paper describes the new tool and its applications. Performance data in targets and under various actual well conditions are presented.

INTRODUCTION

The general acceptance and increasing use of permanent-type well completion by the oil industry has indicated the need for through-tubing perforating equipment with performance comparable to that of conventional casing type perforators.[1,2] To achieve the performance desired, a new, expendable, shaped charge perforator has been developed with adequate power for effectively perforating both 5½-in. and 7-in. casing below tubing. This has been accomplished without resulting severe damage to the casing and can be obtained under extremes of pressure and temperature. The design of this new tool is a radical departure from previous concepts of tubing guns since it was felt that the two major limitations imposed by previous designs severely handicapped performance.

The first of these limitations was the restriction imposed upon the length of the charges by the necessary small inside diameter of the carrier. This resulted from the necessity for compromises in designing a hermetically sealed gun small enough to allow free passage through 2-in. tubing, yet with sufficient wall thickness to withstand some minimum pressure. In an effort to overcome this limitation, the charges were in some cases placed at an angle with the axis of the well with resulting loss in effective depth of penetration.

The second limitation concerned the extreme distance of the charges from the casing when the gun was fired. An example of the latter situation is demonstrated by the fact that a conventional 1¾-in. tubing gun centralized in 5½-in., 17-lb casing has a clearance of more than 1-9/16-in. on all sides. This means that a considerable portion of the force from each charge must be expended in penetrating this 1-9/16-in. of well fluid before it even reaches the casing. With the gun centered in 7-in., 23-lb casing, the amount of fluid penetration required of each jet is in excess of 2¼-in. In a situation where the 1¾-in. gun is touching one side of the 5½-in., 17-lb casing, the jets from the charges on the opposite side have more than 3⅛-in. of fluid to penetrate. A similar situation in 7-in., 23-lb casing necessitates the penetration of more than 4-9/16-in. of fluid. The penetrating effect of the charges is severely impaired in passing through so much fluid. Under such conditions, there is usually insufficient force left to penetrate the casing. Previous studies have shown the decided disadvantage of having to shoot through such an excessive quantity of well fluid.[4,5] The problem, then, was how to position large powerful charges close to the casing prior to firing and still manage free passage through 2-in. tubing.

The solution appeared to be in some method of folding sealed charge units in an open type, expendable, 1¾-in. carrier for travel through the tubing, and unfolding them upon their arrival at the shooting zone in the casing. It was desired to control the mechanism electrically from the surface through the regular shooting cable, making the release of the charges independent of the physical characteristics of the well, yet with a provision to prevent the gun from firing until the

[1]References given at end of paper.

Manuscript received in Petroleum Branch office on Sept. 10, 1954. Paper presented at Petroleum Branch Fall Meeting in San Antonio, Oct. 17-20, 1954.

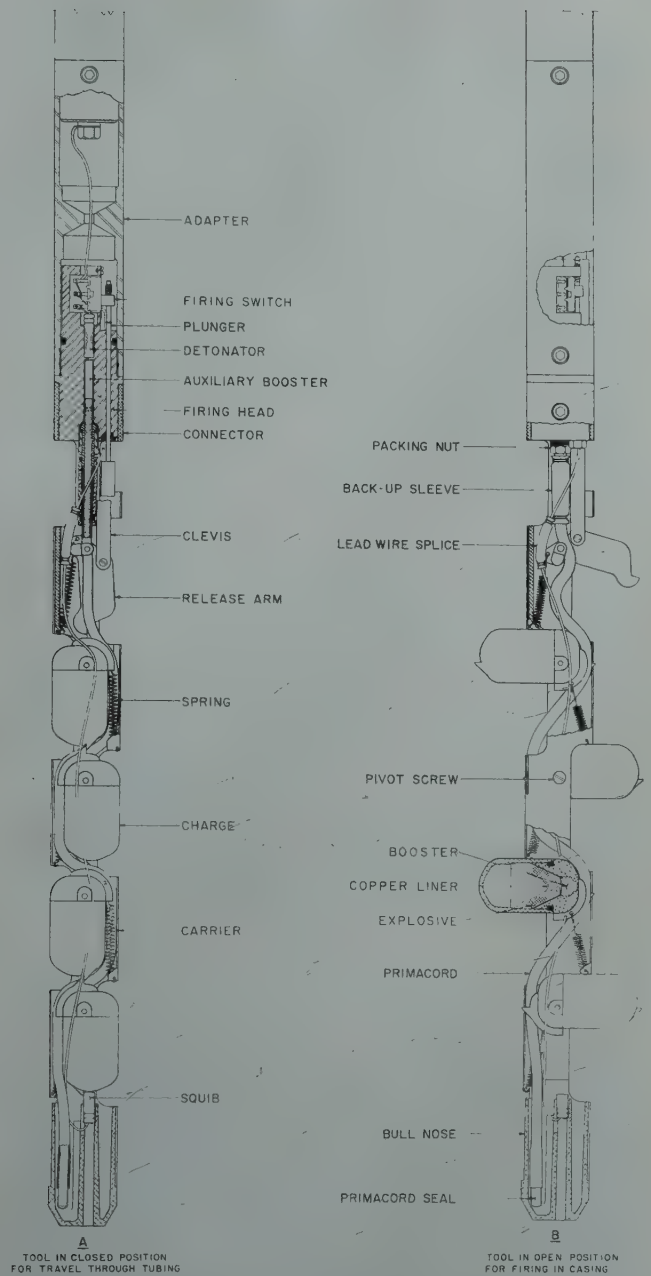

FIG. 1 — TUBING GUN IN CLOSED AND OPEN POSITIONS.

charges were in the proper firing position. Also, with the charges in the open firing position, it must be possible to reposition them and return the gun to the surface through the tubing, without damage to the tubing, should this be desired.

It was felt that any new design should extend the use of the gun over as great a scope of well conditions as possible; therefore, it was decided to design all components to operate at pressures of 10,000 psi and temperatures of 300° F.

This new gun travels through the tubing with the charges locked in a vertical position as shown at A in Fig. 1. When in position in the casing below the tubing, the charges are released at the will of the operator to a horizontal firing position as shown at B in Fig. 1. This innovation of swinging charges provides several distinct advantages, namely:

1. The design of the charge is not restricted by the inside diameter of the gun case, therefore a larger and more powerful charge is possible.

2. Since it is not necessary to angle the charges from the horizontal (unless desired) greater effective depth of penetration is achieved.

3. The spring loaded charges snap open and tend to center the gun in the casing thus distributing the clearance space more equally between the charges on each side of the gun.

4. Since the off-center pivoted charges open from a 1¾-in. diameter to a horizontal position at 180° phasing, resulting in a maximum effective opened diameter of 4⅜-in., they are much closer to the casing, thus minimizing the fluid through which each jet must pass, resulting in larger holes and deeper penetration.

DESCRIPTION OF NEW TUBING GUN

This tubing gun consists of three fundamental components; namely, carrier assembly, bottom release, and safety firing head.

A carrier, charges and connector make up the carrier assembly. The carrier, a brittle, thin wall, 1¾-in. diameter aluminum tube, accommodates four charges per foot at 180° phasing. Small holes are provided in the carrier for the charge pivot screws and the motivating extension springs, while large apertures provide an egress for the charges as they swing from a vertical position when in the tubing to a horizontal position when in the casing. The top of each aperture is placed to provide stops for charges after they have pivoted 90°.

The shaped charges consist of the conventional copper liner, temperature resisting high explosive, and a booster, housed in a die cast aluminum container. Detents at the top and bottom of each container, lock the charges together and allow them to open in a train action after the bottom charge is released.

The carrier assembly is joined to the firing head by a cast aluminum connector which provides a clean break between the expendable and retrievable parts when the gun is fired.

Each charge is detonated by high temperature RDX primacord, tightly covered with Hycar tubing as a protection from well fluids. This primacord originates in the firing head and weaves back and forth between the charges, guided by the groove in each cap which assures contact between the primacord and charges for positive and effective detonation.

The primacord terminates in the bull nose, a die cast unit protecting the bottom of the carrier and guiding it past collars in the tubing. It also holds the electrically detonated release squib in place against the lower detent of the bottom charge, holding it, and thereby all the charges, in position until the squib is sheared off by a current initiated at the surface.

The sequence of events, which allows the charges to be first released and then fired, originates in the expendable, but retrievable, steel firing head. Here, in a sealed compartment, are housed the explosive devices employed in detonating the primacord, and the safety switch mechanism which delivers current to the release squib and the detonator in the proper sequence.

The safety switch is a double pole, double throw switch actuated by a plunger, which is controlled by the release arm. In its down position, the switch grounds the main detonator, as a safety measure, and transmits current only to the release squib, see Fig. 2. In the up position, current is transmitted to the detonator, exploding it, the booster and the primacord successively. To prevent premature actuation of the switch, the release arm is locked in a down position by the top charge until all the charges have been released to assume their firing position. The release arm then swings out of the carrier like a charge, moving through a 70° arc and then closing the switch to the detonator circuit. Any restriction of the arm to less than 70° of travel prevents the gun from arming unless previous adjustments of the firing head has been made to allow firing at a lesser angle. Since the firing head is the sole trigger for the gun and is not dependent upon any part of the tubing or casing to arm it, the gun, in this sense, is independent of the physical characteristics of the well in which it operates. Should an open gun be withdrawn from the casing, back into the tubing, the release arm and charges will be forced back into a vertical position by the bottom of the tubing, returning the detonator circuit to ground and rendering the gun harmless.

A dimensional drawing of the cable head, magnetic casing collar locator, and gun assembly is shown in Fig. 3.

Tandem Carriers

The detail of the tandem connection shown in Fig. 4 illustrates the method of joining carriers to make a single, long gun. By inserting a tandem connector between the carriers, a rigid unit is created, while conventional splicing methods allow continuity of the primacord and the squib lead wire. The system of interlocking charges is maintained by a tandem release arm which replaces a charge at the tandem interval. Several units may be joined to extend the tubing gun to any desired length with no reduction in the efficiency of the gun.

Skipping An Interval

In situations where it is necessary to perforate adjacent zones with a relatively narrow unperforated interval between them in a single run, it is possible to assemble a gun without charges at the interval to go unperforated. To accomplish this and still retain the simple release principle based on interlocking charges, it is necessary to install a blank interval device, Fig. 5. This device consists of two tandem release arms connected by a ⅛-in. OD aluminum rod which transmits the train action of the charges in one group to the charges of the other group, allowing the normal operation of the complete gun, yet keeping the volume of debris to a minimum. A continuous piece of primacord is used to detonate both groups of charges in a method identical to that in a fully loaded gun. It weaves through the grooves of the top group of charges, coils in the blank interval of carrier, (serving upon detonation to break this section into small fragments), and resumes its normal pattern with the bottom charges, terminating in the bull nose.

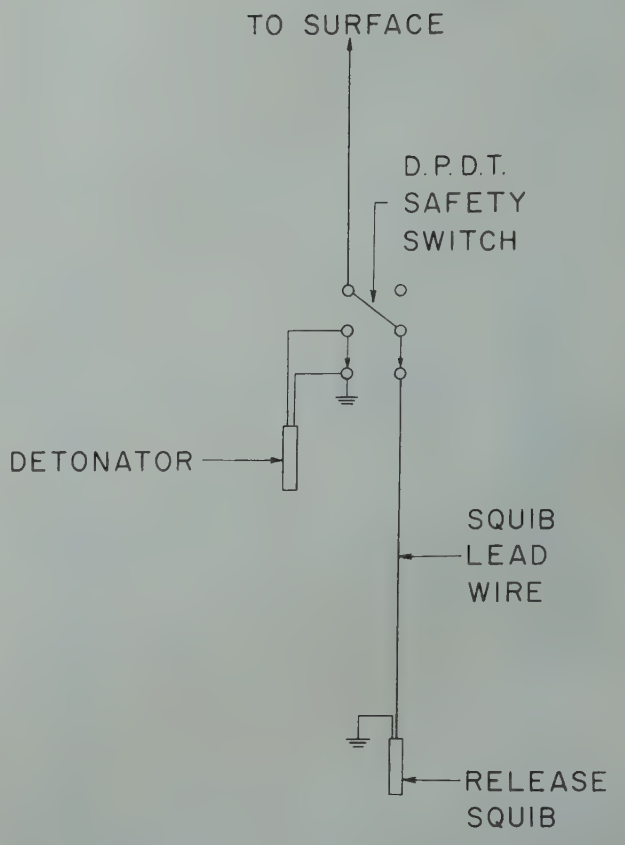

Fig. 2—Schematic Wiring Diagram Showing Safety Switch in Down Position.

SAFETY FEATURES

The swinging charges, which are the unique feature of this gun, are also the key to the safety of the mechanism because without their release it is impossible for the gun to fire. As was previously mentioned, the release arm at the top of the gun controls the firing switch. Prior to the actuation of the firing switch the detonator is grounded. Actuation of the firing switch can take place only after the top charge has released the arm and it has rotated to the set position. To confine the release arm to any position less than the set position, keeps the firing circuit continuously grounded. On the surface, an aluminum safety clamp is kept over the assembly, thus restricting the movement of the charges and the release arm. As soon as the gun enters the confinement of the lubricator, the lubricator takes over this function. At no time while the gun is in the lubricator or the tubing string is it possible for the release arm to swing out far enough to arm the gun.

If, after the gun has left the tubing, the charges are released and for any reason the gun fails to fire, it is an inherent characteristic of the design that they refold themselves into a locked vertical position inside the 1¾-in. carrier upon their re-entry into the 2-in. tubing. This action again grounds the firing circuit and the charges remain in this position until the gun is completely disarmed immediately upon the appearance of the firing head above the lubricator.

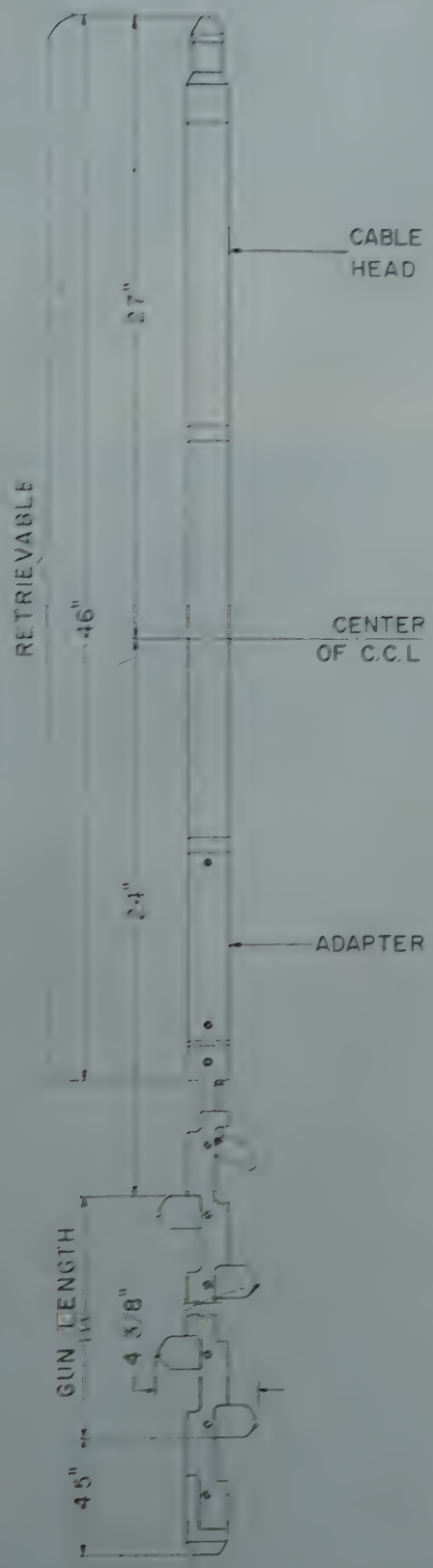

FIG. 3—DIMENSIONAL DRAWING OF COMPLETE TUBING GUN ASSEMBLY.

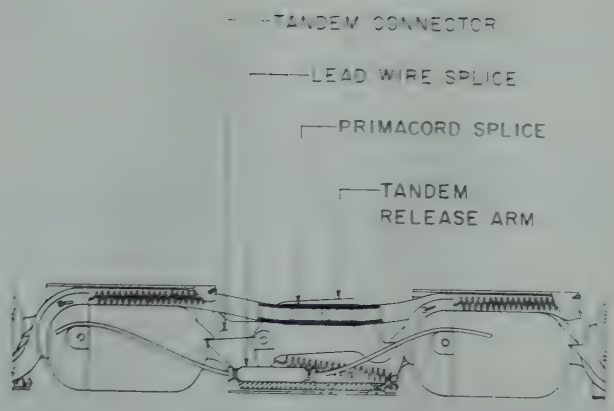

FIG. 4 — TANDEM CONNECTION.

PERFORMANCE

Laboratory tests were run to obtain performance data when firing through the maximum fluid possible in both 5½-in. and 7-in. casing. These tests were fired into prepared targets consisting of ⅜-in. steel plate of analysis and heat treatment similar to API N-80 casing, backed up by 43-day neat cement. Fig. 6 shows the results obtained by firing through ½-in. of fluid which simulates the condition of maximum clearance possible in 5½-in., 17-lb casing. The hole size is ½-in. with 9.1-in. penetration. Fig. 7 displays the results obtained when firing under fluid with 2-in. clearance, simulating the maximum clearance possible in 7-in., 23-lb casing. The entrance hole diameter in this case is 5/16-in. and the depth of penetration is 7.35-in. Fig. 8 illustrates the result of firing at the minimum angle of 45° where the OD of the gun is only 3⅝-in. Note the 0.53 x 0.60-in. diameter hole and 6.9-in. of effective (horizontal) penetration.

In an effort to evaluate the operation and performance of this new gun under actual well conditions together with resulting damage to unsupported casing, a series of field tests were arranged in an abandoned well on the Gulf Coast. This well contained 7-in. casing plugged at 7,000 ft and was filled with 11.6 lb mud. Separate target assemblies consisting of a 12-ft length of 5½-in., 17-lb casing, plugged at the bottom and connected by a perforated swage nipple to 2½-in. tubing, were run successively to depths of 5,000, 4,000, 3,000 and 2,000 ft. In each case a 4-ft section of the new perforating tool was lowered through the tubing on the wire line in the conventional manner and was positioned in the center of the 12-ft length of casing.

After firing, the tubing was pulled which enabled recovery of the debris, examination of position and location of holes and splitting effect on casing. Visual examination of all targets showed two rows of eight perforations 180° apart with all holes over ½-in. in diameter. The astonishing result shown by these tests was the minimum amount of damage to unsupported casing caused by the gun. The maximum splits around the holes were only hairline cracks extending approximately ½-in. from the perforation with many of the holes showing no cracks at all. The debris showed excellent breakup and a minimum fill-up, as expected, and in every case all debris was found in the bottom of the casing. The largest pieces recovered were from the

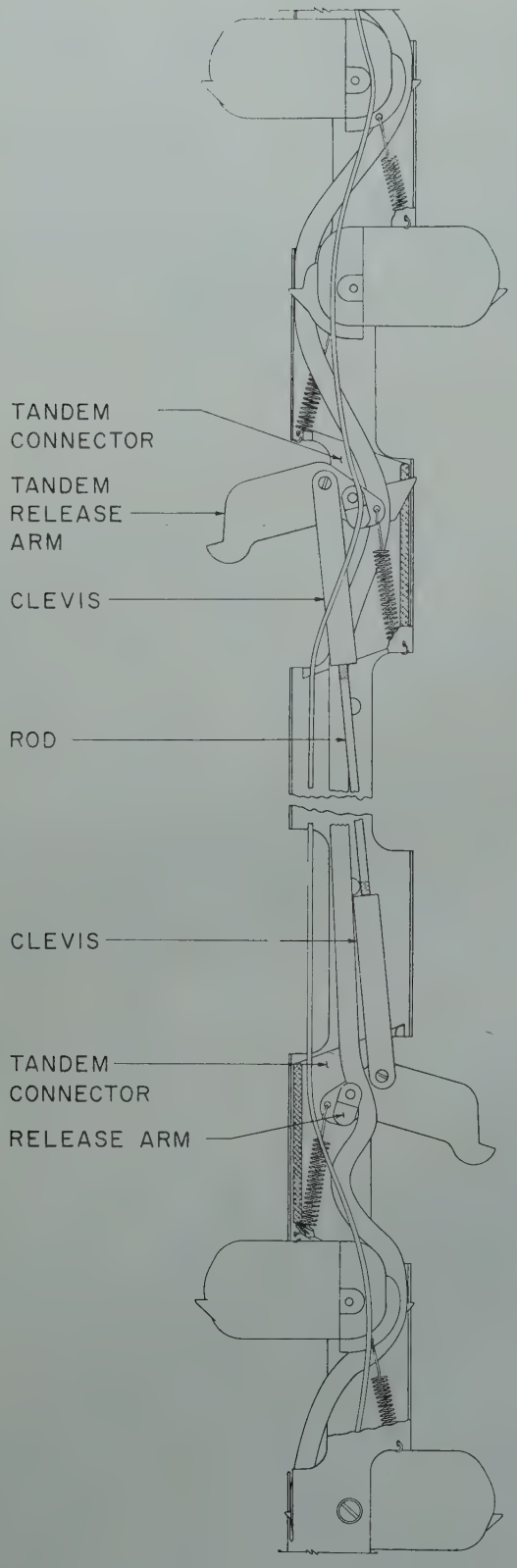

FIG. 5 — BLANK INTERNAL DEVICE.

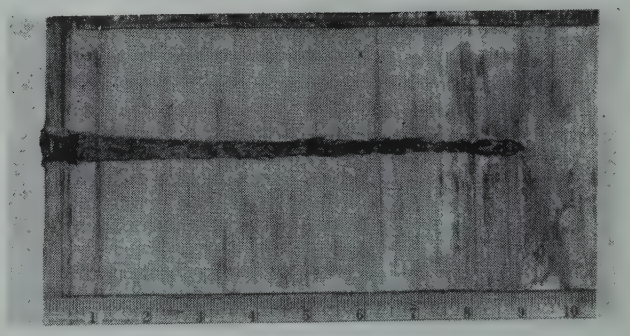

FIG. 6 — TEST SHOT THROUGH ½-IN FLUID AND ⅜-IN STEEL INTO 43-DAY OLD NEAT CEMENT. ENTRANCE HOLE 0.50-IN, PENETRATION 9.1-IN.

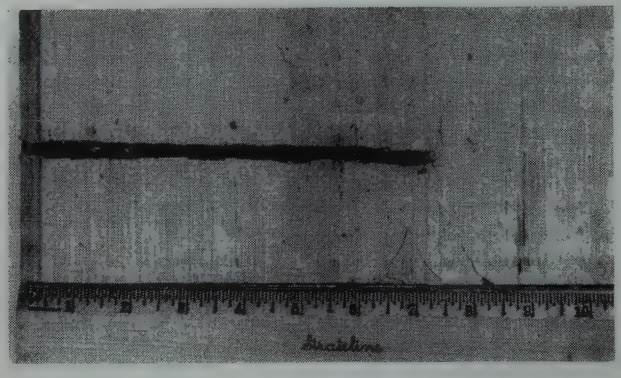

FIG. 7 — TEST SHOT THROUGH 2-IN FLUID (MAXIMUM CLEARANCE FOR THIS GUN IN 7-IN, 23-LB CASING). ENTRANCE HOLE 5/16-IN, PENETRATION 7.35-IN.

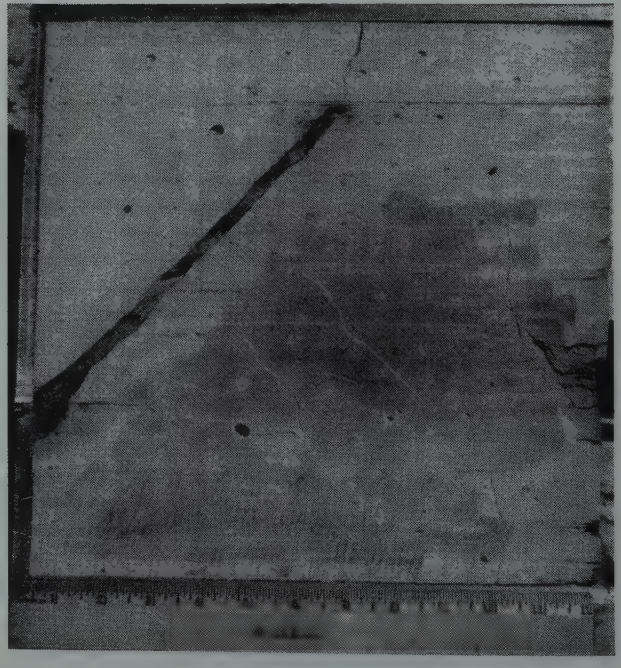

FIG. 8 — TEST SHOT AT 45° ANGLE. ENTRANCE HOLE 0.53-IN X 0.60-IN. TOTAL EFFECTIVE PENETRATION 6.9-IN.

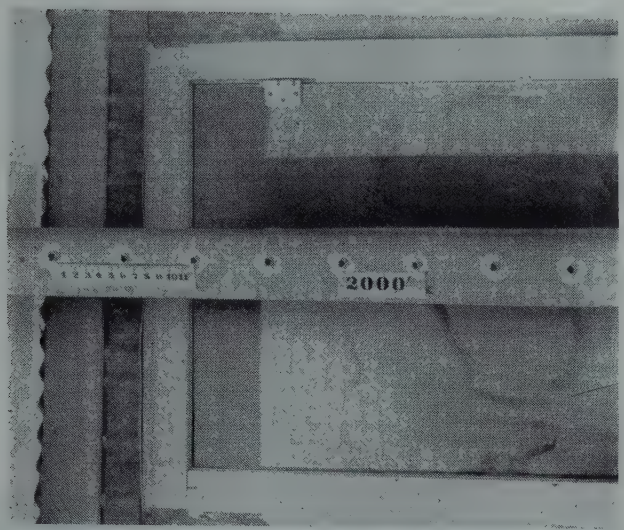

FIG. 9 — CLOSE-UP OF UNSUPPORTED 5½-IN, 17-LB, J-55 CASING SHOT WITH A 4-FT GUN AT 2,000 FT IN 11.6-LB MUD.

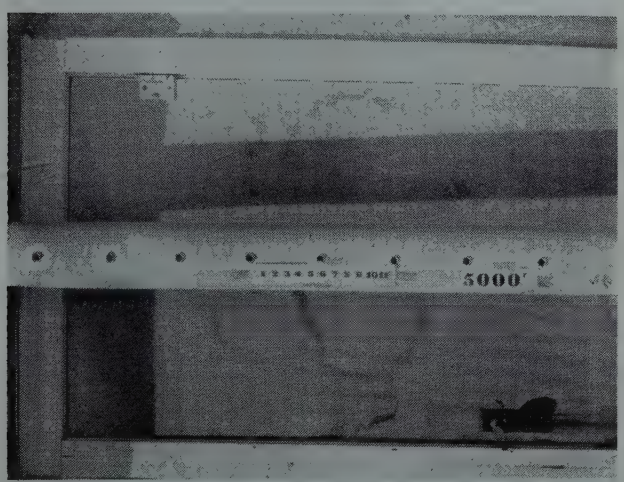

FIG. 10 — CLOSE-UP OF UNSUPPORTED 5½-IN, 17-LB, J-55 CASING SHOT WITH A 4-FT GUN AT 5,000 FT IN 11.6-LB MUD.

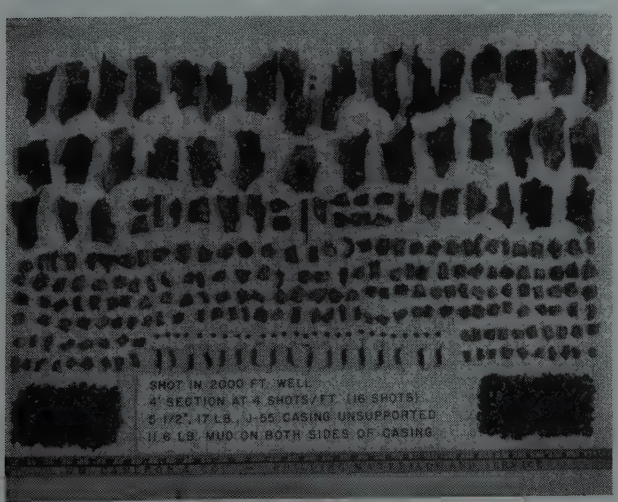

FIG. 11—DEBRIS FROM A 4-FT GUN RECOVERED FROM TEST TARGET SHOWN IN FIG. 9.

sand cast bull nose. This part has subsequently been redesigned as a die casting of one quarter the weight which has resulted in greatly improved breakup characteristics.

Figs. 9 and 10 show the casing from the 5,000 and 2,000-ft tests. Figs. 11 and 12 are photographs of the debris from these tests as removed from the test targets upon return to the surface. Fig. 13 is a composite photograph of all four sections of casing used in the test.

As representative of field results to be obtained with this new gun, the following brief resume of actual case histories are presented:

A well in the Gulf Coast had been perforated in October, 1953 with a conventional type tubing gun and was flowing 25 B/D at 200 psi tubing pressure. After perforating on Feb. 5, 1954 with this new gun, the pressure built up to 700 psi and production increased to 100 B/D where it has remained to date. The recorded bottom hole temperature of this well was 278° F.

In another Gulf Coast field, a major oil company had found all previous attempts to perforate a particularly hard formation with a conventional 1¾-in. tubing gun unsuccessful due to inadequate penetration. They had therefore established the practice of setting 2½-in. tubing to enable the use of the more powerful 2-3/16-in. conventional tubing gun. Upon agreement to use this new 1¾-in. tubing gun in a test, 2-in. tubing was set. Pressure built up immediately after the gun was fired, giving excellent results which were above expectations.

In still another field a well had been perforated twice before with a conventional 1¾-in. tubing gun and production was still unsatisfactory at 40 B/D at 50 to 75 psi flowing pressure. After perforating with 2 ft of the new gun, the tubing pressure built up to 900 psi and the well continued to flow at 90 B/D.

FIELD OPERATION

1. Gauging Tubing—Because of the nature of the construction of this gun it is not feasible to force it, either with weight or by "spudding," through restrictions in the tubing. To guard against possible damage to the gun and assure entry through the tubing to the zone to be perforated, it has proved advantageous to run a 1¾-in. OD tubing gauge equal in length to the gun, up to a maximum of 20 ft, prior to each shooting run. This practice will reveal any crooked or "tight" joints, excessive scale, or restrictions caused by special devices in the tubing and will allow remedial measures to be taken before the gun is run, resulting in lower costs and time saved.

2. Length of Gun—The standard length of this gun is 10 ft; however, the design is such that it can be cut to any desired shorter length. A tandem connector is employed where lengths in excess of 10 ft are required. To date wells have been successfully perforated with guns ranging from 6 in. to 45 ft in length. Fig. 14 is a view of this 45-ft gun in position just prior to being lowered into the well. This is by no means the maximum to which the gun may be extended as there is no reason that a single gun many feet in length could not be successfully fired.

Where guns of extreme length are used, and a derrick is present, they may be raised in one piece and lowered into the well. Where no derrick is available, 30-ft lengths of the gun may be raised with a gin pole and splicing done as the units are lowered into the well.

3. Fittings on Lower End of Tubing—For best performance in retrieving an opened gun, it is recommended that the lower end of the tubing be equipped with expendable tubing plug nipple or left plain. Swage fittings of any size should be avoided because of their detrimental effect upon the locking sequence of the charges.

4. Debris in the Well—Because of the mechanical action of this tubing gun in swinging its charges into firing position, it is desirable that the well fluid be circulated sufficiently to remove pieces of cement, rubber, lost circulation material, and other debris capable of interfering with the free movement of the charges. Removal of this material assures the gun of normal operation. Circumstances may arise in which it is impossible to circulate the well fluid sufficiently to remove this debris. In such cases it is possible to pack the gun with wheel bearing grease to eliminate the deposit of debris in the gun which would interfere with the proper opening of the charges.

5. Well Fluids—Well fluids must also be considered in conditioning the well for the tubing gun. Any acids in the well will have a highly detrimental affect upon the aluminum. Parts of the gun may be completely dissolved by acids left from acidizing operations as a result of insufficient circulation after the job. These acids must be removed or diluted to a degree that will render them harmless to the aluminum.

Extremely heavy mud presents another problem. This gun has been operated successfully in 13-lb, 200-viscosity, oil base mud in which the rate of descent was reduced to as low as 13 ft/min. It is far better, however, to provide a less viscous fluid to allow faster descent and greater ease in opening the charges to the firing position. It is recommended that water or oil be used as a well fluid.

6. Tubing Depth With Relation to the Perforating Zone—To reduce the possibility of complications resulting from the upward surge of force from the detonation of the charges, it is recommended that a minimum clearance of 15 ft be maintained between the bottom of the tubing and the top of the zone to be perforated. When this 15-ft minimum is used, the tubing should be kept full of fluid to provide a cushion.

7. Well Depth With Relation to the Perforating Zone—In its firing position, the bottom charge is less than 6 in. from the bottom of the gun, making it possible to perforate very close to the bottom of the well.

8. Shooting in Restricted Areas—In situations where it is known that the inside diameter of the casing has been appreciably reduced by a sheath of mud, cement, paraffin, or some other material, it is possible to adjust the firing head in the field to fire at intermediary angles below 90°.[6] At the lowest recommended angle of 45°, the outside diameter of the gun is 3⅝-in.

Statistics on the effective penetration perpendicular to the casing when firing at reduced angles of 45° and 70° are shown in Figs. 15 and 16 respectively.

9. Dissolving Debris in the Well—Because of the material and the excellent breakup characteristics of this gun, the fragments are dissolved more rapidly by

FIG. 12—DEBRIS FROM A 4-FT GUN RECOVERED FROM TEST TARGET SHOWN IN FIG. 10.

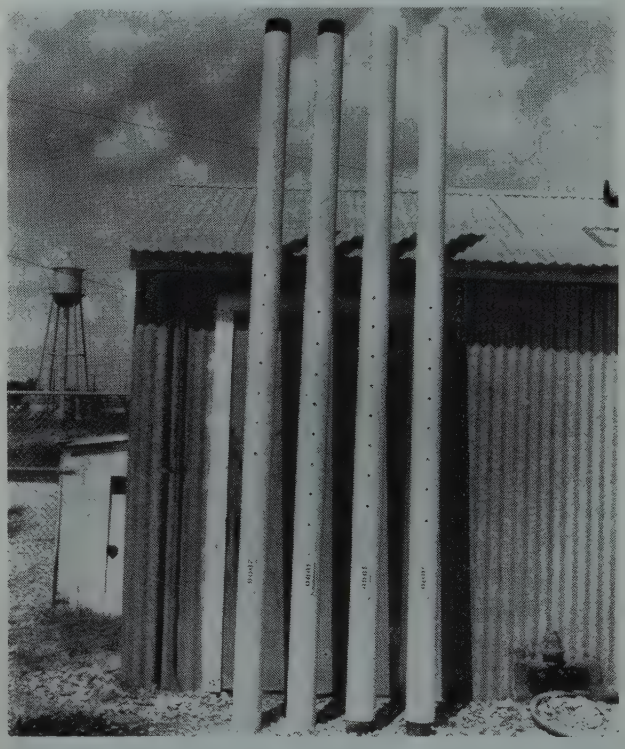

FIG. 13—RESULTS OF TESTS IN UNSUPPORTED 5½-IN, 17-LB CASING.

TABLE 1—SUMMARY OF WORK DATA

Using data compiled from the first 764 jobs performed to Nov. 1, 1954 with this tubing gun, the following information was derived:

Deepest Well	13,310 ft—2-in. tubing—5½, 20-lb casing—120 holes
Shallowest Well	645 ft—2-in. tubing—5½, 11.8-lb. casing—32 holes
Average Depth	6,192 ft.
Type of Completion	60 per cent workover 40 per cent new wells
Longest Gun	45 ft—180 charges at 9,961 ft—9⅞-in. hole—2-in. tubing, 5½-in., 20-lb casing
Shortest Gun	6-in.—2 charges at 5,349 ft—2-in. tubing—5½-in. casing
Average Length Gun	10 ft—40 charges
Greatest Number of Charges Shot in One Well	552
Casing Size	5½-in.—74 per cent 7-in.—20 per cent Other—6 per cent
Highest Recorded Temperature	294° F
Highest Bottom Hole Pressure	8,400 psi
Highest Tubing Pressure at Which Gun Was Lowered Without Pressure Feed in Equipment	900 psi with 3/16-in. line and 600 psi with 7/16-in. line
Highest Tubing Pressure at Which Gun Was Lowered With Grease Tube Type Packoff [7]	2,200 psi
Highest Tubing Pressure at Which Gun Was Withdrawn from the Well	2,750 psi with 3/16-in. line and 1,200 psi with 7/16-in. line

FIG. 14—A 45-FT GUN JUST PRIOR TO ITS ENTRY INTO THE WELL PERFORATED 9,961 FT. WELL FLOWED WITH 1,900 PSI PRESSURE.

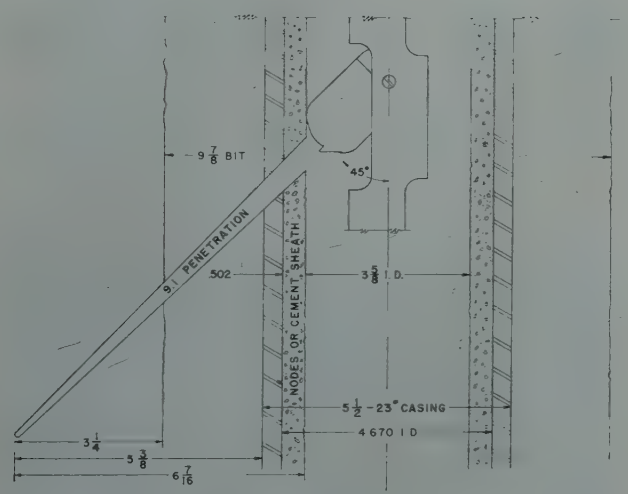

FIG. 15 — LATERAL PENETRATION OF TUBING GUN CHARGE IN RESTRICTED CASING AT 45 DEGREES.

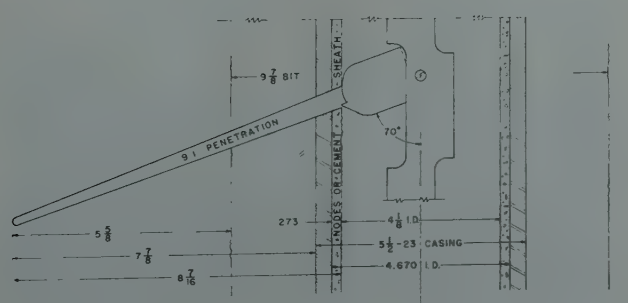

FIG. 16 — LATERAL PENETRATION OF TUBING GUN CHARGE IN RESTRICTED CASING AT 70 DEGREES.

the well fluids. In cases where it is necessary to dissolve the debris immediately, a caustic solution may be used. In one instance, 500 lbs of caustic soda was mixed with 3½ bbl of water and this solution was pumped to the debris and allowed to remain one hour after which the solution was pumped past the debris at the rate of ¼-bbl every 15 minutes. This procedure dissolved the debris and left the casing free for perforating.

10. Wells Containing 1-25/32-in. ID Nipples—Wells containing Otis Type "J" landing nipples or 1-25/32-in. ID pump seating nipples in the tubing string have been successfully shot with this new gun. Because of the flexibility of the opened carrier as compared with the rigid sealed gun tubes in conventional type tubing guns, it is much easier to pass through these restricted areas. To assure the gun will pass through such a nipple, a 1.780-in. ID gauge is passed over the entire length of the assembly prior to running the gun in the well.

CONCLUSIONS

This new tubing gun, utilizing a swinging jet charge, has increased the scope and effectiveness of permanent-type well completion by providing:

1. A larger charge placed closer to the casing, resulting in larger hole size and greater depth of penetration.

2. Equipment capable of operating at pressures up to 10,000 psi and temperatures of 300° F.

3. Increased fragmentation of the expendable aluminum parts.

4. No objectionable casing damage.

5. Extra safety features not provided in any conventional perforators.

ACKNOWLEDGMENT

The authors wish to express their appreciation to the Shell Oil Corp. and the Humble Oil & Refining Co. for their cooperation in field testing this equipment. They also wish to thank the Welex Jet Services, Inc., for permission to publish this data and to John J. Robertson and R. L. Robinson of this organization for their assistance and cooperation.

REFERENCES

1. Huber, T. A., and Tausch, G. H.: "Permanent-Type Well Completion," *Trans.* AIME (1953), **198,** 11.
2. Kastrop, J. E.: "Permanent-Type Well Completion," *World Oil,* (March, 1954).
3. Lebourg, M. P., and Hodgson, G. R.: "A Method of Perforating Casing Below Tubing," *Trans.* AIME (1952), **195,** 303.
4. Reed, J. E., and Carr, F. F.: "Effect of Temperature, Pressure, Standoff Upon Perfo-Jet Penetration," *Oil and Gas Jour.,* (August, 1950), 69.
5. BUSH, R. E.: "Factors Affecting Perforated Completions," *Pet. Eng.,* (November, 1953), B-59.
6. Huber, T. A., Tausch, G. H., and Dublin, J. R.: "A Simplified Cementing Technique for Recompletion Operations," *Trans.* AIME, (1953), **198,** 11.
7. McKinney, H. E.: "A High-Pressure Wellhead Lubricator," *Trans.* AIME, (1952), **195,** 261. ★★★

DISPLACEMENT of OIL from POROUS MEDIA by MISCIBLE LIQUIDS

J. OFFERINGA
C. van der POEL

KONINKLIJKE/SHELL LABORATORIUM
AMSTERDAM

T. P. 3963

ABSTRACT

The report describes scaled model experiments on the recovery of oil from porous sands by the injection of miscible liquids [solvents] and the subsequent recovery of the solvents by water flooding. Special attention has been paid to the scaling problem.

Scaling rules are deduced and their correctness is checked by carrying out experiments in tubes of various sizes.

Data are submitted on the effect of the viscosity ratio oil-solvent on the efficiency of the displacement process, the viscosity ratio varying from 1.5 to 5,000.

Breakthrough recoveries obtained when flooding with kerosene as a solvent, are equal to those obtained in water flooding at the same viscosity ratio, indicating that the phenomenon of viscous fingering is decisive. After breakthrough, however, flooding with a miscible liquid becomes much more efficient than a water flood and this is more pronounced as the viscosity ratio oil-solvent is higher.

Although high oil recoveries are obtained and most of the solvent in the sand can be recovered by a subsequent waterdrive, a straight flood with miscible liquids does not appear economically attractive because of the large quantities of solvent required. Therefore, a circulation process is introduced, the features of which are described in this paper. Though by means of this circulation process the amount of solvent required can be drastically reduced, the process is not yet economic.

Manuscript received in Petroleum Branch Office on Aug. 2, 1954. Paper presented at Petroleum Branch Fall Meeting in San Antonio, Oct. 17-20.

SCOPE OF THE INVESTIGATION

The recovery efficiency by water flood of oils of viscosities exceeding 50 cp is low. As interest in production of these highly viscous oils is growing at the moment, it was considered worthwhile to gain basic information on the feasibility of first flooding such oils with a low viscous miscible liquid [solvent] and subsequently producing the latter in a conventional way, e.g. by water flooding. The method has the obvious drawbacks that return on the investment is delayed until water flooding has begun and that it requires the investment of a more valuable product to produce a less valuable one. On the other hand, it may be expected that the displacement of one liquid by another is more efficient when the two liquids are miscible than when they are immiscible. As laboratory data on this point are scanty, the present investigation seemed justified.

Another argument for carrying out these experiments is that they present a valuable contribution to our concepts of the scaling problem in reservoir engineering studies. Some major difficulties which are encountered in the scaling of the waterflooding process such as the scaling of the capillary forces and the difficulty of obtaining the same permeability characteristics in the model do not present themselves in this case. As the fluids are miscible capillary forces do not play a role and as there is only one fluid phase, Darcy's law is valid in its original form. Consequently it is felt that the scaling rules can be deduced with a greater amount of certainty.

An essential feature of the experiments is that they are scaled model ones, which are, however, somewhat

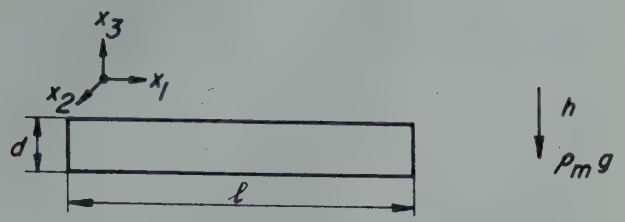

FIG. 1 — DIAGRAM ILLUSTRATING DIRECTION OF GRAVITATIONAL FORCE.

limited in scope in that they represent the rather ideal prototype of a homogeneous loose sand body completely saturated with a viscous oil that is subjected to a linear flood.

The experiments carried out can be divided into two groups:

1. Those carried out to obtain basic information on the displacement process only without considering any economic aspects. These experiments at the same time present a valuable contribution to our conceptions of the scaling problem in reservoir engineering studies.
2. Experiments in which the merits are evaluated of a procedure which aims at reducing the large amounts of solvent required in a straight flood for displacing the viscous oil. A recycling process is described in which the oil viscosity is gradually lowered until a viscosity level is obtained at which water flood can be successfully applied. In this way relatively small amounts of displacing miscible liquid may be sufficient. The cheapest displacing liquid will probably be a low viscous crude.

SCALING RULES

Experiments have been made in various horizontal cylindrical tubes [length l, diameter d], filled with sand of permeability k and completely saturated with oil of viscosity η_o. A miscible liquid [solvent] is injected at a constant rate of q at one end of the tube. The quantities of oil and solvent produced at the other end are measured.

Hydrodynamically our problem is governed by the equations of continuity and Darcy's law. If the oil is considered to be incompressible, the equation of continuity for it, taking diffusion of oil in solvent into account, may be written as:

$$-f\frac{\partial c_o}{\partial t} - \sum_i \frac{\partial}{\partial x_i}[c_o v_i] + fED_o \sum_i \frac{\partial^2 c_o}{\partial x_i^2} = 0 \quad (1)$$

where $i = 1, 2, 3$.

Equation 1 obtains for an elementary cube, the dimensions of which are large compared to those of the pores. The v_i in the equation denotes a mean velocity component in a certain direction; in the pores, however, the direction of flow may be at angles to this mean flow direction. Thus the actual distance along which diffusion must occur is longer than in a non-porous medium. For this reason in the third term of Equation 1 the effective diffusion coefficient is indicated by ED_o, where D_o is the normal diffusion coefficient in a non-porous medium and E is a dimensionless factor which will be smaller than one and which depends on the pore configuration.

Apart from this addition of the factors E and f, Equation 1 is identical to the equation of continuity for fluid flow in a non-porous medium. The factor f has been added to take into account that v_i is defined as the superficial velocity in accordance with reservoir engineering practice.

By substituting

$$x_i = X_i d \text{ and } t = T\frac{d^3}{q} \quad . \quad . \quad . \quad . \quad . \quad . \quad (2)$$

we can write the above equation in a dimensionless form:

$$-f\frac{\partial c_o}{\partial T} - \sum_i \frac{\partial}{\partial X_i}\left[\frac{c_o v_i d^2}{q}\right] + \frac{fED_o d}{q}\sum_i \frac{\partial^2 c_o}{\partial X s_{i2} + e + X_i^2} = 0 \quad . \quad . \quad . \quad (3)$$

A similar equation obtains for the solvent component, which can easily be found by replacing the index o in Equation 3 by s.

Also Darcy's law obtains

$$v_i = -\frac{k}{\eta_m}\left[\frac{\partial p}{\partial x_i} + \delta_i \rho_m g\right] \quad . \quad . \quad . \quad . \quad . \quad (4)$$

where $i = 1, 2, 3$ and $\delta_1 = \delta_2 = 0$ and $\delta_3 = 1$ [Fig 1].

By introducing the same transformation (2), equation 4 can be written in a dimensionless form as follows:

$$\frac{v_i d^2}{q} = -\frac{\partial}{\partial X_i}\left[\frac{kpd}{q\eta_m}\right] - \delta_i \frac{\rho_m g k d^2}{q\eta_m} \quad . \quad . \quad (5)$$

From equations 2, 3 and 5 it is seen that the following dimensionless products pertain to our problem:

a. independent variables: $\frac{x_i}{d}$ and $\frac{qt}{d^3}$

b. dependent variables: $\frac{v_i d^2}{q}$ and $\frac{kpd}{q\eta_m}$

c. coefficients: $\frac{\rho_m g k d^2}{q\eta_m}$, $\frac{q}{D_o d}$, $\frac{q}{D_s d}$

Instead of the last two coefficients we may also introduce one of them and the ratio of the two viz. D_o/D_s.

It should be noted that f, c_o, c_s and E are dimensionless. Consequently, they may be left out of the dimensionless products if we consider it as an obviously necessary condition that porosity, initial saturation and pore configuration are the same in model and prototype. If this is done and scaling is correct according to the dimensionless products derived, then c_o and c_s will have the same value at each scaled time and in each scaled point in model and prototype. If, f, C_o, C_g and E are not identical in model and prototype, they should be included in the dimensionless groups in the same way as the other parameters.

The following relations also hold:

$$c_s = 1 - c_o \quad . \quad . \quad . \quad . \quad . \quad . \quad . \quad . \quad . \quad (6)$$

$$\rho_m = c_o\rho_o + c_s\rho_s \quad . \quad . \quad . \quad . \quad . \quad . \quad . \quad . \quad (7)$$

$$\eta_m = \eta_m[c_o, \eta_o, \eta_s] \quad . \quad . \quad . \quad . \quad . \quad . \quad . \quad (8)$$

From equations 6 and 7 it follows that:

$$\frac{\rho_m}{\rho_o} = c_o + [1 - c_o]\frac{\rho_s}{\rho_o} \quad . \quad . \quad . \quad . \quad . \quad . \quad (9)$$

Consequently ρ_m in $\frac{\rho_m g k d^2}{q\eta_m}$ may be replaced by ρ_o if the group $\frac{\rho_s}{\rho_o}$ is introduced as c_o will nowhere differ from its prototype value.

According to Equation 8 η_m can be written as $\eta_m = \Phi\left[\frac{\eta_o}{\eta_s}, \eta_s, c_o\right]$, where Φ is some [complicated] function. Therefore, in groups which contain η_m, it may be replaced by η_o if a new group η_o/η_s is introtroduced and η_s is taken equal to its value in practice, c_o being everywhere the same in prototype and model.

As the ratios η_o/η_s, ρ_o/ρ_s and D_o/D_s and in addition η_s must be the same in model and in prototype, *it is almost imperative to use the same liquids in both cases.*

One may wonder why the density of the mixture ρ_m can be replaced in the dimensionless group by ρ_o introducing only the ratio ρ_s/ρ_o, while η_m cannot be replaced by η_o without setting both the ratio η_o/η_s and η_s. The reason for this is that ρ_m/ρ_o is a function of ρ_s/ρ_o only, whereas such a simple relation does not exist between η_m/η_o and η_s/η_o.

The variables $\frac{v_1 d^2}{q}$ cannot easily be measured in our experiments as it involves a determination of the flow velocity components in each point of the tube. However, for the outflow end of the tube $\frac{v_1 d^2}{q}$ can be transformed into a more practical form. This is seen by multiplying with the dimensionless factor $1/4\pi c_o$, giving $\frac{1/4\pi d^2 c_o v_1}{q}$. The nominator of this group presents the oil production per unit time [q_o]. Thus the variable $\frac{q_o}{q}$ has been introduced, which is applied in its integrated form $\frac{\int q_o dt}{\int q dt} = \frac{R}{Q}$ where R is the quantity of oil produced and Q the total production [oil and solvent]. Both quantities are reported as percentages of the original amount of oil in place [= pore volume of the sand for an initial oil saturation of 100 per cent]. As oil and solvent are considered to be incompressible p can be replaced by $\triangle p$ [pressure difference across the tube].

Consequently, the result of an experiment can be reported by giving the dependent variables R [recovery] and $\frac{k \triangle pd}{q\eta_o}$ [dimensionless pressure number] as functions of the independent variable $\frac{qt}{d^3}$ [dimensionless time number]. Expressed in this way model and prototype should yield identical results, provided that the following dimensionless coefficients are the same:

$$\frac{q}{D_o d}, \quad \frac{\rho_o g k d^2}{q\eta_o}, \quad \frac{\eta_o}{\eta_s}, \quad \frac{\rho_o}{\rho_s}, \quad \frac{D_o}{D_s}$$

It will be clear that in order to have the same value in model and prototype the independent variables $\frac{x_i}{d}$ require the geometrical similarity between model and prototype.

TABLE 1 — VALUES OF THE VARIABLES FOR CORRECT SCALING OF VARIOUS FLOODING EXPERIMENTS WITH OIL (300 CP) AND KEROSENE (1.2 CP)

l	d	q	k
1.03 m	0.064 m	0.67×10^{-6} m³/sec	203×10^{-12} m² (203 D)
1.60 m	0.100 m	1.02×10^{-6} m³/sec	150×10^{-12} m² (150 D)
3.00 m	0.186 m	2.02×10^{-6} m³/sec	74×10^{-12} m² (74 D)

Assuming the linear dimensions of the model in which the same liquids are used as in the prototype, to be scaled down by a factor of a [$a > 1$] the first coefficient shows that q must be scaled down by the same factor, and the second coefficient shows that k must be scaled up by a. The dimensionless time number shows that t is scaled down by a^2, while from the pressure number it follows that $\triangle p$ is scaled down by a.

It is therefore possible to satisfy the scaling rules when using the same liquids as in the prototype.

SCALED EXPERIMENTS WITH VARYING LINEAR DIMENSIONS

To check the correctness of the scaling conditions discussed in the preceding section, experiments in which all of the dimensionless coefficients had the same value have been made in cyclindrical tubes of different lengths. The lengths of the tubes were 1.03, 1.60 and 3.00 m; their diameters were chosen so as to give equal $\frac{l}{d}$ ratios. The tubes were placed in a horizontal position and were all fully saturated with the same oil of 0.3 N sec/m^2 [300 cp].*

The displacing liquid was kerosene, viscosity 1.2 x 10^{-3} N sec/m^2 [1.2 cp]. The injection rates and the permeabilities were chosen in such a way that both $\frac{q}{d}$ and $k.d$ were [nearly] equal in all cases. It is easy to see that in that case also the dimensionless coefficients are [nearly] equal.

The values of q and k in the various experiments are given in Table 1.

The porosities of the sand were almost the same in the three cases [33 per cent to 36 per cent].

Fig. 2 shows the values of the dimensionless pressure $\left[\frac{k \triangle pd}{q\eta_o}\right]$ and the recovery of the original oil in place [R] plotted against the dimensionless time $\left[\frac{qt}{d^3}\right]$ for the three cases. It appears that the curves for the two largest tubes coincide satisfactorily, but that those for the smallest tube show appreciable deviations. The reason for this may possibly be that the diameter of the 103-cm tube [6.4 cm] is too small as compared to the grain size of the sand [0.07 cm].

To apply these results to a practical case, let us assume a scaling factor $a = 100$ for the 3.00-m tube.

*In the system used in this paper the units of mass, length, and time are kilogram, meter, and second, respectively. The corresponding unit of force is kg m/sec² called Newton (N).
1 N = 10^5 dyne; 1 N/m² = 10 dyne/cm² = 1.45×10^{-4} psi.
1 N sec/m² = 10 dyne sec/cm² = 10 poise.
1 m² = 1.013×10^{12} darcy.

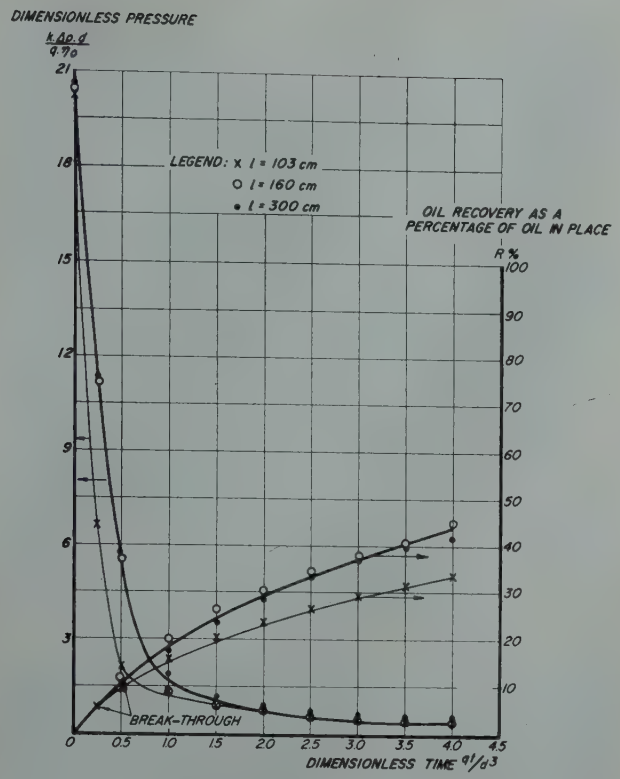
DIMENSIONLESS PRESSURE
LEGEND: x l = 103 cm
o l = 160 cm
• l = 300 cm
OIL RECOVERY AS A PERCENTAGE OF OIL IN PLACE
R %
BREAK-THROUGH
DIMENSIONLESS TIME

FIG. 2 — DIMENSIONLESS PRESSURE NUMBER AND OIL RECOVERY AS A PERCENTAGE OF OIL ORIGINALLY IN PLACE VS DIMENSIONLESS TIME NUMBER FOR SCALED KEROSENE FLOODING EXPERIMENTS IN CYLINDRICAL TUBES.

The above results then obtain, for a linear flow in an oil sand of 300 m length, a thickness of 19 m, having a permeability of 750 md in which the injection rate is 17 m^3/day. Breakthrough for this case will occur after about seven months.

From the figure it is seen that the pressure necessary to maintain the constant injection rate decreases very rapidly in the pre-breakthrough period. After that moment the decrease is far less pronounced.

EXPERIMENTS WITH VARYING VISCOSITY RATIO

According to results obtained by Croes and Schwarz[1] in water drive experiments, the viscosity ratio η_o/η_s can be expected to have a great effect on the recovery efficiency. To check this point, tests were carried out with η_o/η_s varying from 1.5 to 5,000. Again a kerosene viscosity 1.2 cp was used as the displacing fluid. In view of the results described above, these tests were made in the 1.60-m tube. To obtain a good comparison with the water drive experiments mentioned, the same sand having a permeability of 200 x 10^{-12} m^2 [200 D] and the same linear velocity [v = 2.3 x 10^{-4} m/sec corresponding to q = 1.8 x 10^{-6} m^3/sec] were used. Results are given in Fig. 3 where the oil recovery is plotted against log η_o/η_s at different stages of production. As parameter for characterizing the production stage, the total production of oil and kerosene as a percentage of the pore volume (Q) is issued. The figure also shows some curves obtained in the waterdrive tests referred to above.

[1]References given at end of paper.

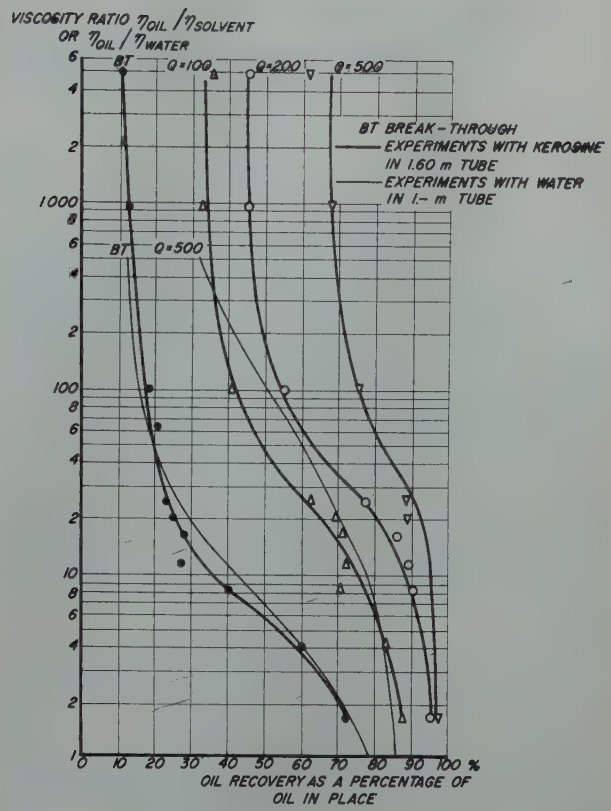

FIG. 3 — OIL RECOVERY WITH SOLVENT FLOODING, AS DEPENDENT ON THE VISCOSITY RATIO OF OIL AND SOLVENT COMPARED WITH OIL RECOVERY FROM WATER FLOODING TESTS ACCORDING TO CROES AND SCHWARZ. SOLVENT USED: KEROSENE, VISCOSITY 1.2 CP. CURVES ARE GIVEN FOR VARIOUS VALUES OF THE GROSS PRODUCTION Q [OIL + KEROSENE OR WATER] EXPRESSED AS A PERCENTAGE OF THE OIL ORIGINALLY IN PLACE.

It is seen that the breakthrough recoveries are nearly the same in both cases. Thus it is concluded that in this range the breakthrough recoveries are determined by the same phenomenon, namely, viscous fingering. After breakthrough of the displacing liquid, however, flooding with a miscible liquid becomes much more efficient than a water flood and this is the more pronounced as the viscosity ratio is higher. Apparently diffusion does not play an important role in the pre-breakthrough period, and can only make itself felt after prolonged flooding.

It has been claimed[2] that when displacing an oil by a miscible liquid a region exists in which the oil concentration increases gradually from zero to one in the direction of flow. The length of this transition zone is said to remain unaltered while it travels through the sand, thus acting as a plunger between the displacing and the displaced liquids. The length of this zone under field conditions is claimed to be of the order of 10 m, which is small compared to a well-distance of say 300 m.

As the results of the experiments in the two largest tubes tend to prove the correctness of the scaling rules, the length of the transition zone should consequently be of the order of 0.10 m for our 3.00-m tube. Accordingly a breakthrough recovery of the order of $\frac{300\text{-}10}{300}$

TABLE 2 — RESULTS OF FLOODING EXPERIMENTS WITH OIL AND KEROSENE FOLLOWED UP BY A WATER DRIVE

η_o/η_s	Total amount of kerosene used in per cent of pore volume	Ultimate oil recovery after water flooding in per cent of pore volume	Amount of kerosene in per cent of pore volume left in sand pack after water flooding
24	650	95	15
103	650	82	10
925	650	77	11
4960	650	68	17

or 96 per cent should be expected. The breakthrough recoveries found in our experiments are much lower in the whole range of viscosity ratios investigated. As, moreover, flooding phenomena in the pre-breakthrough period appear to be similar to those in water-oil displacement tests where no plunger action exists, it is concluded that the assumption of a transition zone is not valid in displacements of oil by miscible fluids for the range of viscosity ratios larger than one.

After injection of an amount of kerosene of 6.5 times the pore volume, water was injected at the same rate. This produced a mixture of oil and kerosene, which, however, largely consisted of kerosene. Water flooding was continued until the water/oil mixture ratio equalled 20.

Results are shown in Table 2, where the produced quantity of viscous oil and the amount of kerosene left in the sand pack are given.

Evidently, high ultimate oil recoveries are obtained, also in the case of very viscous oils. Further, most of the solvent [kerosene] in the sand is recovered by the water flood.

However, a straight flood as applied in these experiments requires large quantities of solvent. A method by which to reduce these amounts, will be described below.

EXPERIMENTS WITH RECIRCULATION OF PRODUCED MIXTURE

When considering the results given in Table 2 it should be borne in mind that they were obtained after prolonged flooding with kerosene. Consequently, if we think of a commercial process, enormous amounts of kerosene would have to be injected, which afterwards would have to be separated again from the oil by distillation, thus rendering the whole process uneconomic.

In the flooding experiments described above it was found that after breakthrough the kerosene content of the mixture produced increases rapidly.

The economy of the process can therefore be improved by introducing the following procedure: After breakthrough of the solvent part of the outflow is reinjected, the remaining part is withdrawn from the circuit [bleeding] and replaced by the same amount of pure kerosene. This recycling process is continued until the viscosity of the resulting mixture in the sand has been lowered sufficiently for successful application of a water flood. Results of an experiment are given in Fig. 4.

Before breakthrough the outflow is homogeneous and its viscosity equals that of the original oil, then suddenly "schlieren" occur and the mean viscosity of the [inhomogeneous] outflow drops from 1.10 to 45 x 10^{-3} N sec/m^2 [1,100 cp to 45 cp]. Without recirculation this decrease in viscosity would continue; if, however, recirculation starts as in the test of Fig. 4, the viscosity of the outflow rises again owing to the increase in viscosity of the displacing fluid. Consequently, the viscosity

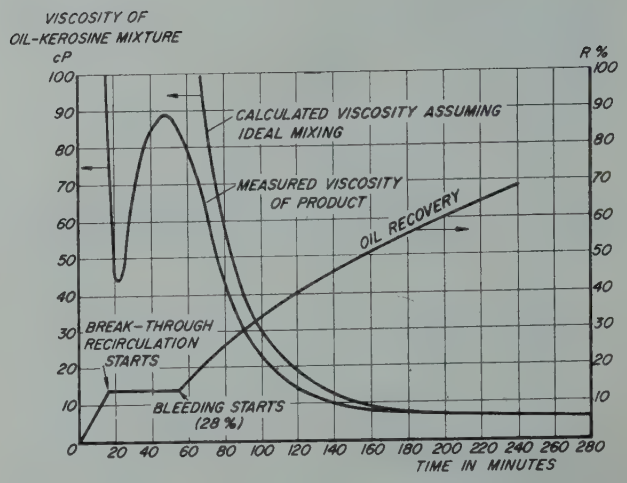

FIG. 4 — RESULTS OF A RECIRCULATION EXPERIMENT.

INITIAL OIL VISCOSITY 1100 cP
KEROSINE VISCOSITY 1.2 cP
BEFORE BREAK-THROUGH q = 37 ml/min.
AFTER BREAK-THROUGH q = 110 ml/min.

ratio of oil in place and displacing liquid will drop, which in its turn results in a more effective production of viscous oil.

As soon as bleeding is started and fresh kerosene is added to the inflow the viscosity of the outflow will again decrease rapidly. In Fig. 4 a curve is also drawn representing the viscosity of the mixture in the sand pack, calculated on the assumption that the pure kerosene injected is completely mixed up with the remaining original oil. It is seen that already after 170 minutes the two viscosity curves coincide, indicating that at that moment mixing was almost complete. Continuing recirculation would now become less effective as the viscosity drops only slowly and depends on the amount of fresh kerosene injected into the system. At this stage water drive should be started.

A series of experiments were carried out to study the influence of two variables, viz. the time of recirculation until bleeding starts and the fraction of the outflow which is continuously withdrawn from the circuit after bleeding has started.

From these experiments the following conclusions were drawn:

1. There is only a slight difference in results when bleeding started immediately after breakthrough and when it is started after 100 per cent PV has been recirculated. There is, however, a distinct influence of the degree of bleeding, less bleeding resulting in a markedly smaller amount of kerosene needed, without appreciably diminishing the ultimate recovery.

2. Water flooding should start as soon as possible, i.e., as soon as more or less homogeneous mixing of viscous oil and kerosene has been obtained. It is of interest to compare also the viscosity curves in Fig. 4, from which it is seen that as soon as 170 minutes after the beginning of the test practically homogeneous blending occurs.

3. The most salient fact, however, is that the economy of the procedure is much greater when applying recirculation.

From Table 2 it is seen that without recirculation 650 per cent PV of kerosene had to be used to reach an oil recovery of 77 per cent PV for a 1,100 cp oil,

while with recirculation a recovery of 81 per cent with only 48 per cent PV of kerosene could be obtained; the amount of kerosene lost was practically the same in both cases [11 per cent and 10 per cent respectively]. Yet the above figures show that to produce 100 m^3 of a highly viscous oil 59 m^3 of kerosene [or low viscous crude] must be used, of which 47 m^3 can be recovered by distillation and 12 m^3 are lost.

Though consequently the process may not be attractive for the moment it should be borne in mind, that the production of viscous oils will always involve extra costs. The process may further be of value for obtaining a bypass to start some other recovery process [underground combustion].

CONCLUSIONS

1. Model experiments on the displacement of oil by miscible liquid [solvent] should not be carried out on too small a scale. In the tests reported results with tubes of 1.60 and 3.00 m length were in good agreement, whereas those with a 1.03-m tube showed appreciable deviations.

2. Breakthrough recoveries obtained when flooding oils of different viscosities with kerosene as a solvent in unconsolidated sands are equal to those obtained in water flooding. When continuing the flooding process kerosene yields appreciably higher recoveries than water especially in the case of higher viscous oils. The drawback of a "straight" kerosene flood is, however, that large quantities of this solvent are required.

3. By applying a procedure in which after breakthrough the outflowing liquid is recirculated for some time, the amount of kerosene required can be drastically reduced without decreasing the oil recoveries. Though the procedure may be a potential bypass to start some other recovery process it is not yet an economic proposition.

ACKNOWLEDGMENT

The authors are greatly indebted to Jan van Heiningen for many valuable discussions, to A. Achterberg, J. A. van Benten, and J. Toornvliet for carrying out the experiments and to the management of N. V. De Bataafsche Petroleum Maatschappij, The Hague, for their permission to publish this work.

NOMENCLATURE

f	= porosity
c_o, [c_s]	= concentration of oil [solvent] in the mixture oil-solvent [m^3/m^3]
η_o, [η_s] [η_m]	= viscosity of oil, [solvent] [mixture] [N sec/m^2]
ρ_o, [ρ_s] [ρ_m]	= density of [oil], [solvent], [mixture] [kg/m^3]
D_o, [D_s]	= diffusion coefficient of oil [solvent] into solvent [oil] [m^2/sec]
E	= ratio of diffusion coefficient in a porous medium and the normal diffusion coefficient in a non porous medium
k	= one-phase permeability [m^2]
x_1, x_2, x_3	= Cartesian coordinates
X_1, X_2, X_3	= dimensionless coordinates
l	= length parallel to flow direction [m]
d	= length perpendicular to flow direction [m]
t	= time [sec]
T	= dimensionless time
q	= flow rate [m^3/sec]
g	= acceleration of gravity [m/sec^2]
p	= pressure [N/m^2]
$\triangle p$	= pressure difference [N/m^2]
v_1, v_2, v_3	= components of flow velocity [m/sec]
R	= oil recovery as a percentage of original oil in place
Q	= cumulative production [oil and solvent] as a percentage of original oil in place

REFERENCES

1. Croes, G. A., and Schwarz, N.: "Dimensionally Scaled Experiments and the Theories of the Water-Drive Process," Paper 332-G, Presented at the Petroleum Branch, AIME, Fall Meeting [October 1953], Dallas, Tex.
2. Morse, R. A.: [Stanolind Oil and Gas Co.] "Recovery of Oil from Reservoirs," German patent No. 849534 [July 1952].

DISCUSSION

R. A. MORSE
MEMBER AIME

STANOLIND OIL & GAS CO.
TULSA, OKLA.

The authors conclude that in a miscible fluid drive in the range of viscosity ratios larger than one, there is no transition zone formed separating the injected and in-place fluids. This conclusion is based on the results of scale experiments in which a large prototype is studied by means of a small model. Our opposite conclusion has been reached based on laboratory tests on long core systems, flooded at oil field rates. Thus no scaling down of either time or distance is involved.

In core systems up to 100 ft in length, a more viscous oil was driven with a less viscous hydrocarbon (solvent). It was found that a transition zone was formed, which separates the in-place oil from the solvent. This zone was observed to grow rapidly at first, then gradually the rate of growth fell off to where it became nearly stabilized. As an example, in a 100-ft core system in which a 1.2 cps viscosity oil was pushed at a rate of advance of 2 ft per day by a solvent having 0.24 cps viscosity (viscosity ratio = 5), the transition zone was 5 ft long after traveling 10 ft, but after traveling 100 ft the zone was only about 10 ft long. The length of this zone was found to be influenced by its rate of advance, distance traveled, but most of all by the viscosity ratio and absolute viscosity of the fluids. Permeability of the porous material was found to have only a small effect on the length of the transition zone. Tests were run in an unconsolidated core system (2 darcys) and two consolidated core systems (400 md and 12 md).

It is a possibility that the work of the authors' is a study of the initiating stage of development of the transition zone. Our experience agrees with that of the authors for this phase of miscible fluid displacement in that the behavior during the initial phase is similar to immiscible fluid displacement. The scaling criteria that were used apparently are not complete enough to include the factors which control the formation of a transition zone.

AUTHORS' REPLY to R. A. MORSE

R. A. Morse's experiments are very valuable, especially as they are carried out in such very long cores.

There seems to be, however, an explanation which agrees with both our and his experimental results. In a cylindrical core with laminar flow in the longitudinal direction, diffusion has two effects. In the longitudinal direction it prevents the formation of a clear interface; in the radial direction, however, it helps in removing the original liquid which is trapped between "fingers" of the solvent. This promotes the formation of a more-or-less clear interface or transition zone. In the present case longitudinal diffusion can be safely neglected with respect to the large convection in that direction.

Consequently, the results we get will largely depend on whether the time which is required for diffusion to reduce radial variations of concentration to a negligible amount is small or large compared to the time necessary for longitudinal transport to produce such variations or fingers. This viscous fingering is likely to be especially important for high viscosity contrasts. Once fingers have been formed, some of them may grow rapidly to large dimensions until they are either confined by the boundaries of the reservoir or by other fingers. Thus, we believe the lateral dimensions of the fingers will be greater, the greater the width of the reservoir. Spreading out the finger boundary within which the concentration variation occurs must proceed by radial diffusion. Thus, the time required to eliminate the fingers will be proportional to d^2/D_o where d is diameter of the tube and D_o is the diffusion coefficient. Also, the time to produce a finger will be proportional to L/v where v is linear velocity and L the length the displacing fluid has traveled along the tube. The governing dimensionless group is consequently d^2v/D_oL. If this number is small, radial diffusion is relatively important and promotes the formation of a transition zone within which there is little or no radial variation in concentration. If it is large, diffusion will not play a significant role; and the effect achieved equals that obtained with immiscible liquids, i.e., viscous fingering.

Now, in Morse's experiment the values of v, D_o, and L are of the same order of magnitude as those in the field, but the lateral dimension d is greatly reduced as he uses a core, and this decreases the magnitude of the dimensionless number. Consequently, after traveling some length through the core a transition zone as described can develop. This, however, would not occur in the field where d is much larger and lateral diffusion cannot make itself felt over such a large distance in the time available. In the long core experiment the longitudinal distance is not scaled down, but the lateral distance is scaled down by a large factor. By giving both d/l *and* q/D_od the values occurring in the field, we gave also the number d^2v/D_oL the right value ($q = \frac{1}{4}\pi d^2v$).

This also explains why in the initiating stage Morse's results agree with those given in the paper. The length L over which the fluid is displaced is still very short and the number d^2v/D_oL has still a low value; radial diffusion has not yet had time to make itself felt, and radial variations in concentrations or fingers still exist. Or, in other words, the ratio d/L still complies with that used by us.

In the later stage of Morse's experiment radial variations in concentrations are negligible, and there results a continuous concentration variation in longitudinal direction forming a transition zone between pure solvent and pure oil. Such a transition zone has a stabilizing effect in that it will prevent further viscous fingering. Viscous fingering can only be expected if there exists a large contrast in viscosity between two adjacent fluids, and this condition only occurs at the start of Morse's experiment.

It is, however, exactly that initiating stage which will occur in the field, and the stabilizing transition zone will not get time to develop before breakthrough to the production well occurs. ★★★

FURTHER DISCUSSION of PAPERS PUBLISHED in TRANSACTIONS, VOLUME 201 (1954)

THE MECHANICS of FORMATION FRACTURE INDUCTION and EXTENSION

W. J. McGUIRE, JR.
MEMBER AIME
EUGENE HARRISON
W. F. KIESCHNICK, JR.
JUNIOR MEMBER AIME

THE ATLANTIC REFINING CO.
DALLAS, TEX.

(Published as T. P. 3916, Page 252)

DISCUSSION

ROSCOE C. CLARK, JR., MEMBER AIME, THE WESTERN CO., MIDLAND, TEX.
HENRY F. COFFER, CONTINENTAL OIL CO., PONCA CITY, OKLA.

W. J. McGuire, et al, are to be commended for their undertaking of a mathematical solution of a very difficult problem.

Unfortunately, however, a mathematical approach requires the application of several assumptions. These assumptions appear to be unrealistic and lead to answers which do not describe what actually happens when hydraulically fracturing oil and gas wells.

Considering laboratory confirmation of breakdown phenomena, the authors appear to have tested their theories only on cement specimens and on samples of Austin limestone, much too small to provide any fracture system. This work resulted in the formation of vertical fractures. If the authors had tried similar experiments on thick walled cylinders made from almost any sandstone cores, they would have found that, using crude oil as the breakdown fluid, horizontal fractures would almost always occur, and at pressures much lower than any calculated. They would also find that by confining the fluid to within the bore (using oil base mud for example) on similar samples, the pressures required to burst the cylinders would be considerably higher and most of the fractures would be vertical. This breakdown pressure behavior has been duplicated in wells in Texas, Oklahoma, Kansas and in Wyoming.

Considering field data the phenomena of different breakdown pressures for different breakdown techniques can be further illustrated. Most production and service personnel will agree that a breakdown can be more easily obtained if injection into a formation can be established prior to the occurrence of the breakdown. This is true whether the formation being treated is completed as open hole or as a perforated interval. This is clearly illustrated by a Lakota well in Wyoming, completed open hole at a total depth of 7,358 ft. An attempt to vertically fracture this well failed when a bottom hole pressure of 10,326 psi was insufficient to break down the formation. A non-penetrating type fluid (oil base mud) was in the well at the time the breakdown was tried.* The oil base mud was then cleaned out of the well and replaced by a 30° API gravity crude oil. With this oil in the hole the formation breakdown was easily accomplished at a bottom hole pressure of 3,607 psi. This large difference in fracture pressures would be impossible according to the theories presented by McGuire, et al.

The authors have used as an example the breakdown pressures experienced when acidizing Permian Basin wells. During acid treatments of limestone and dolomite the "breakdown" (drop-off in pressure) seldom occurs until some injection of acid has been accomplished. In these cases the breakdown is most likely to result from the chemical reaction of acid and rock in already existing vugs and fractures rather than from making a new fracture by hydraulic pressure. If this is true, then results in the Permian basin should not be used to validate the authors' calculations. ★★★

*Several attempts were made to accomplish the breakdown.

AUTHORS' REPLY to ROSCOE C. CLARK and HENRY F. COFFER

The purpose of our laboratory experiments in which thick-walled rock cylinders were hydraulically fractured was to determine the validity of the "thick pipe" formula for brittle materials, and not *to predict nor demonstrate directly* the orientation of field fractures. Our conclusions concerning field results resulted from calculations involving the "thick pipe" relationship as well as considerations of overburden stresses, rock strengths, and the geometry and dimensions of the field system. Clark suggests that had the models been more porous or contained weak bedding planes, horizontal fracturing would have occurred. This is undoubtedly true provided external stresses similar to those in the earth's crust *are not imposed*. However, if we were going to design experiments to represent directly the field case we would impose the proper stresses on the models. It is generally recognized that the vertical compressive stress in the earth's crust arising from the weight of the overburden is approximately 1 psi/ft of depth. Then, as an example, even though a horizontal bedding plane has zero strength, the formation cannot be separated to form a horizontal fracture unless the hydraulic pressure exceeds the stress due to overburden. And in those cases in which the stress resisting vertical fracturing is significantly less than that resisting horizontal fracturing, vertical fractures should result, notwithstanding horizontal plane weaknesses.

We agree that breakdown pressure will be less if the fracturing fluid penetrates the formation. In Appendix III of our paper it is shown that leak-off reduces the pressure necessary to initiate either a horizontal or vertical fracture. It would be difficult to attempt to

explain the failure to breakdown of the Lakota well without complete data. If the state of stress in the formation is dominated by tectonic forces such that horizontal stresses are higher than vertical stresses, for example, our analysis might explain the failure to breakdown at this high pressure.

The majority of the breakdown pressures which we cited were from wells completed in a Devonian field which does not have interconnected vugs or fractures. Further, vugs and fractures in this formation are of microscopic size, so that we can not visualize breakthrough into any native system with enough volume to cause pressure "breakbacks" of the magnitude of these observed in the field. ★★★

THE MECHANICS of FORMATION FRACTURE INDUCTION and EXTENSION

W. J. McGUIRE, JR.
MEMBER AIME
EUGENE HARRISON
W. F. KIESCHNICK, JR.
JUNIOR MEMBER AIME

THE ATLANTIC REFINING CO.
DALLAS, TEX.

(Published as T. P. 3916, Page 252)

DISCUSSION

GEORGE C. HOWARD, *MEMBER AIME, STANOLIND OIL & GAS CO., TULSA, OKLA.*

As far as we know, theoretical investigations such as those by Miles and Topping* made in the past concerning hydraulic fracturing of formations overlooked the important fact that these formations are porous and permeable. The authors of this paper are to be commended for their attempt to analyze the validity of the assumption that the rock may be considered impermeable, insofar as calculation of stresses is concerned. They conclude in Section III of the Appendix that such an assumption is valid. We think this conclusion may have overlooked some factors.

The stress distribution was calculated by the authors under conditions of flow from the wellbore into a permeable formation. The boundary conditions imposed are correct both at the bore where the radial compressive stress is equal to the pressure in the hole and also far away from the bore where the radial compressive stress vanishes. However, it appears that the proper boundary conditions along the plane interfaces between permeable and impermeable formations that occur in a well were not considered. Instead of imposing such boundary conditions, the problem is solved for cases of plane stress and plane strain. It is incorrectly stated that the solution of the problem under consideration is intermediate between the two simple cases mentioned above.

It is believed that this problem can be correctly solved by super-imposing the stresses which would satisfy the boundary conditions along the permeable-impermeable formation interface upon a two-dimensional stress distribution. This additional stress must not disturb the already satisfied conditions along the cylindrical boundaries. This stress vanishes some distance away from the plane boundaries and is greatest at these interfaces.

This may be visualized by stating that the additional stress has both normal and shearing components along the plane boundaries between the permeable and impermeable formation. Calculation of the additional stress is not a two-dimensional problem, but a much more complicated problem of axial symmetry, the solution of which we have not found in the literature.

This additional stress distribution, the result of leak-off, has a definite effect on the induction of hydraulic fractures. This conclusion differs from that of the authors. We feel that such leak-off affects fracture orientation.

Consider, for example, the circular cylinder with concentric hole shown in Fig. A. The cylinder is made of a permeable rock (the size of the pores being exaggerated in the figure for illustration). If such a cylinder is provided with impermeable covers for the ends, the cylinder can be considered equivalent to a permeable formation bounded by impermeable formations above and below.

If fluid could not flow out of the axial hole, pressure applied in the hole would result in the well-known stress distribution, with vertical (or axial) components of stress being nil and the tangential components being tensile. Such a stress distribution, if of sufficient magnitude, would tend to produce a vertical fracture.

If, on the other hand, the fluid can leak away, with a resulting pressure buildup in the pores, then the stress distribution is very complex. An insight into the phenomenon may be obtained by considering the extreme case of constant pressure throughout the pores, i.e., of having the same pressure applied to the outer wall of the cylinder as to the bore itself. Then the *stress* components *in* any *horizontal direction* are equal and they are *compressive*. On the other hand, pore pressure results in vertical forces F, shown in Fig. A, which act on the impermeable flat ends and subject the cylinder to a *vertical tensile stress*. Therefore, a horizontal fracture may be expected.

The above example describes a cylinder of finite outer radius with equal pressure in the pores, i.e., subjected to a zero gradient of pressure. In a formation, i.e., in a cylinder of an infinite outer radius, the gradient of pressure around the wellbore may be made as small as desired by choosing a sufficiently low rate of injection. Therefore it would appear that there may be a critical value of injection rate above which fractures would be expected to be vertical and below which they would probably be horizontal. This critical value would be affected by many factors such as viscosity of the fracturing fluid, depth, thickness and permeability of the formation, and vertical variation in permeability. Since viscosity is a factor also affecting the leak-away rate, it would appear that the lower the viscosity the greater is the likelihood of horizontal fracturing. This is in agreement with the results of laboratory experiments published by Scott et al**.

Fracturing pressures generally increase with depth. For a given available pump power, this would indicate that the injection rate would decrease with depth. For the same pump power, therefore, it would be expected that the likelihood of vertical fracturing would be greater in shallow wells and the likelihood of horizontal

*Miles, A. J., and Topping, A. D., "Stresses Around a Deep Well," JOUR. PET. TECH., Nov., 1948.

**Reference 8, "The Mechanics of Formation Fracture Induction and Extension."

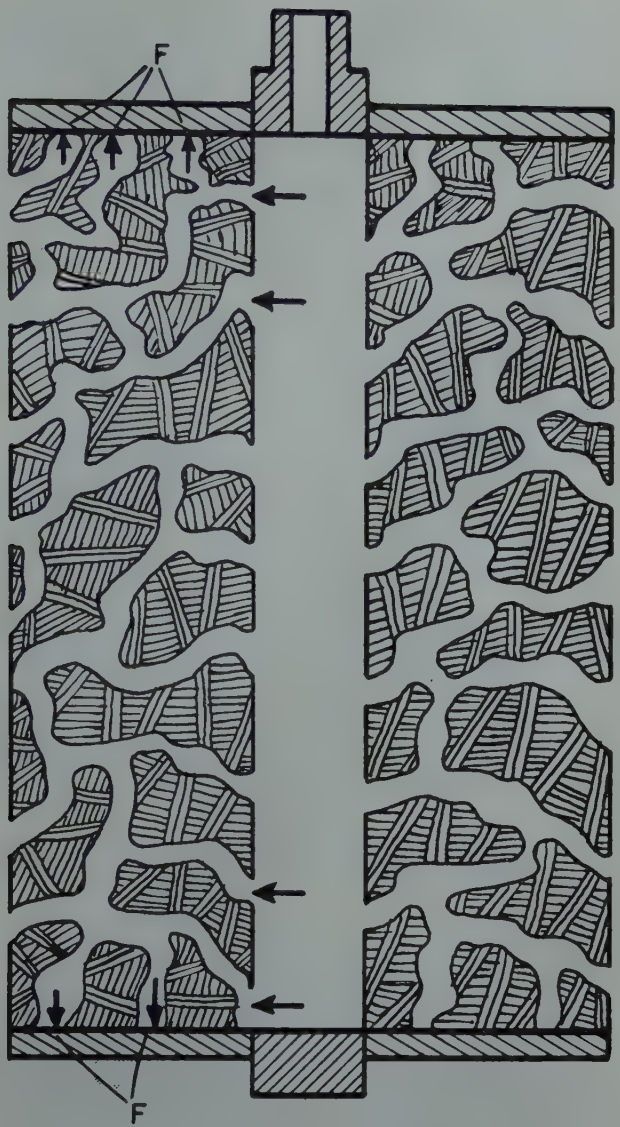

FIG. A — VERTICAL STRESS IN POROUS MEDIA.

fracturing greater in deep wells. This is opposite to the conclusions reached in the paper.

In Fig. 1 of the paper, tensile strength calculated using the thick cylinder formula varies for the same rock between 240 and 3,500 psi. This wide variation in rupturing pressure is explained as due to random distribution of points of weakness in the material. Experimental data which we have obtained make us question this conclusion. Specimens of rock of constant ratio of internal to external radii and with varying diameter of the internal bore were fractured. In these tests the borehole diameter varied from ⅜ in to 4 in. It was observed that these variations in bore diameter did not appreciably affect the bursting pressures. On the other hand, as previously reported**, variations in the penetrating characteristics of the fracturing fluid resulted in a marked variation in fracturing pressure.

If, as these experiments would indicate, the stresses in the rock depend in part on the flow of the fluid into it, it would appear that parting of the rock near the bore or considerably removed from it must be examined with this fact in view. Therefore, a study of fracture extension or rock parting after the initial fracture based upon formulae of the elasticity of impermeable bodies should, in our opinion, be viewed with caution. The

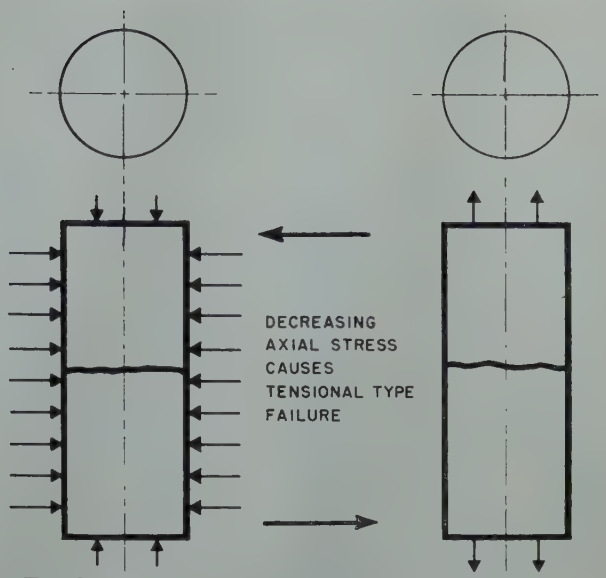

FIG. B — FAILURE RESULTING FROM VARIATION IN PRINCIPLE STRESS.

same comment should be made regarding the results of photoelastic experiments with gelatin. Here again the effect of permeability of the media is excluded by the nature of the experiment.

In the portion of the paper dealing with fracture orientation, it is stated that fracturing may occur only as the stress in the direction perpendicular to the fracture passes from compression to tension. Experiments performed by P. W. Bridgman*** indicate that the above conclusion may have overlooked some considerations. A solid impermeable cylinder shown in Fig. B was first subjected to the same high pressure on the curved surface and on the flat ends. Then the pressure was somewhat decreased on the flat ends only. When the difference in pressures acting on the curved surface and on the flat ends reached some value, the cylinder broke as if subjected to an axial tension although the axial stress was compressive.

This phenomenon may also be illustrated by the idealized test machine in Fig. C. Here the plane ends and the round surface of an impermeable specimen in rod form, having a tensile strength of 1,000 psi and a cross-sectional area of 1 sq in, may be subjected to different hydraulic pressures shown as P_1 and P_2 respectively. The sample is held in two packing seals which react on the rod with a negligible force. If P_1 is equal to P_2, say 10,000 psi, then rod is subjected to a compressive stress of 10,000 psi and will not rupture. However, in accordance with Bridgman's experiments, if the pressure P_1 is reduced to a value of about 1,000 psi below P_2, the rod will part. A "tension type" failure would be produced even though the specimen was still under 9,000 psi compressive stress.

In light of experimental evidence, it does not appear that a formation must be in tension for hydraulic fracturing to occur. Until more direct evidence is available, it would appear that the conclusion of the authors that horizontal fractures are impossible below around 3,000 ft may be in conflict with other known facts as outlined below.

The section of the paper entitled "Direct Evidence of Fracture Orientation" is a good review of the very

***Bridgman, P. W., *Studies in Large Plastic Flow and Fracture*, McGraw-Hill Book Co., Inc., 1952, and *The Physics of High Pressure*, G. Bell and Sons, Ltd., London, England, 1931.

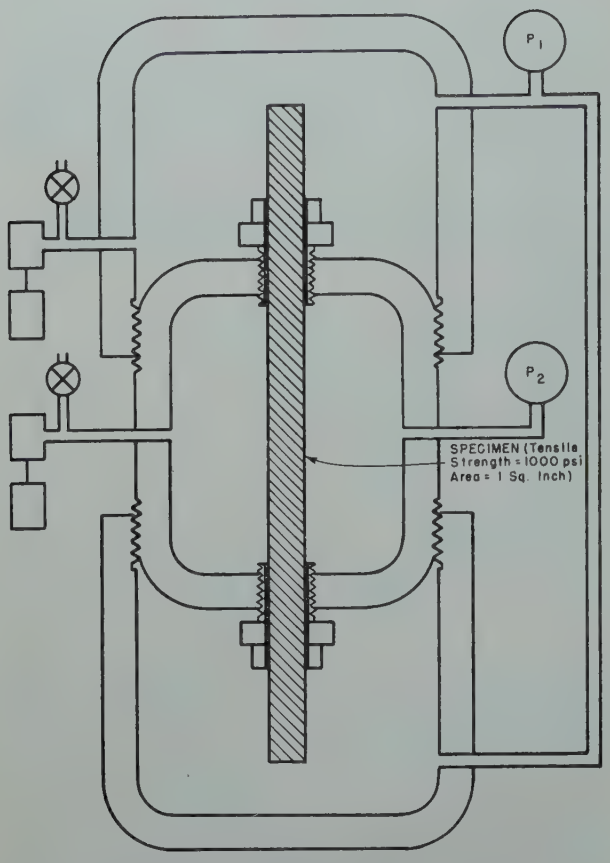

FIG. C — APPARATUS TO ILLUSTRATE TENSIONAL TYPE FAILURE DUE TO COMPRESSIVE STRESS.

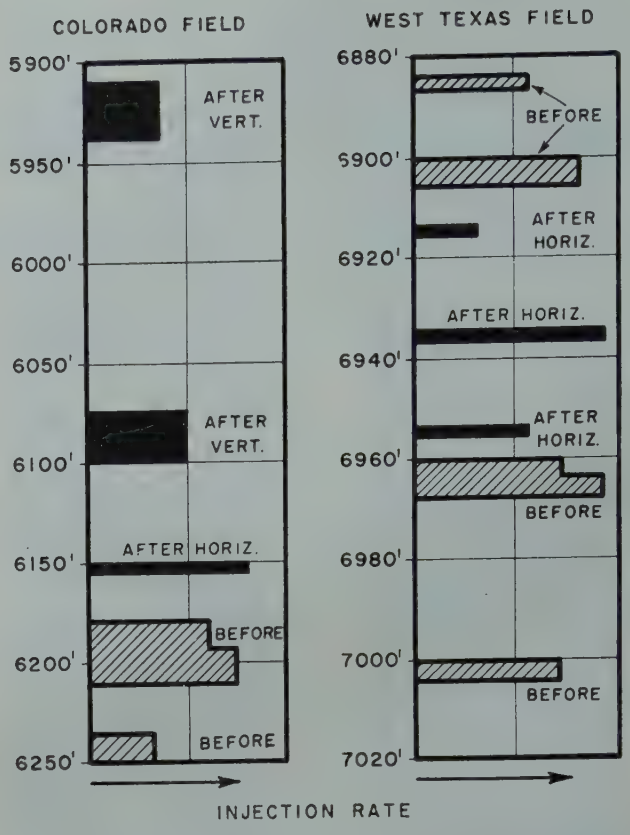

FIG. D — PERMEABILITY PROFILE EVIDENCE OF VERTICAL AND HORIZONTAL FRACTURES.

majority of hydraulic fracturing jobs are successful in producing primarily oil, even in thin formations where another phase (water or gas) is present, seems to indicate that fractures are generally horizontal. Further evidence of the creation of horizontal fractures has been obtained from permeability profiles conducted before and after hydraulic fracturing treatments.

As an example, two profiles are shown on Fig. D, one from a well in a West Texas field and one from a well in a Colorado field. In the Colorado well, the profiles were interpreted to indicate one horizontal and two vertical fractures. In the West Texas field, the profiles indicated three horizontal fractures. Both of the wells were open hole completions.

The laboratory experiments on Austin limestone cylinders, described by the authors, resulted in vertical fracturing. Similar experiments described last year by Scott et al** which were made with other rock resulted in production of both horizontal and vertical fractures. Since both conditions are possible, it seems to us that a very thorough understanding of all factors concerned is required before conclusions can be reached as to the circumstances under which each is normally produced.

★★★

AUTHORS' REPLY to GEORGE C. HOWARD

George C. Howard raises a number of points in his criticism, and for clarity we shall first re-state his important points and then deal with them in order. We believe that his main points consist of the following:

1. That there is error in our theoretical analysis showing that a consideration of rock porosity and permeability will not change conclusions derived from an analysis of an impermeable system.

2. That our analysis of the relationship between bursting pressure and size of borehole in small models is not confirmed by his data.

3. That we have omitted the consideration of porosity and permeability from our fracture extension studies.

4. That experiments by Bridgman are a basis for questioning our criterion for rock failure.

5. That direct evidence concerning the orientation of fractures in the field is furnished by spinner data and that this evidence contradicts our conclusions.

6. That results of laboratory experiments by Scott contradict conclusions drawn from results of our laboratory experiments.

We submit the following comments in answer to these points:

1. It is pointed out that we have omitted consideration of the proper boundary conditions along the plane interfaces between permeable and impermeable formations. This consideration is of interest, of course, for two reasons: (a) due to the fluid pressure bearing against such a barrier, tensile stresses will be set up, tending to cause horizontal fracturing; and (b) a shear stress will exist on this boundary, tending to restrict radial displacement of a formation being fractured and complicating the three dimensional stress distribution.

We believe that we have dealt with (a) in our Appendix III by demonstrating that the magnitude of the pressure which would lead to horizontal fracturing by this mechanism is greater than the pressure required to induce vertical fracturing. Concerning (b), it is true that we have omitted a boundary condition which should be a consideration in the problem. However, we can demonstrate that taking this into account will not

lead to any appreciable effect upon the analysis. We cite the work of Nadai* who has shown in laboratory experiments that the pressure required to rupture relatively short, thick-walled cylinders is actually slightly reduced by restraining or capping the ends. We believe that by dealing with this objection our assumption that the true solution lies intermediate between the cases of plane strain and plane stress will be acceptable.

Howard uses a cylindrical model with a porous outer boundary to demonstrate how, in the extreme case, horizontal fracturing would be expected as a result of severe leak-off. If an actual reservoir could be represented by such a model we would agree with his conclusion that in the extreme example cited, that is, when the entire reservoir has been pressured up, a horizontal fracture could be created. We would agree, further, that there would be some critical injection rate above which fractures would be expected to be vertical and below which they would be horizontal. However, this critical rate is certainly beyond practical operating conditions. For example, it may be recalled that the breakdown pressures in actual field operations occur after the injection of a very small volume of fluid and during a period when there is certainly a large horizontal pressure gradient. Further, with respect to this critical injection rate, we believe that our steady-state leak-off analysis can shed some light. Even though we did not use the same assumptions as Howard did in his analysis, our steady-state leak-off analysis could be thought of as a special case involving injection into his model at the time at which the pressure wave just reaches the outer porous boundary. Even in this case of extreme leak-off penetration and relatively flat pressure gradient, vertical fractures are predicted.

2. We are not sure how to reconcile our data with those of Howard. We do believe, however, that the generality that measured tensile strength is a function of the volume of material placed under tension is well established, and it is interesting to note that some of the data published by Clark** seem to demonstrate the same relationship between bursting pressure and borehole diameter which we observed in our work.

3. Concerning the effect of leak-off upon our analysis of fracture extension, we did not believe at the time of the study that this would affect our conclusions. It can be demonstrated that the only consideration to be made here is that of the influence of the leak-off upon failure at the outer tip of the fracture. The effect of a leak-off would be in the direction of lowering the extension pressure. However, we do not believe that this is a significant effect because we would predict that the leak-off rate would be quite small relative to the rate of fracture extension.

4. Some experiments by P. W. Bridgman are cited as casting doubt on our criterion of failure, namely, that fracturing may occur only as a stress in the direction perpendicular to the fracture passes from compression to tension. The most important point to be made here is that Bridgman *did not obtain open fractures* and certainly *could not* under the circumstances. In our case we are certainly concerned with fractures which must be opened sufficiently for a stream of fluid to pass through. However, confining our attention merely to the criterion for failure, we believe it is important to observe that these experiments were carried out at extremely high pressures, in the magnitude of several hundred thousand pounds per square inch, and in the words of Bridgman*** "under these pressures all ordinary theories as to behavior of elastic solids break down completely . . ." We cannot be sure of an explanation for this phenomenon, but it seems possible that nonuniform transmittal of compressive stress, or internal adjustments, or other such considerations could explain the phenomenon.

5. We have been concerned about the difficulties of interpreting spinner surveys for the purpose of discriminating between vertical and horizontal fractures. Without examining the raw data which went into the bar graphs presented we cannot make useful comment about these examples. It should be noted that our concepts could lead to predicting horizontal fractures in the locations cited *if* high horizontal stresses were present due to tectonic forces.

Frequently in the literature or in discussions concerning this controversial issue of fracture orientation, reference is made to spinner data as direct evidence of fracture orientation. We have not seen such reliable data. We believe that those who base their conclusions upon such data could perform a useful service in publishing this type of information for the industry, not in simplified bar graph form, but in raw form along with analysis and conclusions. For our part, we are attempting to gain more insight into this complex question by obtaining radioactive tracer data on downhole fracture orientation and vertical extent.

6. We believe that the first paragraph of our answer to the comment of Clark and Coffer adequately deals with this point. ★★★

*Nadai, A.: *Theory of Flow and Fracture of Solids*, (1950), 205.
**Clark, R. C., Jr.: "Hydraulic Fracturing of Oil and Gas Wells," *Oil and Gas Jour.* (Sept. 1953), 52.
***Bridgman, P. W., *Philosophical Magazine* (July 1912), XXIV, 63.

SOLUTION OF THE EQUATIONS OF UNSTEADY STATE TWO-PHASE FLOW

W. J. WEST
W. W. GARVIN
J. W. SHELDON
CALIFORNIA RESEARCH CORP.
LA HABRA, CALIF.

(Published as T. P. 3892, Page 217)

DISCUSSION

LOYD R. KERN, *MEMBER AIME, THE ATLANTIC REFINING CO., DALLAS, TEX.*

Future progress in reservoir engineering will be greatly influenced by the recent development of high speed, digital computers; the work of the authors is an excellent example of computer application to this field of endeavor.

The worth of computers may be illustrated by comparing the work of Miller, Brownscombe, and Kieschnick[1] with the present work. The equations which were solved by the authors of the present paper were solved in 1948 by Miller, Brownscombe, and Kieschnick to determine the effect of production rate on ultimate recovery in solution gas driven reservoirs. The actual numerical computations in the present work were obtained in 30 minutes on the computer. Miller et al labored for nearly 1½ man-years on a desk calculator to obtain their solution. The solution, no doubt, would have required many years had not special procedures been devised to allow the use of fairly large zones and time intervals at the sacrifice of some accuracy.

Economical and accurate studies of the two-phase flow equations as well as other complex equations are now possible with the development of modern computers. ★★★

EFFECT of GAS SLIP on UNSTEADY FLOW of GAS through POROUS MEDIA — EXPERIMENTAL VERIFICATION

G. C. WALLICK
J. S. ARONOFSKY
MEMBER AIME

MAGNOLIA FIELD RESEARCH LABORATORIES
DALLAS, TEX.

ABSTRACT

This paper presents an experimental verification of numerical solutions of the differential equation describing the transient flow of an ideal gas through a porous material including gas slip effects. Several experiments previously proposed by one of the authors are described together with the correlation of the experimental results with the numerical solutions. Excellent agreement is shown between experiment and theory, thus demonstrating the validity of both the basic assumption made in the derivation of the differential equation and of the numerical solutions of the differential equation.

INTRODUCTION

In a recent paper,[1] one of the authors has discussed a numerical solution of the differential equation describing the unsteady flow of an ideal gas through a porous material. This paper was primarily concerned with the effect of gas slip on the flow behavior. In steady state measurements, Klinkenberg[2] and others have observed that the apparent gas permeability k_a of a porous material may be expressed as a linear function of the reciprocal average pressure $1/\bar{P}$ of the form,

$$k_a = b + m/\bar{P} \quad . \quad . \quad . \quad . \quad . \quad . \quad . \quad . \quad . \quad (1)$$

where the intercept b is a constant for a given porous material and the slope m is a constant for a given porous material-gas combination. Aronofsky[1] assumed that Equation (1) could be used to describe transient flow if $\bar{P}$ was replaced by the average pressure in an infinitesimal volume element. A number of numerical solutions of the resultant differential equation were presented and specific flow experiments were proposed as a means of testing the numerical solutions. The purpose of the present paper is to describe the results of several of these experiments and the correlation of the experimental data with the results of the numerical analysis. Reference should be made to the previous paper[1] for details of the mathematical and numerical analysis.

EXPERIMENTAL PROCEDURE

A simplified schematic drawing of the experimental apparatus is shown in Fig. 1. An 8.89 cm diameter limestone core of length $L = 14.82$ cm was mounted in a conventional rubber sleeve permeameter cell. The external sleeve pressure in this cell was maintained equal to 500 psig during all experimental tests, thus permitting only longitudinal flow through the core. One end of the core, $X = L$, was connected to an adjustable cavity of volume V as well as a pressure gauge or manometer. The other end of the core, $X = O$, was connected to a Nullmatic pressure regulator which was in turn connected to a nitrogen cylinder or vacuum pump. In each experiment, the core and adjacent dead volume were charged with nitrogen to a uniform gas pressure P_i. The pressure at $X = O$ was then suddenly raised or lowered to a constant pressure P_f and the resulting pressure buildup or pressure decline at $X = L$ was recorded as a function of the time.

The porosity ϕ and the permeability constants m and b were determined using the transient method which was suggested by the results of the numerical analysis and which was described in the earlier paper.[1] The following average values for these constants were obtained as a result of 19 separate evaluations: $m = 0.259 \pm 0.005$ md-atm; $b = 0.374 \pm 0.008$ md; and $\phi = 0.098 \pm 0.005$*. It should be noted that in order that transient phenomena will be slow enough to be observed conveniently, it is desirable to use a porous material of very low permeability, e.g., less than 1 md. Moreover, it is in this low permeability range that the gas slip effects are most significant. Thus, such a low permeability sample is very suitable for use in an experimental verification of the numerical solutions previously described.

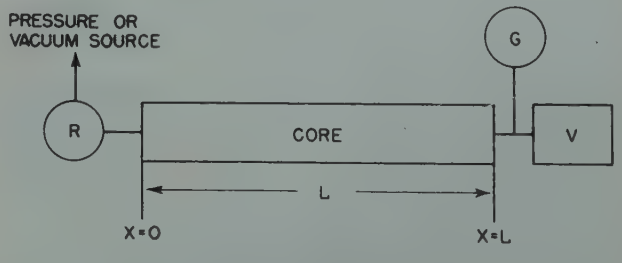

FIG. 1 — SCHEMATIC OF EXPERIMENTAL APPARATUS.

[1]References given at end of paper.

Manuscript received in Petroleum Branch offices on Aug. 19, 1954.

*These values as obtained by the transient method were in agreement with values obtained by steady state measurements to within the accuracy of the steady state measurements (approximately 10 per cent).

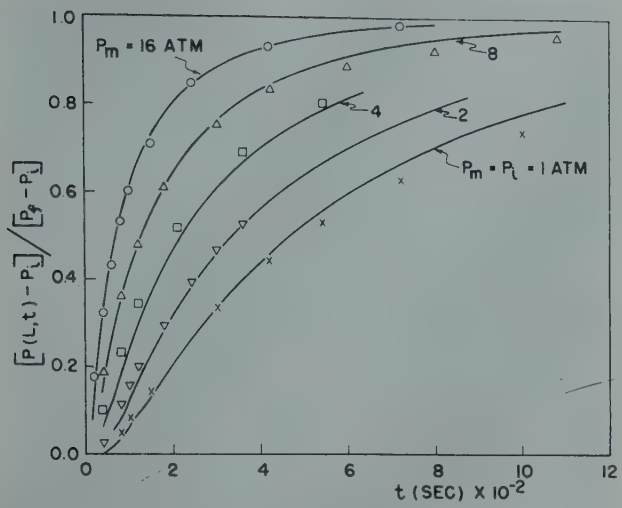

FIG. 2 — INFLUENCE OF MAXIMUM PRESSURE $P_m = P_i$ ON PRESSURE HISTORY AT $X = L$. COMPARISON OF EXPERIMENTAL DATA WITH NUMERICAL SOLUTIONS. $P_f/P_i = 0.1$.

The following experiments, suggested in the previous paper, have been carried out and the data thus obtained correlated with numerical solutions in which the above values for m, b, and ϕ were used.

1. The factors m and b and the ratio of dead volume to pore volume V/V_p were held constant. The maximum pressure P_m in the system was then varied in a series of experiments by starting at different initial pressures for the fixed value of $P_f/P_i = 0.10$.

2. The factors m, b, V/V_p, and P_m were held constant, while the ratio P_f/P_i was varied.

3. The factors m, b, P_m, and P_f/P_i were held constant, while the ratio V/V_p was varied by adjusting V.

These three experiments, investigating the effects of variation of each of the three factors P_m, P_f/P_i, and V/V_p could be carried out using only one gas and one porous core, and it is such a series of experiments which is described in the present paper. In order to investigate the effects of the factors m and b it would be necessary to employ several different cores and different gases. Such an extensive experimental program was considered to be beyond the scope of this investigation.

CORRELATION OF EXPERIMENT AND THEORY

The analysis of the numerical solutions of the transient gas flow equation indicated that, in a series of depletion experiments carried out with a fixed ratio of P_f/P_i, the rate of pressure decline in the core would be strongly dependent upon the value of the maximum pressure P_m in the system. (For $P_f/P_i < 1.0$, $P_m = P_i$; for $P_f/P_i > 1.0$, $P_m = P_f$). Five depletion experiments were carried out to investigate this dependence. The same ratio of $P_f/P_i = 0.1$ was used in each test and the initial pressure in the system, $P_i = P_m$, was set successively at 1, 2, 4, 8, and 16 atmospheres.

A comparison of the experimentally observed pressure history curves at $X = L$ with the pressure curves predicted by the numerical analysis is shown in Fig. 2. In this figure the solid curves are the numerical solutions and the individual points represent the experimental data. A different symbol has been used to represent the experimental data corresponding to each of the five values of P_m, e.g., the circles represent the data for $P_m = 16$ atm. The agreement between experiment and theory is very satisfactory with the exception of the case where $P_m = 1$ atm. Since there is no apparent factor in the calculation procedure which would render one numerical solution less accurate than another, this deviation is probably due to small errors in the low pressure measurements. There is a deviation of the experimental data from the theoretical curves during the early transient period in each of the five cases. Several factors may have contributed to this deviation. The shape of the experimental decline curves could very well have been influenced by the time required to open the valve isolating the core from the pressure regulator. In addition it is likely that the pressure regulator could not maintain a constant pressure at the end of the core, $(X = O)$, during the initial transient period. It is also possible that inertial effects, neglected in the original formulation of the problem, may have been important in the early transient period.

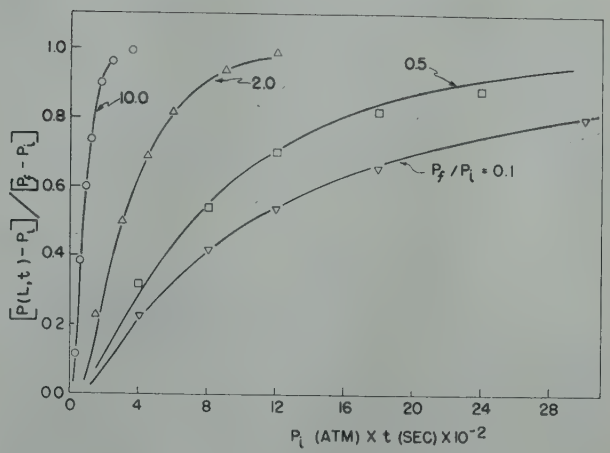

FIG. 3 — INFLUENCE OF RATIO OF FINAL PRESSURE TO INITIAL PRESSURE P_f/P_i ON PRESSURE HISTORY AT $X = L$. COMPARISON OF EXPERIMENTAL DATA WITH NUMERICAL SOLUTIONS. $P_m = 10.0$ ATM.

It is significant that for the five pressure history curves shown there is no consistent type of deviation of the experimental data from the theoretical curves. This more or less random deviation indicates that the observed discrepancies between experiment and theory may for the most part be attributed to experimental error.

The numerical solutions indicated that the rate of pressure increase or decline within a core in an injection or depletion experiment is very dependent upon the ratio P_f/P_i. To investigate this dependence experimentally, the factors m, b, V/V_p, and P_m were held constant in each of two injection experiments and two depletion experiments and only the ratio P_f/P_i was varied. In each of these tests, a maximum pressure $P_m = 10$ atm. was used and the ratio P_f/P_i was established successively equal to 10.0, 2.0, 0.5, and 0.1. The resultant pressure buildup and decline curves are shown in Fig. 3. In this figure the solid curves are the numerical solutions and the individual points represent the experimental data. A different symbol has been used to represent the experimental data corre-

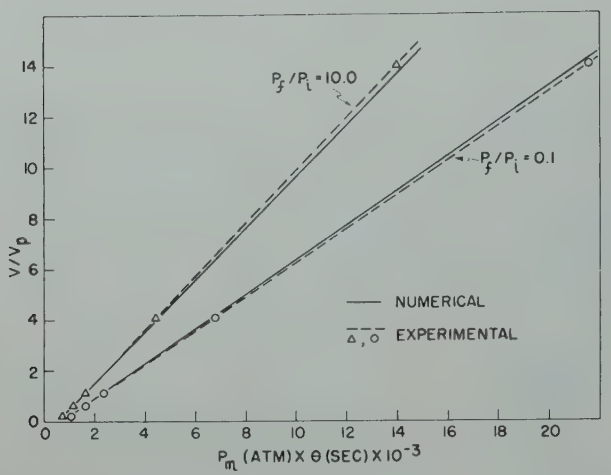

FIG. 4 — INFLUENCE OF CAVITY VOLUME TO PORE VOLUME RATIO V/V_p ON PRESSURE HISTORY AT $X = L$. $P_m = 10.0$ ATM: Θ = TIME REQUIRED FOR $P(L, t)$ TO REACH 0.55 P_m.

sponding to each of the four values of P_f/P_i. With the exception of the early transient period, there is excellent agreement between experiment and theory. The possible reasons for this initial deviation are the same as those discussed in connection with Fig. 2.

In the previous paper it was shown that for a series of depletion experiments with constant values for the factors m, b, P_m, and P_f/P_i, the time Θ in seconds required for the pressure at the end of the core, $X = L$, to reach 55 per cent of P_m could be expressed approximately in terms of the cavity volume to pore volume ratio V/V_p as

$$P_m\Theta = A + B(V/V_p) \quad . \quad . \quad . \quad . \quad . \quad (2)$$

This dependence of Θ on the ratio V/V_p was investigated experimentally for both injection and depletion, setting P_f/P_i equal to 0.1 for depletion and equal to 10.0 for injection. The method of least squares was applied to the experimental values for the intercept A and the slope B of the straight line described by Equation (2). The numerical solutions indicated that Equation (2) was also valid for injection if different values for A and B were introduced. Therefore, the same method was used to obtain experimental values for A and B for injection. The method of least squares was also used to obtain the best theoretical values for A and B for depletion and corresponding values for injection.

The results of this investigation are summarized in Fig. 4. In this figure, the solid lines represent the theoretical predictions; the individual points, the experimental data; and the broken lines, the best straight lines through the experimental points as determined by the method of least squares. The agreement between experiment and theory is seen to be very satisfactory. For both the depletion and injection experiments, it was found that the theoretical values for the constants A and B were in agreement with the experimental values to within 2.0 per cent. This close agreement is very significant in view of the fact that the largest value for V/V_p used in the theoretical determination of these constants was $V/V_p = 2.0$ while the largest experimental value for this ratio was $V/V_p = 14.0$.

The correlation of experiment and theory, represented in Figs. 2, 3, and 4, provides strong evidence of the validity of the numerical solutions described in the earlier paper. Moreover, since the transient method for determining m, b, and ϕ was based upon the numerical solutions, the consistency of the method and the reasonable agreement of the results of the method with steady state measurements may be considered as a further verification of the numerical solutions. It is believed that a refinement of the experimental techniques employed in this investigation would result in an even more satisfactory correlation. At the same time, deviations in experiment and theory in the earlier transient period indicate that further refinements may be needed in the theoretical formulation to extend the range of validity to higher gas flow velocities.

ACKNOWLEDGMENTS

Acknowledgment is made to the management of the Field Research Laboratories, Magnolia Petroleum Co., for permission to publish the results of this investigation. The authors also wish to express their appreciation to N. Stein for his supervision of the experimental work and to O. D. Ferris for his aid in the numerical calculations.

REFERENCES

1. Aronofsky, J. S.: *Jour. Appl. Phys.* (1954), **25**, 48.
2. Klinkenberg, L. J.: *Drilling and Production Practice* (API, 1941).

★★★

TECHNICAL NOTE **244**

A ROTATIONAL HIGH PRESSURE VISCOSIMETER

MURRAY F. HAWKINS, JR.
MEMBER AIME

MARION L. KIMMEL
JUNIOR MEMBER AIME

LOUISIANA STATE UNIVERSITY
BATON ROUGE, LA.

INTRODUCTION

Sage[1] appears to have been the first (1933) to design a rolling ball viscosimeter for the express purpose of measuring the viscosity of oils with natural gas in solution, i.e., under reservoir conditions. In 1940 Hocott and Buckley[2] further refined the rolling ball instrument in both design and method of operation, and their instrument, known as the Humble type, was the forerunner of present day viscosimeters used in petroleum production and research laboratories. They also initiated the technique of charging the viscosimeter with a sample directly from a bottom hole sampler.

In 1948 the committee on engineering research of the Petroleum Division of the AIME in Part 3 (1) of

Manuscript received in Petroleum Branch offices on May 6, 1954.

[1]References given at end of paper.

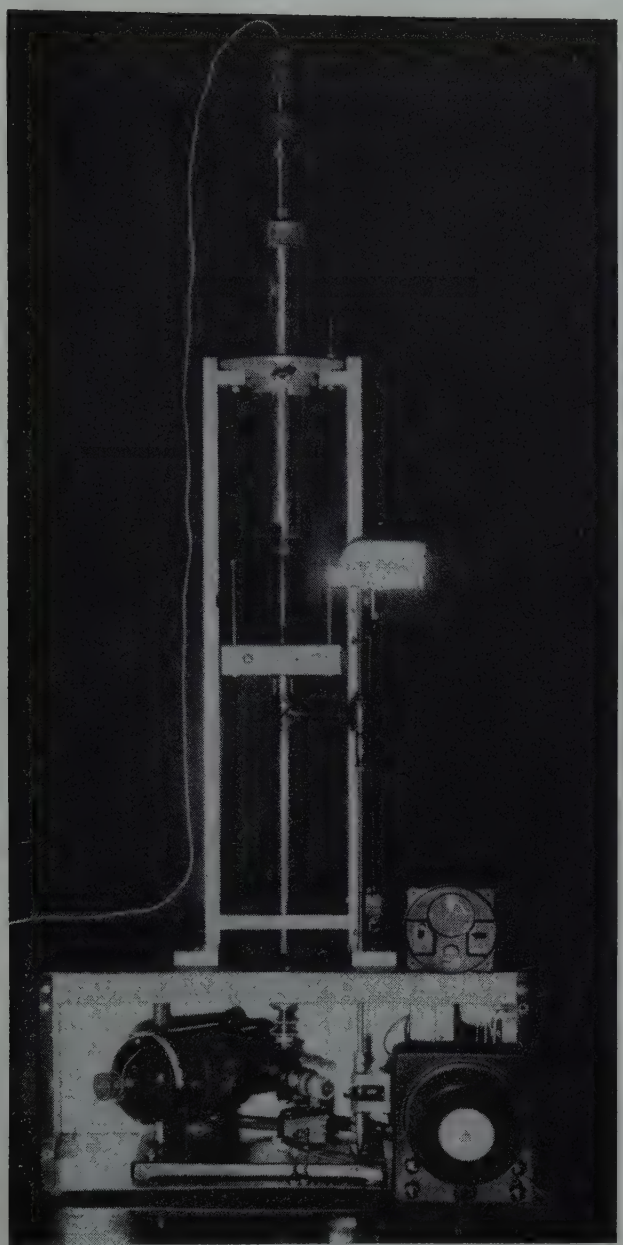

FIG. 1 — PHOTOGRAPH OF THE HIGH PRESSURE ROTATIONAL VISCOSIMETER.

the Physical-Chemical Topics of Table 1 suggested the "development of improved and simpler methods of measuring viscosity of reservoir fluids." This note will describe a rotational, high pressure viscosimeter which has been developed in response to this suggestion but whose relative merits are yet to be determined fully.

THE INSTRUMENT

Fig. 1 is a photograph and Fig. 2 is a cross sectional drawing of the instrument. It consists of a non-magnetic, stainless steel rotor about 4 in. in length and 1 in. in diameter centered axially within a non-magnetic, stainless steel, pressure vessel of cylindrical bore. The rotor is mounted on miniature, precision ball bearings and has a radial clearance of about 1/64 in. Alnico magnets are inserted perpendicular to the axis of rotation on either end of the rotor, those at the top to serve as indicator magnets, those at the bottom, as the driven magnets which turn the rotor. A constant (but variable) speed motor outside the pressure vessel turns the rotor by means of a driving magnet attached to the motor shaft. The motor speed is checked using an aircraft type, precision, spring-wound interval timer and an electric impulse counter to record revolutions by means of an electric contactor on the motor shaft.

FLUID VISCOSITY MEASUREMENT

The fluid viscosity is measured at constant rotational speed in terms of the distance (screw turns) the driving magnet must be withdrawn from the rotor magnets before a break in the magnetic linkage occurs, that is, when the viscous torque exerted by the fluid on the rotor just exceeds the torque between the magnets. This break is precipitous and is easily detected by observing the motion of a magnetized needle suspended outside the pressure vessel near the indicator magnets in the top of the rotor.

Rotor speeds and clearance between rotor and stator were selected from tests[3] to insure laminar flow, which generally obtains in the reservoir. While the upper and lower limits of the viscosity range are yet to be determined, it is known that they can be extended considerably beyond those indicated in Fig. 3 by changing the clearance, using insert cylinders for example, and/or by changing the speed of rotation. The instrument has a capacity of about 40 cc and is designed to measure absolute viscosity.

The pressure coefficient in the present instrument was made negligible for the range of pressures used by selecting a pressure vessel of sufficient wall thickness (½ in), as an alternative to using an insert cylinder on which internal and external pressures may equalize. The temperature coefficient was made small by manufacturing the rotor and stator of the same material. The

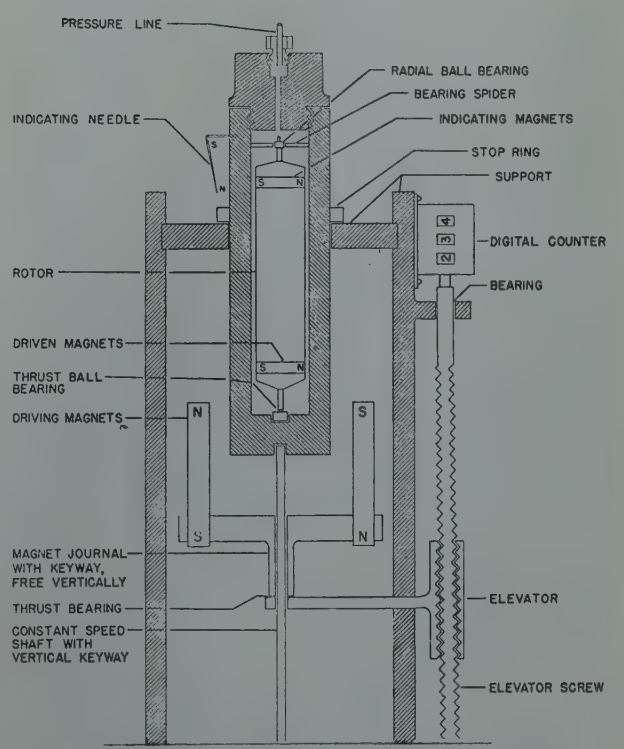

FIG. 2 — SKETCH OF PRESSURE VISCOSIMETER.

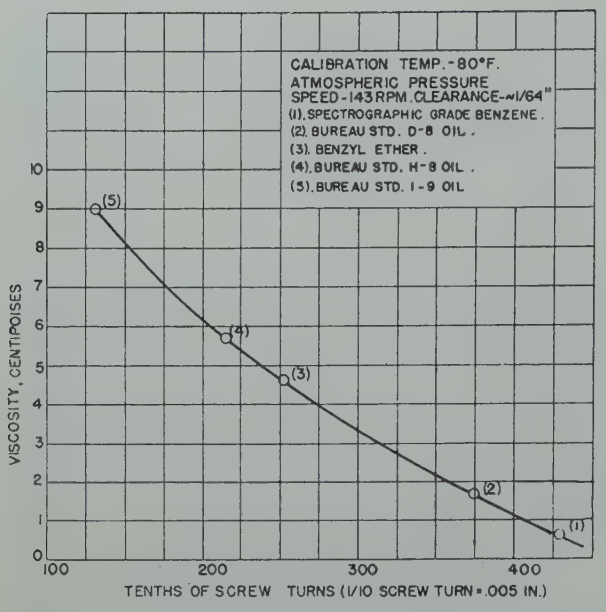
CALIBRATION TEMP. - 80°F.
ATMOSPHERIC PRESSURE
SPEED - 143 RPM. CLEARANCE - ~1/64"
(1). SPECTROGRAPHIC GRADE BENZENE.
(2). BUREAU STD. D-8 OIL.
(3). BENZYL ETHER.
(4). BUREAU STD. H-8 OIL.
(5). BUREAU STD. I-9 OIL
VISCOSITY, CENTIPOISES
TENTHS OF SCREW TURNS (1/10 SCREW TURN = .005 IN.)

FIG. 3 — CALIBRATION CHART FOR ROTATIONAL HIGH PRESSURE VISCOSIMETER.

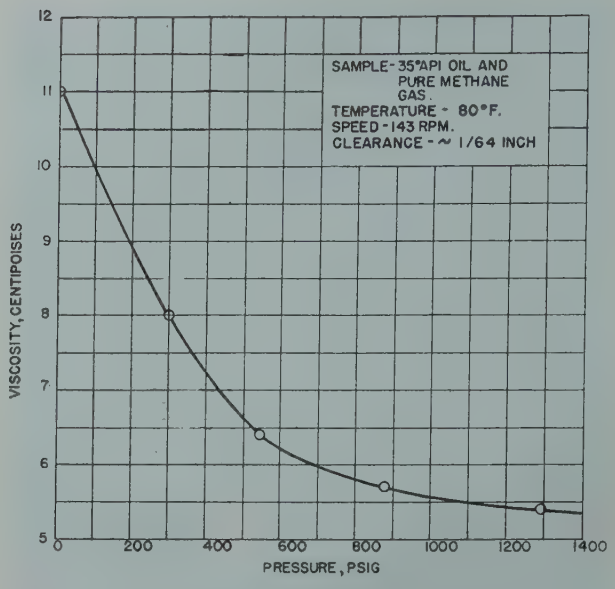
SAMPLE - 35° API OIL AND PURE METHANE GAS.
TEMPERATURE - 80°F.
SPEED - 143 RPM.
CLEARANCE - ~ 1/64 INCH
VISCOSITY, CENTIPOISES
PRESSURE, PSIG

FIG. 4 — VISCOSITY OF A 35° API OIL WITH METHANE SOLUTION GAS AS A FUNCTION OF SATURATION PRESSURE.

aging coefficient of the Alnico magnets is known to be very low; however, bearing wear, although not observed in some 50 hours of testing, will certainly call for periodic calibration.

CALIBRATION CURVE

Fig. 3 is a calibration curve performed at atmospheric pressure and room temperature using fluids supplied by the U. S. Bureau of Standards and other fluids of known viscosities. No temperature controlled jacket was provided for the present instrument, and all measurements were made at room temperature. Corrections for small temperature variations from 80° F were made using known or estimated temperature coefficients of viscosity for the liquids.

Fig. 4 is a measurement at elevated pressures on a 35° API oil sample using pure methane for the dissolved gas. As the gas was dissolved in the oil in the instrument, pressures above saturation were not obtainable without mercury entering the vessel. This limitation would not exist, of course, in the case of a sample transferred from a bottom hole sampler or storage vessel. Check measurements with a Humble type rolling ball instrument at the higher pressures gave satisfactory agreement. Tests indicate a rapid attainment of equilibrium following a pressure change during which the rotor was kept in motion. No difficulties were encountered with escaped gas bubbles lodging between the rotor and stator. The five measurements of Fig. 4 were completed in less than an hour, several duplicate readings of good reproducibility having been taken at each point.

While no claim is made for a finished, commercial instrument, and while several refinements, improvements, and simplifications are now obvious, tests indicate that a new type pressure viscosimeter has been developed which satisfactorily measures reservoir oil viscosity.

ACKNOWLEDGMENT

Appreciation is expressed to the Humble Oil and Refining Co., who, although in no way connected with this work, established a graduate fellowship in the Petroleum Engineering Department under which this study was conducted.

REFERENCES

1. Sage, B. H.: "Measurements of Viscosities of Liquids Saturated with Gases at High Pressures," *Ind. Eng. Chem.*, Anal. Ed., V (1933), 261.
2. Hocott, C. R., and Buckley, A. E.: "Measurement of the Viscosity of Oils Under Reservoir Conditions," *Pet. Dev. and Tech.*, CSLII (1941).
3. Kimmel, M. L.: "The Development of a High Pressure Viscosimeter," a thesis submitted in partial fulfillment for the M.S. degree in Petroleum Engineering, Louisiana State University (1952), 52.

★★★

INDEX

Petroleum Transactions, Volume 201

(Plus References to Articles and Technical Notes Published in JOURNAL OF PETROLEUM TECHNOLOGY *in 1954)*

A

ALLEN, T. O., and ATTERBURY, J. H., JR.: *Effectiveness of Gun Perforating,* 8 (Jan. JPT, 34)

AREAL SWEEP PATTERNS: potentiometric model studies of vertically fractured reservoir, 192 (Aug. JPT, 41)

ARONOFSKY, J. S., and JENKINS, R.: *Simplified Analysis of Unsteady Radial Gas Flow,* 149 (July JPT, 23)

ARONOFSKY, J. S., and WALLICK, G. C.: *Effect of Gas Slip on Unsteady Flow of Gas through Porous Media —Experimental Verification* (Tech. Note) Oct. JPT, 27

ASHBY, W. H., et al.: *Pressure Maintenance by Gas Injection in the Brookhaven Field, Mississippi,* 97 (April JPT, 43)

ATTERBURY, J. H., JR., and ALLEN, T. O.: *Effectiveness of Gun Perforating,* 8 (Jan. JPT, 34)

B

BEARDEN, W. G., and WILSEY, L. E.: *Reservoir Fracturing — A Method of Oil Recovery for Extremely Low Permeability Formations,* 169 (Aug. JPT, 21)

BERRY, V. J., JR., et al.: *Role of Bubble Formation in Oil Recovery by Solution Gas Drives in Limestones,* 294 (Dec. JPT, 21)

BERTUZZI, A. F., et al.: *Phase and Volumetric Behavior of Natural Gases at Low Temperatures and High Pressures,* 245 (Oct. JPT, 37)

BLOMBERG, C. R., et al.: *Pressure Maintenance by Gas Injection in the Brookhaven Field, Mississippi,* 97 (April JPT, 43)

BOBO, R. A., and HOCH, R. S.: *Mechanical Treatment of Weighted Drilling Muds,* 93 (April JPT, 39)

BRADENHEAD SQUEEZING, 17 (Jan. JPT, 43)

BRANNON, H. R., JR., et al.: *Interrelation of Resistivity and Potential of Shaly Reservoir Rock,* 176 (Aug. JPT, 29)

BRONS, F., et al.: *Method for Determination of Average Pressure in a Bounded Reservoir,* 182 (Aug. JPT, 35)

BROOKHAVEN FIELD, MISSISSIPPI: five years of unitized pressure maintenance basis for optimistic outlook, 97 (April JPT, 43)
Geology, 97 (Apr. JPT, 43)

BROWNE, W. H., et al.: *Optimum Sand Concentrations in Well Treatments,* 273 (Nov. JPT, 35)

BUBBLES: gas, in solution gas drive of limestone reservoirs of non-uniform porosity, role in oil recovery, laboratory study and indicated possibilities, 294 (Dec. JPT, 21)

BUNDRANT, C. O., et al.: *Optimum Sand Concentrations in Well Treatments,* 273 (Nov. JPT, 35)

BUREAU OF MINES: water-tracer laboratory studies at Bartlesville, 210 (Sept. JPT, 118)

BURROWS, D. B., et al.: *Viscosity of Hydrocarbon Gases under Pressure,* 264 (Oct. JPT, 47)

C

CALDWELL, B. M., and OWEN, H. D.: *New Tool for Perforating Casing below Tubing,* 302 (Dec. JPT, 29)

CALIFORNIA RESEARCH CORP.'s model oil well, filtration measurements, 29 (Feb. JPT, 30)

CALLAWAY, F. H., et al.: *Comparison of Methods for Analyzing a Water Drive Field, Torchlight Tensleep Reservoir, Wyoming,* 197 (Sept. JPT, 105)

CAPILLARY PRESSURE: measurement in experiments on displacement of oil and water in alundum core, 57 (March JPT, 21)

CARR, N. L., et al.: *Viscosity of Hydrocarbon Gases under Pressure,* 264 (Oct. JPT, 47)

CASSINGHAM, R. W., et al.: *Pressure Maintenance by Gas Injection in the Brookhaven Field, Mississippi,* 97 (April JPT, 43)

CAUDLE, B. H., et al.: *Oil Production after Breakthrough as Influenced by Mobility Ratio,* 81 (April JPT, 27), correction, June JPT, 38

CEMENTING: simplified technique for recompletion operations: theory, surface experiments, process, field results, 1 (Jan. JPT, 27)

CEMENT SLURRIES: clay bubbles reduce weight safely to 10 pounds, 146 (June JPT, 35)
Kerosene-cement for plugging off water in fractured formations, 132 (June JPT, 21)

CENTRIFUGE, decanting type useful in treatment of weighted drilling muds, 93 (April JPT, 39)

CHALKLEY FIELD, Southwest Louisiana Coastal area: drilling mud control, 87 (April JPT, 33)

CLARK, R. C., JR., et al.: *Ten-pound Cement Slurry for Oil Wells,* 146 (June JPT, 35)
Discussion of TP3916, 317

CLAUS, C. R., and STANDISH, G. A.: *Drilling Mud Control in Southwest Louisiana Coastal Area,* 87 (April JPT, 33)

CLAY-BUBBLE CEMENT, 146 (June JPT, 35)

COFFER, H. F., et al.: *Ten-pound Cement Slurry for Oil Wells,* 146 (June JPT, 35)
Discussion of TP3916, 317

COLDWATER OIL FIELD, Isabella County, Michigan: development and performance, 22 (Feb. JPT, 23)

Collins, R. E., and Crawford, P. B.: *Estimated Effect of Vertical Fractures on Secondary Recovery,* 192 (Aug. JPT, 41)
Conductive solids. See Electric Logging
Conpernick, 204 (Sept. JPT, 112)
Core: liquid saturation, determination by magnetic susceptibility method, 203 (Sept. JPT, 111)
Corrosion and corrosion fatigue of sucker rods, damaging effects and their relationship to microstructure of rods, 73 (March JPT, 37)
Crawford, P. B., and Collins, R. E.: *Estimated Effect of Vertical Fractures on Secondary Recovery,* 192 (Aug. JPT, 41)
Criss, C. R., and McCormick, R. L.: *History and Performance of the Coldwater Oil Field, Michigan,* 22 (Feb. JPT, 23)

D

Davis, P. C., et al.: *Phase and Volumetric Behavior of Natural Gases at Low Temperatures and High Pressures,* 245 (Oct. JPT, 37)
Dehlinger, Peter, et al.: *Optimum Sand Concentrations in Well Treatments,* 273 (Nov. JPT, 35)
Dewees, E. J., et al.: *Measurement of Resistance to Flow of Fluids in Natural Gas Wells,* 279 (Nov. JPT, 41)
De Witte, Leendert: *Resistivity Logging in Thin Beds,* 155 (July JPT, 29)
Dirty sand: (see also Electric Logging): synthetic, method of making, 46 (Feb. JPT, 47)
Displacement: air-liquid, gas-liquid, and liquid-liquid in microscopic capillaries, 162 (July JPT, 37)
  Oil-water, experiments in alundum core, 57 (March JPT, 21)
Drainage boundaries, determination, 186 (Aug. JPT, 39)
Drilling fluids: clay-water, pumping experiments and calculation of pressure losses, 287 (Nov. JPT, 49)
  Pressure losses, calculation in pumping experiments on clay-water fluids, 287 (Nov. JPT, 49)
Drilling mud: Control in Southwest Louisiana Coastal area, 87 (April JPT, 33)
  Filtration hypotheses, 31 (Feb. JPT, 32)
  Filtration loss during drilling, 29 (Feb. JPT, 30)
  Weighted, treatment with decanting centrifuge improves quality and reduces necessity for chemical treatment, 93 (April JPT, 39)
Dublin, J. R., III, et al.: *Simplified Cementing Technique for Recompletion Operations,* 1 (Jan. JPT, 27)
Dyes, A. B.: *Production of Water-driven Reservoirs below Their Bubble Point,* 240 (Oct. JPT, 31)
Dyes, A. B., et al.: *Oil Production after Breakthrough as Influenced by Mobility Ratio,* 81 (April JPT, 27) correction, June JPT, 38

E

Electric analyzer, comparison with other methods for analyzing water-drive field, 197 (Sept. JPT, 105)
Electric logging: dirty sands (conductive solids), experimental investigation of S. P. and resistivity phenomena, 43 (Feb. JPT, 44)
  Estimation of oil and gas content in shaly rocks and porosity of shaly sands, 179 (Aug. JPT, 32)
  Laterolog-limestone curve combination, 157 (July JPT, 31)
  Shaly reservoir rock, interrelation of resistivity and potential, 176 (Aug. JPT, 29)
  In thin beds, 155 (July JPT, 29)
Electric logs: interpretation of data from shaly sands, 138 (June JPT, 27)
Electrolytic model, blotter type: determination of areal sweep patterns in oil recovery by in-situ combustion, 119 (May JPT, 35)
Electronic digital method: solution of equations of unsteady state two-phase flow in oil reservoirs, 217; Summary, Sept. JPT, 125
Erickson, R. A., et al.: *Oil Production after Breakthrough as Influenced by Mobility Ratio,* 81 (April JPT, 27), correction, June JPT, 38

F

Ferguson, C. K., and Klotz, J. A.: *Filtration from Mud during Drilling,* 29 (Feb. JPT, 30)
Filtration. See Drilling Mud
Flow: air-liquid, gas-liquid, and liquid-liquid displacements in single uniform Pyrex capillaries of microscopic size, 162 (July JPT, 37)
  Fluid, "friction coefficient" and "friction factor" replaced by "resistance coefficient" and "transmission factor," 279 (Nov. JPT, 41)
  Fluid saturation in porous core, determination by magnetic susceptibility method, 203 (Sept. JPT, 111)
  Oil and gas to wells underground, supersaturation study, 230 (Sept. JPT, 127)
  Oil and water in alundum core, breakthrough recoveries, 57 (March JPT, 21)
  Two-phase unsteady state, solutions of equations by electronic digital method, 217; Summary, Sept. JPT, 125; Discussion, 321
  Unsteady, ideal gas through porous media, numerical solution of differential equation, including effect of gas slip (Tech. Note) Oct. JPT, 27
Fluid saturation of porous core, determination by magnetic susceptibility method, 203 (Sept. JPT, 111)
Formation factor, significance of term when applied to dirty sands, 49 (Feb. JPT, 50)
Formation fractures: gel-sand or oil-sand well treatments, abrasion tests, 277 (Nov. JPT, 39)
  Induction as means of increasing recovery of oil from formations of very low permeability, 169 (Aug. JPT, 21)
  Induction and extension, mechanics, 252; Summary, Oct. JPT, 45; Discussion, 317
  Plugging off water with kerosene-cement slurry, 132 (June JPT, 21)
  Repair by squeeze-cementing, 6 (Jan. JPT, 32)
  Sand as propping agent, optimum sand concentrations in gel-sand or oil-sand well treatments, laboratory study, 273 (Nov. JPT, 35)
  Vertical, effect on secondary recovery, potentiometric model studies, 192 (Aug. JPT, 41)
Friction coefficient and friction factor, terms replaced by resistance coefficient and transmission factor, respectively, 279 (Nov. JPT, 41)

G

GARVIN, W. W., et al.: *Solution of the Equations of Unsteady State Two-Phase Flow in Oil Reservoirs,* 217; Summary, Sept. JPT, 125; Discussion, 321

GASES. See Hydrocarbons; also Natural Gas

GAS INJECTION: application of laboratory data to field performance, 85 (April JPT, 31)
- Oil production after breakthrough as influenced by mobility ratio, 81 (April JPT, 27), correction, June JPT, 38
- Pressure maintenance at Brookhaven field, 97 (April JPT, 43)

GEFFEN, T. M., et al.: *Role of Bubble Formation in Oil Recovery by Solution Gas Drives in Limestones,* 294 (Dec. JPT, 21)

GLADFELTER, R. E., et al.: *Comparison of Methods for Analyzing a Water Drive Field, Torchlight Tensleep Reservoir, Wyoming,* 197 (Sept. JPT, 105)

GORE, T. L., et al.: *Phase and Volumetric Behavior of Natural Gases at Low Temperatures and High Pressures,* 245 (Oct. JPT, 37)

GRANT, B. F., and SZASZ, S. E.: *Development of an Underground Heat Wave for Oil Recovery,* 108 (May JPT, 23)

GRAVEL PACKING: essentials for success, 15 (Jan. JPT, 41)
- Histories of wells, 20 (Jan. JPT, 46)
- Pressure pack technique, essentials for success, 16 (Jan. JPT, 41)
- Pressure pack technique, procedure, 17 (Jan. JPT, 43)
- Reasons for, 16 (Jan. JPT, 42)

GUERRERO, E. T., and KENNEDY, H. T.: *Effect of Surface and Interfacial Tensions on Recovery of Oil by Water Flooding,* 124 (May JPT, 41)

GUN PERFORATORS: bullet and jet types, test results, 9 (Jan. JPT, 35)
- Effectiveness, 8 (Jan. JPT, 34)
- Penetration tests, equipment, procedure, and evaluation of data, 10 (Jan. JPT, 36)

H

HARRISON, EUGENE, et al.: *Mechanics of Fracture Induction and Extension,* 252; Summary, Oct. JPT, 45; Discussion, 317

HAVENAAR, I.: *Pumpability of Clay-water Drilling Fluids,* 287 (Nov. JPT, 49)

HAWKINS, M. F., JR., and KIMMEL, M. L.: *Rotational High Pressure Viscosimeter* (Tech. Note) Nov. JPT, 31

HAZEBROEK, P., et al.: *Method for Determination of Average Pressure in a Bounded Reservoir,* 182 (Aug. JPT, 35)

HEAT WAVE, combustion-supported, for increasing oil production, concept and field experiments, 108 (May JPT, 23)

HIGGINS, R. V.: *Study of Undersaturation during Repressuring and Supersaturation during Flow of Oil to Wells,* 230 (Sept. JPT, 127)

HOCH, R. S., and BOBO, R. A.: *Mechanical Treatment of Weighted Drilling Muds,* 93 (Apr. JPT, 39)

HOWARD, G. C., and SCOTT, P. P., JR.: *Plugging Off Water in Fractured Formations,* 132 (June JPT, 21); Discussion of TP3916, 318

HUBER, T. A., et al.: *Simplified Cementing Technique for Recompletion Operations,* 1 (Jan. JPT, 27)

HUNT, E. B., JR., et al.: *Role of Bubble Formation in Oil Recovery by Solution Gas Drives in Limestones,* 294 (Dec. JPT, 21)

HURST METHOD of analyzing water-drive fields, simplified, comparison with other methods, 197 (Sept. JPT, 105)

HYDRATES: formation from mixtures of hydrogen sulfide and methane, 237 (Sept. JPT, 135)

HYDROCARBONS: gas mixtures, viscosity, computation from gas analysis or gas gravity, 264 (Oct. JPT, 47)
- Viscosity, correlation of effect of pressure, temperature, and composition, 265 (Oct. JPT, 48)

HYDROGEN SULFIDE, mixture with methane: hydrate formation, 237 (Sept. JPT, 135)

J

JENKINS, R., and ARONOFSKY, J. S.: *Simplified Analysis of Unsteady Radial Gas Flow,* 149 (July JPT, 23)

JUSTUS, J. B., et al.: *Pressure Maintenance by Gas Injection in the Brookhaven Field, Mississippi,* 97 (April JPT, 43)

K

KATZ, D. L., and NOAKER, L. J.: *Gas Hydrates of Hydrogen Sulfide-Methane Mixtures,* 237 (Sept. JPT, 135)

KENNEDY, H. T., and GUERRERO, E. T.: *Effect of Surface and Interfacial Tensions on Recovery of Oil by Water Flooding,* 124 (May JPT, 41)

KERN, L. R.: Discussion of TP3892, 321

KEROSENE-CEMENT SLURRY for plugging off water in fractured formations, 132 (June JPT, 21)

KIESCHNICK, W. F., JR., et al.: *Mechanics of Fracture Induction and Extension,* 252; Summary, Oct. JPT, 45; Discussion, 317

KIMMEL, M. L., and HAWKINS, M. F., JR.: *Rotational High Pressure Viscosimeter* (Tech. Note) Nov. JPT, 31

KLOTZ, J. A., and FERGUSON, C. K.: *Filtration from Mud during Drilling,* 29 (Feb. JPT, 30)

KOBAYASHI, RIKI, et al.: *Viscosity of Hydrocarbon Gases under Pressure,* 264 (Oct. JPT, 47)

KURATA, F., et al.: *Phase and Volumetric Behavior of Natural Gases at Low Temperatures and High Pressures,* 245 (Oct. JPT, 37)

L

LEVINE, J. S.: *Displacement Experiments in a Consolidated Porous System,* 57 (March JPT, 21)

LIMESTONE RESERVOIRS of non-uniform porosity, definition, 294 (Dec. JPT, 21)
- Solution gas drive, role of gas bubbles, laboratory study and indicated possibilities, 294 (Dec. JPT, 21)

LOUISIANA: Southwest Coastal area: drilling mud control, 87 (April JPT, 33)
- Geology, 88 (April JPT, 34)

LOW-TEMPERATURE SEPARATION PROCESSES: application of data on phase and volumetric behavior of gas mixtures, 245 (Oct. JPT, 37)

LOY, M. E., et al.: *Contribution to Electrical Log Interpretation in Shaly Sands,* 138 (June JPT, 27)

M

MAGNETIC susceptibility, determination of liquid saturation in porous materials, 203 (Sept. JPT, 111)

MAGNOLIA PETROLEUM CO.: drilling mud control in Southwest Louisiana Coastal area, 87 (April JPT, 33)

MAGNOLIA RESEARCH LABORATORIES: schemes for injecting heat into oil formations, 117 (May JPT, 32)

MARDOCK, E. S., and WATKINS, J. W.: *Use of Radioactive Iodine as a Tracer in Water-flooding Operations,* 209 (Sept. JPT, 117)

MATTHEWS, C. S., et al.: *Method for Determination of Average Pressure in a Bounded Reservoir,* 182 (Aug. JPT, 35)

MCCORMICK, R. L., and CRISS, C. R.: *History and Performance of the Coldwater Oil Field, Michigan,* 22 (Feb. JPT, 23)

MCGLASSON, R. L., and RADD, F. J.: *Corrosion-Metallurgical Aspects of Sucker Rods and Their Oil Well Service Performance,* 73 (March JPT, 37)

MCGUIRE, W. J., et al.: *Mechanics of Fracture Induction and Extension,* 252; Summary, Oct. JPT, 45; Discussion, 317.

METHANE: mixture with hydrogen sulfide, hydrate formation, 237 (Sept. JPT, 135)

MICHIGAN: history and performance of Coldwater oil field, 22 (Feb. JPT, 23)

MISCIBLE LIQUIDS. See Oil Recovery

MISSISSIPPI: Brookhaven field. See Brookhaven

MOBILITY RATIO IN SOME IN-SITU COMBUSTION OPERATIONS: determination of areal sweep by blotter-type electrolytic model, 120 (May JPT, 36)

MODEL: electrolytic, blotter-type: advantages and disadvantages, 119 (May JPT, 35)

Determination of areal sweep patterns in oil recovery by in-situ combustion, 119 (May JPT, 35)

Experiments in recovery of oil from porous sands by injection of miscible liquids (solvents) and subsequent water flooding, 310 (Dec. JPT, 37)

Oil well: filtration measurements, 29 (Feb. JPT, 30)

Potentiometric: fractured system analog for study of effect of vertical fractures on secondary recovery, 192 (Aug. JPT, 41)

MORSE, R. A.: Discussion on Displacement of Oil from Porous Media, 315 (Dec. JPT, 42)

N

NABOR, G. W., and RAMEY, H. J., JR.: *Blotter-Type Electrolytic Model Determination of Areal Sweeps in Oil Recovery by In-situ Combustion,* 119 (May JPT, 35)

NATURAL GAS: conditions for forming hydrates with water when hydrogen sulfide, carbon dioxide, and paraffin hydrocarbons are present, 237 (Sept. JPT, 135)

Flow strings in six fields, measurement of transmission factors, 279 (Nov. JPT, 41)

Ideal, unsteady flow through porous media, numerical solution of the differential equation, including effect of gas slip (Tech. Note) Oct. JPT, 27

Mixtures: Phase and volumetric behavior at low temperatures and high pressures, 245 (Oct. JPT, 37)

Unsteady radial flow in reservoirs, numerical method of prediction, 149 (July JPT, 23)

NITROGEN: separation from hydrocarbons by low-temperature distillation, application of data on phase and volumetric behavior of gas mixtures at low temperatures and high pressures, 245 (Oct. JPT, 37)

NOAKER, L. J., and KATZ, D. L.: *Gas Hydrates of Hydrogen Sulfide-Methane Mixtures,* 237 (Sept. JPT, 135)

O

OFFERINGA, J., and VAN DER POEL, C.: *Displacement of Oil from Porous Media by Miscible Liquids,* 310 (Dec. JPT, 37)

OIL RECOVERY: by in-situ combustion: determination of areal sweeps by blotter-type electrolytic model, 119 (May JPT, 35)

Fracture of formations as means of increasing, 169 (Aug. JPT, 21)

Heat wave method, development, 108 (May JPT, 23)

From fractured formations: conditions affecting, 170 (Aug. JPT, 22)

From porous media by injection of miscible liquids (solvents) and subsequent water flooding, model experiments, 310 (Dec. JPT, 37)

OWEN, H. D., and CALDWELL, B. M.: *New Tool for Perforating Casing below Tubing,* 302 (Dec. JPT, 29)

P

PERFORATOR: tubing gun using a swing jet charge for perforating casing below tubing, 302 (Dec. JPT, 29)

PERKINS, F. M., JR., et al.: *Interrelation of Resistivity and Potential of Shaly Reservoir Rock,* 176 (Aug. JPT, 29)

PIROS BURNER: construction and use in thermal recovery of oil from reservoir, 110 (May JPT, 25)

PLUGGING AGENT: kerosene-cement slurry for plugging off water in fractured formations, 132 (June JPT, 21)

POUPON, A., et al.: *Contribution to Electrical Log Interpretation in Shaly Sands,* 138 (June JPT, 27)

PRESSURE. See Reservoir Pressure

PRESSURE MAINTENANCE. See Gas Injection, etc.

R

RADD, F. J., and MCGLASSON, R. L.: *Corrosion-Metallurgical Aspects of Sucker Rods and Their Oil Well Service Performance,* 73 (March JPT, 37)

RADIOACTIVE IODINE as tracer in water flooding, 209 (Sept. JPT, 117)

RAMEY, H. J., JR., and NABOR, G. W.: *Blotter-Type Electrolytic Model Determination of Areal Sweeps in Oil Recovery by In-situ Combustion,* 119 (May JPT, 35)

RECOMPLETION: benefits from simplified cementing technique, 1 (Jan. JPT, 27)

RELATIVE PERMEABILITY: dynamic, calculation in experiments on oil-water displacement in alundum core, 57 (March JPT, 21)

Oil-water: determination of liquid saturation of porous core by magnetic susceptibility method, 203 (Sept. JPT, 111)

REPRESSURING: undersaturation where some effective permeability to gas exists, 230 (Sept. JPT, 127)

RESERVOIR FLUID containing 35 mole per cent hydrogen sulfide: equilibrium vaporization ratios of other components, 67 (March JPT, 31)
Pressure-volume relationships, 67 (March JPT, 31)
Published correlations on physical properties of fluids can lead to gross errors, 67 (March JPT, 31)
RESERVOIR PERFORMANCE: natural gas: numerical prediction of unsteady radial flow, 149 (July JPT, 23)
RESERVOIR PRESSURE: bounded reservoir: determination of average, 182 (Aug. JPT, 35)
RESERVOIR ROCK: shaly: estimation of oil or gas content by electric logging, 179 (Aug. JPT, 32)
Interrelation of resistivity and potential, 176 (Aug. JPT, 29)
RESISTANCE COEFFICIENT, definition, 279 (Nov. JPT, 41)
RESISTIVITY LOGGING: in thin beds, 155 (July JPT, 29)
REYNOLDS, J. J., et al.: *Ten-pound Cement Slurry for Oil Wells,* 146 (June JPT, 35)
RODGERS, C. J.: *Some Practical Aspects of Gravel Packing,* 15 (Jan. JPT, 41)

S

SANDSTONE, thin-bedded formations, resistivity logging, 155 (July JPT, 29)
SCHILTHUIS, modified method for analyzing water-drive field, comparison with other methods, 197 (Sept. JPT, 105)
SCHNEIDER, F. N., et al.: *Role of Bubble Formation in Oil Recovery by Solution Gas Drives in Limestones,* 294 (Dec. JPT, 21)
SCOTT, P. P., JR., and HOWARD, G. C.: *Plugging Off Water in Fractured Formations,* 132 (June JPT, 21)
SECONDARY RECOVERY: estimated effect of vertical fractures in reservoir, 192 (Aug. JPT, 41)
SHALY SANDS: identification of oil-bearing sands qualitatively and quantitatively from electric logs, 138 (June JPT, 27)
Porosity: estimation by electric logging, 180 (Aug. JPT, 33)
SHELDON, J. W., et al.: *Solution of the Equations of Unsteady State Two-phase Flow in Oil Reservoirs,* 217; Summary, Sept. JPT, 125; Discussion, 321
SINCLAIR RESEARCH LABORATORIES: development of an underground heat wave for oil recovery, 108 (May JPT, 23)
SMITH, R. V., et al.: *Measurement of Resistance to Flow of Fluids in Natural Gas Wells,* 279 (Nov. JPT, 41)
SOLUTION GAS DRIVE: in limestone reservoirs of nonuniform porosity: role of gas bubbles, laboratory study and indicated possibilities, 294 (Dec. JPT, 21)
SOUTHWICK, P. F., and WYLLIE, M. R. J.: *Experimental Investigation of the S. P. and Resistivity Phenomena in Dirty Sands,* 43 (Feb. JPT, 44)
STANDISH, G. A., and CLAUS, C. R.: *Drilling Mud Control in Southwest Louisiana Coastal Area,* 87 (April JPT, 33)
STEEL: major factors affecting service life in oil field sucker rods, 73 (March JPT, 37)
STEWART, C. R., et al.: *Role of Bubble Formation in Oil Recovery by Solution Gas Drives in Limestones,* 294 (Dec. JPT, 21)
STEWART, F. M., et al.: *Comparison of Methods for Analyzing a Water Drive Field, Torchlight Tensleep Reservoir, Wyoming,* 197 (Sept. JPT, 105)
SUCKER RODS: corrosion and corrosion fatigue damage, 73 (March JPT, 37)
Corrosive agencies, 73 (March JPT, 37)
Design and selection of steels for, 78 (March JPT, 42)
Performance affected by manufacturing variables, 79 (March JPT, 43)
Service life affected by microstructure of rods, 73 (March JPT, 37)
SZASZ, S. E., and GRANT, B. F.: *Development of an Underground Heat Wave for Oil Recovery,* 108 (May JPT, 23)

T

TAUSCH, G. H., et al.: *Simplified Cementing Technique for Recompletion Operations,* 1 (Jan. JPT, 27)
TEMPLETON, C. C.: *Study of Displacements in Microscopic Capillaries,* 162 (July JPT, 37)
TEXAS PETROLEUM RESEARCH COMMITTEE: estimated effect of vertical fractures on secondary recovery, 192 (Aug. JPT, 41)
THERMAL ENERGY: application to oil-bearing reservoirs to increase oil recovery, 108, 117 (May JPT, 23, 32)
TIXIER, M. P., et al.: *Contribution to Electrical Log Interpretation in Shaly Sands,* 138 (June JPT, 27)
TORCHLIGHT TENSLEEP RESERVOIR, WYOMING: analysis, comparison of methods, 197 (Sept. JPT, 105)
TRACERS: characteristics required, 209 (Sept. JPT, 117)
Radioactive. See Radioactive
TRANSMISSION FACTOR, definition and methods of computing, 279 (Nov. JPT, 41)
Flow strings of six gas fields, measurement, 279 (Nov. JPT, 41)
TUBING GUN: swinging jet charge: description and field operation, 302 (Dec. JPT, 29)

U

UNITIZATION: Brookhaven field, Mississippi, five years of pressure maintenance indicates continued successful operation, 97 (April JPT, 43)

V

VAGTBORG, HAROLD, JR.: *Equilibrium Vaporization Ratios for a Reservoir Fluid Containing a High Concentration of Hydrogen Sulfide,* 67 (March JPT, 31)
VAN DER POEL, C., and OFFERINGA, J.: *Displacement of Oil from Porous Media by Miscible Liquids,* 310 (Dec. JPT, 37)
VAN EVERDINGEN, et al., 1952 method for analyzing water-drive field, comparison with other methods, 197 (Sept. JPT, 105)
VISCOSIMETER: high pressure rotational (Tech. Note) Nov. JPT, 31

W

WALLICK, G. C., and ARONOFSKY, J. S.: *Effect of Gas Slip on Unsteady Flow through Porous Media — Experimental Verification* (Tech. Note) Oct. JPT, 27

WATER CONING: control: comparative efficiencies of horizontal and vertical barriers, 133 (June JPT, 22)

WATER-DRIVE FIELD: methods for analyzing, comparison, modified Schilthuis, simplified Hurst, van Everdingen, et al., and electric analyzer, 197 (Sept. JPT, 105)

WATER FLOODING: effects of surface tension of brine and interfacial tension between oil and brine on recovery of oil, 124 (May JPT, 41)

Gas decreases effect of interfacial and surface tensions of liquids on oil recovery, 129 (May JPT, 46)

Oil production after breakthrough as influenced by mobility ratio, 81 (April JPT, 27), correction, June JPT, 38

Production of reservoirs below bubble point, effect on recovery, 240 (Oct. JPT, 31)

Radioactive iodine as tracer, 209 (Sept. JPT, 117)

Recovery of oil from porous sands first treated with a miscible liquid (solvent), circulation process, model experiments, 310 (Dec. JPT, 37)

WATKINS, J. W., and MARDOCK, E. S.: *Use of Radioactive Iodine as a Tracer in Water-flooding Operations,* 209 (Sept. JPT, 117)

WELL COMPLETION: gun perforating, effectiveness, 8 (Jan. JPT, 34)

Recompletion, simplified cementing technique for, 1 (Jan. JPT, 27)

WELL TREATMENTS; gel-sand or oil-sand: abrasion tests, 277 (Nov. JPT, 39)

Sand as propping agent, optimum sand concentrations, laboratory study, 273 (Nov. JPT, 35)

WEST, W. J., et al.: *Solution of the Equations of Unsteady State Two-phase Flow in Oil Reservoirs,* 217; Summary, Sept. JPT, 125; Discussion, 321

WHALEN, J. W.: *Magnetic Susceptibility Method for Determination of Liquid Saturation in Porous Materials,* 203 (Sept. JPT, 111)

WILLIAMS, R. H., et al.: *Measurement of Resistance to Flow of Fluids in Natural Gas Wells,* 279 (Nov. JPT, 41)

WILSEY, L. E., and BEARDEN, W. G.: *Reservoir Fracturing — A Method of Oil Recovery for Extremely Low Permeability Formations,* 169 (Aug. JPT, 21)

WINSAUER, W. O., et al.: *Interrelation of Resistivity and Potential of Shaly Reservoir Rock,* 176 (Aug. JPT, 29)

WYLLIE, M. R. J., and SOUTHWICK, P. F.: *Experimental Investigation of the S. P. and Resistivity Phenomena in Dirty Sands,* 43 (Feb. JPT, 44)

WYOMING, TORCHLIGHT TENSLEEP RESERVOIR, analysis, comparison of methods, 197 (Sept. JPT, 105)

Z

ZOMA TANNER PROPERTY: field trials of combustion-supported heat wave for increasing recovery of oil, 109 (May JPT, 24) ★★★